Advanced Triaxial Testing of Soil and Rock

Donaghe/Chaney/Silver
editors

STP 977

ASTM

STP 977

Advanced Triaxial Testing of Soil and Rock

Robert T. Donaghe, Ronald C. Chaney, and Marshall L. Silver, editors

ASTM
1916 Race Street
Philadelphia, PA 19103

Library of Congress Cataloging-in-Publication Data

Advanced triaxial testing of soil and rock/Robert T. Donaghe, Ronald C. Chaney, and Marshall L. Silver, editors.
(STP; 977)
"The symposium on advanced triaxial testing of soil and rock was presented at Louisville, Kentucky on 19–20 June 1986 sponsored by ASTM Committee D-18 on Soil and Rock"—Foreword.
ASTM publication code number (PCN) 04-977000-38.
Includes bibliographies and index.
ISBN 0-8031-0983-0
1. Soils—Testing—Congresses. 2. Rocks—Testing—Congresses. I. Donaghe, Robert T. II. Chaney, Ronald C. III. Silver, Marshall L. IV. ASTM Committee D-18 on Soil and Rock. V. Title: Advanced Triaxial testing of soil and rock. VI. Series: ASTM special technical publication: 977
TA710.5.A38 1988 88-19070
624.1'5136'0287—dc19 CIP

NOTE

The Society is not responsible, as a body,
for the statements and opinions
advanced in this publication.

Peer Review Policy

Each paper published in this volume was evaluated by three peer reviewers. The authors addressed all of the reviewers' comments to the satisfaction of both the technical editor(s) and the ASTM Committee on Publications.

The quality of the papers in this publication reflects not only the obvious efforts of the authors and the technical editor(s), but also the work of these peer reviewers. The ASTM Committee on Publications acknowledges with appreciation their dedication and contribution of time and effort on behalf of ASTM.

Printed in Baltimore
November 1988

Foreword

The symposium on Advanced Triaxial Testing of Soil and Rock was presented at Louisville, Kentucky on 19–20 June 1986 sponsored by ASTM Committee D-18 on Soil and Rock. Robert T. Donaghe, U.S. Army Corps of Engineers, Ronald C. Chaney, Humboldt State University, and Marshall L. Silver, University of Illinois, served as chairmen of the symposium and editors of the resulting publication.

Contents

TEST METHODS

TEST INTERPRETATION AND ERRORS

Overview

Although the triaxial compression test is presently the most widely used procedure for determining strength and stress-deformation properties of soils, there have been no books published on triaxial testing since the 1962 second edition of the landmark work *The Measurement of Soil Properties in the Triaxial Test* by Bishop and Henkel. It is apparent there is a need to document advances made in triaxial testing since publication of Bishop and Henkel's book and to examine the current state of the art in a forum devoted solely to triaxial testing. Because of increasing versatility brought about by recent developments in testing techniques and equipment, it is also important that the geotechnical profession be provided with an up-to-date awareness of potential uses for the triaxial test.

Along with a better understanding of the current state of the art of triaxial testing is the need to evaluate whether recent developments should be incorporated in standard triaxial test methods. Although modern equipment allows testing to be customized to fit many types of design problems, most triaxial testing is still routine and follows standardized procedures. Procedures for standard triaxial tests have been developed by authors of texts, university laboratory instructors, federal and state agencies, and many engineering consulting firms. A major objective of ASTM is to eliminate possible design problems resulting from misleading interpretation of results obtained through the use of different testing procedures by developing widely used standard test methods. To achieve this objective, it is important to keep ASTM standard test methods current and to develop new standard test methods when research and use indicate a need.

With the preceding in mind, Subcommittee D18.05 on Structural Properties and Subcommittee D18.09 on Dynamic Properties suggested to the Executive Committee of Committee D-18 on Soil and Rock that ASTM sponsor a symposium on triaxial testing. As a result, the symposium on Advanced Triaxial Testing on Soil and Rock was held in Louisville, Kentucky on 19–20 June 1986.

The symposium was held in four sessions (two sessions per day) with an evening poster session held at the end of the first day. Topics for the poster session papers were taken from those for the daily sessions. The daily session program format and participants were as follows.

Session 1—Equipment

Chairman	Willard L. DeGroff, McClelland Engineers, Inc., Houston.
State-of-the-art speakers	Marshall L. Silver, University of Illinois, Chicago
	F. Tatsuoka, University of Tokyo, Tokyo, Japan
Invited speakers	D. Negussey, University of British Columbia, Vancouver, B.C.
	H. W. Olsen, U.S. Geological Survey, Denver
	C. K. Chan, University of California, Berkeley

Session 2—Test Methods

Chairman	Richard S. Ladd, Woodward-Clyde Consultants, Clifton, New Jersey
State-of-the-art speakers	S. LaCasse (for Toralv Barre), Norwegian Geotechnical Institute, Oslo, Norway
	G. Baldi, ISMES, Bergamo, Italy
Invited speakers	R. S. Ladd, Woodward-Clyde Consultants, Clifton, New Jersey
	P. C. Lambe, North Carolina State University, Raleigh
	J. C. Evans, Bucknell University, Lewisburg, Pennsylvania
	J. L. Colliat, Institut de Mecanique de Grenoble, France

Session 3—Test Interpretation and Errors

Chairman	H. F. Hanson, Los Angeles City Department of Water and Power, Los Angeles
State-of-the-art speakers	J. F. Peters, U.S. Army Corps of Engineers, Waterways Experiment Station, Vicksburg, Mississippi
	J. T. Germaine, Massachusetts Institute of Technology, Cambridge, Massachusetts
Invited speakers	R. Kitamura, Kagoshima University, Kagoshima, Japan
	N. D. Dennis, U.S. Military Academy, West Point, New York
	H. Dendani, Institut de Mecanique de Grenoble, Grenoble, France
	W. Z. Savage, U.S. Geological Survey, Denver

Session 4—New Varieties of Tests

Chairman	Ronald C. Chaney, Humboldt State University, Arcata, California
State-of-the-art speakers	A. S. Saada, Case Western Reserve University, Cleveland
	J. R. F. Arthur, University College London, London, England
Invited speakers	G. F. Bianchini, Case Western Reserve University, Cleveland
	V. Janoo, University of Colorado, Boulder
	V. Silvestri, Ecole Polytechnique, Montreal, Canada

Papers are presented in this STP under the topics of the four sessions. State-of-the-art papers are given first, followed by invited and poster papers. Papers include examples of equipment designed to meet unusual applications, as well as the most recent examples of the use of computers and special equipment to automate standard tests. In the area of test methods, there are papers detailing methods for testing hard to handle soils such as marine clays and contaminated soils. Also under this topic are papers relating the latest information on routine test methods developed by some of the best laboratories in the world. Under test interpretation and errors are papers on the influence of test conditions and specimen preparation techniques on results. In addition, there are papers on the meaning of results relative to design conditions. In this context, an important finding pointed out in several papers is that results from standard unconsolidated undrained triaxial tests on saturated soils may be meaningless relative to the design problems for which they are normally used. Finally, there are papers describing new varieties of tests including true triaxial, directional shear, and hollow cylinder tests.

It is the hope and belief of the organizers of this symposium, that this STP will serve as a valuable tool for engineers and researchers who seek knowledge concerning triaxial testing and its application, and that it will serve as a basis for improving existing and developing new ASTM triaxial testing standards.

The editors wish to thank all those who participated in the symposium and who contributed to this STP. Special thanks go to the reviewers of the papers, to ASTM Committee D-18 on Soil and Rock for sponsoring the symposium, and to members of Subcommittees D18.05 on Structural Properties and D18.09 on Dynamic Properties. Finally, the editors would like to thank the ASTM staff for their assistance in preparing for the symposium and in the preparation of this STP. The high quality of ASTM publications would not be possible without their efforts.

Robert T. Donaghe
U.S. Army Corps of Engineers, Waterways Experiment Station, Vicksburg Miss.; symposium cochairman and coeditor

Ronald C. Chaney
Telonicher Marine Laboratory, Humboldt State University, Arcata, California; symposium cochairman and coeditor

Marshall L. Silver
Department of Civil Engineering, University of Illinois, Chicago, Illinois; symposium cochairman and coeditor

Equipment

Fumio Tatsuoka[1]

STATE-OF-THE-ART PAPER

Some Recent Developments in Triaxial Testing Systems for Cohesionless Soils

REFERENCE: Tatsuoka, F., "**Some Recent Developments in Triaxial Testing Systems for Cohesionless Soils,**" *Advanced Triaxial Testing of Soil and Rock, ASTM STP 977,* Robert T. Donaghe, Ronald C. Chaney, and Marshall L. Silver, Eds., American Society for Testing and Materials, Philadelphia, 1988, pp. 7–67.

ABSTRACT: The stress states and their changes that can be attained in the conventional triaxial testing method are reviewed and compared to those attained in other more sophisticated testing methods. These advanced tests have been developed to extend the ranges of the stress states and the changes in these states that can be controlled. In conventional triaxial testing on solid cylinder specimens σ_2' is equal either to σ_1' or to σ_3' and only a jump rotation of 90° in the principal stress directions can be achieved. It is argued that in spite of this limitation the triaxial testing method is still a useful means to measure the strength and deformation characteristics of soils. The results, however, should be corrected to account for the actual states of stress in the field. Furthermore, some recent advances in the methods and equipment for triaxial testing and other related kinds of testing are reviewed with an emphasis on the importance of automation and simplification. Several examples are presented where automated controlled stress and/or strain path tests can be performed by means of a simple triaxial apparatus using various electronic transducers, microcomputers, and pneumatic pressurizing systems.

KEY WORDS: soils, shear strength, laboratory testing equipment, triaxial test, plane strain test, simple shear, torsional shear, true triaxial, anisotropy, triaxial cell, electronic transducers, automated measurements, controlled stress paths, external pressure cell

Nomenclature

A_s	cross-sectional area of sample
a	sealing area of piston rod
b	$(\sigma_2' - \sigma_3')/(\sigma_1' - \sigma_3')$
DP	differential pressure measured with a differential pressure transducer
e	void ratio
p	$(\sigma_1' + 2\sigma_3')/3$ in triaxial compression, $(\sigma_3' + 2\sigma_1')/3$ in triaxial extension
q	$\sigma_1' - \sigma_3'$ in triaxial compression, $\sigma_3' - \sigma_1'$ in triaxial extension
R	σ_1'/σ_3'
$u(u_w)$	pore water pressure
u_A	pore air pressure
Δu	excess pore water pressure
v	$\epsilon_1 + 2\epsilon_3$ in triaxial compression, $\epsilon_3 + 2\epsilon_1$ in triaxial extension
γ	$\epsilon_1 - \epsilon_3$ in triaxial compression, $\epsilon_3 - \epsilon_1$ in triaxial extension
γ_{at}	shear distortion in torsional shear
γ_{hv}	shear distortion in direct simple shear

[1] Associate professor, Institute of Industrial Science, University of Tokyo, 22-1, Roppongi 7, Minato-ku, Tokyo 106, Japan.

δ angle of σ_1 direction from bedding plane ($= 90° - \omega$ when $\xi = 90°$)
$\epsilon_1, \epsilon_2, \epsilon_3$ principal strains (positive in compression)
ϵ_a, ϵ_r axial and radial strains in a sample
ξ angle of normal to bedding plane from $\sigma_1' - \sigma_2'$ plane
$\sigma_1', \sigma_2', \sigma_3'$ effective principal stresses (positive in compression)
σ_a', σ_r' effective axial and radial stresses in a sample
σ_c cell (air) pressure
σ_{BP} back (air) pressure
σ_v, σ_h vertical and horizontal stresses in direct simple shear
τ_{at} shear stress in torsional shear
τ_{hv} shear stress in direct simple shear
φ $\arcsin \{(\sigma_1' - \sigma_3')/(\sigma_1' + \sigma_3')\}_{max}$
ω angle of normal to bedding plane from σ_1' direction ($= 90° - \delta$ when $\xi = 90°$)

Introduction

The objective of this paper is to review some recent advances in testing methods and equipment mainly of the triaxial testing method. The plane strain and simple shear testing methods are also reviewed but to a lesser extent. In the first part of the paper, laboratory strength testing methods for soils are classified in terms of stress states and their changes that can be achieved in each testing method (refer to Refs *1* and *2* for a comprehensive review). This classification is presented to show the extent and limitation of the conventional triaxial testing method. In the second part of the paper, some recent progress in both the structure of apparatus and the methods of controlling and measuring loads, pressures, displacements, and volume change is discussed. In some cases, equipment or testing methods have become very complicated in order to extend the stress or strain states that can be attained. Consequently they have failed to achieve widespread use. Therefore, examples in which equipment and testing methods have become simplified without losing both the accuracy and the versatility of testing are discussed as well.

Because the details of equipment and testing methods are not fully described in most of the reviewed literature, many important examples may be missed in this paper. Furthermore, most of the equipment and testing methods discussed can be applied equally to clays and to sands. The scope of the present paper is restricted, however, to cohesionless materials.

Stress States in Laboratory Strength Testing of Soils

In laboratory shear tests such as the triaxial compression and extension tests, the plane strain tests, and the true triaxial tests, only normal stresses are controlled or measured. While the normal stresses are not exactly equal to principal stresses due to friction at rigid or flexible boundaries, these normal stresses can be approximated as principal stresses on the average in most cases. In these testing methods, the principal stress direction does not rotate continuously, that is, only a jump rotation of 90° can be achieved. In other types of tests, such as the simple shear tests, the torsional shear tests, and the tests by means of the directional shear cell [*3,4*], the directions of two among three principal stresses can be continuously rotated in a subjective or controlled manner. These two principal stresses can be defined when normal and shear stresses on two orthogonal planes are given. Accordingly, different laboratory shear testing methods may be classified in terms of the relative magnitudes and the directions of principal stresses and the manner of their changes which can be attained in each testing method.

Most soils have anisotropic strength and deformation characteristics. When an anisotropic soil element is stressed, the magnitudes and directions of principal strain increments of the soil element depend on the directions of both current principal stresses and principal stress increments. When a soil element has an axis or axes of symmetry in the sense that the properties of the soil element are the same in all directions at right angles to the axis, then the directions of the axis or axes of symmetry can be defined in terms of angles relative to the principal stress directions. Most inherently anisotropic soils have one axis of symmetry and in this case these soils are called cross-anisotropic. Typical examples are sands produced either by pluviating sand particles through static air or static water, or by one-dimensional static or dynamic compaction.

For cross-anisotropic soils, the direction of the axis of symmetry can be defined only by such two angles as ω and ξ as shown in Fig. 1*a*; ω and ξ are the angle of the axis of symmetry from the σ_1' direction and the angle of its projection on the σ_2'–σ_3' plane from the σ_2' direction. When $\omega = 0°$, the angle ξ need not be defined. Further, when $\sigma_1' = \sigma_2'$, the direction of the axis of symmetry can be defined only by a single angle $\theta = \arcsin\{\sin \omega \cdot \sin \xi\}$. The relative magnitudes of three principal stresses can be represented by, among others, the following two parameters: (1) the principal stress ratio $R = \sigma'_1/\sigma_3'$ and (2) the b parameter $= (\sigma_2' - \sigma_3')/(\sigma_1' - \sigma_3')$. Because R is the common variable in all laboratory shear tests, the stress states of soil in these tests can be classified in terms of the parameters (b, ω, and ξ) and their increments ($\dot{b}$, $\dot{\omega}$, and $\dot{\xi}$) as shown in Table 1 and Figs. 1*b* and 1*c*.

In Table 1 and Fig. 1, the direct shear testing method is excluded although some interesting work has been done studying the strength anisotropy of sands (see for example, Refs *65* and *66*). This is because both strains and principal stresses are difficult to evaluate in this testing method. True triaxial testing methods with the use of cubic samples are thoroughly reviewed by Arthur [*2*] and are not discussed here.

The ring shear apparatus developed by Yoshimi and Oh-Oka [*67*] is another version of the torsional shear apparatus where plane strain condition is mechanically achieved by means of a stack of inner disks and outer rings. However, this is not classified either as TSI (for explanation of this and other classifications, see Table 1) or as TSD in Table 1 because both inward and outward horizontal stresses are not measured.

In Table 1, figures without the asterisk (*) mean the parameters which can be controlled to be so at will, whereas those with the asterisk (*) mean the parameters which are subjective (cannot be controlled to be so at will). Only representative references among many others are listed in Table 1. In Figs. 1*b* and 1*c*, only the stress states in terms of b, ω, and ξ at failure are shown and the state paths in the (b, ω, ξ) space during shear are not shown for simplicity. Each solid line segment having two arrows at both its ends either on the $\omega = 0$ plane or on the $b = 0$ plane represents a testing method where the angle ξ cannot or need not be defined. Each broken line segment having two arrows at both its ends represents the range of possible stress state in each testing method. Furthermore, the coordinates of b in the testing methods denoted as PS, PSA, and SS (see Table 1) are rather arbitrarily given because this value is subjective in these tests.

In the tests denoted as TTH, TSI, and TSD, hollow cylindrical specimens are used. Therefore, the stress distribution across the wall thickness of the sample is inherently nonuniform. In TSI, the stress nonuniformity across the thickness can be minimized by making the walls as thin as possible. However, in TTH and TSD, the degree of stress nonuniformity across the wall thickness of the sample becomes very large when the pressures applied inside and outside the cylinder vary greatly. In this case, only stresses averaged across the thickness of the sample can be defined.

It is to be noted that another kind of anisotropy, different from the inherent one, is induced by straining the soil element. The axis of symmetry for the induced anisotropy, if

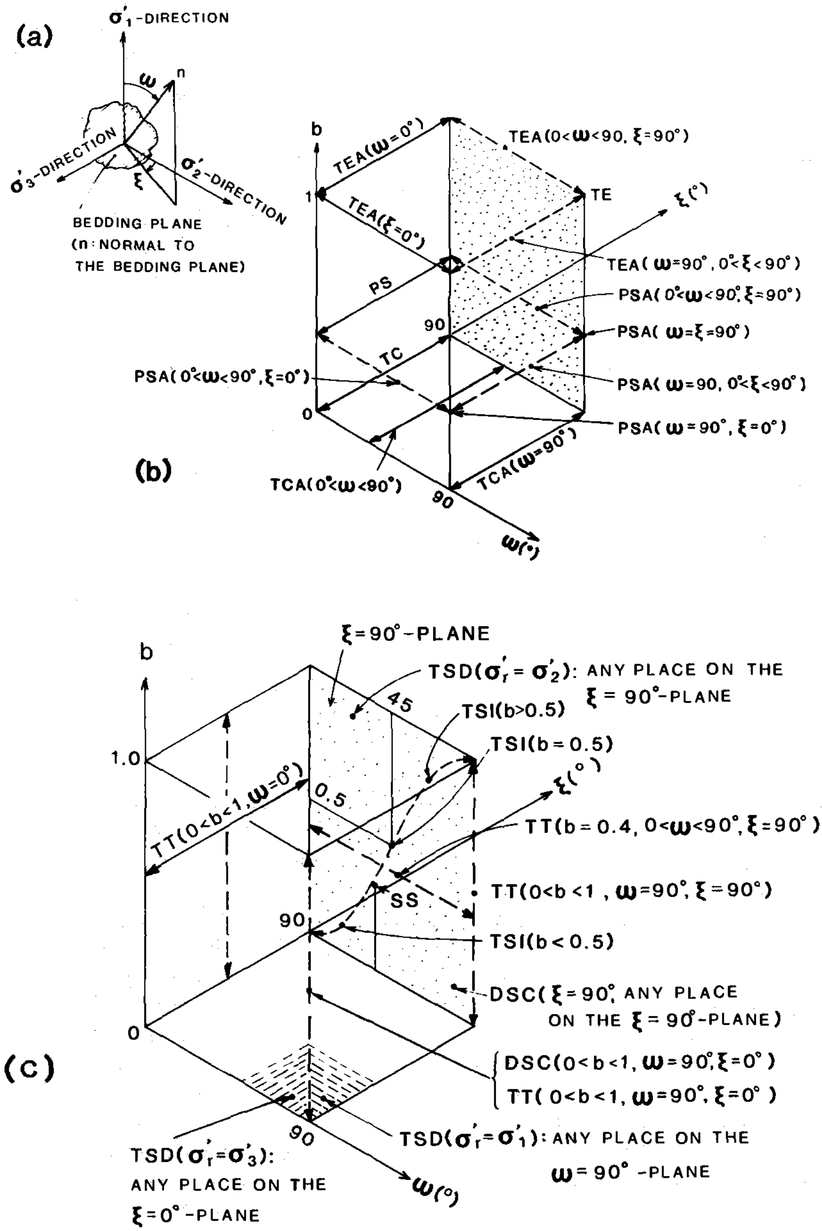

FIG. 1—*Stress states at failure of soil in various laboratory shear testing methods.*

it exists, may be different from that for the inherent anisotropy. When both kinds of anisotropy, inherent and induced, have different axes of symmetry, the stress state cannot be represented only by (b, ω, and ξ) and ($\dot{b}$, $\dot{\omega}$, and $\dot{\xi}$), that is, other parameters are needed.

Fig. 2*a* shows the angle of internal friction $\varphi = \arcsin\{(\sigma_1' - \sigma_3')/(\sigma' + \sigma_3')\}_{max}$ of air-pluviated dense and loose Toyoura sand, in the plane strain condition at $\xi = 90°$, as a function of ω. In Fig. 2*a*, δ is equal to $90° - \omega$. All the samples were sheared from the isotropic stress condition at various confining pressures σ_c' by using the apparatus shown in Fig. 25. In Fig. 2*a*, φ at a certain angle $\omega = 90° - \delta$ is divided by the value at $\omega = 0°$ ($\delta = 90°$). It may be seen that the strength anisotropy is considerable and is rather independent of σ_3' for a wide stress range ($\sigma_3' = 0.05$ to 4.0 kgf/cm^2). Figure 2*b* shows φ of air-pluviated dense Toyoura sand at $\sigma_3' = 1.0$ kgf/cm^2 represented as a function of b, ω, and ξ, and Fig. 2*c* shows the values of ϕ in the plane strain compression [17]. The void ratio value $e_{0.05}$ or $e_{0.3}$ is defined when the specimen is isotropically compressed at $\sigma_3' = 0.05$ or 0.3 kgf/cm^2. These values of b, ω, and ξ shown in Figs. 2*b* and 2*c* are the ones at the failure of sand.

In general, the effect of the strain and stress history on φ, in addition to the effect of the stress state at failure in terms of b, ω, ξ, and others, cannot be completely ignored. However, the effects of the strain and stress history prior to failure on φ can be considered small as shown by Tatsuoka and Ishihara [68], Hight et al. [49], and Wong and Arthur [62]. The results presented in Fig. 2*b* were obtained by means of drained strain-controlled tests denoted as TC, TE, PS, TCA, TEA, and PSA in Table 1.

Three values of φ were obtained for $b = 1.0$ (that is, triaxial extension, TE and TEA); one is the lowest strength value when a shear band is formed through two opposite flexible σ_1' planes, the second is an intermediate strength value when a shear band intersects with either the top or the bottom rigid σ_3' plane, and the last is the highest strength value when a shear band intersects with both the top and bottom rigid σ_3' plane. Because the strength data were obtained only when either ω or ξ was 0 or 90°, strength values when both ω and ξ were neither 0 nor 90°, shown in Fig. 2*c*, were estimated by interpolation. It may be seen from Figs. 2*a*, 2*b*, and 2*c* that φ is, at least, a complicated function of b, ω, and ξ. This result clearly indicates that to take into account solely the effect of b parameter or strength anisotropy is not sufficient to define the value of φ but at least both should be considered in a combined manner. It may also be seen in Figs. 2*b* and 2*c* that very limited values of φ can be obtained by means of the conventional testing methods, which are denoted as TC, TE, and PS in Table 1 and are represented by ①, ⑦, and ② in Figs. 2*b* and 2*c*.

In most field loading and unloading problems, the principal stress directions rotate continuously with varying magnitudes of rotation. This continuous rotation can be attained only in limited testing methods. These methods are generally much more sophisticated than those in which the continuous rotation of principal stress direction cannot be attained. The first examined deformation mode where principal stress directions rotate continuously is the simple shear deformation which is considered prevailing in the field condition. Among other research organizations, simple shear tests in which the magnitudes and directions of principal stresses can be defined have been performed at the Cambridge University by means of a series of box-type simple shear apparatus [39,42,43,46]. Figure 3*a* shows a typical result of drained simple shear test performed by Stroud [39]. It may be seen that in this monotonic loading test the angle ω rotates very fast in the early stage of straining, that is, ω starts from zero and approaches a constant value of 50 to 55° before shear distortion α becomes 1%. Figure 3*b* shows the rotation of σ_1' direction during a drained cyclic straining simple shear test with a constant shear distortion amplitude of $\pm 5\%$ performed by Budhu [42] and Wood and Budhu [69]. In Fig. 3*b* the angle ω is the measured one and the angle ψ is the one predicted as $\psi = \arctan(\tau_{hv}/\sigma_v)/\kappa$ with a constant value of 0.575 for κ. A good coincidence

TABLE 1—*Classification of laboratory shear testing methods on cohesionless soils.*

Test Name	Description	b[a]	ω, degrees	ξ, degrees	$\dot{b}$[b]	$\dot{\omega}$[c]	$\dot{\xi}$[c]	*IA?*[e]	References[f]
Triaxial compression, TC	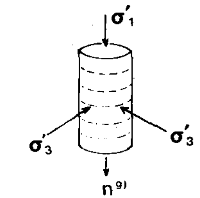	0.0	0	——[h]	0	0	——	No	[*5–9*]
Triaxial extension, TE	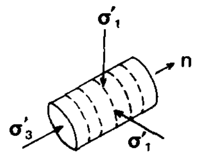	1.0	90	90	0	0	0	No	[*5,10,11*]
Plane strain, PS	$\dot{\varepsilon}_2 = 0$ 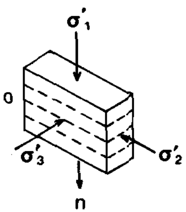	≑0.3*[i]	0	——	≠0*[j]	0	——	No	[*12–15*]
Triaxial compression to investigate strength antisotropy, TCA	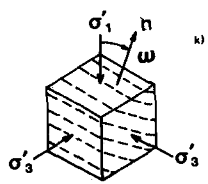	0.0	0–90	——	0	0	——	Yes	[*16–20*]

Triaxial extension to investigate strength anisotropy, TEA^{l}	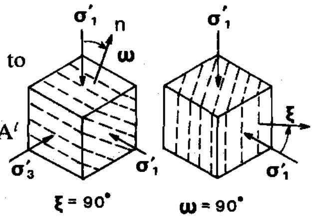	1.0	0–90 90	90 0–90	0	0	0	Yes	[*9,17,20*]
Plane strain to investigate strength anisotropy, PSA	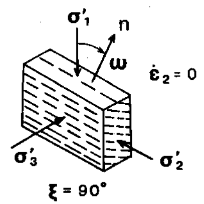	≑0.3*	0–90	90	≠0*	0	0	Yes	[*21–24*]
	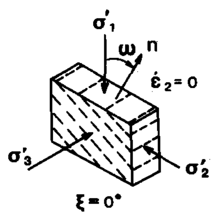	≑0.3*	0–90	0	≠0*	0	0	Yes	[*17*]
	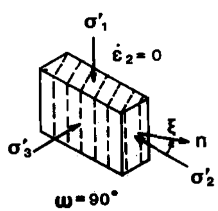	≑0.3*	90	0–90	≠0*	0	0	Yes	[*17*]

TABLE 1—*Continued.*

Test Name	*Description*	b^a	ω, degrees	ξ, degrees	$\dot{b}^b$	$\dot{\omega}^c$	$\dot{\xi}^c$	*IA?*[e]	References[f]
	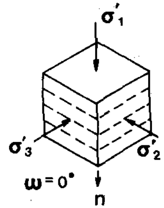		0	——	≠0	0	0	No	
True triaxial, TT[m]	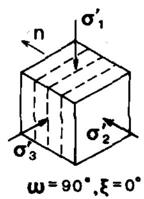	0–1.0	90	0	≠0	0	0	Yes	[*11,16,25–36*]
	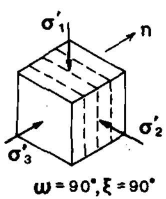		90	90	≠0	0	0	Yes	
True triaxial by means of hollow cylinder apparatus, TTH	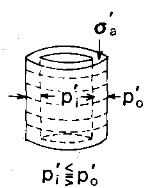	0–1.0	0 or 90	0 or 90	0	0	0	Yes	[*37,38*]

Simple shear, SS	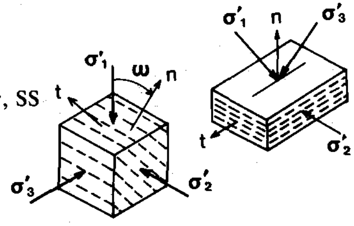 $\dot{\varepsilon}_t = 0^*, \dot{\varepsilon}_2 = 0^*$		≒ 0.3*ⁿ	= 45*	90	≠0*	≠0*	0	Yes	[39–47]
Torsional shear with identical inner and outer pressures, TSI[o]	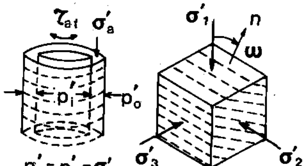 $p_i' = p_o' = \sigma_2'$		$\sin^2\omega$ 0.5	0–90 45	90 90	0 or ≠0 0	0 or ≠0 0	0 0	Yes Yes	[48–59]
		$(\sigma_1' =)\ \sigma_2'$	0–1.0	0–90	90	≠0	≠0	0	Yes	
Torsional shear with different inner and outer pressures, TSD[p]	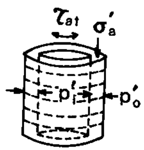 $p_i' \lesseqgtr p_o'$	σ_1'	0–1.0	90	0–90	≠0	0	≠0	Yes	[49,57,60,61]
	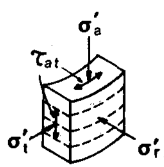	σ_3'	0–1.0	0–90	0	≠0	≠0	0	Yes	

TABLE 1—*Continued.*

Test Name	*Description*	b^a	ω, degrees	ξ, degrees	$\dot{b}^b$	$\dot{\omega}^c$	$\dot{\xi}^c$	*IA?*[e]	References[f]
	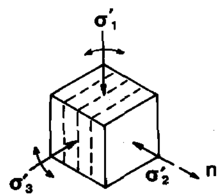	(b^{*r} for PS) or (0–1.0)	90	0 90	$\neq 0^*$ or $\neq 0$ or 0	0^s	0	Yes	[*3,4,21,62–64*]
Directional shear cell, DSC[q]	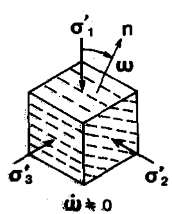	(b^{*n} for PS) or (0–1.0)	0–90		0	0 or $\neq 0$	0	Yes	[*62*]

[a] $b = (\sigma_2' - \sigma_3')/(\sigma_1' - \sigma_3')$ at failure.
[b] Increment of b during shear.
[c] Increment of ω during shear.
[d] Increment of ξ during shear.
[e] Is another anisotropy induced having a different axis of symmetry than that for inherent anisotropy?
[f] Only representative ones are listed here among many other references.
[g] Normal to the bedding plane (axis of cross-symmetry).
[h] No need to define.
[i] Subjective (unable to control).
[j] Parameters that are subjective (cannot be controlled to be so at will).
[k] The shape of specimen is either cylindrical or prismatic.
[l] Tests at ($\omega = 0°$ with any ξ) and tests at ($\xi = 0°$ with any ω) are categorized as the same kind of test.
[m] There is a large variety in loading methods through either rigid, flexible, or mixed boundaries. By means of TT, tests for any point either on the surface or within the "*b*–ω–ξ cubic" *without* the continuous rotation of principal stresses can be performed.
[n] $\sigma_2' = 0.37\ (\sigma_1' + \sigma_3')$ at failure [39]. The values of b and ω cannot be measured in most Norwegian Geotechnical Institute (NGI) type simple shear apparatus unless a calibrated wire-reinforced membrane is used [*40–42*].
[o] The same pressure is applied inside and outside the cylinder.
[p] Stress states attainable are restricted when serious stress nonuniformity is avoided. $\sigma_r' = \sigma_2'$ in most tests reported so far.
[q] Currently this is restricted to stress-controlled testing at relatively low stress levels.
[r] The value of b so as to achieve the plane strain condition; $\sigma_2' = 0.39\ (\sigma_1' + \sigma_3')$ at failure [*62*].
[s] The direction of σ_1' and σ_3' can be continuously rotated during shear with respect to the test material. In this case, the stress condition cannot be described only in the (b–ω–ξ) space.

between the two angles ω and ψ means that the equation proposed by Oda and Konishi [70] for monotonic simple shear deformation

$$\frac{\tau_{hv}}{\sigma_v} = \kappa \tan\omega \tag{1}$$

(κ = a constant) is also valid for cyclic simple shear deformation.

We obtain from Eq 1 the following equation

$$\sigma_1'/\sigma_3' = (1 + \kappa \cdot \tan^2\omega)/(1 - \kappa) \tag{2}$$

The relationship between σ_1'/σ_3' and ω obtained from Eq 2 is similar to the one shown in Fig. 3*a* in the sense that ω increases very fast only at low σ_1'/σ_3'. The result seems to suggest that under cyclic loading, as well as under monotonic loading, a major part of plastic strain is induced at a rather constant angle of ω.

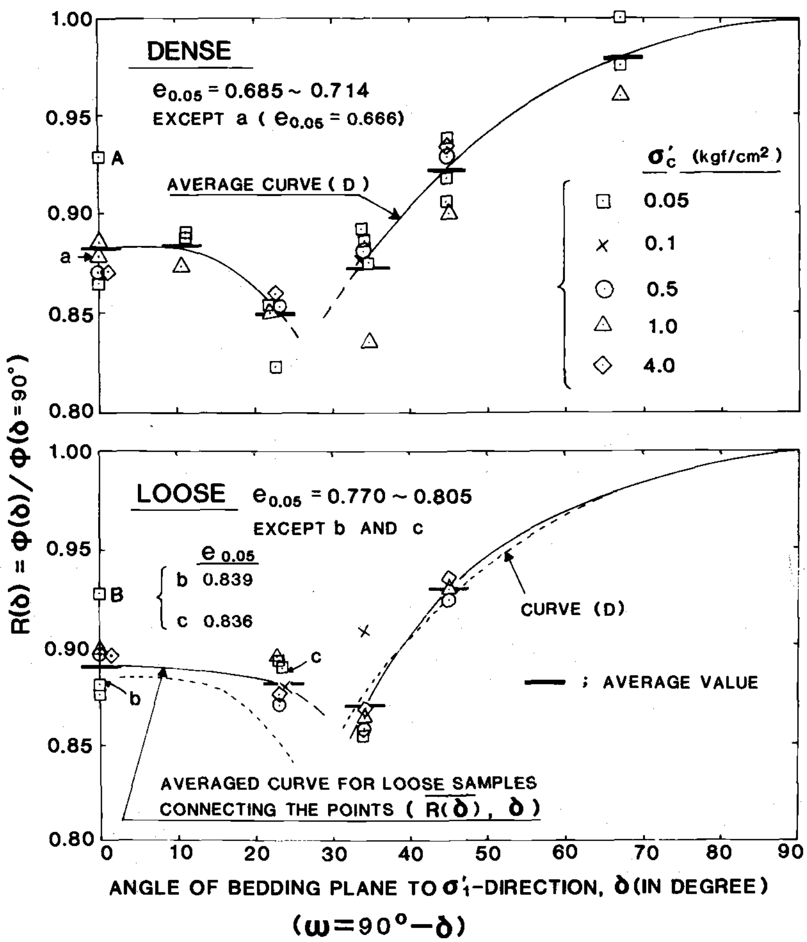

FIG. 2*a*—φ = *arcsin* $\{(\sigma_1' - \sigma_3')/(\sigma_1' + \sigma_3')\}_{max}$ *of air-pluviated dense Toyoura sand in plane strain at* ξ = *90° as a function of* ω [24].

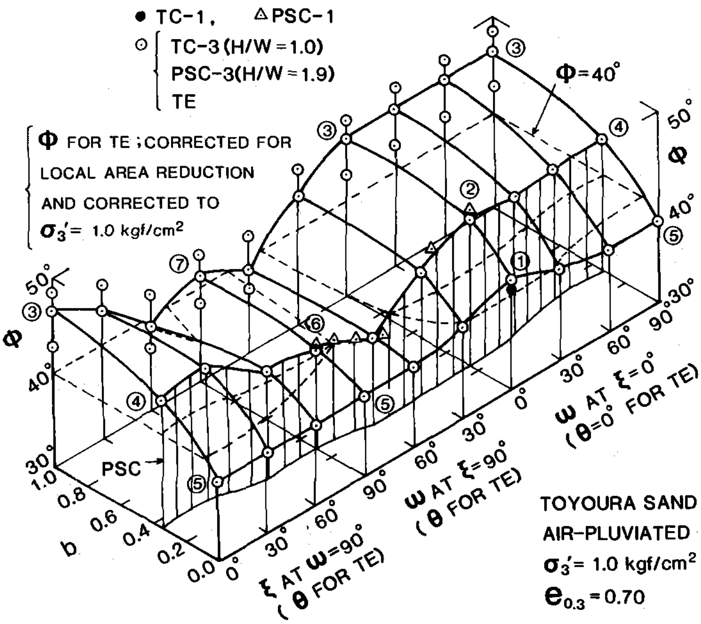

FIG. 2b—φ = *arcsin* $\{(\sigma_1' - \sigma_3')/(\sigma_1' + \sigma_3')\}_{max}$ *of air-pluviated dense Toyoura sand as a function of* (b, ω, *and* ξ) *at failure* [17].

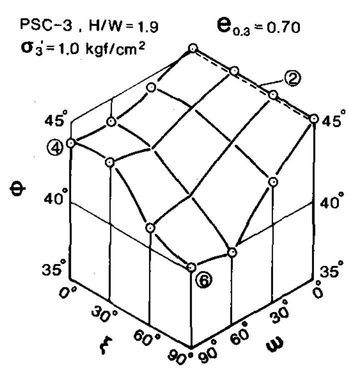

FIG. 2c—φ = *arcsin* $\{(\sigma_1' - \sigma_3')/(\sigma_1' + \sigma_3')\}_{max}$ *of air-pluviated dense Toyoura sand in the plane strain compression* [17].

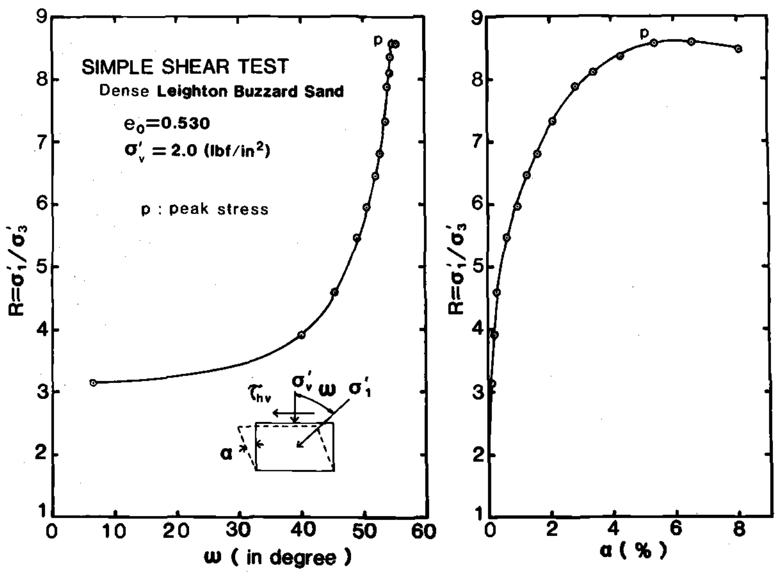

FIG. 3*a*—*Rotation of* σ_1' *direction during a drained monotonic straining simple shear test by Stroud* [39].

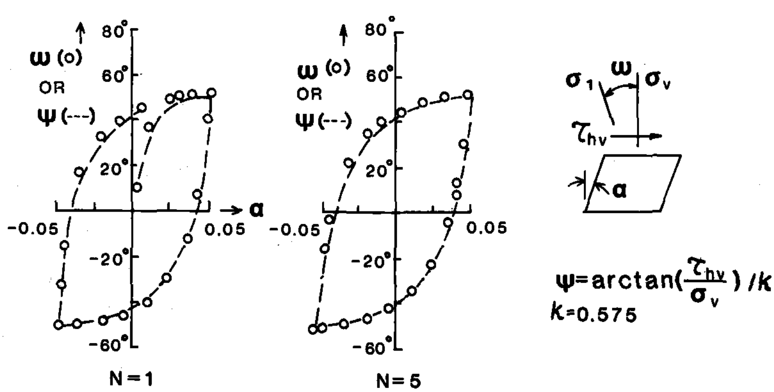

FIG. 3*b*—*Rotation of* σ_1' *direction during a drained cyclic straining simple shear test* (σ_v' = *1.0 kgf/cm*^{2}, e_0 = *0.53* [42]); *Leighton Buzzard sand for both tests.*

It may further be seen in Fig. 3*b* that the value of ω changes very fast after the loading direction is reversed. This means that the principal stress directions rotate largely only when the principal stress ratio σ_1'/σ_3' is low; however, they rotate at a very small rate at higher levels of σ_1'/σ_3'. It can also be seen from Fig. 3*b* that the value of ω changes between around +45° and around −45°. This behavior is similar to that in the cyclic triaxial test where both the triaxial compression and extension stress conditions are attained in the sense that the directions of principal stresses change by 90° (or around 90°).

The behavior of sand in the constant-volume cyclic simple shear deformation has been studied using the Cambridge University simple shear apparatus by Finn and his co-workers [*44,71,72*] (see Fig. 4). The boundary stresses are measured by a stiff load transducer and pressure transducers. This testing method was developed to reduce to a very low value the errors due to system compliance.

The cyclic undrained simple shear behavior of sand can be examined also by cyclic torsional shear tests. Because a detailed comparison of the torsional shear test and the simple shear test has been given in Ref *1*, this will not be discussed here. It seems worthwhile to point out, however, that a cyclic undrained torsional shear test on a saturated sample can be performed in a rather simple manner as in the cyclic undrained triaxial testing, together with sensitive stress measurements with an accuracy of, say 1.0 gf/cm^2, as shown below.

This paper will examine results of two cyclic undrained torsional shear tests on loosely and densely packed sand samples in which the test material does not change the volume and the length, as shown in Figs. 5 through 18. This testing method has been used by Saada and his coworkers for clays [*1*]. In such tests, the cross-sectional area of the hollow cylindrical sample is kept constant as in the simple shear test. This feature is not completely the same

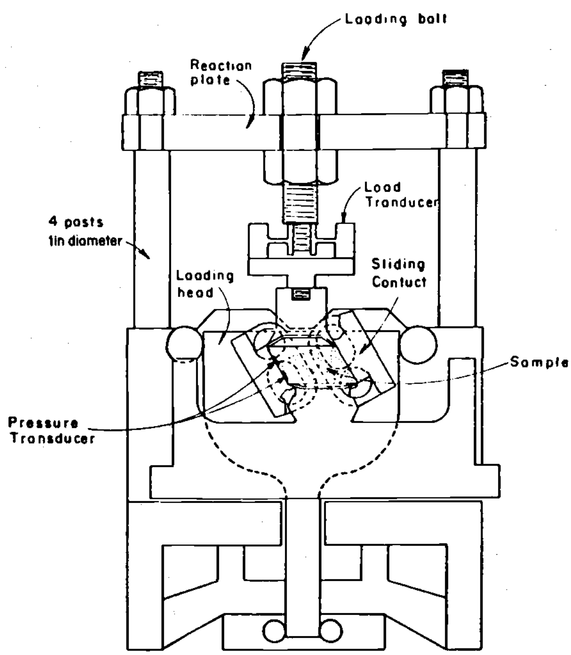

FIG. 4—*Constant volume cyclic simple shear apparatus at the University of British Columbia* [72].

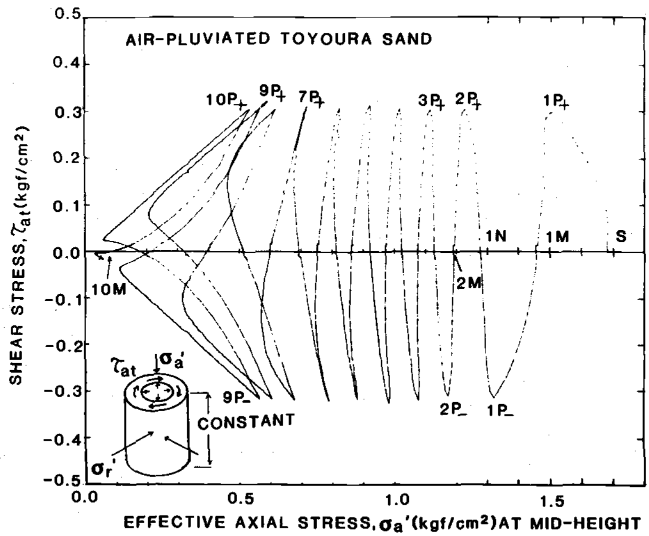

FIG. 5—*Effective stress path in terms of* τ_{at} *and* σ_a' *in a cyclic undrained torsional test on air-pluviated loose Toyoura sand* [73].

as that in the simple shear deformation because the two orthogonal normal strains are zero in the horizontal plane in the simple shear deformation whereas this condition is not ensured in the torsional shear tests. However, it is very likely that in this kind of torsional shear test horizontal normal strains are much smaller than shear strain. Therefore, an idea as to the stress state in the field cyclic undrained simple shear deformation may be obtained from this test result. In fact, it has been confirmed by the author and his co-workers that the results shown in Figs. 5 through 18 are very similar to those obtained by the cyclic undrained torsional shear tests where the condition of simple shear deformation was satisfied rather rigorously. The results will be reported elsewhere in the future.

Figures 5 through 18 show the results of two strain-rate-controlled cyclic undrained torsional shear tests ($\dot{\gamma}_{at}$ = 0.5/min) with a constant shear stress amplitude in each test using

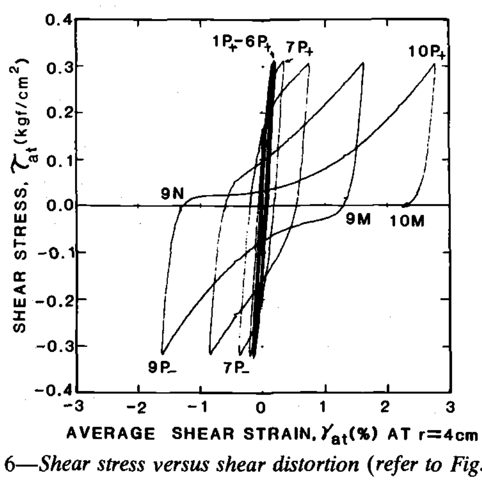

FIG. 6—*Shear stress versus shear distortion (refer to Fig. 5).*

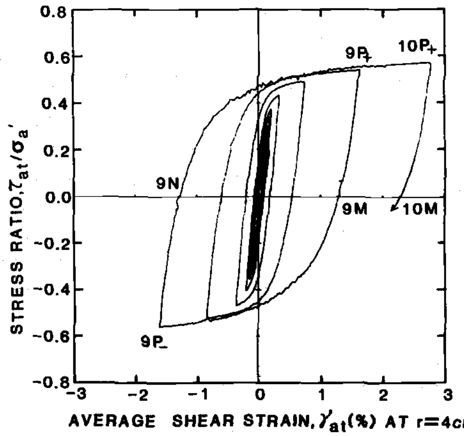

FIG. 7—*Shear stress/effective axial stress ratio versus shear distortion (refer to Fig. 5).*

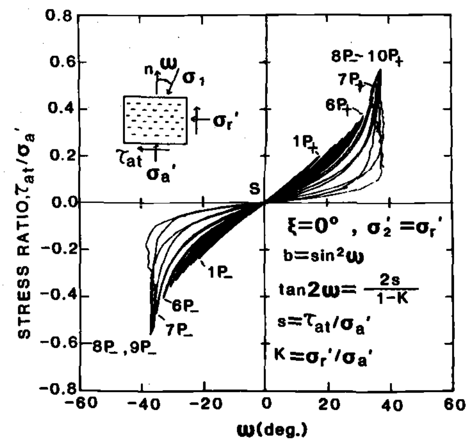

FIG. 8—*Shear stress/effective axial stress ratio versus angle of σ_1' direction from axial direction ω (refer to Fig. 5).*

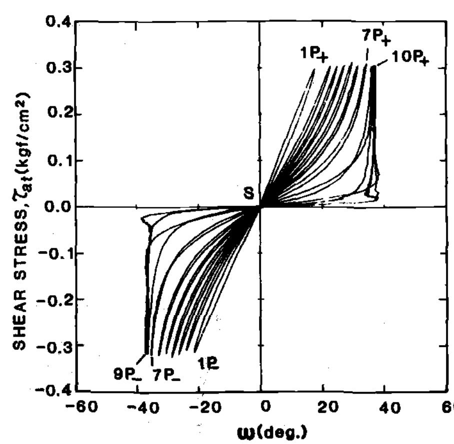

FIG. 9—*Shear stress versus angle of σ_1' direction from axial direction ω (refer to Fig. 5).*

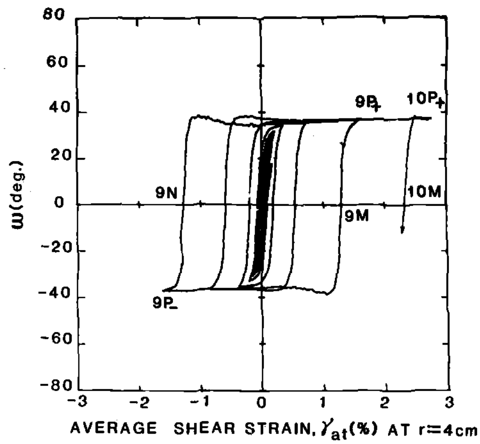

FIG. 10—*Angle of σ_1' direction from axial direction ω versus shear distortion (refer to Fig. 5).*

air-pluviated Toyoura sand [73]. Fully saturated hollow cylindrical loose and dense specimens with a height of 10 cm, an outer diameter of 10 cm, and an inner diameter of 6 cm were first anisotropically compressed to a stress state with an axial stress of $\sigma_a' = 1.69$ kgf/cm^2 and a lateral stress of $\sigma_r' = 0.66$ kgf/cm^2 for the loose sample, or $\sigma_a' = 1.78$ kgf/cm^2 and $\sigma_r' = 0.62$ kgf/cm^2 for the dense sample. The ratios are similar to the K_0 values measured for this kind of specimen by Okochi and Tatsuoka [74]. The consolidated void ratios were

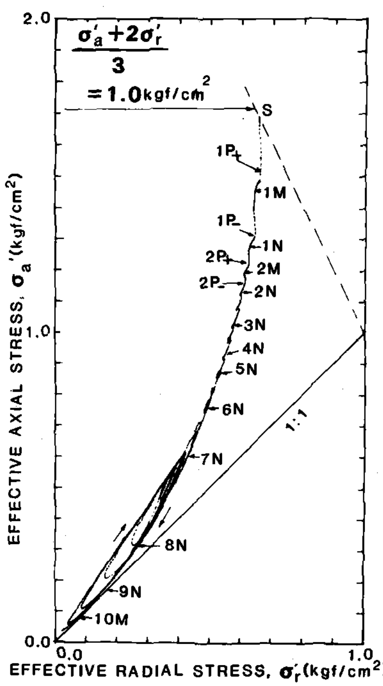

FIG. 11—*Effective stress path in terms of σ_a' and σ_r' (refer to Fig. 5).*

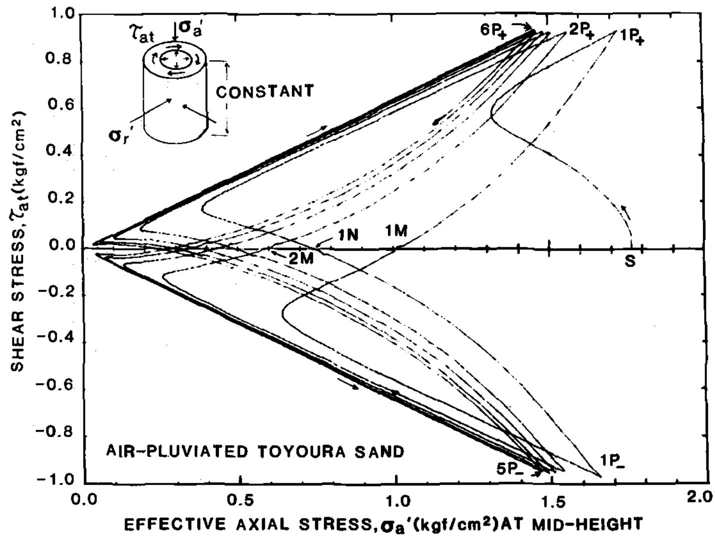

FIG. 12—*Effective stress path in terms of* τ_{at} *and* σ_a, *air-pluviated dense Toyoura sand* [73].

0.734 and 0.663 as compared with e_{max} = 0.977 and e_{min} = 0.605. Great care was exercised in measuring all the stresses; axial and radial effective stresses σ_a' and σ_r' and shear stress τ_{at} (for further details refer to Ref *59*), as will be discussed again in the later part of this paper. In these tests, the length of a sample was kept constant by means of a simple cramping device shown in Fig. 23*b*. The falling of the loading ram was prevented by a thrust bearing which allowed free rotation of the loading ram. The upward movement of the loading piston was prevented by applying a sufficient amount of axial load to the top end of the loading piston. The same method has been used for load-controlled cyclic undrained torsional shear tests [*58,75,76*].

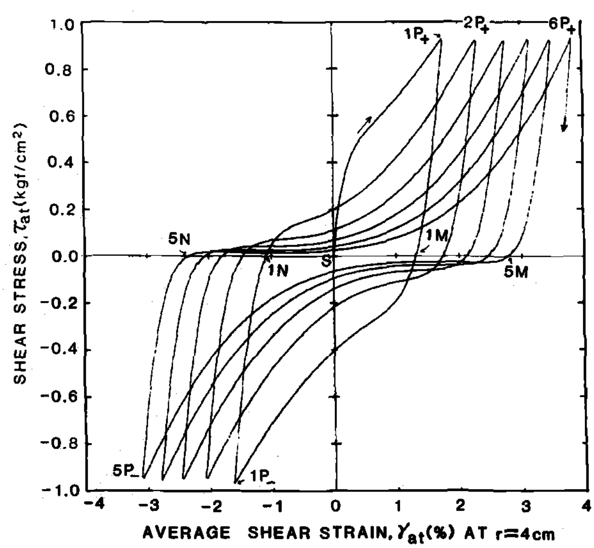

FIG. 13—*Shear stress versus shear distortion* (*refer to Fig. 12*) [73].

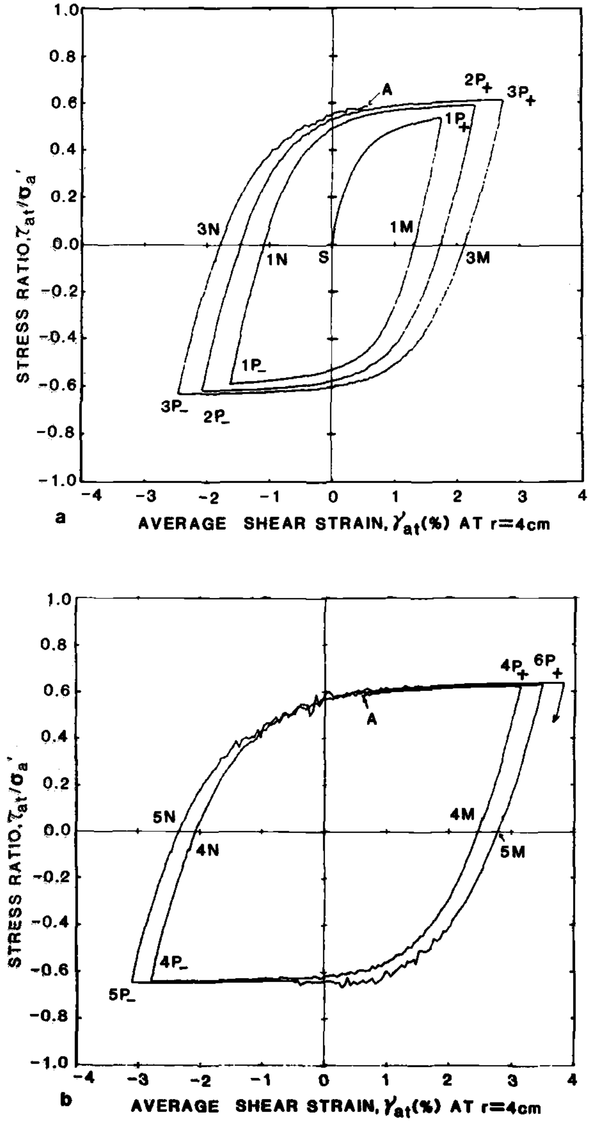

FIG. 14—*Shear stress/effective axial stress ratio versus shear distortion (refer to Fig. 12)* [73].

Figures 5 and 12 show the effective stress paths in terms of shear stress τ_{at} and effective axial stress σ_a' defined at the midheight of the specimen. Figures 6 and 13 show the stress–strain relationships in terms of shear stress τ_{at} and shear distortion γ_{at}. Figures 7*a*, 7*b*, and 14 show the stress–strain relationships in terms of τ_{at}/σ_a' and γ_{at}. It may be seen in these figures that the relationships are of strain-hardening type as those obtained by a drained (or σ_a'-constant) cyclic shear test. Note that to obtain such relationships the stress measurements should be extremely accurate when effective stresses are extremely low.

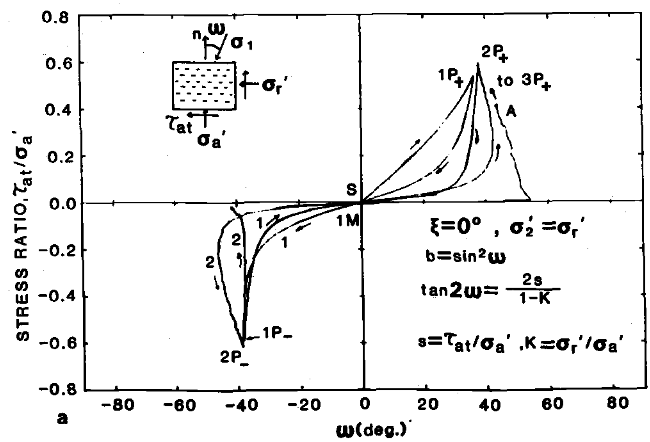

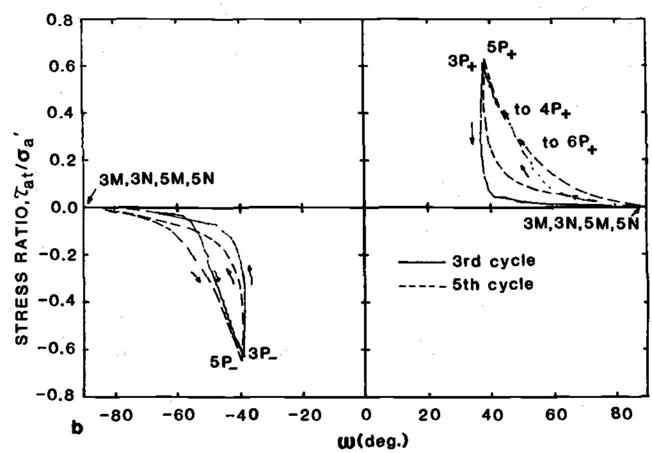

FIG. 15—*Shear stress/effective axial stress ratio versus* ω (*refer to Fig. 12*) [73].

Figures 8 and 15 show the relationships between the angle of σ_1' direction from the vertical ω and stress ratio τ_{at}/σ_a', and Figs. 9 and 16 show those between ω and shear stress τ_{at}. Figures 10 and 17 present the relationship between ω and shear distortion γ_{at} as shown in Fig. 3*b* (γ_{at} is equivalent to α in Fig. 3). All these figures indicate that both in the first loading from the point S to the point $1P_+$ for the loose and dense samples and during cyclic straining at small strain amplitudes in the first seven cycles for the loose sample, the angle ω changes almost in proportion to the change in τ_{at}/σ_a'. On the other hand it may be seen that during cyclic straining at larger strain amplitudes, for example, larger than about $\pm1\%$, the angle ω is rather constant around $\pm45°$ as in the case of drained cyclic simple shear test (Fig. 3*b*). It may also be seen that at larger strain amplitudes most of the rotation of principal stress directions occurs just after the loading is reversed and is associated with very small shear distortion. The reason for this phenomenon is that at larger strain amplitudes the effective stress ratio σ_r'/σ_a' at the neutral stress condition ($\tau_{at} = 0$) has changed from K_0 to approximately unity with cyclic straining (see Figs. 11 and 18).

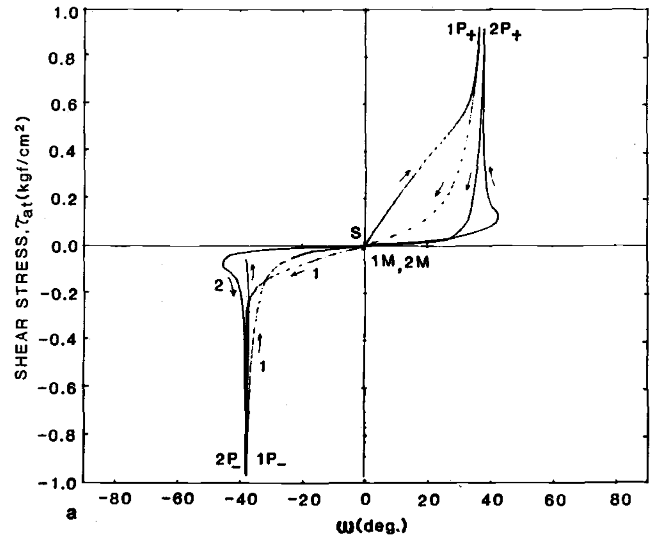

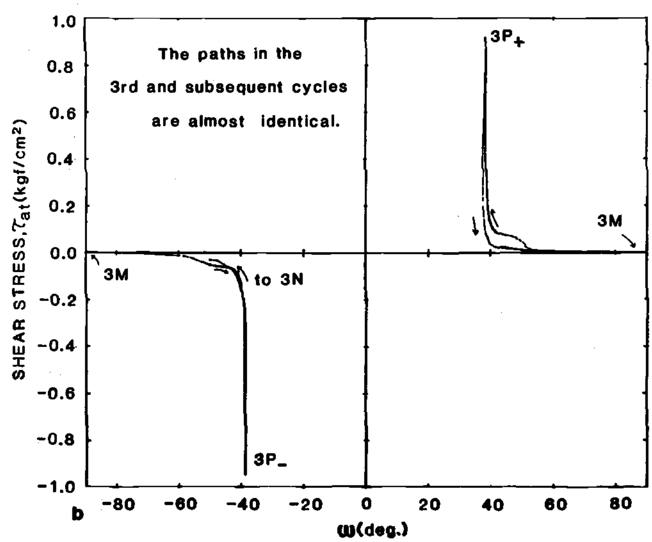

FIG. 16—*Shear stress versus* ω (*refer to Fig. 12*) [73].

Furthermore, the reason why the dense sample the angle ω becomes larger than 45° at smaller values of τ_{at}/σ_a' in the third and subsequent cycles is that σ_r' becomes larger than σ_a' at $\tau_{at}/\sigma_a \fallingdotseq 0$ as represented by the points 3M through 6M in Fig. 18. Such a phenomenon as that σ_r' becomes larger than σ_a' with the decrease in effective stresses is similar to the one observed in a static K_0-rebound test. It has also been found that in cyclic undrained simple shearing on a K_0-consolidated sample, principal stress directions rotate at a very reduced rate at high principal stress ratios σ_1'/σ_3'. (The results will be reported elsewhere in the future.)

In summary, in triaxial tests and plane strain compression tests, which are considered to

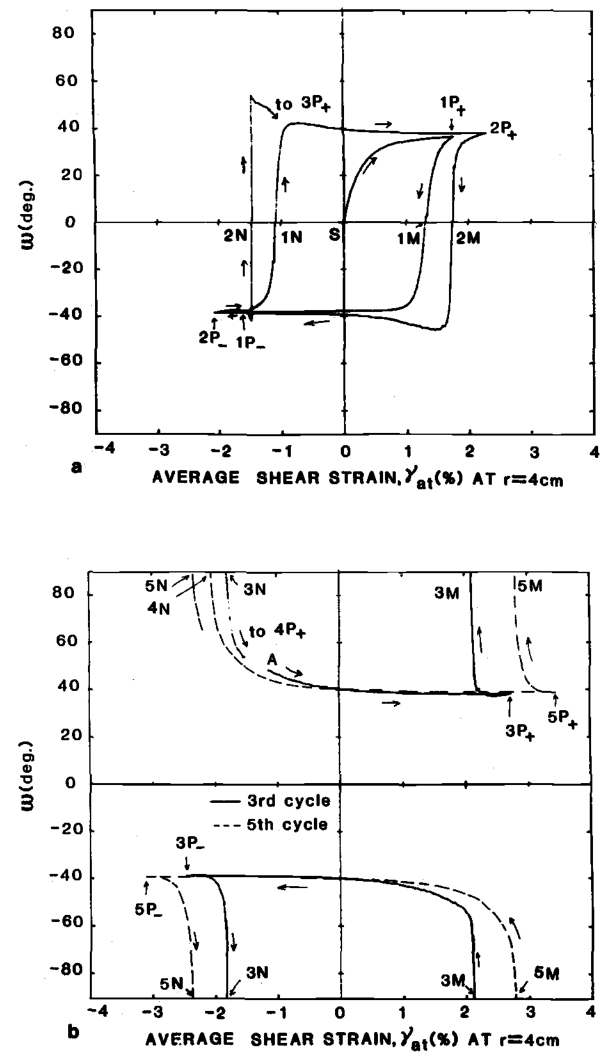

FIG. 17—ω *versus shear distortion* (*refer to Fig. 12*) [73].

be rather established conventional testing methods, the ranges of stress states which can be attained are very limited with respect to the *b* value, its change, and the continuous rotation of principal stress directions. In spite of this limitation, these testing methods have an advantage that stresses or strains or both can be controlled in relatively simple and accurate ways.

Continuous rotation of principal stress directions and changes in the relative magnitude of the intermediate principal stress are features of the stress paths associated with most field loading and unloading problems. In the simple shear deformation among various field deformation modes, principal stress directions rotate and the *b* value changes in a subjective manner. The behavior of soils in the simple shear deformation can be examined only by means of well-controlled simple shear tests or in an approximated way, by means of torsional shear tests. Tests with controlled variable *b* values or principal stress directions can be

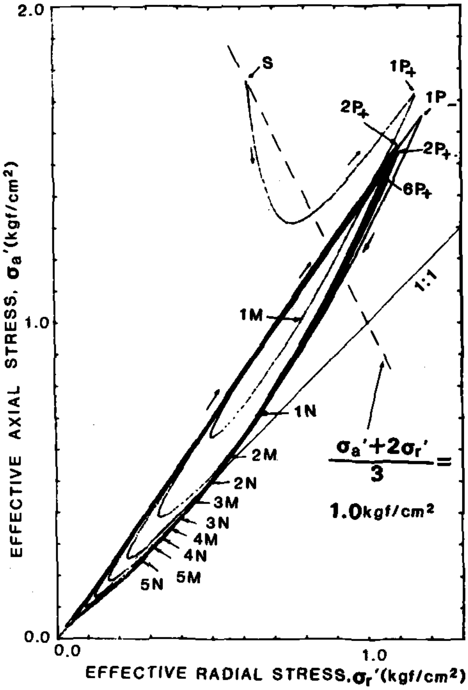

FIG. 18—*Effective stress path in terms of σ_a' and σ_r' (refer to Fig. 12)* [73].

performed only by means of very sophisticated testing methods which seem very difficult to perform as routine testings. On the other hand, it has been found for the simple shear deformation in monotonic loading that in the first stage of shearing the rotation of principal stress directions is not associated with a large change in the principal stress ratio σ_1'/σ_3' and further these directions rotate only very slightly at large plastic strains. It has also been found that under cyclic simple shear loadings, fast rotation of around 90° in the σ_1' and σ_3' directions occurs just after the reverse of shear direction from a relatively high level of stress ratio σ_1'/σ_3' associated with very small magnitude of plastic strains. Consequently, it may be reasonable to consider that in most field problems the effects of the change of the principal stress ratio $R = \sigma_1'/\sigma_3'$ on the shear deformation and strength characteristics of soils are still much larger than those of the continuous rotation of principal stress directions, which of course cannot be totally ignored. Therefore, it seems that major features of the deformation and strength characteristics in both monotonic and cyclic field loading problems can be examined even by a simple means of the triaxial tests where no rotation or only a 90° jump rotation in principal stress directions is attained. Usually, in practice, the field strength and deformation characteristics of soils have been examined first by the triaxial tests and, if necessary, with the results being corrected for the effects of the *b* value, its change, the principal stress directions, and their continuous rotation. To clarify the extent of these effects more research work is needed.

Structure of the Triaxial Cell

Only one major feature of the triaxial cell's structure will be discussed. To attain the triaxial extension condition, to prevent the cap rotation, or to apply torque to a specimen for a torsional shear test, it is necessary to fix the cap to the loading piston. For such a

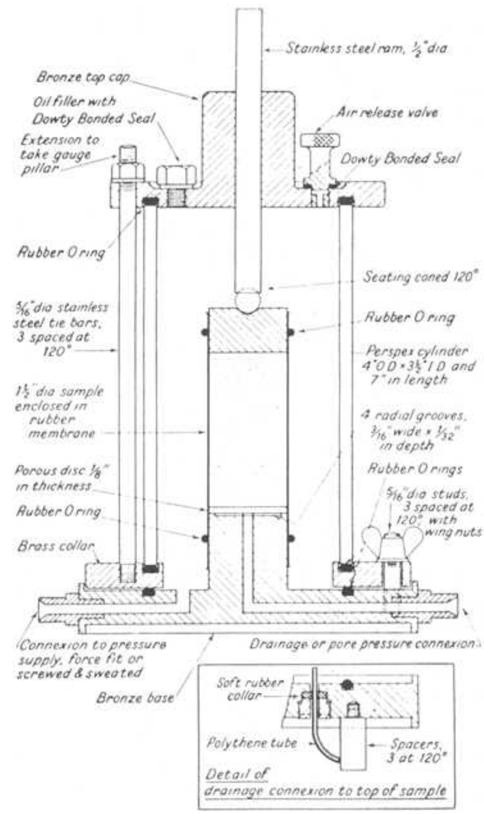

FIG. 19—*The triaxial cell for 1-1/2-inch-diameter samples* [7].

triaxial cell, as illustrated in Fig. 19, the loading piston is connected, if needed, only after the remaining parts of the triaxial cell, including the pressure cell, have been assembled. This remote connection may cause sample disturbance when the alignment between the loading piston and the sample is not good. Furthermore, for this triaxial cell, without this connection, the change in sample height during isotropic compression cannot be measured accurately. Many methods for this remote connection technique have been developed for triaxial extension tests as described by Bishop and Henkel [7]. A method utilizing a suction cap (see Fig. 20) was also developed at Imperial College by Skinner [77]. A connection

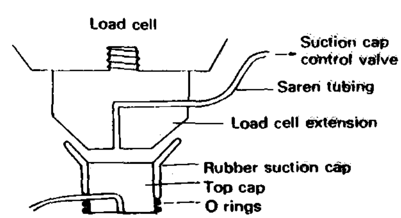

FIG. 20—*An exaggerated view of a triaxial sample before connection of load cell and suction cap developed by Skinner* [77].

method using three pots filled with a liquid polyester resin placed on the sample top plate for torsional shear tests is described in Hight et al [49]. The bolts from the loading piston enter the pots after the triaxial cell is assembled. The hardened resin transmits the required forces between the loading piston and sample. This connection method seems appropriate for research purposes.

Another type of triaxial cell is illustrated in Fig. 21. It has been used in many laboratories mainly for routine and research-oriented cyclic undrained triaxial testing. For this type of triaxial cell, the pressure cell is located outside the internal three or more tie rods. Consequently, the loading piston can be connected to the sample cap in any manner, that is, either rigidly or allowing rotation by direct hand operation before the pressure cell is assembled. For triaxial testing, generally the sample cap has been connected to the piston cap before a specimen is set in the cell. This type of triaxial cell has been built not only for samples having a diameter less than 10 cm but also for samples having a larger diameter. Alva-Hurtado and co-workers [78] built a triaxial cell of this type for samples with a diameter of 15.24 cm. Figure 22*a* shows a similar type of triaxial cell for samples having a diameter of 30 cm [79]. This triaxial cell was built for both static and cyclic tests. Figure 22*a* shows a Toyoura sand sample prepared for a cyclic undrained triaxial test standing under a suction. Figure 22*b* represents a typical result of a test performed at a loading frequency of 1/20 Hz. A pneumatic cyclic loading system similar to the one developed by Chan [80] was used with an increased capacity using giant boosters, large air-pressure accumulator tanks, and a large double-action air cylinder. The structure and tubing arrangement of this triaxial cell and its associated testing method are principally the same as for the smaller triaxial cells. A 35-mm-diameter piston is used for fast cyclic tests; this is replaced by a 50-mm-diameter piston for static tests.

The same type of small triaxial cell with an external pressure cell has been widely used for torsional shear tests as well (at least in Japan); Fig. 23 shows a typical example [59]. In this case the pressure cell is assembled after the load cell (LC) is connected to the sample

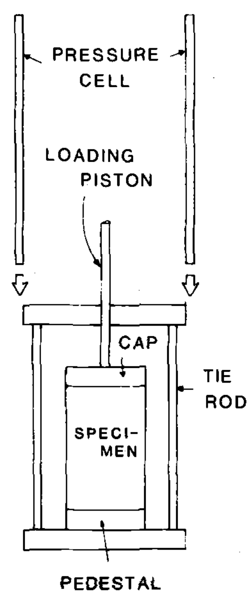

FIG. 21—*The triaxial cell with a pressure cell outside tie rods.*

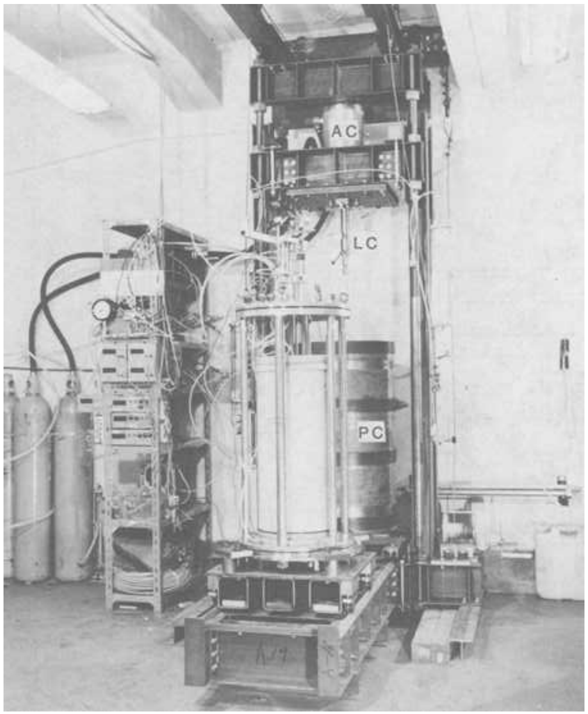

FIG. 22a—*Large triaxial cell for 30-cm-diameter samples with a pressure cell outside six tie rods built at Institute of Industrial Science, University of Tokyo (LC = load cell, PC = pressure cell, AC = double-action air cylinder).*

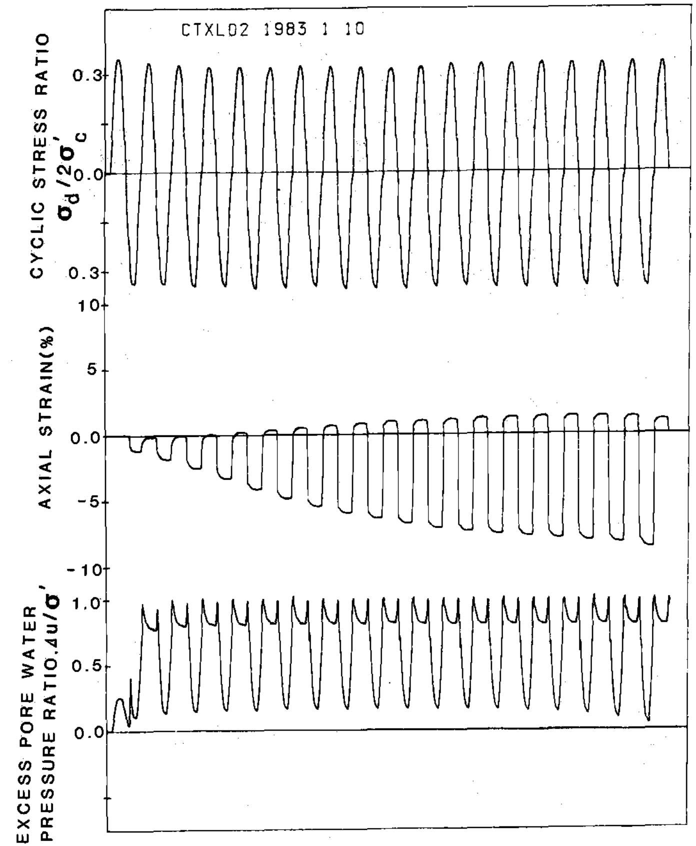

FIG. 22b—*A typical result of cyclic undrained triaxial test* (D_r = *79.1*, σ_c' = *1.0 kgf/cm²*, D = *30 cm*, H = *63 cm*).

cap by direct hand operation. Note that the triaxial cell shown in Fig. 23 was designed so that both triaxial and torsional shear tests, which may be static or cyclic, can be performed by changing only the loading piston, the bearing house, the sample cap, and the pedestal.

The problem of improper alignment between the loading piston, the sample cap, and the sample, which is sometimes associated with a type of triaxial cell such as that shown in Fig. 19, can be effectively avoided for a triaxial cell with an external pressure cell. In the case where the loading piston is connected to the sample cap, proper axial load should be applied to the loading piston to compensate for the uplift by the cell pressure so as to ensure the isotropic stress condition. This procedure is not needed when a triaxial cell such as that shown in Fig. 19 is used and the loading piston is not connected to the cap. When the loading piston has such a small diameter as shown in Figs. 21–23, this compensating axial load can be applied simply by dead weight. It should be noted that such triaxial cells have a slightly complicated structure and are somewhat larger in size for the same sample dimensions than that shown in Fig. 19. In addition, one may consider that a specimen that has been connected to the loading piston may be disturbed by possible deformation of the triaxial cell associated with the assembling of the pressure cell. This kind of disturbance can be reduced to a negligible value by proper design and careful manufacturing of the triaxial cell. Furthermore

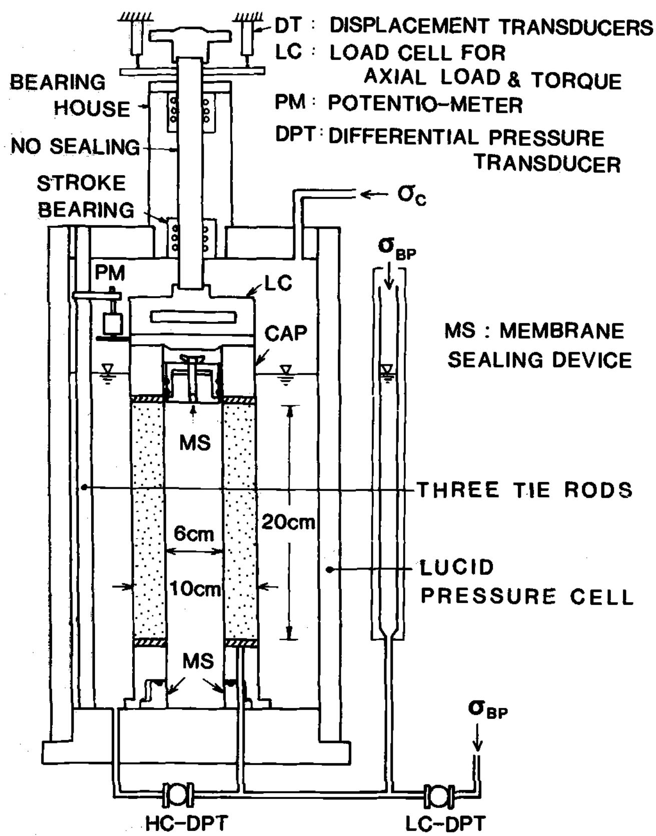

FIG. 23a—*Triaxial cell built at Institute of Industrial Science, University of Tokyo for both triaxial and torsional testing. In this figure a hollow cylindrical sample is set for a torsional shear test* [59].

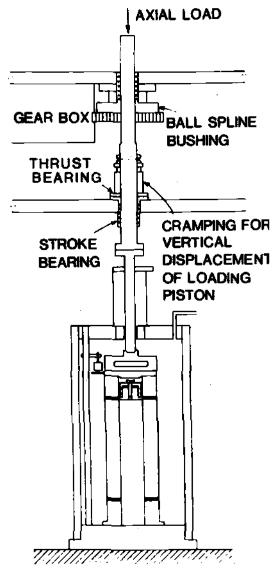

FIG. 23*b*—*Loading system for static torsional shear testing* [59].

this disturbance can be avoided by assembling the pressure cell with unclamping the loading ram against the piston guide [*81*].

In summary, triaxial cells having external pressure cells outside the internal tie rods are getting more popular primarily because the connection of the loading piston and the sample cap can be achieved in a very simple manner, and thereby the proper alignment between the loading piston, the cap, and the sample can be ensured easily.

Pressure and Load Measurements

Only methods of measuring pressures and loads by means of electronic pressure transducers and load cells (load transducers), respectively, will be discussed because manual measuring methods are becoming less popular.

Pressure Measurement

The effective confining pressure of a saturated sample can be measured accurately and directly by a liquid–liquid differential pressure transducer (DPT) such as those shown in

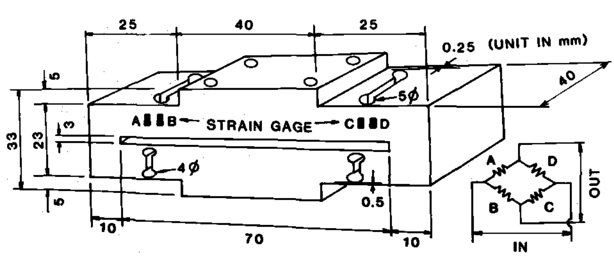

FIG. 23*c*—*Two-component* (*axial load and torque*) *load cell. The upper portion is for measuring torque and the lower portion is for measuring normal load* (*see Fig. 25*) [59].

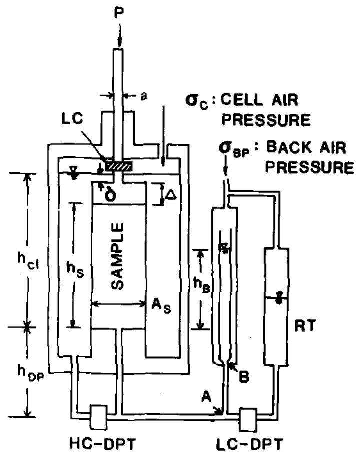

FIG. 24—*Schematic diagram of triaxial apparatus with the use of an HC-DPT and an LC-DPT.*

Figs. 23, 24, 27*b*, and 49. In Figs. 23*a* and 24, this transducer is denoted as HC (high capacity)-DPT because another kind of DPT having a lower capacity (LC-DPT) is used in this case for the automated volume change measurement. This direct method of measuring the effective confining pressure has been used by Castro [82] for the study of liquefaction of sands. When both cell liquid and pore liquid in a sample are water, the effective confining pressure σ_r' at any level in a sample is defined in the case shown in Fig. 24 as

$$\sigma_r' = p_h - u + \Delta\sigma_{r_m} \tag{3}$$

where

p_h = $\sigma_c + (h_{cl} + h_{DP})\gamma_w$, the liquid pressure applied on the high pressure face of the HC-DPT
σ_c = cell air pressure
h_{cl} = height of cell water from the sample bottom
h_{DP} = distance of the HC-DPT down from the specimen bottom
γ_w = unit weight of water
u = $\sigma_{BP} + (h_B + h_{DP})\gamma_w$, the pore water pressure applied on the low pressure face of the HC-DPT
σ_{BP} = back air pressure
h_B = height of burette water surface from the sample bottom
$\Delta\sigma_{r_m}$ = stress correction for membrane forces

It is obvious that a highly accurate measurement of σ_r' may not be ensured either when the values of σ_c and σ_{BP} are measured separately or when the values of p_h and u are measured separately. On the other hand, the differential pressure *DP* measured by the HC-DPT is given as

$$DP = p_h - u \tag{4}$$

Consequently, the value of σ_r' is obtained as

$$\sigma_r' = DP + \Delta\sigma_{r_m} \tag{5}$$

This measuring method is superior especially for a test at a high back pressure, because the resolution in the output of DPT is independent of the back pressure whereas the accuracy of measured value of σ_r' decreases when the pressures p_h and u are measured separately.

At the Geotechnical Laboratory, Institute of Industrial Science, University of Tokyo, several units of liquid–liquid DPT of capacitance type having a capacity of differential pressure either between 0.32 and 3.2 kgf/cm^2 or between 3.0 and 30.0 kgf/cm^2 have been used over 5 years for triaxial compression tests at $\sigma_r' \fallingdotseq 0.02$ to 2.0 kgf/cm^2 [*83*], for plane strain compression tests at $\sigma_r' \fallingdotseq 0.05$ to 1.0 kgf/cm^2 [*24*], and for torsional shear tests (TSI) at $\sigma_r' \fallingdotseq 0.3$ to 2.0 kgf/cm^2 [*59*]. Note that for the same value of σ_r' the accurate measurement of σ_r' is more important in the torsional shear tests than in the triaxial or plane strain compression tests because in the torsional shear test, σ_3' can be much less than σ_r'; for example in the case of TSI where $p_o' = p_i'$ (Table 1), $\sigma_3' = \sigma_r' - \tau_{ai}$ is obtained.

The effective axial stress σ_a' at a level z from the sample bottom is obtained by means of a load cell, which is placed either outside or inside a triaxial cell, as

$$\sigma_a' = (\sigma_a \text{ at } z) - (u \text{ at } z) + \Delta\sigma_{am} \tag{6}$$

where

$\Delta\sigma_{am}$ = stress correction for membrane forces,
$(\sigma_a \text{ at } z)$ = total axial stress at the level z, and
$(u \text{ at } z)$ = $\sigma_{BP} + (h_B - z)\gamma_w$, pore water pressure at the level z.

When the value of DP is measured, σ_a' is given for the same cross-sectional area of the cap and the sample as follows:

1. For an external load cell [*83*]:

$$\sigma_a' = (P_a + W \pm F_r)/A_s + DP - (\sigma_c + \delta \cdot \gamma_w)a/A_s - \Delta \cdot \gamma_w + \gamma_s' \cdot (h_s - z) + \Delta\sigma_{am} \tag{7}$$

where

P_a = load cell reading
W = combined weight of cap, loading piston, and other attachments
F_r = loading piston friction
A_s = cross-sectional area of the specimen and the cap
Δ = thickness of the cap
δ = depth of cell water above the cap
a = cross-sectional area of the loading piston (the same sealing area is assumed)
γ_s' = effective unit weight of the sample
h_s = length of the sample

2. For an internal load cell:

$$\sigma_a' = LC/A_s + DP - \delta \cdot \gamma_w \cdot a/A_s - \Delta \cdot \gamma_w + \gamma_s' \cdot (h_s - z) + \Delta\sigma_{am} \tag{8}$$

where LC is the load cell reading of which the zero value is defined in the atmosphere with the cap and the other attachments being fixed to the load cell. For example when the strength of sand is measured in terms of $R_{max} = (\sigma_1'/\sigma_3')_{max}$ by the triaxial or plane strain compression tests, the axial stress σ_a' is equal to σ_1'. Therefore, it is not so difficult to ensure the accurate measurement of σ_1' as compared to the accurate measurement of σ_r'. Of course, great care should be exercised in measuring σ_a' in compression tests at low stress levels. On the other hand, in triaxial or plane strain extension tests, even at relatively high levels of σ_r', σ_a' should be measured very carefully because it is equal to σ_3' which is needed more accurately. For example, suppose that in a triaxial extension test $\sigma_c = 4$ kgf/cm^2, $\sigma_{BP} = 2$ kgf/cm^2, and thereby $\sigma_1' = \sigma_r' = 2$ kgf/cm^2 ($\Delta\sigma_{rm}$ is ignored). In this case $\sigma_3' = \sigma_a'$ may decrease to a value of the order of 0.3 to 0.5 kgf/cm^2 which is much less than the values of σ_c and σ_{BP}. As has been shown it is very difficult to ensure the accurate measurement of σ_a' when σ_c and σ_{BP} are measured separately, that is, without the use of a DPT. In this case, the measurement based on Eq 8 seems appropriate.

Load Measurement

Various types of load cells have been developed in many laboratories to measure (1) axial load in triaxial testing and plane strain testing, (2) horizontal normal load in plane strain testing, (3) normal and tangential loads in simple shear testing, or (4) axial load and torque in torsional shear testing. Desirable features of load cells may be summarized as follows: (1) high linearity, (2) small hysteresis, (3) small zero drifting, (4) high resolution, (5) high rigidity (low compliance), (6) low coupling effect (low effect of load components other than the one to be measured), (7) temperature insensitivity, (8) tightness against pressurized water, (9) compactness, (10) high degree of versatility (the same basic structure can be adapted for many different testing purposes), (11) high durability, (12) insensitivity against hydrostatic pressure, (13) ability to measure multiple load components, if needed, (14) simple calibration procedure, (15) low cost, and (16) simple structure (easy to design and manufacture). Many load cells that satisfy most, if not all, of the above requirements are now available. Pressure-insensitive load cells built based on the original idea of Tani et al. [*84*] have been used over 5 years at the author's laboratory for many different testing purposes, such as static and cyclic triaxial tests, static plane strain tests (Fig. 25), static and cyclic torsional shear tests (Fig. 23), and model tests. The results shown in Figs. 5 through 18 were obtained from tests using the load cell shown in Fig. 23c. In Fig. 25 the following notation is used: LC1 is for axial load, LC2 is for horizontal load, and LC3 and LC4 are for vertical friction on the vertical surfaces of the confining plates. It may be seen in Fig. 25 that with the use of these compact load cells the plane strain compression apparatus has been very much simplified.

Any load cell shown in Figs. 23 and 25 is comprised of four active gauges in a full Wheatstone bridge configuration, without using dummy gauges, and thereby the rigidity as compared to the capacity is considerably increased and the coupling effects are remarkably reduced. The load cells currently used at the author's laboratory have compliances of the order of 2.4×10^{-3} mm/kgf (2.4×10^{-4} mm/N) for a capacity of 20 kgf (200 N), 2.0×10^{-4} mm/kgf (2.0×10^{-5} mm/N) for a capacity of 300 kgf (3 kN), and 2.5×10^{-5} mm/kgf (2.5×10^{-6} mm/N) for a capacity of 5 tonf (50 kN). These values seem to be comparable to those reported as low compliance values in literature (for example, Ref *77*). Figure 26 shows the result of calibration for a one-component (normal load) load cell having a capacity of 20 kgf, LC1 shown in Fig. 25 [*81*]. It may be seen that the output of the Wheatstone bridge consisting of the four active gauges, denoted as a, b, c, and d, is very insensitive to either load eccentricity or thrust force, although the output of each individual gauge is influenced by these. This low coupling effect has two advantages as compared to other multicomponent load cells which have a large coupling effect (for example, load cells developed at the University of Cambridge [*39,43*]). First, the calibration becomes very simple. Second, the load components to be measured can be shown on real time without any data

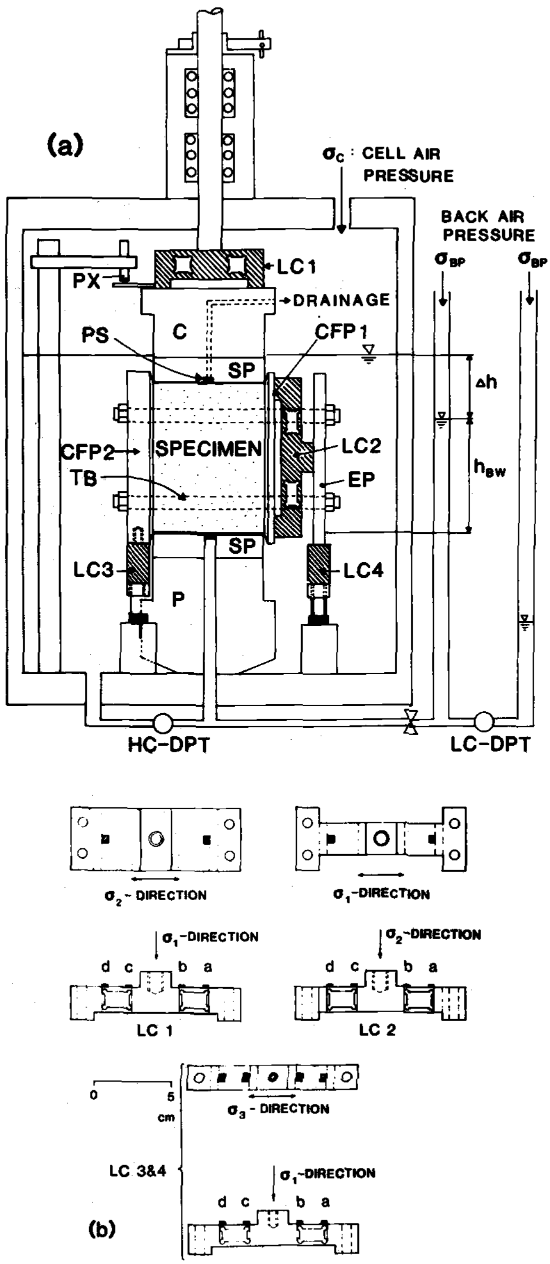

FIG. 25—*Plane strain compression apparatus with four internal load cells: (a) triaxial cell; (b) load cells* [24].

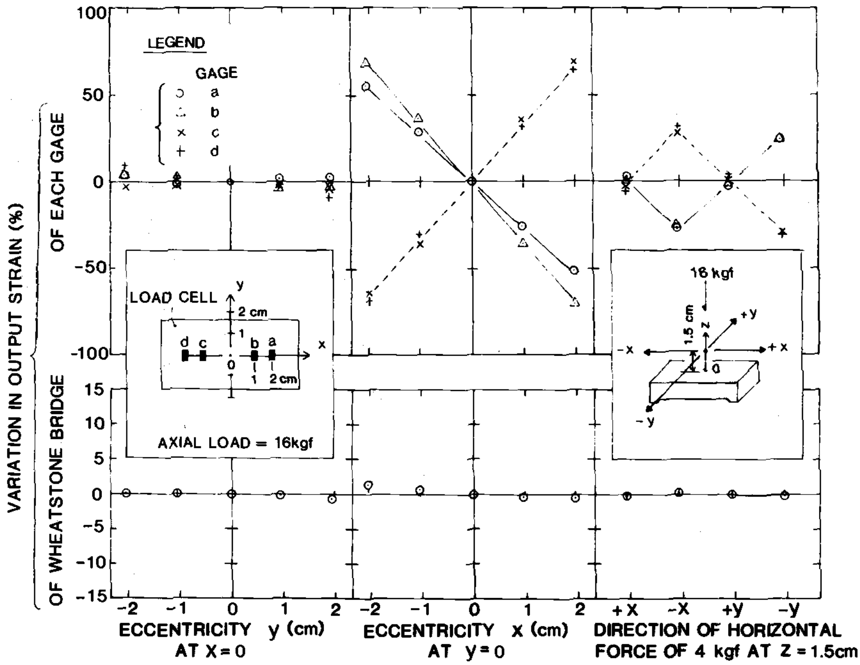

FIG. 26—*Result of calibration loading for a load cell LC1 shown in Fig. 25* [81].

processing on such displays as digital voltmeters or a visual display unit after analog-to-digital (A-D) conversion. Also, one can see that the structure of these load cells is very simple. Further details are described in Refs *24, 59, 81*, and *84*.

Another advantage in using an internal load cell is the ability to control the stress path of a specimen at extremely low stress levels, for example less than 5 kN/m^2 (0.05 kgf/cm^2), during the sample preparation stage before isotropic compression. Figure 27*a* shows such a stress path which was controlled and measured during the sample preparation stage for an air-pluviated sample tested in a highly accurate triaxial system (Fig. 27*b*), developed at Delft Soil Mechanics Laboratory (now called Delft Geotechnics) [*85–87*]. The numbers in Fig. 27*a* indicate the following distinct stages: (1) pluviation of the sand, (2) application of the cap contact force, (3, 4) before and after clamping of the piston, (5) application of a small vacuum pressure to the sample, (6) removal of the mold, (7) assembling the cell, (8) filling of the cell with water, (9) replacing the vacuum pressure with cell air pressure, (10, 11) before and after saturation of the sample, (12) closing the drainage valve, (13) connection of the drainage line to the balance, and (14) unclamping the piston (this is the end of the preparation stage). A similar result has also been obtained by Tatsuoka et al. [*81*]. Such great care as outlined above is needed to study the deformation and strength characteristics of sands at low stress levels. Furthermore even for shear tests at relatively high stress levels this care is necessary because the strain history of the sample during the sample preparation stage does not completely fade by a small amount of compression, especially for sands. It is the author's opinion that a significant part of large unaccountable scattering in data, if it exists, can be attributed to uncontrolled different stress and strain histories during the sample preparation stage.

Others

Stress corrections for membrane forces are needed for tests at low stress levels. For example, it may be seen in Figs. 28 and 29 that the dependency of φ on σ_3' of Toyoura sand is very small for $\sigma_3' < 0.5$ kgf/cm^2 when stresses are corrected for membrane forces in both triaxial compression tests and torsional shear tests whereas it is not the case otherwise [*59,83*]. These stress corrections were made based on the theory of elasticity together with the assumption that the membrane has not buckled. The equations are given in Refs *59* and

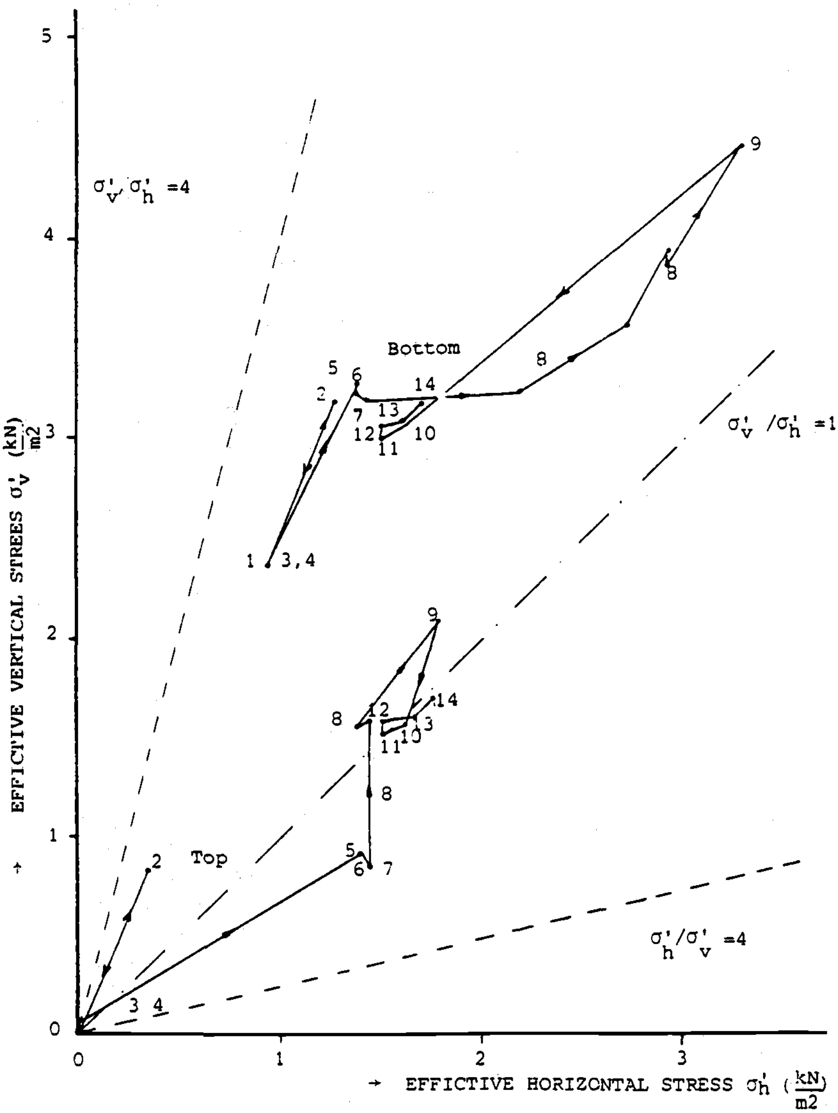

FIG. 27*a*—*Typical stress conditions during the various stages of the preparation of a sample as calculated both for top and bottom level of the sample.*

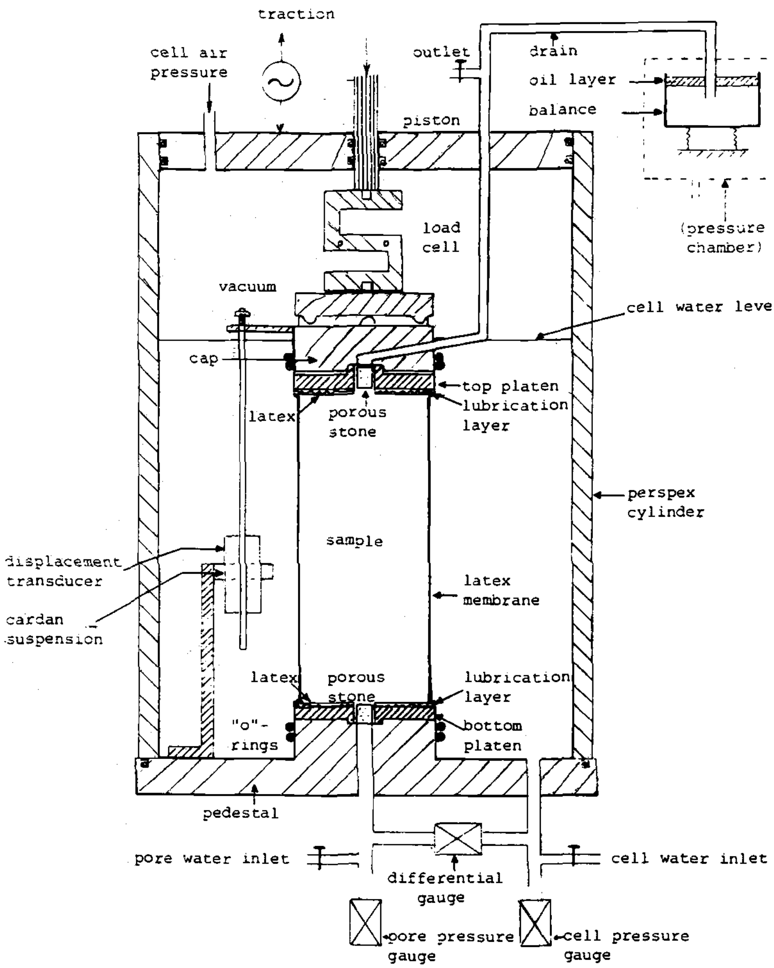

FIG. 27*b*—*Schematic view of the triaxial apparatus* [85–87].

83. A similar result has been obtained for plane strain tests (Fig. 30). The results shown in Figs. 5 through 18 have been corrected for membrane forces as well. This problem has been discussed by many researchers (see Refs *83*, *88* to *92* among others for triaxial testing, Refs *24* and *89* among others for plane strain testing, and Ref *59* for torsional shear testing).

The lubrication of end platens is also very important in reducing the end restraint. The method employing grease layer(s) and latex rubber disk(s) used by Rowe and Barden [*93*] and Bishop and Green [*6*] is known to be very effective. It is, however, to be noted that the errors in both boundary axial displacements and volume change associated with this lubrication method should be accounted for if necessary. Furthermore, it is very important to examine the quality of a lubrication layer under the test condition for which it is used in an element test. The effects of normal stress, duration of loading, displacement rate, stress history, and others on the lubrication quality were investigated by means of a direct shear test by Lee [*94*], Arthur and Dalili [*95*], Tatsuoka et al. [*96*], and Tatsuoka and Haibara [*97*]. This experimental confirmation is essential because no universal method of good

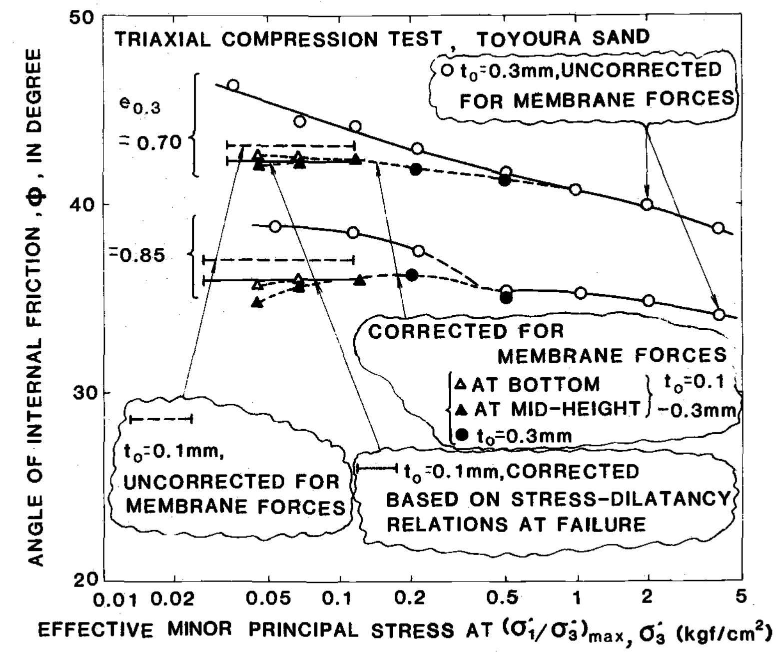

FIG. 28—*Effects on φ of membrane restraint in triaxial compression tests* (D = *7 cm*, H = *15 cm with lubricated fixed ends* [83]).

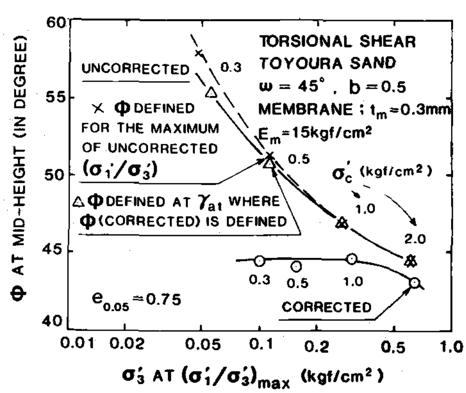

FIG. 29—*Effects on φ of membrane restraint in torsional shear tests* (D_0 = *10 cm*, D_i = *6 cm*, H = *20 cm* [59]).

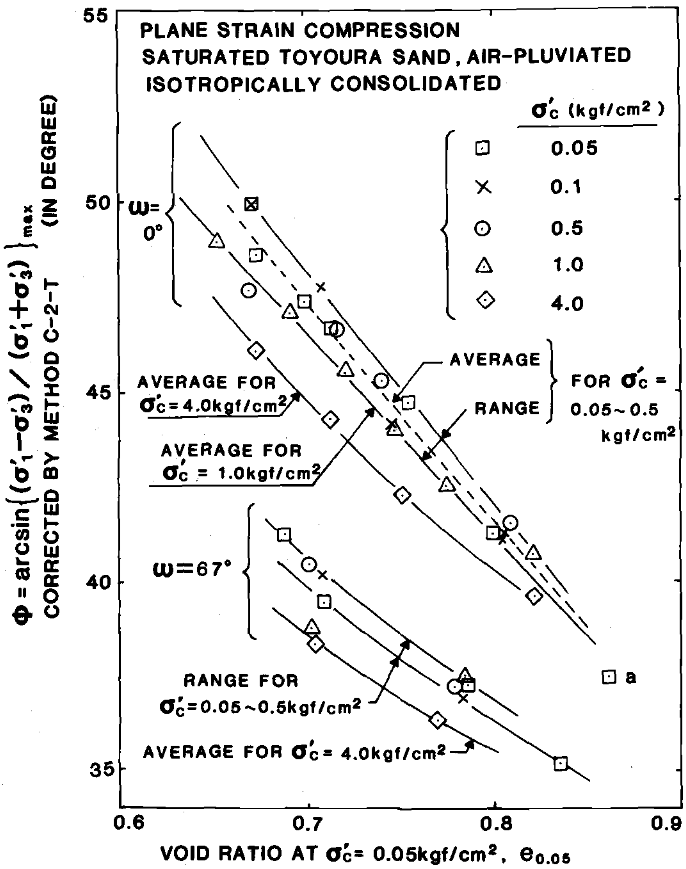

FIG. 30—φ *in plane strain compression; the values of* φ *have been corrected for membrane restraint* [24].

lubrication, which is always effective at varying test conditions, exists. The composition of lubrication layer (the number of grease layers and latex rubber disks, the thickness of grease and latex disk, the amount, dimensions and properties of fine fillers in grease, the viscosity of oil in grease, and others) should be carefully selected depending on the test condition.

Displacement and Volume Change Measurements

Axial Displacement

The necessity for very accurate measurement of extremely small axial strains, say less than 10^{-4}, has increased during the last two decades, primarily for the following two purposes: (1) small deformation analysis of soil masses under monotonic loadings, and (2) earthquake response analysis of soil masses. To accomplish accurate measurement of very small axial deformation of a sample, two main methods have been developed: (1) to measure the vertical relative displacement between the cap and the pedestal, with corrections for bedding errors if needed, and (2) to measure the local vertical compression on the sample lateral surface. Figure 27*b* shows an example of the first method in which average vertical displacement of the cap is obtained from the readings of three displacement transducers located at 120° centers in a horizontal plane. When lubricated ends are used, the correction for bedding errors is essential. This point, however, is beyond the scope of this paper.

Figure 31 shows another example of a technique developed to obtain equivalent shear moduli and hysteretic damping coefficients of clays and sands under cyclic loading for a wide range of strain (between 10^{-6} and 10^{-2}) [*98*]. The cap displacement is measured by means of a pair of two diametrically opposed proximity transducers. In this method, ends are not lubricated so as to minimize the bedding error at the ends. Figure 32*a* shows a typical hysteresis curve for a very soft Tokyo Bay clay sample at an axial strain in single amplitude of 2.12×10^{-5}, obtained by a cyclic undrained triaxial test at a loading frequency of 0.1 Hz [*99*], using the same testing method as shown in Fig. 31. The sample had a diameter of 7.3 cm and a height of 15 cm. For this data, the equivalent shear modulus G_{eq} is 35.7 kgf/cm^2, and the hysteretic damping coefficient h is 0.037. Suppose that the axial load is measured by means of a load cell outside the triaxial cell and an error of as small as ±5 gf is involved due to the piston friction. The measured values of G_{eq} and h increase then to 37.6 kgf/cm^2 and 0.054, respectively. Note that this test was performed in a framework of routine soil testing, using a commercially available load cell with a capacity of 20 kgf and two proximity

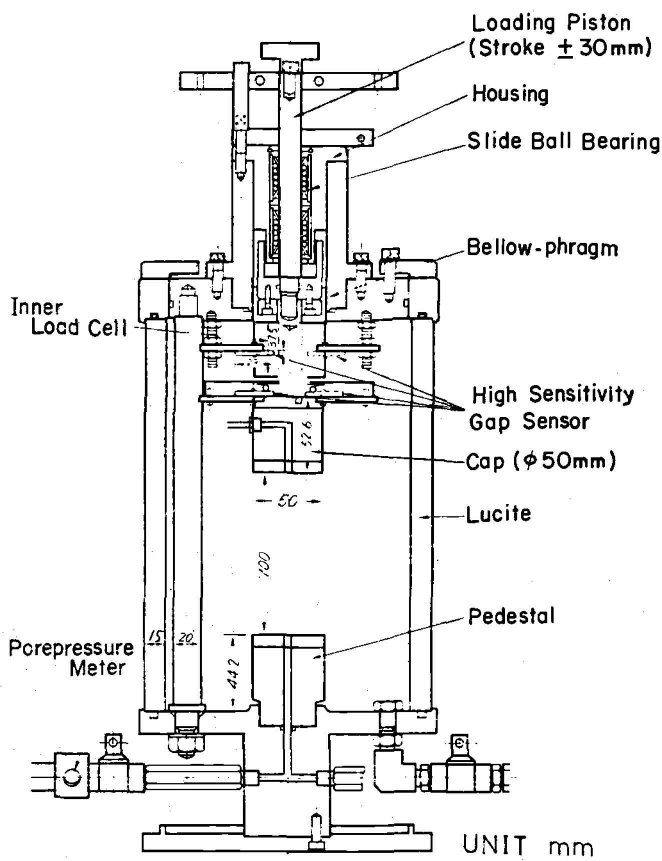

FIG. 31—*Triaxial cell with an internal load cell and two proximity transducers developed to measure cyclic deformation properties for a wide strain range* [98].

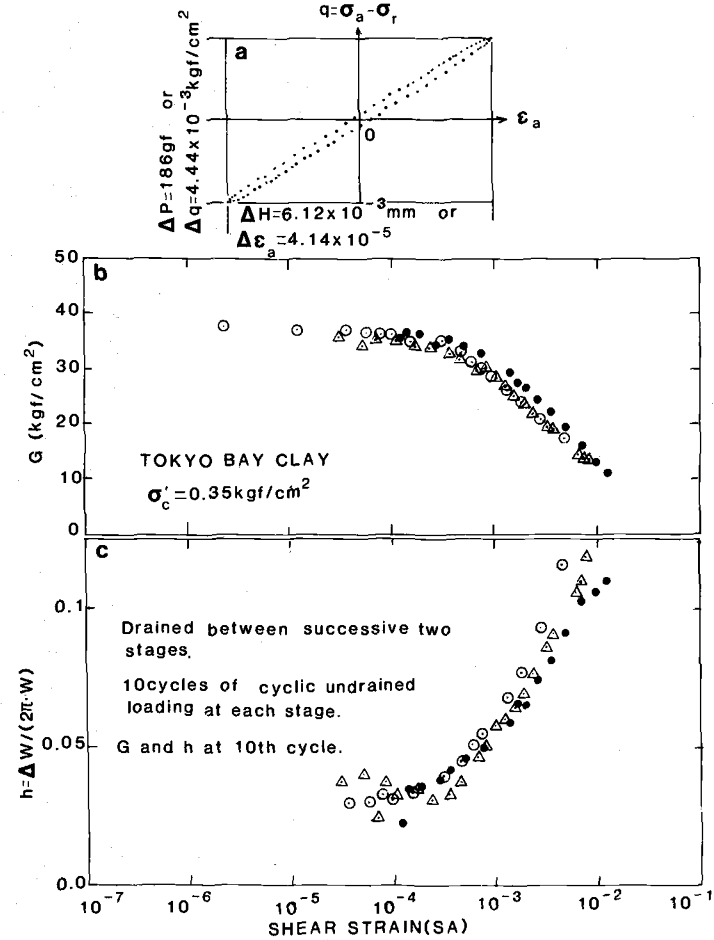

FIG. 32—a, *Typical hysteresis loop,* b, *G–γ* relation, and c, *h–γ relation of soft Tokyo Bay clay obtained by cyclic triaxial tests* [99].

transducers with measuring ranges of 1.5 mm and 8 mm. Figures 32*b* and 32*c* show the summary of the results for three similar tests.

It is clear now that even in routine soil testing using conventional triaxial apparatus, accurate cyclic deformation properties of various types of soils subjected to strain levels less than 10^{-4} can be obtained. It is known, however, that the deformation properties of soils at small strain levels are rather strain-rate independent (see, for example, Ref *100*) (Fig. 33). Consequently, quasistatic or slow cyclic testing methods are now replacing such dynamic soil testing methods as the resonant-column testing method and the pulse method. This is true at least in Japan. This change is because quasistatic cyclic testing methods are much simpler both in instrumentation and in testing operation than the dynamic testing methods. Furthermore, these tests are versatile in the sense that by using the same device and type of sample, other kinds of cyclic test, such as liquefaction test or static loading test, can be performed.

For evaluation of cyclic deformation properties of soils, quasistatic cyclic triaxial testing

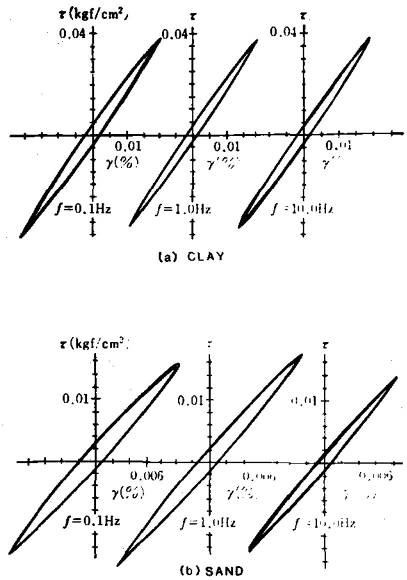

FIG. 33—*Frequency-independence of deformation properties by cyclic simple shear tests for* a, *a clay* ($\sigma_v' = 1.68$ *kgf/cm*^{2}, e = *1.75*, PI = *63.7*) *and* b, *a sand* ($\sigma_v' = 0.31$ *kgf/cm*^{2}, e = *0.67*) [100].

has been widely performed. However, quasistatic cyclic torsional shear testing or simple shear testing are occasionally performed mainly for research purposes (see, for example, Refs *47*, *100* to *102*). Figure 34 presents typical quasistatic test results for a partly saturated sand utilizing the apparatus shown in Fig. 35 [*103*]. These tests were performed for the response analysis of shaking table tests on small models of earthfill dams. Therefore the stress levels at these tests were very low. Because the apparatus shown in Fig. 35 has been used primarily for stress-controlled liquefaction tests of sands [*58,75,76*], the part prepared particularly for this property test is the device to measure the rotational displacement by means of a proximity transducer which is designated by the number 12 in Fig. 35. The load cell denoted as 11 is the same as the one shown in Fig. 23*c*.

In testing rock samples, bedding errors at sample ends can induce large unaccountable errors. These errors may occur even with the use of ground cylindrical seated platens at sample ends because of possible poor flatness and parallelism of specimen ends [*104*]. Burland and Symes [*105*] and Jardine et al. [*104*] developed a new technique to avoid the above errors (Fig. 36). The mean axial strain over a central gauge length is given by half the sum of the output of two diametrically opposed electrolytic levels, and the sample tilt is given by half the difference of the outputs. The device can resolve to less than 1 μm over a range of 15 mm and is not damaged when the sample is taken to failure.

While the method shown in Fig. 36 is very powerful for highly accurate measurements of axial deformation of the sample, this method may be overly sophisticated to be used in a laboratory. Compared with this method, the method shown in Fig. 37 is much simpler [*106*] and can be reproduced in most laboratories. In this method two strain gauges are attached to each of two thin strips of phosphor bronze to measure the bending strain of the strips. This simple device can resolve to around 1 μm without large difficulties. However, the measuring range is not large (about 1.5 mm in the case shown in Fig. 37). For larger axial compression, the strips should be taken off by some measures in order not to damage the

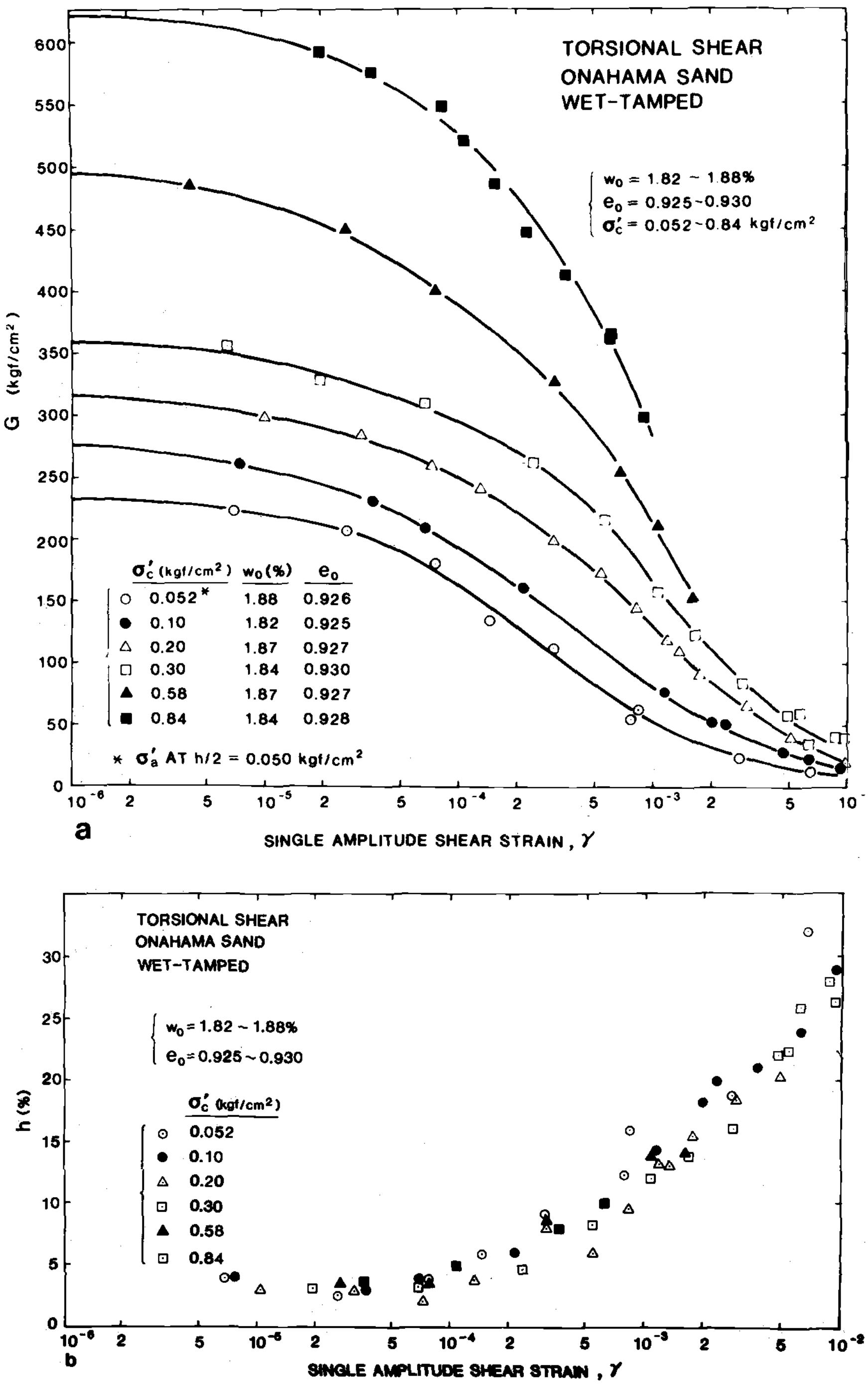

FIG. 34—*Typical results of quasistatic cyclic torsional shear tests* (D_0 = *10 cm*, D_i = *6 cm*, H = *10 cm*, f = *0.1 Hz, isotropically consolidated wet sand: (a) Shear modulus; (b) hysteretic damping coefficient* [103]).

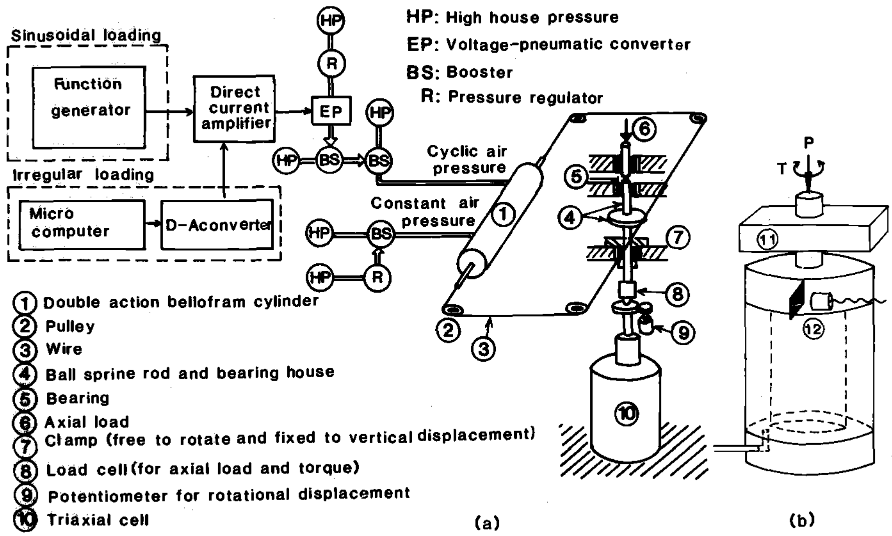

FIG. 35—*Load-controlled cyclic torsional shear apparatus:* a, *general and* b, *specimen* ((11) *load cell and* (12) *proximity transducer*) [76].

device. Furthermore, the relationship between the local axial compression of sample and the output of the device is nonlinear. In spite of the above drawbacks, very accurate small local axial strains can be measured with this device.

Horizontal Displacement

It is extremely difficult to accurately measure local radial deformations of a sample by methods similar to those shown in Figs. 36 and 37 because the horizontal planes of the sample at the ends are usually not exposed. Hight et al. [*49*] used the method illustrated in Fig. 38 to measure radial displacements of the inner and outer surfaces of a cylindrical sample for torsional shear tests. This method seems to be very accurate unless the sample deformation is nonuniform and the bedding error between the target aluminum foil and sample is large due to the change in the effective stress. The bedding error should be very carefully evaluated because the cylinder wall thickness or sample diameter is usually small. This kind of bedding error can be reduced to a much smaller value by using a location stud shown in Fig. 39 [*107*]. Boyce and Brown [*107*] attached small LVDTs to the studs to measure axial strain and flexible strain-gauged rings to measure radial strain of a triaxial sample. Targets for proximity transducers can be attached to these studs also if needed. However, the use of such a location stud seems to complicate sample preparation very much.

Volume Change

The automated volume change measurement by means of an electronic transducer is the most difficult among other kinds of automated instrumentation in triaxial testing and others. Various automated methods of measuring the volume change of a saturated specimen are reviewed in Ref *108*. One simple automated volume change measurement method, which is appropriate for a back-pressurized saturated specimen, utilizes a low-capacity differential pressure transducer (LC-DPT) as shown in Figs. 23*a*, 24, and 25*a*. The one shown in Figs.

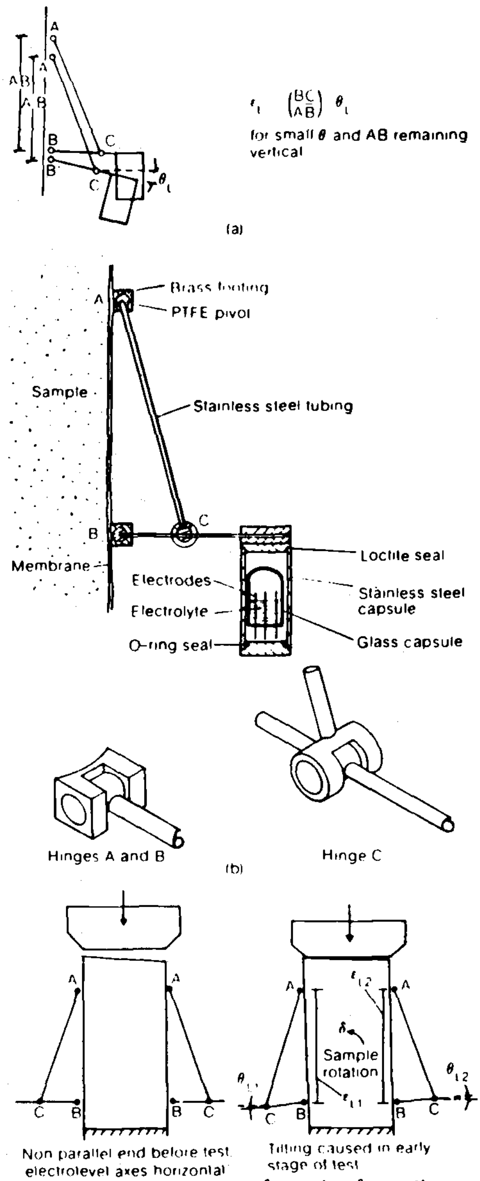

θ_{L1} positive, θ_{L2} negative

For similar triangles experiencing small rotations, with angles in radians

$$\theta_{L1} = \delta + \epsilon_{L1}\left(\frac{AB}{BC}\right)$$

$$\theta_{L2} = -\delta + \epsilon_{L2}\left(\frac{AB}{BC}\right)$$

$$\epsilon_L = \frac{\epsilon_{L1} + \epsilon_{L2}}{2} = \frac{\theta_{L1} + \theta_{L2}}{2}\left(\frac{BC}{AB}\right)$$

(c)

FIG. 36—a, *Conversion of axial strain to rotation of electrolevel capsule,* b, *construction of electrolevel gauges, and* c, *effects of tilting* [104].

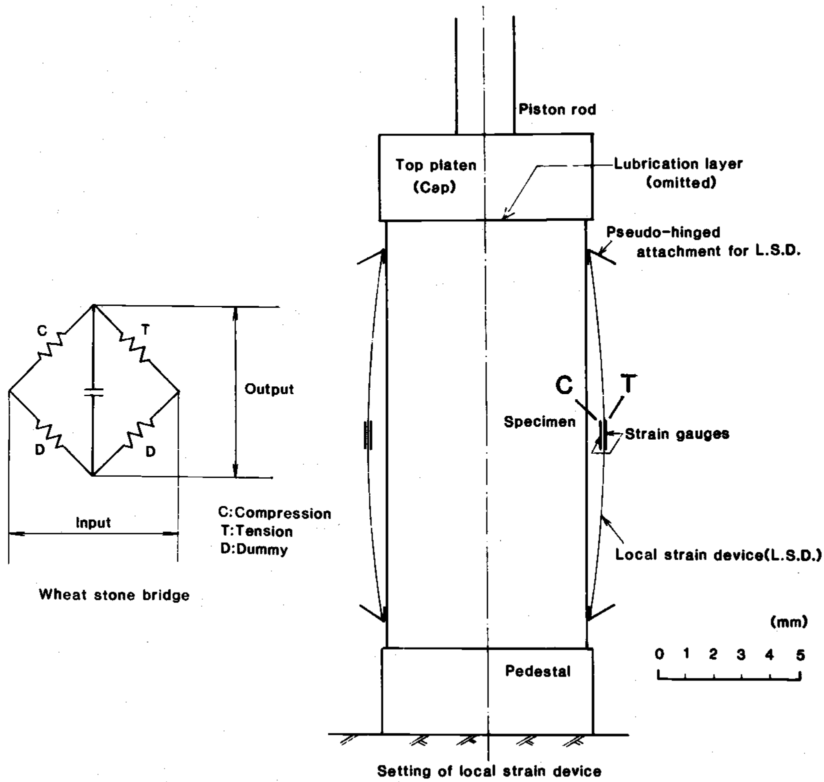

FIG. 37—*A simple method to measure local axial compression of sample* [106].

23*a* and 25*a* is of capacitance type and has an adjustable measuring range of differential pressure between 2.5 cm and 25 cm in water head [*109*]. While this method seems to be getting popular in practice primarily due to the simplicity in handling and its relatively high accuracy, the following two points should be noted. First, the evaporation of water in a burette induces an error especially in a long-duration test. The rate of water evaporation

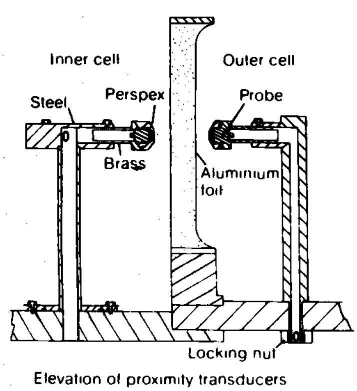

FIG. 38—*Method of measuring horizontal displacement by means of proximity transducers* [49].

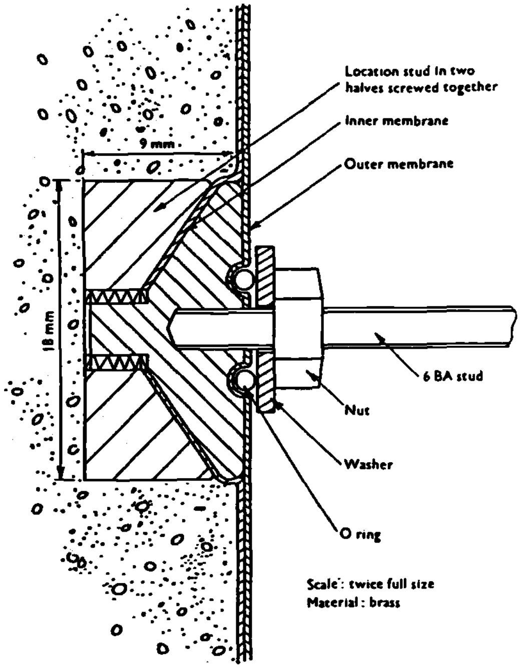

FIG. 39—*Location stud embedded in a sample* [107].

in a burette, however, can be reduced by applying a back pressure [*110*]. Furthermore, this problem can be effectively solved by using a reference tube as shown in Fig. 24. Because the effects of the water evaporation in the burette and the reference tube are canceled out, the output of the LC-DPT is compensated for evaporation. In the method shown in Fig. 24, the measured differential pressure can be kept in the measuring range by adjusting the vertical position of the reference tube. Second, some hysteresis effect may occur in this method largely due to the friction between water and tube wall above the point denoted as A in Fig. 24. This effect can be reduced to a negligible value by reducing the tube length between points A and B or by increasing the tube diameter [*110*].

Errors in measured volume change due to membrane penetration at the sample lateral surface and bedding error at the sample ends should be considered for accurate volumetric strain determination. This point, however, is beyond the scope of this paper.

A more direct method for the volume change measurement of a saturated sample is the one in which the weight of water expelled or soaked in by the sample is directly measured by means of either a load cell [*111*] or an electronic balance such as shown in Figs. 27*b* and 49 [*85,86,110*]. Other advantages of a weighing system with an electronic balance are that the ratio of measuring capacity/measuring accuracy can be easily increased to a value larger than 10^4 and that evaporation of the pore water can be prevented without influencing the measurement accuracy by covering the water with a layer of suitable oil (see Fig. 27*b*). Because this method is complicated as compared to the method using the LC-DPT, the latter method is preferable in most practical cases unless an extremely accurate volume change measurement is needed such as for cyclic drained tests.

Measuring the volume change of partly saturated soil is more complicated. In the method shown in Fig. 40, a sample is surrounded with mercury to avoid transfer of air between the

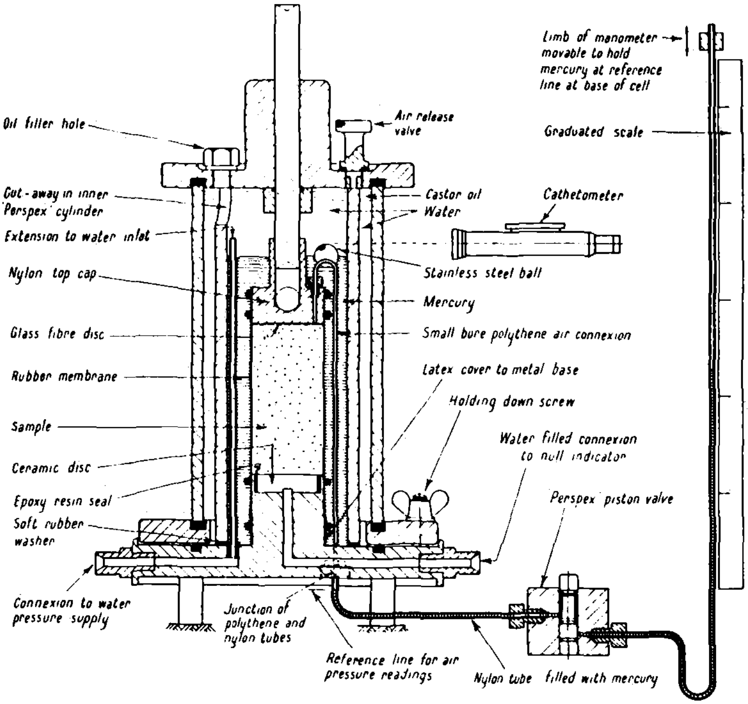

FIG. 40—*Arrangement of triaxial cell when using a mercury to surround the rubber membrane (Fig. 134 of Ref 7).*

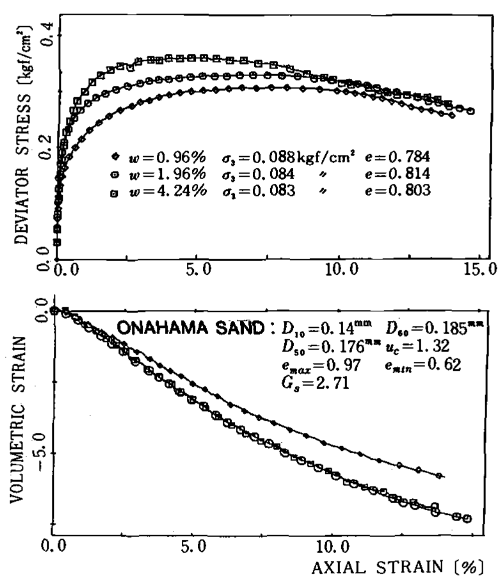

FIG. 41—*Examples of drained triaxial compression on a partly saturated sand* (D = *7.5 cm*, H = *10.7 cm, fixed lubricated ends*) [112].

pore space of the soil and water in the triaxial cell [7]. This is needed for a test in which both air and water are undrained. To measure sample volume change, the rise and fall of the mercury level is measured by a cathetometer on a nylon or stainless steel float. The mercury level can be measured by reading a pressure difference between the cell water surrounding the inner perspex cylinder and the mercury by means of a differential pressure transducer. In many practical cases associated with partly saturated soils, the pore air is under the drained condition and the pore water is under the drained or partly undrained or fully undrained condition. In this case, the transfer of air between the pore space of the soil and the cell water is not a serious problem because air can drain at will. The mercury shown in Fig. 40 can be replaced with water and thereby many technical problems associated with handling mercury can be avoided. Then the volume change of a sample can be determined by measuring a pressure difference between the cell air pressure and the cell water within the inner perspex cylinder by means of a LC-DPT in the same manner as shown in Fig. 24 (refer to Fig. 46). Figure 41 shows an example of triaxial compression test results on partly saturated sand samples where both air and water were drained and the sample volume change was measured by the method described above [*112*]. The LC-DPT used had a measuring range of 25 cm in water height.

Automated Strain and Stress Control

The automated data acquisition with the use of electronic transducers and a microcomputer has been reviewed in Ref *113* and will not be repeatedly discussed here. Many difficulties in apparatus design, manufacturing, and testing operation associated with manual control of stresses or strains can be solved by using both a microcomputer and a pneumatic stress control system. One important advantage of introducing the above improvement is that a simple triaxial cell, which had been used for routing soil testing without an automated strain- or stress-controlling system, can also be used for tests with automated control. Another advantage is that many complicated mechanical devices become unnecessary.

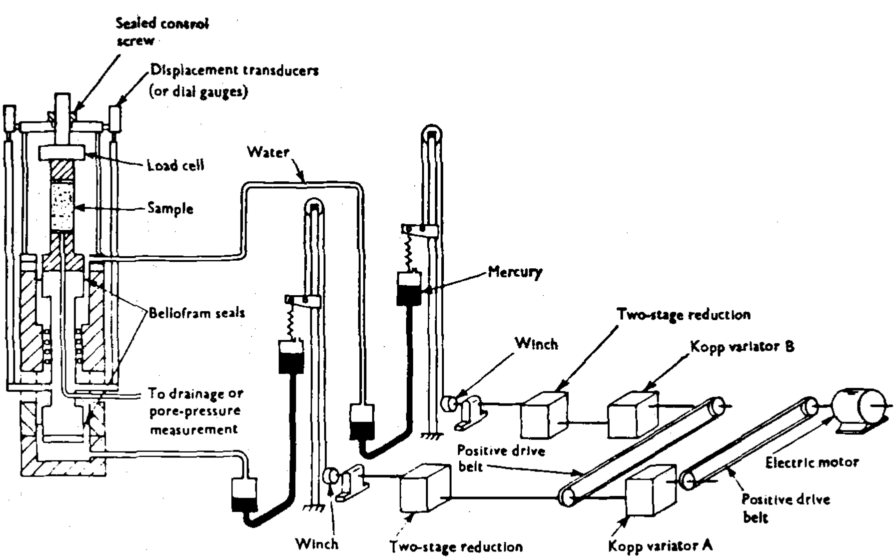

FIG. 42—*Differential hydraulic stress path control system developed by Bishop and Wesley* [114].

The hydraulic triaxial apparatus for controlled stress path testing (Fig. 42), developed by Bishop and Wesley [*114*], has two main features. First, the stress path is controlled hydraulically by means of a mechanical method without the use of a microcomputer. Second, a special triaxial cell (the Bishop and Wesley stress path cell) is used of which the sealing portion of the loading piston is achieved with the use of Bellofram seals. In this case the axial stress σ_a is given by

$$\sigma_a = p\frac{a}{A_s} + \sigma_r\left(1 - \frac{a}{A_s}\right) - \frac{W}{A_s} \tag{9}$$

where σ_r is the cell pressure, p is the pressure in the lower pressure chamber, A_s is the sample area, a is the Bellofram seal area for both seals, and W is the weight of the loading ram. The advantage claimed is that both the triaxial compression and extension stress conditions can be attained by controlling only one pressure (p). Disadvantages of using Bellofram seals are (1) the structure of triaxial cell becomes complicated, (2) the friction of Bellofram seal is not small (in general, of the order of 0.5 kgf), generally much larger than that for a small-diameter loading piston guided by two linear-motion bearings (Figs. 22*a* and 23*a*), and (3) the frequent need for maintenance. It is to be noted that if the seal has the same area as the sample ($A_s = a$), σ_a becomes independent of σ_r (see Eq 9). The mechanical parts of this stress-controlling system have been simplified by replacing the hydraulic pressurizing method with a pneumatic one which is controlled electrically either with or without a microcomputer [*115*] (see Fig. 43). The triaxial cell used is the Bishop Wesley stress path cell.

Although triaxial cells with a piston sealing area the same as the sample are more complicated to design and manufacture than triaxial cells having pistons with smaller diameters, these cells have been used for the ease of independent control of axial and radial stresses in K_0-consolidation tests [*74,116*] (see Figs. 44 and 45). The apparatus shown in Fig. 44 has a special, very rigid, pressure cell. The cell water should be well deaired so that the lateral

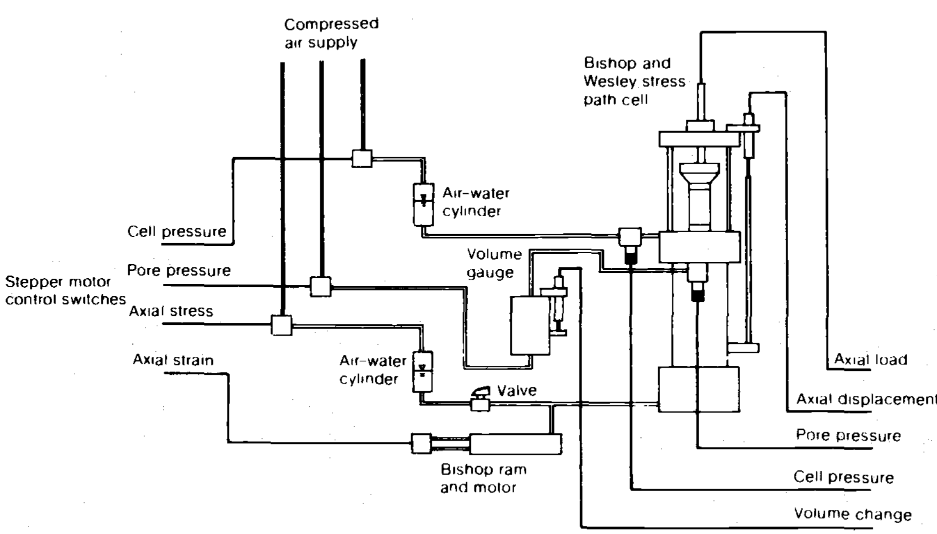

FIG. 43—*Loading method for a hydraulic cell for triaxial stress-controlled and strain-controlled tests and for stress path tests* [115].

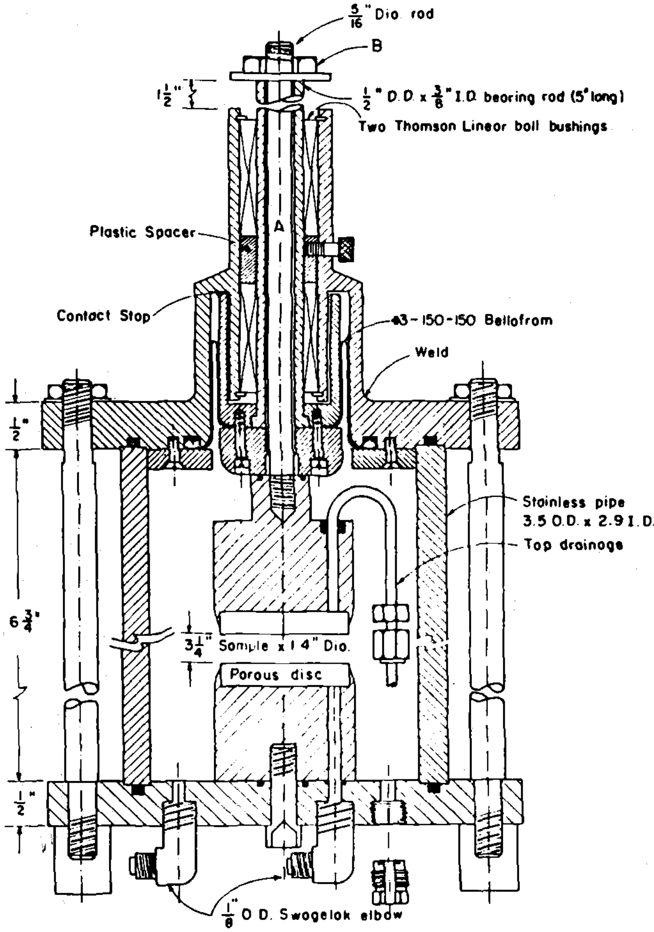

FIG. 44—K_0 *triaxial apparatus with an internal pressure cell developed by Campanella and Vaid* [116].

strain of sample is kept at zero during axial loading or unloading with a constant cell water volume. In the apparatus shown in Fig. 45 the condition of compression with zero lateral strain is achieved by maintaining the level of the deaired water in the annular space between the inner cell and the top cap which is the same cross-sectional area as the sample. This is the similar method as used by Bishop et al. [*6*], but Bishop used mercury. The change in the water level at the annular space is detected by a LC-DPT. These apparatuses are not versatile because the sample diameter cannot be different from the piston sealing diameter.

On the other hand, when such a pneumatic circuit as shown in Fig. 46, which is in principle similar to the one developed by Saada et al. [*53–56*], is introduced into a system with a triaxial cell having a smaller diameter piston, the axial stress becomes independent of the change of the lateral stress. In both systems shown in Figs. 45 and 46, the condition of axial compression with zero lateral strain was achieved by the manual controlling of the cell air pressure so that the output of the LC-DPT was constant. However, this operation can be automated by controlling the cell air pressure σ_c responding to the change of the LC-DPT using a microcomputer and an electric-to-pneumatic transducer (that is, a complete servo

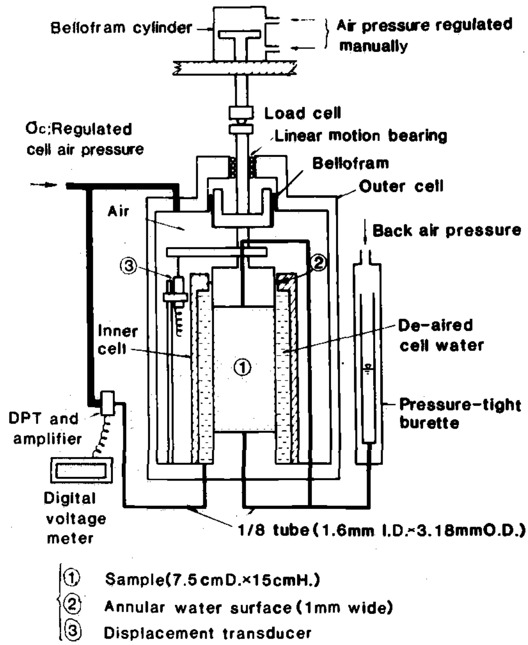

FIG. 45—*Double-cell triaxial cell having a seal area equal to sample area used for* K_0-*compression test* [74].

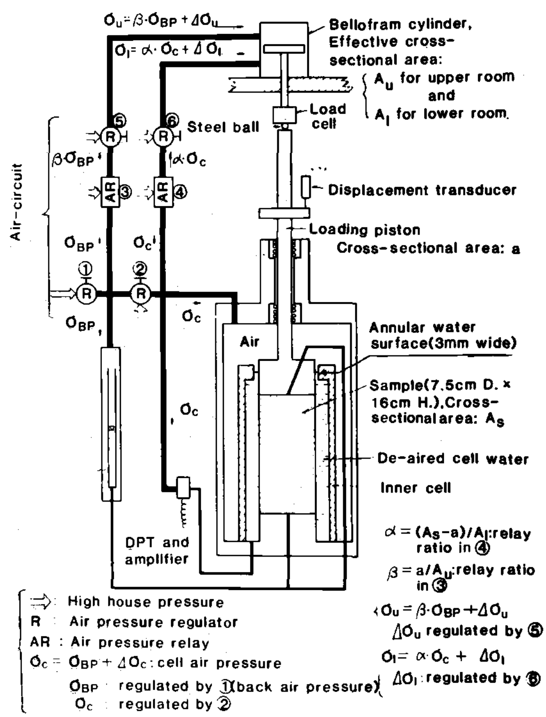

FIG. 46—*Schematic diagram of double-cell* K_0 *triaxial apparatus having a small-diameter piston* [74].

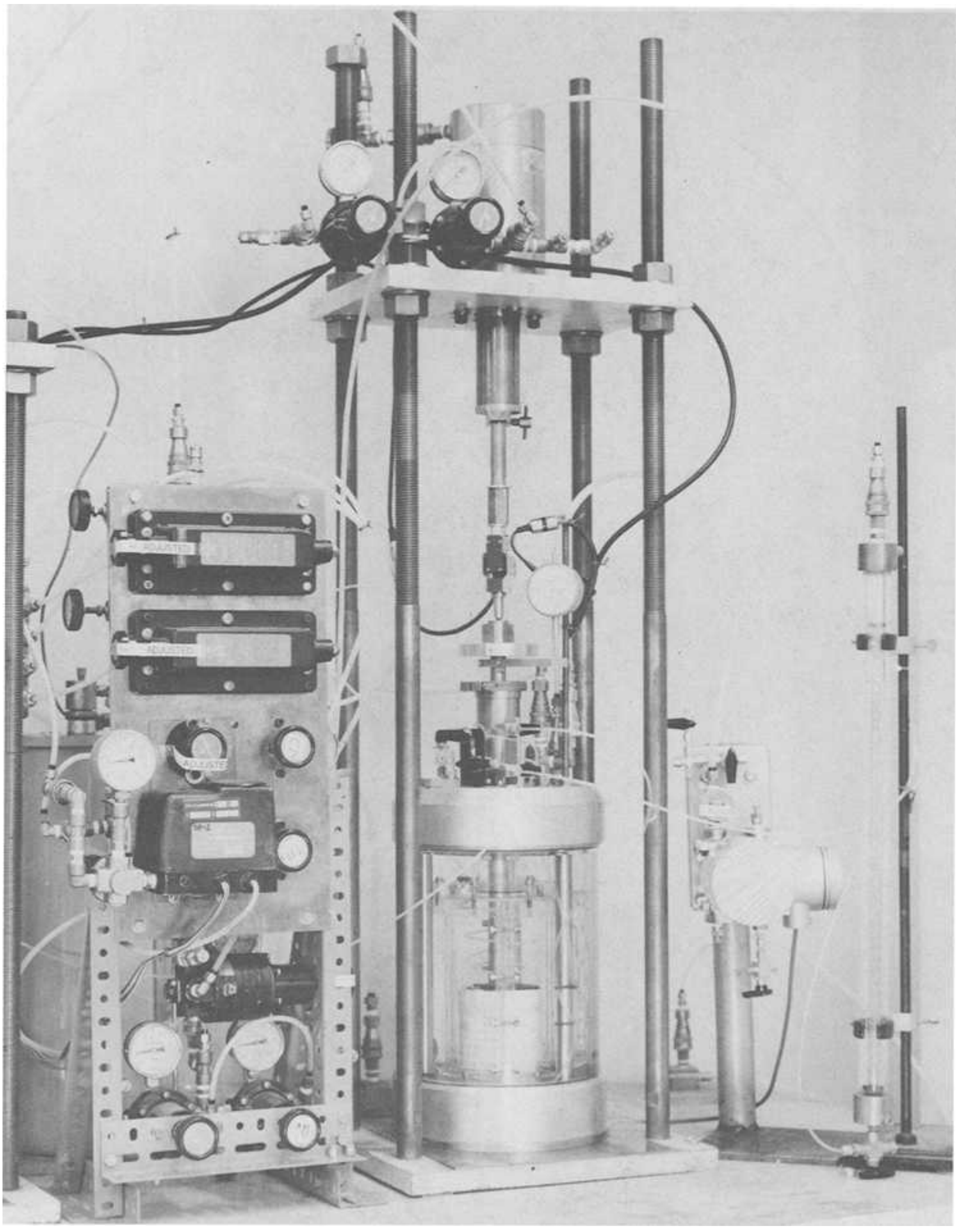

FIG. 47—*Automated double-cell* K_0 *triaxial apparatus having a small-diameter piston; the air-regulator denoted as 2 in Fig. 46 has been replaced by the air-circuit denoted as AC in Fig. 50. In this particular test a short sample is used* [117].

system). Currently the system shown in Fig. 47 with the regulator denoted as 2 (shown in Fig. 46) replaced by the air circuit denoted as AC (shown in Fig. 49) is used in the author's laboratory.

Figure 48 shows typical results of automated K_0-compression tests on partly saturated silty clay samples (D = 7.5 cm, H = 7.5 cm, silty clay; *LL* (liquid limit) = 34%, *PI* (plasticity index) = 13) performed by means of an apparatus shown in Fig. 47 [*1*]. Both samples A and B are K_0-compressed from the point S to the points A_1 and B_1 by increasing the total axial stress σ_a and decreasing the pore water pressure u_W at a constant pore air pressure u_A = 2.0 kgf/cm². Then the sample A was K_0-unloaded from the point A_1 to the point A_2 by decreasing σ_a at constant values of u_A and u_W (= 1.4 kgf/cm²). The sample B was K_0-unloaded from the point B_1 to the point B_2 by increasing u_W at constant values of σ_a and u_A. This process is called "collapse" in the one-dimensional deformation. At the stress point B_2, the sample became almost saturated. It may be seen that the effective stress path in terms of $\sigma_a' = \sigma_a - u_W$ and $\sigma_r' = \sigma_r - u_W$ during collapsing is different from that during K_0-rebounding by the unloading of axial stress.

Automated stress path control tests, other than K_0-compression tests, can be performed by means of this system (Fig. 47). In particular, the method of volume change measurement by means of a double-cell triaxial cell is appropriate for partly saturated soils. For saturated soils, this method of volume change measurement can be replaced by other methods where the change of pore water volume is measured (Fig. 49).

When a soil specimen is strained at a controlled axial displacement rate along a controlled stress path, a pneumatic circuit for controlling axial load independently of σ_r (shown in Fig.

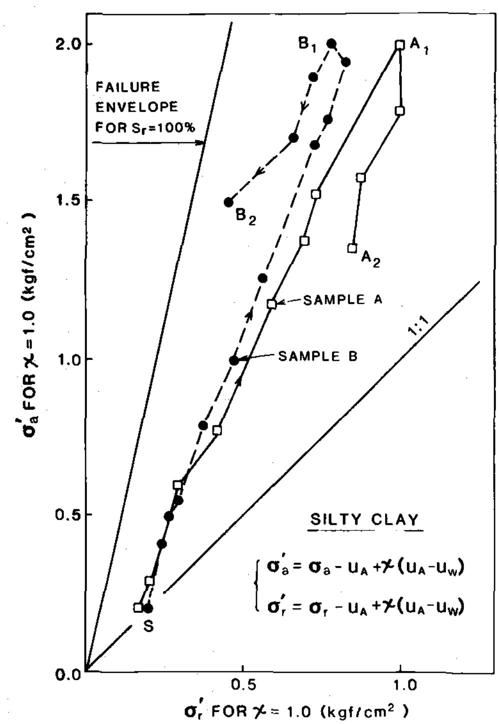

FIG. 48—*Typical results of automated K_0-compression tests of partly saturated silty clay by means of the apparatus shown in Fig. 47* [117].

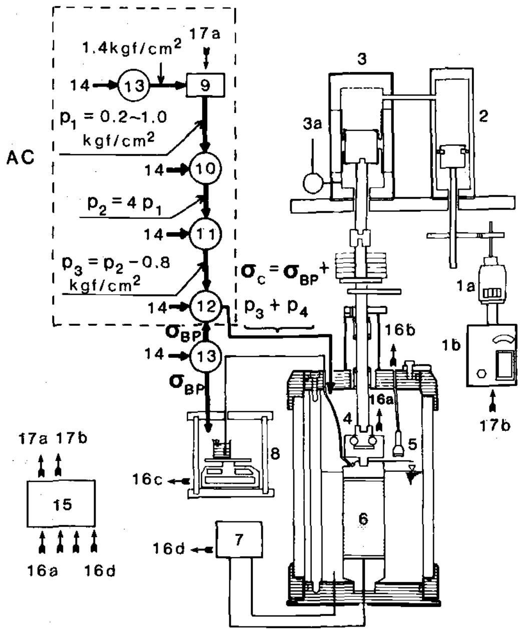

FIG. 49—*Schematic diagram of servo system for controlled stress path tests* [119]*: 1a = reversible motor, 1b = controller of reversible motor, 2 = control cylinder, 3 = double-action cylinder, 3a = regulated air pressure, 4 = internal load cell, 5 = displacement transducer, 6 = soil sample, 7 = HC-DPT, 8 = electronic balance, 9 = electric-to-pneumatic* (*E/P*) *transducer, 10 = booster, 11, 12 = bias-relay, 13 = air pressure regulator, 14 = high house air pressure, 15 = microcomputer + analog-to-digital* (*A/D*) *converter + digital-to-analog* (*D/A*) *converter, 16a–16d = outputs from transducers to microcomputer through amplifiers, 17a, b = outputs from microcomputer.*

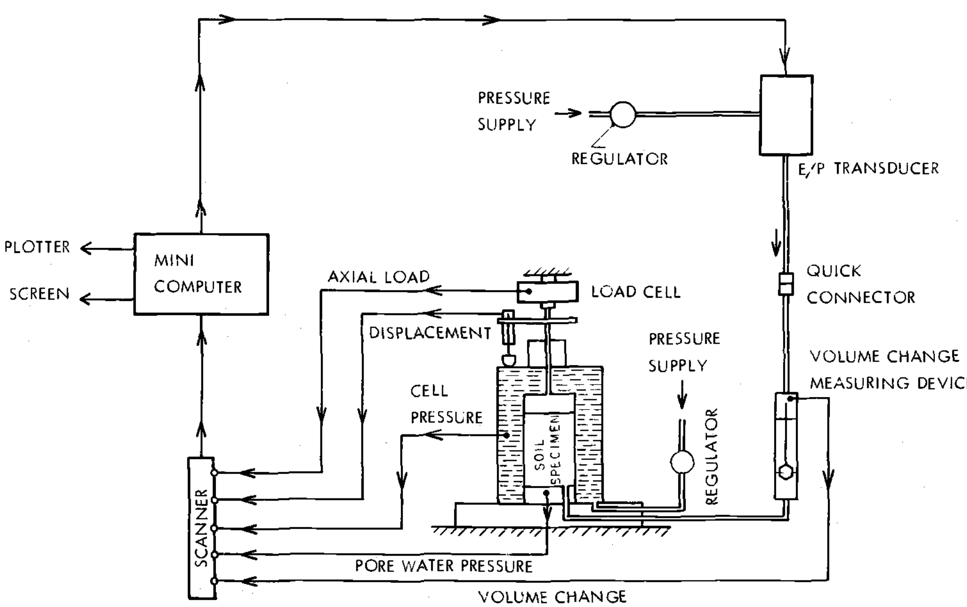

FIG. 50—*Schematic diagram of servo system for controlled stress path tests* [118].

46) becomes unnecessary even when a small-diameter piston is used. Among many variations, Law [*118*] and Molenkamp et al. [*85–87*] have developed such systems (Fig. 50). Figure 49 shows another example developed by Mohri et al. [*119*]. This system has two main features:

1. The triaxial cell has a small-diameter piston and is not a special one. This cell can be used for ordinary triaxial compression tests and cyclic triaxial tests and for static and cyclic torsional shear tests by replacing only the piston, the piston guide, the cap, and the pedestal.
2. Physical quantities are measured very accurately in a similar way as shown in Fig. 27*b*.

Figure 51 shows typical results of a controlled stress path test at a controlled axial strain rate. It may be noted that very smooth results have been obtained. Post-peak stress paths as well as pre-peak ones can be accurately controlled by this method.

More recently, a simpler pneumatic control system with a stepper motor has been developed for the pneumatic pressurizing control (see, for example, Fig. 43, Refs *49* and *115*). In this method, the rotation of the ranged screw of an air regulator is controlled by the stepper motor, which, in turn, is controlled by a microcomputer. The air circuit denoted as AC in Fig. 49 can be replaced by a set of stepper motors and air regulators.

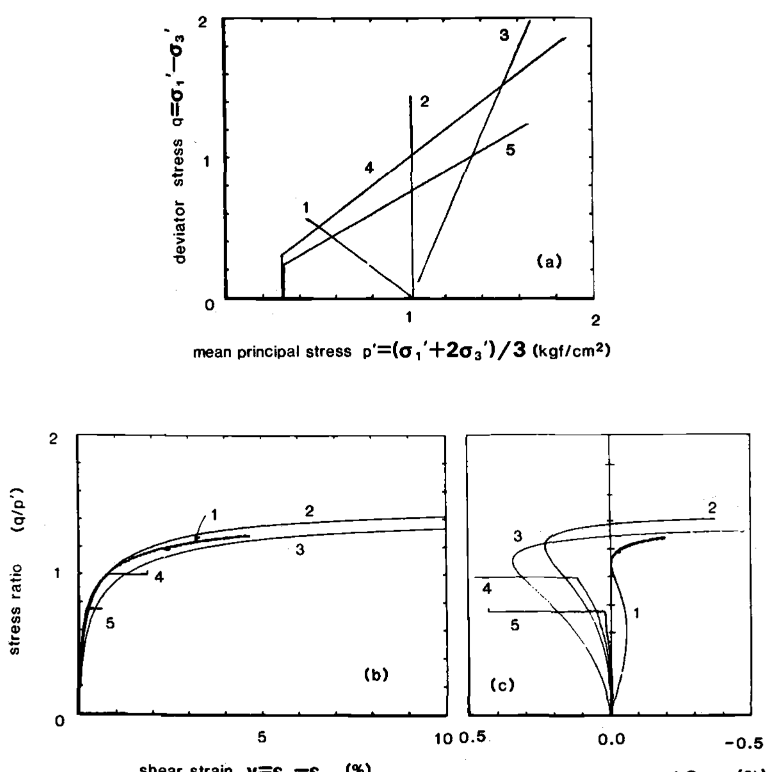

FIG. 51—*Typical results of controlled stress path test at a controlled axial strain rate:* a, *measured stress paths,* b, q/p – γ *relations* (q = σ_a' – σ_r', p = (σ_a' + 2σ_r')/3), *and* c, q/p–v *relations* (D = *7.5 cm,* H = *15 cm, Toyoura sand,* e = *0.83 to 0.87, fixed regular ends* [119]).

Conclusions

The following remarks regarding the triaxial testing apparatus and method may be drawn based on the information presented herein and the author's experience.

The stress states and their changes that can be achieved in the triaxial testing method with the use of solid cylinder specimens are restricted: σ_2' is equal to either σ_3' or σ_1' and the principal stress directions cannot rotate continuously. Several sophisticated testing methods to extend the ability of controlling stress states or strain states have been developed. Such very sophisticated equipment is not often used in practice largely owing to (1) a lack of simple stress- or strain-controlling and measuring system, and (2) a relatively high cost for manufacturing and operating such equipment.

There are data showing that the effects of continuous rotations of principal stress directions on the strength and deformation characteristics cannot be ignored. At the same time, some other data have shown that the continuous rotation of principal stress directions become small at larger plastic strains under the monotonic and cyclic simple shear loading. Therefore, it seems still very useful to perform triaxial testing in practice. However, the effects of the b value and the continuous rotation of principal stress directions, based on the results obtained from research work by means of more sophisticated testing methods, should be accounted for. Of course, such sophisticated testing should be performed in practice when its use is justified.

Triaxial systems with pressure cells located outside the tie rods are becoming popular mainly because of the convenience in connecting the loading piston and the sample cap.

Automated measurements of loads, pressures, displacements, and volume change are now prevailing in practice as well as in research works. Some new but simple methods for accurate measurement of these physical quantities were discussed. The methods presented herein may be introduced into ordinary triaxial testing systems without large modifications. The importance of evaluating errors in stress and strain measurements due to membrane restraint, bedding errors, and membrane penetration at top and bottom ends and at lateral surfaces was discussed only to a limited extent.

The method of automated stress and strain path controlling was also discussed. By means of a microcomputer together with a pneumatic pressurizing system, a mechanically simple system, with an ordinary triaxial cell having a small-diameter piston, can be used for automated stress or strain control tests.

Acknowledgment

The author wishes to acknowledge the cooperation provided by T. Sato, Tej B. S. Pradhan, W.-K. Lam, and M. Torimitsu in preparing this manuscript. The author also gratefully acknowledges M. L. Silver for his valuable suggestions as to the instrumentation of triaxial testing and D. Leshchinsky for his kind review of the manuscript.

References

[1] Saada, A. S. and Townsend, F. C., "State of the Art; Laboratory Strength Testing of Soils," in *Laboratory Shear Strength of Soil, ASTM STP 740,* American Society for Testing and Materials, Philadelphia, 1980, pp. 7–77.

[2] Arthur, J. R. F., "Cubical Devices: Versatility and Constraints," in this volume, pp. 743–765.

[3] Arthur, J. R. F., Chua, K. S., and Dunstan, T., "Induced Anisotropy in a Sand," *Geotechnique,* Vol. 27, No. 1, 1977, pp. 13–30.

[4] Arthur, J. R. F., Chua, K. S., Dunstan, T., and Rodriguez, del C. J. I., "Principal Stress Rotation: A Missing Parameter," *Proceedings,* American Society of Civil Engineers, Vol. 106, No. GT4, 1980, pp. 419–433.

[5] Bishop, A. W. and Eldin, A. K. G., "The Effect of Stress History on the Relation Between φ and the Porosity of Sand," *Proceedings*, Third International Conference on Soil Mechanics and Foundation Engineering, Switzerland, Vol. 1, 1953, pp. 100–105.
[6] Bishop, A. W. and Green, G. E., "The Influence of End Restraint on the Compression Strength of a Cohesionless Soil," *Geotechnique*, Vol. 15, No. 3, 1965, pp. 243–266.
[7] Bishop, A. W. and Henkel, D. J., *The Measurement of Soil Properties in the Triaxial Test*, Arnold, London, 1962.
[8] Hettler, A. and Vardoulakis, I., "Behaviour of Dry Sand Tested in a Large Triaxial Apparatus," *Geotechnique*, Vol. 34, No. 2, 1984, pp. 183–198.
[9] Lade, P. V., "Localization Effects in Triaxial Tests on Sand," *Proceedings*, International Union of Theoretical and Applied Mechanics Conference on Deformation and Failure of Granular Materials, Delft, 1982, pp. 461–471.
[10] Barden, L., Ismail, H., and Tong, P., "Plane Strain Deformation of Granular Material at Low and High Pressures, *Geotechnique*, Vol. 19, No. 4, 1969, pp. 441–452.
[11] Green, G. E. and Reades, D. W., "Boundary Conditions, Anisotropic and Sample Shape Effects on the Stress–Strain Behavior of Sand in Triaxial Compression and Plane Strain, *Geotechnique*, Vol. 25, No. 2, 1975, pp. 233–256.
[12] Barden, L. and Khayatt, A. J., "Incremental Strain Rate Ratios and Strength of Sand in the Triaxial Test," *Geotechnique*, Vol. 16, No. 4, 1966, pp. 338–357.
[13] Cornforth, D. H., "Some Experiments on the Influence of Strain Condition on the Strength of Sand," *Geotechnique*, Vol. 32, No. 4, 1982, pp. 291–303.
[14] Ichihara, M. and Matsuzawa, H., "Behavior of Dry Sand in Plane Strain and Triaxial Compression," *Journal of the Japanese Society of Civil Engineers*, No. 173, 1970, pp. 47–59 (in Japanese).
[15] Lee, K. L. and Seed, H. B., "Drained Strength Characteristics of Sands," *Journal, SMF Division, Proceedings, ASCE*, Vol. 93, No. SM6, 1967, pp. 117–141.
[16] Arthur, J. R. F. and Menzies, B. K., "Inherent Anisotropy in a Sand," *Geotechnique*, Vol. 22, No. 1, 1972, pp. 115–129.
[17] Lam, W.-K. and Tatsuoka, F., "Effects of Initial Anisotropic Fabric and σ_2 on Strength and Deformation Characteristics of Sand," *Soils and Foundations*, Vol. 28, No. 1, 1988, pp. 89–106.
[18] Oda, M., "Initial Fabrics and Their Relations to Mechanical Properties of Granular Material," *Soils and Foundations*, Vol. 12, No. 1, 1972, pp. 18–36.
[19] Oda, M., "The Mechanism of Fabric Changes during Compressional Deformation of Sand," *Soils and Foundations*, Vol. 12, No. 2, 1972, pp. 1–18.
[20] Shankariah, D. B. and Ramamurthy, T., "Axisymmetric Compression and Extension of Anisotropic Sand," *Indian Geotechnical Journal*, Vol. II, 1980, pp. 77–81.
[21] Arthur, J. R. F. and Assadi, A., "Ruptured Sand Sheared in Plane Strain," *Proceedings*, Ninth International Conference, SMFE, Tokyo, Vol. 1, 1977, pp. 19–22.
[22] Oda, M., Koishikawa, I., and Higuchi, T., "Experimental Study on Anisotropic Shear Strength of Sand by Plane Strain Test," *Soils and Foundations*, Vol. 18, No. 1, 1978, pp. 25–38.
[23] Oda, M., "Anisotropic Strength of Cohesionless Sands," *Journal, GE Division, Proceedings, ASCE*, Vol. 107. No. GT9, Sept., 1981, pp. 1219–1231.
[24] Tatsuoka, F., Sakamoto, M., Kawamura, T., and Fukushima, S., "Strength and Deformation Characteristics of Sand in Plane Strain Compression at Extremely Low Pressures," *Soils and Foundations*, Vol. 26, No. 1, 1986, pp. 65–84.
[25] Green, G. E., "Strength and Deformation of Sand Measured in an Independent Stress Control Cell," *Proceedings*, Roscoe Memorial Symposium, Cambridge, England, 1971, pp. 285–323.
[26] Ko, H. Y. and Scott, R. F., "Deformation of Sand in Shear," *Journal, SMFE Division, Proceedings, ASCE*, Vol. 93, No. SM5, 1967, pp. 283–310.
[27] Lade, P. V. and Duncan, J. M., "Cubical Triaxial Tests on Cohesionless Soil," *Journal, SMF Division, Proceedings, ASCE*, Vol. 99, No. SM10, 1973, pp. 793–811.
[28] Matsuoka, H. and Nakai, T., "A New Failure Criterion for Soils in Three-dimensional Stresses," *Proceedings*, International Union of Theoretical and Applied Mechanics Symposium on Deformation and Failure of Granular Materials. Delft, 1982, pp. 253–263.
[29] Miyamori, K., "Shear Strength and Deformation Characteristics of Sand under Three Dimensional Stress Condition," *Journal of the Japanese Society of Civil Engineers*, No. 225, 1976, pp. 81–91 (in Japanese).
[30] Nagaraj, T. S. and Somashekar, B. V., "Shear Strength of Soils under General Stress Field," *Proceedings*, Ninth International Conference on Soil Mechanics and Foundation Engineering, Tokyo, Vol. 1, 1977, pp. 225–228.
[31] Procter, D. C. and Barden, L., "Correspondence," *Geotechnique*, Vol. 19, No. 3, 1969, pp. 424–426.

[32] Ramamurthy, T. and Rawat, P. C., "Shear Strength of Sand under General Stress System," *Proceedings*, Eighth International Conference on Soil Mechanics and Foundation Engineering, Moscow, Vol. 1.2, 1973, pp. 339–342.
[33] Reades, D. W. and Green, G. E., "Independent Stress Control and Triaxial Extension Tests on Sand," *Geotechnique*, Vol. 26, No. 4, 1976, pp. 551–576.
[34] Sutherland, H. B. and Mesdary, M. S., "The Influence of the Intermediate Principal Stress on the Strength of Sand," *Proceedings*, Seventh International Conference on Soil Mechanics and Foundation Engineering, Mexico, Vol. 1, 1969, pp. 391–399.
[35] Wu, T. H., Loh, A. K., and Malvern, L. E., "Study of Failure Envelopes of Soils," *Journal, SMF Division, Proceedings, ASCE*, Vol. 89, No. SM1, 1963, pp. 145–181.
[36] Yamada, Y. and Ishihara, K., "Anisotropic Deformation Characteristics of Sand under Three Dimensional Stress Condition," *Soils and Foundations*, Vol. 19, No. 2, 1979, pp. 79–94.
[37] Frydman, S., Zeitlen, J. G., and Alpan, I., "The Yielding Behavior of Particulate Media," *Canadian Geotechnical Journal*, Vol. 10, No. 341, 1973, pp. 341–362.
[38] Kirkpatrick, W. M., "The Condition of Failure for Sands," *Proceedings*, Fourth International Conference on Soil Mechanics and Foundation Engineering, London, Vol. 1, 1957, pp. 172–178.
[39] Stroud, M. A., "The Behavior of Sand at Low Stress Levels in the Simple Shear Apparatus," Ph.D. thesis, University of Cambridge, 1971.
[40] Youd, T. L. and Craven, T. N., "Lateral Stress in Sands During Cyclic Loading, Technical Note," *Journal, GE Division, Proceedings, ASCE*, Vol. 101, No. GT2, 1975, pp. 217–221.
[41] Moussa, A., "Radial Stress in Sand in Constant Volume Static and Cyclic Simple Shear Tests," Norwegian Geotechnical Institute Internal Report, 51505-10, 1974.
[42] Budhu, M., "Simple Shear Deformation of Sand," Ph.D. thesis, University of Cambridge, 1979.
[43] Cole, E. R., "The Behaviour of Soils in the Simple-Shear Apparatus," Ph.D. thesis, University of Cambridge, 1967.
[44] Finn, W. D. L., Pickering, J., and Bransby, P. L., "Sand Liquefaction in Triaxial and Simple Shear Test," *Journal, SMF Division, Proceedings, ASCE*, Vol. 97, No. SM4, April, 1971, pp. 639–659.
[45] Peacock, W. H. and Seed, H. B., "Sand Liquefaction under Cyclic Loading Simple Shear Conditions," *Journal, SMF Division, Proceedings, ASCE*, Vol. 94, No. SM3, 1968, pp. 689–708.
[46] Roscoe, K. H., "An Apparatus for the Application of Simple Shear to Soil Samples," *Proceedings*, Third International Conference on Soil Mechanics and Foundation Engineering, Zurich, Vol. 1, 1953, pp. 186–191.
[47] Silver, M. L. and Seed, H. B., "Deformation Characteristics of Sands under Cyclic Loading," *Journal, SMF Division, Proceedings, ASCE*, Vol. 97, No. SM8, 1971, pp. 1081–1098.
[48] Drnevich, V. P., "Undrained Cyclic Shear of Saturated Sand," *Journal, SMF Division, Proceedings, ASCE*, Vol. 98, No. SM8, 1972, pp. 807–825.
[49] Hight, D. W., Gens, A., and Symes, M. J. P. R., "The Development of a New Hollow Cylinder Apparatus for Investigating the Effects of Principal Stress Rotation in Soils," *Geotechnique*, Vol. 33, No. 4, 1983, pp. 183–198.
[50] Ishibashi, I. and Sherif, M. A., "Soil Liquefaction by Torsional Simple Shear Device," *Journal, GE Division, Proceedings, ASCE*, Vol. 100, No. GT8, 1974, pp. 871–887.
[51] Ishihara, K. and Yasuda, S., "Sand Liquefaction in Hollow Cylinder Torsion under Irregular Excitation," *Soils and Foundations*, Vol. 15, No. 1, 1975, pp. 45–59.
[52] Lade, P. V., "Torsion Shear Apparatus for Soil Testing," in *Laboratory Shear Strength of Soil, ASTM STP 740*, American Society for Testing and Materials, Philadelphia, 1980, pp. 145–163.
[53] Saada, A. S., "A Pneumatic Computer for Testing Cross Anisotropic Materials," *Materials Research and Standards*, Vol. 8, No. 1, 1968, pp. 17–23.
[54] Saada, A. S. and Ou, C. D., "Strain–Stress Relations and Failure of Anisotropic Clays," *Journal, SMF Division, Proceedings, ASCE*, Vol. 99, No. SM12, 1973, pp. 1091–1111.
[55] Saada, A. S. and Bianchini, G. F., "Strength of One-dimensionally Consolidated Clays," *Journal, GE Division, Proceedings, ASCE*, Vol. 101, No. GT11, pp. 1151–1164.
[56] Saada, A. S. and Zamani, K. K., "The Mechanical Behaviour of Cross Anisotropic Clays," *Proceedings*, Seventh International Conference on Soil Mechanics and Foundation Engineering, Mexico City, Vol. 1, 1969, pp. 351–359.
[57] Symes, M. J. P. R., Hight, D. W., and Gens, A., "Investigating Anisotropy and the Effects of Principal Stress Rotation and of Intermediate Principal Stress Using a Hollow Cylinder Apparatus," *Proceedings*, International Union of Theoretical and Applied Mechanics Symposium on Deformation and Failure of Granular Materials, Delft, 1982, pp. 441–449.
[58] Tatsuoka, F., Muramatsu, M., and Sasaki, T., "Cyclic Undrained Stress–Strain Behavior of Dense

Sands by Torsional Simple Shear Test," *Soils and Foundations,* Vol. 22, No. 2, June, 1982, pp. 55–70.
[59] Tatsuoka, F., Sonoda, S., Hara, K., Fukushima, S., and Pradhan Tej, B. S., "Failure and Deformation of Sand in Torsional Shear," *Soils and Foundations,* Vol. 26, No. 4, 1986, pp. 79–97.
[60] Ishihara, K. and Towhata, I., "Sand Response to Cyclic Rotation of Principal Stress Directions as Induced by Wave Loads," *Soils and Foundations,* Vol. 23, No. 4, 1983, pp. 11–26.
[61] Miura, K., Miura, S., and Toki, S., "Deformation Behavior of Anisotropic Dense Sand Under Principal Stress Axes Rotation," *Soils and Foundations,* Vol. 26, No. 1, 1986, pp. 36–52.
[62] Wong, R. S. K. and Arthur, J. R. F., "Induced and Inherent Anisotropy in Sand," *Geotechnique,* Vol. 35, No. 4, 1985, pp. 471–481.
[63] Arthur, J. R. F. and Dunstan, T., "Discussion," *Soils and Foundations,* Vol. 18, No. 4, 1978, pp. 105–106.
[64] Sture, S., Ko., H.-Y., Budiman, J. S., and Ontuna, A. K., "Development and Application of a Directional Shear Cell," *Proceedings,* Eleventh International Conference on Soil Mechanics and Foundation Engineering, San Francisco, Vol. 2, 1985, pp. 1061–1064.
[65] Mahmood, A. and Mitchell, J. K., "Fabric–Property Relationships in Fine Granular Materials," *Clays and Clay Minerals,* Vol. 22, 1974, pp. 397–408.
[66] Dunstan, T., "The Influence of Grading on the Anisotropic Strength of Sand, Technical Note," *Geotechnique,* Vol. 22, No. 3, 1972, pp. 529–532.
[67] Yoshimi, Y. and Oh-Oka., "A Ring Torsion Apparatus for Simple Shear Tests," *Proceedings,* Eighth International Conference on Soil Mechanics and Foundation Engineering, Moscow, Vol. 1.2, 1973, pp. 501–506.
[68] Tatsuoka, F. and Ishihara, K., "Drained Deformation of Sand Under Cyclic Stresses Reversing Direction," *Soils and Foundations,* Vol. 14, No. 3, 1974, pp. 51–65.
[69] Wood, D. M. and Budhu, M., "The Behaviour of Leighton Buzzard Sand in Cyclic Simple Shear Test," *Proceedings,* International Symposium on Soils under Cyclic and Transient Loading, Swansea, Vol. 1, 1980, pp. 7–11.
[70] Oda, M. and Konishi, J., "Rotation of Principal Stresses in Granular Material in Simple Shear," *Soils and Foundations,* Vol. 14, No. 4, 1974, pp. 39–53.
[71] Finn, W. D. L. and Vaid, Y. P., "Liquefaction Potential from Drained Constant Volume Cyclic Simple Shear Tests," *Proceedings,* Sixth World Conference on Earthquake Engineering, New Delhi, 1977.
[72] Finn, W. D. L., Bhatia, S. K., and Pickering, D. I., "The Cyclic Simple Shear Test," in *Soil Mechanics—Transient and Cyclic Loads,* Pande and Zienkiewicz, Eds., Wiley, New York, 1982, pp. 583–607.
[73] Tatsuoka, F., Hara, K., and Pradhan, T. B. S., "Stress–Strain Relation of Saturated Sand Subjected to Cyclic Undrained Simple Shear," *Seisan-Kenkyu, Journal of Institute of Industrial Science,* University of Tokyo, Vol. 38, No. 9, pp. 28–31 (in Japanese).
[74] Okochi, Y. and Tatsuoka, F., "Some Factors Affecting K_0-Values of Sand Measured in Triaxial Cell," *Soils and Foundations,* Vol. 24, No. 3, 1984, pp. 52–68.
[75] Tatsuoka, F., Maeda, S., Ochi, K., and Fujii, S., "Prediction of Cyclic Undrained Strength of Sand Subjected to Irregular Loadings," *Soils and Foundations,* Vol. 26, No. 2, 1986, pp. 73–90.
[76] Tatsuoka, F., Ochi, K., Fujii, S., and Okamoto, M., "Cyclic Undrained Triaxial and Torsional Shear Strength of Sands for Different Sample Preparation Methods," *Soils and Foundations,* Vol. 26, No. 3, 1986, pp. 23–41.
[77] Atkinson, J. H. and Evans, J. S., "Discussion," *Geotechnique,* Vol. 35, No. 3, 1985, pp. 378–382.
[78] Alva-Hurtado, J. E., McMahon, D. R., and Stewart, H. E., "Apparatus and Techniques for Static Triaxial Testing of Ballast," in *Laboratory Shear Strength of Soil, ASTM STP 740,* American Society for Testing and Materials, Philadelphia, 1980, pp. 94–113.
[79] Tatsuoka, F., Toki, S., Miura, S., Kato, H., Okamoto, M., et al., "Some Factors Affecting Cyclic Undrained Triaxial Strength of Sand," *Soils and Foundations,* Vol. 26, No. 3, 1986, pp. 99–116.
[80] Chan, C. K., "An Electropneumatic Cyclic Loading System," *Geotechnical Testing Journal,* Vol. 4, No. 4, 1982, pp. 183–187.
[81] Tatsuoka, F., Goto, S., and Sakamoto, M., "Effects of Some Factors on Strength and Deformation Characteristics of Sand at Low Pressures," *Soils and Foundations,* Vol. 26, No. 1, 1986, pp. 105–114.
[82] Castro, G., "Liquefaction of Sands," *Harvard Soil Mechanics Series,* No. 81, Harvard University, Cambridge, MA, 1969.

[83] Fukushima, S. and Tatsuoka, F., Strength and Deformation Characteristics of Saturated Sand at Extremely Low Pressures," *Soils and Foundations*, Vol. 24, No. 4, 1984, pp. 30–48.
[84] Tani, Y., Hatanaka, Y., and Nagao, T., "Development of Small Three Component Dynamometer for Cutting Force Measurement," *Bulletin of Japanese Society of Mechanical Engineers*, Vol. 26, No. 214, April, 1983, pp. 650–658.
[85] Hjortnaes-Pedersen, A. G. I. and Molenkamp, F., "Accuracy and Reproducibility of Triaxial Tests," *Proceedings*, International Union of Theoretical and Applied Mechanics Conference on Deformation and Failure of Granular Materials, Delft, 1982, pp. 391–401.
[86] Hjortnaes-Pedersen, A. G. I. and Molenkamp, F., "Computer Program for Analysis for Triaxial and True Triaxial Tests," Report of Delft Soil Mechanics Laboratory, 1983.
[87] van Deventer, J. M. M. and Molenkamp, F., "Prediction of the Stiffness of Shallow Foundations by Means of Plate Loading Tests and Triaxial Tests," Report of Delft Soil Mechanics Laboratory, CO-234508/3, 1984.
[88] Henkel, D. J. and Gilbert, G. C., "The Effect of Rubber on the Mechanical Triaxial Compression Strength of Clay Samples," *Geotechnique*, Vol. 3, 1952, pp. 20–29.
[89] Duncan, J. M. and Seed, H. Bolton, "Corrections for Strength Test Data," *Journal, SMF Division, Proceedings, ASCE*, Vol. 93, No. SM5, 1967, pp. 121–137.
[90] Ponce, V. M. and Bell, J. M., "Shear Strength of Sand at Extremely Low Pressures," *Journal, SMF Division, Proceedings, ASCE*, Vol. 97, No. SM4, 1971, pp. 625–638.
[91] Molenkamp, F. and Luger, H. J., "Modelling and Minimization of Membrane Penetration Effects in Tests on Granular Soils," *Geotechnique*, Vol. 31, No. 4, 1981, pp. 471–486.
[92] Berre, T., "Triaxial Testing at the Norwegian Geotechnical Institute," *Geotechnical Testing Journal*, Vol. 5, No. 12, 1982, pp. 3–17.
[93] Rowe, P. W. and Barden, L., "Importance of Free Ends in Triaxial Testing," *Journal, SMF Division, Proceedings, ASCE*, Vol. 90, No. SM1, Jan. 1964, pp. 1–27.
[94] Lee, K. L., "End Restraint Effects on Undrained Static Triaxial Strength of Sand," *Journal, GE Division, Proceedings, ASCE*, Vol. 104, No. GT6, June, 1978, pp. 687–704.
[95] Arthur, J. R. F. and Dalili, A., "On the Lubrication of Rubber Surfaces, Technical Note," *Geotechnique*, Vol. 29, No. 1, 1979, pp. 96–98.
[96] Tatsuoka, F., Molenkamp, F., Torii, T., and Hino, T., "Behavior of Lubrication Layers of Platens in Element Tests," *Soils and Foundations*, Vol. 24, No. 1, 1984, pp. 113–128.
[97] Tatsuoka, F. and Haibara, O., "Shear Resistance Between Sand and Smooth or Lubricated Surfaces," *Soils and Foundations*, Vol. 25, No. 1, 1985, pp. 89–98.
[98] Kokusho, T., "Cyclic Triaxial Test of Dynamic Soil Properties for Wide Strain Range," *Soils and Foundations*, Vol. 20, No. 2, 1980, pp. 45–60.
[99] Tatsuoka, F., Yamada, S., and Sato, T., "Design and Manufacturing of Shear Testing Apparatuses for Soils No. 6—Methods of Controlling and Measuring Stress and Loads No. 3, Chishitsu-to-chosa, Journal of Japanese Association of Geotechnical Consultants, No. 1984-1," 1984, pp. 56–62 (in Japanese).
[100] Hara, A. and Kiyota, Y., "Study on Dynamic Properties of Soils for Response Analysis of Grounds—Frequency-dependency of Shear Moduli and Damping Coefficients," *Proceedings*, Fourteenth Annual Japanese Domestic Symposium on Soil Mechanics and Foundation Engineering, 1979 (in Japanese).
[101] Hardin, B. O. and Drnevich, V. P., "Shear Modulus and Damping in Soils; Measurement and Parameter Effects," *Journal, SMF Division, Proceedings, ASCE*, Vol. 98, No. SM6, 1972, pp. 603–624.
[102] Hardin, B. O. and Drnevich, V. P., "Shear Modulus and Damping in Soils; Design Equations and Curves," *Journal, SMF Division, Proceedings, ASCE*, Vol. 98, No. SM7, July, 1972, pp. 667–692.
[103] Kong, X. J., Tatsuoka, F., and Pradhan, Tej B. S., "Dynamic Deformation Properties of Sand at Extremely Low Pressures," *Proceedings*, Seventh Japan Earthquake Engineering Symposium, 1986, pp. 631–636.
[104] Jardine, R. J., Symes, N. J., and Burland, J. B., "The Measurement of Soil Stiffness in the Triaxial Apparatus," *Geotechnique*, Vol. 34, No. 3, 1984, pp. 323–340.
[105] Burland, J. B. and Symes, M., "A Simple Axial Displacement Gauge for Use in the Triaxial Apparatus, Technical Note," *Geotechnique*, Vol. 32, No. 1, 1982, pp. 62–65.
[106] Goto, S. and Tatsuoka, F., "Influence of the Testing Condition on Strength and Deformation Characteristics of Granular Material," *Proceedings*, Twenty-first Annual Japanese Symposium on Soil Mechanics and Foundation Engineering, Vol. 1, 1986, pp. 237–240 (in Japanese).
[107] Boyce, J. R. and Brown, S. F., "Measurement of Elastic Strain in Granular Material, Technical Note," *Geotechnique*, Vol. 26, No. 4, 1976, pp. 637–640.

[*108*] Alva-Hurtado, J. E. and Selig, E. T., "Survey of Laboratory Devices for Measuring Soil Volume Change," *Geotechnical Testing Journal,* Vol. 4, No. 1, 1981, pp. 11–18.
[*109*] Tatsuoka, F., "A Simple Method for Automated Measurement of Volume Change in Laboratory Tests, Technical Note," *Soils and Foundations,* Vol. 21, No. 3, 1981, pp. 104–105.
[*110*] Pradhan, Tej B. S., Tatsuoka, F., and Molenkamp, F., "Accuracy of Automated Volume Change Measurement by Means of a Differential Pressure Transducer, Technical Note," *Soils and Foundations,* Vol. 26, No. 4, 1986, pp. 150–158.
[*111*] Kiekbusch, M. and Schuppener, B., "Membrane Penetration and Its Effect on Pore Pressures," *Journal, GE Division, Proceedings, ASCE,* Vol. 103, No. GT11, 1977, pp. 1267–1279.
[*112*] Han, G.-C., Sato, T., Tatsuoka, F., and Tamura, C., "Study on Strength and Deformation of Unsaturated Sand Under Low Lateral Pressure," *Seisan-Kenkyu, Journal,* Institute of Industrial Science, University of Tokyo, Vol. 34, No. 9, 1982, pp. 35–38 (in Japanese).
[*113*] Silver, M. L., "Automated Data Acquisition, Transducers, and Dynamic Recording for the Geotechnical Testing Laboratory," *Geotechnical Testing Journal,* Vol. 2, No. 4, Dec. 1979, pp. 185–189.
[*114*] Bishop, A. W. and Wesley, L. D., "A Hydraulic Triaxial Apparatus for Controlled Stress Path Testing," *Geotechnique,* Vol. 25, No. 4, 1975, pp. 657–670.
[*115*] Atkinson, J. H., "Simple and Inexpensive Pressure Control Equipment for Conventional and Stress Path Triaxial Testing of Soils, Technical Note," *Geotechnique,* Vol. 35, No. 1, 1985, pp. 61–63.
[*116*] Campanella, R. G. and Vaid, Y. P., "A Simple K_0 Triaxial Cell," *Canadian Geotechnical Journal,* Vol. 9, 1972, pp. 249–260.
[*117*] Abe, H. and Tatsuoka, F., "Behavior of Partly Saturated Soil at Wetting in K_0-Triaxial Test," *Proceedings,* Fortieth Annual Symposium of Japanese Society of Civil Engineers, Sept. 1985, pp. 547–548 (in Japanese).
[*118*] Law, K. T., "A Servo System for Controlled Stress Path Tests," in *Laboratory Shear Strength of Soil, ASTM STP 740,* American Society for Testing and Materials, Philadelphia, 1980, pp. 164–179.
[*119*] Mohri, Y., Pradhan, Tej B. S., and Tatsuoka, F., "Automated Control of Stress Path in Triaxial Tests," *Proceedings,* Twenty-first Annual Japanese Symposium on Soil Mechanics and Foundation Engineering, Vol. 1, 1986, pp. 303–306 (in Japanese).

Harold W. Olsen,[1] Roger H. Morin,[1] and Roger W. Nichols[1]

Flow Pump Applications in Triaxial Testing

REFERENCE: Olsen, H. W., Morin, R. H., and Nichols, R. W., **"Flow Pump Applications in Triaxial Testing,"** *Advanced Triaxial Testing of Soil and Rock, ASTM STP 977,* Robert T. Donaghe, Ronald C. Chaney, and Marshall L. Silver, Eds., American Society for Testing and Materials, Philadelphia, 1988, pp. 68–81.

ABSTRACT: New testing capabilities can be added to a conventional triaxial system by using a commercially available flow pump to control the rate and amount of pore fluid movement to or from the ends of a test specimen. These capabilities include measurements of equipment compliance, constant-rate-of-deformation consolidation, very-small-strain compressibility, permeability, coefficient of consolidation, and strain-path control with arbitrary combinations of vertical and volumetric strain rates. These capabilities are of interest not only in themselves; they facilitate a testing strategy that reduces the amount of equipment and the number of replicate specimens needed to define the permeability, compressibility, and strength of a soil.

KEY WORDS: flow pump, triaxial, compliance, consolidation, compressibility, permeability, coefficient of consolidation, strain-path control, K_o consolidation, shear strength, stage testing

This paper presents an overview of capabilities that can be added to a conventional triaxial system by using a commercially available flow pump to control liquid movement to and from the ends of a test specimen. The paper includes flow pump applications that can be achieved by generating arbitrary constant flow rates without the use of servo-mechanisms and computers, but it does not address complex applications of digitally controlled flow pumps, such as the digital pressure controller developed by Menzies, Sutton, and Davies for automation of laboratory consolidation and triaxial testing equipment [*1*].

The applications described here arise from the ability of a flow pump to control volume change and pore-fluid transport processes in a test specimen. Volumetric control of these processes has a fundamental advantage over the stress-controlled approach employed currently. The generation of very low flow rates and the measurement of pressures and forces with transducers in the volume-controlled approach can be accomplished more easily and accurately than the measurement of very low flow rates and the control of pressures and forces involved in the stress-controlled approach.

This advantage was first exploited with the introduction of the flow pump method for conducting permeability measurements on a rigidly confined test specimen [*2–4*]. Subsequently, the flow pump method has been used in both research and practice for conducting permeability tests in oedometers [*5–7*]. The technical and practical advantages of the flow pump method for permeability measurements in a triaxial system were demonstrated recently [*8*].

During and since the latter study, the authors recognized several additional applications of a constant-rate flow pump in triaxial testing. This paper describes the applications we

[1] Research civil engineer, research geophysicist, and civil engineering technician, respectively, United States Department of the Interior, Geological Survey, Box 25046, M.S. 966, Denver Federal Center, Denver, CO 80225.

have identified to date, and summarizes our progress in their development. These applications include measurements of equipment compliance, constant-rate-of-deformation (CRD) consolidation, very-small-strain compressibility, permeability, and the coefficient of consolidation. They also include strain-path control with arbitrary combinations of vertical and volumetric strain rates.

Equipment: Set-up and Testing

Figures 1 and 2 present a photograph and a scheme, respectively, of the authors' experimental equipment. A triaxial cell (T), mounted in a loading frame, is equipped with a permeant control manifold which interconnects the base pedestal and top cap of a test specimen (E) with the flow pump (P), the differential transducer (D), the gage transducers (G), and the permeant-fluid standpipes (S). The triaxial cell is also connected to the chamber-fluid standpipe (C). A deaired solution reservoir (V) is connected to the manifold and to the permeant-fluid standpipes. Details concerning the flow pump and the differential transducer are documented elsewhere [8]. The left and right sides of the manifold are symmetric, and they are connected, respectively, to the base pedestal and to the top cap of the test specimen within the triaxial cell. Each side of the manifold is connected to a gage transducer, a standpipe, and one side of the differential transducer. The flow pump is connected so that it can infuse liquid into or withdraw liquid from either side of the manifold, or both sides simultaneously.

The triaxial system is tested for leaks by determining whether the system can retain

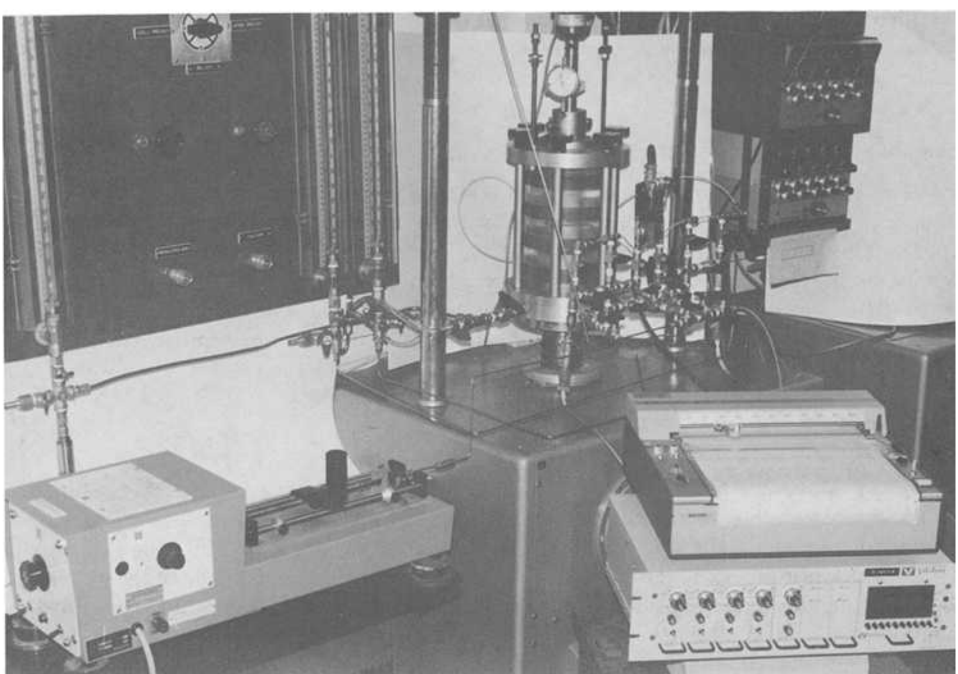

FIG. 1—*Photograph of the equipment.*

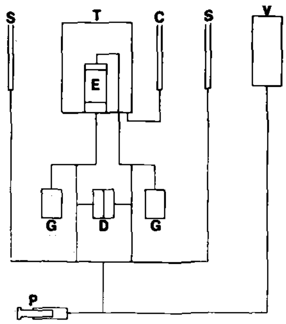

FIG. 2—*Scheme of the equipment.*

elevated pressure or vacuum for substantial periods of time, for example a few days. Leaks are located by using the valves and transducers to isolate and test zones within the system.

Before mounting a test specimen, the entire permeant subsystem is filled with deaired permeant and tested for undissolved air as follows. First, vacuum is applied simultaneously to the reservoir of permeant solution and to the permeant subsystem, to remove dissolved air from the permeant solution and entrapped air in the subsystem. Second, while the vacuum is maintained on both the deaired solution reservoir and the subsystem, the deaired solution is allowed to flow under gravity from the reservoir into the subsystem. Third, the vacuum is removed from, and pressure applied to, the subsystem to drive any remaining undissolved air into solution. Fourth, the subsystem is tested for undissolved air by measuring its compliance, as described below. Finally, the subsystem design enables any undissolved air, if identified in the compliance measurement, to be dissolved either by further elevating the pressure in the permeant, or by exchanging the permeant with fresh deaired solution from the reservoir.

Compliance of the Permeant System

The compliance of the permeant system is defined herein as the amount by which the volume of liquid contained within the system (dV) varies in response to a change in the head within the system (dh). It follows that the compliance can be measured by using the flow pump to introduce liquid into or withdraw liquid from the manifold at a constant rate, $Q = dV/dt$, and monitoring the consequent head variation with time, dh/dt, with the transducers. Thus, letting the compliance of the permeant system be represented by S_{ps},

$$S_{ps} = \frac{dV\ (\text{cm}^3)}{dh\ (\text{cm H}_2\text{O})} = \frac{dV/dt\ (\text{cm}^3/\text{s})}{dh/dt\ (\text{cm/s})} \tag{1}$$

Figure 3 illustrates data from a compliance measurement wherein the left side of the manifold is connected to the flow pump and the right side is connected to its pressure-controlled standpipe. The time scale on the abscissa in Fig. 3 shows when the flow pump is shut off, is infusing liquid into, or is withdrawing liquid from, the left side of the manifold. The ordinate shows the pressure difference between the left- and right-hand sides of the manifold, which was measured directly with the differential transducer. When the data in Fig. 3 are introduced into Eq 1, the compliance, S_{ps}, equals 2.39×10^{-4} cm^3/cm H_2O.

A basis for using such a compliance measurement to evaluate the presence of undissolved air in the permeant system is presented in Fig. 4, which shows compliance measured as a

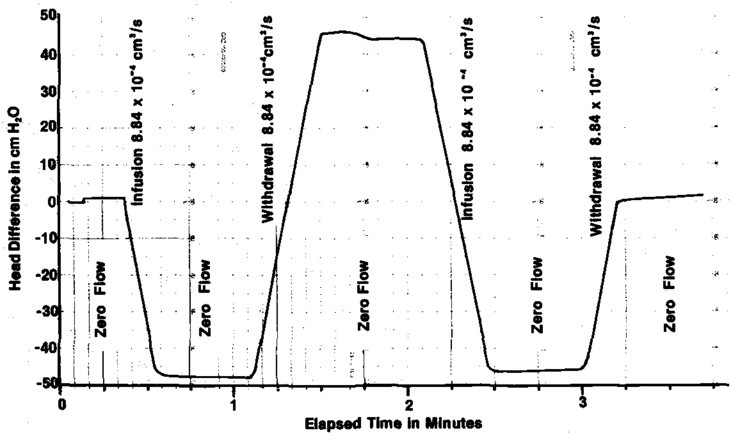

FIG. 3—*A typical compliance measurement.*

function of the pressure in the manifold. The compliance decreases with increasing pressure and approaches a constant value asymptotically. The minimum value is the compliance of the system when it is fully saturated and free of undissolved air.

Constant-Rate-of-Deformation (CRD) Consolidation

Figure 5 presents CRD consolidation data on a triaxial specimen of soft and silty clay. The vertical axis shows the volume decrease of the specimen generated by withdrawing pore fluid from the base of the specimen with a flow pump. The horizontal axis shows the effective stress calculated from periodic readings (usually daily) of the gage transducers connected to the cell pressure and the pore pressure at the base of the specimen. The table in Fig. 5 shows that the data were obtained in a sequence of steps wherein different flow rates (Q) were used to change the volume of the specimen. This table also shows, for each step, the

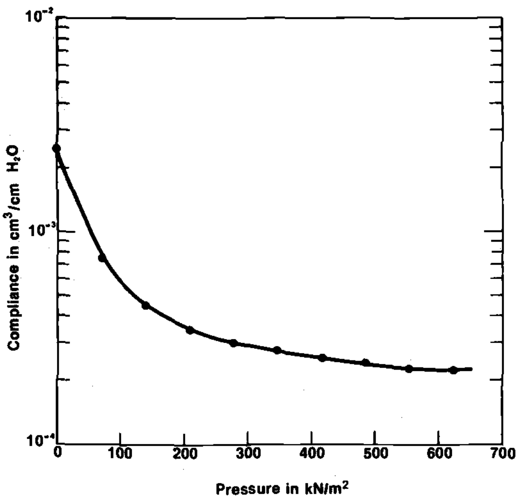

FIG. 4—*Variation of compliance with pressure.*

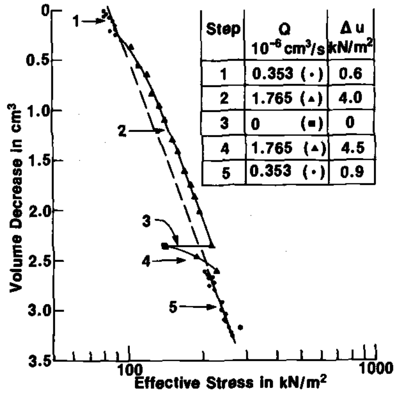

FIG. 5—*Constant-rate-of-deformation consolidation data.*

pore-pressure difference (Δu) induced across the specimen by the applied flow rate (Q). Note that the values of Δu are very small compared with the effective-stress values plotted on the abscissa. Hence, the variation of effective stress within the specimen is also very small compared with the effective-stress values calculated from the gage transducer readings of the cell pressure and the pore pressure at the base of the specimen.

The data in Fig. 5 are generally consistent with published data obtained using step loading and existing CRD consolidation methods in that the sample volume varies linearly with the log of the effective stress for a given rate of loading, and the position of the volume change versus log effective-stress relation shifts to the left with decreasing rates of pore-fluid withdrawal or volumetric deformation [*9*].

Very-Small-Strain Compressibility and Temperature Effects

During and following the period when the data for step 5 in Fig. 5 were being obtained, the differential-pressure transducer was used to monitor the variation of the pore pressure at the base of the specimen relative to a constant external reference. Therewith, substantially more sensitive consolidation, rebound, and recompression data were obtained; these data are presented in Fig. 6 together with data on the associated ambient temperatures in the laboratory.

Figure 6 shows that the slopes of the consolidation and rebound curves are clearly defined. However, the effective stress varies not only with the decrease in volume of the specimen but also cyclically in direct response to variations in the ambient temperature of the laboratory. Thus, it appears that a flow pump is a convenient tool for conducting very-small-strain compressibility measurements on a triaxial specimen in both normally consolidated and overconsolidated states. But the usefulness of this capability is limited by the temperature control of the environment in which it is located.

Another important phenomenon shown in Fig. 6 is the extent to which the rebound and recompression data are reversible. Between effective stresses of 230 and 245 kN/m², reversibility occurs while the room temperature is decreasing. In contrast, the deformations are irreversible at effective stresses above 245 kN/m². When the room temperature begins to rise, the deviations from reversibility grow with succeeding cycles of ambient temperature variations. It appears that the irreversibility arises from the deformations caused by variations in effective stress which are caused by variations in the ambient temperature. These cyclically

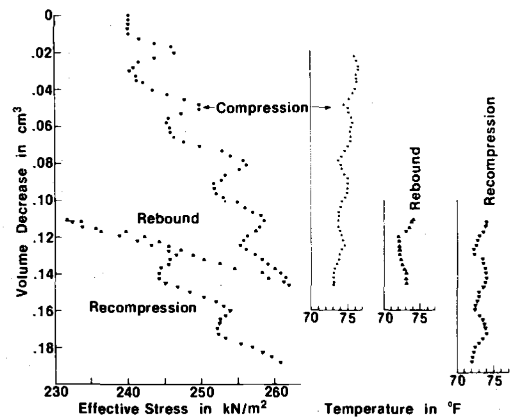

FIG. 6—*Very-small-strain compressibility data.*

induced irreversible deformations may be experimental artifacts which are clearly evident in the highly sensitive data in Fig. 6, but which cannot be distinguished in less sensitive data, such as those in Fig. 5, and those customarily obtained in engineering practice.

Permeability and Response Time

Compared with conventional constant-head and falling-head methods, a flow pump provides the following advantages for conducting permeability measurements in a triaxial system: (1) direct flow-rate measurements are avoided, together with the associated errors that arise from the effects of contaminants on capillary menisci and the long periods of time involved in flow-rate measurements; (2) permeability measurements can be obtained much more rapidly and at substantially smaller gradients; (3) errors from the small intercept in the otherwise linear flow rate versus hydraulic gradient relationship, and also from seepage-induced permeability changes, can easily be recognized and avoided or minimized; and (4) the initial transient response of a specimen preceding the steady-state condition needed for a permeability measurement can extend over a substantial period of time, and errors in permeability measurements from this transient response can easily be avoided with the flow pump method, but not with constant-head and falling-head methods [*8*].

We have learned that the sensitivity of the flow pump method for low-gradient permeability measurements is fundamentally limited by experimental errors caused by environmental temperature variations such as those shown with the consolidation and rebound data in Fig. 6. In addition, we have been investigating the significance of the transient response that precedes the steady-state condition needed for a permeability measurement. The following summarizes our current understanding of these issues.

Figures 7 and 8 illustrate the results of flow-pump permeability tests on sand and silty clay specimens, respectively. A flow pump was used to generate arbitrary constant flow rates across the base of each specimen while the pore fluid at the top of the specimen was maintained at a constant pressure and the head difference induced across the specimen was monitored with the differential transducer and continuously recorded as a function of time. Figure 7 shows that the response time for sand is very short and that very small head differences across the specimen, on the order of a few centimeters of water or less, can be measured with both high resolution and accuracy. In contrast, Fig. 8 shows that the response time for clays can be substantial. Moreover, the measured head difference across a clay

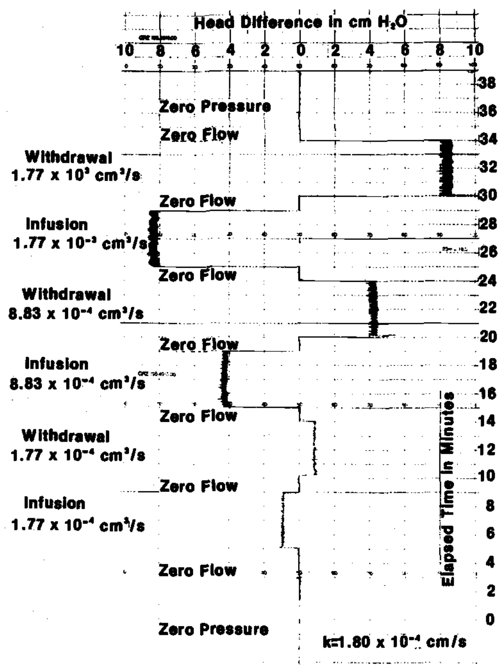

FIG. 7—*Flow-pump-permeability and coefficient-of-consolidation data for sand.*

specimen also includes a small head difference, on the order of a few centimeters of water, which is present during the zero-flow condition. Furthermore, this residual head difference can vary somewhat with time.

Our recent experience shows that the small residual head differences shown in Fig. 8 arise, in large measure, from room temperature variations such as those shown in Fig. 6. It has also been suggested that they could be generated by geochemical sources of osmosis within a test specimen [*10*]. Unfortunately, these sources of experimental error limit the sensitivity of the flow-pump method for very low gradient permeability measurements on clays. Nevertheless, these experimental errors are not of sufficient magnitude to compromise the very substantial advantages of the flow pump method, compared with conventional methods, for conducting permeability measurements on clays in a triaxial system.

Response Time and the Coefficient of Consolidation

Regarding the response time, its cause in constant-head permeability tests was recognized as seepage-induced consolidation nearly 20 years ago [*11–13*]. For example, Al-Dhahir and Tan [*12*] showed how Terzaghi's [*14*] governing equation for one-dimensional consolidation can be used, with analogous heat-conduction theory from Carslaw and Jaeger [*15*], to interpret the coefficient of consolidation from the initial transient phase of a constant-head permeability test. For a flow pump permeability test, the response time can be similarly described with analytic solutions in Carslaw and Jaeger [*15*] of Terzaghi's governing equation for the models in Fig. 9. The flow model on the left side of Fig. 9 represents a test wherein the flow rate to or from the specimen is changed instantaneously from zero to a constant

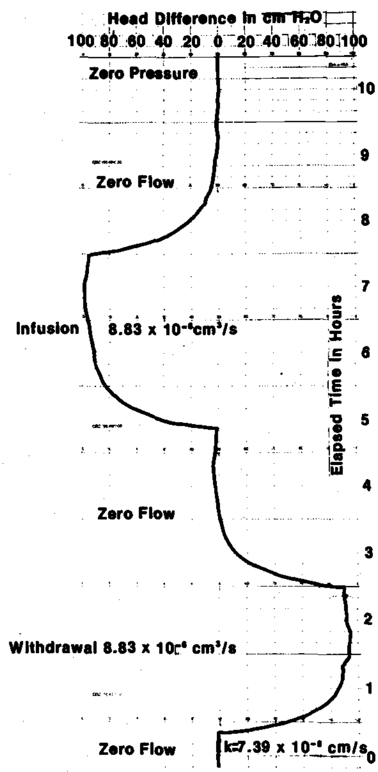

FIG. 8—*Flow-pump-permeability and coefficient-of-consolidation data for clay.*

value, and the head difference induced thereby across the length of the specimen changes with time from an initial value of zero to a final constant value when the steady-state condition has been established. This latter condition also serves as the initial condition for the decay model illustrated on the right side of Fig. 9. Therein, the flow rate is changed instantaneously from a constant steady-state value to zero, and, thereafter, the head difference across the length of the sample decays with time until the head difference due to the initial steady-

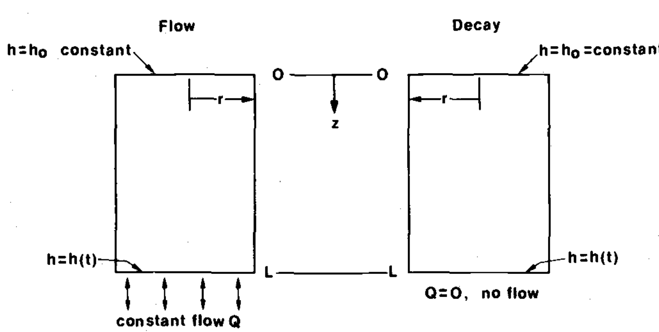

FIG. 9—*Models for analyzing flow-pump transport-property test data.*

state flow rate has fully dissipated. According to Carslaw and Jaeger [15], the analytic solutions for these models are:

For the flow model,

$$\Delta h = \frac{QL}{kA}\left\{1 - \frac{8}{\pi^2}\sum_{n=0}^{\infty}\frac{e^{-\alpha(2n+1)^2\pi^2 t/4L^2}}{(2n+1)^2}\right\} \tag{2a}$$

For the decay model,

$$\Delta h = \frac{8\,\Delta h_s}{\pi^2}\sum_{n=0}^{\infty}\frac{e^{-\alpha(2n+1)^2\pi^2 t/4L^2}}{(2n+1)^2} \tag{2b}$$

where

k = permeability (cm/s)
s = compressibility (cm^{-1})
α = k/s = the coefficient of consolidation (cm^2/s)
Δh = differential head across sample, $(h - h_o)$ (cm)
Δh_s = steady-state differential head across the sample, $(h_1 - h_o)$ (cm)
t = time (s)
L = length of sample (cm)
Q = constant flow rate (cm^3/s)
A = cross-sectional area of sample (cm^2)

Figure 10 illustrates that the time response behavior for the flow model in Fig. 9, according to Eq 2a, is governed by the coefficient of consolidation, α, which equals the permeability, k, divided by the compressibility, s. Equation 2b shows that the same parameters govern the time response for the decay model in Fig. 9.

In applications of the above, the nature of the seepage-induced deformations that occur when a flow pump is used to conduct permeability and coefficient-of-consolidation tests needs to be considered [16–18]. These deformations are illustrated in Fig. 11. During an infusion test, the pore pressure increases and the effective stress decreases at the base of the specimen until a steady state is reached. In consequence, the specimen expands both axially and radially by an amount that varies from zero at its top to a maximum at its base. Conversely, a withdrawal test causes deformations similarly distributed but opposite in sign. In other words, a test specimen rebounds during an infusion test and reconsolidates when the infusion test is terminated (decay). Similarly, a test specimen consolidates during a withdrawal test and rebounds when the withdrawal test is terminated (decay).

Experimental data shown in Fig. 12 illustrate the above concepts. The data are from the same specimen used to obtain the consolidation and compressibility data in Figs. 5 and 6. The upper part of Fig. 12 shows an infusion test conducted shortly after the data in Figs. 5 and 6 were collected. Subsequently, after further consolidation of the specimen using the flow pump, the withdrawal test shown in the lower part of Fig. 12 was run. In Fig. 12, the effective stress, σ', and the permeability, k, are noted to indicate the changes in the state of the specimen during the course of these experiments.

Figure 12 shows that the time response for the withdrawal test is relatively long, compared with the time responses for the infusion test and also for the decay parts of both the withdrawal and the infusion tests. This difference clearly reflects the high compressibility of the specimen in virgin compression during the withdrawal test, compared with the relatively low compressibility of the specimen in rebound and recompression during the infusion test and also during the decay parts of both the withdrawal and infusion tests.

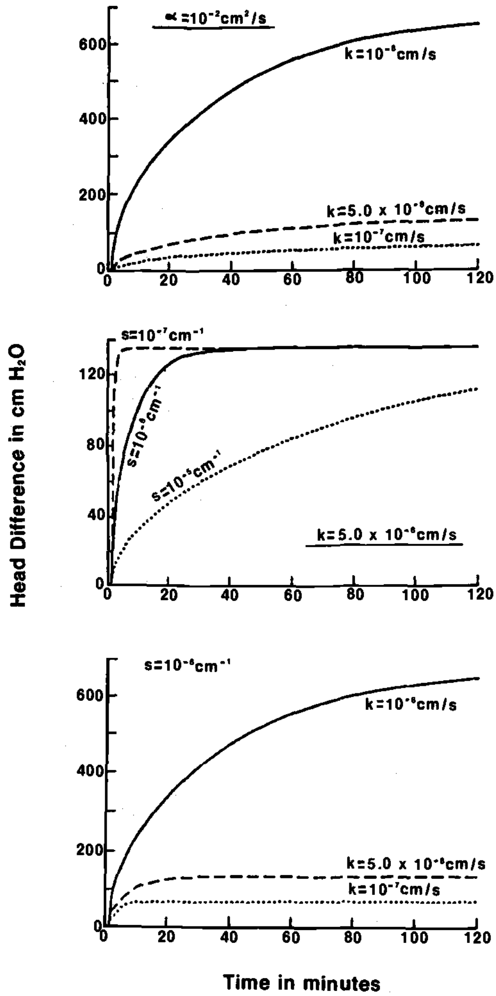

FIG. 10—*Variation of time response with the permeability, the compressibility, and the coefficient of consolidation.*

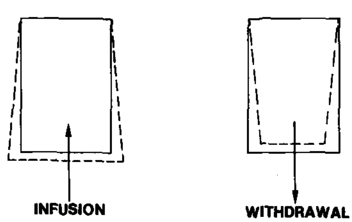

FIG. 11—*Variation of specimen deformation with flow direction.*

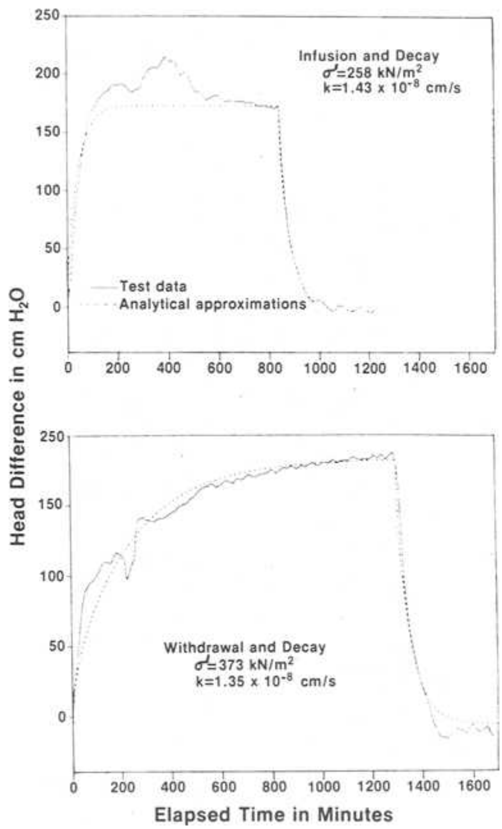

FIG. 12—*Variation of time response with flow direction for normally consolidated and overconsolidated clay specimens.*

Figure 12 further shows analytic approximations of the experimental data based on Eq 2a and 2b. The fitted response curves are displayed for comparison with the experimental curves. The discrepancies between the experimental and fitted response curves appear to be caused by the same room temperature variations responsible for the small residual-head variations in Fig. 7, and the cyclic variations in effective stress in Fig. 6.

The above applications of Eq 2a and 2b are not exact, at least in part, because they are solutions of a one-dimensional diffusion equation, whereas the deformations in the test specimen during flow pump permeability tests involve both axial and radial components. Nevertheless, the use of Eq 2a and 2b appears to be reasonable, at least as a first approximation. This is suggested by the consistency of the theoretical curves with the experimental data in Fig. 12, and further by the results in Table 1.

Table 1 shows the compressibility values interpreted from flow pump permeability and coefficient-of-consolidation tests in Fig. 12 are generally consistent with those obtained from the direct measurements in Fig. 6. For both the direct and indirect determinations, the compressibility for virgin compression is on the order of 10×10^{-6} cm^{-1}, whereas the compressibility for rebound and recompression is on the order of 2×10^{-6} cm^{-1}. The ratio of the compressibility for virgin compression to that for rebound or recompression is on the order of about five for both the direct and indirect measurements.

TABLE 1—*Comparison of compressibility values from direct measurements and from flow pump transport-property measurements.*

	Effective Stress, kN/m^2	Compressibility, cm^{-1}		
		Compression	Rebound	Recompression
Values from direct measurements in Fig. 6	250	8.69×10^{-6}	1.59×10^{-6}	
Values from the flow pump transport data in Fig. 12	258		1.84×10^{-6}	2.14×10^{-6}
	373	9.88×10^{-6}	2.16×10^{-6}	

Other Potential Applications

The use of a flow pump to control the rate and amount of pore fluid movement to the ends of a test specimen also enables capabilities other than those described above. Additional capabilities can be obtained by applying a constant rate of vertical deformation to a triaxial specimen (using, for example, a controlled-deformation-rate loading press) while simultaneously changing its volume with a flow pump [*8*]. Arbitrary combinations of vertical and volumetric deformation rates can be used for controlling strain paths during either consolidation or shear phases of a triaxial test.

One special case of strain-path control, which yields one-dimensional consolidation of a triaxial specimen (the K_o condition), can be achieved by synchronizing the rate of vertical deformation with the rate at which the specimen volume is reduced such that the average cross-sectional area of the specimen remains constant during the consolidation process (that is, the rate of volume change produced by axial deformation equals the rate of volume change produced by the flow pump). This case follows when the ratio of the volume change rate (dV/dt) to the axial-length-change rate (dz/dt) equals the average cross-sectional area (A) of the test specimen. In other words,

$$\frac{dV}{dt} = A\left(\frac{dz}{dt}\right) \tag{3}$$

The significance of this criterion becomes evident when it is compared with the general case

$$\frac{dV}{dt} = A\left(\frac{dz}{dt}\right) + z\left(\frac{dA}{dt}\right) \tag{4}$$

It follows from Eq 3 and 4 that

$$\frac{dV}{dt} - A\left(\frac{dz}{dt}\right) = 0 = z\left(\frac{dA}{dt}\right) \tag{5}$$

and hence that A remains constant.

Conclusion

The capabilities of a conventional triaxial system can be expanded by using a commercially available flow pump to control the rate and amount of pore fluid movement to or from the ends of a test specimen. These capabilities include measurements of equipment compliance, constant-rate-of-deformation consolidation, very-small-strain compressibility, low-gradient permeability, and coefficient of consolidation. Additional capabilities can be obtained by combining the use of a flow pump with established methods for controlling axial deformations in a specimen. Arbitrary combinations of vertical- and volumetric-deformation rates can be used to control strain paths. One special case of strain-path control yields one-dimensional consolidation of a triaxial specimen (the K_o condition).

These flow pump applications are of practical interest, in part, because they facilitate the acquisition of data of better quality than can be obtained with conventional methods. Examples of this advantage include (1) the capability to obtain one-dimensional consolidation test data on a triaxial specimen free from the side friction that occurs in a conventional oedometer and (2) the capability to obtain rapid permeability and compressibility data in response to low gradients and very small deformations.

These flow pump applications reduce the equipment and the number of replicate specimens needed for determining the permeability, compressibility, and strength of a given soil. For example, the above applications enable the permeability and the compressibility of a single triaxial test specimen to be determined over a range of conditions while being consolidated under K_o conditions prior to shear. Thereafter, stage testing can be used to determine strength parameters on the same specimen.

References

[1] Menzies, B. K., Sutton, H., and Davies, R. E., "A New System for Automatically Simulating K_o Consolidation and K_o Swelling in the Conventional Triaxial Cell," *Geotechnique,* Vol. 27, No. 4, 1977, pp. 593–596.

[2] Olsen, H. W., "Darcy's Law in Saturated Kaolinite," *Water Resources Research,* Vol. 2, No. 6, 1966, pp. 287–295.

[3] Olsen, H. W., "Simultaneous Fluxes of Liquid and Charge Through Saturated Kaolinite," *Proceedings of the Soil Science Society of America,* Vol. 33, No. 3, 1969, pp. 338–344.

[4] Olsen, H. W., "Liquid Movement Through Kaolinite Under Hydraulic, Electric, and Osmotic Gradients," *Bulletin of the American Association of Petroleum Geologists,* Vol. 56, 1972, pp. 2022–2028.

[5] Pane, V., Croce, P., Znidarcic, D., Ko, H.-Y., Olsen, H. W., and Schiffman, R. L., "Effects of Consolidation on Permeability Measurements for Soft Clays," *Geotechnique,* Vol. 33, No. 1, 1983, pp. 67–72.

[6] van Zyl, D., "Design, Construction, and Field Testing of a Heap Leach Clay Pad," Symposium on Uranium Mill Tailings, Fort Collins, CO, 1982, pp. 521–535.

[7] van Zyl, D., "Construction and Investigation of a Clay Heap Leach Pad," in *Gold and Silver Heap and Dump Leaching Practice,* J. B. Hiskey, Ed., American Institute of Mechanical Engineers, New York, 1984, pp. 59–68.

[8] Olsen, H. W., Nichols, R. W., and Rice, T. L., "Low-Gradient Permeability Measurements in a Triaxial System," *Geotechnique,* Vol. 35, No. 2, 1985, pp. 145–157.

[9] Mitchell, J. K., *Fundamentals of Soil Behavior,* Wiley, New York, 1976, 342 pp.

[10] Olsen, H. W., "Osmosis—A Cause of Apparent Deviations from Darcy's Law," *Canadian Geotechnical Journal,* Vol. 22, No. 2, 1985, pp. 238–241.

[11] Gibson, R. E., "A Note on the Constant Head Test to Measure Soil Permeability in Situ," *Geotechnique,* Vol. 16, No. 3, 1966, pp. 256–259.

[12] Al-Dhahir, Z. A. and Tan, D. I. C., "A Note on One-Dimensional Constant-Head Permeability Tests," *Geotechnique,* Vol. 18, No. 4, 1968, pp. 499–505.

[13] Wilkinson, W. B., "Constant Head in Situ Permeability Tests in Clay Strata," *Geotechnique,* Vol. 18, No. 2, 1968, pp. 172–194.

[14] Terzaghi, K., *Theoretical Soil Mechanics,* Wiley, New York, 1943, 510 pp.

[15] Carslaw, H. S. and Jaeger, J. C., *Conduction of Heat in Solids,* 2nd ed., Oxford University Press, London, 1959, 510 pp.

[16] Morin, R. H. and Olsen, H. W., "Determining Specific Storage of Sediment Using Data from a Constant Flow Rate Permeability Test" (abstract), *EOS, Transactions, American Geophysical Union,* Vol. 65, No. 45, 1984, p. 889.
[17] Morin, R. H. and Olsen, H. W., "Theoretical Analysis of the Transient Response from a Flow-Pump Permeability Test," *Water Resources Research,* Vol. 23, No. 8, Aug. 1987, pp. 1461–1470.
[18] Olsen, H. W. and Morin, R. H., "Comparison of Direct and Indirect Approaches for Determining Specific Storage in a Triaxial System" (abstract), *EOS, Transactions, American Geophysical Union,* Vol. 67, No. 7, 1986, p. 84.

Bruce K. Menzies[1]

A Computer Controlled Hydraulic Triaxial Testing System

REFERENCE: Menzies, B. K., "**A Computer Controlled Hydraulic Triaxial Testing System,**" *Advanced Triaxial Testing of Soil and Rock, ASTM STP 977,* Robert T. Donaghe, Ronald C. Chaney, and Marshall L. Silver, Eds., American Society for Testing and Materials, Philadelphia, 1988, pp. 82–94.

ABSTRACT: A computer controlled hydraulic triaxial testing system is introduced. A desktop computer is linked to a hydraulic triaxial cell via three microprocessor controlled hydraulic actuators and two subsystems, one for the measurement of axial deformation and the other for the measurement of pore pressure. The separate system elements and subsystems are described in detail. The operation of the system is described, and control algorithms are explained with particular reference to K_0 consolidation and swelling and automatic testing rate by controlled hydraulic gradient. System performance is illustrated by reference to published data describing K_0, stress path, cyclic loading, and triaxial extension tests. The advantages of the system are summarized.

KEY WORDS: computer control, digital controller, saturation ramps, isotropic and anisotropic consolidation, conventional tests, triaxial extension, K_0 consolidation and swelling, stress paths, cyclic loading, automatic drained testing rate, data presentation, repeatability, software based

System Layout

As shown in the schematic diagram in Fig. 1, a desktop computer is linked to a hydraulic triaxial cell via three microprocessor controlled hydraulic actuators called "digital controllers" [*1–4*]. The controllers precisely regulate pressure and volume change of deaerated water supplied to the cell to control axial load or axial deformation, cell pressure, and back pressure. The system also measures axial deformation indirectly by volume change into the lower chamber of the cell or by direct measurement of displacement using a digital indicator. Pore pressure may be measured by the back-pressure controller (locked for the undrained condition so there is no volume change) or by a solid state pressure transducer plumbed directly into the base pedestal. The digital controllers, pore pressure indicator, axial deformation indicator, printer, and plotter are connected by interface bus cables to the IEEE 488 standard parallel interface of the computer.

System Elements

The Triaxial Cell

The triaxial compression/extension cell is based on the design of Bishop and Wesley's [*5*] hydraulic triaxial apparatus for controlled stress path testing developed at Imperial College

[1] Director, GDS Instruments Ltd., Unit 12 Eversley Way, Thorpe Industrial Estate, Egham, Surrey, England TW20 8RG.

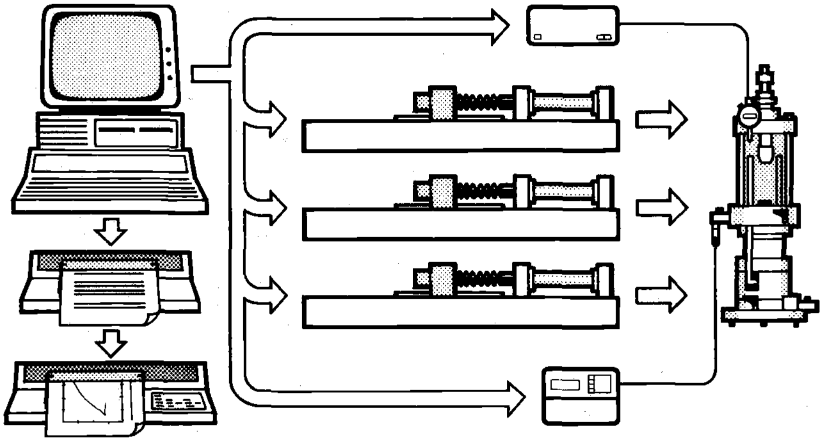

FIG. 1—*Diagrammatic layout of the system.*

of Science and Technology, London. Note that any test, including a conventional test, may be referred to as a "stress path test."

Although Bishop and Wesley set out to design "a simple form of triaxial apparatus in which the stress paths encountered in engineering practice can be approximated more readily than in conventional equipment," their versatile cell is equally adept at carrying out classic "standard" tests as well as advanced tests.

As shown in the schematic diagram in Fig. 2, axial force is exerted on the test specimen by means of a piston fixed to the movable base pedestal. The top cap of the test specimen is fixed in position by an adjustable rod passing through the top of the cell. The piston moves vertically up and down in a linear guide comprising a cage of ball bearings housed in a turret joining the cell to the base. The piston is actuated hydraulically from an integral lower chamber in the base of the cell which contains deaerated water. The piston is sealed into the upper cell and the lower chamber by matched Bellofram rolling diaphragms which sweep equal volumes of water. Accordingly axial ram friction is very small and normally less than 5 kPa of deviator stress.

The statics of the cell are very simple. By considering the equilibrium of the loading ram, the following relationship is obtained:

$$\sigma_a = p(a/A) + \sigma_r(1 - a/A) - W/A \tag{1}$$

where

σ_a = the average axial total stress,
σ_r = the radial total stress or cell pressure,
p = the pressure in the lower chamber,
A = the current average cross-sectional area of the test specimen (defined as the area of the volumetrically equivalent right cylinder),
a = the effective area of the Bellofram rolling diaphragm, and
W = the weight of the loading ram.

The computer continuously computes the average axial total stress using Eq 1, and so an external or internal load cell is not required and not supplied with the system.

As can be seen from the photograph in Fig. 3, there are two versions of the cell—the

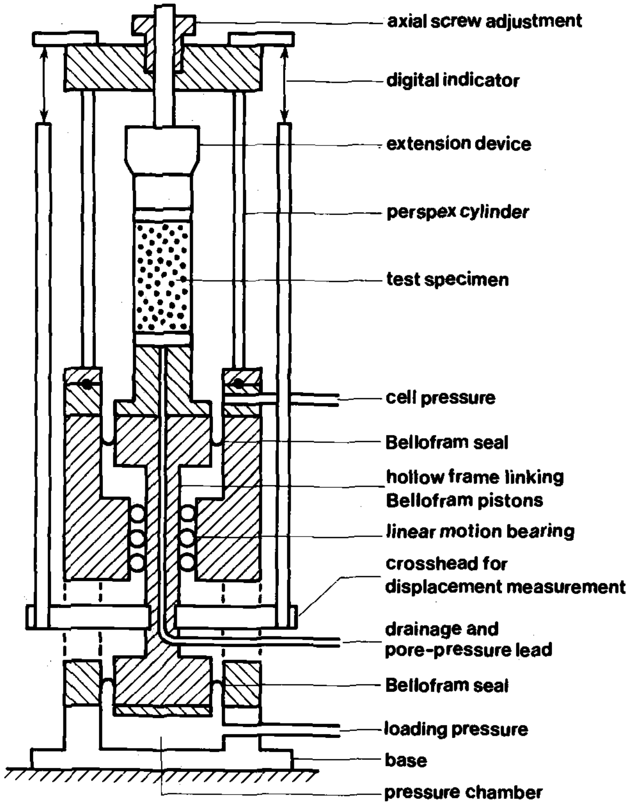

FIG. 2—*Diagrammatic layout of the hydraulic triaxial apparatus (after Bishop and Wesley [5]).*

smaller one for test specimens of 38-mm diameter, and a larger cell which accommodates 50-, 70-, and 100-mm diameter test specimens by interchangeable base pedestals and top caps.

The Extension Device

The extension device is fitted to the triaxial cells in place of the redundant load cell. The object of the extension device is to allow axial stress to be reduced below radial stress. In conventional triaxial cells this is normally not possible because the radial stress or cell pressure acts vertically on the top cap. Indeed, in many types of conventional cell, a small hole is drilled through the side of the loading ram and into the conical end socket to avoid any possibility of partial pressures between the end of the ram and the ball seating of the top cap. This ensures that the vertical component of cell pressure acts with equal intensity, thus simplifying the statics.

As shown in the schematic diagram in Fig. 4, the hollow adjustable reaction rod passes through the top of the cell. Fixed to the bottom of the rod is a truncated conical fitting which mates with the plane top cap of the triaxial test specimen. The top cap is fitted with a bell mouthed surgical PVC dip molded sleeve.

The cell is filled with water, with air being purged out through the hollow reaction rod.

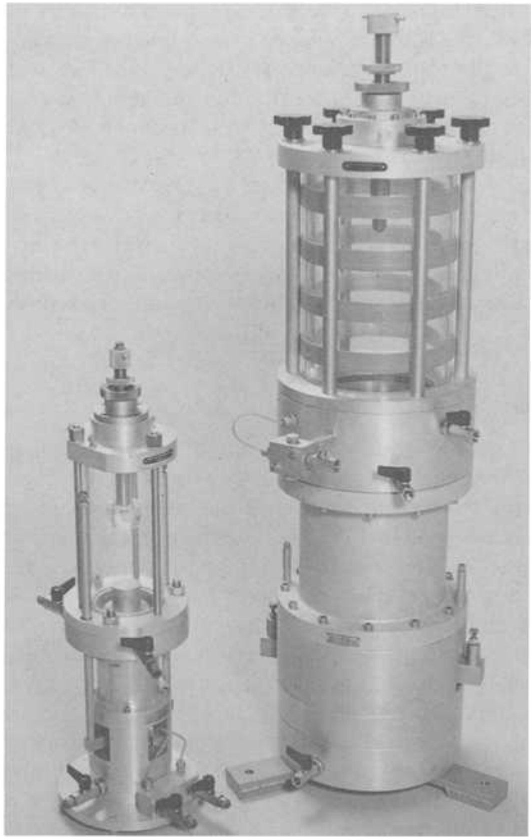

FIG. 3—*Hydraulic triaxial cells for test specimen diameters of 38 mm (small) and 50, 70, 100 mm (large) by interchangeable base pedestals and top caps.*

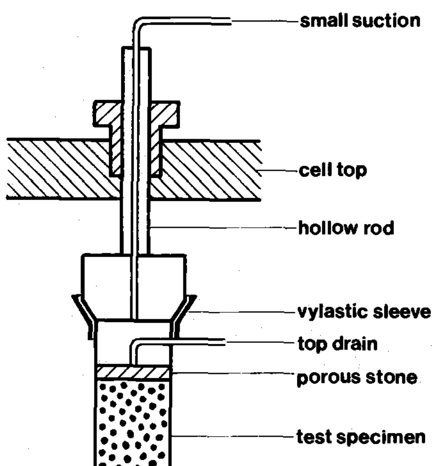

FIG. 4—*The extension device.*

The reaction rod is then adjusted to dock the plane and conical parts together. Lightly smearing the angled surfaces with soft silicone grease ensures good contact. A small suction can then be applied to the top of the hollow reaction rod to cause the sleeve to seal the interface. Cell pressure is then applied. As the top cap is now sealed to the fixed reaction rod, cell pressure does not act vertically on the test specimen. Accordingly, axial stress can be reduced to below cell pressure.

Provided axial stress always remains positive, there is always a positive load between the mating parts which, therefore, will not move apart. Smooth transitions between compression and extension of course are essential in an advanced triaxial testing system, for example, for stress paths simulating excavations, surcharge removal, emptying of storage tanks, and so forth, or for K_0 consolidation and swelling to a high overconsolidation ratio during SHANSEP procedures.

The Digital Controller

The digital controller shown in the photograph in Fig. 5*a* is a microprocessor controlled hydraulic actuator for the precise regulation and measurement of liquid pressure and liquid volume change. For the triaxial testing of soils the volumetric capacity is 200 or 1000 cm^3 and the pressure range is 0 to 2000 kPa. Pressure measurement is resolved to 0.2 kPa, and pressure is controlled to 0.5 kPa. For rock mechanics applications the volumetric capacity is nominally 200 cm^3 and the pressure ranges are 7, 10, 20, 32, and 64 MPa.

The principles of operation are shown in the schematic diagram in Fig. 5*b*. Deaerated water in a cylinder is pressurized and displaced by a piston moving in the cylinder. The piston is actuated by a ball screw turned in a captive ball nut by a stepping motor and gearbox that move rectilinearly on a ball slide.

Pressure is detected by means of an integral solid state pressure transducer. Control algorithms are built into the programmable memory to cause the controller to seek to a target pressure or step to a target volume change. Volume change is measured by counting the steps of the stepping motor. Knowing the number of steps per revolution of the motor, the gearbox ratio, and the pitch of the ball screw, the bore of the pressure cylinder may be found such that one step of the motor equals 1 mm^3.

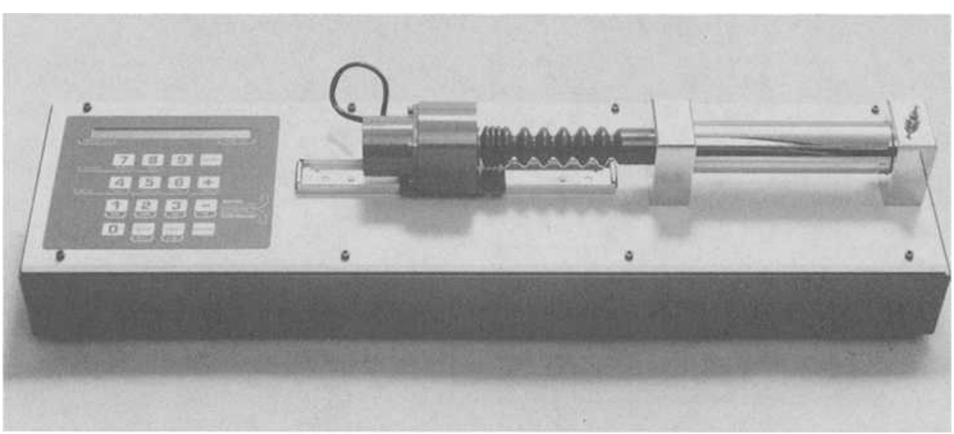

FIG. 5 (a)—*Digital controller.*

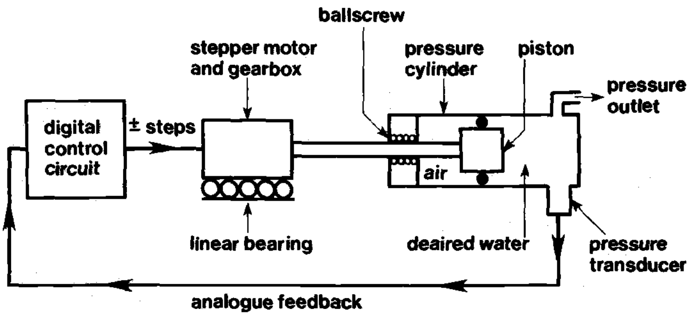

FIG. 5 (b)—*Diagrammatic layout of digital controller.*

In stand-alone mode the instrument is a general purpose constant pressure source, a volume change gauge, a pore pressure measuring system, a flow pump (or screw pump), and a digital pipette. As a constant pressure source it can be used to replace mercury column, compressed air, pumped oil, and dead weight devices. It can be programmed through its own control panel to ramp and cycle pressure and volume change linearly with respect to time.

In computer control mode it is a computer peripheral via the standard IEEE 488 computer interface. The user interface is a control panel comprising a liquid crystal display and membrane touch keypad. This is used in stand-alone mode for entering target pressure, target volume, ramping data, and other functions including access to on-board diagnostics for checking out each of the major hardware components of the system.

The Axial Deformation Digital Indicator

The axial deformation digital indicator is similar in size and appearance to a conventional dial gauge. In place of the dial is a liquid crystal display. In place of the indicating pointer there is an internal optoelectronic linear encoder and large-scale integration (LSI) counter gauging the movement of a finely graduated glass plate actuated by the external spindle.

The advantages of the axial deformation digital indicator over conventional displacement transducers of the inductive, resistive, and capacitive type are:

- The indicator is an inherently digital device and not subject to thermal and electronic drift.
- The digital indicator displays its own reading.
- The digital indicator does not require any calibration whatsoever.

The subsystem uses an axial deformation digital indicator connected to a multiplexer with an IEEE interface. Axial deformation is resolved to 0.001 mm over a range of 12.7 mm.

Pore Pressure Measuring System

A solid-state pressure transducer is plumbed directly into the pore water ducts leading to the base pedestal. The transducer is connected to a digital pressure indicator with an IEEE interface. The subsystem resolves pore pressure to ±0.2 kPa over a range of 2000 kPa.

System Operation

Test Control

Continuously and at a frequency typically less than once a second, the computer:

- takes a set of readings from the digital controllers and the axial deformation and pore pressure measuring subsystems,
- calculates the current test parameters and stores them as required, and
- gives new commands to the digital controllers to keep the selected test on the chosen stress path or strain path.

Using this general approach in a series of standard subroutines, a range of tests can be made available by selection from a test menu.

Test Menu

The test menu of the system is as follows:

- saturation by simultaneous ramps of cell pressure and back pressure;
- incremental and ramped evaluation of pore pressure parameter B;
- isotropic and anisotropic consolidation;
- unconsolidated-undrained compression/extension;
- consolidated-undrained compression/extension with pore pressure measurement;
- consolidated-drained compression/extension, volume change resolved to 1 mm^3;
- K_0 consolidation and swelling for saturated soils;
- continuous linear stress paths, mixed drained and undrained, mixed compression and extension;
- cyclic loading by axial stress controlled square, sinusoidal, and triangular wave forms; periods down to sea wave periods; and
- permeability by constant hydraulic gradient or by constant rate of flow [6].

The system has a "loop-round" facility enabling any series of the above tests to be sequentially carried out on the one test specimen with changed height and diameter being passed on from the end of one test to the beginning of the other, for example, unconsolidated-undrained after K_0 gives a SHANSEP capability.

Test Control Algorithms

The on-board intelligence of the digital controller provides useful functions (seek to target pressure, step to target volume change, ramp pressure, ramp volume change) which facilitate the design of the test control algorithms. Generally, for tests most simply described by a stress path, the controllers are continually set and reset to ramped pressure control (for a stress path test per se, this refers to the axial and radial stress controllers). For tests most simply described by a strain path (for example, a U-U test) the controllers are continually set and reset to ramped volume change control (for the U-U test this would be the axial controller only). There are two notable exceptions to this approach—K_0 consolidation and swelling, and automatic drained testing rate by controlled hydraulic gradient, as discussed below.

K_0 *Consolidation and Swelling*

Here the test control rule is that the volume change in the pore water duct must at all times be equal to the volume of the axial deformation times the original average cross-sectional area. This rule is only applicable to saturated soils. Continuously, and at a frequency typically less than once a second, the computer:

- calculates the volume of the axial deformation times the original average cross-sectional area;
- commands the back-pressure controller (which is under volume change control) to step an equal and opposite volume change, that is, extract pore water if consolidation is required, infuse water if swelling is required; and
- commands the cell pressure controller to adjust cell pressure to keep the back pressure constant at the predetermined value.

The test is only valid if the chosen testing rate is such that unacceptable excess pore pressures do not develop (for example, during consolidation, it is possible to imagine contraction of the test specimen adjacent to the base porous stone while bulging occurs in the middle third of the test specimen). Accordingly, it is highly desirable to regulate the testing rate by controlling the hydraulic gradient throughout the height of the test specimen as discussed in the following section.

Automatic Drained Testing Rate

One of the biggest problems associated with any form of triaxial testing is the question of testing rate. This is particularly so in effective stress testing, that is, testing where a complete knowledge of the pore water pressure regime is required.

For the particular case of drained tests (conventional, stress path, K_0) where a constant back pressure is applied to the base pedestal or to the top cap, if the testing rate is too high the back pressure may be significantly different from the average pore pressure throughout the test specimen. Accordingly, chosen testing rates tend to err on the side of caution and, in many cases, are far too low. This slows down test throughput and reduces productivity.

An alternative is to measure the difference in pore pressure from one end of the test specimen to the other and to control the testing rate to restrict the difference to an acceptable level. As shown in the schematic diagram in Fig. 6, the system applies a constant back pressure to the top drain and measures the pore pressure at the base pedestal. Axial loading can now be controlled such that the difference in end pore pressures—the excess pore pressure—is either a fixed value, say 5 kPa, or, more logically perhaps, a fixed proportion of axial total stress, say 5%. Referring to Fig. 6, these control criteria may be expressed algebraically as

$$u - u_0 = \Delta u = 5 \text{ kPa} \tag{2}$$

or

$$\Delta u / \sigma_a = 5\% \tag{3}$$

In this way the soil is tested at the optimum testing rate for the chosen criteria, automatically adjusting to changing soil conditions such as permeability, while the state of effective stress is continuously controlled and measured.

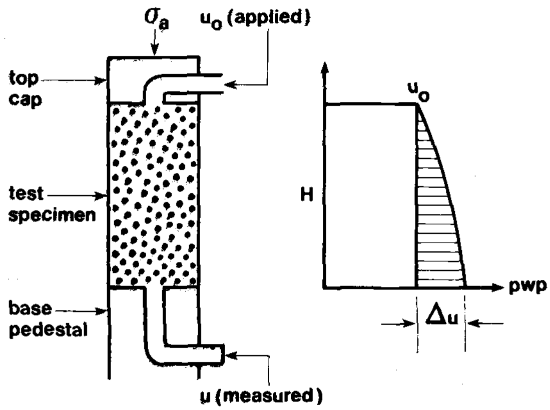

FIG. 6—*Diagrammatic representation of variation of pore pressure in a top-drained triaxial test specimen.*

Data Presentation

The system reduces the data into SI units. Optionally, the system can tabulate or plot saved data. The list of parameters available for data presentation are as follows:

- pressure and volume change from each controller,
- time,
- percent axial strain,
- axial stress,
- radial stress,
- effective axial stress,
- effective radial stress,
- deviator stress (Cambridge q),
- stress ratio,
- mean stress (MIT p),
- mean effective stress (MIT p'),
- average radial strain,
- average diameter change,
- pore water pressure,
- volume change,
- change in length,
- square root of time,
- $\log_{10}$ (time),
- $\log_{10}$ (effective axial stress),
- maximum shear stress (MIT q),
- maximum shear strain,
- spherical pressure (Cambridge p), and
- effective spherical pressure (Cambridge p').

Any one parameter can be plotted against any other. Scaling can be automatic or overridden to allow families of curves to be plotted within the same set of axes or to enlarge particular features. Data can also be smoothed using a cosine weighted moving average.

System Performance

For an assessment of the performance of the system, reference can be made to Coatsworth and Hobbs [2] who carried out advanced tests to provide design parameters for a variety of construction projects. Their tests are summarized below.

Stress Path Testing

In situ ground deformation parameters were required for predicting the movement of a proposed immersed tube tunnel river crossing in Wales. Stress path tests were carried out on selected piston samples of glacial lake clays from beneath the proposed tunnel. As shown in Fig. 7, each test specimen was consolidated under a small all-round stress (point A in Fig. 7) to give it some stability. The specimen was then K_0 consolidated to the maximum

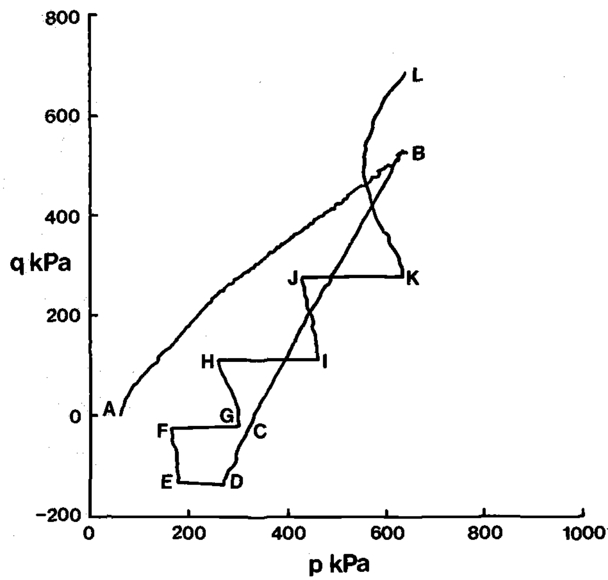

A–B	K_0 consolidation	Representing
B–C	Drained stress path	geological history
C–D	Undrained unloading	Representing
D–E	Swelling	excavation of the trench
E–F	Undrained loading	Representing
F–G	Consolidation	the placing
G–H	Undrained loading	of the
H–I	Consolidation	immersed
I–J	Undrained loading	tube
J–K	Consolidation	tunnel
K–L	Undrained compression to failure	To determine the soil strength after construction

FIG. 7—*Stress path test on glacial clay (from Coatsworth and Hobbs* [2]).

previous consolidation pressure (stage A–B in Fig. 7). The final stage in the reimposition of the in situ stresses was to impose a drained stress path while allowing swelling to occur (stage B–C). The specimen was then subjected to undrained unloading to simulate excavation (stage C–D). Drainage was then allowed to occur at constant total stresses (stage D–E). The increments in vertical stress corresponding to tunnel construction were applied in a number of undrained stages, usually three (E–F, G–H, I–J), each undrained stage being followed by a drainage interval (F–G, H–I, J–K) during which the total stresses were maintained constant.

These tests provided deformation moduli significantly different from those obtained from conventional oedometer tests, even allowing for Skempton and Bjerrum's [7] correction, a general conclusion also reached by Simons and Som [8] who tested London clay.

Cyclic Loading Tests

A series of tests were performed to model the behavior of normally consolidated sand below the center of a foundation subjected to repeated loading. The breadth of the foundation was large compared to the depth of sand, and so conditions of zero lateral strain were assumed. As shown in Fig. 8, the loading sequence to model conditions below the foundation were simplified into three stages, zero lateral strain conditions being maintained for both loading and unloading paths, as follows:

- initial consolidation of the sand under effective vertical overburden pressure,
- application of the dead load of the structure and application and removal of the proof load, and
- repeated application and removal of the live load during operational life of the structure.

The tests were carried out on samples of gravelly medium and coarse sand from Monkey Island, Bray, Berkshire, England. For clarity, the results given in Fig. 8 are for selected cycle numbers only. The control algorithm was written by the authors.

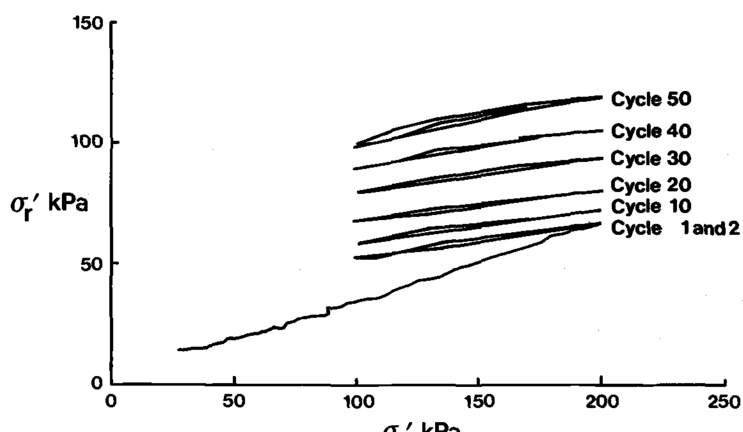

FIG. 8—*Cyclic loading test on dense sand (from Coatsworth and Hobbs* [2]).

Extension Tests

A series of consolidated-undrained extension tests were carried out on overconsolidated silty clay to investigate the stability of the base of a deep excavation in the Middle East. The results of 1 set of tests on a stiff to very stiff silty clay overconsolidated by desiccation are given in Fig. 9 in which the strain contours show the mobilization of strength. In all, 24 tests were completed in 48 days with just 1 cell.

System Features

Some major features of the system are summarized below:

Cell

- Specifically designed to facilitate stress path testing
- Ram friction negligible and corrected for by computer anyway
- Plane top cap reduces bedding and alignment errors

Digital Controllers

- Pressure measured to 0.2 kPa, pressure controlled to 0.5 kPa
- Volume change measured and controlled to 1 mm^3
- On-board intelligence enables ramping of pressure and volume change

Software

- Repeatability of tests
- Automatic data recording, data reduction, and data presentation to standard format
- Advanced tests can be carried out as routinely as conventional tests

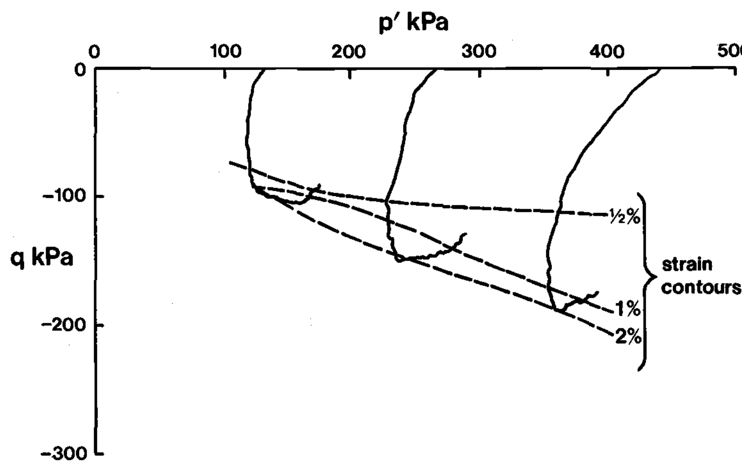

FIG. 9—*Undrained extension tests on overconsolidated silty clay (from Coatsworth and Hobbs* [2]).

Changing the triaxial cell for a hydraulic consolidation cell of the Rowe and Barden type [9] and changing the software package converts the system into a computer controlled consolidation testing system. The test menu includes classic step loading, constant rate of deformation, constant rate of loading, controlled hydraulic gradient, and permeability by constant rate of flow.

Because it is software based, the system repertoire may readily be updated to incorporate new techniques (for example, strain path testing) without changes in hardware. At the time of writing, over 50 systems are currently in use worldwide with the users providing an invaluable data bank of experience and suggestions. This feedback is reflected in periodic releases of software enhancements.

Acknowledgments

The author thanks the editor of *Ground Engineering* and the directors of Soil Mechanics Ltd. for their permission to reproduce Figs. 7, 8, and 9.

References

[1] Menzies, B. K., "Soil Testing System," *Geotechnical News,* Vol. 1, No. 3, 1984, pp. 38–39.
[2] Coatsworth, A. M. and Hobbs, N. B., "Computer Controlled Triaxial Soil Testing Equipment in a Commercial Laboratory," *Ground Engineering,* Vol. 17, No. 7, 1984, pp. 19–23.
[3] Linenberger, M. J., "Microcomputer Controlled Cyclic Triaxial Testing System," Project Report NSF83-297p for Master of Science Degree, University of Massachusetts–Amherst, 1983.
[4] Hsieh, K. H., "Techniques for Investigation of Sand Behaviour Under Cyclic Loading," Project Report OUR85-321p for Master of Science Degree, University of Massachusetts–Amherst, 1985.
[5] Bishop, A. W. and Wesley, L. D., "A Hydraulic Triaxial Apparatus for Controlled Stress Path Testing," *Geotechnique,* Vol. 25, No. 4, 1975, pp. 657–670.
[6] Olsen, H. W., Nichols, R. W. and Rice, T. L., "Low Gradient Permeability Measurements in a Triaxial System," *Geotechnique,* Vol. 35, No. 2, 1985, pp. 145–157.
[7] Skempton, A. W. and Bjerrum, L., "A Contribution to the Analysis of Foundations on Clay," *Geotechnique,* Vol. 7, No. 4, 1957, pp. 168–178.
[8] Simons, N. E. and Som, N. N., "Settlement of Structures on Clay with Particular Emphasis on London Clay," Report 22, CIRIA, London, 1970.
[9] Rowe, P. W. and Barden, L., "A New Consolidation Cell," *Geotechnique,* Vol. 16, No. 2, 1966, pp. 162–170.

X. S. Li,[1] *Clarence K. Chan,*[2] *and C. K. Shen*[1]

An Automated Triaxial Testing System

REFERENCE: Li, X. S., Chan, Clarence K., and Shen, C. K., "**An Automated Triaxial Testing System,**" *Advanced Triaxial Testing of Soil and Rock, ASTM STP 977,* Robert T. Donaghe, Ronald C. Chaney, and Marshall L. Silver, Eds., American Society for Testing and Materials, Philadelphia, 1988, pp. 95–106.

ABSTRACT: This paper describes a recently developed automated triaxial testing system. Loading is controlled by a closed-loop feedback scheme capable of performing stress- or strain-controlled tests in the standard triaxial environment. The system has two control channels allowing separate control of both the axial load and the chamber pressure.

Software written especially for this system can control back pressure saturation, consolidation, shear loading, cyclic loading, and a number of special loading programs. Each software package is well documented with complete notes for interactive dialogue with the computer.

The data retrieving and plotting software is capable of processing data and converting it to 20 variables commonly used in geotechnical engineering. These variables can be plotted with different combinations for display and detailed study. Typical test results for a fine sand are included to demonstrate the abilities of the system.

The system is well suited for research purposes, however it can also be used effectively in geotechnical material testing in consulting laboratories. The computer-based testing system is simple in operation, rapid in sampling, accurate in performance, and reasonable in cost.

KEY WORDS: data acquisition, microcomputer control, sand, triaxial testing system

Nomenclature

The following symbols are used in the figures:

Q	deviator stress $= \sigma_1 - \sigma_3$
P	mean normal stress $= \frac{1}{3}(\sigma_1 + 2\sigma_3)$
P'	effective mean normal stress $= \frac{1}{3}(\sigma_1' + 2\sigma_3')$
EPSILON Q (ϵ_Q)	shear strain $= \frac{2}{3}(\epsilon_1 - \epsilon_3)$
EPSILON V (ϵ_V)	volumetric strain $= \epsilon_1 + 2\epsilon_3$
D_r	relative density
σ_{30}'	initial consolidation pressure

Introduction

The triaxial testing apparatus is the most widely used testing device in geotechnical laboratories; it is used to study soil responses under both static and dynamic loadings. The device, practical in design and versatile in control, is capable of performing tests of controlled stress or strain rate of loading, or different types of prescribed stress paths under both drained and undrained conditions. The system described here is a modification and extension

[1] Associate development engineer and professor, respectively, Department of Civil Engineering, University of California, Davis, CA 95616.

[2] Research engineer, Department of Civil Engineering, University of California, Berkeley, CA 94720.

of the CKC cyclic triaxial testing system initially designed for studying the liquefaction potential and seismic mobility of soils. In the automated triaxial testing system, the computer-programmed electronic signal for frequency and magnitude of loading is applied to an electropneumatic transducer which then controls pneumatic amplifiers for the application of loads. All modes of loading are controlled by closed-loop feedback schemes. The system is designed for performing both static and dynamic testing. Two control channels allow independent and synchronized adjustment of axial load and chamber pressure. The system is best used for precision measurements of stress–strain relationships, for constitutive model calibration, for pore pressure development under cyclic loading, and for measurement of the response to various stress paths.

Triaxial System

A photograph and a schematic diagram of the automated system are shown in Figs. 1 and 2, respectively. The system includes a loading frame, a triaxial cell, a load piston, a volume-measuring device with three pressure transducers, a dual channel pneumatic loading unit, a signal-conditioning unit, a process interface unit, a TRS-80 Model IV microcomputer, and a dot-matrix printer. Brief descriptions of the various elements are given below.

Controller

The system uses two feedback control loops: one for the axial actuator and the other for the lateral actuator. Under software control, the two loops can work individually or synchronously. As an example, Fig. 3 shows the block diagram of the axial feedback loop. It has five major parts: computer, process interface, pneumatic loader, test apparatus with

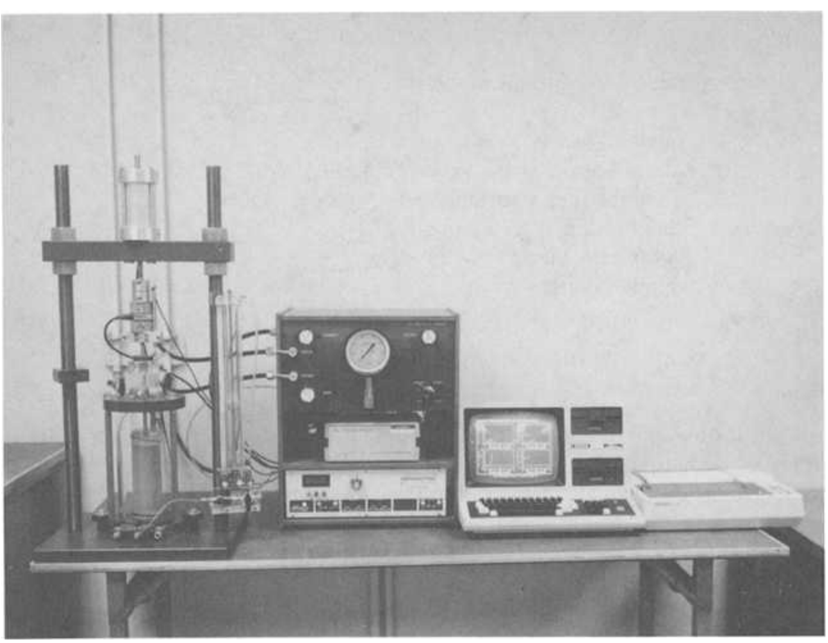

FIG. 1—*The automated triaxial testing system.*

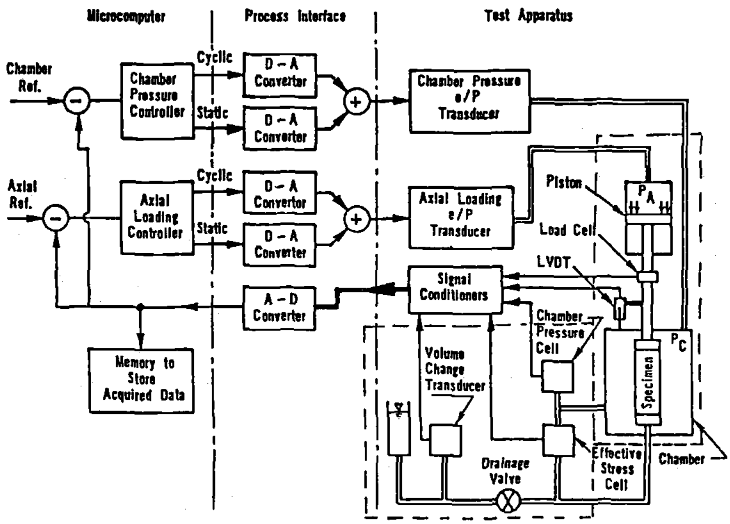

FIG. 2—*Schematic diagram of the automated triaxial testing system.*

soil specimen, and sensors. The computer plays the role of loop control by means of software so that the loop behavior can be easily modified by changes in the program. From Fig. 3 it can be seen that four control parameters are needed to specify the operation of the loop. First, the loop switch turns on or off the feedback path. Second, the loop selector selects the mode of control (either load or displacement). Third, the reference specifies the expected value of the selected mode, and fourth, the optimizer adjusts the dynamic range of the analog-to-digital (A–D) converter and correspondingly the coefficients of the discrete proportional-integral-differential (PID) controller. Proper selection of parameters for each con-

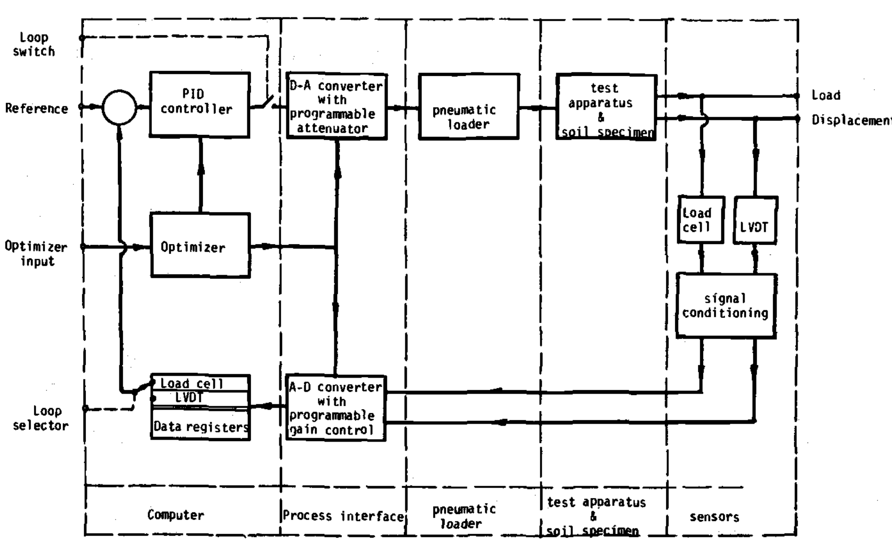

FIG. 3—*Block diagram of the loading system.*

trol loop in testing provides considerable flexibility. For instance, an initially stress-controlled shear loading test can be easily converted to a strain-controlled test at a later stage.

Loading System Components

A dual channel electropneumatic (e/p) system is used to convert the command electronic signal to pneumatic pressure, which in turn applies the axial load (P_A) and the lateral pressure (P_c). The entire system is shown schematically in Fig. 4. The e/p transducer essentially balances the force on the torque bar caused by the pressure at the end of a nozzle against the electronically controlled moving coil. The backup pressure is then amplified by pneumatic relay and volume booster in order to perform the work. The test gauge is used to monitor pressures being generated (that is, cyclic and lateral pressure) or controlled by regulators (that is, steady and back pressure). Clean dry compressed air is required to keep the system trouble-free. A more complete description on the electropneumatic system is given in Ref *1*.

The load frame is a two-post frame with adjustable cross bar and a flat plate base. Double-acting (push/pull) actuators of various sizes are used with the loader and are made with low friction seals. The lower chamber of 155-cm² (24 in.²) actuator is filled with oil so that strain-controlled testing on strain-softening specimen can be performed. A double swivel coupler is used to allow for minor misalignment between the guided loading rod and the guided triaxial rod. The hold down clamps for the triaxial cell are threaded on to the base plate.

Triaxial Cell and Volume Change Device

The triaxial cell is equipped to test 35.5 and 71-mm (1.4 and 2.8 in.) diameter specimens up to a chamber pressure of 689 or 1378 kPa (100 or 200 psi) for acrylic and aluminum chambers, respectively. The cell is built with the latest low friction piston rod seal [2] (air and diffusion control), three external tie rods, and straight-through tube fitting on the pore fluid lines to the specimen cap and base.

The volume change device uses three different size tubes with a valve manifold to select the range required for the particular test condition calculated in the software. The height of the water column under back pressure is measured by a sensitive differential pressure transducer.

Transducer and Signal Conditioner

A total of five sensors are used in the system: the 13.3-kN (3000-lb) load cell is sized to the largest loading piston for the anticipated static load test. The shape of the load cell is selected so that the mounting of the linear variable differential transformer (LVDT) can be as close to the center of the specimen as possible to give reliable low strain readings. To measure the vertical displacement a ±38-mm (±1.5-in.) LVDT with its small case size is selected to minimize the inertia loading on the sample and allow mounting close to the center of the specimen. Three pressure transducers are used to detect the chamber pressure, the effective pressure, and the volume change; the differential pressure transducer is a wet-to-wet type.

The signal-conditioning unit accommodates five channels for five sensors: the load cell, the three pressure transducers, and the LVDT. The output signals of these sensors are conditioned and then received by the process interface unit.

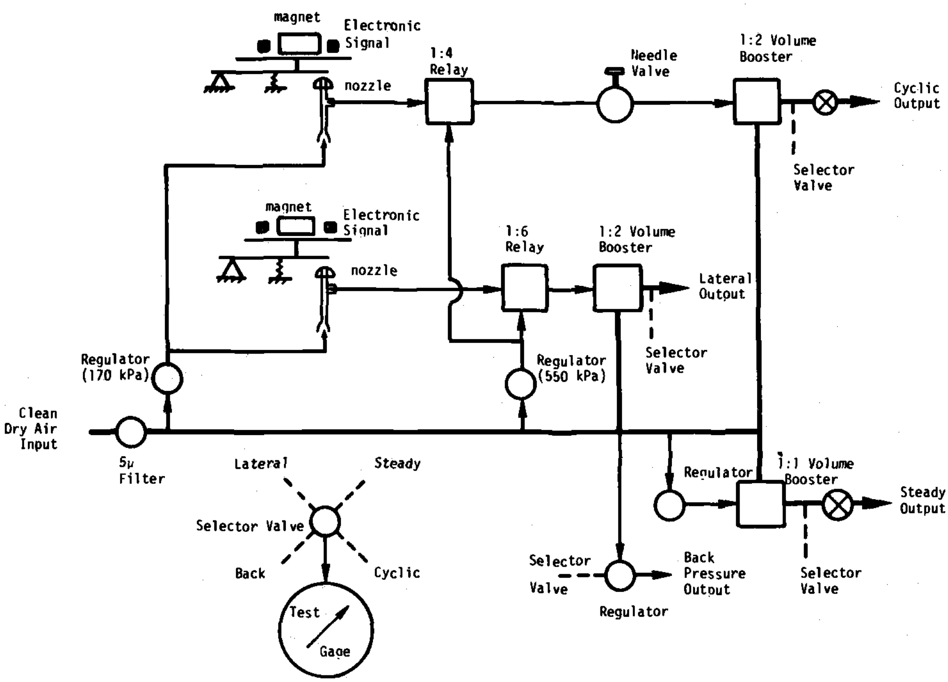

FIG. 4—*Schematic diagram of the loading system.*

Interface Unit

The process interface forms the communication link between the computer and the loading/sensor system. It is a compact and powerful unit which can be used to interface with many different types of laboratory loading and measuring systems for material testing. The unit consists of a 16-channel, 12-bit, high speed A–D converter, 8 channels of 12-bit, high speed digital-to-analog (D–A) converters, and a 24-line digital input/output port. The D–A converter channels can also be configured as gain controllers to suit specific purposes of a designed system.

For the automated triaxial testing system, seven channels of the A–D converters are employed. Five channels are used to monitor the signals from the five sensors equipped with the system, one is used to sense the state of the drainage valve, and another one is grounded as a zero reference to minimize the zero shift of the system. The digital input/output port is not used in this system.

Computer and Printer

The Tandy TRS-80 Model IV microcomputer with two disk drives controls the whole system. It receives and stores the real-time data in its memory and issues control signals to regulate the test. The keyboard and display screen provide an effective and convenient means of communication between the operator and the testing system. The computer also performs other functions such as data reduction and data processing.

The Epson FX-80 printer is used to record the output from the system. It prints out hard copies of test results in tabular or graphic form.

Software

The software written for this system includes the following packages:

Back pressure saturation (B value check)
Consolidation (isotropic, anisotropic, and K_o—confined state)
Shear loading (stress, strain, and stress/strain control; drained and undrained)
Shear stress path loading
Cyclic loading (up to 1 Hz, stress or strain programmed)
A number of special loading programs
Data retrieving and plotting

The software integrates three function blocks: CALIB, TEST, and PLOT. The CALIB program is used for input of the calibration coefficients of the five sensors. Any change of the sensitivities detected by periodic calibration check can be fed into the computer through CALIB. The TEST program is the major building block of the package and performs all the real-time tasks specified by the user. It has three subdivisions. The first one is in charge of test managing, system optimization, and loading control. The second one takes care of data acquisition and generates disk files of the test data. The third one performs the tasks of data display featuring a digitized multichannel load/pressure gauge monitoring system and an on-line high resolution graphics display of up to four different plots of the test results. The PLOT program as a postprocessor loads test data from disk data files, converts them to 20 quantities commonly used in geotechnical engineering, and plots curves of any two parameters selected by the user. Both log scale and linear scale are available for plotting with the options of either automatic scale adjustment or user-specified scale. Curves are displayed on the computer's high resolution screen and can be printed out on a dot-matrix

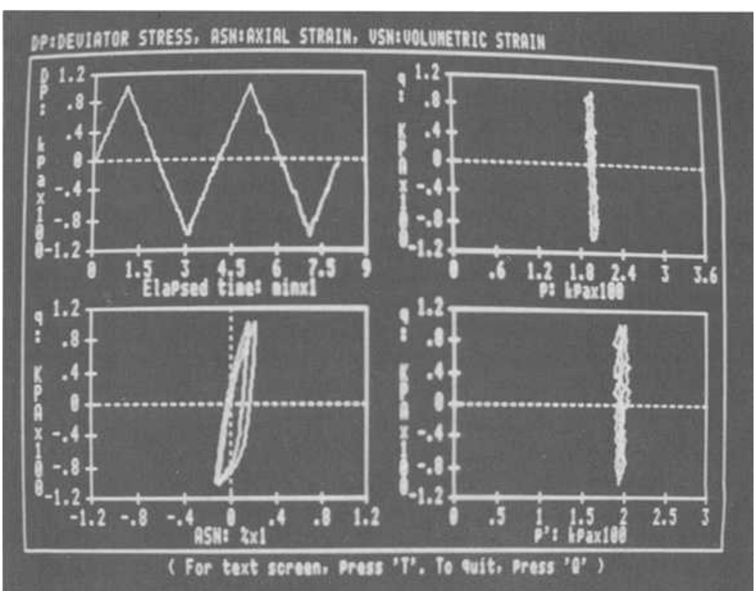

FIG. 5—*Real-time screen display of test results.*

printer. Additional features include a variable time-constant digital filter for data smoothing and a zooming option for greater detail of a specified portion of a curve.

The software is written in menu-driven mode and is user friendly. All operation steps involved in tests are displayed on the screen; a photograph of a typical real-time screen display of the data is shown in Fig. 5. Most of the interactions between the system and the operator are printed in a report-ready hard copy for documentation. The software is also modularly set up with a few spare slots to easily integrate any customized testing programs.

Typical Test Results

The automated triaxial testing system has been used in laboratory research for the past 3 years. Recently, an extensive testing program on the Leighton Buzzard 120/200 sand was carried out using this system. The Leighton Buzzard sand is a relatively uniform fine sand of subangular particles, the physical properties of which are tabulated in Table 1. The maximum and minimum void ratios are 1.03 and 0.65, respectively. Specimens of different densities were prepared by dry pluviation and were saturated using the high vacuum evacuation chamber. The B values of all the specimens tested were greater than 0.98. The cylindrical specimens were 63.5 mm (2.5 in.) in diameter and approximately 152 mm (6 in.) in height. A single 0.3-mm (0.012-in.) membrane was used. Because the D_{50} sand particle size is 0.09 mm, the problem of membrane penetration, according to Frydman and coworkers [3], can be ignored in pore water pressure response measurements.

Figures 6 through 12 show a variety of results for drained, undrained tests in compression, extension, or cyclic loadings. Results are plotted in the critical soil mechanics stress or strain spaces [4]. These plots are obtained from the plotter using the data retrieving and plotting software developed for this system.

In the shear loading tests shown in Figs. 6 through 12 the total mean normal stress was kept constant throughout each test. Figures 6, 7, and 8 give the response of a relatively loose specimen (D_r = 40%) under stress-controlled monotonic loading condition. Depending on the drainage conditions, either the pore pressure (Fig. 6 $\mu = P - P'$ measured between the total stress path of P = constant and the effective stress path) or the volume change (Fig. 7) readings were measured. The results clearly indicate that before reaching the phase transformation line, shearing of a specimen can cause decrease in volume (Fig. 7) or a corresponding increase in pore pressure (Fig. 6). However, as the specimen approaches failure, further loading will cause increase in volume and a corresponding decrease in pore pressure. Figure 8 depicts the response of an identical specimen in drained monotonic extension test. Comparing results in Figs. 7 and 8 it can be seen that the specimen failed at a lower load in extension than in compression, and consequently the failure envelopes in compression and in extension are different. Furthermore, no reversal of volume change during shearing is noticed in extension.

TABLE 1—*Physical properties Leighton Buzzard 120/220 sand.*[a]

D_{50} = 0.09 mm	
C_u = 1.29	
specific gravity = 2.65	
e_{max} = 1.03	
e_{min} = 0.65	
Unified Soil Classification:	SM

[a] C_u = uniformity coefficient; D_{50} = diameter at which 50% of the soil is finer; e_{max} = void ratio of soil in loosest condition; e_{min} = void ratio of soil in densest condition.

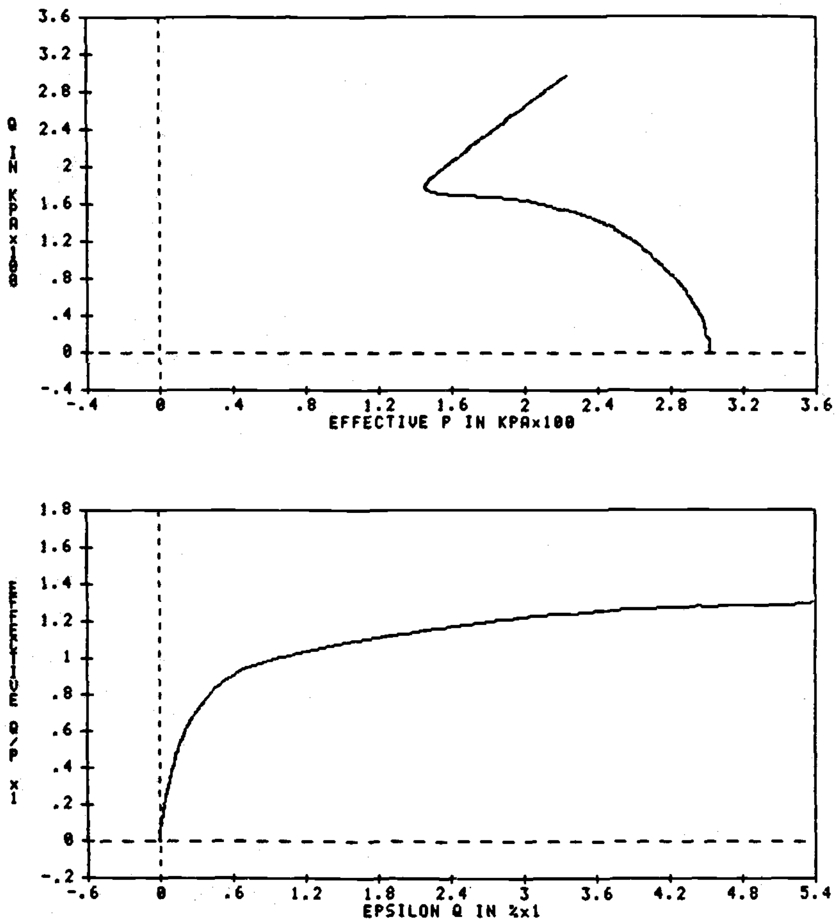

FIG. 6—*Undrained monotonic compression test—stress control* (D_r = *40%*, σ_{30}' = *300 kPa*).

Figures 9 and 10 are strain-controlled undrained test results under monotonic loadings. Figure 9 shows the response of a dense specimen (D_r = 80%). A very rapid rise in shear resistance is shown at the beginning followed by a large buildup of pore pressure, thus a reduction in effective confinement. However, as it reaches the phase transformation state, the pore pressure decreases with further deformation causing an increase in shear resistance. Figure 10 shows the results of a very loose and unstable specimen (D_r = 5%). Such information is best obtained by strain-controlled testing. The shear stress–shear strain curve shows the peak shear resistance and the sudden drop of resistance (softening) as the unstable assembly of particles collapsed. The effective stress path in the P'–Q space indicates a continuous decrease in shear resistance as a result of pore pressure buildup (or a reduction in effective confinement) in the specimen. At zero confinement, a small amount of shear resistance (approximately 7.5 kPa) is maintained. It is worthy to note that the peak shear resistance for this specimen is associated with a small shear strain (less than 0.5%). It would be difficult to record the response accurately if no feedback control and electronic data acquisition systems were used.

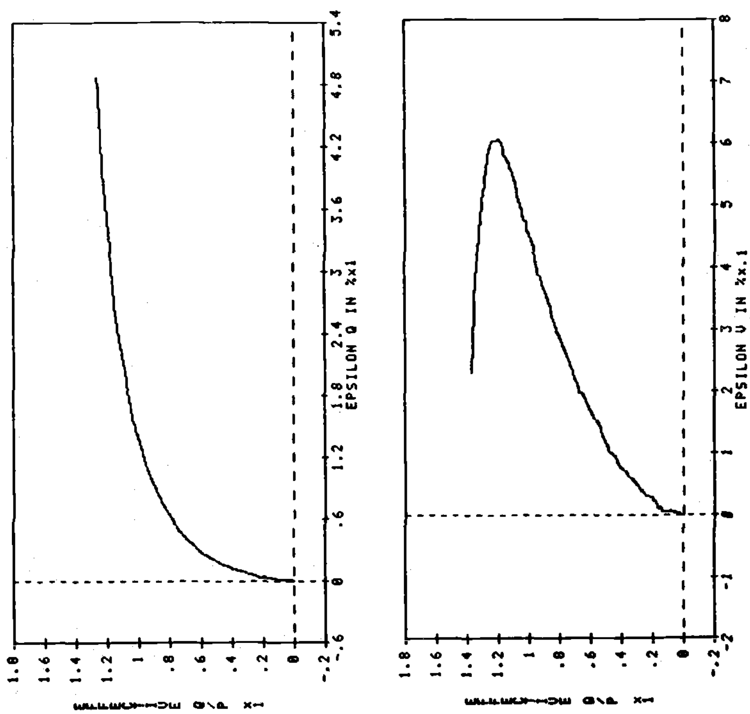

FIG. 7—*Drained monotonic compression test—stress control* (D_r = *40%*, σ_{30}' = *300 kPa*).

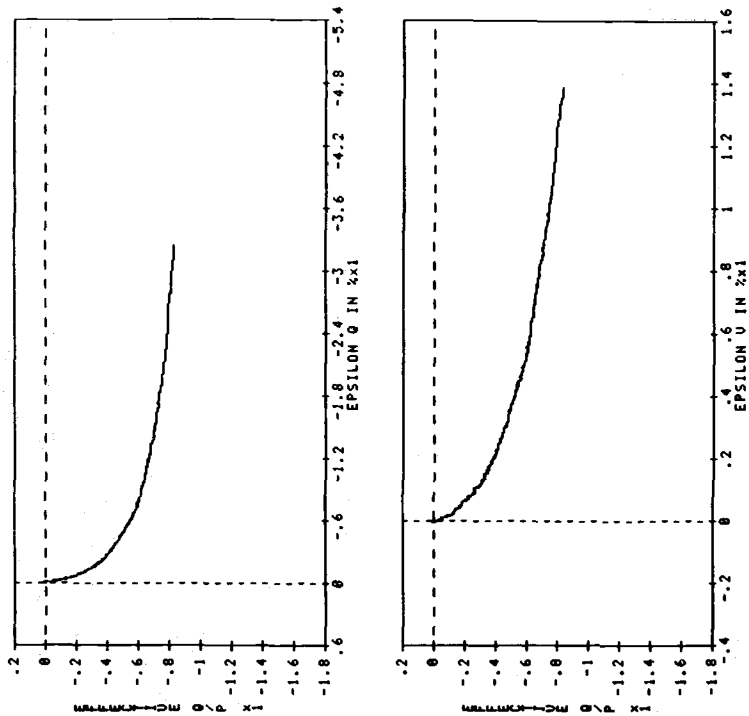

FIG. 8—*Drained monotonic extension test—stress control* (D_r = *40%*, σ_{30}' = *300 kPa*).

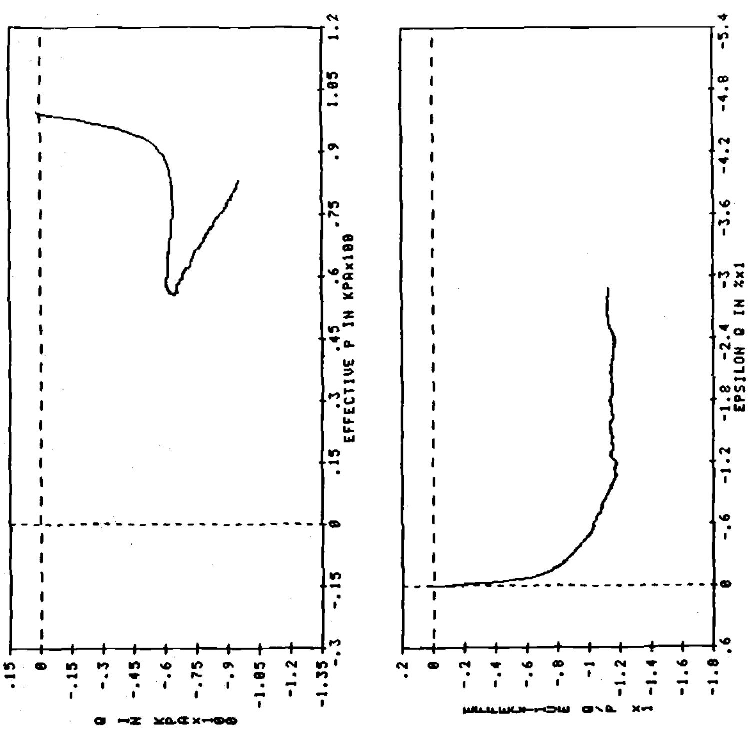

FIG. 9—*Undrained monotonic extension test—strain control* (D_r = 80%, σ_{30}' = 100 kPa).

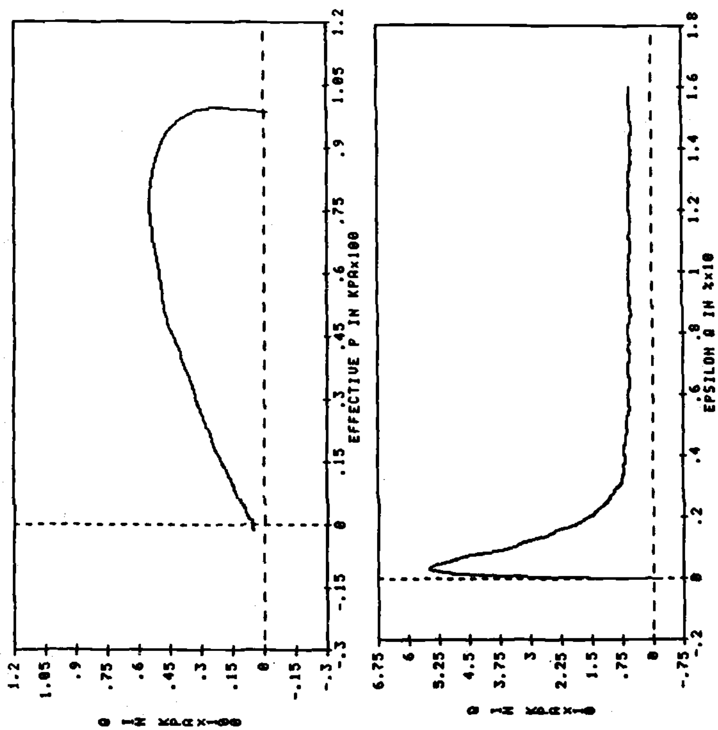

FIG. 10—*Undrained monotonic compression test—strain control* (D_r = 5%, σ_{30}' = 100 kPa).

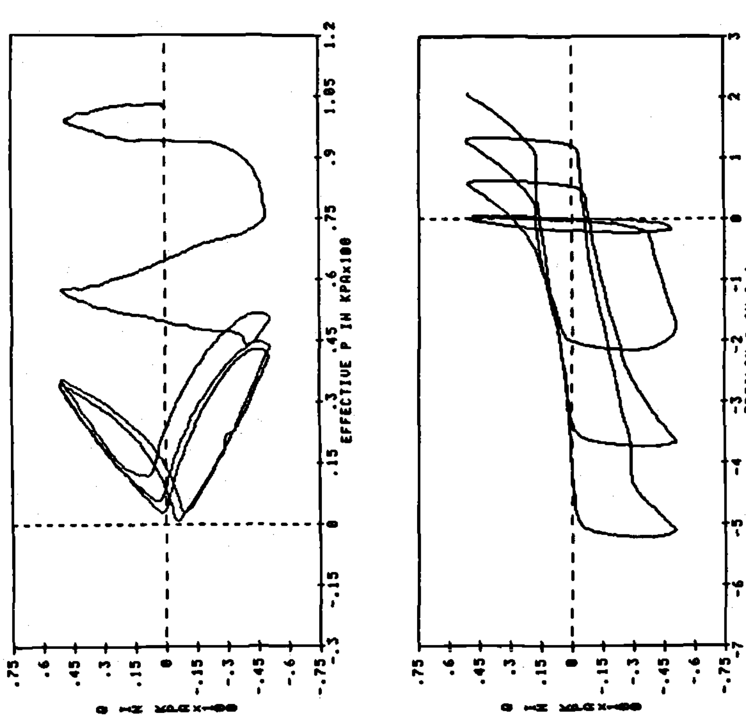

FIG. 11—*Constant P undrained cyclic loading test—stress control* (D_r = 40%).

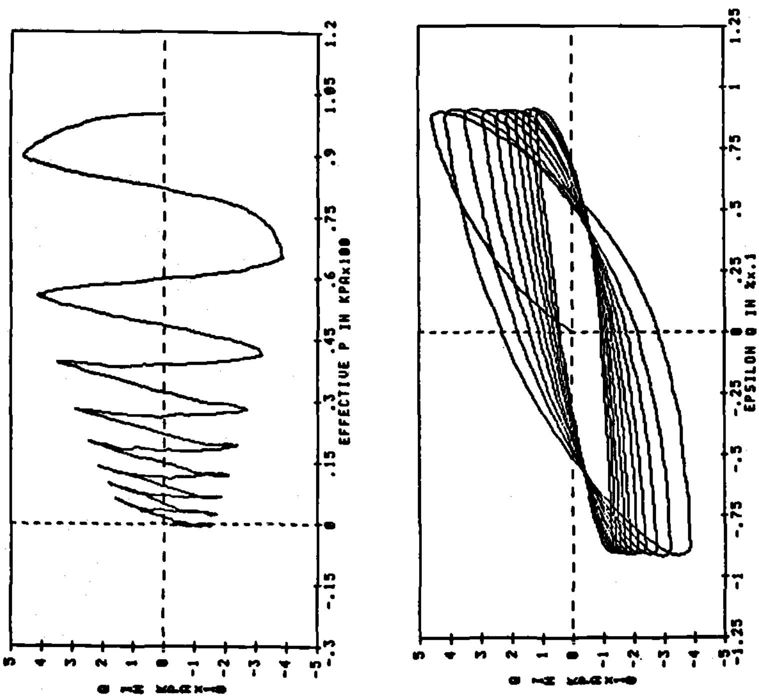

FIG. 12—*Constant P undrained cyclic loading test—strain control* (D_r = 40%).

Figures 11 and 12 are examples of cyclic shear loading test results (p = constant). Preliminary investigation on pore pressure measurements indicates that a frequency of loading of one cycle per minute or slower is needed to ensure equalized pore pressure readings; therefore, all cyclic loading tests were performed at a loading rate of one cycle per minute. Figure 11 is the result of a stress-controlled test on a loose specimen. The effective stress paths and the shear stress–shear strain loops are presented. Large shear strains are associated with stress paths approaching the phase transformation line under very small effective confinement. The shear strain buildup is slow and gradual before that. Figure 12 shows the results of an identical specimen tested under strain-controlled cyclic shear loading. The reduction in shear resistance with increasing loading cycles is evident.

The examples illustrated above are typical results of commonly prescribed tests for triaxial testing. Other less traditional tests, such as the constant stress ratio (Q/P') path test or more complex stress path tests can also be performed using the automated system.

Conclusion

This paper describes a new development in triaxial testing of geotechnical materials. The adoption of microprocessor-controlled loading conditions and the use of electronic instrumentation for data acquisition and processing using specially written software programs have elevated the practice of laboratory testing in geotechnical engineering to a new environment. This is particularly significant because more detailed stress–strain relations and sophisticated stress paths are required in the development of constitutive models for soils. Because the system is simple in operation and the cost is affordable (approximately $25 000), the geotechnical material testing laboratories can also benefit from the new system.

The software package is capable of handling almost all the routine work involved in triaxial testing (that is, loading, data recording, data processing, plotting, and graphing). It thus has changed the nature of the labor-intensive geotechnical laboratory work to a high-tech type operation. Indeed, the authors envision that microcomputers can be used to benefit all aspects of the geotechnical profession; however, its major impact lies in the development of portable and versatile systems suitable for laboratory and field use.

Acknowledgments

This research was partially supported by grants from the National Science Foundation (CEE-8311722, CEE-8507402). The authors are grateful for the support. The authors would also like to express their appreciation to H. W. Yang and Z. J. Shi for performing the laboratory tests.

References

[1] Chan, C. K., "An Electropneumatic Cyclic Loading System," *Geotechnical Testing Journal, ASTM*, Vol. 4, No. 4, Dec. 1981, pp. 183–187.
[2] Chan, C. K., "Low-Friction Seal System," *Journal of Geotechnical Engineering Division, ASCE*, Vol. 101, No. GT9, Sept. 1975, pp. 991–995.
[3] Frydman, S., Zeitlen, J. G., and Alpan, I. "The Membrane Effect in Triaxial Testing of Granular Soil," *Journal of Testing and Evaluation*, Vol. 1, No. 1, Jan. 1973, pp. 37–41.
[4] Schofield, A. M. and Wroth, C. P. *Critical State Soil Mechanics*, McGraw-Hill, London, 1968.

Malcolm Reeves[1]

Microcomputer-Based Data Acquisition Systems for Triaxial Testing of Soft Yielding Rocks

REFERENCE: Reeves, M., "**Microcomputer-Based Data Acquisition Systems for Triaxial Testing of Soft Yielding Rocks,**" *Advanced Triaxial Testing of Soil and Rock, ASTM STP 977,* Robert T. Donaghe, Ronald C. Chaney, and Marshall L. Silver, Eds., American Society for Testing and Materials, Philadelphia, 1988, pp. 107–118.

ABSTRACT: The structure and design of a generic, device-independent, set of software data acquisition and control routines for long-term rock mechanics monitoring are described. The routines are designed for an Intel 8086/8088-microprocessor-based microcomputer running under the MS-DOS[R] (Microsoft Disk Operating System). It is assumed that the rock will undergo long-term, slow deformation rather than rapid elastic rupture, and the routines are designed primarily for low strain rate and creep/consolidation testing.

The main features of the package include instrumental drift compensation, inputs from multiple interfaces, on-line configuration changes, complex control functions based on multiple sensor values, automatic elimination of erratic sensors, background acquisition and control, and on-line real-time graphics.

KEY WORDS: data acquisition and control, microcomputer, software, rock mechanics testing, creep, consolidation

All data acquisition and control (DA&C) systems consist of two distinct, strongly interdependent parts: hardware (microprocessors, sensors, amplifiers, counters, and so forth) and software (protocols, instructions, and so forth). Although good software can compensate for many hardware deficiencies, excellent hardware can be crippled by inadequate software.

In very general terms, the prime design requirement for testing soft rocks at low strain rates is long-term reliability rather than raw acquisition speed. A second important consideration is economy. Many of the elements used to build a system (transducers, signal conditioners, dumb loggers, and so forth) may be available from previous projects; important cost savings can be made by making full use of pre-existing resources.

The Geological Engineering Laboratories of the University of Saskatchewan (GELUS) have cooperated with the Saskatchewan Research Council (SRC) to develop and test various microcomputer-based DA&C systems for triaxial testing of soft yielding rocks.

A basic DA&C system comprises six stages: signal acquisition, signal conditioning, analog-to-digital (A–D) conversion, signal transmission, signal processing, and data storage. Much of the detailed design work is device or system specific and as such is not of general interest. An attempt has been made to discuss the problems in generic terms and to avoid detailed descriptions of the idiosyncracies of specific instrumentation. One exception to this rule is the discussion of microcomputers. Discussion assumes that an IBM-PC or compatible mi-

[1] Professor of Geological Engineering, University of Saskatchewan, Saskatoon, Saskatchewan, Canada S7N 0W0.

crocomputer, running under MS-DOS, is used to operate the various DA&C devices [1–5].

Objectives

The primary objective of the ongoing study is to develop a largely device-independent collection of DA&C software to log and control a wide variety of experimental laboratory tests on soft rocks. The adjective "soft" implies that the system must record large strains and long-term, time-dependent, creep/consolidation response for weak yielding materials. A somewhat different approach is needed for collecting data and controlling tests on elastic rocks in which very rapid strain-softening behavior is anticipated.

There are some major advantages in developing flexible device-independent software. It is extremely cost-effective to train research students and technicians to use a single software package which readily interfaces with all sensors and instruments in the laboratory and can be used for every experiment. Device-independence means that the laboratory is not tied to a single equipment supplier and that independent comparisons can be made of hardware combinations.

A second reason for developing custom software is that much vendor-provided software imposes limits on hardware performance and does not support all hardware configurations. That is, flexibility is lost when such software is used. This may not matter for many routine applications but in research laboratories flexibility is essential.

A number of independent software vendors have attempted to provide generic DA&C packages to perform simple logging and control. The usual difficulty with such packages is their relatively limited flexibility in experimental control. Control algorithms must be very simple, and for many rock mechanics tests this is not the case (especially if the control variables are effective stresses). A further difficulty can arise with such packages if it is necessary to use data from several different logging and control devices in the same experiment.

Despite these limitations, custom software is a last resort if and only if neither the vendor-supplied software nor a generic package will perform the necessary acquisition and control tasks. If such packages fully meet the laboratory need it is foolish (and very expensive) to write custom software.

Rock Mechanics Testing Equipment

Three rock mechanics test rigs have been instrumented to various degrees for automatic data acquisition and/or control. In all cases the axial and confining pressures are applied through independent gas-pressurized, hydraulic-oil systems. Although the three test rigs vary in their operational pressure ranges, specimen-size capability, and the degree of control and monitoring currently possible, from a DA&C viewpoint they are conceptually very similar and all can be (and have been) controlled by the same generic software.

The SRC large specimen triaxial test facility [6] comprises ten large pressure cells capable of testing specimens with diameters up to 200 mm and lengths up to 400 mm. Axial pressures of up to 70 MPa can be applied through hydraulic pistons, and confining cell pressures of up to 50 MPa can be attained. Pressures may be controlled by air-actuated solenoid valves which switch to a series of pressure accumulators and bleed lines. Axial and radial strain measurements can be made, and rudimentary room temperature control (heat but no refrigeration) is possible. The practical limit of axial strain measurement is in excess of 25%.

The GELUS laboratories have a single large sample triaxial test rig which can test specimens of up to 100 mm in diameter with lengths of up to 200 mm. Axial and confining stresses up to 70 MPa are possible with a maximum practical axial strain of 10%. Axial and confining pressures may be controlled by manual air regulators. Pore pressures and volume change measurements are possible, but temperature control is not available for this cell at the present time.

The small triaxial test rigs [7] will test specimens with diameters up to 50 mm and lengths of up to 100 mm. The rigs are housed in a controlled-temperature room which can be maintained at temperatures between +40 and −40°C with a precision of less than 0.1°C. Axial, confining, and pore pressures may be controlled by nitrogen regulators or by solenoid valves through independent pressure accumulators. Pore pressure can be measured automatically, but volume change measurement has yet to be automated.

Figure 1 shows a composite system illustrating all logging and control possibilities in the three test rigs combined. Software development has proceeded under the assumption that all test rigs may eventually be equipped with all control and logging sensors shown in Fig. 1.

Data Acquisition and Control Hardware

The GELUS system uses the Tecmar Labmaster TM40-PGL card which has analog and digital input/output (1/O) analog-to-digital (A–D) conversion, and five independent timers. The card plugs directly into the microcomputer bus and is attached to an external analog-to-digital converter (ADC) module which receives the signal cables.

The SRC laboratory uses a DAS-Keithley Series 500 system, a modular DA&C system which has analog input and conditioning, digital 1/O, and A–D conversion capability on separate modular cards linked through a proprietary bus to the PC bus.

Both systems can be memory-mapped so that instructions to the DA&C system are sent to user-selectable specific addresses in the PC. The Tecmar card can also be 1/O mapped through user-selectable port addresses. Although the systems provide enormous flexibility in configuration options, in both cases the software provided by the vendors does not fully support this flexibility.

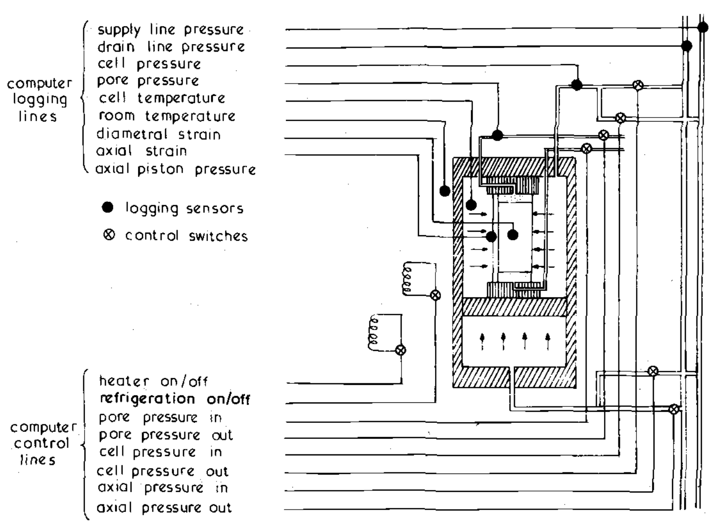

FIG. 1—*Composite schematic of logging sensors and control switches for experimental control.*

Signal Acquisition—A wide variety of sensors are used in the SRC and GELUS laboratories with analog signal output ranges from 10 V to as little as 30 mV. Sensor precisions are between 1 and 0.25% of full range. Excitation voltages are supplied using stabilized 10 or 15-V variable power supplies. All "floating" differential signals are provided with a resistor to ground to prevent absolute voltages drifting outside the range of the ADC.

Signal Conditioning—Signals in both GELUS and SRC laboratories are routinely acquired through a low-pass filter prior to amplification to remove "mains noise" [*2,5,8*]. Additional filters are implemented, either in hardware or software, to prevent the aliasing of low frequencies due to high-frequency noise. Both commercial and "in-house" signal-conditioning units are used. Some signals are preamplified, but all signals pass through a second-stage, multiplexed, software-controlled, variable-gain amplifier immediately prior to A–D conversion. Very low-level signals (less than 100 mV full scale), such as strain gauges and some pressure transducers, are conditioned by bridge amplifiers.

Analog-to-Digital Conversion—Both systems have 12-bit A–D conversion capability and will accept signals with input ranges as low as +20 mV and have a maximum input range of +10 V. Both systems seem to lose about one to two significant bits because of problems with linearity and hysteresis (especially at very high amplifier gains) although the problem may lie in the "in-house" part of the signal-conditioning system. Such losses are not unexpected and do not cause any real concern.

Very few rock mechanics applications require precision better than 0.5% (of full-scale) which can be achieved readily with any 12-bit system. The same precision can be obtained with an 8-bit system by using a computer-controlled analog output signal as a variable dc offset. This technique of changing the range in which a sensor is read is useful in long-term strain measurements in which a precise time derivative rather than accurate absolute strain value can become important. Problems can arise with this procedure if the offset voltage and the signal to which it is applied are not closely grounded. The offset voltage must also be very stable. Some analog output signals may not be satisfactory in terms of long-term stability.

RS-232C Serial Transmission—In addition to the ADC I/O card, both SRC and GELUS DA&C systems use RS-232C serial loggers and instruments to acquire data. These devices have to be interrogated using device-specific codes and sometimes even require different cables.

The RS-232C interface is a bit-serial interface which has been used widely for direct digital output from many instruments including data loggers. Because such devices (especially data loggers) often provide excellent analog signal conditioning, multichannel simultaneous sample and hold capabilities, and A–D conversion, it is often very cost-effective to incorporate them into a DA&C system.

Many microcomputers are provided with RS-232C communications ports as standard, so a complete RS-232C network can be configured from existing equipment without any capital outlay if loggers and microcomputers are available from previous projects.

RS-232C interfaces have some major limitations and disadvantages to weigh against their widespread availability [*1*]. There is no real RS-232C standard so cabling and communications protocols may be different for each individual device. The ability to verify transmitted data is limited, and in many cases no checking is possible. Because data are transmitted bit by bit, transmission is slow. Despite these problems, RS-232C transmission has a very important advantage in that information can be transmitted over long distances using inexpensive cables or telephone lines.

For rock mechanics applications, transmission of digital data from several remote, multichannel loggers to a distant central microcomputer may make an excellent DA&C system. Such an option is particularly attractive if existing data loggers and aging microcomputers can be used as the remote devices and incorporated into a laboratory-wide system reducing the rate at which equipment must be discarded.

GPIB (IEEE-488, HPIB) Transmission—The general purpose interface bus (GPIB) is a byte-serial, bit-parallel interface with a bus structure which has become widely available as a digital interface for many data loggers and instruments since its introduction in 1978. It has four very important advantages as a communications interface [*1*]. It is very resistant to electromagnetic noise, allows true simultaneous data acquisition and control, is fast (throughputs > 75 kHz for 12-bit data), and is a true standard (all GPIB cables are pin compatible and bus signal protocol is standardized).

The interface has the disadvantage that cables can be no longer than 20 m unless expensive line-drivers are used, and thus, in common with ADC I/O cards which plug into the microcomputer bus, it requires the computer to be close to the sensors.

For many rock mechanics applications, the real advantages of the GPIB cannot be exploited because problems with speed, true concurrent readings, and noise-free transmission are not usually serious limitations. One major advantage of the GPIB is the large amount of tried and tested hardware and software already available.

Although no GPIB-interfaced equipment is used in the GELUS and SRC laboratories at present and none of the laboratory computers have GPIB ports, the generic software package is being developed to support this interface. Many generic software packages support GPIB I/O in a variety of high level languages.

Control Aspects—Control systems, as opposed to simple logging systems, can make decisions based on the incoming data and act on those decisions. The action may often be simply to change the sampling frequency for some sensors or to save or discard a particular set of logged data. More sophisticated decisions may involve abandoning sensors that give erratic data or signaling an alarm condition. Such actions may involve output from an RS-232C port or GPIB port or just setting a single logic voltage high or low to trigger a switch.

Both the Tecmar and DAS-Keithley ADC I/O cards have digital I/O (and even analog output) capability. Digital I/O capability is important so the computer can set and read logical signals (switches). These I/O signals can be used to trigger or read the status of hardware switches.

In the control system logic for long-term testing it is important that the computer has a preprogrammed reaction for every possible condition. Because it is difficult to think of every possible combination of events, the equivalent is achieved in practice by having a default action if none of the preprogrammed conditions occur. The GELUS software relinquishes all control but continues to log all channels if an unforeseen control condition occurs. As experience is gained, more conditions will be preprogrammed and fewer default conditions will occur.

Signal Processing—Software must be able to read and store data in random access memory (RAM) as fast as it can be presented to the microcomputer interface by the ADC.

By writing many frequently used low-level routines in assembler, there is considerable scope for data processing during acquisition because neither the central processing unit (CPU) nor the data bus are "busy." This is a possibility only for low-frequency acquisition and control and requires careful programming to avoid wasting processor time. Reasonably efficient software can exercise very complex and reliable control at frequencies of around 1 Hz.

Real-time graphics are possible for pressure, stress, strain, displacement, and similar low-frequency data. As data acquisition frequencies increase, the scope for such options is diminished.

Data Storage—The speed of the system is determined by the maximum rate at which all the necessary data channels can be read and, where appropriate, stored; and all the control triggers can be tested and, where appropriate, action taken. It is a combination of hardware and software performance.

For an on-board A–D interface on an 8086/8088-based PC the frequency with which a single channel can be read is typically 20 kHz for 12-bit data so that information is provided at the rate of (20 × 12 =) 240 Kbaud (Kbits/s).

For an RS-232C serial logger with on-board 12-bit A–D conversion, data transmission will involve at least 5 ASCII (American Standard Code for Information Interchange) bytes per channel (40 bits assuming no channel identification codes are sent and minimal message checking). Thus assuming a data transmission rate of 9.6 Kbaud, the corresponding acquisition frequency is less than (9.6/(5 × 8) =) 0.24 kHz. For long distance transmission a more realistic baud rate is 1.2 Kbaud, and data acquisition throughput is reduced to 30 Hz or less.

A GPIB can send or acquire data by direct memory access (DMA) at rates in excess of 2 Mbaud corresponding to a sampling rate of (2000/(2 × 8) =) 125 kHz for binary data or about (2000/(5 × 8) =) 50 kHz for ASCII transmission. These transmission rates assume that they are supported by the logger signal conditioning and A–D conversion hardware. A realistic expectation for throughput is 30 kHz.

An ADC I/O bus card and a GPIB-interfaced logger have comparable acquisition capabilities of between 20 and 30 kHz, whereas ASCII RS-232C serial devices at 1.2 Kbaud are limited to less than 30 Hz.

Maximum data sampling rates were estimated for acquiring data in random access memory (RAM), not onto disk. The longest continuous sampling period is limited by the size of the computer RAM which is typically between 512 and 640 KB.

Maximum disk transfer rates to save data are 300 Kbaud for floppies and 5 Mbaud for hard disks although typical transfer rates are somewhat less than these maxima. Where speed is important, data must be buffered in RAM because every disk start/write operation has an overhead (300 ms for floppy disk; 15 to 100 ms for hard disk).

These hardware considerations are by no means insignificant when estimating the overall performance of a DA&C system, particularly for GPIB and ADC I/O data bus cards (where the potential acquisition rates are comparable with hard disk transfer rates). For bus systems, the disk transfer rate limits continuous acquisition rates to permanent disk storage. For RS-232C serial acquisition, the disk transfer rates can be ignored because the transmission baud rate is the factor limiting the effective acquisition rate.

Software Design

The software under development has been tested on the IBM-PC and a number of compatible microcomputers under various versions of MS-DOS. The software package comprises six modules, each containing routines with specific purposes:

(1) system description,
(2) data acquisition,

(3) signal sampling,
(4) control functions,
(5) data storage, and
(6) on-line display.

Figure 2 shows the generalized structure of the software package. There are several data areas and buffers which are read from and written to by various modules. In general only one module has write access to each data area although many routines can read the data from the various buffers. The disk output buffer is eventually physically written to disk by the operating system and forms the permanent record of the experiment. All other buffers are circular, operating on the first in first out (FIFO) principle.

Background Processing—It is possible to run some low-level logging and control tasks in "background" on the 8086/8088 processor by using an interrupt to switch between "tasks."

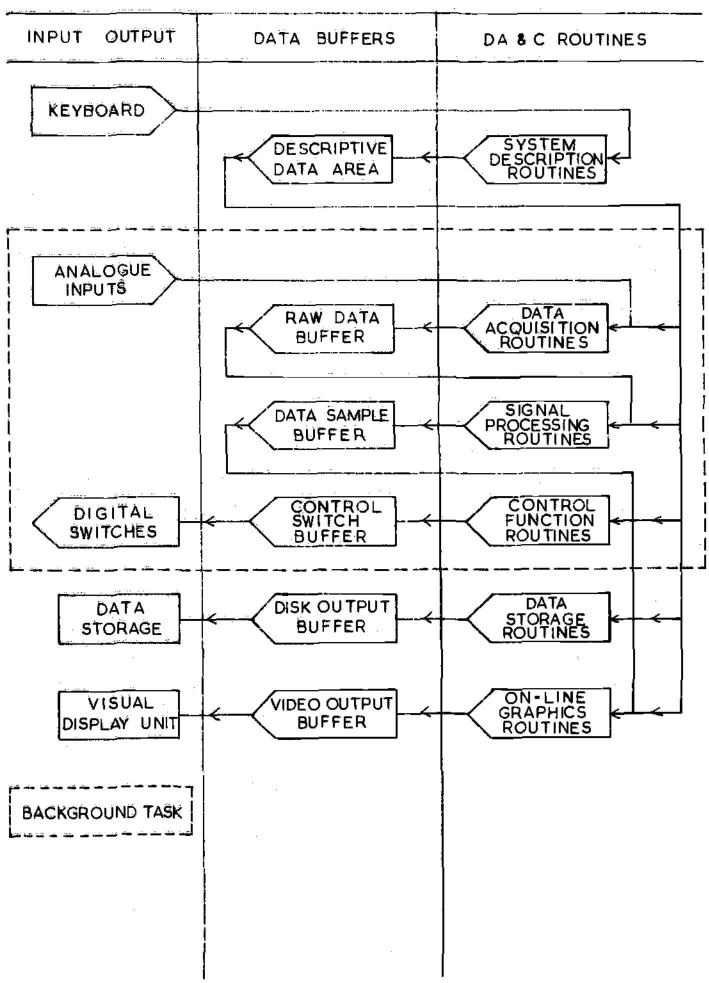

FIG. 2—*Generalized flow-chart for data acquisition and control software.*

This "time-slicing" procedure allows the PC to switch between logging and control routines and the main program which either displays on-line graphics or accepts keyboard input. The user clock tick interrupt which is automatically called 18.2 times per second by the ROM-BIOS time-of-day clock can be used for this purpose [9]. The GELUS logging and control routines "capture" this interrupt and provide the DA&C services.

For logging and control, the clock tick interrupt vector points to a routine including a call instruction which is reset by each DA&C routine on exit to point to the next step in the DA&C cycle. This sequencing can be disrupted if a nonmaskable interrupt (NMI) is received as the call instruction is changed. To avoid this, a second copy of the call instruction is provided for use as a check. The NMI is active in DMA and 8087 usage.

System Description Routines—The system description routines prompt the user to describe the hardware in use and the experiment to be carried out. A series of interactive menu-driven routines allow the user to provide the system with a description of loggers, controllers, sensors, and test procedures.

The description of the system is a fairly complex data structure and is most readily programmed in a language that readily accepts such structures. For microcomputer implementation the Pascal or C languages are obvious choices.

The system description routines interrogate the user for data which are placed in the various data areas or buffers for reference by other routines.

Data Acquisition Routines—Because each sensor may be attached to any I/O memory-mapped logger channel, the data acquisition (DA) routines must be provided with this information by reading from the appropriate data area. Low-level routines are required to perform the very frequent tasks of checking the time, addressing a sensor, and acquiring a value or series of values ("burst"). The DA routines write bursts of data into a number of buffers which are read by the sampling routines.

The major requirement for the acquisition algorithms is that they execute very quickly. Such routines are generally written in assembler and are usually supplied by equipment vendors. Whether a device is memory mapped or I/O mapped, acquisition routines involve assembly of one or more data bytes which are written or sent to port or memory addresses. These bytes identify the channel and sometimes the amplifier gain setting, and start the A–D conversion. Other addresses are read to check whether the data are available and then to recover the data.

A generic acquisition routine has been written which can be customized for various devices by supplying the appropriate addresses and data bytes through the system description routines. The routine will also read and write to an RS-232 serial port, an 8-bit parallel port, and a GPIB parallel port when supplied with the correct sequence of addresses and data bytes.

Additional routines have been written for setting and reading a time-of-day clock and calendar and to enable interval timing using up to five counters. One timer can be used to generate a periodic hardware interrupt to drive the foreground/background "multitasking" instead of the BIOS clock tick interrupt.

To allow continuous calibration of the variable gain amplifier, one logging channel per logging device may be devoted to monitoring an analog voltage of known level which can be varied under computer control. This allows some continuous compensation for instrumental drift and provides a check that the analog I/O functions are operating consistently. Switching off the analog input voltage for this channel can be programmed to cause immediate suspension of all control functions (because the computer thinks the sensor has failed). It also (fortuitously) provides a useful "panic" button to rapidly shut down an experiment without losing data because logging will continue uninterrupted. Unused analog input channels must be shorted to ground and may be read by the computer through the variable gain amplifier to check for zero shift.

Signal Sampling Routines—Sampling A–D channels at low frequency involves calling the DA routines repeatedly. Collection of a burst (an uninterrupted sequence of values) may be triggered by a timer, a control signal, or the time-of-day clock. A sample is defined as a group of bursts separated in time which are combined to give a single sample value. The sampling routines read from the raw data buffers and write sample values and time derivatives to the sample buffer.

There are a large number of ways in which bursts can be collected and combined to give a sample value. The simplest is of course to collect only one burst comprising one value. The GELUS software collects sufficient data in a burst to provide reliable estimates of first and second time derivatives because these values are used to check sensor performance and integrity.

Sensors attached to RS-232 devices will degrade overall throughput unless they are interrogated less frequently than the faster bus devices. Many RS-232 loggers are sufficiently intelligent to transmit time-averaged samples (not values), and these can be passed directly to the sample buffer.

The number of bursts, the length of a burst, the frequency with which bursts are collected, and the way in which bursts are combined to arrive at sample values and derivatives can be determined by experiment but are ultimately limited by the amount of time available for signal acquisition between samples. Low-frequency DA&C (for example, less than 0.1 Hz) allows a considerable amount of flexibility in this area.

Sampling algorithms involve significant amounts of floating-point arithmetic which is tedious (but not impossible) in assembler. Because control in rock mechanics experiments does not have to be exceptionally fast, these algorithms use the 8087 math coprocessor through FORTRAN-77, which provides a large library of tried and tested signal processing routines for averaging and filtering.

Control Function Routines—Control algorithms are used to decide on the settings of digital switches which open and close hydraulic and electric circuits. The control routines use the sampling routines (which in turn use the low-level acquisition routines) to determine the value of a control function. Because such functions run the experiment, the data passed from the sampling routines to the control routines must be as reliable as possible. The derivatives collected by the sampling routines are read from the sample buffer and are used to predict the expected next value, and control functions will only operate if the control request is consistent with the prediction. The verified control data are written to the control switch buffer and then to the appropriate port or memory addresses.

The routines work well with yielding and creeping materials because the expected stress and strain versus time behavior is reasonably continuous. Control has been maintained for continuous periods of several months without operator intervention.

For recording and controlling elastic failure the GELUS routines require some modification to increase the speed of execution. This is not a serious problem in the GELUS and SRC laboratories because the control solenoid valves on the hydraulic lines do not respond fast enough to follow the postfailure behavior of a hard rock. The switching hardware limits control frequencies to no more than about 0.1 to 0.5 Hz.

Control limits may be the actual value V or the first derivative dV/dt. In the case of gradient control, the second derivative is used to predict the next value of dV/dt. This enables control of total or effective stress rates and linear or volumetric strain rates as well as stresses and strains.

Several control functions can be active simultaneously, but the system description routines will refuse to accept experiments with mutually exclusive control functions. Constant temperature deformation, with no volume change at constant axial strain rate, is acceptable if and only if all the necessary sensors for control have been described.

Even if the control routines have had the necessary sensors and switches described, if a control function cannot be calculated, perhaps due to sensor failure or when a control operation ceases to provide the expected response, the experiment will be abandoned. Abandonment involves the cessation of all control operations having ensured that all switches are in their preprogrammed "failsafe" condition. All logging functions continue until aborted by the user.

Such problems are inevitable so the experiment description routine allows the user to specify what to do if any of the control functions are lost. That is, some control functions can be identified as critical and others as expendable.

Data Storage—Data is stored temporarily in circular RAM buffers and more permanently on hard or floppy disk. Circular buffers are used to collect bursts of data which are processed to give sample values and derivatives. The sample values are copied from the sample buffer to the disk buffer when predetermined trigger conditions are satisfied. The disk buffer is physically written to disk by MS-DOS and is not flushed for every software write operation. This involves a slight risk in that the buffered data will be lost in a power failure.

A–D conversion data are acquired as 12 bits but are stored in a temporary buffer as a 2-byte integer. When written to disk with a high level language in a form suitable for post-processing, the data use up to 6 bytes of ASCII code. It is all too easy to acquire vast amounts of irrelevant data.

The system description routines convert all control variables to 12-bit integers for the signal processing and control routines so that all "fast" operations use raw signal values. Conversion to engineering units can be optionally requested prior to output to disk. This is not recommended because time is lost in conversion and valuable disk space is wasted. Postprocessing programs can readily carry out such conversions and for long-term experiments (even without expansion) data volumes can be very large.

In the GELUS program, the user can select the variable that controls when data are saved and written. Equal intervals of time, stress, strain, volume change, temperature, and so on can be specified. The default is time intervals of 6 minutes, but both the interval and the trigger variable are changed easily at any time during an experiment and are automatically adjusted when the program detects a problem.

On-line Display—Data can be displayed on-line as a "strip-chart" type graph or as a "odometer" type counter or both. All graphics calls use "in house" Turbo Pascal routines which support a variety of video devices including the IBM color graphics, adapter, Hercules graphics card, AT&T PC 6300 adapter, and the IBM-enhanced graphics adapter.

Up to eight channels can be displayed at one time during logging and control operation. The channels displayed can be changed during an experiment, or the display can be suppressed. For high-frequency data, on-line graphics limit the effective logging rate to about 10 Hz when eight channels are displayed as a "strip chart." No facility is provided for hard copy because the display is mainly intended for testing sensor response and calibration. About 600 samples are displayed on the screen at any time for each channel.

The video display can be reduced to show a single channel and magnified to increase the signal amplitude. This is useful in seeking out "noisy" sensors and checking response sensitivity.

The on-line graphics routines use by far the most time in the logging and control cycle. The GELUS software assigns internal priorities to requests for logging, control, permanent data storage, and on-line data display. The strategy is to abandon data display when more urgent tasks require processing time so that as more sensors are added, the time available for on-line graphics is reduced. The programs tell the user whether or not the requested functions are possible in the available time and suggest options.

Postprocessing—Data are transferred to the disk buffer and eventually to disk for permanent storage. The data are written in a simple compact form readily accepted by most spreadsheet programs as comma-separated values (CSV). No headers or any other nonessential data are written, but such files can readily be expanded. Because spreadsheet programs provide a powerful means of processing and displaying multichannel data, the GELUS DA&C package does not include any postprocessing arithmetic or graphics routines.

Summary and Conclusions

A generic set of data acquisition and control routines are under active development for long-term triaxial testing of soft yielding rocks. The routines are designed to be as device independent as possible so that data from many diverse sources can be collected and used for control. Whenever possible, existing software has been incorporated into the package (for example, signal processing, graphics, and postprocessing).

Because rock mechanics triaxial data are low frequency, a large amount of real-time signal processing can be incorporated to enable sophisticated experimental control. Sensor readings can be anticipated by extrapolation techniques, and extensive performance checking can be carried out.

User-selectable default instructions may be executed when the specified experiment can no longer be continued (due to sensor and/or specimen failure). Unpredictable sensors can be eliminated from control calculations, and self-test and calibration routines are available to check the correct functioning of signal-conditioning hardware and to compensate for drift.

Pseudosimultaneous control may be exercised over several simple functions of stress, effective stress, pore pressure, axial strain, diametral strain, volumetric strain, or temperature, and their first time derivatives (provided such functions are not mutually exclusive).

Control of elastic failure cannot be achieved with the GELUS or SRC laboratory control valve systems although the DA&C software and hardware can operate at much higher speed than that necessary for control of yield and creep failures.

References

[1] Clune, T. R., "Interfacing for Data Acquisition," *Byte*, Vol. 10, No. 2, 1985, pp. 269–282.

[2] Englemann, W. and Abraham, M., "Personal Computer Signal Processing," *Byte*, Vol. 9, No. 4, 1984, pp. 94–113.

[3] Ford, L. E., "Laboratory Interfacing," *Byte*, Vol. 10, No. 2, 1985, pp. 263–266.

[4] Gates, S. C., "Laboratory Data Collection with an IBM PC," *Byte*, Vol. 9, No. 5, 1984, pp. 366–378.

[5] Wyss, C., "Planning a Computerized Measurement System," *Byte*, Vol. 9, No. 4, 1984, pp. 114–123.

[6] Reeves, M. J., "Evaluation Large Sample Triaxial Test Facility: A Progress Report," *Proceedings*, Twenty-sixth U.S. Symposium on Rock Mechanics, Rapid City, SD, 1985, pp. 1033–1040.
[7] Penner, L. A. and Reeves, M. J., "Fracture Patterns, Strength, and Hydraulic Conductivity in Saskatchewan Tills," *Proceedings*, International Association of Hydrogeologists, Third Canadian Conference, Saskatoon, 1986, 22 pp.
[8] Sheingold, D. H., Ed., *Transducer Interfacing Handbook*, Analog Devices, Norwood MA, 1980, 260 pp.
[9] *IBM-PC Technical Reference Manual*, rev. ed., International Business Machines Corporation, Boca Raton, FL, IBM Part #1502234, April 1983.

Y. P. Vaid,[1] *D. Negussey,*[1] *and M. Zergoun*[1]

A Stress- and Strain-Controlled Monotonic and Cyclic Loading System

REFERENCE: Vaid, Y. P., Negussey, D., and Zergoun, M., **"A Stress- and Strain-Controlled Monotonic and Cyclic Loading System,"** *Advanced Triaxial Testing of Soil and Rock, ASTM STP 977,* Robert T. Donaghe, Ronald C. Chaney, and Marshall L. Silver, Eds., American Society for Testing and Materials, Philadelphia, 1987, pp. 119–131.

ABSTRACT: A combination hydraulic-pneumatic loading system for triaxial testing of soils under a variety of loading modes is described. The system permits both monotonic and cyclic loading under stress or strain control. Anisotropic consolidation and stress path control during monotonic or cyclic shear are important features of the system. A combination stress- and strain-controlled loading on the same specimen can also be carried out. Typical test results are presented in support of the capabilities of the loading system.

KEY WORDS: loading system, triaxial test, strain control, stress control, stress path, cyclic loading

Triaxial testing of soils under a variety of loading modes is often necessary to simulate field loading conditions or in fundamental studies of material response. Monotonic loading under strain control yields postpeak behavior necessary in analyses of progressive failure. Similar loading under stress-controlled conditions has been used to study time effects in clay deformation. Earthquake effects on soils are simulated by stress-controlled cyclic loading, whereas similar loading under strain control has proved useful in fundamental studies of volume change induced by cyclic loading and hence an understanding of pore pressure development if undrained conditions prevail. A combination of strain and stress control on the same test specimen may be needed for investigating effects of prior strain history on the response of contractive sands during subsequent earthquakes. Stress path control is used in the study of path dependence of soil behavior.

Triaxial loading systems with front-end computer control and some servo-controlled electrohydraulic loop systems are capable of simulating most of the loading patterns described above. But these systems are generally quite complex and expensive. This paper describes a simple combination hydraulic-pneumatic loading system developed over several years of research at the University of British Columbia. The loading system permits stress- or strain-controlled monotonic or cyclic loading, enables switching from stress to strain control or vice versa part way into the test, and also enables stress path control.

Description of the Apparatus

A schematic diagram of the loading system is shown in Fig. 1. The axial load is applied to the soil specimen by a rolling diaphragm (Bellofram) double-acting, water-saturated

[1] Professor, Natural Science and Engineering Research Council of Canada (NSERC) Industrial Research Fellow, and graduate student, respectively, Department of Civil Engineering, University of British Columbia, Vancouver, British Columbia, Canada V6T 1W5.

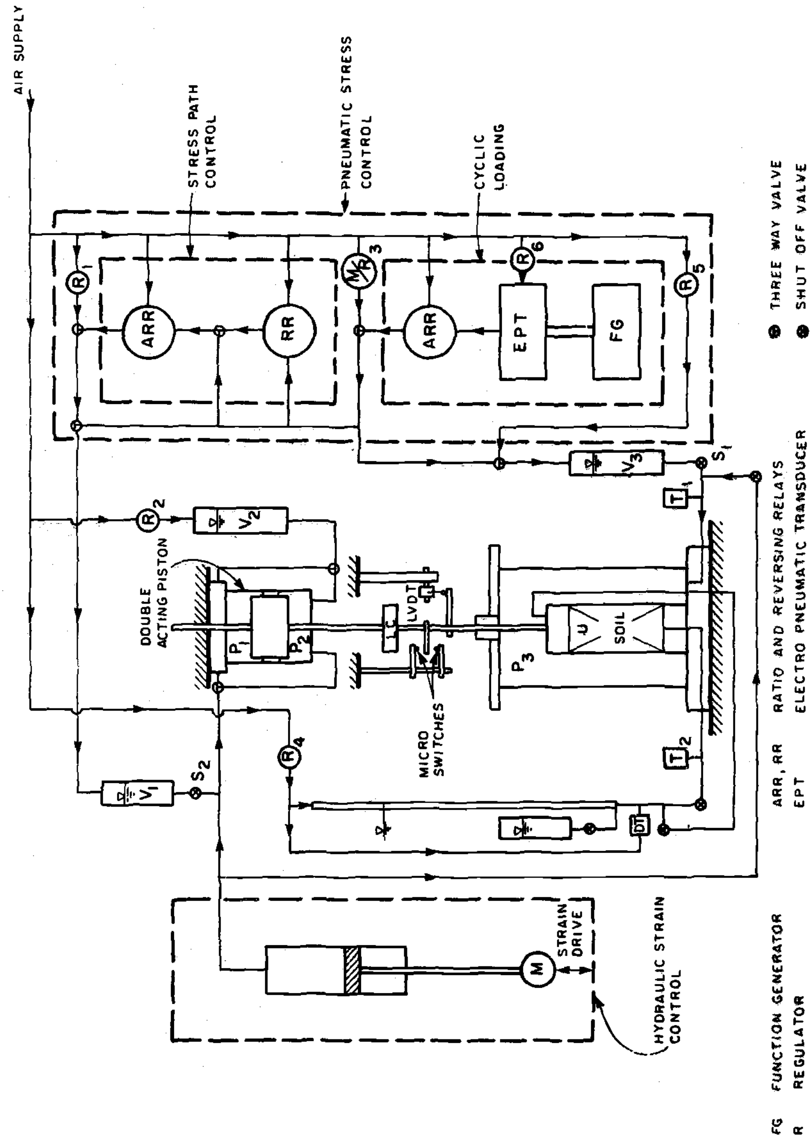

FIG. 1—Schematic layout of loading system.

piston. When the piston is not transmitting any load, it is kept pressurized with a base pressure P_0 in both chambers. Each side of the piston is connected to the hydraulic strain control as well as the pneumatic stress control. The strain control unit consists of a saturated displacement plunger activated by a strain drive. The plunger feeds water at a constant rate to the loading piston resulting in a constant rate of axial strain loading. For axial compression loading, water is fed into the upper chamber of the loading piston while the lower chamber drains freely to a constant pressure (controlled by regulator R_2) in the small reservoir V_2. The operations on the two chambers are reversed if extension loading is desired. When connected to a low compliance triaxial chamber, the strain control unit also enables a constant rate of radial or volumetric strain test. The technique of strain-controlled loading by moving water at a constant rate into a loading piston or triaxial cell was first used by Vaid in 1969 [*1*].

Axial stress control is achieved by delivering a desired air pressure to the loading piston through reservoir V_1. Pressure can be admitted either to the top or bottom chambers of the piston while the other side drains freely to a constant pressure in reservoir V_2. The stress control unit also supplies the cell pressure P_3 through the reservoir V_3. Independent incremental changes in axial stress or cell pressure are applied respectively through pressure regulators R_1 and M/R_3. These changes can be applied monotonically at a controlled rate if the regulators are motorized. Monotonic changes in axial load by regulator R_1 are all that are needed for conventional triaxial testing in which cell pressure is held constant.

Stress Path Control

For stress path control, increments in radial stress σ_h and axial stress σ_v are coupled. σ_h, which equals cell pressure, is then the control independent pressure. By routing cell pressure through the stress path subunit before delivery to the loading piston at V_1, the dependent axial stress is obtained. The stress path control consists of two pneumatic relays—a reversing relay (RR) and an adjustable ratio relay (ARR). The relays transform the signal pressure P_3 into an output pressure P in the following manner

$$\text{Ratio Relay:} \quad P = RP_3 \tag{1}$$

$$\text{Reversing Relay:} \quad P = K - P_3 \tag{2}$$

in which R and K are continuously adjustable positive constants. If the reversing relay is used in series and ahead of the ratio relay, the output pressure obtained will be

$$P = R(K - P_3) \tag{3}$$

In Eqs 2 and 3, $K > P_3$ because all pressure must be positive. Constants R and K would be prescribed by the sample size, system features, stress state, and intended path as shown in the subsequent section. It will also be shown that anisotropic consolidation under constant effective stress ratio can be achieved by using ARR only. Both RR and ARR are required in series for exercising stress path control during shear loading.

Cyclic Loading

The cyclic loading subunit of the stress control consists of an electropneumatic transducer (EPT) driven by a function generator (FG). Similar techniques of cyclic loading have been proposed previously [2,3]. The electropneumatic transducer converts the input voltage signal to a proportional pressure output, enabling choice of cyclic loading pulse shape, amplitude, and frequency by appropriate selection of electrical signal on the function generator. The adjustable ratio relay amplifies the output of the electropneumatic transducer for feeding directly into the loading piston for conventional cyclic loading tests in which cell pressure is held constant. On the other hand, if cyclic stress path control is required, the output of the cyclic loading subunit is fed as the cell pressure, and the same signal is routed through the stress path control subunit before delivery to the loading piston.

For completeness, other instrumentations related to triaxial testing are also illustrated in Fig. 1. These include cell and pore pressure transducers T_1 and T_2, axial load transducer LC, linear variable differential transformer LVDT, and differential pressure transducer DT for volume change measurements.

Operation of the Apparatus

There are two distinctly different stages in triaxial (or other test systems) testing—(1) consolidation and (2) shear. Consolidation of the specimen may be required either under isotropic or anisotropic stresses. In certain situations consolidation under constant rate of strain may be of interest. Shear loading may be drained or undrained, monotonic or cyclic, under stress- or strain-controlled conditions. In addition, stress path control may be required during shear loading.

Consolidation

After the triaxial specimen has been set up and connected to the volume change/pore pressure measuring device, it is under a small hydrostatic effective stress σ_0' (Point E in Fig. 2). This effective stress is a consequence of a small vacuum needed for confining reconstituted sand specimens or is due to the residual capillary tension in clay specimens. This stress state E is therefore the initial state from which the consolidation phase commences.

Isotropic—The desired cell pressure and back pressure for stress-controlled consolidation are applied by regulators R_5 and R_4, respectively. The small uplift of the loading rod due

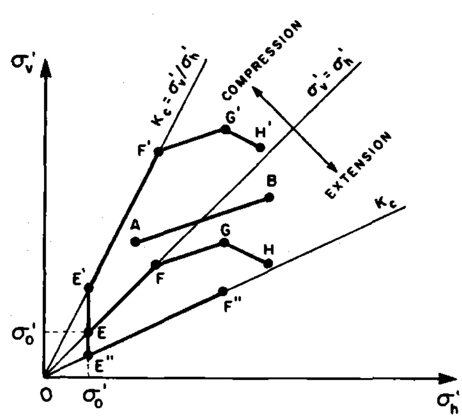

FIG. 2—*Examples of specific and arbitrary stress paths.*

to the cell pressure may be compensated, if needed, by incrementing the base pressure P_0 in the upper piston chamber. Motorized control on regulator R_5 may be used if consolidation under monotonically increasing stresses is desired.

Strain-controlled consolidation under isotropic stresses is initiated by connecting the triaxial cell to the strain control unit and shutting off valve S_1. A triaxial cell of low compliance would be needed to maintain a constant rate of volumetric strain [*1*]. By permitting drainage at one end and pore pressure measurements at the other, clay consolidation under hydrostatic loading may be studied [*4,5*].

Anisotropic—It can be readily shown from consideration of vertical equilibrium of the specimen that

$$\sigma_v' = (P_1 - P_2)\frac{A}{A_s} + P_3\left(1 - \frac{A_r}{A_s}\right) - u_0 \tag{4}$$

Also

$$\sigma_h' = P_3 - u_0 \tag{5}$$

where

P_1 = pressure in upper piston chamber
P_2 = pressure in the lower piston chamber
A = area of piston
A_s = current area of sample
A_r = area of sample loading rod
u_0 = back pressure

From Eq 4 it is easy to determine the way in which P_1 or P_2 must be varied in relation to P_3 in order to follow the required consolidation stress path. To do this, it is convenient to write Eqs 4 and 5 in terms of stress increments and neglecting contributions arising from changes in sample area. Noting that the back pressure u_0 is constant during this drainage loading,

$$\Delta\sigma_v' = (\Delta P_1 - \Delta P_2)\frac{A}{A_s} + \Delta P_3\left(1 - \frac{A_r}{A_s}\right) \tag{6}$$

$$\Delta\sigma_h' = \Delta P_3 \tag{7}$$

During anisotropic consolidation, such as along path E′F′ in Fig. 2, the constant stress ratio $K_c = \sigma_v'/\sigma_h' = \Delta\sigma_v'/\Delta\sigma_h'$. From Eqs 6 and 7, the following expression can be developed:

$$\Delta P_1 - \Delta P_2 = \left[\frac{A_s}{A}\left(K_c - 1 + \frac{A_r}{A_s}\right)\right]\Delta P_3 = C\,\Delta P_3 \tag{8}$$

For compression paths ($K_c > 1$), C is positive and P_2 is held constant. Then Eq 8 becomes

$$\Delta P_1 = C\,\Delta P_3 \tag{9}$$

For extension paths ($K_c < 1$), C is negative and P_1 is held constant. Then Eq 8 becomes

$$\Delta P_2 = |C|\,\Delta P_3 \tag{10}$$

in which $|C|$ represents the absolute value of C. The desired coupling of P_1 or P_2 with P_3 expressed by Eqs 9 and 10 is made possible by the stress path control unit with ratio relay only (see Eq 1). Clearly, $|C|$ equals the R constant of the relay.

Because the initial stress state E of the sample is hydrostatic, it would first be necessary to bring its stress state to the desired K_c ratio prior to initiating consolidation along the K_c line, such as E′F′. This is most conveniently achieved by following a vertical stress path EE′ and merely involves reduction in base pressure P_0 in the lower piston chamber. Furthermore, P_0 in the upper piston chamber must be selected such that at stress state E′

$$P_{1E'} = P_0 = |C|P_{3E'} = |C|\,(\sigma_0' + u_0) \tag{11}$$

in which $P_{1E'}$ and $P_{3E'}$ are respectively the values of P_1 and P_3 at E′. Once the specimen is at stress state E′, control of P_1 is switched from regulator R_1 to the stress path control. Consolidation beyond E′ along E′F′ is now automatically achieved by monotonically increasing P_3 while P_2 is held constant.

Consolidation under extension K_c values, such as along E″F″, can be carried out in a similar manner. For such paths, monotonic increase in P_3 controls the variations in P_2 through the stress path control, while P_1 is held constant.

Stress changes for anisotropic consolidation of clays must be applied slowly to avoid build-up of significant excess pore pressures. Pressure regulators coupled to variable speed motors with gear reduction are used for simulation of extremely slow loading rates.

Monotonic Shear Loading

Conventional Compression and Extension Tests—In these tests cell pressure is held constant and axial stress is monotonically increased (compression) or decreased (extension). This is done by increasing (compression) or decreasing (extension) P_1 while P_2 is held constant. Alternatively P_2 may be varied while P_1 is held constant. If the sample has been anisotropically consolidated, P_1 or P_2 output from the stress path control is first switched to regulator R_1. Incremental or monotonic stress-controlled compression or extension loading is then accomplished by changing P_1 or P_2 with regulator R_1 while the pressure in the other side of the piston is held constant by R_2. If strain-controlled loading is desired, valve S_2 is shut off and the hydraulic strain control unit feeds water to the upper (compression) or lower (extension) piston chamber while the other side drains to a constant pressure controlled by R_2.

Stress Path Control, Undrained—It may be shown theoretically that for saturated soils, only the sign and magnitude of $\sigma_v - \sigma_h$ determines the effective stress path and thus deformation response of the sample. The shape of the total stress path under undrained loading does not influence response, provided compression and extension modes of deformation are considered separately.

This is demonstrated by the total and effective stress paths and the stress–strain curves illustrated in Fig. 3. Four identical samples of an undisturbed clay from the same block were K_0 normally consolidated (in a special K_0 cell [*1*]) to a vertical effective stress σ_{vc}' of about 600 kPa. Specimens A and B were then brought to failure in undrained compression, A with σ_h constant and σ_v increasing, and B with σ_v constant and σ_h decreasing. Specimens C and D were brought to failure in undrained extension, C with σ_h constant and σ_v decreasing, and D with σ_v constant and σ_h increasing.

It may be noted that undrained compression tests have essentially identical effective stress paths and stress–strain curves. Likewise, the extension tests have essentially identical ef-

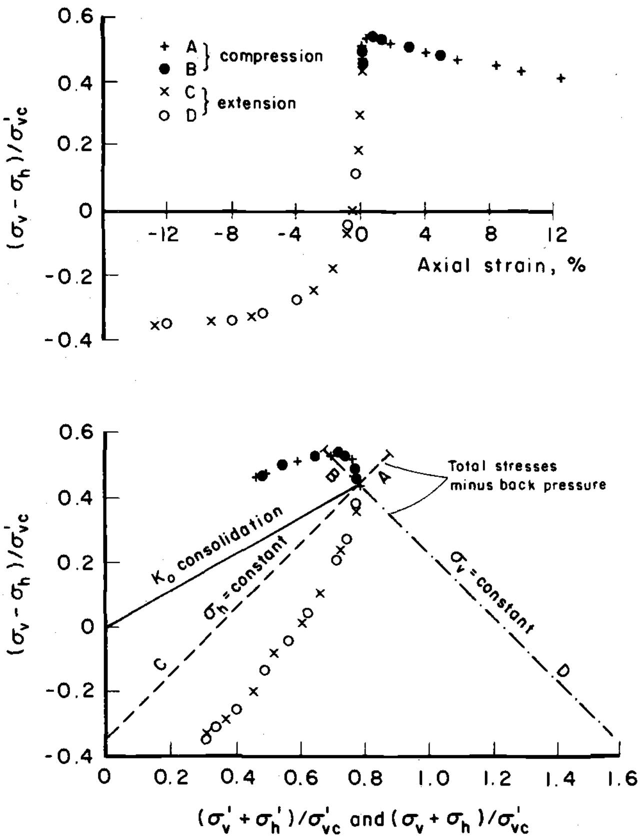

FIG. 3—*Undrained response of saturated clay to different total stress paths.*

fective stress paths and stress–strain curves, although the total stress paths for each pair of tests are radically different. This invariance of the behavior of saturated clays to undrained total stress path has also been demonstrated by others [6–8]. Thus, an arbitrary control of total stress path under undrained loading is not necessary. The unique compression or extension loading behavior can be determined by conventional triaxial tests with either stress or strain control.

Stress Path Control, Drained—Linear drained stress paths are used most commonly in both research and practice. An arbitrary stress path, if needed to be followed, can be approximated by a series of successive linear segments (see for example path F′G′H′ in Fig. 2). Each linear segment represents stress changes $\Delta\sigma_v'$ and $\Delta\sigma_h'$ (which also equal $\Delta\sigma_v$ and $\Delta\sigma_h$ with back pressure remaining constant during drained loading). If the ratio $\Delta\sigma_v'/\Delta\sigma_h' = \Delta\sigma_v/\Delta\sigma_h$ is designated as $\tan\theta$, the manner in which P_1 or P_2 must be varied in relation to P_3 along a desired stress path may be written in incremental form by analogy to Eq 8 as

$$\Delta P_1 - \Delta P_2 = \left[\frac{A_s}{A}\left(\tan\theta - 1 + \frac{A_r}{A_s}\right)\right]\Delta P_3 = C_1\,\Delta P_3 \tag{12}$$

For a given loading system and specimen size, the term C_1 in square brackets is a function of only the direction of stress increment θ. Because A_r/A_s is small, it can be neglected in calculating C_1 value. For all θ values other than $90° > \theta > 45°$ and $270° > \theta > 225°$, C_1 is negative. For these stress path directions, P_2 is held constant and therefore Eq 11 becomes

$$\Delta P_1 = -|C_1|\,\Delta P_3 \tag{13}$$

And for stress path directions $90° > \theta > 45°$ and $270° > \theta > 225°$, C_1 is positive. For these stress path directions P_1 is held constant and therefore Eq 12 becomes

$$\Delta P_2 = -|C_1|\,\Delta P_3 \tag{14}$$

where $|C_1|$ is the absolute value of C_1. Assume AB (Fig. 2) represents the linear stress path increment to be applied. If P_{1_A}, P_{1_B}, P_{3_A}, and P_{3_B} represent piston and cell pressures at A and B, respectively, Eq 12 becomes

$$P_{1_B} - P_{1_A} = -|C_1|(P_{3_B} - P_{3_A})$$

or

$$P_{1_B} = |C_1|(D_1 - P_{3_B}) \tag{15}$$

in which

$$D_1 = \frac{P_{1A}}{|C_1|} + P_{3_A} \tag{16}$$

is a positive quantity. It may be noted that the relationship expressed by Eq 14 is identical to Eq 3. Thus, choosing constants $R = |C_1|$ and $K = D_1$ relevant to the stress increment on the relays of the stress path control would enable pursuing stress path directions for which P_2 is held constant. Relationships similar to Eqs 15 and 16 can be written for pursuing stress path increment directions for which P_1 is held constant

$$P_{2_B} = |C_1|\,(D_2 - P_{3_B}) \tag{17}$$

and

$$D_2 = \frac{P_{2A}}{|C_1|} + P_{3_A} \tag{18}$$

Shearing stress paths initiate from end of consolidation states, such as F′ (Fig. 2). For the small linear segment F′G′, the constants C_1 and D of the relays are computed using Eqs 12 and 16 or 18 depending on the θ value. The control of pressure in reservoir V_1 is temporarily switched to regulator R_1 if stress path control was used during consolidation. The computed constants $|C_1|$ and D are now selected on the relays. This enables the stress path control to deliver a pressure unchanged from the previous value. The control of pressure in V_1 is now switched back to the stress path control. The desired stress path segment F′G′ may then be followed by monotonically varying P_3 until the stress state at G′ is reached. The next linear segment of stress path, for example G′H′, is followed in a similar manner after new relay constants applicable to G′H′ are selected. In this manner, the entire stress path can be traversed.

Similar to anisotropic consolidation, stress increments during stress path testing of clays must be applied slowly to avoid build-up of significant excess pore pressure. Once again this is conveniently achieved by using motorized regulators for applying pressures at very slow rates.

Cyclic Loading

In the most common form of stress-controlled cyclic loading, the deviator stress $\sigma_v - \sigma_h$ is varied symmetrically about the ambient end of consolidation value, while the cell pressure is held constant. At the conclusion of the consolidation phase, the control of cell pressure is switched from R_3 to R_5 (Fig. 1) and that of pressure at V_1 to the cyclic loading control. The latter is achieved by adjusting the dc offset on the function generator until the system delivers the desired pressure before the switch is made. Amplitude, pulse shape, and frequency of cyclic load are controlled by selecting appropriate settings on the function generator. It is useful to have a gate mode on the function generator which allows the operator to start and stop the cyclic loading at the ambient deviator stress level about which cyclic loading is carried out. The pressure is cycled about the ambient value only on one side of the loading piston while the other side is kept freely draining to a constant pressure.

Stress-controlled cyclic loading under undrained conditions has been of most interest in practice. The loading system, however, can also be used to apply cyclic loading under drained conditions at a sufficiently low frequency to avoid build-up of significant excess pore pressures. This requirement often restricts the use of cyclic drained loading to sandy soils.

Stress path control during cyclic loading can be exercised in a manner similar to that under monotonic loading, provided the cyclic path is linear. Like the monotonic undrained response, cyclic undrained response of a saturated soil is invariant to the changes in total stress path for identical oscillations of deviator stress. Thus undrained stress path control is not necessary and the conventional test in which the cell pressure is held constant is all that is needed. To control drained stress path during cyclic loading, the control of cell pressure is first switched from regulator R_3 to cyclic loading control. This is done by adjusting dc offset on the function generator until the system delivers the desired pressure before the switch is made. The control of pressure at V_1 is switched to R_1. This would be necessary if consolidation was anisotropic. For the given cyclic loading path direction, θ, the constants C_1 and D on stress path control are computed and set on the respective relays. The control of pressure at V_1 is now switched back to the stress path control, and cyclic loading about ambient values of both axial stress and cell pressure is then initiated. Amplitude, frequency, and waveform are selected on the function generator.

For constant strain amplitude cyclic loading, the cell pressure is held constant at the end of consolidation value by regulator R_5. Cyclic strain pulses are applied by moving water in or out of the upper (or lower) piston chamber by forward or reverse movements of the strain drive. Reversal in the direction of strain drive is triggered by a microswitch whose position controls the strain amplitude. Cyclic strains may be applied undrained or drained. In the latter case, restrictions on the ability of soil to drain without developing significant excess pore pressure apply, as in the case of stress-controlled monotonic loading.

Performance and Typical Results

Some typical results selected from a variety of tests performed using the loading system are now described to illustrate some of the capabilities of the apparatus. It would not be possible to carry out such tests with simpler triaxial loading systems.

The modular nature of the system provides considerable flexibility in its loading capacity. For a given specimen size, axial loading capacity can be increased by a mere increase in the size of the loading piston. The maximum limit on pressures in the stress-controlled mode is the available line air pressure (normally 700 to 800 kPa). In the strain-controlled mode, however, the maximum pressure in the loading piston, and hence the axial load, is limited only by the working pressure rating of the Bellofram (1400 to 1500 kPa).

The pneumatic cyclic loading system can operate up to a maximum frequency of about 1 Hz without any loss to the set magnitude of load, provided the soil stiffness does not change abruptly. If soil stiffness does change abruptly, as in liquefaction studies, the loading piston must move at a very high velocity. This would result in degradation of the load trace because the fluid could not be supplied to the piston through piping restrictions at a rate compatible with the fast movement of the piston. Liquefaction studies can be carried out by replacing the water piston with an air piston. Addition of volume booster relays on both sides of the piston will prevent degradation of load trace if abrupt change in soil stiffness may occur [9].

Constant Rate of Strain Hydrostatic Consolidation

Results of such a test on an undisturbed marine clay are shown in Fig. 4. A standard triaxial specimen, 3.5 cm in diameter × 7.0 cm high, and a rigid stainless steel cell were used. The average rate of volumetric strain imposed was 4.2×10^{-7}/s. Consolidation was carried out to a maximum hydrostatic effective stress of about 1100 kPa. The loading system, however, does not impose any limit on the level of hydrostatic consolidation stress because the hydraulic strain control is a closed system. Results were analyzed as discussed in Refs *4* and *5*.

Constant Stress Ratio Anisotropic Consolidation

Results of consolidation of a sand specimen under $K_c = 2$ are shown in Fig. 5. Excellent agreement can be seen between the intended linear consolidation path (solid line) and the path actually followed (data points). Use of a large size loading piston in relation to the 6.5-cm-diameter specimen together with a pressure multiplier for cell pressure enabled consolidation to high, $\sigma_v' = 5000$ kPa and $\sigma_h' = 2500$ kPa, stresses.

Anisotropic K_0 *Consolidation*

Anisotropic K_0 consolidation requires a special K_0 cell [*1*]. Results of a cyclic K_0 consolidation test on an undisturbed marine clay are shown in Fig. 6. The test was carried out

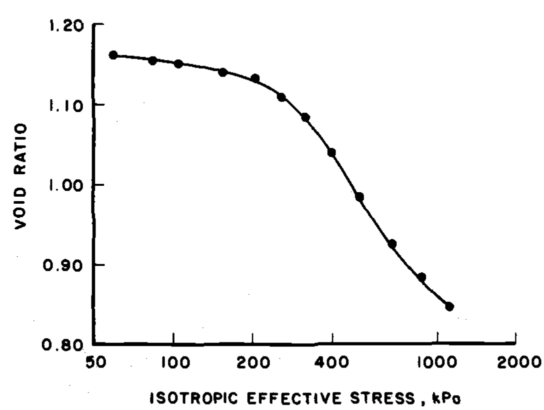

FIG. 4—*Constant rate of strain hydrostatic compression of a clay sample.*

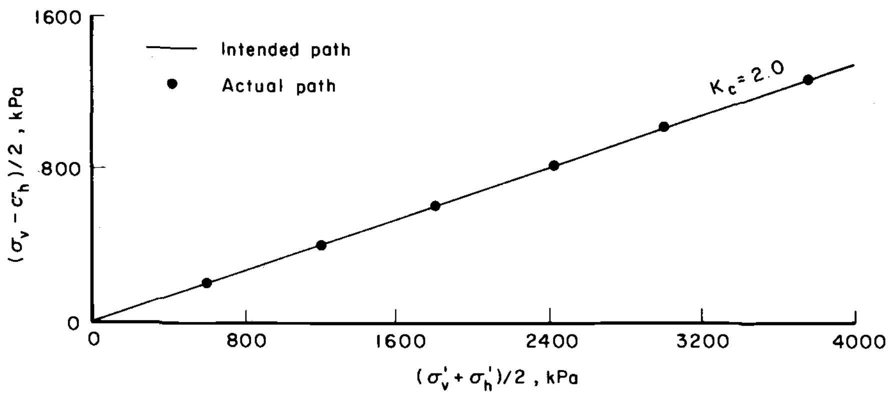

FIG. 5—*Anisotropic consolidation of a sand specimen.*

under strain-controlled conditions on a 3.5 cm diameter × 7.0 cm high specimen. A constant value of K_0, a well-known characteristic of normally consolidated clay, may be noted. The large range of σ_v' values possible by the loading system may also be observed.

Drained Stress Path Controlled Shear

Figure 7 shows comparison between the stress paths desired (solid lines) and those actually applied (data points) in two drained triaxial tests on identical samples of a sand. The stress paths chosen represent a wide spectrum from conventional compression (A_1B_1, OA_2), constant stress ratio (A_2B_2), constant shear stress under increasing (B_1C_1), (B_2C_2) and decreasing (E_1F_1) mean normal stress, and constant mean normal stress (C_1E_1, C_2D_2). It may be noted that excellent reproduction of desired stress paths is obtained by the stress path control.

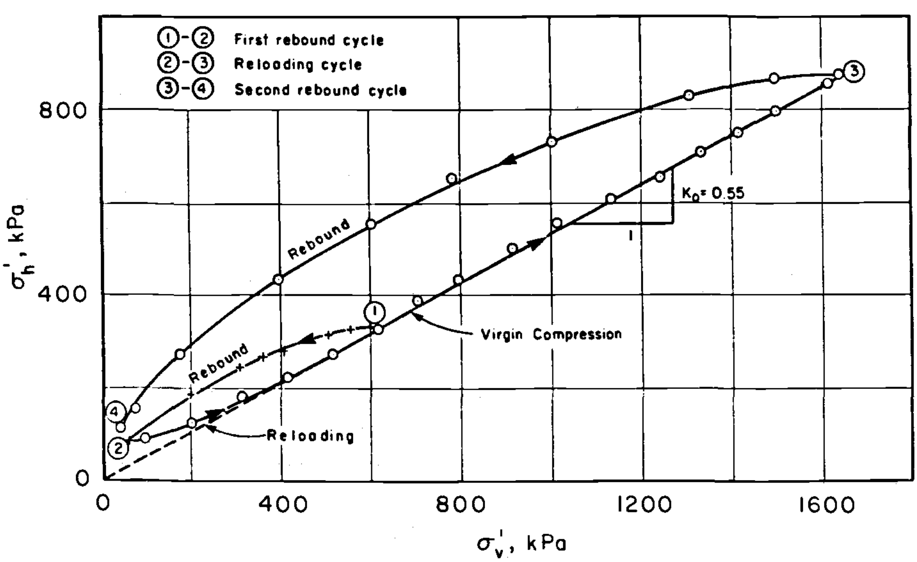

FIG. 6—K_0 *consolidation and rebound of a clay.*

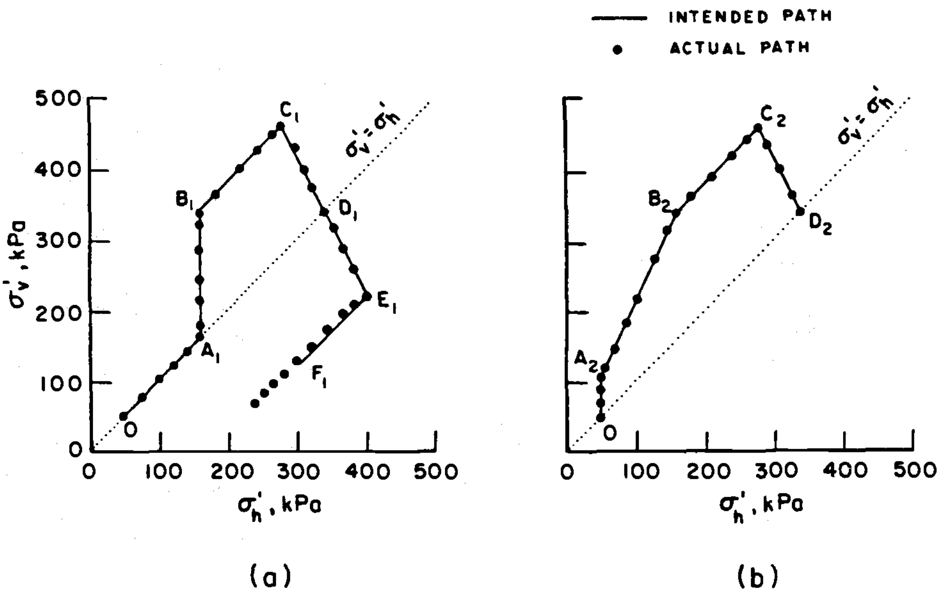

FIG. 7—*Drained stress-path-controlled shearing of sand.*

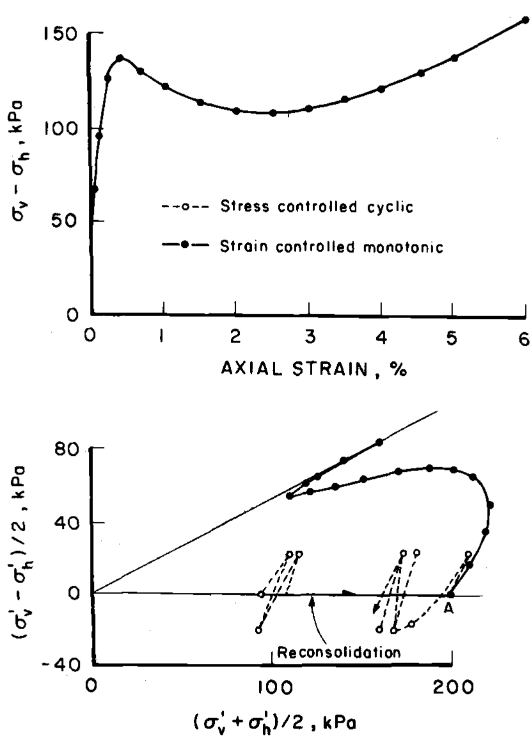

FIG. 8—*Cyclic stress loading followed by monotonic strain-controlled undrained loading of a sand.*

Sequential Stress- and Strain-Controlled Loading

Figure 8 shows the results of a stress-, then strain-controlled loading test on a contractive saturated sand specimen. The sample had a relative density of 36% and was hydrostatically consolidated to point A. It was then cyclically loaded under stress-controlled conditions using a cyclic stress ratio of 0.1 until it developed a residual strain of about 0.15%. The excess pore pressure developed was about 70% of the initial confining pressure. Cyclic loading was then terminated, and the specimen was reconsolidated to the initial effective stress, point A. It was then loaded under monotonic strain-controlled undrained compression. The results show that the sand still shows contractive behavior, although it had been subjected to a prior cyclic strain history. Thus, its resistance to subsequent cyclic loading is not improved [*10*]. If the sand is initially dilative, substantial increase in cyclic loading resistance is observed due to small cyclic strain history.

Conclusions

A simple triaxial loading system, which is neither computer-based nor servo-controlled, is capable of simulating most of the loading mode patterns in practical as well as research needs. The system can apply monotonic or cyclic loading under either stress- or strain-controlled conditions, permits switch from one to the other type part way into the test, and also enables stress path control. The modular construction of the loading system uses commercially available components and provides unlimited flexibility in loading capacity and selection of loading patterns.

Acknowledgments

This research was supported by a grant from the Natural Science and Engineering Research Council of Canada. Kelly Lamb typed the manuscript, and Richard Brun drafted the illustrations. Their assistance, together with the technical assistance of the staff of the Civil Engineering Workshop, is gratefully acknowledged.

References

[*1*] Campanella, R. G. and Vaid, Y. P., *Canadian Geotechnical Journal*, Vol. 9, No. 3, 1972, pp. 249–260.
[*2*] Motherwell, J. T. and Wright, S. C., *Journal of the Geotechnical Engineering Division, American Society of Civil Engineers*, Vol. 104, No. GT7, 1978, pp. 1036–1039.
[*3*] Chan, C. K., *Geotechnical Testing Journal, American Society for Testing and Materials*, Vol. 4, No. 4, 1981, pp. 183–187.
[*4*] Wissa, A. E. Z., Christian, J. T., Davis, E. H., and Heiberg, S., *Journal of the Soil Mechanics and Foundation Division, American Society of Civil Engineers*, Vol. 97, No. SM10, 1971, pp. 1393–1413.
[*5*] Vaid, Y. P. and Campanella, R. G., *Journal of the Soil Mechanics and Foundation Division, American Society of Civil Engineers*, Vol. 98, No. SM5, 1972, pp. 508–510.
[*6*] Henkel, D. J., "The Shear Strength of Saturated Remolded Clays," Presented at American Society of Civil Engineers Research Conference on Shear Strength of Cohesive Soils, Boulder, CO, 1960, pp. 533–554.
[*7*] Parry, R. H. G., *Geotechnique*, Vol. 10, 1960, pp. 166–180.
[*8*] Bishop, A. W. and Wesley, L. D., *Geotechnique*, Vol. 25, No. 4, 1975, pp. 657–670.
[*9*] Chan, C. K. and Mulilis, J. P., *Journal of the Geotechnical Engineering Division, American Society of Civil Engineers*, Vol. 102, No. GT3, 1976, pp. 277–282.
[*10*] Chung, E., "Effects of Stress Path and Prestrain History on the Drained Monotonic and Cyclic Loading Behavior of Saturated Sand," M.A.Sc. thesis, University of British Columbia, Vancouver, Canada, 1985.

Jean-Michel Dupas,[1] Alain Pecker,[2] Pierre Bozetto,[3] and Jean-Jacques Fry[4]

A 300-mm-Diameter Triaxial Cell with a Double Measuring Device

REFERENCE: Dupas, J.-M., Pecker, A., Bozetto, P., and Fry, J.-J., **"A 300-mm-Diameter Triaxial Cell with a Double Measuring Device,"** *Advanced Triaxial Testing of Soil and Rock, ASTM STP 977,* Robert T. Donaghe, Ronald C. Chaney, and Marshall L. Silver, Eds., American Society for Testing and Materials, Philadelphia, 1988, pp. 132–142.

ABSTRACT: A large-diameter triaxial cell (ϕ 300 mm) is presented. Its uniqueness lies in the double measuring system of all parameters: axial strain, volumetric strain, and pore pressures. Owing to this system, accurate measurements can be taken, enabling the determination of the soil constitutive relationships from very small strains (elastic behavior) to failure strains. The cell can be used either under quasistatic monotonic or cyclic dynamic loadings. The apparatus has been used to evaluate the accuracy of the measurements and the influence of sample size on elastic Young's modulus, Poisson's ratio, and variation of secant modulus with strain.

Preliminary results show that, as opposed to conventional testing, significantly improved results are obtained with the double measuring system.

KEY WORDS: triaxial cell, axial strain, radial strain, volumetric strain, pore pressures, measurements, elastic behavior, failure, dynamic loading, static loading

When building nuclear power plants, it is necessary, during the construction and the life time of the plant, to impose very low values on settlements and rotations of the works.

To obtain the variation of the settlement as a function of the load history, it has been necessary to develop an accurate triaxial device. Therefore, the Design Department for Thermal and Nuclear Projects (SEPTEN) ordered a ϕ 300-mm cell to test gravelly soils under static and dynamic loads.

The design was to be based on the work of El Hosri [*1,2*] who had equipped a ϕ 70-mm triaxial with proximity transducers and had obtained remarkable results.

As shown by Flavigny [*3*], the use of frictionless ends in a triaxial test to avoid end restraint has a significant influence on the value of the moduli. The bedding effect (badly compacted upper layer, for instance) also affects the measurements by overestimating the total vertical strains. So, to cancel these two problems proximity transducers were used to measure strains in the central third of the sample.

The dimensions of the sample and the study of drained or undrained conditions required the exact knowledge of the pore pressure. A needle was inserted in the middle of the sample. A device with a double system of measurements of vertical strains, volume, and pore pressure

[1] Managing director, Mécasol SA, 8 Rue Eugène Oudiné, Paris 75013, France.
[2] Manager, Géodynamique et Structure SARL, 8 Rue Eugène Oudiné, Paris 75013, France.
[3] Engineer, Electricité de France, Septen, Villeurbanne 69628, France.
[4] Engineer, Design Dam Unit, Electricité de France, Real, Chambery 73010, France.

was then obtained. All parameters could now be measured and thus decrease the range of the error.

The applications of this triaxial device consist mainly in determining the laws of variation of moduli and damping as a function of the shear strain. These parameters, defining the viscoelastic linear model (QUAD4, FLUSH codes), enable the further study of soil–structure interaction of nuclear power plants [*4*] and of the seismic response of dams.

Other interests arise from the determination of the constitutive relationships in the low strains range: the calculation of foundation settlements and behavior of backfills and of road deflections.

Description of the Cell

The cell (see Fig. 1) was built to contain cylindrical samples 300 mm in diameter and 600 mm in height. This allows the testing of materials with particles up to 50 mm.

This cell has the versatility of a standard triaxial cell, including independent control of the lateral and axial stresses, existence of a drainage system at the top and the base of the sample, and the possibility to apply a high back pressure to the sample. It is made to withstand pressures up to 10 MN/m^2.

To perform static, cyclic, or dynamic tests, the cell is placed under an INSTRON hydraulic

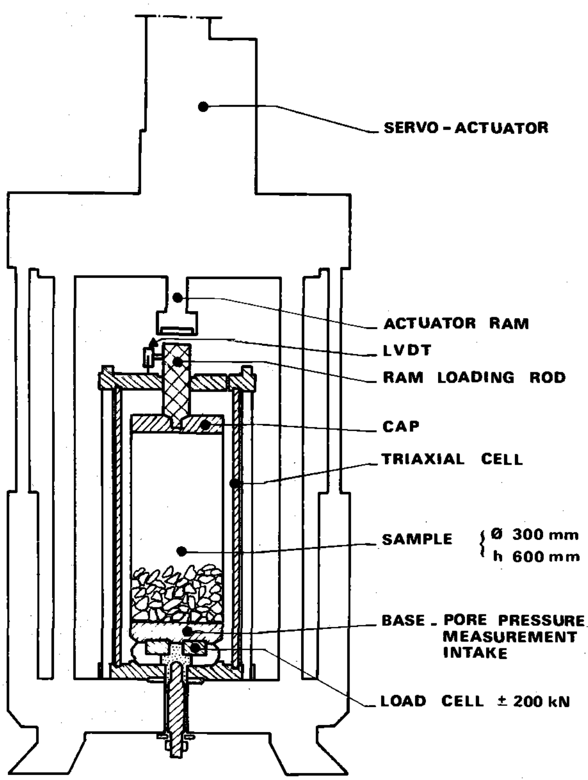

FIG. 1—*ϕ 300-mm triaxial apparatus.*

press, equipped with a ±100-kN jack and generated by a unit of 0.042 m^3/min power. Tests can be carried out at frequencies ranging from 0 to 50 Hz and can be force or strain controlled, or for undrained tests on saturated samples, strain controlled by means of a transducer performing automatically the correction of section resulting from the variation of the sample height. Achieved frequencies depend on the solicitation amplitude, because of the power limitation of the INSTRON test frame.

Measurement Devices

Like any triaxial cell, the cell is equipped to measure the load applied to the sample, the length variation of the sample, and the pore pressure. Its uniqueness lies in the existence of a double system of measurements of the axial strain and the pore pressure, and the ability of measuring the radial strain of the sample.

Measurement of the Load

Measurement of the load is performed with a force transducer with strain gauges in full bridge, whose characteristics are a rated range of ±20 000 daN and sensitivity of 1 mV/V.

Because the cell is used for the study of the material behavior under low strain (elastic condition) or at failure, it is imperative to know with accuracy the load applied to the sample. For that purpose, the force transducer is placed inside the cell at the base of the sample (Fig. 1). The force measurement is therefore not altered by friction caused by the seal placed at the entrance of the ram inside the cell. The same load cell is used through the test and is accurate enough to measure less than 1 daN, which is a value consistent with very low strains.

Axial Strain ϵ Measurements

A linear variable differential transformer (LVDT) type transducer is put on the axis of the ram outside the cell. Given the stiffness of the ram and of the mechanical assembly, the measured displacement corresponds to a shortening (or lengthening) of the sample only. Because of its position, this transducer measures the average displacement of the sample on its total height. In particular, the contact displacements between the sample and its support are included in the obtained value. Under low strains, these strains cannot be ignored and it is necessary to measure the strain of the sample in an area free of end restraint or other surface effect.

A second measurement device (see Fig. 2) has been added with a proximity transducer placed at the central third of the sample. This transducer and its target are linked to the sample, each by two points, which penetrate the material through the membrane to form a link between the transducer or its target and the material [2]. To rigidly link the supports of the transducers to the sample, they are inserted into a uniform fine sand finger placed in the sample and compacted to 100% relative density.

This type of transducer measures static and dynamic displacements without mechanical contact with the moving part. It can be used in a liquid medium submitted to a high pressure. The transducer is composed of an inductive coil, generated by a 5-kHz alternative power, and a receptive coil. The introduction of a metallic target in the magnetic field of the inductive coil modifies the magnetic permeability of the transducer environment and creates a phase displacement in the receptive coil. At this stage, displacement is linked to a variation of the tension directly associated to the variation of the air-gap, therefore to the displacement.

The sensitivity varies with the air-gap and the nature of the target. Displacements of 0.2

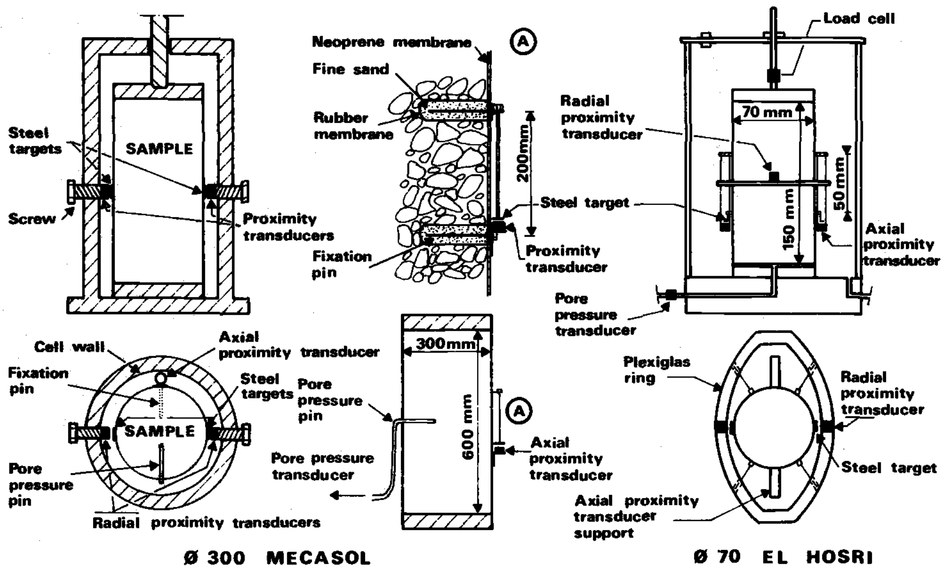

FIG. 2—*Strain measurement devices in the ϕ 70-mm cell and ϕ 300-mm cell.*

μm, or strains lower than 10^{-6} can theoretically be detected. In practice, the strains obtained can be trusted for values of 5.10^{-6} to 10^{-5}. The positioning is made before consolidation, so as to have a maximum sensitivity after consolidation.

The two systems of measuring the displacement are simultaneously used during a test. They enable accurate judgment of the strain values obtained between 5.10^{-6} and 10^{-2}, the proximity transducer being unable to make measurements greater than 10^{-2}; anyway, for the latter, strain differences between both systems are small.

Radial Strain Measurement ϵ_3

Radial strain measurement is made with proximity transducers identical to those described above. As opposed to El Hosri who fixed the radial strain transducers on a Plexiglas® ring just opposite their targets stuck on the samples, it was thought more practical to position the two radial strain transducers on the body of the cell. For that, holes were made to screw the transducer on, after having first glued the target on the sample through the hole. The adjustment of the transducer with regard to the target is done from outside. This enables the adjustment of accuracy to its optimum value. The two transducers are diametrically opposed.

This design limits the measurement at strains lower than 10^{-2}, but it eases largely the initial adjustments. This obviously helps in studying low variations of volume of unsaturated samples.

The presence of large particles and the local characteristic of the measurement render scattered results below 10^{-5}. The comparison between the two transducers helps the interpretation by revealing local abnormalities.

Pore Pressure Measurements

For undrained tests, pore pressure measurements are traditionally taken at the end of the sample (top or base). But in order to determine the behavior of the sample with more

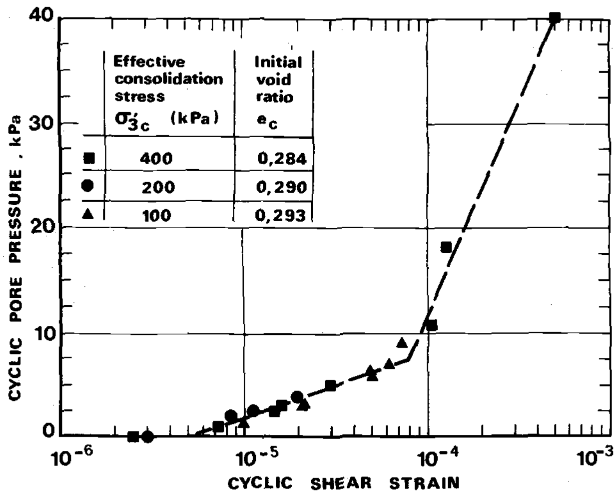

FIG. 3—*Cyclic pore pressure versus cyclic shear strain.*

accuracy, measurement is taken in the middle of the sample with a needle penetrating the membrane 11 cm horizontally (Fig. 2).

This system gives evidence of the development of the pore pressure from the lowest strains ($<10^{-5}$) (see Fig. 3). It also enables the verification of the shear rate of the drained tests. The drained tests had to be abandoned in the case of unsaturated samples taken from the core of the Grand Maison dam (located in the Alps, France). The extreme slowness of the dissipation for a saturation degree of 85% was noticed. The permeabilities are, for the unsaturated sample, 20 times lower than for the saturated sample.

Monitoring System

All the measurements were taken either manually for the quasistatic drained tests, or recorded on an analogic paper for the dynamic or cyclic undrained tests. A digital recording system with automatic processing of the data was then under study and is now available.

Comparison Among Strain Measurements

Modulus at Low Strains

Since the utilization of the cell, various types of tests have been carried out on different types of materials:

- Cyclic undrained tests on gravelly sand and sandy gravel from Malville nuclear power plant (in the Rhone Valley, France) [*5*].
- Consolidated undrained tests at 1 Hz on a clayey silty gravel, slightly plastic (IP $\leq$ 10%) forming the core of the Grand Maison dam. These tests on the material of La Cochette (Grand Maison dam core) have been carried out under different experimental conditions of saturation (100 and 85%) and consolidation (normally consolidated or overconsolidated) of the material.

- Consolidated drained tests on the same material as La Cochette.
- Consolidated drained tests on material of Matemale dam (located in the Eastern Pyrenees, France) (slightly plastic clayey gravel).

Of all these tests, only 35 test samples on which axial strain measurements have been performed with LVDT transducers and proximity transducers have been kept. For each test, we have computed the ratio:

$$\lambda = \frac{E_p - E_t}{E_p}$$

where

E_p = value of the modulus computed with proximity transducers
E_t = value of the modulus computed with LVDT transducers

The value of this ratio, λ, is shown as a function of the consolidation confinement in Fig. 4. For most values, λ is positive, therefore $E_p > E_t$. The value of λ does not rely on the confinement ($26\ \mathrm{kN/m^2} \leq \sigma_3' \leq 800\ \mathrm{kN/m^2}$), the type of test, or the density of the material. It can be retained as an average value of $\lambda = 0.17$, which corresponds to an E_p modulus greater than 20% of modulus E_t, with a standard deviation of 0.15.

Variation of E/E_{max} *as a Function of* ϵ

The comparisons (Fig. 5) among variations of moduli as a function of the vertical strain are made for the same tests as in the above paragraph. The λ factor, previously defined,

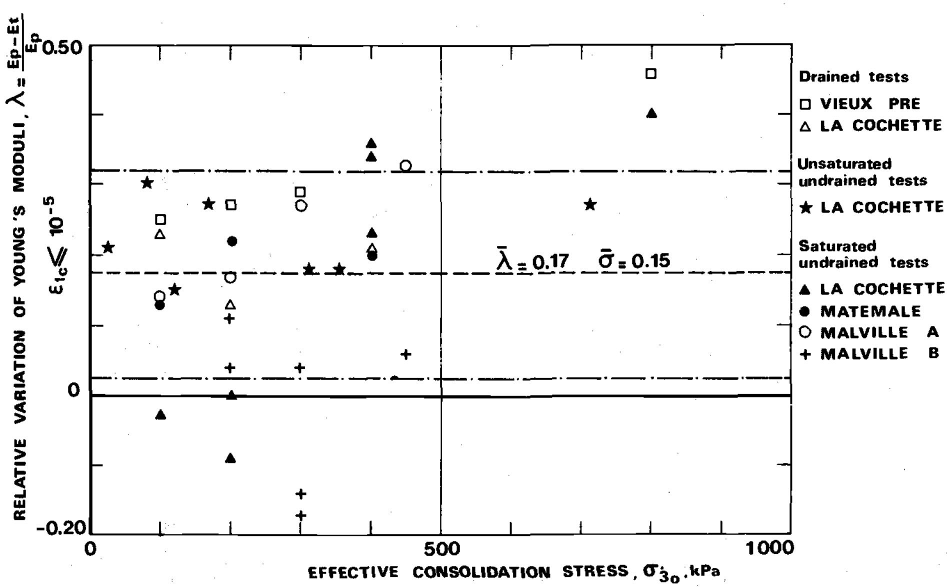

FIG. 4—*Influence of effective consolidation stress on small strain Young's moduli measured by LVDT and by proximity transducers.*

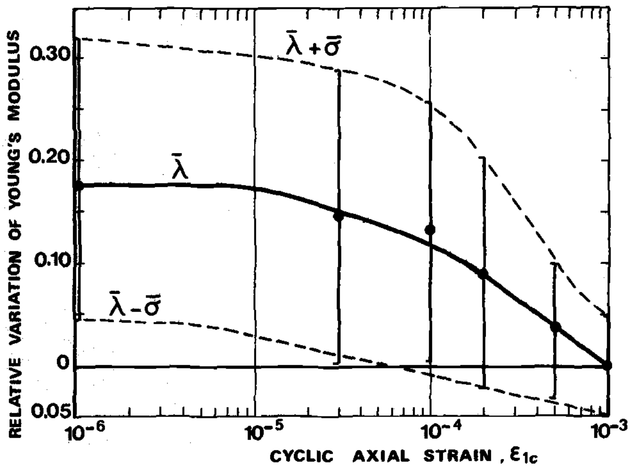

FIG. 5—*Influence of axial strain on secant Young's moduli measured by LVDT and by proximity transducers.*

decreases and tends to zero as the axial strain increases and the deviation from the mean value decreases. At large strains, the influence of the parasite strains therefore diminishes.

Variation of Volume and Irreversible Strain

It is possible to add the local measurements of strain to find the volume variation and to compare it with that given by the burettes during drained tests. Figure 6 shows the comparison between the two systems on a cyclic drained path. The path consists in applying a compression-extension cycle with a maximum increasing deviator. We see that the strain paths are

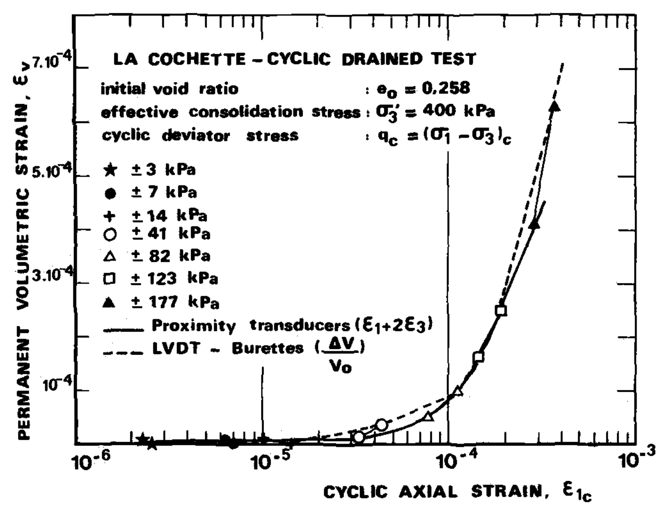

FIG. 6—*Permanent volumetric strains generated by drained cyclic loading with increasing cyclic deviator stress.*

identical, but the total variations of volume are up to 50% higher than the variations computed from proximity transducers.

Influence of the Sample Sizes

Modulus at Low Strains

To compare results obtained from the ϕ 300-mm cell to those obtained in triaxial cells of standard dimensions, cyclic tests have been carried out on the same material and in the same experimental conditions. The sand of Fontainebleau was used (d_{10} = 0.125 mm, d_{50} = 0.17 mm, d_{60}/d_{10} = 1.48), set in place at a dry unit weight of 15.4 kN/m^3 and consolidated isotropically under 300 kN/m^2. Samples of 38-, 54-, 120-, and 300-mm diameter with a slenderness ratio of 2 have been tested. Young's moduli measured at low strain ($\epsilon < 10^{-5}$) and a strain of $7 \cdot 10^{-4}$ are shown in Fig. 7. To be compared, all the strain measurements are made with LVDT transducers set outside the cell.

Apart from the tests on ϕ 38-mm samples, the maximum difference among the different values is, at the most, 30% under low strain. This difference is smaller but stays significant when the strain increases (20% at $\epsilon = 7 \cdot 10^{-4}$). We see on the other hand that the greater the diameter of the sample, the higher the moduli are and the closer they come to the value of the resonant column.

For small-diameter samples, these results show the influence of the height of the sample. This is explained when an axial strain of 10^{-4} corresponds to an axial displacement of 8 μm for ϕ 38-mm sample, 11 μm for ϕ 54 mm, 24 μm for ϕ 120 mm, and 60 μm for ϕ 300 mm. It can therefore be considered that parasite contact displacement around the top of the sample, which should be practically independent from the height of the sample, causes greater errors if the height is low. This hypothesis is confirmed by the fact that the difference among the values obtained in the four cells decreases when the strain increases.

To conclude, it appears therefore that a ϕ 300-mm cell leads to results of greater accuracy

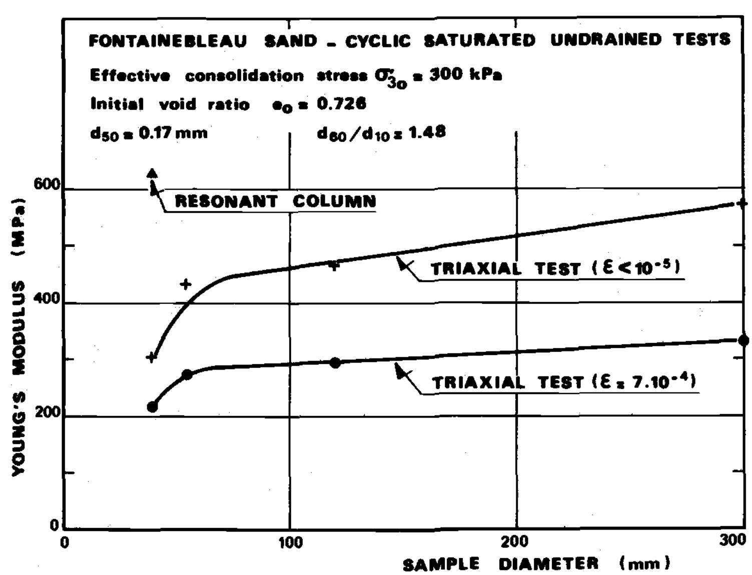

FIG. 7—*Young's modulus versus sample diameter.*

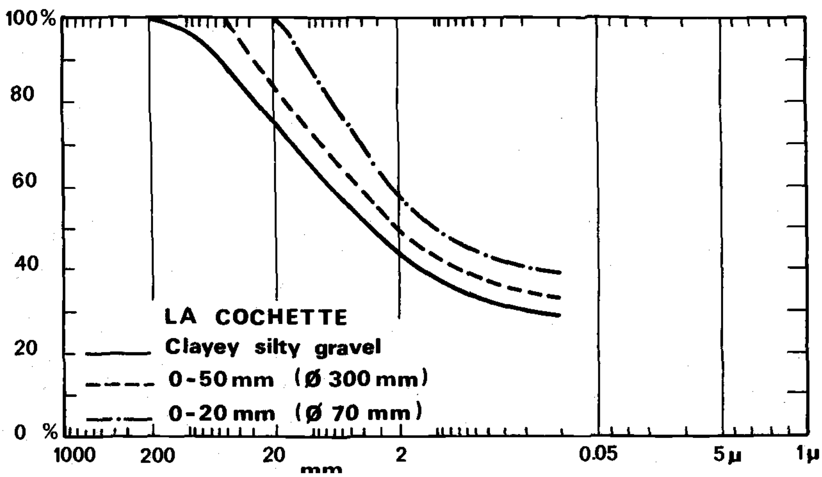

FIG. 8—*Grain size distribution for Grand Maison core material.*

than those obtained on small-diameter samples. This accuracy can be improved by the use of proximity transducers.

Other comparisons have been made for the construction of Grand Maison dam on the gravel core. The moduli of the 0/20 mm fraction tested on the ϕ 70-mm cell were compared to moduli of the 0/50-mm fraction tested on ϕ 300-mm cell (Fig. 8). The moduli found in ϕ 300-mm cell are two times higher than that determined on the ϕ 70-mm cell and are very close to values found by geophysics (Fig. 9).

By linking this result to those obtained on Fontainebleau sands (E_L = 570 MN/m^2, $E_{\text{resonant column}}$ = 630 MN/m^2), it can be concluded that the modulus computed from proximity transducers corresponds to an elastic modulus of the material.

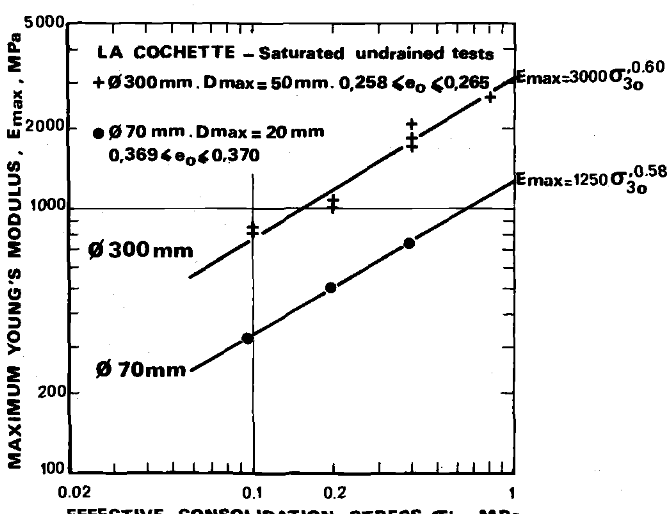

FIG. 9—*Effect of the maximum grain size on Young's modulus.*

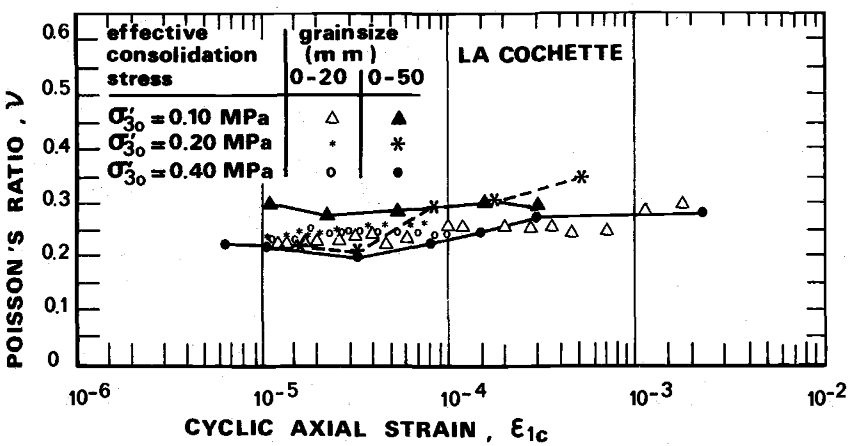

FIG. 10—*Poisson's ratio versus cyclic axial strain.*

E/E_{max} *as a Function of Vertical Strain*

The comparison among variations of moduli as a function of the vertical strain, obtained from proximity transducers, has given the same curve for the 0/20-mm fraction of φ 70-mm cell as for the 0/50-mm fraction of φ 300-mm cell.

Poisson's Ratio

The results obtained on the Grand Maison gravel from φ 300-mm triaxial cell have confirmed those of φ 70-mm cell. Poisson's ratio is practically constant between 10^{-6} and

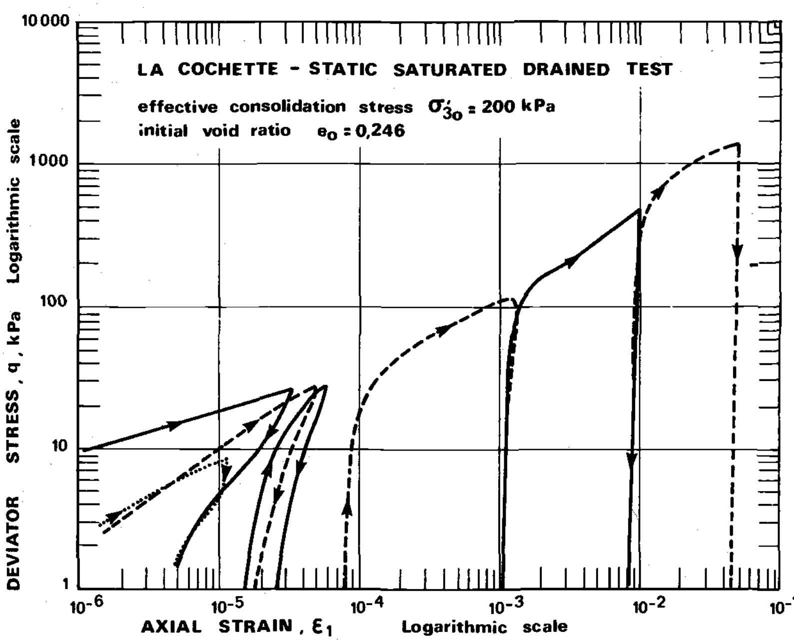

FIG. 11—*Drained stress–strain path from very small strains up to failure.*

10^{-3} and is independent from the consolidation strain (100 kPa < σ_3' < 400 kPa). Poisson's ratio does not seem to be affected by the large particles (20 to 50 mm) (Fig. 10).

Prospects for the Future

Compared to standard triaxial cells, the ϕ 300-mm cell presents the great advantage that, with one single apparatus, it is possible to study material behavior within the elastic domain (strains lower than 10^{-5}) up to failure (Fig. 11).

Results obtained in the field of small strains have been used already in order to fit nonlinear constitutive models for stress–strain behavior of soils. Complementary results are needed to generalize these models.

In the future, metrology will have to be improved to measure the wave velocity and the shape of signal after shock with sound detectors to compare them with the proximity transducer measurements. It may be possible to achieve more accurate measurements in the field of very small strains (10^{-6}).

The double measuring device solves the twofold problem of obtaining trustworthy measurement and of setting representative grain size distribution. It is an indispensable tool in the field of dam or nuclear power projects.

References

[1] El Hosri, M. S., "Contribution à l'étude des propriétés mécaniques des matériaux en régime non permanent," Thèse de docteur ingénieur, Ecole Centrale des Arts et Manufactures, Châtenay-Malabry, France, 1979.
[2] El Hosri, M. S., "Contribution à l'étude des propriétés mécaniques des matériaux," Thèse d'état, Université de Paris VI, 1984.
[3] Flavigny, F., "Sur les conditions d'essais," Rapport interne EDF, Electricité de France, Villeurbanne, France, 1984.
[4] Idriss, I. M. and Kennedy, R. P., "Analysis for Soil Structure Interaction Effects for Nuclear Power Plants," Report by Ad Hoc Group on Soil Structure Interaction. Committee on Nuclear Structures and Materials of the Structural Division of ASCE, 1980.
[5] Pecker, A., "Etude expérimentale du comportement dynamique d'alluvions dans une cellule triaxiale ϕ 300 mm," *Proceedings du Premier Colloque National de Génie Parasismique,* Vol. I, 1986, pp. 3–13.

Fred A. Donath,[1] Jon T. Holder,[2] and Lester S. Fruth[1]

Simultaneous Hydraulic/Physical Parameter Measurement on Rock Specimens Subjected to Triaxial Conditions

REFERENCE: Donath, F. A., Holder, J. T., and Fruth, L. S., "**Simultaneous Hydraulic/Physical Parameter Measurement on Rock Specimens Subjected to Triaxial Conditions,**" *Advanced Triaxial Testing of Soil and Rock, ASTM STP 977,* Robert T. Donaghe, Ronald C. Chaney, and Marshall L. Silver, Eds., American Society for Testing and Materials, Philadelphia, 1988, pp. 143–154.

ABSTRACT: The apparatus described provides for laboratory studies of stress-coupled parameters, with simultaneous measurement of mechanical deformation, permeability, electrical resistivity, and compressional wave velocity in 10- by 20-cm (4- by 8-in.) cylindrical test specimens with pore fluid pressure and subjected to triaxial test conditions. The compact collar-coupled design facilitates specimen installation and apparatus mobility. Axial and volumetric strains are determined using external linear displacement transducers, and differential axial stress is determined by a load cell which is an integral part of the loading column. Hydrostatic pressures in the confining fluid and in the pore fluid reservoirs up- and downstream from the test specimen are measured with pressure transducers. Data acquisition and servocontrol of the confining pressure and axial loading are performed by a microcomputer system, and test results are cross-correlated with the applied differential axial stress. Transient pulse techniques are used to determine the permeability of specimens in the range of 10^{-20} to 10^{-16} m^2 (10 nanodarcies to 100 microdarcies). The electrical resistivity measurements incorporate phase-sensitive detection with a four-terminal configuration. Transducers in the specimen end caps generate and detect mechanical pulses for wave velocity measurements. The apparatus is designed to operate with corrosive pore fluids such as brine. System performance is illustrated by representative results from tests on a specimen of domal salt during equilibration, and during and after deformation.

KEY WORDS: rock mechanics, stress-coupled hydraulic/physical tests, automated triaxial testing, permeability, electrical resistivity, wave velocity, rock salt

Laboratory testing is very useful and in many instances required for the characterization of geologic materials. Natural environmental conditions can be simulated in laboratory apparatus and altered in a carefully controlled fashion. In many cases, complex interactive systems can be analyzed in sequences of simpler, more understandable subsets of test conditions. For laboratory studies to be able to provide meaningful data, the test system must be capable of realistically simulating in situ environmental conditions. For most geologic systems, this requires at least the imposition of representative hydromechanical test conditions—triaxial states of stress with pressurized pore fluids. Because of the intimate relationships between pore fluid transport and the mechanical properties of fluid–rock systems,

[1] Vice president for Research and Development and principal geoscientist, respectively, The Earth Technology Corporation, 3777 Long Beach Boulevard, Long Beach, CA 90807.
[2] Research geophysicist, CGS, Inc., 2405 Spring Creek, Austin, TX 78704.

simultaneous permeability measurements are valuable supplements to mechanical deformation measurements.

Laboratory characterizations of geologic materials are considerably enhanced if coupled petrophysical measurements are carried out simultaneously with hydromechanical deformation measurements. Wave velocity and electrical resistivity measurements are especially useful because they provide correlations with properties routinely measured in the field. Wave velocity is sensitive to the pore structure of materials (see, for example, Ref *1*) and provides an indication of deformation-induced microfracture. The dc electrical conductivity in fluid–rock systems is generally dominated by electrolytes dissolved in the pore fluid, and it is therefore influenced by many of the same factors important for pore fluid permeability. The development of predictive microscopic models of the relationship between pore structure variation and velocity variation (see, for example, Ref *2*) and between ionic conductivity and pore fluid permeability (see, for example, Ref *3*) are important topics in many geophysical and geotechnical areas. The quantitative assessment of these models through controlled laboratory testing is critical to their development.

The apparatus described below has been developed to measure simultaneously the axial stress, axial and volumetric strains, pore-fluid pressure, permeability, compressional wave velocity, and electrical resistivity of saturated 10- by 20-cm (4- by 8-in.) cylindrical test specimens during triaxial deformation. The permeability measurement system is designed to accommodate very low permeability specimens, which are relevant to such diverse geotechnical areas as radioactive waste management, hazardous material disposal, borehole stability, and petroleum reservoir performance. Because many of the pore fluids of interest in these subject areas are corrosive, the testing system is designed to minimize apparatus corrosion and pore fluid contamination.

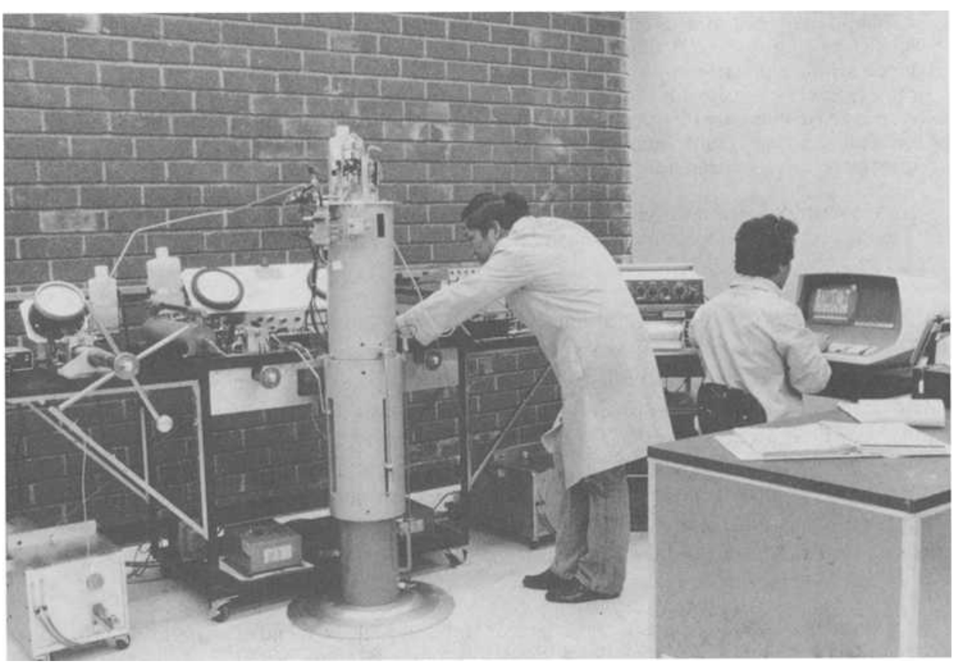

FIG. 1—*CGS Series 150 triaxial pressure apparatus for testing of 10- by 20-cm (4- by 8-in.) cylindrical test specimens.*

Apparatus and Procedures

Triaxial Test System

Figure 1 shows the CGS Series 150 Triaxial Testing System set up for coupled physical measurements of a saturated rock specimen subjected to triaxial compression; the loading column of the triaxial testing system is diagrammed in Fig. 2. The system consists of a triaxial pressure vessel coupled to a 150-ton hydraulic ram by a steel collar. The unit is capable of applying differential axial stress to 165 MPa (24 000 psi) on 10- by 20-cm (4- by 8-in.) or 585 MPa (85 000 psi) on NX-size cylindrical test specimens, and confining pressure and pore pressure to 100 MPa (15 000 psi). Deformation of the larger specimens can be up to 30% axial strain. A stress equalizer incorporated in the apparatus eliminates the effect of confining pressure on the loading column and facilitates the maintenance of constant confining pressure during axial loading. The hydraulics for the axial loading, confining pressure, and pore pressure systems are shown schematically in Fig. 3.

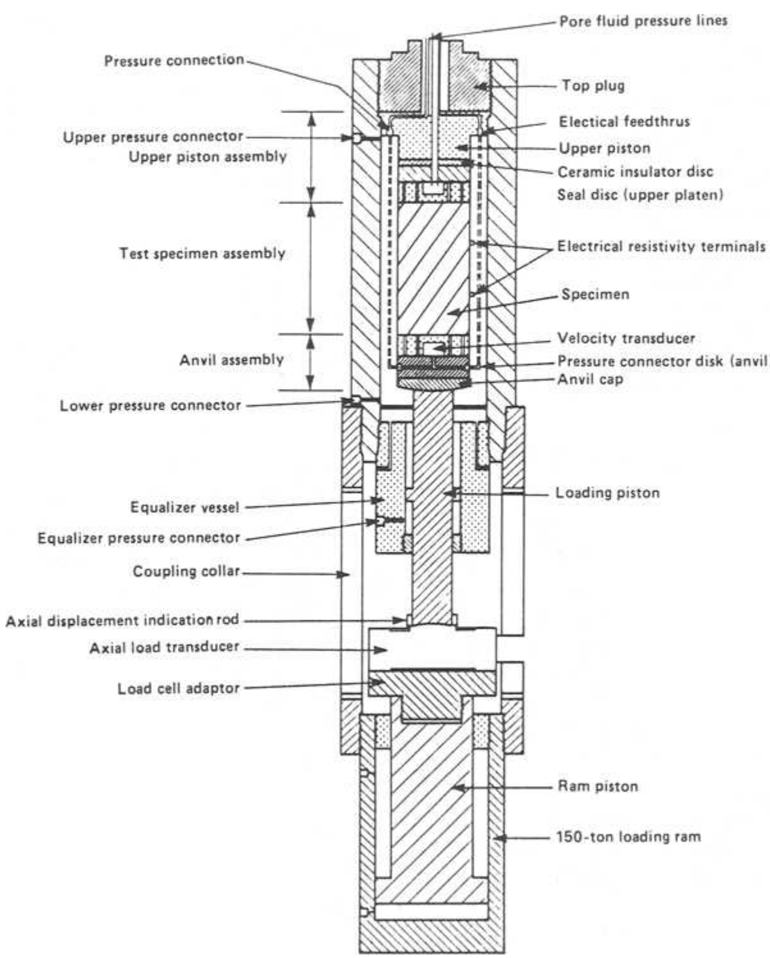

FIG. 2—*Cross-section of the triaxial test apparatus loading column. For reference, the dimensions of the specimen shown are 10 cm (4 in.) in diameter by 20 cm (8 in.) in length.*

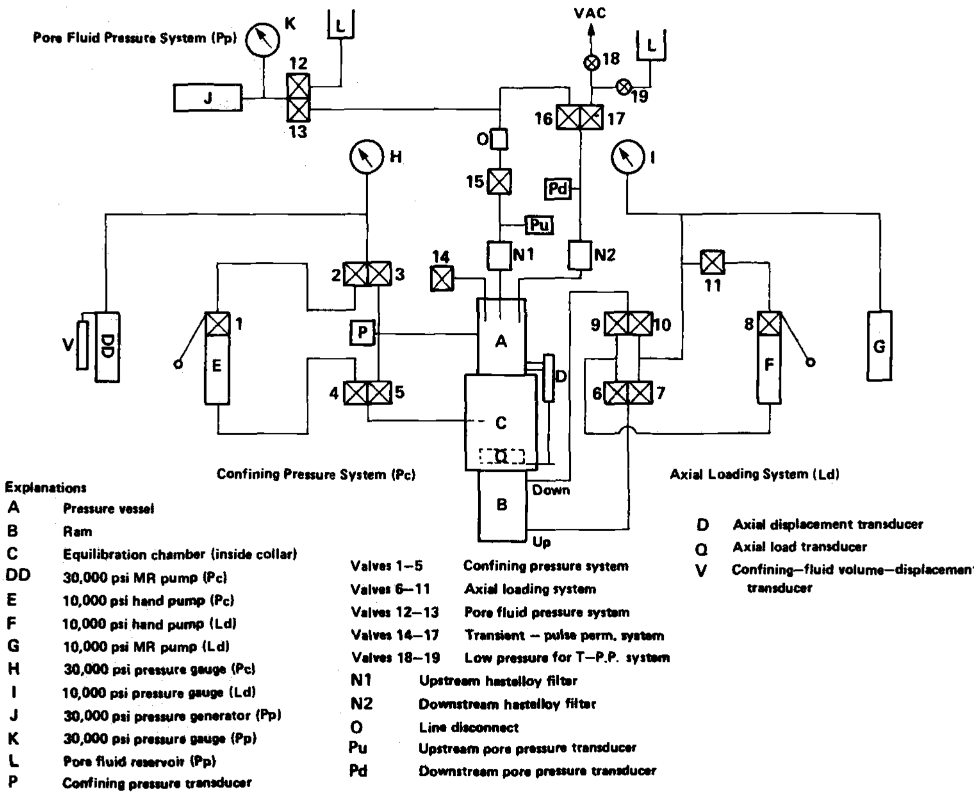

FIG. 3—*Schematic layout of the hydraulics for the axial load, confining pressure, and pore fluid pressure systems.*

The applied differential axial load is indicated by the output of the load cell in series with the load piston (Fig. 2). Axial deformation of the specimen is determined from the output of a linear displacement transducer, corrected for the measured apparatus distortion. Data reduction procedures and apparatus distortion corrections for the calculation of true axial stress and strain are described in Ref *4*. Volumetric strain is determined from the output of a linear displacement transducer attached to the piston of a multiple-rate syringe pump used for confining pressure control; a correction for the measured apparatus volume change caused by the application of axial load is incorporated into the volumetric strain calculation. Total volumetric displacement of up to 50 cc can be accommodated without recharging the syringe pump; this is the equivalent of 2.5% volumetric strain for 10-cm (4-in.) diameter specimens or 20% volumetric strain for NX-size specimens. Voltage outputs from the confining pressure transducer, up- and downstream pore pressure transducers, the load transducer, and the outputs from linear displacement transducers attached to the axial load piston and the confining pressure pump are monitored, stored, and printed by a microcomputer-based data acquisition system. Outputs from the load transducer, pore pressure transducers, confining pressure transducer, and confining fluid displacement transducer are recorded on a strip chart recorder; differential axial load and axial displacement are recorded on an *x–y* recorder. The axial load ram pressure, confining pressure, and pore pressure are also indicated by pressure gauges. The microcomputer system provides closed-loop servocontrol of confining pressure, pore pressure, and axial strain rate.

The basic collar-coupled load design concept, which allows convenient loading of the specimen assembly through the top of the vessel, was introduced in the early 1960s and a description can be found in Ref *5*. Specimen preparation and installation procedures are simplified by the use of external and load measurement transducers which provide more than adequate resolution of measured results for most testing needs. Velocity and dilatometric measurement and microcomputer-based servocontrol system enhancements are described in Ref *6*. The entire testing system is compact and sufficiently mobile that it has been used in remote field locations.

All metal components in contact with the pore fluid in the region between, and including, the up- and downstream pore fluid reservoirs are constructed from the highly corrosion-resistant alloy Hastelloy C-276.[3] Corrosion processes can detrimentally affect the mechanical integrity of system components, and spurious permeability measurements resulting from apparatus corrosion products have been demonstrated. Observed decreases of permeability in sandstone specimens were directly related to fouling of the test specimen with colloidal iron hydroxides which had formed from minor corrosion of stainless steel apparatus components by distilled water [*7*]. A comprehensive discussion of design considerations and corrosion-resistant materials for pore fluid systems is in Ref *8*.

Permeability Measurements

The present system is designed for the measurement of permeability in relatively impermeable materials by transient pulse decay techniques [*9–11*]. The mathematical formalism required for transient permeability determinations is straightforward; a summary of the formalism is given in the Appendix at the end of this paper. Permeability measurements in our system are carried out by isolating the two pore fluid reservoirs from the remainder of the respective up- and downstream pore fluid system components and manually effecting a small (10% of ambient pore pressure) pressure step change into one of the reservoirs. The permeability is determined by comparing the measured pore pressure decay to the calculated variation.

The finite difference program of Trimmer [*11*], modified to operate with Microsoft Mbasic[4] on a microcomputer, is used to calculate the family of type curves for our permeability determinations. Although pressure variations in both the up- and downstream pore fluid reservoirs are measured in the testing system, and both should conform to calculated variations, the permeability determinations are based primarily on measured differences between the up- and downstream pore pressures. This is done because test conditions, such as ambient temperature, might cause pressure variations in each reservoir, but these do not significantly affect the measured differences between the up- and downstream pressures. A family of pressure difference curves calculated for brine flow through specimens with a permeability of 10^{-19} m^2 (100 nanodarcies) and a range of effective porosities in our test apparatus is shown in Fig. 4. As noted in the Appendix, curves for other specimen permeabilities are obtained by the translation of these curves along the log(time) axis by the quantity $\log(k/k_o)$, where k is the desired permeability and k_o is the value of 10^{-19} m^2 (100 nanodarcies) used for the model calculations. Trimmer [*11*] notes that the region between normalized pressure differences of 0.1 and 0.6 is relatively insensitive to the effective porosity and should be most heavily weighted in the fit to experimental data.

[3] Hastelloy C-276 is a trademark of Cabot Corporation, Kokomo, IN 46901.
[4] Microsoft Mbasic is a trademark of Microsoft Corporation, Redmond, WA.

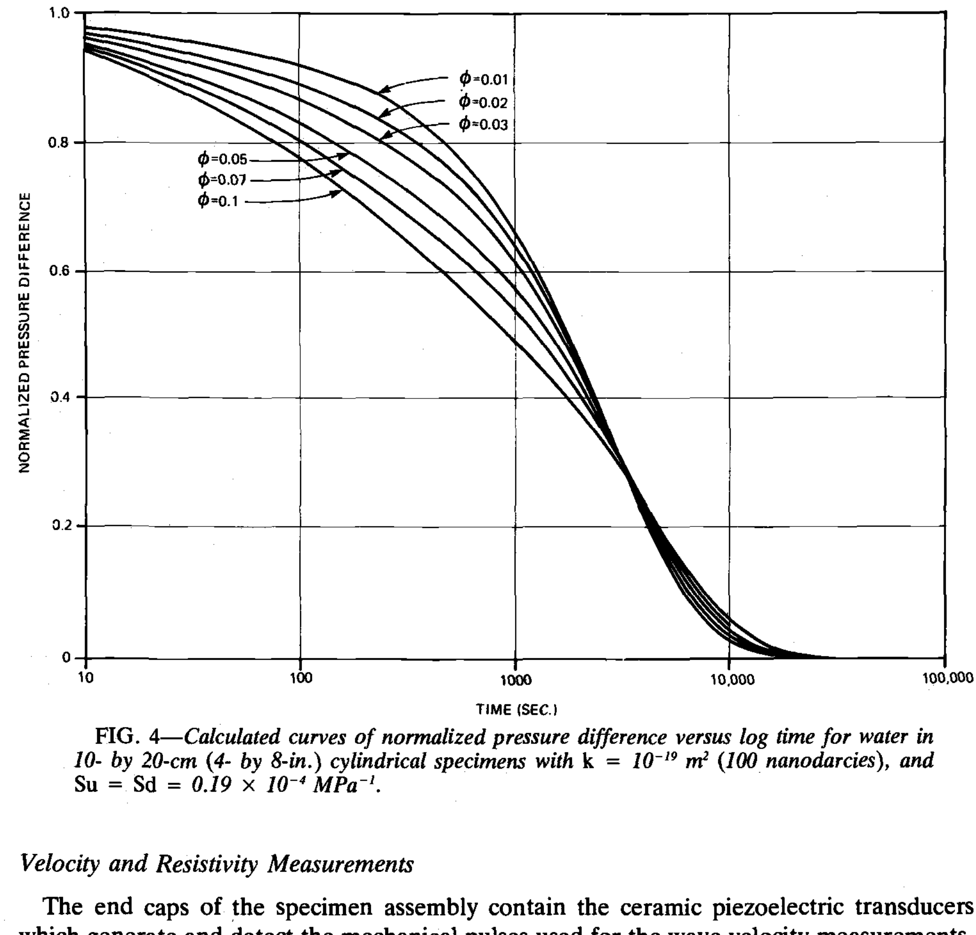

FIG. 4—*Calculated curves of normalized pressure difference versus log time for water in 10- by 20-cm (4- by 8-in.) cylindrical specimens with* k = 10^{-19} *m*^{2} *(100 nanodarcies), and* Su = Sd = 0.19×10^{-4} MPa^{-1}.

Velocity and Resistivity Measurements

The end caps of the specimen assembly contain the ceramic piezoelectric transducers which generate and detect the mechanical pulses used for the wave velocity measurements. The velocity is determined from oscilloscope measurements of the transit time for pulses generated by one transducer to travel the axial length of the specimen and be detected by the other transducer, after correction for the calibrated transit time within the end caps.

The specimen end caps are also used as current electrodes to generate a uniform axial current density for electrical resistivity measurements. The upper piston is electrically isolated from the remainder of the triaxial vessel by a high strength ceramic spacer-disk between the piston and the top plug and by a Teflon sleeve around the upstream pore fluid tube. The two potential electrodes extend through the specimen jacket and are also constructed of Hastelloy C-276.

A four-terminal phase-sensitive detection system (Fig. 5) is used to measure the electrical resistance of the specimen. The in-phase voltage difference across the potential electrodes is measured with a phase-sensitive lock-in amplifier operating at 20 Hz. The voltage readings are translated directly to the corresponding resistances of the specimen region between the potential electrodes by using, as the reference signal, the voltage across a calibrated decade resistance box in series with the test specimen. This configuration effectively eliminates any effects caused by nonohmic processes within the specimen or by contact potentials at sample-electrode interfaces, and provides a reliable measure of the absolute values as well as the relative changes in electrical resistivity of the specimen.

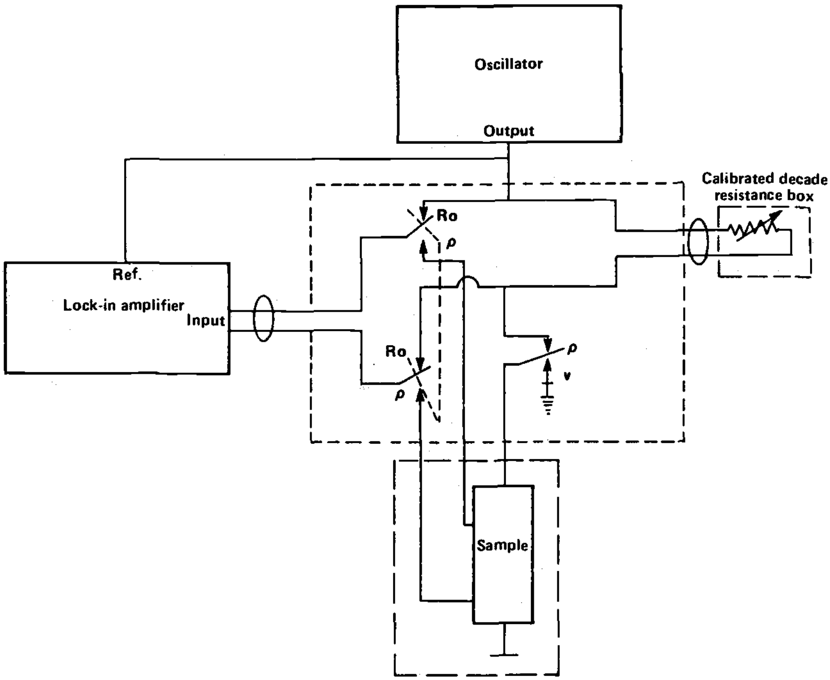

FIG. 5—*Block diagram of the four-terminal resistivity measurement and phase-sensitive detection system.*

Specimen Preparation

Considerable care is required to prepare low-permeability specimens for tests in which transient permeability measurements are carried out. It is particularly important to avoid irregular edges around the specimen end surfaces and to ensure a good contact seal between the specimen and jacket to eliminate pore fluid bypass along the specimen–jacket interface.

Prior to all end cuts and surface grinding in the preparation of our test specimens, the outer specimen diameter adjacent to the end is coated with silicone adhesive, and a 12.7- to 25.4-mm (½ to 1-in.) length of heat-shrink Teflon tubing (preshrunk to the specimen diameter) is placed over the specimen end and clamped with a jacket clamp. This procedure eliminates virtually all grain-scale chipping along the end surface edges, even for large-grained salt specimens for which grain plucking during specimen preparation is particularly troublesome.

For test specimens with smooth cylindrical surfaces, soft jacketing materials such as Viton[5] or rubber membrane will conform to the surface sufficiently to prevent bypass flow. However, most as-cored specimens have surface variations on the order of a few tenths of a millimetre, and the Viton and rubber membrane jackets are not adequate if specimen permeabilities are less than about 10^{-18} m^2 (1 microdarcy). For our test specimens, a thin even coat of silicone adhesive is applied to the outer specimen surface and allowed to set for 1 hour before jacketing. The specimen is then jacketed with a rubber membrane, and the assembly is allowed to set for 8 to 12 h before installation in the test vessel. Pore fluid equilibration times faster than those corresponding to permeabilities of 10^{-20} m^2 (10 nanodarcies) have been observed for salt specimens assembled in this way.

[5] Viton is a trademark of E. I. du Pont de Nemours & Co., Inc., Newark, DE 19711.

Representative Results

The following data illustrate the operation and performance of the testing system. The test specimen was a 10- by 20-cm (4- by 8-in.) cylinder of domal salt cored with brine and maintained in a near-saturated state by waxing the core for shipment. Brine was also used as a lubricant for specimen preparation, and specimen preparation was completed within 24 hours of extraction from the site. The prepared specimen assembly was sealed into the triaxial vessel, and air in the pore fluid and specimen was removed by evacuating the entire pore fluid system for a period of 1 h. A pore pressure of 2.76 MPa (400 psi) was applied while maintaining an effective pressure of less than 350 kPa (50 psi); the confining pressure was then raised from 3.1 to 6.2 MPa (450 to 900 psi). The system was allowed to equilibrate for approximately 24 h, during which compressional wave velocity, electrical resistance, and pore pressure were periodically measured.

Constant resistance readings would indicate specimen saturation and pore fluid equilibration [*11*], as well as specimen mechanical stability. Although the pore pressure variations stabilized to within the range of temperature-induced changes (less than 14 kPa or 2 psi per hour), the specimen resistivity continued to increase in a steady fashion; the resistance across the specimen region between the potential electrodes increased from approximately 2 to over 10 kΩ in the 24-h period. This behavior could indicate chemical nonequilibrium in the pore fluid, but it is more likely the result of continuing interconnective crack healing. The

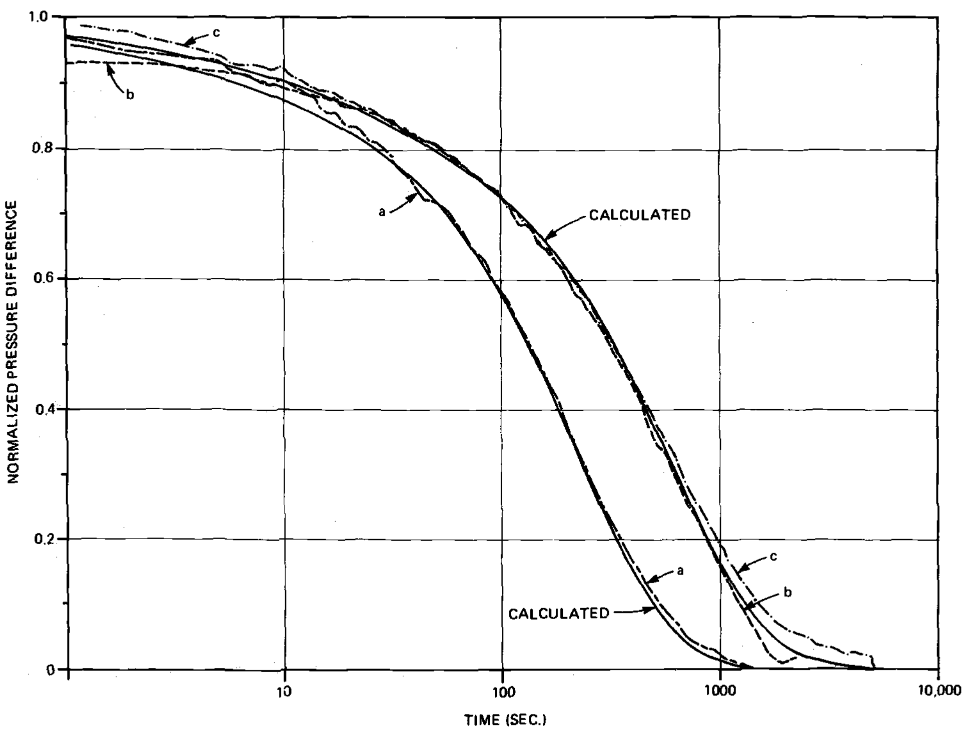

FIG. 6—*Measured pressure differences, normalized to the initial pore pressure change, versus log time. The solid curves are the best-fit calculated variations. Refer to the text for an explanation of the designations a, b, and c.*

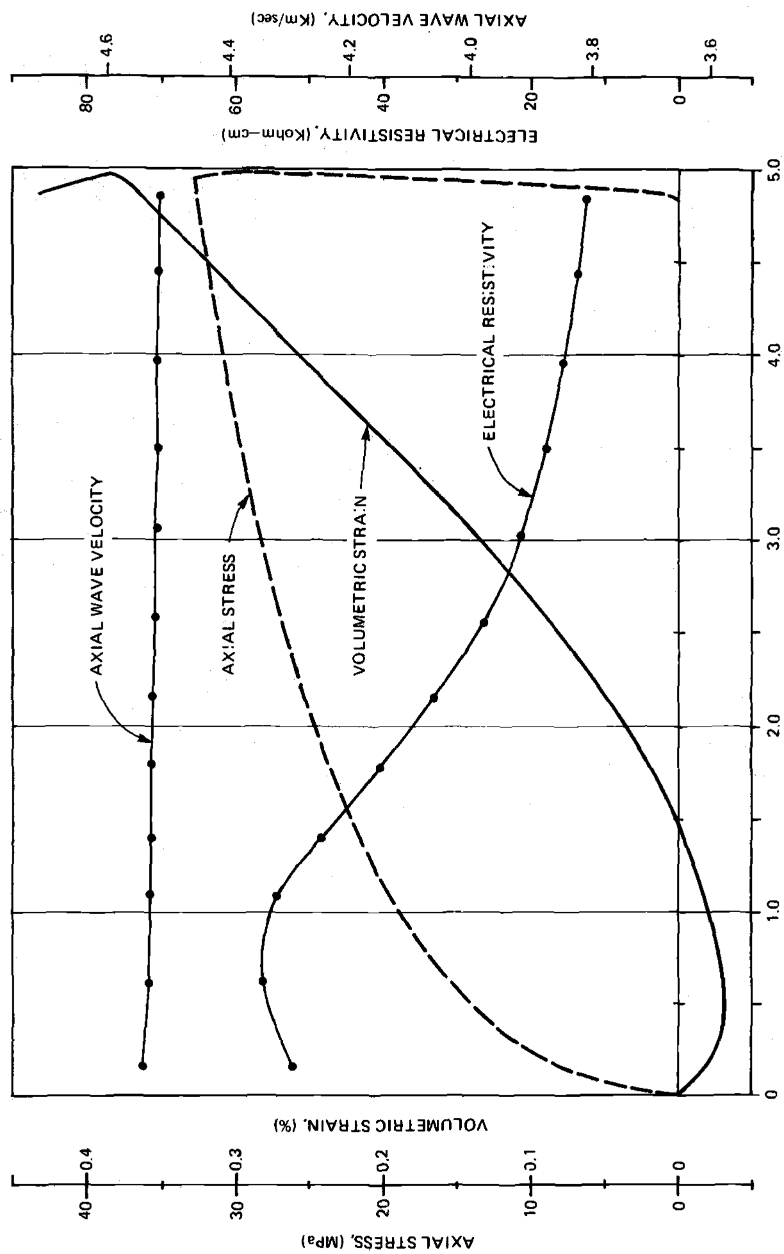

FIG. 7—*Measured variation in differential axial stress, volumetric strain, electrical resistivity, and compressional wave velocity as a function of axial strain during triaxial deformation to 5% axial strain. The confining pressure is 6.2 MPa (900 psi) and the pore pressure is 2.76 MPa (400 psi).*

compressional wave velocity remained approximately constant throughout the equilibration period.

Three sets of permeability measurements were carried out during the equilibration period. The corresponding pore pressure decay curves, following the initial pore pressure steps, are shown in Fig. 6. The pressure differences are normalized to the initial pressure change (decrease for curves a and c, increase for curve b) of approximately 0.28 MPa (40 psi) in the upstream pore fluid reservoir, and plotted as a function of the logarithm of the time after the initial change in pore pressure. Data for curve a were measured after the specimen had equilibrated for only 12 h at the test conditions. The measurements corresponding to curves b and c were carried out within a short period (10 min) of one another after the specimen had equilibrated an additional 12 h. Calculated curves representing best fits to the data are also shown; both were computed for a permeability of 10^{-19} m^2 (100 nanodarcies) and translated forward along the abscissa to their indicated positions.

The measured variations for the two closely spaced test measurements are very reproducible, particularly in the "critical region." The widely spaced test measurements indicate that permeability decreased from $1.18 \pm 0.05 \times 10^{-18}$ m^2 to $5 \pm 0.2 \times 10^{-19}$ m^2 (1.18 microdarcies to 500 nanodarcies) during the last 12 hours of specimen equilibration, while the effective porosity increased from 2 to 3%. During this same time period the confining fluid displacement indicated a total specimen volume increase of approximately 0.1% and the electrical resistivity more than slightly doubled.

The variations in axial stress, volumetric strain, electrical resistivity, and compressional wave velocity are shown in Fig. 7 as a function of axial strain during the triaxial deformation of the specimen at a constant strain rate of 10^{-5} per second. Data for the axial stress and volumetric strain curves were collected automatically at axial strain intervals of 0.02%. The resolution of the reduced data curves (less than 0.01% for the volumetric strain) illustrates the sensitivity attainable with this approach.

The electrical resistivity and compressional wave velocity measurements were performed manually; twelve measurements of each were carried out during the deformation. The electrical resistivity during deformation closely mimics the volumetric strain; both indicate substantial microfracturing for axial strains above 1.5%. Little variation in compressional wave velocity is observed in these saturated specimens. The compressional wave velocity in the pore fluid does not differ substantially from that in the intact rock, and the predominantly axial microfractures generated by the deformation of crystalline salt specimens are oriented such as to have little influence on wave velocity.

A transient pulse measurement carried out 24 hours after the deformation indicates a permeability of $7 \pm 2 \times 10^{-17}$ m^2 (70 ± 20 microdarcies). The permeability increase of two orders in magnitude is consistent with the observed resistivity decrease and volumetric strain increase associated with deformation-induced dilatancy. This permeability is near the upper limit of the range for which transient pulse techniques can be used, and the large uncertainty in the measured permeability reflects the difficulty in fitting pore pressure decay curves for the very rapid equilibration time (on the order of 20 s).

Summary

The triaxial apparatus and testing system described in this paper have been developed to permit the simultaneous measurement of mechanical and pore fluid transport properties, compressional wave velocity, and electrical resistivity in low-permeability material saturated with corrosive pore fluid. The system design is compact and facilitates specimen installation and operation at remote locations. Representative test results from a study of brine-saturated salt specimens illustrate the operation and excellent performance of the system.

Appendix

Transient Pore Fluid Behavior

Fluid flow through a permeable specimen with a cross-sectional area, A, can be generally described by Darcy's law:

$$Q = (kA/\mu) * (dp/dx) \tag{1}$$

where Q is the volume rate of flow, k is the specimen permeability, μ is the fluid viscosity, and dp/dx is the pressure gradient across the specimen. The dimensions of k, permeability, are length squared (m^2). For reference, 10^{-12} m^2 is the equivalent of 1 darcy; if the fluid is pure water under standard conditions, the hydraulic conductivity of a specimen having a permeability of 10^{-18} m^2 (1 microdarcy) would be 10^{-11} m/s.

Prior to the establishment of steady state conditions, the time rate of pore pressure change is given by the ratio of the rate of pore fluid volume change to the storage capacity of the specimen pore volume (the change in pore fluid volume with pore pressure). Using Eq 1 for the net rate of pore fluid volume change along the specimen, and defining an effective specimen porosity, ϕ, as the ratio of pore volume storage capacity to the product of specimen volume and pore fluid compressibility, β, the differential equation for the pore pressure within the specimen is

$$d^2p/dx^2 = (\mu\beta\phi/k) * dp/dt \tag{2}$$

The boundary conditions at the ends of the specimen are

$$dp/dx|_{x=o} = Q|_{x=o}/Su \tag{3}$$

$$dp/dx|_{x=L} = Q|_{x=L}/Sd \tag{4}$$

Su and Sd are the storage capacities of the up- and downstream reservoirs, respectively, which reflect the compressibility of the pore fluid and the yielding of the pore fluid apparatus; both they and the effective specimen porosity must be determined experimentally for each test specimen/apparatus configuration.

The set of differential equations in Eq 2–4 has no closed form solution, but numerical solutions to the complete transient-response equations have been developed [*11*], and Hsieh et al. [*10*] have derived a series solution. Permeability appears in the equations only as a product with time, so that the solutions for any permeability, k, and a given specimen geometry and pore fluid reservoir configuration are obtained by a translation of solutions for one set of curves calculated for a particular permeability, k_o, by the quantity $\log(k/k_o)$. The pore pressure decay curves shown in Fig. 4 were calculated with Trimmer's finite difference algorithm for a permeability of 10^{-19} m^2 and the indicated parameters appropriate for our test system configuration.

The calculated transient pressure responses for a wide range of specimen/apparatus configurations indicate that the pore pressure decays to within one-tenth the initial pressure difference in a common equilibration time, τ, on the order of

$$\tau = 1.5 * (\mu LSu/kA) \tag{5}$$

This parameter represents the typical time required for a transient pulse measurement.

References

[1] Johnston, D. H. and Toksoz, M. N., *Journal of Geophysical Research*, Vol. 85, 1980, pp. 925–936.
[2] Cheng, C. H. and Toksoz, M. N., *Journal of Geophysical Research*, Vol. 84, 1979, pp. 7533–7544.
[3] Thompson, A. H., *Bulletin of the American Physical Society*, Vol. 31, 1986, p. 267.
[4] Donath, F. A. and Guven, N., *Contributions to Geology*, Vol. 10, 1971, pp. 89–123.
[5] Donath, F. A., *Testing Techniques for Rock Mechanics, ASTM STP 402*, American Society for Testing and Materials, Philadelphia, 1966, pp. 41–51.
[6] Schrodt, J. K. and Holder, J., "Rock Mechanics: Theory–Experiment–Practice," in *Proceedings, Twenty-fourth U.S. Rock Mechanics Symposium*, 1983, pp. 449–468.
[7] Potter, J. M., Dibble, W. E., and Nur, A., *Journal of Petroleum Technology*, Vol. 33, 1981, pp. 905–907.
[8] Johnson, C. B. and Holder, J., "Rock Mechanics: Key to Energy Production," in *Proceedings, Twenty-seventh U.S. Rock Mechanics Symposium*, 1986, pp. 632–639.
[9] Brace, W. F., Walsh, J. B., and Frangos, W. T., *Journal of Geophysical Research*, Vol. 73, 1968, pp. 2225–2236.
[10] Hsieh, P. A., Tracy, J. V., Neuzil, C. E., Bredehoeft, J. D., and Silliman, S. E., *International Journal of Rock Mechanics and Mining Science Geotechnical Abstracts*, Vol. 18, 1981, pp. 245–252.
[11] Trimmer, D., *Reviews of Scientific Instruments*, Vol. 53, 1982, pp. 1246–1254.

James R. Baleshta[1] *and Maurice B. Dusseault*[1]

Triaxial Testing of Intact Salt Rocks: Pressure Control, Pressure Systems, Cell and Frame Design

REFERENCE: Baleshta, J. R. and Dusseault, M. B., **"Triaxial Testing of Intact Salt Rocks: Pressure Control, Pressure Systems, Cell and Frame Design,"** *Advanced Triaxial Testing of Soil and Rock, ASTM STP 977,* Robert T. Donaghe, Ronald C. Chaney, and Marshall L. Silver, Eds., American Society for Testing and Materials, Philadelphia, 1988, pp. 155–168.

ABSTRACT: An extensive laboratory for intact salt rock behavior research (the WATSALT Laboratory) was conceived at the University of Waterloo in 1982, and by 1984 researchers here were producing results of high quality. At present, six high capacity test stations for creep behavior are operating on a continuous basis. The designs were developed to meet the requirements of constant pressure, environmentally stable creep testing. Self-regulating pressure control systems have been designed, and they are performing effectively. The WATSALT systems can test a range of specimen sizes to 100 mm in diameter, at stresses of 200 MPa axial, and 70 MPa lateral. Creep test durations have extended to 6 months on an individual specimen. The automated control systems keep temperatures constant to 0.1°C and pressure fluctuations to within 0.1%. This paper describes the approach to design, the triaxial cell and axial load frame configuration, an alternate internal axial piston cell, temperature and pressure control systems, instrumentation, and data acquisition.

KEY WORDS: triaxial cell, loading frames, temperature control, pressure control, data acquisition, salt

This paper describes the design, development, and systematic use of triaxial equipment related to potash and salt research at the University of Waterloo. Extensive triaxial testing on intact salt specimens required the design of specialized research equipment and the implementation of instrumentation, data acquisition, and control systems.

Laboratory studies of creep behavior tend to be long-term projects. Tests on an individual specimen can extend over 6 months, and creep strains can approach 15%. For the 48- to 102-mm-diameter specimens tested at length-to-diameter (L/D) ratios of 2:1, this translates to axial shortening of 14 to 31 mm. In addition, experience indicated that normal laboratory temperature fluctuations of ±2°C can create a 0.5-MPa confining pressure deviation in a cell. The design procedure required an accommodation of these parameters, solving the problems of stability for long-term tests, and generating an economic design.

Design Approach

In light of these constraints, a general approach or "philosophy of design" was conceived. The major components required for each complete test system were divided into the fol-

[1] Research/design engineer and professor, respectively, Department of Earth Sciences, University of Waterloo, Waterloo, Ontario, Canada N2L 3G1.

lowing subgroups: triaxial cell, axial load frame, axial and lateral pressure control, temperature control, instrumentation, and data acquisition.

Personnel safety was always of primary concern, therefore it was imperative to minimize the pressurized volumes, to use competent materials with ample reserves of strength beyond the working stresses, and to design proper electrical and pressure circuits.

The next most important design criterion was versatility so that the equipment could be adapted readily to other modes of testing. To enhance this versatility, each system, or creep station, required an axial stress capability of 200 MPa (over a range of specimen diameters to 100 mm) and a confining pressure capability of 70 MPa. It was also desirable to minimize the possibility of losing a specimen in the midst of several months of testing because of the failure of one component in the system.

Design for extended test duration included automated data acquisition (with electronic instrumentation) and some "closed loop" form of process control to regulate temperatures and pressures. Finally, the complete system was to be as compact and economical as possible.

Triaxial Cell Design

Separate triaxial cells were designed to test 44-, 48-, and 54-mm specimens. These cells were designed to withstand confining pressures to 70 MPa. A cross-sectional view of a typical cell is shown in Fig. 1.

The triaxial cells operate in a similar fashion to the common Hoek-Franklin cell [*1*]. Confining pressure is applied to cylindrical test specimens with hydraulic oil. The specimens are isolated from the pressurized oil by a urethane sleeve. These sleeves are oil resistant, leakproof, and reusable. Although the inner diameter has been set by the mandrel diameter on which the membrane was made (plus 0.7% typical shrinkage), the outer diameter of the membrane can be ground to tolerances of about ±0.4 mm. For specimen diameters of 54 mm and smaller, our experience is that the optimum urethane durometer rating is 70.

Monobloc 4340 steel was used to construct the pressure cylinders. The vessels were machined to approximate size, heat treated to a Rockwell C hardness (HRC) of 30 to 32, then machined to final dimensions. The heat treatment imparts a greater uniformity in material properties, refines the grain size, and increases the strength of the vessel [2]. The Rockwell C value specified for the 4340 steel brings the ultimate strength of the material to 960 MPa and the yield strength to 825 MPa, while maintaining ductility.

The cylinders were designed with a minimum inside diameter, after taking lateral specimen expansion (as high as 8% at 15% axial strain) into account. A reduced inner diameter reduces the pressurized fluid volume which enhances safety, requires less vessel wall thickness for sufficient tangential strength, and reduces overall vessel weight and manufacturing cost. The margin of safety employed for the working stress of the vessels followed Section 8 of the American Society of Mechanical Engineers (ASME) Pressure Vessel Code [*3*].

Pressure seals are of the positively actuated lip or cup seal geometry. With our seal arrangement a vessel which may have required four to eight O-rings can be sealed with two seals, each one serving multiple purposes. The seals are located between the bore and the membrane to keep hydraulic oil from penetrating the specimen, exiting the vessel, and seeping through the clearance at the axial piston. Machining of seal installation chamfers and selection of a beveled edge style seal greatly facilitated cell assembly. To save user time and trouble, seal retainers were implemented so that specimens could be changed without draining the hydraulic oil.

Threaded end caps are used to enclose the vessel. With the use of hook spanner wrenches the vessels can be assembled easily. Assembly is further facilitated because the lip seal does not require an initial torque for sealing. Studies have shown that the tensile strength of a

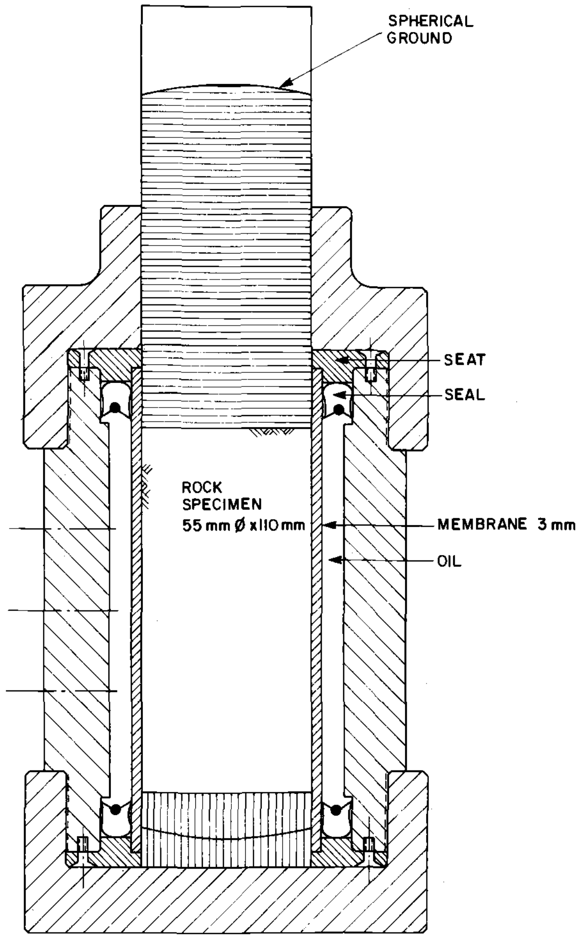

FIG. 1—*Triaxial creep cell, cross-sectional view.*

threaded rod is roughly equal to an unthreaded rod of diameter equal to the pitch diameter of the thread [*4*], hence with threads on the outer diameter of the vessel, the enclosures can be very strong when used under static or low cycle loading. However, stress concentrations in threads can be as much as 3.85, which was considered when evaluating the applied stresses in this region [*5*].

The ram and lower platen which contact the specimen are of 304 or 316 stainless steel. One system has been modified to include flow-through capability. To deal with sample end nonparallelism, a spherical seat has been incorporated at the bottom platen. A second spherical seat is used outside the vessel to account for any nonparallelism between the axial piston and the load frame actuator. A close sliding fit (0.012-mm clearance) was provided for the piston, with a guide length one and one-half times the piston diameter. This reduces side friction and binding but is not a pressure seal.

The surfaces of the piston and lower platen are sprayed with a thin layer of dry lubricant before testing to minimize specimen end restraint created by platen friction and to reduce the amount of barrelling.

Loading Frame

Compressional load frames were required to apply axial load to the triaxial cells described in the previous section. They are semiportable, easily dismantled, constructed of inexpensive and readily available materials, and adjustable to accommodate various sizes of triaxial cells.

The alternative selected as best suited to these purposes was a bolted frame design using standard structural steel. Design analysis followed the provisions of the structural steel Canadian Standards Association Standard S16.1 [*6*]. The design used stiffened 200- by 200-mm wide flange sections for the upper and lower beam members and two 100- by 100-mm wide flange sections as columns.

Steel plates, 25 mm × 200 mm, were welded to the column members for additional stiffness. The frame was assembled by bolting these sections to plates which were welded onto the ends of the beam members. Two rows of three 16-mm Class 5 bolts were used at each connection. Additional bolt holes were drilled to permit height adjustment. The bolted connections were designed so that friction between the sandblasted plates would be sufficient to withstand full actuator load. This prevents slippage during testing and avoids the possibility of applying excess shear to the first bolt to come into bearing. As an additional precaution, the connections were designed so that the shear plane would not intersect the threads of the bolts. Transverse and 45°-oriented stiffening plates were added to prevent web crippling, local flange buckling, and shearing of the beam members, and to resist moment-induced thrust in the columns.

Compact, commercially available hydraulic cylinders are used to supply the compressive force for each load frame. These actuators were secured to the upper beam member of the frame. A 200-mm circular hardened steel disk has been mounted to the lower beam as a platen. The facing flange surfaces of the beams were machined flat to ensure parallelism between the platen and the ram. The platens also act as bearing plates and distribute the vertical load applied to the beams. This increases the local bearing resistance of the flanges on which these plates are mounted. To complete the design, angular sections were bolted to the outer column flanges to prevent toppling.

Frames were tested by repeated cycling to full load capacity. To calibrate the hydraulic cylinders, accurate load cells were inserted in the frames. Dial gauges were used to check frame stiffness by determining deflections resulting from column extension and beam bending. At full capacity a maximum deflection of only 0.6 mm was found.

In the completed form, the frames are 1150-mm-high "bench top" units capable of withstanding 450 kN of compressive force, with an adjustable working space of 430 by 530 mm. A third frame was later constructed of larger members but of the same overall design for 900-kN capacity. Figure 2 shows 450-kN frame with temperature chamber and triaxial cell.

Internal Piston Cell

In 1985 an expanding program of laboratory research required the construction of three additional creep stations for testing 100-mm-diameter intact salt specimens. An alternative cell/frame system was developed. Instead of the usual triaxial cell with an external compression frame providing axial load reaction, these cells were designed to incorporate both axial load and confinement pressure in a compact integral unit. This resulted in savings in materials, labor, implementation time, and space requirements in the laboratory. The vessels were designed to be capable of applying 210 MPa axial stress and 70 MPa confinement stress on 100 mm × 200 mm cylindrical specimens.

In many respects, the upper portion of this design was similar to the triaxial cell described

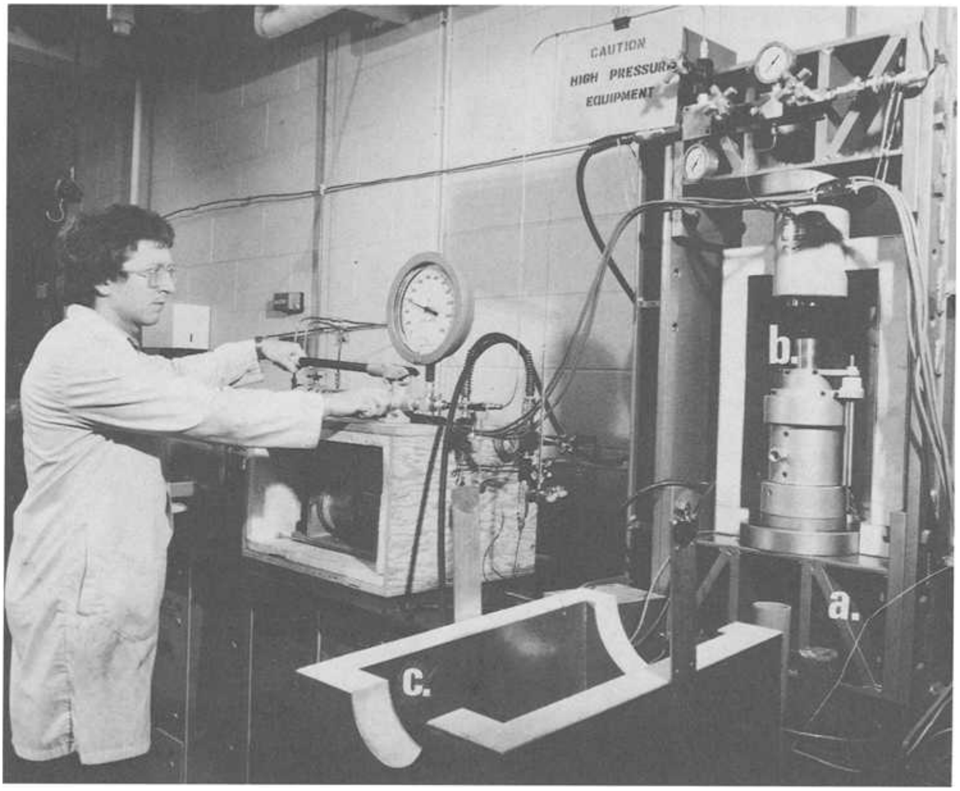

FIG. 2—*Example of a 450-kN frame, with triaxial cell and temperature chamber.* a = *compression frame,* b = *triaxial cell,* c = *temperature chamber.*

earlier (albeit upside-down) in that the membrane, spherical seat, and sealing method were retained. The membrane thickness was 3.2 mm, as before; however, for the larger 100-mm diameter, a urethane durometer of 80 was used. An additional chamber with an internal axial load piston was incorporated at the lower end of the cell to apply the axial load. The larger diameter (178 mm) of this chamber was required to achieve the desired 1750-kN axial load under a hydraulic actuation pressure of 70 MPa. The axial load piston was constructed of aluminum for reduction in weight and ease of machining. The tall profile of this piston was designed to reduce side loading, and wear rings and a low-friction lip seal were incorporated to minimize break-away friction stick-slip. As a result the piston moves quite readily, requiring only about 7 kPa to initiate movement. This created a responsive system which quickly adjusts to creep movement. The piston has a stroke length of 40 mm which can accommodate up to 19% strain in the specimen. Axial force calibration was accomplished by inserting a load cell in place of the upper (confinement) chamber.

A single set of end plates encloses both vessels, and a series of ten threaded tie rods (32 mm in diameter) holds the entire system together. An intermediate ring separates the two chambers, provides cylinder alignment, seal seating and additional bearing for the piston, and protects the tie rods from errant lateral blows during assembly. Materials for the vessel included 4340 steel for the enclosures and cylinders (again heat treated to HRC 30), and a cold worked steel called "Stressproof" for the tie rods. The ram and platen were machined from 304 stainless steel.

Three cells were built in this fashion (Fig. 3). They form compact 355- (diameter) by 760-mm units and require about 40% less laboratory space than an equivalent external frame system (Fig. 4). The cost savings in construction for this integral type of creep station over the former were approximately 35%, and the capabilities are considerably greater.

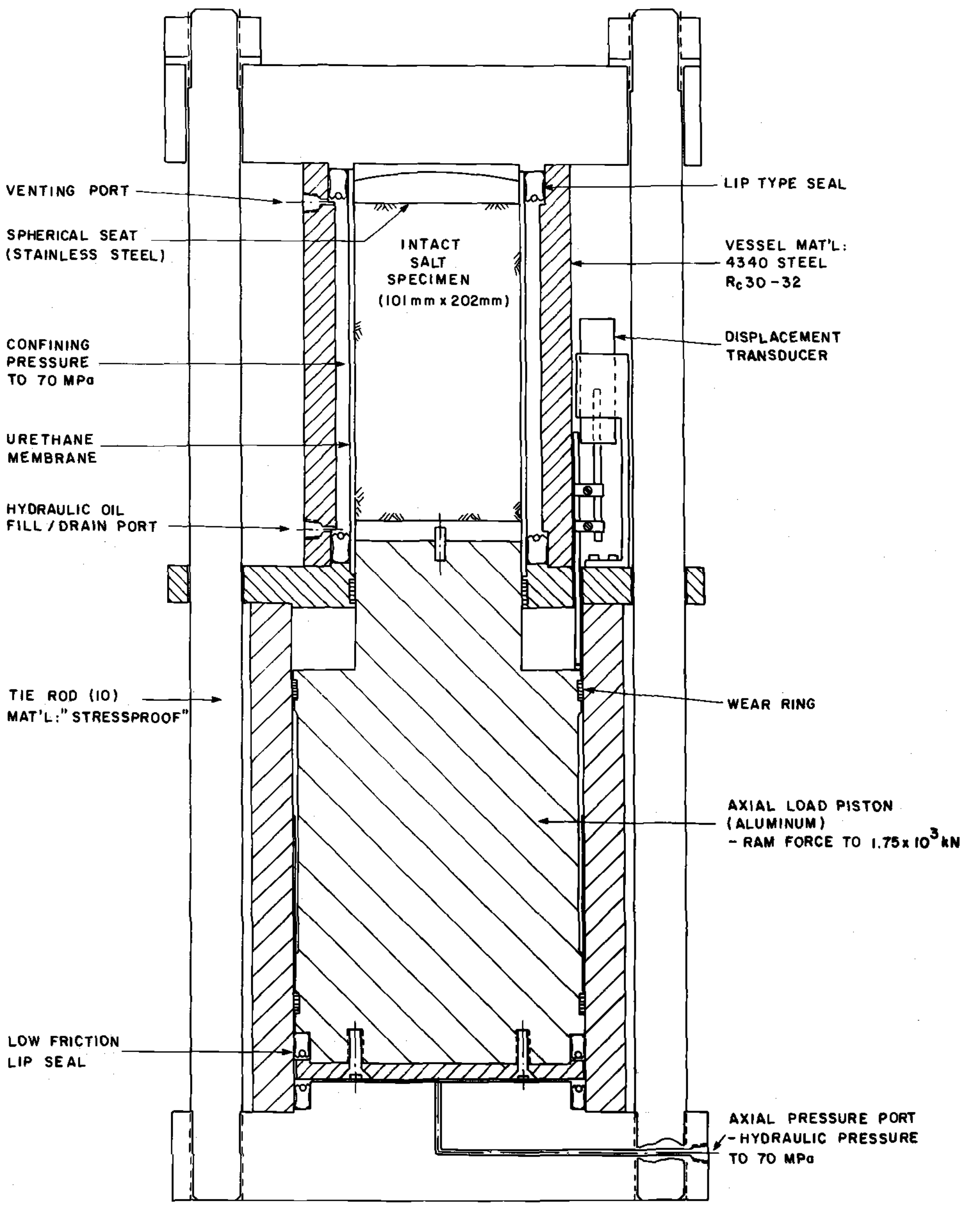

FIG. 3—*Internal piston creep cell, cross-sectional view.*

FIG. 4—*Three internal piston cells in the laboratory.*

Pressure Application and Control

Fluctuation of lateral and axial pressures are induced by changes in air temperature, minute leaks through fittings, and by creep deformation of the specimen. Due to the 24 h/day extended nature of testing, manual pressure adjustment was not feasible, hence an automated system was required to accurately and reliably control hydraulic pressures. The risk of failure of the pressure system (resulting in a loss of perhaps several weeks of testing) was to be minimized.

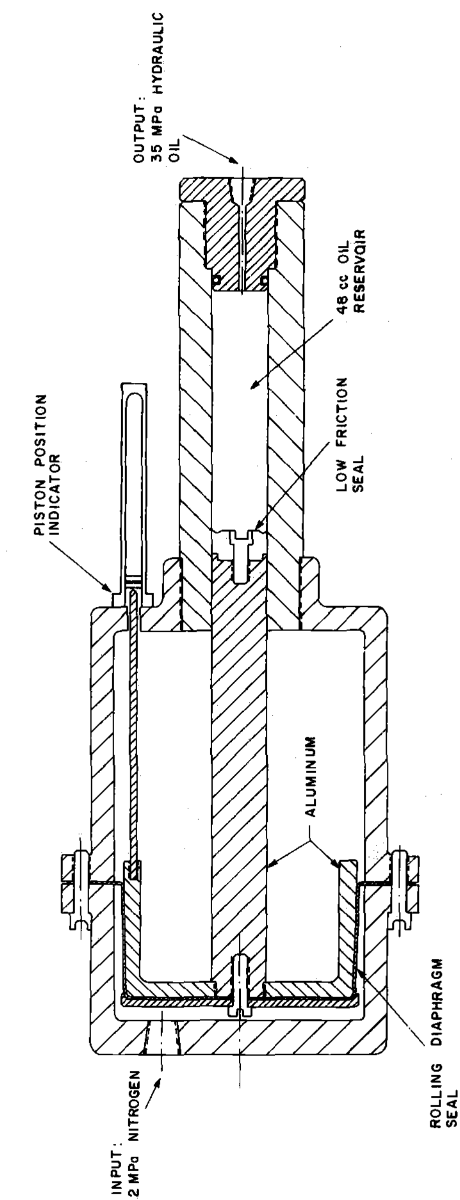

FIG. 5—*Intensifier-accumulator.*

A combination "intensifier-accumulator" was designed to reduce these pressure deviations. This device is an accumulator because it stores a quantity of compressed nitrogen to buffer pressure fluctuations induced by changes in the pressurized volume. It is also an intensifier because the output hydraulic oil pressure side of the device is boosted from the 2.0-MPa nitrogen pressure to 70 MPa due to a cross-sectional reduction of the bore.

A major objective in the design of this intensifier-accumulator was to reduce the breakaway friction and drag during operation. To achieve this, a rolling diaphragm seal was used at the low pressure, nitrogen end of the device. This seal confines the nitrogen in a 100-mm-diameter bore and can take working pressures to 2.0 MPa. At the high pressure end of the intensifier-accumulator a 17.5-mm rod transmits the force applied by the compressed nitrogen and pressurizes the hydraulic oil. A low friction lip seal is used to contain the high pressure oil. The volume of oil stored is set by the stroke length of the diaphragm seal and diameter of the high pressure bore. The volumes are 48 cc for a 35-MPa output version and 24 cc for a 70-MPa design. An outside indicator on the intensifier-accumulator reveals the piston location. When the piston has completed 90 to 95% of its stroke, the intensifier-accumulator can be restroked (using a small hydraulic hand pump) in 45 s or less, with no fluctuation of system pressure. This may happen every few days in rapid creep testing, but more commonly every few weeks. A cross-sectional view of the intensifier-accumulator is shown in Fig. 5.

To regulate pressures automatically and accurately, a closed-loop (self-regulating) system was designed. Pressure is monitored by a pressure transducer at the high pressure, hydraulic

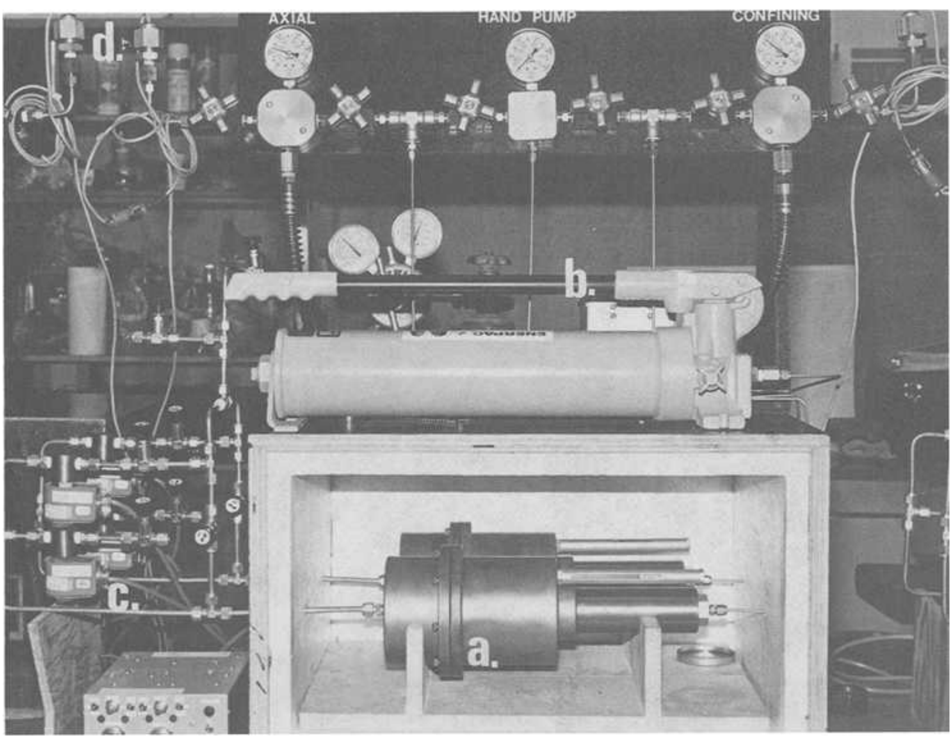

FIG. 6—*Pressure control system for an individual creep station.* a = *intensifier-accumulator,* b = *hydraulic hand pump,* c = *solenoid valves,* d = *pressure transducers.*

oil end of the system. The pressure transducer signal is fed to either an analog control unit or a microprocessor, and is compared to a selected reference. If the pressure is low a solenoid valve in line with the nitrogen source opens to increase system pressure. Alternatively, if pressure is excessive, a second solenoid valve opens to vent some nitrogen gas to the atmosphere, which lowers the system pressure. Needle valves are placed in series with the solenoid valves to throttle (buffer) the amount of nitrogen flow into or out of the system to give it a high degree of stability. Typically, a single bottle of nitrogen lasts for 6 months of continuous testing because the system is leak-free and requires no continuous bleed-by.

Two complete pressure control systems are required for each creep station: one for axial load, one for confining pressure. Pressure can be constantly maintained to within $\pm 0.1\%$ of the selected operating pressure. Since 1983 fifteen of these systems, including intensifier-accumulators, have been used at the University of Waterloo. Twelve of these systems are used to control the six creep stations in the WATSALT Laboratory. A dual pressure control system for one creep station is shown in Fig. 6.

The design of the pressure system explicitly sacrifices rapid loading capability. The most rapid reasonable strain rate that can be applied by controlling the pressure system with a microprocessor is about 10^{-5} s^{-1}, and this would require relatively frequent recharging by hand. However, the savings generated by the current design as compared to a commercial

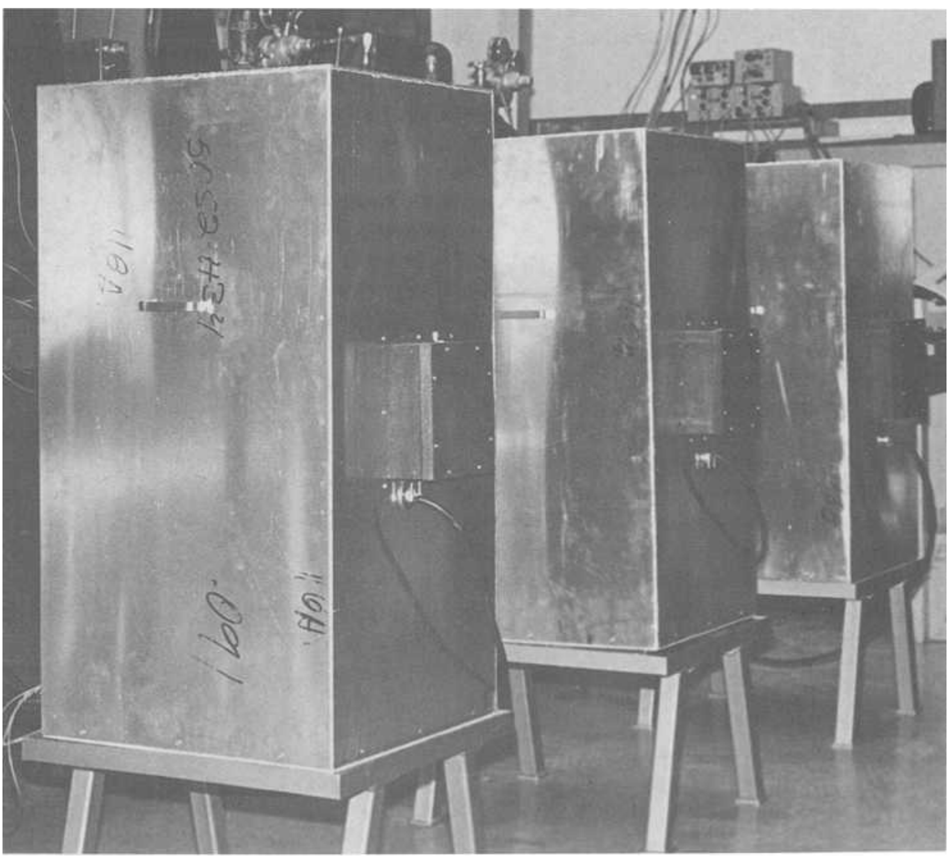

FIG. 7—*Internal piston cells with temperature control chambers in place.*

servo-controlled system are on the order of \$30K to \$100K (Canadian) depending on which system is purchased.

Because the system uses pistons of the same diameter as specimens, triaxial extension tests can be carried out. Also, microprocessor pressure control permits programming any stress path, providing strain rates are relatively slow.

Temperature Control

Experience has shown that changes in temperature can cause significant hydraulic pressure fluctuation in the test cells. Separate temperature chambers were built for the six creep stations, each with individual temperature control.

The temperature boxes are constructed of 50 mm of extruded polystyrene foam insulation with interior and exterior aluminum sheet casing. They are typically 0.13 m^3 in volume. The units for the external frame/cell systems are detachable in two components (Fig. 2), whereas the boxes for the internal piston cells are single units and are lowered directly onto the cell (Fig. 7). All boxes are lightweight and can be installed by hand.

The heaters for these chambers are two 100-watt light bulbs. A thermistor monitors the interior temperature, and an analog control unit turns the light bulbs on to heat the box as required. A squirrel cage fan circulates the air in the chamber when the light bulbs are on. Temperatures are adjustable to 50°C with this device and are controlled to ± 0.1°C. Replacing the bulbs with higher wattage devices or direct heating coils would allow the chambers to operate up to a design limit of 75 to 80°C.

Room temperature air (typically 20 ± 2°C in the laboratory) is used as the cooling medium. However, one design has incorporated a cooling unit consisting of thermal-electric modules and can lower the chamber temperature to 10°C if desired.

A dual Plexiglas window is included in each chamber for visual monitoring of the test operation without removal of the temperature chamber. Hydraulic hoses and electric cables that run into the box are sandwiched between layers of soft foam rubber to provide a thermal seal.

Instrumentation and Data Acquisition

Data required routinely from each creep station include axial and confining pressures, specimen axial deformation, and cell temperature. Electronic instrumentation is used to monitor these parameters. Output signals from this instrumentation are recorded at regular intervals.

The transducers used in the pressure control loops are also the indicators of axial and confining pressure. These pressure transducers were selected for their ability to withstand long-term pressure application as opposed to quick cycling or fatigue. Our work has found that strain-gauged, welded metal diaphragm-style transducers tend to be well suited for this purpose.

The axial deformation of the specimens is monitored by a single linear variable differential transformer (LVDT) mounted inside the temperature-controlled environment. The LVDTs were mounted directly to the cell piston to be as unaffected as possible by any deflection in the system other than the contraction of the specimen. Aluminum dummy specimens were tested in each cell to determine the extent of equipment effect so it could be subtracted from the actual readings. The LVDTs used were of the range ±25 mm to cover the entire range of specimen deformation during an extended test. Currently, work is being done using a ±1.3-mm LVDT in addition to the longer stroke unit, for enhanced resolution. This shorter stroke LVDT can be reset as required. Displacements of a few microns in a day can be

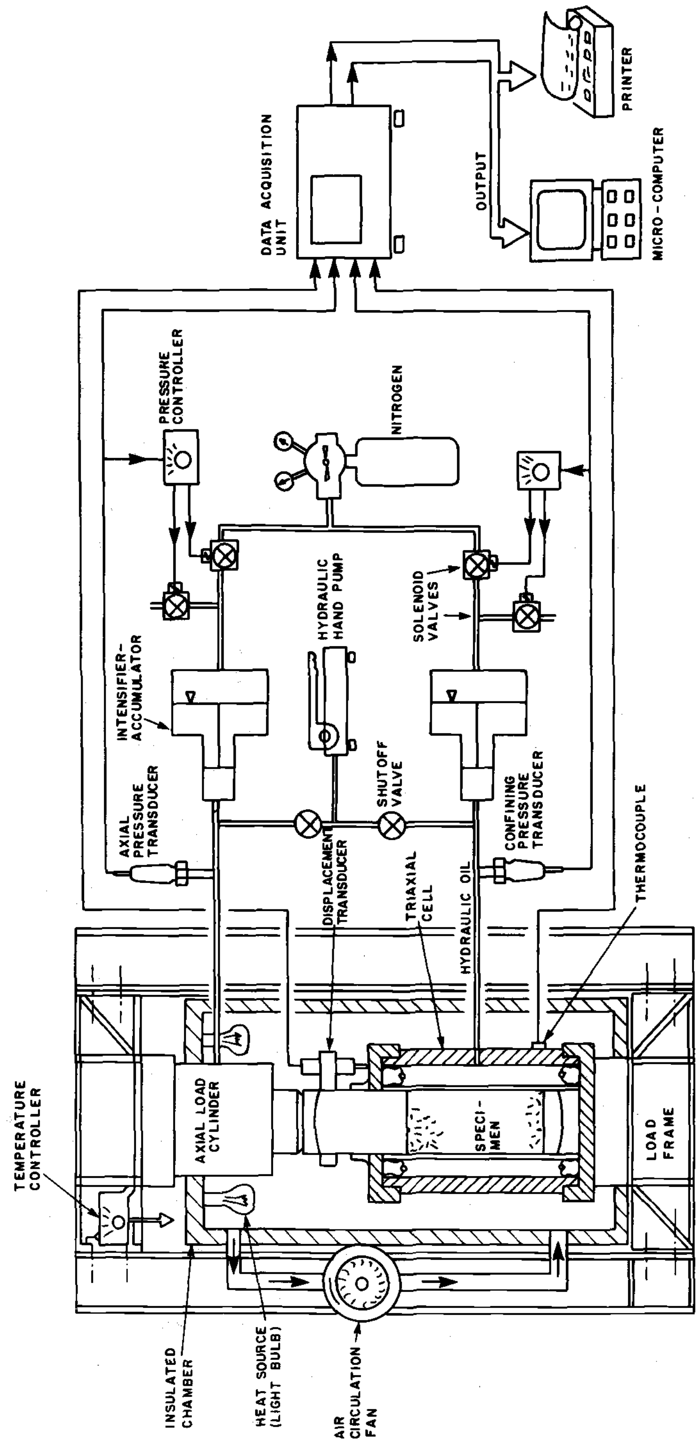

FIG. 8—*Major components of an individual creep station.*

detected, and the systems have been monitoring creep tests at strain rates of $5 \times 10^{-10}\ s^{-1}$ on 200-mm-long specimens with no serious problems.

The commercial data acquisition device selected for use in the WATSALT Laboratory contains an integral screen for multichannel output. The complete data for each creep station can be displayed on the screen as a "page" of information containing all relevant channels. It is possible to configure the input voltages so they read in the direct units desired, for example, MPa for the pressure transducers. Another design feature of this data acquisition system is its capability of internally providing both power source and signal conditioning for the instruments. Hence only a single cable for each instrument is necessary to send power and return the output signal. This eliminates the costs for power supplies, additional connectors, and amplifiers; reduces installation labor; and decreases the possibility of poor electrical connections. In the extensive equipment configuration of the WATSALT Laboratory, reducing the myriad of wires which typically surround a multichannel electronically instrumented system allows a more efficient operation and reduces the likelihood of damage.

Finally, the output readings for each system are sent through a RS-232 port on the data acquisition system to a personal computer which outputs the data to both a hard copy printer and magnetic storage medium (floppy disk) at regular predetermined intervals.

Figure 8 is a schematic diagram of the major components of an individual creep station.

Summary

An extremely compact and economical system for triaxial creep testing of cylindrical specimens has been designed and is in continous use. It provides most of the capabilities of much larger systems at literally a fraction of the cost because of several straightforward but novel design concepts. The precision and reliability of the system is very high, and the entire assembly has been shown to be stable for months.

The major novel aspects of the system are the pressure sealing method, the pressure control system which incorporates the intensifer-accumulator, and the integral reaction cell. The entire system can emulate all functions of commercial systems costing up to five times as much, except for rapid loading or cycling.

Acknowledgments

The authors thank John Unrau and Mike Souliere for their work in implementing the designs and systems described in this paper. The authors also appreciate the work and advice of machinists Heinz Birkenhauer and Jacques Pronovost, and Arie DeGroot of The Mechanical Engineering Department at the University of Waterloo. Thanks are extended to Sue Andrews, Barry Hannah, and Nadia Bahar for preparation of the manuscript and figures. Financial support from the Natural Sciences and Engineering Research Council of Canada is gratefully acknowledged, and thanks are extended to D. Mraz of MPC Limited for getting us involved in the first place.

References

[1] Hoek, E. and Franklin, J. A., "A Simple Triaxial Cell for Field and Laboratory Testing of Rock. *Transactions of the Institute of Mining and Metallurgy*, (*G.B.*), Vol. 77, 1968, pp. A22–A26.

[2] Jastrezebski, Z. D., *The Nature and Property of Engineering Materials*, 2nd ed., Wiley, New York, 1976, pp. 317–320.

[3] *ASME Boiler and Pressure Vessel Code,* American Society of Mechanical Engineers, New York, 1974, Section VIII, Division I.
[4] Shigely, J. E. and Mitchell L. D., *Mechanical Engineering Design,* 4th ed., McGraw-Hill, New York, 1983, p. 359.
[5] Harvey, J. F., *Theory and Design of Modern Pressure Vessels,* 2nd ed., Van Nostrand Reinhold, New York, pp. 351–353.
[6] Gilmor, M. I., Ed., *Limit States Design Steel Manual,* 1st ed., Canadian Institute of Steel Construction, Toronto, 1977.

John F. Peters[1] *and Daniel A. Leavell*[1]

Relationship Between Tensile and Compressive Strengths of Compacted Soils

REFERENCE: Peters, J. F. and Leavell, D. A., "**Relationship Between Tensile and Compressive Strengths of Compacted Soils,**" *Advanced Triaxial Testing of Soil and Rock, ASTM STP 977*, Robert T. Donaghe, Ronald C. Chaney, and Marshall L. Silver, Eds., American Society for Testing and Materials, Philadelphia, 1988, pp. 169–188.

ABSTRACT: A direct-pull tension test was developed to study the behavior of compacted soils in total stress tension. A comprehensive series of tension and unconsolidated undrained compression tests was performed on Vicksburg silty clay; the data from these tests were supplemented with published data. Analysis of the data was based on relating the tensile strength parameter of the Griffith-Brace theory for brittle fracture to the suction-derived cohesion term of the Fredlund-Morgenstern failure law for partially saturated soils. Application of the analysis was demonstrated by relating tensile and compressive strengths to water content and void ratio.

KEY WORDS: compacted soils, tensile strength, shear strength, partially saturated soils, critical state theory, triaxial test, unconsolidated undrained test, tensile test, soil suction, brittle fracture

The tensile strength of soil generally is considered small for engineering applications. Yet there are a number of problems in which even a small amount of tensile strength can have significant influence on computational results. For example, the tensile strengths of clays are significant in problems involving low mean normal stresses. Motivation for studying tensile strength comes indirectly from the study of partially saturated soils, because the tensile strength is derived presumably from the suction potential of the soil. This paper presents data for compacted Vicksburg silty clay for uniaxial tension and unconsolidated undrained triaxial compression tests propose a theory to relate tensile and compressive strengths for partially saturated materials.

Test Methods

Different test configurations and methods have been used to determine the tensile strength of soil [*1,2*]. But most of this work did not consider the complete stress–strain response of soil in tension. Also, the most common test methods involve loading configurations that create inhomogeneous stress conditions from which the tensile stress at failure must be computed indirectly. Indirect tests suffer the disadvantages of (1) requiring a stress analysis for determining strength which in turn requires the stress–strain properties of the material and (2) creating mixed compression and tension which invokes a complex failure mode.

The direct tensile test [*3*] has the advantage that it is the only test in which, in principle,

[1] Research civil engineers, Geotechnical Laboratory, U.S. Army Engineer Waterways Experiment Station, Civil Engineer, Vicksburg, MS 39180.

all induced stresses and strains are homogeneous and can be computed from direct measurements without making assumptions about the material's stress–strain response. In practice, the test has the drawback that it is virtually impossible to apply a tensile stress to a specimen's ends without inducing a nonuniform stress field. Thus the major challenge in designing a direct tensile loading device is to develop a suitable end-gripping technique.

Failure Laws

Despite the large number of tensile strength investigations, relatively little systematic theory has been developed on the failure of soils in tension. The majority of tensile tests measure total stresses rather than effective stresses, making it difficult to develop a comprehensive theory. This deficiency comes in part from the interest in determining the tensile strength of partially saturated compacted materials. Thus, deficiencies in understanding tensile strength parallel the deficiencies in understanding partially saturated materials.

Various researchers have attempted to predict the tensile strength of soil and rock using classic failure criteria such as Mohr-Coulomb, Griffith, and modified Griffith [*4,5*]. Most found that the Mohr-Coulomb criterion overpredict tensile strength whereas the Griffith criterion underpredict the cohesive strength. A more applicable approach was outlined by Lee [*4*] who used the Griffith criterion with modifications by McClintock and Walsh and Brace (modified Griffith theory). Bishop and Garga [*6*] and Shen [*7*] used the modified Griffith failure criterion to predict the failure of blue London clay and lateritic clay, respectively, and found the criterion to work quite well.

Experimental Program

Tensile Test Equipment

The direct tensile test equipment consists of two gripping jaws, a rigid base, a slide table, a linear variable differential transformer (LVDT), an electrical load cell, and a loading mechanism. One of the gripping jaws is rigidly attached to the base while the other is attached to the slide table. The slide table provides a precise alignment of the pulling force along the longitudinal axis of the specimen. The LVDT is mounted along a reduced section of the specimen at a gage length of 5.0 cm and provides a means of measuring axial displacement. The load cell is attached to the jaw mounted on the slide table ensuring that the load measured is that which is actually applied to the specimen. The assembled test device with its loading system is shown in Fig. 1.

Sample Preparation

Material for a test series was batched at a specified water content and allowed to cure for a minimum of 24 h. Predetermined weights were taken from the batched material and evenly distributed into seven water-tight containers. From this preweighed material, a specimen consisting of seven layers was compacted in a rectangular mold 7.6 cm high, 5.1 cm wide, and 22.9 cm long, using a miniature pneumatic kneading compactor having a square compactor foot with an area of 6.45 cm^2. Compaction was accomplished with 40 tamps per layer, which was sufficient to completely cover the layer surface three times. The compacted specimen was then trimmed to produce a reduced center section 3.80 by 6.35 by 5.0 cm long, as shown in Fig. 2, and allowed to cure in a sealed container for another 24-h before

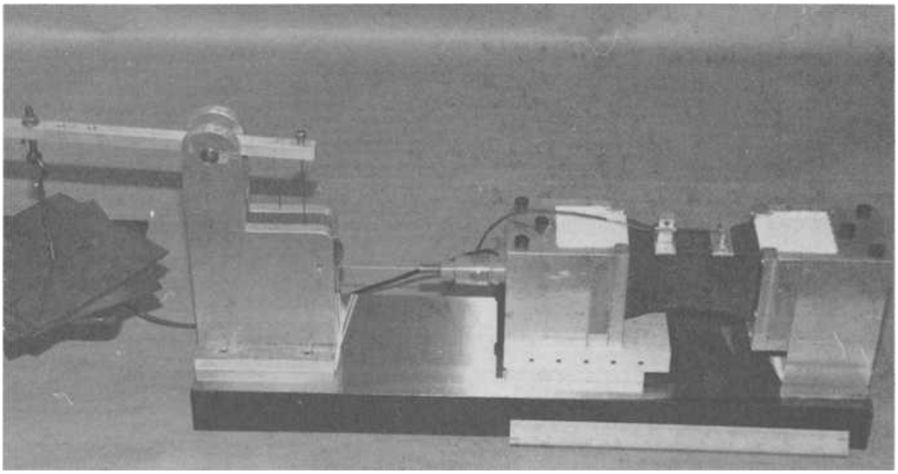

FIG. 1—*Tensile testing apparatus and dead weight loading system.*

testing. The curing time tends to promote a uniform distribution of water throughout the specimen.

Tensile Test Procedure

The specimens were incrementally loaded at 1-min intervals with load and deformation readings being monitored continuously until failure occurred. A somewhat arbitrary standard loading program was selected to ensure that all tests would be comparable even though other loading schemes might better match field conditions. At the conclusion of the tensile

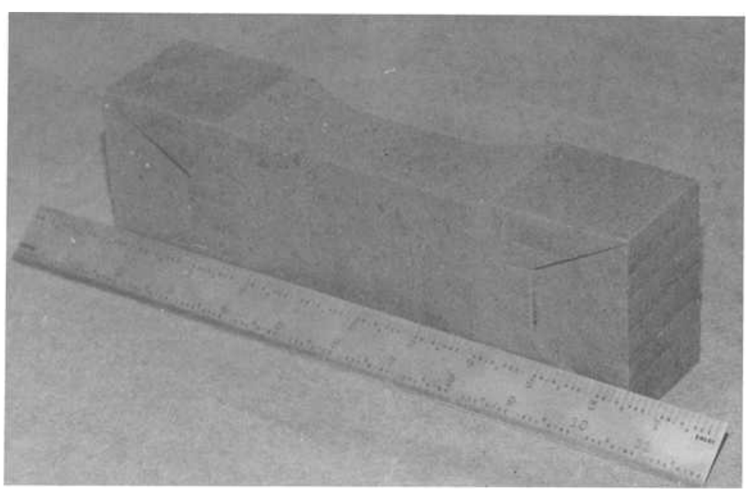

FIG. 2—*Configuration of tensile specimen after trimming procedure.*

test, a water content specimen was obtained from the fracture zone which was normally in the central portion of the specimen.

Compression Tests

Unconsolidated undrained triaxial compression tests were performed on cylindrical specimens trimmed from rectangular samples compacted in the tensile test mold. A series of three specimens from each rectangular sample were tested using confining pressures of 50, 145, and 290 kN/m^2. The specimens were trimmed so that the longitudinal axis was perpendicular to the compaction layers. Thus the maximum principal stress in the unconsolidated undrained test corresponded to the zero stress direction in the tensile test. The specimens were tested under strain control using procedures presented in Ref *8*.

Material Tested

General Description

Vicksburg silty clay was used in the test program so data could be correlated with work done by Al-Hussaini and Townsend [*9*] and Seed et. al. [*10*]. The Vicksburg silty clay used by other researchers differs slightly from that used in this study. Tensile test results reported in this paper and in Ref 9 are for a material having a liquid limit of 34, plastic index of 13, specific gravity of 2.68, and a gradation of 98% passing the No. 200 sieve with 20% being finer than 0.005 mm. The material used for compression tests in Ref *10* had a liquid limit of 35 and a plastic index of 19. Vicksburg silty clay was also used as the standard (CL) soil in a round robin compaction test series performed by nine U.S. Army Engineer Division laboratories and the Kansas City District laboratory [*11*] which allows comparison of different compaction methods.

Compaction Characteristics

The compaction curves for this material, shown in Fig. 3, were obtained using the pneumatic kneading compactor and compaction mold used for compacting the tensile specimens. A standard Proctor curve is also presented for comparison (Fig. 3). The optimum water contents and maximum dry densities for compaction efforts 345, 518, and 690 kN/m^2 were 17.6% and 16.93 kN/m^3, 16.6% and 17.15 kN/m^3, and 15.9% and 17.37 kN/m^3, respectively. Comparing these compaction curves to the standard Proctor curve for Vicksburg silty clay, it is noted that they are steeper and attain a higher degree of saturation at their optimum water content (85 versus 80%, respectively). It is interesting that although the optimum water content occurs at different degrees of saturation for the two compaction methods, the maximum degree of saturation is the same, approximately 90%. There appears to be a maximum degree of saturation the material can attain which is independent of the compaction method.

Tensile tests performed at compactive efforts of 173 and 1035 kN/m^2 provide additional compaction data. Compaction curves for these efforts were sketched based on the shapes of the other compaction curves to obtain estimates of the optimum water contents and densities. In constructing these curves, it was assumed that all compaction curves have generally the same shape. The assumption is considered valid when the same compaction equipment and technique (mold size and configuration and compaction procedure) are used for all tests.

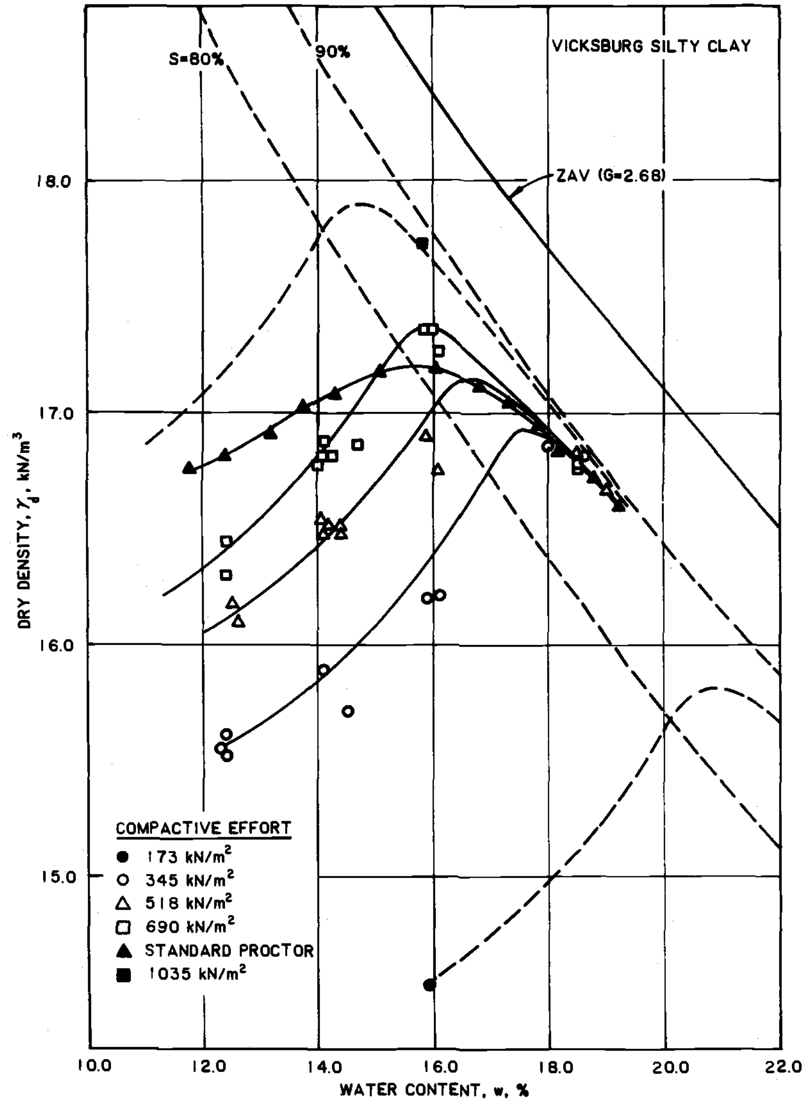

FIG. 3—*Compaction curves for Vicksburg silty clay.*

Suction–Water Content Relationship

In studying the tensile strength of unsaturated compacted materials, it is normally assumed that they derive strength from their suction potential. Therefore, comparisons between suction data and compressive and tensile strengths were made to determine if such a correlation could be verified. The relationship between suction potential and water content was developed for tensile test specimens compacted at water contents of 10, 12, 14, and 18%, using a compaction effort of 345 kN/m². The specimens were trimmed into small cubes, and the suction potential was determined with psychrometers using the procedure outlined by

TABLE 1—*Suction potential test data.*

Test Number	Water Content (w), %	Void Ratio (e)	Degree of Saturation (S), %	Suction Potential (τ), kN/m^2
CM-10-50-1a	8.84	0.752	31.8	1571.2
CM-10-50-1b	9.32	0.735	34.2	864.2
CM-10-50-1d	9.35	0.752	33.5	916.5
CM-10-50-1f	9.20	0.764	32.4	549.9
CM-10-50-1g	9.37	0.734	34.5	419.0
CM-10-50-1h	9.25	0.752	33.2	392.8
CM-10-50-1i	9.37	0.739	35.0	523.7
CM-12-50-2a	11.83	0.776	41.1	614.7
CM-12-50-2b	11.39	0.780	39.4	614.7
CM-12-50-2d	13.00	0.795	44.1	481.1
CM-12-50-2f	11.23	0.822	36.9	588.0
CM-12-50-2g	11.01	0.808	36.8	534.6
CM-12-50-2h	11.06	0.790	37.8	427.6
CM-12-50-2i	10.78	0.793	36.7	855.3
CM-14-50-3a	14.30	0.707	54.6	294.9
CM-14-50-3b	14.10	0.704	54.0	268.1
CM-14-50-3d	14.30	0.687	56.2	402.1
CM-14-50-3f	14.12	0.682	55.9	375.3
CM-14-50-3g	14.08	0.692	54.9	375.3
CM-14-50-3h	14.44	0.675	57.8	160.8
CM-14-50-3i	14.08	0.683	55.6	348.5
CM-18-50-4a	17.50	0.625	75.6	184.9
CM-18-50-4b	17.69	0.627	76.2	158.5
CM-18-50-4d	17.64	0.610	78.1	264.2
CM-18-50-4f	17.88	0.630	76.7	184.9
CM-18-50-4g	17.72	0.628	76.2	158.5
CM-18-50-4h	17.72	0.603	79.3	158.5
CM-18-50-4i	17.59	0.603	78.7	184.9

Johnson [*12*]. A disadvantage of the psychrometer method is that the resolution of measurement is on the order of 100 kPa, making necessary the use of several psychrometers per water content. Considerable scatter was observed among different psychrometers at each water content, however, all psychrometers indicated the same basic trend. Suction potential test data are summarized in Table 1. Figure 4 shows the average suction potentials for the compacted water contents relative to the optimum water content. A steady decline is observed in the suction potential as the water content is increased until optimum is reached. At optimum, the suction potential becomes very low. Sufficient data were not obtained to determine the influence of compactive effort on the suction versus water content relationship.

Test Results

Test Program

The test data from the main series of direct tensile tests performed on Vicksburg silty clay are presented according to specimen water content in Table 2. The main series was separated into four groups with material in each group being batched at water contents of 12, 14, 16, and 18%. Each group contained a minimum of two specimens at each of compactive efforts 345, 518, and 690 kN/m^2. In general, the test data shown in Table 2 appear

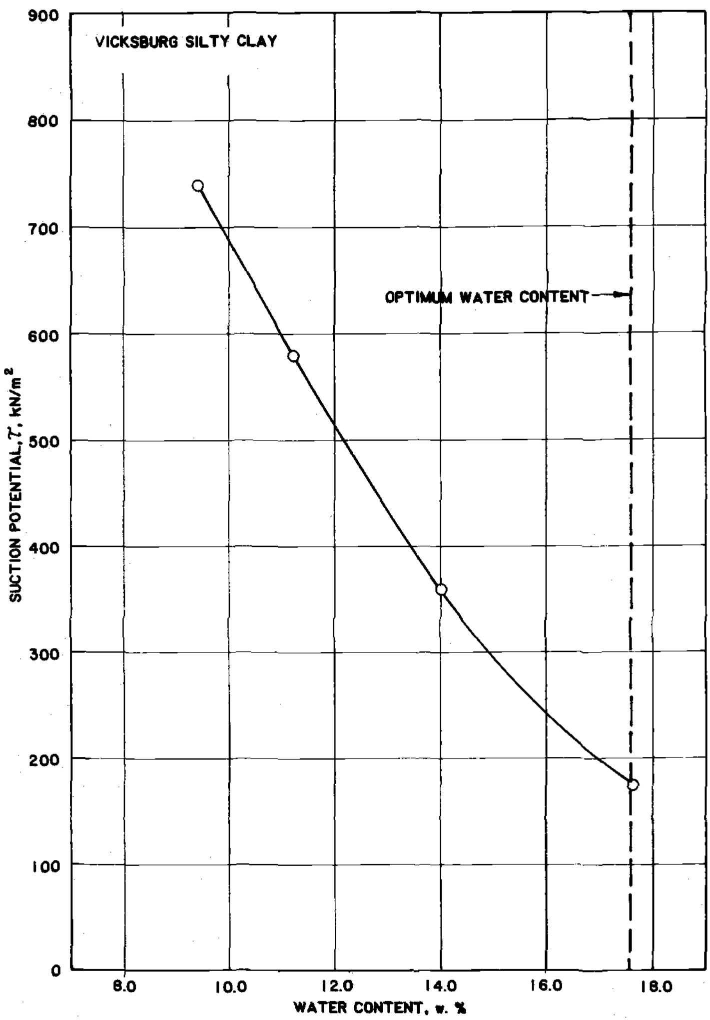

FIG. 4—*Suction potential versus water content for Vicksburg silty clay.*

to be consistent and repeatable. An observed decrease from the initial to the final water content is attributed to moisture loss during specimen compaction, trimming, and setup.

Strength Versus Suction

Figure 5 shows an increase in tensile strength as the material's suction potential increases, indicating that tensile strength depends on suction potential. Figure 6 shows a reduction in tensile strength with the transition of the water content from dry to wet of optimum. Thus the suction–strength relationship consists of two parts: (1) dry of optimum where the strength is nearly constant and (2) wet of optimum where the strength falls off rapidly. The extrapolation of behavior to zero suction is based on the general relationship between water content

TABLE 2—*Direct tension test data at failure.*

Test Number	w_i, %	w_f, %	Effort, kN/m^2	γ_d, kN/m^3	ϵ_t, 10^{-4}	σ_t, kN/m^2
CM-12- 50- 1	12.3	12.2	345.0	15.55	3.5	37.3
CM-12- 50- 2	12.4	11.6	345.0	15.61	4.0	37.3
CM-12- 50- 3	12.4	11.9	345.0	15.52	7.3	40.0
CM-12- 75- 4	12.5	12.0	517.5	16.18	5.6	51.8
CM-12- 75- 5	12.6	11.9	517.5	16.10	5.0	51.1
CM-12-100- 6	12.4	...	690.0	16.31	6.5	64.2
CM-12-100- 7	12.4	11.8	690.0	16.45	2.0	62.1
CM-14- 50- 8	14.1	13.7	345.0	15.90	6.8	37.3
CM-14- 50- 9	14.5	13.9	345.0	15.72	5.4	35.2
CM-14- 75-10	14.1	13.5	517.5	16.53	3.5	43.5
CM-14- 75-11	14.1	13.4	517.5	16.48	3.0	49.7
CM-14- 75-12	14.4	13.0	517.5	16.49	1.0	61.4
CM-14- 75-14	14.4	13.4	517.5	16.51	2.0	49.0
CM-14- 75-16	14.2	13.4	517.5	16.51	2.3	53.1
CM-14- 75-33	14.3	13.8	517.5	16.32	2.3	38.6
CM-14- 75-34	14.1	13.9	517.5	16.37	9.5	38.6
CM-14-100-13	14.2	13.5	690.0	16.82	6.2	53.1
CM-14-100-15	14.1	13.4	690.0	16.89	...	49.7
CM-14-100-17	14.1	13.5	690.0	16.82	4.5	53.1
CM-14-100-18	14.0	13.4	690.0	16.78	11.8	60.7
CM-14-100-32	14.7	13.9	690.0	16.87	...	53.2
CM-16- 25-35	16.1	15.9	172.5	14.53	2.1	13.8
CM-16- 50-19	15.9	15.6	345.0	16.20	12.8	34.5
CM-16- 50-20	16.1	15.5	345.0	16.21	9.6	35.2
CM-16- 75-21	16.1	15.5	517.5	16.75	4.4	38.6
CM-16- 75-22	15.9	15.6	517.5	16.90	9.8	43.5
CM-16-100-23	16.1	15.6	690.0	17.26	10.3	49.7
CM-16-100-24	15.9	15.2	690.0	17.36	17.5	53.8
CM-16-100-25	16.0	15.3	690.0	17.36	...	45.5
CM-16-150-36	16.2	15.8	1035.0	17.74	...	35.2
CM-18- 50-26	18.0	17.2	345.0	16.86	...	23.5
CM-18- 50-27	18.6	17.4	345.0	16.82	7.0	27.6
CM-18- 75-28	18.5	17.7	517.5	16.82	...	20.0
CM-18- 75-29	19.0	18.0	517.5	16.68	14.0	19.3
CM-18-100-30	18.5	17.6	690.0	16.79	...	19.3
CM-18-100-31	18.5	18.1	690.0	16.78	6.0	17.3

[a] w_i = initial water content, w_f = final water content, effort = compactive effort, γ_d = dry density, ϵ_t = tensile strain, and σ_t = tensile strength.

and strength observed for specimens at other compactive efforts for which suction measurements were not obtained.

Strength Versus Kneading Pressure

Figure 6 shows that the tensile strength increases with compactive effort until the water content is wet of optimum, where a sharp decrease in tensile strength occurs. The strength loss on the wet side of optimum is often related to "overcompaction" which occurs when degree of saturation is great enough to permit excess pore pressures to develop. It was also observed that when compacting wet of optimum, the compaction foot tended to push material laterally rather than compress material in a punching manner as for the dryer material. The shearing action in the wet material may damage the specimen and make it weaker as the

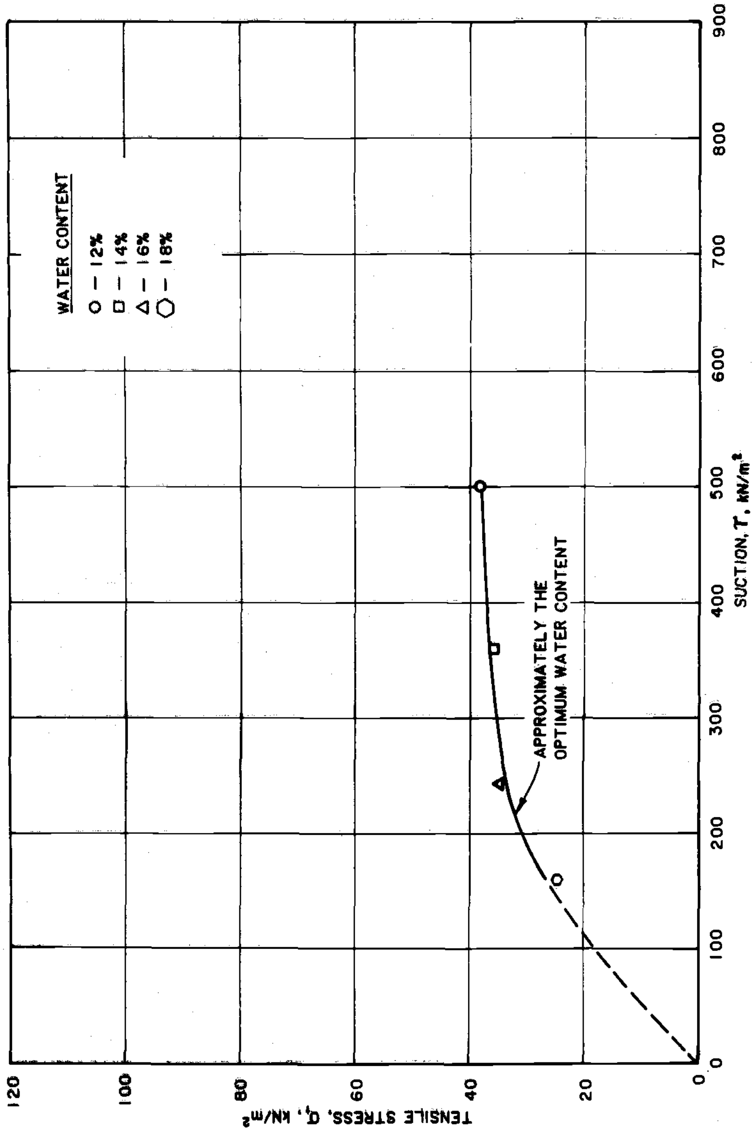

FIG. 5—*Tensile stress at failure versus suction potential for Vicksburg silty clay (compactive effort = 345 kN/m$_2$).*

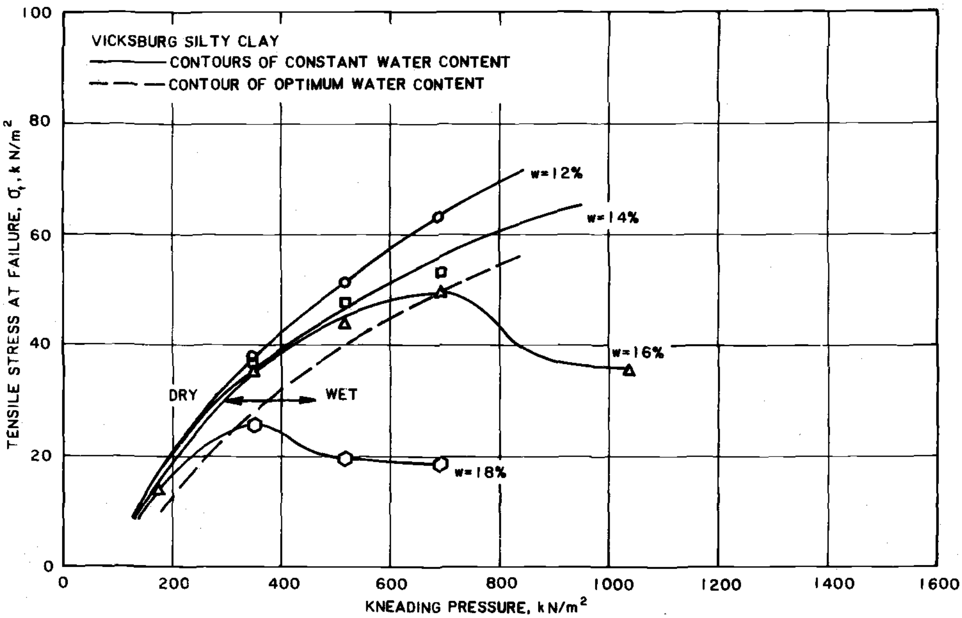

FIG. 6—*Tensile stress at failure versus kneading pressure for Vicksburg silty clay contoured with respect to water content.*

compactive effort is increased. Note that the size of the compaction foot and thickness of compaction layer are large relative to the specimen size, and strength reduction as a result of the damage effect may not be observed at a prototype scale.

Stress–Strain Characteristics

Figure 7 shows typical stress–strain data obtained from the direct tension test. The strain used to plot the curve corresponds to the accumulated strain at the end of a load step. The response of the specimen to a load application consisted of two parts, an initial and creep response, which created a stair-stepped load-deformation curve. The initial strain was typically small and was approximately the same for all load steps including those near failure. The creep response represents the strain due to the sustained load between each step which became greater as failure was approached. Therefore, it is to be expected that the measured stress–strain curve would be quite sensitive to the rate of loading.

Ductility was defined as the strain a specimen could withstand prior to rupture. The strains at failure, given in Table 2, display considerable variability as a result of the load-control method of testing. To obtain a more definitive measure of ductility, a strain control device is preferable. However, based on general observations of specimen behavior, a clear picture of the relative ductility emerged. It appeared that ductility, like tensile strength, was directly related to the compacted water content relative to optimum water content. There was a gradual increase in ductility from dry of optimum to optimum and a large increase from optimum to approximately two percentage points wet of optimum. At two percentage points wet of optimum, the material's ductility became small, possibly a result of the greatly reduced strength of the wetter specimens. As most of the ductility was derived from creep strains, the observations of the influence of compactive effort and water content on ductility also apply to creep.

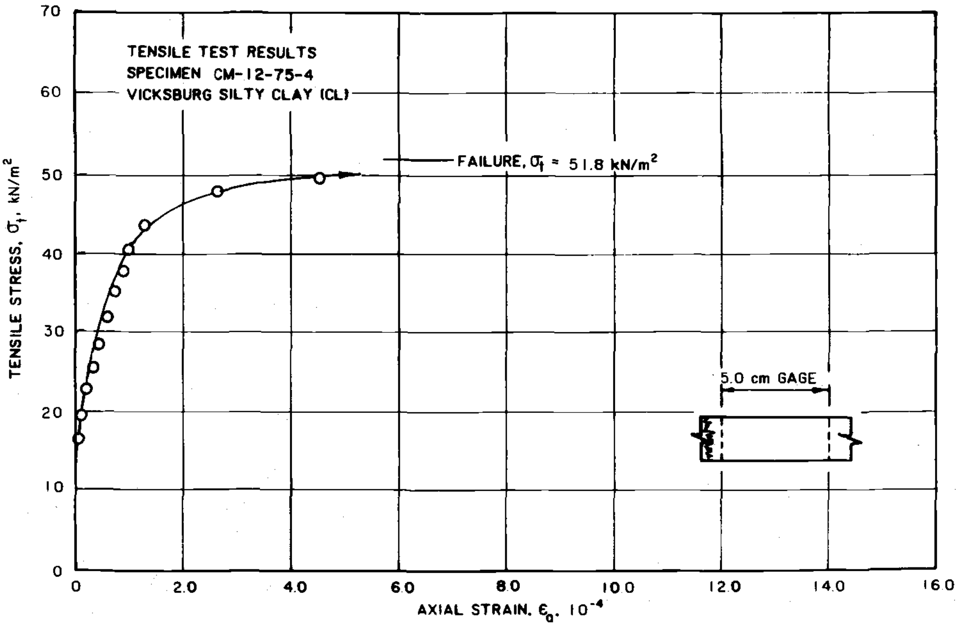

FIG. 7—*Typical stress–strain curve for direct tensile test on Vicksburg silty clay.*

TABLE 3—*Triaxial compression test data at failure.*

Test Number	w, %	Effort, kN/m²	γ_d, kN/m³	ϵ_1, %	$\frac{\sigma_1 - \sigma_3}{2}$, kN/m²	$\frac{\sigma_1 + \sigma_3}{2}$, kN/m²
CM-12- 50- 1C	11.7	345.0	15.32	5.0	133.9	182.2
CM-12- 50- 2C	11.6	345.0	15.43	10.0	225.9	370.8
CM-12- 50- 3C	11.6	345.0	15.41	15.0	359.3	649.1
CM-14- 50- 4C	14.0	345.0	15.80	6.0	124.8	173.1
CM-14- 50- 5C	13.9	345.0	16.04	10.0	225.9	370.8
CM-14- 50- 6C	13.8	345.0	16.02	15.0	360.7	650.5
CM-16- 50- 7C	16.6	345.0	16.24	6.0	135.9	184.2
CM-16- 50- 8C	16.6	345.0	16.07	20.0	194.6	339.5
CM-16- 50- 9C	16.6	345.0	16.34	20.0	345.0	634.8
CM-16-100-10C	16.3	690.0	17.42	5.0	220.1	268.4
CM-16-100-11C	16.3	690.0	17.39	8.0	329.1	474.0
CM-16-100-12C	16.3	690.0	17.69	10.0	500.9	790.7
CM-18- 50-13C	18.2	345.0	16.71	9.5	151.1	199.4
CM-18- 50-14C	18.2	345.0	16.67	15.0	229.8	374.7
CM-18- 50-15C	18.3	345.0	16.76	15.0	331.2	621.0
CM-18-100-16C	18.5	690.0	16.07	15.0	92.5	140.8
CM-18-100-17C	18.3	690.0	16.34	15.0	115.9	260.8
CM-18-100-18C	18.3	690.0	15.94	15.0	220.1	509.9

Note: Dry densities were based on weights of compression test specimens and are generally less accurate than those reported in Table 2.

For the specimen shown in Fig. 7, failure was outside the gage length and in the tapered portion of the specimen. However, the stress–strain curve, which is indicative of conditions within the gage length, shows the entire specimen to be in a state of failure. This implies that strains are relatively uniform within the specimen up to the point of rupture. Note that of the 36 specimens tested, 28 failed in the gage length. However, the failure plane in all specimens occurred as a planar fracture running perpendicular to the specimen's longitudinal axis.

Triaxial Compression Test Data

The triaxial test data presented in Table 3, combined with the tensile test data, permitted construction of a complete failure envelope for uniaxial loading; these data are summarized in Fig. 8. The compressive strengths correlated with tensile strengths, in that specimens having the greater compressive strengths also had the greater tensile strengths. All the compression test specimens compacted dry of optimum display approximately the same tan ϕ_u, indicating that these specimens all behaved as partially saturated. The ϕ_u of 27° is lower than the 33° measured in drained tests on Vicksburg silty clay [*13*], which suggests that a moderate pore pressure response was created even in the dry specimens.

The compression test data, supplemented by the test results of Seed et. al. [*10*], were used to construct Fig. 9. The relationships among strength, water content, and compactive effort are identical in form to those for tensile strength. The failure envelopes for the compression test results are nearly parallel, indicating that differences in strength are the result of differences in the cohesion intercept. Therefore, the factors influencing the cohesion parameter appear to be the same as those influencing tensile strength.

Discussion of Results

Implications to Strength Theories

The observed trends in tensile test data outlined in previous sections point to a consistent picture of the mechanisms governing the tensile strength of compacted soils. These data also present a clear picture of how the tensile strength should be modeled for purposes of analysis. Consider these observations:

1. In every case, failure occurred as a planar fracture running perpendicular to the specimen's longitudinal axis.
2. Tensile strength fell below the Mohr-Coulomb envelope as defined from the compression test. The ratio of tensile to compressive strength ranged from 0.2 to 0.4.

It is quite common to account for the failure behavior of soil in tension by defining a tensile "cutoff" to the failure envelope on the tension side of the effective stress origin. Also, it is common to treat the strength component due to suction by defining an equivalent effective stress axis:

$$\sigma' = (\sigma - u_a) + \chi\,(u_a - u_w) \tag{1}$$

where

σ = total stress
σ' = effective stress
u_a = pore air pressure
u_w = pore water pressure
χ = factor that depends on the degree of saturation (for example, see Ref *14*)

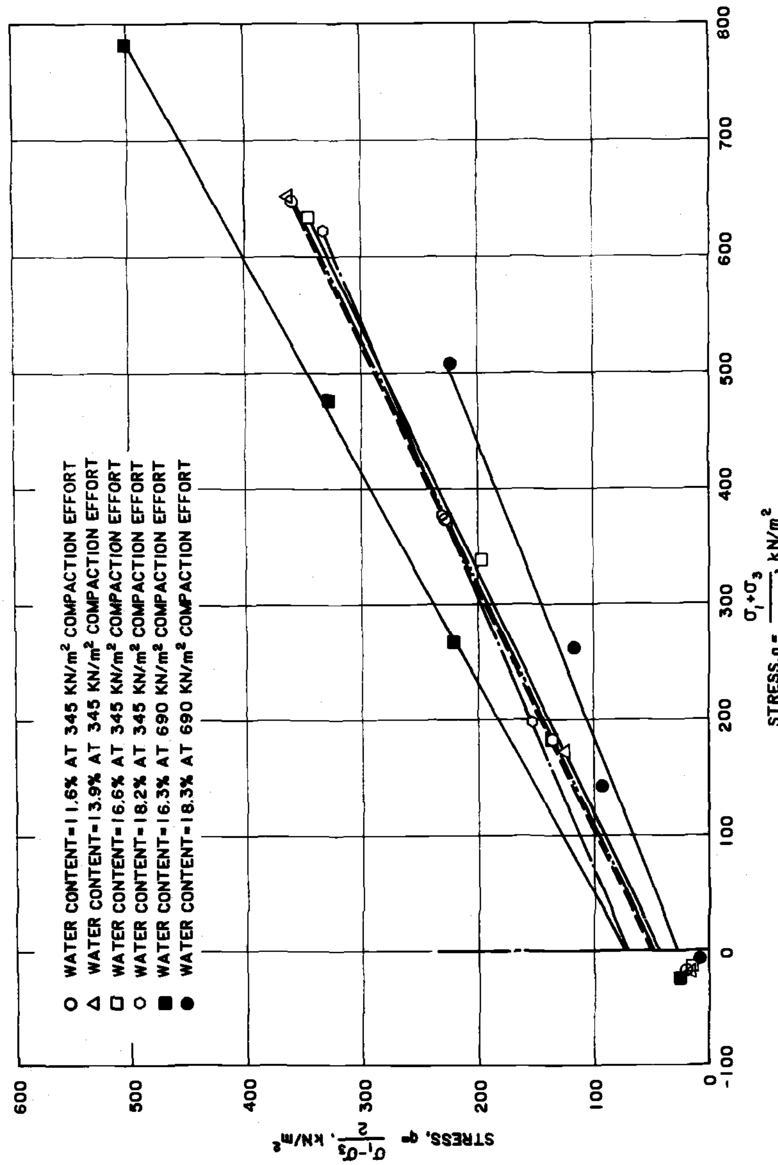

FIG. 8—*Strength data for tension and compression tests on Vicksburg silty clay.*

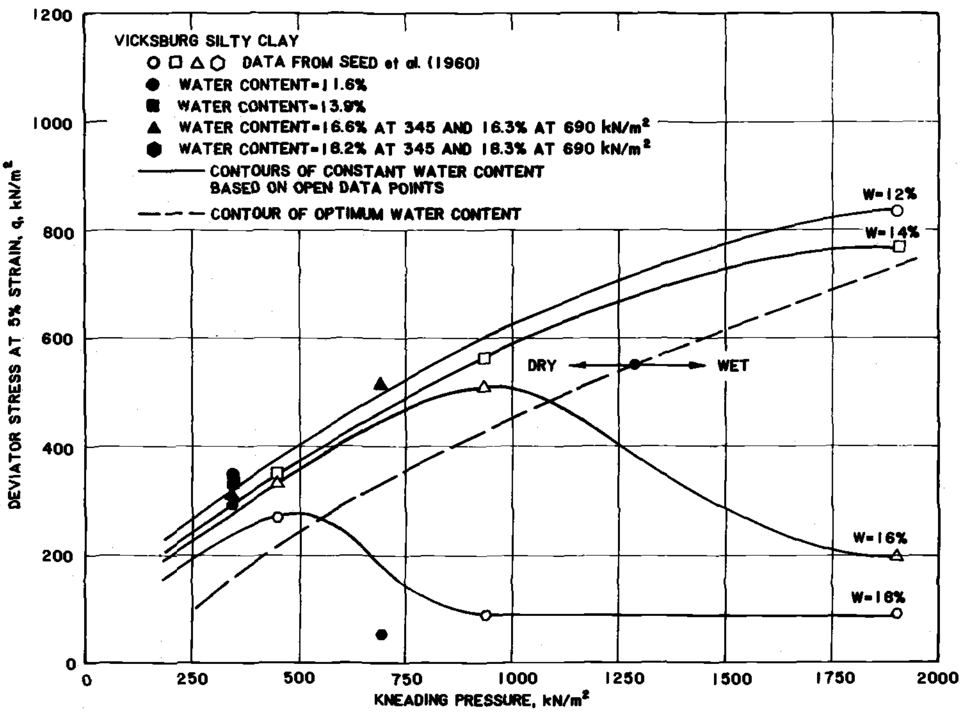

FIG. 9—*Strength at 5% strain versus kneading pressure for Vicksburg silty clay contoured with respect to water content* [*10*].

The two observations cited at the beginning of this section were used to show that, in general, tensile strength should not be defined in terms of effective stress and that the use of an equivalent effective stress is inadequate even for compressive strength.

First, the use of Eq 1 in conjunction with the Mohr-Coulomb failure law is inconsistent with the observed tensile fracture. The use of a χ factor in a definition of effective stress implies that the effective stress strength envelope is simply shifted to the tensile side by the amount $\chi(u_a - u_w)$. Therefore, failure of a partially saturated soil in tension should be similar to failure of a saturated soil in an undrained extension test—failure should occur as either necking or formation of shear planes. From the first observation, failure was never observed to be of the Mohr-Coulomb type, and the only report in the literature of ductile failure modes involved natural clayey soils which were most likely saturated and thus behaved as undrained extension tests [*15*]. In general, the use of Eq 1 will lead to incorrect prediction of ductile shear failure in the tensile region.

The second observation leads to the conclusion that the strength of the compacted soil is modeled well by a Griffith-type theory which predicts different failure modes in tension and compression. Several researchers have in fact proposed application of the modified Griffith theory to compacted soil with some success [*7,8*]. To apply the theory to partially saturated (noncemented) soils, the question of effective stress must be addressed because the tensile strength becomes negligible when the material is saturated. This implies that the tensile strength is derived from capillary tension which evidently makes suction an important variable.

Incidentally, another inconsistency appears when applying the effective stress concept to partially saturated soils in compression. Suppose several saturated, overconsolidated specimens are to be tested in drained triaxial compression. If the specimens are consolidated at low confining pressures and then sheared, they will tend to be dilative and to fail in a brittle fashion. In contrast, specimens consolidated to a sufficiently high stress to return the specimens to a normally consolidated state will be contractive and appear ductile. Specimens consolidated to intermediate stress levels will correspondingly display failure mechanisms ranging from dilative-brittle to contractive-ductile. If a specimen is desaturated by drying or by introducing air pressure u_a, Eq 1 indicates that it should become more ductile because the extra effective stress due to suction brings the specimen closer to being normally consolidated. Experience indicates that if desaturation influences behavior at all, the tendency is toward becoming more brittle upon drying. It is again seen that the strength derived from suction is not due simply to an increase in intergranular stress but also must be due to the strength of the water surface tension acting as cementation.

Correlation Between Effective Stress and Suction

The difficulty with applying the effective stress concept to partially saturated soils is that the relationship between mechanical behavior and suction is more complex than implied by Eq 1. Olsen and Langfelder [*16*] found that the negative pore pressure of a compacted soil depends strongly on water content but not on degree of saturation. If strength is derived directly from soil suction, there should be a direct correspondence between water content and strength. For example, the compaction curve, which could be viewed as an indicator of resistance to compaction (density) versus water content, clearly indicates that degree of saturation plays a greater role than would be indicated by a relationship based on suction alone. Therefore, the contribution of suction to shear strength involves a mechanism more complicated than simply adding a component to the effective confining pressure.

Fredlund [*17*] applied the state variable concept to obtain the shear strength law:

$$\tau = c' + (\sigma - u_a)\tan\phi' + (u_a - u_w)\tan\phi'' \tag{2}$$

where

τ = shear stress at failure
c' = effective stress cohesion intercept
ϕ' = angle of internal friction related to normal stresses
ϕ'' = angle of internal friction related to matrix suction

Eq 2 can be criticized in the same fashion as Eq 1. In fact, if χ is taken to be constant, then the above equation reduces to the Bishop theory with $\tan\phi'' = \chi\tan\phi'$. However, the essence of Fredlund's relationship does not rest in the Mohr-Coulomb form of Eq 2, but rather in the fact that the contribution of suction is independent of the other stress quantities [*18*]. That is, rather than incorporating suction into an equivalent effective stress, it should be treated as an independent state variable whereby the failure law would take the form

$$\tau = c' + f_1(\sigma - u_a) + f_2(u_a - u_w) \tag{3}$$

where f_1 and f_2 are functions to be determined experimentally. Equation 1 is, of course, a particular case of Eq 3. An alternative failure law consistent with the state variable approach is described in the following paragraphs. The proposed relationship is equivalent to Eq 2 for compressive stress states but also predicts the correct failure mechanism in tension.

Using the Griffith theory for fracture and the modification by Brace [19], three distinct failure criteria based on stress state can be identified. Consider a specimen subjected to the stresses σ_t and σ_c (shown in Fig. 10), in which stresses are negative in tension. From Griffith theory, criteria 1 and 2 follow:

1. For $-\sigma_t > -\sigma_c$ and $(3\sigma_t + \sigma_c) < 0$:

$$\sigma_t = -T_o \tag{4a}$$

2. For $-\sigma_t > -\sigma_c$ and $(3\sigma_t + \sigma_c) > 0$:

$$(\sigma_t - \sigma_c)^2 = 8T_o\,(\sigma_t + \sigma_c) \tag{4b}$$

where T_o is the positive tensile strength parameter. From the Brace modification to Griffith theory, criterion 3 follows:

3. For $\sigma_t < \sigma_c$ and $\sigma_t \geq 0$, $\sigma_c \geq 0$:

$$-\mu\,(\sigma_c + \sigma_t) + (\sigma_c - \sigma_t)\sqrt{1 + \mu^2} = 4T_o \tag{4c}$$

where $\mu = \tan\phi$, and ϕ is the friction angle between the crack faces.

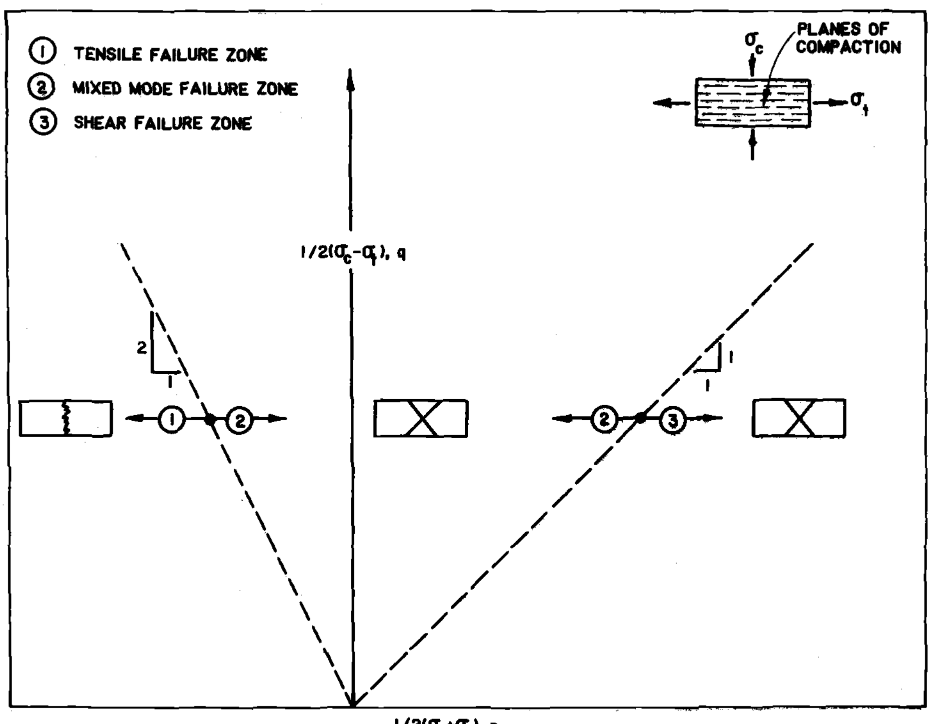

FIG. 10—*Failure zones dictated by the Griffith-Brace theory and the failure mechanism associated with each zone.*

The stress states corresponding to each criterion are shown in Fig. 10 along with the failure mechanism that should be observed for each case. Failure in the direct tensile test is controlled by criterion 1 whereas failure in the unconsolidated undrained triaxial compression test is controlled by criterion 3. The boundary between criteria 2 and 3 correspond to the unconfined compression test. The stress conditions corresponding to criterion 2 involve both compression and tension and were not produced by any of the tests performed in this study.

Equation 4c is clearly equivalent in form to the Mohr-Coulomb criterion in which the cohesion intercept is proportional to the tensile strength parameter. Therefore, a correspondence can be made between the tensile strength measured in the direct tensile test and the cohesion intercept of the failure envelope for the compression tests. If the value of the cohesion intercept is denoted as a_o in q-p coordinates and c_o in τ-σ coordinates, T_o can be computed from the compression test data using Eq 5:

$$T_o = \tfrac{1}{2}\, a_o \sqrt{1 + \mu^2} = \tfrac{1}{2}\, c_o \tag{5}$$

For simplicity, it is assumed that the response of pore pressures u_w and u_a is insignificant for all tests; this is equivalent to assuming that the normal stress axes correspond to $(\sigma - u_a)$ with $u_a = 0$. Also, it will be assumed that $c' = 0$ and $\mu \approx \tan\phi_u$. In view of criterion 3 and Eq 2, the tensile strength is related to Fredlund's failure criterion by

$$2T_o = (u_a - u_w) \tan\phi'' \tag{6}$$

The effects of suction can also be accounted for by noting that the relationship between suction and water content is typically found to plot as a straight line on a semilogarithmic plot suggesting the form

$$\log(u_a - u_w) = aw + b \tag{7}$$

where w is the water content and a and b are constants. By substituting Eq 6 into Eq 7, a semilogarithmic relationship between strength and water content can be obtained. If the water content in the relationship is replaced with the difference between the water content and the water content at maximum density $(w - w_{opt})$, the semilogarithmic trend should be unaffected. It is further proposed that the strength increase due to higher kneading pressure, shown in Figs. 6 and 9, can be related to density. It was found that the effects of density could be accounted for by normalizing T_o by a function of void ratio P_e. The complete empirical relationship for strength is given by

$$\log\,(T_o/P_e) = a(w - w_{opt}) + \text{constant} \tag{8}$$

The function P_e is given by

$$P_e = P_a \exp[(e_a - e)/\lambda] \tag{9}$$

where

P_a = atmospheric pressure
λ = slope of virgin curve on $e - \log_e(p)$ plot for saturated soil under isotropic compression
e_a = void ratio on virgin compression curve at P_a
e = void ratio of soil

A plot of ($w - w_{opt}$) versus $\log(T_o/P_e)$ is shown in Fig. 11. For the tension test, T_o is simply the failure stress; for the compression test, T_o is computed from Eq 5. Values of $\lambda = 0.07$ and $e_a = 0.71$ (based on isotropic consolidation tests on saturated specimens) were used to compute P_e. It is seen that (1) the proposed empirical relationship is supported by the experimental data and (2) the T_o computed from the compression test data agrees well with strengths measured directly in the tension test.

Summary

Data from a comprehensive test series performed on Vicksburg silty clay were supplemented with published data. An analysis of the data was based on relating the tensile strength parameter of the Griffith-Brace theory for brittle fracture to the suction-derived cohesion term of the Fredlund-Morgenstern failure law for partially saturated soils. The application of the proposed analysis was demonstrated by relating tensile and compressive strengths to water content and void ratio.

Conclusions

The conclusions drawn from this study are

1. For a given kneading pressure the tensile strength is governed primarily by the water content relative to optimum. It was noted that the tensile strength gradually decreased as the water content was increased until optimum, then a sharp reduction in the tensile strength occurred beyond optimum.

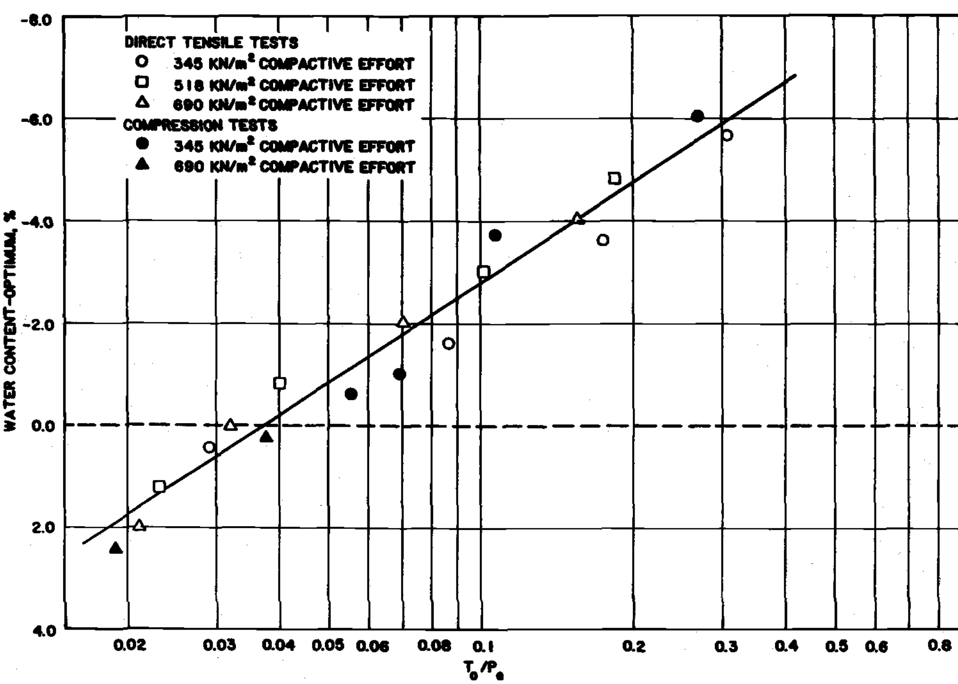

FIG. 11—*Plot of normalized tension versus water content using strength based on the Griffith-Brace theory for Vicksburg silty clay.*

2. The relationships among strength, water content, and density observed for the tensile test were also observed for the compression test. A semi-empirical relationship was developed accounting for water content and density that is valid for tensile strengths measured either by direct tension or computed from the cohesion intercept extrapolated from compression test data.

3. One of the most important conclusions to be reached from this study is that it may be possible to develop a general failure theory for partially saturated soils that not only accounts for the influence of suction but also predicts the correct type of failure mechanism. The theory is similar to a critical state model in that it is based on a state surface which contains both void ratio and water content as state variables. The "line of optimums" obtained from a series of compaction tests represents a projection of the surface onto the e-w axes. The appropriate stress state variable for the theory would be $(\sigma - u_a)$, which would reduce to the effective stress as conventionally defined, when degree of saturation increases to the point where the air phase takes the form of occluded air bubbles and $(u_a - u_w)$ equals zero.

4. Considerable work and more detailed testing of other soil types are required to develop the theory fully. In particular, an investigation is needed on noncompacted partially saturated soils to determine if a reference state equivalent to w_{opt} can be identified. Conceptual work is needed to identify the mechanical basis of using the modified Griffith theory for granular materials such as Vicksburg silty clay. Also, the role of excess pore pressures and influence on μ requires study. Future studies on tensile strength should be performed using strain-controlled loading to better define behavior near failure.

Acknowledgments

The research presented in this paper was performed at the U. S. Army Engineer Waterways Experiment Station (WES), Vicksburg, MS and funded under Civil Works Investigation Study (CWIS), Work Unit 31211, "Material Characterization and Analysis of Cracking in Embankment Dams." The Office, Chief of Engineers is gratefully acknowledged for authorizing publication of this paper.

References

[*1*] Haefeli, R., "Investigations and Measurements of the Shear Strengths of Saturated Cohesive Soils," in *Proceedings*, Conference on the Measurement of the Shear Strength of Soils in Relation to Practice, *Geotechnique*, Vol. 2, No. 2, 1950, pp. 186–208.

[*2*] Al-Hussaini, M. M., and Townsend, F. C., "Tensile Testing of Soils, A Literature Review," Miscellaneous Paper S-73-24, U. S. Army Engineer Waterways Experiment Station, Civil Engineer, Vicksburg, MS, 1973.

[*3*] Leavell, D. A. and Peters, J. F., "Uniaxial Tensile Test for Soil," Technical Report GL-87-10, Department of the Army, Waterways Experiment Station, Corps of Engineers, April 1987.

[*4*] Lee, I. K. and Ingles, O. G., "Strength and Deformation of Soil and Rock," in *Soil Mechanics Selected Topics*, I. K. Lee, Ed., Elsevier, New York, 1968, pp. 268–283.

[*5*] Obert, L., and Duvall, W. I., "Mechanical Properties and Behavior of Rock," in *Rock Mechanics and the Design of Structures in Rock*, Wiley, New York, 1967, pp. 301–317.

[*6*] Bishop, A. W., and Garga, V. K., "Drained Tension Tests on London Clay," *Geotechnique*, Vol. 19, No. 2, 1969, pp. 309–313.

[*7*] Shen, X., "The Tensile Behaviors of Compacted Cohesive Soils (in Chinese)," in *Collected Research Papers*, Water Conservancy and Hydroelectric Power Research Institute, Vol. 8, 1982, pp. 63–73 (translated by Tse-Shan Hsu).

[*8*] Department of the Army, Office, Chief of Engineers, "Laboratory Soils Testing," Engineering Manual 1110-2-1906, Washington, DC, 1970, pp. X-18–X-27.

[9] Al-Hussaini, M. M., and Townsend, F. C., "Investigation of Tensile Testing of Compacted Soils," Miscellaneous Paper S-74-10, U. S. Army Engineer Waterways Experiment Station, Civil Engineer, Vicksburg, MS, 1974.
[10] Seed, H. B., Mitchell, J. K., and Chan, C. K., "The Strength of Compacted Cohesive Soils," in *Research Conference on Shear Strength of Cohesive Soils*, American Society of Civil Engineers, University of Colorado, Boulder, CO, 1960, pp. 877–964.
[11] Strohm, W. E., Jr., "Preliminary Analysis of Results of Division Laboratory Tests on Standard Soil Samples," Miscellaneous Paper No. 3-813, U. S. Army Engineer Waterways Experiment Station, Civil Engineer, Vicksburg, MS, 1966.
[12] Johnson, L. D., "Psychrometric Measurement of Total Suction in a Triaxial Compression Test," Miscellaneous Paper S-74-19, U. S. Army Engineer Waterways Experiment Station, Civil Engineer, Vicksburg, MS, 1974.
[13] Peters, J. F., "Constitutive Theory for Stress–Strain Behavior of Frictional Materials," Ph.D. dissertation, University of Illinois at Chicago, 1982.
[14] Bishop, A. W., Alpan, I., Blight, G. E., and Donald, I. B., "Factors Controlling the Strength of Partly Saturated Cohesive Soils," in *Research Conference on Shear Strength of Cohesive Soils*, American Society of Civil Engineers, University of Colorado, Boulder, CO, 1960, pp. 503–532.
[15] Thorne, C. R., Tovey, N. K., and Bryant, R., "Recording Unconfined Tension Tester," *Journal of the Geotechnical Engineering Division, American Society of Civil Engineers*, Vol. 106, No. GT11, 1980, pp. 1269–1273.
[16] Olsen, R. E., and Langfelder, L. J., "Pore Pressures in Unsaturated Soils," *Journal of the Soil Mechanics and Foundations Division*, American Society of Civil Engineers, Vol. 91, No. SM4, 1965, pp. 127–150.
[17] Fredlund, D. G., "Appropriate Concepts and Technology for Unsaturated Soils," Second Canadian Geotechnical Colloquium, *Canadian Geotechnical Journal*, Vol. 16, No. 1, 1979, pp. 121–139.
[18] Fredlund, D. G., and Morgenstern, N. R., "Stress State Variables for Unsaturated Soils," *Journal of the Geotechnical Engineering Division, American Society of Civil Engineers*, Vol. 103, No. GT5, 1977, pp. 447–466.
[19] Brace, W. F., "An Extension of the Griffith Theory of Fracture to Rock," *Journal of Geophysical Research*, Vol. 65, 1960, p. 3477.

Serge Leroueil,[1] *François Tavenas,*[1] *Pierre La Rochelle,*[1] *and Michel Tremblay*[2]

Influence of Filter Paper and Leakage on Triaxial Testing

REFERENCE: Leroueil, S., Tavenas, F., La Rochelle, P., and Tremblay, M., **"Influence of Filter Paper and Leakage on Triaxial Testing,"** *Advanced Triaxial Testing of Soil and Rock, ASTM STP 977,* Robert T. Donaghe, Ronald C. Chaney, and Marshall L. Silver, Eds., American Society for Testing and Materials, Philadelphia, 1988, pp. 189–201.

ABSTRACT: A significant problem, especially in long-term tests, is leakage through the fittings and membrane. To avoid the first of these two sources of error, a cell with fittings enclosed in a back pressure chamber has been developed. To reduce leakage through the membrane, various cell fluids have been considered and tested in normal triaxial test conditions but with a dummy in place of the specimen. The results show that silicone oil minimizes the leakage.

Filter papers are used in triaxial testing to accelerate the consolidation process and the equalization of effective stresses within the specimen during shearing. The drainage capacity of five different filter papers was measured, and their effect on the consolidation and shear processes was evaluated by comparative tests. The results show that in the overconsolidated range, the filter papers are efficient; however, due to the high coefficient of consolidation of natural clays in this range, they are not really useful. In the normally consolidated range, the efficiency of the filter drains during consolidation is considerably less than expected; contrary to what has been observed by other researchers, no effect of the filter drains on shear strength was found.

KEY WORDS: triaxial, consolidation, shear strength, leakage, cell fluids, membrane, filter paper drains

In the last four decades, the triaxial test has become the laboratory test most commonly used to investigate soil behavior and to determine the soil parameters necessary for design purposes. During the 1950s and 1960s, considerable research was done to improve the triaxial apparatus and its use [*1–5*]. Since that time, attention has been centered on the development of new testing methods, and little research has been carried out on topics related to the common triaxial test. However, geotechnicians working in industrial and research laboratories have accumulated experience and developed techniques which can benefit the profession; Berre's summary of the triaxial testing practice at the Norwegian Geotechnical Institute (NGI) [*6*] is a good example. This paper and a companion paper by La Rochelle et al. [*7*] discuss some practical aspects of the triaxial test and its interpretation, and suggest some improvements.

Among the practical problems associated with the performance and interpretation of a triaxial test, leakage through fittings and membrane, the use and selection of filter strips around the specimen, the correction of test results for the effects of filter strips, the mem-

[1] Department of Civil Engineering, Laval University, Quebec, Canada G1K 7P4.
[2] Geotechnical engineers, Roche Ltd., 2535 Bd Laurier, Ste-Foy, Canada G1U 4M3.

brane, and the changes in cross-sectional area are probably the most important. This paper discusses the problems of leakage and filter strips, while the membrane and area corrections are treated in the companion paper by La Rochelle et al. [7].

Leakage in the Triaxial Test

In the triaxial test installation, a rubber membrane surrounds the soil specimen to isolate it from the cell fluid, and tubings and fittings are provided to either isolate the specimen from the atmospheric pressure (undrained tests) or to connect it to volume change measuring devices. However, as demonstrated by Poulos in his extensive study on control of leakage in the triaxial test, the efficiency of membrane, fittings, and tubings in providing a tight environment for the specimen is far from perfect [8]. Figure 1 schematically presents the main sources of exchange between the pore water of the specimen and the surrounding fluids: leakage in the external fittings (① in Fig. 1) and in fittings within the cell (②); osmosis and diffusion through the membrane and tubings (③); saturation of the membrane (④); and leakage and diffusion within the back pressure burette (⑤). All these phenomena introduce fluid movements which result in an inflow or an outflow, the importance of which depends on the fittings, the membrane, the cell fluid, the cell pressure, and, of course, on the duration of the test.

In drained tests, these uncontrolled fluid movements result in errors in the measurement of volume changes and eventually prevent the analysis of long-term creep tests [9], but, fortunately, the soil behavior remains unaffected. This is not the case in undrained tests in which changes in pore water volume modify the effective stresses and, consequently, the soil behavior.

If the soil is a normally consolidated clay (point A, Fig. 2), an uncontrolled outflow only slightly affects the effective stress and the soil response (case 1); on the contrary, an uncontrolled inflow (case 2) in a normally consolidated clay specimen, or both inflow and outflow in an overconsolidated clay (cases 3 and 4) or a cohesionless soil may considerably

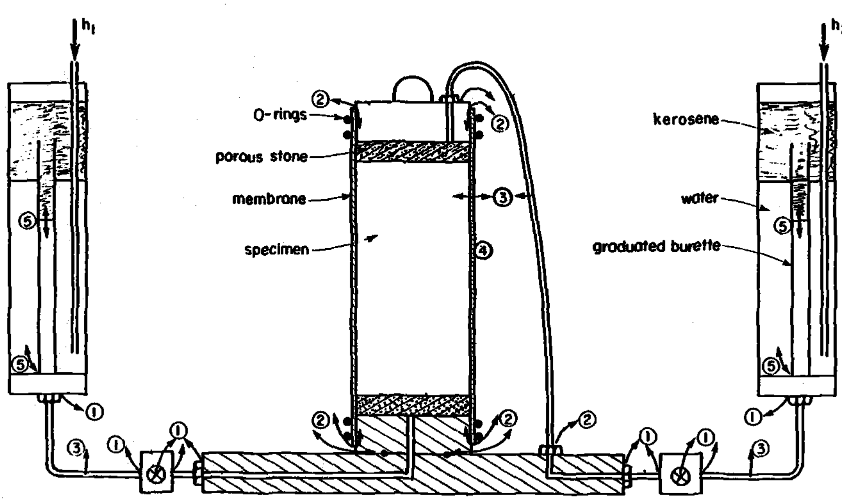

FIG. 1—*Sources of errors in triaxial test installation.* ① = *Leakage in external fittings.* ② = *Leakage in fittings within the cell.* ③ = *Osmosis and diffusion through membranes and lines.* ④ = *Saturation of membrane.* ⑤ = *Leakage and diffusion within the back pressure burette* [11].

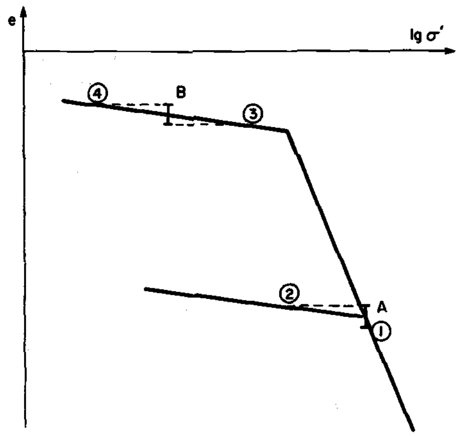

FIG. 2—*Effects of leakage on effective stress.*

modify the effective stresses and thus the soil behavior, even if the volume changes involved are very small. It is thus important, especially for long-term tests, to reduce the fluid exchanges to a minimum.

External fittings represent a significant source of leakage; their number should be reduced to a minimum or, ideally, completely eliminated. To this end, a triaxial cell with the back pressure burette directly attached to the base and with all the fittings enclosed in the back pressure chamber has been developed at Laval University in Quebec (Fig. 3). By enclosing the valves and connections in the back pressure chamber, this system completely eliminates the leakage through fittings due to hydraulic gradients, as shown in Fig. 4. Cells equipped in this manner have been used successfully for long-term drained creep tests [*10*] or, with two burettes connected, for permeability tests on intact overconsolidated clays [*11*].

Leakage may also occur between the membrane and the pedestal or the cap. It can be

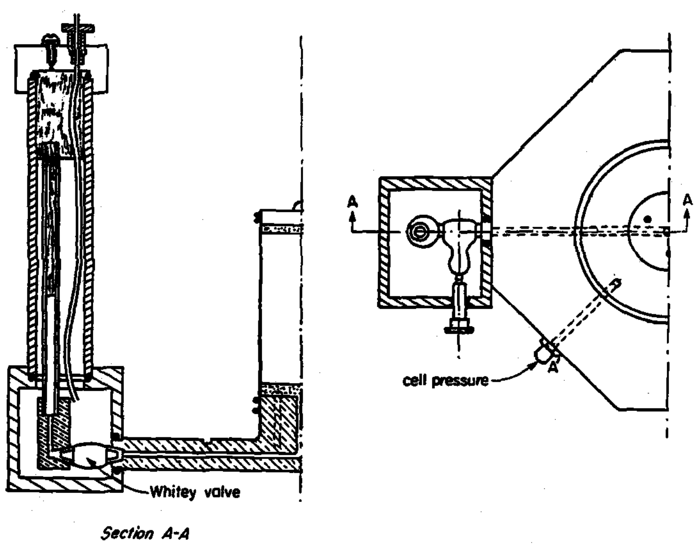

FIG. 3—*The new triaxial cell.*

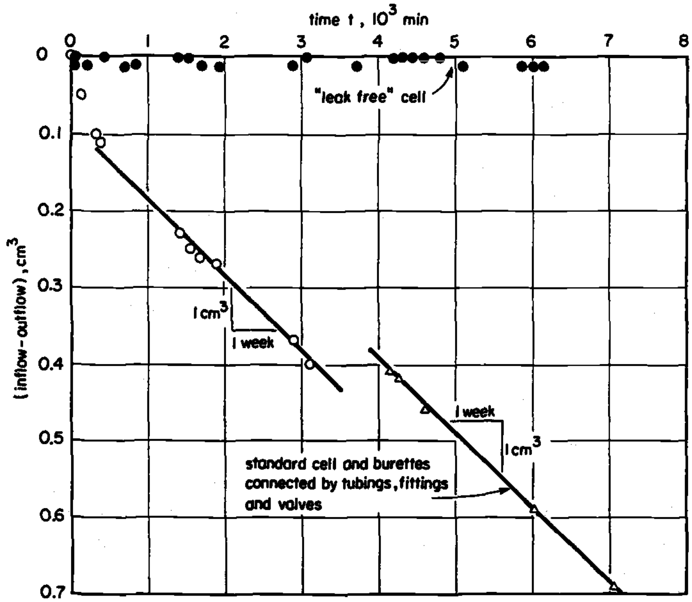

FIG. 4—*Observed leakage in a conventional and in the new triaxial cell* [11].

considerably reduced by polishing the surfaces of the cap and pedestal and by applying a thin layer of silicone grease on them before positioning the membrane and the O-rings.

Leakage may also result from the combined effects of hydraulic pressure difference and osmotic pressure difference between the pore pressure and the cell fluid through the membrane. Depending on the chemical compositions of the pore fluid and cell fluid and on the applied effective stress, inflow of cell fluid into the specimen or outflow of pore water may occur. Various tests were carried out to examine the influence of the cell fluid on the flow rate through the membrane. A dummy, 5 cm in diameter and 10 cm high, completely surrounded by filter paper, was installed in a cell such as the one shown in Fig. 3. The cap and the pedestal were coated with silicone grease before the membrane and the O-rings were installed. The membranes used, supplied by Soiltest (membrane T 604) and Wykeham Farrance (membrane WF 10510), are made of latex rubber and have a thickness of about 0.3 mm. The following cell fuilds were considered: deaired water, glycerin, castor oil, paraffin, and silicone oil (350 Cs. viscosity). The test results obtained for an effective stress of 100 kPa are summarized in Table 1; because several tests were carried out under similar conditions, range of values is given.

When deaired water was used as cell fluid, the measured flows varied between +0.25 cm^3/week (inflow) and −0.23 cm^3/week (outflow). While the mounting of the membrane could have influenced the test results, these variations probably are due mainly to the chemical characteristics of pore and cell waters; however, no control of the chemical compositions of these waters was performed to explain these differences.

Flow of pore water toward the cell and flow of cell liquid toward the specimen could be limited or avoided by selecting a cell liquid in which the water would not be miscible and which would have molecules larger than the pores of the membrane. Various types of oils have been proposed.

Kerozene, liquid paraffin, and silicone oil satisfy both conditions relatively well and have been tested. Kerozene attacks latex rubber, rapidly leading to leakage; therefore it cannot

TABLE 1—*Flow through the membranes.*

Type of Membrane	Cell Liquid	Range of Measured Flow Through the Membrane, cm^3/week[a]
Rubber latex membrane	Deaired water	-0.23 to $+0.25$
$t = 0.3$ mm[b]	Glycerin	-1.45 to -1.76
$\phi = 5$ cm[b]	Castor oil	-0.25 to -0.41
$H = 10$ cm[b]	Liquid paraffin	-0.04
	Silicone oil	-0.04 to -0.05
Ramses membranes	Deaired water	$+0.01$
$t = 0.07$ mm		
$\phi = 3.8$ cm		
$H = 7.6$ cm		

[a] + = flow from the cell to the specimen (inflow).
− = flow from the specimen to the cell (outflow).
[b] t = membrane thickness; ϕ = specimen diameter; H = specimen height.

be used. Liquid paraffin, recommended by Berre [6] for tests without membranes, gives very small flows (Table 1); however, when in contact with paraffin, the membrane swells, creases as shown in Fig. 5, and becomes very brittle, this leading possibly to leakage, as observed by Trak et al. [12]. Moreover, these authors have shown that, in the absence of evident leakage, the pore pressure measured in isotropically consolidated undrained (CIU) triaxial compression tests (strain rate of 0.5%/h) with paraffin was smaller (at least 20% in four pairs of tests) than that measured when water was used as cell liquid; they explain this phenomenon by the presence of folds [12]. Therefore, paraffin cannot be recommended for tests in which membranes are used.

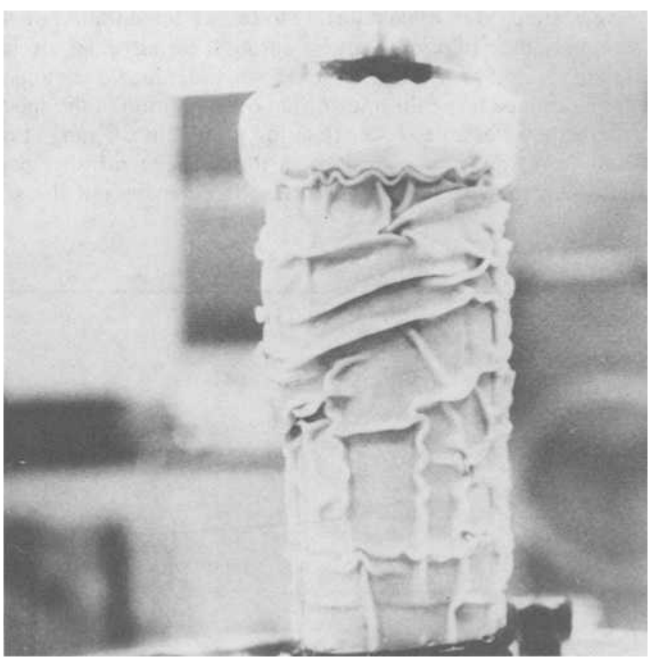

FIG. 5—*Effects of liquid paraffin on rubber latex membrane.*

Silicone oil does not seem to have any detrimental effect on the membranes. As shown in Table 1, very small rates of outflow have been observed, suggesting that silicone oil is suited ideally for use as a cell fluid. Silicone oil has been used consistently and with great success for long-term tests at Laval University for about 10 years. Its only shortcoming is its high cost; it must be recovered and filtered after each test.

Glycerin is often advertised as the ideal cell fluid by soil testing equipment companies; tests performed in the present study suggest quite the contrary. As shown in Table 1, outflow rates between 1.4 and 1.8 cm^3/week were observed for pressure differences between 50 and 340 kPa, indicating that glycerin is sucking the water out of the specimen through the membrane at rates greater than those observed with any of the fluids tested. This may be explained by the high miscibility of water and glycerin and consequent high attraction forces; because the large glycerin molecules have difficulty penetrating the membrane pores, the pore water is sucked out. Figure 6 clearly evidences the poor performance of glycerin in contrast to silicone oil: in the same test, glycerin was first used as a cell fluid, leading to outflow rates of 1.75 cm^3/week; the cell was then drained and filled with silicone oil, which reduced outflow rate to 0.18 cm^3/week; when the cell was filled again with glycerin, the outflow rate increased again to 1.4 cm^3/week. Glycerin is not recommended as a cell fluid.

The choice of the membrane itself is certainly an important factor in controlling the rate of flow, and the common latex rubber membranes used in this study are probably not of the highest quality in terms of impermeability. Ramses prophylactic membranes tested by Poulos [*8*] and in two tests in the present study (Table 1) seem to give a much lower rate of leakage. While such membranes would appear preferable, they are available only in one size suitable for tests on 3.8-cm (1.5-in) diameter specimens.

Influence of Filter Paper Drains on Consolidation and Shear Strength

Filter paper drains are used in triaxial testing to reduce the duration of consolidation and to accelerate the equalization of pore pressures during shearing of the specimen. In common practice they are considered completely effective when defining durations of consolidation and rates of shear in drained tests; this means that consolidation of the specimen is assumed to develop approximately 100 times faster than for specimens draining at one end only [*3*]. Bishop and Gibson have shown analytically that the efficiency of filter papers depends on the ratio between the drainage capacities of the filter papers and the soil, the drainage

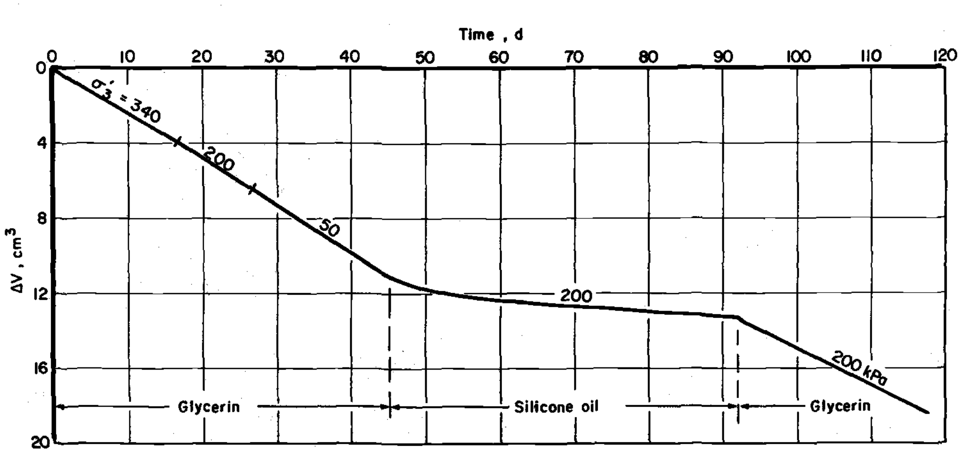

FIG. 6—*Leakages through a rubber latex membrane.*

capacity being equal to the permeability multiplied by the cross-sectional area [5]. However, to the authors' knowledge, very few experimental studies show the actual efficiency of the drains in common use.

The influence of filter papers on the consolidation process of typical Champlain Sea clays has been investigated in this study. Five types of filter paper drains have been used (Table 2). Their thickness varies between 0.11 mm for the Whatman No. 50 and 0.20 mm for the Whatman No. 40. Their strength, measured in tension after 10 min in boiling water and 1 day at rest, is 0.8 and 1.1 N/cm width for the Whatman No. 1 and No. 40, while it is 4.4 and 6.7 N/cm width for the Whatman No. 50 and No. 54 specified as hardened; the strength of Schleicher and Schuell 595 filter paper is intermediate at 3.3 N/cm width.

The drainage capacity of the filter papers was first determined by setting six 1-cm-wide strips on the curved surface of a dummy, 3.8 cm in diameter and 7.6 cm high, as in a standard triaxial test. A cell pressure was applied for 1 to 3 days before carrying out a permeability test by circulating water between the pedestal and the cap. For each type of paper, three or four cell pressures varying between 50 and 400 kPa were used; the long duration between the application of the cell pressure and the test has been imposed by the fact that the filter papers have a permeability that significantly decreases with time, especially during the first hours. The test results (Fig. 7) show that the drainage capacity, also defined as the ratio of the flow rate to the hydraulic gradient, typically decreases by a factor of 100 when the confining stress increases from 50 to 400 kPa. The Whatman No. 40 and No. 54 give the highest drainage capacities, slightly above the values obtained with the Schleicher and Schuell and Whatman No. 50 papers. The drainage capacity of the Whatman No. 1 is lower, particularly at large stresses, and this type of paper will be disregarded in the rest of the study on consolidation.

The efficiency of the filter paper drains was analyzed on four intact clays; overall, 60 consolidation tests on 28 specimens were carried out. The geotechnical properties of the tested clays are shown in Table 3; the plasticity indices vary between 6 and 41; the permeabilities at the initial void ratio, obtained from falling head tests, are between 10^{-9} and 5×10^{-9} m/s, which are typical for Champlain sea clays [*13*].

Comparative consolidation tests with and without lateral drains were carried out on 3.8-cm-diameter and 7.6-cm-high specimens cut from 20-cm-diameter samples taken with the Laval sampler [*14*]. In tests with lateral drainage, six 1-cm-wide strips of filter paper were used; in all tests, drainage was allowed only from the top cap, and the pore pressure was measured at the base. In this way, it was possible to evaluate the efficiency of the drains from volumetric change-time consolidation curves and from the pore pressure dissipation curves.

In Figure 7, the drainage capacity of the specimens, equal to the permeability (given on the right side of Fig. 7) multiplied by the section area, is plotted versus the effective stress. The drainage capacity of the filter drains Whatman No. 40 and Whatman No. 54 is typically 10 to 60 times higher than the drainage capacity of the soils. From the analytical work by

TABLE 2—*Side drain characteristics.*

	Thickness, mm	Tensile Strength, N/cm width
Schleicher and Schuell 595	0.14	3.3
Whatman No. 1	0.16	0.8
Whatman No. 40	0.20	1.1
Whatman No. 50	0.11	4.4
Whatman No. 54	0.16	6.7

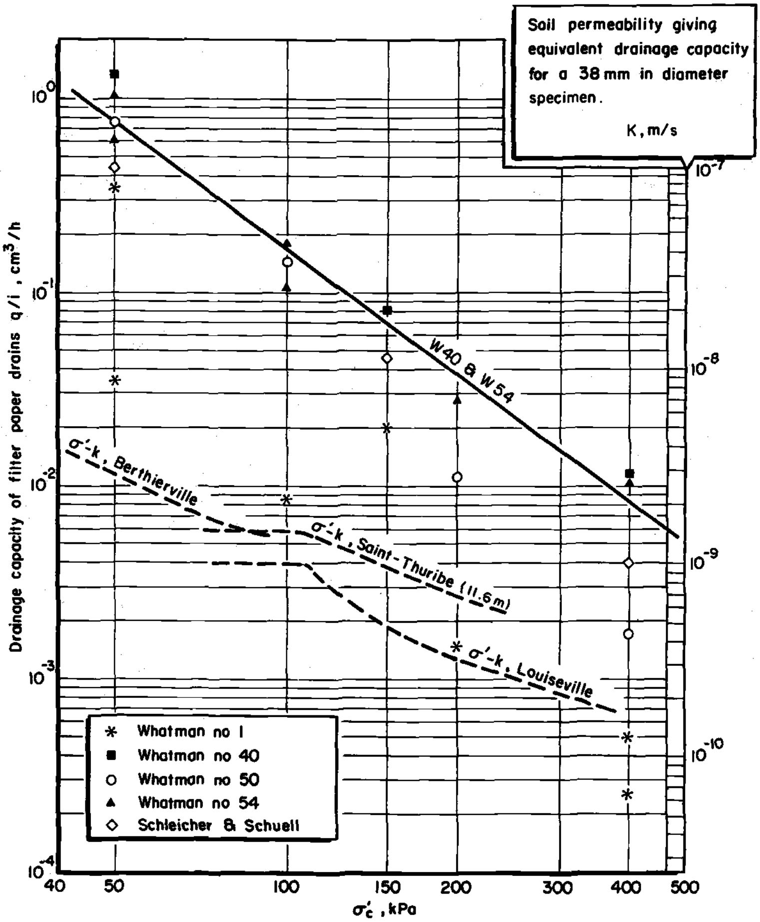

FIG. 7—*Drainage capacities of lateral filter drains and studied soils.*

Bishop and Gibson [5] and taking into account the fact that the filter drains cover only half of the lateral surface of the specimen, the consolidation time should be reduced by a factor of five to ten with these filter drains. It would be less for other drains with smaller drainage capacities.

Typical consolidation test results are presented in Figs. 8 and 9. From all the data, the following comments can be made. When the clay is consolidated in the overconsolidated range, the filter paper drains reduce the consolidation time by a factor varying between 5

TABLE 3—*Geotechnical characteristics of the tested clays.*

Site	Depth, m	w, %	I_p	I_L	<2 μm	σ_p', kPa	k_o, m/s	$C_k = \Delta e/\Delta lgk$
Saint-Thuribe	5.8	51	22	1.3	43	175	1.2×10^{-9}	0.56
Saint-Thuribe	11.6	42	6	4.5	30	175	1.8×10^{-9}	0.50
Louiseville	12.4	66	41	1.0	85	185	10^{-9}	0.90
Berthierville	4.0	58	19	1.9	34	054	5×10^{-9}	0.75

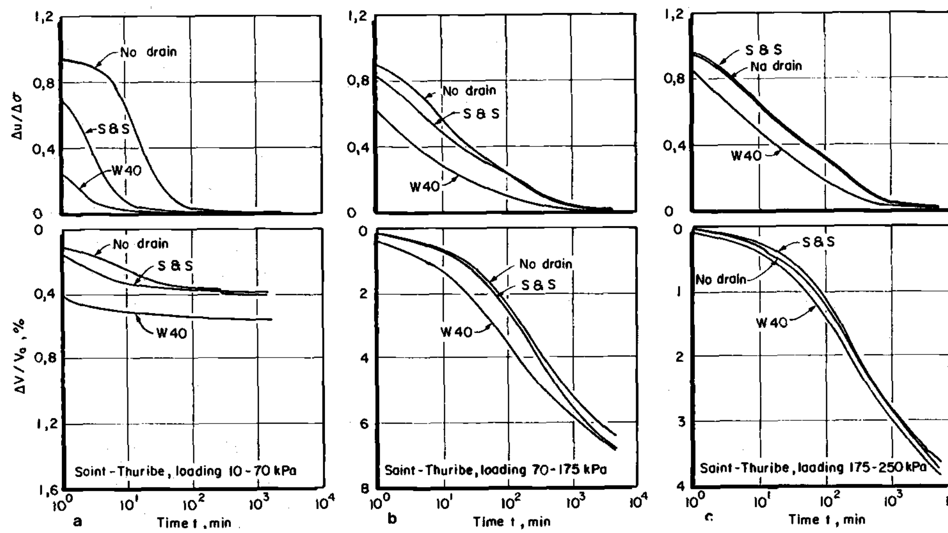

FIG. 8—*Consolidation of soil specimens with and without lateral filter drains (Saint-Thuribe clay) 11.6 m.*

and 25 and can thus be considered as perfectly efficient (Fig. 8*a*). When the clay is in the normally consolidated range, as in Figs. 8*c* and 9, their efficiency is considerably reduced; there is no test in which the consolidation time has been reduced by a factor greater than 2.5, which is considerably less than expected. The most efficient filter papers are the Whatman No. 40 and No. 54 as shown in Figs. 8 and 9. Finally, for loading steps straddling the yield stress of the clay, the behavior is generally somewhere in between those observed for in overconsolidated and normally consolidated ranges. The poor performance of the filter

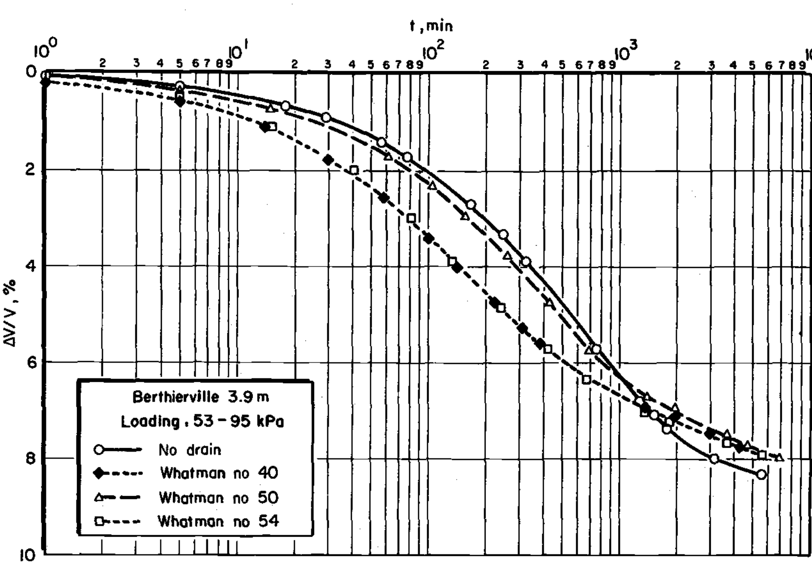

FIG. 9—*Consolidation of soil specimens with and without lateral filter drains (Berthierville clay).*

paper drains with normally consolidated clays is attributed to a clogging phenomenon which is confirmed by the gray color of the filters after testing. With the overconsolidated clays, the volumetric strains are much smaller and the clogging phenomenon is almost nonexistent. In summary, for the clay tested, filter papers used as lateral drains appear to be efficient only for tests on overconsolidated clays, for which the rate of consolidation is naturally so high that drains are of little interest. For tests on normally consolidated clays which show a slow natural rate of consolidation the efficiency of the drains is much smaller than what is normally assumed, making the use of such drains questionable.

After consolidation under the last step of loading, the specimens were sheared under undrained conditions at a strain rate of 0.5% per hour. Only one set of comparative curves is presented here, in Fig. 10. The Saint-Thuribe clay was normally consolidated under an isotropic effective stress of 245 kPa, and its volumetric strain was about 11%; one specimen was set up without a drain, one with a Schleicher and Schuell drain, one with a Whatman No. 40, and the last one with a polyester drain having a strength of 55 N/cm of width (that is, about ten times stronger than the stiffest paper filter).

The results show no difference in terms of deviatoric stress for strains as high as 16%, indicating that, for clays which have undergone large volume changes, the strength of the drains is not mobilized and thus does not change the stress–strain relation. This behavior has been confirmed by other series of tests on normally consolidated clays, as shown in Fig. 11. These results are in disagreement with those previously obtained on remolded clays by Henkel and Gilbert [1] and Olson and Kiefer [15], which indicates that the effect of the

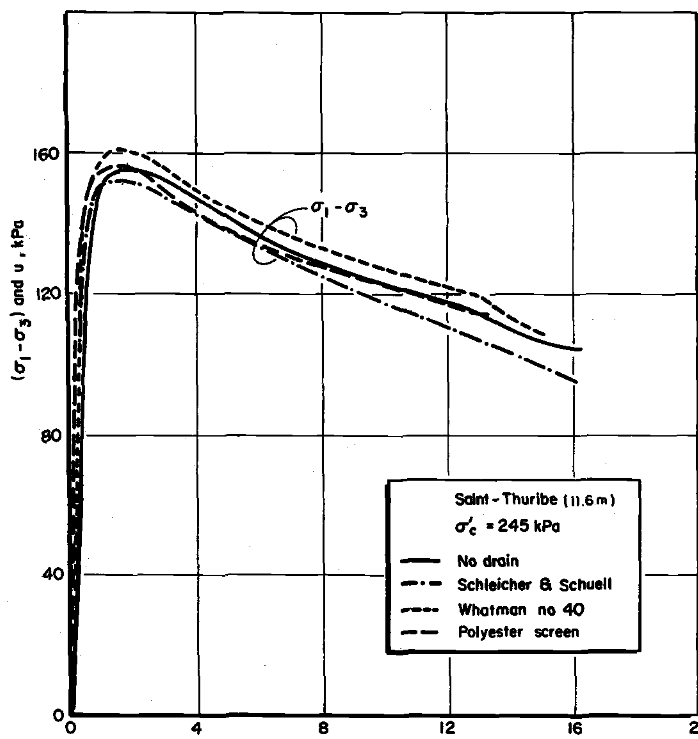

FIG. 10—*CIU tests on normally consolidated clay specimens with and without lateral filter drains.*

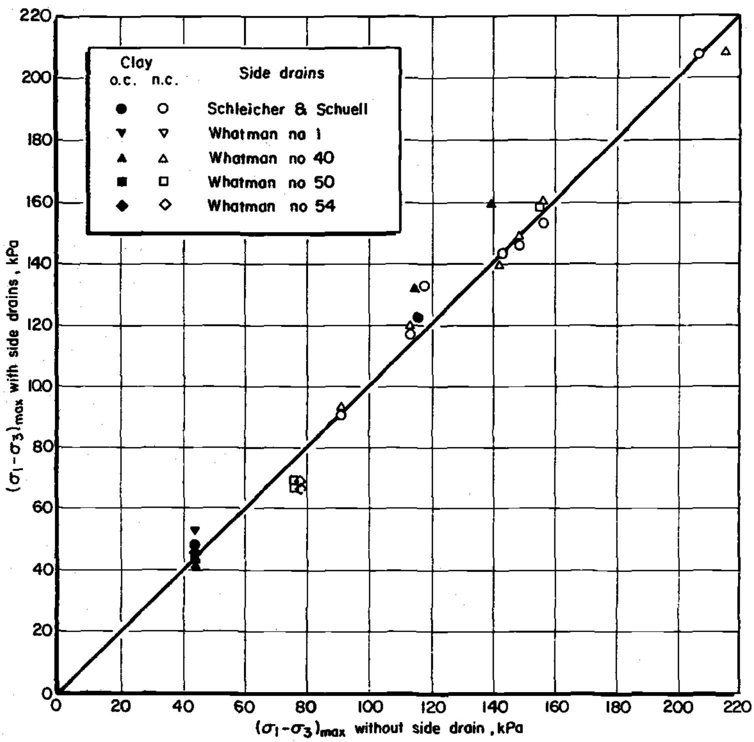

FIG. 11—*Comparison between undrained shear strengths obtained with and without lateral filter drains.*

filter drains could depend on numerous factors such as the type of soil, the accumulated volumetric strain before shearing, the type of failure, and the effective stresses. In such conditions, it is better to try to minimize the eventual effect of the drains by using a filter paper of low strength, such as the Whatman No. 1 or Whatman No. 40. Because the Whatman No. 40 is also one of the most efficient drains during the consolidation, in the authors' opinion it is preferred.

Only a few undrained shear tests were carried out in the overconsolidated range. Tests on the Saint-Alban clay ($\sigma_1 - \sigma_3 = 44$ kPa in Fig. 11) do not show any significant effect of filter paper drains on the undrained shear strength. However, two other series of results shown in Fig. 11 indicate that the Whatman No. 40 paper increases the shear strength in a significant manner, by 15 and 20 kPa. This is surprising because the strength of this paper is rather small (1.1 N/cm width, Table 2) and the mobilization of the full resistance of three of the six strips would theoretically increase the strength of the specimen by only 3 kPa. These two test results could be due to the natural variability of the specimens. More tests would be necessary to be conclusive, but the problem is not that important because, in the overconsolidated range, most natural clays have a high coefficient of consolidation and consolidate rapidly, making the use of filter paper drains unnecessary.

Practical Conclusions

Although the triaxial test was developed four decades ago, there is still place for improvement of the technique and its use. This paper examines two of the important aspects of triaxial testing: leakage and the role of the filter paper drains during the consolidation and shear processes.

For long-term tests, leakage could have significant effects on soil behavior and test interpretation. Therefore, leakage must be as small as possible; beyond this general requirement, criteria for acceptable leakage rates cannot be given because they vary with such parameters as soil type and behavior, test type and duration. There is no perfect solution to prevent leakage, but there are some actions which can be taken to minimize them:

- The number of fittings must be minimized. One solution is proposed—attaching the burette directly to the base of the cell, with the fittings in a back pressure chamber.
- The pedestal and the top cap must be polished and coated with a thin layer of silicone grease before installing the membrane and the O-rings.
- The choice of the membrane is important. Prophylactic membranes, such as the Ramses membrane, seem to have a lower permeability. Moreover, as shown in the companion paper by La Rochelle and co-workers [*7*], these membranes of small thickness and stiffness minimize the membrane correction to be applied for the interpretation of the test.
- The membrane should be saturated by soaking it in deaired water for at least 3 days before the test [*6*].
- For various reasons, deaired water, paraffin, kerozene, and glycerin should not be used as cell fluid. Silicone oil is recommended for use in long-term tests.

The efficiency during consolidation and the effect on shear strength of various filter paper drains have been examined. The tested soils are typical Champlain sea clays. The conclusions can be summarized as follows:

- In the overconsolidated range, filter papers are very efficient during consolidation. However, at such stresses, the coefficient of consolidation of natural clays is high, consolidation is rapid, and lateral drains are not really useful. It is preferable in these conditions not to use filter paper drains.
- In the normally consolidated range, lateral filter papers have a limited effect: the most efficient papers, the Whatman No. 40 and the Whatman No. 54, reduce the time of consolidation by a factor of less than 2.5. As for the influence of filters on shear strength, no effect was found. This is contrary to what has been found by other researchers, which would indicate that the influence of the drains could depend on the type of soil, the type of failure, and the accumulated volumetric strain before shearing. In this context, it seems preferable to use a filter paper with low strength to reduce a possible effect. The Whatman No. 40 fulfills this condition and, moreover, is one of the most efficient during consolidation; it is thus the one to prefer for testing normally consolidated clays. However, it must be recognized that for the tested clays, consolidation would be faster with double drainage than with drainage at one end only and lateral drains.

The efficiency of the filter paper drains is smaller than expected. Consequently, the coefficient of consolidation of a clay calculated from the rate of consolidation as suggested by Bishop and Henkel [*3*] may be in error when lateral filters are used, unless their efficiency has been checked experimentally for the type of soil and test conditions considered.

Acknowledgments

The authors wish to acknowledge J. P. Dussault, J. Y. Julien, and S. Paré, technicians, and all the graduate students for having carried out the necessary tests for this study. The research was supported by grants from the programme "Formation de chercheurs et action concertée" (FCAC) and Natural Science and Engineering Research Council of Canada (NSERC) operating grants A7379, S1503, and A7724.

References

[*1*] Henkel, D. J., and Gilbert, G. D. "The Effect of the Rubber Membrane on the Measured Triaxial Compression Strength of Clay Samples," *Geotechnique*, Vol. 3, 1952, pp. 20–29.

[*2*] Gibson, R. E., and Henkel, D. J., "Influence of Duration of Tests at Constant Rate of Strain on Measured 'Drained' Strength," *Geotechnique*, Vol. 4, 1954, pp. 6–15.

[*3*] Bishop, A. W., and Henkel, D. J., "The Measurement of Soil Properties in the Triaxial Test," 2nd ed., Edward Arnold, London, 1962, 228 pp.

[*4*] Andresen, A., and Simons, N. E., "Norwegian Triaxial Equipment and Technique," *Proceedings*, American Society of Civil Engineers Research Conference on Shear Strength of Cohesive Soils, Boulder, CO, 1960, pp. 695–709.

[*5*] Bishop, A. W., and Gibson, R. E., "The Influence of the Provisions for Boundary Drainage on Strength and Consolidation Characteristics of Soil Measured in the Triaxial Test," in *Laboratory Shear Testing of Soils, STP 361*, American Society for Testing and Materials, Philadelphia, 1964, pp. 435–451.

[*6*] Berre, T., "Triaxial Testing at the Norwegian Geotechnical Institute," *Geotechnical Testing Journal, ASTM*, Vol. 5(1/2), 1982, pp. 3–17.

[*7*] La Rochelle, P., Leroueil, S., Trak, B., Blais, L., and Tavenas, F., "Observational Approach to Membrane and Area Corrections in Triaxial Tests," in this volume, pp. 715–731.

[*8*] Poulos, S. J., "Control of Leakage in the Triaxial Test," Harvard Soil Mechanics Series No. 71, 1964, 230 pp.

[*9*] Leroueil, S., "Quelques considérations sur le comportement des argiles sensibles," Ph.D. thesis, Department of Civil Engineering, Laval University, Québec, 1977.

[*10*] Tavenas, F., Leroueil, S., La Rochelle, P., and Roy, M., "Creep Behaviour of an Undisturbed Lightly Overconsolidated Clay," *Canadian Geotechnical Journal*, Vol. 15(3), 1978, pp. 402–423.

[*11*] Tavenas, F., Leblond, P., Jean, P., and Leroueil, S., "The Permeability of Natural Clays—Part I—Methods of Laboratory Measurement," *Canadian Geotechnical Journal*, Vol. 20(4), 1983, pp. 629–644.

[*12*] Trak, B., Blais-Leroux, L., and La Rochelle, P., "Etude de la correction de membrane et de surface dans les essais de cisaillement non drainés," Report GCT-81-06, Department of Civil Engineering, Laval University, Quebec, 1981.

[*13*] Tavenas, F., Jean, P., Leblond, P., and Leroueil, S., "The Permeability of Natural Clays—Part II—Permeability Characteristics," *Canadian Geotechnical Journal*, Vol. 20(4), 1983, pp. 645–660.

[*14*] La Rochelle, P., Sarrailh, J., Tavenas, F., Roy, M., and Leroueil, S., "Causes of Sampling Disturbance and Design of a New Sampler for Sensitive Soils," *Canadian Geotechnical Journal*, Vol. 18(1), 1981, pp. 52–66.

[*15*] Olson, R. E., and Kiefer, M. L., "Effect of Lateral Filter Drains on the Triaxial Shear Characteristics of Soils," in *Laboratory Shear Testing of Soils, STP 361*, American Society for Testing and Materials, Philadelphia, 1964, pp. 482–491.

Paul Ferguson Linton,[1] *Michael C. McVay,*[2] *and David Bloomquist*[2]

Measurement of Deformations in the Standard Triaxial Environment with a Comparison of Local Versus Global Measurements on a Fine, Fully Drained Sand

REFERENCE: Linton, P. F., McVay, M. C., and Bloomquist, D., **"Measurement of Deformations in the Standard Triaxial Environment with a Comparison of Local Versus Global Measurements on a Fine, Fully Drained Sand,"** *Advanced Triaxial Testing of Soil and Rock, ASTM STP 977,* Robert T. Donaghe, Ronald C. Chaney, and Marshall L. Silver, Eds., American Society for Testing and Materials, Philadelphia, 1988, pp. 202–215.

ABSTRACT: Deformation measurement devices are reviewed. Measurements obtained using linear variable differential transformers attached to the middle third of a specimen and the standard burette–piston system are compared. Results are presented for hydrostatic and standard compression tests run on a fully saturated, fully drained, poorly graded fine sand—Reid-Bedford, Unified Soils Classification System group SP. The effects of end restraints and membrane penetration are discussed in regard to the test results. In addition, a new technique is presented for measuring specimen saturation on coarse grain soils.

KEY WORDS: standard triaxial compression, end effects, saturation, deformation, data acquisition, axial strain, radial strain, drained fine sand, Reid-Bedford sand, standard compression, hydrostatic compression, strain gauges, linear variable differential transformer, inductive device, pneumatic device, membrane penetration, burette

Laboratory testing is usually carried out to characterize the stress–strain–strength behavior of in situ soil. There are experimental limitations on laboratory equipment's ability to emulate actual field conditions. This, combined with the difficulties in obtaining high quality samples, has resulted in more frequent use of in situ testing devices.

Yet laboratory testing remains superior in some areas of work for at least two reasons. First, the laboratory environment provides the ability to vary both the loading and measurement methods. Second, many projects may require evaluation of the behavior of soils before modification or placement. Construction of embankments for roads or dams are typical examples.

The problem becomes twofold: (1) manufacturing a laboratory specimen which has the same properties as in the field, and (2) loading and monitoring movement without significantly affecting its behavior. This latter problem has been studied by a number of researchers,

[1] Staff engineer, Dames S. Moore, 350 W. Camino Gardens Blvd., Boca Raton, FL 33432.
[2] Associate professor and research engineer, respectively, University of Florida, 345 Weil Hall, Gainesville, FL 32611.

[1,2] and an overview has been presented by Saada and Townsend [3]. Basically, the studies conclude that if uniform deformation field throughout the specimen (that is, homogeneous axial strains) and tangential strains equal to radial strains are desired, a combination of rubber sheeting and silicone grease should be used to develop near frictionless ends. Otherwise, the use of rough platens may result in the development of quasi-rigid zones at the specimen's ends [2].

The use of grease and rubber sheeting between the specimen and its end caps poses a number of problems in determining axial strain in the conventional piston and platen deformation system [4]. Consequently, to include frictional reducers and improve accuracy of measurements, trends are toward instrumentation that either attaches or scans the specimen from inside the triaxial cell.

This report addresses one such set of measuring devices, hermetically sealed direct current linear variable differential transformers (DCDTs), which are affixed to the specimen.

Because a study of instrumentation influences on specimen response is also warranted, both DCDTs and the conventional burette–piston measuring system were employed during testing. The DCDT system was waterproof, and water was used as the chamber fluid facilitating the standard burette readings. In an attempt to reduce the effect of frictional end caps, platens were made from polished aluminum blocks and coated with Teflon, and porous steel insets were used for drains.

The tests investigated monotonic and cyclic conventional triaxial compression (CTC) and hydrostatic compression, all on dense, fully drained sand. Results show that both measuring systems give nearly identical vertical strain measurements in the case of the CTC, but significantly different lateral strains for all other tests. This difference may be attributed to specimen bulging, resulting from friction between the soil and the end caps. The hydrostatic compression study revealed that if the burette–piston measuring system was used, specimen deformation may be masked by membrane penetration.

This report begins with a brief overview of available measuring devices, the monitoring and data acquisition equipment selected, and necessary software reduction algorithms. Additional sections on the soil tested, specimen preparation, and method of determining specimen saturation are presented. Finally, DCDT and conventional burette–piston measurement systems are compared.

Deformation Measurements

Strain Gauges

A strain gauge, a common component in many devices used for contact measurement of specimen deformations, is used to determine the flexural strains in a simply supported beam attached to the specimen. Figures 1*a* and *b* are a simplified plan and a cross-sectional view of a proposed device consisting of three brackets affixed to the specimen in the vicinity of its middle third. Epoxied to the central aluminum beam of each bracket are two pairs of gauges (two on each side). They are subsequently wired to form an unbalanced Wheatstone bridge circuit, with the individual resistors (legs) in the bridge connected to produce the greatest imbalance for the smallest strain.

Using an aluminum strip 5 mm (0.2 in.) wide by 0.5 mm (0.02 in.) thick, specimen deformation on the order of 0.0025 mm (0.0001 in.) is measurable, if the resolution of the voltmeter is on the order of 200 μV [5]. A typical data acquisition system (for example, Hewlett-Packard's HP 3497A) is capable of measuring on the microvolt scale. Cost of raw material in the brackets, gauges, and calibration micrometer is on the order of $1500. Devices similar to the one discussed have been used by a number of researchers [6].

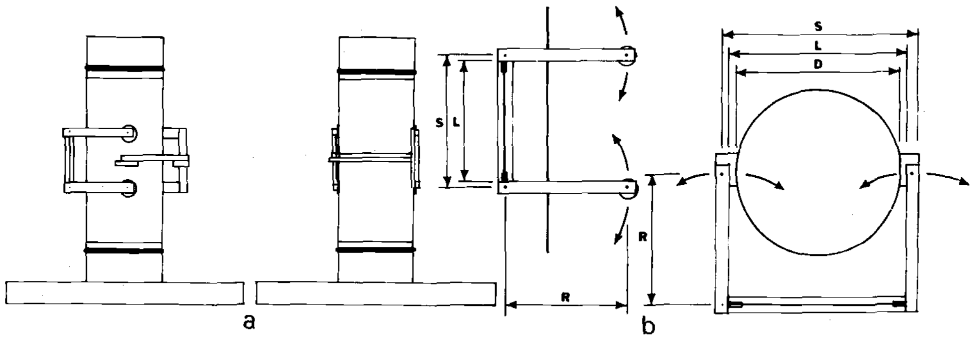

FIG. 1—*Proposed strain gauge device:* (a) *plan view and* (b) *cross-sectional view.*

Some disadvantages of this form of measurement are: (1) to record deformation, the aluminum bar has to flex, thereby applying a stress traction on the specimen on the order of 7 kN/m^2 (1 psi) [*5*]; (2) the necessity of periodic calibration; (3) the uncertainty of waterproofing the gauges; and (4) the possibility of equipment destruction (induced permanent deformation) due to large specimen deformations.

Noncontact Devices

Noncontact measurement instruments generally fall into one of four categories: inductive, ultrasonic, optical, and pneumatic. Possibly due to increase in demand, the accuracy of all representative devices has improved within the last two years. Ultrasonic and pneumatic instruments are generally ruled out due to a lack of sensitivity (0.05 mm or 0.002 in.) in the case of the former, and size constraints, as well as ability to perform submerged, in the case of the latter. Optical techniques such as lasers look promising with the aid of microcomputers and robotics; however, the capital expenditures required to develop holographic equipment are presently prohibitive. Inductive equipment, both small and fully immersible has found use in monitoring shaft or plate thickness, but only recently have there been attempts to monitor soil response.[3] Inductive measurement of distance uses the eddy currents generated in a metallic target through high-frequency excitation to stimulate the impedance of a coil. This reaction is then conditioned and linearized to produce a direct, but not linear, relationship between position and output voltage [*7*].

Linear Variable Differential Transformers

The final option investigated was the use of linear variable differential transformers (LVDTs). Available in alternating or direct current (DCDTs), the LVDTs work by exciting a primary coil placed between two symmetrical secondary coils which are in an opposing series circuit. Electrical potential between the primary and secondary coils is then monitored and converted to deformation. However, the alternating current devices require an additional unit to convert AC to DC before the display of deformations. LVDTs have many valuable attributes for measurement [*8*]:

(a) near frictionless measurement
(b) long mechanical life
(c) extremely high resolution
(d) core and coil separation
(e) null repeatability

[3] A. S. Saada, personal communication, 1985.

Even though the AC devices are much smaller than their DC counterparts, the authors found them questionable for the following reasons:

1. Erratic readings often developed due to outside power sources.
2. The instruments had to be continuously recalibrated due to drift.

Consequently, standard DCDTs with ranges of 13 and 25 mm (0.5 and 1.0 in.) were used. This resulted in a full range output of about 3.2 and 1.6 V/mm (80 and 40 V/inch). A proposed DCDT system to monitor vertical and horizontal deformations in a soil specimen's middle third is presented in Figs. 2*a* and *b*. Note that all brackets are designed with sliding rods within stainless steel sleeves (top and bottom, Fig. 2*b*), or a combination of DCDTs (middle, Fig. 2*b*), to result in linear deformations and prevent the transfer of normal forces onto the specimen. The weight of the brackets and DCDTs will result in an average vertical shear stress of approximately 7 kPa (1 psi) over the contact surface. However, this may be reduced to zero if flotation is employed. Estimated total cost of DCDTs and brackets is $1600.

Because of cost, previously discussed benefits, and limited determents, the authors decided to construct and compare the LVDT measuring system to the conventional burette and dial gauge system [*9*].

With the aid of the data acquisition system described below, the authors evaluated several measurement techniques. For several test samples the data from each device were measured and recorded. Because the specimen showed very little or no creep, the authors chose to use a simple measurement cycle. For the local devices (Fig. 2), the vertical strain was obtained by measurement of the vertical deformation of the middle third of the specimen, on opposite sides, using the vertical DCDT brackets. Specifically, the original vertical spacing of the brackets as measured and recorded for each side. Then during the test the deformation and the corresponding initial length were used to calculate a strain on one side. These two vertical strains were recorded individually and then averaged and recorded as the local vertical strain. The individual strains were recorded to check against detachment or malfunction of individual DCDTs. The local radial strain was measured in a similar fashion. If the results from DCDTs were significantly different, the test was aborted.

Data Capture and Reduction

Monitoring both the local (DCDT) and macro (burette and dial gauge) measurements consisting of approximately eight instruments for 200 different loadings (cyclic testing) or

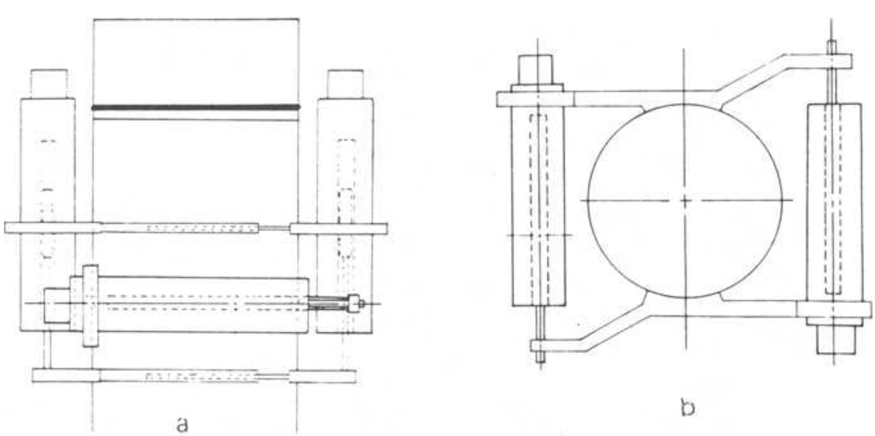

FIG. 2—*DCDT measurement device:* (a) *plan view and* (b) *cross-sectional view.*

1600 data entries, the benefits of an automated data acquisition and reduction package are readily evident. A large number of hardware-specific software packages are commercially available for such tasks. However, the system developed incorporated hardware (equipment) commonly found in soils laboratories. The package shown in Fig. 3 consists of:

(a) a microcomputer and monochromatic CRT (screen)
(b) a multiprogrammer and interface
(c) a 3.25-in. (8.25-cm) floppy drive unit
(d) a two-pen plotter
(e) a dot matrix printer

The multiprogrammer (voltmeter), controlled by a microcomputer software package (TRI-TEST) developed at the University of Florida, automatically scans eight channels after the application of each load increment: four DCDTs associated with the local measurement system (Fig. 2), one DCDT to monitor movement of top platen attached to the specimen, two pore pressure transducers (one for the cell, the other for the specimen), one load cell to monitor axial load, and a volumetric burette reading (inputted manually). All of the measuring devices were read every two minutes.

The captured data are immediately reduced and stored on both hard and soft media (floppy disk drive unit). Examples of available results are.

(a) individual LVDT deformations
(b) local (Fig. 2) and macro (computed from burette and platen movement) vertical, horizontal, and volumetric strains
(c) effective vertical and horizontal stresses
(d) P' $((\sigma_1' + \sigma_2' + \sigma_3')/3)$, and Q' $(\sigma_1' - \sigma_3')$
(e) $\bar{\epsilon}$ $(\epsilon_1 - \epsilon_3)$

FIG. 3—*Photograph of the computer system.*

Through the course of the test, the operator has the option of viewing the measured response by a hard copy (printer), or by plots (CRT or plotter), or both. Several graphs (local and macro Q' versus $\bar{\epsilon}$) may also be viewed concurrently. These latter options were implemented to assess the performance of all instrumentation during the test [5].

Soil-Sample Preparation–Back Saturation

The soil tested, commonly referred to as Reid-Bedford sand, is composed of 89% quartz, 9% feldspar, 2% ferromagnesians and heavies. Particle shapes range from subrounded to subangular with a coefficient of uniformity, C_u, of 1.8, and a coefficient of curvature, C_c, of 1.0. The Unified Soil Classification System identifies Reid-Bedford as a fine sand with a group symbol of SP. The average of five relative density tests (ASTM D-2049) indicates that the void ratio ranges from 0.59 to 0.91. These void ratios correspond to a maximum dry unit weight of 16.3 kN/m^3 (104.0 pcf) and a minimum dry unit weight of 13.6 kN/m^3 (86.6 pcf), respectively. All reported tests were run on specimens with a void ratio of 0.67 (that is, a relative density of 75%). Testing began with the preparation of a specimen 15.1 cm (5.95 in.) high by 7.11 cm (2.8 in.) in diameter, with a volume of 600 cm^3 (36.6 in.^{3}). The necessary soil mass for the given volume and dry unit weight was first determined, then deposited through aerial pluviation with a drop height of 18 to 23 c (7 to 9 in.). No vibration was necessary if the operator established a coherent stream of falling sand particles instead of a spray. Measurements of the average specimen height were checked during pluviation to ensure uniform specimen density.

The specimen end caps (Fig. 4) were polished aluminum platens with porous steel insets for drainage. In addition, each platen was coated with Teflon spray to reduce friction between the sand grains and the metal. Before attachment of DCDTs, the specimen mold was removed after subjecting the specimen to a vacuum of 34 kPa (5 psi).

Attachment of the DCDTs was a three-step process (Fig. 5). First, the central bracket (local horizontal measurement device) was attached to the specimen; a quick-drying epoxy was used to provide a base which molds to the specimen, then a cyanoacrylate adhesive was used to firmly attach the epoxy to the membrane (step A in Fig. 5). Second, the bottom bracket of the vertical measuring system was affixed (step B) through a similar process, followed by the top bracket containing the DCDTs (step C). Care must be exercised in aligning the vertical DCDTs with their respective cores. The whole process placement of brackets, cementing, and hardening takes approximately 30 min.

Following the placement of the local measurement system, the specimen was saturated with water by repeatedly applying a vacuum to the top of the specimen followed by deaired water entry through the bottom and subsequent back pressuring. In addition to the normal

FIG. 4—*Polished aluminum platen.*

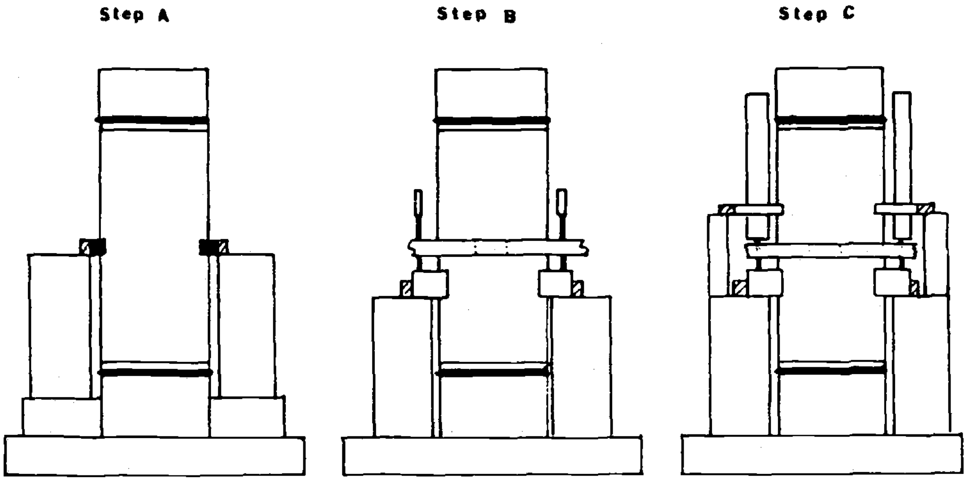

FIG. 5—*Steps for attaching the DCDTs.*

method of measuring saturation through a *B*-value reading [*10*], saturation was also determined by subjecting the specimen to an arbitrary raise in cell and back pressure so that no effective stress changes occur within the specimen. The volume of fluid entering the specimen (burette) is subsequently used to determine the degree of saturation.

The saturation equation was obtained from Boyle's law, as laid out in 1610 [*11*], and a phase diagram. The latter approach was taken over the conventional *B* test [*10*] until the degree of saturation was at least 90% in order to reduce the load applied during the *B*-value test and thereby the influences of stress-induced anisotropy. Because conventional (burette) volume measurements [*12*] were to be employed, *B* values of at least 95% were maintained for all tests.

More specifically, the saturation process occurs by two mechanisms. First, the trapped air is reduced in volume due to the increase in total pressure, and second, the air dissolves in the water. Assuming isothermal conditions, the first processes can be accurately described by Boyle's law as shown below. This equation, combined with the use of a fine burette to apply the back pressure, can be used to check the saturation as shown below.

$$P_1V_1 = k = P_2V_2 \tag{1}$$

where

P_1 = pressure at state 1
P_2 = pressure at state 2
V_1 = volume of gas at state 1
V_2 = volume of gas at state 2
k = constant

Because the volume change is known from the burette

$$V_1 - V_2 = \Delta V \longrightarrow \tag{2}$$

Substituting Eq 1 into Eq 2 results in

$$V_2 = \left\{\frac{P_1}{P_2 - P_1}\right\} \Delta V \tag{3}$$

Using the definition of saturation defined for the final state

$$S = \frac{V_v - V_2}{V_v} 100 \tag{4}$$

From a phase diagram

$$V_v = \left\{\frac{e}{1 + e}\right\} V_t \tag{5}$$

Inserting Eq 5 into Eq 4 and rearranging

$$S = \frac{V_t - \left\{\frac{1 + e}{e}\right\} V_2}{V_t} 100 \tag{6}$$

Substituting Eq 3 into Eq 6 results in

$$S = \frac{V_t - \left\{\frac{1 + e}{e}\right\}\left\{\frac{P_1}{P_2 - P_1}\right\} \Delta V}{V_t} 100 \tag{7}$$

where

S = saturation at the final state
V_t = volume of the specimen
e = void ratio of the specimen
P_1 = pore pressure at state 1
P_2 = pore pressure at state 2

Note: The cell pressure should be changed to keep the effective confining stress constant.

Triaxial Test Results

The first results reported are those from a combination monotonic and cyclic triaxial compression test performed at a constant confining pressure of 207 kN/m^3 (30 psi). Q' $(\sigma_1 - \sigma_3)$ versus the local vertical strain (ϵ_v) measured from the DCDTs is plotted in Fig. 6*a*, whereas Fig. 6*b* depicts Q' versus the macro axial strain as determined from end platen movement. It is evident from a comparison of the two figures that the axial strains are remarkably close with the local being slightly larger than the macro values, but not by more than 10% anywhere. For this one particular test in which the vertical macro deformations were manually recorded, readings recorded by the DCDTs for the local response were noted.

Figures 7*a* and *b* present the macro and local respectively, volumetric strain versus $\bar{\epsilon}$ $(\epsilon_1 - \epsilon_3)$ for the same triaxial test. Cambridge stress and strain nomenclature was used because the variables are three-dimensional invariants. A comparison of Fig. 7*a* and *b* reveals that the results tend to diverge once dilation initiates, and the macro readings both lag and average out the local response. The lateral strain for the burette system was obtained by calculating the new volume and height from cap and burette readings. The height and volume of the specimen were used to calculate an average sample diameter and resulting radial strain. For the DCDT system, the volumetric strain was obtained using a right circular

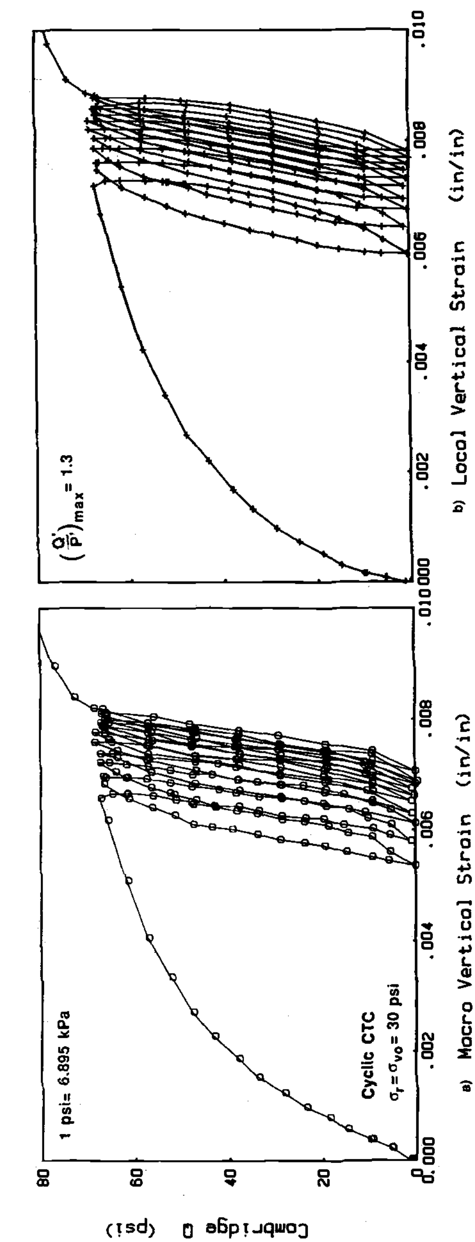

FIG. 6—*Q' versus vertical strain:* (a) *macro measurement and* (b) *local measurement.*

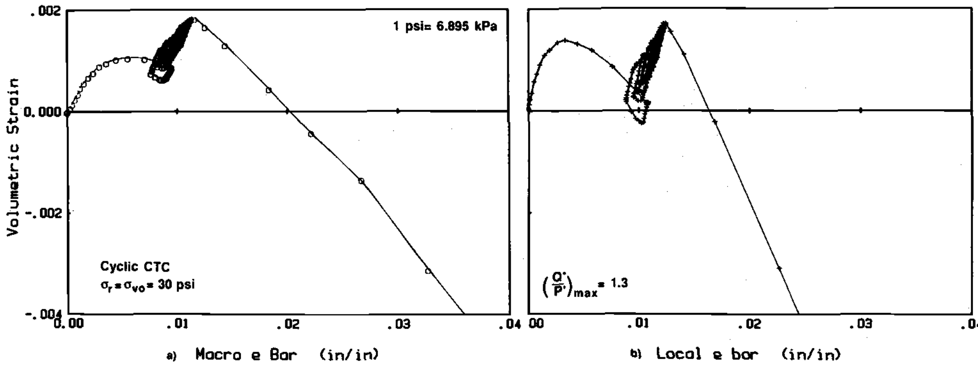

FIG. 7—*Volumetric strain versus* $\bar{\epsilon}$: (a) *macro measurements and* (b) *local measurements.*

cylinder assumption. The authors selected this method because for small strain, even with bulging, the middle third of the specimen closely resembles a right cylinder. However, because the vertical strains measured with the two systems were very close, the differences can be attributed to lateral response. One possibility is that the local measurement equipment was influencing the lateral behavior (that is, DCDT brackets failing to open or close properly). However, because the major divergence was noted when the specimen was dilating (that is, deformations occurring radially outwards), it was ruled out, leaving specimen bulging (that is, frictional development between end caps and soil grains) as the only rational explanation.

Similar results of approximately six other CTC monotonic and cyclic tests concur with this behavior. Even though a number of the specimens had pronounced (visual) slip surfaces at failure, specimen bulging was evident. The results of these tests indicate that while larger height to diameter (H/D) ratios free more of the specimen, they do not necessarily yield uniform stress and deformation fields within the specimen.

Depicted in Figs. 8*a* and *b* are the macro and local, respectively, mean pressure, P' $((\sigma_1 + \sigma_2 + \sigma_3)/3)$, versus volumetric strain from a hydrostatic compression test. As expected, both indicate decreasing volumetric response with increasing mean pressure (below particle crushing level). However, also evident is a pronounced slope variation with the macro (burette-piston) device recording almost twice the local's volumetric response at peak monotonic load. The permanent deformation measured in the unloading phase of any cyclic

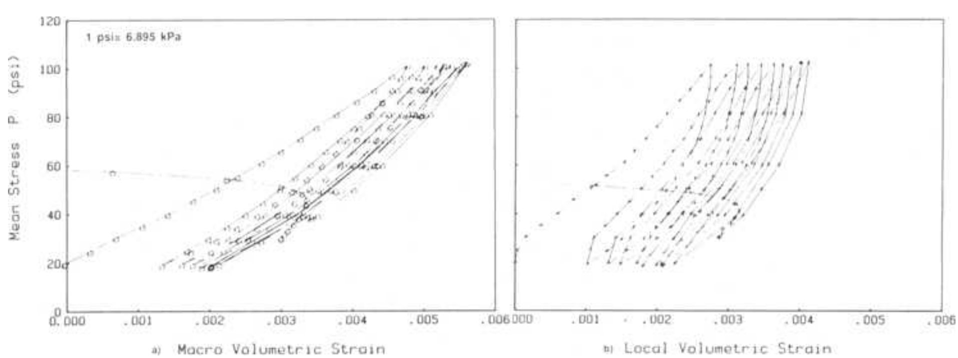

FIG. 8—*Mean pressure versus volumetric strain:* (a) *macro measurements and* (b) *local measurements.*

portion is quite similar, whereas the values recorded at maximum load are much smaller for the macro system. Results of four other hydrostatic compression tests [5] (not depicted), both with and without the DCDT measuring system attached, show similar response as presented, and no influence of DCDTs. Consequently, the difference could be explained only in terms of (1) membrane penetration, (2) frictional end cap effects, and (3) specimen inhomogeneity. Because considerable effort was expended to control specimen homogeneity, it is the authors' opinion that approximately only 10% of the anomalous behavior could be attributed to variation in density. Furthermore, for hydrostatic compression, end effects should make the local reading higher for both vertical and radial strains. It should be noted that the DCDT system has almost no membrane penetration (that is, DCDT brackets actually span from soil grain to soil grain).

In an attempt to estimate the effects of membrane penetration on burette readings, the following equations are presented. However, the results of these computations are only very crudely quantitative; the intent is to provide an indicator of the need to run a membrane correction test. Because membrane penetration was a primary concern, several tests were run to quantify the amount of membrane penetration.

Assuming that the average particle size is D_{10}, then a crude approximation of the penetration between four surface grains, by the membrane, is depicted in the cross-section and planar view of Fig. 9.

Assuming that the membrane is pushed down into the space between four adjacent spheres arranged in a hexagonal close-packed structure,

$$v = D_{10}^2 \left\{ \frac{1}{2} - \frac{\pi}{12 \cdot \text{Cos } 30°} \right\} \tag{8}$$

The number of volumes penetrated by the membrane equals the total surface area divided by the surface area required for each penetration.

$$N = \frac{A}{a} = \frac{H \, \pi \, D}{\frac{1}{2} \cdot D_{10}^2 \text{ Cos } 30°} \tag{9}$$

The entire volume of membrane penetration equals the sum of all of the individual penetrations.

$$\delta V = N \cdot v \tag{10}$$

$$\delta V = \pi \, D_{10} \, H \, D \left\{ \frac{1}{2} - \frac{\pi}{12 \cdot \text{Cos } 30°} \right\} \tag{11}$$

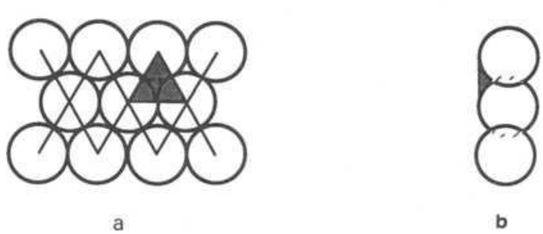

FIG. 9—*Interstitial membrane penetration:* (a) *plan view and* (b) *cross-sectional view.*

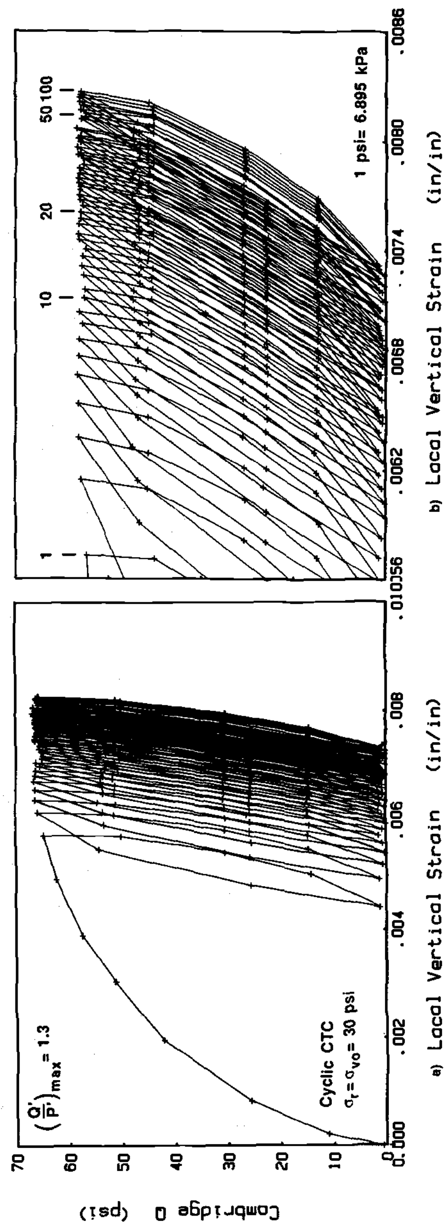

FIG. 10—*100-cycle CTC.*

Calculating the volumetric strain due to membrane penetration

$$\epsilon_{vol} = \frac{\delta V}{V_o} = 4 \cdot \frac{D_{10}}{D} \left\{ \frac{1}{2} - \frac{\pi}{12 \cdot \text{Cos } 30°} \right\} \tag{12}$$

Using the given specimen dimensions and the average particle grain size, the volume change associated with membrane penetration is 5.4 cm^3 (0.27 in.^{3}) or a volumetric strain of 0.0018. If this value were to be added to the recorded DCDTs' response at peak monotonic load, it would explain the discrepancy between the measuring systems. However, because the permanent deformation recorded in the unloading phase of the cyclic portion is quite similar for both tests (Fig. 7), but much less (macro) at peak load, frictional influences associated with higher pressures are also definitely present. Consequently, the DCDT and macro response would be quite similar if both membrane and frictional effects could be accounted for in the latter test.

The membrane penetration was also calculated by using the unload portion (from 483 to 207 kPa; 70 to 30 psi) of a hydrostatic test [*13*]. The specimen was assumed isotropic and the vertical strain was multiplied by three to obtain the volumetric strain at both the peak and bottom of the unload curve. This method resulted in a membrane penetration of approximately 0.0012, which is on the same order as the value from the equation.

Finally, the benefits of using DCDTs over the conventional burette–piston measuring system in terms of resolution are presented in Fig. 10. The test, a 100-cycle CTC, shows the gradual shakedown of a dense granular soil (Fig. 10*a*) and the DCDTs' excellent ability to monitor such phenomena (Fig. 10*b*).

Conclusions and Recommendation

A number of significant conclusions can be drawn from the results reported herein. First, the influence of friction associated with the end caps is minimal on the axial strain behavior, at least for CTC which employ polished end caps and Teflon spray. However, its effects on lateral or volumetric behavior are more pronounced, and the use of a greased membrane between the soil grains and platens is recommended.

The conventional triaxial monitoring method of burette and piston is not recommended for two reasons: (1) the use of friction reduction materials on platens makes piston monitoring impossible, and (2) the use of volume-monitoring devices forces the determination of the influence of membrane penetration on any test in which the cell pressure is changing.

Contact or noncontact specimen-monitoring systems are improving. Of those investigated, the DCDT system had one of the best resolutions and the fewest determinants. The benefits of using such a system over conventional monitoring are

1. The specimen doesn't need to be saturated because exterior movement is measured directly.
2. The influence of membrane penetration is minimal (device spans soil grains).
3. The deformations determined by the DCDTs if end cap friction is present are much closer to the response that would be measured if end effects were eliminated.
4. The resolution is only a function of the sensitivity of the voltmeter used.

The use of a data acquisition and reduction system is recommended because (1) the course of the test may be more closely monitored, and (2) a number of readings for the same load step may be obtained and averaged, resulting in a smoothing process from which trends are more evident.

It is recommended that further research be directed to the development of improved specimen-monitoring techniques and methods of reducing frictional end effects.

References

[1] Rowe, P. W. and Barden, L., "The Importance of Free-Ends in the Triaxial Test," *Journal of the Soil Mechanics and Foundation Division, American Society of Civil Engineers,* Vol. 90, No. SM1, 1964, pp. 1–27.

[2] Kirkpatrick, W. M. and Belshaw, D. J., "On the Interpretation of the Triaxial Test," *Geotechnique,* Vol. 18. No. 3, 1968, pp. 336–350.

[3] Saada, A. S. and Townsend, F. C., "State of the Art Laboratory Strength Testing of Soils," *STP 740, Laboratory Shear Strength of Soil,* American Society for Testing and Materials, Philadelphia, 1981.

[4] Hettler, A., Gudehus, G., and Vardoulakis, I., "Stress–Strain Behaviour of Sand in Triaxial Tests," in *International Workshop on Constitutive Relations for Soils,* Grenoble, France, A. A. Balkema, 1982.

[5] Linton, P. F., "A Study of a Sand in the Standard Triaxial Chamber Equipped with a Computerized Data Acquisition System," M. S. thesis, University of Florida, Dept. of Civil Engineering, Gainesville, 1986.

[6] Boyce, J. R., "Measurement of Stress and Strain During Repeated Load Triaxial Tests on a Crushed Rock," in *UROMECH 157—Quality of Mechanical Observations on Particulate Media,* 1983.

[7] Bristol Industrial & Research Associates Ltd, *Non-Contact Measurements,* P.O. Box 2, Portishead, Bristol, England, BS20, 9JB.

[8] Herceg, E. E., *Handbook of Measurement and Control,* Pennsauken, NJ, Schaevitz Engineering, 1985, pp. 3–14.

[9] Johnson, H. V., "The Effects of End Platens, Method of Loading, and Specimen Size in Monotonic Triaxial ∂ Tests," U.S. Army Engineering Waterways Experiment Station, Vicksburg, MS, 39180, 1982.

[10] Lambe, T. W. and Whitman R. V., *Soil Mechanics,* 11th ed., Wiley, New York, 1969.

[11] Young, J. E., *The New Science of Skin and Scuba Diving,* Follett Publishing Co., New York, 1974, p. 26.

[12] Bishop, A. W. and Henkel, D. J., *The Measurement of Soil Properties in the Triaxial Test,* Edward Arnold, London, 1962.

[13] Vaid, Y. P. and Negussey, D., "A Critical Assessment of Membrane Penetration in the Triaxial Test," *Geotechnical Testing Journal,* Vol. 7, No. 2, 1984, pp. 70–76.

Test Methods

Gualtiero Baldi,[1] David W. Hight,[2] and Gregory E. Thomas[1]

STATE-OF-THE-ART PAPER

A Reevaluation of Conventional Triaxial Test Methods

REFERENCE: Baldi, G., Hight, D. W., and Thomas, G. E., **"A Reevaluation of Conventional Triaxial Test Methods,"** *Advanced Triaxial Testing of Soil and Rock, ASTM STP 977,* Robert T. Donaghe, Ronald C. Chaney, and Marshall L. Silver, Eds., American Society for Testing and Materials, Philadelphia, 1988, pp. 219–263.

ABSTRACT: A practical reevaluation of some aspects of conventional triaxial test methods is made, based on Bishop and Henkel's book *The Measurement of Soil Properties in the Triaxial Test* (2nd ed., Edward Arnold, London, 1962). Some advances in measurement techniques, methods of preparing, installing and saturating specimens, and the measurement of the initial effective stress are discussed, with particular emphasis on potential sources of disturbance and methods to reduce this. The use of unconsolidated undrained tests and various stress paths in relation to current needs is represented.

KEY WORDS: triaxial test, state-of-the-art review, test procedures, specimen disturbance, measurement, saturation, initial effective stress, consolidation, stiffness, shear strength, unconsolidated undrained tests, consolidated tests, stress path testing

One of the purposes of this review paper is to reevaluate some triaxial test methods, described in *The Measurement of Soil Properties in the Triaxial Test* by Bishop and Henkel [*1*] and still followed in routine work, to identify where changes are due.

There is no doubt that the "Triaxial Book," as it is referred to here, established the state of the art in triaxial testing of cylindrical soil specimens and has been the standard reference for the triaxial test from its publication (1957) until the present (1988). Part I of the book, which describes the basic principles underlying strength and deformation measurement in relation to practical problems, has become the "engineer's guide" to triaxial testing while Parts II to IV have become the "technician's guide." In practice, only the following triaxial tests, described in Part I, are routinely carried out:

(a) unconsolidated undrained (UU) triaxial compression test without measurement of pore pressure [*1*, pp. 10–11]
(b) isotropically consolidated undrained (CIU) triaxial compression test, which may be performed with or without measurement of pore pressure [*1*, pp. 15–18]
(c) isotropically consolidated drained (CID) triaxial compression test [*1*, pp. 18–21]

[1] Head of the Soil Mechanics Laboratory and engineer, Soil Mechanics Laboratory, respectively, ISMES, Viale Giulio Cesare, 29, 24100 Bergamo, Italy.
[2] Principal, Geotechnical Consulting Group, London, and Visiting Research Fellow, Imperial College, London, England.

Limitations of these particular tests, as well as the more general limitations of the triaxial test on cylindrical specimens, are well covered in the book. For example, regarding the UU test, it states

> The routine undrained test on undisturbed samples is often performed in about 10 minutes. The direct use of these results in the total stress analysis involves a . . . number of compensating factors as both c' and ϕ' and the pore pressure change determine the final result. Current practice in this respect is justified largely on empirical grounds [*1*, p. 32].

Despite this and other statements (for example, Ref *1*, p. 11), strengths measured in conventional UU tests are often taken as *the* undrained strength in the ground and the scatter of data from the tests is often taken as an indication of natural variability.

With regard to isotropically consolidated tests, Bishop and Henkel state

> In the field consolidation of the soil generally occurs under conditions in which the major and minor principal stresses are not equal; for example, under Ko conditions in level ground, or under the particular stress system obtaining in a slope. For a full investigation of these cases it is necessary to consolidate the specimens under stress ratios similar to those occurring in the field [*1*, p. 106].

Again, despite this and other very clear statements (for example, Ref *1*, p. 8), the use of isotropic consolidation rather than anisotropic consolidation prevails.

For a proper review of the "Triaxial Book" and to identify areas for change, the following points must be recognized:

1. There was a preoccupation with the measurement of strength in the late 1950s and early 1960s, with less emphasis being paid to the measurement of detailed stress-strain properties. Even when differences in stress-strain properties resulting from varying the consolidation path were observed, for example as clearly shown by Ladd and Lambe [*2*], the significance was not fully appreciated in practice. The conventional triaxial test was perfectly suitable for measuring triaxial strength, but its potential and limitations in measuring stiffness were, perhaps, not fully understood.
2. Much of Bishop and Henkel's research at that time was directed toward understanding the behavior of compacted, partially saturated soils. There was, as a result, less emphasis in the book on the handling and testing of "undisturbed" (tube and block) clay samples, and no reference is made to "undisturbed" samples of sand.
3. At that time, all measurements were made by mechanical transducers mounted externally to the triaxial cell.
4. Stress path testing had not been formalized, and simple control of stresses, now feasible with hydraulic, mechanical, or pneumatic systems, was not available then.

This reevaluation will concentrate on topics not sufficiently covered in the "Triaxial Book," for the reasons given above, and on subjects in the book often used inappropriately or requiring modification. The topics considered are inextricably linked with developments in equipment, measurement techniques, data logging, and computer control. A number of the methods now available are only feasible because of these developments while others have only been identified as a result of our widening understanding of soil behavior in general, including the effects of soil sampling.

After a brief review of advantages and limitations of triaxial testing on cylindrical specimens, the following topics are discussed:

(a) methods of measurement, including axial load, pore pressure, and axial displacement, with special emphasis given to axial deformation measurements;
(b) methods of preparing and installing specimens;
(c) measurement of initial effective stress in cohesive soils;
(d) methods of specimen saturation;
(e) unconsolidated undrained testing; and
(f) stress path testing.

The discussion will be restricted to the conventional triaxial test on cylindrical specimens. Many topics, such as partially saturated soils, cyclic testing, the effects of end restraint and bifurcation, membrane and drain restraint, membrane penetration, multistage testing, and methods of radial measurements are not included here.

To prepare the paper, the writers have drawn on their combined experience in research laboratories (including the Imperial College laboratory where Bishop and Henkel developed many of the methods described in the book), in commercial laboratories, and in the practical use of triaxial test results. This paper is not meant to be a comprehensive state of the art on conventional triaxial test methods, but only aims to emphasize some of the areas the writers feel deserve attention.

Advantages and Limitations of the Triaxial Test on Cylindrical Specimens

The main advantages of the conventional triaxial test are

(a) relative simplicity of drainage control and measurement of pore pressure;
(b) ability to apply principal stresses in known directions;
(c) ease of measuring axial and volumetric strains;
(d) use of solid cylindrical specimens which can be conveniently obtained from standard tube samples; and
(e) versatility of the equipment which may be used for a variety of determinations besides triaxial strength and stiffness (consolidation and permeability parameters, wave velocity, and so forth).

The triaxial test, however, has limitations [*1*, pp. 27–32]. The fundamental limitation is related to the stress states that can be applied to the specimens, where one is restricted to:

1. Triaxial *compression*, in which

$$\begin{aligned} &\sigma_V, \text{ vertical stress} &&= \sigma_1, \text{ major principal stress} \\ &\sigma_H, \text{ horizontal stress} &&= \sigma_3, \text{ minor principal stress} \\ & &&= \sigma_2, \text{ intermediate principal stress} \end{aligned}$$

In triaxial compression, α, the angle between σ_1 and the vertical direction, $= 0°$, and

$$b = (\sigma_2 - \sigma_3)/(\sigma_1 - \sigma_3) = 0$$

2. Triaxial *extension*, in which

$$\sigma_V = \sigma_3$$
$$\sigma_H = \sigma_1 = \sigma_2$$

and therefore $\alpha = 90°$ and $b = 1$.

In drained triaxial compression and extension, any combination of σ_V' and σ_H' can be applied so that maneuvers within the triaxial plane in stress space shown in Fig. 1 are unlimited. However, because the use of specimens cut at different angles and tested in the triaxial cell to assess anisotropy [*1*, p. 28] can be questioned [*3*] and because α and b are linked and α can only be 0° or 90°, neither anisotropy nor the effects of principal stress rotation can be properly investigated in the triaxial test.

The increasing bank of data obtained through more sophisticated laboratory tests (using the hollow cylinder apparatus, directional shear cell, and true triaxial apparatus), through *in situ* testing, and through measurements of field performance has allowed a better insight into both the anisotropy of soils and the importance of b. These tests also show that drained and undrained strength and stiffness parameters all vary with α and b.

Hypothetical variations of the undrained shear strength (S_u), effective friction angles (ϕ'), and undrained compression secant stiffness at 0.1% strain ($E_{u0.1}$) with α and b are shown as examples in Fig. 2. (Only the simple case in which the directions of σ_1 and σ_3 vary in a single plane is considered.) Figure 2 illustrates that from a specimen at an initial condition the triaxial test can furnish data at only two points on the surface representing all possible variations in strength or stiffness. Therefore, triaxial results should be related to other laboratory or field results by reference to surfaces of the form shown in Fig. 2.

Even if other limitations of the test, such as rate effects and end restraint, are ignored, the direct use of triaxial data in analysis of most engineering problems (in which in general α and b deviate from those in the triaxial test), therefore, involves reliance on experience.

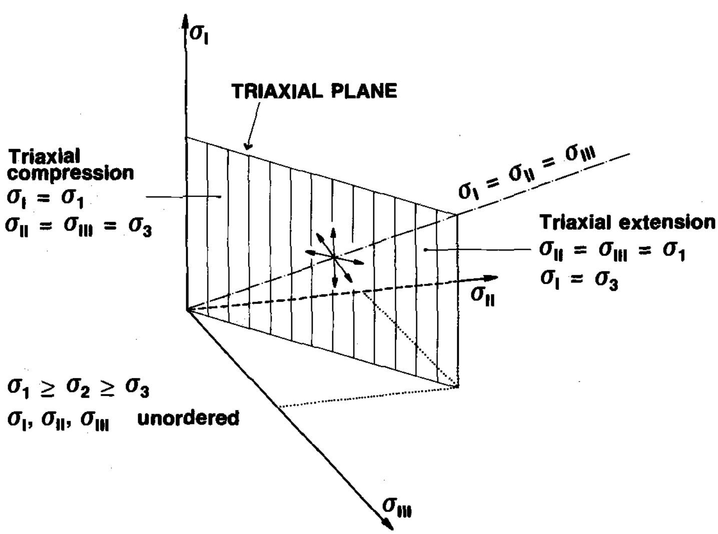

FIG. 1—*Triaxial plane.*

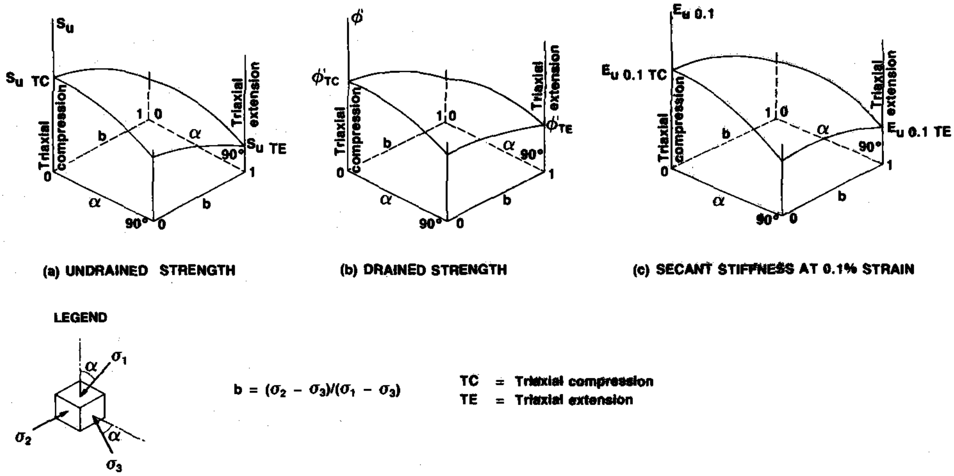

FIG. 2—*Hypothetical surfaces representing strength and stiffness parameters versus* α *and* b *axis.*

For example, when using triaxial compression/extension data to estimate plane strain behavior, one may decide to [*4*]

a) use triaxial results directly because they should provide a conservative evaluation of plane strain parameters
b) use results published in the literature to adjust triaxial values
c) use constitutive models which can predict plane strain behavior from input data obtained from triaxial results

Most situations are less studied and in these cases the application of triaxial results to practical problems requires a substantial amount of experience and engineering judgment.

Methods of Measurement in the Triaxial Test

The advent and widespread use of electrical transducers has had an important influence on methods of triaxial testing and on the quality of the results. The use of these transducers has allowed an increase in the precision of measurements, facilitated measurements inside the triaxial cell, enabled the use of automatic data logging, and provided feedback in control systems.

Potential uses of closed loop feedback systems are described here. The increased precision and the use of automatic data logging have a number of obvious advantages. Some of the advantages of electrical transducers, particularly for internal measurements, are illustrated here for the cases of axial load, pore pressure, and axial displacement measurements.

Measurement of Axial Load

Load measurements are typically taken outside the triaxial chamber. Even if a low friction piston seal system is used, such as those described by Berre [*5*] or Chan [*6*], there may be an error in the load measurements, especially when low loads are being measured or when high bending loads on the piston are present. This problem can be overcome by internal load measurements.

Since the introduction, at the end of the 1960s, of the submersible load cell designed by Skinner and described by Bishop and co-workers [*7*], a variety of other load cells have been developed. Cells suitable for triaxial measurements should be insensitive to eccentricity of load and not affected by changes in cell pressure.

To correct for the additional axial compliance internal load cells introduce into the system, calibration curves must be relied on or internal measurements of displacements must be made.

Measurement of Pore Pressure

Two alternative approaches for accurate measurements of pore pressure are [*1*, p. 30]

1. Run the test at such a rate that the pore pressure is uniform throughout the specimen and measure the pore pressure at the specimen ends.
2. Make internal local measurements of pore pressure in the anticipated failure zone, as applied by Taylor [*8*].

Usually, the first solution is adopted on the grounds of simplicity and reliability. The second solution requires more skill and a fast response measuring system [*1*, p. 30].

The null indicator was the standard device for measuring pore pressure when the "Triaxial Book" was published. The advent of the electrical pressure transducer and the use of double drainage connections to the platens have greatly facilitated the measurement of pore pressure.

The combination of a base and midheight measurement of pore pressure is extremely valuable in the automation of triaxial testing and for the control of consolidation loading rates, as discussed later, and allows one to determine when uniform conditions have been reached within the specimen. The availability of miniature pressure transducers has facilitated local measurements of pore pressure as illustrated by the midheight piezometer probe described by Hight [*9*] and shown in Fig. 3. Because midheight pore pressure measurements

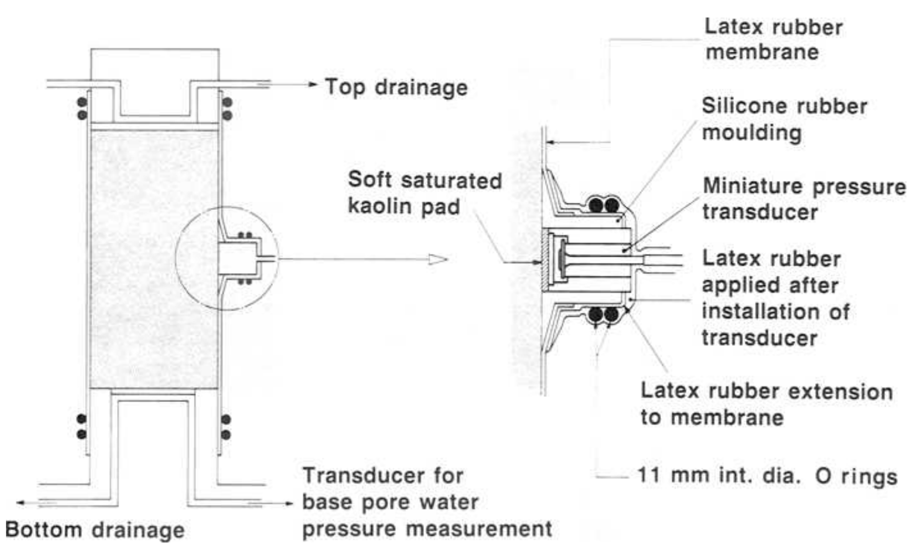

FIG. 3—*Midheight piezometer probe.*

are made where the influence of end restraint is small, as long as interference between the piezometer and specimen is also low, continuous measurements of pore pressure at relatively fast shear rates are possible. Figure 4 compares the effective stress paths from tests on similar specimens taken to failure in UU tests in 30 and 1383 min, using the piezometer probe illustrated in Fig. 3.

Measurement of Axial Displacement

Axial displacements of a triaxial specimen are generally measured external to the cell by means of the relative displacement between the load piston and the triaxial cell. The introduction of submersible electrical displacement transducers has facilitated measurements of axial displacement made inside the cell.

The ability to make more accurate measurements of axial displacement, especially locally on the central part of a triaxial specimen [*10–14*], has highlighted the following:

1. Soils have a high initial stiffness, even under slow monotonic loading, and highly nonlinear stress–strain properties [*13*]. Figure 5 presents the stiffness determined with local measurements of displacement on a low plasticity clay (overconsolidation ratio [OCR] = 1.5) reconsolidated to its estimated *in situ* stress state.
2. Yielding often occurs at strains less than 0.1%, making accurate measurement of small strains important.
3. Failure strains, especially after anisotropic consolidation, tend to be considerably lower than those quoted in Table 8 of the "Triaxial Book" [*1*, p. 127] (and widely used as a guide to calculate times to failure).
4. Lack of initial alignment, and therefore specimen tilting, is common.

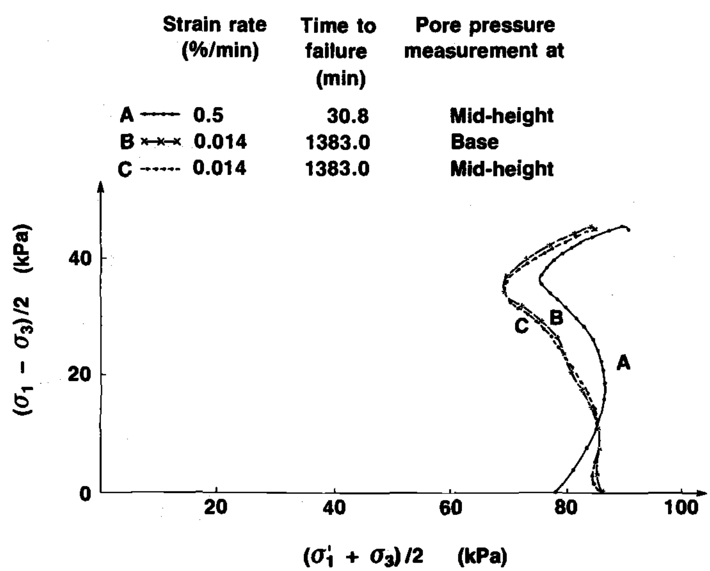

FIG. 4—*Effective stress paths in unconsolidated undrained tests performed with different strain rates and with different pore pressure transducer positions.*

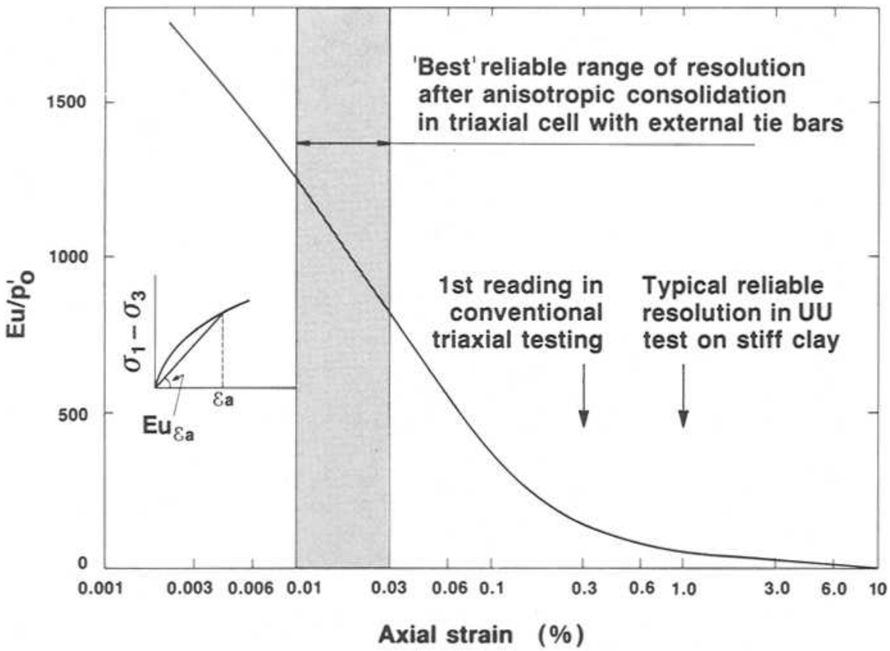

FIG. 5—*Typical stiffness curve obtained by local measurements of axial displacement.*

5. The error involved in the conventional external measurement of axial displacement can be substantial, depending, inter alia, on
   a) initial lack of fit and alignment
   b) whether or not consolidation is carried out prior to shear
   c) consolidation path
   d) stiffness of the soil and, therefore, the ease with which lack of fit can be consolidated out

Sources of Measurement Error—Because external axial deformation measurements are most commonly used, a brief summary of potential sources of error is given here and indicated in Fig. 6, using the notation of Jardine and co-workers [*13*]. Typical errors comprise:

(a) seating errors due to the closing of gaps between ram/internal load cell and platen, and platens and porous stone;

(b) alignment errors which may result from equipment and specimen nonconformity;

(c) bedding errors caused by lack of fit or surface irregularities at the interfaces (top and bottom) between the specimen and loading surfaces (platens or porous stones);

(d) compliance errors which may occur in:

- the tie bars as they extend and cause relative displacement of the cell top with respect to the piston
- an internal load cell as it deflects under load
- the loading system in the hydraulic triaxial cell [*15*], as it deforms under increasing load
- lubricated ends, when these are used

(e) nonuniform strains along the specimen height resulting from end restraint.

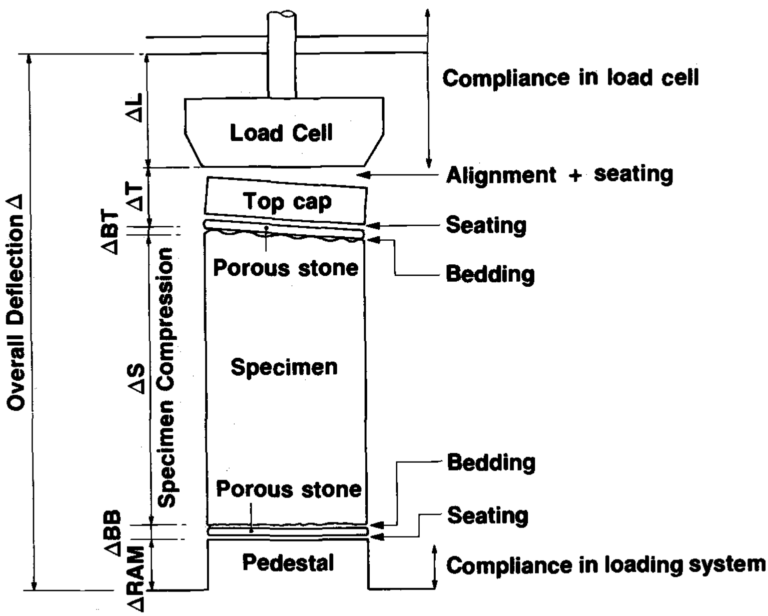

FIG. 6—*Sources of errors in external axial deformation measurements.*

Errors Due to Misalignment—One of the most serious errors in axial strain measurements results from misalignment between the triaxial cell and the specimen. Errors due to misalignment will, therefore, be considered in detail here. It is necessary first to separate the sources of misalignment associated with the specimen from those associated with the apparatus.

Misalignment associated with the specimen arises from improper positioning or ends not perpendicular to the specimen axis. Misalignment associated with the apparatus may result from

(a) porous stones of nonuniform thickness
(b) nonverticality of the loading ram
(c) eccentricity of the ram
(d) nonhorizontality of the platen surfaces

In considering misalignment, it is helpful to distinguish between triaxial cells with external tie bars and those with internal tie bars [*5,14*] as shown in Figs. 7*a* and *b*, respectively.

In *cells with external tie bars* (Fig. 7*a*), the connection between the loading ram and specimen top cap is made after the cell top has been placed. Some common forms of connection are shown in Fig. 8.

Bishop and Henkel noted that with the steel ball and coned seating, shown in Fig. 8*a*, there is some freedom of movement which allows the specimen to be brought into line as the load is applied. However, this causes uncertainty in the definition of strains at the beginning of the test [*1*, p. 37]. The definition at the start of the test may be improved with the halved steel ball and flat-ended ram connection (Fig. 8*b*), but misalignment will persist so that great care must be given to trueing the ends of the specimen and centering it [*1*, p. 37]. A simple connection, commonly used in practice, is presented in Fig. 8*c*. The problems of this connection are similar to those mentioned above.

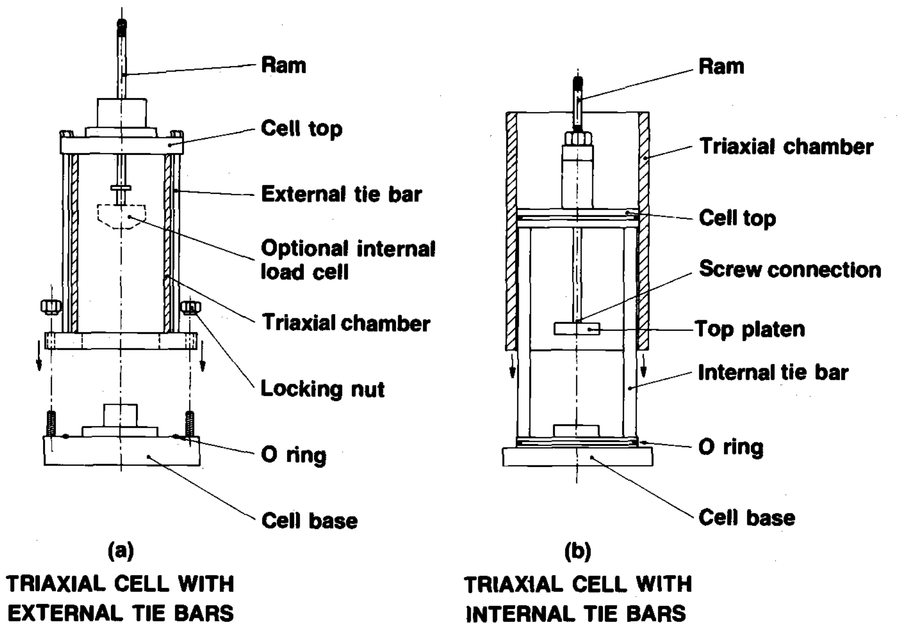

FIG. 7—*Triaxial cells with external and internal tie bars.*

Examples of misalignment associated with this type of connection are illustrated in Fig. 9. With cells with external tie bars the misalignment will not be consistent between tests but will depend on the uniformity of clamping pressure applied and on the seating of the O-ring seal often used in the cell base.

In *cells with internal tie bars* (Fig. 7*b*), the connection between the loading ram and top cap generally involves a platen rigidly connected to the ram, as with the screw connection shown in Fig. 10*a*. In this case, the ram and platen alignment is fixed, is consistent between tests, and can be easily checked. Either the equipment alignment (without specimen) or the system alignment (with specimen) can be checked with these details by lowering the upper platen close to the mating surface. (A similar mating between the ram and top cap occurs

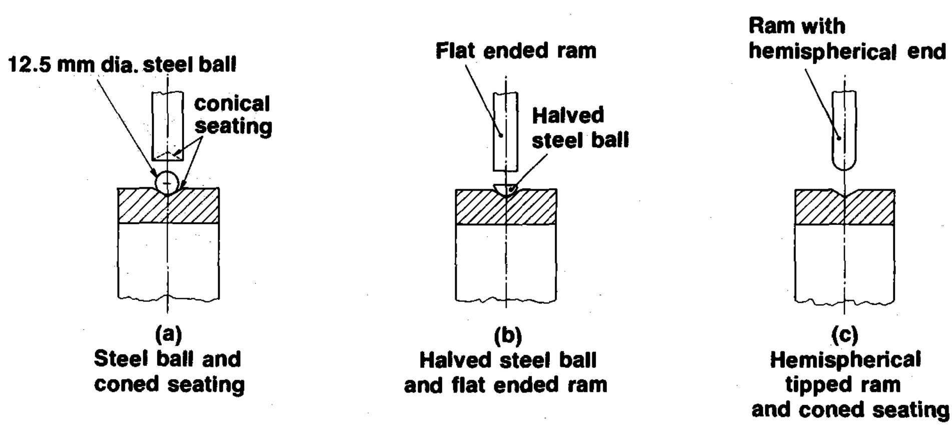

FIG. 8—*Examples of connections typically used with triaxial cells with external tie bars.*

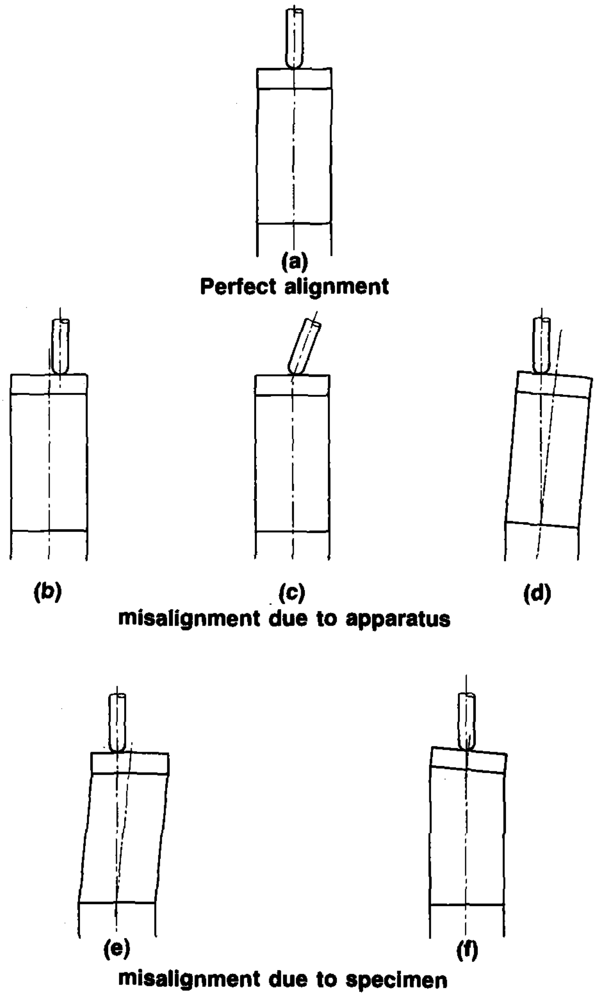

FIG. 9—*Examples of possible initial misalignment with coned seating connections.*

when a load cell is used in a triaxial cell with external tie bars [Fig. 7*a*] but in this case the variations in alignment between tests remain.)

The corresponding misalignment is illustrated in Fig. 11. Minor eccentricities (Figs. 11*c* and *e*) are probably accommodated within the specimen, but nonparallel load platen and specimen surfaces are certainly of consequence.

Improper mating may be "ironed out" either when the connection is made or after the start of the test. Forcing the specimen alignment prior to testing will cause specimen disturbance. This can be illustrated by reference to testing experience with a low plasticity clay and with the suction cap connection shown in Fig. 10*b*, which was designed by Skinner[3] for use in cyclic triaxial compression–extension tests. Disturbance of the specimen, due to its being forced into alignment when the vacuum was applied to create the connection, caused

[3] Personal communication, 1974.

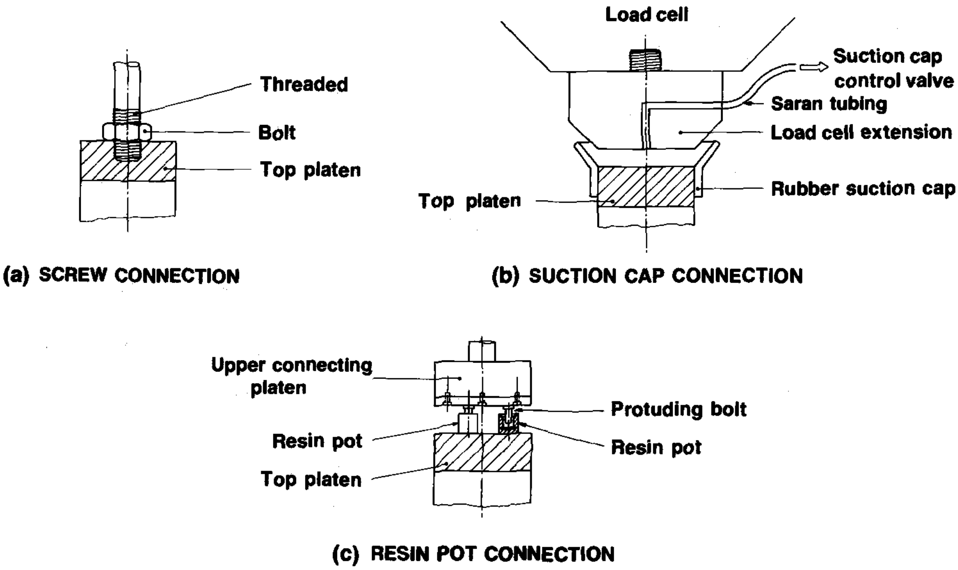

FIG. 10—*Examples of possible connections for compression/extension tests.*

reductions in initial effective stress of up to 50% and strains that depended on the initial lack of alignment and initial stiffness of the soil.

The importance of misalignment during shearing may be seen from the test results shown in Fig. 12. UU tests on 102-mm-diameter specimens of stiff clay, using a connection of the type shown in Fig. 8*c*, were carried out with external and with midheight measurements of axial displacement. These measurements have shown that nonuniform deformations due to initial misalignment persist until a significant shear stress is applied. The shear stress at which equal incremental displacements were measured at each side of the specimen was found, not surprisingly, to relate to the undrained strength of the specimen. Prior to this shear stress being reached, substantial tilting of the specimen was taking place, with subsequent yielding at the ends.

Specimen misalignment can be eliminated by precise trimming or, for example, by casting the specimen ends in resin or plaster, or by use of special details, such as the connection shown in Fig. 10*c* which does not force alignment [*16*].

Equipment misalignment can be improved only by using equipment with better tolerances. This is most easily attained in triaxial cells using internal tie bars. Figure 13 compares the results of two isotropically consolidated undrained tests on lightly overconsolidated reconstituted specimens of a silty clay from Pontida, Italy. For one specimen, a triaxial cell with external tie bars was used, and the ram-top connection was made using the detail of Fig. 8*b*. In the other, a cell with internal tie bars and the screw connection shown in Fig. 10*a* was adopted. A higher initial stiffness and a more credible variation in stiffness are achieved with the cell with internal tie bars and the screw connection.

Because it is difficult to completely avoid misalignment, it may be preferable if the resulting nonuniform strains are monitored with internal displacement gauges mounted on the specimen. The amount of misalignment can then be evaluated and the average value of axial strain can be defined.

Evaluation of Stiffness with Internal and External Measurements—Referring to the typical stiffness characteristics shown in Fig. 5, it is of interest to examine to what extent these may

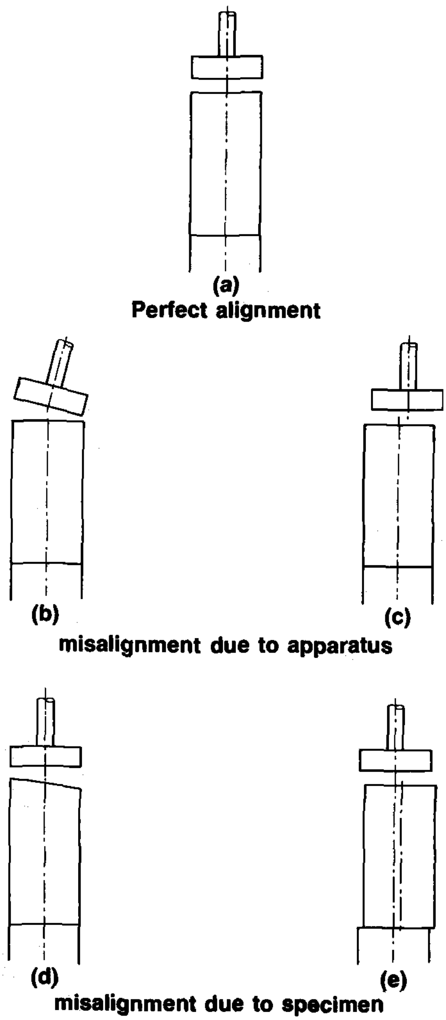

FIG. 11—*Examples of possible initial misalignment with screw and suction cap connections.*

be determined using conventional external measurements of displacement. It will be assumed that seating errors have been avoided and that errors resulting from compliance have been calibrated out. (It is unlikely that compliance errors associated with the use of lubricated ends can be calibrated out because they depend, *inter alia*, on loading time, cell pressure, and loading direction [*17*].)

In UU tests on stiff to hard clays, typical alignment and bedding errors are likely to result in serious errors in the external strain measurements for values less than 1%. This strain will increase when the steel ball and coned seating connection (Fig. 8*a*) is used. Taking the characteristics shown in Fig. 5 to be representative of a stiff clay specimen, much of the initial response of the specimen is not detected correctly.

In consolidated tests, anisotropic consolidation is generally more effective than isotropic consolidation in reducing bedding and seating errors as well as solving some misalignment errors during the consolidation phase, rather than during the shear phase. In carefully prepared anisotropically consolidated undrained (CAU) tests undergoing substantial con-

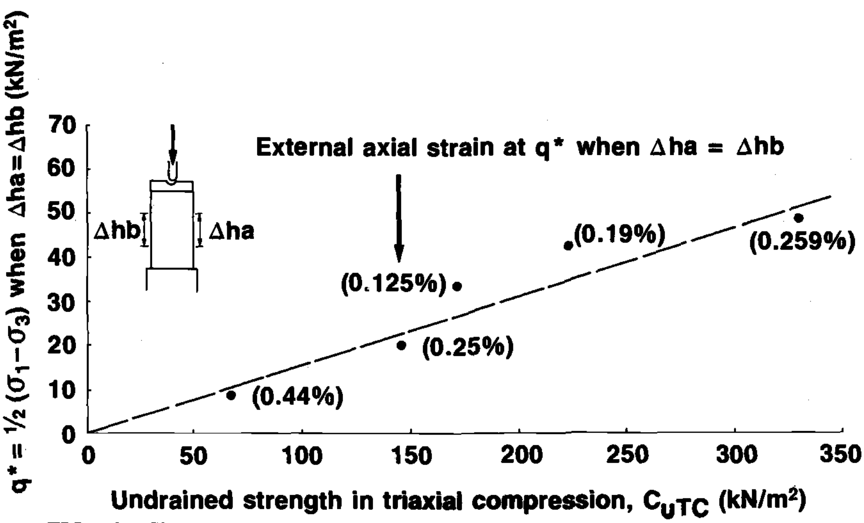

FIG. 12—*Shear stress causing strain equalization in UU tests after nonuniform strains resulting from initial misalignment.*

solidation and limited swelling, reliable resolutions of up to 0.01% strain may be obtained. However, swelling after anisotropic consolidation, and especially when the horizontal stress is greater than the vertical, may reintroduce errors [*11,18*].

Currently used methods of specimen preparation and current tolerances on alignment in triaxial apparatus are unlikely to eliminate these errors. Thus detection of the high initial stiffness of soils and their degradation with strain is prevented.

Presently, accurate measurements of axial displacement may be made easily by local measurements with transducers mounted in the cell on the specimen periphery. With the addition of an internal load cell for accurate measurement of low loads and with allowance of time for pore pressure equalization, the determination of the initial part of the stress–strain curve can be improved considerably.

The monitoring intervals suggested by Bishop and Henkel (for example, Ref *1*, p. 95) for routine tests, giving a first reading at an axial strain of 0.3%, are totally inadequate for initial stiffness measurements. Earlier measurements are required and if standard strain rates are used, faster logging rates are necessary. Alternatively, very slow strain rates or, as suggested by Atkinson and Evans [*19*], initial stress control may be used to obtain the required initial data. In these cases, the results might be affected by the different strain rates adopted. However, for typical strain rates these effects are probably of minor importance.

Specimen Preparation and Installation

Disturbance due to shear strains and water content changes must be minimized if a specimen representative of the field is to be obtained [*1*, p. 83]. Laboratory disturbance during specimen preparation and installation is superimposed on those previously caused by sampling, transport, and storage.

For clays, the shear strains occurring during undrained tube sampling have been quantified approximately by Baligh [*20*] using the strain path method. The effect of the predicted strain paths for normally and overconsolidated clays has been examined by Hight and co-workers

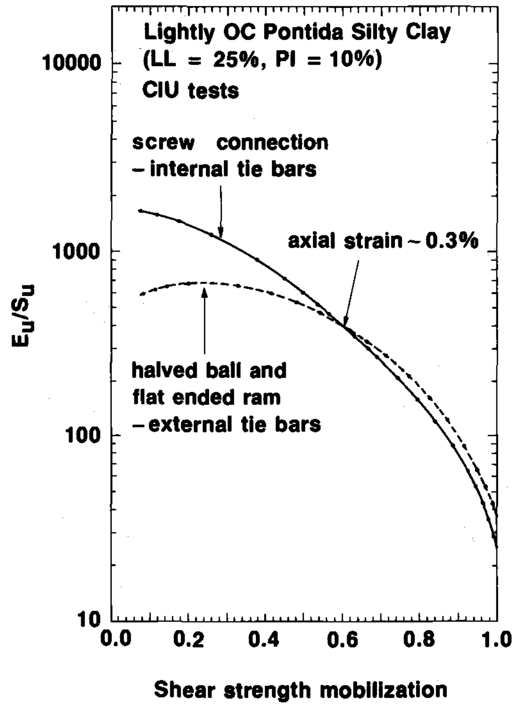

FIG. 13—*Comparison of stiffness measurements with different types of test details.*

[21]. These studies show that substantial changes in effective stress occur in the samples, and nonuniform pore pressures exist within them immediately after sampling. In most cases, water migration during the delay between clay sampling and laboratory testing *[22]* will allow equilibration of pore pressures within the tube, but storage may result in further changes in the mean effective stress in the sample. This has been shown for laboratory reconstituted samples *[23]*, but the process involved requires further investigation.

The starting point in the laboratory is, generally, a tube sample having a mean effective stress within it which may be higher or lower than that *in situ* *[21]*, depending on the soil's stress history and sensitivity. Figure 14 presents some sources of possible disturbance during sampling, storage, preparation, and installation, and indicates the direction in which the mean effective stress may change. The relative importance of the changes is shown speculatively by the length of the arrows.

Cohesionless soils can sustain, at most, only a limited suction. Therefore, the effective stress *in situ* is often almost totally lost due to stress relief during conventional sampling. Experimental evidence shows that standard sampling techniques significantly affect the mechanical properties of sands *[24,25]*. The major cause of disturbance seems to be the shear stress and strain history involved in tube sampling and in subsequent handling. The stress relief alone has minor influence *[22,26,27]*, but the reduction of the effective stress makes the sample very sensitive to disturbance. Disturbance may consist of possible changes in density and fabric. Both types of disturbance have to be minimized because a change in either will cause different static and cyclic properties *[28,29]*.

No theoretical method has yet been applied to predict, at least approximately but in a quantitative manner, the effect of sampling in sand. Indirect measurements such as the formation factor *[28]*, the initial dynamic shear moduli, or the shear wave velocity *[26,30]*,

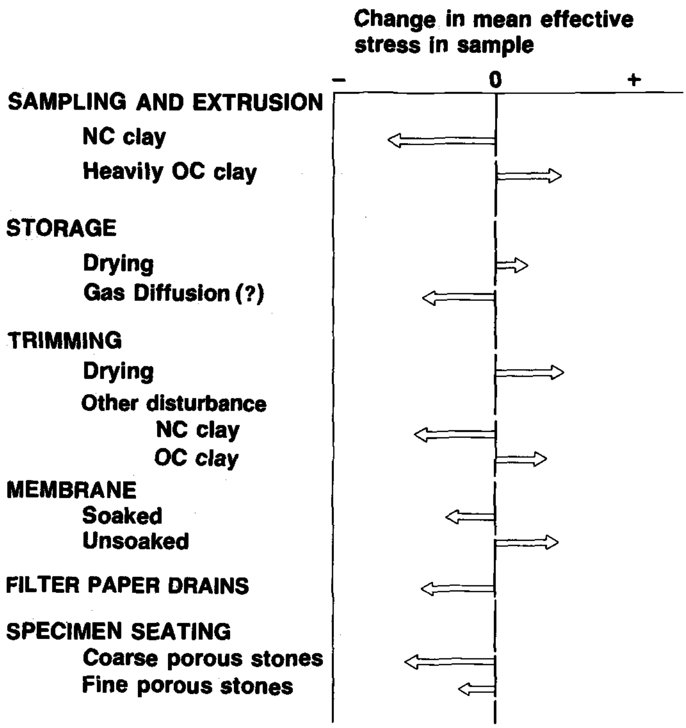

FIG. 14—*Factors affecting the initial mean effective stress in cohesive materials.*

may provide empirical methods to evaluate disturbance, but the degree of sensitivity of these parameters to the various sources of disturbance still requires study.

To try to reduce sampling disturbance, alternative methods of sampling such as those based on impregnation [*31*] or *in situ* freezing have been developed [*32*]. One of the most recent versions is the *in situ* radial freezing technique [*33*]. Comparisons of cyclic results from the laboratory with field behavior and indirect evidence, such as shear wave velocity measurements, show *in situ* radially frozen samples of dense sand are significantly less disturbed than tube samples [*26,30,34*]. Freezing has also been applied to samples after retrieval from the ground to reduce possible disturbance during transport and laboratory handling [*35–37*]. However, freezing can only be applied to sands with a limited fines content, and frozen samples are subject to disturbance by variables such as temperature fluctuations (including those that may occur in frost-free freezers) and sublimation [*38*].

Sample Extrusion

Sample extrusion is only mentioned briefly by Bishop and Henkel during their discussion on clay specimen preparation [*1*]. Even now, the effects of sample extrusion are poorly understood and are largely based on the limited data available for clays [*22,27,39*]. There is little doubt that the sample can be significantly strained during extrusion, especially if

(a) high friction values exist between the soil and the sample tube or support during extrusion
(b) there is inadequate support of the sample as it leaves the tube
(c) significant time has elapsed since sampling

Clearly there may be advantages in avoiding extrusion. Existing methods for this include using plastic or stocking (as in the Delft sampler) liners or presplit tubes, and splitting the tube. However, none of these methods is in widespread use.

Disturbance during extrusion may be decreased in the following ways:

1. Typical techniques to reduce friction between the soil and tube include the use of smooth internal surfaces in the tube, paint or Teflon coatings, and so forth. The friction between the soil and support may be minimized with a thin application of a lubricant, or a liner which accompanies the soil as it leaves the tube. For this, a band of aluminum foil [*40*] or plastic foil has been used.

   To reduce the force required for extrusion, the sample tube may be cut into shorter sections to reduce the total wall friction. Attention should be paid during cutting because the tube may distort (disturbing the sample) if it is not clamped in shape.
2. The alignment of the internal tube surface to the support for horizontal extrusion or to the vertical for vertical extrusion must be carefully checked to avoid dragging or bending of the sample.
3. For clays there may be advantages in immediate extrusion and trimming of the sample perimeter before there has been significant water content redistribution [*22*]. For contractive clays there may also be an advantage in performing extrusion immediately after sampling, before strengths adjacent to the tube can recover and increase the resistance to extrusion. The extruded soil then could be stored in suitable containers which provide support but do not require further extrusion. Whether this will prove truly advantageous still requires investigation.

The choice of sample extrusion technique depends on, *inter alia,* material sampled, sampling method, sample quality, time since sampling, and specimen preparation technique to be used.

Generally, samples are extruded with relative tube-to-sample movements in the same direction as during sampling. This eliminates the problem of extruding past the cutting edge, which normally has a smaller inner diameter than the rest of the tube, and maintains the sample strains in one direction. Any disturbed sections of the sample should be removed prior to testing. Conventionally, if obviously disturbed sections are not present, at least one and a half tube diameters from the head and toe of the sample should not be used for triaxial tests [*40*]. In cohesive soils, pocket penetrometer or torvane results may help in evaluating the extent of disturbed zones.

Samples that can stand unsupported are often extruded horizontally. This allows the complete sample to be seen, described, and photographed, and the most appropriate section for specimen use can be chosen. Sensitive samples, or those with low cohesion, are normally extruded vertically. With these materials, only a limited height of material can be extruded without support. Some arrangements allow the material to enter directly into a trimming tube, as described later in the section dedicated to cohesive specimen preparation. In this case, direct examination of the sample is difficult and other techniques, such as radiography, may be even more desirable.

In conclusion, it must be remembered that disturbances during extrusion are usually concentrated at the sample boundaries and that significant pore pressure gradients may be established in cohesive soils.

Test Preparation for Cohesive Soils

Specimen Preparation—Several preparation techniques were mentioned in the "Triaxial Book," and others have been developed and used since then. These methods include subsampling, trimming with guide parts, trimming with manually guided ring cutters, and the use of lathe trimmers. Only some of them will be discussed here.

One method described in detail in the book involves a subsampling process [*1*, pp. 83–84]. Three brass tubes are simultaneously pressed into the sample, which is laterally confined in a larger tube, to provide three subsamples of 38-mm (1.5-in.) diameter (satisfying the requirement for a set of three specimens for a triaxial test). Subsampling tubes made with internal diameter of 38 mm (1.5 in.) and wall thicknesses of either 0.76 mm (0.03 in.) or 1.59 mm (0.0625 in.) are referred to. For these tubes, the ratios of outside diameter, B, to wall thickness, t, are 52 and 26, respectively.

This method of preparation is still used occasionally. However, there is a tendency for the thicker-walled tube, which had originally been intended for stiff clays, to be adopted. Predictions of strains due to tube sampling by Baligh show a strong dependency of strain magnitude at the centerline of the sample on the ratios of B/t [*20*]. For a B/t value of 26, unacceptably large strains are likely. In view of this potential for serious disturbance, this technique should be discontinued. Where it is used, it should be recognized that subsampling may establish strains and pore pressure gradients in the specimen similar to those existing from tube sampling [*21*].

Cohesive or slightly cohesive self-supporting specimens may be trimmed with thin-walled tubes in which the specimen is trimmed to size ahead of the trimming tube as it is advanced by a manual press. This operation typically takes about 15 min, and final trimmed surfaces are immediately covered, thus reducing drying. Details of a similar method are described by Eischens, who used a variable speed compression machine to control the trimming rate [*41*].

As with the subsampling method previously described, this technique will cause some surface disturbances but the resulting strains and pore pressure increases will be much smaller.

Specimens that cannot stand unsupported can be prepared by vertically extruding the specimen into a trimming ring, while the excess material is trimmed away ahead of the ring, as previously described. In this case a short trimming ring is used, and the specimen enters directly into the membrane which is expanded in a mold connected to the trimming ring (Fig. 15). Similar systems are described in the literature [*37,40*].

Full size specimens (that is, having the same diameter as the sample) may also be used. This reduces disturbance due to trimming, but edge disturbance caused by sampling may not be removed. In general, the authors believe the disturbance of a carefully trimmed specimen from a tube sample is less than that of an untrimmed specimen. Therefore, the authors prefer some trimming of the edges of the specimen to remove the zone most severely distorted by tube sampling.

Pore Pressure Gradients During Specimen Preparation—Pore pressure gradients, caused by cutting and drying, develop during specimen preparation and installation. A reduction of pore pressure gradients due to cutting may be obtained by minimizing the thickness of the cut, especially as the final diameter of the specimen is approached. Quantitative data to support this statement are, however, lacking.

As shown in Fig. 16, a high potential for drying from the specimen surface exists unless precautions are taken during specimen preparation and installation, such as working in a controlled-humidity environment. The effect of drying on the initial effective stress in clays, p_o', has been monitored with internal pressure probes by Wesley [*42*] and evaluated approximately by Sandroni [*43*] using measured changes in water content combined with the volumetric compressibility of the clay. The last method involves the assumption that the specimen remains fully saturated during evaporation. Changes of p_o' due to drying may be

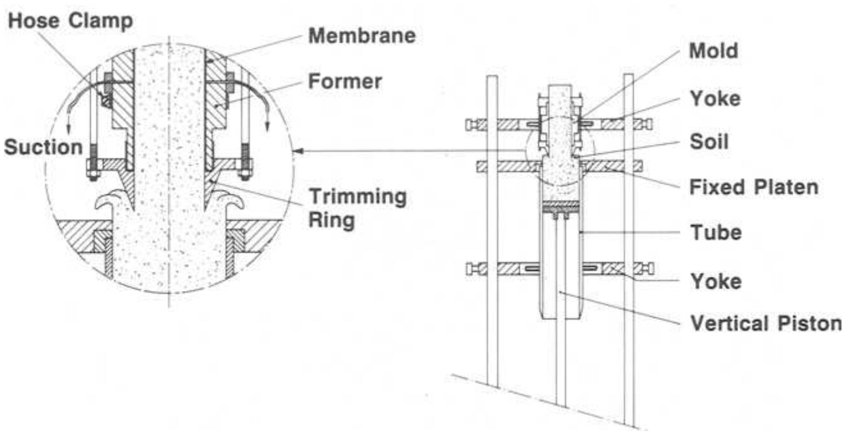

FIG. 15—*Apparatus for specimen preparation during vertical extrusion.*

significant, as shown in Fig. 17, and depend on specimen dimensions (surface area/volume), clay compressibility, and evaporation time.

Soils should not be left exposed to air except for the time strictly necessary for working. Enclosure of the specimen halts the evaporation process, and equilibration of pore pressure gradients may then occur.

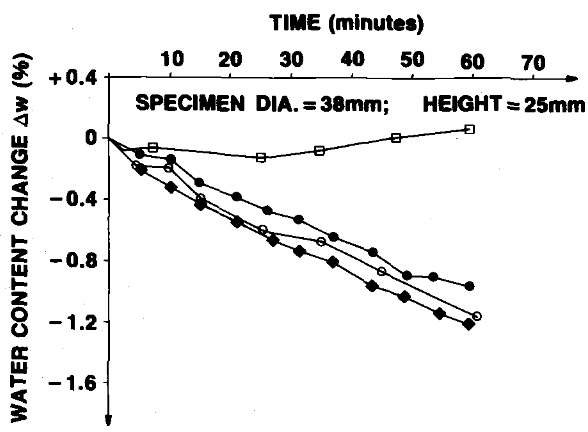

SOIL TYPE	SYMBOL	RELATIVE HUMIDITY (%)	TEMPERATURE (°C)
RECONSTITUTED PONTIDA SILTY CLAY (INITIAL WATER CONTENT = 26.0 %)	□	97	24
	○	60	24
UNDISTURBED PO VALLEY STIFF SILTY CLAY (INITIAL WATER CONTENT = 24.5 %)	●	60	24
	◆	49	27.5

FIG. 16—*Examples of water content changes due to drying.*

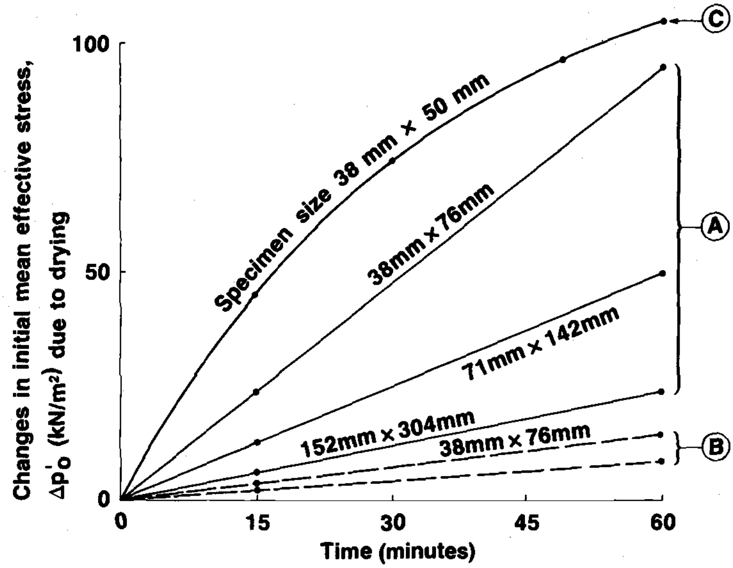

Ⓐ : Estimates for samples of stiff London Clay by Sandroni (1977)

Ⓑ : Measurements of $\Delta p_o'$ in soft Mucking clay by Wesley (1975)

Ⓒ : Estimates for samples of Pontida Silty Clay

A and B – temperature controlled at 20° C

C – temperature controlled at 23°C, relative humidity 75%

FIG. 17—*Effects of drying on the initial mean effective stress in cohesive soils.*

Water Exchange Between Specimen and Membrane—Membranes will absorb water and soften during prolonged immersion [*1*, p. 39]. The amount of water absorbed varies with membrane batch, type, and time of immersion (Fig. 18). The permeability of the rubber appears to be reduced during absorption, and the amount of water absorbed correlates with the initial permeability of the membrane [*17*]. The ability to absorb water means that there is a potential for water transfer between the membrane and specimen. In Fig. 19, a comparison is presented of the changes in initial effective stress, p_o', that occur with time after placing a soaked and an unsoaked membrane on specimens of low plasticity clay. Although the low compressibility of this clay may have emphasized the differences, there is no doubt that transfer of water between membrane and specimen causes some changes in p_o'.

There appears to be an advantage in using presoaked membranes, both to minimize changes in p_o' and to further reduce subsequent leakage. However, in soil with a high negative pore pressure, the specimen might absorb water from the membrane. For some applications, lubricated prophylactics, which typically seem to absorb less water (Fig. 18), may be useful.

Water Exchange Between Specimen and Filter Paper—When filter paper is used either to facilitate radial drainage or to protect the porous stones from clogging, water exchange between the specimen and filter paper will take place until the suctions in each balance. The resulting gradients in specimen pore pressure will exist until equilibrium is reached.

The suction that can be established in filter paper is related to its water content [*44*].

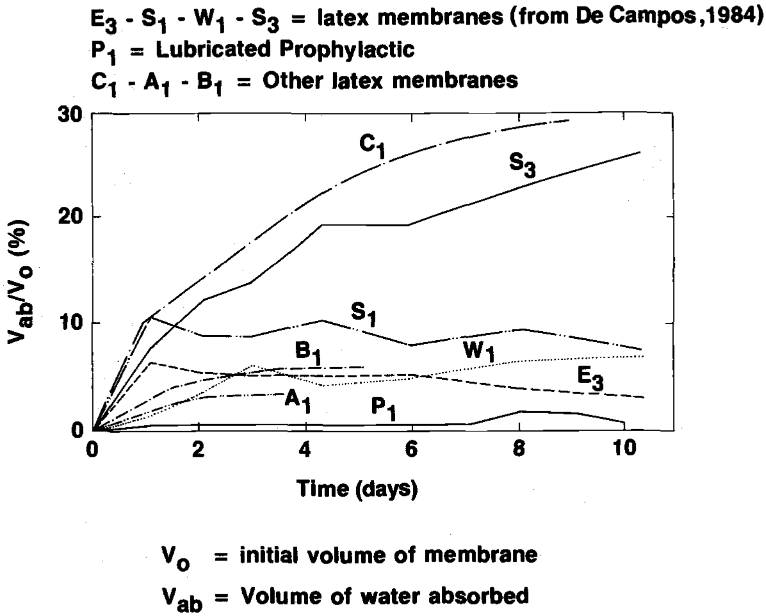

FIG. 18—*Water absorption in different membranes.*

There is some scope, therefore, for minimizing water exchange between the specimen and paper by initial adjustment of the water content of the filter paper to obtain a suction near to that expected from the specimen. It should be noted that the use of radial filters may introduce water content inhomogeneities in the specimen [*45*].

Water Imbibed from Pore Pressure Measurement/Drainage System—When the specimen is brought into contact with porous stones, the suction in the soil, $-u_s$, is established in the

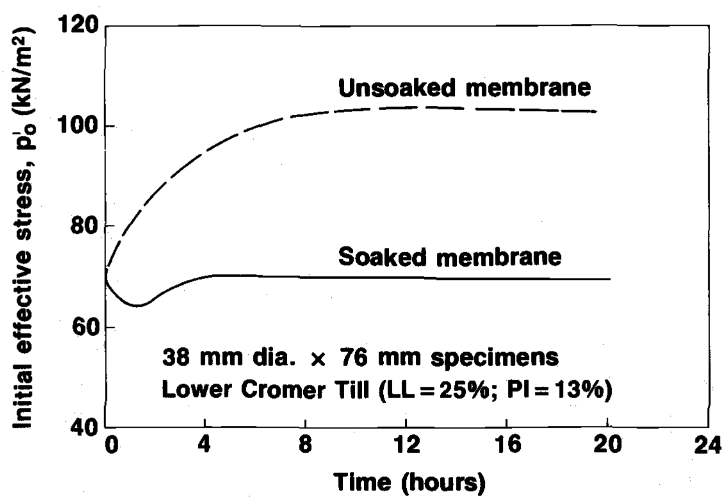

FIG. 19—*Effects of unsoaked and soaked membranes on the initial mean effective stress as measured at the middle of the specimen.*

stones, the cavities behind them, and in the drainage lines up to the first closed valve. If this suction cannot be maintained, cavitation will occur. In view of their relative dimensions, cavitation will probably take place in cavities or drainage lines before it can occur in the porous stones. Once cavitation has occurred, a pore pressure gradient exists and water flow into the specimen can occur. The amount of water transferred depends on, *inter alia*

(a) volume of water available in the measuring system (including top and bottom drainage lines)
(b) time before the confining stress is applied to the specimen
(c) coefficient of consolidation of the soil
(d) whether or not cavitation occurs in the porous stones (if cavitation does not occur in the stone, then water will not be drawn from the stone itself)

Methods to minimize the potential for water transfer to the specimen obviously center around

(a) having a small volume of water available in the pore pressure measuring system (this is, of course, consistent with the requirements of a stiff measuring system); in UU tests with pore pressure measurement, solid ends and a stiff piezometer probe may be used
(b) using high air entry porous stones inset into the pedestal, as shown in Fig. 131 of the "Triaxial Book," when cavitation in coarser stones is likely [*1*, p. 184]
(c) minimizing the time during which the installed specimen is under zero total stress
(d) avoiding the availability of free water

A technique sometimes employed to minimize the available water during mounting is to use coarse dry filter stones (usually used with soft soils) or saturated stones with an air entry value higher than the negative pore pressure (in stiff specimens) and with a cavity behind them which is left dry [*5,46*]. Flushing of the coarse stones or the empty cavity behind the high entry value porous stone is performed after an increase of cell pressure about equal to the initial suction in the specimen.

Bishop experienced with the "fuse-wire" technique [*47*] in which the specimen is separated from the porous stone during installation by a loop of thin wire (Fig. 20). Only on undrained application of the confining stress, when the pore pressure in the specimen has been elevated to a positive value, is the specimen brought into contact with the porous stone as the applied stress embeds the wire into the base of the specimen. A similar technique can be used to separate surface-mounted piezometer probes from the specimen until pore pressures are positive [*9*]. However, these techniques increase compliance and the potential for air entrapment.

Test Preparation for Cohesionless Soils

In the "Triaxial Book" only the preparation of reconstituted cohesionless specimens is covered. Increased interest in problems related to sands, such as liquefaction, has promoted both the use of reconstituted specimens and of "undisturbed" specimens from tube samples, block samples, or "intact" frozen samples.

Reconstituted Specimens—The preparation method used greatly influences the fabric of the sand and thus its mechanical properties. A summary of methods for reconstitution of

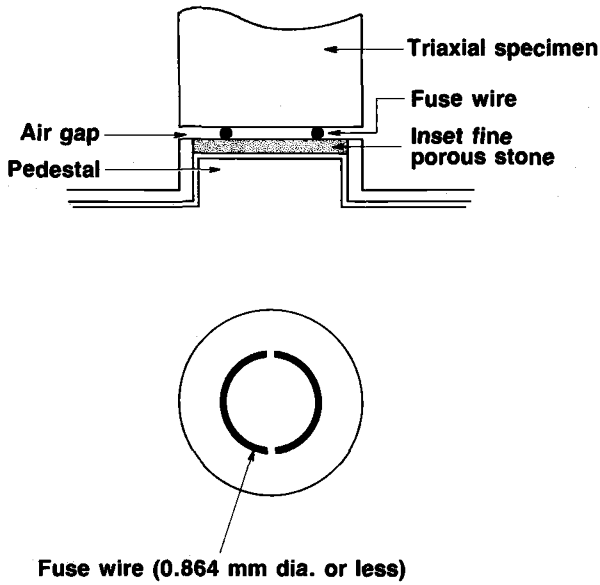

FIG. 20—*Fuse wire technique.*

sand specimens is given by Mulilis and co-workers [*28*]. The most commonly used techniques are pluviation and tamping.

1. Pluviation—Basic principles of pluviation are given by Kolbuszewski [*48*] and various modifications to the method are described in the literature [*28,29,32,49,50*]. With these techniques it is possible to prepare specimens having a wide range of relative densities (usually from 10–15% to 90–95%), thus avoiding the use of vibrations to obtain high densities as described in the "Triaxial Book" for the funnel method [*1,90–92*]. Improvements in saturation procedures make wet pluviation unnecessary. Specimens can be prepared dry and saturated subsequently. Pluviation of sand specimens is fast and thus particularly useful when large specimens are to be prepared. However, it is difficult to prepare uniform specimens [*51*], and the method, up to now, is not suitable for use with materials having a large grain size distribution because particle segregation, particularly when fines are present, may occur.
2. Tamping—A basic undercompaction tamping method has been described by Ladd [*52*]. This technique is relatively easy to follow, and, when properly performed, provides very consistent specimens, even from material having a large grain size distribution.

   When circumstances permit, the complete method including the determination of the optimum undercompaction value by cyclic or extension tests should be followed. However, this often is not practical. Experience at ISMES has shown an initial estimate can be obtained as follows:

(a) The undercompaction percentage may be obtained from the estimate

$$\text{Uni} = (95 - D_d)(D_d)^{2/3}/100\%$$

where *Uni* is the percentage undercompaction in the first layer and D_d is the relative density of the compacted specimen (in percent) before consolidation. This is based on experience in the preparation of specimens as loose as 20% D_d. The percentage undercompaction calculated by this formula may correspond to a dry density near or below the minimum dry density of the material. This is usually possible due to the bulking behavior of the moist material, but care is required in the preparation process. If it is not possible to prepare a layer at the desired density, a lower percentage of initial undercompaction is used.

(b) The initial water content to be used can be estimated by placing a known weight (dry weight plus water content) in a plastic bag and then slowly adding water while kneading until the material starts to cling together, but without free water sticking to the bag.

(c) Material for undercompaction may be prepared by weighing the dry soil for each layer and adding water later, rather than weighing it from the bulk wet soil for the entire specimen. This avoids possible errors in dry density due to nonuniform water content.

For any reconstitution technique, it is important to inspect the specimen during preparation, consolidation, and testing to see if any part is displaying unusual behavior. If any differences are seen, the preparation procedure should be adjusted for subsequent specimens to remove this behavior.

Undisturbed Unfrozen Samples—Unfrozen sand specimens have been prepared from tube samples in the following ways:

1. By free draining the sample tube, negative pore pressures can be developed. A short column of soil, extruded vertically, can be self-supporting for a short time, especially if some fines are present. This soil column may be tested directly (after trimming of the ends) or it may be trimmed to a smaller diameter.
2. By vertically extruding the specimen into a mold, using a method similar to that described for cohesive specimens, essentially continual support for the specimen is provided. This method also works for clean sands and has been used successfully for a large number of specimens and types of materials and is comparatively easy to perform. However, the potential for significant disturbance increases with reduction of the fines content.

Before preparing any sand specimens from a tube sample, the material within the tube should be inspected. Settlement of the sand or free water indicates major disturbance.

Undisturbed Frozen Samples—A number of different techniques to prepare frozen specimens are available [*38*]. Specimens may be successfully prepared using a single-wall core barrel with a diamond-tip coring device and direct circulation. Liquid carbon dioxide is generally used as a circulating fluid and to help keep the system cool. Details of a similar technique have been described by Singh and co-workers [*32*]. Experience shows that liquid carbon dioxide behaves better than liquid nitrogen because the latter tends to freeze the cored sample to the barrel. Good specimens can be prepared this way, but the procedure is not easy and the diamond bits are expensive.

Good results have been obtained also from frozen tube samples by placing the tube in a hot oven for a very short time. Melting occurs along the sample boundaries while the central core remains frozen. The sample may then be extruded and trimmed using previously described methods. The use of an electric wire saw, in which the normal wire is replaced by a resistance wire which will melt the specimen along the cut, may facilitate the preparation and the trimming process. The specimen can be refrozen during the trimming process by applying liquid nitrogen.

The Measurement of Initial Effective Stress in Clays

The measurement of the initial effective stress, p_o', in undisturbed clay specimens after installation in the triaxial cell is not routinely performed. Yet p_o' is an extremely important parameter, valuable in

(a) assessing the amount of specimen disturbance, particularly in soft clays [*2*]
(b) interpreting the results of unconsolidated undrained tests in which there is no reliable measurement of pore pressure during shear [*53*]
(c) providing an estimate of the *in situ* horizontal stress in stiff clays [*54*], particularly when p_o' has not been seriously modified by sampling, drying, and so forth
(d) determining the appropriate path to follow during reconsolidation [*5*]

An estimation of the initial effective stress may be made by

(a) attempting to measure the negative pore pressure or suction, $-u_s$, in the specimen while it is subjected to zero total stress
(b) applying a confining stress under undrained conditions to elevate the pore pressure to an easily measurable value and assume that the difference between cell pressure and pore pressure is equal to p_o'
(c) adjusting the chamber pressure to eliminate the tendency for volume change of the specimen. The cell pressure which prevents volume change is considered to be approximately equal to p_o'. This procedure is performed by initial application of a confining pressure roughly equal to the initial negative pressure, or enough to cause a small initial axial deformation of the specimen. The pore pressure measuring system is flushed then, and volume changes are monitored and kept to zero by subsequent adjustment of the cell pressure.

The first approach is adopted, for example, at Massachusetts Institute of Technology (MIT) where a pedestal with an inset high air entry value porous stone and a carefully deaired measuring system is used. Limitations to the value of suction that can be registered are set by cavitation occurring in the system at around -70 kN/m^2 [*46*].

The accuracy of the second approach depends on the assumption of an initially saturated specimen and measuring system. The evaluation may be improved by measurements of pore pressure resulting from increasing undrained steps in total stress. These values are used to extrapolate back to the p value (p_o') corresponding to zero total confining stress. In any case, this method depends on the prior elimination of trapped air in the system.

In the third approach, which is adopted by Norwegian Geotechnical Institute (NGI) [*5*] and which can be considered a modification of a method proposed by Skempton [*54*], the effective stress is assumed from the volume change tendency.

The time taken for an equilibrium pore pressure to become established in the specimen to allow the measurement of p_o' depends on a number of factors. These include specimen size, method of pore measurement, the coefficient of consolidation, and gradients caused by specimen disturbance, such as those discussed previously. Typical examples of the equilibration time for 38-mm-diameter by 76-mm-high specimens, using measurements at the base and midheight, are shown in Fig. 21.

Saturation

To avoid errors in the measurement of specimen volume changes or the pore pressure changes representative of a fully saturated soil, full saturation of the specimen and the pore water measurement system, including drain lines, is required. Usually, the degree of satu-

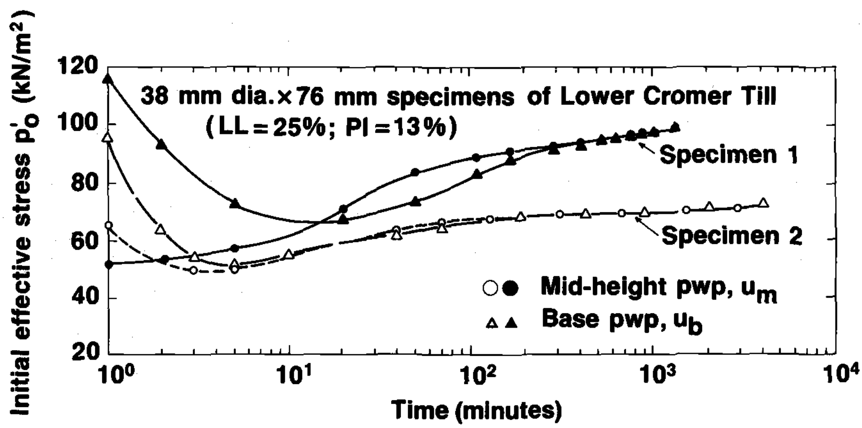

FIG. 21—*Example of time required for equalization of initial mean effective stress.*

ration is monitored in terms of Skempton's pressure parameter B, where a B value of 1 is taken to demonstrate complete saturation. However, it must be remembered that the parameter relevant for triaxial testing is the degree of saturation, which is related to B through the porosity and compressibility of the pore fluid and soil structure. The same B parameter, say 0.95, may mean 99.9% saturation in a stiff soil, but only 96% in a soft soil [*55*].

Therefore, some types of soils (typically very dense cohesionless soils or overconsolidated stiff clays) may have a high percentage of saturation even though they show B values less than one. For these cases, other methods of determining saturation must be used rather than attempting to obtain a B close to 1. These include the use of piezoelectric crystals inset in the platens to determine the compression wave velocity in the specimen [*56*], which is very sensitive to the presence of air or, more usually, monitoring changes of B with increasing back pressure at constant effective stress. Further changes of B will not occur when full saturation is achieved [*57*].

B values indicating acceptable levels of saturation for the aim of the test have to be related, therefore, to soil compressibility. The use of a simple criterion, such as obtaining a B value greater than 0.95, may not be valid in all cases.

Potential Causes of Gas in the System

Incomplete saturation means the presence of gas, usually air, in the system (specimen and pore pressure lines). It is helpful to examine the causes of air within the system (illustrated in Fig. 22):

1. Air within the specimen as a result of
   (a) partial saturation *in situ* (that is, prior to sampling)
   (b) partial saturation of the specimen after reconstitution in the laboratory
   (c) gases exsolving on reduction in pore pressure
   (d) cavitation when the suction level exceeds that sustainable in the pore space
2. Air within the measuring system (that is, top and bottom porous stones, drainage lines, and pressure transducer) which has collected because of
   (a) inadequate deairing initially
   (b) cavitation under $-u_s$
3. Air trapped
   (a) between the membrane and specimen
   (b) between the membrane and porous stones and top platen
4. Air diffusion through the membrane into the specimen.

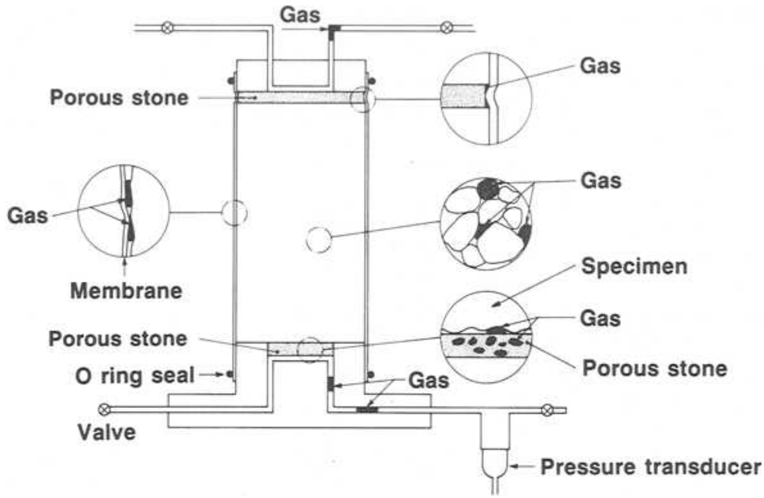

FIG. 22—*Possible gas entrapment within the system.*

Saturation of the specimen itself is not desirable in the case of 1, a) and, while desirable in the cases of 1, b), c), and d), it can only be achieved by changing either the water content or the effective stress in the specimen, as discussed later.

Clearly, elimination of air occurring from 2), 3), and 4) is desirable. In most cases this can be achieved without modifying the effective stresses in the specimen.

Flushing of deaired water beneath the pedestal will remove air within the measurement system. Where top drainage is used, a similar flushable system should be used.

Perhaps greater attention could be paid to eliminating the air trapped between the membrane and specimen, top cap, and porous stones during installation. Potential air traps around the porous stone can be avoided by using porous stones inset into the pedestal and top cap. It may be helpful to unroll the stretched membrane with its end anchored at the pedestal, rather than enveloping the specimen in one step by releasing the vacuum in a membrane stretcher which inevitably traps air. Buri [*58*] had considerable success in reducing trapped air by inserting a small hollow plastic tube between the specimen and membrane and withdrawing this when assembly was complete. An alternative technique is to allow the assembled specimen to stand in a cell filled with deaired water so air may diffuse out through the membrane from around the specimen. Diffusion of air can take place between the cell water and the specimen because the rubber membrane is relatively permeable to air.

The use of deaired water in the cell, especially when used in conjunction with a remote air–water interface, helps to slow air migration from the cell into the specimen [*59*]. When tests of long duration are planned, oil may be used instead as confinement fluid to reduce migration, but oil–membrane compatibility should be considered.

Methods of Saturation

Because full saturation is, at best, difficult to maintain during installation, subsequent saturation methods are used. These usually consist of a combination of flushing and back pressuring.

Flushing—Flushing is usually used to remove gas bubbles from the triaxial system, but it is not very effective on its own for achieving saturation. In the past, particularly before the use of back pressure was adopted, flushing was used in the saturation process for clays [*60*].

Now, however, the practice is limited to sands, mainly due to time limitation. Flushing can be applied either to the complete system (specimen and connecting lines, and so forth) or limited to the lines outside the specimen up to the porous stone. Typically, the flushing fluid is deaired water. In some cases, a preliminary flushing with a gas more soluble in water than air, such as carbon dioxide, may be used to displace the air [*61*].

Potential problems with flushing involve

(a) reduction of the initial effective stress with consequent swelling if flushing is performed under too low an effective stress
(b) piping
(c) consolidation or swelling of one part of the specimen with respect to the other causing a nonuniform void distribution
(d) leaching of soluble salts from the specimen
(e) transport of fines with possible clogging of the drainage lines
(f) undesired chemical reactions occurring between the flushing fluid and the soil, for example, when carbon dioxide is used and lime or limestone components are present [*61*]

Sometimes clay specimens are flushed around their periphery before the membrane is sealed, as described by Bishop and Henkel [*1*, p. 67, 109] for soft clays. When this procedure was developed, flushing after specimen assembly was more difficult than now due to the use of null indicators. Therefore, a high degree of initial saturation was essential. With techniques available today, subsequent saturation is possible. This procedure of flushing around the specimen periphery should be avoided because the problems associated with it (swelling and p_o' changes) are usually higher than the benefits it may provide.

When flushing is used, it should be performed

(a) under a proper effective stress within the specimen
(b) under minimized gradient
(c) using the same water as exists in the pores when leaching is suspected
(d) without the use of carbon dioxide when reaction with soil components is possible

Back Pressure—Saturation by back pressure, as it is referred to in the literature, actually involves increases in the specimen pore pressure to obtain saturation. This method is based on the compressibility (controlled by Boyle's law) and solubility (controlled by Henry's law) of air in water, which both increase with the applied back pressure. Basic principles and suggestions for the use of back pressure to saturate specimens and criteria for evaluating back pressure values and time of application have been described elsewhere [*1,40,55,60*].

Two basic techniques are used for specimen saturation by back pressure. While the basic techniques are easy to perform, the implications of the methods are quite complicated. To help clarify this, the basic methods are illustrated here.

1. Saturation may be obtained by an increase in the cell pressure with drainage to the specimen closed. This is illustrated in Fig. 23*a*), in which the dashed line is used to represent the pore pressure present in the specimen as the cell pressure is increased. Each incremental increase of cell pressure will cause a corresponding incremental increase in the pore pressure, from which the B value may be determined. When the resulting pore pressure change is less than the change in cell pressure, the effective stress applied to the specimen will be increased.

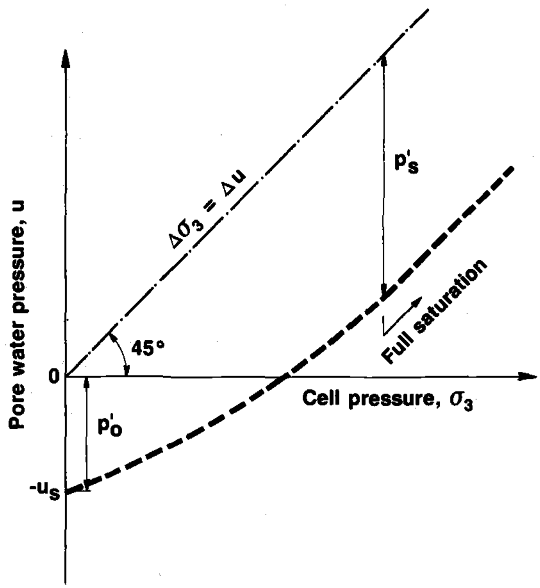

(a) SATURATION BY INCREASING σ_3 UNDRAINED ($\Delta w = 0$, $\Delta p' > 0$)

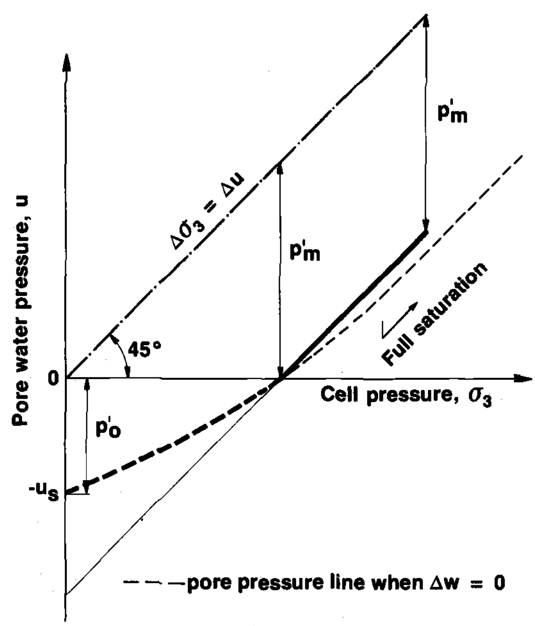

(b) SATURATION BY INCREASING σ_3 AND u_b ($\Delta w > 0$, $\Delta p'_m = 0$)

FIG. 23—*Saturation techniques by back pressure.*

This process of incremental increases may continue until

(a) saturation is achieved, at which point, if required, drainage is opened to an applied back pressure equal to the existing pore pressure and the remaining consolidation stress is applied

(b) the maximum desired effective stress is applied; saturation may be continued by the next method presented.

2. The second method involves saturation with drainage open to maintain a set effective stress. The heavy line in Fig. 23*b* represents the pore pressure present in the specimen during this process. As the figure shows, this procedure usually consists of an initial undrained increase in cell pressure, as in method 1, to bring the pore pressure to zero or a positive value. Drainage is then opened to the desired back pressure. This may be equivalent to the existing pore pressure (to maintain the current effective stress, p_M' as in the figure), or to the value required to obtain the effective stress desired.

   This effective stress difference (p_M' in Fig. 23*b*), is then maintained by simultaneous increases in the back pressure and the cell pressure, with drainage open. In practice, this method is usually performed in small undrained stages so that *B* values may be determined, with the drainage occurring between stages.

A variation of these classic procedures is described by Rad and Clough [*62*] who used an initial vacuum in the specimen and in the cell to facilitate saturation.

Method 1 will minimize swelling of the specimen because free water is not available to enter the specimen, but there is no choice in the effective stress during the process. Also, it is not very effective if initial saturation is low because application of a confining stress increase will cause a much smaller increase in the pore pressure. The choice of effective stress to maintain during method 2 is important because the specimen is subject to swelling if too low a value is used.

Both methods involve some change in the effective stress acting on the specimen before saturation is attained. Specimen volume changes due to this effective stress change cannot be accurately measured by a burette connected to the specimen because the accuracy of this requires a saturated system. Instead, they may be estimated from changes in specimen dimensions.

As described, the methods are based on specimens under an isotropic state of stress. Although somewhat more cumbersome, the methods are also applicable to specimens under anisotropic stress states.

Unconsolidated Undrained Tests

For convenience in presentation, unconsolidated undrained tests in clays are considered here separate from other types of triaxial testing.

Bishop and Henkel point out that as a result of the modified stress history caused by sampling, the *A* value measured in a UU test is very different from the value *in situ* under a similar change in shear stress [*1*, p. 11]. They add that, for this reason, pore pressure measurements are not usually made during UU tests on saturated samples. Although the book does not suggest performing the UU test this way, these statements seem to represent the philosophy behind the current test methods, namely of running a UU rapidly without the measurement of p_o' and of pore pressures during shear.

Current criticisms of the test concentrate on the basic shortcomings of the method for determining the undrained shear strength, S_u, rather than on current test procedures. Some of the shortcomings mentioned include shearing starting from an isotropic state of stress and significant changes in effective stress from *in situ* conditions [*4*]. The inconsistency of results obtained by the standard UU test procedure shows that some criticism of the test is justified. However, improvements in the test methods are possible, and can lead to a reduction in scatter of experimental data and to a better interpretation of the test. With current methods, the following limitations exist:

1. Several stages in the preparation and installation of cohesive specimens for triaxial testing, during which pore pressure gradients can be established in the specimen, were previously identified. Unless time is allowed for their equilibration after installation of the specimen, pore pressure gradients will affect specimen behavior, and the resulting variation will be superimposed on those caused by changes in the mean p_o' value due to sampling disturbance. The consequent scatter of data can be reduced only by allowing time for the equalization of the initial pore pressure differences. Unpublished commercial data from UU tests, with and without delay periods, have demonstrated a reduction in scatter due to pore pressure equalization before shear.
2. Having simply the shear strength from a UU test does not provide the necessary information for the interpretation of the test; the starting point (p_o') and the effective stress path followed are also required. The situation is similar to having, as a result of a consolidated undrained test, the failure point only. Most geotechnical engineers would not accept this from a CU test because it is not possible to judge if the result is reasonable or has to be rejected. Similarly, in interpreting standard UU results, one does not know what the initial effective stress is and, consequently, how close it is to the mean effective stress *in situ*. There is a range of mechanical overconsolidation ratios (typically about 4 to 8) for which the mean effective stress *in situ* is quite close to the residual effective stress of high quality samples. There are also soils, namely overconsolidated stiff sandy clays, that have an undrained shear strength mainly controlled by water content and not very sensitive to limited changes in initial effective stress (Fig. 24). In these circumstances, if the quality of the sample is high and no major additional disturbance is added in the laboratory, then a reasonable estimate of S_u may be obtained from UU tests. In other cases, namely in normally consolidated or in lightly overconsolidated soils or when soils are severely disturbed, the differences from *in situ* conditions may be so large as to prevent the use of UU tests to determine S_u [21]. The additional knowledge of pore pressure during shearing allows a better insight into the specimen response and helps to distinguish between different types of soil behavior.

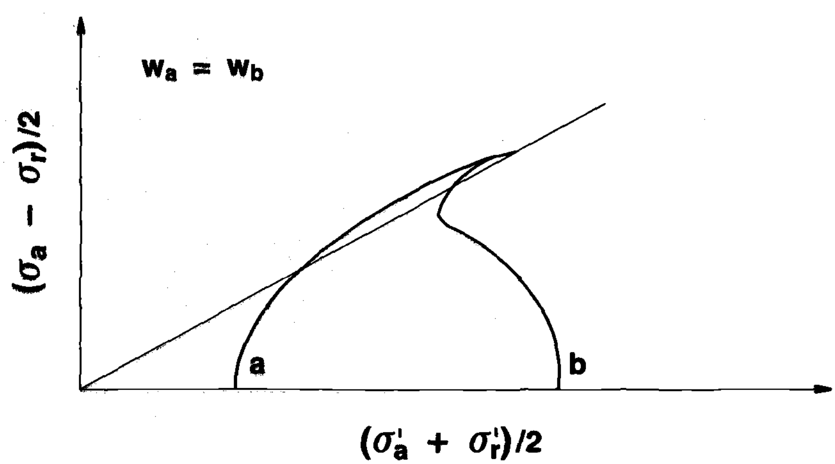

FIG. 24—*Examples of effective stress paths of UU tests on stiff sandy clay specimens having different initial effective stresses and the same water content.*

Certainly the UU test is subject to basic limitations if one wants to use it to measure the undrained shear strength in compression applicable to *in situ* conditions. In this respect, other procedures are, in general, superior (see the following section). However, it should be recognized that

1. The UU test is simple and, when using a midheight pore pressure probe to measure pore pressure during shear, remains relatively quick, even with the introduction of an initial delay to allow pore pressure equalization.
2. Our understanding of the effects of sampling are improving and some allowance can be made for these effects, especially in stiff clays in which the effects can be less severe.
3. The additional disturbance caused by volumetric strains during reconsolidation is avoided, thus increasing the possibility of identifying the effects of bonding and aging which may have survived the sampling process.
4. The UU test provides a rapid method for distinguishing between different types of stiff clay behavior (for example, plastic clays and sandy clays).
5. In some particular cases the UU tests may provide reasonable estimates of S_u resulting from *in situ* stress conditions.
6. With correct measurement of pore pressure during shear, an estimate of the effective stress failure envelope can also be defined in some instances.
7. In some practical circumstances, the UU test may represent the only viable test method; for instance, in the testing of large specimens of clay in which consolidation times would otherwise be excessive.

Based on these factors and depending on the soil type, the UU test may have a place in practice, provided that equalization of pore pressure gradients after installation is allowed and the initial effective stress p_o' is measured.

The addition of saturation before shear and correct measurements of pore pressure during shear may also increase the accuracy of the test and improve its interpretation.

By use of the above, the complexity, duration, and cost of the test are increased, but the quality and the practical use of the results are incomparably higher. Without improvements, the standard UU test is often of little more value than a pocket penetrometer test.

Stress Path Testing

Control of the stress path is possible during either the consolidation phase, the shearing phase, or both. The paths followed for the standard consolidated triaxial compression or extension tests (CIU and CID) represent just two of the possible triaxial stress paths.

Stress Path Test Methods

While a standard pressure system and a displacement-controlled loading frame are sufficient to follow the stress paths for standard isotropically consolidated tests, both in compression loading and in extension unloading, other stress paths require some form of integrated control of the vertical, σ_V', and the horizontal stress, σ_H'.

When the "Triaxial Book" was published, methods of controlling stress were somewhat cumbersome and not amenable to automation. Bishop himself made a major contribution to rectifying this when he introduced the hydraulic triaxial cell [*15*]. This apparatus, with suitable control systems, enables the principles of stress path testing, formalized by Lambe [*63*], to be put into practice relatively simply.

Methods with the Hydraulic Triaxial Cell—The hydraulic triaxial cell (HTC) allows both the vertical and horizontal stress to be controlled while retaining the ability to control drainage and run constant rate of strain tests. It is the simple and independent control of the confining pressure and the deviator stress that gives the HTC the flexibility to follow with relative ease the full range of stress paths in triaxial space (Fig. 1), but, perhaps more importantly, it allows the use of anisotropic reconsolidation stress paths to be performed routinely.

The basic HTC requires operator control for general stress paths. Soon after its introduction, Bishop instigated the development of computer-control systems. A system was operational at Imperial College in London in the mid-1970s [*64*].

The philosophy behind this system is illustrated in Fig. 25. Feedback from electrical transducers measuring the horizontal stress, σ_H, the axial load, L, the midheight pore pressure, u_m, the base pore pressure, u_b, the axial displacement, Δh, and the radial displacement, Δr, enables the current state of the specimen to be defined and its response to

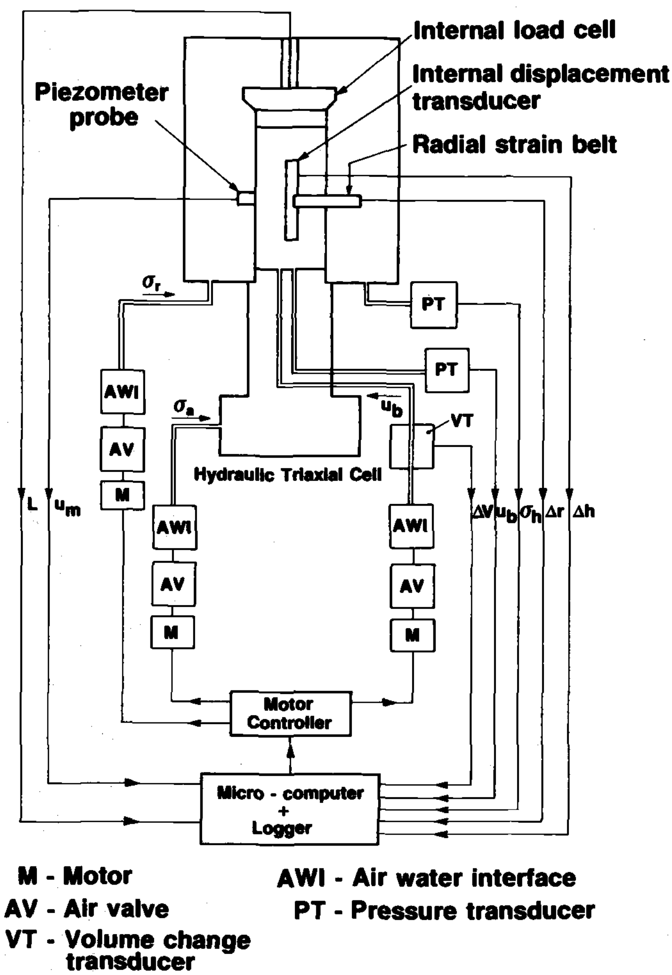

FIG. 25—*Schematic of the computer-controlled HTC system at Imperial College, London.*

a change in stress or displacement to be measured. Control over σ_V, σ_H, and, in drained tests, back pressure (u_b), is achieved using air valves rotated by motors under the direction of the microcomputer.

The system shown is capable, in principle, of running any triaxial stress path test. Reconsolidation to estimated *in situ* stresses is relatively straightforward as, of course, are stress history and normalized soil engineering properties (SHANSEP) procedures [*65*]. The use of internal measurements, and in particular, the midheight and base measurements of pore pressure are key features of the design. During anisotropic consolidation, measurement of u_b and u_m allows pore pressure differences along the specimen height to be maintained within predefined limits by control of the rate of stress change. Similarly, rates of strain during conventional drained testing can be controlled automatically, without predefining these on the basis of assumed failure strains and pore pressure distributions. Combined with feedback from the radial strain belt, the information on u_b and u_m enables various methods of K_o consolidation to be carried out (stress controlled, rate of strain controlled, and so forth).

A similar system has been used by Atkinson [*66*] but with an external measurement system. A different approach to computer-controlled triaxial testing has been adopted by Menzies [*67*] who used ram pumps to control σ_V, σ_H, and u_b in a HTC system which relies on feedback from the pressure sources and not directly from the measured values of load or displacement at the specimen. The use of the Menzies system in a commercial laboratory is described by Coatsworth and Hobbs [*68*].

Methods with Conventional Triaxial Cell—Stress path testing is also feasible in conventional triaxial equipment. For example, in a standard triaxial cell, a deviator stress may be applied by dead loads on the ram [*1*, p. 78]. Alternatively, a standard displacement-controlled loading press may be easily modified to apply a controlled deviator stress by use of a double-acting pneumatic actuator attached to the reaction bar of the frame (Fig. 26). A combination of the two methods has proved to be practical. For example, during anisotropic consolidation, the initial consolidation may be performed by dead weights of limited mass which are thus easily manageable, keeping the press free. The final consolidation, which requires larger weights, may be carried out in the press, reducing disturbance and allowing a more accurate start to the test. The detail shown in Fig. 26 allows a simple change from stress- to displacement-controlled loading for use either in compression or in extension.

Computer control for automatic stress path testing with modified conventional equipment can be developed by simply controlling, by the computer, the confining pressure or the back pressure, while a standard displacement-controlled loading frame applies a displacement to cause a deviator stress. Law describes a system in which only the back pressure is adjusted during shearing to follow the desired stress path [*69*]. With systems of this type, the deviator stress is not directly controlled.

The addition of direct control of the axial load makes the system more flexible. For example, a system based on a load frame capable of controlling both load and displacement offers most of the advantages of an HTC-based system. The addition of a computer, analog-to-digital (A/D) converters, and so forth allows automatic stress path testing to be performed.

Consolidation/Reconsolidation

One of the most important stress paths to control in triaxial testing is that followed when bringing a specimen from the installed state to the final consolidation state because the path chosen will affect the specimen behavior during shear.

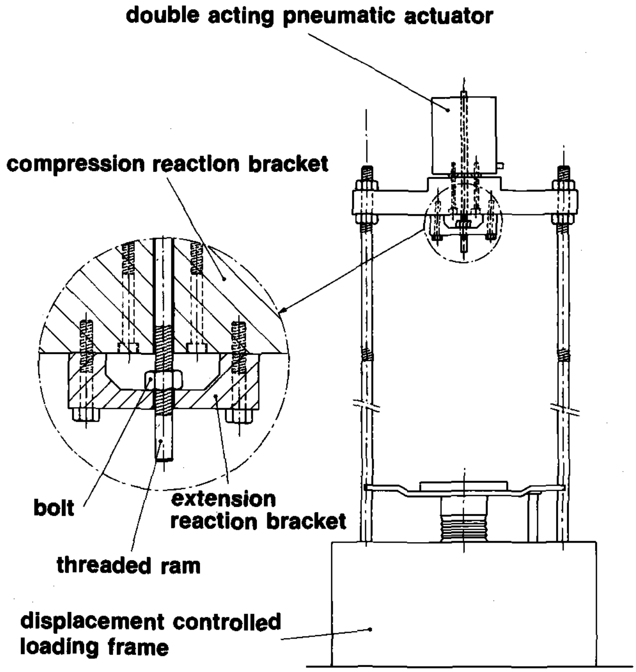

FIG. 26—*Displacement-controlled loading frame equipped with a double-acting pneumatic actuator for stress- or strain-controlled tests.*

Clays—Alternative consolidation paths are illustrated schematically in Fig. 27 for the case of a normally consolidated reconstituted clay for which sampling was performed in laboratory. The improved fit between *in situ* and specimen behavior when anisotropic consolidation is used is obvious. However, water content reduction during reconsolidation may introduce subtle changes to behavior. There may also be significant residual effects due to sampling [*4*], such as the effects of aging and cementation, so that anisotropic reconsolidation is not the panacea for all sampling problems.

Water content changes during reconsolidation should be minimized. They are restricted by keeping the reconsolidation path inside the yield surface (that is, paths abc, agc for a normally consolidated clay in Fig. 28, as opposed to path adc or any other path crossing the yield surface).

A further constraint on the reconsolidation path is imposed when attempting to measure the small strain response of specimens from retrieved samples. This is illustrated in Fig. 29 for the case of a lightly overconsolidated soil and uses the idea of mobile small strain zones introduced by Jardine [*70*] and applied to the sampling problem by Hight and co-workers [*21*]. The small strain zone may be considered as a region around a point in stress space, within which strains accompanying stress changes from that point are less than some small limiting value, say 0.1%. The location of the small strain zone relative to the current stress state is determined by the recent stress path direction and time. Its location, and therefore the measured small strain response, will be different for the two reconsolidation paths, abc and adec shown in Fig. 29. In this case, path adec, which includes a unloading leg, more closely restores the *in situ* small strain region.

The reconsolidation paths shown in Figs. 28 and 29 avoid exceeding the preconsolidation pressure, σ_{VC}'. In the SHANSEP procedure, reconsolidation paths deliberately exceed σ_{VC}'

by some 1.5 to 2 times to erase the effects of sampling [65]. Swelling back to the estimated *in situ* OCR (Fig. 30, path abcd) is assumed to restore the *in situ* behavior for soils in which behavior is normalizable. Otherwise, the effects of cementation, quick structures, aging, and so forth are, of course, largely eliminated so that a "lower bound" strength is obtained. Experience suggests that small strain stiffnesses are restored using SHANSEP procedures, mainly because the appropriate stress path directions are involved.

In general terms, the appropriate reconsolidation path to follow will depend on p_o', the soil stress history, and the material to be tested. The duration of the secondary consolidation at the final consolidation point should last the same time for each specimen to minimize the difference of possible secondary effects on the initial part of the stress–strain curve.

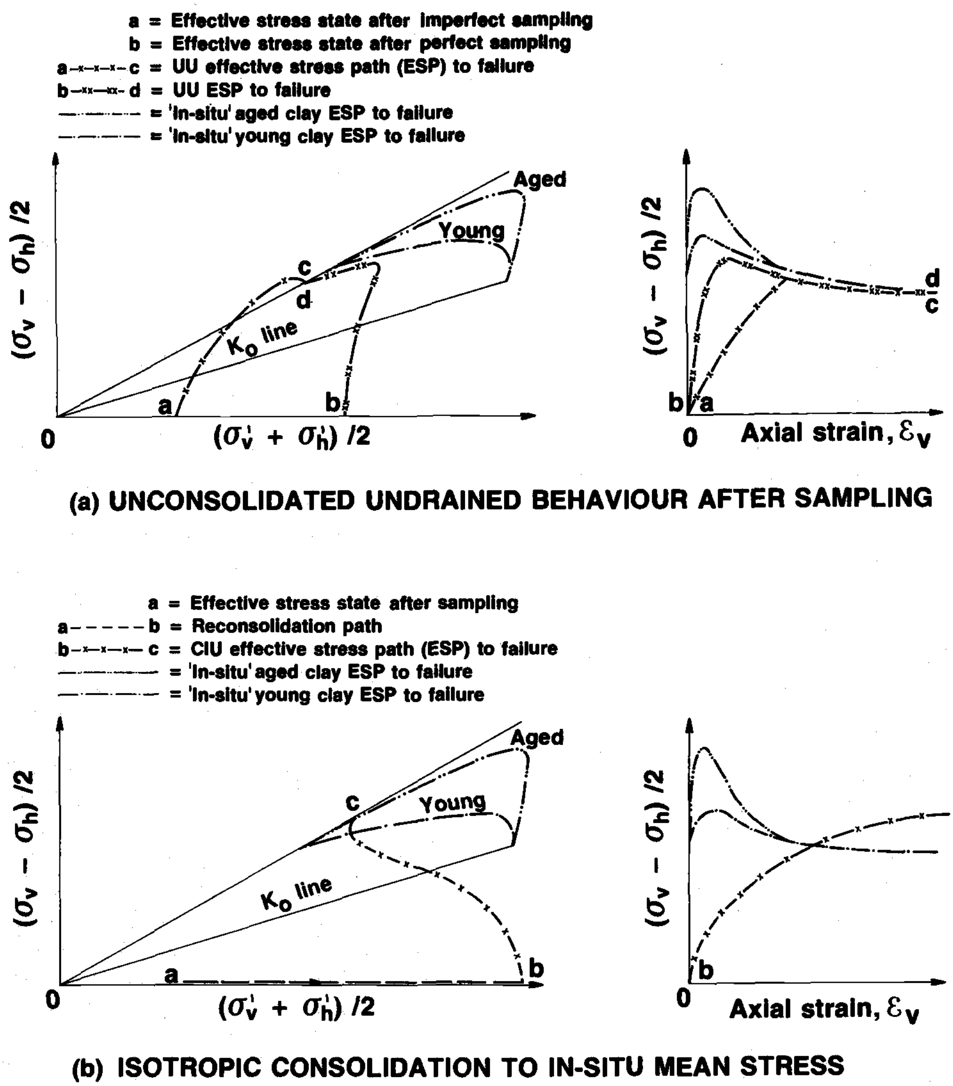

FIG. 27—*Effects of different consolidation paths on stress–strain behavior of a normally consolidated clay.*

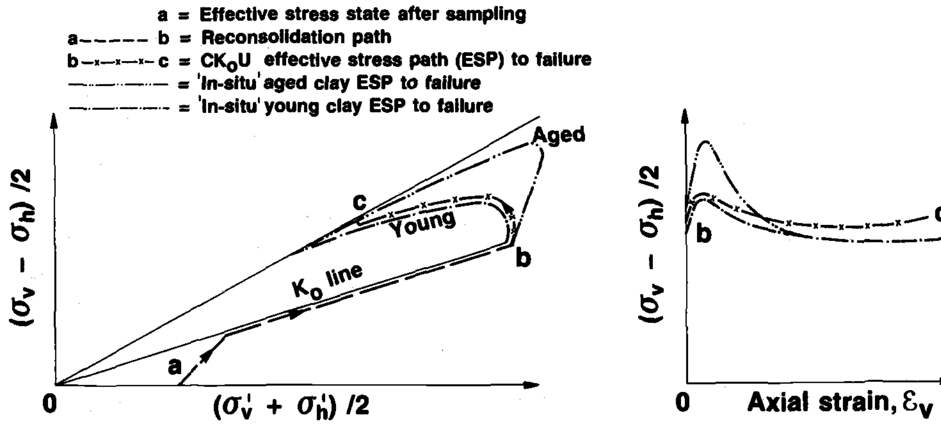

(c) ANISOTROPIC CONSOLIDATION TO IN-SITU STRESSES

FIG. 27—*Continued.*

Sands—In most cases, the consolidation path for sands starts from the isotropic effective stress imposed on the specimen during the installation to maintain the specimen size and shape. In practice, consolidation paths usually follow either the isotropic line or the K_o line. As in clays, these two different consolidation paths produce quite different stress–strain curves (Fig. 31), but the same failure envelope [*71*].

In most practical applications, the major problem remains the retention or the duplication of the fabric and the density existing *in situ,* as previously discussed. In general, it is unlikely that simple reconsolidation of specimens from tube samples or reconstitution to the *in situ*

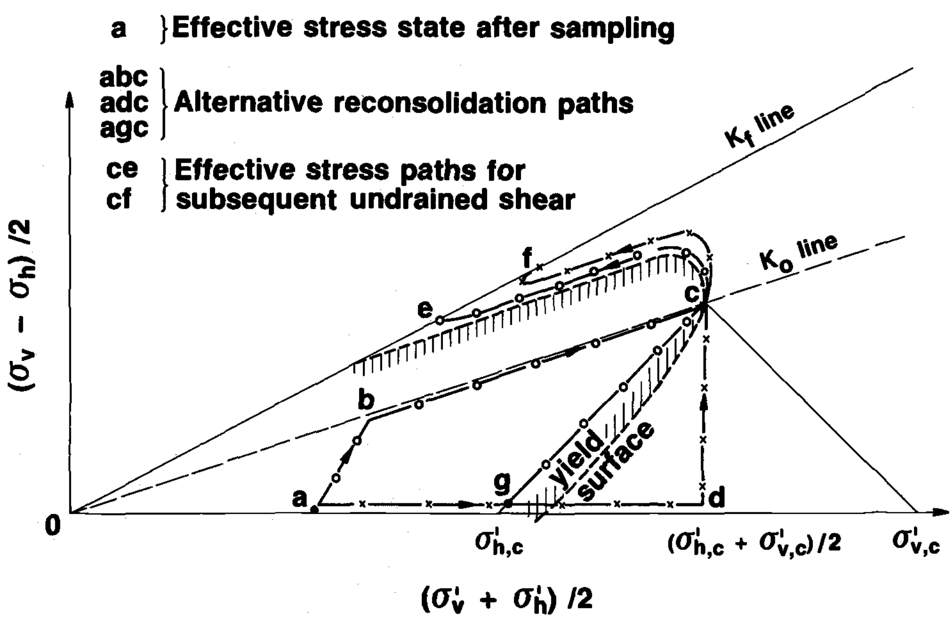

FIG. 28—*Alternative stress paths for* K_o *consolidation.*

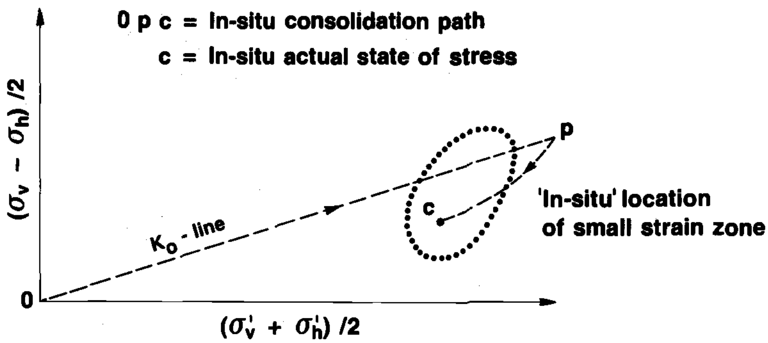

(a) MECHANICALLY LIGHTLY OVERCONSOLIDATED SOIL IN-SITU

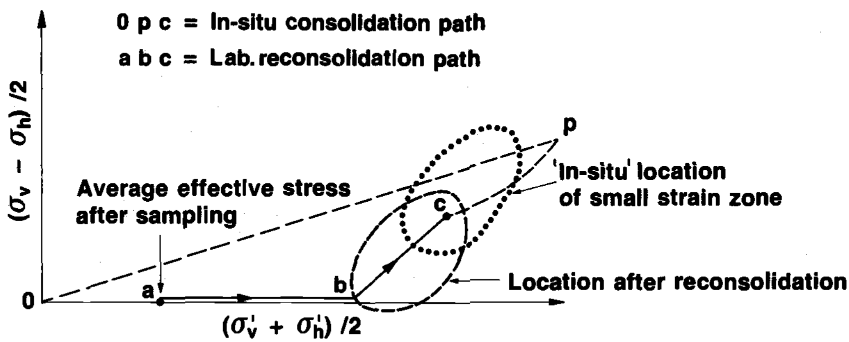

(b) RECONSOLIDATION TO IN-SITU STRESS AFTER SAMPLING

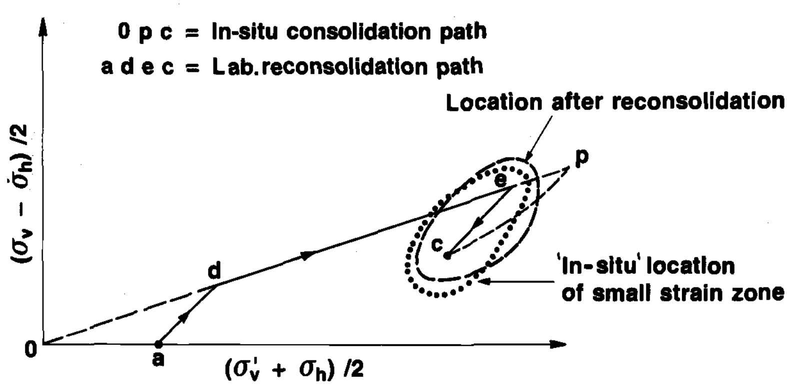

(c) RECONSOLIDATION TO IN-SITU STRESS AFTER SAMPLING

FIG. 29—*Effects of consolidation paths on location of small strain zone.*

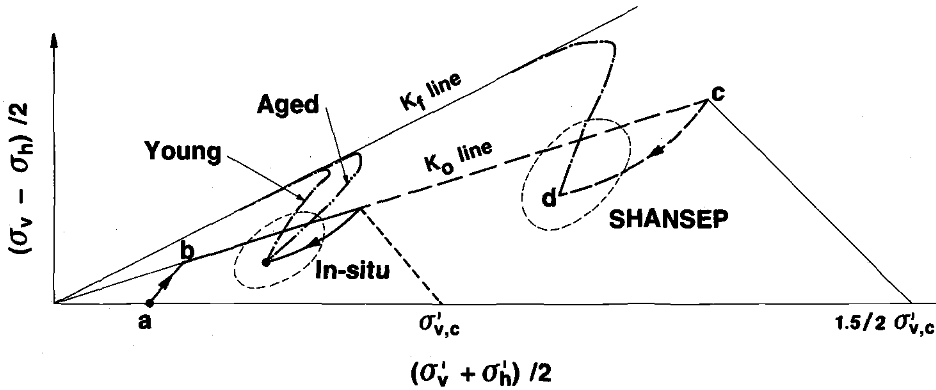

FIG. 30—*SHANSEP reconsolidation method.*

density will reproduce general stress–strain properties representing *in situ* behavior [*24–26,30*]. However, after a cyclic stress history has been applied to reconstituted dense specimens, prepared close to the *in situ* density, to cause them to have the same shear wave velocity as *in situ,* the response of the specimens from radially frozen samples and from reconstituted specimens has been quite similar [*26*]. This may mean that by matching the shear wave velocities to those *in situ,* laboratory specimens could be used to reproduce to an acceptable level the mechanical properties of the intact sand [*26,72*]. The duplication in the laboratory of the *in situ* shear wave velocity might be an improvement over existing techniques for dealing with reconstituted and standard tube sand specimens. However, evidence for this is limited at this time. Additional studies are necessary, mainly to investigate the sensitivity of the shear wave velocity to all aspects of disturbance and the relationships among shear wave velocities, cyclic stress history, and the mechanical behavior of sands.

Shear wave velocities may be derived from low amplitude cyclic loading tests, as performed by Tokimatsu and Hosaka [*26*], but this requires very accurate load and deformation measurements and the assumption of the value of Poisson's ratio. Alternatively, direct shear wave velocity measurements may be obtained by using piezoelectric transducers inserted in the platens. Preliminary experience at ISMES shows that both piezoelectric shear crystals and benders give similar initial shear moduli (G_{max}) (Fig. 32), and compare well to those obtained from resonant column tests (Fig. 33), as also shown in the literature [*73*].

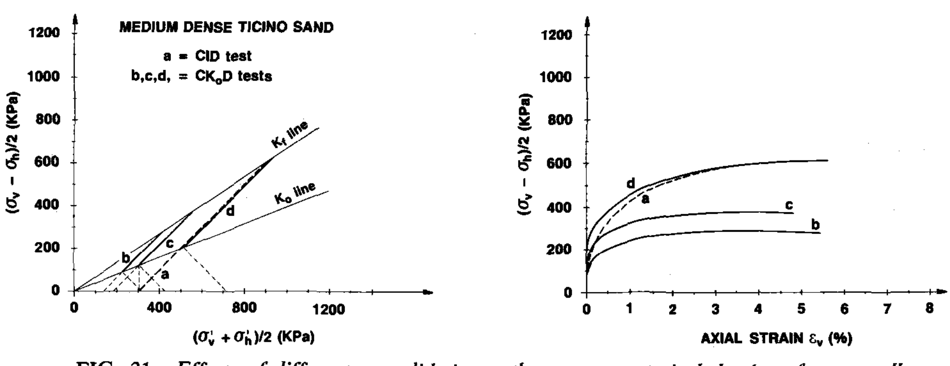

FIG. 31—*Effects of different consolidation paths on stress–strain behavior of a normally consolidated sand from the Ticino River, Italy.*

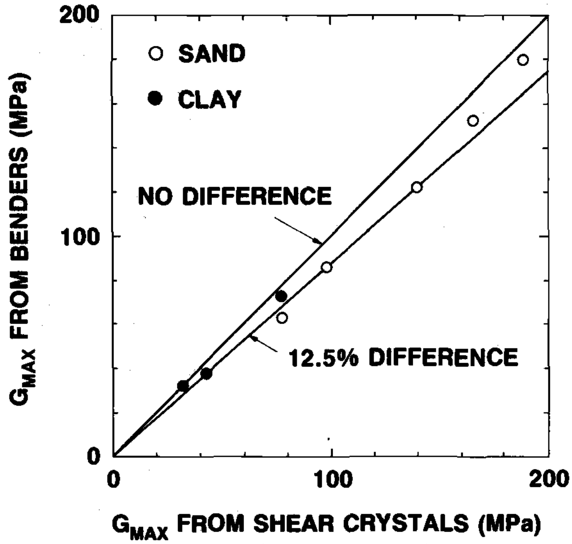

FIG. 32—*Comparison of initial shear moduli from shear wave measurements obtained from piezoelectric shear crystals and benders.*

Stress Paths to Failure

For undrained tests on fully saturated soils, each total stress path for compression gives the same effective stress path. The same holds for extension. Therefore, conventional equipment can be used for shearing the specimen. In drained tests, an infinite choice of effective stress paths within the triaxial plane are possible, and more elaborate systems may be necessary to follow the stress path chosen.

An example of the advantages of stress path testing can be seen by considering the stress path followed in the conventional CID test (paths ab and cd in Fig. 34). This path is particularly unsuitable for the determination of the strength parameters c' and ϕ' at the low stresses relevant to many field problems (for example shallow slope stability). Having a stress path system available, alternative, more appropriate, stress paths may be followed, for example:

(a) paths ae and ch in Fig. 34 in which σ_V' is held constant while σ_H' is reduced, or
(b) path fg in Fig. 34 in which σ_V' and σ_H' are maintained constant while u_b is increased, to simulate swelling in an unloaded slope.

A computer-controlled stress path system should allow switching smoothly from stress to stain control. Such a change can be made as failure is approached to avoid instability of the system. This technique has been used extensively with the HTC to investigate the failure envelope at low stresses by Gens [*74*] and is advocated by Atkinson.[4] The use of stress control initially also allows full drainage to be ensured while passing through the small strain zone.

Concluding Remarks

The triaxial test on cylindrical specimens is one of the most popular methods for determining the strength and stiffness characteristics of soils. The basic principles and methods

[4] Personal communication, 1986.

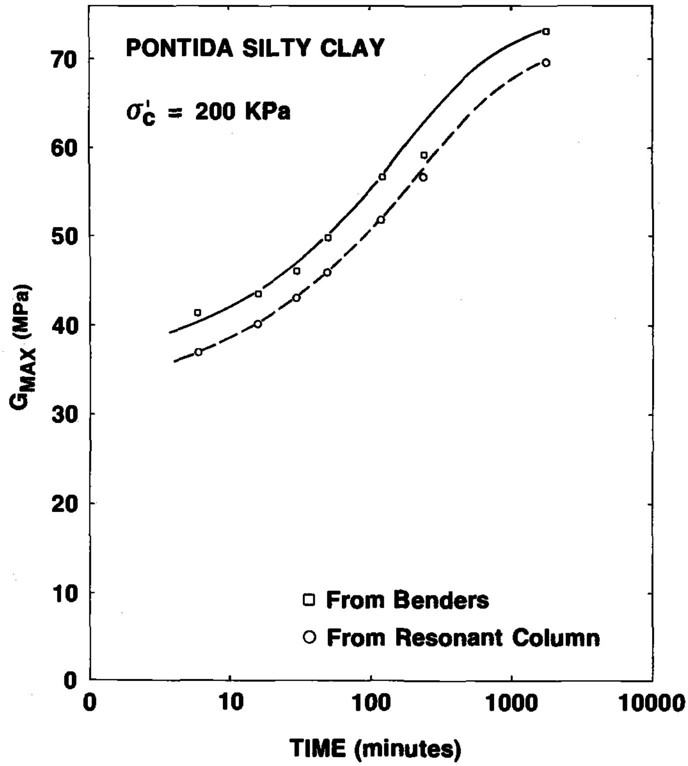

FIG. 33—*Comparison of initial shear moduli obtained from benders and resonant column measurements on reconstituted specimens of a lake bed sediment taken near Pontida, Italy.*

underlying the test were admirably described in *The Measurement of Soil Properties in the Triaxial Test* by Bishop and Henkel [*1*]. A number of other test methods have been developed since the publication of the "Triaxial Book," some of which have been presented here.

The main points discussed may be summarized under the following broad categories:

1. Triaxial test results depend on the degree of soil disturbance. In cohesive soils, the use of undisturbed samples and of appropriate laboratory methods allows a reasonable determination of *in situ* properties. By the adoption of appropriate test details, additional disturbance due to specimen preparation, drying, and water exchange between the specimen and membrane, filter paper, and pore pressure measuring and drainage systems can be reduced.

   For testing undisturbed cohesionless specimens, major problems lie in the phases before the samples arrive at the laboratory. Disturbance is usually more severe than for cohesive soils and greatly affects the soil properties. Promising developments to reduce disturbance include the adoption of new sampling and handling techniques, such as freezing and, hopefully in the future, impregnation. New methods such as those based on shear wave velocity measurements or other indirect parameters may help in assessing disturbance and in promoting the use of reconstituted specimens to represent field behavior.
2. Improvements in equipment, and especially in measurement methods, have been developed. Electrical transducers increase measurement precision, and enable measure-

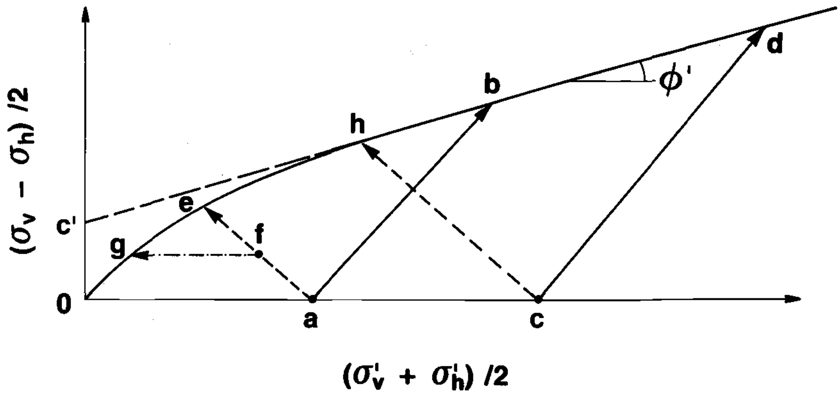

FIG. 34—*Examples of possible drained stress paths.*

ments to be made inside the cell, the use of automatic data logging, and automatic test control by means of computers and feedback systems.

New details in equipment and the use of pore pressure transducers have facilitated the saturation of the specimen and the measurement of the initial effective stress.

3. Measurements made within the triaxial cell have shown that measurement errors during triaxial testing can be severe, particularly for axial deformation measurements. Internal measurements, improvements in specimen preparation, and better tolerances in equipment enable a more accurate definition of the yield and stiffness characteristics of the soils, especially during the initial part of the stress–strain curve. Use of a pore pressure probe located at the midheight of the specimen, in conjunction with the classic measurement made at the base, can demonstrate pore pressure equalization during shear, and differences in readings can be used for the definition of the strain rate.
4. Although the general use of UU tests has been questioned in the literature, a properly performed UU test can provide, in some circumstances, useful information. Some of the scatter of UU results is due to the test methods conventionally used rather than from the natural variability of soils. More consistent results may be obtained by allowing the equalization of pore pressure prior to shear. A better interpretation of test results may be obtained with the measurement of the initial effective stress, p_o', and of pore pressures during shear.
5. An appropriate stress path both for consolidation and shearing will provide a better reproduction of *in situ* stress–strain properties. For instance, K_o consolidation provides a considerable improvement over isotropic consolidation for the representation of many *in situ* conditions.

It is important that developments in equipment and methods of tests be considered and adopted in practice if the viability of triaxial testing is to be maintained. Unfortunately, many valuable testing techniques have not yet been adopted in routine activities.

Acknowledgments

The ISMES Soil Mechanics Laboratory wishes to thank Ente Nazionale Energia Elettrica (ENEL), in particular the Direzione Studi Ricerche-Centro Ricerche Idrauliche e Strutturali (DSR-CRIS) Division, and Ente Nazionale Energia Alternative (ENEA), for the support they provide to our research activities.

Dr. Hight wishes to acknowledge the support of the Science and Engineering Research Council who awarded his research fellowship.

References

[1] Bishop, A. W., and Henkel, D. J., *The Measurement of Soil Properties in the Triaxial Test,* 2nd ed., Edward Arnold, London, 1962, pp. 8, 10, 11, 15–21, 27–32, 37, 39, 67, 78, 83, 84, 90–92, 95, 106, 109, 127, 184.

[2] Ladd, C. C. and Lambe, T. W., "The Strength of Undisturbed Clay Determined from Undrained Tests," *ASTM Symposium on Laboratory Shear Testing of Soils, Ottawa, STP 361,* American Society for Testing and Materials, Philadelphia, 1963, pp. 342–371.

[3] Saada, A. S., "Testing for Anisotropic Clay Soils," *Journal of the Soil Mechanics and Foundation Division, American Society of Civil Engineers,* Vol. 96, No. SM5, 1970, pp. 1847–1852.

[4] Jamiolkowski, M., Ladd, C. C., Germaine, J. T., and Lancellotta, R., "New Developments in Field and Laboratory Testing of Soils—Theme Lecture," *Proceedings,* Eleventh International Conference on Soil Mechanics and Foundation Engineering, San Francisco, Vol. 1, 1985, pp. 57–153.

[5] Berre, T., "Triaxial Testing at the Norwegian Geotechnical Institute," *Geotechnical Testing Journal, ASTM,* Vol. 5, No. 1/2, 1982, pp. 3–17.

[6] Chan, C. K., "Low Friction Seal System," *Journal of the Geotechnical Engineering Division, American Society of Civil Engineers,* Vol. 101, No. GT9, 1975, pp. 991–995.

[7] Bishop, A. W., Kumapley, N. K., and El-Ruwayih, A., "The Influence of Pore-Water Tension on the Strength of Clay," Philosophical Transactions of the Royal Society of London, No. 278, 1975, pp. 511–554.

[8] Taylor, D. W., "10th Progress Report for the Cylindrical Compression Research Program," Soil Mechanics Laboratory, Massachusetts Institute of Technology, Cambridge, MA, 1944.

[9] Hight, D. W., "A Simple Piezometer Probe for the Routine Measurement of Pore Pressure in Triaxial Tests on Saturated Soils," Technical Note, *Geotechnique,* Vol. 32, No. 4, 1982, pp. 396–401.

[10] Brown, S. F., Austin, G., and Overy, R. F., "An Instrumented Triaxial Cell for Cyclic Loading of Clays," *Geotechnical Testing Journal, ASTM,* Vol. 3, No. 4, 1980, pp. 140–152.

[11] Costa-Filho, L. M., "A Laboratory Investigation of the Small Strain Behaviour of London Clay," Ph.D. thesis, University of London, 1980.

[12] Symes, M. J., and Burland, J. B., "Determination of Local Displacements on Soil Samples," *Geotechnical Testing Journal, ASTM,* Vol. 7, No. 2, 1984, pp. 49–59.

[13] Jardine, R. J., Symes, M. J., and Burland, J. B., "The Measurement of Soil Stiffness in the Triaxial Apparatus," *Geotechnique,* Vol. 34, No. 3, 1984, pp. 323–340.

[14] Tatsuoka, F., "Some Recent Developments in Triaxial Testing Systems for Cohesionless Soils," in this volume, pp. 7–67.

[15] Bishop, A. W., and Wesley, L. D., "A Hydraulic Triaxial Apparatus for Controlled Stress Path Testing," *Geotechnique,* Vol. 25, No. 4, 1975, pp. 657–670.

[16] Hight, D. W., Gens, A., and Symes, M. J., "The Development of a New Hollow Cylindrical Apparatus for Investigating the Effects of Principal Stress Rotation in Soils," *Geotechnique,* Vol. 33, No. 4, 1983, pp. 355–383.

[17] De Campos, T. M. P., "Two Low Plasticity Clays under Cyclic and Transient Loading," Ph.D. thesis, University of London, 1984.

[18] Daramola, O., "The Influence of Stress History on the Deformation of Sand," Ph.D. thesis, University of London, 1978.

[19] Atkinson, J. H., and Evans, J. S., Discussion on Jardine R. J., Symes, N. J., and Barland, J. B., "The Measurements of Soil Stiffness in the Triaxial Apparatus," (1984), *Geotechnique,* Vol. 35, No. 3, 1985, pp. 378–382.

[20] Baligh, M. M., "Strain Path Method," *Journal of the Geotechnical Engineering Division, American Society of Civil Engineers,* Vol. 3, No. 9, 1985, pp. 1108–1136.

[21] Hight, D. W., Gens, A., and Jardine, R. J., "Evaluation of Geotechnical Parameters from Triaxial Tests on Offshore Clay," *Proceedings,* International Conference on Offshore Site Investigation, London, 1985, pp. 253–268.

[22] La Rochelle, P., Sarrailh, J., Roy, M., and Tavenas, F. A., "Effect of Storage and Reconsolidation on the Properties of Champlain Clays," in *Soil Specimen Preparation for Laboratory Testing, ASTM STP 599,* American Society for Testing and Materials, Philadelphia, 1976, pp. 126–146.

[23] Kirkpatrick, W. M., and Khan, A. J., "The Reaction of Clays to Sampling Stress Relief," *Geotechnique,* Vol. 34, No. 1, 1984, pp. 29–42.

[24] Mori, K., Seed, H. B., and Chan, C. K., "Influence of Sample Disturbance on Sand Response of Cyclic Loading," *Journal of the Geotechnical Engineering Division, American Society of Civil Engineers,* Vol. 104, No. GT3, 1978, pp. 323–339.

[25] Seed, H. B., Singh, S., Chan C. K., and Vilela T. F., "Consideration in Undisturbed Sampling

of Sands," *Journal of the Geotechnical Engineering Division, American Society of Civil Engineers,* Vol. 108, No. GT2, 1982, pp. 265–283.

[*26*] Tokimatsu, K., and Hosaka, Y., "Effects of Sample Disturbance on Dynamic Properties of Sand," *Soils and Foundations,* Vol. 26, No. 1, 1986, pp. 53–64.

[*27*] Arman, A., and McManis, K. L., "Effects of Storage and Extrusion of Sample Properties," in *Soil Specimen Preparation for Laboratory Testing, ASTM STP 599,* American Society for Testing and Materials, Philadelphia, 1976, pp. 66–87.

[*28*] Mulilis, J. P., Seed, H. B., Chan, C. K., Michell, J. K., and Arulanandan, K., "Effects of Sample Preparation on Sand Liquefaction," *Journal of the Geotechnical Engineering Division, American Society of Civil Engineers,* Vol. 103, No. GT2, 1977, pp. 91–108.

[*29*] Miura, S., and Toki, S., "A Sample Preparation Method and Its Effect on Static and Cyclic Deformation—Strength Properties of Sand," *Soils and Foundations,* Vol. 22, No. 1, 1982, pp. 61–77.

[*30*] Tokimatsu, K., Yamazaki, T., and Yoshimi, Y., "Soil Liquefaction Evaluation by Elastic Shear Moduli," *Soils and Foundations,* Vol. 26, No. 1, 1986, pp. 25–35.

[*31*] Schneider, H., "Undisturbed Sampling of Cohesionless Soils by Chemical Impregnation," Ph.D. thesis, Purdue University, 1985.

[*32*] Singh, S., Seed, H. B., and Chan, C. K., "Undisturbed Sampling of Saturated Sands by Freezing," *Journal of the Geotechnical Engineering Division, American Society of Civil Engineers,* Vol. 108, No. GT2, 1982, pp. 247–264.

[*33*] Yoshimi, Y., Hatanaka, M., and Oh-oka, H., "Undisturbed Sampling of Saturated Sands by Freezing," *Soils and Foundations,* Vol. 18, No. 3, 1978, pp. 59–73.

[*34*] Yoshimi, Y., Tokimatsu, K., Kaneko, O., and Makihara, Y., "Undrained Cyclic Shear Strength of a Dense Niigata Sand," *Soils and Foundations,* Vol. 24, No. 4, 1984, pp. 131–145.

[*35*] Ishihara, K., and Silver, M. L., "Large-Diameter Sand Sampling to Provide Specimens for Liquefaction Testing," *Proceedings,* Ninth International Conference on Soil Mechanics and Foundation Engineering, Specialty Session 2, Tokyo, Japan, 1977, pp. 1–6.

[*36*] Walberg, F. C., "Freezing and Cyclic Triaxial Behavior of Sands," Technical Note, *Journal of the Geotechnical Engineering Division, American Society of Civil Engineers,* Vol. 104, No. GT5, 1978, pp. 667–671.

[*37*] Hanzawa, H., Matsuda, E., and Makoto, H., "Evaluation of Sample Quality of Sandy Soil Obtained by the Modified Bishop Sampler," *Soils and Foundations,* Vol. 20, No. 3, 1980, pp. 17–32.

[*38*] Baker, T. H. W., "Transportation, Preparation, and Storage of Frozen Soil Samples for Laboratory Testing," in *Soil Specimen Preparation for Laboratory Testing, ASTM STP 599,* American Society for Testing and Materials, Philadelphia, 1976, pp. 88–112.

[*39*] Kimura, T., and Saitoh, K., "The Influence of Disturbance Due to Sample Preparation on the Undrained Strength of Saturated Cohesive Soil," *Soils and Foundations,* Vol. 22, No. 4, 1982, pp. 122–128.

[*40*] Berre, T., "Suggested International Code of Soil Engineering Practice for Consolidated Triaxial Tests," Norwegian Geotechnical Institute, Internal Report 56103-30, February 1986. 1985.

[*41*] Eischens, G. R., "Suggested Method for Trimming Undisturbed Samples," *Geotechnical Testing Journal, ASTM,* Vol. 3, No. 3, 1980, pp. 131–133.

[*42*] Wesley, L. D., "Influence of Stress Path and Anisotropy on the Behaviour of a Soft Alluvial Clay," Ph.D. thesis, University of London, 1975.

[*43*] Sandroni, S. S., "The Strength of London Clay in Total and Effective Stress Terms," Ph.D. thesis, University of London, 1977.

[*44*] Chandler, R. J., and Gutierrez, C. I., "The Filter Paper Method of Suction Measurement," *Geotechnique* Technical Note, Vol. 36, No. 2, 1986, pp. 265–268.

[*45*] Houlsby, G. T., and Nageswaran, S., "A Study of Consolidation with Radial Drainage," presented at Critical State Soil Mechanics Workshop, Cambridge University, 1982.

[*46*] Germaine, J. T., "Laboratory Measurement of Clay Behavior," Lecture 4, MIT Special Summer Course I.608 on Recent Developments in Measurement and Modeling of Clay Behavior for Foundation Design, Department of Civil Engineering, Massachusetts Institute of Technology (MIT), Cambridge, MA, 1985.

[*47*] Davies, P., "Creep Characteristics of Three Undisturbed Clays," Ph.D. thesis, University of London, 1975.

[*48*] Kolbuszewski, J. J., "An Experimental Study of the Maximum and Minimum Porosities of Sands," *Proceedings,* Second International Conference on Soil Mechanics and Foundation Engineering, Rotterdam, Vol. 1, 1948, pp. 158–165.

[*49*] Chaney, R. C., and Mulilis, J. P., "Suggested Method for Soil Specimen Remoulding by Wet-Raining," *Geotechnical Testing Journal, ASTM,* Vol. 1, No. 2, 1978, pp. 107–108.

[50] Battaglio, M., Bellotti, R., and Pasqualini, E., "Pluvial Deposition for the Preparation of Sand Specimens," (in Italian), *Rivista Italiana di Geotecnica,* Anno XIII, No. 2, 1979.
[51] Gilbert, P. A., "Investigation of Density Variation in Triaxial Test Specimens of Cohesionless Soil Subjected to Cyclic and Monotonic Loading," Technical Report GL-84-10, U.S. Army Waterways Experiment Station, Vicksburg, MS, 1984.
[52] Ladd, R. S., "Preparing Test Specimens Using Undercompaction," *Geotechnical Testing Journal, ASTM,* Vol. 1, No. 1, 1978, pp. 16–23.
[53] Hight, D. W., "Laboratory Testing: Assessing BS5930." *Proceedings,* Twentieth Regional Meeting of Engineering Group of the Geological Society, University of Sidney, Vol. 11, 1984, pp. 79–85.
[54] Skempton, A. W., "Horizontal Stresses in an Overconsolidated Eocene Clay," *Proceedings,* Fifth International Conference on Soil Mechanics and Foundation Engineering, Paris, Vol. 1, 1961, pp. 351–357.
[55] Black, K. D. and Lee, K. L., "Saturating Laboratory Samples by Back Pressure," *Journal of the Soil Mechanics and Foundation Division, American Society of Civil Engineers,* Vol. 99, No. SM1, 1973, pp. 75–93.
[56] Strachan, P., "Alternative Test Method for Ensuring Full Saturation in Triaxial Samples," *Geotechnical Testing Journal, ASTM,* Vol. 8, No. 1, 1985, pp. 43–46.
[57] Wissa, A. E. Z., "Pore Pressure Measurement in Saturated Stiff Soils," Proceedings, Paper 6670, *Journal of the Soil Mechanics and Foundation Division, American Society of Civil Engineers,* Vol. 95, No. SM4, 1969, pp. 1063–1073.
[58] Buri, B. P., "The Influence of Secondary Consolidation on Overconsolidation on the Behaviour of a Soft Alluvial Clay," Ph.D. thesis, University of London, 1978.
[59] Pollard, W. S., Sangrey, D. A., and Poulos, S. J., "Air Diffusion Through Membranes in Triaxial Tests," *Journal of the Geotechnical Engineering Division, American Society of Civil Engineers,* Vol. 103, No. GT10, 1977, pp. 1169–1173.
[60] Lowe, J., and Johnson, T. C., "Use of Back Pressure to Increase Degree of Saturation of Triaxial Test Specimens," *Proceedings,* Research Conference on Shear Strength of Cohesive Soils, American Society of Civil Engineers, 1960, pp. 819–836.
[61] Chaney, R. C., Stevens, E., and Sheth, N., "Suggested Test Method for Determination of Degree of Saturation of Soil Samples by B value Measurement," *Geotechnical Testing Journal, ASTM,* Vol. 2, No. 3, 1979, pp. 158–162.
[62] Rad, S. N., and Clough, G. W., "New Procedure for Saturating Sand Specimens," *Journal of the Geotechnical Engineering Division, American Society of Civil Engineers,* Vol. 110, No. 9, 1984, pp. 1205–1218.
[63] Lambe, T. W., "Stress-Path Method," *Journal of the Soil Mechanics and Foundation Division, American Society of Civil Engineers,* Vol. 93, No. SM6, 1967, pp. 309–331.
[64] Hight, D. W., "Laboratory Investigations for Sea-bed Clays," Ph.D. thesis, University of London, 1983.
[65] Ladd, C. C., and Foott, R., "New Design Procedure for Stability of Soft Clays," *Journal of the Geotechnical Engineering Division, American Society of Civil Engineers,* Vol. 100, No. GT7, 1974, pp. 763–786.
[66] Atkinson, J. H., "Simple and Inexpensive Pressure Control Equipment for Conventional and Stress Path Triaxial Testing of Soils," *Geotechnique,* Vol. 35, No. 1, 1985, pp. 61–63.
[67] Menzies, B. K., "Soil Testing System," *Geotechnical News,* Vol. 1, No. 3, 1984, pp. 38–39.
[68] Coatsworth, A. M., and Hobbs, N. B., "Computer Control Triaxial Soil Testing Equipment in a Commercial Laboratory," *Ground Engineering,* Vol. 17, No. 7, 1984, pp. 19–23.
[69] Law, K. T., "A Servo System for Controlled Stress Path Tests," in *Laboratory Shear Strength of Soil, ASTM STP 740,* American Society for Testing and Materials, Philadelphia, 1981, pp. 164–179.
[70] Jardine, R. J., "Investigations of Pile-Soil Behaviour with Special Reference to the Foundations of Offshore Structures," Ph.D. thesis, University of London, 1985.
[71] Baldi, G., Bellotti, R., Ghionna, V., Jamiolkowski, M., and Pasqualini, E., "Cone Penetration Testing and Experience on O.C. Sands," presented at American Society of Civil Engineers National Convention, St. Louis, 1981.
[72] De Alba, P., Baldwin, K., Janoo, V., Roe, G., and Celikkol, B., "Elastic-Wave Velocities and Liquefaction Potential," *Geotechnical Testing Journal, ASTM,* Vol. 7, No. 2, 1984, pp. 77–87.
[73] Dyvik, R., and Madshus, C., "Lab Measurements of G_{max} Using Bender Elements," presented at American Society of Civil Engineers National Convention, Detroit, Oct. 1985.
[74] Gens, A., "Stress–Strain and Strength Characteristics of a Low Plasticity Clay," Ph.D. thesis, University of London, 1982.

Suzanne Lacasse[1] and Toralv Berre[1]

STATE-OF-THE-ART PAPER

Triaxial Testing Methods for Soils

REFERENCE: Lacasse, S. and Berre, T., "**Triaxial Testing Methods for Soils,**" *Advanced Triaxial Testing of Soil and Rock, ASTM STP 977,* Robert T. Donaghe, Ronald C. Chaney, and Marshall L. Silver, Eds., American Society for Testing and Materials, Philadelphia, 1988, pp. 264–289.

ABSTRACT: The paper presents the 1986 practice at the Norwegian Geotechnical Institute (NGI) for triaxial testing of soils that are fully saturated in situ. The test procedures for specimen mounting, saturation, consolidation, and static and cyclic shearing are outlined. Sample disturbance, specimen height, end friction, and anisotropic consolidation are discussed at length. Simplified procedures for anisotropic consolidation according to soil types are proposed. Sources of error are mentioned. A new method to measure the initial shear modulus in triaxial soil specimens is described.

KEY WORDS: triaxial test, procedures, consolidation, trimming, shear, cyclic load, test error, initial shear modulus

Triaxial tests were originally used to determine shear strength parameters when the vertical stress increased while the horizontal stress was kept constant. It was gradually realized that laboratory specimens ought to be subjected more closely to the same stresses and stress changes as in the field. Equipment and procedures were then developed so that any combination of vertical and horizontal stress could be applied.

This paper presents the 1986 practice at the Norwegian Geotechnical Institute (NGI) for triaxial testing of soils. The authors' aim was not to deal in detail with all aspects of triaxial testing. Rather, several specific topics were selected for discussion because of their difficulty and impact on soil parameters. Sample disturbance, specimen height, end friction, and anisotropic consolidation are discussed at length. Simplified anisotropic consolidation procedures are proposed as a function of soil type. General guidelines are offered with respect to triaxial equipment, specimen mounting procedures, data presentation, and sources of errors in the triaxial test. A new method to measure the initial shear modulus in triaxial soil specimens is presented. Recommendations for further developments are made.

Triaxial Equipment

Figure 1 presents the layout for a triaxial test. The specimen, enclosed in a rubber membrane, is loaded by the piston through the top of the cell by either a motor-driven press, deadweights on a hanger, or by an air-operated double-acting piston on top of the loading frame.

Valve selector blocks for cell pressure and pore pressure are connected to the triaxial cell

[1] Research engineer and head of laboratory, respectively, Norwegian Geotechnical Institute, P.O. Box 40 Taasen, N-0801 Oslo 8, Norway.

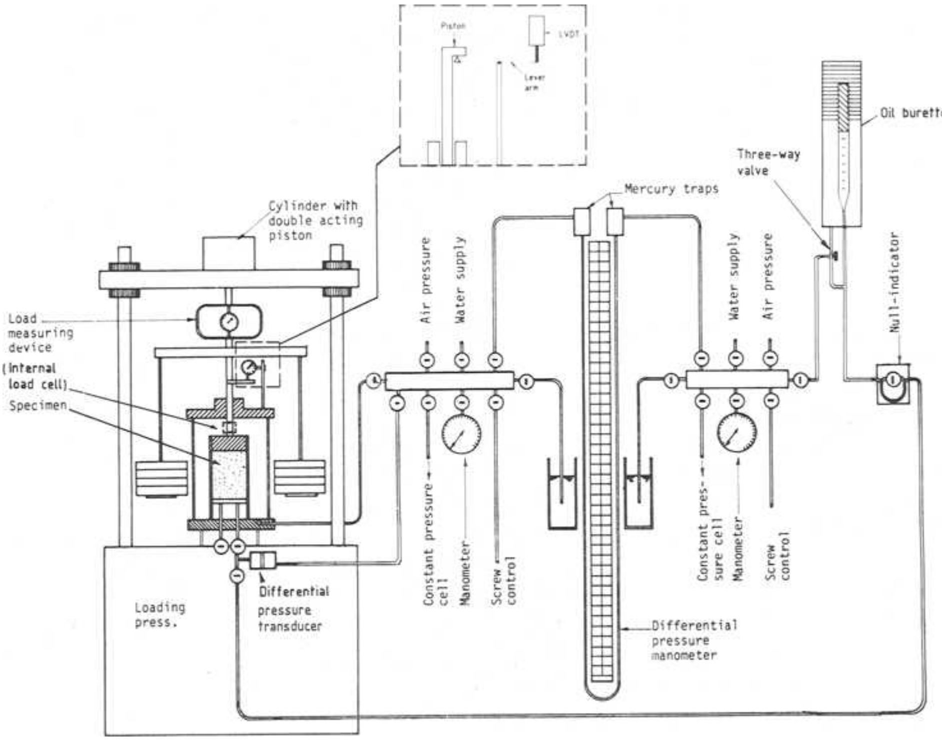

FIG. 1—*Layout of a typical triaxial test unit (additional consolidation units not shown).*

with outlets to a screw control, a Bourdon gauge, a constant pressure cell, and an air pressure supply.

A mercury differential manometer can measure the difference between the cell and pore pressures very accurately. The triaxial test unit is also equipped with electronic transducers for automatic data logging.

For maximum utilization of a loading press and its auxiliary equipment, two extra consolidation units can be included in the triaxial test unit. A consolidation unit consists of a triaxial cell where the piston can be locked, a cell pressure unit, and hangers for application of deadweights on the piston.

Two types of triaxial cells are in use at NGI, one for static loading and one for cyclic loading. Andresen and Simons [*1*] and Berre [*2,3*] have described the equipment, including recent improvements. The cell for cyclic loading is also superior for static loading and will probably gradually replace the cells presently used for static loading.

Sampling Disturbance

To obtain reliable stress–strain strength and pore pressure parameters from undisturbed specimens, the quality of the specimens must be reasonably good. Material at the ends of the sample within 1.5 or preferably 3 times the sample diameter should not be used for triaxial testing unless X-ray inspection indicates that the material is really undisturbed [*4*].

For clays, the volumetric strain when consolidating the specimen to the in situ effective stresses, ϵ_o, can be used as an indication of the sample quality. Berre [*3*] suggested the following criterion to evaluate sample quality from the volumetric strain of soft sensitive onshore clay specimens, measured during anisotropic consolidation to the in situ stresses:

ϵ_o, %	Test Quality
<1	very good to excellent
1–2	good
2–4	fair
4–8	poor
>8	very poor

The results of oedometer tests at two offshore sites (Fig. 2*a*) were used to evaluate this criterion. If one uses a volumetric strain of, for example, 1.5% as the maximum allowable strain, one would reject 78% of what are considered high quality specimens in the case of a soft clay deposit and 20% in the case of a stiff clay deposit. (The preconsolidation stresses were obtained by averaging Casagrande's and Janbu's methods). A criterion of 1.5% volumetric strain for soft clays may thus be too strict in practice. Data compiled by Kleven[2] at NGI show that one should consider allowable strain as a function of stress history (ratio p'_c/p'_o) and depth (Fig. 2*b*) [5].

Table 1 summarizes the results of an investigation carried out at NGI on the effect of sample disturbance on the undrained shear strength at small strain [6–8]. The soil samples were Drammen clay, consolidated anisotropically past their preconsolidation stress, and all were unloaded to an overconsolidation ratio of 2.5. Reference specimens, sheared without any kind of disturbance, were called "perfect." The diameter of the reference specimens was 80 mm.

The specimens denoted "sampled" in Table 1 were quickly unloaded and taken out of the triaxial cell, trimmed to a smaller diameter (54 mm), mounted into a new triaxial cell, and then reconsolidated. "Sampled, fully remolded" means that the specimens were "sampled" as described above, and in addition completely remolded before being formed into new specimens and remounted into the cells. "Strongly deformed but not sampled" means that the specimens were disturbed by deforming them about 7% under undrained conditions and thereafter reconsolidated to the same consolidation stresses. The compression tests were deformed +7% and the extension tests −7% before reconsolidation.

After the sampling treatment described above, some of the specimens were reconsolidated to p'_o (Test Series 1), that is, loaded anisotropically to the same stresses as they carried after the laboratory overconsolidation, while some were consolidated anisotropically to p'_c and then unloaded anisotropically to p'_o (Test Series 2). The stress p'_c here is the maximum vertical stress the specimens were subjected to during the first consolidation. Table 1 also gives the volumetric strain ϵ_{vol} which took place during the reconsolidation.

The test results show that

1. $p'_c \rightarrow p'_o$-consolidation tends to give too high strengths and may lead to unconservative designs.
2. The undrained shear strength in triaxial extension can be overpredicted by as much as 60 to 80% because of disturbance.

Hight et al. [9], in their discussion of the effect of sampling disturbance, referred to a strain path analysis of the tube sampling process made by Baligh [10]. According to Baligh,

[2] A. Kleven, Private communication, NGI, July 1985.

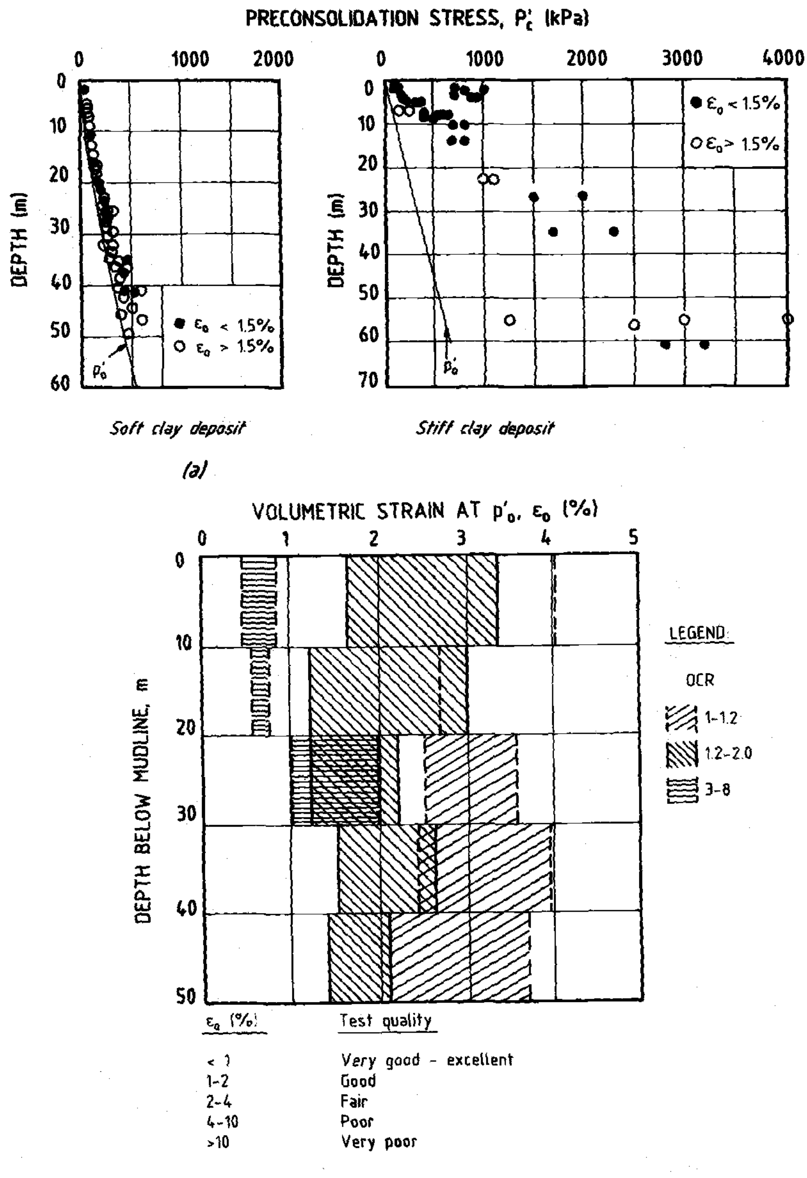

FIG. 2—(a) *Preconsolidation stress from high quality clay specimens.* (b) *Strain at in situ overburden stress from oedometer tests on high quality clay samples* [5].

the degree of disturbance at the centerline of a sampling tube is a function of the ratio between the diameter of the tube and the wall thickness. For the 3-in. (7.6-cm) tubes used in the North Sea, this ratio is about 40. According to Baligh's data, an element on the centerline of the tube should, during the sampling process, first be compressed axially about 1%, then be extended back to zero strain and further to −1% axial strain, and finally be compressed back to zero strain.

TABLE 1—*Effect of sample disturbance. Drammen clay, OCR = 2.5,* I_p *= 27%.*

		Reconsolidation			
		Test series 1, p'_o-consolidated		Test series 2, $p'_c \rightarrow p'_o$-consolidated	
Test Specimen	Stress System	ϵ_{vol}, %	τ/τ_{ref}	ϵ_{vol}, %	τ/τ_{ref}
Sampled, undisturbed	compression	0.7	0.89	0.6	1.03
	extension	0.9	1.02	1.0	1.12
Sampled, fully remolded	compression	12.4	0.41	15.4	1.09
	extension	15.7	1.00	14.6	1.20
Strongly deformed, but not sampled	compression	1.3	0.96	3.6	1.24
	extension	1.8	1.64	5.5	1.79

τ = Undrained shear resistance at 2% axial strain or the peak value if this occurred before 2% axial strain.

τ_{ref} represents "perfect" sample.

Figure 3 shows the results of eight triaxial tests on plastic clay from Drammen. All specimens were first K_o consolidated to a common stress well above their in situ preconsolidation stress. Then four of the tests were used to study the effect of sampling disturbance at an overconsolidation ratio (OCR) of 1, and four were K_o unloaded to an OCR of 2.5 before the study of the effects of sampling disturbance. The tests marked "disturbed" were strained according to Baligh's data and allowed to drain at the same stresses as they carried before the straining, and then sheared undrained. This process should, in principle, duplicate what happens when a tube sample is taken in the field and the material later reconsolidated back in the laboratory to the in situ stresses. The stress-strain plots should indicate the effect of the sampling disturbance on the undrained shear strength behavior of reconsolidated specimens. The tests in Fig. 3 experienced the following volumetric strains during reconsolidation:

OCR	ϵ_{vol}, %
1.0	≈1.0
2.5	≈0.13

The following preliminary conclusions can be drawn from Table 1 and Fig. 3:

1. *Compression tests* (OCR = 1 and 2.5)—The peak shear strength is about the same for the disturbed and the undisturbed tests while the initial moduli are much lower for the disturbed tests. For OCR = 1, the shear resistance at high strains is much higher for the disturbed test.

2. *Extension tests* (OCR = 1 and 2.5)—The ultimate shear strengths and the initial moduli are higher for the disturbed than for the undisturbed tests.

Specimen Mounting

General

If the specimen is extruded with the sampling tube in a horizontal position, then the surface on which the sample is extruded must be lined up with and be at exactly the same

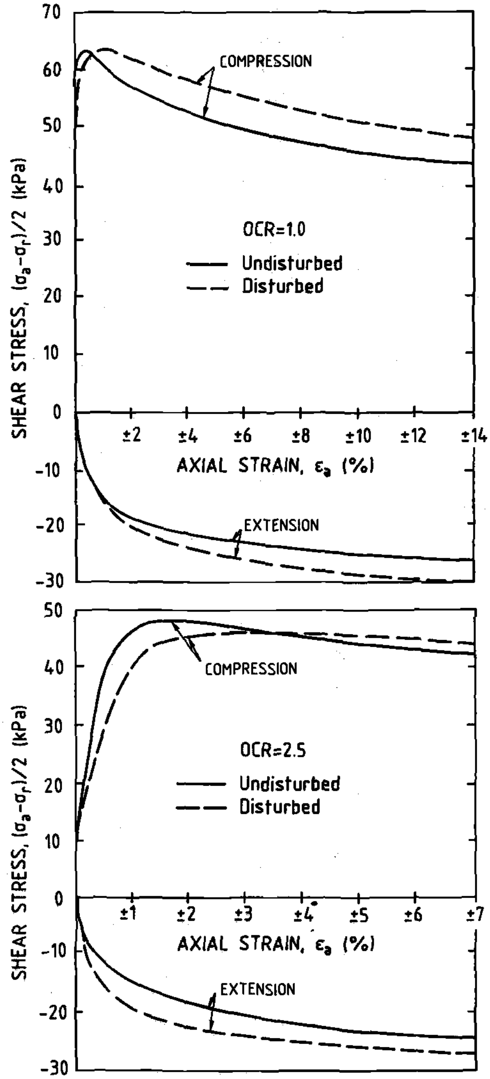

FIG. 3—*Comparison of triaxial tests on undisturbed and disturbed specimens. Drammen clay, OCR = 1.0 and 2.5.*

level as the sampling tube. The sliding friction between sample and table must be eliminated. The sample is extruded toward the top of the sampling tube. Foreign or disturbed material in the tube is discarded. At the top and bottom of the sampling tube, material within 1.5 or preferably 3 times the sample diameter is not used for triaxial testing. Extreme care is taken to avoid, as much as possible, deforming the specimen during the mounting process. The mounting is done in a cabinet with humidity around 90% to minimize evaporation from the specimen.

Undisturbed specimens, if less than 80 mm in diameter, are usually mounted with full cross section. Larger specimens are trimmed down to a diameter of preferably 54, 71, or 80 mm, and never less than 35 mm. If no provisions are made to reduce end friction, the specimen height is from 1.85 to 2.25 times the diameter. For well graded materials, the maximum dimension of the largest soil particle should not exceed 1/6 of the specimen diameter. For other materials, the maximum particle size should not exceed 1/10 of the specimen diameter. Grooves and holes in the ends of the specimens are filled with remolded material if they cannot be removed by further trimming and if a new sample cannot be trimmed. Grooves and holes in the ends greater than about 1/10 of the specimen diameter are cast in with gypsum. The end surfaces should be plane and perpendicular to the longitudinal axis of the specimen. The angle between an end surface and the longitudinal axis should not deviate from a right angle by more than ±0.6°. The height of the specimen is measured within ±0.1 mm with a height measuring device. To obtain the average diameter of the specimen, one measures the circumference at top, midheight, and bottom to the nearest ±0.1 mm with a flat strip. The entire sample preparation is done under such conditions that the volume of water evaporating during the process does not exceed 0.3% of the total volume of the specimen.

Coarse filter disks are kept dry during mounting to prevent swelling of the specimen by sucking in water from the filters. High air entry value filter disks are always kept saturated. For soils with a strong tendency to suck in water, the compartments behind high air entry value filter disks are filled with air.

The triaxial cell is usually filled with castor oil. Problems with leakage through the rubber membrane are then reduced. The castor oil also acts as a lubricant for the piston through the top of the cell.

The specimen is usually confined by one membrane made of natural rubber. Such membranes have very good mechanical properties. However, they tend to absorb some water especially when they are new. The initial absorption can be reduced if the membrane is stored in water some days before its use.

Normally and Slightly Overconsolidated Clay Specimens

The specimen is trimmed with a wire saw. If the clay is quick or extremely soft, extrusion is done vertically from the sampling tube directly into a cutting cylinder [*11,12*]. In a new version of the cutting cylinder [*3,13*], the membrane is mounted inside it. The sample is then pushed directly into the rubber membrane, and a small suction can be applied to the specimen before the cutting cylinder is removed. This procedure is used when the sample contains so much silt and sand that the specimen cannot stand upright unless supported laterally.

Tests carried out at NGI indicate that end friction is of minor importance for soft clays. Therefore, no attempts are made to reduce end friction for such clays.

Filter paper strips (four strips in spiral, see under *Heavily Overconsolidated Clay Specimens*) on the sides of the specimen are used for offshore samples, which are sheared at higher rates than onshore samples (see under *Static and Cyclic Shearing*). For both offshore and onshore testing, filter disks with two drainage tubes are placed both at the top and the bottom of the specimen.

For compression tests on very soft homogeneous clays, the paraffin method is often used [*14*]: the cell is filled with liquid paraffin, and no rubber membrane is used around the specimen. The interfacial tension between paraffin and pore water completely prevents the paraffin from penetrating into the pores of either the clay or the high air entry value filters. The rubber membrane correction, which for very soft clays can account for more than 10% of the measured shear stress at high strains, is completely avoided. The paraffin method has not given water–paraffin interface leakage problems in soft homogeneous clays, for effective horizontal stresses up to 100 kPa. Preliminary tests indicate that castor oil may be used instead of liquid paraffin.

Heavily Overconsolidated Clay Specimens

Jacobsen [*15*] found that the undrained shear strength for very stiff boulder clay increased by about 50% when decreasing end friction by the technique recommended by Roscoe [*16*] and Rowe and Barden [*17*] and using a height/diameter ratio equal to 1. According to Lee [*18*], the importance of using smooth ends increases with increasing tendency for dilatancy of the soil and is more important for cyclic than for static testing. To reduce end friction, heavily overconsolidated clays are always mounted between polished, stainless steel plates covered with silicone grease and one rubber membrane, as shown in Fig. 4. In special cases, three rubber membranes with grease in between have been used at each end to reduce end friction. However, very stiff specimens may tend to split up vertically at the ends if too many membranes are used.

Reducing end friction has two advantages:

1. Stresses and strains at large strains are much more homogeneously distributed over the whole specimen height. Pore pressure during undrained shearing can then be accurately measured for much higher rates of strain.
2. Too early formation of shear planes in "unstable," strongly dilatant soils can be prevented by using frictionless ends and *reducing the height* of the specimen. This may be more correct in cases where shear planes in the field cannot be formed easily [*15,19*].

Two aspects important for heavily overconsolidated clay specimens are looked at in more detail: (1) specimen height and (2) filter paper.

Specimen Height—Following Jacobsen's [*15*] work, Berre [*5,20,21*] obtained the following results from anisotropically consolidated undrained triaxial compression tests on plastic Drammen clay (I_p = 27%) (Table 2).

The term "rough" means that the filter and the test specimen have the same diameter and that no attempt was made to reduce end friction. The term "smooth" means that polished metal plates with silicone grease and rubber sheets (or membranes) were used at the ends instead of filter disks. To extend Berre's observations, the effects of height/diameter ratio

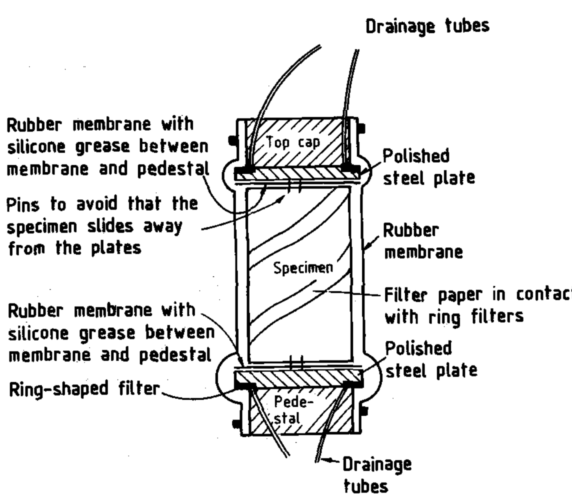

FIG. 4—*Reduction of end friction in triaxial tests.*

TABLE 2—*Effect of end friction and height/diameter* (H/D) *ratio in triaxial tests on Drammen clay with OCR between 1 and 4.*

Consolidation	Overconsolidation Ratio (OCR)	H/D Ratio	Conclusions
Anisotropic to p'_o	1.2–1.5	1.62	Tests with smooth ends and rough ends agree.
Anisotropic to 1.3 p'_c	1.0	1.11 1.85	Tests with different H/D agree, both had rough ends.
Isotropic K_o = 1.0	4.0	1.85	Tests with smooth ends and rough ends agree.

and end friction were investigated on Drammen clay specimens with an overconsolidation ratio of 40. Figure 5 presents the test results obtained for triaxial compression and triaxial extension tests. Figure 6 reproduces the early portion of the stress–strain curve (axial strain between 0 and 1%) at a much larger scale.

The results show that

1. The use of smooth ends and a height/diameter ratio of 1 instead of 2 resulted in a higher strength in compression, but only at axial strains higher than 10%.
2. In triaxial extension, no differences were seen for specimens with height/diameter ratios of 2 and 1. Rough ends were used for both the high and the low specimens.
3. The initial part of the stress–strain curve for the compression test on the low specimen with the rough ends is steeper than for the high specimen with rough ends, indicating that false deformations are less pronounced for rough-end tests. The curves for the tests with smooth ends indicate that false deformations are higher for smooth-end tests than for rough-end tests. The determination of the modulus at low strain level appears therefore to be more reliable from tests with high specimens and rough ends.

Filter Paper—Four strips of filter paper are placed in spiral on the side of the specimen and down to the ring filter. The inclination of the spirals is chosen such that they do not affect the deformation of the specimen when it is sheared undrained.

Shear Mode	Inclination of Filter Strip
Undrained compression	1:1.3 (1 is vertical distance and 1.3 is distance along the specimen perimeter.)
Undrained extension	1:1.5
Undrained two-way cycling	1:1.4

The filter paper is soaked in water at approximately the same salt concentration as the pore water of the clay, but free water on the surface of the paper is wiped away before it is placed on the specimen. Teflon® tape is placed over the edge of the rubber membrane on the smooth end plates where the filter papers come on the plates to avoid the silicone grease clogging the filter paper drain. The inclination of the filter paper strips is chosen such that there should be a minimum of deformation of the strips during shearing. However, in zones with intense straining (for example, necking zones in extension tests), the strips have been observed to fail in tension.

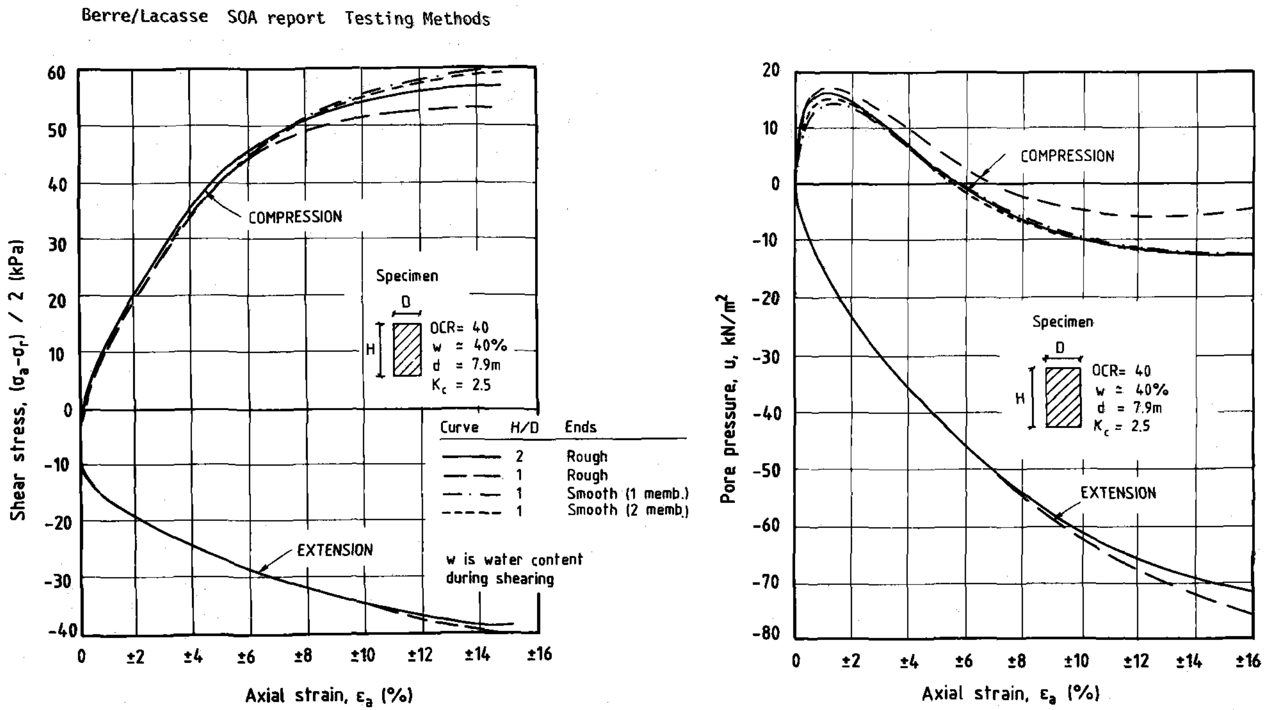

FIG. 5—*Effects of end friction and height/diameter ratio in triaxial compression and extension tests on Drammen clay, OCR = 40.*

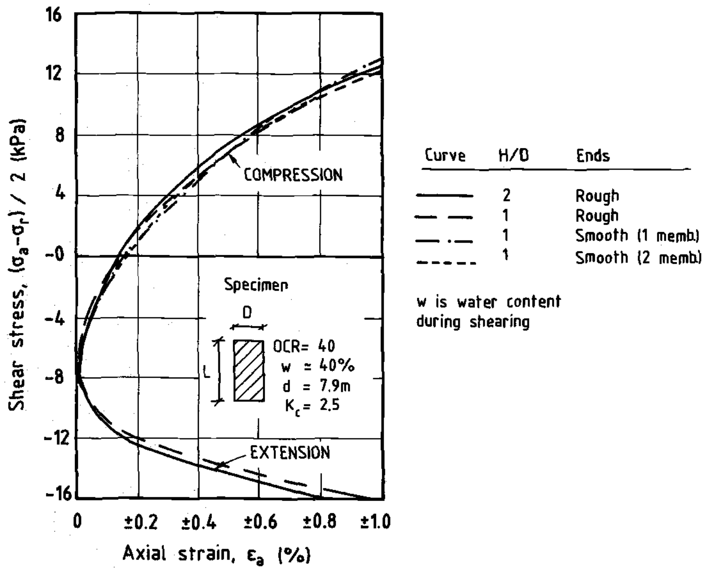

FIG. 6—*Detailed stress–strain curves at low strains showing effects of end friction and height/diameter ratio.*

Reconstituted Specimens (Sand and Silt)

The specimen is built in by tamping, vibrating, or raining the material into a cylindrical split mold stretching the rubber membrane on its inside. To ensure a uniform porosity in tamped or vibrated specimens, it is usually necessary to compact or vibrate the initial layers to higher porosities than the succeeding layers (undercompaction [*22*]).

A small variation to this procedure is, however, implemented at NGI: a constant height of soil is used in each layer rather than a constant mass.[3] Pluvial compaction is also used, especially for sands with a uniform grading, but it has proved difficult to obtain very low porosities with this method [*23*]. The free-end technique is not used for routine testing of reconstituted sand specimens.

Regardless of the method used to build in the specimen, extreme care should be taken to measure the initial diameter, height, and total dry mass of the specimen. The specimen should be saturated by first flushing carbon dioxide through the specimen and then deaired water. Before removing the split mold, a suction should be maintained until a cell pressure of about +5 kPa has been applied.

After shearing, it should be checked that the upper and lower halves of the specimen have been deformed approximately equally. Otherwise, the mounting specifications should be adjusted to achieve this in subsequent tests.

If a sand specimen does not collapse under its own weight, the mounting is done in the same manner as for clays.

Application of Initial Cell Pressure

When the triaxial cell has been filled with fluid, a cell pressure equal to the estimated initial negative pore pressure in the specimen is applied. The dry filters (and the dry compartments behind high air entry value filter disks) are flushed with water at approximately

[3] C. Chan, Private communication to R. S. Ladd, 1985.

the same salinity as the pore water of the specimen. With a mercury null-indicator connected to the specimen, the volume change is monitored. The cell pressure is continuously adjusted until no more volume change takes place. The cell pressure at this time is called the "swelling" pressure. For a fully saturated material, the swelling pressure is equal to the initial negative pore pressure in the specimen. The devices for measuring vertical displacement and volume change of the specimen should now be set to zero. The cell pressure is then increased to twice the swelling pressure, but never higher than the specified maximum radial consolidation stress. The specimen is allowed to consolidate fully, usually overnight, under this pressure.

Saturation

Because the specimens tested are fully saturated in the field, it is attempted, after application of the initial cell pressure, to saturate as well as possible the specimens, the filter disks, and pore pressure measuring system. This is done partly by increasing the initial saturation as much as possible and partly by applying a back pressure prior to further consolidation.

Initial Saturation

To increase the initial degree of saturation for sand and silt specimens, specimens may be flushed first with carbon dioxide and thereafter with deaired water. Flushing with CO_2 replaces the air in the test specimen with a gas of greater solubility in water. The volume of carbon dioxide passing through the material to be saturated should not be less than twice the volume of voids in the material. For very loose specimens, care must be taken to ensure that the carbon dioxide stream does not destroy the specimen. The gas pressure should not exceed 2 kPa, and the carbon dioxide drainage tube should be kept under water. These requirements are usually satisfied if the gas stream is left on for at least 20 min and if about three bubbles evacuate per second.

If the specimen is so loose that it is likely to change volume when saturated with water, the saturation with CO_2 is done during the mounting, usually just before the split mold is removed. For "undisturbed" sand and silt specimens, the permeability usually is too low to flush CO_2 through the specimen. However, it may still help to saturate parts of the specimen if only the filter disks are flushed with CO_2.

Rad and Clough [*24*] described a new technique to increase the initial saturation of sand specimens. The method first applies a high vacuum to the soil while avoiding increasing the effective stresses. After water percolation through the sand and a short waiting period under vacuum, the sand is saturated under back pressure.

Application of Back Pressure

During application of back pressure the difference between cell pressure and pore pressure is kept constant, equal to the initial cell pressure σ'_{ri} (which usually is equal to twice the swelling pressure). Deadweights are applied on the piston to keep it just in contact with the top cap. The back pressure is applied so slowly that usually almost no deformations take place. Based on earlier experience at NGI, the maximum allowable deformation during application of back pressure should be as small as possible and never greater than

$$H_i \cdot 0.001 \cdot \frac{\sigma'_{rcmax}}{\sigma'_{ri}}$$

where

H_i = initial specimen height,
σ'_{rcmax} = maximum effective radial consolidation stress, and
σ'_{ri} = initial effective cell pressure (usually equal to twice the swelling pressure).

The dial gauge is placed so that it is not influenced by the magnitude of the cell pressure.

For drained tests, a back pressure of 100 to 200 kPa is used. For undrained tests, it is attempted to reach a B-value equal to about 0.95 for static tests and 0.98 for cyclic tests. For soft clays, a back pressure of about 200 kPa may be sufficient. For very stiff clays and dense sands, back pressures up to 1500 kPa may be required. It seems to be more important to obtain a high B-value for dilatant than for nondilatant materials. For soft clays, B-values as low as 90% seem to be acceptable for static testing. If it proves difficult to obtain a satisfactory B-value, a constant volume test may be carried out instead of an undrained test.

Consolidation

Triaxial tests are usually consolidated under the same effective stresses as those carried out in the field before sampling. The cell pressure is increased such that the difference between the cell and the pore pressure becomes equal to the desired effective radial consolidation stress, and the piston force is increased or decreased until the axial stress is equal to the desired value of the axial effective consolidation stress.

K_o *Versus Simplified Consolidation Procedure*

During K_o consolidation, the stresses are applied such that no radial deformation of the specimen takes place. To consolidate to the in situ stresses and reach a correct ratio between radial and axial stress for an overconsolidated material by K_o consolidation, the specimen must first be K_o loaded to the preconsolidation stress, p'_c, and then K_o unloaded to the in situ stresses. Although excellent for research purposes, K_o consolidation is very time-consuming and therefore prohibitive in practice. In addition, consolidation through p'_c may lead to an overestimate of the undrained shear strength, as indicated by Table 1. Therefore, the specimen is consolidated anisotropically, directly to the in situ effective stresses, σ'_{ho} and σ'_{vo}. Originally this was done by a number of stress increments keeping, for each increment, the ratio between radial and axial stress equal to $\sigma'_{ho}/\sigma'_{vo}$, both for normally and overconsolidated materials. However, this procedure was found to be too time-consuming in practice. Berre [7] investigated the effect of the number of consolidation increments on the shear behavior in triaxial tests. He used good quality undisturbed Drammen clay specimens consolidated to about 1.2 times the preconsolidation stress. The plasticity index of the clay was about 27%.

Figure 7 presents the results of four triaxial tests, two sheared in compression, two sheared in extension. In one test series, consolidation to the *in situ* stresses was carried out in 18 increments to follow exactly the K_o line; in the second test series, only 2 stress increments were used to reach the same state of anisotropic effective stress. For triaxial compression, the test data show practically the same stress–strain curves, pore pressure–strain curves, and effective stress paths for the two methods of consolidation. For triaxial extension, the shear resistance is slightly higher for the test with the simplified procedure.

The above evidence combined with recent experience with overconsolidated and normally

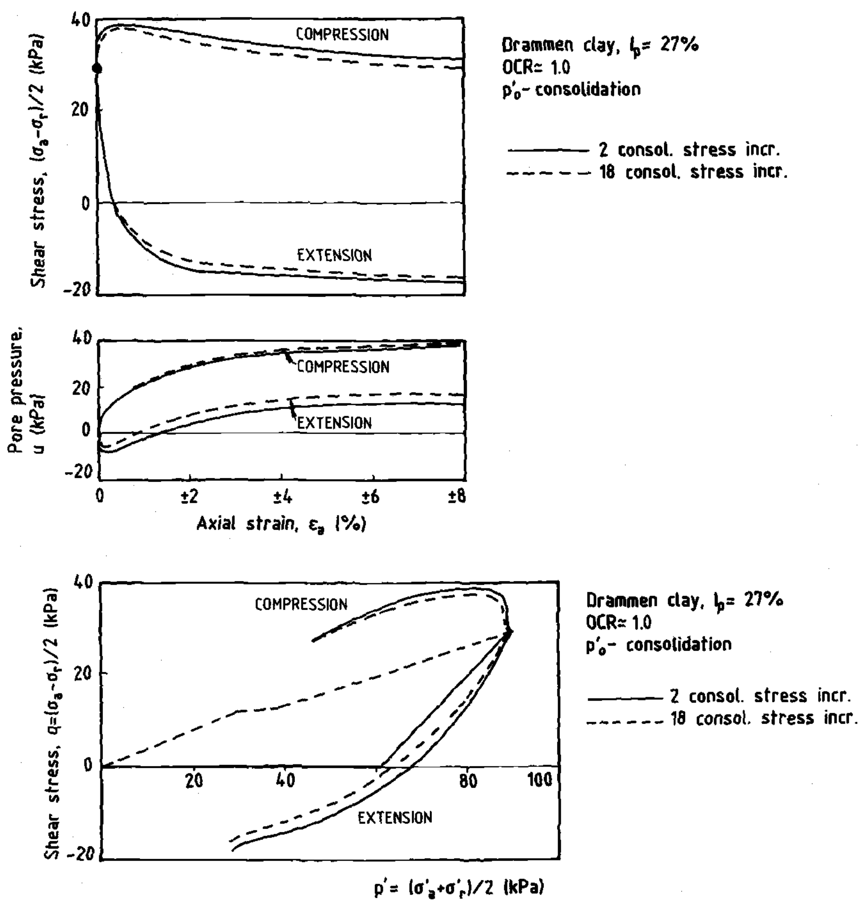

FIG. 7—*Comparison of* K_o *consolidation and simplified anisotropic consolidation in triaxial compression and extension tests on Drammen clays.*

consolidated clays from the North Sea leads NGI to propose the following simplified consolidation procedure:

1. For *clays and clayey materials with overconsolidation ratio less than 1.5 and other loose materials, load to the in situ stresses* in two increments of radial stress (OA and BC) and two increments of the deviatoric stress (AB and CD), as shown in Fig. 8*a*. The first isotropic effective stress cell increment plus the initial cell pressure (about twice the swelling pressure) should be no more than 0.5 times the in situ effective horizontal stress, σ'_{ho}, especially if large volumetric strains are expected. An isotropic effective stress greater than 0.5 times the in situ effective vertical stress risks loading the clay outside the yield surface, as illustrated in Fig. 8*b*. The conceptual behavior shown applies to a lightly overconsolidated clay. The position of the yield locus depends on the preconsolidation stress. Hight et al. [9,25] first expressed concern in this respect for low overconsolidation, low plasticity clays.

The deviatoric loading is usually done in four to six steps. A new step is not applied until the rate of axial strain is less than or equal to about 0.08%/h. Normally the deviatoric

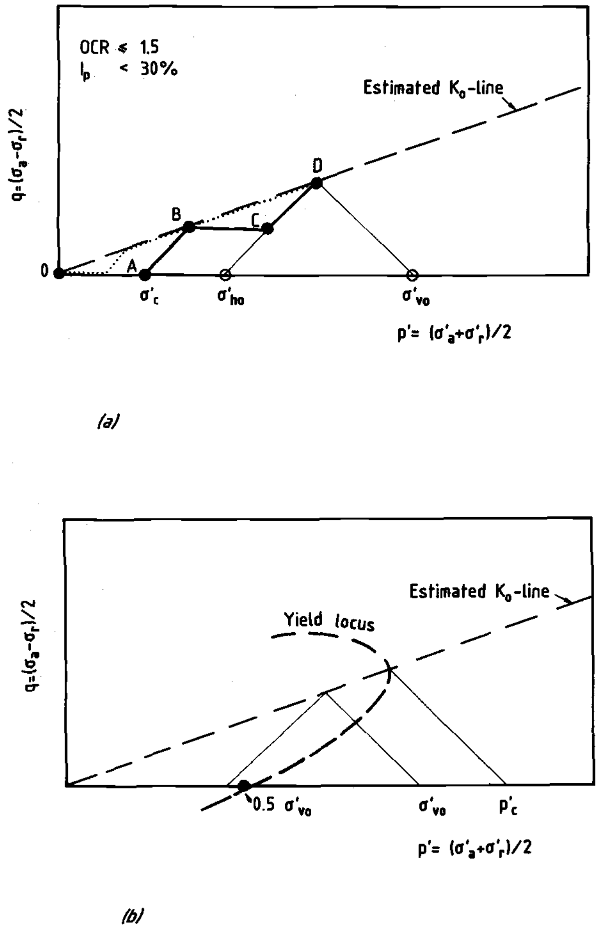

FIG. 8—*Proposed simplified consolidation stress path for lightly overconsolidated clays.* (a) K_o *versus simplified consolidation for lightly overconsolidated clay.* (b) *Hypothetical yield locus for lightly overconsolidated clay.*

loadings (AB and CD) take one day each. The second cell pressure increment is usually applied in the evening the same day as the deviatoric loading AB is finished.

2. For p'_o consolidation of *all other materials,* where little water expulsion is expected (that is, <2% volumetric strain), a "one-step" consolidation is used, with application firstly of a cell pressure equal to the in situ effective horizontal stress and secondly of a deviator stress equal to the deviatoric stress in situ.

The latter procedure applies also to heavily overconsolidated clays with in situ coefficient of earth pressure at rest greater than 1.0, as illustrated in Fig. 9. This approach is believed preferable to a procedure applying an effective cell pressure equal to the effective overburden stress and then increasing the mean effective stress to reach the in situ effective stresses (path OBA in Fig. 9). Along path OBA, swelling may occur, and load application is very cumbersome. Along path OCA, negligible additional compression occurs for a highly overconsolidated clay, and the actual load application is simpler.

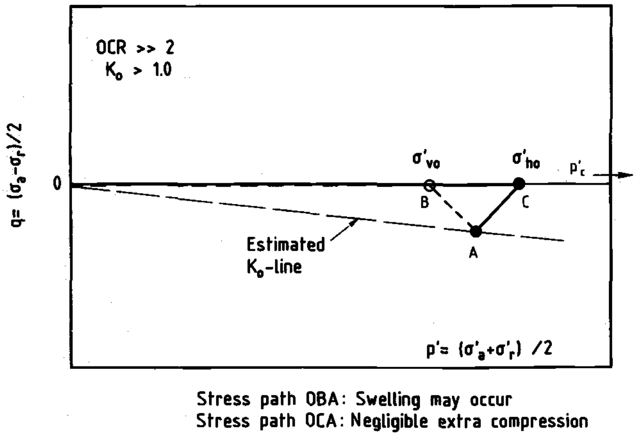

FIG. 9—*Proposed simplified consolidation stress path for highly overconsolidated clays.*

Testing of Shallow Samples of Normally Consolidated Soil

In the case of geotechnical design for pipelines, extremely low stresses need to be applied to soil specimens. Figure 10 illustrates one such case, where the difference between cell pressure and back pressure may be 1 to 10 kPa, the back pressure about 5 kPa, the piston load to be applied during consolidation may be negative, and the deviatoric load at failure only 1 kg. In the case shown, the specimen was tested without a membrane with the paraffin method.

Static and Cyclic Shearing

Before the start of shearing, one checks that practically no movement of the mercury in a 1.2-mm² boring null indicator takes place over a time interval of 2 min.

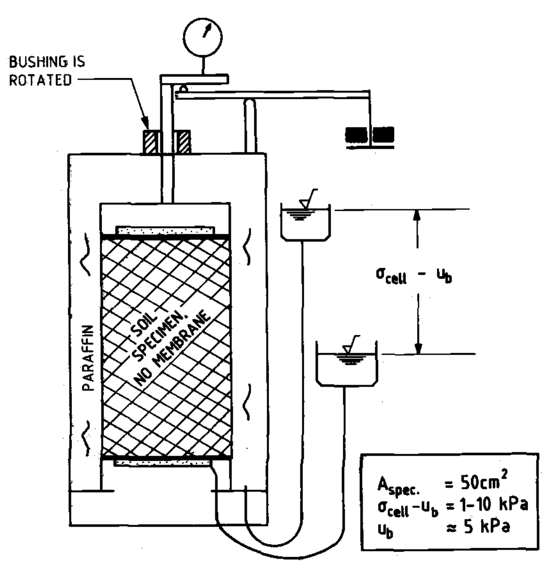

FIG. 10—*Stresses for triaxial testing of very shallow specimens.*

Static Tests

Figures 11 and 12 present the typical results plots for undrained triaxial compression and extension tests. (One can also combine these figures.) The specimens were anisotropically consolidated to the in situ effective stresses. Shear stress–strain and pore pressure–strain curves and two types of effective stress paths are provided. The consolidation test data are usually not exploited in routine testing, but consolidation stress increments and the respective axial and volumetric strains are tabulated.

For *undrained* tests on offshore clay specimens, the rate of axial strain is about 2%/h. The specimen is then surrounded by four filter paper strips in spiral, and the total axial strain during shearing is about 20%. For *undrained* tests on onshore clay specimens, the rate of axial strain is about 0.8%/h. No filter paper strips are used, and the total axial strain during shearing is about 7.5%. The reason for shearing onshore specimens more slowly is partly that failure may take place at very small strains for sensitive onshore clays and partly that loading in the field usually is much slower onshore. The strain rates given above apply to specimens with diameter 54 mm and height 110 mm.

Drained tests must be run so slowly that the excess pore pressure at the midheight of the specimen at failure is less than 2% of the radial effective consolidation stress.

Cyclic Tests

Figures 13 and 14 give examples of four plots prepared specifically for presentation of cyclic test results. Pore pressure and axial strain are presented as a function of number of cycles for both the preshearing and the undrained cycling parts of the test. Preshearing consists of consecutive parcels of, for example, 100 waves applied under undrained condi-

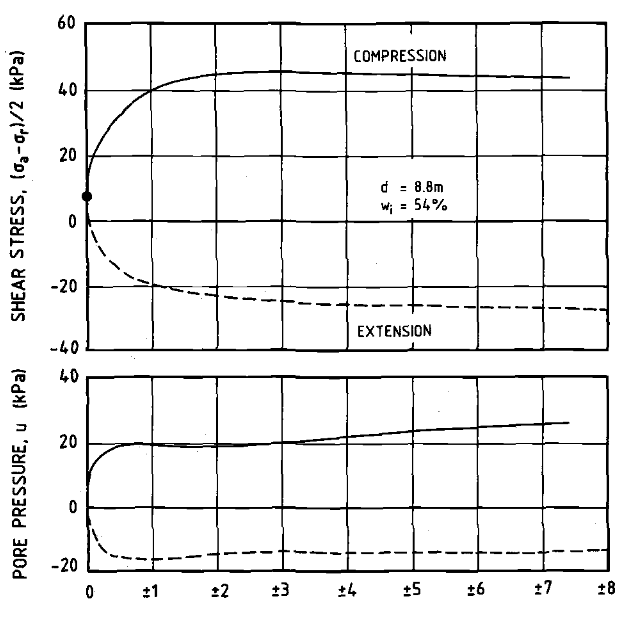

FIG. 11—*Typical results of static undrained triaxial tests on soft clay: stress–strain curves.*

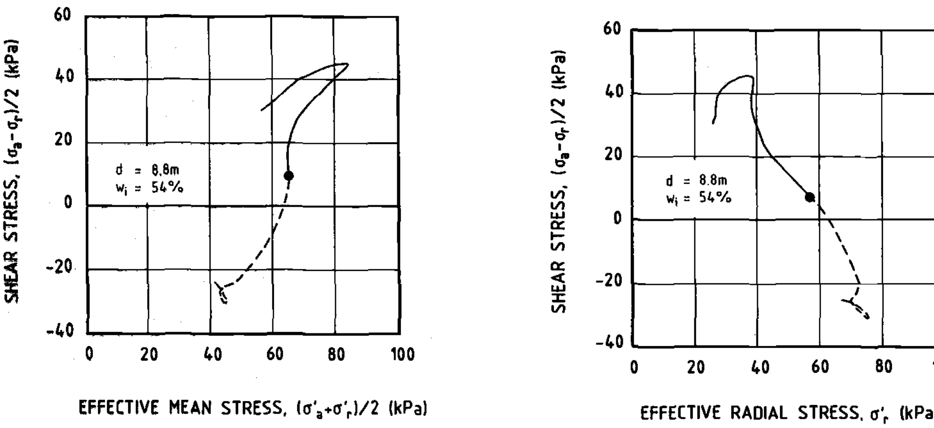

FIG. 12—*Typical results of static undrained triaxial tests on soft clay: effective stress paths.*

tions. Drainage is allowed between each parcel. The cyclic shear stress level during preshearing is very low (5% of effective consolidation stress, for example). Undrained cycling is the application of the actual cyclic stresses to be modeled, under undrained conditions. As part of the cyclic test results, the effective stress path and the detail of the cyclic pore pressure during cycling are also given. The sequence of each load cycle can also be given as a function of axial strain.

Load periods between 5 and 15 have been used so far, with 10 s most common for duplicating North Sea waves. Moreover, when frictionless end plates are used in connection with cyclic triaxial tests, the pore pressures will still be unevenly distributed to some degree within the specimen due to the rapid variation in the vertical stress. To allow the pore pressure to equalize, the cyclic loading is stopped after 500 and 1500 cycles. Equalization takes at least 15 min for clay specimens.

After undrained cycling has been completed, a monotonic undrained compression or extension test is run to study the effect of cyclic loading on the static shear strength. No drainage is allowed between the cycling and the monotonic loading, but the pore pressures reach equilibrium before the monotonic test is started.

Undrained Creep Tests

No perfect solution has been found for keeping the water content of the specimen sufficiently constant for undrained tests lasting several days. The best test technique consists probably of using the paraffin method with no rubber membrane around the specimen [*12*]. However with today's knowledge, this technique works well only for compression tests on soft homogeneous clays when the effective radial stress is less than about 100 kPa. If a rubber membrane is required, membranes made of natural rubber latex in combination with castor oil in the cell probably give a minimum of water migration. Castor oil in the cell seems to be preferable to deaired water because water tends to leak through the membrane and the leakage cannot easily be detected. Castor oil (resinous oil) in the cell seems to give a very small migration of water from the specimen into the membrane.

For undrained creep tests lasting several weeks, automatic data logging often results in an undesirable quantity of test data. The daily readings of strain and pore pressure are still best if taken manually.

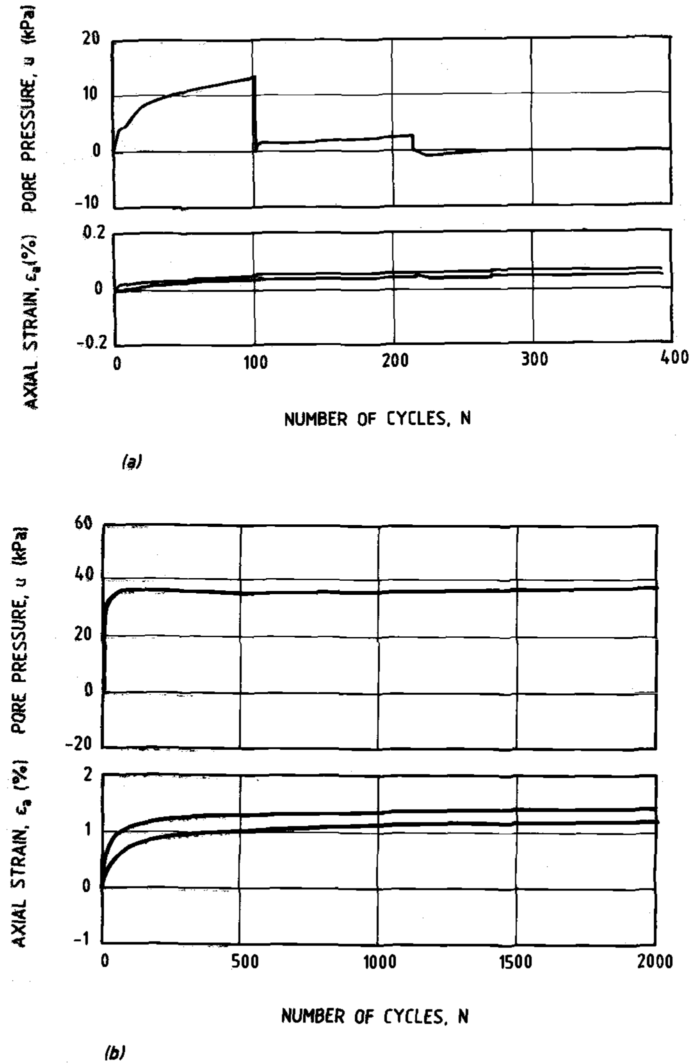

FIG. 13—*Typical results of cyclic undrained triaxial tests on dense sand: axial strain and pore pressure during* (a) *preshearing and* (b) *cycling.*

Strain Measurements

For ordinary tests the axial compression during shearing is still measured outside the cell, but two improvements have been made:

1. The piston through the top of the cell tilts slightly as a result of the rotation of the bushing. The vertical movement of the piston must therefore be measured as close to the axis of the piston as possible. To achieve this the movement of the piston is measured through a lever arm as shown in Fig. 1.
2. The linear variable differential transducer (LVDT) is no longer fixed to a dial gauge, because the variation in the dial gauge spring force probably tends to disturb the measurement of very small movements.

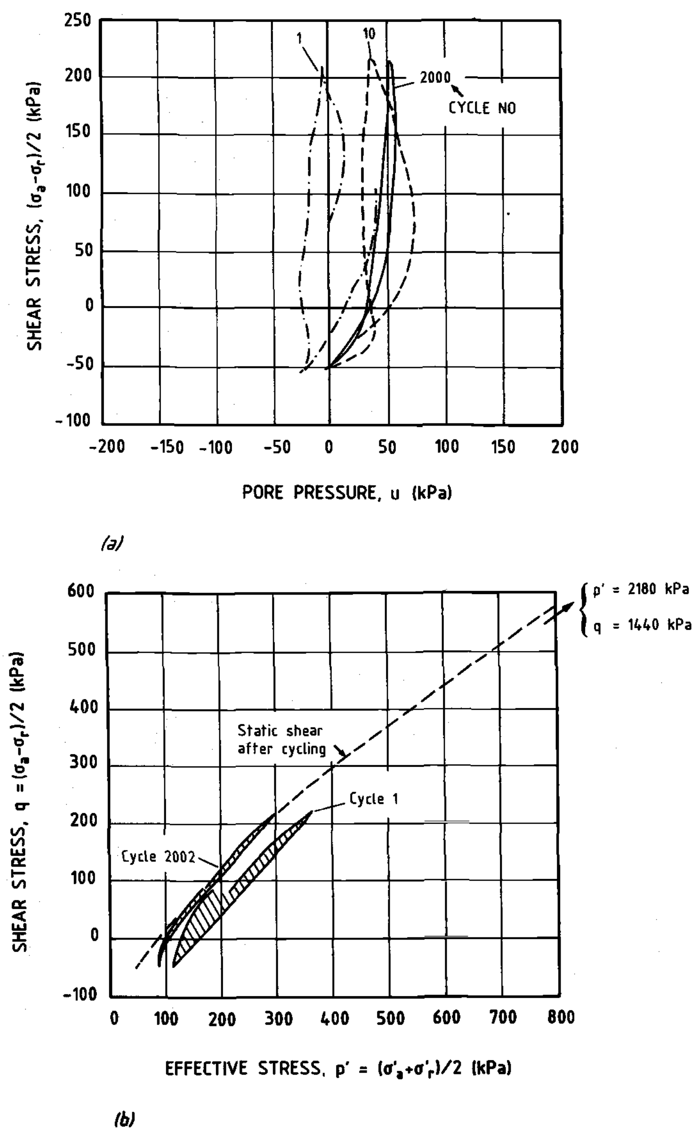

FIG. 14—*Typical results of cyclic undrained triaxial tests on dense sand:* (a) *cyclic pore pressure and* (b) *effective stress paths during cycling.*

The measurement of strains in the range 10^{-3} to 10^{-1}% has long been unsatisfactory until the recent work at Imperial College by Burland and his coworkers [*26–30*]. At NGI, work has recently been initiated in this area to measure displacements inside the cell directly on the specimen. A simpler and possibly as accurate approach as that at Imperial College, using flexible strain gauged strips of spring metal mounted on footings glued to the membrane, is being developed at NGI. An initial study[4] indicates that accurate measurements can be obtained during static and cyclic loading.

[4] N. S. Rad, Private communication, NGI, July 1986.

Sources of Error

To minimize *piston friction,* the pistons and rotating bushings used at NGI are nitrid hardened. The bushing is rotated by a small electric motor. To check the magnitude of piston friction, several comparisons of inner and outer deviatoric load measurements were made. They showed that the friction between piston and bushing is negligible.

According to Silver [31], *top cap tilt* may lead to scattering in test results when testing rigid materials, especially for cyclic tests. A rigid connection between piston and top cap should be considered in this case. Such a connection will make it easier to avoid false deformation at this point.

Using "*smooth end*" techniques can cause problems with membrane sample–end plate contact at each end of the specimen and with false deformations. Whenever possible, one should try to keep the test technique at its simplest, with respect to end restraint, filter paper, and so forth.

Part of the vertical load applied in the triaxial test is carried by the *rubber membrane.* In general, during consolidation, rubber membrane corrections are negligible in relation to the effective consolidation stresses. The widely used Duncan and Seed [32] formulas for membrane corrections assume no slippage between specimen and membrane. Visual observations made during consolidation and undrained shearing of plastic clay from Drammen confirmed that the membrane and specimen for this clay deform together, up to axial strains of about 15%. This axial strain is a total strain, that is, the sum of the axial strains during consolidation and shear. At higher strains, the membrane showed signs of folding. To avoid the problem of membrane folding and to avoid an uncertainty in the effective stresses just before the start of shearing, especially for rebounded clay specimens having deformed significantly during consolidation, a method for pretensioning rubber membranes is in use at NGI. This method more or less eliminates membrane stresses at the end of consolidation. The pretensioning method has, so far, only been used for SHANSEP-type tests on clay that have been highly overconsolidated in the laboratory. In this case, the final consolidation stresses are small, the consolidation strains are very large, and the rubber membrane correction is, therefore, very important relative to the final consolidation stresses.

False deformations can represent a large portion of the measured deformation at low strain levels. The problem is especially important in static extension and cyclic tests when the shear stress passes through zero. False deformation should be considered and corrected for when evaluating shear modulus and damping at low strain levels.

The *duration of each consolidation increment* should be kept approximately constant for research tests run for comparison purposes. Deviations may be acceptable for the early consolidation steps, but it is important that the last two consolidation increments have consistent reference times.

Initial Shear Modulus from Bender Elements

Piezoceramic bender elements were first used in soil testing by Shirley [33] and Shirley and Hampton [34]. The bender element, a plate which protrudes cantilevered into the soil specimen, bends from side to side pushing the soil. It has a large coupling factor with the soil and produces a shear wave which propagates perpendicularly to the soil particle motion. Shultheiss [35–37] and Hamdi and Taylor-Smith [38] used bender elements mounted in various laboratory apparatus to measure the shear wave velocity in a soil specimen. NGI installed the bender elements in its geotechnical testing devices and compared the results with results from the resonant column device.

A piezoceramic bender element is an electromechanical transducer capable of converting mechanical energy (movement) either to or from electrical energy. The element itself consists

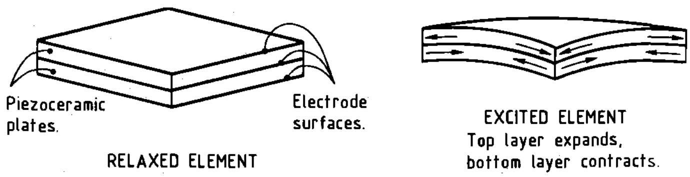

FIG. 15—*Piezoceramic bender element before and after excitation voltage is applied* [39].

of two thin piezoceramic plates rigidly bonded together with conducting surfaces between them and on the outer surfaces (Fig. 15). The polarization of the ceramic material in each plate and the electrical connections are such that when a driving voltage is applied to the element, one plate elongates and the other shortens. The net result is a bending displacement which is greater in magnitude than the length change in either of the two layers (plates). When the element is forced to bend, one layer goes into tension and the other into compression. This results in an electrical signal which can be measured through wire leads. Figure 15 shows the shape of an element before and after a driving voltage is applied [*39*].

The bender element is placed in a slot in the pedestal or top cap in the triaxial cell as shown in Fig. 16. The soil particles move in the same back and forth movement as the cantilevered tip of the element, resulting in shear waves propagating through the specimen in a direction parallel to the length of the relaxed element. There is good impedance match between the cantilevered bender element and the soil.

Figure 17 describes the measurement technique with the piezoceramic bender elements. The bender element at one end of the triaxial specimen generates the shear wave pulse. A second element is used to determine the arrival time of the shear wave at the other end of the specimen, and gives a direct measurement of shear wave velocity. The measurement is simpler than that for a resonant column test and can be made in any of the standard geotechnical testing devices. A very fast electronic switch or a function generator is used

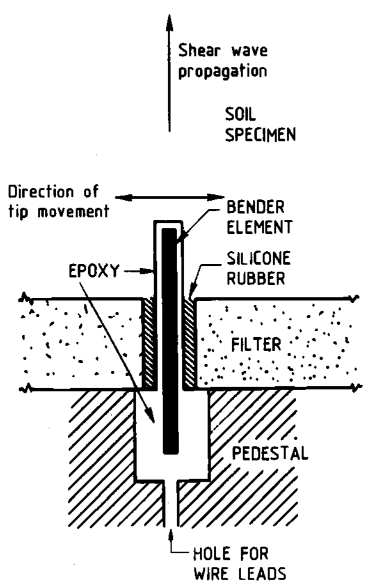

FIG. 16—*Bender element mounted in triaxial pedestal* [39].

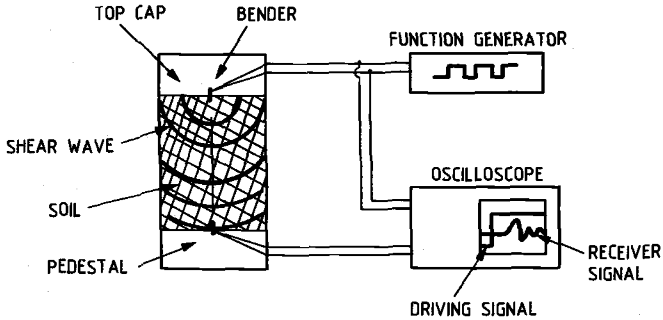

FIG. 17—*Measurement of initial modulus by piezoceramic bender elements* [39].

to provide the excitation voltage to the bender element. Because of the very short travel time of the shear waves from one end of the specimen to the other, an oscilloscope of very high resolution and accuracy is needed to record the results.

The shear wave velocity (V_s) and initial shear modulus (G_{max}) for the soil specimen can be determined from:

$$V_s = L_t/T_t \quad (1)$$

$$G_{max} = \rho(V_s)^2 \quad (2)$$

where

L_t = consolidated height of specimen minus protrusion of bender elements (protrusion ≈ 7% of specimen height for a 100-mm high triaxial specimen),
T_t = travel time, and
ρ = mass density of soil.

Figure 18 compares the initial shear modulus, G_{max}, measured on five clays with the resonant column and the piezobender techniques. For this comparison, the piezoceramic

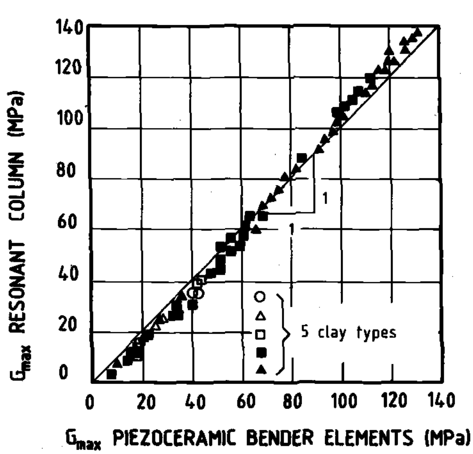

FIG. 18—*Comparison of initial shear modulus from resonant column and bender element techniques* [39].

elements were mounted in the resonant column cell. The G_{max} values presented apply to shear strain levels of 10^{-3}% and below. The agreement between the two devices is excellent. NGI has now implemented bender elements in other laboratory devices, including the oedometer and simpler shear tests.

Further Developments

Among the more pressing issues, one should note

- Improve measurements of strains at stress levels less than 5% of the failure stress.
- Investigate further effects of sample disturbance, end friction, and reconsolidation to the in situ effective stresses.
- Investigate pore pressure nonuniformity in cyclic tests and the need for small pore pressure probes inserted into the test specimen.
- Investigate effect of top cap tilt on test results, especially for cyclic tests on rigid material.
- Improve data acquisition systems from the points of view of noise levels and logging rapidity.
- Develop "intelligent" loggers and data processors that can select and reduce only the meaningful data, especially for cyclic tests.
- Use desk computers to steer different stages of triaxial tests.

Acknowledgments

The authors are indebted to their NGI colleagues who have contributed to the data presented here, including laboratory testing, data reduction, and test interpretation. Special recognition is addressed to S. Bakke and E. Heier for the improvement of the strain measurement, E. Moen for his work on sources of error, and K. Iversen, T. S. Olsen, and G. Sandbækken for programming data reduction routines.

References

Abbreviations

ASCE	American Society of Civil Engineers
ASTM	American Society for Testing and Materials
ICSMFE	International Conference of Soil Mechanics and Foundation Engineering
ISSMFE	International Society of Soil Mechanics and Foundation Engineering
JGE	*Journal of Geotechnical Engineering*
JGED	*Journal of the Geotechnical Engineering Division*
JSMFD	*Journal of the Soil Mechanics and Foundation Division*

[1] Andresen, A. and Simons, N. E., "Norwegian Triaxial Equipment and Technique," American Society of Civil Engineers, Research Conference on Shear Strength of Cohesive Soils, Boulder, CO, 1960, pp. 695–709.

[2] Berre, T., "Triaxial Testing at the Norwegian Geotechnical Institute," *Geotechnical Testing Journal,* Vol. 5, No. 1/2, 1982, pp. 3–17.

[3] Berre, T., "Suggested International Procedure for Triaxial Compression Tests," Submitted to ISSMFE Subcommittee on Soil Testing. Also NGI Internal Report 56103-30, Feb. 1986 (unpublished).

[4] Lacasse, S., Iversen, K., Sandbækken, G. and Morstad, P., "Radiography Offshore to Assess Sample Quality," NGM (Northern Geotechnical Conference), Linköping, Sweden, 1984, *Proceedings* Vol. 2, pp. 575–584.

[5] Lacasse, S., "Testing of Special Soils: Ocean Floor Soils," Panel discussion, Session 2B. Eleventh ICSMFE, San Francisco, CA, 1985.

[6] Berre, T., "Effect of Different Testing Procedures and Sampling on Isotropically Consolidated Stiff Clay Specimens," NGI Internal Report 56103-15, 11 Sept. 1978 (unpublished).
[7] Berre, T., "Sources of Error for Undrained Tests on Soft and Medium Stiff Clay," Nordiska Geoteknikermötet, NGM-79, Esbo, 1979, pp. 597–603.
[8] Berre, T., "Effect of Sampling Disturbance on Undrained Static Triaxial Tests on Plastic Drammen Clay," NGI Internal Report 56001-3, 9 Oct., 1986 (unpublished).
[9] Hight, D. W., Gens, A., and Jardine, J., "Evaluation of Geotechnical Parameters from Triaxial Tests on Offshore Clay," Society of Underwater Technology, Offshore Site Investigation 85, London, Vol. 3, 1985, pp. 253–268.
[10] Baligh, M. M., "The Strain Path Method in Geotechnical Engineering," MIT Report 84-01, Cambridge, MA, 1984.
[11] Landva, A., "Equipment for Cutting and Mounting Undisturbed Specimens of Clay in Testing Devices," Norwegian Geotechnical Institute, Publication 56, 1964, pp. 1–5.
[12] Berre, T., "Preparation of Very Soft Clay Specimens for 50 cm^2 Conventional Triaxial Tests," *Proceedings,* 7th ICSMFE, Mexico, Vol. 3, 1969, pp. 517–518.
[13] "Forslag till geotekniska laboratorieanvisningar, del 9: skjuvhållfasthet," Svenska Geotekniske Forening (Swedish Geotechnical Society), Linköping, 1980.
[14] Iversen, K. and Moum, J., "The Paraffin Method; Triaxial Testing Without a Rubber Membrane," *Géotechnique,* Vol. 24, No. 4, 1974, pp. 665–670.
[15] Jacobsen, M., "The Undrained Shear Strength of Preconsolidated Boulder Clay, Geotechnical Conference Shear Strength Properties of Natural Soils and Rocks," *Proceedings,* Vol. 1, Oslo, 1967, pp. 119–122 (Also published in Danish Geotechnical Institute, Bulletin 26, 1967).
[16] Roscoe, K. H., "An Apparatus for the Application of Simple Shear to Soil Samples," Third ICSMFE, Zürich, Vol. 1, 1953, pp. 186–191.
[17] Rowe, P. W. and Barden, L., "Importance of Free Ends in Triaxial Testing," ASCE, JSMFD. *Proceedings,* Vol. 90, No. SM 1, 1964, pp. 1–27.
[18] Lee, K. L., "End Restraint Effects on Undrained Static Triaxial Strength of Sand," ASCE, JGED. *Proceedings,* Vol. 104, No. GT 6, 1978, pp. 687–704.
[19] Jacobsen, M., "New Oedometer and New Triaxial Apparatus for Firm Soil. Strength and Deformation Properties of Preconsolidated Moraine Clay. Time Dependence of Settlements," Danish Geotechnical Institute, Bulletin 27, 1970.
[20] Berre, T., "Effect of End Friction on Results of Triaxial Tests on Plastic Clay from Drammen," NGI Internal Report 56103-9, 1 July 1977 (unpublished).
[21] Berre, T., "Effect of Rubber Membrane, Sidedrain and Specimen Height on Results of Triaxial Tests," NGI Internal Report 56103-10, 25 April 1978 (unpublished).
[22] Ladd, R. S., "Preparing Test Specimens Using Undercompaction," *Geotechnical Testing Journal,* Vol. 1, No. 1, 1978, pp. 16–23.
[23] Kildalen, S. and Stenhamar, P., "NGI Laboratory Sand Rainer," NGI Internal Report 51505-15, 1977 (unpublished).
[24] Rad, N. S. and Clough, G. W., "New Procedures for Saturating Sand Specimens," ASCE, JGED. *Proceedings,* Vol. 110, No. G19, 1984, pp. 1205–1218.
[25] Hight, D. W., Gens, A. and Jardine, J., "Discussion of the Reaction of Clays to Sampling Stress Relief," *Geotechnique,* Vol. 35, No. 1, 1985, pp. 86–89.
[26] Burland, J. B., "Recent Developments in Laboratory Equipment," Panel discussion, Session 2B Eleventh ICSMFE, San Francisco, CA, 1985.
[27] Jardine, R. J., Symes, M. J. and Burland, J. B., "The Measurement of Soil Stiffness in the Triaxial Apparatus," *Geotechnique,* Vol. 34, No. 3, 1984, pp. 323–340.
[28] Jardine, R. J., Fourie, A., Mascowswe, J. and Burland, J. B., "Field and Laboratory Measurements of Soil Stiffness, Eleventh ICSMFE, San Francisco, CA, Vol. 1, 1985, pp. 511–514.
[29] Burland, J. B. and Symes, M., "A Simple Axial Displacement Gauge for Use in the Triaxial Apparatus," *Geotechnique,* Vol. 32, No. 1, 1982, pp. 62–65.
[30] Symes, M. J. and Burland, J. B., "Determination of Local Displacements on Soil Samples," *Geotechnical Testing Journal,* Vol. 7, No. 2, 1984, pp. 49–59.
[31] Silver, M. L., "Laboratory Triaxial Testing Procedures to Determine the Cyclic Strength of Soils," U.S. Nuclear Regulatory Commission, Report NUREG-0031 (unpublished).
[32] Duncan, J. M. and Seed, H. B., Corrections for Strength Test Data," ASCE, JSMFD. *Proceedings,* Vol. 93, No. SM 5, Pt. 1, 1967, pp. 121–137.
[33] Shirley, D. J., "An Improved Shear Wave Transducer," *Journal of the Acoustical Society of America,* Vol. 63, No. 5, May 1978, pp. 1643–1645.
[34] Shirley, D. J. and Hampton, L. D., "Shear-Wave Measurements in Laboratory Sediments," *Journal of the Acoustical Society of America,* Vol. 63, No. 2, 1978, pp. 607–613.

[35] Schultheiss, P. J., "Development of Seismic Shear Wave Devices," Report, Marine Science Laboratories, Gwynedd, U.K., 1981.
[36] Schultheiss, P. J., "Simultaneous Measurement of P & S Wave Velocities During Conventional Laboratory Soil Testing Procedures," *Marine Geotechnology,* Vol. 4, 1981, pp. 343–367.
[37] Schultheiss, P. J., "The Influence of Packing Structure and Effective Stress on V_s, V_p and the Calculated Dynamic and Static Moduli in Sediments," Conference Acoustics and the Sea-Bed, *Proceedings,* 1983, pp. 19–27.
[38] Hamdi, F. and Taylor-Smith, D., "The Influence of Permeability on Compressional Wave Velocity in Marine Sediments," *Geophysical Prospecting,* No. 30, 1982, pp. 622–640.
[39] Dyvik, R. and Madshus, C., "Laboratory Measurements of G_{max} Using Bender Elements," ASCE National Convention, Detroit, MI, Oct. 1985.

Jean Louis Colliat-Dangus,[1] Jacques Desrues,[2] and Pierre Foray[2]

Triaxial Testing of Granular Soil Under Elevated Cell Pressure

REFERENCE: Colliat-Dangus, J. L., Desrues, J., and Foray, P., "**Triaxial Testing of Granular Soil Under Elevated Cell Pressure,**" *Advanced Triaxial Testing of Soil and Rock, ASTM STP 977,* Robert T. Donaghe, Ronald C. Chaney, and Marshall L. Silver, Eds., American Society for Testing and Materials, Philadelphia, 1988, pp. 290–310.

ABSTRACT: A study of triaxial testing under elevated cell pressure is presented. The influence of test conditions, namely end lubrication and slenderness ratio, on such tests is discussed. Results of a tomodensitometric investigation of internal homogeneity are given. The main results of the high pressure study are presented, including time effects on isotropic compression.

KEY WORDS: triaxial test, high pressure, lubricated ends, slenderness ratio, calcareous sand, density, x-ray, tomodensitometer, time effect

Some classic geotechnical engineering field problems, including high embankment dams, piles, and deep tunneling, involve mean pressures significantly higher than those found in common practice. A new interest in this subject stems from specific offshore geotechnical problems, especially ones in which long piles and/or marine calcareous sand deposits are concerned.

The purpose of this study, undertaken as part of a research program on offshore piling, was to characterize and compare the behavior of two sands, a marine calcareous one and a siliceous one, under high confining stresses. Within this work, a preliminary study was conducted to evaluate the influence of the experimental conditions of the specimen end restraint and slenderness ratio on the result of drained compression triaxial tests performed under both low and elevated confining pressures.

Two main types of specimens are considered: (1) the conventional specimen (rough ends, length-to-diameter ratio $[L/D] = 2$) and (2) the specimen using lubricated ends and a slenderness ratio reduced to 1. Two kinds of granular materials of different mineralogic composition are used: a siliceous sand and a marine calcareous sand. Besides current triaxial experiments on these specimens, original tests were performed using an x-ray scanner apparatus to investigate the internal homogeneity of the specimens.

The behavior of granular materials under elevated cell pressures is discussed for both stages of the triaxial test: isotropic compression and triaxial shear. Special attention is paid to the effects of time on this behavior.

In this paper, the words *low pressure* and *high pressure* will be used; a numerical definition of the threshold between these two domains cannot be given because the sensitivity of

[1] Project engineer, GEODIA Offshore Geotechnical Consultants, 16, rue Médéric, Paris, France.
[2] Chargé de recherche Centre National de la Recherche Scientifique (CNRS) and maitre de conférences, GEONUM team, respectively, Institut de Mécanique de Grenoble, BP 68, 38402 St. Martin d'Hères, France.

granular materials to mean stress is significantly dependent (as will be shown) on the mineralogy of the sand particles, among other factors. For siliceous materials, the cell pressures used in common practice of triaxial testing (lower than 1 MPa) can be considered as defining a low-pressure range, while higher pressure will be considered as the high-pressure range.

Effects of End Lubrication and Slenderness Ratio on Drained Compression Triaxial Tests: Low- and High-Pressure Range

Previous Works

End Restraint in Triaxial Testing—The basic requirements for reliable triaxial testing are controlled specimen preparation to ensuring reproducible initial state, complete saturation of the specimen, well-centered axial load, negligible friction on the loading ram, well-controlled cell and pore pressures, and accurate measurements of axial load, axial deformation, and volumetric change. These requirements are easily fulfilled as far as research tests in the low-pressure range are concerned. However, less satisfactory test conditions can be encountered when dealing with industrial tests or with high-pressure apparatus.

Beyond these basic requirements, additional specifications to improve the homogeneity of the test have been proposed by several workers. End restraint was recognized, a long time ago, to be responsible for strong heterogeneous responses, such as barreling and localization of deformation along failure planes. Bishop and Henkel discussed this point in their classic book [*1*]; it was also underlined by Sowers in the introductory paper of the ASTM symposium on laboratory testing of soils in 1963 [*2*]. Roscoe and co-workers conducted a series of triaxial compression and extension tests, with measurements of axial and radial strains, revealing severe nonuniformities throughout the specimen [*3*]. Kirkpatrick and Belshaw showed experimentally the existence of rigid cones inside the specimen due to end restraint [*4*].

Because the triaxial test is an elemental test, performed to obtain mechanical properties, the specimen should be perfectly homogeneous. From a more technical point of view, the area correction that is necessary to take into account the radial variation of the specimen during the test in order to calculate the actual axial stress (and estimate the membrane action on the actual lateral pressure) can be obtained from axial and volumetric strains only as long as the specimen shape remains cylindrical. In other cases, additional assumptions must be made: cylinder of average area [*5*] or more realistic generant shapes, such as parabolic or sinusoidal ones.

Lubricated End Platens and Slenderness Ratio—Antifriction devices were designed and tested in order to suppress end-restraint effects. The most popular device is lubricated end platens, using one or several rubber disks, coated with silicone grease in contact with the polished steel platens. Such devices were developed by Bishop and Green [*5*], Rowe and Barden [*6*], Biarez [*7*], and others.

If the antifriction device works, the slenderness ratio (length to diameter) should have no effect on the test results; actually, the value of this ratio varies over a wide range from one author to another. Most authors recommend use of rather short specimens, with enlarged lubricated ends [*6,8–14*] essentially because this arrangement allows one to suppress the rigid cones, and then to improve the homogeneity of the test up to large axial strains. A theoretical study by Vardoulakis indicated that, regarding the bifurcation from the homogeneous deformation mode (cylindrical shape) to an axisymmetric diffuse heterogeneous mode, the bifurcation stress generally increases by decreasing the slenderness ratio; hence, shorter specimens would tend to shear more homogeneously up to large strains [*15*].

A typical result of the improved boundary conditions in triaxial tests on dense cohesionless materials is to smooth out the pronounced peak observed commonly in classic tests. Most published results of lubricated-end tests on dense sand show a soft maximum in the curved stress ratio (σ_1/σ_3) versus axial strain, followed by a slight softening. Some authors consider that this softening is due to remaining imperfections and present results from improved tests without any decrease in stress ratio [*9*].

Strength Parameters—Regarding the influence of the modified test conditions on the strength parameters, various opinions are expressed in the literature. Bishop and Green, concluding a very detailed experimental study in 1965 on that question, estimated that, as long as the slenderness ratio is 2, conventional and frictionless ends give the same friction angle at peak stress; shorter specimens give higher angles, unless perfect end lubrication is provided [*5*]. The value corresponding to $L/D = 2$ is estimated to be the "true" friction angle. Many authors disagree with these conclusions and conclude from their own experiments that the friction angle with conventional ends is always slightly higher [*6,11,16,17*]. Drescher and Vardoulakis, in a theoretical analysis based on a static method of slices, corroborate these findings [*18*].

Bedding Error—Although there is general agreement on the use of lubricated platens and a slenderness ratio reduced to 1 (essentially because of the improved homogeneity of the test), another specific problem concerns experimentalists—the so-called bedding error. Bedding error is related to the measurement of the axial strain at the very beginning of the test; it is due to the deformation of the antifriction device which is generally much more compressible than the specimen. Several recent works are devoted to this problem [*9,16,19*]. For drained compression tests, using specimens with a slenderness ratio of 2, the bedding error can lead to initial moduli 60% lower if frictionless conditions are used [*5,6,11,14*]. However, the end-restraint effect can, in turn, induce an overestimation in the modulus [*17*]. Goldscheider attempted to determine a correction to be applied to the axial strain by evaluating the difference between conventional and lubricated tests [*19*]; the scatter of the results is significant. Other authors use a local measurement of the axial strain in the central part of the specimen for calculating the initial modulus [*9*].

Current works devoted to bedding error by the authors' research team will not be discussed here. (This topic is reviewed in Ref *20*; related information can also be found in Ref *21*.)

Experiments

Description of the Problem—The experiments reported in the first part of this paper were performed as a preliminary study, with the intention of determining what test conditions should be used in an experimental program on calcareous sand tested in drained triaxial compression under elevated cell pressures. To the authors' knowledge, the only work on soils for pressure ranges up to 10 MPa was published by Roy and Lo in 1971 [*14*]. The conclusions of that work were favorable to the use of improved test conditions for the same reasons as apply to the low-pressure range: improving the specimen shape (cylindrical) at the end of the test and preventing the premature development of predominant failure surface. Nevertheless, the idea that test refinements are unnecessary for high-pressure range still remains common; in the last 20 years, many high-pressure tests have been performed with conventional conditions, namely rough platens and $L/D = 2$ [*22–27*].

Hence, the purpose of the preliminary study was to control the effects of improved test conditions, especially into the high-pressure range.

Moreover, the recent theoretical and experimental advances related to bifurcation analysis (diffuse heterogeneous mode, localization) gave a new motivation in questioning the homogeneity of tests, as attested by recent work *[15,18,28–31]*. A number of experimental techniques have been used to control the homogeneity of tests and detect actual localization; however, in the classic triaxial test performed on cylindrical specimens only the external surface of the specimen can be directly observed. How can one be sure that an apparent homogeneous deformation mode (cylindrical shape) does not actually conceal a heterogeneous mode of any kind? Tomodensitometry, a recent technique using an x-ray scanner, can provide an insight into the internal homogeneity. Original tests performed using this technique are reported hereafter.

Test Procedure—The test conditions compared were: (1) conventional ends, $L/D = 2$; (2) lubricated ends, $L/D = 2$; (3) lubricated ends, $L/D = 1$. The material used in this preliminary study is Hostun (Drôme, France) RF sand, a fine angular siliceous sand, uniformly graded (Fig. 1), with $D_{50} = 0.32$ mm, uniformity coefficient = 1.70, minimum and maximum volumetric weights of 13.24 and 15.99 kN/m^3, respectively, and grain specific gravity of 2.7.

Some tests in the preliminary study and half of the tests in the high-pressure study reported in the second part of this paper were performed on a calcareous sand, referred to here as SC. Figure 1 shows the grain size distribution of this second material, a well-graded sand, with $D_{50} = 0.17$ mm, $C_u = 2.80$, γ_d ranging from 9.81 to 13.01 kN/m^3, and $G_s = 2.67$.

The specimens were air pluviated at a constant drop height, from zero (relative density about 20%) to 1 m (relative density of 90%). This technique ensures homogeneity and reproducibility of the initial density.

The radius of the specimens was 100 mm for the low-pressure tests. The specimens were axially strained at 1%/min in drained conditions. The membrane was 0.4 mm thick. Membrane correction was applied. The antifriction device used consisted of polished steel platens (larger than the specimen) and two rubber disks, 0.4 mm thick, coated with silicon grease. Drainage was ensured by a 18-mm central porous stone on each platen (see Fig. 7). Axial and volumetric strains were calculated from the global height and volume, as $\epsilon_1 = -\text{Log}(H/H_0)$ and $\epsilon_v = -\text{Log}(V/V_0)$ (positive compression).

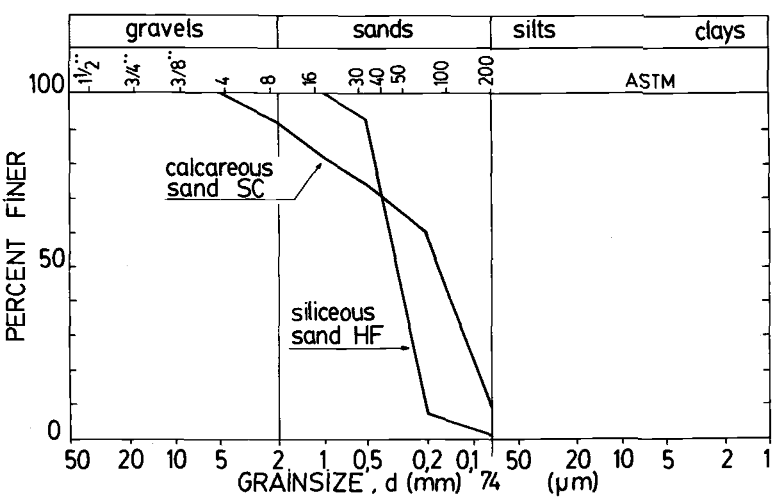

FIG. 1—*Grain size distribution for both sands.*

Hereafter, the "loose" and "dense" densities refer to the relative densities given in the preceding paragraph.

Strength Parameters and General Features—Figure 2 illustrates the typical stress ratio versus strain curves obtained for dense and loose specimens under 90 kPa of lateral pressure for various test conditions.

In good agreement with previous works, the main features observed are:

1. Conventional test conditions (nonlubricated ends, $L/D = 2$) on dense specimens lead to a pronounced stress peak (Fig. 2*a*, dashed line); shear banding can be seen on the specimen. Simultaneously, the increase of the volumetric strain is abruptly stopped (Fig. 2*b*, dashed line). Moreover, these conventional tests are very sensitive to imperfections. For example, the dotted line in Figs. 2*a* and *b* gives the results for a second conventional test, identical to the first one except that it had a slight centering fault of the specimen; the peak stress is significantly lower, and furthermore the volumetric strain stops much sooner, indicating very early localization effects.

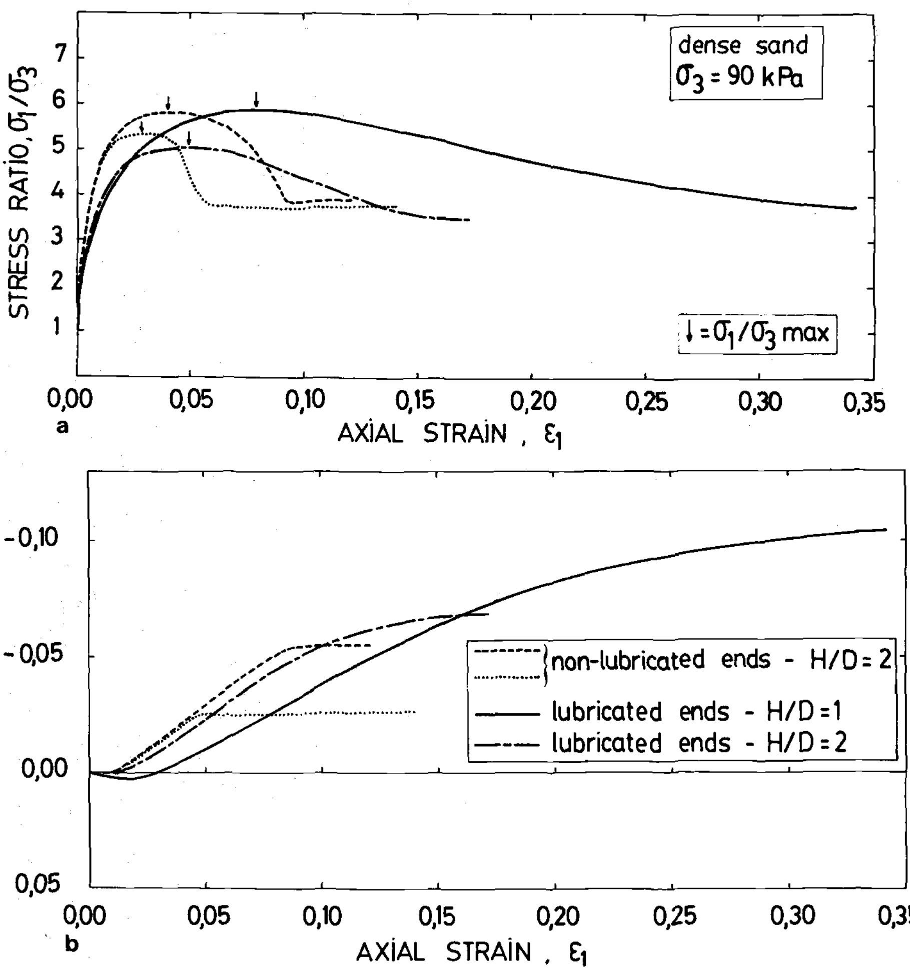

FIG. 2—*Influence of the test conditions on the stress ratio and volumetric strain curves,* (a, b) *for dense sand and* (c, d) *for loose sand.*

2. Lubricated platens and reduced slenderness ratio give a much smoother curve in both diagrams (Figs. 2*a* and *b*, solid lines). The specimen remains nearly cylindrical, although a diffuse heterogeneous mode of deformation can be observed in some cases (conic shape). Improved homogeneity is attested by the much larger dilatancy strain at the end of the test; on the other hand, the peak strength and the residual strength are not significantly different from those obtained in classic tests.

3. Classic slenderness $L/D = 2$ associated with lubricated ends leads to less reproducible results than reduced slenderness ratio. This is due to the development of an axisymmetric mode of diffuse heterogeneous deformation, extended to only a part of the specimen (upper or lower part). This produces a strength underestimation (Fig. 2*a*, mixed line), and a truncated volumetric strain evolution (Fig. 2*b*).

For loose specimens, Figs. 2*c* and *d* show only slight differences between the tests conducted with lubricated ends and $L/D = 1$ or 2. The results of the conventional test are somewhat different, showing much less contractancy and a slight softening.

Figure 3*a* is a summary of the effects of test conditions on strength (peak stress), in terms of friction angle versus mean normal stress. Two sets of points can be distinguished, referring

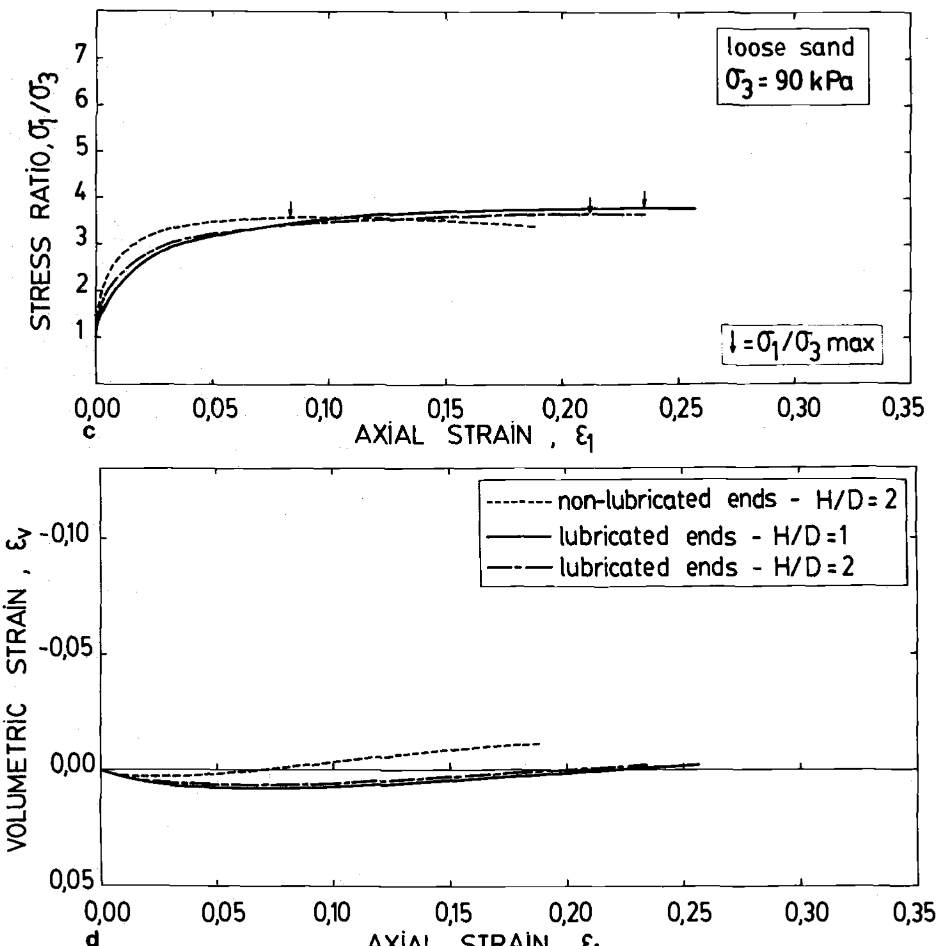

FIG. 2—*Continued.*

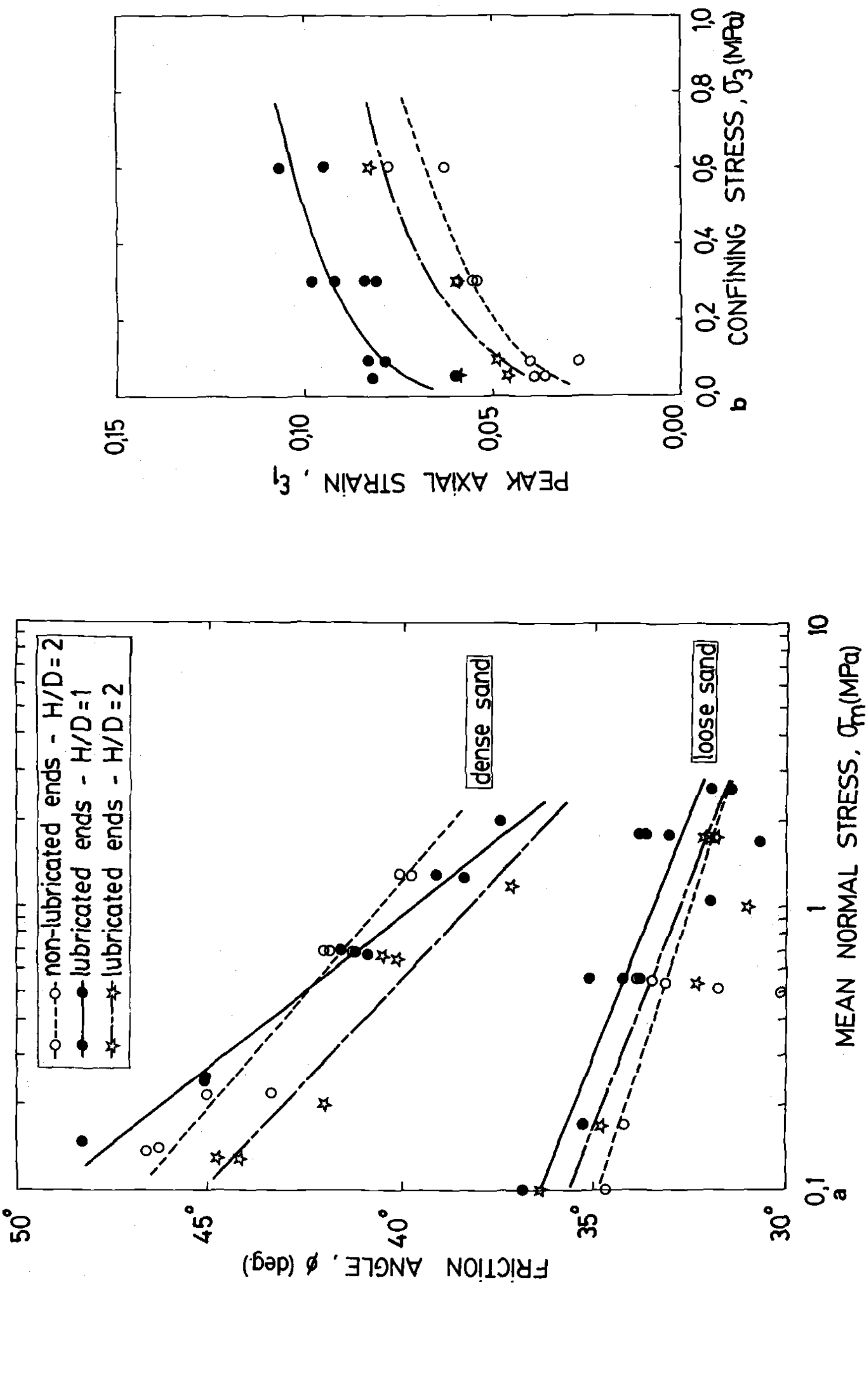

FIG. 3—*Influence of the test conditions on:* (a) *friction angle,* (b) *peak axial strain,* (c) *final volumetric strain, and* (d) *peak dilatancy rate.*

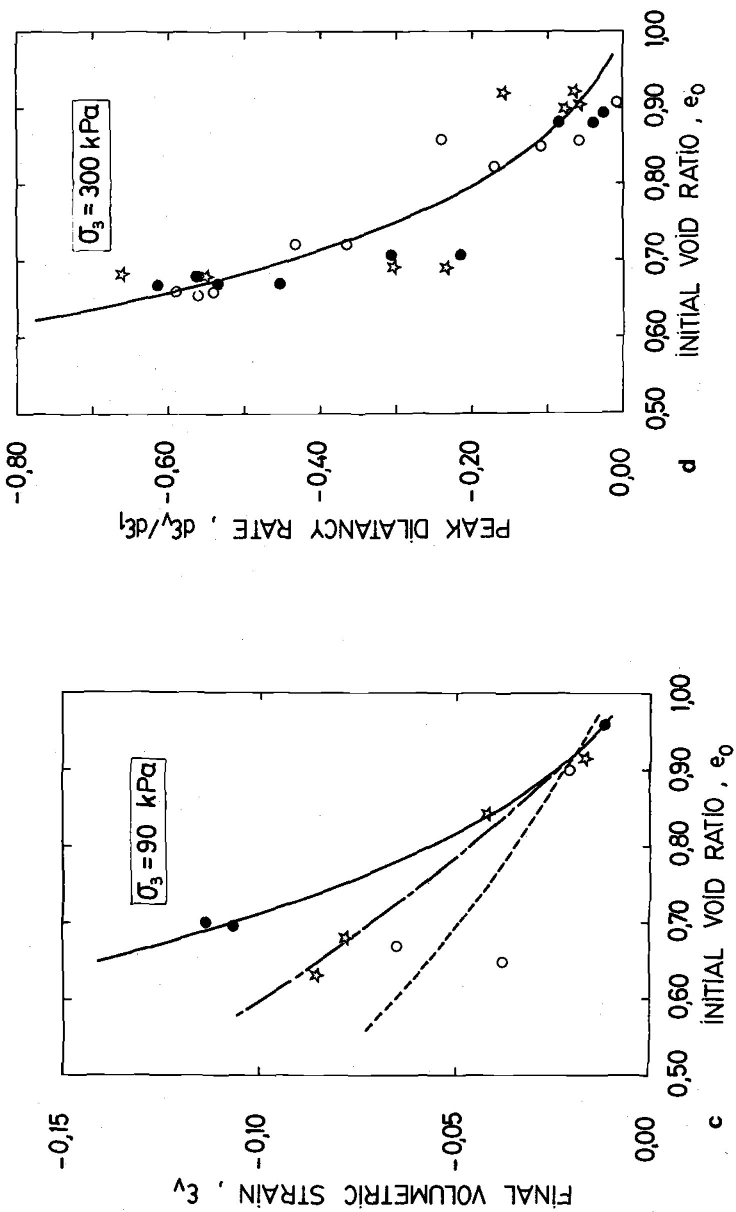

FIG. 3—*Continued.*

to dense and loose specimens. In both cases, the most prominent feature is the decrease of the friction angle with the mean stress; the influence of the test conditions is limited to a few degrees (maximum 4°) on the friction angle, while the error due to reproducibility of the tests, especially in conventional tests and at very low mean pressure, is of the same order. However, significant variation of the peak axial strain is shown in Fig. 3*b*, depending on the test conditions; rough ends induce earlier peaks, as was illustrated in Figs. 2*a* and *c*. In the same way, but much more marked in dense specimens, the volumetric strain at the final stage of the test is sensitive to the test conditions (Fig. 3*c*). This sensitivity is due to almost unavoidably truncated volumetric strain evolution in the conventional tests (due, in turn, to the localization). This leads to nonsignificant final volumetric strains, as confirmed by the large scatter observed for conventional tests on the figure. With regard to the dilatancy rate at peak (Fig. 3*d*), despite a moderate scatter, it can be concluded that there is no significant influence of the test conditions.

These results can be summarized as follows: rough ends induce restraint, leading to (1) slightly increased initial modulus and peak strength (if no premature localization) and (2) strong tendency to localize, from which neither reliable final volumetric strain nor peak strength can be determined; dilatancy rate under all conditions is more or less the same before localization occurs. Reduced slenderness ratio allows improved specimen homogeneity with regard to the diffuse modes.

High-Pressure Range—From a comparison of Figs. 2*a* and *b* (dense, dilatant) with Figs. 2*c* and *d* (loose, contractant), one can hypothesize that the end lubrication and slenderness effects have less and less influence at higher pressures (inducing lower dilatancy). Actually this is not true, as was shown by comparative tests performed at a 10-MPa cell pressure, on both siliceous and calcareous sands.

The test procedure is described in the second part of this paper. Quite similar results were obtained for this comparison on loose and dense, HF or SC sands; only the HF dense case will be presented.

The comparison between the improved test (solid line) and the conventional test (dashed line) is shown in Fig. 4. In the latter, marked barreling was observed, followed by a multisurface localization. The stress ratio versus axial strain curve has a maximum followed by a slight softening. In the improved test, the specimen remained cylindrical up to 50% axial strain, without discernable localization. The stress–strain curve shows a monotonic increase in this case. This could be stated to be the "true" elementary response of the material.

The initial modulus is, again, higher in conventional tests (up to 30%). The volumetric strain curves do not have systematic differences; as in the low-pressure range, the volumetric strain mobilization seems to be faster, leading here to slightly higher contractancy, despite the heterogeneity (barreling, localization). The heterogeneity of the volumetric strains in high-pressure tests will be discussed in the next section.

Tomodensitometric Survey of the Internal Homogeneity—The x-ray scanner, well known for its medical applications, is beginning to be used in the engineering domain. For dry sand specimens, a simple correlation can be established between the local x-ray attenuation and the local compactness; proper calibration for each specific material is required if quantitative measurements are desired.

Briefly, an x-ray scanner irradiates the object to be examined, through a range of angles of incidence. Only a thin slice of the object is irradiated. For each incidence, the transmitted x-ray beam is recorded behind the object by detectors, giving a profile of the integrated local attenuation along parallel paths inside the slice. From the combination of these profiles, one can compute the local attenuation in elementary volumes ("voxels"). The attenuation

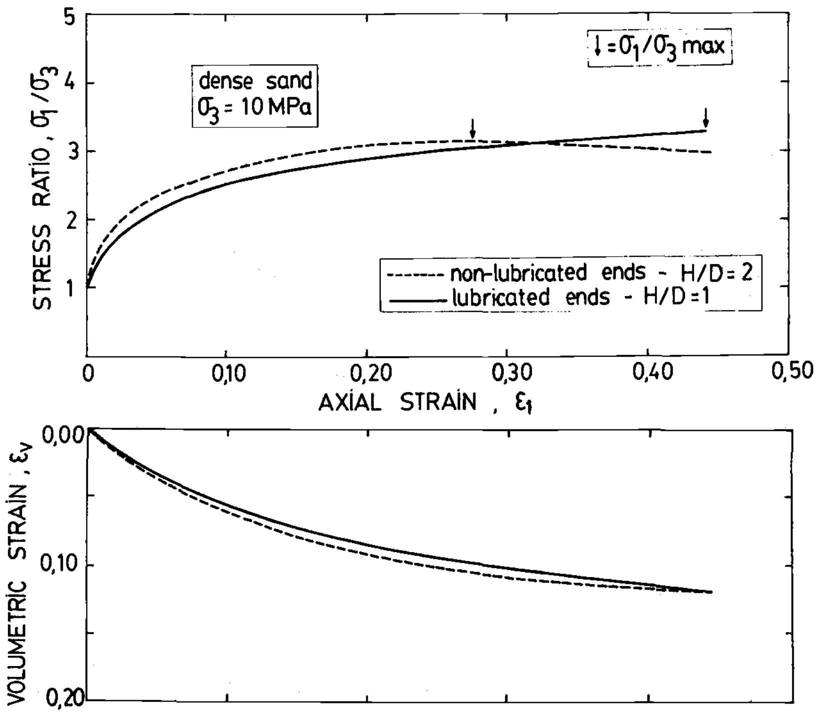

FIG. 4—*Conventional and improved tests under high cell pressure.*

is affected by the mass density, depending on compactness and mineral density. Because the mineral density is unaffected, the degree of compactness is the variable governing the attenuation. A map of the compactness in a cross-section of the sand specimen (averaged over the thickness of the slice) can then be obtained.

Practically, some difficulties in the numerical process can result from complicated geometric shapes or very dense inclusions. This leads to completely distorted pictures. The cylindrical shape of the authors' specimens is the optimum. Another difficulty is due to the modification of the spectrum of the x-ray beam in the first millimeters of their path inside the material. The less penetrating part of the radiation is absorbed in this zone, while the remainder goes through the sample; this "skin effect" gives an overestimated attenuation (compactness) near the boundary of the section; it can be avoided by special devices, or corrections, but the results presented here were obtained without any special disposition. Hence, the easily discernable external white halo should be neglected when evaluating the results.

All the figures presented were directly photographed on a cathode ray tube (CRT) display. They can be interpreted as classic x-ray photographs. In the picture, the darker a zone is, the looser the material inside that zone is. When profiles are shown, they concern the attenuation along the zone indicated by dotted lines on the picture. Differences in lightness and darkness are to be interpreted in relative terms, because the system was not calibrated.

1. Conventional versus improved test conditions on dense HF sand

A special apparatus, designed to allow the tomodensitometric survey of a specimen during a triaxial test, consists of a rather rustic, manually operated mechanical press. The confining pressure is produced by atmospheric pressure on the dry specimen under vacuum. After a given loading step, the specimen can be unloaded and, still under vacuum, removed from the apparatus and placed in the scanner. It is then possible to control the homogeneity of the compactness over the specimen at several stages of the test.

Figures 5*a* and *b* show the density inside the conventionally tested specimen, rough ends and $L/D = 2$, at 10% axial strain. At this stage, a typical failure surface could be directly observed outside the specimen. In Fig. 5*a* a cross-section is shown at the middle height of the specimen ($Z = 10$ cm); the failure surface appears clearly as a dark straight line on the picture. Darker means looser, so this figure confirms the strong dilatancy observed inside the shear bands under low mean pressure, reported in a number of works about strain localization [*28,30,31*]. In Fig. 5*b* another cross-section is shown, a few centimeters below the upper platen ($Z = 15$ cm). The brighter central zone, surrounded by a gray ring, is the section of the less deformed central cone, induced by end restraint (little dilatancy). Moreover, the failure surface appears to be distorted; this indicates that, during its development, the surface could not penetrate the rigid zone, but had to pass around it. To the authors' knowledge, this observation is original. Although indicating only relative values, the density profiles deserve comment: the lower density, recorded inside the failure surface, is quite the same in both sections (1670 units); the mean value outside the surface, in the central section of Fig. 5*a*, is about 1730, while the value in the rigid cone, in Fig. 5*b*, is markedly denser (1880). (These units are uncalibrated, but in monotonic increase with compactness.)

For the improved tests (lubricated ends, $L/D = 1$), a question arises: does a specimen that remains cylindrical after deformation conceal some strong internal heterogeneities? As

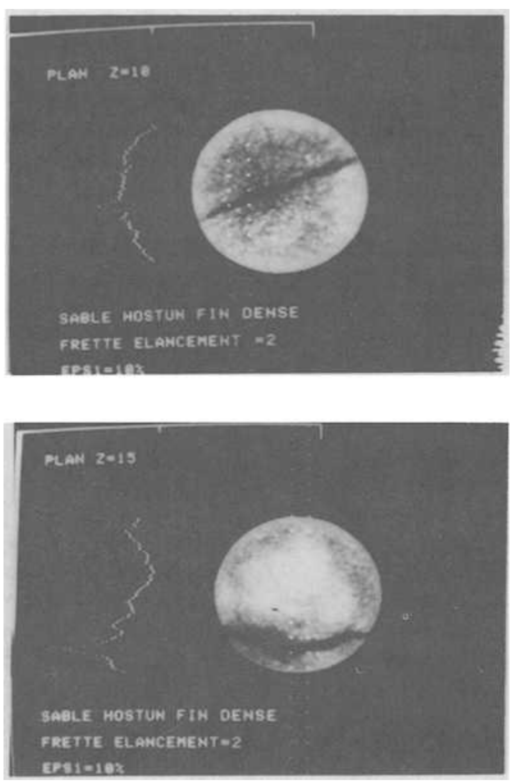

FIG. 5—*Conventional test:* (top) Z = *10 cm,* (bottom) Z = *15 cm.*

will be discussed, some heterogeneities do exist, but these are much smaller and limited than in the conventional test.

Figure 6*a* shows a section from just beneath the upper lubricated platen; this rather surprising picture reveals that a very small rigid cone is generated by the small porous stone placed for drainage at the center of the platen. In Fig. 7, a schematic of the actual arrangement, the cone is bordered by a failure surface, clearly identified by its high void ratio (dark circle in Fig. 6*a*). The density measure is, again, about 1650 units. The half angle of this cone can be estimated at 25° from another cross-section, 1 cm beneath, as shown in Fig. 7. This cone, being only a local perturbation, cannot affect significantly the overall measurements.

Figure 6*b* shows the central cross-section (Z = 5 cm) of the specimen sheared at 20% axial strain. No failure surface is revealed inside the specimen, despite the large axial strain. However, a diffuse heterogeneity is observed, namely a denser small zone in the middle of the specimen (1800). The remainder is in a more or less homogeneous loose state, only slightly denser (1700) than the density measured inside the failure surfaces. This supports the idea of a critical void ratio, which can be reached immediately after localization inside the shear bands, or at large strains in the homogeneous specimens. No clear explanation of the denser central zone is proposed; further experiments are needed to clarify that point.

2. High pressure tests on calcareous sand

The SC specimens, once consolidated and strained under 10-MPa cell pressure, remain sufficiently cohesive to be easily handled. It is then possible to put them, once dried, inside

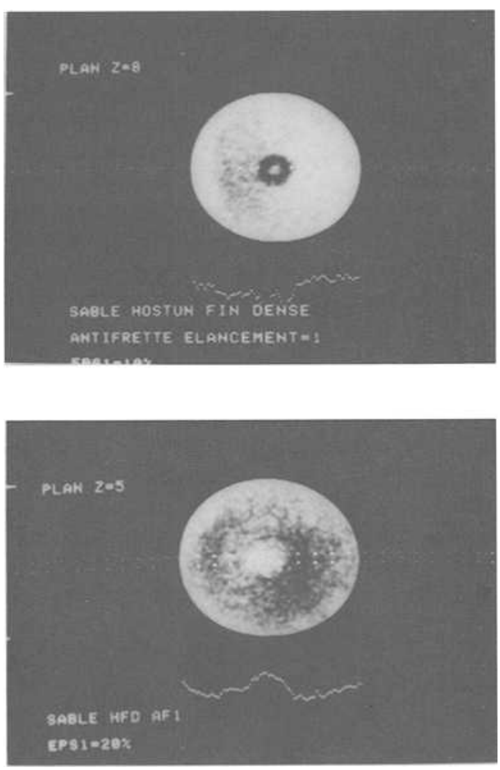

FIG. 6—*Improved test:* (top) Z = *8 cm,* (bottom) Z = *5 cm.*

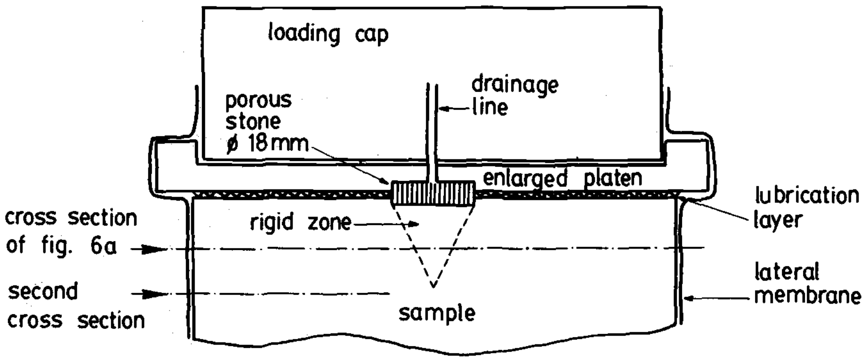

FIG. 7—*Lubricated end, porous stone and x-ray cross-sections.*

the scanner. Figure 8 shows a section of such a specimen, along its axis (not a cross-section). The specimen was sheared to extreme strain (50%). A typical barrel-like shape is observed, but the most interesting result is the effect of end restraint: the "rigid" cones remain significantly looser than the other parts of the specimen. This result is quite reasonable because the material in these cones undergoes less stress and strain, and therefore less contractancy; however, it is commonly assumed that high mean pressure erases any restraint effect. It is shown here that the heterogeneity of strains, and therefore of particle crushing and alteration, is severely affected by restraint.

These tomodensitometric results confirm in a unique way that the lubricated ends and reduced slenderness ratio ensure improved (but not perfect) homogeneous behavior in triaxial tests, in both the low- and high-pressure ranges.

High-Pressure Triaxial Tests

Test Procedure

Consolidated drained (CD) compression triaxial tests were performed under elevated cell pressures (up to 15 MPa) on both materials already used in the preliminary study: the siliceous HF sand and the calcareous SC sand.

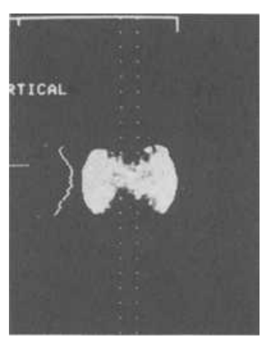

FIG. 8—*Transverse section of a specimen tested under high pressure and under conventional conditions.*

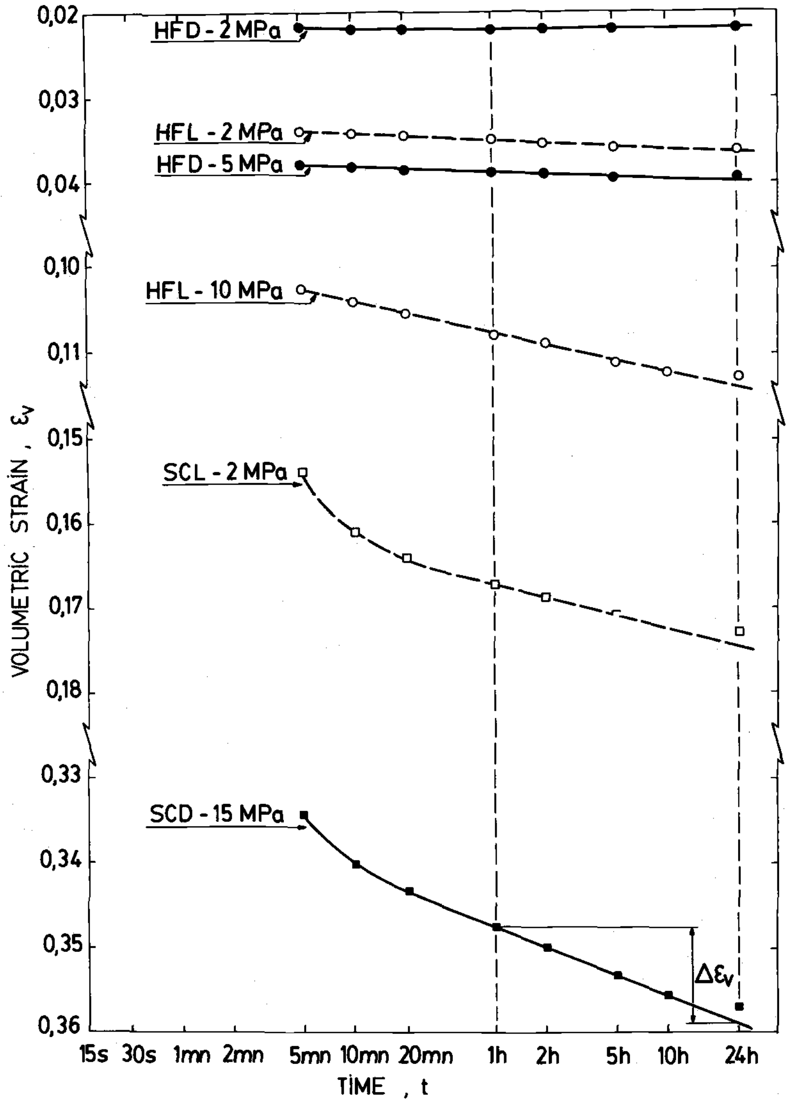

FIG. 9—*Volumetric strain versus time in isotropic creep tests.*

The conclusions of the preliminary study led to the choice of short specimens (L/D = 1) with lubricated end platens.

Great attention was paid to the measurement of significant volume changes; for this reason, large specimens were used, namely

D = 100 mm for σ_3 between 1 and 5 MPa

D = 70 mm for σ_3 between 5 and 10 MPa

D = 50 mm for σ_3 between 10 and 15 MPa

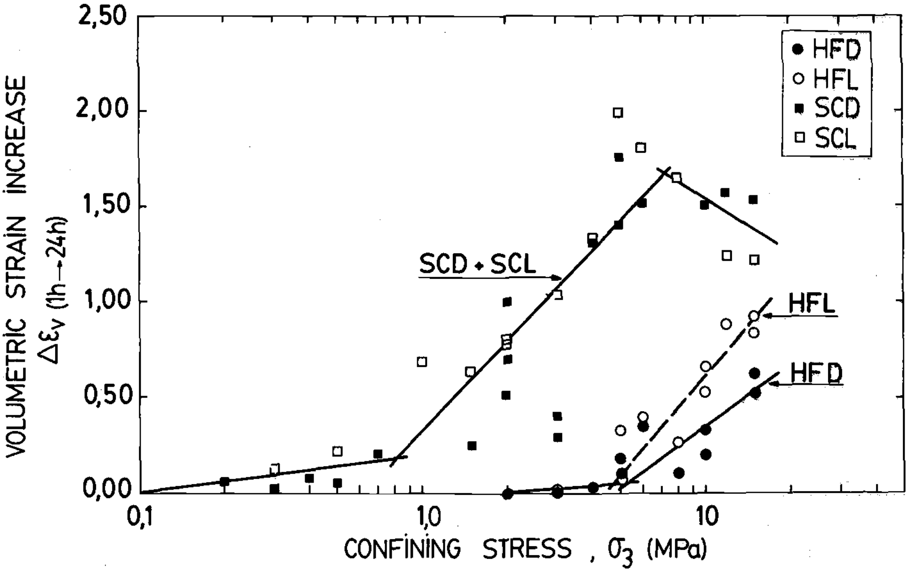

FIG. 10—*Evolution of creep rate versus isotropic stress.*

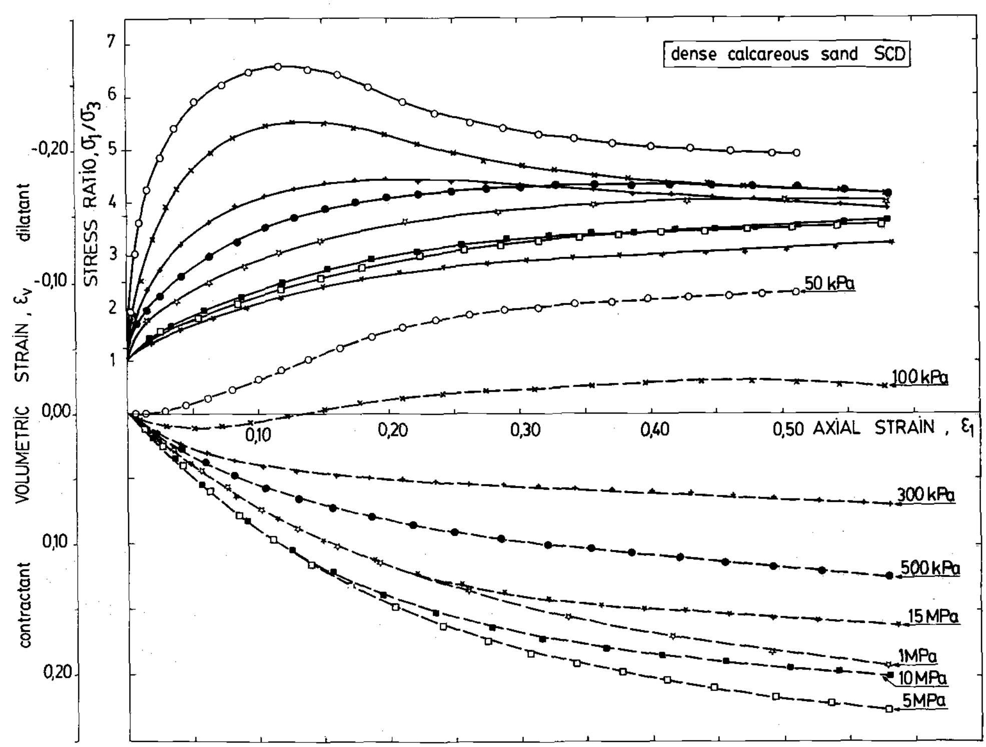

FIG. 11—*Stress-strain-volume change curves—dense calcareous sand.*

All tests were performed on saturated specimens. Full saturation of the specimen was achieved by a precirculation of carbon dioxide gas and application of a back pressure of 300 kPa; this back pressure was kept constant during the test by a self-compensating mercury-pot system.

All tests were performed under constant confining pressure. Specimens tested at confining pressure below 5 MPa were enclosed in a high-quality neoprene membrane, 0.5 mm thick; for higher pressures, two membranes were used. No membrane correction was applied.

Except in some specific cases, all the specimens were sheared at constant strain rate 1%/min, up to large axial strains (50%).

Test Results

The behavior of granular materials was studied for both stages of the triaxial test: isotropic compression and triaxial shear. The specimens will be referred to as HFD, HFL, SCD, SCL with D and L for dense and loose, respectively, initial compactness.

Time Effects on Granular Materials Under Isotropic Compression—Previous work has shown that under elevated confining pressures the compression of sand is not instantaneous but continues at an ever-decreasing rate over a long period of time, in a way similar to the phenomenon of secondary compression observed in clays [*11,22*].

"Creep" tests, in which the confining pressure was kept constant for 24 h, were performed to characterize time effects on the compression of granular materials. Typical results, presented in the classic semi-log graph (ϵ_v versus Log t), are given in Fig. 9. A time effect is clearly shown, analogous to a viscous phenomenon at a macroscopic scale.

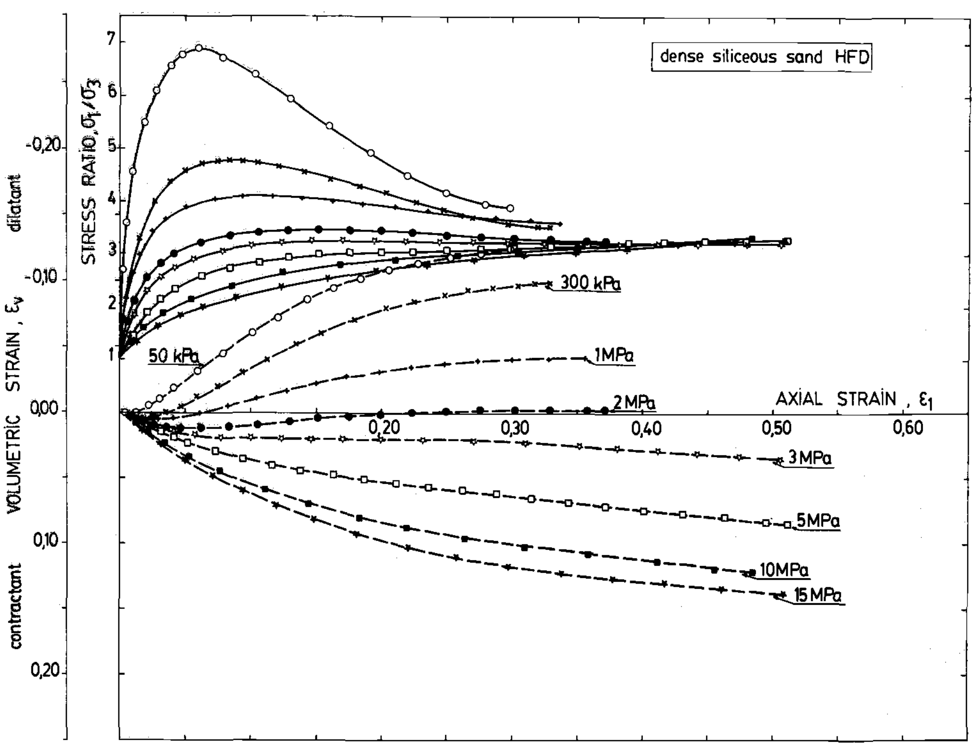

FIG. 12—*Stress-strain-volume change curves—dense siliceous sand.*

The slope of the "secondary compression" (that is, the increase in volumetric strain, $\Delta\epsilon_v$, measured between 1 h and 24 h of consolidation), is represented versus the confining pressure in Fig. 10. Despite a certain extent of scattering in the results obtained, it is shown that this time effect increases with the confining pressure. For siliceous sand HF, the compression may be considered instantaneous as long as the pressure is lower than 2 MPa, while, for calcareous sand SC (composed of fragile particles), time effects occur even at very low confining pressures.

From these results, a threshold in stress level can be defined, corresponding to a sharp increase in time effect: about 0.8 MPa for the calcareous sand and 6 MPa for the siliceous one. This threshold can be called a "creep stress," with reference to the so-called creep load defined from static pile loading tests.

Grain size analyses, performed at successive stages of the creep tests, showed that time effects are correlated to grain crushing [32]. Hence, the propagation of the rupture of particles may be the physical factor responsible for time effects on the compression of granular materials under elevated stresses. Further research is needed to give firm conclusions on that point; nevertheless, it can be stated that the mineralogy of the particles affects the value of the "creep stress."

Triaxial Shearing Under High Pressures—Figures 11 and 12 give typical stress–strain–volume change behavior for dense HF and SC sands. The decrease of the friction angle when increasing the mean stress applied to the specimen is shown in Fig. 13. It is worth comparing the friction angle measured in the high-pressure range with the so-called char-

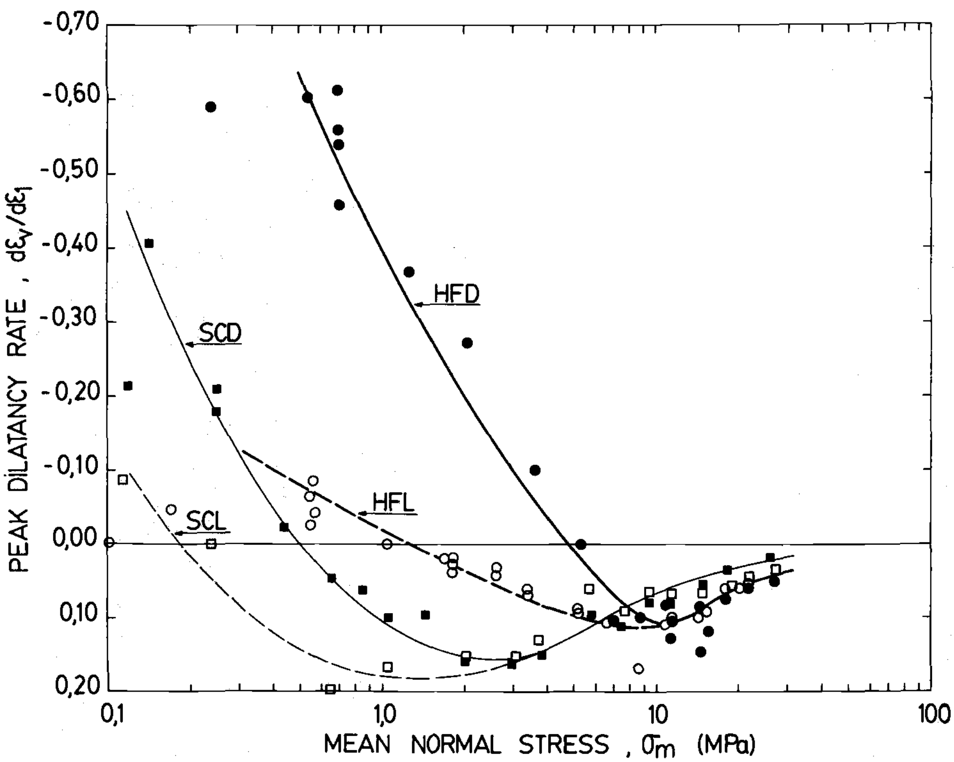

FIG. 13—*Stress peak friction angle evolution with mean pressure.*

acteristic angle and the interparticle friction angle. The characteristic angle is defined by Luong and Touati as the mobilized friction angle when the minimum in volume change is reached in the first stage of low-pressure triaxial tests on dense material [27]. As far as siliceous sand is concerned, the actual friction angle does not decrease below these bounds (32°). On the other hand, for calcareous sand, friction angles obtained at high mean pressures are clearly smaller than the characteristic angle (ϕ_c = 39°), and than the interparticle friction angle (ϕ_μ = 38°), the latter determined indirectly on the basis of Rowe's stress dilatancy theory. This means that, for calcareous sands, with high compressibility linked with intraparticle porosity and brittleness of their grains, the interparticle friction angle, ϕ_μ, cannot be considered as a lower limit for the friction angle.

Figures 11 and 12 show that the compressibility of granular materials under triaxial shear reaches a maximum value and then decreases in the high-pressure range. This behavior is also shown in Fig. 14 giving the evolution of the rate of volume change at peak stress: at very high pressures, the rate of volume change at peak becomes zero. This reduction of sand compressibility at the peak is related to the transformation of the material that occurred during the consolidation stage, as pointed out by Billam [33]. If the total volume changes due to both confining stage and shear stage of the test are considered, a monotonic increase with increasing pressure is observed (as expected).

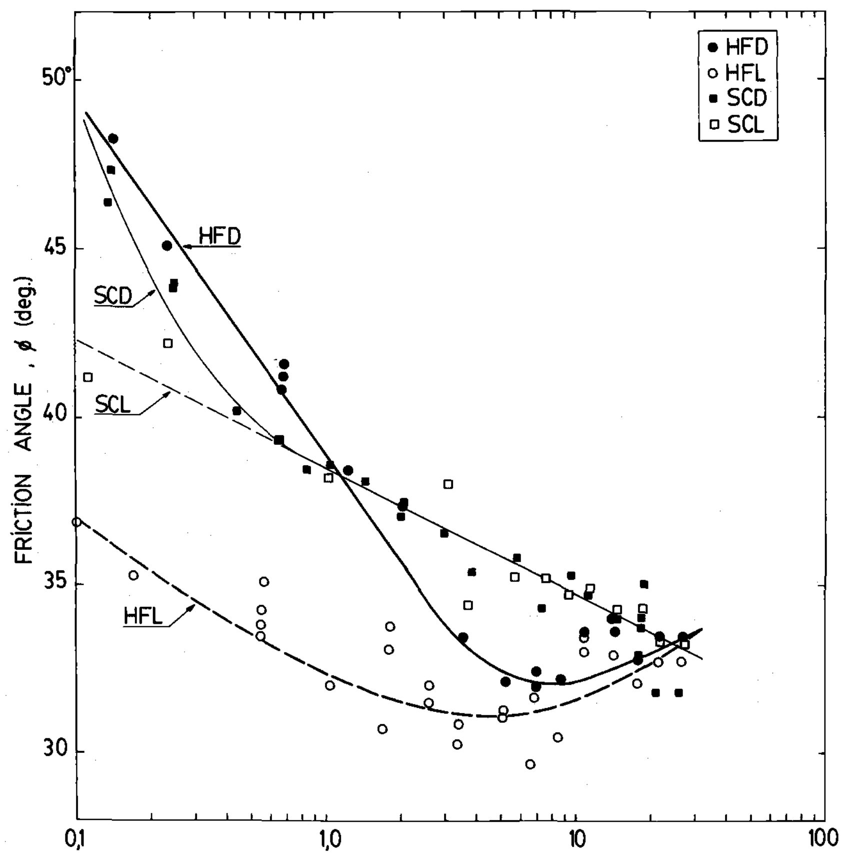

FIG. 14—*Stress peak dilatancy rate evolution with mean pressure.*

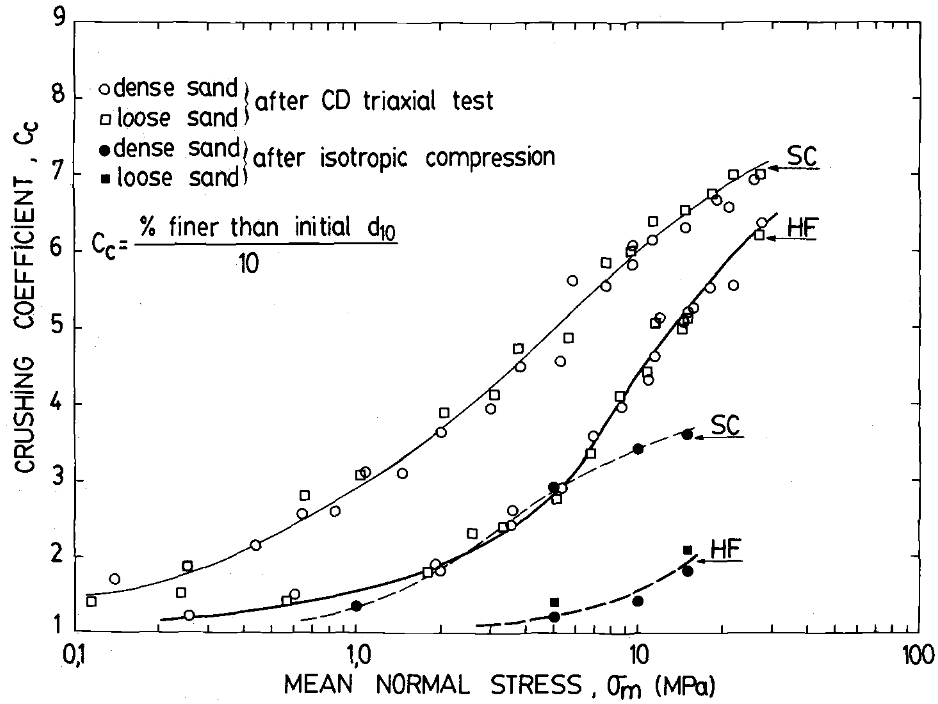

FIG. 15—*Grain crushing evolution with mean pressure.*

For granular materials, grain crushing is the main cause of compressibility under elevated pressures. Figure 15 gives typical features of both siliceous and calcareous sands. The classic behavior is recognized here (that is, the main part of grain crushing occurs during the shearing stage of the triaxial test). The magnitude of crushing is expressed in terms of a crushing coefficient, C_c, defined as 0.1 times the percentage of particles finer than D_{10} of the original sand. For both sands, grain crushing begins at very low pressure, because of the brittleness of the calcareous particles and the angularity of the siliceous particles. With higher pressures, the rate of grain crushing decreases, which is responsible for the decrease in compressibility already described.

Conclusions

The use of short specimens ($L/D = 1$) with lubricated ends in the compression triaxial test is preferable to the use of conventional specimens (nonlubricated ends, $L/D = 2$) for the determination of stress–strain parameters, because of the improved homogeneity. This improvement was discussed along these lines, on the basis of global considerations (global response, specimen shape), and local measurement (x-ray scanner).

Despite the problem of bedding error, these modified experimental conditions were estimated to be particularly advantageous, with regard to the following objectives:

- Uniform distribution of stress inside the specimen, for the study of grain-crushing effect
- Homogeneous deformation of the specimen, for measurement of significant volume changes
- Large axial strains (> 10%)
- Elevated confining pressures (> 1 MPa)

Classic behavior was obtained for two types of granular materials of different mineralogic composition, tested under elevated confining pressures: decrease of the friction angle and high compressibility related to grain crushing.

In the case of calcareous sands, characterized by a very high compressibility, due to the intraparticle porosity and the brittleness of their grains, the friction angle may decrease far below the interparticle friction angle, previously considered as a lower limit.

Finally, time effects (creep) observed during the confining stage of triaxial tests increase with the increasing pressure applied to the specimen and seem to be related to the propagation of the rupture of particles.

Acknowledgment

Thanks are due to Pleybert and Martin, who gave us access to and operated the x-ray scanner of LETI, Centre d'études Nucléaires de Grenoble, France.

References

[*1*] Bishop, A. W. and Henkel, D. J., *The Measurement of Soil Properties in the Triaxial Test,* Edward Arnold, London, 1957.
[*2*] Sowers, G. H., *Laboratory Shear Testing of Soils, STP 361,* American Society for Testing and Materials, Philadelphia, 1963, pp. 3–21.
[*3*] Roscoe, K. H., Schofield, A. N., and Thurairajah, A., *Laboratory Shear Testing of Soils, STP 361,* American Society for Testing and Materials, Philadelphia, 1963, pp. 111–128.
[*4*] Kirkpatrick, W. M. and Belshaw, D. J., *Geotechnique,* Vol. 18, 1968, pp. 336–350.
[*5*] Bishop, A. W. and Green, G. E., *Geotechnique,* Vol. 15, 1965, pp. 243–266.
[*6*] Rowe, P. W. and Barden, L., *Journal of the Soil Mechanics and Foundations Division, American Society of Civil Engineers,* Vol. 90, 1964, pp. 1–64.
[*7*] Biarez, J., "Contribution à l'étude des sols et des matériaux pulvérulents," Thèse de doctorat es sciences, Université de Grenoble, 1962.
[*8*] Bouvard, D. and Stutz, P., *Geotechnical Testing Journal,* Vol. 9, 1986, pp 10–18.
[*9*] Hettler, A. and Vardoulakis, I., *Geotechnique,* Vol. 34, 1984, pp. 183–198.
[*10*] Lee, K. L., *Journal of the Geotechnical Engineering Division, American Society of Civil Engineers,* Vol. 104, 1978, pp. 687–704.
[*11*] Lee, K. L. and Seed, H. B., *Journal of the Soil Mechanics and Foundation Division, American Society of Civil Engineers,* Vol. 90, 1964, pp. 173–175.
[*12*] Olson, R. E. and Campbell, L. M., *Journal of the Soil Mechanics and Foundation Division, American Society of Civil Engineers,* Vol. 90, 1964, pp. 167–173.
[*13*] Raju, V. S., Sadasivan, S. K., and Ventakaraman, M., *Soils and Foundations,* Vol. 12, 1972, pp. 35–43.
[*14*] Roy, M. and Lo, K. Y., *Canadian Geotechnical Journal,* Vol. 18, 1971, pp. 579–588.
[*15*] Vardoulakis, I., *Acta Mechanica,* Vol. 32, 1979, pp. 35–54.
[*16*] Tatsuoka, F., Molenkamp, F., Torii, T., and Hino, T., *Soils and Foundations,* Vol. 24, 1984, pp. 113–128.
[*17*] Lade, V., *Proceedings,* IUTAM Conference on Deformation and Failure of Granular Material, Delft, 1982, pp. 461–471.
[*18*] Drescher, A. and Vardoulakis I., *Geotechnique,* Vol. 32, 1982, pp. 291–303.
[*19*] Goldscheider, M., *Results of the International Workshop on Constitutive Relations for Soils,* 6–8 Sept. 1982, Gudehus, G. et al., Eds., Balkema, Rotterdam/Boston, 1984, pp. 11–54.
[*20*] Dendani, H., Flavigny, E., and Fry, J. J., in this volume, pp. 486–500.
[*21*] Colliat-Dangus, J. L., Desrues, J. and Flavigny, E., *Revue Française de Géotechnique,* No. 34, 1986, pp. 41–55.
[*22*] Vesic, A. S. and Clough, G. W., *Journal of the Soil Mechanics and Foundations Division, American Society of Civil Engineers,* Vol. 94, 1968, pp. 661–688.
[*23*] Bishop, A. W., Webb, D. L., and Skinner, A. E. in *Proceedings,* Sixth International Congress on Soil Mechanics and Foundation Engineering, Montreal, University of Toronto Press, 1965, pp. 170–174.

[24] Ramamurthy, T., Kanitkar, V. K., and Prakash, K., *Indian Geotechnical Journal*, Vol. 4, 1974, pp. 39–63.
[25] Ramamurthy, T. and Lal, R. S., *Journal of the Indian National Society SMFE*, Vol. 9, 1970, pp. 305–321.
[26] Miura, N. and Yamanouchi, T., *Soils and Foundations*, Vol. 15, 1975, pp. 23–34.
[27] Luong, M. P. and Touati, A., *Revue Française de Géotéchnique*, No. 24, 1983, pp. 51–64.
[28] Vardoulakis, I. and Graf, B., *Proceedings*, IUTAM Conference on Deformation and Failure of Granular Material, Delft, 1982.
[29] Lanier, J., in this volume, pp. 859–869.
[30] Desrues, J., Lanier, J., and Stutz, P., *Engineering Fracture Mechanics*, Vol. 21, 1985, pp. 909–921.
[31] Desrues, J., "La Localisation de la déformation dans les Matériaux Granulaires," Thèse de doctorat es sciences, Université de Grenoble, 1984, pp. 177–188.
[32] Colliat-Dangus, J. L., "Comportement des matériaux Granulaires sous fortes contraintes," Thèse de doctorat de spécialité, Université de Grenoble, 1986, pp. 170–173.
[33] Billam, J., *Proceedings*, Roscoe Memorial Symposium, Cambridge, England, March 1971, pp. 69–80.

Philip C. Lambe[1] *and William T. Heartz*[2]

Consolidated Drained Triaxial Testing of Piedmont Residual Soil

REFERENCE: Lambe, P. C. and Heartz, W. T., **"Consolidated Drained Triaxial Testing of Piedmont Residual Soil,"** *Advanced Triaxial Testing of Soil and Rock, ASTM STP 977,* Robert T. Donaghe, Ronald C. Chaney, and Marshall L. Silver, Eds., American Society for Testing and Materials, Philadelphia, 1988, pp. 311–320.

ABSTRACT: The paper describes problems encountered in performing consolidated drained triaxial tests on Piedmont residual soil specimens trimmed from both Shelby tube samples and block samples. The micaceous silty soil has steeply dipping layers, planes of weakness, and granular seams. These characteristics complicate trimming and cause specimens to bend during consolidation and shearing. Because some specimens failed at strains of 14% to 20%, the nonuniformities influence the estimation of peak shear strength. To cope with variability, a multistage test on one specimen was compared to behavior measured on three single-stage tests performed on three specimens; all four specimens were trimmed from the same block. Comparative results were inconclusive.

KEY WORDS: residual soil, triaxial tests, shear strength, testing procedures

This paper describes the consolidated drained triaxial testing of Piedmont residual soil samples—the procedures used for trimming samples, performing tests, and finally reducing test results, and the problems encountered. The overall research objective [*1*] was to determine the soil properties at a North Carolina State University (NCSU) test site and to evaluate how well different in situ equipment types measure the properties of Piedmont residual soil. The triaxial test was the primary tool for evaluating the shear strength, compressibility, and permeability of the sampled soils with depth at the test site.

Tests were run on both Shelby tube samples and block samples. During the 2-year project 24 Shelby tube samples were taken from three boreholes, and nine 0.3- by 0.3- by 0.3-m block samples were trimmed from a 3.7-m-deep test pit. These samples were sealed in wax and stored in a humid room until trimming for tests.

In all, 15 triaxial tests were performed on specimens trimmed from Shelby tube samples and 13 tests were run on specimens trimmed from the block samples. Observed behavior of specimens during both initial consolidation and shear to failure indicated nonuniform strains.

Soil Characteristics

The soils underlying the test site have weathered from gneiss and schist bedrock. Parker [*2*] says these rocks dip 60° to the northwest. This site has 15 to 17 m of Piedmont residual soil underlain by 3 to 4.6 m of partially weathered rock before reaching sound bedrock. Sowers and Richardson [*3*] have described typical properties for Piedmont residual soils.

[1] Assistant professor of civil engineering, North Carolina State University, Raleigh, NC 27695.
[2] Research engineer, Rockwell International, 189 Wildwood Court, Richland, WA 99352.

Triaxial tests were performed on specimens taken from the upper 12.2 m of the residual soil profile having standard penetration test blow counts less than 25. The soils were visually classified as micaceous clayey silts, micaceous sandy silts, and micaceous silts. Specimens above 3 m had liquid limits of 70 to 90 and plasticity index values of 30 to 40 to classify by the Unified Soil Classification System (USCS) symbol MH. For specimens deeper than 3 m liquid limits varied from 35 to 50 and plastic limit tests were difficult to run. Linear shrinkage limit tests [*4*] measured plasticity index values of less than 7 to classify by either the USCS symbols ML or SM soils depending on the percentage of fines. The tested soils had specific gravity values varying from 2.7 to 2.85 with an average value of 2.8.

In their natural state the soils are multicolored with predominately red and brown in the upper 1.5 to 3 m; gold, brown, and tan down to the water table at 10 m; and gray, green, and tan below the water table. The micaceous soils underlying the upper 1.2 m of clayey soils have a banded appearance like the parent bedrock with 2.5 to 7.6-cm-thick bands distinguished by both color and textural differences. The soil surface polishes easily when rubbed because of the high mica content. In the side of the 3.7-m-deep test pit and in the block samples 0.6- to 1.9-cm clay nodules were observed. In many of these nodules were 0.16- to 0.64-cm-diameter cavities up to 5 cm long.

The soil samples deeper than 1.2 m have thin tan, red, and black lines. These lines do not always parallel the thicker bands and may represent old joints. The black lines often are planes of weakness as samples fall apart on slickenside surfaces. St. John and co-workers [*5*] hypothesized that the slickensides formed from strains induced by differential expansion of the bedrock during weathering. Some soil samples have 0.16 to 1.2-cm-thick quartz seams. The size of the quartz fragments increases with depth.

Figure 1 shows profiles of void ratio, saturation, percentage of fines (minus #200 sieve),

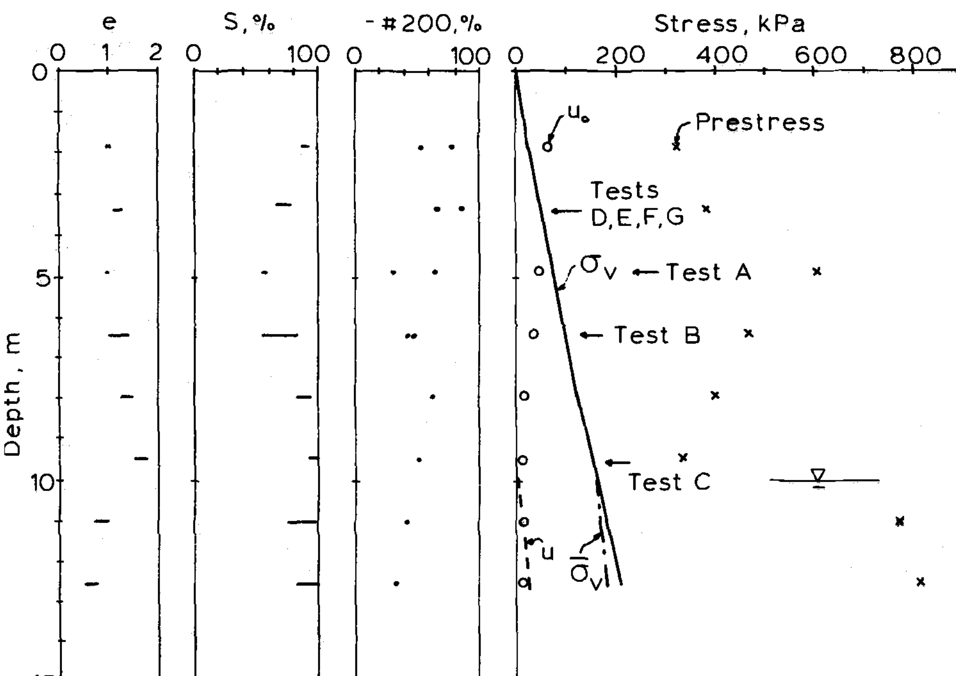

FIG. 1—*Profile of research site.*

and in situ vertical stresses based on measurements on Shelby tube samples. The upper 5 m have more than 50% fines, void ratios of 1 to 1.3, and saturation values decreasing from 90 to 60%. For samples from 5 to 10 m deep the void ratios increase with depth and vary from 1 to 1.75, about 50% fines, and the saturation increases with depth from 60 to 100% at the water table. For samples below the water table the void ratio decreases with depth from 0.85 to 0.65, the saturation varies between 80 and 100%, and the samples had a decreasing percentage of fines.

The stress plot portrays the total vertical stress, the in situ pore pressure measured below the water table, the effective vertical stress below the water table, the residual negative pore pressures, and the prestress pressures measured in consolidation tests. The open circles on the plot show the residual negative pore pressures, u_o, measured as described in Ref *6*. Because an unconfined sample has a zero total stress, the residual negative pore pressure represents the effective stress. The difference between the in situ vertical effective stress and u_o provides a measure for the stress unloading experienced by the sample. Because the in situ pore pressure for samples above the water table was not measured, the total vertical stress is used as a reference. The measured u_o values decrease with increasing depth although the effective vertical stresses increase. Vaughan [*7*] reports that the grain size distribution for residual soils often limits the maximum negative pore pressure that samples can hold and therefore causes samples to swell. The Shelby tubes sampled below the water table were observed to expand enough that the mechanical seals were sometimes pushed out the end of the tube. Samples would swell 1 to 3% based on measured recompression index values and stresses changing from in situ vertical effective stress to the residual pore pressure. This swelling takes place both in the tube and after sample extrusion. No quantitative measurements of the observed swelling were made. The Xs on the stress plot in Fig. 1 indicate the prestress pressures determined from consolidation tests using the Casagrande procedure [*8*]. While the stress history causing a prestress pressure in residual soils differs from the stress history experienced by sedimentary soils, the prestress pressure still plays an important role in the estimation of field settlements. Above the water table the pressures varied from 300 to 500 kPa with one value of 600 kPa at 5 m deep. The samples below the water table had prestress pressures of almost 800 KPa.

The Piedmont residual soils at this research site are micaceous nonplastic silts with varying color and texture. The presence of weakness planes, quartz seams, and the steeply inclined dip of the soil layers affects specimen trimming and testing.

Testing Procedure

The residual soil specimens with permeabilities greater than 10^{-5} cm/s could be tested in drained triaxial tests of moderate duration. The unsaturated specimens were saturated before testing by means of back pressure and permeation to provide accurate volume change measurements. This program represented an initial effort at testing residual soil specimens in the NCSU laboratories so test procedures closely followed those proposed by Bishop and Henkel [*9*]. Sample dimensions and equipment details were based on the existing NCSU laboratory facilities. The observed features reported in this paper will influence the procedures used in future testing. To minimize the influence of specimen variability on measured strength envelopes, multistage testing was performed on three specimens trimmed from blocks following the procedure described in Ref *10*. The other 25 specimens were sheared to failure at only one consolidation stress.

To minimize breakage along weakness planes, samples were confined during trimming by a 12.5-cm-long and a 3.8-cm-inner-diameter cylindrical steel tube having a 0.3-cm-long and 3.6-cm-inner-diameter cutting shoe. Before final trimming the Shelby tube samples were cut into 6-in. (15.2-cm) lengths, extruded, and sealed. The block samples were cut into octants by first halving them with a serrated wire saw and then quartering each half using a band saw. Each octant of the full block, which was sealed in wax for later use, yielded four 7.6- by 7.6- by 15.2-cm blocks for use in triaxial tests, making a total of 32 triaxial specimens per block. Before advancing the trimming tube over the coarsely trimmed samples, they were roughly trimmed to size with a knife in the manner described in Ref *11*. The trimmed samples' surface had small pockmarks left by quartz fragments and by trimming against the grain. The samples behave as if they had a grain as observed in wood because of the oriented mica particles. When breaks occurred along weakness planes the samples were abandoned, therefore tests generally measured properties of the stronger samples.

The 3.6-cm-diameter and 7.9-cm-long specimens were tested in a Wykeham Farrance triaxial cell and loaded to failure by a Wykeham Farrance load frame. The cell pressure and back pressure were applied by an air compressor and measured by Data Instruments Model AB pressure transducers. The vertical load was measured by a 900-N Wykeham Farrance proving ring. The piston met the specimen top cap at a ball joint which allowed the top cap to rotate. The specimen was contained by two Trojan prophylactics. No membrane correction was made to the measured axial load. Volume changes during both consolidation and drained shear were measured by burettes having an internal circular cross-sectional area equal to 0.735 cm^2.

The triaxial specimens were consolidated to an isotropic initial stress after sitting for 1 day at an initial isotropic effective stress of 6.9 to 13.8 kPa and a 345-kPa back pressure, which was reached in three steps: 138, 241, and 345 kPa. The specimens were then isotropically consolidated to pressures of between 52 and 621 kPa in one to four increments depending on the magnitude of the final stress. Isotropic consolidation was used for this preliminary program; future testing will examine the influence of K_o consolidation. After each consolidation increment, the specimen permeability was measured in a falling head test and 0.3 to 1.0 void volumes of distilled water flowed through the specimen. After the final consolidation increment, several permeability tests were performed and 1 to 5 void volumes flowed through the specimens. The measured permeability decreased with each consolidation increment and from the beginning to the end of consolidation specimens

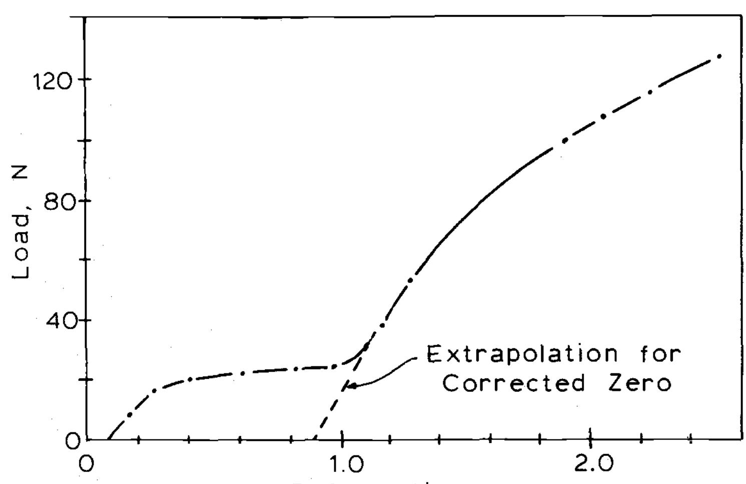

FIG. 2—*Correction for initial seating error.*

experienced a twofold to fivefold decrease in permeability. The measured values varied from 10^{-3} to 10^{-4} cm/s for vertically oriented specimens.

During consolidation at pressures less than the prestress pressure, the specimens consolidated more perpendicular to the plane of layering than parallel to it. Therefore, as specimens consolidated they often tilted. For one specimen in particular the top cap moved laterally 0.6 cm to 0.95 cm representing a tilt of 5 to 7°. This tilt caused problems at the start of shearing when the piston was moved into contact with the top cap. Figure 2 shows the plot of load versus deformation for one such test at the start of shearing. These results were corrected visually by taking the first two data points that show a concave downward trend and extrapolating them back to the horizontal axis. For the test pictured in Fig. 2, the zero deformation reading used in evaluation was 0.9 mm instead of the measured 0.1 mm.

The isotropically consolidated specimens were sheared to failure under a compression loading stress path at a rate of 0.0046 cm/min or about 0.06%/min. The specimens were drained at the bottom while pore pressure was measured at the sealed top. The pore pressure measurements indicated that specimens were strained sufficiently slowly to ensure full drainage. For some specimens, shear led to bending of the specimen. The 15 Shelby tube specimens failed in three failure modes. Four of the specimens failed in a symmetrical bulging mode, four specimens failed along foliation or weakness planes without tilting of the top cap, and seven specimens experienced top cap tilting. Of the seven specimens that experienced bending, four showed slight bending while the other three experienced severe bending. Figure 3 shows one specimen that failed in symmetrical bulging and one that experienced severe bending.

Results

The specimens that experienced bending during shear felt both nonuniform stresses and strains. The effect of these nonuniformities can be investigated qualitatively by comparing the test results measured for specimens that behaved in the different failure modes. Figure

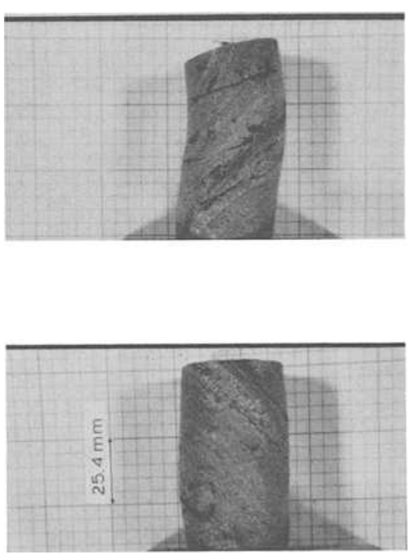

FIG. 3—*Photographs of two failed specimens.*

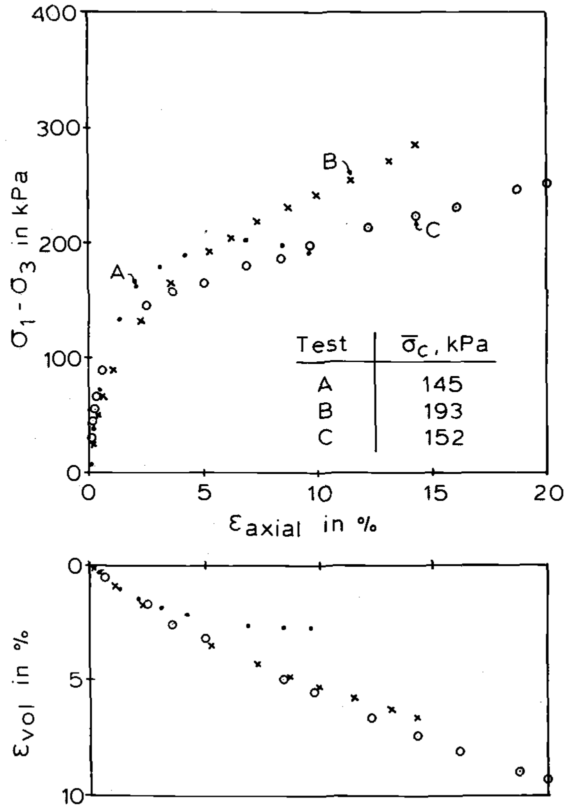

FIG. 4—*Stress–strain curves for tests on Shelby tube specimens.*

4 compares three tests that failed in different modes. Test A on a specimen taken from 5 m deep was consolidated to an isotropic stress of 145 kPa, which was two times the in-place vertical total stress and one quarter of the prestress pressure; the Test B specimen came from 6.4 m deep and was consolidated to a stress of 193 kPa, which was two times the vertical total stress and one half of the prestress pressure; and the Test C specimen came from 9.4 m deep and was consolidated to a stress of 152 kPa, which was equal to the vertical total stress and one half of the prestress pressure. Although these three specimens were consolidated to about the same stress, they represent different soil and observed behavior differences must be attributed to differences in both failure mode and soil characteristics. In Test A the top cap tilted slightly and the specimen experienced moderate bending; in Test B the tilting and bending were more severe; in Test C the top cap tilted little and the specimen bulged symmetrically. The specimen in Test A also failed along a weakness plane inclined at less than 30° to the horizontal, while the specimens in Tests B and C were not observed to fail along a plane.

Figure 4 compares the results in plots of deviator stress versus average axial strain and volumetric strain versus axial strain. The stress–strain curve for Test A specimen rises to a peak at 7% strain and then decreases while the stresses for both Test B and C specimens increase almost linearly at strains greater than 2 to 4%. Test B and C specimens were still carrying increasing stress at average strains of 14 and 20%. The measured volumetric strain

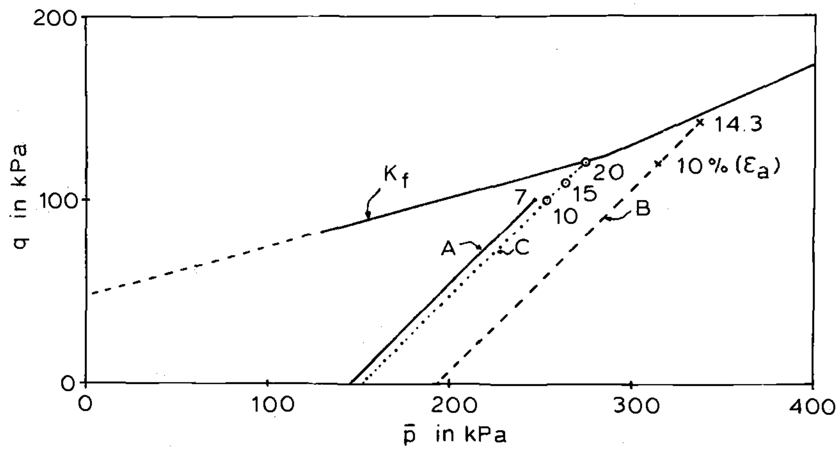

FIG. 5—*Stress paths for tests on Shelby tube specimens.*

plots appear similar for all three tests at axial strains less than 2%. The specimen for Test A has a larger prestress pressure and experienced a weakness plane; these factors combine with the different failure mode to explain the measured behavior different from Test B and C specimens. At low strain all three tests have about equal moduli with Tests A and C being slightly stiffer than Test B.

Figure 5 compares the stress paths for Tests A, B, and C on a plot with the K_f line, which represents failure on a p–q plot, determined from the maximum stress measured at less than or equal to 20% strain for all 15 tests performed on Shelby tube specimens. The specimen for Test A, which failed at a strain of 7%, falls below the K_f line, while specimens for Tests B and C only reach the line at strains of 14 to 20%. Therefore this failure line may be influenced by the nonuniformities apparent at large strain.

Figure 6 compares the test results for a multistage triaxial test performed on Specimen G with the results of three single-stage triaxial tests performed on Specimens D, E, and F. All the specimens were trimmed from one block taken at a depth of 3.4 m and tested at consolidation stresses equal to the vertical total stress (Specimens D and G1), two times the vertical total stress (Specimens E and G2), and four times the vertical total stress (Specimens F and G3). These stresses equal approximately 0.1, 0.2, and 0.4 times the prestress pressure of 550 kPa. All six tests show stresses rising to a peak and then decreasing. The failure strain increases with increasing consolidation stress. Tests G1 and D have similar slopes and fail at 1.5%; Tests G2 and E also have similar slopes but Test E fails at 1.5% strain instead of 2% for the multistage Test G2; and the high stress Test G3 failed at 5% strain and a 28% lower maximum stress than Test F which failed at 12.5% strain. The multistage Test G3 showed a higher modulus than Test F. The Test G specimen experienced severe bending which got progressively worse with each stage and the errors should be most severe during the final stage, G3. Figure 7 compares the stress paths for Tests D, E, F, G1, G2, and G3 with the K_f line based on the tests performed on vertically oriented specimens taken from 3.4-m-deep block samples. The strength results for the multistage test during Stages G1 and G2 fall within 10% of the results for the single-stage tests, while the error exceeds 30% for stage three when bending is severe. Multistage testing was abandoned early in the test program because of the brittle behavior observed on specimens consolidated to low effective stress. These results are inconclusive, but the potential payoff for determining the strength envelope in highly variable soils suggests further investigation is worthwhile.

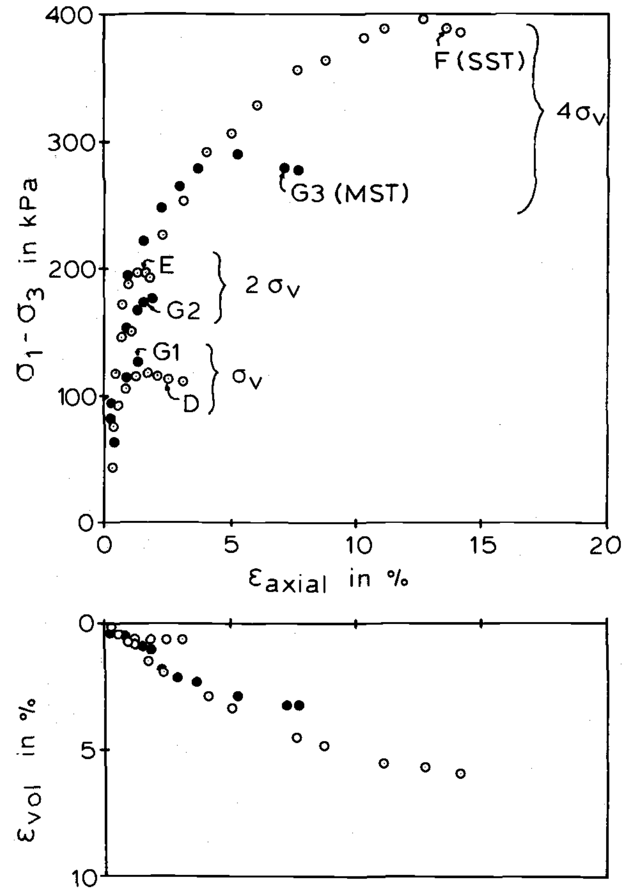

FIG. 6—*Stress–strain curves for tests on block specimens.*

Summary and Conclusions

The characteristics of residual soil affect the trimming of triaxial samples and their subsequent testing. Samples taken at this site had steeply dipping foliation inclining the axis of symmetry for anisotropy about 60° from the vertical axis. These samples exhibited spacial variability with weakness planes, quartz seams of medium-sand-sized grains, and an apparent grain direction caused by the high mica content. The samples were trimmed using a tube to provide some confinement. Even with confinement some of the samples broke along weakness planes so that test results only represent the stronger samples.

The steeply dipping foliation caused specimens to bend during both isotropic consolidation and shearing to failure. Bending affects the uniformity of stresses and strains in the triaxial specimens. This influence should get larger and larger with increasing strains. Because both test B and C specimens failed at strains of 14 to 20% these nonuniformities can significantly influence the estimation of a peak shear strength. Future tests need to examine the influence of a fixed top cap and of frictionless end platens on measured results. Other variables that should be investigated include sample size and anisotropic consolidation.

The variability of the residual soils makes multistage testing an attractive alternative so that the complete failure line can be determined on one soil specimen. The example of

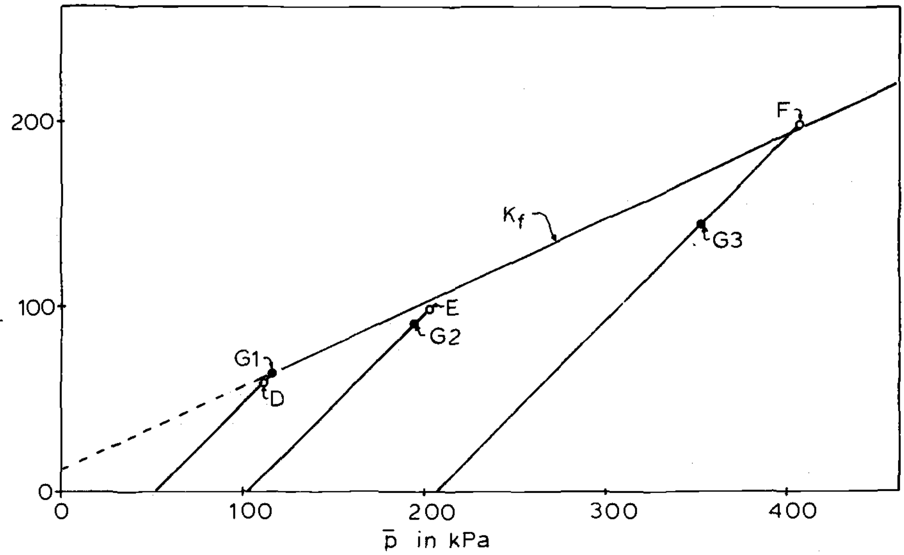

FIG. 7—*Stress paths for tests on block specimens.*

multistage testing described in this paper was inconclusive. During the first two stages, the multistage test specimen failed at stresses within 10% of the single-stage test specimen. But for the third stage of the multistage test, the specimen bent severely and failed at a 30% lower stress than measured for the single-stage test. More extensive comparison of multistage and single-stage testing is necessary to establish the value of this technique for Piedmont residual soils.

The triaxial test will remain a valuable tool for studying the behavior of residual soils, but the characteristics of these soils will increase the variability of test results over those reported for sedimentary deposits, and care must be taken to observe the behavior during consolidation and shearing.

Acknowledgments

Funds for this research were provided by the National Science Foundation Grant no. CEE-8307208. The authors would also like to acknowledge the contributions of STS Consultants Ltd. and Soil and Material Engineers Inc. who provided drilling help.

References

[1] Heartz, William T., "Properties of a Piedmont Residual Soil," Ph.D. Thesis, North Carolina State University, 1986.
[2] Parker, John M. III, "Geology and Mineral Resources of Wake County," Bulletin 86, North Carolina Department of Natural Resources, Geological Survey Section, 1979.
[3] Sowers, G. F. and Richardson, T. L., "Residual Soils of the Piedmont and Blue Ridge," Transportation Research Record 919, Transportation Research Board, 1983, pp. 10–16.
[4] Head, K. H., *Manual of Soil Laboratory Testing, Volume 1,* Halstead Press, 1980.
[5] St. John, B. J., Sowers, G. F., and Weaver, C. E., "Slickensides in Residual Soil and Their Engineering Significance," *Proceedings,* Seventh International Conference on Soil Mechanics and Foundation Engineering, Mexico City, Vol. 2, 1969, pp. 591–597.
[6] Lambe, T. W., "Residual Pore Pressures in Compacted Clay," *Proceedings,* Fifth International Conference on Soil Mechanics and Foundation Engineering, Paris, Vol. 1, 1961, pp. 207–211.

[7] Vaughan, P. R., "Mechanical and Hydraulic Properties of In-Situ Residual Soils," presented at First International Conference in Geomechanics in Tropical Lateritic and Saprolitic Soils, Brasilia, Brazil, 1985.
[8] Casagrande, A., "The Determination of the Pre-Consolidation Load and Its Practical Significance," Discussion D-34, *Proceedings,* First International Conference on Soil Mechanics and Foundation Engineering, Cambridge, MA, Vol. 3, 1936, pp. 60–64.
[9] Bishop, A. W. and Henkel, D. J., *The Measurement of Soil Properties in the Triaxial Test,* St. Martins, New York, 1962.
[10] Parker, J. C., Amos, D. F., and Sture, S., "Measurement of Swelling, Hydraulic Conductivity, and Shear Strength in a Multistage Triaxial Test," *Soil Science Society American Journal,* Vol. 44, 1980, pp. 1133–1138.
[11] Gibbs, H. J., Hilf, J. W., Holtz, W. G., and Walker, F. C., "Shear Strength of Cohesive Soils," presented at the American Society of Civil Engineers Soil Mechanics and Foundation Division Conference, Boulder, CO, 1960.

Vincent Silvestri,[1] Michel Soulié,[1] Ziad Touchan,[1] and Bernard Fay[2]

Triaxial Relaxation Tests on a Soft Clay

REFERENCE: Silvestri, V., Soulié, M., Touchan, Z., and Fay, B., "**Triaxial Relaxation Tests on a Soft Clay,**" *Advanced Triaxial Testing of Soil and Rock, ASTM STP 977,* Robert T. Donaghe, Ronald C. Chaney, and Marshall L. Silver, Eds., American Society for Testing and Materials, Philadelphia, 1988, pp. 321–337.

ABSTRACT: Results of consolidated undrained triaxial relaxation tests on a soft sensitive clay of eastern Canada are presented and discussed. The initial consolidation phases of the triaxial tests are carried out under both isotropic and anisotropic stress conditions.

The results show that pore water pressures remain approximately constant during the relaxation phases of the tests. The phenomenological model developed by Prevost (Journal of the Geotechnical Engineering Division, ASCE, Vol. 102, No. GT12, 1976, pp. 1245–1259) describes the observed response quite well. In addition, because the clay possesses a well-defined volumetric yield curve, the position of this curve should be taken into account when analyzing the results. Finally, triaxial test procedure and equipment modifications used in the laboratory investigation are fully described.

KEY WORDS: triaxial tests, relaxation, undrained, sensitive clay, phenomenological model

The effects of time and deformation behavior of clays have been the subject of numerous investigations, in particular during the last two decades. As a result of the classic separation between strength and settlement problems, various types of time effects have been separately defined and studied: creep, stress relaxation and steady-state deformation as related to stability problems, and secondary consolidation as related to settlement problems. Only a few attempts have been made to develop a unified approach that encompasses all time-related phenomena.

In the earlier studies of time effects, different mechanical or rheologic models were proposed for the stress–strain–time response behavior of clays [*1–6*]. Linear and nonlinear springs and dashpots, and sliders were combined to provide a reasonable approximation of the behavior for certain soils and loading conditions. Mathematical relationships were developed to describe creep, stress relaxation, steady-state deformation, and secondary consolidation, in terms of the models' parameters. The accuracy of these models to predict both laboratory and field response depended on the proper formulation of the parameters and the boundary conditions.

In recent years, it became evident that more and more complex models were needed to properly represent clay response. The mathematical difficulties associated with the analysis of these models and their inherent limitations led some investigators to consider phenomenological approaches in which creep, stress relaxation, and steady-state deformation are simply considered to be different manifestations of the same basic phenomenon, that is, the dependence of clay response on time [*7–9*].

[1] Professor, professor, and graduate research assistant, respectively, Civil Engineering Department, École Polytechnique, Montreal, Quebec, Canada H3C 3A7.

[2] Chief, Soil Mechanics Laboratories, École Polytechnique, Montreal, Quebec, Canada H3C 3A7.

Most laboratory investigations of the time effects associated with undrained shear strength of soft clays use triaxial creep tests [*10*]. Results reported in Refs *7*, *8*, and *10* to *14* illustrate quite well the time dependence of clay response.

Although triaxial stress relaxation tests are of shorter duration [*15*] than creep tests, they have not been used as extensively as the latter for the study of time effects on clay response. This is probably due to technical difficulties associated with the running of true stress relaxation tests. However, in spite of the paucity of data reported in the literature, it appears that the various relationships derived from creep tests may equally be used to describe relaxation phenomena [*3,8,16,17*]. It has been shown that, even though the deviator stress decreases with time, the pore water pressure remains more or less constant [*3,8,16,17*]. This is in accord with the hypothesis of Lo [*18,19*] and others that pore water pressures depend almost exclusively on strain.

With the technical facilities existing today, relaxation tests may be as easily performed as creep tests. In addition, in the authors' opinion, relaxation tests provide better insight into the mechanisms that control the mobilization of the shear strength in clays than creep tests provide. Indeed, the relaxation test is the only test to find the long-term strength of the soil skeleton as it is. In an undrained creep test, because both the effective stresses and the soil structure continuously change as a result of increasing strains, it is difficult to relate the applied stress to the nonhomogeneous strain state throughout the specimen. In addition, in a drained creep test it is quite difficult to separate primary consolidation effects from those due to creep.

This paper presents the results of a laboratory investigation on the stress relaxation phenomenon observed in both isotropically and anisotropically consolidated undrained triaxial tests. The soil used in this study is a soft sensitive clay from Louiseville, Quebec, Canada. Problems encountered with triaxial stress relaxation tests are presented, and the solutions adopted are discussed. In addition, the analysis of the experimental data is performed with reference to the phenomenological model of Prevost [*9*].

Soil Properties

The soil used in this study was obtained from a test trench excavated on the outskirts of Louiseville, a town located about 100 km northeast of Montreal. The site is located along Highway 40, on the north shore of Lake St-Peter.

Undisturbed blocks of clay were recovered below the weathered crust, at a depth varying between 3 m and 5 m. The general properties of the Louiseville clay are summarized in Table 1.

Triaxial Relaxation Test Procedures

Both isotropically consolidated and anisotropically consolidated undrained triaxial tests were performed on the Louiseville clay. The specimens used in the study measured 50 mm in diameter by 100 mm in height. Top and bottom porous stones, as well as filter paper side drains, were used to speed up consolidation and equalization of pore pressure. A back pressure of 200 kPa was applied in all the tests. For the initial consolidation phase, a dead weight system was used for the application of the axial load.

For the isotropically consolidated undrained (CIU) tests, three confining pressures, σ_c', were used: 30, 58, and 96 kPa. These particular values were chosen in such a way that, while at 30 kPa and 58 kPa the soil remained overconsolidated and sensitive, at 96 kPa, it became normally consolidated and insensitive. Indeed, the preconsolidation pressure was found to be about 90 kPa under isotropic consolidation conditions.

TABLE 1—*Geotechnical properties of the Louiseville clay.*

Natural water content	82%
Liquid limit	59%
Plastic limit	26%
Plasticity index	33%
Liquidity index	1.7
Silt content	22%
Clay content	78%
Activity	0.4
Field vane strength	30 kPa
Sensitivity (by field vane)	20
Oedometric preconsolidation pressure, σ_{po}'	100–120 kPa
Vertical strain at σ_{po}'	3–4%
Isotropic preconsolidation pressure, σ_{pi}'	80–100 kPa
Volumetric strain at σ_{pi}'	6–8%

For the anisotropically consolidated undrained (CAU) triaxial tests, the specimens were initially consolidated under a stress state (σ_{1c}', $\sigma_{3c}' = K_0\sigma_{1c}'$), where an average value of about 0.70 was retained for K_0, the coefficient of the lateral pressure at rest. This value of K_0 was based on the plasticity and the degree of overconsolidation of the clay [*20*]. Three initial consolidation stress states (σ_{1c}', σ_c') were used in the CAU tests: (35 kPa, 21 kPa), (77 kPa, 53 kPa), and (103.5 kPa, 75 kPa). For the first two of these, the specimens remained overconsolidated throughout the shearing process, whereas for the last, the effective stress path during the subsequent undrained loading was such that it approximately followed the volumetric yield surface of the clay.

Table 2 presents a summary of the tests performed and the volumetric strains experienced by the soil specimens at the end of the consolidation phases.

Once the consolidation phases of both the CIU and CAU tests were completed, the specimens were sheared at a constant strain rate $\dot{\epsilon}$ of 0.33%/h, for a period of time t_1, up to a predetermined strain level ϵ_1, corresponding to a deviatoric stress q (ϵ_1, t_1). When this level of strain was reached, the press was stopped and a relaxation test was performed. During the relaxation test the strain of the specimen was kept constant. Both the decay of the deviatoric stress and the pore water pressure were monitored throughout the relaxation process. After 24 hours of relaxation, the test was resumed up to another strain level and an additional relaxation test was performed. In some of the tests reported here, up to seven relaxation phases were carried out on the clay specimens.

TABLE 2—*Triaxial test consolidation information.*

Type of Test	Test Number	Consolidation Stresses σ_{1c}', kPa	Consolidation Stresses σ_{3c}', kPa	Volumetric Strain at End of Consolidation, ϵ_{vc}, %
	CIU-30	30.0	30.0	2.56
CIU	CIU-58	58.0	58.0	3.31
	CIU-96	96.0	96.0	10.43
	CAU-21	35.0	21.0	2.17
CAU	CAU-53	77.0	53.0	2.83
	CAU-75	103.5	75.0	6.93

Standard Piston Cell

At the beginning of this investigation, a standard triaxial cell was used. The axial load was recorded by means of a very stiff load cell in contact with the top of the piston, at the exterior of the triaxial chamber. However, it was soon discovered that when the press was stopped to perform a relaxation test, there was some unforeseen relaxation in the press mechanism, resulting in a substantial decrease of the axial load. It then became impossible to separate the decrease of the axial load due to the relaxation of the soil specimen from that due to the press.

Modified Piston Cell

To solve the problem of the relaxation of the press, various approaches were tried. In each of these, efforts were made to keep the length of the soil specimen constant by monitoring its displacement through a linear variable differential transformer (LVDT) and manually adjusting the press platen to annul the measured displacement.

After several trials, it became evident that the most effective way of keeping the length of the soil specimen constant was to physically prevent it from deforming. This was achieved by clamping the piston to a fixed rigid frame attached to the triaxial cell. With such an arrangement, the piston was prevented from moving either in an upward or a downward direction. The axial load was then monitored by means of a very stiff load cell which was an integral part of the piston and of the same diameter. This load cell was screwed to the bottom end of the piston, in contact with the top cap of the soil specimen inside the triaxial cell. For an additional check on the constant strain condition, an LVDT was placed on the top of the piston to monitor any possible displacement.

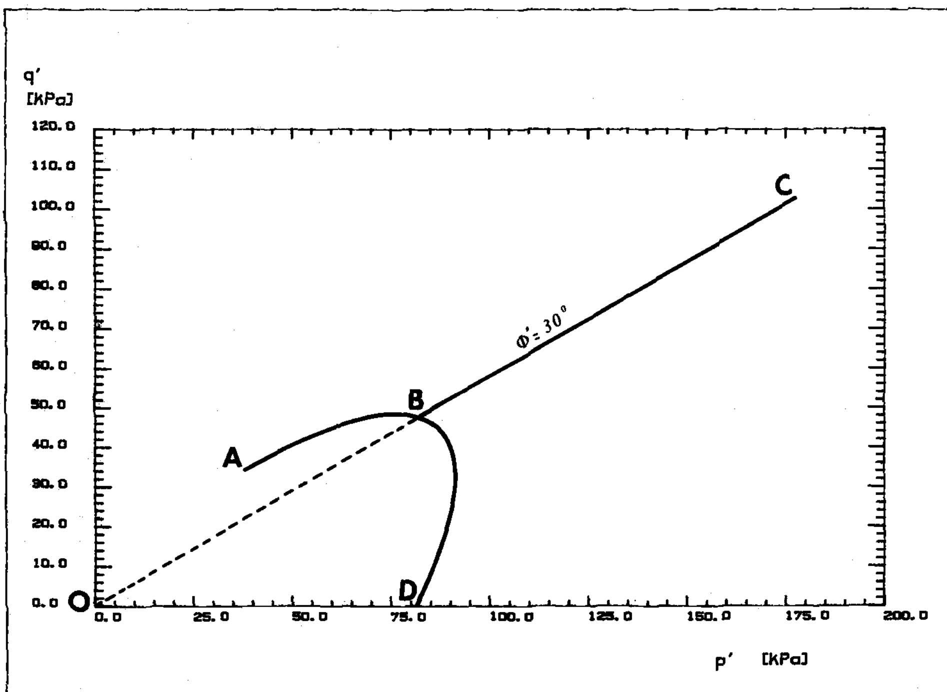

FIG. 1—*Yield and failure envelopes of the Louiseville clay.*

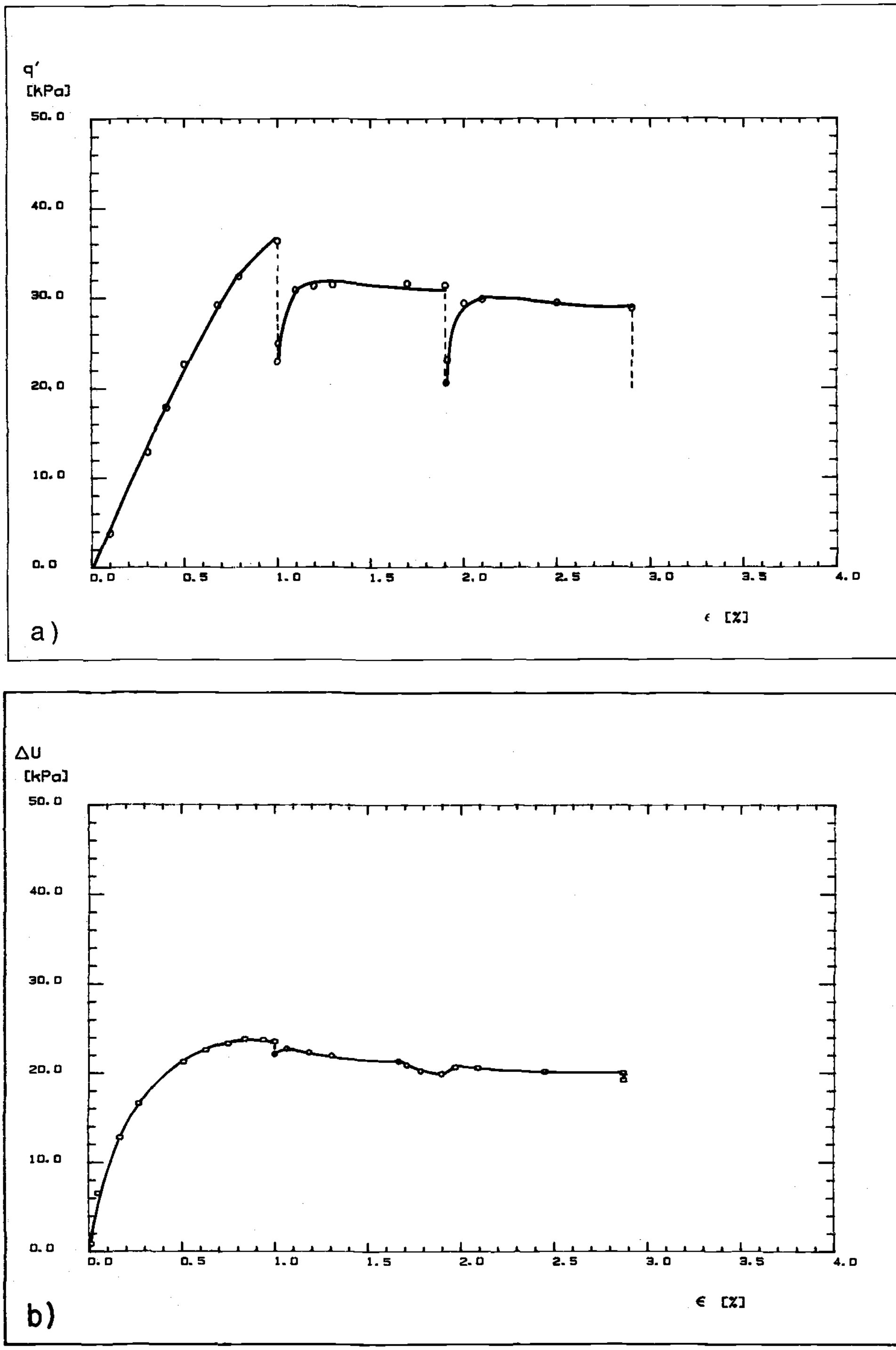

FIG. 2—*Results of CIU triaxal test* ($\sigma_c' = 30$ *kPa*).

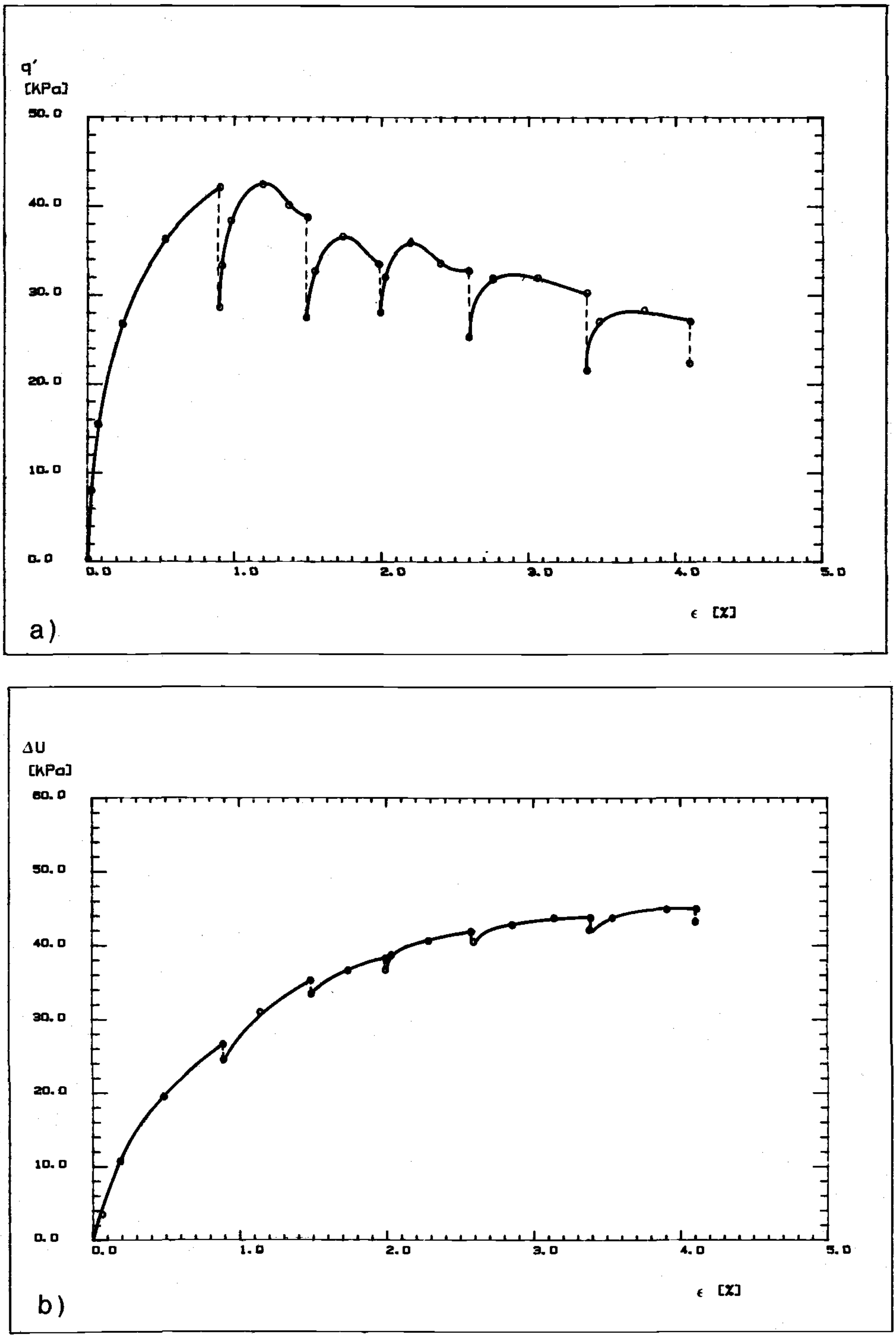

FIG. 3—*Results of CIU triaxial test* ($\sigma_c' = 58$ *kPa*).

TABLE 3—*CIU relaxation test results.*

Test Number	Relaxation Phase Number	Axial Strain During Relaxation Phase, %	Maximum Pore Water Pressure Drop During Relaxation, kPa
CIU-30	1	1.00	3.0
	2	1.90	0
	3	2.90	0.9
CIU-58	1	0.85	1.7
	2	1.54	2.2
	3	1.96	1.0
	4	2.55	2.6
	5	3.37	2.0
	6	4.10	2.1
CIU-96	1	0.63	0.8
	2	0.95	2.9
	3	1.62	1.1
	4	2.42	3.9
	5	3.44	2.9
	6	4.30	2.4
	7	5.10	1.4

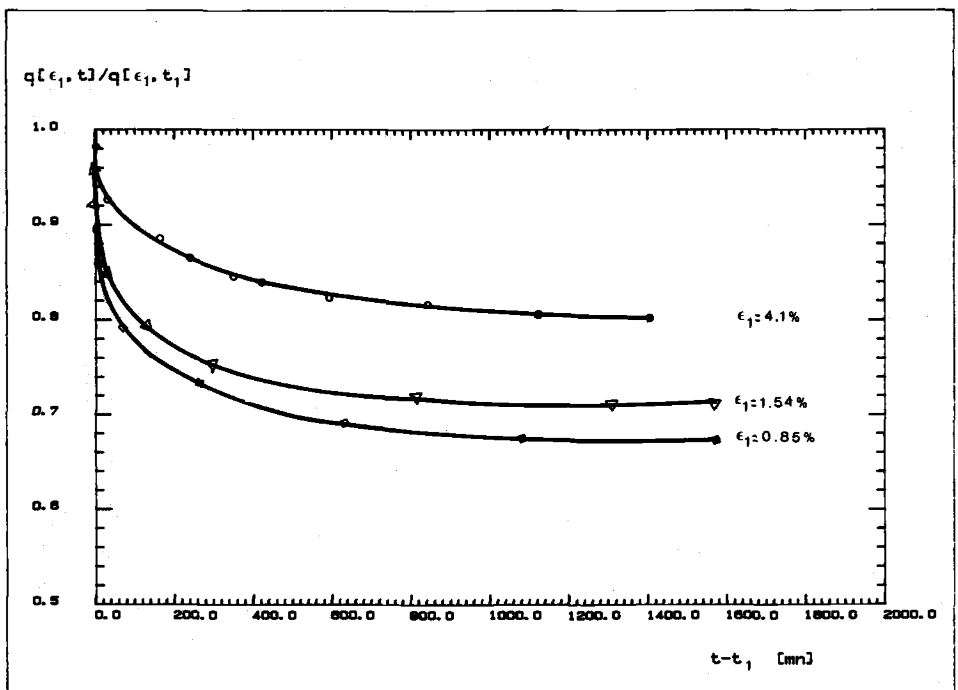

FIG. 4—*Normalized behavior (σ_c' = 58 kPa).*

All the tests reported in this paper were carried out with the modified piston cell just described.

Analysis and Discussion of Test Results

Structured Clay

Before discussing the results obtained in the relaxation tests, it is necessary to present the volumetric yield and failure surfaces of the Louiseville clay. Figure 1 summarizes the results of a series of CIU triaxial tests performed at different consolidation pressures at a strain rate $\dot{\epsilon}$ = 0.33%/h. In this figure, as long as the clay is subjected to an effective stress state which is located inside the curved surface ABD, the soil remains overconsolidated and its structure remains intact. In this case, the portion AB of the failure envelope represents the locus of the stress conditions causing the failure of the overconsolidated clay. Once the clay is subjected to a stress state that crosses the volumetric yield surface BD, the soil gradually becomes normally consolidated, its initial structure is destroyed, and it slowly "forgets" its past. In this case, the portion BC and its extrapolation BO represent the failure envelope of the normally consolidated clay, because the surface AB no longer exists. It should be noted, however, that the position of the yield and failure surface, ABD, of the clay shown in Fig. 1 is not fixed in stress space; rather, it depends on the value of the strain rate used in the triaxial tests, as indicated also, for example, by Tavenas and Leroueil [*21*]. When one deals with a behavior similar to that shown in Fig. 1, it should be expected that the stress–strain response of a clay specimen depends a great deal on the position of the stress state relative to that of the yield surface BD. Such a response will be shown at the end of this section.

Results obtained in the CIU tests performed at σ_c' = 30 and 58 kPa are shown in Figs. 2 and 3. The experimental data reported in the figures indicate that there is a small drop in pore water pressure during the relaxation tests. Table 3 summarizes the maximum drops in pore water pressures observed in all the CIU tests. Examination of the values reported in this table reveals that the maximum drops vary from 0 to about 3.9 kPa, with an average value of about 2 kPa. These findings, albeit somewhat larger than those reported by previous investigators [*3,8,16,17*], tend to indicate that the pore water pressure mobilization depends almost exclusively on strain.

To determine whether different physical relaxation mechanisms are operational at different strain levels, the deviatoric stress q (ϵ_1, t) measured during the relaxation process at any $t > t_1$ has been normalized with respect to the values of the deviatoric stress, q (ϵ_1, t_1), acting at the beginning of each relaxation phase. The results obtained at σ_c' = 58 kPa, shown in Fig. 4, indicate that similar relaxation mechanisms are probably present, in view of the similarity of the experimental curves.

Results obtained in the CAU tests are shown in Figs. 5 to 7. Once again the data show that the pore water pressure remains approximately constant during the relaxation phases, as found in the CIU tests. More specifically, it was observed that the maximum values of the pore water pressure drops varied between 0 and 3.7 kPa in the CAU relaxation tests. The results, shown in Table 4, compare well with those found in the CIU relaxation tests.

For the test specimen initially consolidated at (σ_{1c}', σ_{3c}') equal to (77 kPa, 53 kPa), the results have been normalized in the manner of Fig. 4 and are shown in Fig. 8. Because the shapes of the curves shown in Fig. 8, which refer to a CAU test, are quite similar to those shown in Fig. 4, which refer to a CIU test, it is believed that similar relaxation mechanisms are present in both types of test. This is in accordance with the observations made by Lacerda

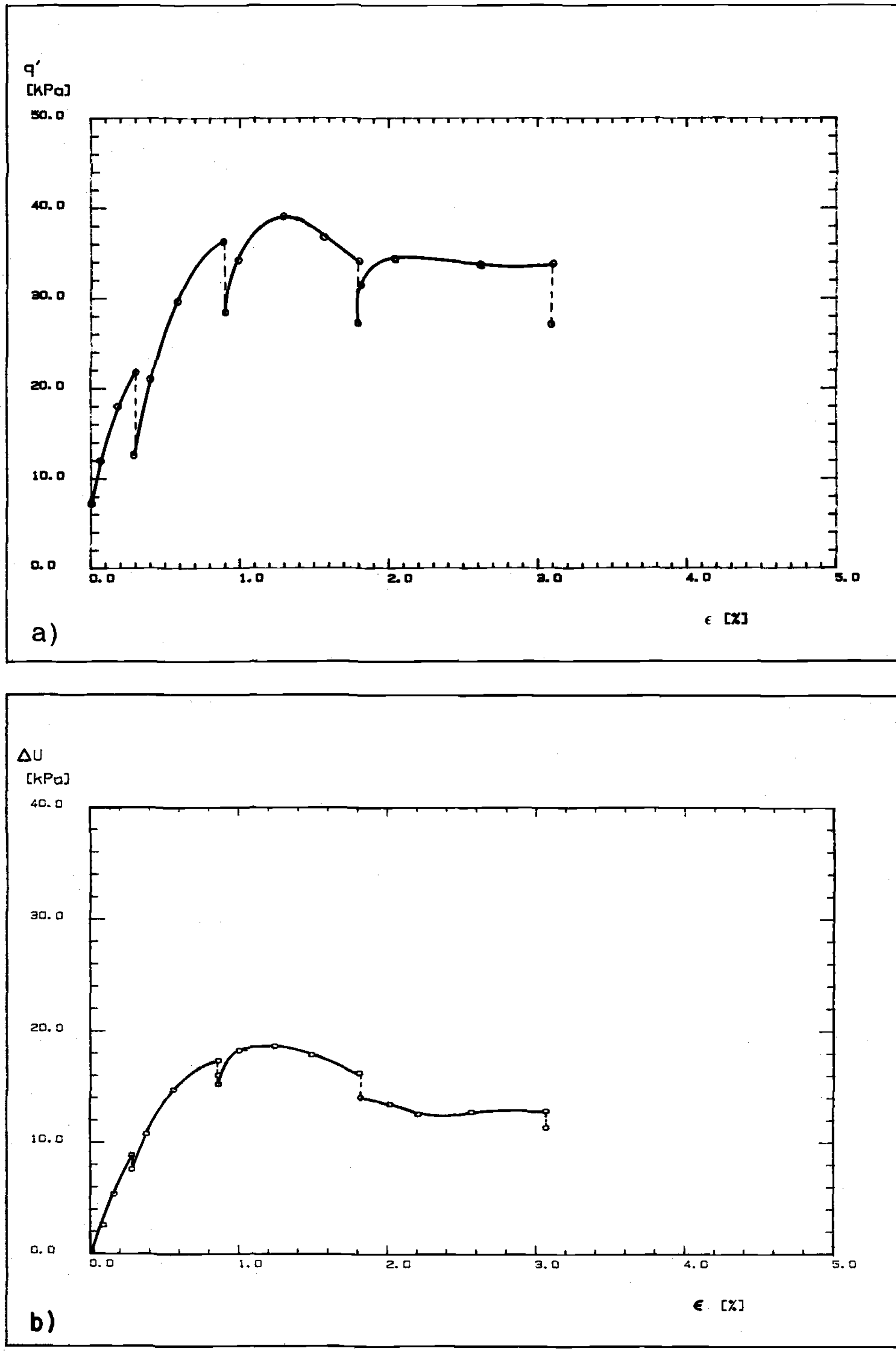

FIG. 5—*Results of CAU triaxial test* ($\sigma_{1c}' = 35$ *kPa*, $\sigma_{3c}' = 21$ *kPa*).

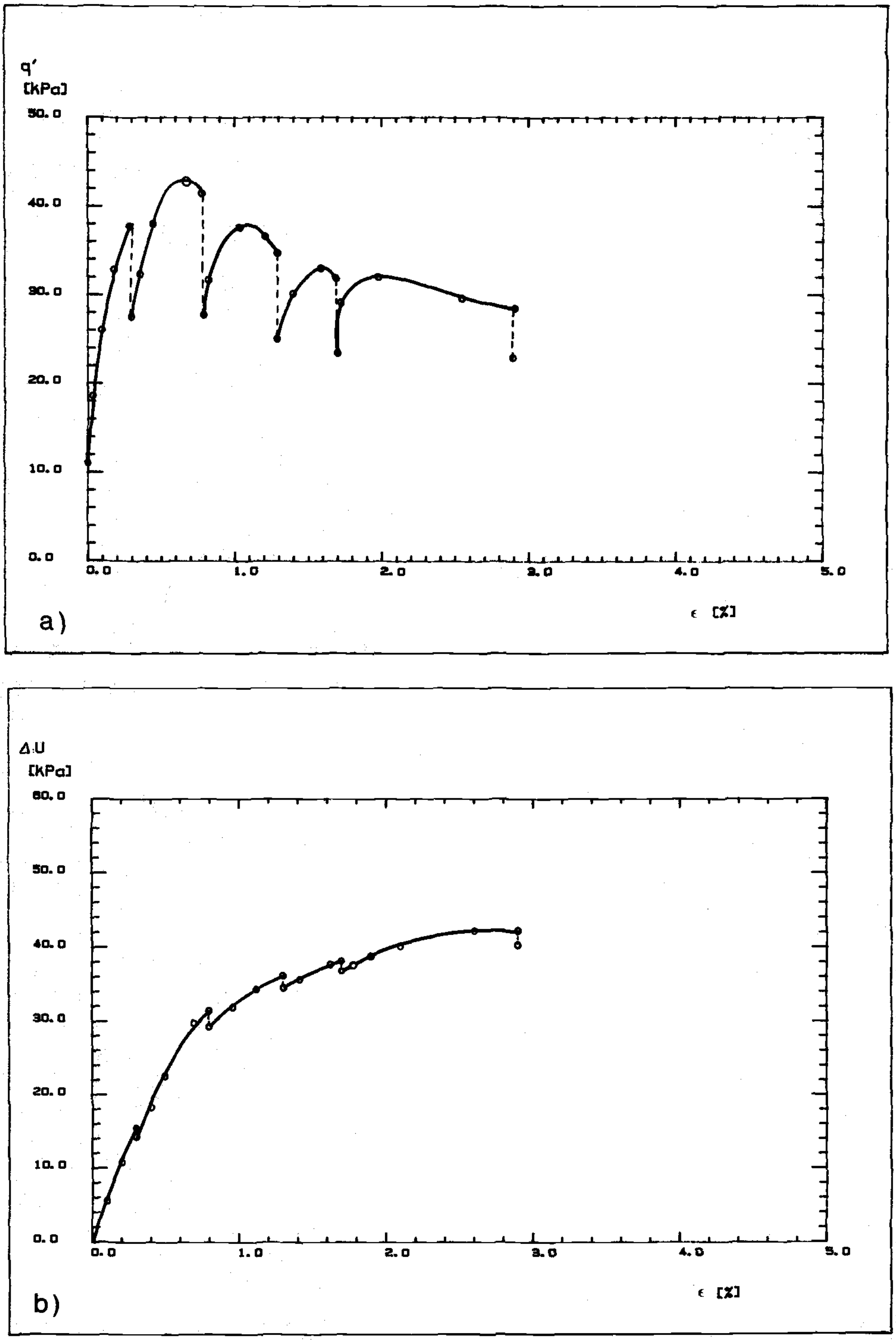

FIG. 6—*Results of CAU triaxial test (σ_{1c}' = 77 kPa, σ_{3c}' = 53 kPa).*

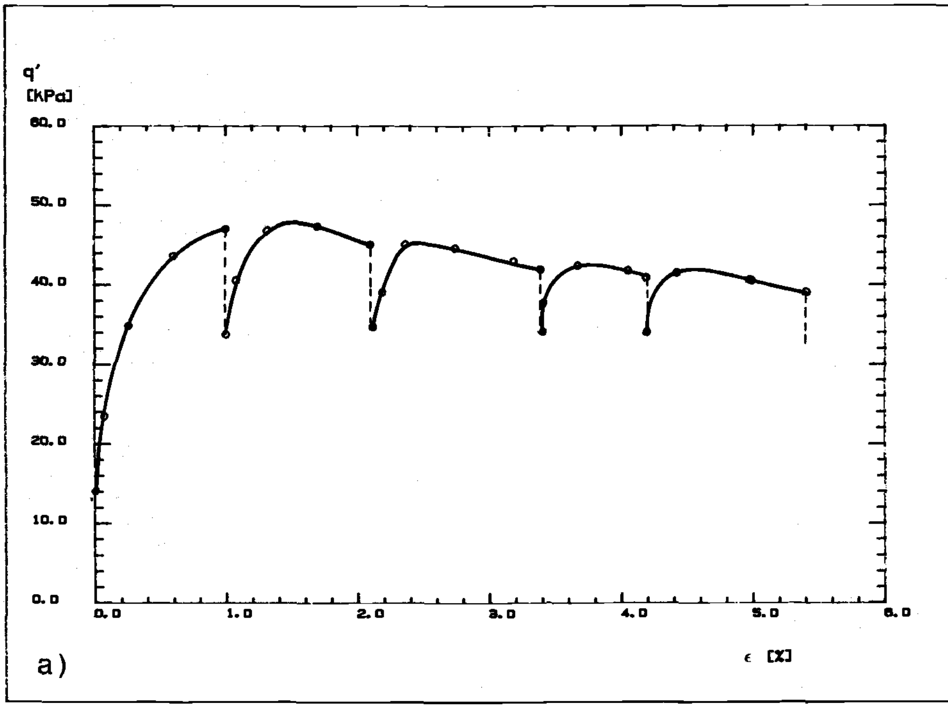

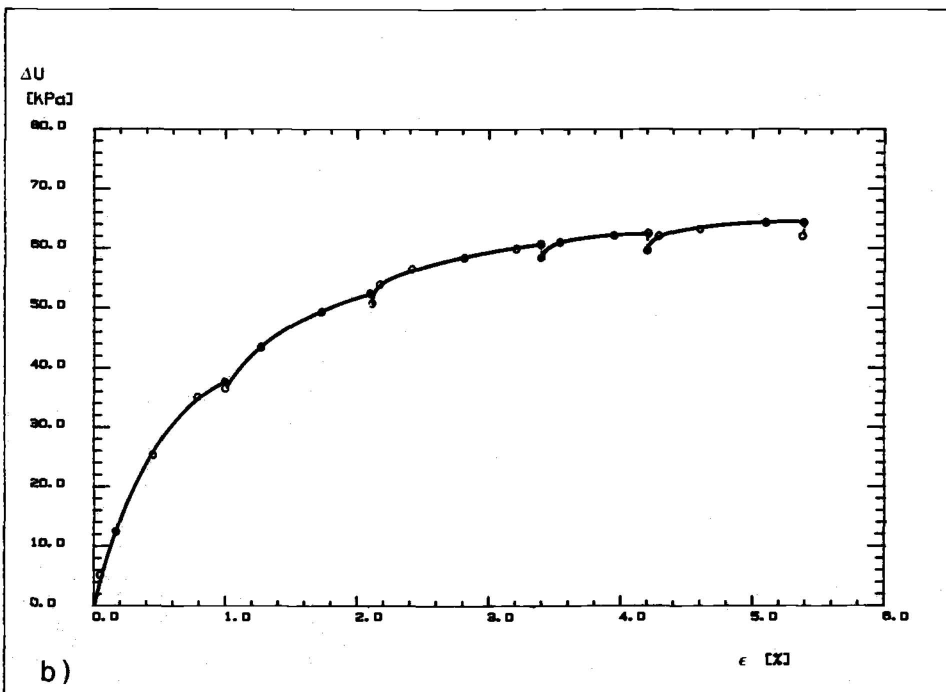

FIG. 7—*Results of CAU triaxial test* ($\sigma_{1c}' = 103.5$ *kPa*, $\sigma_{3c}' = 75$ *kPa*).

TABLE 4—*CAU relaxation test results.*

Test Number	Relaxation Phase Number	Axial Strain During Relaxation Phase, %	Maximum Pore Water Pressure Drop During Relaxation, kPa
CAU-21	1	0.28	1.1
	2	0.86	2.0
	3	1.81	3.0
	4	3.07	0
CAU-53	1	0.34	0.3
	2	0.80	2.5
	3	1.30	3.7
	4	1.71	2.3
	5	2.88	2.0
CAU-75	1	1.00	0.5
	2	2.11	1.4
	3	3.41	2.8
	4	4.20	3.0
	5	5.37	2.9

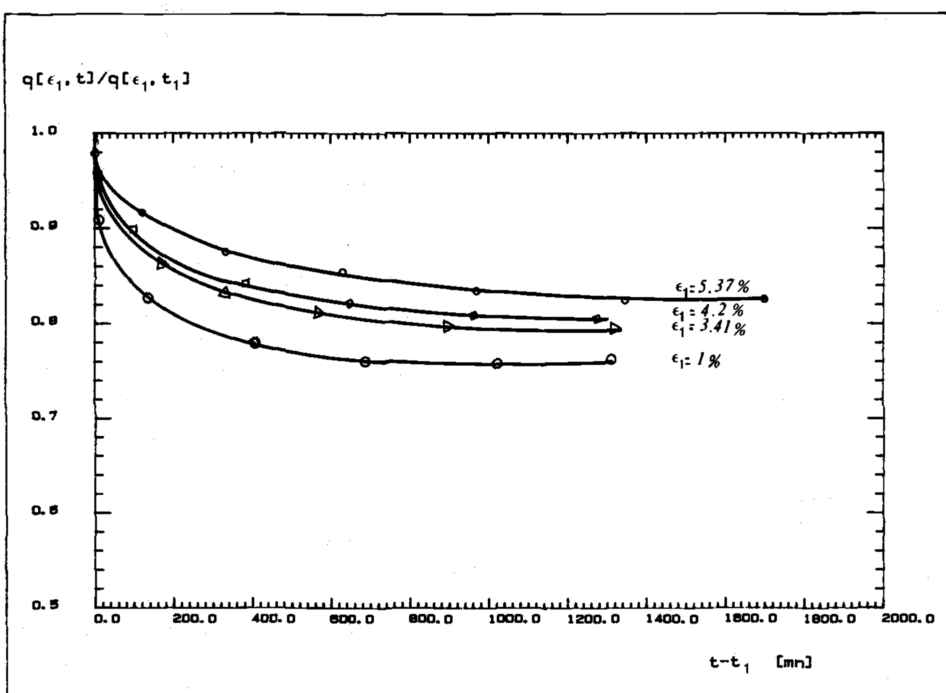

FIG. 8—*Normalized behavior (σ_{1c}' = 103.5 kPa, σ_{3c}' = 75.0 kPa).*

and Houston [16] and is in contrast with the large effect of anisotropic consolidation on creep [13].

To compare the observations made in both types of test, the experimental results obtained on overconsolidated soil specimens in both the CIU and CAU tests are shown in Figs. 9 and 10, respectively. In these figures, $p' = (\sigma_1' + \sigma_3')/2$ and $q = (\sigma_1' - \sigma_3')/2$. Because of the small variation in the excess pore water pressure during the relaxation phases of each test, the effective stress paths followed by the soil specimens in these tests are along lines inclined at 45° with respect to both axes. The relaxation test phases appear as broken lines in these diagrams. The general behaviors shown in these figures are similar to those observed by other investigators [8,9,16,22].

The results shown in Figs. 4 and 8 indicate that in most of the relaxation tests the deviatoric stress had reached a constant limiting value after a period of time of less than 1 day. For some of the tests shown in these figures, for example the test corresponding to an axial strain of 4.1% in Fig. 4 and that corresponding to an axial strain of 5.37% in Fig. 8, a longer period of time would have been necessary for the deviatoric stresses to reach constant values or limiting stress states. The curve obtained by joining these limiting stress states would represent the "static" effective stress path, as proposed also in Refs *8*, *9*, *22*, and *23*. It should be noted that the data obtained by Larsson [14] confirm the existence of a limiting stress curve for a number of soft Swedish clays. This "static" curve may be obtained either experimentally by performing very slow undrained triaxial tests or analytically by using, for example, Cam-Clay theory, as proposed in Ref *8*.

The analysis of some of the results reported in the preceding figures has been made with

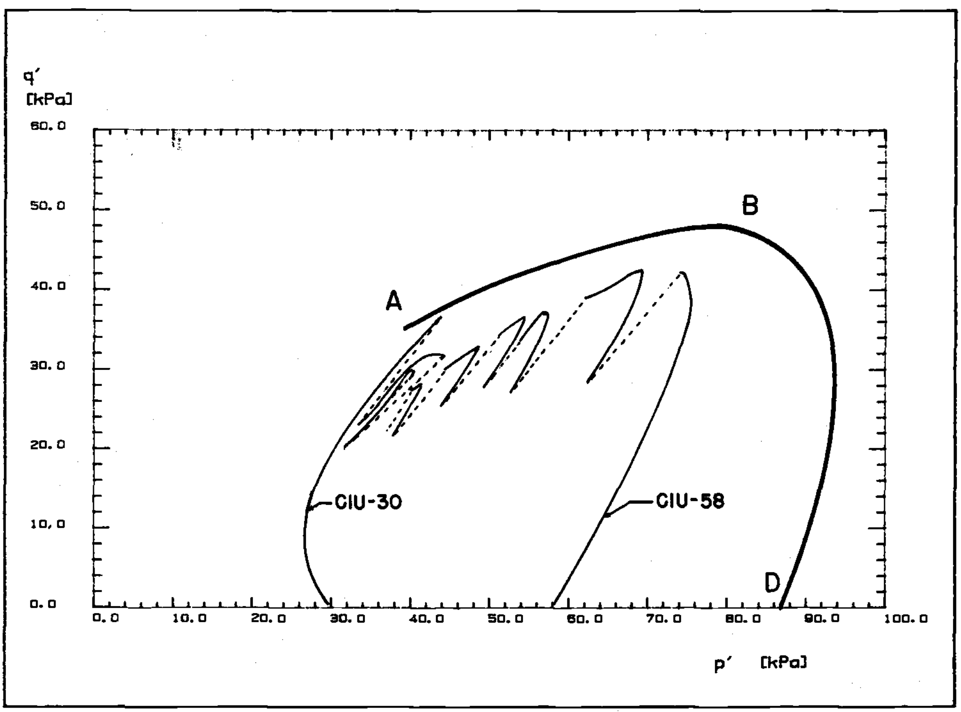

FIG. 9—*CIU test results.*

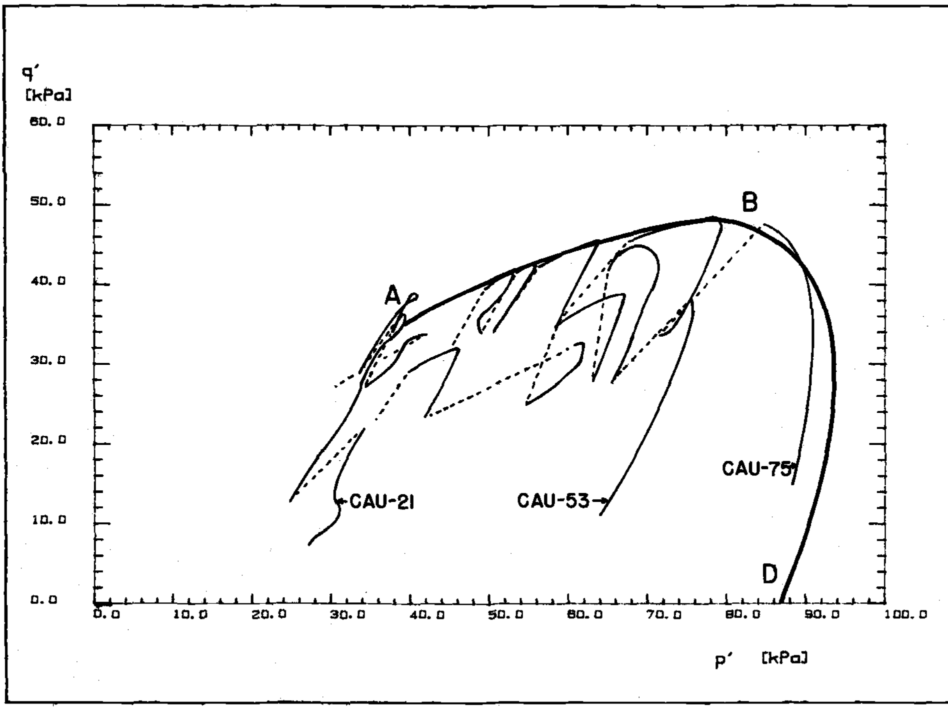

FIG. 10—*CAU test results.*

reference to the phenomenological approach developed by Prevost [*9*]. In the case of relaxation tests, the relationship suggested by Prevost reduces to the following expression:

$$q(\epsilon_1, t) = q(\epsilon_1, t_1) - [q(\epsilon_1, t_1) - q(\epsilon_1, 0)] \tanh [b \ln(t/t_1)] \quad (1)$$

where

$q(\epsilon_1, t)$ = deviatoric stress acting at strain ϵ_1 and time $t > t_1$
$q(\epsilon_1, t_1)$ = deviatoric stress state acting at the beginning of relaxation and reached by shearing the specimen with a constant strain rate $\dot{\epsilon} = a$ up to a strain level ϵ_1 attained in a time t_1, that is, $\epsilon_1 = at_1$
$q(\epsilon_1, 0)$ = deviatoric stress at a strain ϵ_1 in a "static" undrained test
b = experimental constant
a = a reference strain rate
t = time
t_1 = time at which relaxation begins

Figure 11 presents preliminary theoretical curves corresponding to Eq 1 and the experimental results obtained in the CIU-58 test and the CAU-75 test. Because the exact value of the parameter b appearing in Eq 1 is not known in advance, various numerical values were tried to obtain a good fit to the experimental results. In addition, the value of the limiting "static" deviatoric stress was taken as that acting after 24 h of relaxation. The results

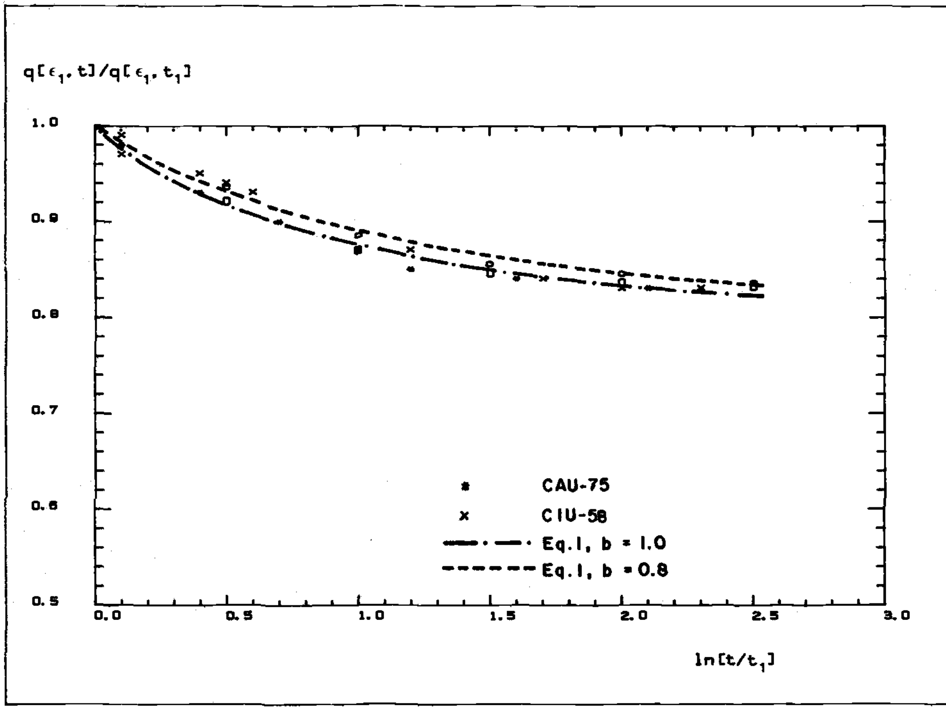

FIG. 11—*Relaxation curves.*

shown in this figure indicate that a value of b in the range of 0.8 to 1.0 may be considered representative of the clay response, at least for the conditions existing in these tests. The time t_1 at which relaxation begins is taken to be the time it takes to reach the strain level ϵ_1 at a constant strain rate of 0.33%/h. For example, for the CIU-58 test, the first relaxation phase was performed at an axial strain of 0.85%. This strain level was reached at t_1 = 0.85%/0.33%/h = 2.58 h. In addition, because the relaxation process lasted for 1580 minutes or 26.33 h, the maximum value of the time t is equal to (2.58 + 26.33) h or 28.91 h. In Eq 1 and Fig. 11 the final value of ln (t/t_1) is thus equal to ln (28.91/2.58) or 2.41, that is, the last reading in Fig. 11 for the CIU-58 first relaxation test. Intermediate values were obtained in a similar fashion. Additional tests and analyses are presently being carried out to get a more complete soil response.

Finally, to show that the clay behavior depends to a large extent on the position of the effective stress path relative to that of the volumetric yield curve of the clay, the results obtained in the CIU test performed at σ_c' = 96 kPa are compared to those observed in the CAU test consolidated at $(\sigma_{1c}', \sigma_{3c}')$ equal to (103.5 kPa, 75.0 kPa), as shown in Fig. 12. In this figure is also shown the critical state curve of the Louiseville clay of Fig. 1. In the CAU test, the clay specimen which is still overconsolidated follows quite closely the critical state curve of the clay; whereas, in the CIU test, the intact soil structure has been partially destroyed and the soil has become normally consolidated. The two stress paths shown in Fig. 11 illustrate well the dramatic changes the normally consolidated soil specimen must have experienced due to the collapse of the once intact structure. These changes must always be taken into account when analyzing the test results.

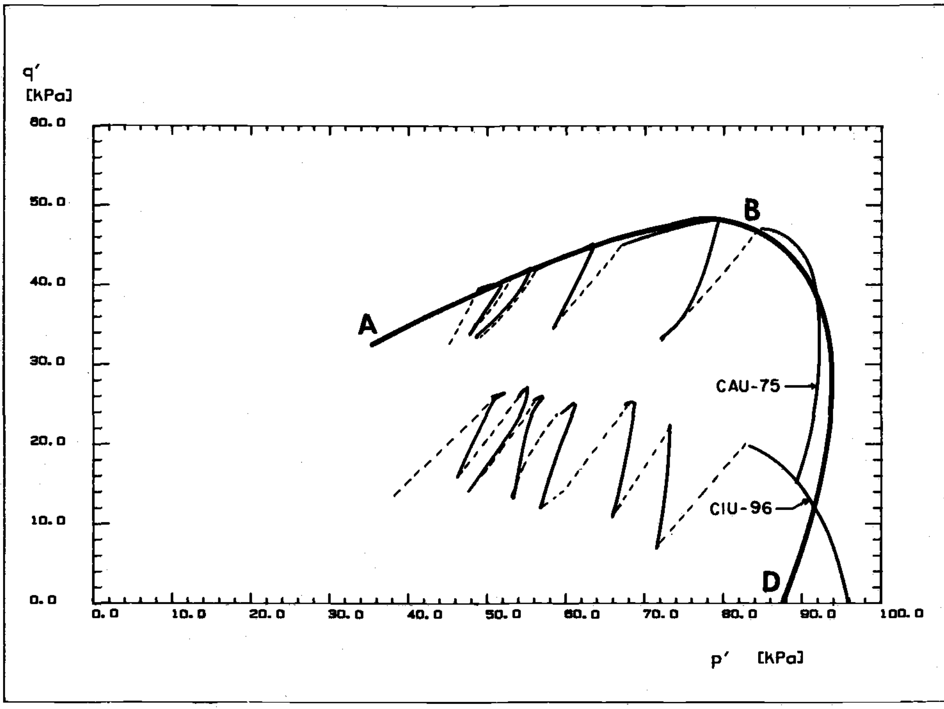

FIG. 12—*Effect of destructuration on relaxation behavior.*

Conclusions

On the basis of the findings of this study, the following principal conclusions have been drawn:

1. The results of both CIU and CAU tests performed on specimens of sensitive clay show that the pore water pressure drops somewhat during the relaxation processes. The maximum drop in the pore water pressure was found to be about 4 kPa with an average value of 2 kPa.
2. For some of the relaxation tests reported in this paper, constant values of the deviatoric stresses were reached in a period of time of less than 1 day. The phenomenological model developed by Prevost [9] is found to adequately describe soil response during relaxation.

Acknowledgments

The authors gratefully acknowledge the support received from the National Research Council of Canada and the Department of Education of Quebec.

References

[1] Geuze, E. and Tan, T. K., in *Proceedings,* Second International Congress of Rheology, Oxford, England, 1953, pp. 247.
[2] Gibson, R. E. and Lo, K. Y., *A Theory of Consolidation for Soils Exhibiting Secondary Compression,* Norwegian Geotechnical Institute, Publication No. 41, 1961, 16 pp.

[3] Murayama, S. and Shibata, T., in *Rheology and Soil Mechanics,* J. Kravtchenko and P. M. Sirieys, Eds., Springer-Verlag, Berlin, 1966, pp. 99–141.
[4] Schiffman, R. L., Chen, A. T.-F., and Jordan, J. C., *Journal of the Soil Mechanics and Foundations Division, American Society of Civil Engineers,* Vol. 95, No. SM1, 1969, pp. 285–312.
[5] Barden, L., *Journal of the Soil Mechanics and Foundations Division, American Society of Civil Engineers,* Vol. 95, No. SM1, 1969, pp. 1–31.
[6] Christensen, R. W. and Wu, T. H., *Journal of the Soil Mechanics and Foundations Division, American Society of Civil Engineers,* Vol. 90, No. SM6, 1964, pp. 125–157.
[7] Singh, A. and Mitchell, J. K., *Journal of the Soil Mechanics and Foundations Division, American Society of Civil Engineers,* Vol. 94, No. SM1, pp. 21–46.
[8] Akai, K., Adachi, T., and Ando, N., *Soils and Foundations,* Vol. 15, No. 1, 1975, pp. 1–16.
[9] Prevost, J.-H., *Journal of the Geotechnical Engineering Division, American Society of Civil Engineers,* Vol. 102, No. GT12, 1976, pp. 1245–1259.
[10] Tavenas, F., Leroueil, S., LaRochelle, P., and Roy, M., *Canadian Geotechnical Journal,* Vol. 15, No. 3, 1978, pp. 402–423.
[11] Kavazanjian, E. and Mitchell, J. K., in *Proceedings,* Ninth International Conference on Soil Mechanics and Foundation Engineering, Tokyo, Specialty Session 9, 1977, pp. 113–120.
[12] Arulandandan, K., Shen, C. K., and Young, R. B., *Geotechnique,* Vol. 21, No. 4, 1971, pp. 359–375.
[13] Campanella, R. G. and Vaid, Y. P., *Canadian Geotechnical Journal,* Vol. 11, No. 1, 1974, pp. 1–10.
[14] Larsson, R., "Drained Behaviour of Swedish Clays," Swedish Geotechnical Institute, Report No. 12, 1981, 157 pp.
[15] Salencon, J., *Viscoelasticity,* Presses de l'Ecole Nationale des Ponts et Chaussées, Paris, 1983, 92 pp.
[16] Lacerda, W. A. and Houston, W. N., in *Proceedings,* Eighth International Conference on Soil Mechanics and Foundation Engineering, Moscow, Vol. 1.1, 1973, pp. 221–227.
[17] Lacerda, W. A., in *Proceedings,* Ninth International Conference on Soil Mechanics and Foundation Engineering, Tokyo, Vol. 1, 1977, pp. 177–179.
[18] Lo, K. Y., *Canadian Geotechnical Journal,* Vol. 7, No. 3, 1969, pp. 383–394.
[19] Lo, K. Y., *Canadian Geotechnical Journal,* Vol. 7, No. 3, 1969, pp. 395–412.
[20] Wroth, C. P., in *Proceedings,* American Society of Civil Engineers Specialty Conference on In-Situ Measurement of Soil Properties, Raleigh, NC, Vol. 2, 1975, pp. 181–230.
[21] Tavenas, F. and Leroueil, S., in *Proceedings,* Ninth International Conference on Soil Mechanics and Foundation Engineering, Tokyo, Vol. 1, 1977, pp. 319–326.
[22] Adachi, T. and Okano, M., *Soils and Foundations,* Vol. 14, No. 4, 1974, pp. 55–73.
[23] Murayama, S. and Shibata, T., in *Transactions,* Japanese Society of Civil Engineers, Vol. 74, 1961, pp. 74–75.

Gretchen Rau[1] *and Ronald C. Chaney*[2]

Triaxial Testing of Marine Sediments with High Gas Contents

REFERENCE: Rau, G. and Chaney, R. C., **"Triaxial Testing of Marine Sediments with High Gas Contents,"** *Advanced Triaxial Testing of Soil and Rock, ASTM STP 977,* Robert T. Donaghe, Ronald C. Chaney, and Marshall L. Silver, Eds., American Society for Testing and Materials, Philadelphia, 1988, pp. 338–352.

ABSTRACT: Gas types, zonation present in marine sediments, the corresponding mechanism of bubble formation, and methods of performing triaxial tests on gassy sediments are discussed. Gases (methane and hydrogen sulfide; methane gas predominates) may be found either in solution or in the bubble phase in the sediment. A method to estimate the amount of gas that theoretically comes out of solution is shown. The result of gas bubbles is a reduction in the bulk modulus of the pore fluid. The bulk modulus of a gas–water mixture decreases with increasing fluid pressure. Results of decreasing bulk modulus are shown to reduce the pore pressure increment per application of a load increment. Triaxial testing techniques are recommended when (1) gas is in solution, (2) gas is in the bubble phase, and (3) gas is still evolving.

KEY WORDS: gas, pore pressure, marine, sediments, triaxial

Marine sediments are composed of a three-phase system of solid, liquid, and gas. A problem that usually is unimportant onshore, but very critical offshore, is the change in total stress state on a marine solid when sampled. One of the major results of large stress release on samples of marine soil is that gases can come out of solution and expand within the soil sample. This phenomenon is well known and has been described in many references to soils from all over the world [*1–4*]. When gas expands within a sample of marine soil, changes in physical and engineering properties occur. The unit weight and degree of saturation decrease due to the increasing volume, and the strength and compressibility are irreversibly altered. For the practicing geotechnical engineer investigating deep marine soils, the problem of soil containing gas, either free or in solution, will result in samples that may be significantly disturbed (unless special procedures are utilized).

The gases in marine sediments are O_2 (oxygen), CO_2 (carbon dioxide), N_2 (nitrogen), H_2S (hydrogen sulfide), CH_4 (methane), and others [*5–7*]. Natural gases in marine sediments arise from several sources, the most important of which is the biogenic degradation of organic matter during early diagenesis. Other sources include the atmosphere, the thermolytic cracking of more complex molecules, and submarine or geothermal processes [*8*]. A summary of typical gas types and contents in the marine environment as reported in the literature is presented in Table 1.

Research over the last few years has indicated that the distribution of gases in marine

[1] Undergraduate student, Department of Environmental Resources Engineering, Humboldt State University, Arcata, CA 95521.

[2] Professor and director, Humboldt State University Marine Laboratory, Trinidad, CA 95570.

TABLE 1—*Typical gas types and contents of the marine environment.*

Reaction	Example	Depth of Burial	Water Column Depth, m	Gas Concentration	Other
Oxygen reduction	Equatorial red clay and calcareous oozes [9]	upper 50 cm		0–0.09 mM[a]	
				50 μM	
Denitrification		0.01–0.15 m		0–0.04 mM	
	Chesapeake Bay [10]	0–1 m		2–11 ml/L	
Mn(IV)-Mn(II)		0.01–0.3 m		0.027–0.27 + mM/g	
Fe(III)-Fe(II)		0.01–0.2 + m		0.35–0.7 + mM/g	
Sulfate reduction		0.1+ m		0–30 mM	
	Cariaco Trench				
	[11]	0–5 m			
	[12]	0.45–0.50 m			
	South Guymas Basin, Gulf of California [13]	0–2 m			
	Santa Barbara Basin				
	[14]	0–1 m			
	[16]	2–3 m			
	Chesapeake Bay [17]	0.2–0.3 m			
	Limfjorden [18]	0–0.014 m			
Methanogenesis		25+ cm			
	Southern Louisiana Coastal Marsh [19]	0.5 m	0.3	1.1 mM/kg	20°C
	Southern California Coastal Marsh [6]	0.2–0.3 m	0.3	0.002–0.01 mM/kg	20°C
	Chesapeake Bay [17] [10]	1.0 m	15.2	4.3 mM/kg	15°C
		0.9 m	30	6.5 mM/kg	15°C
			15.2	85 ml/L	
			30.4	150 ml/L	
	Santa Barbara Basin [6]	3.8 m	585	10.4 mM/kg	
	Cariaco Trench [20]	45–180 m		86%–99% of gas in pockets analyzed	

[a] mM = millimole.

sediments is governed by changes in microbiologic populations over time and, hence, by depth [7,8]. The competition for the available organic material is awarded to the organisms that obtain the greatest metabolic energy from it. The most efficient organisms will live in the top sedimentary layers, and the less efficient organisms will live in deeper layers.

In the top sedimentary layer, oxygen is available for aerobic respiration. In the process, inorganic compounds are used as electron acceptors. Carbon, sulfur, nitrogen, and phosphorus are converted to carbon dioxide, sulfate, nitrate, and phosphate, respectively [7]. When the oxygen demand exceeds the rate of replenishment, the environment becomes anaerobic. When this occurs, sulfate-reducing bacteria become dominant, because the concentration of sulfur in sea water is high. In this process, sulfate ion is reduced to hydrogen sulfide. Some bacteria, which are capable of living under conditions other than the usual, switch from aerobic respiration to anaerobic respiration (or fermentation). These organisms use nitrate or inorganic sulfur compounds as electron acceptors in limited zones. When sulfur is depleted, methane-producing (carbonate-reducing) processes occur. Methane is produced in a two-stage process of first becoming a liquid (nonmethanogenic) and then a gas (methanogenic). Methane-producing bacteria are obligate microorganisms and cannot grow in the presence of dissolved sulfate. Necessary conditions for anoxic (without oxygen) conditions to be established and methane production to occur are rapidly deposited sediments ($\simeq$50 m/my) and sufficient organic carbon (>0.5%) [14]. Ultimately, the substrate is reduced to where metabolic energy can no longer be released, and the final products accumulate in

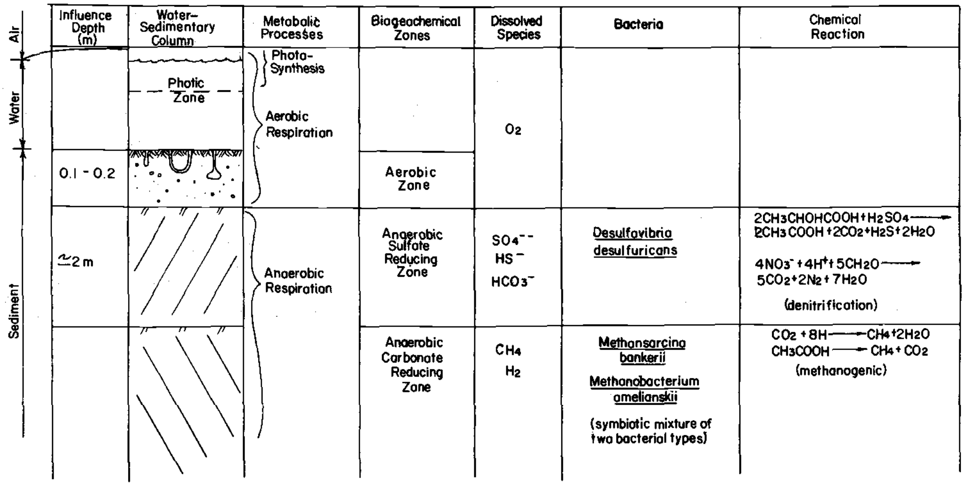

FIG. 1—*Generalized cross-section of an open ocean sedimentary/chemical environment.*

the sediment. A generalized cross-section of an open ocean sedimentary/chemical environment is presented in Fig. 1. This figure is an expanded version of a previous figure by Whelan et al. [*15*].

Although these biogeochemical zones and the idea of ecologic succession are widely accepted at this time, some research has not been in agreement. Marty, investigating sediments in the Gulf of Aden and the Oman Sea (Egypt), reports on anaerobic bacteria that depend on food from organic material (heterotrophic) and are the first to disappear with depth, before heterotrophic aerobic bacteria, sulfur-reducing bacteria, and methane-producing bacteria [*21*]. Marty also notes the coexistence of sulfur-reducing and methane-producing bacteria in the same layers. Marty proposes that, instead of homogenous zones of differing environmental conditions and bacterial populations, microniches that support these different populations exist within any sediment layer.

The form of gas present in sediments is important when considering their response to pressure and temperature. Gases in sediments are found (1) dissolved in the interstitial pore water, (2) as free gas bubbles or pockets, or (3) as solid gas hydrates, as shown in Fig. 2. Gas bubbles are formed when the quantities of gas exceed the saturation limit for pore water based on the phase relationship between pressure and temperature. The bubbles are very small when formed by microbial activity, and their movement is by molecular diffusion; being too small to push aside particles and too slow to coalesce, they may remain trapped in the sediment for years [*22*].

The existence in nature of natural gas hydrates has been acknowledged since about 1935, when they were found clogging gas pipelines. Natural gas hydrates are a type of clathrate compound, which is a crystal lattice containing cages or voids that incorporate a guest molecule. When the crystal lattice is composed of water, it is called a hydrate. Gas hydrates are formed when water and certain gases are mixed at high pressures [*8,23*] or low temperatures if the gas is supersaturated.

The gas hydrates found in deep sea sediments incorporate either methane, carbon dioxide, ethane, hydrogen sulfide, and perhaps propane, isobutane, or carbon monoxide. Initial studies have concentrated on areas of extensive permafrost. Gas hydrates have been suggested in other areas too, however. Stoll suggests that hydrate formation is possible over a large percentage of the ocean bottom [*24*]. The presence of hydrates has been indicated by anomalous acoustical data, but the drilling and sampling technology for gas hydrate zones

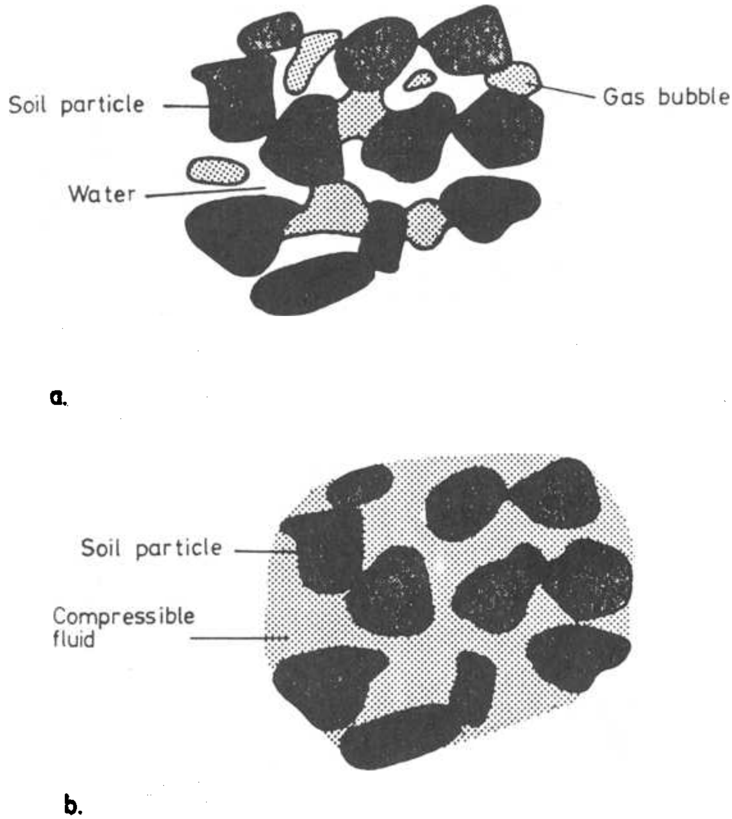

FIG. 2—*Schematic of partially saturated soil.* a, *Partially saturated soil with gas bounded by soil particles and minisci.* b, *Idealized model of partially saturated soil.*

is still primitive. A major reason for the lack of physical evidence is the release of gas from a hydrate state as a core is brought up from depth [*23*].

A chemical equilibrium exists between interstitial gas bubbles in the sediment and the gases dissolved in the pore water. The general gas law governs the relation between temperature and pressure for an ideal gas. If a sample is moved from an ocean floor temperature of 0°C (273 K) to a laboratory temperature of 20°C (293 K), its temperature has only changed by a factor of 1.07 (the ratio of absolute temperatures). In contrast, a sediment at a depth of 2200 m (7216 ft) is under a hydrostatic pressure of 22.1 MPa (3207 psi). When this sediment is brought to the ocean surface, its confining pressure has been reduced by a factor of 220 to atmospheric pressure. The change is large when compared with the factor of 1.07 for the corresponding temperature change [*25*].

The response of the bulk density of the sample to changes in confining pressure is a time-dependent property. Reduction of pressure on a sand sample for a specified time followed by repressurization to the original confining pressure was conducted by Chace [*26*]. If the duration of the pressure reduction is less than 4 hours, the sand samples return to approximately the same density. Reducing the pressure for over 5 hours, however, resulted in failure to attain the initial pressurized density [*26*].

In the following sections, the mechanism of gas bubble formation will be discussed along with an analysis of the theoretical effect of saturation on pore water response to load application. This discussion will be concluded with a summary of the various triaxial testing techniques available to handle gassy marine sediments.

Mechanism of Gas Bubble Formation

The complete relationship between sediment geochemistry, biogenic gas production, gas phase, and pore water pressure is not completely understood at present. Enough information is now available, however, to allow the development of a general model of how gas may influence soil strength. When biogenic gas is produced in situ, it is contained in solution with the pore water of the saturated soil. As more gas is produced and the saturation limit is exceeded, nucleation of free gas occurs. At this point, the pore water pressure will tend to increase. The resulting pore water pressure will be the sum of the partial pressures of the gas and water phases. As more gas is generated, the pore pressure will continue to increase in situ or, in the case of a triaxial specimen in which the back pressure is maintained constant, the sample will become less and less saturated (Fig. 3). The amount of gas that can come potentially out of the solution is a function of the liquid's saturation potential at its existing temperature and can be estimated using the generalized gas law.

$$P_g V_g = nRT \tag{1}$$

where

n = number of moles of gas
R = molar gas constant
T = temperature (degrees Kelvin)
P_g = absolute pressure of gas
V_g = volume of gas

At constant temperature and for a fixed mass of gas, Eq 1 can be written as shown in Eq 2, known as Boyle's law.

$$P_g V_g = \text{constant} \tag{2}$$

Equation 2 can be altered to reflect the prospect that part of the volume of gas will remain in solution (V_{dg}).

$$P_g (V_g + V_{dg}) = \text{constant} \tag{3}$$

Then, using Henry's coefficient of solubility (H), a relationship can be written relating V_{dg}

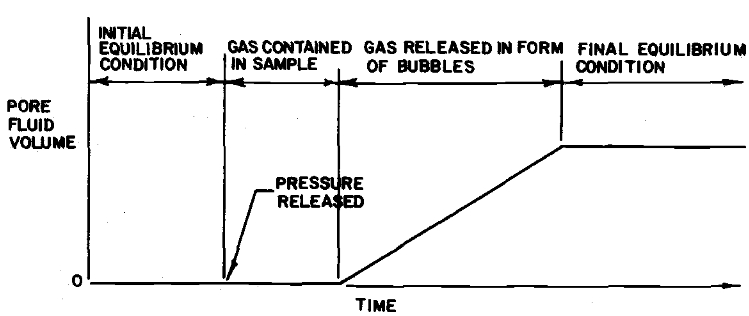

FIG. 3—*Process of gas release in soil.*

to V_w.

$$V_{dg} = HV_w \tag{4}$$

where

V_w = volume of liquid.

Combining Eqs 3 and 4 and assuming V_w is a constant gives

$$P_g (V_g + HV_w) = \text{constant} \tag{5}$$

$$P_g (V_g/V_w + H) = \text{constant} \tag{6}$$

Then, equating an initial state (indicated by subscript 1) to a final state (indicated by subscript 2) gives Eq 7.

$$P_{g1} (V_{g1}/V_w + H) = P_{g2}(V_{g2}/V_w + H) \tag{7}$$

$$V_{g2}/V_w + H = P_{g1}/P_{g2}(V_{g1}/V_w + H) \tag{8}$$

$$V_{g2}/V_w = P_{g1}/P_{g2}(V_{g1}/V_w + H) - H \tag{9}$$

If there is no initially free gas present in the pore fluid then

$$V_{g1}/V_w = 0 \tag{10}$$

then rewriting Eq 9 gives

$$V_{g2}/V_w = H(P_{g1}/P_{g2} - 1) \tag{11}$$

Because porosity $n = V_w/V_T$, where V_T is equal to the total volume, and void ratio can be equated to $n = e/(1 + e)$, then Eq 11 can be rewritten

$$V_{g2}/V_T = (eH/1 + e)(P_{g1}/P_{g2} - 1) \tag{12}$$

Reviewing Eq 12 shows the amount of gas that potentially can come out of solution from a soil sample's pore water during testing is a function of (1) total volume of the sample $-V_T$, (2) void ratio $-e$, (3) Henry's coefficient of solubility H, and (4) the ratio of the total pressure change experienced by the gas $-P_{g1}/P_{g2}$. Graphs showing the theoretical volume of either methane or hydrogen sulfide gas that can come out of solution in a soil sample versus the initial depth of water at which the soil sample came from as a function of void ratio are shown in Figs. 4 and 5. A review of Figs. 4 and 5 shows that a larger amount of hydrogen sulfide gas potentially can come out of solution as compared to methane gas.

The presence of the free gas in the laboratory specimen will increase the compressibility of the soil, which will influence the response of the soil to distortion or shear stresses. It is logical to expect that a soil that contains free gas will not develop significantly higher additional pore pressures caused by the application of shear stresses. Of particular importance is the response of these soils, whether granular or cohesive, to repeated loading. In contrast to the large build-up of pore pressures in saturated soils, the build-up of pore pressures in soils containing free gas should be quite small, perhaps negligible. Consequently, gassy soils should be less vulnerable to repeated loading than are saturated soils of equal strength [*4,27*].

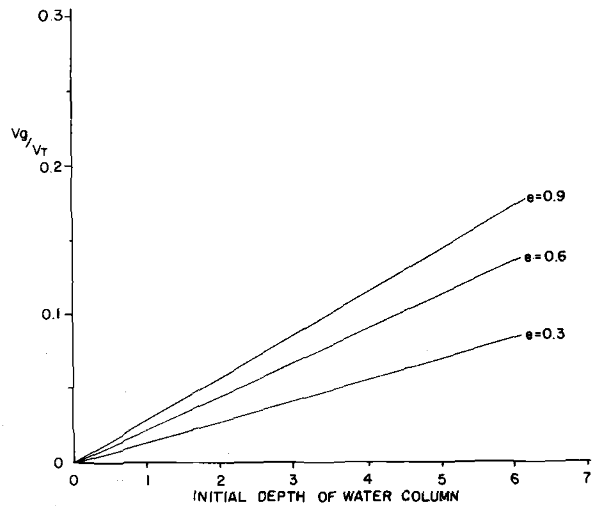

FIG. 4—*Theoretical volume of methane gas that can come out of solution as a result of pressure decrease,* H = *0.002.*

Theoretical Effect of Saturation On Pore Water Pressure Response

The amount of increase in pore water pressure increment per increment of load application is a function of the density of the soil material, bulk modulus of the pore water fluid, rebound tangent modulus, and the reduction in volume of soil structure. The bulk modulus of the pore water fluid in turn is dependent upon the amount of gas present. A relation has been presented by Martin et al. [*28*] relating the increase in residual pore water pressure for each addition of a load increment to the rebound tangent modulus, porosity, bulk modulus of the gas–water mixture, and the volumetric strain. This relationship is given by Eq 13.

$$\Delta u/\epsilon_{vd} + 1/(1/E_r + n/K_{aw}) \tag{13}$$

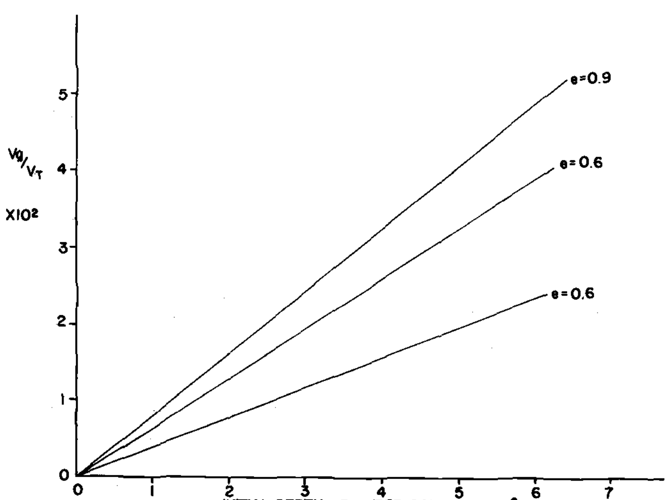

FIG. 5—*Theoretical amount of hydrogen sulfide* (H_2S) *gas that can come out of solution as a result of pressure decrease,* H = *4.67.*

where

E_r = rebound tangent modulus of the one-dimensional unloading curve at a point corresponding to the initial vertical effective stress (approximately 10^4 psi)
K_{aw} = bulk modulus of air–water mixture
Δu = increase in pore pressure increment per load cycle
ϵ_{vd} = reduction in volume of soil structure due to slip deformation per load increment
n = porosity

Equation 13 shows that the ratio $\Delta u/\epsilon_{vd}$ decreases as the bulk modulus of a gas–water mixture decreases or as the porosity increases. The bulk modulus (K_{aw}) of a combined air-water mixture for small changes of pressure can be theoretically determined by employing a relation presented by Richard, et al. [29]. This relation, presented in Eq 14, shows that the bulk modulus of a gas–water mixture is a function of the bulk modulus of water, bulk modulus of gas at a given absolute pressure (P_a), and the degree of saturation of the mixture.

$$K_{aw} = K_w/(1 + V_a/V)(K_w/K_a - 1) \tag{14}$$

where

K_w = bulk modulus of water (2.85×10^5 psi)
K_a = bulk modulus of gas bubble
V_a/V_T = $1 - S_r$ = amount of entrained air

By substituting in Eq 14 for various conditions of gas pressure and degree of saturation (S_r), the resulting effects of these changes on the bulk modulus of the gas–water mixture may be presented graphically as shown in Fig. 6. A review of Fig. 6 shows that the bulk modulus of a gas–water mixture decreases with (1) increasing amounts of gas present and (2) decreasing solution pressure. Note that P_a is approximately equal to water pressure for bubble radii 0.9 mm.

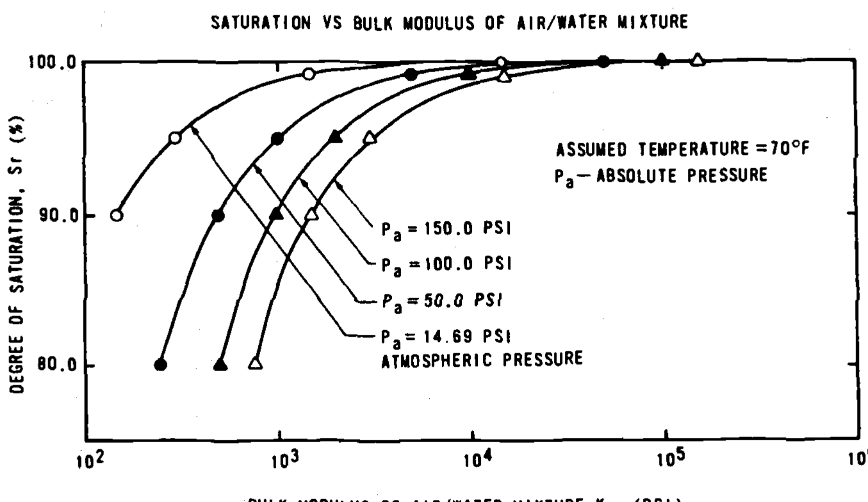

FIG. 6—*Effect of back pressure on the bulk modulus of an air–water mixture as a function of degree of saturation. (From Chaney, R. C., "Saturation Effects on the Cyclic Strength of Sands,"* Proceedings, *Earthquake Engineering and Soil Dynamics, American Society of Civil Engineers, Pasadena, CA, 1978, pp. 342–348).*

Assuming various values of ϵ_{vd} (values typically range from 0.01% to 0.2%) and substituting a value of K_{aw} at P_a = 50 psi (absolute pressure) for various saturation levels in Eq 13, a qualitative presentation of the effects of saturation on the pore pressure change per load increment can be made as presented in Fig. 7. Decreasing degrees of saturation and decreasing volumetric change are shown in Fig. 7 to decrease the corresponding pore pressure increment (Δu) per load increment. The smaller the u per load increment, the smaller the total pore pressure change will be. The practical significance of this behavior is shown in Figs. 8 and 9. Both figures represent results on soil samples from the Mississippi Fan in the Gulf of Mexico in water depths of approximately 2200 m. In Fig. 8 results from an isotropically consolidated undrained triaxial test for a sample from a depth of 2.2 m (7.2 ft) in the soil column is shown. A review of Fig. 8 shows a typical nonlinear pore pressure change (convex upwards plot) versus axial strain graph. The nonlinear graph is caused by the variations in volumetric change experienced by the soil structure during shearing. The ability of the pore water pressure to reflect the small variations in volumetric strain is due to the low compressibility (high saturation) of the fluid. In contrast, Fig. 9 shows a linear pore pressure change versus axial strain graph which is due primarily to the high compressibility (low saturation) of the pore fluid. Because of this high compressibility, the magnitude of the pore water pressure at failure is decreased and it does not reflect accurately the volumetric change behavior.

Triaxial Testing Technique

The type of triaxial testing technique used on gassy sediments will depend on two principal factors: (1) whether the gas is present in solution or bubble form and (2) whether the gas is still evolving as the result of bacterial growth. It should be emphasized that the gassy sediments may be undergoing any one or all three conditions at any one time.

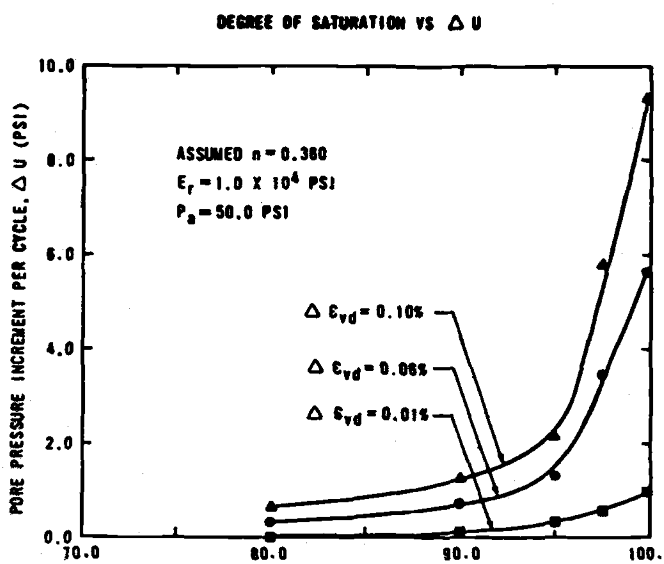

FIG. 7—*Change in pore pressure per load increment as a function of degree of saturation. (From Chaney, R. C., "Saturation Effects on the Cyclic Strength of Sands,"* Proceedings, *Earthquake Engineering and Soil Dynamics, American Society of Civil Engineers, Pasadena, CA, 1978, pp. 342–348).*

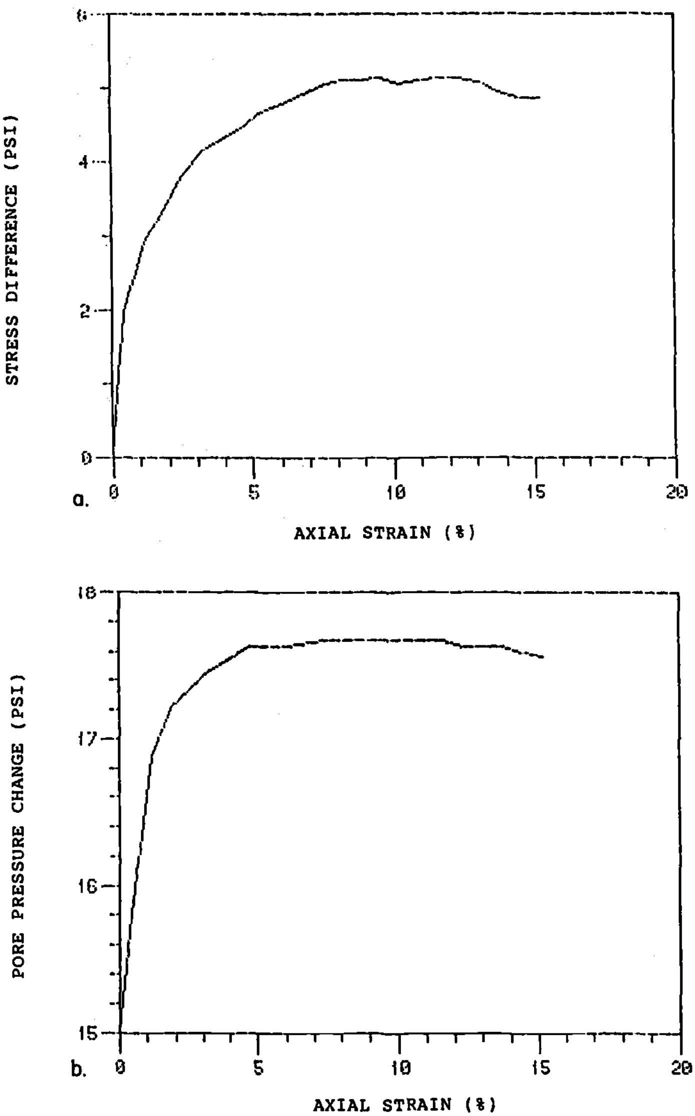

FIG. 8—*Stress difference and pore pressure change versus axial strain, isotropically consolidated undrained (ICU) triaxial, Leg 96, Core 1, Section 2, Depth 2.2 m (7.2 ft),* σ_{3c} = *21 kPa (3 psi).* Note: *6.9 kPa = 1 psi.*

Gas Initially in Solution

If gas is still in solution, then the test technique will be based on the principle that gas under a compressive process goes to equilibrium more quickly than the expansion sequence. The explanation proposed is that the diffusion gradient is generally larger from a bubble into a nonsaturated fluid than it is when gas is moving from a saturated solution into a bubble [*26*]. The practical consequence of this behavior is that it may be possible to test quickly and obtain a reasonable strength estimation. For studies where no specialized equip-

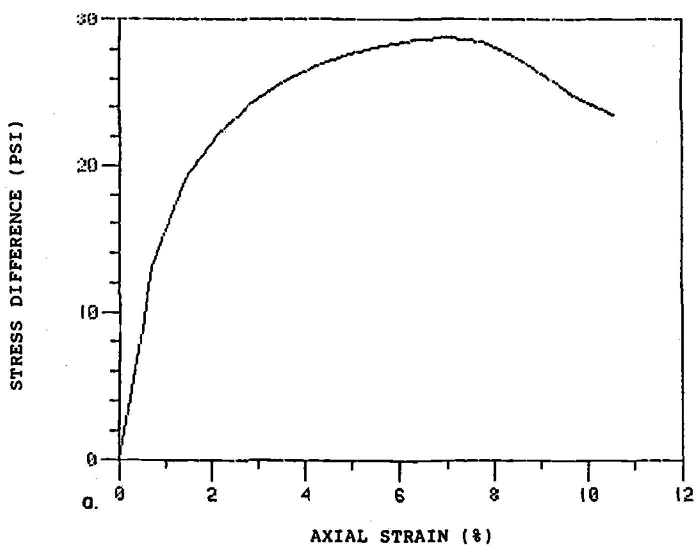

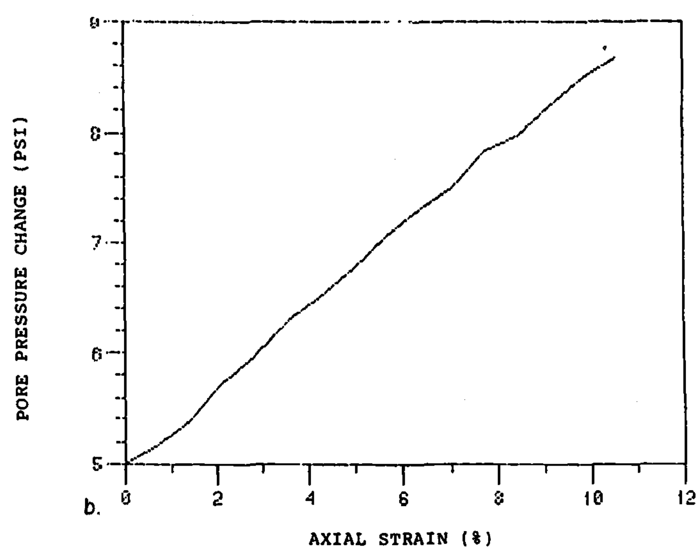

FIG. 9—*Stress differences and pore pressure change versus axial strain, ICU triaxial, Leg 96, Core 6, Section 3, Depth 49.6 m (163 ft),* σ_{3c} *= 827 kPa (120 psi).* Note: *6.9 kPa = 1 psi.*

ment is available, the best approach, therefore, appears to be to perform strength index tests rapidly [*25*]. In contrast, if the samples are returned to a shore laboratory and gas is present in the bubble phase, it may be possible to resaturate the sediment by applying large back pressures. Esrig and Kirby [*25*] report using back pressures between 1.5 MPa (217 psi) and 2 MPa (289 psi) to saturate a sediment from 100 m of water. Consolidation stresses should be applied for a long period before testing to allow at least some redevelopment of bonds in the disrupted fabric [*30*]. A third method would be to sample the soil *in situ* using a pressurized core barrel and then to store it in a pressurized container prior to testing [*31*].

Gas Initially in Bubble Phase

The fabric initially developed *in situ* has already been altered, to some unknown degree, due to the presence of gas bubbles. Removal of the sediment to the surface will cause a pressure decrease resulting in an increase in bubble size. This increase in bubble size will subsequently cause an additional amount of alteration of the soil fabric. One method to handle this condition is to decrease the bubble size by applying large back pressures. Consolidation stresses should probably be applied for a long period of time before testing to allow at least some redevelopment of bonds in the disrupted fabric [*30*]. A second approach would be to sample the soil in situ using a pressurized core barrel and then to store it in a pressurized container [*31*].

Gas Evolving

The primary task is to prevent or retard growth of bacteria that produce gas. Under natural conditions a species of bacteria maintains itself by continuous multiplication, a balance being established between the rates of death and multiplication. This balance can be upset by changes in moisture content, availability of oxygen and of nutrients, the presence of inhibitory agents, competition with other species, and other factors encountered in the environment. In the marine environment, a direct correlation has been observed between survival at increased hydrostatic pressure, temperature, and the salinity of the medium [*32*]. The methods that can be employed to cause the death of bacteria are [*33,34*]:

(a) Injecting a chemical, such as formaldehyde, into the sample
(b) X-raying the sample at high intensity prior to testing
(c) Exposing sample to radiation
(d) Testing using an inert gas, such as nitrogen, to restrict available oxygen
(e) Testing at a temperature below 10 or above 20°C
(f) Increasing pore water salinity by flushing

The injection of a chemical into the sample to prevent the growth of microorganisms has been used previously by Allison in a study of permeability with mixed results [*35*]. One difficulty with this technique is possible interference with the original pore water chemistry.

A summary of pore gas behavior due to bacteria in marine sediments and possible mitigating procedures in triaxial testing is presented in Fig. 10.

Summary and Conclusions

Gases present in marine sediments, methane and hydrogen sulfide (H_2S), are due predominantly to organic matter. The two gases do not coexist but can be found in discrete zones. Hydrogen sulfide typically exists in the upper 2 m of depth in the sediment column, overlying the methane gas. The methane gas, however, predominates in the soil column. The zonation of the gases can be altered by mass movements of the sediments or another similar process. This alteration can take the form of producing pockets of individual species of gas within a predominant zone of the other gas or a reversal of the layering sequence.

Choice of triaxial testing techniques depends on whether the gas is in solution, in the bubble phase, or is still evolving. Any one or all three processes may be occurring at the same time on a sample. For samples having gas present in solution, the test techniques rely on the principle that gas comes out of solution slowly and that it may be possible to limit the alteration of the *in situ* sediment fabric by either (1) testing the sample quickly, (2) applying large back pressures quickly to resaturate the sample, or (3) sampling and testing the specimen in a pressurized environment.

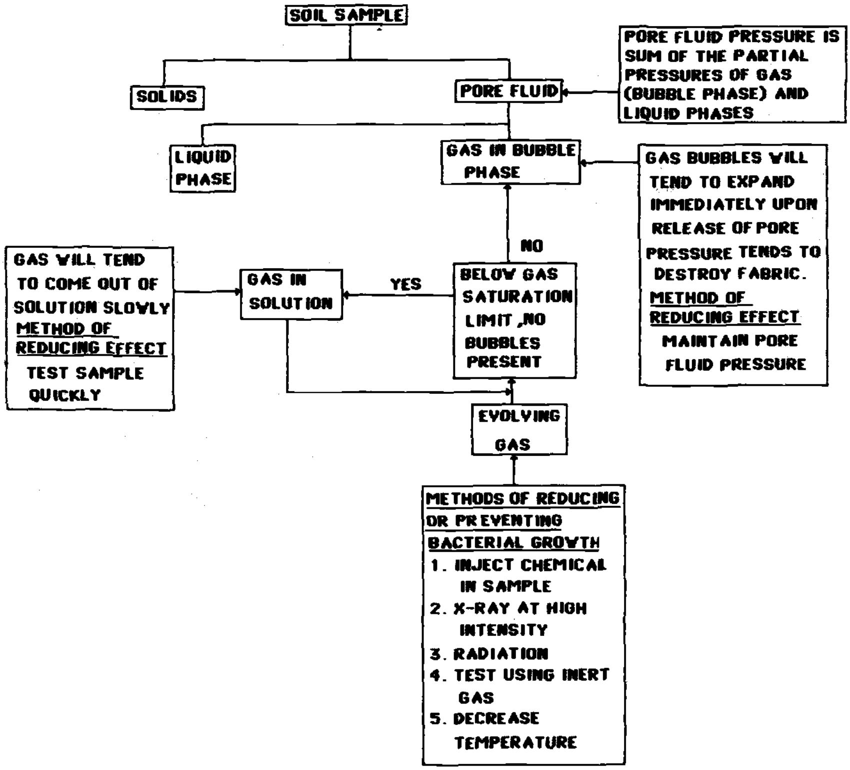

FIG. 10—*Summary of pore gas behavior due to microorganisms in marine sediments.*

In contrast, if the gas is already in the bubble phase in situ, it can be assumed that the original sediment fabric has already been altered. The problem in the laboratory is then to reproduce that altered soil fabric from the highly modified recovered sediment by either (1) resaturating the sample under high back pressure, or (2) sampling and testing in a pressurized environment.

If gas is still evolving, the primary emphasis is to prevent or retard growth of microorganisms that produce gas by (1) injecting a chemical, (2) X-raying sediment at high intensity, (3) irradiating sediment, (4) testing in inert gas, or (5) testing at a reduced temperature.

Acknowledgment

The authors would like to acknowledge the extensive comments and assistance of Dr. Adrian F. Richards in the development of ideas expressed in this paper.

References

[1] Richards, A. F. and Parker, H. W., "Surface Coring for Shear Strength Measurements," in *Proceedings of the Conference on Civil Engineering in the Oceans,* American Society of Civil Engineers, San Francisco, 1967, pp. 391–417.

[2] Roberts, H. H., Cratsley, D. W., and Whelan, T., "Stability of Mississippi River Delta Sediments as Evaluated by Analysis of Structural Features in Sediment Borings," *Proceedings, Eighth Annual Offshore Technology Conference,* Vol. 1, Houston, TX, 1976, pp. 10–15.

[3] Lee, H. J., "State of the Art: Laboratory Determination of the Strength of Marine Soils," in *Strength Testing of Marine Sediments: Laboratory and* In Situ *Measurements, ASTM STP 883*, R. C. Chaney and K. R. Demars, Eds., American Society for Testing and Materials, Philadelphia, 1985, pp. 181–250.
[4] Sangrey, D. A., "Marine Geotechnology—State of the Art," *Marine Geotechnology*, Vol. 2, 1977, pp. 45–80.
[5] Waksman, S. A., "Aquatic Bacteria in Relation to the Cycle of Organic Matter in Lakes," in *Symposium on Hydrobiology*, University of Wisconsin Press, Madison, 1941, pp. 86–105.
[6] Emery, K. O., and Hoggan, D., "Gases in Marine Sediments," *American Association of Petroleum Geologists Bulletin*, Vol. 42, 1958, p. 2174.
[7] Mechalas, B. J., "Pathways and Environmental Requirements for Biogenic Gas Production in the Ocean," in *Natural Gases in Marine Sediments* (Marine Science, Vol. 3), I. R. Kaplan, Ed., Plenum Press, New York, 1974, pp. 11–26.
[8] Kaplan, I. R., "Introduction," in *Natural Gases in Marine Sediments* (Marine Science, Vol. 3), I. R. Kaplan, Ed., Plenum Press, New York, 1974, pp. 1–10.
[9] Murray, J. W. and Grundamanis, V., "Oxygen Consumption in Pelagic Marine Sediments," *Science*, Vol. 209, No. 4464, 26 Sept. 1980, pp. 1527–1530.
[10] Schubel, J. R., "Gas Bubbles and the Acoustically Impenetrable or Turbid Character of Some Estuarine Sediments," in *Natural Gases in Marine Sediments* (Marine Science, Vol. 3), I. R. Kaplan, Ed., Plenum Press, New York, 1974, pp. 99–135.
[11] Hammond, D. E., "Dissolved Gases in Cariaco Trench Sediments: Anaerobic Diagenesis," in *Natural Gases in Marine Sediments* (Marine Science, Vol. 3), I. R. Kaplan, Ed., Plenum Press, New York, pp. 71–90.
[12] Reeburgh, W. S., "Methane Consumption in Cariaco Trench Waters and Sediments," *Earth and Planetary Science Letters,* Vol. 28, 1976, pp. 337–344.
[13] Goldhaber, M., "Kinetic Models of Sulfur Diagenesis in Recent Marine Sediments," *EOS*, (*American Geophysical Union Transactions*), Vol. 55, No. 7, 1974, pp. 696–697.
[14] Claypool, G. E. and Kaplan, I. R., "The Origin and Distribution of Methane in Marine Sediments," in *Natural Gases in Marine Sediments* (Marine Science, Vol. 3), I. R. Kaplan, Ed., Plenum Press, New York, 1974, pp. 99–140.
[15] Whelan III, T., Coleman, J. M., Suhayda, J. N., and Garrison, L. E., "The Geochemistry of Recent Mississippi River Delta Sediments: Gas Concentration and Sediment Stability," in *Proceedings 7th Offshore Technology Conference,* Vol. 3, Paper 2342, 1975, pp. 71–84.
[16] Sholkovitz, E., "Interstitial Water Chemistry of the Santa Barbara Sediments," *Geochimica et Cosmochimica, Acta*, Vol. 37, 1973, pp. 2043–2073.
[17] Reeburgh, W. S., "Observations of Gases in Chesapeake Bay Sediments," *Limnology and Oceanography*, Vol. 14, 1969, pp. 368–375.
[18] Jorgensen, B. B., "Bacterial Sulfate Reduction Within Reduced Microniches of Oxidized Marine Sediments," *Marine Biology*, Vol. 41, 1977, pp. 7–17.
[19] Whelan, T., "Methane, Carbon Dioxide, and Dissolved Sulfate from Interstitial Waters of Coastal Marsh Sediments," *Estuarine and Coastal Marine Science,* Vol. 2, 1974, p. 407.
[20] Lyon, G., "Geothermal Gases," in *Natural Gases in Marine Sediments* (Marine Science, Vol. 3), I. R. Kaplan, Ed., Plenum Press, New York, 1974, pp. 141–150.
[21] Marty, D., "Distribution of Different Anaerobic Bacteria in Arabian Sea Sediments," *Marine Biology,* Vol. 63, No. 3, 1981, pp. 177–281.
[22] Hulbert, M. H. and Bennett, R. H., "Electrostatic Cleaning Technique for Fabric SEM Samples," *Clays and Clay Minerals*, Vol. 23, 1975, p. 331.
[23] Hand, J. H., Katz, D. L., and Verma, V. K., "Review of Gas Hydrates with Implication for Ocean Sediments," in *Natural Gases in Marine Sediments* (Marine Science, Vol. 3), I. R. Kaplan, Ed., Plenum Press, New York, 1974, pp. 179–194.
[24] Stoll, R. D., "Effects of Gas Hydrates in Sediments," in *Natural Gases in Marine Sediments* (Marine Science, Vol. 3), I. R. Kaplan, Ed., Plenum Press, New York, 1974, pp. 235–248.
[25] Esrig, M. I. and Kirby, R. C., "Implications of Gas Content for Predicting the Stability of Submarine Slopes," *Marine Geotechnology*, Vol. 2, 1977, pp. 81–100.
[26] Chace Jr., A. B., "Pressure Release Disturbance in Simulated Marine Cores as Indicated by a Laboratory Gamma-Ray Densitometer," in *Strength Testing of Marine Sediments: Laboratory and* In Situ *Measurements, ASTM STP 883*, R. C. Chaney and K. R. Demars, Eds., American Society for Testing and Materials, Philadelphia, 1985, pp. 154–165.
[27] Sills, G. C. and Nageswaran, S., "Compressibility of Gassy Soils," in *Proceedings Oceanology International*, Society for Underwater Technology, Brighton, United Kingdom, 1984, 18 pp.
[28] Martin, G. R., Finn, W. D. L., and Seed, H. B., "Fundamentals of Liquefaction Under Cyclic

Loading," *Journal of the Geotechnical Engineering Division, American Society of Civil Engineers,* Vol. 101, No. GT5, Proc. Paper 1128, 1975, pp. 423–438.

[*29*] Richart, F. E., Hall, J. R., and Wood, R. D., *Vibrations of Soils and Foundations,* Prentice-Hall, Englewood Cliffs, NJ, 1970, 414 pp.

[*30*] Bea, R. G. and Aurora, R. P., *Proceedings, Thirteenth Annual Offshore Technology Conference,* Paper No. 3975, Houston, 1981, pp. 223–240.

[*31*] Denk, E. W., Dunlap, W. A., Bryant, W. R., Milberger, L. J., and Whelan, T. J. "A Pressurized Core Barrel for Sampling Gas-Charged Marine Sediments," in *Proceedings, Thirteenth Annual Offshore Technology Conference,* OTC 4120, Houston, 1981, pp. 43–52.

[*32*] Litchfield, C. D., "Editor's Comments On Papers 23 through 25," in *Marine Microbiology,* Dowden, Hutchinson and Ross, Inc., Stroudsburg, PA, 1976, pp. 221–230.

[*33*] Clifton, C. E., *Introduction to Bacterial Physiology,* McGraw-Hill, New York, 1957, 414 pp.

[*34*] Zobell, C. E., *Marine Microbiology: A Monograph on Hydrobacteriology,* Chronica Botanica Co., Waltham, MA, 1946, 240 pp.

[*35*] Allison, L. E., "Effect of Micro-organisms on Permeability of Soil Under Prolonged Submergence," *Soil Science,* Vol. 63, 1947, pp. 439–450.

Maurizio Soranzo[1]

Results and Interpretation of Multistage Triaxial Compression Tests

REFERENCE: Soranzo, M., "**Results and Interpretation of Multistage Triaxial Compression Tests,**" *Advanced Triaxial Testing of Soil and Rock, ASTM STP 977*, Robert T. Donaghe, Ronald C. Chaney, and Marshall L. Silver, Eds., American Society for Testing and Materials, Philadelphia, 1988, pp. 353–362.

ABSTRACT: The procedure for performing and interpreting multistage triaxial compression tests is described. The results obtained from unconsolidated undrained and isotropically consolidated undrained tests on normally consolidated alluvial clay and overconsolidated colluvial gravelly clay are presented.

A direct comparison of the results of single stage and multistage compression tests, performed on homogeneous samples, indicates that the latter procedure may be applied to soil specimens that reach failure with vertical strain greater than 8 to 10%.

To demonstrate the similarity between the two procedures and to interpret the tests when only a limited percentage of strain is available for each compression stage, stress versus strain, normalized stress versus strain, normalized tangent modulus versus stress, and Kondner's hyperbolic criterion were used in the analysis.

KEY WORDS: soil mechanics, triaxial test, compression, shear strength, stress–strain behavior, cohesive soils

Triaxial testing of cylindrical soil specimens is common because they allow a wide range of mechanical parameters to be examined during consolidation and shear phases. When the aim of analysis of a defined natural soil is to determine the shear strength (that is, c, ϕ), the most common type of test, for cohesive soil, is undoubtedly consolidated triaxial compression, in which the specimen is tested in undrained conditions. Undrained testing is usually accompanied by the measurement of the pore water pressure to obtain shear strength parameters in terms of effective stresses.

In traditional tests, each specimen undergoes a phase of consolidation and shearing and thus supplies a single stress versus strain trend and of course only one state of stress at failure. A series of three or four specimens, consolidated at various stress levels, supplies an ensemble of stress data allowing identification of a failure envelope and thus shear strength parameters. Sometimes it is impossible to have a set of homogeneous specimens, for economic reasons or because some soil formations may be difficult to sample (for example, gravelly or boulder clay, laminated soil).

This study refers in particular to the shear strength measurements of a normally consolidated alluvial and an overconsolidated colluvial soil formation. Referring to the latter soil type, various authors have shown that the measured strength of plastic and fissured clays depends on the size of the tested specimen [*1–3*]. For this reason the diameter of the specimen is often equal to the diameter of the bored sample (which depends on the sampler—usual range is 7 to 10 cm). This is also the case of clays containing gravelly elements.

[1] Senior research engineer, University of Padova, Via Ognissanti 39, Padova, Italy 35100.

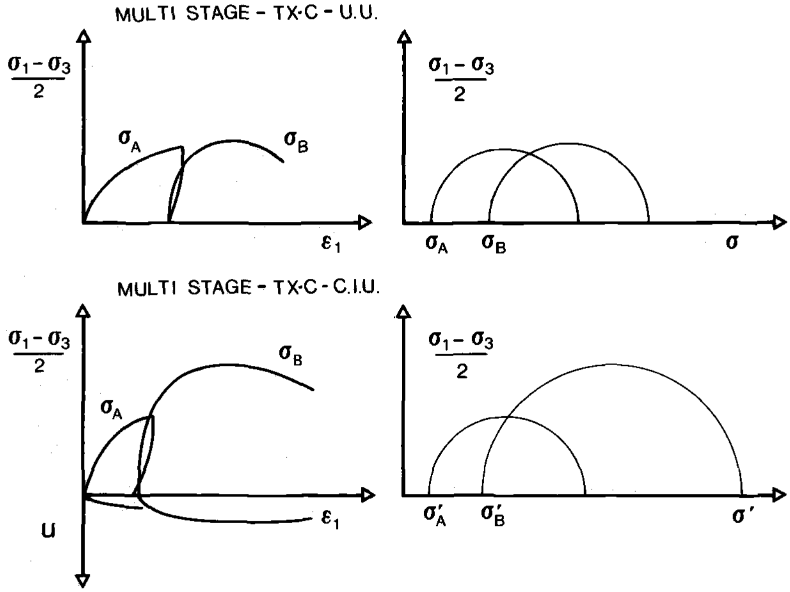

FIG. 1—*Shear stresses versus vertical strains and Mohr's circles at failure for unconsolidated (UU) and consolidated ($\overline{CIU}$) multistage triaxial compression tests (TX-C).*

If this procedure is adopted, it is highly improbable that two identical specimens from the same level can be obtained, unless several borings are made at the same site, which is very expensive. In these circumstances, it is important and sometimes necessary to have a large quantity of information from each single specimen.

The above reasons justify the development of triaxial tests which give more than one stress state at failure for each specimen. This is possible by using a technique of multiple consolidations and shearings within traditional triaxial apparatus and appropriate interpretation of test results. The method enables substantial homogeneity of results and appreciable cost savings.

Various authors have already shown the possibility of carrying out such tests to define undrained shear strength [*4*] or effective shear strength both in unsaturated [*5*] and saturated soils [*6*].

This paper presents the results of multistage unconsolidated undrained (UU) and isotropically consolidated undrained ($\overline{CIU}$) triaxial compression tests on natural complex clayey soils, with special emphasis on analysis and interpretation of test results.

Multistage Procedures

A multistage triaxial compression test induces more than one consolidation and shearing on the same soil specimen loaded inside a triaxial cell.

Specimen preparation and initial test stages of saturation (if required, by means of appropriate back pressure) or imbibition (soaking) are identical to those of traditional triaxial compression tests of various types (UU or consolidated undrained [$\overline{CU}$]).

During the shearing stage the specimen is strained to produce a significant amount of shear stress. Then the specimen is released from deviatoric stress and subjected to a higher confining (or consolidating) pressure before the following shearing stage takes place.

A double confining and compression stage is suggested for triaxial compression (TX-C)

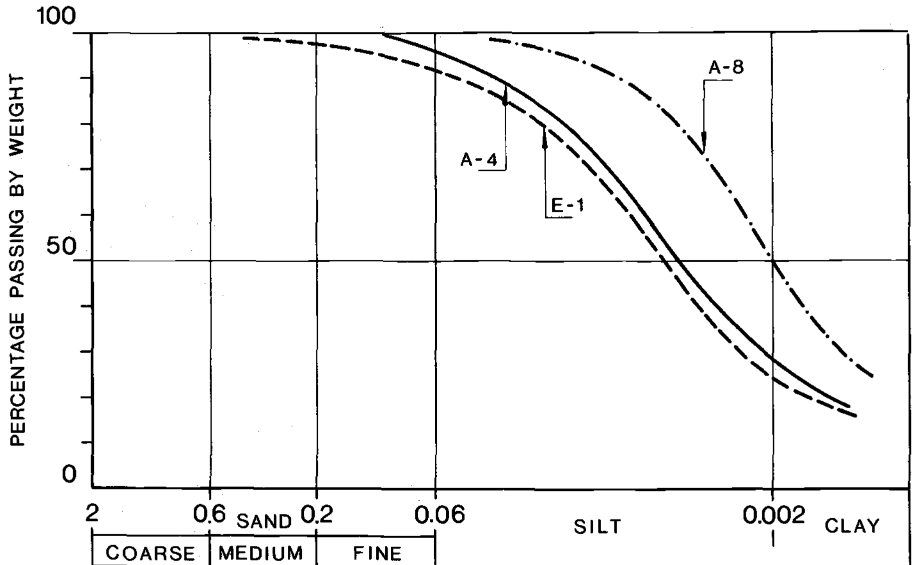

SITE	SAMPLE	γ (kN/m^3)	W (%)	W_L (%)	PI (%)	σ'_c (kPa)
CERVIA	A - 4	18.6	30	51	25	130
CERVIA	A - 8	19.0	38	79	46	190
EUGANEI	E - 1	19-21	22	51	26	250

FIG. 2—*Particle-size distribution curves of examined soils. Table shows unit weight, water content, liquid limit, plasticity index, and consolidation pressures for each soil sample.*

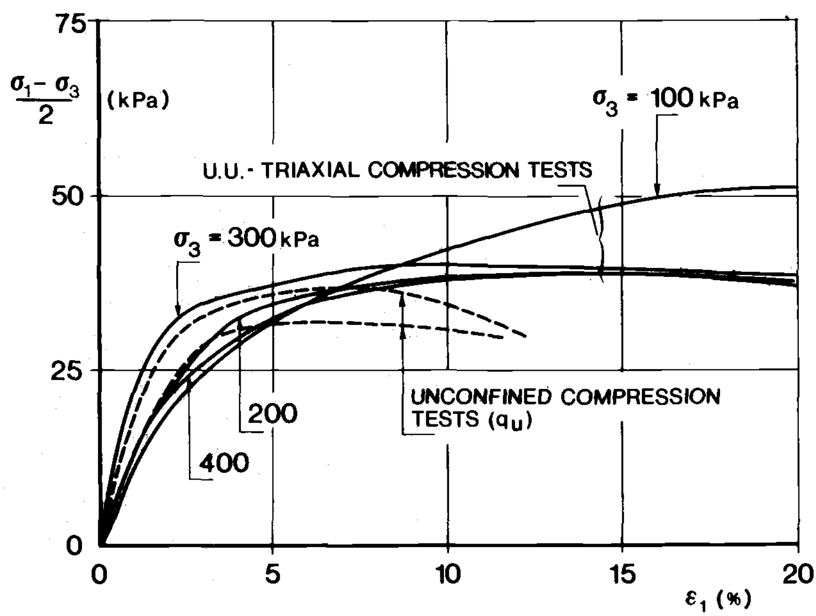

FIG. 3—*Shear stresses versus axial strains of a set of undrained compression tests.*

UU tests and a double or triple set of consolidation-shearing is allowed for TX-C $\overline{\text{CIU}}$ tests, if peak shear stress is not expected for axial strains of at least 8%. In $\overline{\text{CIU}}$ tests, after each consolidation phase, the new volume and height of the specimen are computed and assigned to it for the next compression stage.

Figure 1 shows the main results of multistage UU and $\overline{\text{CIU}}$ triaxial compression tests on isotropically confined specimens. For each test, stress–strain curves and the state of stress at failure for the first and second compression stages are plotted. Isotropic stresses σ_A and σ_B are the confining (UU) or consolidation ($\overline{\text{CIU}}$) stresses for each stage. The strain is of the order of 5% for each compression stage in the unconsolidated test and 3% for the consolidated one. In both cases, peak values of shear strength are expected for strain values greater than 8%, as is the case of many clayey and silty-clayey soils of medium to low plasticity.

Although we suggest that at least 5% of compression strain should be reached in the first compression stage, we will show here that, with appropriate interpretation of test results, this limitation may be reduced. However, the proposed method is not generally applicable for soil formations which reach "failure" at very small axial strain values (sometimes less than 3%), as is the case for sensitive clays [*7–9*] or stiff fissured clays [*10*].

Soil Specimens Examined

The soil specimens used were taken from high-quality borings, using an Osterberg piston sampler.

Two types of soil were tested: an alluvial silty clay from Cervia (central Italy) in the Po Plain and a colluvial gravelly-silty clay from the volcanic Euganean Hills (northeastern Italy). The main characteristics and grain-size distribution curves of these soils are given in Fig. 2.

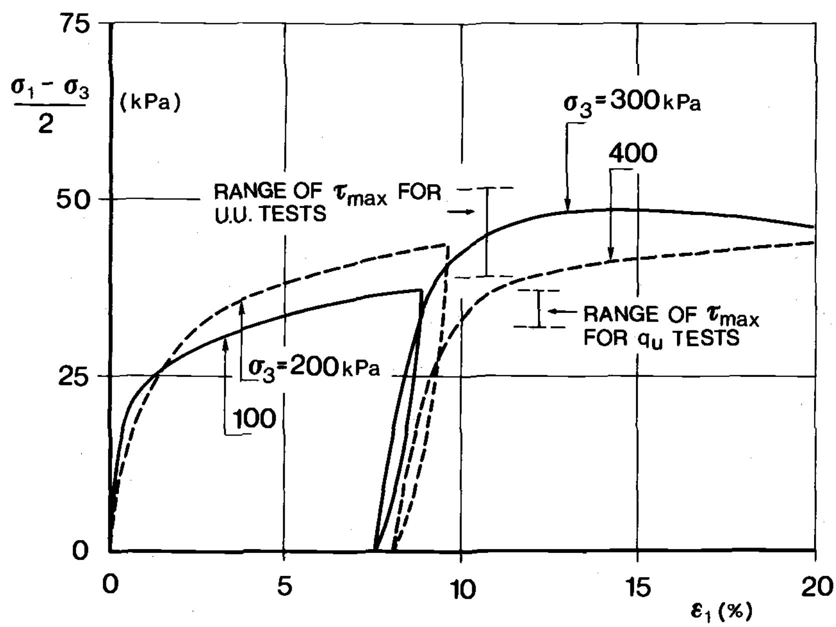

FIG. 4—*Results of unconsolidated undrained multistage triaxial compression tests.*

At each elevation, the Cervia alluvial clay gave very uniform samples and was used for comparing the results of the various triaxial techniques. On the other hand, each sample from the Euganei site was bored at different elevations and, because of the complex nature of the gravelly clay, only one specimen with the same diameter as the sampler per sample was prepared. In this case, no attempt was made to compare the results of the various test techniques.

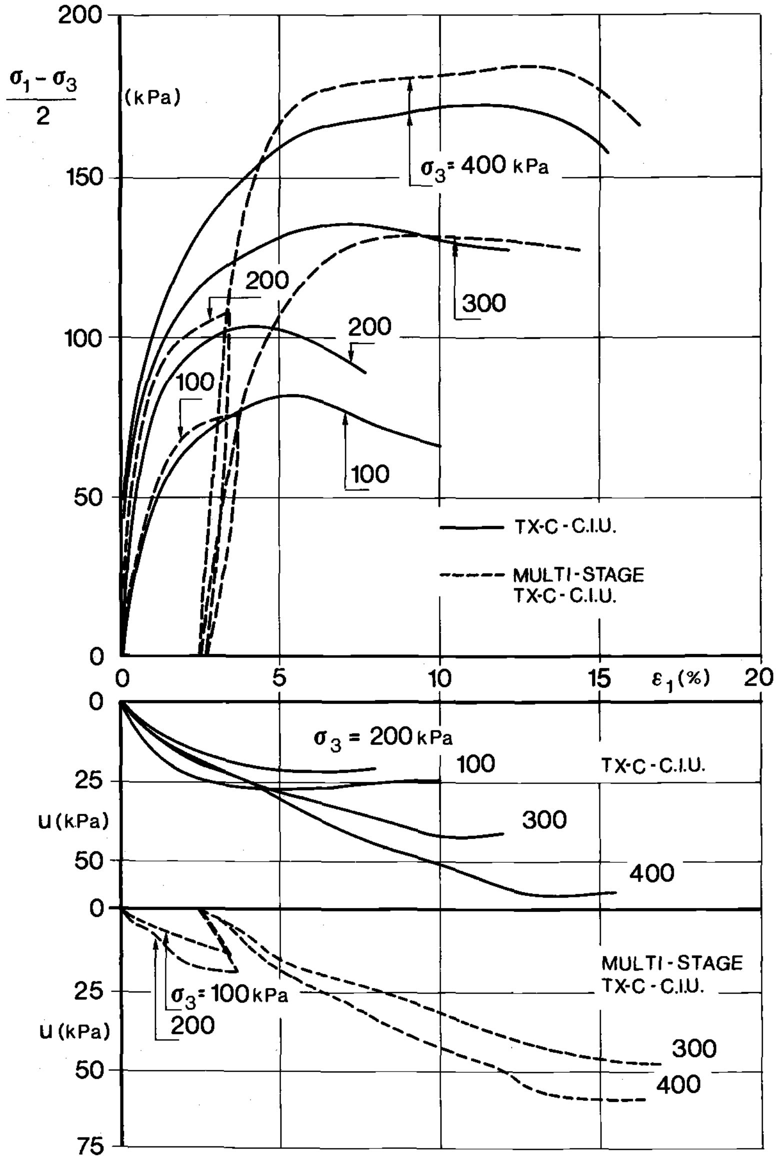

FIG. 5—*Comparison of stress versus strain curves of traditional and multistage TX-C-CIU tests.*

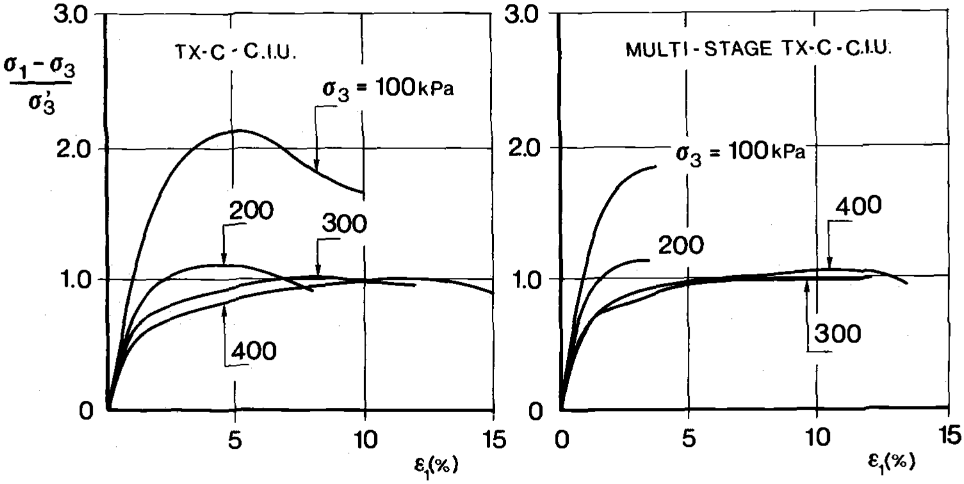

FIG. 6—*Normalized deviatoric stress versus strain curves for traditional and multistage TX-C-$\overline{CIU}$ tests.*

Test Results

Unconsolidated Undrained Triaxial Compression Test (TX-C-UU)

The multistage UU triaxial test may be run according to two techniques:

1. The initial confining pressure (σ_3) is kept constant to a very high compressive strain (15 to 20%) and then two or three successive increases of σ_3 are made to allow the multistage test to be performed.

   In these last phases, each increase in σ_3 is kept for a few units of strain (that is, 1 to 2%). This technique does not allow analysis of stress–strain behavior within this small range of strains, and thus the shear stresses given must be considered as "failure" values, no other interpretation being possible. This technique was proposed by Anderson [*4*] and will not be treated here.
2. Alternatively, the test may be run by increasing σ_3 when a sufficient degree of available shear stress has been mobilized. This usually corresponds to strains of 5 to 10%. Thus, the method is not applicable to brittle soils that reach failure with strains of less than 5%.

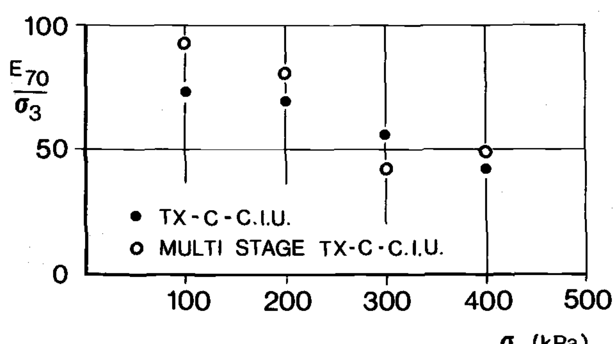

FIG. 7—*Comparison of normalized tangent undrained moduli for single and multistage TX-C-$\overline{CIU}$ tests.*

The results of eight undrained compression tests carried out on specimens trimmed from the same A-4 Cervia sample are reported in Figs. 3 and 4. Figure 3 shows the results of four TX-C-UU tests and two unconfined compression tests (q_u) on the Cervia silty clay, plotted in the shear stress versus strain plane. Figure 4 shows the results of two multistage TX-C-UU tests on the same soil and at the same depth. The range of the peak shear stresses of the previous six compressions are also shown in this figure. An increase in confining pressure took place at strains of 8.9 and 9.6%, after complete unloading of the shear stress acting on the specimen. The new σ_3 was given time to act before the subsequent compression stage took place. A complete double-stage TX-C-UU test took 10% longer than one conventional UU compression test.

In alluvial and colluvial soils without fissures or particular structures, it is sometimes possible to perform triple-stage UU tests. In this case, some judgment is required to define the limit strain for each stage.

It is advisable to plot the test results throughout the test and to use some simple analytical tool to define the approach of a failure condition (see next section).

Isotropically Consolidated Undrained Triaxial Compression Test (TX-C-$\overline{CIU}$)

The multistage technique applied to $\overline{CIU}$ tests requires a number of consolidation phases which occur by raising the value of the hydrostatic confining pressure in the triaxial cell.

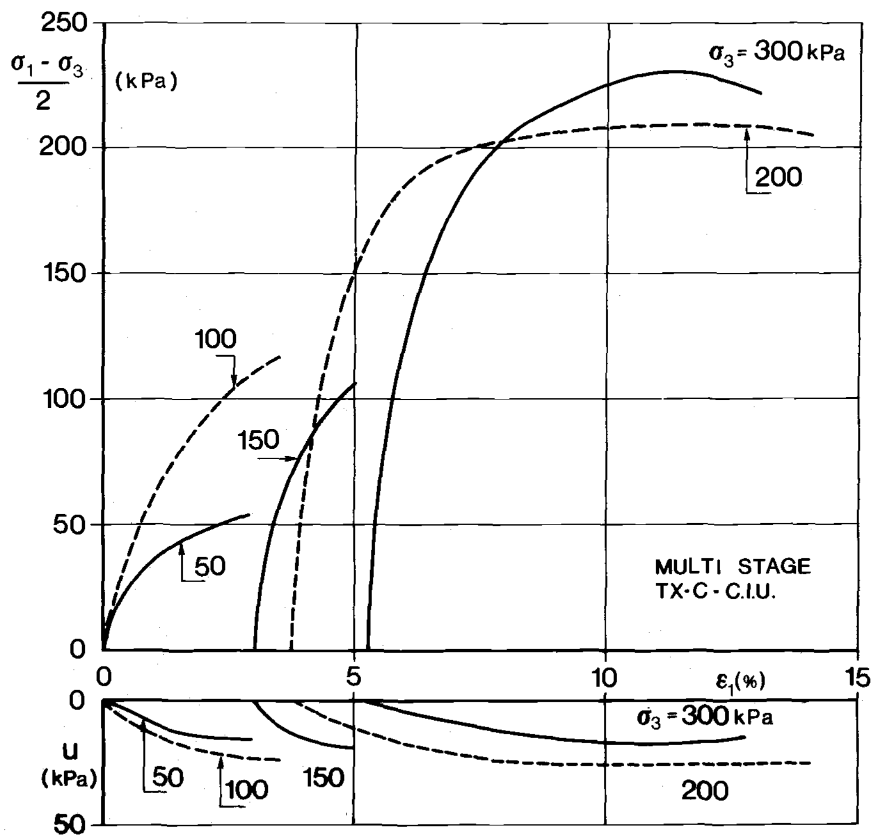

FIG. 8—*Shear stress versus strain curves for two multistage ($\overline{CIU}$) triaxial compression tests.*

Each consolidation stage does not seem to affect the stress–strain curve for stress levels higher than those previously reached (Fig. 5). The shear stresses $(\sigma_1 - \sigma_3)/2$ versus strain for traditional and multistage CIU tests carried out on the Cervia specimens are plotted in the same diagram. The six specimens were trimmed from the central part of a very uniform sample taken with a 102-mm Osterberg sampler.

Tests were performed on specimens taken at a depth of about 24 m, where the consolidation pressure, determined with an oedometer, was estimated to be 190 kPa. Consolidation pressure in the triaxial cell was selected at 100, 200, 300, and 400 kPa, so that one specimen (and one stage of the multistage test) would show overconsolidated behavior, while the other ones would follow normally consolidated behavior.

The plots of Fig. 5 give comparable results: the first phase of each multistage test almost covers the corresponding traditional tests.

More convincing evidence may be achieved by plotting the results in a normalized plane such as $(\sigma_1 - \sigma_3)/\sigma_3'$ versus ϵ_1, as done in Fig. 6. In this way the effective stress behavior and the overconsolidation effect are shown. The curve of each stage of the multistage test is represented in the above figure starting with a strain equal to zero. In both sets of results, the specimens consolidated to 100 kPa, due to their overconsolidation with respect to cell pressure, show normalized resistance almost double that of the other specimens, whose normalized strength falls in a very narrow range. The shape of the curves was also analyzed by plotting a normalized tangent modulus E_{70}/σ_3 (that is, tangent moduli calculated at 70% of soil strength) versus consolidation pressure (Fig. 7). This direct comparison shows that the scatter among the results, which turned out to be 20 to 25% at various consolidation pressures, must be considered within usual experimental practice on natural soils. These moduli (E_{70}) were chosen at a high shear strength level in order to exceed stress levels encountered in the first stage of the test, so they must be considered loading moduli.

If a strong softening effect is feared after reaching peak strength, each compression stage

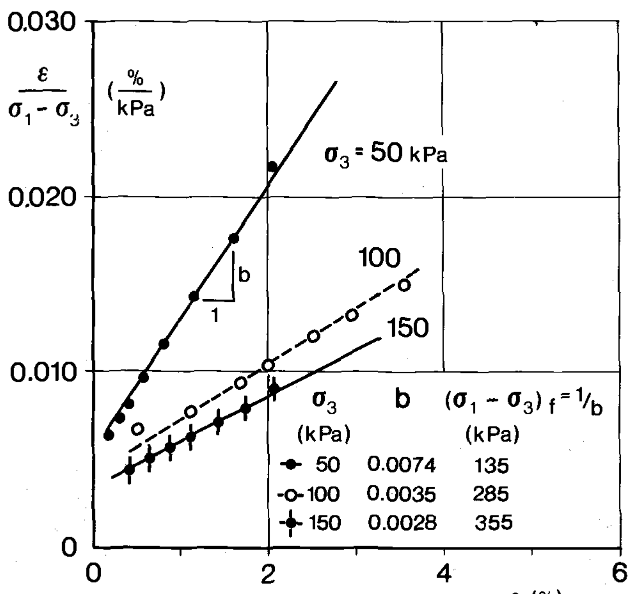

FIG. 9—*Kondner's hyperbolic interpretation for first stages of multiple compression tests.*

may be stopped at low strain values (2 to 3%). In this case, doubts may exist as to whether peak shear has been reached, and the limited stress–strain curve may have to be interpreted.

It was found that Kondner's [*11,12*] "hyperbole" criterion defining a failure condition was useful for the soils tested. Stress–strain data, plotted on a plane $\epsilon/(\sigma_1 - \sigma_3)$ versus ϵ, approximate a hyperbola which has a linear trend in such a plane. The inverse of slope b of the line gives the "at failure" value $(\sigma_1 - \sigma_3)_f$ of the soil. This procedure of data interpretation was used to define the strength of the first stages of the TX-C-CIU tests performed on the complex colluvial clay of the Euganei site (Fig. 8). In this case, these are one triple-stage compression and one double-stage compression at consolidation stresses ranging from 50 to 300 kPa. Only the loading stages are shown.

Kondner's criterion on the stages with confining pressure of 50, 100, and 150 kPa was used, as shown in Fig. 9.

Lastly, the five stress conditions at failure, evaluated from the compression of two specimens, are shown in the Terzaghi-Mohr space in terms of effective stresses (Fig. 10). Again, the test technique and its interpretation gave a homogeneous view of soil strength. In this case, no comparison with the one-stage test was possible because only two samples of complex natural soil were available.

Discussion and Conclusions

Test results demonstrate that it is possible and convenient to perform multistage triaxial compression tests on natural soil to measure shear strength.

Both UU and $\overline{\text{CIU}}$ tests were carried out using the multistage technique and , as shown, the results are highly comparable to those of traditional triaxial tests.

No particular interpretation is needed if it is possible to reach strain levels so that failure stresses are definitely indicated for each stage of consolidation or loading. This is the case of soils that reach peak strength at compression strains higher than 8 to 10% and that do not tend to exhibit brittle behavior after having reached peak strength. In this case, two or possibly three different confining (UU tests) or consolidation ($\overline{\text{CIU}}$ tests) pressures may be used.

As pointed out, when brittle behavior occurs at low strain values (less than 4%), as happens for heavily overconsolidated fissured soil formations and cemented or sensitive clays, the described procedure is not recommended. On the other hand, if for some reason brittle behavior is feared at intermediate strains (that is, 5 to 6%), failure should not be approached too closely. In this case, previous experiences on similar soils help in program-

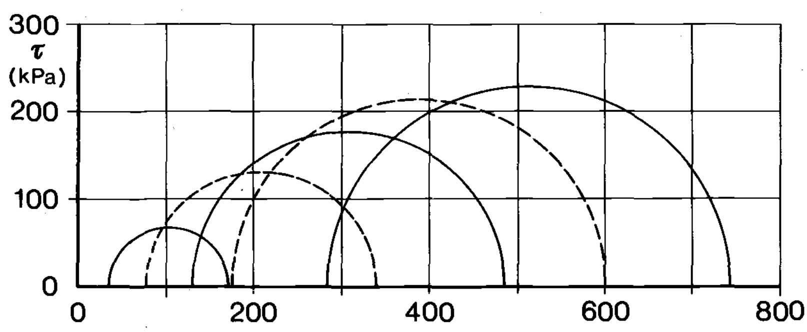

FIG. 10—*Complete set of Mohr's circles at failure of multistage tests shown in Fig. 8.*

ming tests, and some interpretation is needed to define the shear stress at failure of the initial stage(s).

The simple Kondner model is proposed to overcome this difficulty.

Because of successive consolidations, multistage $\overline{\text{CIU}}$ tests also allow the stress–strain curves to be used to evaluate some of the deformation characteristics of the examined soil, if these curves are evaluated at stress levels higher than those reached in the previous stage.

Lastly, the described procedure was found to be economically feasible, because test time is shortened due to reduced manual intervention during specimen preparation in the laboratory.

References

[1] Skempton, A. W., and La Rochelle, P., "A Short-Term Failure in London Clay," *Geotechnique,* Vol. 15, No. 3, 1965, pp. 221–242.

[2] Lo, K. Y., "The Operational Strength of Fissured Clays," *Geotechnique,* Vol. 20, No, 1, 1970, pp. 57–74.

[3] Morgenstern, N. R., Blight, G. E., Janbu, N., and Resendiz, D., "State-of-the-Art Report: Slopes and Excavations," in *Proceedings,* Ninth International Conference on Soil Mechanics and Foundation Engineering, Tokyo, Vol. 2, 1977, pp. 547–603.

[4] Anderson, W. F., "The Use of Multi-Stage Triaxial Tests to Find the Undrained Strength Parameters of Stony Boulder Clay," in *Proceedings,* Institution of Civil Engineers, Pt. 2, Vol. 57, Thomas Telford Ltd., London, 1974, pp. 367–373.

[5] De Beer, E. E., "The Cell Test," *Geotechnique,* Vol. 2, No. 2, 1950, pp. 162–172.

[6] Kenney, T. C., and Watson, G. H., "Multiple-Stage Triaxial Tests for Determining c' and ϕ' of Saturated Soils," in *Proceedings,* Fifth International Conference on Soil Mechanics and Foundation Engineering, Paris, Vol. 1, 1961, pp. 191–195.

[7] Skempton, A. W., and Northey, R. D., "The Sensitivity of Clays," *Geotechnique,* Vol. 3, No. 1, 1952, pp. 30–53.

[8] Yong, R. N., and Tabba, M. M., "On the Random Aspect of Shear Strength in Laboratory Shear Strength of Soil," in *ASTM STP 740,* American Society for Testing and Materials, Philadelphia, 1981, pp. 485–501.

[9] Loiselle, A., Massiera, M., and Sainani, U. R., "A Study of the Cementation Bonds of the Sensitive Clays of the Outardes River Region," *Canadian Geotechnical Journal,* Vol. 8, No. 4, 1971, pp. 479–498.

[10] Marsland, S., "The Shear Strength of Stiff Fissured Clays," in *Proceedings,* Roscoe Memorial Symposium, Cambridge, England, G. T., Faules & Co. Ltd., 1971, pp. 59–68.

[11] Kondner, R. L., "Hyberbolic Stress–Strain Response: Cohesive Soil," *Journal of the Soil Mechanics and Foundation Division, American Society of Civil Engineers,* Vol. 89, No. SM1, Feb. 1963, pp. 115–143.

[12] Kondner, R. L., and Zelasko, J. S., "Void Ratio Effects on the Hyperbolic Stress–Strain Response of a Sand," in Laboratory Shear Testing of Soils, ASTM STP 361, American Society for Testing and Materials, Philadelphia, PA, 1964, pp. 250–257.

Hamed S. Saeedy[1] *and Mohammed A. Mollah*[2]

Application of Multistage Triaxial Test to Kuwaiti Soils

REFERENCE: Saeedy, H. S. and Mollah, M. A., "**Application of Multistage Triaxial Test to Kuwaiti Soils,**" *Advanced Triaxial Testing of Soil and Rock, ASTM STP 977,* Robert T. Donaghe, Ronald C. Chaney, and Marshall L. Silver, Eds., American Society for Testing and Materials, Philadelphia, 1988, pp. 363–375.

ABSTRACT: Forty-eight soil samples taken from twelve different locations in Kuwait City and the Jahra area were used in four series of drained and undrained triaxial compression tests using multistage and conventional test techniques on undisturbed and remolded specimens. Classification tests indicated that the Kuwaiti soil is predominantly sandy with various content of fines. The fines content includes silt and clay, and also clay-size particles of calcareous and gypsiferous matter. Strength test results indicated that the cohesion and angle of friction determined from both techniques are in agreement and hence the multistage principle can be applied to determine the shear strength parameters of Kuwaiti soils. Specific recommendations on applying the multistage technique on cemented soils, occasionally encountered in Kuwait, are also included.

KEY WORDS: triaxial test, multistage test, conventional triaxial test, calcareous soil, drained triaxial test, undrained triaxial test, shear strength, cohesion, angle of friction, cemented soil

A comprehensive investigation for the evaluation of geotechnical properties of soil from various areas of Kuwait was made between 1984 and 1986 in the Building Department of the Kuwait Institute for Scientific Research [*1*]. An intensive field and laboratory testing program was implemented. This included tests which have not yet been standardized by international institutions. Among these, the most prominent was the multistage triaxial compression test being used to determine the shear strength parameters.

The subsoil of Kuwait is characterized as being predominantly sandy but occasionally calcareous. During the investigation, considerable variations of soil properties were noticed even within small zones. The evaluation of the drainage characteristics of soil, which was one of the primary objectives of the 30-month project, indicated that the subsoil ranged from fair draining to impervious material. The ranges of various geotechnical properties of these soils have been reported elsewhere [*2*]. While dealing with these soils, various problems were faced. Certainly, the foremost problem encountered was the selection of truly representative specimens during testing.

In Kuwaiti soils, variation of strength from specimen to specimen was noticed. This occasionally led to multiple choice of failure envelopes wherein cohesion (c) and angle of

[1] Researcher, Civil Engineering and Building Department, Engineering Division, Kuwait Institute for Scientific Research, P. O. Box 24885, 13109 Safat, Kuwait.

[2] Senior geotechnical engineer, Government Lab and Testing Station, Ministry of Public Works, P.O. Box 8, Safat, Kuwait.

friction (ϕ) values varied by 0 to 100 kPa and 2 to 14°, respectively.[3] Such variation was, to a large extent, attributed to the presence of calcareous and gypsiferous matter (resulting in local cementation), cemented conglomerates, and pockets of silt and clay particles in various contents. Sampling and preparation of specimens posed a very serious challenge in testing, particularly in triaxial compression. Sampling of Kuwaiti soils was generally difficult. A pitcher sampler, 73 mm in diameter and 900 mm in length, was used to extract soil samples from the boreholes. In some instances, the recovery of samples was discouraging. Usually, recovery ranged between 20 and 40 cm (rarely exceeding 60 cm), which was not sufficient to conduct a normal triaxial test. Specimens of smaller diameter were tried but were not found feasible, as a result of the granular nature of particles which did not permit obtaining good specimens. Moreover, specimens were found to crumble even with utmost care. These factors (poor recovery and nonavailability of sufficient homogeneous specimens) compelled the use of the multistage principle. However, before the final decision was made, several trials were conducted using conventional and multistage techniques on specimens of fairly homogeneous soils having satisfactory recovery.

This paper reports the application of the multistage principle to Kuwaiti soils. The program of testing included shearing a total of 48 samples from areas in Kuwait City and Jahra, at a constant rate of strain under undrained and drained conditions.

Shear Strength of Soil

The shear strength of soil is generally determined using the Mohr-Coulomb's equation, given by

$$\tau_f = c + \sigma_f \tan \phi \tag{1}$$

where

τ_f = shearing resistance of soil,
c = the intercept on the axis representing shear stress,
σ_f = normal stress on the failure plane, and
ϕ = angle of shearing resistance.

In a saturated soil, the normal stress acting across the plane of failure is not necessarily equal to the effective stress. In terms of effective stress, a concept introduced by Terzaghi [3], the above equation can be rewritten as

$$\tau_f = c' + \sigma_{f'} \tan \phi' \tag{2a}$$

and

$$\tau_f = c' + (\sigma_f - u_f) \tan \phi' \tag{2b}$$

where

u_f = pore water pressure developed and
c' and ϕ' are same as in Eq 1 but in terms of effective condition.

The above equations specifically apply to direct shear test. In a triaxial test, the failure envelope in terms of effective stress is generally drawn on (q', p') plot to be represented

[3] Government Laboratories and Testing Station, "Laboratory Soil Testing for Sub-Surface Water Rise in Kuwait and Suburbs Project," Second Bimonthly Report, Kuwait (Unpublished), 1985.

by the following equation [4]:

$$q_f' = a' + p_f' \tan \alpha' \tag{3}$$

where

$$q' = \frac{\sigma_1' - \sigma_3'}{2} = \frac{\sigma_1 - \sigma_3}{2} \tag{4a}$$

$$p' = \frac{\sigma_1' + \sigma_3'}{2} \tag{4b}$$

σ_1', σ_3' are major and minor principal effective stresses, respectively, and

q_f', p_f' represent the values of (q', p') corresponding to peak points of the stress–strain curves.

a', α' are the modified strength parameters defined by

$$a' = c' \cos \phi' \tag{5a}$$

and

$$\alpha' = \tan^{-1} (\sin \phi') \tag{5b}$$

Multistage Test

A conventional triaxial test using three or more specimens is normally used to determine the shear strength parameters of soil. A multistage test is a modified version of the conventional test and is becoming increasingly popular. The test technique comprises shearing a single specimen to near failures at several elevated lateral pressures, while measuring the corresponding deviator stresses at which the failures occur. The multistage test is mainly used when the soil available for testing is scarce or they are nonhomogeneous.

The relative advantages and disadvantages of the multistage principle over the conventional have been discussed in detail by Lumb [5]. The principal advantages include the reduction of the laborious and often delicate job of specimen preparation and test set-up. This is, in particular, important for brittle or cemented soils as well as saturated sands, where sampling is not only difficult but costly too. Moreover, a drained triaxial test is generally time-consuming. As such, a multistage test would be economical provided it can be used properly for the particular type of soil. On the other hand, compliance to a predefined failure criterion during shear is the most difficult task when applying the multistage principle. This requires immediate data reduction in addition to a standard procedure to define failure. The other shortfalls include (1) the selection of representative specimens for testing and (2) the straining limit of ordinary commercial cells.

Early research work on the multistage test was very limited. A brief review of literature has been offered by Kenney and Watson [6]. Since its first application in 1950, the technique drew attention of few researchers who were reported to have successfully utilized the principle on different soils for the determination of shear strength parameters [5–10].

Physiographic Condition of Kuwait

Kuwait is a small country located at the northwestern part of the Arabian Peninsula. It is bordered by Iraq on the north, by Saudi Arabia on the south and west, and by the Arabian Gulf on the east. The topography of the state of Kuwait is generally flat. The land surface slopes northeastward at an average gradient of 1:500 with elevations ranging from sea level in the east to about 300 m in the southwestern corner of the country.

The area in the state of Kuwait is covered by various types of sedimentary deposits ranging in age from Eocene to Recent [11]. The surficial deposit consists of wind-blown sand and sediments comprising silicious sands and gravels with varying content of silt and clay, and gypsum band, wherein the original sand belongs to Dibbibba formation. The climate of Kuwait is characterized by an extreme hot and dry summer lasting several months. Evaporation is high throughout the year with very little runoff into the sea. The evaporation in excess of the rainfall leads to a general upward movement of groundwater with increased concentration of soluble salts at or near surface, enriching the top layers with gypsum and carbonates, and ultimately leading to cementation. Such soils are locally known as "Gatch" [12].[4]

The study areas were two relatively recent developed urban zones, namely, Kuwait City and its suburbs, and Jahra. The city of Kuwait, at 29° 25′ N latitude and 48° E longitude, is located on Kuwait Bay whereas Jahra is an oasis on the main road to Basra City in Iraq about 40 km southwest of Kuwait City.

Sampling and Testing Program

Soils used for this investigation were collected at depths of 1.5 to 8.0 m from a total of twelve boreholes. Seven of these boreholes were located in Kuwait City and its suburbs, and the remainder were located in the Jahra area (Fig. 1). All boreholes, 100 mm in nominal diameter, were advanced by rotary wash technique using bentonite slurry except above water table where casing was used to protect side walls. The samples were extracted using 73-mm inside diameter (ID) and 900-mm length pitcher samplers.

The testing program included first determining the physical and index properties of all samples. To obtain parameters that could be used in comparing the multistage with the conventional triaxial test, four series of tests were performed under drained and undrained conditions. A total of twelve sets, each comprising three conventional tests and one multistage test were conducted using both undisturbed and remolded specimens. The remolded specimens were prepared to have the same moisture content and density as the natural soil.

The testing program, detailed in Table 1, was implemented using a cell and machine manufactured by Wykeham Farrance. The soil samples exhibiting limited variation in properties and having ample recovery were used. The specimens, with nominal dimension of 73-mm diameter (ID) and 150-mm length, were tested employing a back pressure of 345 kPa. The sequences of isotropically applied consolidation pressures were 69, 207, 414 kPa and 207, 414, 621 kPa. To prepare a test specimen, the sample from the pitcher sampler was pushed hydraulically to standard laboratory tubes of the same ID and 150 mm in length. This practice ensured obtaining good specimens with the least disturbance. (Earlier attempts at taking specimens of smaller dimension ended in failure because of the type of soil, which is characterized by its loose structure and bulky shaped grains.) The true dimension of each individual specimen was recorded after its extraction from the standard tube. End and radial drainage was allowed by using porous stones and filter strips, respectively. In the beginning of the first stage, the specimens were left for 24 h under full back pressure and slightly elevated cell pressure to ensure saturation, followed by application of the consolidation pressure. Each specimen was checked for a degree of saturation ranging from 90 to 100%. After allowing for full consolidation, the specimens were sheared at a constant rate of strain of 0.5 and 1% per hour in drained and undrained tests, respectively. During the shearing stage, a continuous record of load and volume change for drained/pore water pressure for undrained tests were taken at a deformation interval of 0.1 mm.

[4] J. Al-Sulaimi, M. I. El-Sayed, Y. Youash, M. Matti, A. Akber, et al., "Study of the Gatch Deposits in Kuwait City and Suburbs," Research Report 1399, Kuwait Institute for Scientific Research, Kuwait (Unpublished), 1984.

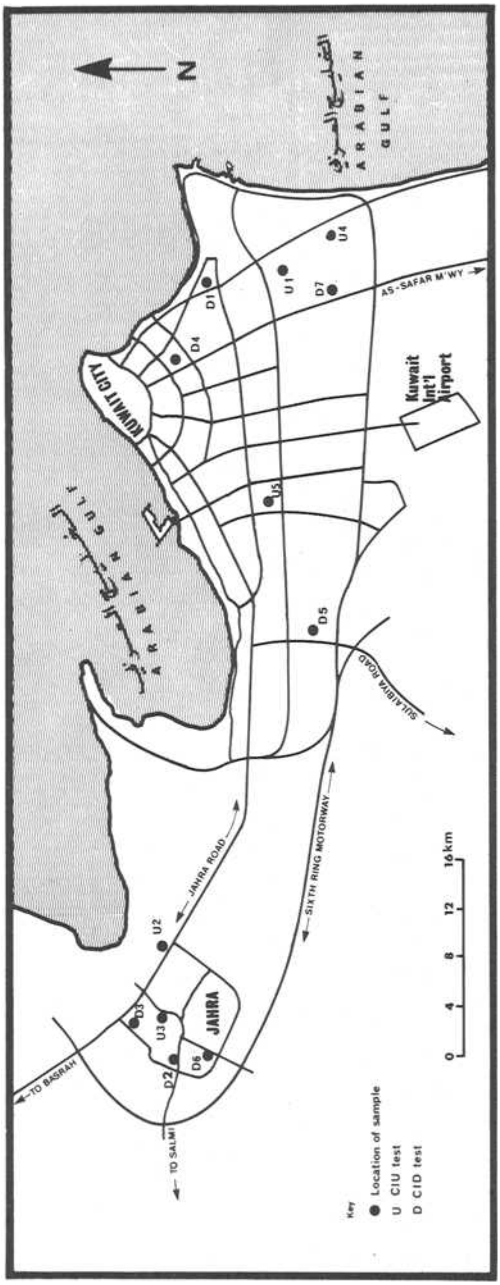

FIG. 1—*Location of sampling sites.*

TABLE 1—*Details of test program.*

Test Set	Test Series	Sample Identification	Sample Depth, m	Sampling Area	Confining Pressure Range, kPa	Type of Samples
1		D1	2.0	East Hawalli	207, 414, 621	disturbed (remolded at in situ moisture content and density)
2	CID-I[a]	D2	1.5	Jahra		
3		D3	6.5			
4		D4	4.0	Qadisiya		
5		D5	1.5	Firdous	69, 207, 414	undisturbed
6	CID-II	D6	1.5	Jahra		
7		D7	1.8	Mushrif		
8		U1	1.5	Bayan	69, 207, 414	undisturbed
9	CIU-I[b]	U2	6.5	Jahra		
10		U3	6.5			
11	CIU-II	U4	6.5	Mushrif	207, 414, 621	undisturbed
12		U5	1.5	Rai		

[a] CID = isotropically consolidated drained.
[b] CIU = isotropically consolidated undrained.

For the purpose of this study, a specimen in multistage test was considered to have reached the failure during Stages 1 and 2 at the point where two consecutive observations showed negligible increase (<0.05%) in the deviator stress. During these stages, the shearing was stopped immediately after failure and was followed successively by closing the drainage valve (in drained test) and unloading the specimen. The confining pressure was then increased to the level required for the next stage. After waiting for sufficient time to allow pore water pressure (PWP) in the specimen to stabilize, the drainage valve was let open to achieve complete dissipation of the PWP. The specimens were sheared as usual, but the test data were analyzed immediately to determine the deviator stress ($\sigma_1 - \sigma_3$). In the third and final stage, however, the shearing was continued beyond failure point to at least 20% axial strain.

Basic Properties

The physical and index properties determined, including natural moisture content, in situ density, Atterberg limits, and specific gravity of soil solids, are given in Table 2. The grain size distribution of all samples was determined using both the sieve and hydrometer methods. The limiting boundaries of all grain size distribution curves are given in Fig. 2. The results indicated that the soil was predominantly sandy and the contents of fines ranged between 12 and 40%. Further, the grain size distribution of coarse fraction was noticed to be similar, unless the sample contained cemented fragments. The natural moisture contents, which ranged between 9 and 17%, were all below their corresponding values of shrinkage limit. This has indicated a general moisture deficiency and possible sensitivity to saturation. Seven out of twelve samples were found to be nonplastic (NP), while the remaining samples were only slightly plastic with a range of plasticity index values less than 12%. According to Unified Soil Classification System (USCS), these soils can be grouped as silty sand to clayey sand (SM-SC), the majority of them belonging to SM. The samples were generally dense to very dense, as indicated by the Standard Penetration Test (SPT) values ($N > 50$), with the degree of saturation varying from 47 to 91%.

TABLE 2—*Physical and index properties of test samples.*

Test Set	Sample Identification	Natural Moisture Content, %	Bulk Density, kg/m³	Passing U.S. No. 200 Sieve, %	Average Grain Size D_{50}, mm	Liquid Limit, %	Plastic Limit, %	Shrinkage Limit, %	Specific Gravity of Soil Solids	Degree of Saturation, %	Unified Soil Classification[a]
1	D1	9.0	1935	21.4	0.30	33.6	24.8	21.9	2.69	47.0	SM
2	D2	14.8	2060	17.4	0.25	NP[b]	NP	NA[c]	2.68	80.3	SM
3	D3	16.8	2077	12.7	0.55	NP	NP	NA[c]	2.65	90.9	SM
4	D4	16.2	1991	20.2	0.27	NP	NP	NA[c]	2.68	77.0	SM
5	D5	16.8	2014	25.9	0.30	25.4	21.2	14.8	ND[d]	81.3	SM-SC
6	D6	16.6	2074	18.7	0.23	NP	NP	NA[c]	2.66	89.2	SM
7	D7	13.2	2063	19.2	0.42	NP	NP	NA[c]	2.67	75.8	SM
8	U1	12.4	2040	20.4	0.24	23.4	18.4	16.0	2.67	70.3	SM-SC
9	U2	12.7	2065	28.1	0.20	28.2	17.2	14.4	2.71	71.9	SC
10	U3	13.3	2117	40.4	0.15	27.5	16.3	14.1	2.71	80.1	SC
11	U4	12.8	2075	24.6	0.60	NP	NP	NA[c]	2.67	75.8	SM
12	U5	9.5	2010	11.6	0.42	NP	NP	NA[c]	2.69	55.0	SM

[a] SM = silty sand, and SC = clayey sand.
[b] NP = nonplastic.
[c] NA = not applicable.
[d] ND = not determined.

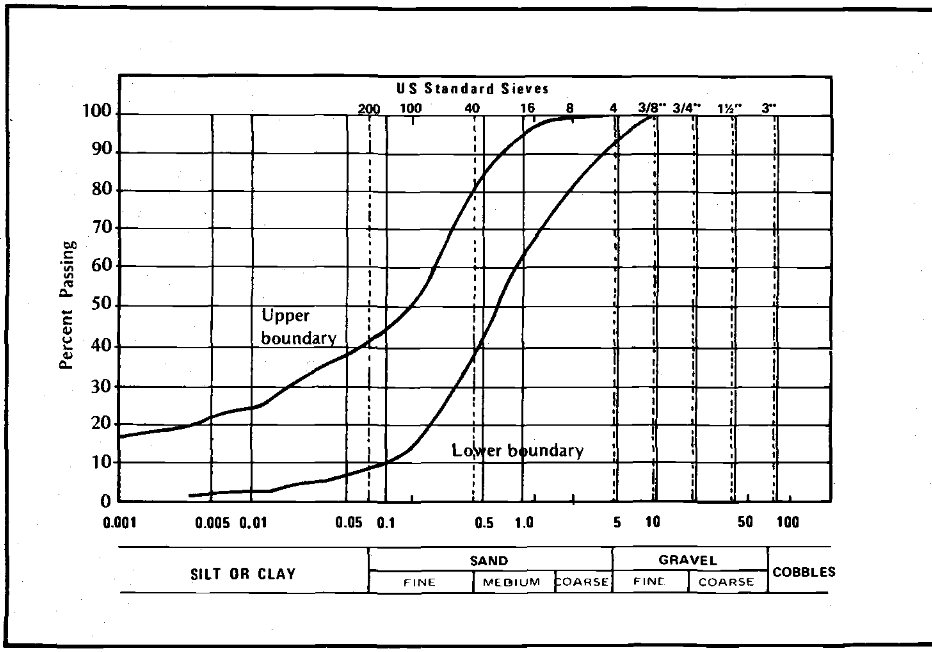

FIG. 2—*Particle size distribution band for tested soil samples.*

Results and Discussion

Two series of drained tests were performed on seven sets of samples taken from different sites. Of these samples, four sets were disturbed and the remainder were undisturbed samples. The disturbed specimens were remolded to the in situ density at the natural moisture content of the sample. The remolded specimens served two purposes, namely, compensation of the lack of undisturbed specimens and comparison of results with those of undisturbed samples.

A typical set of stress–deformation relationships, obtained from both multistage and conventional triaxial tests, is given in Fig. 3. The data were obtained from drained compression tests performed using the confining pressure sequence of 207, 414, 621 kPa. The data presented in Fig. 3 show that the stiffness and peak strength of all specimens increase with confining pressures. Volume changes during shear were measured, and the observations were also plotted in Fig. 3. The volume changes as well as failure strains were generally small. All samples, irrespective of the type of testing, were noticed to fail by slight bulging with the development of failure planes indicating transitional response, a behavior usually displayed by brittle-to-ductile material. The reason for the transition from brittle-to-ductile failure modes appears to be related to the relative contributions to the soil strength response by the cementation and frictional components of the deformation resistance mechanism. Similar observations were noted in the undrained test series performed on five sets of undisturbed samples taken from different sites in which the sequence of lateral pressures were varied from 69, 207, 414 kPa to 207, 414, 621 kPa and records of load, deformation, and changes of pore water pressure during shear were recorded (Fig. 4).

Stress–deformation relationships for multistage versus conventional triaxial test can be compared in Figs. 3 and 4. From these figures, it is clear that during the first stage shearing, the stress–strain curve in the multistage test fairly matches the conventional test. But de-

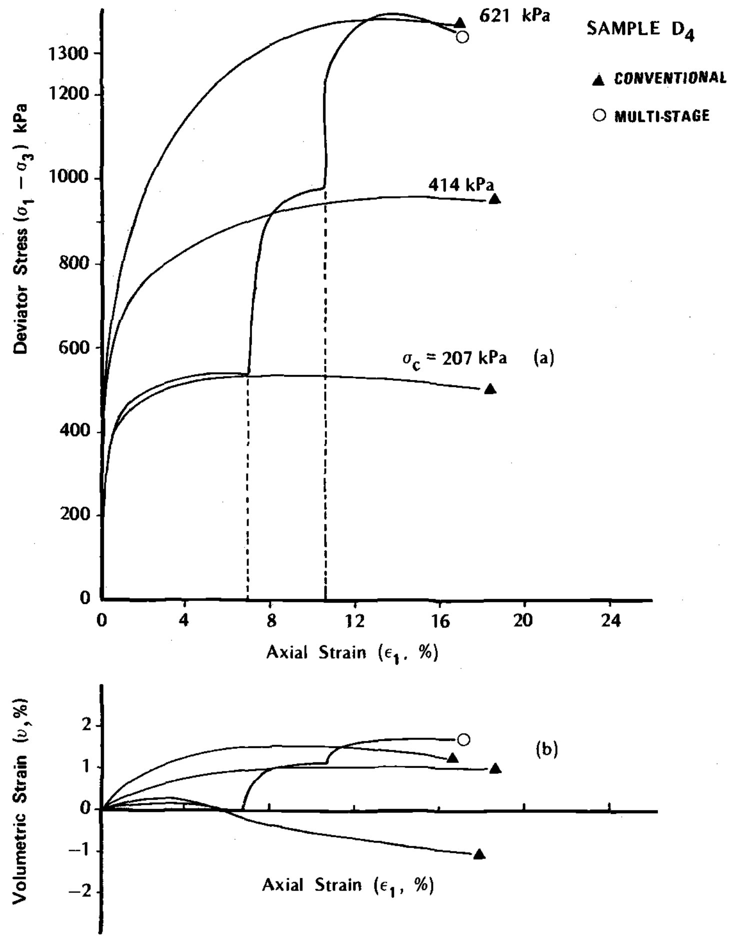

FIG. 3—*Typical stress–strain and volumetric strain relationship for drained test.*

viations are noticed between the two techniques at subsequent stages of shearing with regard to the values of axial strain and corresponding pore water pressure in undrained series and volumetric strain in drained test series. The lack of agreement in Stages 2 and 3 is possibly attributed to the difference in the physical state of specimens before shearing at the relevant stage. Generally, in stages other than Stage 1, the stiffening of soils as a result of further consolidation resulted in smaller failure strains. Figure 4 indicated that multistage tests have provided a much faster rate of excess pore pressure dissipation. This could be attributed to the formation of internal failure planes within the soil sample. These observations confirm the findings of Lumb [5] that true reproduction of stress–strain behavior is not possible in multistage tests.

To compare the shear strength for multistage versus conventional test, the values of deviator stress at failure condition $(\sigma_1 - \sigma_3)_f$ for both the drained and undrained series are plotted in Fig. 5*a* and *b*. In these figures $(\sigma_1 - \sigma_3)_f$ values refer to specimens tested at the same confining pressure. These figures are self explanatory because almost all data lie on the 45° line.

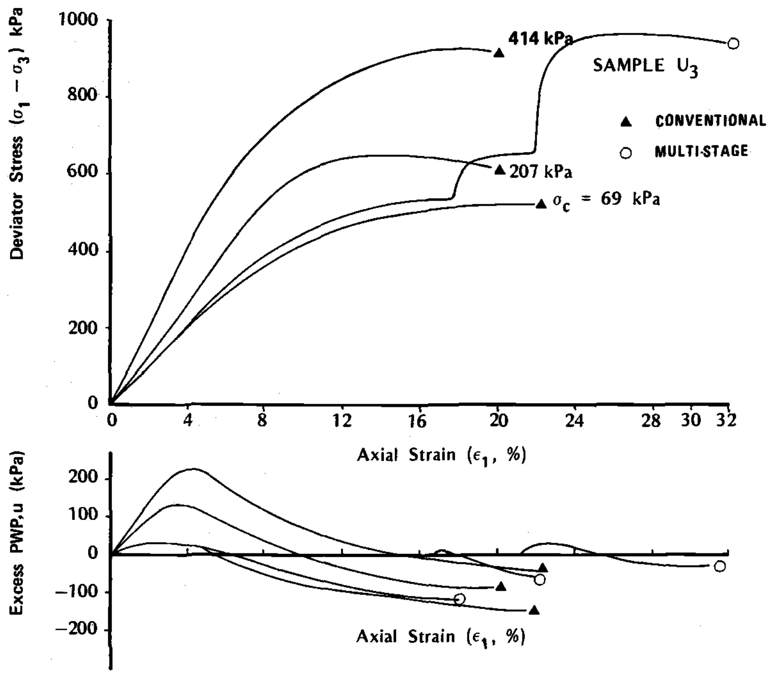

FIG. 4—*Typical stress–strain and excess pore water pressure relationship for undrained test.*

The strength parameters, c′ and ϕ', are given in Table 3. To obtain these parameters, the test results, in terms of effective stress, were plotted on (q', p') plots. The criterion for failure envelope was based on the peak values (q_f', p_f'). These have produced reasonably consistent test results which is often unusual with Kuwaiti soils. The reason of such consistency possibly may be explained by the fairly homogeneous samples selected for testing.

It was further observed in Table 3 that for both undrained and drained series there was a reasonable agreement between the multistage and conventional triaxial tests so far as the strength parameters were concerned. This observation was in agreement to those reported on other soils (decomposed granite and rhyolite [*3*] and glacial till and estuarine soils [*4*]). On the other hand, axial strain and volumetric strain/excess pore water pressure did not show a satisfactory agreement.

Conclusions

The subsoil of Kuwait is predominantly sandy but calcareous. The percentage passing through a No. 200 U.S. sieve (<75 μm) ranged between 12 and 40%. The subsoil is generally heterogeneous, often turning plastic because of calcareous or clay content. There is a general moisture deficiency in the soil which makes it vulnerable to saturation, causing swelling.

Undrained and drained tests conducted on various specimens indicated that the shear strength parameters determined from the multistage and conventional tests are in good agreement while other test parameters (such as axial and volumetric strain/PWP) varied widely because they are functions of the soil's physical conditions before shearing. Hence, as far as the strength parameters are concerned, the multistage technique can be applied. These remarks hold true irrespective of the test conditions such as applied pressure range, degree of saturation of soils, and the type of test (drained or undrained).

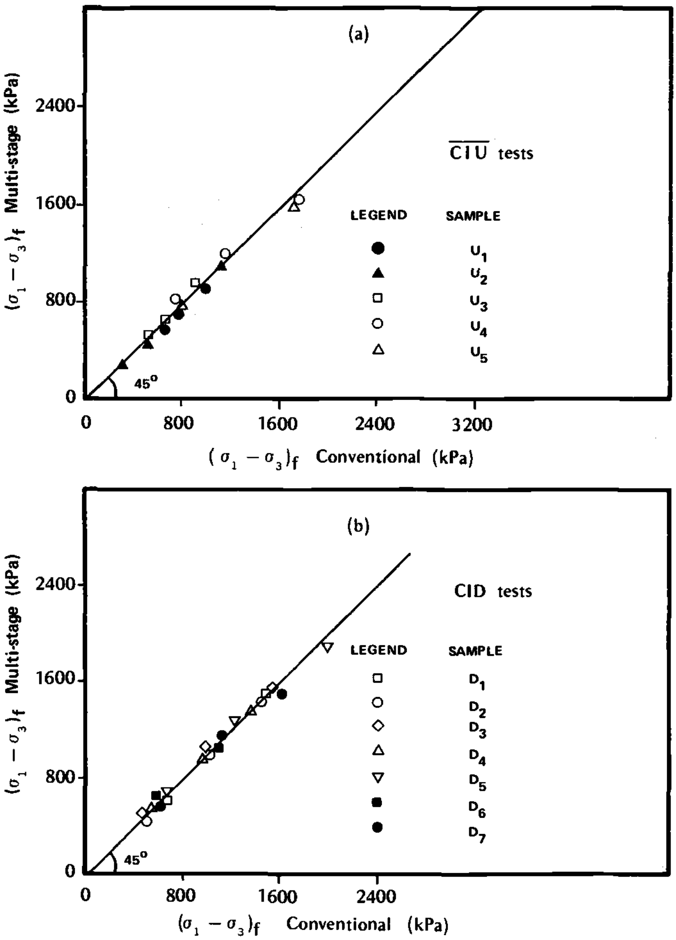

FIG. 5—*Comparison of deviator stress for multistage versus conventional test.*

However, multistage principle should be applied cautiously to strongly cemented (brittle) soil which was not dealt with in depth during this study. This was due to difficulty encountered in obtaining satisfactory recovery, as the soil formation was of a very hard type. These soils are occasionally encountered in Kuwait. Continuation of test beyond failure in either of the first two stages in these soils may induce severe distortion or total collapse of the soil structure. In such soils, it is recommended that the tests at the end of Stages 1 and 2 should be stopped just before the failure, and then proceed to the next stage of confining pressure. To spot failure manually is extremely difficult, but with the aid of computerized testing devices, such difficulty may be overcome. An alternative procedure may be to shear specimens during the first two stages, to a very small strain (say 0.2%). In the last stage, shearing may be continued beyond failure. An initial line connecting the (q', p') values corresponding to the selected small strains should be drawn. The final strength envelope shall be drawn parallel to this line but passing through (q_f', p_f').

Very loose samples usually have large axial failure strains, consequently attainment of failure in multistage tests using ordinary commercial cells may not be possible.

TABLE 3—*Comparison of strength parameters at failure condition.*

Test Set	Test Series	Sample Identification	Cohesion, kPa: Conventional Test	Cohesion, kPa: Multistage Test	Angle of Friction, deg: Conventional Test	Angle of Friction, deg: Multistage Test
1	CID-I[a]	D1	69	59	30.8	31.2
2		D2	12	0	31.6	32.2
3		D3	0	12	33.7	33.4
4		D4	35	23	30.6	30.0
5	CID-II	D5	13	13	36.9	36.0
6		D6	69	58	30.0	30.0
7		D7	36	47	32.7	32.2
8	CIU-I[b]	U1	23	35	31.5	31.2
9		U2	0	13	33.7	34.0
10		U3	34	57	28.6	28.3
11	CIU-II	U4	24	24	33.0	33.0
12		U5	24	24	32.9	32.9

[a] CID = isotropically consolidated drained.
[b] CIU = isotropically consolidated undrained.

Acknowledgments

The testing program was carried out at the soil laboratory of Government Laboratories and Testing Station, Ministry of Public Works, Kuwait. The authors express their deep gratitude to Dr. Abdulmajid Jeragh of the Ministry of Public Works and Ms. Sarah Al-Omar of the Ministry of Electricity and Water.

References

[1] Saeedy, H. S., Azzouz, A., and Mollah, M. A., "Sub-surface Water Rise in Kuwait and Suburbs," Vol. 4—Final Report, Kuwait Institute for Scientific Research, Kuwait, 1986.

[2] Saeedy, H. S. and Mollah, M. A., "Geotechnical Study of North and Northwest Coast of the Arabian Gulf," Paper submitted for publication to *Southeast Asian Geotechnical Society, Geotechnical Engineering Journal*, 1986.

[3] Terzaghi, K., *Erdbaumechanik*, Wien, Deuticke, 1925.

[4] Lambe, T. W. and Whitman, R. V., *Soil Mechanics*, Wiley Eastern Private Limited, New Delhi, 1973, p. 141.

[5] Lumb, P., "Multi-stage Triaxial Tests on Undisturbed Soils," *Civil Engineering and Public Works Review*, Vol. 59, 1964, pp. 591–595.

[6] Kenney, T. C. and Watson, G. H., "Multi-stage Triaxial Test for Determining c' and ϕ' of Saturated Soils," *Proceedings of the Fifth International Conference on Soil Mechanics and Foundation Engineering*, Vol. 1, Paris, International Society for Soil Mechanics and Foundation Engineering, 1961, pp. 191–195.

[7] Folque, J. and Pinto, F. J. C., "Influence of Mean Stress on the Strength Characteristics Evaluated by One Specimen Tests," *Proceedings of the Seventh International Conference on Soil Mechanics and Foundation Engineering*, Mexico, Vol. 1, 1969, pp. 127–130.

[8] Anderson, W. F., "The Use of Multi-Stage Triaxial Tests to Find the Undrained Strength Parameters of Stony Boulder Clay," Technical Note TN 89, *Journal of the Institution of Civil Engineers*, London, 1974, pp. 367–372.

[9] HO, D. Y. F. and Fredlund, D. G., "A Multi-Stage Triaxial Test for Unsaturated Soils," *Geotechnical Testing Journal,* Vol. 5, No. 1/2, 1982, pp. 18–25.

[10] Bishop A. W. and Henkel, D. J., *The Measurement of Soil Properties in the Triaxial Test,* 2nd ed., Edward Arnold Ltd., London, 1962.

[11] Fuch, F., Gattinger, T. E., and Holzer, H. F., "Explanatory Text to the Synoptic Geologic Map of Kuwait," in *Geological Survey of Austria,* Vienna, 1968, pp. 1–87.

[12] Fookes, P. G. and Higginbottom, I. E., "Some Problems of Construction Aggregates in Desert Area, with Particular Reference to the Arabian Penisula; 1. Occurrence and Special Characteristics, 2. Investigation, Production and Quality Control," *Proceedings of the Institution of Civil Engineers, London,* Part 1, Institution of Civil Engineers, 1980, pp. 39–67, 69–90.

Peter J. Millar[1] *and David R. Murray*[1]

Triaxial Testing of Weak Rocks Including the Use of Triaxial Extension Tests

REFERENCE: Millar, P. J. and Murray, D. R., "**Triaxial Testing of Weak Rocks Including the Use of Triaxial Extension Tests,**" *Advanced Triaxial Testing of Soil and Rock, ASTM STP 977,* Robert T. Donaghe, Ronald C. Chaney, and Marshall L. Silver, Eds., American Society for Testing and Materials, Philadelphia, 1988, pp. 376–386.

ABSTRACT: The strength parameters of New Zealand Tertiary weak rocks are found to be intermediate between soil and rock. The nonlinear strength envelopes of these materials for the range of stresses encountered in engineering structures mean that the strength parameters cannot be adequately defined using standard triaxial compression tests.

The strength properties can be established at low stress levels by the triaxial extension test which allows tensile stresses to be developed in the neck of truncated specimens. At high stress levels a high stress triaxial cell is used with confining pressures up to 15 MPa.

KEY WORDS: triaxial compression, triaxial extension, high stress, nonlinear envelopes, weak rock

Triaxial test methods have been developed to define the nonlinear strength characteristics of the Tertiary siltstones and sandstones found extensively in the central North Island of New Zealand. These include triaxial extension tests, which allow a tensile axial stress component in truncated specimens, and high stress triaxial compression tests with confining pressures of up to 15 MPa.

During formation the weak rocks have been subjected to overburden stresses of up to 10 MPa, but stress relief during erosion (unloading) has resulted in residual preconsolidation pressures, as a result of cementing and interparticle "locking," generally in the range of 3 to 5 MPa.

Within the low stress ranges, the material strength characteristics are typical of rocks, exhibiting curved failure envelopes with moderate tensile strength, while at higher stress levels they behave as highly overconsolidated soils. The transition of this rock–soil behavior occurs at stress levels close to the residual preconsolidation pressure of the material.

To determine the strength properties of these weak rocks at low stress levels, a triaxial extension test method was developed. Here an isotropically consolidated, truncated specimen is tested to failure at low values of mean principal stress. When the axial load on the top of the sample is reduced, the confining stress acting on the shoulders induces a tensile axial stress component in the neck.

The conventional triaxial compression test is limited in that no tensile stresses can be developed and failure of the weak rock specimens occurs at high normal stress levels. Also the failure envelope for these materials may exhibit significant curvature at low stress levels, and extrapolation to the shear stress axis is not possible using triaxial compression test results alone.

[1] Geomechanics engineer and senior technical officer, respectively, Ministry of Works and Development, P.O. Box 30-845, Wellington, New Zealand.

Further, at higher stress levels there is a transition in the failure envelope as the interparticle "locking" is broken down and the material fails in ultimate compression.

Test Methods

Triaxial Extension Test

As described by Bishop and Garga [1], the triaxial extension test method involves the unloading of the axial load applied to the top of an isotropically consolidated truncated specimen (see Fig. 1).

During axial unloading the cell pressure (σ_c') acting on the shoulders of the specimen

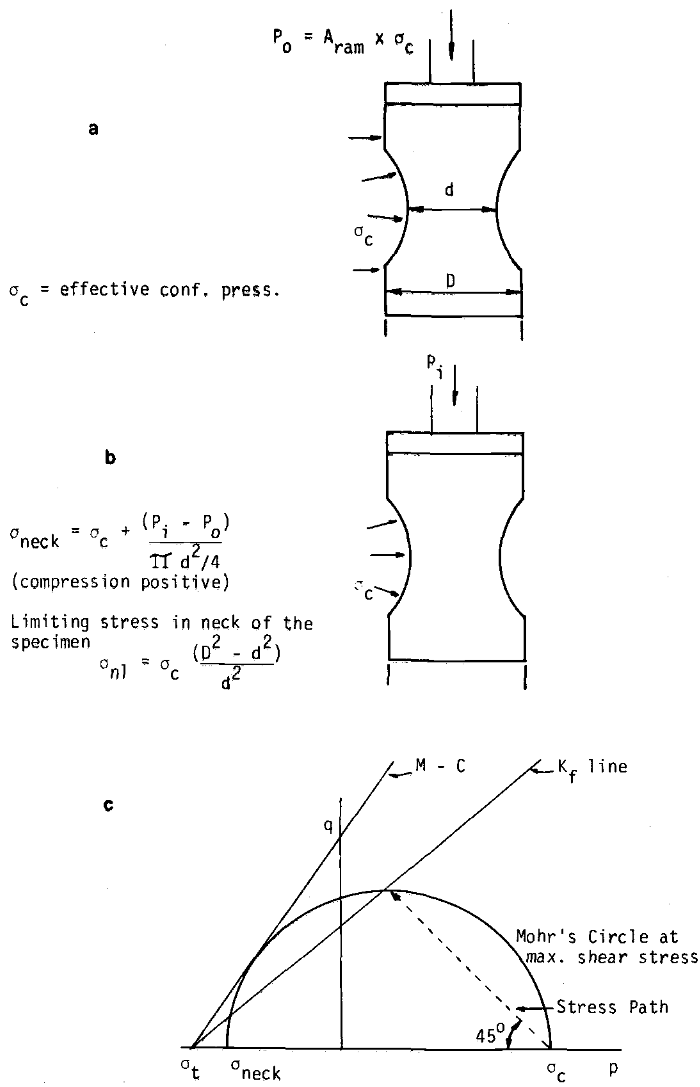

FIG. 1—*Triaxial extension test.* (a) *Consolidation stage, isotropic consolidation.* (b) *Extension test.* (c) *Stress path during drained triaxial extension test.*

initially reduces the compressive stresses and then induces a tensile stress in the neck. The axial stress (σ_{ni}) in the neck at any stage of the test is given by the equation

$$\sigma_{(\text{neck } i)} = \sigma_c' + \frac{4(Pi - Po)}{\pi d^2}$$

where

Po = initial ram load,
Pi = ram load at any stage (i) of the test, and
d = diameter of the reduced section (neck).

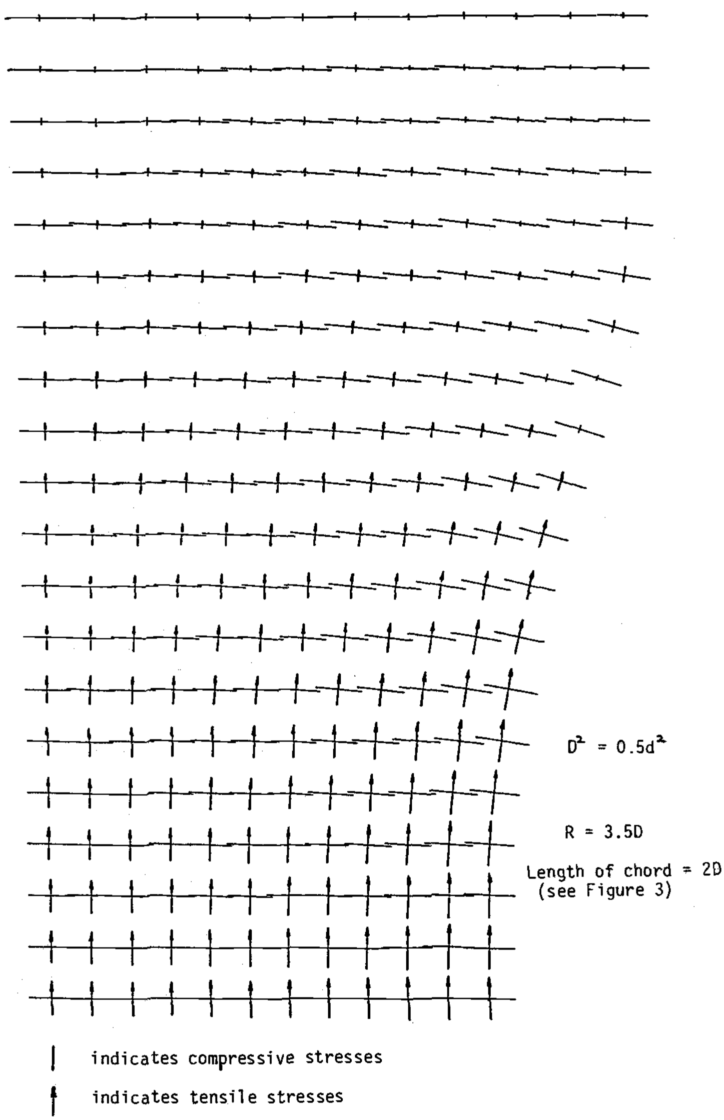

FIG. 2—*Schematic diagram of stress distribution in truncated specimen at the limiting stress point during an extension test.*

The limiting tensile stress that can be applied is the stress at which the top platen separates from the specimen

$$\sigma_{(\text{neck limit})} = \sigma_c' \times \frac{(D^2 - d^2)}{d^2}$$

where D = major diameter of specimen.

In a drained extension test the stress path is a negative 45° line (see Fig. 1C). If a specimen does not fail before achieving the limiting stress, the confining pressure may be increased with a stress path gradient given by

$$\text{stress path gradient} = +\frac{D^2}{(2d^2 - D^2)}$$

(If $d^2 = 0.5D^2$, that is, the area of neck = area of shoulder, then gradient is vertical; and if $d^2 < 0.5D^2$ then gradient is negative.)

A combination of unloading and variation in the cell pressure on a truncated specimen provides the conditions in which any required stress path testing may be modeled.

Specimen Models—A finite element model analysis by the authors determined that a spiral transition over a length greater than twice the difference in the diameter, $2(D - d)$, is the optimum shape for the shoulders of the specimen to minimize stress concentrations and provide the most uniform tensile stress distribution through the neck.

However, for practical purposes an arc with a chord length of $2D$ is a close approximation and simplifies preparation of the specimen (see Figs. 2 and 3).

Preparation of Extension Specimens—For weak rocks, specimens are prepared by axial mounting in a jig and trimming with a motorized wire wheel (Fig. 3).

It has been found that the preparation of the truncated specimens using a motorized wire

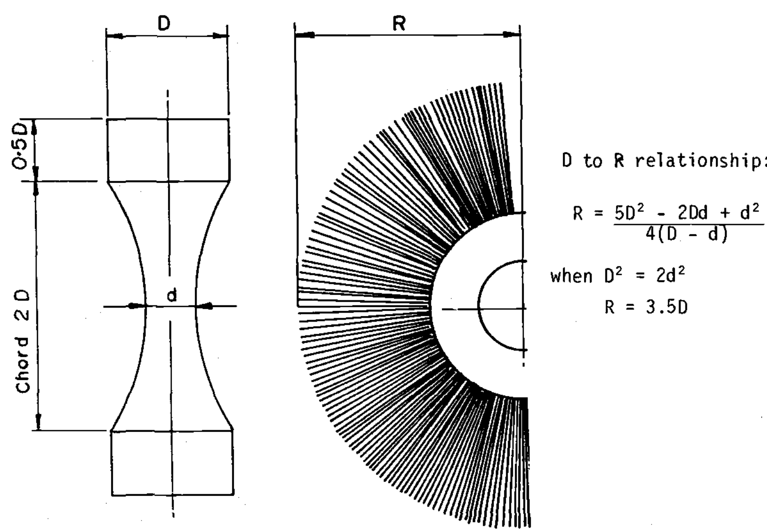

FIG. 3—*Schematic diagram showing specimen preparation with wire wheel.*

wheel facilitates rapid preparation and avoids the problems of heating and drying of the specimen that occur when using a soil lathe.

The squaring and trimming of the ends are usually carried out before the wasting of the center section.

Test Equipment—The specimen is set up in a standard triaxial cell that has the following modifications:

1. The top platen is fixed to the loading ram with a spherical joint within the cell to allow for any misalignment of the ends which may induce premature failure as a result of eccentric loading on the shoulder of the specimen.
2. The loading equipment used to date has been primarily a stress controlled system with a ramp function load generator, but other options including strain control are available. The former allows for a clear definition of the failure point which is accompanied by a rapid increase in the axial displacement. In a strain controlled system, failure should be defined by a rapid unloading, but this has not been as clearly defined in tests carried out to date.

Usually the test is carried out under drained conditions to avoid problems of nonuniform pore pressure distribution. Because tensile failure in weak rocks occurs at low values of strain, volume changes within the system are small, and volume change corrections to the strength parameter calculations are generally insignificant. Also the stress path is subnormal to the failure envelope, minimizing creep.

High Stress Triaxial Compression Test

The requirement to investigate the strength parameters of weak rocks at higher confining pressure necessitates the use of a high stress triaxial cell. A diagram of the equipment developed for this purpose is shown in Fig. 4. This system can develop confining pressures up to 15 MPa.

The high pressure system is operated using a dry nitrogen gas bottle and an accumulator adapted to provide an air–water interface. The accumulator includes a self-closing valve, which, in the event of leakage in the high pressure system, limits the volume change to the quantity of water in the accumulator. The back pressure system is standard but includes a preset pressure relief valve in case of leakage from the high pressure system past the membrane.

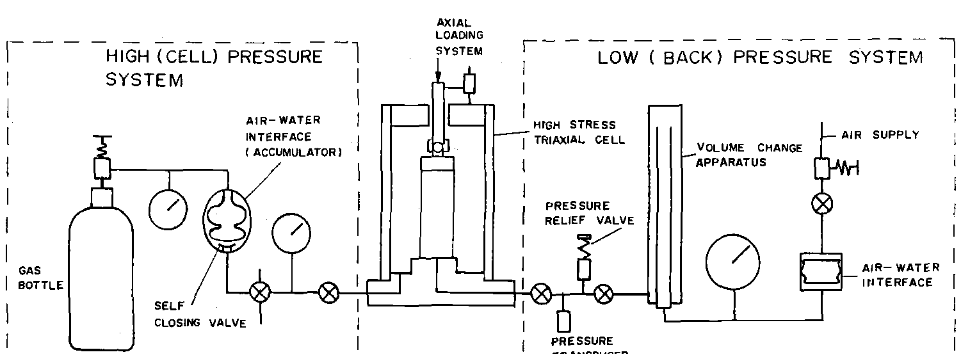

FIG. 4—*Layout of the high stress triaxial test system.*

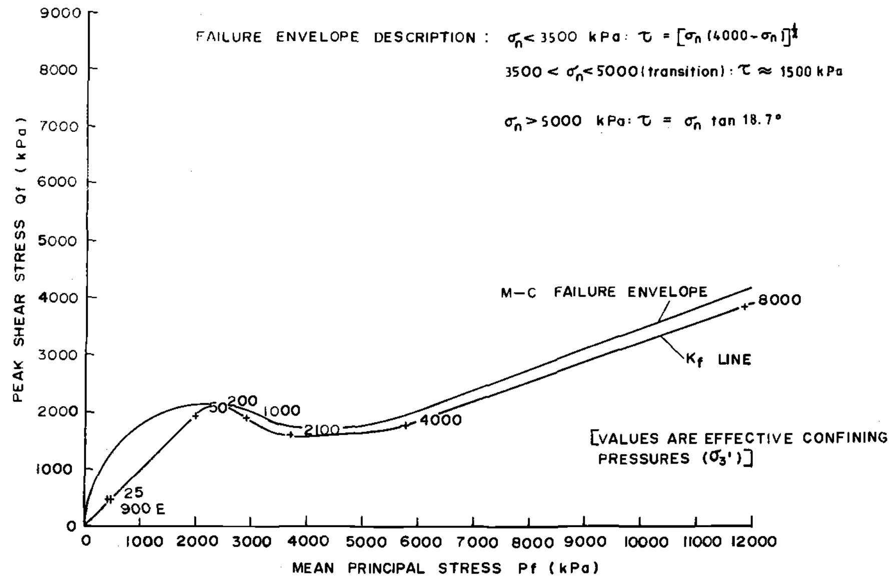

FIG. 5—*Strength parameters and failure envelope Sample 2850.*

Strength Properties of Weak Rocks

The strength properties of a range of typical central North Island weak rocks are shown in Figs. 5, 6, and 7. A summary of these test results and the physical properties and measured residual preconsolidation pressures are given in Tables 1 and 2.

The nonlinear failure envelopes suggest that the strength characteristics are complex and not well defined by standard triaxial compression testing over the usual range of confining pressures 20 to 1000 kPa.

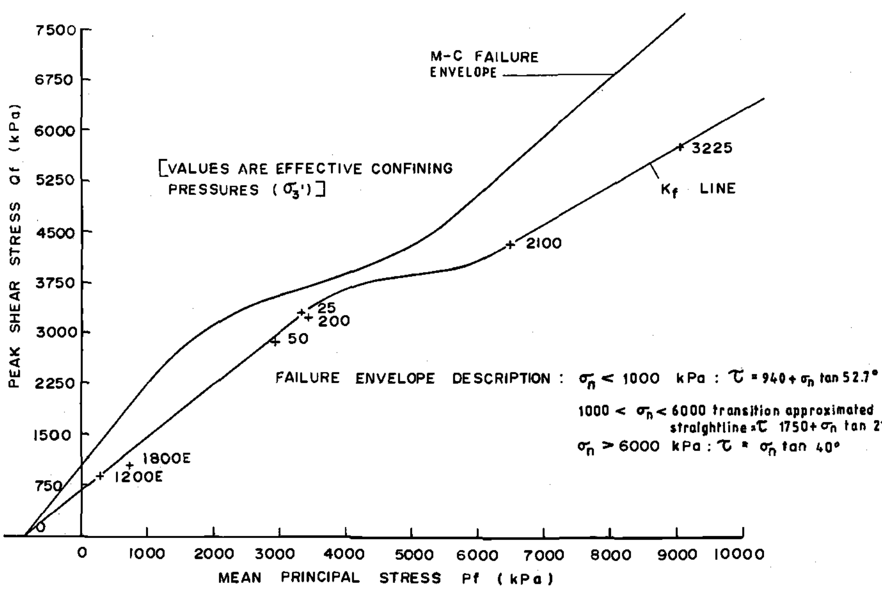

FIG. 6—*Strength parameters and failure envelope Sample 2884.*

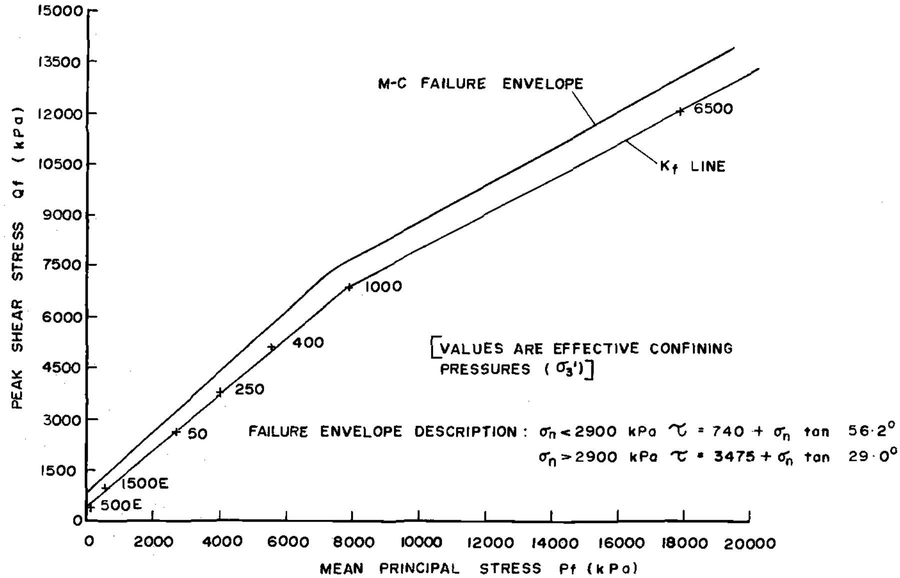

FIG. 7—*Strength parameters and failure envelope Sample 85-220-221.*

In drained triaxial compression tests, the stress path has a positive 45° gradient and intercepts the K_f line at high stress levels. A large extrapolation of the results is required to define the cohesive strength such that the confidence limits are poor.

The volumetric strain in drained tests (Fig. 8*b*) and the pore pressure response in undrained tests are greatly affected by the historic stress relief (effects of unloading as a result of erosion, wetting and drying, swelling and shrinkage, and sampling). Although the materials are dilatant at higher shear strains, there is typically an initial compressive response as the materials reconsolidate and microfractures close at low strains. In an undrained test the positive pore pressure developed at low strain reduces the mean principal stress such that the material, which has low tensile strengths, may effectively fail in uniaxial compression before the development of any significant dilatant response. Hence a series of undrained triaxial compression tests at low confining pressures may produce results giving a K_f line close to 45° ($\phi \cong 90°$). This reflects the influence of the initial reconsolidation of the specimens at increasing confining pressures, that is, a series of effective uniaxial compression tests with Mohr's circles coincident at the origin.

At high confining pressures where the mean principal stress levels developed during tests greatly exceed the preconsolidation pressure of the materials, the strength is purely frictional and specimens fail in ultimate compression (independent of stress history).

The transition between the strength characteristics at stress levels below the residual preconsolidation pressure and failure in ultimate compression is particularly marked in the siltstones, where ultimate friction angles of less than 30° mean that a reduction in strength may be recorded as the influence of interparticle "locking" is lost and crushing occurs (see Fig. 5). Similar behavior has been observed in other triaxial series on siltstones [*2,3*]. These results are also consistent with many other triaxial test results on weak rocks where results of specimens tested at confining pressures of 1000 to 2000 kPa have given low shear strengths relative to the extrapolated failure envelopes of tests at lower confining pressures [*4,5*].

Lee and Seed [*6*] report transitions in the shear strength of highly overconsolidated soils as a result of the changing influence of dilation, crushing, and rearrangement of grains. The

TABLE 1—*Physical properties of central North Island weak rocks.*

Sample	Material Description	Dry Density, $\rho_d(t/m^3)$	Natural, $w\%$	e	Particle Size Distribution			Atterberg Limits		Residual Preconsolidation Pressure, MPa
					Clay, %	Silt, %	Sand, %	L.L.	P.L.	
2850	sandy siltstone	1.68	22.0	0.63	8	59	33	57	25	3–5
2884	silt-claystone	1.98	14.0	0.38	47	43	10	51	24	3–5
85-220	sandstone	2.15	8.8	0.26	1	21	78	nonplastic		8

TABLE 2—*Triaxial test results of central North Island weak rocks.*

		Values at Peak Shear Stress			
Sample	Effective Cell Pressure, kPa	$\frac{1}{2}(\sigma_1' - \sigma_3')$, kPa	$\frac{1}{2}(\sigma_1' + \sigma_3')$, kPa	Strain, %	Vol. Strain, %
CL2884	25	3 320	3 345	1.9	1.0
Silt-	50	2 890	2 940	2.0	0.93
claystone	200	3 250	3 450	2.3	1.13
	2100	4 370	6 470	2.6	0.19
	3225	5 810	9 035	3.0	1.07
	1200 Ext	900	300	−0.52	...
	1800 Ext	1 050	750	−0.72	...
CL2850	25	470	495	1.9	0.96
Sandy	50	1 940	1 990	1.3	0.66
siltstone	200	2 095	2 295	1.9	1.09
	1000	1 895	2 895	2.7	1.80
	2100	1 590	3 690	2.6	0.64
	4000	1 770	4 770	3.4	...
	8000	3 840	11 840	8.1	...
	900 Ext	475	425	...	...
CL85-220	50	2 625	2 675	0.7	−0.49
Sandstone	250	3 760	4 010	0.8	−0- −.88
	400	5 100	5 500	0.7	−0.25
	1000	6 840	7 840	1.1	−0.59
	6500	12 015	18 515	2.4	...
	500 Ext	395	105	...	...
	1500 Ext	950	550	...	...

authors are not aware of other published triaxial compression test results showing a reduction in shear strength with increasing mean principal stress, but Latjai [7] reports shear box tests on cast plaster specimens having irregular planes of weakness where similar mechanisms of failure and reductions in strength are shown.

The triaxial test results shown in Figs. 5 and 6 also indicate that the failure envelope of weak rocks at low stress levels cannot be defined with adequate confidence using extrapolation of standard triaxial compression tests. The triaxial extension test on truncated specimens provides a means of more accurately defining the cohesive strength intercept. In Fig. 6, extrapolation of the standard triaxial compression test results on the clay-siltstone would indicate a straight line best-fit envelope with a cohesive strength of 1.9 MPa and angle of frictional resistance of 27°. The extension test results, however, show this to be a significant overestimate with the cohesive strength being defined as 1.0 MPa.

Conclusion

The Tertiary weak rocks in New Zealand exhibit strength properties that are intermediate between soils and rocks. The strength properties at low stress levels are typical of rocks with a significant tensile strength component and curved failure envelope. At stresses approaching the "residual" preconsolidation pressure, the influence of interparticle locking and cementing is reduced and the strength envelope undergoes a transition before failure occurs in ultimate compression.

The nonlinear strength envelopes obtained over the range of stresses encountered in

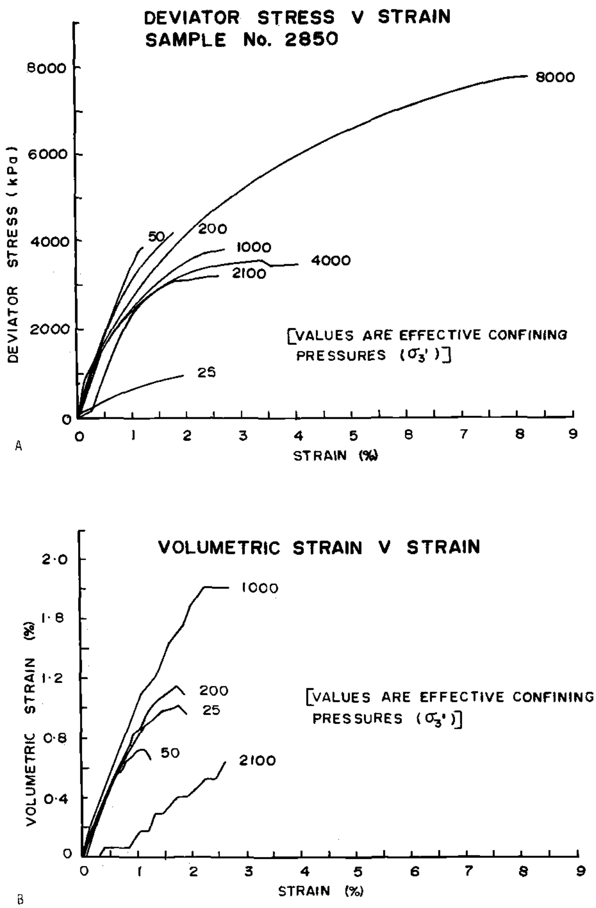

FIG. 8—*Specimen behavior during triaxial loading.*

engineering structures mean that the strength characteristics cannot be adequately defined using standard triaxial compression tests alone. The triaxial extension test on truncated specimens provides good definition of the tensile properties and cohesive strength, while the high stress triaxial test gives additional information on the performance of materials over their transition in strength characteristics from soil to rocklike properties.

References

[1] Bishop A. W. and Garga, V. K., "Drained Tension Tests on London Clay," *Geotechnique*, Vol. 19, No. 2, 1969, pp. 309–313.

[2] Murray, D. R., "Rotowaro Opencast Prospect—Part 3," Report 2-87/4, Central Laboratories, MWD, Lower Hutt, NZ, 1987.

[3] Millar, P. J., "Waikato Coal Fired Power Station Laboratory Testing," Report 2-85/8, Central Laboratories, MWD, Lower Hutt, NZ, 1985.

[4] Murray, D. R. and Millar, P. J., "Mohaka River Power Investigations: Testing of Core and Block Samples from the Raupunga Site," Report 2-83/4, Central Laboratories, MWD, Lower Hutt, NZ, 1983.

[5] Murray, D. R., "Mohaka River Investigations—Classification and Strength Testing of Core Material from M42 and M55," Report 2-86/7, Central Laboratories, MWD, Lower Hutt, NZ, 1986.
[6] Lee, K. L. and Seed, H. B., "Drained Strength Characteristics of Sands," *Journal of Soil Mechanics and Foundations Division*, Vol. 93, No. SM5, Nov. 1967, pp. 117–142.
[7] Latjai, E. Z., "Strengths of Discontinuous Rocks in Direct Shear," *Geotechnique*, Vol. 19, No. 2, 1969, pp. 218–233.

Jeffrey C. Evans[1] and Hsai-Yang Fang[2]

Triaxial Permeability and Strength Testing of Contaminated Soils

REFERENCE: Evans, J. C., and Fang, H.-Y., "**Triaxial Permeability and Strength Testing of Contaminated Soils,**" *Advanced Triaxial Testing of Soil and Roçk, ASTM STP 977,* Robert T. Donaghe, Ronald C. Chaney, and Marshall L. Silver, Eds., American Society for Testing and Materials, Philadelphia, 1988, pp. 387–404.

ABSTRACT: As a consequence of hazardous and toxic waste disposal in the subsurface environment, triaxial permeability and strength tests on contaminated soils or with hazardous pore fluids must be conducted for extended time periods. The determination of hydraulic conductivity and shear strength of contaminated soils (or of uncontaminated soils using contaminated permeants) requires equipment and procedures different from those required for conventional triaxial permeability and strength testing.

The application of a back pressure works well to maintain saturation for short-term testing but may be insufficient for long-term testing. Procedure and equipment modifications are required to maintain saturation. Reservoir modifications may be made to dissolve contaminants at the solubility limit. Frequent replacement of influent permeant may maintain saturation and influent equilibrium. Equipment modifications may be required due to the chemical nature of the permeant and its incompatibility with the equipment. Long-term testing variables also include gradient, effective stress, particle migration, differential consolidation, diffusion through the membrane, and changes in water chemistry. Due to the need to permeate the specimen with at least one pore volume of permeant, gradients higher than those typically encountered in the field are used. This results in high effective stresses and differential consolidation. The volatile nature of certain permeants may cause diffusion through the membrane and changes in influent chemistry throughout the test.

KEY WORDS: laboratory testing, hydraulic conductivity, hazardous waste, soil mechanics, geotechnology, clays, triaxial, permeameters, compatibility

Disposal of hazardous wastes in the subsurface environment has led to the widespread application of geotechnology to control contaminant migration. This in turn has resulted in the need to conduct triaxial permeability and strength tests on contaminated soils. The effect of contaminants in the subsurface on the long-term permeability and strength characteristics of soils often needs evaluation. Studies of soil behavior in an adverse environment frequently require tests to be conducted for time periods as long as several months. The determination of hydraulic conductivity and shear strength of contaminated soils (or of uncontaminated soils using hazardous permeants) requires equipment and procedures different from those required for conventional triaxial permeability and strength testing.

A multi-year study has investigated the fundamental soil behavior in response to permeation with hazardous fluids. Triaxial testing for soil strength and hydraulic conductivity was an integral part of this research program. This paper describes the findings of this study

[1] Associate professor, Department of Civil Engineering, Bucknell University, Lewisburg, PA 17837.
[2] Professor and director, Geotechnical Engineering Division, Department of Civil Engineering, Lehigh University, Bethlehem, PA 18015.

with regard to triaxial test procedures and their influence on triaxial test results. The emphasis of this paper is to present differences in both procedure and equipment required to effectively conduct long-term triaxial permeability and strength tests.

Several recent papers have described methods of laboratory testing of the permeability of soils [*1–8*]. Several researchers describe the use of the procedures and equipment for both short-term and long-term permeability testing [*1,5,7,8*]. Because there are many aspects of the equipment and procedures that affect the measurement of hydraulic conductivity in a triaxial test, the discussion here focuses on those aspects relating to long-term permeability and strength testing conducted to investigate changes in hydraulic conductivity and strength in response to changes in pore fluid chemistry. For short-term triaxial permeability testing, the above citations (Refs *1–8*) may be referenced.

The studies described in this paper used a soil–bentonite material typical of the backfill used in slurry trench cutoff walls. Detailed analyses of the test results and the interpretation of those results with respect to pore fluid–clay interactions are presented elsewhere [*9–12*]. Aspects of long-term testing influenced by the soil–bentonite materials being tested will, however, be discussed. In addition, the equipment and procedures described here have also been used for long-term permeability testing of conventional clay liner materials [*13*].

The constant of proportionality between velocity and hydraulic gradient is termed the hydraulic conductivity. The hydraulic conductivity is a property of both the material and the fluid and has units of velocity. Hydraulic conductivity may be converted to the intrinsic permeability by incorporating the viscosity and unit weight of the permeant into the calculations. Because the exchange of the "natural" pore fluid with a contaminated pore fluid results in a gradual change in permeant properties, this study will focus on the measurement of hydraulic conductivity in a triaxial permeability test. The term flexible wall permeability test has recently been used to describe triaxial permeability tests [*5,8*].

This paper examines the equipment and procedures necessary to determine changes in the hydraulic conductivity and strength of low-permeability soils in response to permeation with hazardous liquids. The testing is long-term in nature and may require many months to complete a single test. Although the shearing of the specimen may be completed relatively quickly, the length of time required to permeate the specimen prior to shear makes the strength testing a long-term test as well.

Experimental Program

Materials

The specimens for these studies were prepared in the laboratory. Procedures were developed to prepare laboratory specimens representative of backfill in soil–bentonite slurry trench cutoff walls. The "base" soil was a New Jersey bar sand described as a clean, medium to fine sand. Grain size distribution analyses were conducted, and the materials were found be be about 5% medium sand, about 93% fine sand, and generally less than 2% silt. The New Jersey bar sand represents a naturally occurring deposit frequently encountered along the eastern United States coastal plain. To simulate the use of these clean sands as soil-bentonite backfill, specimens were prepared using 7% bentonite by dry weight. The air-dried, powdered bentonite was added to sand at its natural moisture content. The final specimen moisture content was achieved through the mixing of stabilized bentonite–water slurry to the mixture of dry bentonite powder and sand. The bentonite–water slurry consisted of 95% water and 5% bentonite by weight and had a stabilized Marsh viscosity of 35 Marsh seconds. The slurry was mixed and fully hydrated prior to use in specimen preparation. The resulting moisture content of the mix was typically 50 to 55% at slump of 4 to 6 in. (101.6

to 152.4 mm) (typical of field-mixed samples of soil–bentonite backfill). The bentonite was an untreated sodium bentonite provided by IMC Corporation.

Permeant

The natural pore water was used as the initial permeant to establish steady state equilibrium. Potable water was used for both mixing and initial permeation. It is believed that variations in the potable water chemistry are inconsequential. After the establishment of equilibrium flow conditions, alternate pore fluids were used to investigate long-term hydraulic conductivity changes. These fluids included concentrated and dilute solutions of both organics and inorganics including sodium hydroxide, hydrochloric acid, acetic acid, aniline, acetone, carbon tetrachloride, and leachate obtained from a municipal solid waste landfill.

Equipment

The measurement of hydraulic conductivity using hazardous permeants was done with triaxial equipment specifically designed and constructed for that purpose [*14*]. Details of the equipment are shown in Figs. 1 and 2.

The permeability testing system included a triaxial cell developed to be compatible with a wide range of liquids. Where structural rigidity was required, the cell was constructed of stainless steel and aluminum. Contamination resistance for long-term testing was obtained through the use of Teflon for all parts in the system where the equipment came in contact with the permeant. The structural rigidity of steel and aluminum was combined with the contamination resistance of Teflon. The triaxial cells included two drainage lines to each of the two platens (top cap and bottom pedestal) to permit sampling of influent and effluent. Friction is minimized during the loading of the samples by Thompson bearings placed in the aluminum caps of the triaxial cell.

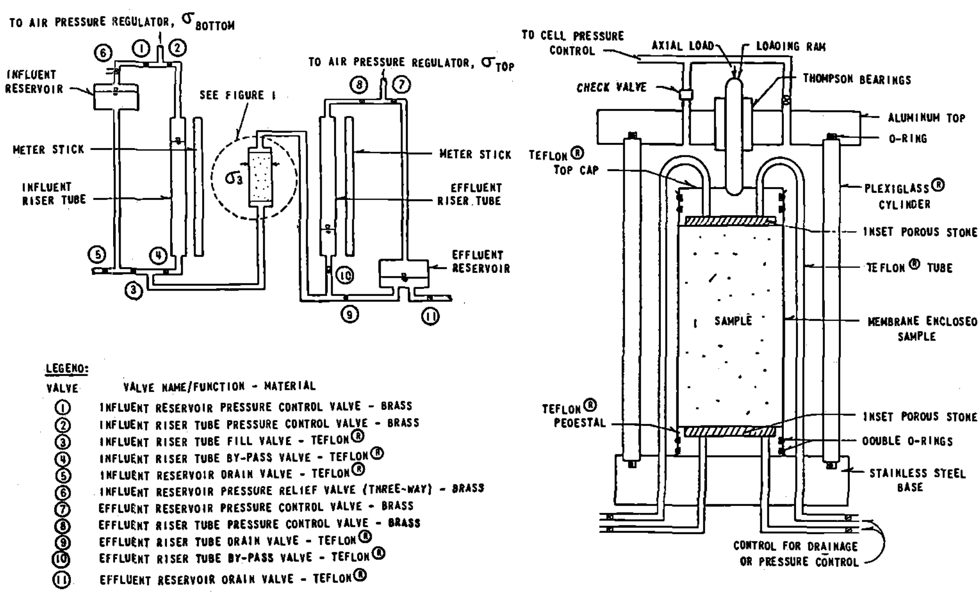

FIG. 1—*Schematic of the triaxial permeameter system:* (left) *permeameter board and* (bottom) *triaxial cell schematic.*

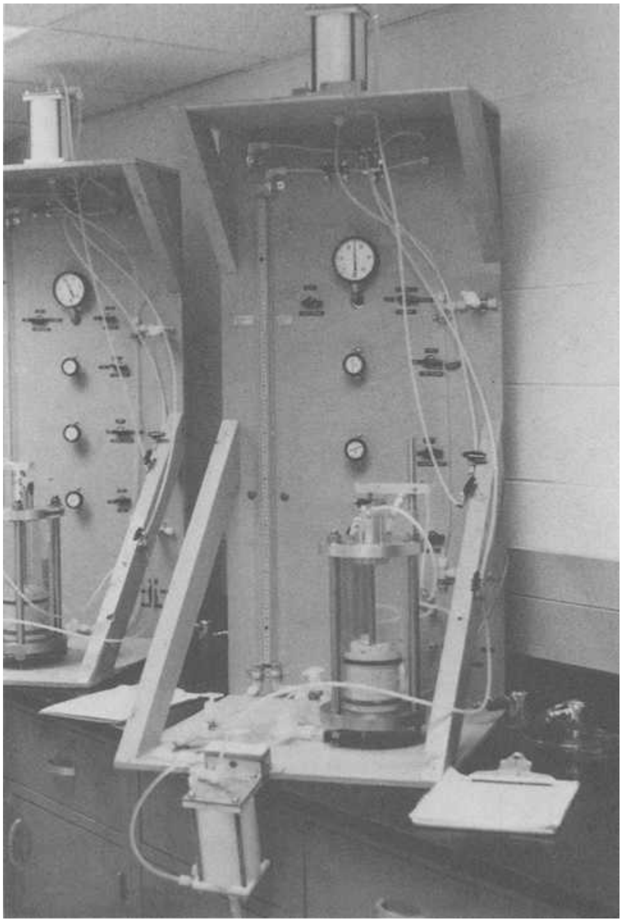

FIG. 2—*Triaxial permeameter system.*

The permeability board and control panel permit readings to be taken on both the inflow riser pipe and the outflow riser pipe (see Fig. 1 left). The permeability board is designed to allow permeants to be changed and inflow-outflow riser pipes either to be filled or emptied without changing the state of stress on the specimen. To maintain sufficient experimental accuracy, small changes in volume of fluid that permeates the sample must be read. As a result, the inflow and outflow riser pipes are quickly emptied and filled, respectively. Because it is necessary to refill the inflow riser pipe (and empty the outflow riser pipe) frequently throughout the testing period, influent and effluent reservoirs were incorporated into the pressure system.

Procedure

The numerous procedures for the determination of hydraulic conductivity in a triaxial cell permeameter [*1–8*] have much in common including specimen setup, consolidation, and permeation. Discussed in the following paragraphs are procedural details specifically related to long-term permeation; when methods are considered "standard practice," other references are cited.

The first step in triaxial testing of soils is the specimen setup. For the studies described here the soil–bentonite backfill material was prepared at the consistency of high slump concrete. It was therefore necessary to "mold" the soil into a 7-cm (2.8-in.) diameter by 14-cm (5.6-in.) long specimen. Alternately, when tests were conducted on compacted clay, specimen preparation included determination of compaction method, moisture content, and density. Conventional triaxial compaction molds form the specimen within the membrane enclosure. The materials were added to the mold in three lifts and rodded in place to reduce the potential for entrapped air. The specimens were vacuum consolidated until they gained adequate strength to be self-supporting. At this point, the triaxial cell assembly was completed and an isotropic state of stress was applied through the cell fluid to consolidate the specimens. Anisotropic consolidation stresses can be applied by supplying additional axial stress through the loading piston.

Back pressure consolidation of the specimen is accomplished by one of two different methods. First, the back pressure applied through the top and bottom platens is applied equally throughout the consolidation and back pressure phase of the test. Alternately, a slight gradient is applied during the consolidation and back pressure phase by employing a lower pressure at the top platen than at the bottom platen. For the tests described here, both methods of back pressure and consolidation were used. The difference in results will be subsequently discussed. A 345-kPa (50-psi) back pressure was used for these studies, and an average effective stress of 207 kPa (30 psi) was used for each of the specimens.

Seepage is induced by elevating the bottom platen pressure with respect to the top platen. Typically, a gradient of 100 was used for long-term permeability testing. Based on typical specimen length of 14 cm, a gradient of approximately 100 is achieved when the differential pressure between the top and bottom platen is approximately 138 kPa (20 psi). Acquisition of flow data is begun immediately on application of the seepage gradient. This flow is unsteady, and the calculation of hydraulic conductivity is technically "incorrect." But, the results of the calculation may be used for initial performance monitoring. Once an equilibrium hydraulic conductivity is reached with the natural pore water, this fluid is removed from the influent reservoir and replaced with the fluid under study. Through the use of the supplemental drainage lines, the remaining permeant in the system can be replaced, and permeation begins with the fluid under study. The tests are typically continued until a minimum of one pore volume of fluid is displaced.

When permeation is complete, the shear strength is determined. The specimen is fully consolidated after permeation. Shearing can be conducted using either drained or undrained loading conditions. The undrained test may be with or without pore pressure measurements. For this study shear strength testing was conducted with drainage lines closed, yielding consolidated undrained total stress strength parameters.

Variables associated with the procedures summarized above and their impact on long-term permeability test results are discussed below. The variables affecting short-term triaxial permeability tests are summarized in Ref *6*.

Long-Term Triaxial Permeability Testing Variables

Gradient

To conduct long-term pore fluid permeability tests a minimum of one pore volume of fluid must pass through the specimen [7]. Further, to determine the shear strength of the specimen, the minimum length-to-diameter ratio required is two. With a specimen diameter of 7 cm the minimum length is 14 cm. For the given specimen size (at a void ratio of 0.50), the relationship between the testing time required for a pore volume displacement of one and gradient as a function of hydraulic conductivity is shown in Fig. 3. For example, to test a specimen having a hydraulic conductivity of 1 × 10^{-8} cm/s in one month, a gradient of about 200 is required. The gradient is not representative of those encountered in the field. For a typical 1-m-thick slurry trench cutoff wall of soil–bentonite, a gradient of 200 is only achieved if there is a differential head across the cutoff wall of 200 m. This is very unlikely.

What is the effect of gradient on the measured value of permeability? For Darcy's law to be considered valid, the coefficient of hydraulic conductivity does not change with gradient. Some studies have shown this to be the case [*15*], whereas others have shown decreases in hydraulic conductivity with increasing gradient [*1,6*]. This observed decrease has generally been attributed to a corresponding increase in effective stress and the resulting specimen consolidation. The primary purpose of long-term permeability testing is, however, to evaluate the effect of *changes* in the hydraulic conductivity due to pore fluid changes. To determine more reliably the hydraulic conductivity with a natural pore water permeant for

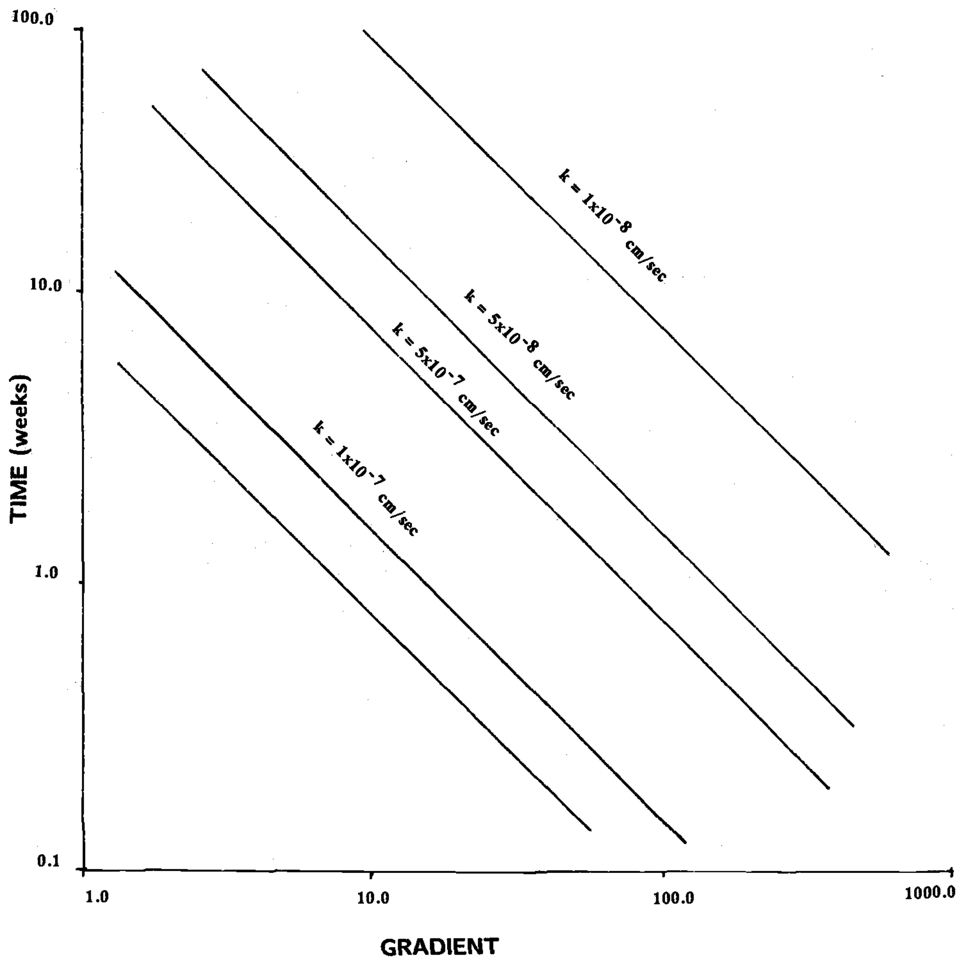

FIG. 3—*Test duration.*

design, field scale tests or triaxial tests at stress levels more representative of those encountered in the field should be used. The use of a high gradient to minimize test duration should not affect *significantly* the results of a study to determine pore fluid–soil interactions.

Effective Stress

An increase in effective stress will result in a decrease in the coefficient of hydraulic conductivity [*1,6*]. It has also been demonstrated that increasing the effective stress reduces the change in the hydraulic conductivity of soils induced by changes in the chemistry of the permeant [*7*]. Thus, at relatively high confining stresses, the soil response is subdued compared to the response observed at low confining stresses.

It has already been demonstrated that it is necessary to use high gradients to conduct the test in a reasonable length of time. For a gradient of about 100, the differential pressure across a 14-cm-long specimen is 138 kPa. For a back pressure of 345 kPa, the influent platen pressure must be 483 kPa (the outflow platen pressure would be 345 kPa). Hence, a cell pressure of greater than 483 kPa is required to maintain a positive effective stress at the influent end of the specimen. The minimum effective stress would be 138 kPa on the effluent end of the specimen, and the average specimen effective stress for the specimen would be 69 kPa. Thus, the use of a triaxial cell for permeability testing results in the need to apply high effective stresses as compared to those one would encounter in the field. Further, there is an effective stress distribution, and, for very soft samples such as those tested for this study, differential consolidation occurs along the sample length.

Particle Migration

Migration of fines can lead to a decrease in hydraulic conductivity during a long-term permeability test. As noted, the materials under study were a mixture of medium to fine sand and bentonite. The mixture was homogeneous and isotropic at the start of testing. During permeation it is postulated that (1) additional consolidation at the top of the specimen occurs and (2) particles migrate downgradient until they get "stuck" and can migrate no further. To investigate this phenomenon, grain size distribution analyses were conducted on portions of the specimen after the completion of permeability tests. Each specimen was split into thirds, and grain size distribution analyses were conducted. Although the initial grain size distributions were uniform, fines migrated from the lower third of the specimen toward the middle third. The upper third of the specimens also had a higher fines content than the lower portion (but lower than the middle of the specimen). It is clear that fines are migrating upward through the specimen (in the direction of flow).

To further investigate this phenomenon, tests were conducted using a gradient during the back pressure and consolidation phase. Some particle reorientation occurs during the consolidation and back pressure phase (prior to the acquisition of hydraulic conductivity data). Figure 4 shows the relationship between hydraulic conductivity and pore volume displacement for a specimen initially permeated with natural pore fluid (later concentrated aniline is added). This specimen was consolidated and back pressured without a gradient. The calculated hydraulic conductivity of the specimen shown in Fig. 4 reduced from 9.0 to 3.7×10^{-8} cm/s before stabilizing. A similar specimen was tested using a gradient of 10 during consolidation and back pressure, and the results are shown in Fig. 5. The hydraulic conductivity changes from about 3.2 to 2.5×10^{-8} cm/s before stabilizing. Although the equilibrium coefficient of hydraulic conductivity for both samples was essentially the same, particle migration appears to cause a considerable decline in the initial hydraulic conductivity.

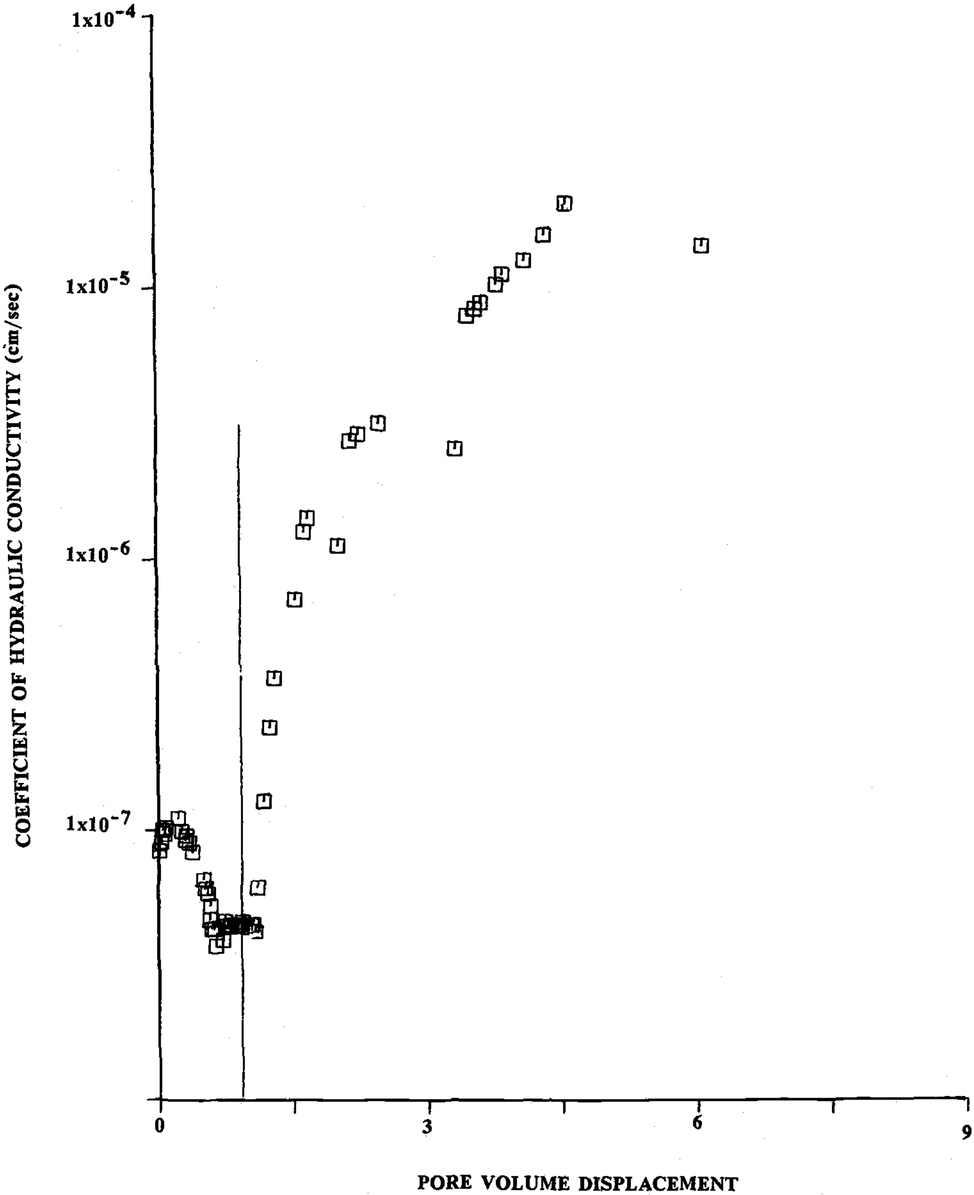

FIG. 4—*Permeability test results (back pressure without gradient).*

Differential Consolidation

As a result of the application of a uniform cell pressure and differential pore water pressures within the specimen (back pressure and driving pressure), the effective stress varies across the length of the specimen. For short specimens or very stiff specimens, this variation in effective stress may be inconsequential with respect to sample dimensions and the resulting consolidation. But, for soft clays or soft materials such as the soil–bentonite backfill investigated here, the differential state of effective stress results in differential

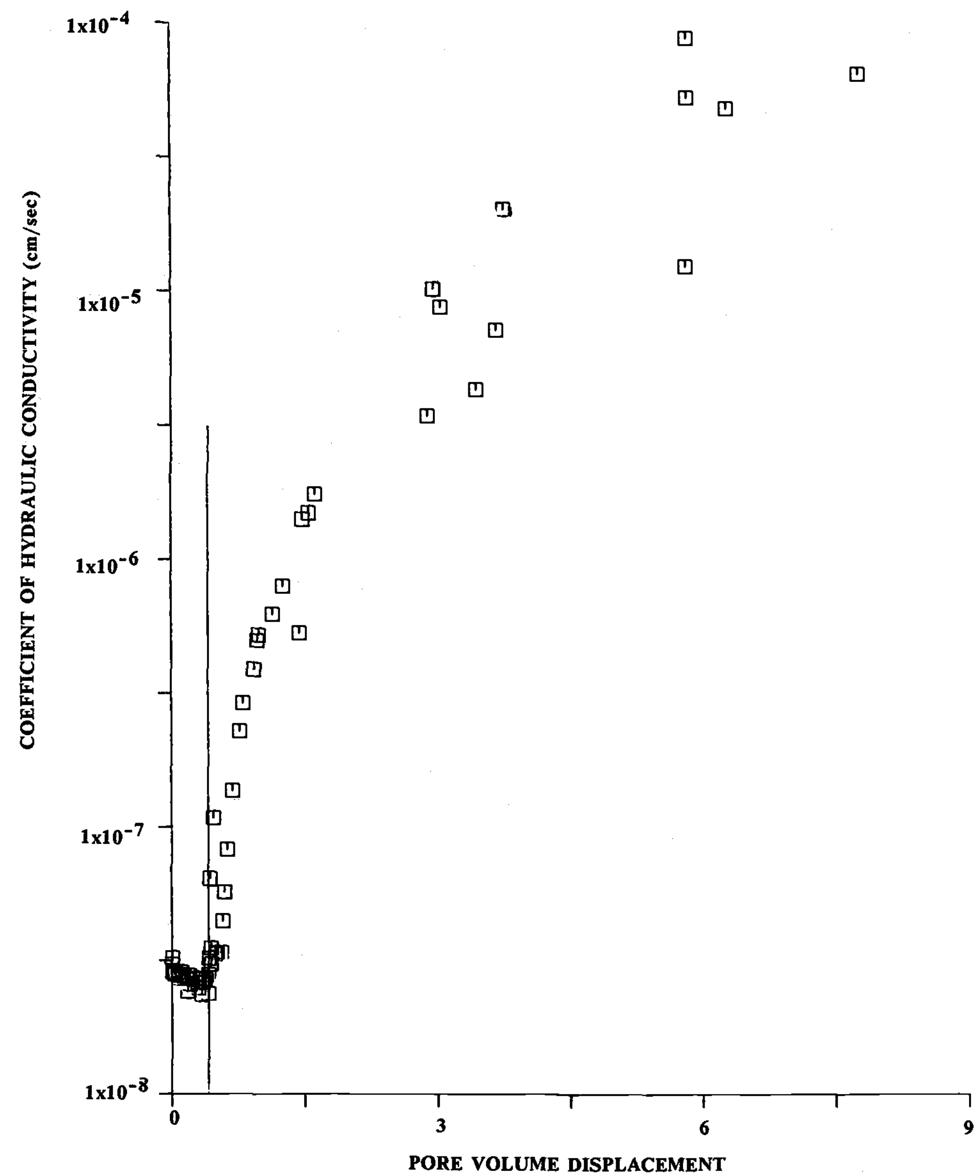

FIG. 5—*Permeability test results (back pressure with gradient).*

consolidation. For soft soils, the upper portion of the specimen has a smaller effective diameter than the lower portion (reflecting the higher state of effective stress at the upper part of the specimen). Using triaxial cell (flexible wall) permeameters for hydraulic conductivity and strength testing makes this phenomenon unavoidable.

Maintaining Saturation

Saturation is typically achieved in triaxial testing through the use of a back pressure [*16*]. With many triaxial cell systems, the back pressure is applied with compressed air. For short-term triaxial testing, this is an adequate method of elevating pore water pressures. However, if an air-water interface is maintained for a long time (such as required for long-term permeability testing), a new equilibrium air content is established. That is, the air content of the influent permeant is at equilibrium with the elevated pressure conditions, and the permeant becomes saturated with air at the influent pressure. As permeant passes through the specimen, a head loss is experienced. As a result, at the exit point of the specimen, the pore water pressure is reduced. Thus, under the lower pressure conditions, dissolved air may come out of solution. Air bubbles will form in the specimen and in the exit lines of the triaxial cell permeameter. This incomplete saturation causes a reduction in the measured hydraulic conductivity. The results of a test conducted to demonstrate this phenomenon are shown in Fig. 6. The air-water interface was maintained throughout the testing period, and, at test termination, air was observed in the effluent lines. Test results showing a steady decline in hydraulic conductivity should always prompt close examination of the testing procedure and equipment.

There are several ways to maintain saturation during long-term permeability testing. The authors replaced the inflow permeant frequently with "fresh permeant." The inflow riser pipes shown in Fig. 1 contain only enough permeant to conduct the test for about one day. The riser pipes therefore need to be refilled daily. The influent reservoirs contain permeant at atmospheric pressure. While the influent riser pipe is being replenished with fresh permeant, the reservoir is momentarily pressurized. The gravimetric head difference permits refilling of the riser pipe without any change of stress on the specimen. In this way, the specimen remains saturated. Other methods to prevent air from dissolving in the influent permeant have been described [*1,5,17*]. These may be equally successful and offer some increasing degree of complexity to the testing apparatus.

Influent Equilibrium

To assess the impact of a pore fluid on a soil material a constant influent chemistry must be maintained. The pore fluid may be provided to the laboratory as representative of the

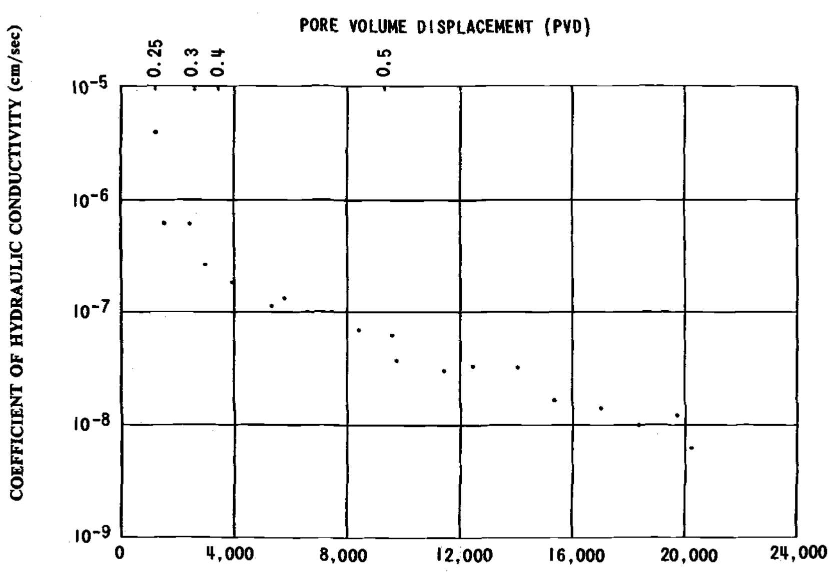

FIG. 6—*Permeability test results without maintenance of saturation.*

fluid chemistry to be encountered in the field or it may be prepared to meet certain experimental constraints. It is difficult to maintain a "constant" influent chemistry throughout the long-term permeability test. The daily replenishment of permeant described above assists in providing uniformity of influent permeant. Difficulty arises when one is testing volatile organics, particularly at concentrations near the solubility limit.

A recent study reported a method to maintain volatile organics at the solubility limit [*17*]. Using a conventional flexible wall permeability system (where an air pressure was applied directly to samples of the volatile organic mixed with water at the solubility limit), analyses were conducted to determine (after some period of the elapsed time) the actual concentration of the volatile organic. For this study, the organic, perchloroethylene (PCE), was mixed at the solubility limit of approximately 150 mg/L. Within hours, the concentration of PCE had dropped to about 10% of its original concentration. At lower concentrations (on the order of 1% to 10% of the solubility limit), only small changes in volatile organic concentrations were measured. To maintain the concentration of PCE at or near the solubility limits, the influent reservoir was modified as shown in Fig. 7. Pure PCE (denser than water) was first added to the reservoir. The reservoir was then filled with water. The chemical concentration

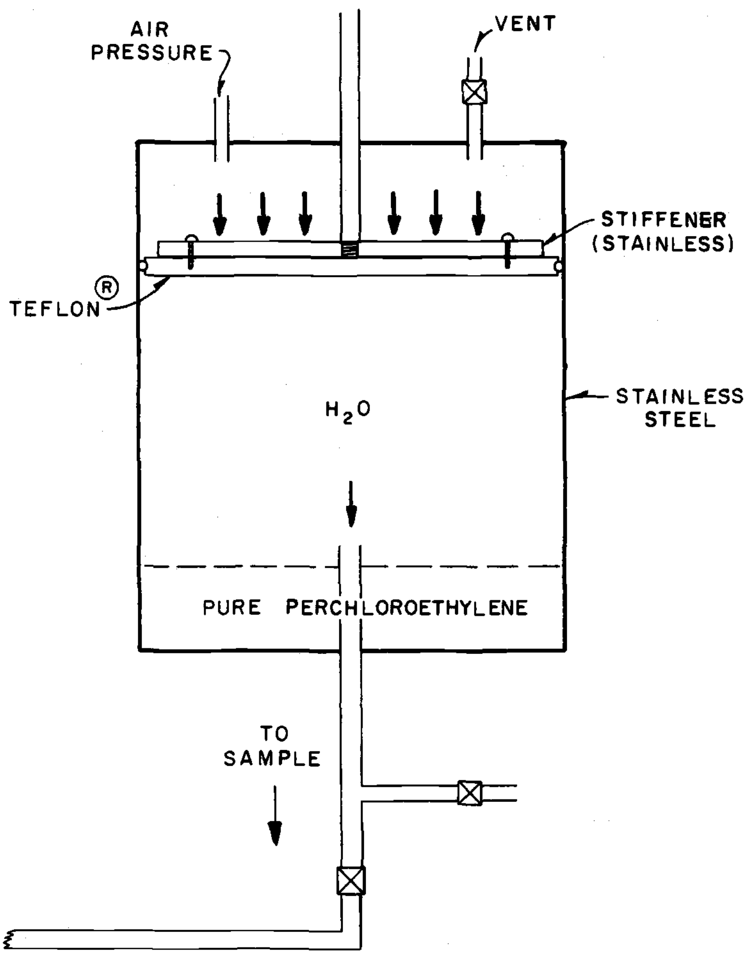

FIG. 7—*Modified influent reservoir.*

gradient results in the water becoming saturated with PCE. Because the air pressure is applied through a piston, the concentration is maintained. This technique is particularly suitable for testing of volatile organics at the solubility limit.

It is important to emphasize, however, that at low concentrations, the change in concentration of volatile organics over many days is relatively small even with an air pressure directly applied to the permeant [17]. For example, the concentration data for the study described above are presented in Table 1. It is important, however, to sample and analyze the influent as well as the effluent during the permeability testing program to document that the influent chemistry is being maintained during the long-term test.

Diffusion Through the Membrane

As the permeant migrates through the soil, solute is carried along at a rate equal to the fluid velocity by a process called advection. This uniform transport rate is altered by hydrodynamic dispersion and molecular diffusion. Just as solute migrates through the soil due to molecular diffusion, it can likewise migrate through the membrane used to encapsulate the specimen in a triaxial cell permeability test. As a result of molecular diffusion through the membrane, the concentration of the contaminant may decrease as the fluid migrates through the specimen. This phenomenon is particularly important when considering permeation with volatile organic compounds.

Figure 8 shows the relationship between pore volume displacement and the change in

TABLE 1—*Samples from perchloroethylene cylinders.*

Date of Sample	Detected Concentration, mg/L
11/28/83	9.5[a]
12/19/83	9.7[a]
12/20/83	0.9[b]
12/21/83	0.86[b]
	5.8[a]
	10.0[c]
12/21/83	1.10[b]
	21.0[c]
1/3/84	0.80[b]
1/6/84	0.80[b]
	134.0[c] (cylinder put in)
1/9/84	1.16[b]
	7.5[a]
	108.0[c]
1/11/84	140.0[c]
1/13/84	84.5[c]
1/16/84	150.0(+)[c]
1/18/84	99.5[c]
1/20/84	0.88[b]
	8.7[a]
1/25/84	150.0(+)[c]
1/30/84	0.69[b]
	9.0[a]
	76.3[c]
2/15/84	0.75[b]
	150.0[c]

[a] From 10 mg/L.
[b] From 2 mg/L.
[c] From 150 mg/L.

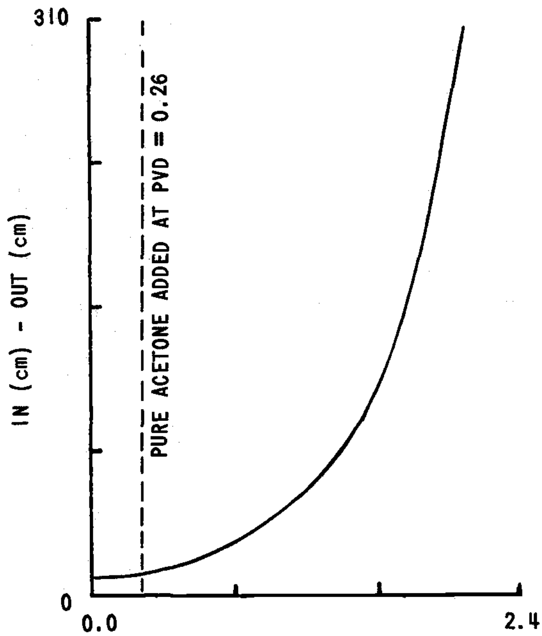

FIG. 8—*Relationship between inflow and outflow riser readings.*

volume as evaluated by the difference in readings between the inflow and outflow riser pipes for a long-term permeability test using acetone. If it is clear that there is more permeant going in than coming out, one needs to ascertain where the excess fluid is going (is the specimen swelling, are there leaks in the system, or is there diffusion through the membrane wall?). Although precise measurements were not made, the level of the fluid within the triaxial cell (between the membrane and the Plexiglas cell walls) was continually rising for the test shown in Fig. 8. When the specimen was dismantled, a sample of cell water was obtained, and a head space analysis with an organic vapor analyzer indicated a concentration of volatile organics of 1000 mg/L. Thus, due to molecular diffusion, acetone migrated through the membrane during permeability testing. Similar results were obtained using other organic fluids. The significance of diffusion through the membrane is twofold. First the durability of the membrane and the triaxial cell must be considered. Some membranes degrade in the presence of certain fluids. The diffusion rate can be minimized by using multiple layers of membrane (including Teflon wrap materials), a film of silicone grease, and silicone oil as the cell fluid [*4*]. Equally important, however, is the change in permeant chemistry occurring throughout the long-term permeability test. With inevitable diffusion through the membrane wall, the concentration of solute in the influent is affected. For a concentrated organic permeant (as in the case shown using concentrated acetone fluid), the diffusion through the membrane has little impact on the influent chemistry. The influent remains 100% concentrated with or without diffusion through the membrane. The measured rate of permeation will, however, be slightly greater than the actual rate due to fluid lost through the membrane. Alternately, for permeants with solutes in water at or below the solubility limit, the concentration of the solute may decrease as it migrates through the specimen due to diffusion through the membrane. As noted, this diffusion through the membrane may be limited by filling the cell with a fluid other than water, such as silicone oil. Analysis and comparison of the solute in both the influent and effluent will provide insight into the net change in contaminant concentration during permeation.

Biologic Activity

Studies have reported biologic growth during long-term permeability tests [*18*]. Bacterial growth may result in the plugging of the flow channels, resulting in a gradual decline in the measured hydraulic conductivity. This has not been a factor in the testing program described above because the contaminants used are generally toxic to biologic activity. However, in studies using landfill leachate, the presence of bacterial growth must be considered.

Type of Water

As previously described, potable water was used for these studies. The potable water has a range of naturally dissolved anions and cations which will interact with the clay minerals during the specimen formation. Changes in soil behavior would not be expected due to initial permeation with the same water because there is no change in the pore fluid chemistry. Other researchers have used a "standard water" consisting of 0.01 N calcium sulfate ($CaSO_4$) [*16*]. Alternatively 0.005 N calcium sulfate and 1 g/L of magnesium sulfate heptahydrate have been used as a standard water. The use of distilled water is not recommended [*1,2,6*]. The permeant water should be natural pore water to minimize soil–pore fluid chemical interactions during the initial permeation. For example, to study a proposed mix of soil–bentonite, the water proposed for mixing of the soil–bentonite backfill at the site should be used for both laboratory mixing and initial permeation. For an evaluation of an undisturbed soil specimen, ground water should be sampled as representative of natural pore water and used in initial permeation. To study a compacted clay that will not be subsequently subjected to water permeation, it appears reasonable to use a standard water such as 0.01 N calcium sulfate. The advantage to using a standard water is to eliminate this variable between laboratories. Long-term permeation of soil compacted with 0.005 N calcium sulfate indicates little change in hydraulic conductivity [*19*]. Data by others also show there is little change in hydraulic conductivity due to soil–fluid interactions when using 0.01 N calcium sulfate as a standard permeant [*16*]. Thus, within the realm of "order of magnitude accuracy" for permeability testing it appears that either the natural pore water or 0.01 N calcium sulfate or equivalent would represent an adequate permeant for initial water permeation.

Testing at Low Gradients

The procedures described above and the need to exchange a minimum of one pore volume result in tests conducted with gradients on the order of 50 to 100. To determine the hydraulic conductivity at gradients representative of field conditions it may be necessary to use different equipment or procedures than described above. Low gradients, however, are impractical for long-term permeability testing.

Shear Strength

For specimens permeated with water and several organic fluids at differing concentrations the strength testing results indicate that differences in strength due to the natural variability between specimens is greater than the change in strength induced by changes in pore fluid for these studies [*9*]. Thus, it may be beneficial to use specimens with a length-to-diameter ratio of one and reduce the permeation time in half. This can be done if shear strength data are not required.

Health and Safety Considerations

A unique consideration associated with long-term triaxial testing of contaminated soils or with hazardous and toxic permeants is the health and safety aspect. Activities associated with permeability testing include handling, shipping, storing, and labeling of specimens and permeants. To complete this work with an adequate level of protection for employees it is necessary to develop health and safety protocols. The objectives of the health and safety protocols include increasing personnel awareness of the potential hazard and providing personnel with information and skills to reduce the degree of risk. As a minimum, protocols should include [*20*]

- recognition and assessment of hazard,
- employee training,
- personal protective equipment,
- first aid training in the emergency response plans,
- decontamination equipment and procedures,
- use of equipment for monitoring toxic and combustible gas/vapor exposure, and
- medical surveillance program.

The major routes of exposure associated with permeability testing of contaminated soils and hazardous wastes are absorption, ingestion, and inhalation. Exposure can be greatly reduced if testing is done in a well-ventilated fume hood by personnel wearing proper protective equipment.

Summary and Conclusions

Long-term permeability testing requires certain equipment and procedural considerations different from those for short-term determination of hydraulic conductivity. These include gradient, particle migration, maintenance of saturation, type of water, and diffusion through the membrane. The impact of the considerations can be minimized, and triaxial permeability tests can be used to evaluate the interaction between hazardous pore fluids and soils.

Although the equipment and procedures used by the authors have been outlined, it is beyond the scope of this paper to present a detailed recommended test procedure (see Refs *1–8*). Both the U.S. Environmental Protection Agency (EPA) and ASTM are developing standard test procedures. It has been the purpose of this paper to identify and describe the equipment and procedural variables that impact the results of long-term hydraulic conductivity tests. The impact of these variables on the test results and alternative equipment and procedures to minimize their impact are summarized in Table 2.

Acknowledgments

The financial support for these studies was provided by the Professional Development Committee of Woodward-Clyde Consultants, Williams S. Gardner, chairman, and the Plymouth Meeting, PA, office of Woodward-Clyde Consultants, Frank S. Waller, managing principal. Funding for the fabrication of additional permeability testing systems was provided by the U.S. Environmental Protection Agency under Grant No. R810922. This support is gratefully acknowledged. We are indebted to Dr. Irwin J. Kugelman of Lehigh University for the assistance provided throughout these studies. The opinions, findings, and conclusions expressed in this paper are those of the authors and are not necessarily those of the project sponsors.

TABLE 2—*Long-term triaxial permeability testing variables.*

Variable	Typical Cause	Potential Errors	Potential Solutions
Gradient	Typically high (100±) to achieve adequate pore volume displacement in a reasonable testing period	• Does not represent field conditions • May cause migration of fines	Conduct replicate tests at "low" gradients to determine hydraulic conductivity and "high" gradients to determine compatibility
Effective stress	High enough to maintain positive effective stress at influent end of the sample	• May cause differential consolidation • May not represent field stress conditions • May result in hydraulic conductivity measurements lower than actual	• See above
Particle migration/ reorientation	Induced by high gradients	• May result in hydraulic conductivity measurements lower than actual	• See above • Perform grain size distribution analysis after testing to check for migration
Differential consolidation	See above	• Reduced cross-sectional flow area; impeding flow	• See above • Use shorter samples
Maintaining saturation	Consolidation and back pressure typically applied using compressed air; tests	• Steady decrease in hydraulic conductivity observed due to entrapped air	• Refresh permeant frequently • Eliminate air–permeant interface • Other equipment modifications

	may run for many weeks causing air in solution		
Influent/equilibrium	Volatilization of organics from influent	• Permeant chemistry may not represent field conditions	• Refresh permeant frequently • Eliminate air–permeant interface • Other equipment modifications
Diffusion through membrane	Molecular diffusion of contaminants through membrane under chemical diffusion gradient	• See above	• Eliminate diffusion gradient by using contaminated cell water • Use alternative membrane systems • Use silicone oil as cell fluid
Biologic activity	Biologic growth due to long-term nature of tests	• May cause decreases in flow rate due to biologic plugging	• Use biocides
Type of "water"	Distilled water, tap water, 0.01N $CaSO_4$, 0.005N $CaSO_4$ and 1.0 g/L $MgSO_4$ are all "standard" water	• Water may alter hydraulic conductivity due to pore fluid–soil interactions	• Avoid distilled water • Use original pore fluid where possible • 0.01N $CaSO_4$ or 0.005N $CaSO_4$ impact
Low gradients	Used to simulate field conditions	• Not practical for compatibility testing • Equipment precision may be inadequate	• Procedures and equipment needs are different for short-term, low-gradient testing than for long-term, high-gradient compatibility testing

References

[1] Dunn, R. J., and Mitchell, J. K., "Fluid Conductivity Testing of Fine-Grained Soils," *Journal, Geotechnical Engineering Division, American Society of Civil Engineers,* Vol. 110, No. 11, Nov. 1984, pp. 1648–1665.

[2] Olson, R. E., and Daniel, D. E., "Measurement of Hydraulic Conductivity of Fine-Grained Soils," in *Permeability and Groundwater Contaminant Transport, ASTM STP 746,* 1981, pp. 18–64.

[3] Day, S. R., and Daniel, D. E., "Hydraulic Conductivity of Two Prototype Clay Liners," *Journal, Geotechnical Engineering Division, American Society of Civil Engineers,* Vol. 111, No. 8, August 1985, pp. 957–970.

[4] Tavenas, E., Leblond, P., Jean, P., and Leroveil, S., "The Permeability of Natural Soft Clays, Part I: Methods of Laboratory Measurement," *Canadian Geotechnical Journal,* Vol. 20, 1983, pp. 629–644.

[5] Daniel, E., Trautwein, J., Boynton, S., and Foreman, E., "Permeability Testing with Flexible-Wall Permeameters," *Geotechnical Testing Journal,* GTJODJ, Vol. 7, No. 3, Sept. 1984, pp. 113–122.

[6] Carpenter, G. W., and Stephenson, R. W., "Permeability Testing in the Triaxial Cell," *Geotechnical Testing Journal,* GTJODJ, Vol. 9, No. 1, March 1986, pp. 3–9.

[7] Acar, Y. B., Hamidon, A., Field, S. D., and Scott, L., "The Effect of Organic Fluids on Hydraulic Conductivity of Compacted Kaolinite," in *Hydraulic Barriers in Soil and Rock, ASTM STP 874,* A. I. Johnson, R. K. Frobel, N. J. Cavalli, and C. B. Pettersson, Eds., American Society for Testing and Materials, Philadelphia, 1985, pp. 171–187.

[8] Daniel, D. E., Anderson, D. C., and Boynton, S. S., "Fixed-Wall Versus Flexible-Wall Permeameters," in *Hydraulic Barriers in Soil and Rock, ASTM STP 874,* A. I. Johnson, R. K. Frobel, N. J. Cavalli, and C. B. Pettersson, Eds., American Society for Testing and Materials, Philadelphia, 1985, pp. 107–126.

[9] Evans, J. C., Kugelman, I. J., and Fang, H.-Y., "Organic Fluid Effects on the Strength, Deformation and Permeability of Soil–Bentonite Slurry Walls," *Proceedings, Seventeenth Mid-Atlantic Industrial Waste Conference,* Techomic Publishing Co., Lancaster, PA, June 1985, pp. 275–291.

[10] Evans, J. C., Kugelman, I. J., and Fang, H. Y., "Influence of Industrial Wastes on the Geotechnical Properties of Soils," in *Proceedings, Fifteenth Mid-Atlantic Industrial Waste Conference,* Butterworth Publishing, Boston, 1983, pp. 557–568.

[11] Alther, G., Evans, J. C., Fang, H.-Y., and Witmer, K., "Influence of Inorganic Permeants upon the Permeability of Bentonite," in *Hydraulic Barriers in Soil and Rock, ASTM STP 874,* A. I. Johnson, R. K. Froebel, N. J. Cavalli, and C. B. Pettersson, Eds., American Society for Testing and Materials, Philadelphia, 1985, pp. 64–73.

[12] Evans, J. C., Fang, H.-Y., and Kugelman, I. J., "Organic Fluid Effects on the Permeability of Soil–Bentonite Slurry Walls," *Proceedings, National Conference on Environmental Emergencies,* Cincinatti, OH, The Hazardous Materials Control Research Institute (HMCRI) May 1985, pp. 267–271.

[13] Fang, H.-Y., and Evans, J. C., "Long-Term Permeability Tests Using Leachate on a Compacted Clayey Liner Material," *Ground-Water Contamination: Field Methods, ASTM STP 963,* A. G. Collins and A. I. Johnson, Eds., American Society for Testing and Materials, Philadelphia, 1988, pp. 397–404.

[14] Evans, J. C., and Fang, H.-Y., "Equipment for Permeability Testing with Hazardous and Toxic Permeants," *Geotechnical Testing Journal, GTJODJ,* Vol. 9, No. 3, September 1986, pp. 126–132.

[15] Brown, K. W., and Anderson, D. C., "Effects of Organic Solvents on the Permeability of Clay Soils," EPA-600/2-83-016, March 1983, p. 153.

[16] Bishop, A. W., and Henkel, D. J., *The Measurement of Soil Properties in the Triaxial Test,* 2nd ed., Edward Arnold, London, 1962, p. 227.

[17] Evans, J. C., and Manual, E. N., "Geotechnical Property Testing of Hazardous Materials and Contaminated Soils," in *Proceedings, Sixth National Conference on the Management of Uncontrolled Hazardous Waste Sites,* Washington, DC, The Hazardous Materials Control Research Institute, 1985, pp. 249–252.

[18] Allison, L. E., "Effect of Microorganisms on Permeability of Soil Under Prolonged Submergence," *Soil Science,* Vol. 63, 1947, pp. 439–450.

[19] Evans, J. C., "Clay Compatibility Testing," Report to Research Triangle Institute, Research Triangle Park, NC, Aug. 14, 1986.

[20] Steele, J. R., "Safety Plans for Uncontrolled Hazardous Waste Sites," in *Proceedings, Fifth National Conference on Uncontrolled Hazardous Waste Sites,* Washington, DC, The Hazardous Materials Control Research Institute, 1984, pp. 269–272.

Y. P. Vaid[1] *and D. Negussey*[1]

Preparation of Reconstituted Sand Specimens

REFERENCE: Vaid, Y. P. and Negussey, D., "**Preparation of Reconstituted Sand Specimens,**" *Advanced Triaxial Testing of Soil and Rock, ASTM STP 977,* Robert T. Donaghe, Ronald C. Chaney, and Marshall L. Silver, Eds., American Society for Testing and Materials, Philadelphia, 1988, pp. 405–417.

ABSTRACT: Review and assessment of sand sample preparation techniques from both theoretical and experimental viewpoints are presented. Sample densities obtained by air pluviation are shown to be sensitive to rate of pouring and drop height. Terminal velocity is reached at a very small drop height, and homogeneous samples of the same initial density tend to be formed by pluviation of uniform sand in water. Uniformly dense samples obtained by vibration of loose pluviated samples show no detectable difference in behavior when compared to samples densified by control of drop height only. Effective confinement during densification by vibration appears to prevent formation of a loose top layer. A loose top layer in an otherwise dense sample leads to a marked decrease in liquefaction resistance. Preparation of triaxial sand samples by pluviation in water is recommended because it results in initially saturated specimens, and homogeneous samples of desired densities can be replicated without difficulty.

KEY WORDS: density, pluviation, sand, triaxial sample

Testing of homogeneous (uniform) samples under uniform states of stress and strain is required for fundamental studies of soil property characterization. It is also necessary to be able to replicate precisely several homogeneous specimens for such studies. These requirements have promoted the use of reconstituted soils rather than natural materials for fundamental investigations of soil behavior. Uniform and repeatable clay specimens are obtained easily by trimming from a large block consolidated from an initial slurry state. Such a procedure is not possible for sand, and each sand test specimen has to be prepared individually. This makes the control of uniformity and the ability to replicate several specimens considerably more difficult.

Several methods of reconstituting sand specimens have been used. The common objective in each type has been the control of average density. Uniformity is generally assumed. Conscious efforts to verify uniformity by direct measurements of density over the height of the reconstituted sample have been made only in a limited number of cases [*1–4*]. These measurements show that specimens prepared by pluviation in water or air tend to be uniform [*3,4*]. Compaction methods, such as moist tamping, produce samples that are considerably less uniform [*1,2*]. The degree of nonuniformity appears to increase with decrease in average density of the reconstituted sample [*1*]. Some modifications in the form of undercompaction have been proposed in the moist tamping technique in an attempt to promote uniformity

[1] Professor and Natural Science and Engineering Research Council of Canada (NSERC) Fellow, respectively, Department of Civil Engineering, University of British Columbia, Vancouver, British Columbia, Canada V6T 1W5.

[5]. There is, however, no direct confirmation of the effectiveness of such modifications. Available direct evidence appears to suggest that vibration techniques of reconstitution also promote considerable nonuniformity within the specimen [3].

Available evidence, although limited, suggests that reconstitution by pluviation is the most promising technique for obtaining uniform samples in the laboratory. Both the nature of anisotropy and soil fabric obtained by pluviation duplicate those observed in natural alluvial environments [6]. Hence, pluviation approximates a natural deposition process, and this technique of preparing laboratory samples for testing allows a convenient study of mechanical response of natural sands.

Both air and water pluviation techniques for sample preparation have been used in the laboratory. The height from which the sand drops during air pluviation has been used to obtain samples of various relative densities, although researchers have different opinions as to the degree of its success. The influence of increasing height of drop on the relative density obtained has been reported to be significant, minor, or insignificant [7–10]. Pluviation in water, on the other hand, has been reported to yield loose relative densities regardless of the drop height. Higher densities, if desired, are obtained by vibrations following pluviation.

In this paper a convincing case is made in favor of pluviation as a convenient means of preparing uniform and replicable sand samples of controlled density. First, a theoretical framework is presented for explaining rationally the effect of drop height on the relative density of the sand deposit. Then, experimental evidence is presented in support of the ideas developed. The theoretical development is also used to seek a satisfactory resolution to the conflicting conclusions in literature on this issue. Specific details of sample preparation until the point of testing are described. Finally, direct and indirect experimental evidence is presented to demonstrate the uniformity of the pluviated samples and the ease of replication of a series of such samples.

Velocity at Impact

It is postulated that the kinetic energy of sand particles at the instant of impact at deposition controls the relative density achieved. The motion of an isolated spherical particle of mass m undergoing free fall in a fluid of mass density ρ is described by

$$ma = mg - V\rho g - C_d \rho A \frac{v^2}{2} \tag{1}$$

where

a = particle acceleration
g = gravitational acceleration
V = volume of the particle
A = projected area of the particle
v = particle velocity
C_d = drag coefficient, which depends on Reynold's number

The second and third terms on the right side of Eq 1 represent, respectively, the forces of buoyancy and drag on the particle. Assuming the particle starts from rest ($v_o = 0$ and thus $a_o = g(1 - V\rho/m)$), it will decelerate from $a = a_o$ to $a = 0$ when the terminal velocity is reached. Given the properties of the falling sphere and that of the fluid medium, the velocity, acceleration, and displacement of the particle can be determined as a function of time from the equation of motion (Eq 1) and the assumed initial at-rest state. These computations are, however, not straightforward because of the interdependence of velocity and drag coefficient. Hence a trial-and-error procedure is required, which is described in standard fluid mechanics textbooks.

The pluviation of a relatively uniform sand may be idealized as a free fall of spheres of an equivalent diameter, D_{50}. Neglecting interference effect due to simultaneous fall of many particles, the time history of velocity, acceleration, and displacement of particles can be calculated as discussed above. Figure 1 shows results of these computations for quartz sand (G_s = 2.67) with D_{50} = 0.4 mm pluviating through air and also water. The results are shown in the form of velocity attained as a function of the drop height. At equal drop heights, velocities in air are very large compared to those in water. This would result in a much higher kinetic energy at deposition in air as opposed to water. Furthermore, the terminal velocity in water is reached in a mere 0.2-cm drop as compared to a very large drop of 270 cm in air. Consequently, considering a practical range of heights of pouring (for example, up to 2 m used by Kolbuszewski [9]), the velocity at impact (and hence kinetic energy) at deposition in air will vary considerably depending on the drop height. The largest increase in velocity with a given increase in drop height may be seen to be associated in the low end of the drop heights and should consequently have greatest influence on the relative density of the deposited sand. Drop height effects on impact velocity for pluviation in water, on the other hand, are inconsequential, because terminal velocity is reached in a drop height of about 0.2 cm and no further increase in velocity can occur after terminal velocity is attained. Therefore, drop height control is ineffective in obtaining different relative densities using water pluviation.

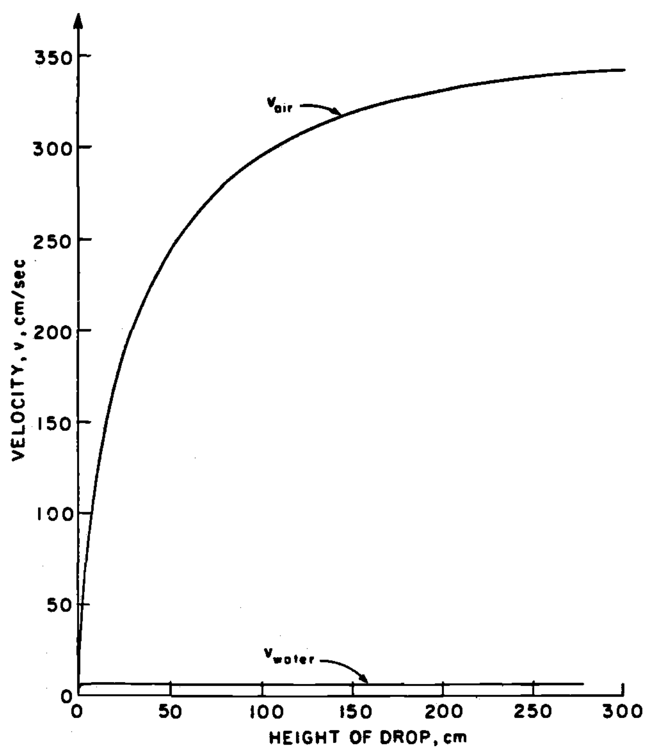

FIG. 1—*Velocity of a free falling sphere in air and water.*

The influence of particle size on impact velocity as a function of drop height in air is shown in Fig. 2. As would be expected, the impact velocity decreases with decrease in particle size at all levels of drop heights. For the conditions examined, the magnitude of terminal velocity attained increases essentially linearly with increase in particle size, but the drop height needed to attain this also increases. A quicker approach to terminal velocity in fine sand implies that the range of drop height in which densification is effective will be smaller.

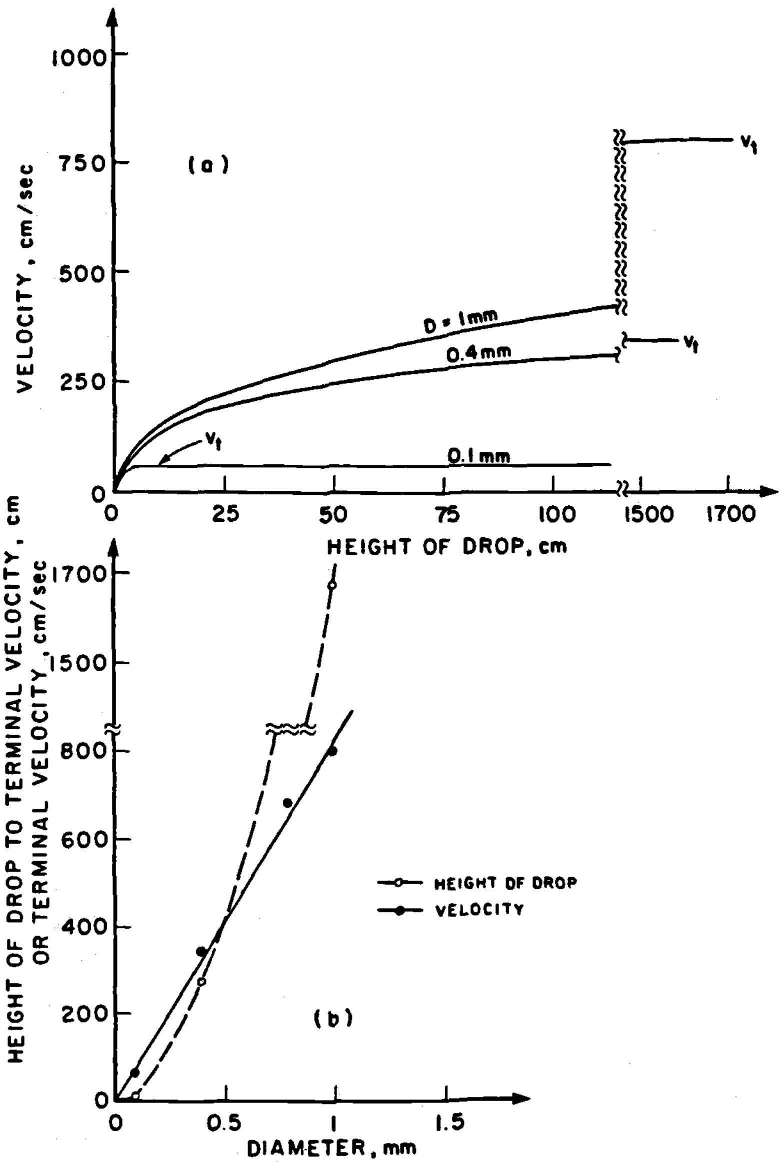

FIG. 2—(a) *Velocity of free falling spheres of different diameters in air.* (b) *Terminal velocity and drop height to terminal velocity as a function of sphere size.*

Results similar to those in Fig. 2 may be obtained for pluviation in water. The drop heights to reach terminal velocity in water, however, are very small. For $D_{50} = 0.4$ mm it was shown to be a mere 0.2 cm and would be less for smaller particle sizes. For 2-mm sand particles this height is less than 2 cm. Consequently, for a variety of sands, the height of the drop in water is generally inconsequential in exercising control on the density of the deposit. The same initial density tends to develop regardless of drop height, and due to low kinetic energy deposition the ensuing relative density will be low.

Experiments on Pluviation

Controlled height of drop in air experiments were carried out on two uniform quartz sands to investigate the relationship between density achieved and height of drop. The sands had the following physical properties.

	D_{50}, mm	e_{max}	e_{min}	C_u
Ottawa sand, ASTM C-109	0.4	0.82	0.50	2.0
Ottawa sand, fine	0.16	0.86	0.56	1.8

Approximately 2.5 kg of sand were deposited each time in a 9.5-cm-diameter Plexiglas container. The sand was poured from a 5-cm-diameter Plexiglas tube having a screened bottom of 1.17-mm sieve opening. The pouring tip was continuously moved up with the surface of the deposit maintaining constant height. Densities obtained by a precise control of drop height were repeatable to within 2%.

Test results presented in Fig. 3 show that higher impact energies associated with increased drop heights lead to compaction and toward a limiting void ratio for both sands. The limiting void ratio reached corresponds closely to the respective minimum void ratios for the sands determined by ASTM method D2049. It may also be noted that the velocity (which is related

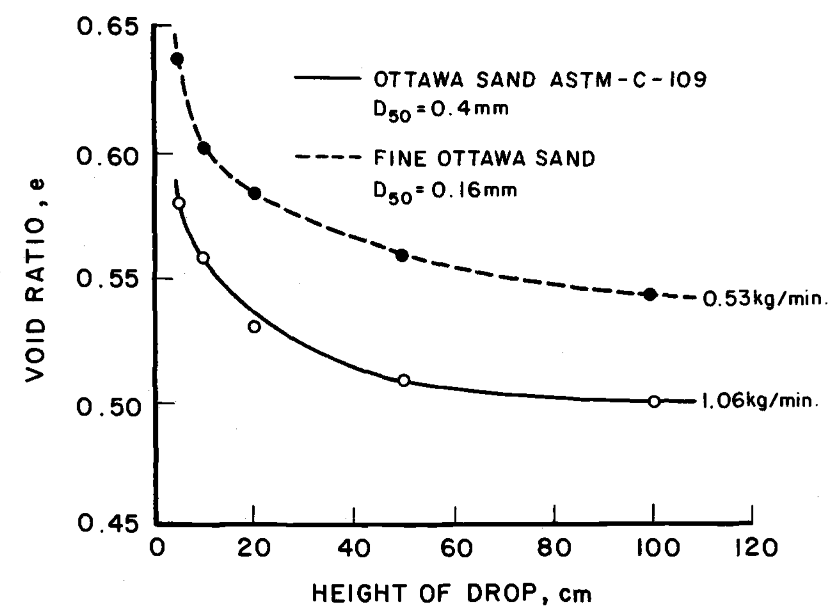

FIG. 3—*Particle size and height of drop effects on void ratio.*

to impact energy) versus drop height trend illustrated in Fig. 1 approximates a mirror image of that shown in Fig. 3, lending support to the theoretical postulate of associating larger densities to larger kinetic impact energies. Figure 3 further shows that the influence of height of drop on densification seems to be most significant in a drop height range of about 0 to 30 cm for the sands studied. This observation is also consistent with the velocity versus drop height relationship of Fig. 1 in the region of smaller drop heights. Although impact energies will keep increasing with increasing drop heights until terminal velocity is reached, it appears from the test results that increase in impact energy beyond a certain maximum magnitude may do little in compacting sand any further. This may explain the results of Miura and Toki [*11*] who observed insignificant changes in void ratio with change in drop height. For the range of drop height they investigated, 30 to 70 cm, the change in void ratio would be small as shown in Fig. 3. Similar arguments may apply to the observations of Mulilis and co-workers [*8*] who noticed only minor effect of drop height on the resulting void ratio.

The arguments presented above are based on the idealized assumption that the sand consists of uniform spheres which undergo free fall without mutual interference. In reality the actual void ratio attained by the sand for a given height of drop will depend on some average particle size, gradation, mass rate of pouring, and characteristics of the container, such as its diameter and surface smoothness, particularly for small diameters. Higher mass rates of pouring would introduce interference effects that may inhibit particles from acquiring the most stable (and hence likely dense) configuration while coming to rest [*10,11*]. Higher mass rates of pouring into a cylindrical former may also trap an air front, the escape of which may cause a counter upward air current. This would likely reduce the impact energy and result in less compaction. A membrane-lined sample former, especially of a smaller diameter, will further inhibit denser packing due to frictional side restraint. Thus, for a given sand and sample former characteristics, the height of fall and mass rate of pouring appear to have opposite effects. Both these effects have been used implicitly to control void ratio of air-pluviated sand samples [*7,11,12*]. Further corroboration of this conclusion may be seen from test results shown in Fig. 4 on the sands used in this study. All factors other than drop height and mass rate of pouring were held constant. A progressively decreasing compaction with increasing mass rate of pouring over the full range of drop heights may be noted for both sands.

If the sand is well graded or contains significant amounts of fines, air pluviation will clearly result in segregation because of the finer particles lagging behind on account of their smaller velocities within the fixed height of drop (Fig. 2). Hence, such pluviated samples may not be homogeneous. Even for a relatively uniform sand, a precise control on drop height is crucial to forming homogeneous samples. The need for precise control of pouring height is apparent in Figs. 3 and 4, which show extreme sensitivity of resulting void ratios to changes in pouring height. Commonly used pouring heights in forming air-pluviated samples may be noted to fall within the sensitive range of drop heights. If low relative densities are desired, a relatively small pouring height would be needed. In such cases the position of the pouring tip must be continuously raised, as the thickness of the deposit builds up, to maintain a constant drop height at all times. This makes the deposition process unnecessarily complex. Samples formed by pluviation in water will not be subject to nonhomogeneity due to variation in height of pouring during deposition. This is because the soil grains reach terminal velocity almost instantly (drop height of 0.2 m for D_{50} = 0.4 mm), and the constant terminal velocity is maintained until deposition, regardless of the height of drop. Initially, water-pluviated samples of a given sand tend to be loose and at essentially the same density. Higher density samples, if desired, may be obtained by vibrations.

As indicated by the theoretical postulates, drop height variations (between 0 and 30 cm) in water for both sands did not result in density changes. The void ratio of each deposit in

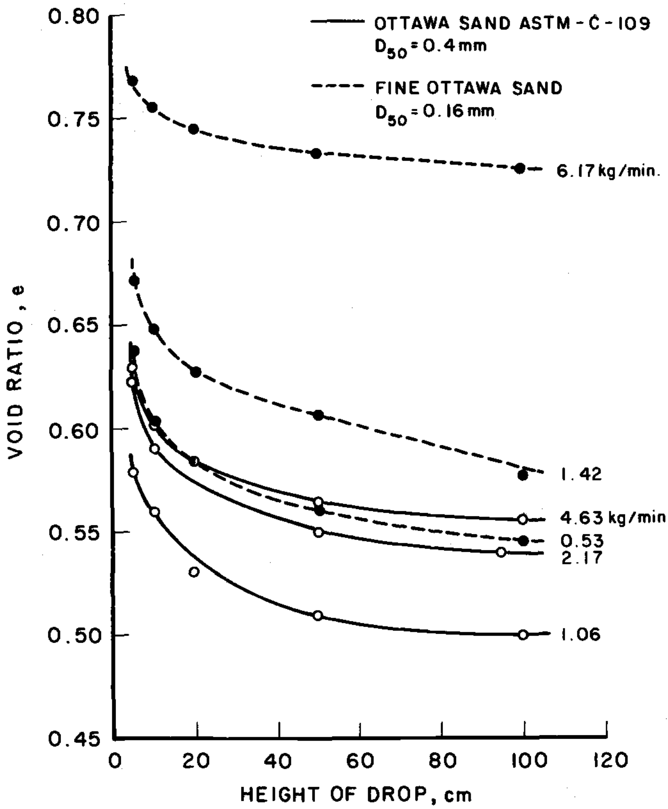

FIG. 4—*Height of drop, mass pouring rate, and particle size effects on void ratio.*

each case was found to be essentially independent of the height of drop. Furthermore, the void ratios obtained correspond to loose relative densities of approximately 28% to 30% for both sands, as would be expected from a low energy water deposition process.

Sample Reconstitution Procedure and Uniformity

Either air or water pluviation techniques may be used for reconstitution of homogeneous sand samples. The latter would be preferable in that a precise control on drop height would not be required. Water pluviation has the additional advantage of providing initially saturated samples. Air pluviation, on the other hand, requires further effort and time for saturating specimens prior to testing. Testing of saturated specimens is generally required for studies of both drained and undrained behavior.

Water pluviation, however, yields specimens of relatively loose densities. Higher relative densities, if desired, have to be achieved by vibrations. The behavior of sand pluviated directly to a given density may or may not be the same as that of sand densified to the same density following loose pluviation. This was investigated by resonant column tests on two dense Ottawa sand ASTM C-109 specimens prepared to identical densities by loose pluviation with subsequent vibrations or direct pluviation in air. The samples were hydrostatically consolidated to an effective stress of 300 kPa. As shown in Fig. 5, Young's modulus versus longitudinal strain relationships for the two samples are essentially identical, and the den-

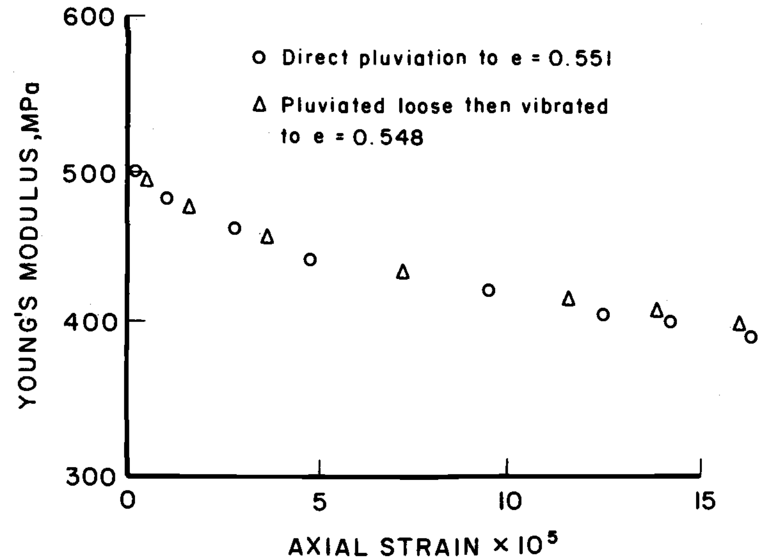

FIG. 5—*Comparison of densification methods by resonant column tests on Ottawa sand, ASTM C-109.*

sification procedure does not appear to have resulted in detectable differences in behavior. This observation, together with advantages already pointed out, supports preference of water pluviation over air pluviation.

Sample Preparation Method

The technique of sample preparation by water pluviation has been described by several researchers [*13–16*]. The procedure basically consists of depositing a known weight of dry sand that has been saturated by boiling with water in a flask and cooled to room temperature. Deposition is made directly into a membrane-lined, deaired-water-filled, split-mold cavity. Sand transfer from the flask to the cavity occurs under water by mutual displacement of sand and water under gravitational influence.

Because the diameter of the mold and membrane thickness are constant, desired relative densities can be obtained easily from the known dry weight of the sand used and controlling specimen heights. Prior to assembling the sample former, a target height is established. Following deposition and leveling, the cap is put in place and the reference height dial gauge is located on top. Then the specimen is densified by high-frequency vibration induced along the top of the cell base maintaining a small seating load on the cap. During densification to the desired height and density, both top and bottom drainage lines are kept open, and change in height is continually monitored. When the target height is approached, densification is terminated. The membrane is then pulled over the top cap and sealed with an O-ring. While the base drainage is kept open, the top drainage line is plugged. A small vacuum is applied to the bottom drainage to give the sample a small effective confinement.

In some procedures the densification of the sand is carried out prior to leveling of the top surface and seating of the loading cap. This appears to lead to formation of a loose layer of sand at the top due partly to disturbance resulting from leveling and seating of the loading cap on the sand surface and partly to the inability of vibrations to densify the unconfined top layers. Such a loose, potentially compressible layer in an otherwise dense sample can lead to a substantial reduction of undrained cyclic resistance of sand samples. In the suggested procedure, the sand is deposited loose and is densified by vibrations with the loading cap placed on the sand surface and by maintaining a small seating load throughout the densification period. The loading cap thus follows the settlement of the sand surface and assumes a proper seating, while the entire sample gets uniformly densified without development of a loose zone at the top. It is believed that this manner of densifying test samples results in the development of full liquefaction resistance of sand at the prepared average density. Such a conclusion is supported by extensive laboratory tests in which a dramatic increase in resistance to liquefaction was noted if dense samples were prepared by the improved technique.

Figure 6 shows data on the resistance to liquefaction of Ottawa sand, ASTM C-109, obtained in the simple shear apparatus. Improved features of sample preparation techniques described above were used in this study. In Fig. 6, the cyclic stress ratio τ_{dy}/σ'_{vo} to cause ±2% shear strain in ten cycles is shown as a function of relative density. The liquefaction resistance increases with relative density and very markedly so for relative densities in excess of about 70%. For relative densities in excess of about 80% it is almost impossible to develop ±2% shear strain in ten cycles even under cyclic stress ratios in excess of 0.40. The numbers in parentheses in Fig. 6 represent the actual number of cycles (not ten cycles) to develop ±2% strain in these dense samples. The vertical asymptotic nature of the liquefaction resistance curve indicates that liquefaction is unlikely to occur irrespective of the level of cyclic stress ratio if sand has a relative density in excess of about 80%. Such a conclusion seems apparent from the analysis of field records of liquefaction [*17,18*]. The weaker response of sands, especially dense sands, to cyclic loading in the laboratory as opposed to field observations [*17,19*] may in part be due to development of zones of nonuniformity. Direct assessment of zones of nonuniformities confined to a few grains' thickness by density measurements over the specimen height is clearly not feasible.

Figure 6 also shows data on liquefaction resistance of the same sand obtained in the triaxial

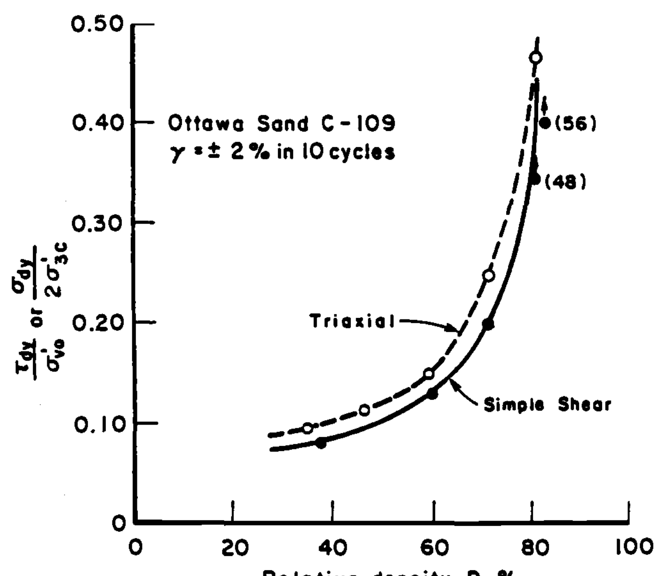

FIG. 6—*Resistance to liquefaction of Ottawa sand, ASTM C-109.*

apparatus. These results were also obtained by using similar careful experimental techniques as used for simple shear results. Again a vertical asymptotic nature of the liquefaction resistance curve may be noted corresponding to a relative density in excess of about 80%.

In shear devices, which require transfer of boundary shear force through one of the loading platens (such as the simple shear or torsional shear devices), ribbed platens are usually necessary for a proper transfer of shear stress to the sample [*14*]. Digging action of these ribs would cause additional loosening of top layers of an otherwise dense sample if densification was done prior to seating of ribbed plate. It is then apparent that these loose zones would cause the sample to have a lower resistance to cyclic loading than a sample that is uniform throughout at the prepared average relative density.

Direct Assessment of Uniformity

Tests were carried out using gelatin solidification method suggested by Emery and coworkers [*4*]. Ottawa sand, ASTM C-109, specimens, 63 mm in diameter and 127 mm high, were formed by pluviation in water containing approximately 3% by weight of gelatin. The specimens were allowed to solidify at room temperature for about 12 h. Each specimen was then cut into four slices along the height for evaluation of the density distribution within the specimen. Such density profiles were determined for specimen as pluviated (loose) as well as vibration-densified specimens following pluviation.

Typical test results are plotted in Fig. 7. Both loose and dense specimens are very uniform. The extreme variation between maximum and minimum relative density is within 3% of the average relative density of the specimens. Thus, not only directly pluviated specimens are uniform but also those which have been densified following pluviation. The results shown in Fig. 7 for loose specimens confirm earlier work of Emery and co-workers [*4*].

Replication

Through procedures described previously, the weight of sand grains and initial sample dimensions can be controlled to enable reproduction of relative density to within 1% of the desired target. Pursuit of an identical reconstituting procedure would replicate grain structure as closely as possible.

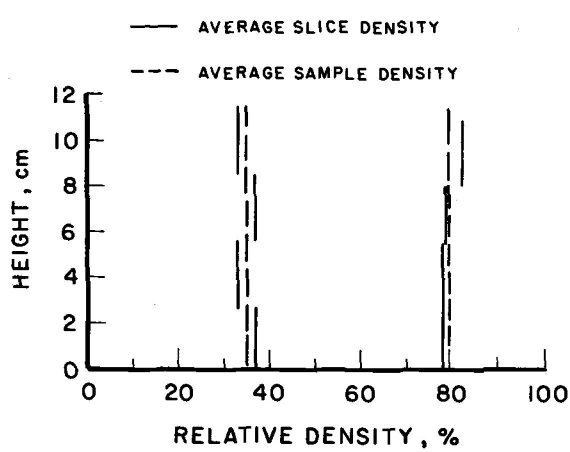

FIG. 7—*Relative density distribution within loose and dense specimens of Ottawa sand, ASTM C-109.*

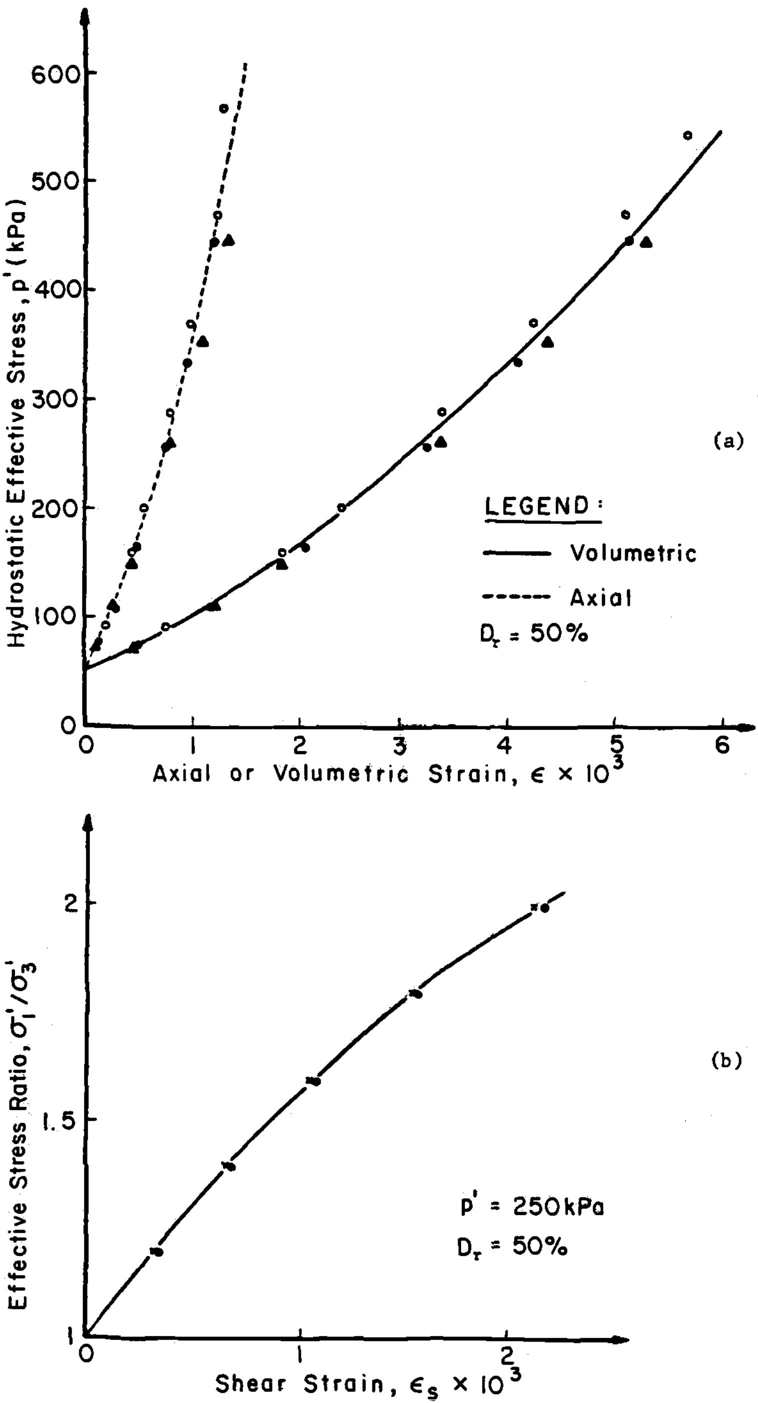

FIG. 8—*Repeatability of test results in hydrostatic compression and constant effective mean normal stress shear.*

The degree to which the pluviation technique enables replication of specimens at a desired density is illustrated in Fig. 8*a*. Results of hydrostatic compression showing hydrostatic effective stress p' versus axial and volumetric strains on three identical samples of Ottawa sand, ASTM C-109, at a relative density of 50% are shown. Excellent repeatability may be noted in the test results, considering the extremely small level of strains developed.

Excellent repeatability of test results showing stress ratio, R (= σ_1'/σ_3'), versus shear strain, ϵ_s (= $\epsilon_1 - \epsilon_2$), from two identical samples under constant effective mean normal stress, p', drained shearing may also be noted in Fig. 8*b*.

Conclusions

A homogeneous sample of a uniform sand can be prepared by pluviation in water or air. Terminal velocity is reached at a very small drop height in water. Regardless of the drop height, the same loose initial density is achieved by pluviation in water. Additional vibration is necessary to densify water-pluviated samples. The drop height required to reach terminal velocity in air is large, and impact velocities vary depending on drop height. A wide range of initial relative densities can be achieved by controlling drop height and pouring rate in air. Thus, careful control of drop height is required to achieve uniform specimens by air pluviation. Differences in behavior between comparable samples densified by either control of drop height or vibration of an initially loose specimen were not observed. Experimental results indicate that densities within pluviated loose as well as vibration-densified samples are uniform. Effective confinement during densification prevents development of a loose top surface and allows uniform contact between the sand and end cap. A loose top surface in an otherwise dense sample appears to contribute to a marked decrease in liquefaction resistance. Sample preparation by pluviation in water is preferable to air pluviation in that it results in initially saturated samples, and replicate samples can be produced much more conveniently.

Acknowledgments

The authors wish to acknowledge financial support of the Natural Science and Engineering Research Council of Canada. R. Brun drafted the figures, and K. Lamb typed the manuscript. P. Lui and J. Christian performed some of the tests. The authors are very grateful for their assistance.

References

[*1*] Castro, G., "Liquefaction of Sands," Ph.D. thesis, Harvard University, Cambridge, MA, 1969.
[*2*] Castro, G., Poulos, S. J., France, J. W., and Enos, J. L., "Liquefaction Induced by Cyclic Loading," Report to National Science Foundation, Washington, DC, 1982.
[*3*] Mulilis, P. J., Seed, H. B., Chan, C. K., Mitchell, J. K., and Arulanandan, K., *Journal of the Geotechnical Engineering Division, American Society of Civil Engineers*, Vol. 103, No. GT2, 1977, pp. 91–109.
[*4*] Emery, J. J., Finn, W. D., and Lee, K. W., *STP 523*, American Society for Testing and Materials, Philadelphia, 1973, pp. 182–194.
[*5*] Ladd, R. S., *Geotechnical Testing Journal*, American Society for Testing and Materials, Philadelphia, Vol. 1, No. 1, 1978, pp. 16–23.
[*6*] Oda, M., Koishikawa, I., and Higuehi, T., *Soils and Foundations*, Vol. 18, No. 1, 1978, pp. 25–38.
[*7*] Tatsuoka, F., Muramatsu, M., and Sasaki, T., *Soils and Foundations*, Vol. 22, No. 2, 1982, pp. 55–70.
[*8*] Mulilis, P. J., Chan, K. K., and Seed, H. B., "The Effect of Method of Sample Preparation on

the Cyclic Stress Strain Behaviour of Sand," Earthquake Engineering Research Center Report No. 75-18, University of California, Berkeley, 1975.
[9] Kolbuszewski, J. J., *Proceedings,* Second International Conference on Soil Mechanics and Foundation Engineering, Rotterdam, Vol. 1, 1948, pp. 158–165.
[10] Kolbuszewski, J. J., *Proceedings,* Second International Conference on Soil Mechanics and Foundation Engineering, Rotterdam, Vol. 7, 1948, pp. 47–49.
[11] Miura, S., and Toki, S., *Soils and Foundations,* Vol. 22, 1982, pp. 61–77.
[12] Ishihara, K., and Towhata, I., *Soils and Foundations,* Vol. 23, 1983, pp. 11–26.
[13] Lee, K. L., and Seed, H. B., *Journal of the Soil Mechanics and Foundations Division, American Society of Civil Engineers,* Vol. 93, No. SM1, 1967, pp. 47–70.
[14] Finn, W. D. L., Pickering, D. J., and Bransby, P. L., *Journal of the Soil Mechanics and Foundations Division, American Society of Civil Engineers,* Vol. 97, No. SM4, 1971, pp. 639–659.
[15] Chaney, R., and Mulilis, P. J., *Geotechnical Testing Journal, ASTM,* Vol. 1, No. 2, 1978, pp. 107–108.
[16] Lee, K. L., and Fitton, J. A., *ASTM STP 450,* American Society for Testing and Materials, Philadelphia, 1968, pp. 71–95.
[17] Seed, H. B., *Journal of the Geotechnical Engineering Division, American Society of Civil Engineers,* Vol. 105, No. GT2, 1979, pp. 201–255.
[18] Castro, G., *Journal of the Geotechnical Engineering Division, American Society of Civil Engineers,* Vol. 101, No. GT6, 1975, pp. 551–569.
[19] Peck, R. B., *Journal of the Geotechnical Engineering Division, American Society of Civil Engineers,* Vol. 105, No. GT3, 1978, pp. 393–398.

Test Interpretation and Errors

John T. Germaine[1] *and Charles C. Ladd*[1]

STATE-OF-THE-ART PAPER

Triaxial Testing of Saturated Cohesive Soils

REFERENCE: Germaine, J. T. and Ladd, C. C., "**Triaxial Testing of Saturated Cohesive Soils,**" *Advanced Triaxial Testing of Soil and Rock, ASTM STP 977,* Robert T. Donaghe, Ronald C. Chaney, and Marshall L. Silver, Eds., American Society for Testing and Materials, Philadelphia, 1988, pp. 421–459.

ABSTRACT: The paper first covers common problems with testing equipment and procedures that cause errors in the measured properties of the soil specimen, with emphasis on consolidated-undrained (CU) and consolidated-drained (CD) triaxial tests. These problems are divided into three categories: errors that can be handled via appropriate corrections; errors that must be avoided; and potential errors that must be evaluated when selecting test procedures or interpreting measured data, the most important being the nonuniform stresses and strains caused by frictional end caps. The paper then assesses the use of triaxial testing in practice to predict undrained stability and deformations for saturated cohesive deposits. Based on considerations of strain rate effects, soil anisotropy, disturbance from tube sampling, and results from case histories of failures, the authors make four recommendations.

1. UU compression tests should not be used as the principal means of estimating in situ undrained strengths because the values can be either significantly too high or too low.
2. CIU compression tests have little value because the measured undrained strength will be unsafe for stability analyses, and the stress–strain data do not simulate in situ behavior.
3. Therefore, more reliance should be placed on CK_oU compression and *extension* tests, which would be aided by the availability of more reliable and less expensive automated "stress path" triaxial cells.
4. Oedometer tests should always be conducted to ascertain the stress history of the deposit.

KEY WORDS: triaxial test, cohesive soils, laboratory testing equipment, testing procedures, corrections, testing errors, undrained strength, anisotropy, sample disturbance, strain rate, stress–strain

Triaxial testing of solid, cylindrical soil samples started during the 1930s [*1*] and evolved to widespread use of equipment similar to that illustrated in Fig. 1. The triaxial apparatus is the principal laboratory shear device used in geotechnical engineering practice for measuring the stress–strain–strength properties of natural cohesive soils and of compacted soils. Triaxial testing is also widely used in research to study basic soil behavioral issues, such as the influence of stress–strain history, strain rate and creep, cyclic loading, and so forth. As with all forms of soil testing, users of the triaxial test should be thoroughly familiar with two potential problems:

1. Regarding the test equipment and procedures per se, do the measured data reflect the

[1] Lecturer and director of the geotechnical laboratory and professor of civil engineering, respectively, Department of Civil Engineering, Massachusetts Institute of Technology, 33 Massachusetts Ave., Cambridge, MA 02139.

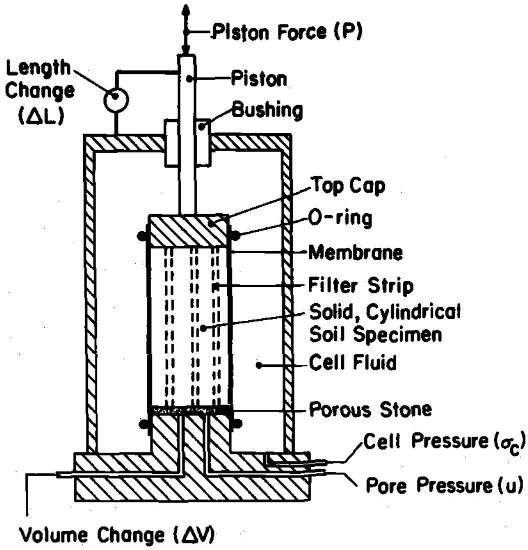

FIG. 1—*Schematic of conventional triaxial test for cohesive soils: components and measurements.*

actual properties of the test specimen under the intended boundary conditions of stress, strain, and drainage?

2. Regarding use of the data in engineering practice, do the properties of the test specimen (even if accurately measured) reflect the in situ behavior of the soil under field conditions?

This paper addresses both questions, but within a framework restricted to triaxial testing of *saturated cohesive* soils and further limited to consideration of stress–strain data from monotonic shearing beyond the "elastic" region (say axial strains greater than 0.1%) and before reaching large postpeak strains associated with the "residual" condition. After summarizing background information regarding basic types of shear tests, conventional triaxial testing procedures and equipment, and error evaluation, the paper gives a fairly comprehensive overview of common problems and typical errors involved with triaxial testing (see the first question cited above). Although essentially all of these potential complications have been well documented in the literature for over 20 years, too many laboratories unfortunately still do not appreciate their impact on measured results. The paper then focuses on the use of *undrained* triaxial testing in design practice (see the second question). Here, the authors draw on more recent information concerning sample disturbance, anisotropy, and strain rate effects to conclude that two common forms of triaxial testing should be largely discontinued and greater emphasis should be placed on performing anisotropically consolidated triaxial compression and *extension* tests.

This paper is not intended to be a scholarly treatise on triaxial testing. Rather, the authors hope to clearly identify ways of avoiding sources of major errors in obtaining triaxial test data on saturated natural and compacted cohesive soils, and give clear guidance on how triaxial testing can be better used for undrained stability problems involving natural cohesive soil. As will be seen, improved techniques for automated testing will greatly benefit the second objective.

Background

Types of Triaxial Shear Tests

The two major variables that can be controlled in the triaxial test are the boundary drainage conditions and the imposed stress path (meaning changes in the axial and radial stresses, σ_a and σ_r, respectively). The first variable leads to the three well-known types of shear tests classified according to the drainage conditions existing during application of the confining stress(es) and then during shear. They are:

(1) consolidated-drained = CD test
(2) consolidated-undrained = CU test
(3) unconsolidated-undrained = UU test

where the first letter designates either complete or zero consolidation under the preshear confining stresses and the second letter obviously denotes either fully drained (no *excess* pore water pressure) or no drainage during the shearing portion of the test. (Note: some refer to these as Q, R, and S tests in reverse order, respectively.)

CD and CU tests will typically have a back pressure of several atmospheres or more, which must be used to achieve complete saturation of the specimen and drainage lines. They may also employ anisotropic preshear consolidation stresses, defined by $K_c = \sigma_{rc}'/\sigma_{ac}'$, leading to notation such as CID for an isotropically consolidated drained shear test and CK_oU for a one-dimensionally ($K_c = K_o$) consolidated undrained shear test. In contrast, UU testing always uses an isotropic preshear confining stress because $\sigma_a \neq \sigma_r$ inherently causes undrained shearing because the test should never allow any drainage. However, some laboratories report results from so-called back pressured UU tests. This practice contradicts accepted basic terminology because such tests actually constitute CIU tests with an unspecified (unknown) preshear consolidation stress.

The triaxial cell configuration requires that failure occur either in *compression* (axial compression) with $\sigma_a = \sigma_1 > \sigma_r = \sigma_2 = \sigma_3$ or in *extension* (axial extension) with $\sigma_r = \sigma_1 = \sigma_2 > \sigma_a = \sigma_3$, where σ_1, σ_2, and σ_3 denote the principal normal stresses. These two failure modes involve both a change in the direction of the major principal stress at failure (that is, vertical for compression and horizontal for extension) and in the *relative* magnitude of the intermediate principal stress as reflected by the value of $b = (\sigma_2 - \sigma_3)/(\sigma_1 - \sigma_3)$ (that is, $b = 0$ and 1 for compression and extension, respectively). This fact complicates assessment of stress–strain–strength anisotropy, as discussed later. However, the real virtue of the triaxial test lies in the variety of stress paths that can be followed during both consolidation and shearing. Figure 2 gives representative examples of drained paths starting from a normally consolidated K_o condition, where $q = 0.5(\sigma_a - \sigma_r)$ and $p' = 0.5(\sigma_a' + \sigma_r')$ will be used in the paper to define the state of stress in triaxial samples. The compression-loading [C(L)] and extension-unloading [E(U)] can be easily followed by simply increasing and decreasing the piston force in Fig. 1, usually by controlled axial deformation. The C(U), E(L), isotropic unloading–loading [I(U/L)] stress paths are somewhat more complex because changes in the cell pressure also affect the axial stress, and these tests generally must be stress- rather than strain-controlled. The K_o stress paths, while conceptually simple, require, in reality, either considerable effort or special automated controls as will be described when discussing triaxial testing in engineering practice.

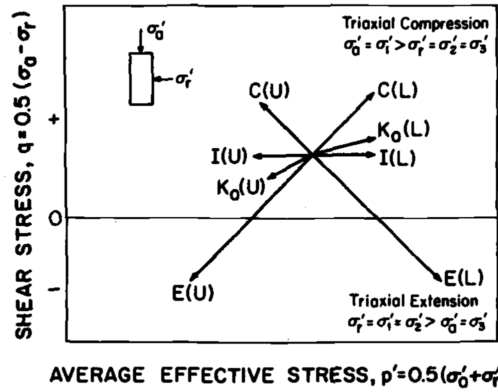

FIG. 2—*Examples of applied effective stress paths during drained triaxial testing.*

Testing Steps and Measurements for CD and CU Testing

The triaxial testing process, like any other shear testing procedure, can be divided into six distinct operations as outlined in Table 1. Each operation has a specific purpose and must be carefully evaluated with respect to the possible sources and consequences of errors. (Note: this paper assumes that pore pressures will be measured in all CU tests.)

The specific details involved in the preparation of a specimen (Operation A) depend on the material type, stress history, and equipment design. While the details vary considerably, the purpose is to define a specimen for subsequent testing. Undisturbed specimens must be trimmed to the required shape without change in water content or structure. In addition, it is usually necessary to remove any disturbed material created during sampling. Reconstituted specimens must have a uniform known density. After specimen preparation, sufficient information (except the weight of solids) must be collected to define completely the phase state and specimen dimensions.

The specifics of assembling (Operation B) vary with the equipment and soil type. The specimen must be mounted in the triaxial cell in such a manner that its condition (geometry, stress state, water content) remains unchanged. Different methods [*2–4*] are required for:

(1) very weak soils which require continuous support
(2) soft soils with low suction potential, and
(3) stiff soils with high suction potential.

At the end of the mounting procedure, a full set of reference readings is required for use in all subsequent calculations of strain and stress.

Obtaining complete saturation (Operation C) of both the specimen and the apparatus is important for CD tests and essential for CU tests or when measuring rates of consolidation. Complete saturation is not necessary if only magnitudes of deformation are required during consolidation (or drained shear) and sufficient time is provided for drainage. However, substantial errors in volume change may result if the degree of saturation increases with time (for example, when specimens are saturated after consolidation). During undrained shear, any macroscopic air within the control volume (specimen and pore pressure measuring system) will change in volume due to changes in pore pressure, resulting in partial drainage. In turn, partial drainage changes the effective stress of the specimen and may also significantly affect the measured pore pressure. The process of saturation, which requires a balance between time and damage to the specimen, is usually achieved by simultaneously increasing

TABLE 1—*Triaxial testing process for CD and CU shear tests.*

Operation	Purpose	Measurements	Results
A. Sample preparation			
i. Natural soil Sample Trim	i. Remove from in situ, form appropriate size, determine specimen state.	Dimensions, weights	Phase relations (w, γ, S, e) Initial dimensions
ii. Reconstituted Compact, press	ii. Prepare a specified size at known *state*: density, fabric, etc.		
B. Assemble apparatus	Put specimen in physical environment without change in *state*.	Zero measuring devices for load deformation, volume, pressure	Set of reference (zero) values for devices
C. Saturate	Increase pore pressure at constant σ' to drive air into solution and prevent cavation.	Stress state B parameter value	Water intake Change in dimensions Check on $S \leqslant 100\%$
D. Consolidate	Change stress system to desired preshear condition.	Stress state Change in specimen geometry	Stress–strain characteristics
E. Shear	Measure stress–strain behavior.		
F. Disassemble apparatus	Remove stresses and measure final specimen *state*.	Final measuring devices Specimen dimensions Weights	Phase relations Water migration Measuring devices Checkpoint

the cell pressure and back pressure in steps such that the effective stress remains constant. This process, which should always include measurements of Skempton's B parameter ($= \Delta u/\Delta\sigma_c$), is discussed further in the section entitled "Saturation."

The processes of consolidation and shear have very similar features and will be the primary topics of this paper. In essence, these processes amount to changes in the stress state while allowing drainage (consolidation or drained shear) or preventing drainage (undrained shear). The many technical issues to resolve or understand in order to obtain accurate stress–strain characteristics will be discussed in the section entitled "Problems, Errors, and Corrections."

Finally, after the specimen has been sheared it must be removed from the apparatus. Operation F should focus on cross checking and evaluation, not preparation for the next test. In particular, the specimen dimensions should be recorded to compare with computed values; the specimen should be sketched, examined, and sectioned to evaluate water content variations and obtain the dry weight; and the reference values of all measuring devices should be recorded and compared to initial values.

The quintessence of the triaxial specimen is its simplicity in geometry and stress state. In 1940, Taylor [5] recognized the potential of Kjellman's [6] true triaxial apparatus, but considered the simplicity of the cylindrical specimen more valuable for investigating soil behavior. Obviously, the profession agreed. But even this simple geometry (Fig. 1) requires five measurements during testing: piston force, cell pressure, pore pressure, axial deformation, and volume change (occasionally augmented by measurements of radial deformation).

Transfer functions, as summarized in Table 2, must then be used to convert these data to relevant engineering parameters. All involve calibration factors (for example, correlation between recorded voltage and resultant force or pressure or length), and several also include correction for the effects of piston friction, presence of filter strips and specimen membranes, and so forth. Uncertainties, such as specimen nonuniformity, imperfect stress application, and changes in specimen geometry, create further complications. As a result of the above factors, these engineering parameters are approximate average values for the simple idealization.

Error Evaluation

An evaluation of errors should be an important aspect of all experimental investigations. However, the geotechnical engineer traditionally has not done this, presumably based on the common belief that soil variability dominates most measurements and hence negates this aspect of a rational, scientific approach. Nevertheless, the authors believe that all users and generators of experimental data should appreciate and understand certain basic concepts (terminology) regarding different sources of error, both to improve testing practice and for

TABLE 2—*Transfer functions to convert triaxial test measurements to engineering parameters.*

Test Measurements (Fig. 1)	Transfer Function	Engineering Parameter
Piston load (P)	F(calibration, area, cell geometry, correction)	σ_a
Cell pressure (σ_c)	F(calibration, correction)	σ_r
Pore pressure (u)	F(calibration)	u
Axial deformation (ΔL)	F(calibration, correction)	ϵ_a
Volume change (ΔV)	F(calibration)	ϵ_v
Radial deformation (not shown)	F(calibration)	ϵ_r
Specimen dimensions and weights	Phase relations	w, e, S, γ_t, γ_d

general perspective. Specifically, one needs to differentiate between three basic sources of error:

(1) *precision*, which expresses the basic scatter in the measurements and is a measure of *repeatability*;

(2) *accuracy*, which expresses the closeness of the measured mean value to the actual value and is a measure of *bias*; and

(3) *resolution*, which reflects the smallest detectable measurement unit and is a measure of *readability*.

Figure 3 illustrates these important differences by the location of holes in targets at a shooting range. Case (a) represents results from a nonexpert using a "good" rifle, which gives significant scatter about a mean lying not far from the center objective. Case (b) reflects results expected from an expert burdened with a poorly calibrated rifle, thus giving little scatter, but all holes have significant bias (deviation from the center). Finally, cases (c) and (d) illustrate results from an expert having "good" rifles of different vintage, say comparing natural vision versus a telescopic lens. From these simple examples, it should be obvious that accuracy is far more important than precision given several data points. And in our age of electronics, the measurement devices should have a resolution (readability) several times smaller than the precision justified by the overall accuracy.

Problems, Errors, and Corrections

Introduction

The function of the triaxial apparatus is to measure the stress–strain–strength characteristics of a cylindrical specimen. In almost all applications the specimen is idealized as a simple element. This section of the paper will review the problems that arise when the conceptually simple element is transformed into the reality of a triaxial specimen with its complex boundary conditions. These problems are most conveniently separated into three categories: corrected using approximate analysis, avoided by experimental design, and evaluated when selecting procedures or interpreting data (Table 3). The correctable problems

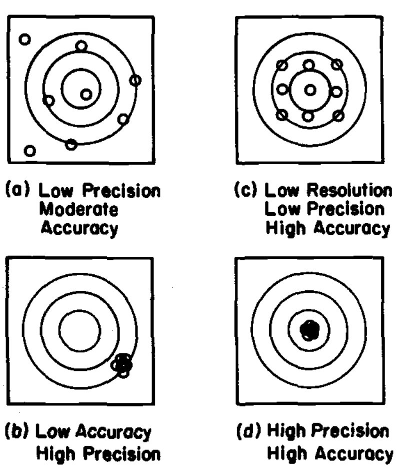

FIG. 3—*Illustration of basic terminology used to evaluate errors.*

TABLE 3—*Sources of problems during triaxial testing.*

	Item of Concern	Engineering Parameter[a]								Type of Test[b]		
		q	σ_a	σ_r	u	ϵ_a	ϵ_v	ϵ_r	e	UU	CU	CD
CORRECT	1. Sensors	C	C	C	C	C	C	C		√	√	√
	2. Apparatus stiffness					C	C				√	√
	3. Membrane resistance	C	C	C						√	√	√
	4. Filter drain resistance	C	C								√	√
	5. Piston friction/uplift	C	C							√	√	√
	6. Specimen geometry	C,N	C,N			N	N	N	N	√	√	√
AVOID	7. Tilting/seating	A,N	A,N			A,N				√	√	√
	8. Saturation				A		A				√	√
	9. Temperature	A,D	A,D		A,D		A,D			*	*	√
	10. Water leakage				A		A		A	*	√	√
	11. Gas leakage				A		A		A	*	√	√
EVALUATE	12. Frictional ends	A,D,N	A,N	A,N	A,D,N	A,N	A,D,N	A,N	A,D,N	*	*	√
	13. Rate of loading[c]				A,D,N		A,D,N		A,D,N	*	*	√
	14. Rupture surfaces	A,N	A,N		A,N		A,N		A,N	√	√	√

[a] A = Must avoid/control; C = Correction required; D = Magnitude depends on soil, must evaluate; N = Nonuniform condition.
[b] √ = Consider; * = Consider if measure u.
[c] For rate-independent material.

(Items 1 to 6 in Table 3) are by no means definitively eliminated. However, these are problems for which approximate analyses have provided numerical results to apply to the measurements, but that still contribute uncertainty in the results. All of these problems are side effects of necessary apparatus components. The avoidable problems (Items 7 to 11) relate to experimental details that cause uncorrectable errors. Results affected by such problems will contain a bias which *cannot* be removed. These problems are solved with proper analysis, elimination, and verification of results. The final category (Items 12 to 14), contains problems that are difficult to correct or avoid and hence must be evaluated when selecting testing procedures or interpreting data. These problems, if ignored or improperly analyzed, can lead to serious errors.

Table 3 presents the *direct* relationships between each problem and the various engineering parameters computed from the measurements. Secondary relationships, although not included in the table, can be equally important to the results. For example, if the pore pressure decreases due to an external leak, the shear stress, vertical stress, and void ratio will all be in error. These secondary relationships are discussed in subsequent sections. The more serious questions of inaccuracy arise due to nonuniform conditions within the specimen, frictional ends being a prime example. This is especially troublesome when the magnitude of the problem is material dependent.

Table 3 also indicates which problems are of importance to the three triaxial test types: UU, CU, and CD. Tests that require pore pressure measurements and/or extended testing times (several days) will require more meticulous attention to the avoidable problems.

Sensors

All measuring devices (sensors) require calibration and should be evaluated in terms of precision and resolution. Proper calibration will make the device accurate. Figure 4 presents an exaggerated schematic of the four parameters commonly used to quantify the performance of a sensor [7]. Stability is the change in output at zero load over time, the magnitude of this zero drift being a function of the device construction (type) and environmental changes (temperature, moisture, corrosion, and so forth). Nonlinearly, hysteresis and repeatability

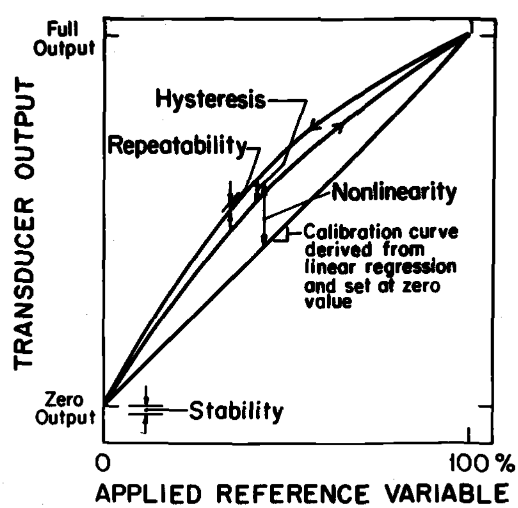

FIG. 4—*Parameters used to quantify the performance of a sensor.*

quantify variations in output as a function of "loading" history. The precision of a sensor will depend on the particular application. For instance, stability should dominate device selection for testing over long periods of time, whereas hysteresis becomes most important for cyclic loading. Resolution is inherent to the device and is specified by the manufacturer.

Mechanical sensors, like load (proving) rings and pressure gauges, have relatively poor performance curves. Such devices must be carefully calibrated and checked before each test program. Nonlinear calibration curves are often necessary to provide reasonable accuracy over the full device range. Mechanical devices may also have undesirable side effects (for example, the compressibility of a load ring causing pronounced variation in the strain rate during loading and strain softening).

Electronic sensors (transducers) have better performance characteristics and fewer side effects, facilitate automatic data logging, and, hence, have largely replaced mechanical sensors in many laboratories. Although most transducer performance specifications exceed our present conventional testing requirements, one should recognize and evaluate the following potential problems:

(1) changes in the performance characteristics due to age, overloading, or corrosion;
(2) the stability of the power supply because the output voltage will be a function of input voltage; and
(3) the performance characteristics of the electronic measuring system (A/D converter, voltmeter, recorder, and so forth).

Typical values for hysteresis, nonlinearity, and repeatability are less than 0.5% of the transducer's capacity. Therefore, linear calibration factors are generally sufficient when working above 10% of the sensor capacity. With sensors having infinite resolution, the dominant performance characteristics will depend on the data recording systems. Finally, electronic sensors have minimal side effects (for example, force and pressure transducers are very rigid).

Apparatus Compressibility

The problem of apparatus compressibility must be explicitly addressed only when testing stiff soils, using very coarse porous stones, requiring small strain response, or using lubricated ends. Calibration curves should be developed relating force and deflection (or pressure and volume) when compressibility can affect axial and volumetric strains. Viscous flow of the grease used with lubricated ends is likely to preclude small strain measurements.

Membrane Resistance

The rubber membrane surrounding the specimen transmits the radial effective stress to the soil grains and establishes the boundary between the cell fluid and pore fluid. The membrane also resists specimen deformation. Henkel and Gilbert [8] originally developed a membrane correction applied to the deviator stress for undrained compression tests. Duncan and Seed [9] extended this work to include the effect of both axial and volumetric strains. The corrections applied to both axial and radial stresses are based on shell theory and assume isotropic linear elastic rubber, with Poisson's ratio of 0.5, continuous support without buckling and uniform cylindrical deformation. The following corrections are approximations of this solution [10].

$$\Delta F_a = -\pi D_{im} t E\left(\epsilon_a + \frac{2}{3}\epsilon_v\right) \quad (1)$$

$$\Delta\sigma_r = 2tE\left(\frac{D_i - D_{im}}{D_i D_{im}}\right) - \frac{4tE}{3D_i}(\epsilon_v) \quad (2)$$

where

t = initial membrane thickness
E = Young's modulus of rubber (≈1400 kPa)
D_i = initial specimen diameter
D_{im} = initial unstressed membrane diameter
ϵ_a = axial strain
ϵ_v = volumetric strain

The axial correction (ΔF_a) is expressed in terms of force so it can be combined with various area corrections. However, the correction is based on the assumption that the specimen remains a right cylinder. Bulging will likely cause a more substantial error in the radial stress than the axial stress correction. The radial stress is corrected for the initial seating of the membrane (first term, Eq 2) and whenever volume change occurs. The initial membrane diameter should be within 10% of the specimen diameter. A reduction in axial stress of 2.5 kPa would be applied to a 10-cm^2 specimen encased by two prophylactic membranes at 10% strain during undrained shear.

Bishop and Henkel [11] present a detailed description of a method to measure the membrane modulus that assumes equal compressive and tensile moduli. Young's modulus, E, is computed by dividing the extension modulus, M, by the initial thickness of the membrane.

Filter Drain Resistance

Filter drains around cohesive specimens accelerate drainage during consolidation (or drained shear) and equalization of excess pore pressure during undrained shear. They are commonly used with frictional ends and always with lubricated ends. The efficiency of the drains is an important issue [12], especially when using measurements during consolidation to compute coefficients of consolidation. The present discussion addresses the influence of the drains on the stress state for two configurations: vertical drains for compression tests, and spiral drains for either compression or extension tests. (Note: although double spirals have been used, they are not recommended unless each spiral is independent.)

The vertical drains carry increasing load until they apparently buckle between 2 or 3% axial strain. The maximum correction [11] applied to the axial force, based on comparative tests on specimens with and without drains, is

$$\Delta F_{am} = -k_{fp} P_{fp} \quad (3)$$

where

k_{fp} = force per perimeter of filter paper (1.3–1.9 N/cm for Whatman #54)
P_{fp} = perimeter of paper

The correction linearly increases from zero to ΔF_{am} at 3% axial strain as referenced to the initial specimen dimensions and is constant thereafter. A typical maximum correction would be 8 kPa for a 10-cm^2 specimen with eight 0.6-cm-wide vertical drains. Spiral drains are assumed to be perfectly flexible and hence require no correction [*2*]. The recommended inclination of the drains is 1:1.3 (vertical:perimeter) for compression tests and 1:1.5 for extension tests [*2*].

An additional consideration when consolidating a specimen with radial drainage is the development of a structural shell in the outer portion of the specimen. This can be especially important when using large consolidation increments and lubricated ends [*13*]. Atkinson [*14*] also reports that radial consolidation and fast loading rates can result in large variations in water content across the specimen.

Piston Friction

Piston friction can potentially cause an important error of unknown magnitude. It occurs within the seal of the triaxial cell and is a function of the type of bearing, type of seal, and lateral force acting on the piston. Two types of bearings are commonly used in triaxial cells: solid and linear ball bushings. Solid bushings, while still common in practice, have a poor performance record. Figure 5 [*15*] plots the net friction (increase in force due to lateral force) force versus lateral force applied to the shaft as it is pushed into the bushing. The stationary solid bushing, in addition to having a high static friction (the stick slip phenomenon), can develop a net dynamic frictional resistance equal to the lateral load. *Ball bushings* dramatically reduce this problem. In fact, the additional frictional force shown in the figure is attributed to the seal friction. The three best performing systems are the rotating solid bushing, the air-sealed ball bushing [*16*], and the ball bushing with a rolling diaphragm seal [*17*]. The rotating solid bushing maintains a high rate of movement which prevents static friction buildup and reduces the vertical frictional component by the ratio of the vertical to

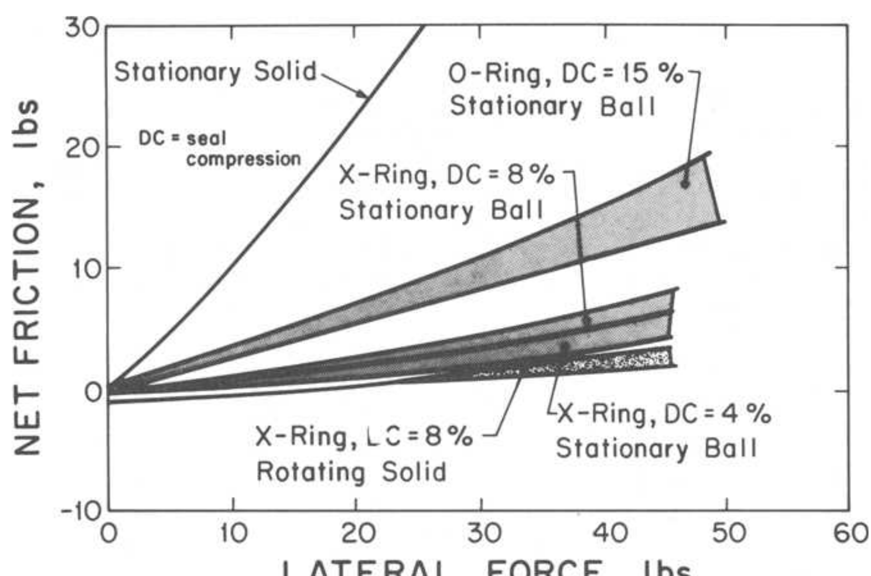

FIG. 5—*Sensitivity of typical piston seals to lateral force* [15].

horizontal displacement rates of the piston. However, the design is complex, and the connection details require careful consideration. The air bushing system bleeds air through a low clearance seal. The air pressurizes the cell fluid and limits friction to the drag force of the air passing through the opening, but has the disadvantage of applying air pressure directly to the cell fluid (see the section entitled "Gas Leakage"). The diaphragm seal has *low friction* characteristics, but rather limited displacement capability.

Table 4 compares the various options. Because the lateral force is unknown during a test, one cannot formulate reliable corrections for stationary bushing systems and they should not be used without internal force measurements. The ball and rotating solid bushing types can provide reasonable accuracy after making a friction correction, which should be obtained by measuring the force required to push the piston in and out of the cell at various pressures and displacement rates. The friction force will be equal to one half the difference between pushing in and pulling out the piston. Such a calibration also provides values of the piston uplift force which is equal to the effective piston area times the cell pressure. This value can be computed as the average of the force required to push in and pull out the piston.

Area Corrections

The axial stress is computed by dividing the piston force (minus corrections for friction, uplift, membrane, and so forth) by an effective area. Because the specimen often deforms substantially during both consolidation and shear, it is necessary to compute a corrected area based on the initial area, the measured axial and volumetric deformations, and an assumed deformation pattern. It is most common to assume that the specimen deforms as a right cylinder (that is, the ideal case for a specimen with frictionless ends). This is often reasonable during consolidation and even during shearing with lubricated platens. However, with frictional ends, the computed area at large axial strains will differ substantially from the actual area in the central portion of the specimen.

In the case of compression tests, the actual cross section will be larger than the computed section, leading to an overprediction of the axial stress. During extension tests, the actual area will be less than that computed, and the axial stress will be underpredicted. The paper focuses on area corrections for specimens that deform "uniformly." Analysis of data obtained on specimens with rupture surfaces requires further research.

Alternate corrections exist when the specimen deforms as a parabola or bulges (Fig. 6). The parabolic correction (developed explicitly for undrained conditions) assumes that the

TABLE 4—*Comparison of various bushing designs used for triaxial testing.*

Type of Bushing			Friction	Sensitivity to Lateral Load	Sensitivity to Disp. Rate
Solid	Stationary	Oil	Moderate	Very high	Stick/slip
		O-/quad ring	High	Very high	
	Rotating	Oil O-/quad ring	Low	Low	Low
Ball	Stationary	O-/quad ring	Moderate	Moderate	Stick/slip
		Rolling diaphragm	Low	Low	Low
		Air	Low	Low	Low

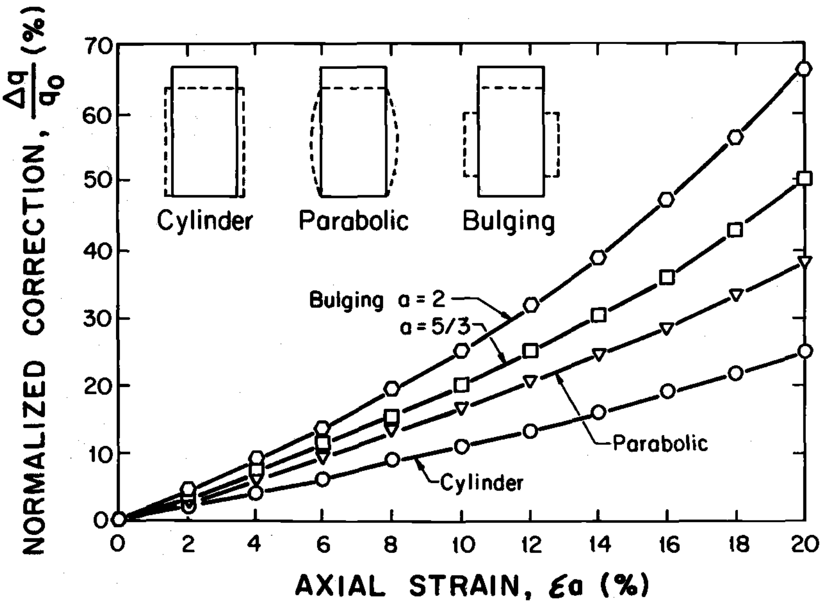

FIG. 6—*Influence of area corrections on computed shear stress for constant volume triaxial compression.*

specimen deforms as a barrel, the area being computed at the largest midplane section. The bulging correction assumes the strains to be concentrated in the central portion of the specimen. The following equations [*18*] apply to the three deformation modes (compressive strains are positive):

$$A_c = A_o \left[\frac{1 - \epsilon_v}{1 - \epsilon_a}\right] \quad \text{cylindrical} \tag{4}$$

$$A_c = A_o \left[-\frac{1}{4} + \frac{\sqrt{25 - 20\epsilon_a - 5\epsilon_a^2}}{4(1 - \epsilon_a)}\right]^2 \quad \text{parabolic} \tag{5}$$

$$A_c = A_o \left[\frac{1 - \epsilon_v}{1 - a\epsilon_a}\right] \quad \text{bulging} \tag{6}$$

where

A_o = area corresponding to zero strain
a = experimental constant, normally between 1 and 2

For the bulging correction, the value of a can be approximated as the ratio of the length of the specimen to the length of the bulging zone. Figure 6 shows the differences in the normalized correction ($\Delta q/q_o$) for various formulas during undrained triaxial compression. The normalized correction is the reduction in shear stress (also equal to percent increase in area) due to the area correction. The figure clearly illustrates the importance of selecting the most appropriate area correction (for example, the difference between the parabolic and cylindrical correction being 6% at 10% strain). Hence, the cylindrical assumption overpredicts the strength by about one-half the axial strain for specimens that form a barrel-like shape. This error can become substantially larger when localized bulging occurs. The most appropriate choice of correction should be based on the observed geometry of the specimen and then compared to that measured at the end of the test.

Relative Importance of Typical Corrections

The foregoing presented typical corrections which must be considered, checked, or applied to triaxial data. Some corrections are too device-specific (for example, piston friction) to quote universal values, while others (for example, vertical filter strips) can be quantified for general use. However, all involve uncertainty (both precision and accuracy), and one should consider the impact of potential errors on the measured parameters. The results in Fig. 7 illustrate their relative importance for the following assumed conditions: undrained compression of a 10-cm^2 specimen with two prophylactic membranes, eight 0.6-cm-wide vertical drains of Whatman #54 paper, 5 N of piston friction (presumed to act at negligible strain), and the cylindrical area correction. The strain contours in Fig. 7*a* show that the total correction increases progressively with strain. For measured strengths above 200 kPa, the corrections are reasonably small (<15% at 10% strain). However, as the strength decreases, the corrections quickly dominate (for example, a correction of 90% at 10% strain for a measured strength of 10 kPa). Figure 7*b* shows the relative importance of the various components at 5% strain. The area correction dominates for measurements above 200 kPa and is independent of strength. The remaining corrections become very important for weak soils leading the Norwegian Geotechnical Institute [*19*] to develop the paraffin method. Also note that these corrections must be minimized because of their approximate nature and not their magnitude.

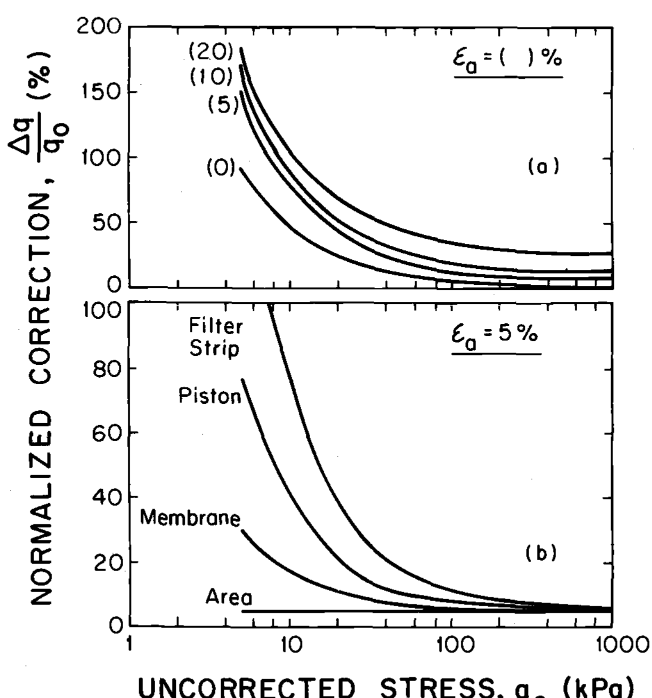

FIG. 7—*Influence of various corrections on computed shear stress for constant volume triaxial compression.*

Seating and Tilting

Imperfect matching of the specimen with the top and bottom caps or the top cap with the piston can cause substantial errors. The first problem, referred to as a bedding error, is caused by rounded, irregular specimen ends, specimens that are not right cylinders, rough stones, or warped stones. Nonparallel ends cause particularly large errors in strain measurements when using fixed top caps which cannot rotate to match the specimen. Bedding imperfections result in excessive deformation [*20*] at early stages of loading, causing large errors in the initial modulus and may even affect the strength of stiff materials due to nonuniform loading.

Specimen ends should be trimmed to be perfectly flat and parallel, several devices being available to facilitate this operation. The split tube jig suggested by Ladd and Dutko [*16*] has proven satisfactory and is easy to fabricate. Minor bedding imperfections can be removed by consolidating the specimen prior to shear and using the fixed top cap design which eliminates the problem of top cap rotation during consolidation and shear. However, the fixed top cap system should not be used with very stiff specimens because the ends are never perfectly parallel and large stress concentrations will result.

The problem of tilting arises from imperfect specimen trimming; misalignment between the piston, top cap, and specimen; and tilting during consolidation due to nonuniformity within the specimen. Tilting can cause large apparent axial deformation during the early stages of loading as with bedding errors. With continued loading, the top cap can be pushed horizontally which increases piston friction (with solid bushings), applies a bending moment to the specimen, and thus reduces the measured strength. If tilting becomes too severe, the test must be terminated. Proper alignment is best maintained by consolidating specimens with the piston and top cap in contact, a rigid connection being preferred to also eliminate top cap rotation.

Saturation

Complete saturation of the entire system (specimen, porous stone(s), drainage lines, and so forth) is desirable for accurate measurements of volume change based on recorded water inflow and outflow during consolidation and shearing, and absolutely essential for reliable data during undrained shear (unless one varies the cell pressure to maintain a constant pore pressure during shear). When pore water fluid is used to measure or control changes in the specimen volume, the presence of macroscopic gas will create errors that depend on test type and specimen stiffness. During drained conditions, the error in measured volume change can be large if the degree of saturation is low, the fluid pressure changes, or the gas/liquid phase is out of equilibrium. Undrained tests require an incompressible pore fluid to assure conditions of no volume change. An unsaturated specimen will follow a partially drained stress path, altering the stress–strain–strength and pore pressure behavior. For contractive soils, partial saturation will often cause significant errors in measured effective stresses whereas dilatant soils may undergo significant volumetric expansion, which can, in the limit, result in a drained condition.

Saturation is achieved by increasing the specimen's pore pressure (referred to as back pressuring) to drive any macroscopic gas into solution. Insufficient measurements are collected during saturation to compute volume changes of the specimen. Therefore, the process must be performed at a constant effective stress which has been equilibrated prior to changing the pore pressure. Thus, the measured water inflow will be mainly due to increasing saturation rather than geometry changes. The post saturation volume is computed from the measured length change and the presaturation area.

The specimen should be saturated under the sampling effective stress, σ_s', whenever possible. This value can be estimated from oedometer data on adjacent specimens or measured directly when using a wet mounting method. Back pressuring at an unequilibrated effective stress above or below σ_s' will result in consolidation or swelling, respectively. The magnitude of the volume change depends on the soil stiffness and stress deviation. When σ_s' is very low (<10 kPa), it may be necessary to isotropically consolidate the specimen to a more workable stress prior to back pressuring.

The saturation process is based on a combination of compression of gas (Boyle's law) and solution of gas (Henry's law). The pressure required for full saturation [*21,22*] depends on the initial pressure, initial degree of saturation, the nature of the gases, and the time provided for saturation. The applied back pressure should equal the saturation pressure plus the maximum negative pore pressure induced during shear so that the absolute specimen pore pressure never drops below the saturation pressure. Note that the shear induced pore pressure depends on both the stress path and overconsolidation ratio of the specimen. A back pressure of 200 to 300 kPa is typical for a nominally saturated soft clay.

The actual saturation process occurs by simultaneously increasing the cell pressure and back pressure, both pressures being applied to the boundaries of the specimen. While the increment in cell pressure acts immediately throughout the specimen, water must flow through the specimen to replace dissolved gas, and hence the rate of pore pressure increase depends on the amount of gas and the permeability of the soil. Therefore, the rate of pressure application should be controlled in order to minimize effective stress increases within portions of the specimen. One of the three back-pressuring procedures should be followed.

1. Apply both pressures in small increments and monitor water inflow. The acceptable rate of inflow will be material-dependent (stiffness and degree of saturation) and hence this approach requires considerable experience.
2. Apply both pressures in small increments with single ended drainage to monitor the pore pressure response at the closed end. This will be slow, but safe, because the effective stress gradient is known.
3. Apply the cell pressure without drainage, measure Skempton's B factor ($\Delta u / \Delta\sigma_c$), then apply back pressure and allow time for drainage. This is optimal because the cell pressure increment can be maximized to the limit of reasonable changes in effective stress.

Temperature

Although variations in temperature generally affect triaxial data, precise temperature control is either expensive or cumbersome. Therefore, one should determine the required temperature control for a given application. Measurement variations as a result of temperature change can be caused by:

(1) changes in the output of measuring devices at constant load, these being a function of sensor type as expressed as a percentage of capacity;
(2) differences in the thermal expansion coefficients of the various materials (water, soil, steel, etc.), which are generally dominated by the behavior of water; or
(3) the thermal coefficient of the soil skeleton, which causes a decrease in volume with increases in temperature [*23*] and is material-dependent.

While it is relatively easy to measure a sensor's temperature sensitivity, it is nearly impossible to apply accurate corrections to data because of the transient nature of temperature variations. Therefore, the problem must be minimized by careful sensor selection and adequate temperature control.

Measurements made during triaxial tests fall in two general categories: deformations at constant stress, and stresses (or forces) at constant deformation (or deformation rate). Deformation measurements are primarily affected by the differences in thermal strains of the various materials. Deformation variation during conventional room temperature control of ±2°C will become important only when measuring small strain behavior (<0.1%) and creep rates. Otherwise, routine measurements of volume change and axial deformation will not require more careful temperature control.

During controlled deformation conditions, the stress variations as a result of temperature are the product of differences in thermal strains and material stiffnesses. The main effect during undrained tests is pore pressure variations which in turn produce changes in effective stress. This variation is amplified by opposite thermal coefficients of the pore fluid and soil skeleton and by the high bulk modulus of water. Mitchell [*23*] quotes normalized pore pressure changes ($\Delta u/\sigma'$) of about 0.015 ± 0.005 per °C for several soft clays. These correspond to a ±3% change in effective stress for a ±2°C temperature fluctuation, which should be acceptable for routine testing. However, pore pressure changes in stiff soils can be several times larger and hence may necessitate closer temperature control. Although temperature fluctuations affect pore pressure during undrained shear and volume changes during drained shear, existing experimental data generally show minor effects on measured peak strengths, at least with relatively soft clays.

Water Leakage

Controlled drainage boundaries are an essential part of triaxial testing. Water leakage alters these intended conditions, the importance of which depends on the leakage location and rate, test duration, and soil stiffness. During undrained shear, water leakage changes the pore pressure and hence the effective stress path, stress–strain characteristics, and the measured strength. It leads to a partially drained test, the results of which *cannot* be corrected to equal undrained conditions. Proper control of leakage is so important that Poulos [*24*] refocused his doctoral studies from undrained rate effects to the control of leakage because the former was not possible without the latter. Water leakage becomes far less severe for drained tests because the measured volume change can be corrected for known rates of leakage.

One needs to distinguish between internal and external leakage. Internal leaks can occur within all pore pressure–drainage connections in contact with the cell fluid, at the membrane seals, and across the membrane itself. They always result in an increase in pore pressure or volume change because σ_c must be greater than u. The rate of leakage depends on the radial effective stress ($\sigma_c - u$), type and condition of the connections, the type and quality of the membrane, and osmotic pressure. Osmotic pressures caused by different pore and cell fluid compositions can develop very substantial seepage gradients. For example, sea water (35 g/L salt) as a pore fluid and distilled water in the cell produce an osmotic pressure of 1500 kPa. Internal leakage can be minimized by adjusting the cell fluid composition to reduce the osmotic pressure, using copper tubing for top drainage with O-ring seal connections and changing the cell fluid in contact with the specimen to mercury (in jacket) or castor oil.

External leaks occur at all connections and valves outside the cell and will decrease the pore pressure or volume change. They can be minimized by using copper tubing, ball valves, and soldering connections. However, leakage cannot be eliminated completely and will be proportional to the back pressure.

In general, water leakage must be measured directly and minimized by equipment design and maintenance. Leakage should be checked periodically by measuring flow rates (for drained tests) and pore pressure changes (for undrained tests) with a solid dummy in place of soil. Every membrane should be checked for holes. In addition, each test should be checked by one or more of the following methods.

1. Monitor the volume change during secondary compression. The rate should decrease linearly versus log time.
2. Close off the drainage line and monitor the pore pressure for one hour prior to shearing. The value of du/dt should decrease with time if caused only by arrested secondary compression.
3. Measure du/dt, as above, after shearing the specimen.

Gas Leakage

Leakage of gas into the specimen causes increases in pore pressure or volume change (similar to internal water leakage), but only if the gas actually forms macroscopic bubbles. Gas can enter the pore fluid by diffusion through the membrane from the cell fluid or through the drain lines from the back pressure system. After proper back pressuring, the existing gas should be dissolved in solution, with the pore fluid having a "gas deficiency" to allow the pore pressure to decrease during shear (and dissolve more gas from diffusion during the test) without developing bubbles. To maintain this condition for tests that last several days, gas–water interfaces should either be avoided or kept sufficiently far from the specimen. The ideal situation is to fill the cell with degassed water and apply both cell pressure and back pressure with mechanisms other than direct gas (mercury pot, screw jack, or gas–water separation).

However, more compact testing systems use gas–water interfaces close to the cell. When gas pressure is applied directly to the back pressure system (as with volume change devices that measure water levels in a standpipe), the gas will diffuse through the lines (within hours) and quickly equilibrate within the specimen. This gas will *not* form macroscopic bubbles unless the pore pressure decreases during the test (for example, undrained shear for all unloading stress paths and for a negative A parameter in loading tests (Fig. 2)). Once the fluid becomes saturated, a small decrement in pressure will cause bubble formation (outgassing).

In systems that apply gas pressure directly to the cell chamber (as with air bushing seals), the gas quickly dissolves into the cell fluid and begins to diffuse through the membrane to the depressed pore fluid. This gas, driven by the higher cell pressure, will come out of solution within the specimen causing increased pore pressure or volume change. Once macroscopic gas develops, the pore fluid compressibility also increases by several orders of magnitude [*25*]. Pollard et al. [*26*] report substantial effects from such diffusion after only one day.

When gas leakage is not prevented by equipment design, restrictions should limit the operating domain as follows.

1. The stress path should be chosen to prevent the pore pressure from decreasing during shear.
2. The total test duration should be limited to one day if gas pressure is applied to the cell chamber.
3. The B parameter should be measured before and after each test. This will identify partial saturation because B reduces significantly if gas bubbles develop within the specimen during the test.

Frictional Ends

In 1940, Taylor [5] wrote:

> The ideal type of shear test must be recognized as one wherein all strains are alike at all points of the sample at any instant during the test. This ideal probably can never be truly reached. . . . The strongest argument for the cylindrical compression test when it recently came into popularity was that it provided a closer approach to uniform conditions. Actually, however, the cylindrical type of test is still so far from the ideal that much could be gained if irregularities of strain could be reduced.

Taylor then went on to describe the problems associated with frictional ends which create a surface traction preventing radial deformation at the specimen ends. While this fact was appreciated in 1940 and has been extensively publicized since [*1,27–29*], the vast majority of tests are still performed with frictional ends. Why? Because efficiency in testing appears to be more important than uncertain errors.

In all tests, frictional ends cause a deviation from the assumption used for analysis that the specimen is a simple element. With the smallest deformation, a surface traction develops at the ends of the specimen resulting in the familiar dead zones. This effect is always present, the magnitude and importance of which depend on the material stress history, type of test, and purpose of test. Table 5 summarizes the reasons for and against the use of frictional and lubricated ends. The primary practical reasons for using frictional ends include faster drainage and simplified, efficient equipment and procedures. The primary technical reason for using frictional ends is to stiffen the system, an important factor for small strain measurements. However, such data can be obtained by internal displacement sensors [*20*]. In contrast, frictional ends create several major technical problems as described below.

The stress state in the dead zones (that is, the conical areas at both ends) is obviously different from that in the specimen center [*1,28*]. During compression loading, the stress state in the dead zones approaches a one-dimensional condition with low shear and high confining stresses. The varying stress states between the dead zones and the center of the specimen cause the following:

(1) increased axial (and hence shear) strains toward the center of the specimen;

(2) significant changes in specimen geometry at large strains causing bulging and further nonuniformity of stresses;

(3) large differences in shear-induced pore pressures or volumetric strains between the middle and the ends of the specimen.

The strain nonuniformity will influence all materials at all strain levels. The error has been evaluated by comparing stress–strain data from specimens tested with frictional and lubricated ends. Such data show that frictional ends stiffen the specimen [*30*], this being consistent with end restraint producing increased confinement. However, this error is relatively small with soft cohesive soils. At larger strains the specimen geometry begins to deviate substantially from a right cylinder. This introduces uncertainty as to the most appropriate correction to use when computing effective areas and can be substantial at strains greater than 10% as discussed in the section entitled "Area Corrections."

The errors caused by the nonuniform pore pressure and volumetric behavior are of most concern, the importance of which depends on the difference between the shearing characteristics along the intended triaxial stress path and that of confined compression (or extension). The following discussion considers a *strain rate-independent* soil and focuses primarily on undrained compression tests.

Figure 8 compares hypothetical effective stress paths from CU tests on two specimens,

TABLE 5—*Comparison of frictional and lubricated triaxial ends.*

Frictional Ends		Lubricated Ends	
Reasons For	Reasons Against	Reasons For	Reasons Against
• East set-up procedures	• Nonuniform stress and strain	• Improves uniformity at *all* strain levels	• More difficult to assemble
• Simple, efficient drainage	• Nonuniform excess pore pressure	• Reduces strain rate effects	• Reduces small strain precision
• Stiff apparatus for axial strain measurement	• Water migration	• Reduces uncertainty in area correction	• Increases consolidation time
• Simple cell geometry	• Larger strain rate effect • Formation of rupture surfaces	• Essential for large strain behavior	

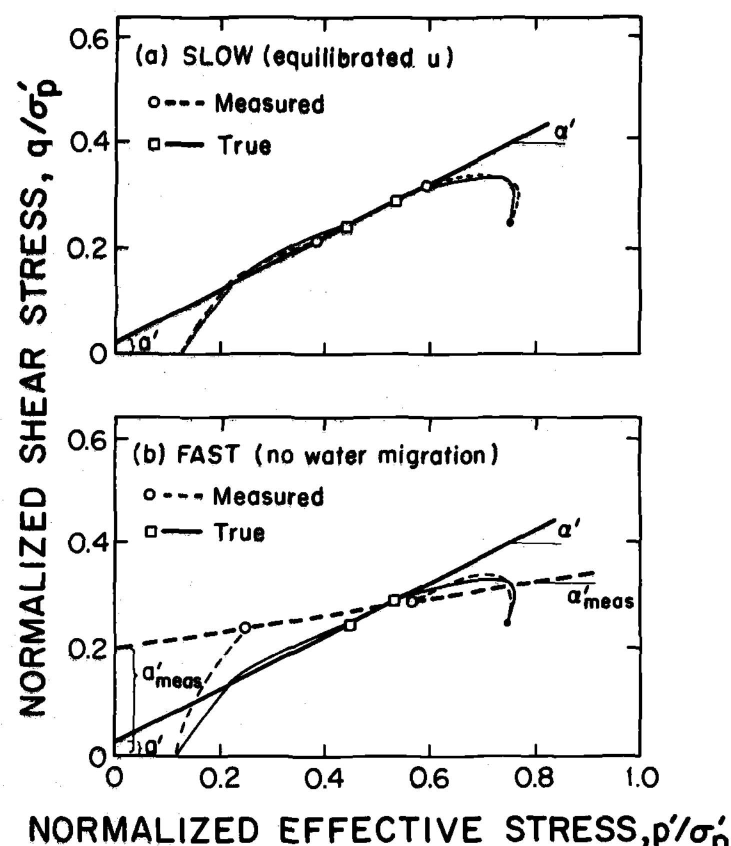

FIG. 8—*Hypothetical stress paths for slow and fast compression tests on rate-independent soil with base pore pressure measurement.*

one normally consolidated and one highly overconsolidated. The "measured" paths correspond to data obtained with frictional ends and pore pressures measured at the end of the specimen (that is, conventional practice). The "true" paths correspond to uniform stresses and strains such as might be obtained with frictionless ends. The results in Fig. 8*a* are for tests performed very slowly to ensure that the pore pressures are equal throughout the conventional specimen. In the dead zones, the confinement tends to produce pore pressure increments that approach the vertical stress increments and hence water must *migrate* within the specimen to equilibrate the pore pressure differences. When the true soil behavior causes shear-induced pore pressures about equal to the vertical stress increment (that is, $A = 1$), there is little migration. Hence, normally consolidated clays should not be significantly influenced by migration of water. But when the soil develops small shear-induced pore pressures, water flows from the dead zones to the specimen center. This migration increases with overconsolidation ratio (OCR) and becomes very substantial for highly dilatant soils. As water migrates to the central zone of high shear, the shearing is now partially drained. Because the stress–strain characteristics are predominantly controlled by the material in the central portion of the specimen, the measured strength will be too low. However, the measured effective stresses at failure should closely approximate the true failure envelope of the material.

Figure 8*b* compares hypothetical results from tests performed sufficiently fast to prevent any water migration. Now the shear-induced pore pressures will be position-dependent, with the conventional base system measuring the pore pressure developed within the dead zones and the overall shearing behavior being mainly controlled by the pore pressure in the center. Similar to the slow test, the error should be small for normally consolidated soil. However, the pore pressure measured in the base of the highly overconsolidated specimen will be much higher than at the center. Thus, very fast tests (that is, minimal internal drainage) give a more correct undrained strength, but the measured effective stress parameters are liable to serious error. In particular, the friction angle will be too low and the cohesion intercept much too high.

Regarding drained tests, several studies [*30,31*] show that end restraint does not significantly affect the failure envelope, but may cause significant changes in the measured volume change behavior, especially with highly dilatant materials [*31*]. End restraint may also contribute to the formation of rupture surfaces as discussed in the section entitled "Rupture Surfaces."

Frictional ends create complex problems such that the data cannot be "corrected" to yield the true soil behavior for a simple element. A more scientific approach to testing would use "frictionless" or more correctly lubricated ends (Table 5). Taylor [*5*] developed a rather complex design for free ends based on the concept of applying numerous point loads on the specimen ends that worked, but it was difficult to use and required an iterative experimental procedure. By the early 1960s, the design for lubricated ends [*13,32,33*] had evolved into a much more compact and practical geometry (Fig. 9). Lubrication was provided by layers of glass, grease, and rubber placed over top caps enlarged by 10 to 20%. Specimens are often shortened to an aspect ratio (height/diameter) of one to increase the lateral stability. Lubricated ends (if effective) can provide near perfect strain fields and hence minimize the "rate effects" illustrated in Fig. 8 because the shear-induced pore pressure should be equal throughout the specimen. However, few laboratories [*33,34*] use lubricated ends for routine testing. Primary technical reasons against lubricated ends are the reduction in small strain precision and increased consolidation time with only radial drainage. However, the strain problem can be resolved using internal contact measuring devices [*20*].

Given the potentially severe problems caused by frictional ends, but the additional practical difficulties associated with using lubricated ends, the authors cannot provide firm recom-

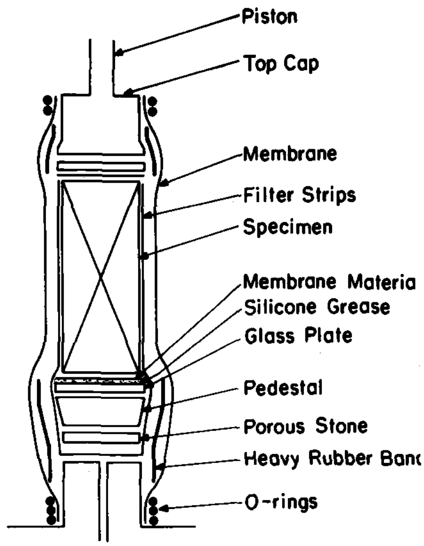

FIG. 9—*Typical schematic of lubricated ends for triaxial tests (after Jackson* [13]).

mendations. However, the following guidelines are offered for consolidated-undrained testing.

1. All tests with frictional ends should be performed slowly enough to allow equilibration of pore pressure (see the section entitled "Rate of Loading"). After shearing, the specimen should be quickly removed from the apparatus and divided into three or four sections for water content measurements to determine the extent of water migration.
2. Lubricated ends should be used when requiring reliable data at large strains (say $\epsilon_a >$ 15%) and for obtaining reliable pore pressure data with minimal water migration when testing highly overconsolidated soils (say OCR > 6).

Rate of Loading

Triaxial test results, both drained and undrained, are sensitive to the rate of loading for two reasons: the time required for flow of water (that is, external drainage during drained shear and internal drainage during undrained shear), and the inherent "viscosity" of the soil skeleton. The former either causes or results from potential testing errors, while the latter reflects true soil behavior. The major concern when selecting a rate of loading should be the time required for the pore pressure to equilibrate throughout the specimen under the requisite drainage conditions. The methods presented by Bishop and Henkel [*11*] to select a proper testing rate still apply today.

During *drained* shear, sufficient time must be provided for water movement throughout the specimen so that the pore pressure everywhere equals the back pressure. Performing the test too quickly causes a partially drained condition with errors in the strength and the effective stress failure envelope. The measured strength will be too low for normally consolidated soil and too high for overconsolidated soil, leading to an overestimate of the cohesion intercept (especially unsafe for slope stability analyses) and the reverse for the friction angle. In contrast, rates slower than needed for complete drainage cause negligible changes in strength [*11*].

Experimental evidence [*11*] shows that 95% dissipation of pore pressure is sufficient to yield accurate drained results. Bishop and Gibson [*12*] used consolidation theory to develop the following approximate solution to estimate the time to failure:

$$t_f = 6.7\ \mathrm{h}^2/c_a \qquad \text{for top and bottom drainage} \tag{7a}$$

$$t_f = 0.5\ \mathrm{h}^2/c_a \qquad \text{for all around drainage} \tag{7b}$$

where

t_f = time to failure
h = ½ height of specimen = diameter of specimen
c_a = coefficient of consolidation

An approximate strain to failure is required to compute the applied displacement rate. The failure strain mainly depends on the OCR, consolidation stress state, and test stress path. Typical values for compression loading of an isotropically consolidated specimen are 20 to 25% at OCR = 1 and decreasing to a few percent at high OCR (>20).

For *undrained* tests, the rate of loading must be sufficiently slow to allow for pore pressure equilibration within the specimen. Pore pressure variations occur as a result of end restraint as discussed in the section entitled "Frictional Ends." Bishop and Henkel [*11*] report an approximate theoretical relationship between the degree of equilibration and the time factor developed by Gibson, which can be used to compute a loading rate. Assuming that 95% equilibration is sufficient, the time to the first significant measurement is

$$t_s = 1.7\ \mathrm{h}^2/c_b \qquad \text{without drains} \tag{8a}$$

$$t_s = 0.07\ \mathrm{h}^2/c_b \qquad \text{with fully effective drains} \tag{8b}$$

The displacement rate will then depend on some selected fraction of the strain to failure which is a function of the type of consolidation, type of loading, and OCR. Strain to failure generally increases with consolidation stress ratio ($\sigma_{hc}'/\sigma_{vc}'$), OCR, and shear in extension.

The use of Eq 7 and Eq 8 has two complications. First, the c_a and c_b are not strictly equal to c_v from an oedometer test, nor do the theories allow for changes during shear. However, they should in all cases be greater than the normally consolidated c_v and hence a value may be taken from oedometer data on similar soil. The second problem relates to the effectiveness of filter drains. Whenever the permeability of the specimen is above about 10^{-8} cm/s, the filter strips do not provide free draining boundaries. Although Eq 7a and Eq 7b can be used to avoid excessive strain rates, an alternate approach uses consolidation data from the last increment prior to shear, thus minimizing both uncertainties. Bishop and Henkel [*11*] recommend an extension of the initial slope of the volume change versus square root of time curve to obtain t_{100} (other methods to determine a nominal end of primary would apply) and use of the following equations:

$$t_f = 16\ t_{100} \qquad \text{for drained tests} \tag{9}$$

$$t_s = 2\ t_{100} \qquad \text{for undrained tests} \tag{10}$$

These equations automatically correct for the effectiveness of the drains, but they ignore changes in c_v during shear. The last consolidation increment also must be sufficiently large to produce a Terzaghi-type consolidation curve. This usually will not be possible during K_o consolidation or when small isotropic increments are applied to avoid development of a soft core (see the section entitled "Filter Drain Resistance").

Rupture Surfaces

Rupture surfaces, which are planes of concentrated strain, often form in triaxial specimens. They usually become visible shortly after reaching the peak deviator stress. The complexity of the stress and strain fields around the rupture surface makes it impossible to analyze the specimen as a simple element. Analysis of the data relative to the slip surface must account for localized membrane and filter strip resistance, the influence of lateral loading on both the piston and specimen, changes in contact area along the surface, and so forth. The mechanics of slip surface formation represent an important aspect of behavior that has received considerable attention recently [*34–37*]. Until the causes and mechanisms of formation are understood, postrupture data probably should not be analyzed quantitatively.

In compression tests, the formation of rupture surfaces is influenced by the boundary conditions, the presence of stress concentrations, and localized areas of weakness within the specimen. They generally form when using frictional ends and almost always in slow tests on overconsolidated specimens. The locations of the surfaces are variable, but most often intersect the edge of one end cap. However, the compression test specimen is relatively stable, which tends to reduce the propagation of such surfaces in low OCR soils. The transition from a more general strain field to a localized slip surface is undoubtedly aggravated by pore water migration.

Rupture surfaces are especially sensitive to zones of weakness during extension tests. The specimen is inherently unstable (similar to the weak link in a chain) which tends to favor slip surface formation. When the first instability begins, it easily grows into a continuous surface. The strain continues to concentrate in this zone of stress concentration and finally forms the familiar neck. Rupture surfaces are much flatter in extension tests. They seldom extend to an end cap, but often pass close to the edge of a dead zone. Rupture surfaces form equally in all types of soils during extension tests.

Interpretation of data from tests that develop rupture surfaces is still a matter of debate. Preformation results should be reasonable when computed using the assumption of a "uniform" strain field. However, the slip surface may initiate long before becoming visible, raising doubts as to when the specimen significantly deviates from a condition of generalized strain. It is also not clear if the presence of rupture surfaces significantly alters the strength or effective stress parameters measured prior to their formation.

Summary

This section covered various aspects of testing equipment and procedures that cause errors in the measured data relative to the properties that should have been obtained from triaxial tests (principally CU and CD tests) conducted with the intended boundary conditions of stress, strain, and drainage. Table 3 lists the 14 problem areas that were considered. The subsections dealing with each issue have attempted to clearly identify the problem and then either offer guidance as to appropriate "corrections" or means for minimizing its effect. Table 6 summarizes the principal conclusions and recommendations for consolidated-undrained triaxial testing. It shows the direction of error in shear stress, pore pressure, axial and volumetric strain caused by the various factors.

TABLE 6—*Typical parameter errors with conventional triaxial equipment used for CU testing (Set-up in Fig. 1 assuming constant temperature and accurate recording instrumentation).*

Parameter		Source of Error	Error Direction	Remarks
1. Maximum shear stress	1.1	Piston friction	$+\Delta q$	Must calibrate correction. Do not use stationary bushing.
$q = \frac{P}{2A}$	1.2	σ_c uplift	$+\Delta q$	Must calibrate correction.
	1.3	Membrane restraint	$+\Delta q$	Apply standard correction.
	1.4	Filter drain restraint	$+\Delta q$	Apply correction (uncertain) or minimize via number and orientation.
	1.5	Nonuniform area due to end restraint	$+\Delta q$ barreling $-\Delta q$ necking	Apply parabolic correction. Terminate test.
	1.6	Nonuniform σ' due to end restraint	$+\Delta q$	Usually small effect.
	1.7	Nonuniform e due to end restraint	$-\Delta q$ usually	Most pronounced at high OCR. Need fast $\dot{\epsilon}$ to reduce Δe, but error in u (see 2.5).
	1.8	Displacement along rupture surface	$\pm\Delta q$	Complex change in area, interaction with membrane and filter strips, lateral force on piston, etc. Therefore terminate test.
	1.9	Tilting of sample	$\pm\Delta q$	Use rigid piston-top cap to minimize.
	1.10	Internal leakage: water and gas	$-\Delta q$	See 2.2 and 2.3.
	1.11	External leakage	$+\Delta q$	See 2.4.
2. Pore water pressure, u	2.1	$S < 100\%$	$\pm\Delta u$	Direction depends on TSP and OCR. Must use back pressure and check B before and after shearing.
	2.2	Internal leakage: water	$+\Delta u$	Check leakage during consolidation and with dummy. Minimize osmotic pressure gradient.
	2.3	Internal leakage: gas	$+\Delta u$	Eliminate gas–water interfaces.
	2.4	External leakage	$-\Delta u$	See 2.2.
	2.5	Nonuniform u distribution due to end restraint and/or rupture zones	$+\Delta u$ usually	Most pronounced at high OCR. Need slow $\dot{\epsilon}$ to equilibrate u.
3. Axial strain, ϵ_a	3.1	Seating	$+\Delta\epsilon_a$	Can be very large at small ϵ and high OCR.
	3.2	Nonuniform area due to end restraint	$-\Delta\epsilon_a$	Terminate tests with necking.
	3.3	Displacement along rupture surface	$-\Delta\epsilon_a$	See 1.8.
4. Volumetric strain, ϵ_v	4.1	Increase in S during back pressuring	$+\Delta\epsilon_v$	Keep σ' constant and assume area is constant.
	4.2	Internal leakage: water and gas	$+\Delta\epsilon_v$	See 2.2 and 2.3.
	4.3	External leakage	$-\Delta\epsilon_v$	See 2.4.

Undrained Triaxial Testing in Engineering Practice

Introduction

Do the properties obtained from laboratory triaxial tests, even if measured accurately, reflect the in situ behavior of the soil under field conditions? The discussion here is restricted to prediction of the initial in situ undrained stress–strain–strength properties of saturated cohesive deposits. To assess the use of triaxial testing for such purposes, the authors first summarize the three major factors that affect results of undrained shear tests run on "undisturbed" specimens, namely: (1) the influence of sample disturbance; (2) the rate of shearing; and (3) the mode of shearing, especially regarding the effects of anisotropy. This review also compares laboratory-derived strengths with those back calculated from case histories of undrained failures. Based on this collective knowledge, the paper examines and illustrates the generally unreliable nature of UU and CIU triaxial compression test results and then recommends how CK_oU triaxial testing can provide more useful data in engineering practice.

Sample Disturbance

Ideally, the laboratory test specimen should have the same preshear water content and values of effective stress (for example, σ_{vo}' and $\sigma_{ho}' = K_o\sigma_{vo}'$) as existed in situ before sampling. But this ideal condition cannot be attained, except possibly with block samples from a soil having K_o equal to unity. Hence, for typical projects involving tube samples from deposits with $K_o \neq 1$, the effects of sample disturbance must be recognized and minimized to the extent possible. Jamiolkowski et al. [*38*] describe three sources of sample disturbance arising from the stress relief (including eventual removal of the in situ shear stress, $q_o = 0.5\sigma_{vo}'(1 - K_o)$); the sampling technique (also see Ref *39* for disturbance effects associated with the straining caused by common thin-walled tube sampling); and the handling procedures (for example, transportation, extrusion, and trimming). Jamiolkowski and coworkers [*38*] also suggest ways of assessing the degree of sample disturbance via radiography, measurement of the sample's effective stress (σ_s'), and evaluation of one-dimensional compression curves. In any case, tube sampling will always alter the in situ soil structure, may involve internal migration of water, and frequently leads to values of σ_s' substantially less than the in situ σ_{vo}' (especially with relatively deep, low OCR materials). Hence, UU type tests can never simulate the in situ stress–strain behavior because shearing a priori starts from an *isotropic* state of stress (σ_s') that differs from the in situ K_o stress condition. (Note: resultant errors in the peak undrained strength may be offset by other factors affecting c_u measurements.) UU tests on specimens having varying degrees of disturbance will also give a misleading indication of spatial variability due to bias in the measurements.

Given the obvious limitations of UU testing, one must therefore employ CU tests to minimize the adverse effects of sample disturbance, where the two principal variables are the vertical consolidation stress (σ_{vc}') and the consolidation stress ratio ($K_c = \sigma_{hc}'/\sigma_{vc}' = \sigma_{rc}'/\sigma_{ac}'$ for triaxial testing). Because K_c should approximate the in situ K_o, both to help restore the in situ soil structure and to give more meaningful stress–strain–strength data, the paper will now focus on the so-called Recompression and SHANSEP techniques developed for CK_oU test programs.

The two techniques are illustrated in Fig. 10, which shows hypothetical in situ and laboratory K_o compression curves for a slightly overconsolidated clay. Points 1 and 2 designate the in situ condition and the sampled condition, respectively (the latter assuming no change in water content during sampling). Point 2 also represents the preshear effective stress of a

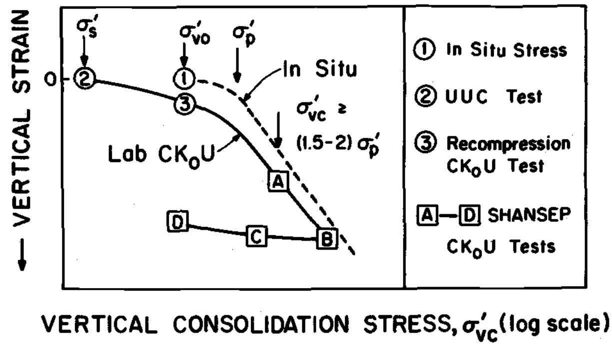

FIG. 10—*Consolidation procedures for laboratory* CK_oU *testing* (*after Ladd et al.* [43]).

UUC test. Test specimens following the Recompression technique are reconsolidated to $\sigma_{vc}' = \sigma_{vo}'$ shown as Point 3, whereas Points A through D correspond to typical stresses used for SHANSEP.

Bjerrum [*40*] and Berre and Bjerrum [*41*] present the rationale underlying the Recompression approach developed at the Norwegian Geotechnical Institute. They quote typical volumetric strains of 1.5 to 4% and conclude that destruction of natural bonding by sample disturbance more than offsets the strength gain due to the lower water content, provided its reduction is not too large. The SHANSEP technique as described by Ladd and Foott [*42*] and Ladd et al. [*43*] involves the following basic steps (for a given layer and mode of failure): (1) oedometer tests to obtain the preconsolidation pressure profile and hence the OCR $= \sigma_p'/\sigma_{vo}'$; (2) CK_oU tests on specimens consolidated beyond the in situ σ_p' to measure the behavior of normally consolidated soil (Points A and B in Fig. 10) and also on specimens rebounded to varying OCR to measure overconsolidated behavior (Points C and D); (3) evaluate and express the results in terms of normalized soil parameters such as c_u/σ_{vc}' versus OCR; and (4) use these relations with the stress history to compute c_u profiles. Although originally developed based on the empirical observation that it gave reasonable results, SHANSEP inherently assumes that the in situ clay exhibits normalized behavior that can be simulated in the laboratory by mechanical overconsolidation.

Although more research is needed to clarify the likely errors and relative merits for both reconsolidation techniques, the authors offer the following recommendations for CK_oU test programs conducted on fixed piston *tube* samples having a diameter of 75 mm. (References *38* and *44* provide further background information.)

The *Recompression* technique:

(1) is more accurate with highly structured, brittle clays such as typical of eastern Canada (where SHANSEP tends to underpredict peak c_u values and especially undrained modulus);

(2) is preferred for cemented soils and for testing weathered crusts and heavily overconsolidated deposits (where SHANSEP is often difficult to apply);

(3) should *not* be used in truly normally consolidated (OCR = 1) deposits because reconsolidation to $\sigma_{vo}' = \sigma_p'$ will clearly overestimate the in situ c_u; and

(4) should always be accompanied by an evaluation of the in situ stress history to check the reasonableness of the measured c_u/σ_{vo}' values and to extrapolate/interpolate the discrete c_u data.

The SHANSEP technique:

(1) is probably preferred for moderate to low OCR deposits of "ordinary" clays, meaning a relatively low sensitivity and precompression mainly because of mechanical-desiccation-secondary compression rather than physico-chemical mechanisms;

(2) relies on an accurate estimate of the in situ σ_p' profile (but if this cannot be reasonably obtained from oedometer tests, Recompression c_u data would also be suspect and may be unsafe); and

(3) generally requires more testing (although the normalized parameters can be used on subsequent projects involving the same deposit).

Both approaches ideally require K_o consolidation, which is especially difficult and time consuming for SHANSEP triaxial testing without automated controls. The paper later discusses special equipment and simplified anisotropic consolidation techniques.

Rate of Shearing

Laboratory UU and CU triaxial tests on cohesive soils show higher strengths with increasing strain rate ($\dot{\epsilon}$) and hence decreasing time to failure (t_f). The effect can be expressed in terms of $\lambda = (\Delta c_u / c_{uo}) / \Delta \log \dot{\epsilon}$, where c_{uo} is the undrained strength at some reference strain rate, say at $\dot{\epsilon} = 1\%/\text{h}$. The thorough literature survey by Lacasse [45] and subsequent research indicate typical trends as follows: (1) CIUC tests on OCR = 1 clays give $\lambda = 0.1 \pm 0.05$ for t_f ranging from several minutes to several hours; (2) λ can be substantially higher in heavily overconsolidated soils; and (3) λ often increases at faster shearing rates, as illustrated in Fig. 11. Although changes in c_u appear related to changes in effective stress

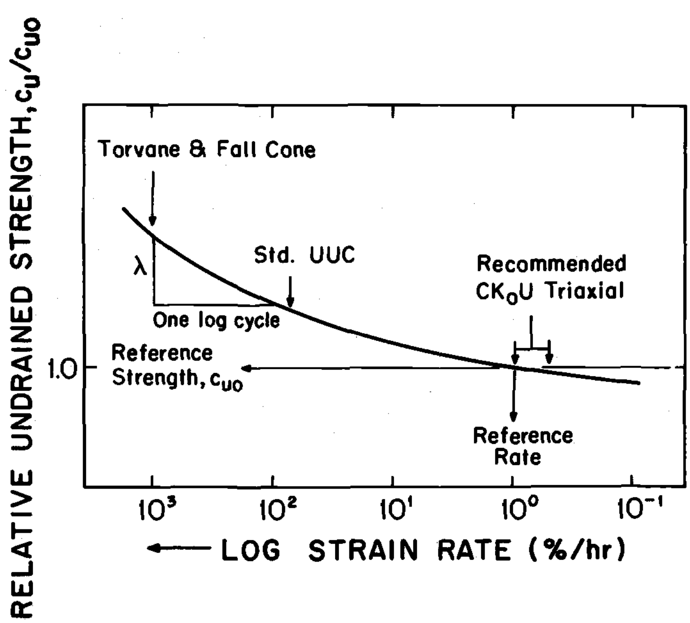

FIG. 11—*Schematic illustration of variation in undrained shear strength with strain rate.*

(for example, higher excess pore pressures at slower rates), the mechanisms responsible for this behavior are both controversial and unclear, for example: membrane leakage (likely at t_f exceeding several days); a "structural viscosity"; particle slippage and reorientation; redistribution of water content (considered important with high OCR soils); or a combination thereof.

Irrespective of the mechanism, rate effects should be considered when comparing c_u data from tests having large differences in t_f and for CK_oU testing. For typical λ values, shearing at the UUC standard of 1%/min will increase c_u by about 20 ± 10% in low OCR clays, and may exceed 50% in some high OCR soils, relative to tests run at $\dot{\epsilon}$ = 1%/h. These differences may even double at shearing rates associated with Torvane and fall cone testing. Although no rational framework exists to select strain rates to replicate in situ behavior, many leading laboratories now use $\dot{\epsilon}$ = 0.5 to 1%/h for CK_oU triaxial tests on soft cohesive soils. As will be seen, this value appears reasonable based on case histories of undrained failures.

Mode of Shearing

When comparing the different modes of shearing that can be achieved in laboratory shear devices, two variables usually suffice to describe the basic differences in the applied stress system, meaning the magnitudes and directions of the three principal stresses. They are: (1) the relative magnitude of the intermediate principal stress as defined by $b = (\sigma_2 - \sigma_3)/(\sigma_1 - \sigma_3)$; and (2) the *direction* of the applied major principal stress relative to the vertical (depositional) direction, denoted by the angle δ. Changes in the values of b and δ lead to different stress–strain responses due to the effects of σ_2 and anisotropy, respectively.

References *38* and *44* discuss the combinations of b and δ that can be achieved by laboratory shear devices and their applicability for engineering practice and research. Ideally, CK_oU testing would shear specimens at representative δ angles to measure the stress–strain–strength anisotropy of the soil while maintaining a constant σ_2 condition (for example, with b = 0.3 to 0.4 to approximate plane strain conditions). However, no existing device has this capability for routine testing of natural clays. Hence, most studies of undrained anisotropy, starting from K_o conditions, have come from the following modes of shearing:

(1) plane strain compression/extension (PSC/E), which can provide reliable data for plane strain shearing at $\delta = 0°$ and $90°$ (for example, Vaid and Campanella [*46*]) but cannot achieve intermediate δ angles;
(2) triaxial compression/extension (TC/TE), which give data at $\delta = 0°$ with $b = 0$ and at $\delta \doteq 90°$ with $b = 1$, and hence involve a change in the σ_2 condition;
(3) direct simple shear (DSS), such as with the Geonor device [*47*], which simulates the horizontal portion of a plane strain failure surface.

Results from CK_oU TC, TE, and Geonor DSS tests will be used to illustrate the effects of anisotropy, even though such data involve complicating factors, namely: triaxial testing generally gives peak strengths less than plane strain testing, by about 5 to 10% in compression and about 15 to 20% in extension [*43*]; and the values of $0.5\,(\sigma_1 - \sigma_3)_f$ and δ are ill-defined in the DSS test due to nonuniform and incomplete stress–strain conditions. Figure 12 plots peak undrained strength ratios from such tests run on a wide variety of normally consolidated clays and silts (but excluding varved clays), where τ_h is the maximum horizontal shear stress applied to the DSS test specimens. The data show: $q_f/\sigma_{vc}' = 0.32 \pm 0.02$ SD in TC having no trend with I_p; generally much lower DSS strengths that tend to decrease with lower plasticity; and even smaller ratios for shear in TE, especially at low I_p with q_f/σ_{vc}' in the

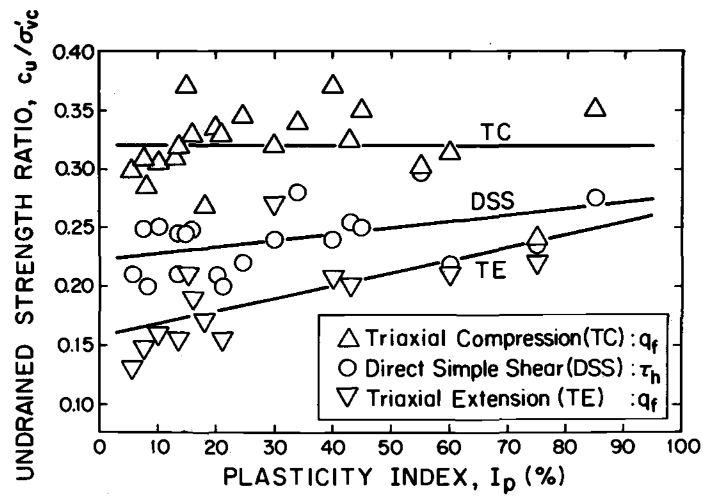

FIG. 12—*Undrained strength anisotropy from CK$_o$U tests on normally consolidated clays and silts* [44].

range of only 0.16 ± 0.03. These results and the general literature clearly demonstrate that most OCR = 1 soils exhibit significant c_u anisotropy that generally becomes most important in lean clays, especially if also sensitive.

Anisotropy can also have a significant effect on undrained stress–strain behavior, as illustrated by the data in Fig. 13 from CK_oU TC and TE tests on OCR = 1 resedimented Boston blue clay (I_p = 15 to 20%). Shearing in compression produces a high peak strength at a very low strain (ϵ_a = 0.3%), followed by pronounced strain softening as the effective stresses decrease and finally reach the maximum obliquity failure envelope. In contrast, the

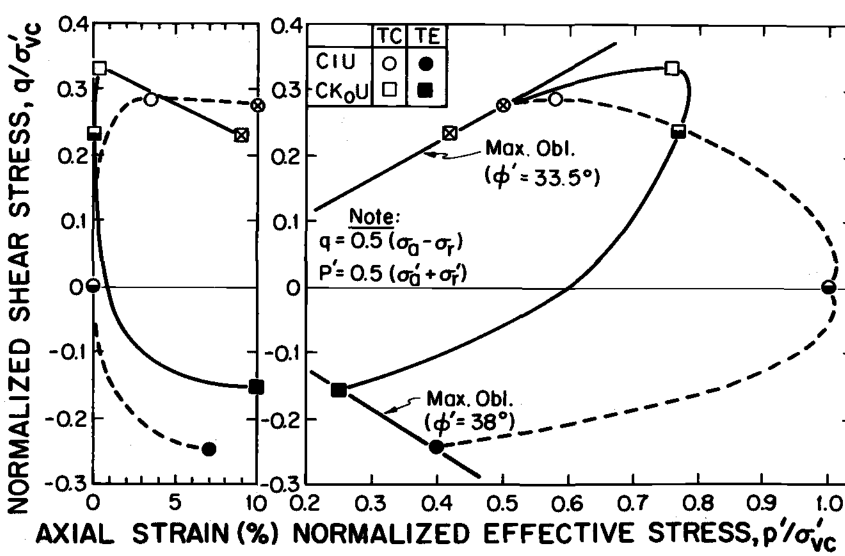

FIG. 13—*Undrained stress-strain behavior for* K$_o$ *and isotropic consolidation of OCR = 1 resedimented Boston blue clay.*

effective stress path is always decreasing during shear in extension, which produces a much lower strength (in spite of the steeper failure envelope) at a very large axial strain. Figure 13 also plots results from CIU tests, which show that isotropically consolidated specimens give completely different behavioral trends (for example, relatively little change in both the strain at failure and the peak strength). This occurs because anisotropic consolidation per se causes most of the anisotropy observed in typical low OCR soils. Hence, CIU testing will generally give a highly misleading picture of soil behavior when the in situ K_o is less than about 0.7 to 0.8. Although not plotted, CK_oUDSS tests on resedimented Boston blue clay give a peak $\tau_h/\sigma_{vc}' = 0.20$ at about 5% shear strain.

In Situ Undrained Strength Ratios for Stability Analyses

Jamiolkowski and coworkers [*38*] and Ladd [*44*] show that overconsolidated soils can also exhibit pronounced undrained stress–strain–strength anisotropy. Hence, any meaningful laboratory test program conducted as part of engineering studies for an undrained stability problem should account for this important aspect of soil behavior. But before making recommendations, results from recent studies of the in situ undrained strength appropriate for circular arc or wedge type stability analyses will first be reviewed. Ladd [*44*] made a detailed comparison of the undrained strength ratios plotted in Fig. 14 and obtained as follows: (1) values of c_u/σ_p' back calculated from case histories of loading failures on low OCR deposits as reported by Larsson [*48*]; (2) values of τ_{ave}/σ_{vc}' obtained from CK_oU compression, direct simple shear and extension tests run on ten normally consolidated soils and treated for *strain compatibility* to account for the effect of progressive failure [*49*]; and (3) the peak τ_h/σ_{vc}' obtained from CK_oUDSS tests run on 25 OCR = 1 nonvarved soils. After distinguishing between soils with Atterberg limits plotting above the A-line (CL and CH soils) versus those falling below the A-line or containing shells and fibers, Ladd reached the following conclusions especially pertinent to this paper:

1. There was good agreement between the three undrained strength ratios for CL and CH soils having $I_p = 25 \pm 15\%$.
2. The more limited data base for silts and organic soils precluded a meaningful comparison but indicated higher and more scattered undrained strength ratios than for inorganic clays.
3. The initial in situ undrained strength appropriate for circular arc stability analyses can be computed using the relationship

$$c_u/\sigma_{vo}' = S(\text{OCR})^m \tag{11}$$

where S equals the normally consolidated value and the exponent m gives the increase resulting from overconsolidation.

4. For nonvarved CL and CH sedimentary clays of low to moderate sensitivity and I_p = 20 to 80%, $S = 0.22$ with a nominal $SD = 0.03$.
5. For sedimentary deposits of silts, organic soils (excluding peats) and clays with shells, $S = 0.25$ with a nominal $SD = 0.05$.
6. The value of m can be estimated as $m = 0.88(1 - C_s/C_c) \pm 0.06\ SD$, where C_s and C_c equal the slope of the oedometer void ratio versus log consolidation stress curve during unloading and virgin compression, respectively, or more simply taken as $m = 0.8$.

Based on the above conclusions, c_u/σ_{vo}' ratios appropriate for stability analyses with CL

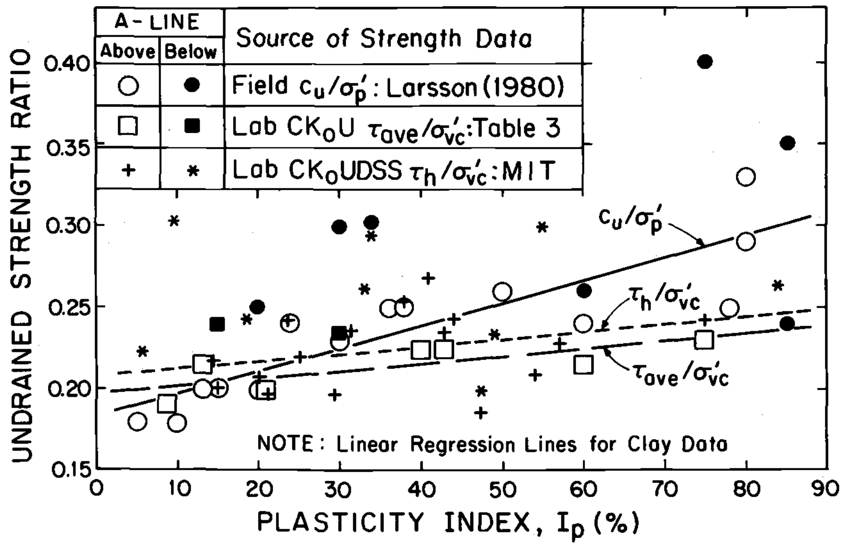

FIG. 14—*Comparison of field and laboratory CK_oU strength ratios for OCR = 1 nonvarved sedimentary soils* [44].

and CH soils would fall within the following ranges based on S = 0.22 ± 0.03 and m = 0.8 ± 0.10:

$$OCR = 1,\ c_u/\sigma_{vo}' = 0.22 \pm 0.03SD$$

$$OCR = 5,\ c_u/\sigma_{vo}' = 0.80 \pm 0.17SD$$

$$OCR = 10,\ c_u/\sigma_{vo}' = 1.40 \pm 0.37SD$$

The paper next examines typical results from UUC and CIUC testing in light of these values.

Conclusions Regarding UU and CIU Triaxial Compression Tests

Reliance on UUC tests to obtain reasonable estimates of the initial in situ undrained strength for stability analyses depends on a fortuitous self-compensation of the three factors reviewed above. In other words, the *increased strength* due to shearing at a very fast strain rate (60%/h) and due to failure in triaxial compression (that is, shearing at $\delta > 0°$ leads to lower strengths because of anisotropy) must be offset by a *strength reduction* due to significant sample disturbance (that is, values of preshear effective stress much less than the in situ effective stresses). These compensating factors cannot be controlled, often produce large scatter, and may cause misleading trends with depth.

Given the continued widespread use of UUC testing, it appears that many practicing engineers still believe that sample disturbance will predominate, such that significant errors in UUC strengths will always be on the safe side. However, the general move in recent years to better sampling techniques (for example, 75-mm fixed piston versus 50-mm pushed or hammered samples) can produce the opposite effect. Table 7 shows four examples of data from sites with high quality sampling and well documented reference strengths. The last two sites are especially notable for having highly unsafe UUC strengths, probably due

TABLE 7—*Examples of unsafe strengths from UUC tests (From Ref 44).*

Location	Soil Type	Depth, m	OCR	q_f(UUC)/c_u	Reference c_u
Atchafalaya, LA	CH deltaic clay I_p = 75%	9–11	1.2	1.15 (mean)	SHANSEP CK_oUDSS and field experience
AGS Offshore NJ	CH marine clay I_p = 43 ± 7%	6–10	4.2 ± 0.9	1.4 ±0.15 (mean)	SHANSEP τ_{ave}
Great Salt Lake Causeway	CH–OH clays I_p = 40 ± 10%	3–18	1.5	1.4–2.4 (typical range)	SHANSEP τ_{ave} and two embankment failures
Smith Bay, AK	CL–CH Pleistocene	3–5	35	4.0 (mean)	SHANSEP CK_oUDSS
	arctic "silt" I_p = 23 ± 4%	9–11	14	3.1 (mean)	

to typical anisotropy combined with abnormally large strain rate effects. Hence, UUC data can be unduly low (say by up to 50%), reasonable or unsafe, and should not be relied on as the principal means of estimating the in situ c_u. All UUC data also should be compared to strengths predicted by Eq 11, which requires an assessment of the stress history at the site.

Mayne [50] gives a comprehensive tabulation of undrained strength ratios measured in CIUC tests run on a wide variety of normally consolidated soils. Using those values judged reliable for natural soils and results on 15 natural soils obtained by researchers at MIT, $q_f/\sigma_c' = 0.33 \pm 0.05SD$ based on 30 soils and showing no trend with I_p which typically varied between 15% and 75%. These values generally fall significantly above undrained strengths considered appropriate for stability analyses as presented in Fig. 14, except perhaps for some silts and organic soils with Atterberg limits plotting below the A-line. Moreover, the data set excluded all q_f/σ_c' ratios greater than 0.45 because these higher values probably occurred from using consolidation stresses too low compared to the in situ preconsolidation pressure. Whereas using σ_{vc}'/σ_p' greater than 1.5 to 2 usually suffices with K_o consolidation to obtain true OCR = 1 behavior, isotropic consolidation often requires stresses about double those values.

Although the above comparison was made for normally consolidated soils, CIUC testing will also yield unsafe strengths for most overconsolidated materials, even with in situ K_o values greater than unity, because of the "inherent" anisotropy resulting from the soil's one-dimensional consolidation stress history. Moreover, the unsafe error will become even larger with CIUC Recompression testing (that is, $\sigma_c' = \sigma_{vo}'$) of low OCR deposits due to the adverse effects of sample disturbance.

In conclusion, the authors find little merit in running CIUC tests for undrained stability problems because the strengths will be unsafe because of anisotropy (especially with lean clays), and also may be due to sample disturbance; and the stress–strain data generally will not simulate in situ behavior, even for a triaxial compression mode of shearing, because K_o is seldom equal to unity (especially in low OCR soils). Hence, only the effective stress failure envelope at maximum obliquity has any physical significance. But these values of c' and ϕ' cannot be reliably used in effective stress analyses to assess *undrained* stability [44].

Role of Undrained Triaxial Testing in Engineering Practice

If one accepts that neither UUC nor CIUC tests should be run, can triaxial testing play any useful role in designs involving undrained stability? The authors believe it can, but only if the profession is willing to use anisotropic consolidation and also to shear specimens in extension as well as compression. This approach obviously entails significant added expense (and experience) which should be compared to the benefits, namely:

1. One can obtain stress–strain data representative of the expected limits for in situ anisotropic behavior, that is, for shearing in compression ($\delta = 0°$) and in extension ($\delta = 90°$).
2. The mean of the peak strengths for failure in compression and extension should give a reasonable estimate of the in situ strength appropriate for circular arc stability analyses, provided that c_u is defined as $\tau_{ff} = q_f \cos\phi'$. (*Note:* This recommendation assumes that the in situ strength reduction due to progressive failure will be offset by using lower triaxial strengths compared to plane strain strengths.)

The above "benefits" do not apply to varved clays such as found in the northeastern region of the United States. These deposits have much lower strengths when sheared parallel to the varves (that is, the DSS mode of failure) than in compression and extension. Ladd [*44*] recommends extensive oedometer testing and use of Eq 11 with $S = 0.16$ and $m = 0.75$ for such soils as being far more reliable than any form of triaxial testing.

Some Recommendations for CK_oU Triaxial Compression and Extension Testing

One-dimensional (K_o) consolidation entails significant increased costs and time compared to isotropic consolidation. The increased costs occur either from capital investment in more expensive automated equipment to facilitate K_o consolidation or from the increased labor costs required to manually achieve the desired stress path during consolidation. This subsection first discusses the manual K_o consolidation technique and simplified approaches that can be adopted to reduce costs, and then describes special modifications needed for shear in triaxial extension. It concludes with a brief overview of some advances in automated consolidation.

True K_o consolidation requires application of many small increments of vertical and radial stress in order to follow a stress path *dictated* by the specimen deformation. The specimen is first isotropically consolidated at σ_s' (and back pressured), and then follows a drained stress path of decreasing K_c as it approaches the normally consolidated condition (the true K_o stress path A in Fig. 15). For actual manual K_o consolidation, increments must be

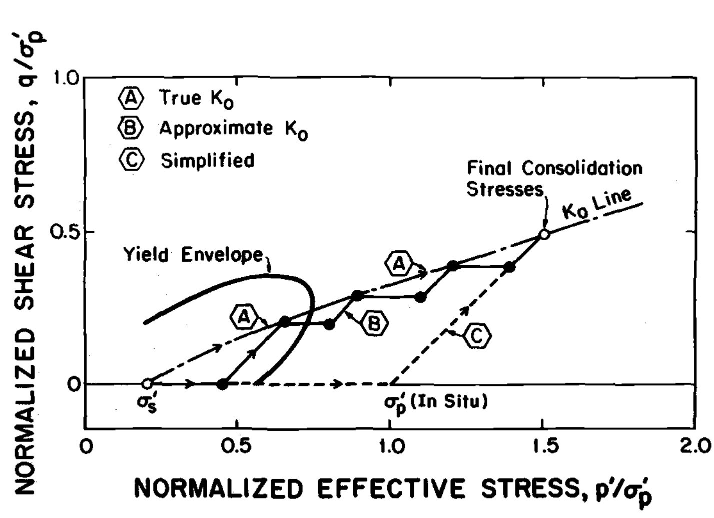

FIG. 15—*Techniques for anisotropic consolidation to OCR = 1.*

sufficiently small (for example, $\Delta\sigma_v \approx 0.2\sigma_v'$) to minimize straining due to undrained shear and must remain long enough to allow full consolidation. At the end of each increment the change in length and volume are used to calculate the present area (or may be measured directly with an internal device) which is compared to the initial area to determine if the selected K_c is too high or too low. Based on this information, a new K_c value is estimated and the next increment is applied. The process continues to the final stress state which often requires 20 or more increments.

Simplified consolidation techniques [*51,52*] have been proposed to reduce labor requirements without expensive equipment additions. Berre [*51*] presented the technique shown as stress path C (Fig. 15) in which the specimen is isotropically consolidated (*Note:* one should limit the load increment ratio to 0.5 when OCR = 1 and using filter drains) to the final radial effective stress, and then the vertical stress is increased such that K_c equals the estimated K_o value. This second stage is equivalent to drained triaxial compression and must be performed relatively slowly (see the section entitled "Rate of Loading"). Once at the K_c value, the vertical stress should be maintained for one cycle of secondary compression prior to undrained shear. This process dramatically decreases the testing period and labor requirements compared to stress path A.

The results for both compression and extension tests [*51,53*] on Drammen clay and a low plasticity silt confirm that the simplified method, while not perfect, yields data comparable to true K_o consolidation. However, isotropic consolidation well beyond the yield envelope may cause a significant change in the "structure" of the soil. Hence, a better approach would select a stress path similar to B in Fig. 15.

The simplified consolidation method offers a viable alternative for engineering practice and can easily be implemented with a few modifications to standard equipment. The following equipment features facilitate these testing techniques and allow for extension testing.

1. A fixed top cap to piston connection maintains alignment during isotropic consolidation and allows extension testing.
2. A moment free tension/compression connector to the load cell is required for extension testing.
3. A fixed connection between triaxial cell base and load frame for extension testing
4. A lightweight hanger for applying constant force to the piston which also allows connection to the load cell. The constant force may be applied by air jack or weights.

Appreciating the benefits of true K_o consolidation (Path A), researchers have developed control systems to automate the consolidation process. Lewin [*54*] developed a very simple analog which makes use of an external volume cylinder with the same diameter as the specimen. The cylinder volume is connected to the specimen drainage, and its piston is attached to the specimen piston. Thus, the displacement volume relationship is identical for specimen and cylinder. A mercury reversing switch controls the direction of the piston movement. Consolidation is performed by increasing the cell pressure at a constant rate and allowing the "feedback" loop to adjust the vertical loading as required.

More complicated and more expensive systems have also been developed. For example, Menzies and coworkers [*55*] developed a double feedback loop which uses pressure control cylinders driven by electric motors. The cylinder providing the cell pressure is linked by the process controls to a transducer which monitors the specimen diameter. As the specimen is loaded axially at a constant displacement rate, the controls adjust the cell pressure to keep the diameter constant.

The hydraulic stress path cell [*56*] provides more general consolidation capabilities. All three pressures (u, σ_c, σ_a) can be computer controlled with complete feedback loops [*57*] allowing controlled gradient or constant rate of strain consolidation. It also provides the capability of performing more generalized consolidation and shearing stress paths.

Conclusions

The paper covers two aspects of UU, CU, and CD triaxial testing of saturated cohesive soils: problems in the testing equipment and procedures that cause errors in the measured properties of the test specimen compared to the intended boundary conditions of stress, strain, and drainage; and changes in conventional triaxial testing practice to provide better estimates of in situ soil behavior under field conditions.

The paper divides testing problems into three categories.

1. Errors that can be reasonably handled by means of *corrections*, such as errors due to membrane and filter drain resistance and piston friction (except that stationary solid bushings should not be used).
2. Errors that can and should be *avoided*, such as incomplete saturation and leakage of water and gas (gas–water interfaces should not be used for tests lasting more than several hours).
3. Errors that are difficult to correct or avoid and hence must be *evaluated* when selecting testing procedures or interpreting measured data. The most important problem is the nonuniform stresses and strains caused by frictional end caps, which frequently lead to serious errors in effective stress parameters obtained from CU tests run too fast for pore pressure equilibration. Although lubricated ends minimize this problem, they are seldom used due to their added complexity. The cause and effects of rupture planes require further study.

Regarding the use of triaxial testing in practice to predict the initial in situ undrained stress-strain-strength properties of saturated cohesive deposits, the paper draws the following conclusions.

1. UU compression tests should not be used as the *principal* means of estimating undrained shear strengths, c_u, because the values can be either seriously too high or too low. This results from the uncontrollable effects of strain rate, anisotropy, and sample disturbance.
2. CIU compression tests have little value because the c_u values will be unsafe for stability analyses because of anisotropy and also sample disturbance, and the stress–strain data seldom simulate in situ behavior because K_o is rarely equal to unity.
3. Therefore, more emphasis should be placed on anisotropically (preferably K_o) consolidated, undrained triaxial compression and *extension* test programs. However, the wider adoption of CK_oU testing in practice requires education of both engineers and clients regarding their enhanced cost–benefit ratio, and the availability of more reliable, relatively inexpensive automated "stress path" triaxial cells.

Furthermore, oedometer tests should also be part of the overall experimental program to ascertain the stress history of the deposit and thus calculate undrained strengths by Eq 11 for comparison with results from UU (if used) and CU testing.

References

[1] Saada, A. S. and Townsend, F. C., in *Laboratory Shear Strength of Soil, ASTM STP 740*, Philadelphia, ASTM, 1981, pp. 7–77.

[2] Berre, T., *Geotechnical Testing Journal*, Vol. 5, No. 1/2, 1982, pp. 3–77.
[3] Landva, A., "Equipment for Cutting and Mounting Undisturbed Specimens of Clay in Testing Devices," *Norwegian Geotechnical Institute Publication 56*, 1964, pp. 1–5.
[4] Berre, T., in *Proceedings*, Seventh ICSMFE, Mexico, Vol. 3, 1969, pp. 517–518.
[5] Taylor, D. W., "Soil Mechanics Research Program on Cylindrical Compression Testing in Cooperation with U.S. Engineering Department," Massachusetts Institute of Technology 3rd Report, Oct. 1940.
[6] Kjellman, W., *Geotechnique*, Vol. 2, 1951, pp. 225–232.
[7] Norton, H. N., *Handbook of Transducers for Electronic Measuring Systems*, 1st ed., Prentice-Hall, Englewood Cliffs, NJ, 1969.
[8] Henkel, D. J. and Gilbert, G. D., *Geotechnique*, Vol. 3, 1952, pp. 20–29.
[9] Duncan, J. M. and Seed, H. B., *Journal of the Soil Mechanics and Foundations Division, ASCE*, Vol. 93, No. SM 5, Pt. 1, 1967, pp. 121–137.
[10] Berre, T., "Suggested International Code of Soil Engineering Practice for Triaxial Compression Tests," Preliminary Draft #3, 1986.
[11] Bishop, A. W. and Henkel, D. J., *The Measurement of Soil Properties in the Triaxial Test*, 2nd ed., Arnold, London, 1962.
[12] Bishop, A. W. and Gibson, R. E., in *Laboratory Shear Testing of Soils, ASTM STP 361*, Philadelphia, ASTM, 1965, pp. 435–461.
[13] Jackson, W. T., "Stress Paths and Strains in a Saturated Clay," SM Thesis, Massachusetts Institute of Technology, Cambridge, MA, 1963.
[14] Atkinson, J. H., Evans, J. S., and Ho, E. W. L., *Geotechnique*, Vol. 35, No. 3, 1985, pp. 353–355.
[15] Olsen, R. E. and Campbell, L. M., *Materials Research and Standards*, Vol. 7, No. 2, 1967, pp. 45–52.
[16] Ladd, R. S. and Dutko, P., *Advances in the Art of Testing Soils Under Cyclic Conditions*, ASCE, Detroit, 1985, pp. 148–165.
[17] Wissa, A. E. Z., Christian, J. T., Davis, E. H., and Heiberg, S., *Journal of the Soil Mechanics and Foundations Division, ASCE*, Vol. 97, No. SM 10, 1971, pp. 1393–1413.
[18] Hedberg, J., "Cyclic Stress–Strain Behavior of Sand in Offshore Environment," Ph.D. Thesis, Massachusetts Institute of Technology, Cambridge, MA, 1977.
[19] Iverson, K. and Moum, J., *Geotechnique*, Vol. 24, No. 4, 1974, pp. 665–670.
[20] Burland, J. B. and Symes, M., *Geotechnique*, Vol. 32, No. 1, 1982, pp. 62–65.
[21] Black, D. K. and Lee, K. L., *Journal of the Soil Mechanics and Foundations Division, ASCE*, Vol. 99, No. SM 1, 1972, pp. 75–93.
[22] Rad, N. S. and Clough, G. W., *Journal of Geotechnical Engineering, ASCE*, Vol. 110, No. 9, 1984, pp. 1205–1218.
[23] Mitchell, J. K., *Fundamentals of Soil Behavior*, 1st ed., Wiley, New York, 1976.
[24] Poulos, S. J., "Control of Leakage in the Triaxial Test," Research Report, Harvard University, 1964.
[25] Fredlund, D. G., *Canadian Geotechnical Journal*, Vol. 13, 1976, pp. 386–396.
[26] Pollard, W. S., Sangrey, D. A., and Poulos, S. J., *Journal of Geotechnical Engineering, ASCE*, Vol. 103, No. GT 10, 1977, pp. 1169–1173.
[27] Shockley, W. G. and Ahlvin, R. G., "Non-uniform Conditions in Triaxial Test Specimen," Research Conference on Shear Strength of Cohesive Soils, ASCE, Boulder, 1960, pp. 341–357.
[28] Rowe, P. W. and Barden, L., *Journal of the Soil Mechanics and Foundations Division, ASCE*, Vol. 90, No. SM 1, 1964, pp. 1–27.
[29] Blight, G. E., in *Laboratory Shear Testing of Materials, ASTM STP 361*, Philadelphia, ASTM, 1965, pp. 173–184.
[30] Duncan, J. M. and Dunlop, P., *Journal of the Soil Mechanics and Foundations Division, ASCE*, Vol. 94, No. SM 1, 1968, pp. 271–290.
[31] Lee, K. L., *Journal of Geotechnical Engineering, ASCE*, Vol. 104, No. GT 6, 1978, pp. 687–704.
[32] Rowe, P. W., *Proceedings of the Royal Society of London*, Series A, Vol. 269, 1962, pp. 500–527.
[33] Sarsby, R. W., Kalteyiotis, N., and Haddad, E. H., *Journal of Geotechnical Engineering, ASCE*, Vol. 108, No. GT 1, 1982, pp. 83–107.
[34] Raju, V. S., Sadsivan, S. K., and Venkataraman, M., "Use of Lubricated and Conventional End Platens in Triaxial Tests on Sands," *Soils and Foundations*, Japanese Society of Soil Mechanics and Foundation Engineering, Vol. 12, No. 4, Japan, 1972, pp. 25–43.
[35] Gudehus, G. and Kolymbas, D., in *Proceedings*, Eleventh ICSMFE, San Francisco, Vol. 2, 1985, pp. 489–494.

[36] Lade, P. V. and Tsai, J., in *Proceedings,* Eleventh ICSMFE, San Francisco, Vol. 2, 1985, pp. 549–552.
[37] LaRochelle, P., Leroueil, S., Trak, B., Blais-Leroux, L., and Tavenas, F., in this volume, pp. 715–731.
[38] Jamiolkowski, M., Ladd, C. C., Germaine, J. T., and Lancellotta, R., in *Proceedings,* Eleventh ICSMFE, San Francisco, Vol. 1, 1985, pp. 57–153.
[39] Baligh, M. M., Azzouz, A. S., and Chin, C.-T., *Journal of Geotechnical Engineering, ASCE,* Vol. 113, No. GT 7, 1987, pp. 739–757.
[40] Bjerrum, L., in *Proceedings,* Eighth ICSMFE, Moscow, Vol. 3, 1973, pp. 111–159.
[41] Berre, T. and Bjerrum, L., in *Proceedings,* Eighth ICSMFE, Moscow, Vol 1.1, 1973, pp. 39–49.
[42] Ladd, C. C. and Foott, R., *Journal of Geotechnical Engineering, ASCE,* Vol. 100, No. GT 7, 1974, pp. 763–786.
[43] Ladd, C. C., Foott, R., Ishihara, K., Schlosser, F., and Poulos, H. G., in *Proceedings,* Ninth ICSMFE, Tokyo, Vol. 2, 1977, pp. 421–494.
[44] Ladd, C. C., "Stability Evaluation During Staged Construction: 22nd Terzaghi Lecture," Submitted for publication in *Journal of Geotechnical Engineering, ASCE,* 1988.
[45] Lacasse, S. M., "Effect of Load Duration on Undrained Behavior of Clay and Sand–Literature Survey," Norwegian Geotechnical Institute, Internal Report 40007-1, 1979.
[46] Vaid, Y. P. and Campanella, R. G., *Journal of Geotechnical Engineering, ASCE,* Vol. 100, No. GT 3, 1974, pp. 207–224.
[47] Bjerrum, L. and Landva, A., *Geotechnique,* Vol. 16, No. 1, 1966, pp. 1–20.
[48] Larsson, R., *Canadian Geotechnical Journal,* Vol. 17, No. 4, 1980, pp. 591–602.
[49] Koutsoftas, D. C. and Ladd, C. C., *Journal of Geotechnical Engineering, ASCE,* Vol. 111, No. GT 3, 1985, pp. 337–355.
[50] Mayne, P. W., *Journal of Geotechnical Engineering, ASCE,* Vol. 106, No. GT 11, 1980, pp. 1219–1242.
[51] Berre, T., "Sources of Error for Undrained Triaxial Tests on Soft and Medium Stiff Clay," Northern Geotechnical Conference, Esbo, Finland, 1979, pp. 597–608.
[52] Kirkpatrick, W. M. and Khan, A. J., *Geotechnique,* Vol. 34, No. 1, 1984, pp. 29–42.
[53] Ayan, K. D. J., "Undrained Triaxial Strength Deformation Behavior of Harrison Bay Arctic Silts," SM thesis, Massachusetts Institute of Technology, Cambridge, MA, 1985.
[54] Lewin, P. I., *Geotechnique,* Vol. 21, No. 3, 1971, pp. 259–262.
[55] Menzies, B. K., Sutton, H., and Davis, R. E., *Geotechnique,* Vol. 27, No. 4, 1977, pp. 593–596.
[56] Bishop, A. W. and Wesley, L. D., *Geotechnique,* Vol. 25, No. 4, 1975, pp. 657–670.
[57] Menzies, B. K. and Sutton, H., *Ground Engineering,* Vol. 13, No. 1, 1980, pp. 22–31.

John F. Peters[1]

Determination of Undrained Shear Strength of Low Plasticity Clays

REFERENCE: Peters, J. F., "**Determination of Undrained Shear Strength of Low Plasticity Clays,**" *Advanced Triaxial Testing of Soil and Rock, ASTM STP 977,* Robert T. Donaghe, Ronald C. Chaney, and Marshall L. Silver, Eds., American Society for Testing and Materials, Philadelphia, 1988, pp. 460–474.

ABSTRACT: Difficulties posed by low plasticity soils including silty and sandy clays, silts, and sands are described. The soils considered are not cemented and generally display the dependence between consolidation state and strength necessary to apply such procedures as Stress History and Normalized Soil Engineering Properties (SHANSEP). Unfortunately, these soils are highly susceptible to sampling disturbance because of the unavoidable low effective stress that remains in specimens after sampling. Sampling disturbance obscures consolidation behavior, making it difficult to estimate the in situ overconsolidation ratio. Also, the low compressibility of these materials makes it difficult to clearly define the virgin compression curve. Improvements in interpretation procedures will come only after a sound mechanical description of sampling disturbance has been developed.

KEY WORDS: triaxial test, undrained shear strength, sample disturbance, stress history, pore pressure, critical state, silt

The science of test interpretation has come a long way in the past three decades, largely spurred by efforts to develop reliable constitutive relationships for soils. The volume change behavior of soil in the triaxial test and the relationship between volume change tendency and pore pressure response are now well understood. Yet, there remains a considerable gap in knowledge when attempting to determine the in situ behavior of soil because the strength and deformation characteristics of soil depend very much on its state. Unless laboratory tests replicate the in situ state, the observed behavior will not be representative of field conditions. Even if the response of the soil can be described precisely by an analytical model, the appropriate starting point of the model prediction is not known. Similarly, the parameters used to calibrate the model must be determined from laboratory tests on specimens that have undergone an extensive stress history during the period between sampling and testing. Often, the stresses applied during sampling are more severe than those expected during field loading. Thus, the engineering response of soil is always clouded by the inability to relate the laboratory and field states.

The problem of relating behavior in the triaxial test to in situ conditions has received considerable attention, and excellent state-of-the-art reviews have been presented recently [*1,2*]. This paper will focus on the problem of strength determination for low plasticity clays and silts.

The occurrence of low plasticity materials is widespread. Often these materials are uncemented and of geologically recent origin and are therefore not considered as problematic

[1] Research civil engineer, Geotechnical Laboratory, U.S. Army Engineer Waterways Experiment Station, Civil Engineer, Vicksburg, MS 39180.

as sensitive or overconsolidated clays. But low plasticity soils are often highly susceptible to sampling disturbance and present difficult problems when an accurate strength determination is required. In many cases, soils that would be classified as plastic clays may still pose problems if they contain silt layers or contain a significant non-clay fraction.

To aid the discussion, the terms disturbance and sensitivity will be given rather restrictive definitions. The term *sampling disturbance* refers to all factors contributing to changes in soil state as a result of sampling, storage, and specimen preparation. *Disturbance* can be viewed as consisting of two components: one related to reversible changes in the pore water pressure and the other related to permanent deformations. In this context, the *sensitivity* of the soil is tied to its susceptibility to nonrecoverable disturbance. A nonsensitive soil will be viewed as a material that can be returned to its in situ state by restoring the correct effective stress. All soils are susceptible to permanent changes during sampling and the distinction between sensitive and nonsensitive depends on the ability to restore the in situ state. This description of sensitivity differs from the traditional definition which relates the strength of the undisturbed soil to that after complete remolding at the same water content. For design purposes, the traditional definition is preferred because it provides an indication of potential strength loss caused by construction activity. The definition adopted here is better suited to describe laboratory behavior. For example, any specimen will display a loss in strength when remolded at constant water content because the remolding action will increase pore pressure. The strength of a nonsensitive soil can be restored by consolidating to the original (before remolding) effective stress condition whereas remolding destroys some essential aspect of the composition of a sensitive soil (such as cementation). All soils are sensitive to some extent because response to loading depends on the previous stress history including stresses imposed by sampling. The validity of strength derived from laboratory data depends on the extent that disturbance is either reversible or that its effects can be removed through application of special laboratory procedures.

This paper is divided into three parts. The first part discusses what stress conditions actually exist in the laboratory specimen, how these stresses relate to the field, and the general deficiency of current practice of using the undrained unconsolidated (UU) test to determine undrained shear strength of low plasticity materials. Although the deficiencies of the UU test are well documented, it is still commonly used and most engineers do not appreciate the magnitude of the errors involved when using the test. The second part of the paper discusses the use of the consolidated undrained (CU) test to replicate in situ conditions and procedures to account for nonreversible sample disturbance. The third part continues the discussion on the CU test by addressing areas still very much in the research stages of development.

Stress Conditions in Laboratory Specimens

Pore Pressure Response During Sampling

The greatest source of error in any determination of stress in a soil is related to the pore pressure. Even if the total stress history of a soil element is known, the pore pressure history may be impossible to predict because of the many factors that enter into the pore pressure response. These factors include the volume change characteristics of the material, pore pressure dissipation, and cavitation. Consider the pore pressure history that occurs as a result of sampling. As the total normal stress is reduced, there is a corresponding reduction in pore pressure. So long as the pore pressure reduction is directly proportional to the changes in total stress, the effective stress state remains unchanged. In fact, sampling also involves shearing the soil which tends to increase pore pressure; thus the reduction in pore pressure due to unloading is partly offset by pore pressure generated during sampling and handling. Further at some point in the unloading, the negative pore pressure will fall below the cavitation pressure which sets a bound on the amount of suction that can be retained in the specimen. The net effect of sampling disturbance is to create residual negative pore pressure which is more positive than the ideal response.

A classic study on the residual effective stress in $\overline{\text{UU}}$ specimens was reported by Ladd and Lambe [*3*]. Results of similar tests on alluvial clay soils from the New Orleans area are shown in Figs. 1 to 5. The tests are conducted similarly to a standard UU test except that the pore pressure in the specimen is measured without back pressure saturation and the rate of loading applied to the specimen is selected based on the criteria generally used for CU tests. As the specimen is initially set up in the cell a suction is measured. As cell pressure is applied, the pore pressure becomes more positive. As shown in Fig. 1, by the time the pore pressure becomes positive, a nearly perfect response is obtained. The effective stress, shown in Fig. 2, is nearly constant.

A plot of residual effective stress is shown plotted as a function of depth in Fig. 3. The effective stress value plotted corresponds to the value measured when the cell pressure was equal to the estimated in situ total stress. Also plotted are results for case histories presented by Ladd and Lambe [*3*]. It appears that, as reported by Ladd and Lambe, the residual effective stress increases with depth at a rate of about 20% of the in situ stress which is consistent with the observation that strength from UU tests increases with sample depth. The departure from the 20% value may be quite large and depends on the plasticity of the sample and the amount of sampling disturbance.

The results shown in Figs. 1 to 3 depend on as-tested conditions in the specimens. Two important questions pertaining to those conditions are (1) does the pore pressure measurement system (which gives the specimen access to water) influence the test results? and (2) how well does the behavior observed in the $\overline{\text{UU}}$ test correspond to the behavior in the $\overline{\text{CU}}$ test? The first question can only be answered statistically by comparing strengths of $\overline{\text{UU}}$ tests to conventional UU tests as shown in Fig. 4. The two types of tests are comparable both in terms of the strength versus depth relationship obtained and the amount of variation

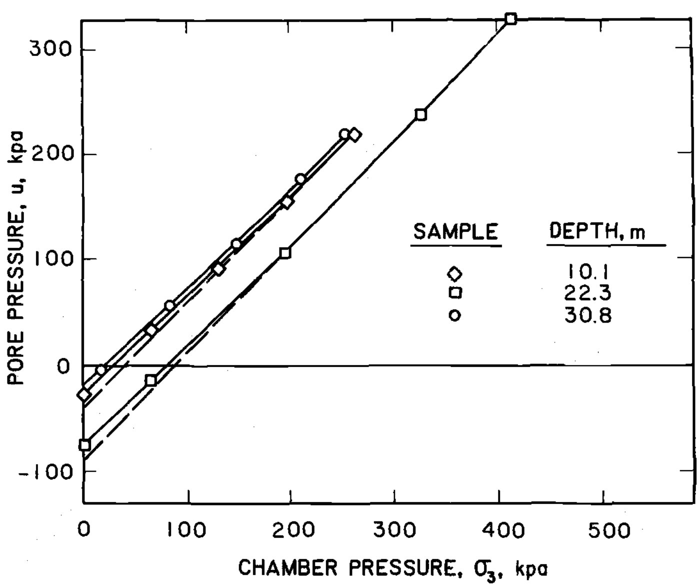

FIG. 1—*Pore pressure induced by cell pressure in UU test.*

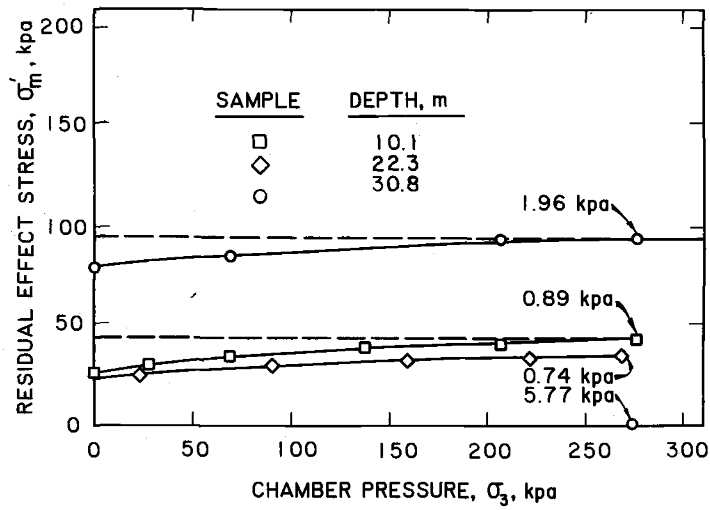

FIG. 2—*Effective stress in $\overline{UU}$ test.*

in the strength data. There is no evidence that measuring pore pressure has any significant influence on the test results.

The stress path data in Fig. 5 illustrate how $\overline{UU}$ and CU tests compare. The CU tests were performed at three consolidation pressures. The lowest consolidation pressure corresponds to the effective stress measured initially in the $\overline{UU}$ test. The intermediate stress corresponds to the average effective stress at the sample depth and the highest pressure corresponds to twice the average in situ pressure. Also plotted is the effective stress path

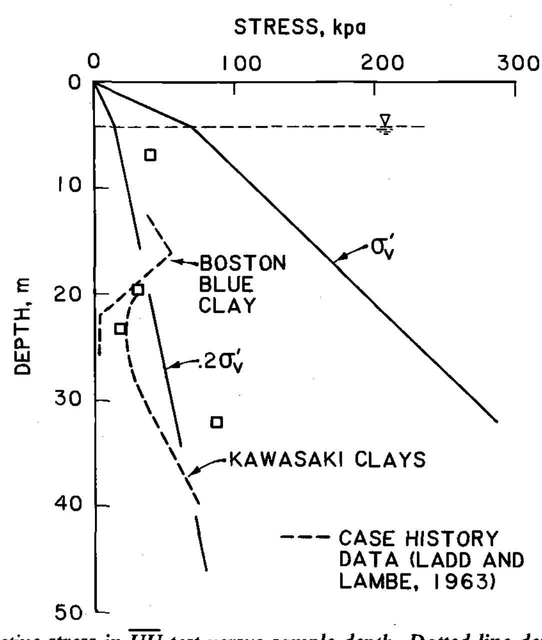

FIG. 3—*Effective stress in $\overline{UU}$ test versus sample depth. Dotted line designates data from Ladd, C. C., and Lambe, T. W.* [3].

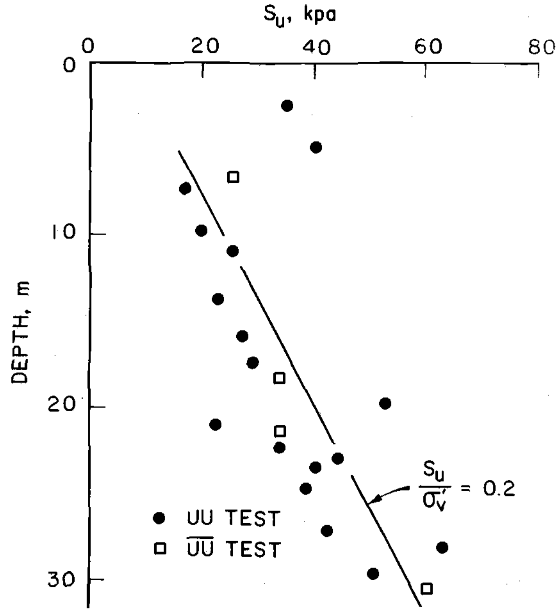

FIG. 4—*Strength versus depth.*

measured in the $\overline{UU}$ test which is nearly identical to the corresponding CU test. The $\overline{UU}$ test is equivalent, therefore, to a CU test, provided both are loaded at comparable rates and have the same initial effective stress state.

The measurement of residual pore pressure in undisturbed specimens clearly shows that pore pressures in the specimens are higher than in the in situ state. However, the comparison with in situ conditions is based on computed total stresses and pore pressure, leaving the

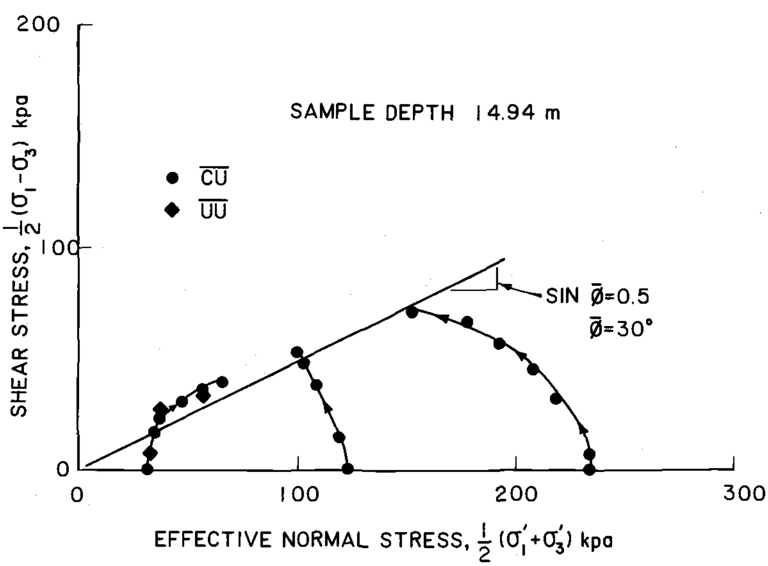

FIG. 5—*Comparison of effective stress paths for* $\overline{UU}$ *and CU test.*

actual mechanism of pore pressure changes open to speculation. These changes were investigated in laboratory-prepared specimens by Kimura and Saitoh [*4,5*] who monitored pore pressures during initial consolidation from a slurry, sampling, trimming, and testing. When the vertical stress was removed from the sample, a corresponding negative pore pressure was induced. The initial suction was gradually lost during the processes of extrusion from the sample tube and trimming. By the time the soil was tested, effective stress remaining in the specimen was only a fraction of its original presampled value. The loss of residual suction was greatest for low plasticity soils. High plasticity clay retained nearly half of the initial suction while low plasticity clay retained only a small fraction of the initial value. This dependence on soil plasticity is consistent with experience in the lower Mississippi valley where it is generally observed that UU strengths of low plasticity soil are lower than expected when compared to their sampling depth.

An important practical question concerning sample disturbance is whether the loss of residual suction is the result of handling the sample or if it is simply time dependent (that is, will residual effective stress be lost over a period of time after sampling regardless of how the specimen is handled?). A series of laboratory tests performed by Kirkpatrick and Khan [*6*] on two clays provides a detailed picture of the effect of storage time on loss of suction. The results are similar to those obtained by Kimura and Saitoh [*4,5*]; there is a loss in suction, after a few days of storage, which is greatest for low plasticity soil. It was also found that the loss in strength is not directly proportional to the loss in effective stress. The specimens became more dilative as the residual suction was lost, leading to a smaller induced pore pressure and higher strength. The correspondence between dilative tendency and residual pore pressure is, of course, a result of the specimen becoming more overconsolidated as the effective stress is reduced. The same trend can be identified from the stress paths shown in Fig. 5. The strength lost as a result of reducing effective stress is thus partly offset by the increasing dilative tendency. The specimens retained up to half of their initial strength (that is, strength before sampling) even though the residual effective stress has fallen to less than 30% of the initial value.

Kirkpatrick and Khan [*6*] also compared strengths for specimens with and without pore pressure measurements to investigate the possible influence of the pore pressure measurement system. As already noted in Fig. 4, the measurement of pore pressure does not appear to influence results significantly.

Implications to Sampling Disturbance

Based on the investigations cited above, three conclusions can be made concerning the condition of samples tested in the laboratory.

1. Sample disturbance increases the pore pressure in specimens. The effect on UU tests is to create a specimen at lower effective stress and higher overconsolidation ratio that is weaker than the in situ soil.
2. The pore pressure increase may be influenced by extrusion from the sampling tube, trimming, and general handling. However, the reduction in suction appears also to be time dependent, which implies that disturbance will occur even with the best sampling and handling procedure.
3. The loss of suction is greatest for low plasticity soils.

The above conclusions have severe implications to interpretation of the UU test because the strength actually obtained is the product of a number of factors. In most cases, pore pressures are not measured in the specimens and it cannot be determined how severe the effects of sampling disturbance may be. Therefore, use of the test carries a greater degree of error than is generally realized in common practice. In many practical cases, this error can have significant influence on the design. For example, considering the strength profile in Fig. 4, the relatively low design strength ratio S_u/σ_v' of 0.2, is higher than indicated by nearly 80% of the UU tests for the project. The use of the UU strength on the basis of conservatism may require millions of dollars of unnecessary earthwork. On the other hand, to ignore the UU strengths goes against considerable precedence and increases the engineer's liability. Therefore, the question of what to do with the UU test represents a practical deficiency in the state of the art.

The alternative to the UU test is the CU test in which the specimen is consolidated to the in situ stress state prior to shearing. Although reconsolidation restores the correct effective stress state to the specimen, the strength obtained may not be appropriate for design. The problem is that sampling disturbance causes strengths in the CU test to be high by an indeterminable amount [7]. Residual pore pressure does not provide a complete measure of disturbance for the CU test because the loss of effective stress cannot be directly related to the disturbance that remains after reconsolidation to in situ stress. Water is the least compressible component of a saturated soil and very little volume change is needed to substantially reduce the negative pore pressure. Therefore, even if the residual effective stress in a sample has been reduced to a minimal value by disturbance, it may still be possible to restore the in situ state by reconsolidation. The problems of interpretation introduced by reconsolidation will be considered in more detail in the next section.

Reconsolidation Effects

It is well known that sampling disturbance influences the reconsolidation behavior of soil. A highly disturbed specimen displays a flatter recompression curve, and the past maximum consolidation pressure determined by the Casagrande method is lower than the in situ value. Methods to correct compression curves are generally based on the concept that the slope of the compression curve depends on the overconsolidation ratio (OCR) and thus the compression curve can be reconstructed from data obtained at higher pressures. Methods to correct shear strength for sampling disturbance are similar to consolidation test corrections in that they depend on a relationship between shear strength and consolidation state. All such methods ultimately depend on the validity of the state surface concept.

State Surface Concept

The idea of a state surface for soil is illustrated in Fig. 6. The virgin curve of the soil represents a limiting stress state whereby a soil cannot support a greater stress than the stress state on the virgin curve, p_e, corresponding to the current void ratio. A measure of how close a soil is to the limiting state is p/p_e, the ratio of the current stress state, p, to the limiting state, p_e. On the traditional plot of e versus $\log(p)$, states of constant p/p_e plot as lines parallel to and to the left of the virgin curve (Fig. 6*a*). The lines of constant p/p_e constitute unique states of the soil as illustrated in Fig. 6*b*. Soils consolidated at low p/p_e values are dilatant; soils consolidated to higher ratios are contractive. Regardless of the actual consolidation stress, the effective stress path will have a unique shape on the normalized plot.

One of the original theories based on the state surface concept was proposed by Hvorslev [8] who defined a failure law for direct shear test.

$$\tau_{ff}/p_e = c_e/p_e + \sigma_{ff}/p_e \tan\phi_e \tag{1}$$

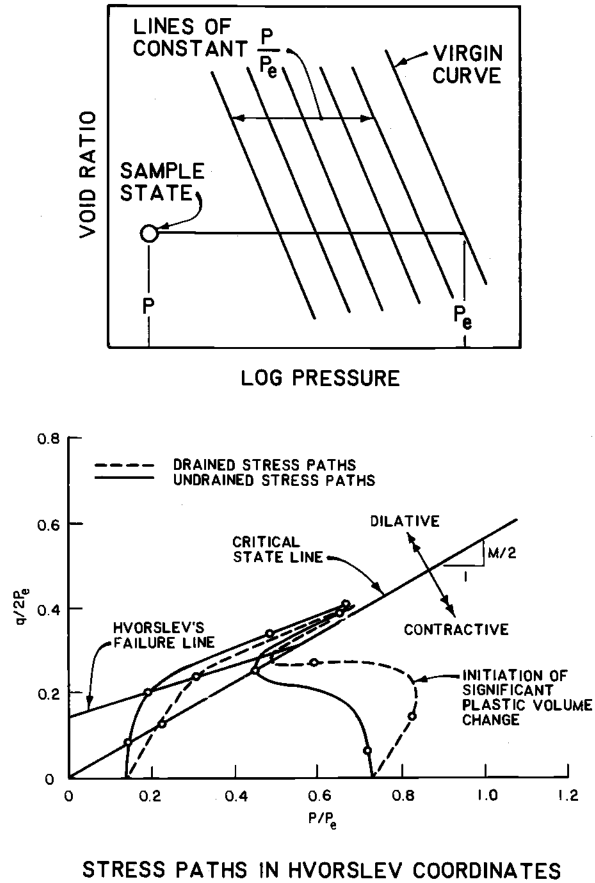

FIG. 6—*Influence of consolidation state on soil behavior.* a, *Contours of state surface on* e-*log*(p) *plot.* b, *Normalized stress path plot.*

The corresponding Hvorslev surface is shown for the triaxial test in Fig. 6*b* in which failure is defined in terms of limiting shear–normal effective stress ratio. The Hvorslev theory became a cornerstone of the critical state theory [*9*] which further assumes the existence of an ultimate state, which occurs at a unique p/p_e value, where the soil deforms without volume change (critical state). Numerous constitutive models have been based on the concept, including the so-called cap models (see, for example Ref *10*) and bounding surface models [*11*]. The tendency for the effective stress path to be uniquely related to the initial p/p_e was exploited by Pender [*12,13*] to develop a relatively simple constitutive model.

The lines of constant p/p_e correspond to lines of constant OCR if the slope of the rebound curve is a constant. A subtle, but important, difference in using p/p_e versus OCR lies in the relationship to stress history [*2*]. Traditionally, the effects of stress history on the behavior of clays has been attributed to the OCR. However, the ratio p/p_e is a measure of distance from the limiting state; no relationship necessarily exists between the limiting state and stress history. For a clay, it may be necessary to load to some past pressure then rebound to obtain an overconsolidated state, in which case OCR and p/p_e become equivalent concepts. In contrast, a sand may be brought to a state left of the virgin compression curve during sample formation without applying pressures even approaching those required to reach the virgin curve. Yet, if loaded to sufficiently high pressure a limiting state is obtained for sand similar to that found for clays (for example, the consolidation data for Sacramento River Sand in Ref *14* clearly show that, regardless of initial density, compression curves tend to converge to one ultimate compression curve). This similarity between sands and clays in hydrostatic compression carries over to the triaxial compression test as illustrated in Fig. 7 in which the different behaviors of dense and loose sand loaded from the same confining pressures reported by Torrey [*15*] can be resolved by normalizing by the limiting pressure, p_e.

The importance of the preceding paragraph to understanding the behavior of low plasticity clays and silts lies in the difficulty in defining the correct normalizing stress. For example,

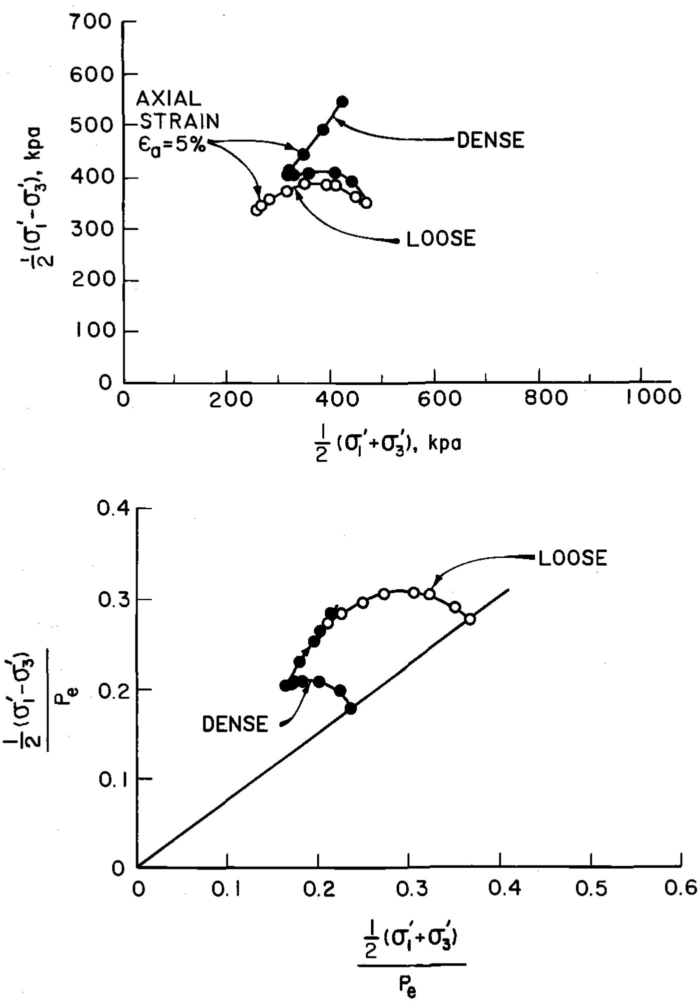

FIG. 7—*Example of normalized behavior in sand.* a, *Stress paths for loose and dense sand starting from same effective stress state.* b, *Normalized stress paths showing difference in initial states.* (*Data from Torrey, V. H., "Some Effects of Rate of Loading, Method of Loading, and Applied Total Stress Path on the Critical Void Ratio of a Fine Uniform Sand," Ph.D. dissertation, Texas A&M University, College Station, TX, 1981.*)

the limiting stress for the sand must be determined from a test on a sand initially at its loosest state, otherwise the perceived virgin curve will be much flatter than the true limiting curve and the limiting pressure p_e will be too low. If the correct p_e is not used, the normalized behavior among several specimens will not display any clear-cut trend, giving the perception that the state surface concept is not valid for sand. Critical state theory has been criticized on the basis that sands do not have a unique virgin curve [*16*].

The use of the state surface concept for low plasticity clays and silts can be as problematic as for sands. Like sands, silty materials tend to have poorly defined recompression curves, and determination of the correct normalizing stress is difficult. In the case of undisturbed specimens, the compression curve is always obtained for void ratios that are lower than the in situ values, and determination of the correct normalizing stress for the in situ condition requires considerable extrapolation back from the compression curve defined at high stresses. Like sands, both the reload and the virgin compression curves are much flatter than those of high plasticity clays, and relatively small errors in the void ratios lead to large errors in the normalizing stress. This last factor makes it extremely difficult to define the limiting state curve from comparisons of groups of samples. Therefore, while it may be concluded that the state surface concept is valid for noncemented soils in general, application of the concept becomes more difficult for silty or low plasticity soils.

Correcting for Disturbance

If the state surface concept can be shown to be valid for a given soil, the effects of sampling disturbance can be accounted for by determining the "normalized behavior." Once the normalized behavior is known, the in situ behavior can be determined by scaling the stress variables to the in situ p_e. In the case of shear strength the method amounts to (1) defining a relationship between s_u/σ_{vc}' and OCR; (2) determining the relationship between OCR, σ_{vc}', and depth; and (3) computing s_u for each depth.

The method was formalized by Ladd and Foott [*17*] as the Stress History and Normalized Soil Engineering Properties (SHANSEP) method. As illustrated in Fig. 8, to determine the strength for the in situ state [1] the specimens would first be consolidated to state [B] then rebounded to states [C] to [D] (to achieve known values of OCR) and tested. By normalizing the strength obtained at each state with the consolidation stress, a plot of s_u/σ_{vc}' can be constructed. Assuming the in situ OCR is known, the correct strength can be obtained by multiplying the appropriate s_u/σ_{vc}' by the in situ σ_{vc}'. The SHANSEP method thus depends on three items: (1) that the relationship between normalized strength s_u/σ_{vc}' and OCR is a unique property of the soil, (2) that the OCR is known, and (3) that the soil is not cemented or sensitive.

The bulk of experimental evidence suggests that the relationship between s_u/σ_{vc}' and OCR is a property of the soil [*17,18,19*]. The principal problem of defining the relationship is the difficulty in correctly determining the consolidation characteristics as discussed previously. It is not clear that in situ OCR is necessarily known, particularly for low plasticity soils which are subject to considerable sampling disturbance.

An interesting approach to the problem of determining OCR was proposed by Mayne [*20*] who applied the well-known result of critical state theory given by Eq 2.

$$s_u/\sigma_{vc}' = \mathrm{OCR}^{-\Lambda_o} \tag{2}$$

Equation 2 is identical to an empirical relationship proposed by Ladd and Edgers [*18*] in which $\Lambda_o = 0.8$ and is derived from the assumption that the effective stress paths all converge to a common point on the critical state line. Mayne collected data from 96 sources and

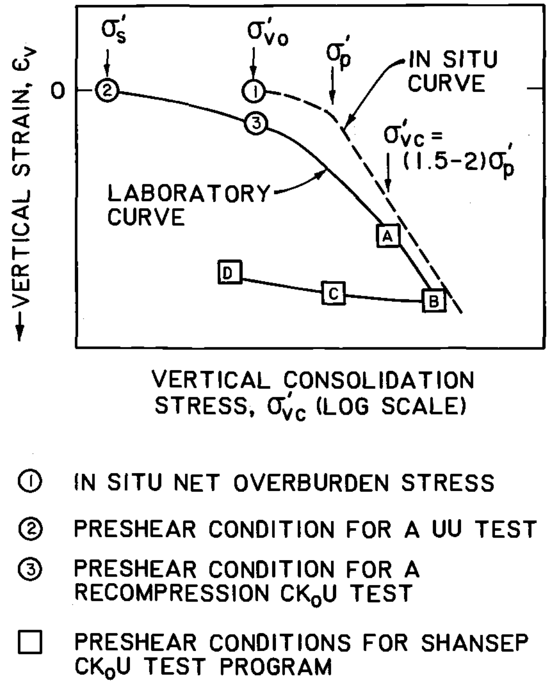

FIG. 8—*Consolidation states for SHANSEP method* [2].

found the relationship to be generally valid although the parameter Λ_o ranged from 0.130 to 0.999. According to critical state theory, Λ_o is related to the ratio between the loading and unloading modulus for compression. Mayne's data showed considerable scatter but appeared to support the theoretical result. Mayne noted that the large data scatter may be the result of inaccurate unloading modulus and that the unload–reload behavior may not be linear on a semi-logarithmic plot.

Equation 2 can be used to estimate OCR based on the fact that OCR $\leq$ 1. The logarithm of normalized strength values should fall on a straight line when plotted versus log (σ_v'), provided the consolidation stress is less than the past maximum consolidation pressure. At confining pressures approaching the past maximum pressure, the normalized strength becomes the constant $(s_u/\sigma_v')_{nc}$. The past maximum pressure is obtained by extrapolation of the straight line portion of the semi-logarithmic plot to the point stress where $s_u/\sigma_v' = (s_u/\sigma_v')_{nc}$. If $(s_u/\sigma_v')_{nc}$ is known or can be estimated, OCR can be estimated without consolidating to the high pressures needed to reach the past maximum pressure.

The straight line relationship between normalized strength and logarithm of consolidation stress provides the information needed to estimate in situ strength, thus avoiding the need to consolidate beyond the past maximum pressure as required for the SHANSEP method. Also the method remains valid for sandy soils or silts which have never been loaded to the past maximum pressure but can be normalized by the limiting pressure p_e. For such soils an apparent past maximum pressure is obtained.

The Mayne procedure does not completely solve the uncertainties created by sampling disturbance. Generally, sampling disturbance causes soils in the CU test to appear more overconsolidated than in the in situ state which, in Mayne's procedure, is reflected as overestimating the past maximum pressure. Therefore, the Casagrande procedure provides a lower-bound estimate of past maximum pressure while Mayne's procedure provides an upper-bound estimate [*21*]. Assuming the straight-line relationship is not greatly affected by sampling disturbance, the two estimates of past maximum pressure can be used to establish bounds on strength. The difference in the bounding values possibly could be developed as a measure of nonrecoverable sampling disturbance.

Summary on Reconsolidation Effects

Sampling disturbance increases the undrained strength of soils by making them more dilative relative to the in situ state. The state surface concept provides a reasonable framework to address the problem for noncemented soils because the relationship between normalized shear strength and OCR is not as greatly influenced as the strength by disturbance. However to apply any of the concepts, it is necessary to estimate the in situ past maximum pressure. Unfortunately, the error in estimates of shear strength are proportional to estimates of maximum past pressure. Therefore, even if the normalized strength versus OCR relationships are known to considerable accuracy, the in situ strength cannot be determined any more accurately than the past maximum pressure. Mayne's procedure is promising because it provides a means to place bounds on the strength values.

Influence of Loading History

In the preceding discussion, disturbance was explained in terms of pore pressure changes that result from sampling, trimming, and reconsolidation. Disturbance to the soil structure induced by sampling was accounted for through the state surface concept which ignores structural changes by assuming that soil behavior is controlled by the initial consolidation stress state and OCR. However, some significant effects of loading history can lead to errors. Although these effects are probably of second order compared to errors inherent in the UU test, research is still limited and loading history will become an important consideration in the future.

Two major problems will be considered. First, the effects of reconsolidation to high stresses will be considered in more detail. Second, the effect of shear stress history will be briefly discussed with special emphasis on the susceptibility of low plasticity soils to shear stresses during sampling.

Consolidation to High Stress

One of the primary assumptions made in application of the state surface concept to reconstruct the in situ state is that the state lines on the e-log(p) plot are parallel to the virgin compression curve. There is nothing inherent in the state surface to guarantee or require that the lines are indeed parallel. The existence of the state surface only depends on the lines being parallel on some form of plot relating void ratio and pressure. Thus, even if the state surface exists, the OCR or p/p_e may not describe it adequately.

Yudhbir and co-workers performed a series of consolidation tests to investigate the relationship between the critical state line and the virgin compression curve [*22*]. Each test was performed at a different effective stress ratio (σ_1'/σ_3' = constant). The compression curves from these tests should be parallel to the state lines shown in Fig. 6*a* because they represent the limiting stress state for a given value of effective stress ratio. The slopes of the lines were found to become systematically flatter as the stress ratio was increased. Therefore, a relationship between normalized strength and OCR developed after stressing to a higher pressure would not be valid for the in situ condition. For a given OCR, the specimens consolidated to the higher pressures and then rebounded would be more dilative and stronger. More recent data indicate that slopes of compression curves in isotropic and K_o loading can be significantly different depending on the soil type [23,24].

It is difficult to determine from available data how much error is introduced by the assumption that the state lines are parallel. There are a number of open questions. For example, is the shift in OCR versus s_u/σ_{vc}' relationship as great as indicated by differences among slopes of isotropic and anisotropic compression curves? What is the effect of soil type on the state line relationship? Are sands and low plasticity soils more susceptible to errors than plastic clays?

Shear-Induced Anisotropy

Another area that requires research is the influence of shear stress history on laboratory strength. The in situ stress state is anisotropic, which potentially leads to the specimen being anisotropic. This initial anisotropy indicates that the state of the soil is not completely defined by the void ratio of the soil and some means of accounting for the shear stress history is needed. Hardin proposed a simple model to depict stress-induced anisotropy [25]. When the specimen is consolidated under isotropic conditions, a yield surface is developed about the hydrostatic axis. If the specimen is loaded to an anisotropic stress state the yield surface shifts and subsequent response of the specimen is relative to a pseudohydrostatic axis established by the previous anisotropic stress state. When a specimen is consolidated isotropically in a triaxial cell, it is actually being loaded into extension relative to the pseudohydrostatic axis that describes the in situ condition. Thus, the state of the soil is described by both void ratio and the position of the pseudohydrostatic axis.

The anisotropy of natural clays was investigated by Graham and coworkers [26,27] who found the actual condition of specimens to be like that depicted by Hardin's conceptual model. The shifted (anisotropic) yield surface was mapped by a series of anisotropic compression tests similar to those used in Yudhbir's experiments. The surface was constructed by plotting the stress states where the past consolidation stress was obtained as indicated by a Casagrande construction. The past maximum pressure was found to be greatest for specimens consolidated under effective stress ratios that approximate the one-dimensional consolidation conditions existing during sample formation.

Apart from the direct comparisons between isotropic and anisotropic consolidation, there are some important ramifications of the tendency for anisotropic consolidation to alter the behavior of soil. It is well known that soil responds to changes in effective stress ratio rather than simply shear stress (see, for example, Ref *28*). For plastic clays, which may retain significant residual effective stress, shear stress caused by sample disturbance produces relatively small changes in effective stress ratio. In contrast, low plasticity soils retain little residual effective stress and even small shear stresses incurred during sampling and preparation cause large changes in stress ratio. The reference or pseudohydrostatic axis of Hardin's model could thus be shifted significantly, causing the specimen to appear more compressible to subsequent laboratory compression. If a mechanistic picture of disturbance could be developed, it may be possible to create a strategy for correcting test results that is comparable to the SHANSEP method. Unfortunately, little systematic data yet exist to support such an interpretation of sampling disturbance.

Conclusions

Interpretation of triaxial test data is made difficult by the obscuring effects of sampling disturbance. The engineer can define fundamental properties of soil with considerable accuracy using modern testing methods but is unable to relate these properties to field behavior because the in situ state of the soil cannot be defined completely. The problem of relating laboratory behavior to field behavior is a particular problem when dealing with low plasticity soils because (1) samples are at a state of low effective stress, (2) the relationship between consolidation state and strength is difficult to determine, and (3) shear stresses induced by sampling may influence laboratory behavior. The loss of effective stress in laboratory specimens appears to be inevitable even under ideal conditions. Therefore, practical methods to improve strength determination of low plasticity soils must come from improved understanding of loading history effects.

Of all techniques for strength determination popular in practice, the least accurate appears to be the UU test. Use of the UU test should be restricted to obtaining strengths of partially saturated or compacted soils; it is not valid for saturated soils having low plasticity, especially when total stress relief exceeds the cavitation pressure of the pore fluid. However, the UU test has precedence and application of undrained strengths from UU tests is much more direct than for the CU test. Therefore considerable effort will be needed to persuade the profession to give the CU test a more dominant role in strength determination. Improvements in the state of the art of triaxial testing will require improvements in education and standardization of test procedures to accompany technical improvements in testing technique and interpretation.

Acknowledgment

The data shown in Figs. 1 to 5 were obtained from special geotechnical studies for the New Orleans District of the U. S. Army Corps of Engineers. Their support is greatly appreciated.

References

[1] Wroth, C. P., and Houlsby, G. T., "Soil Mechanics—Property Characterization and Analysis Procedures," in *Proceedings*, Eleventh International Conference on Soil Mechanics and Foundation Engineering, Vol. 1, San Francisco, A. A. Balkema, 1985, pp. 1–55.

[2] Jamiolkowski, M., Ladd, C. C., Germaine, J. T., and Lancellotta, R., "New Developments in Field and Laboratory Testing of Soils," in *Proceedings*, Eleventh International Conference on Soil Mechanics and Foundation Engineering, Vol. 1, San Francisco, A. A. Balkema, 1985, pp. 57–153.

[3] Ladd, C. C., and Lambe, T. W., "The Strength of Undisturbed Clay Determined from Undrained Tests," *ASTM Symposium on Laboratory Shear Testing of Soils, Ottawa, ASTM STP 361*, American Society for Testing and Materials, Philadelphia, 1963, pp. 342–371.

[4] Kimura, T., and Saitoh, K., "The Effect of Reconsolidation on Undrained Strength of Normally Consolidated Cohesive Soils," *Soils and Foundations*, Japanese Society of Soil Mechanics and Foundation Engineering, Vol. 23, No. 3, 1983, pp. 27–38.

[5] Kimura, T., and Saitoh, K., "The Effect of Sampling Disturbance on Undrained Strength of Cohesive Soils," *Geotechnical Engineering*, Vol. 15, 1984, pp. 37–57.

[6] Kirkpatrick, W. M., and Khan, A. J., "The Reaction of Clays to Sampling Stress Relief," *Geotechnique*, Vol. 34, No. 1, 1984, pp. 29–42.

[7] Johnson, S. J., "Analysis and Design Relating to Embankments: A State-of-the-Art Review," Soils and Pavements Laboratory, U. S. Army Engineer Waterways Experiment Station, Civil Engineer, Vicksburg, MS, Miscellaneous Paper S-75-3, 1975.

[8] Hvorslev, M. J., *Physical Properties of Remoulded Cohesive Soils*, Translation No. 69-5, U. S. Army Engineer Waterways Experiment Station, Civil Engineer, Vicksburg, MS, 1937 (translation published in 1969).

[9] Roscoe, K. H., Schofield, A. N., and Wroth, C. P., "On the Yielding of Soils," *Geotechnique*, Vol. 8, No. 1, 1958, pp. 25–53.

[10] Sandler, I. S., DiMaggio, P. L., and Balidi, G. Y., "Generalized Cap Model for Geologic Materials," *Journal of the Geotechnical Engineering Division, American Society of Civil Engineers*, Vol. 102, No. GT7, 1976, pp. 638–699.

[11] Dafalias, Y. F., and Herrmann, L. R., "A Bounding Surface Formulation of Soil Plasticity" in *Soils Under Cyclic and Transient Load*, G. N. Pande and O. C. Zienkiewicz, Ed., Wiley, New York, 1980, pp. 253–282.

[12] Pender, M. J., "Discussion of Elastoplastic Stress–Strain Theory for Cohesionless Soil," *Journal of the Geotechnical Engineering Division, American Society of Civil Engineering*, Vol. 102, No. GT11, 1976, pp. 1202–1204.

[13] Pender, M. J., "A Model of the Behavior of Overconsolidated Soil," *Geotechnique*, Vol. 28, No. 1, 1978, pp. 1–25.

[14] Seed, H. B., and Lee, K. L., "Undrained Strength Characteristics of Cohesionless Soils," *Journal of the Soil Mechanics and Foundation Division, American Society of Civil Engineers*, Vol. 93, No. SM6, 1967, pp. 333–360.

[15] Torrey, V. H., "Some Effects of Rate of Loading, Method of Loading, and Applied Total Stress Path on the Critical Void Ratio of a Fine Uniform Sand," Ph.D. dissertation, Texas A&M University, College Station, TX, 1981.

[16] Rowe, P. W., "Theoretical Meaning and Observed Values of Deformation Parameters for Soils," in *Proceedings*, Roscoe Memorial Symposium on Stress–Strain Behavior of Soils, Cambridge University, England, R. H. G. Parry, Ed., London, G. T. Foulis, 1971, pp. 143–194.

[17] Ladd, C. C., and Foott, R., "New Design Procedure for Stability of Soft Clays," *Journal of the Geotechnical Engineering Division, American Society of Civil Engineers*, Vol. 100, No. GT7, 1974, pp. 763–786.

[18] Ladd, C. C., and Edgers, L., "Consolidated-Undrained Direct-Simple Shear Tests on Saturated Clays," Research Report R72-92, Soils Publication 284, Department of Civil Engineering, Massachusetts Institute of Technology, Cambridge, MA, 1972.

[19] Ladd, C. C., Foott, R., Ishihara, K., Schlosser, F., and Poulos, H. G., "Stress-Deformation and Strength Characteristics: State of the Art Report, in *Proceedings*, Ninth International Conference on Soil Mechanics and Foundation Engineering, Vol. 2, Tokyo, Japan, 1977, pp. 421–494.

[20] Mayne, P. W., "Cam-Clay Predictions of Undrained Strength," *Journal of the Geotechnical Engineering Division, American Society of Civil Engineers*, Vol. 106, No. GT11, 1980, pp. 1201–1218.

[21] Olsen, H. W., Rice, T. L., Mayne, P. W., and Singh, R. D., "Piston Core Properties and Disturbance Effects," *Journal of the Geotechnical Engineering Division, American Society of Civil Engineers*, Vol. 112, No. 6, 1986, pp. 608–625.

[22] Yudhbir, Mather, S. K., and Kungnathan, V., "Critical State Parameters," Technical Note, *Journal of Geotechnical Engineering Division, American Society of Civil Engineers*, Vol. 104, No. GT4, 1978, pp. 497–501.

[23] Chakrabarti, S., and Horvath, R. G., "Slopes of Consolidation Lines," *Canadian Geotechnical Journal*, Vol. 22, 1985, pp. 254–258.

[24] Peters, J. F., "Constitutive Theory for Frictional Materials," in *Proceedings*, International Conference on Constitutive Laws For Engineering Materials: Theory and Applications, Tucson, AZ, University of Arizona, 1983, pp. 271–282.

[25] Hardin, B. O., "The Nature of Stress–Strain Behavior for Soils," in *Proceedings*, American Society of Civil Engineers Geotechnical Engineering Division, Speciality Conference, Earthquake and Soil Dynamics, Pasadena, CA, Vol. 1, 1978, pp. 3–90.

[26] Graham, J., Noonan, M. L., and Lew, K. V., "Yield States and Stress–Strain Relationships in a Natural Plastic Clay," *Canadian Geotechnical Journal*, Vol. 20, 1983, pp. 502–516.

[27] Graham, J. and Li, E. C. C., "Comparison of Natural and Remolded Plastic Clay," *Journal of Geotechnical Engineering, American Society of Civil Engineers*, Vol. III, No. 7, July 1985, pp. 865–881.

[28] Tatsuoka, F., and Ishihara, K., "Yielding of Sand in Triaxial Compression," *Soils and Foundations*, Japanese Society of Soil Mechanics and Foundation Engineering, Vol. 14, No. 2, 1974, pp. 63–76.

Mladen Vucetic[1] *and Ricardo Dobry*[2]

Cyclic Triaxial Strain-Controlled Testing of Liquefiable Sands

REFERENCE: Vucetic, M. and Dobry, R., "**Cyclic Triaxial Strain-Controlled Testing of Liquefiable Sands,**" *Advanced Triaxial Testing of Soil and Rock, ASTM STP 977,* Robert T. Donaghe, Ronald C. Chaney, and Marshall L. Silver, Eds., American Society for Testing and Materials, Philadelphia, 1988, pp. 475–485.

ABSTRACT: Two series of undrained cyclic triaxial strain-controlled tests were performed on two different Imperial Valley, California, silty sands which liquefied during an earthquake in 1981. Both intact and reconstituted specimens were tested, and the testing procedures are described. The experimental data confirm that cyclic shear strain is the fundamental parameter governing pore pressure buildup, because strain-controlled tests essentially eliminate the influence of specimen fabric and sample disturbance. Also, the results indicate that the cyclic triaxial test can be used to model cyclic simple shear (similar to seismic field conditions), if the cyclic simple shear strain, γ_{cy}, is related to the cyclic triaxial axial strain, ϵ_{cy}, by either of two similar analytical expressions: $\gamma_{cy} = 1.5\,\epsilon_{cy}$ or $\gamma_{cy} = \sqrt{3}\,\epsilon_{cy}$. Consequently, a unique pore pressure model is developed and recommended to simulate the seismic pore pressure buildup at the site. This model is applicable to reconstituted and intact specimens of the two sands, despite their different void ratios and nonplastic silt contents, and is valid for both cyclic triaxial and cyclic simple shear strain-controlled conditions.

KEY WORDS: dynamic loading, liquefaction, model, pore pressure, repeated loading, sample disturbance, sand, simple shear test, triaxial test

Nomenclature

e	Void ratio
F	Pore pressure model experimental constant
n_c	Number of cycles
p	Pore pressure model experimental constant
s	Pore pressure model experimental constant
u	Residual cyclic pore pressure
u^*	Residual cyclic pore pressure normalized to $\bar{\sigma}_c$
γ_{cy}	Cyclic shear strain amplitude
γ_d	Dry unit weight
γ_{tp}	Practical threshold shear strain
ϵ_{cy}	Cyclic axial strain amplitude
$\bar{\sigma}_c$	Isotropic effective consolidation stress
σ_{dc}	Cyclic deviatoric stress amplitude
τ_{cy}	Cyclic shear stress amplitude
τ_{cy}^*	Cyclic shear stress amplitude normalized to $\bar{\sigma}_c$

[1] Assistant professor, Civil Engineering Department, University of California at Los Angeles, Los Angeles, CA 90024-1593.
[2] Professor, Civil Engineering Department, Rensselaer Polytechnic Institute, Troy, NY 12180.

Introduction

In geotechnical engineering practice, many design methods rely on laboratory test results. However, obtaining good quality laboratory data, and particularly results of cyclic testing, requires a sophisticated operation, and its success depends to a great extent on both the researcher's experience and the available equipment. The last 20 years have seen the development of ever more realistic and sophisticated methods for analyzing the seismic response of soil deposits, which have outpaced the development of corresponding laboratory techniques. Some explanations for this trend lie in the complex, painstaking, and time-consuming processes associated with experimental research, plus the economic inertia which tends to block needed changes in established testing procedures and equipment. Also, the numerous factors that influence soil behavior cause conflicting findings followed often by controversy and confusion. On the other hand, as shown elsewhere by Vucetic [*1*], small variations of parameters in the laboratory can sometimes significantly change the calculated seismic response of a soil profile. To obtain reliable soil properties, it is therefore indispensable to develop testing procedures in which the detrimental effects influencing the results can be systematically examined, eliminated, reduced, or accounted for.

There are basically three types of cyclic testing techniques employed today for evaluation of cyclic properties of saturated sands: cyclic triaxial, cyclic simple shear, and cyclic (solid or hollow cylinder) torsional shear technique. While the conceptually more realistic cyclic simple shear and torsional shear methods have been steadily improved, the cyclic triaxial procedure still seems to play a key role in most soil dynamics studies.

Actual seismic loads are highly irregular and three-directional. However, most of the laboratory-based methods presently available simplify this reality and use one-directional uniform cyclic testing, either stress-controlled or strain-controlled. The stress-controlled testing technique, in which the cyclic stress amplitude is kept constant throughout the test, was introduced first. But the unacceptable scatter of test data obtained on reconstituted specimens and the great sensitivity to sample disturbance of the stress-controlled results have induced a critical reexamination of this technique [*2*]. Simultaneously, a substantial body of evidence has shown that pore pressure buildup during cyclic strain-controlled testing, in which the cyclic strain amplitude is kept constant throughout the test, is affected very little by specimen fabric, and only moderately by specimen void ratio (density). This indicates clearly that cyclic shear strain, rather than cyclic shear stress, is a more fundamental parameter governing the seismic response of sand [*1–5*].

This paper presents and discusses cyclic triaxial strain-controlled tests on reconstituted and intact specimens of two different sands. In each of the two corresponding test series, the void ratio was kept practically constant, and the following aspects of the strain-controlled testing were evaluated: repeatability of testing procedure, comparison between results obtained on intact and reconstituted specimens, comparison between results obtained on two different sands, interpretation of pore water pressure buildup by a model previously proposed by Dobry and coworkers [*4*], and comparison with cyclic results on the same sands obtained in the simple shear device.

Sands Tested and Testing Program

Both sands tested here were obtained from the same Wildlife Site deposit, located in the Imperial Valley, Southern California, which liquefied during the 1981 Westmoreland earthquake [*6*]. This saturated deposit is composed of two layers: an upper, looser, sandy silt unit located between 2.6 m and 3.5 m depth, containing more fines (37%) and called here sand A, and the lower, loose to medium-dense sand unit located between 3.5 m and 6.8 m, containing less fines (25%) and called here sand B. The grain size distribution curves are presented in Fig. 1.

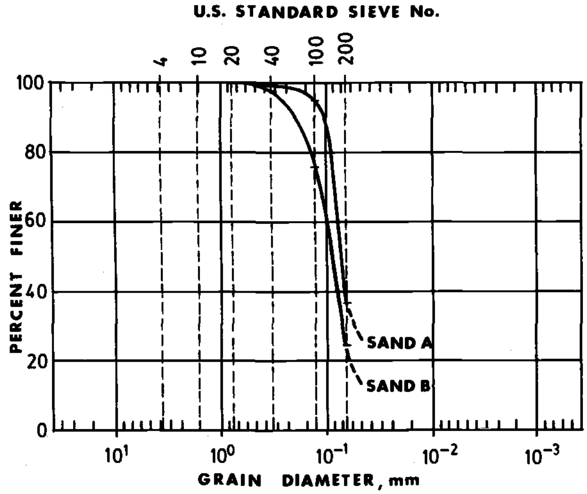

FIG. 1—*Grain size distribution of sands tested.*

The two test series (summarized in Table 1) were conducted by the authors as part of a comprehensive evaluation of the Wildlife Site 1981 liquefaction case history [*1*]. The complete testing program (reported in Ref *1*) also included a series of Norwegian Geotechnical Institute (NGI) cyclic direct simple shear tests, and several slow and fast monotonic triaxial tests.

A total of thirteen strain-controlled tests are analyzed here: six on sand A consolidated to a void ratio $e \simeq 0.85$, and seven tests on sand B consolidated to $e \simeq 0.76$. The cyclic axial strain amplitude used, ϵ_{cy}, ranged between 0.02% and 1.35% at a frequency of 0.2 Hz. Most of the tests were performed on reconstituted specimens, except for one test per sand conducted on an intact specimen (tests 6 and 13). In all tests an isotropic consolidation effective stress, $\bar{\sigma}_c$ = 96 kPa (2 ksf), was used.

Testing Procedure

The intact sand samples used in this investigation were 76.2 mm (3 in.) in diameter, and they were retrieved with an Osterberg piston sampler or a thin-walled Shelby tube sampler.

TABLE 1—*Triaxial testing program.*

Test Number	Layer	Method of Specimen Preparation	Dry Unit Weight (γ_d), g/cm^3	Void Ratio (e)	Cyclic Axial Strain (ϵ_{cy}), %	Cyclic Shear Strain ($\gamma_{cy} = 1.5\epsilon_{cy}$), %
1	A	Reconstituted	1.447	0.852	0.020	0.030
2	A	Reconstituted	1.448	0.851	0.067	0.101
3	A	Reconstituted	1.446	0.853	0.200	0.300
4	A	Reconstituted	1.452	0.846	0.667	1.001
5	A	Reconstituted	1.451	0.847	1.347	2.021
6	A	Intact	1.468	0.826	0.702	1.053
7	B	Reconstituted	1.534	0.751	0.020	0.030
8	B	Reconstituted	1.528	0.757	0.067	0.101
9	B	Reconstituted	1.527	0.759	0.199	0.299
10	B	Reconstituted	1.534	0.751	0.674	1.011
11	B	Reconstituted	1.523	0.764	0.681	1.021
12	B	Reconstituted	1.527	0.759	1.350	2.025
13	B	Intact	1.618	0.660	0.682	1.023

After the tube withdrawal in the field, water was drained from the tubes to generate capillary forces in the silty sand. These forces minimized sample disturbance during transportation and trimming.

The intact specimens were produced in the laboratory by first cutting the tube into smaller sections to minimize the side friction during extrusion. After being vertically extruded from such a short tube, each intact specimen was cut with a sharp edge to a height of approximately two sample tube diameters. The diameter of the specimen obtained in this way was not reduced by trimming. It remained the same as it was after the extrusion. The specimen then was slid carefully onto the fine-grained porous stone fixed into a special horizontal plate. The top porous stone was put on the specimen, and a membrane was placed around it by means of a membrane stretcher and vacuum. The vacuum was then released so that the membrane became slightly pressed against the specimen and also grasped both porous stones. Now supported by the membrane and the porous stones, the specimen was removed from the extrusion frame and placed onto the triaxial cell pedestal. The triaxial cell cap was first mounted by fixing it on the rigid columns located inside the cell, and the top specimen cap was then lowered onto the top porous stone already sitting on the specimen. Finally, the cell was closed by pulling on the cell sleeve. Then the triaxial cell was filled with deaired water to prevent migration of air through the specimen membrane. Following that the specimen was flushed with carbon dioxide (CO_2), filled with deaired distilled water, and back-pressured overnight to 414 kPa (60 psi) (345 kPa [50 psi] in the case of reconstituted specimens), with an effective all-around confining pressure of 17 kPa (2.5 psi). The next day, the specimen was consolidated to the desired effective confining stress, $\bar{\sigma}_c$ = 96 kPa (2 ksf). Volume and height changes were recorded during all consolidation steps.

After consolidation, the triaxial cell was sealed and locked and then transferred from the consolidation table to the cyclic testing frame. Here, the cell was fixed to the base of the frame and attached to the vertical actuator and transducer, volume change burette, and pore pressure transducer. The pore pressure B parameter was then determined to check for the saturation of the soil. This was done by increasing the cell pressure by 28 kPa (4 psi) and by measuring the increase of pore pressure in the specimen. The measured value of B was typically about 98%, and it was always greater than 95%, usually accepted as the minimum value needed to ensure full saturation. The drainage valves were then closed, while the connection between pore pressure transducer and specimen remained open, and the undrained cycling was started.

The reconstituted triaxial sand specimens tested were all solid cylinders, 50.8 mm (2.0 in.) in diameter and 101.6 mm (4.0 in.) in height. They were fabricated by mixing the wet sand extruded from all tubes containing the same type of sand and prepared by the wet tamping undercompaction technique described by Ladd [*7,8*]. Although this procedure most frequently uses undercompaction in six layers with 6% water content, in the present testing, to ensure a higher degree of uniformity within each specimen and between different specimens, the specimens were compacted in eight layers. Also, given the high silt content of the sands tested, the water content of the sand mixture was set somewhat higher, varying between 8 and 12%. The undercompaction used was 2%.

The cyclic strain-controlled tests were conducted in the sinusoidal mode with the servo-hydraulic closed loop system shown in Fig. 2. During cyclic shearing, all parameters were recorded automatically with an oscillographic FO-CRT (fiber-optic cathode-ray tube) strip chart recorder and an X-Y recorder. The strip chart data were preferred for interpretation of the results shown later, because of the practically infinite speed of the FO-CRT recording.

Given the relatively high silt content of 37% for sand A and 25% for sand B, and based on the membrane compliance measurements on similar soils by Hammer [*9*], no membrane compliance correction was considered necessary in the interpretation of the measured pore pressures.

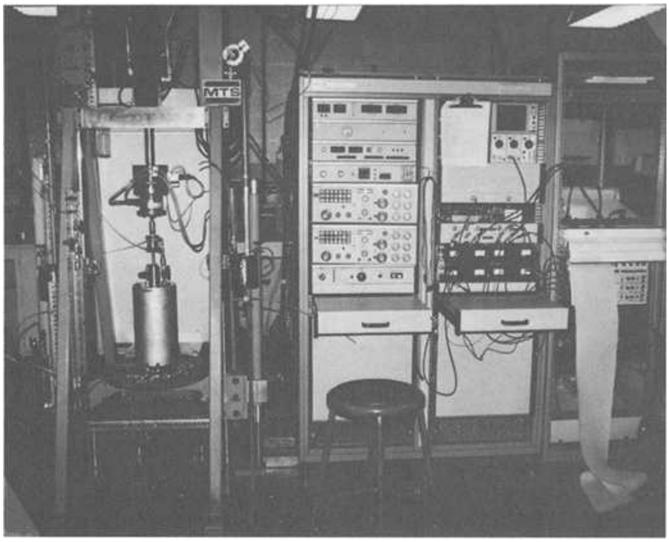

FIG. 2—*Triaxial testing configuration layout.*

Interpretation of Test Results

Selected plots of normalized cyclic shear stress, $\tau_{cy}^* = \tau_{cy}/\overline{\sigma}_c$, and normalized residual pore pressure, $u^* = u/\overline{\sigma}_c$, versus number of uniform strain cycles, n_c, up to $n_c = 30$, are shown in Figs. 3 and 4 for sands A and B, respectively. τ_{cy} above is the amplitude of cyclic shear stress acting on 45° planes within the specimen, with $\tau_{cy} = \sigma_{dc}/2$, where σ_{dc} is the cyclic deviatoric stress amplitude, and u is the accumulated residual cyclic pore pressure at

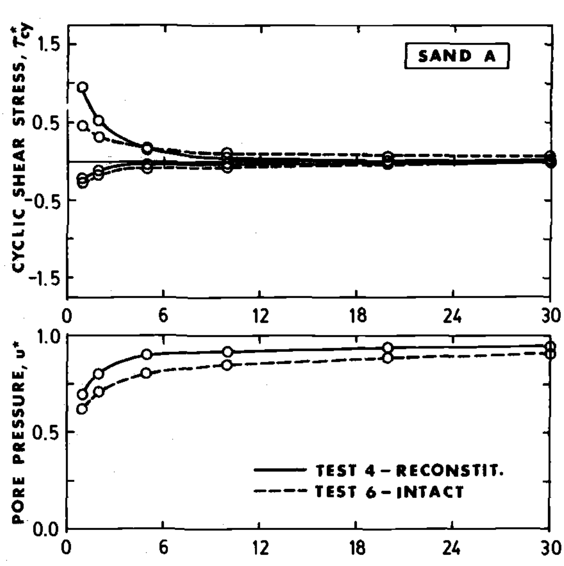

FIG. 3—*Comparison of results obtained on intact and reconstituted specimens of sand A.*

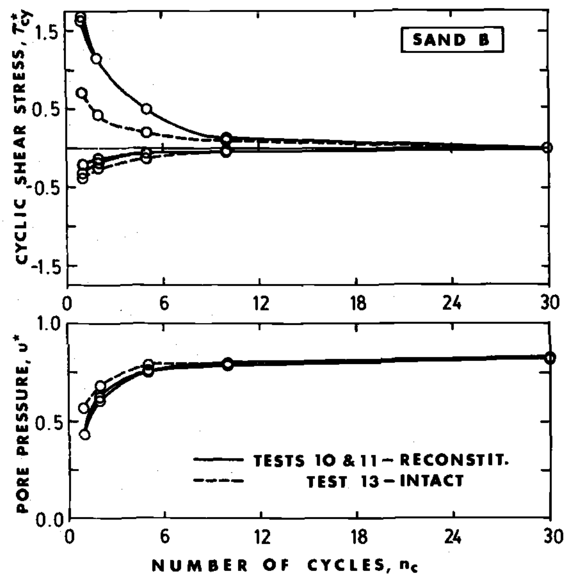

FIG. 4—*Comparison of results obtained on intact and reconstituted specimens of sand B.*

the end of the pertinent strain cycle, derived from measurements at the point of the cycle at which the cyclic stress $\sigma_{dc} = \tau_{cy} = 0$.

The repeatability of the undercompaction, wet-tamping testing technique will be examined first. Figure 4 includes the results of two comparable tests on sand B, tests 10 and 11, which practically plot on top of each other, verifying the high repeatability of the procedure. These results, as well as the consistency of other results, generally confirm the high quality of the experimental data presented in this paper.

The effect of sand fabric, that is, the difference between results obtained on reconstituted and intact specimens, is analyzed next for both sands A and B, with the help of Figs. 3 and 4. It can be readily noticed in these two figures that the residual pore pressures in cyclic triaxial strain-controlled tests are practically unaffected by the change of sand fabric (u^* versus n_c curves), while, on the contrary, soil stiffness is significantly affected (τ_{cy}^* versus n_c curves). This is especially noticeable in Fig. 4, and it confirms similar findings obtained earlier from other available strain-controlled testing [*2*].

The results are further evaluated for the effects of specimen void ratio and silt content, and from the viewpoint of modeling of pore pressure buildup for seismic field analyses. A careful examination and comparison of individual results for both soils reveals that the relationships among ϵ_{cy}, n_c, and residual pore pressure buildup, u^*, are almost identical for the two Wildlife sands. The corresponding comparison for all reconstituted specimen tests is illustrated in Fig. 5. Up to $\epsilon_{cy} = 0.20\%$, there is practically no difference in the rate of pore pressure buildup between the two soils. Given the fact that sands A and B have different silt contents and were prepared at different densities, these results confirm the insensitivity of pore pressure buildup in strain-controlled tests to those two factors. Additional evidence supporting this conclusion is provided elsewhere [*1,2*].

It must also be noticed that the range of cyclic shear stresses measured at a given cyclic strain in Figs. 3 and 4, for the two sands and for the two types of specimen fabric, is quite wide, in contrast to the corresponding range of pore pressures in Fig. 5, which is very narrow. This confirms once again that cyclic shear strain is the fundamental parameter governing

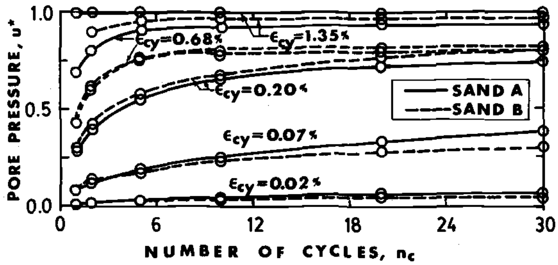

FIG. 5—*Residual pore pressure in reconstituted specimens of sands A and B.*

pore pressure buildup, and that use of strain-controlled testing and of associated analytical modeling represents the most appropriate, as well as the most convenient, approach currently available for evaluation of seismic pore pressures and liquefaction of level ground sites.

To describe such consistent pore pressure buildup obtained in cyclic strain-controlled tests, Dobry and coworkers have developed a simple pore pressure model [*4*], applicable to both cyclic triaxial and cyclic simple shear pore pressure results. The basic form of the model is

$$u^* = \frac{p \cdot n_c \cdot g(\gamma_{cy})}{1 + n_c \cdot g(\gamma_{cy})} \tag{1}$$

where the constant p and function $g(\gamma_{cy})$ can be determined from the measured u^*. Recent results by Vucetic [*1*] further show that a convenient particular form of the model for many sands is

$$u^* = \frac{p \cdot n_c \cdot F \cdot (\gamma_{cy} - \gamma_{tp})^s}{1 + n_c \cdot F \cdot (\gamma_{cy} - \gamma_{tp})^s} \tag{2}$$

where

$$g(\gamma_{cy}) = F \cdot (\gamma_{cy} - \gamma_{tp})^s \tag{3}$$

This means that the relationship between u^*, γ_{cy}, and n_c can be described for one-directional loading by four experimental constants: p, F, γ_{tp}, and s. The constant γ_{tp} is the practical threshold strain, that is, the shear strain below which, for all practical purposes, the residual pore pressure buildup can be taken as zero. It should be mentioned that γ_{tp} is usually somewhat larger than the actual threshold strain, which is for most sands about equal to $10^{-2}\%$ [*2,3,5*].

Based on the results presented in Fig. 5, the following unique pore pressure model, applicable to both Wildlife sands A and B, was obtained:

$$u^* = \frac{1.04 \times n_c \times 2.6 \times (\gamma_{cy} - 0.02)^{1.7}}{1 + n_c \times 2.6 \times (\gamma_{cy} - 0.02)^{1.7}} \tag{4}$$

This expression is graphically portrayed in Fig. 6 as a family of curves for $n_c = 1, 2, 5, 10$, and 30. In Eq 4 and Fig. 6 the transformation $\gamma_{cy} = 1.5\ \epsilon_{cy}$, based on continuum mechanics considerations, was used to plot the cyclic triaxial measurements. This expression is very similar to $\gamma_{cy} = \sqrt{3}\ \epsilon_{cy} = 1.73\ \epsilon_{cy}$, derived by Prevost [*10*] based on the incremental theory of plasticity.

As shown in Fig. 6, the model described by Eq 4 was developed based only on the tests

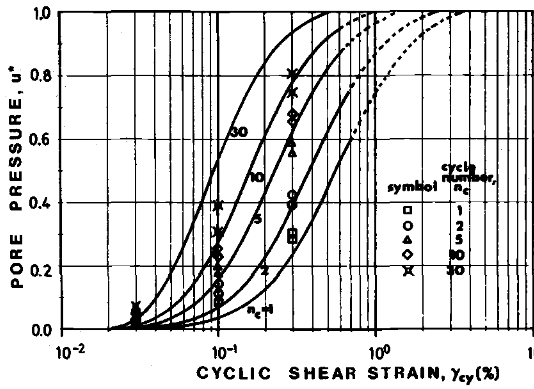

FIG. 6—*Unique pore pressure model for sands A and B based on cyclic triaxial results.*

with $\gamma_{cy} \lesssim 0.3\%$. This was done because the pore pressure results for γ_{cy} = 1 and 2% and the data for smaller γ_{cy} could not be properly fitted together by means of a single $u^* = f(\gamma_{cy},n_c)$ relationship of the form given by Eq 1. A detailed examination of the strip charts and X-Y test records disclosed that in these tests with γ_{cy} = 1 and 2%, the effective stress paths of both sands A and B reached the failure envelope in the very first cycle and then, because the tested sands were dilative, the stress paths followed the envelope upwards until the stress reversed. This kind of behavior of dilative sands subjected to large cyclic strains is exemplified by the deviator vertical load versus pore pressure curve of test 11 conducted on sand B and presented in Fig. 7. This graph can, of course, be interpreted as an effective stress path p'–q plot. In Fig. 7, the two consecutive points in the first cycle, at which the stress path first reaches and then leaves the envelope, are denoted by P and Q respectively. Consequently, after approaching the envelope, beyond point P, while the "stress path" moved between points P and Q, the pore pressure was decreasing instead of increasing, and the shear-stress-versus-time relationship, recorded on the strip chart, did not have the sinusoidal pattern characteristic of all other tests with γ_{cy} smaller than 1%. Because of this inconsistency, the triaxial results for γ_{cy} = 1% and beyond were not used for the development of the pore pressure model described by Eq 1 and 2.

It was mentioned earlier that, as a part of the Wildlife site seismic evaluation, cyclic simple shear tests were also performed on the same sands. The results are reported elsewhere, together with a discussion on the applicability of the simple shear technique to cyclic testing

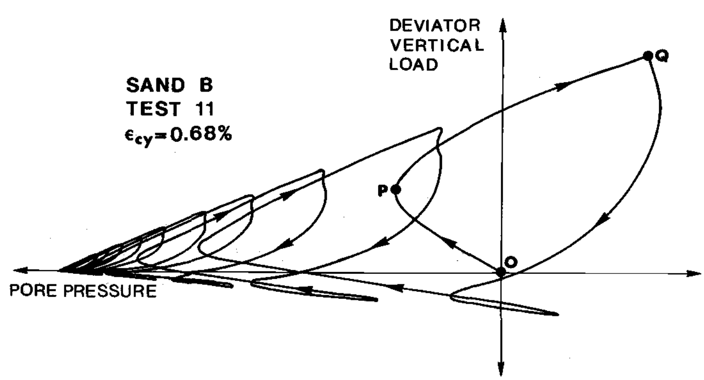

FIG. 7—*Record of deviator vertical load versus pore pressure for test 11.*

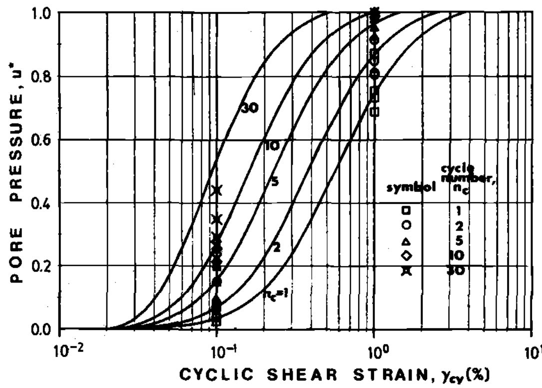

FIG. 8—*Unique pore pressure model for sands A and B based on cyclic simple shear results.*

of sand [1]. The model based on these simple shear tests is reproduced in Fig. 8 and can be compared to the corresponding model in Fig. 6, obtained here from triaxial tests. The two models are identical, despite being derived from two different sets of pore pressure data. The only difference between the two is that the simple shear-based model in Fig. 8 could be applied to cyclic strains up to at least 1%, unlike the model based on cyclic triaxial tests of Fig. 6, which is not valid for such large strains, as discussed above. This is clearly associated with the different loading and boundary conditions in the two types of tests (for more information on this, see Ref 1).

Therefore, the results presented in this paper clearly show that a unique pore pressure model is valid for both Wildlife sands, applicable to both cyclic triaxial and simple shear strain-controlled tests and to both reconstituted and intact specimens. This is a very important conclusion, supportive of the strain approach and consistent with the theory of plasticity formulation suggested by Prevost. It reveals that no empirical factor is necessary to go from pore pressures measured in cyclic triaxial tests to those obtained in cyclic simple shear tests, provided that strain-controlled tests are used in both cases.

Discussion and Conclusions

The test results presented yield a number of significant conclusions concerning the experimental evaluation of seismic pore pressures in saturated sands using cyclic triaxial strain-controlled tests. They show that cyclic strain-controlled testing is a very good tool for quantitative and qualitative evaluation of pore pressures developed in saturated sands subjected to cyclic loading. It was verified that, if sand is tested in the strain-controlled mode, as opposed to the stress-controlled mode, a very consistent picture of pore pressure generation is obtained. Such experimental findings confirm that cyclic shear strain is the fundamental parameter governing undrained pore pressure buildup in saturated sands, as previously concluded by Dobry and coworkers [3]. An important practical consequence is that the residual pore pressure buildup, for a given shear strain and number of cycles, is relatively insensitive to the initial values of sand stiffness, strength, and confining pressure, as well as to sample disturbance.

In this work, results on two Wildlife sands, tested in intact and reconstituted state and using triaxial and simple shear testing techniques, were evaluated. An identical pore pressure model was derived independently from experiments using two different testing techniques, and this model was found to be valid for both intact and reconstituted specimens. This verifies the conclusion that the pore pressure model proposed by Dobry and coworkers [4] can be successfully developed based on results obtained on reconstituted specimens only, which greatly simplifies the whole procedure of evaluating pore pressure and liquefaction of level sandy sites subjected to earthquakes.

The results also show that for the development of the pore pressure model, the undercompaction method proposed by Ladd [7], if properly applied, is a good method for building reconstituted specimens. In this procedure, however, care must be taken when determining the percentage of undercompaction and the water content of the sand mixture. Also, to ensure good uniformity, the specimen should be built using the maximum possible number of layers.

With regard to the selection of the appropriate testing technique for evaluating the seismic characteristics of saturated sand deposits, it must be emphasized that the NGI simple shear testing procedure, if the equipment is available, can be simpler and more economical than triaxial testing. There are also other reasons to support the use of the simple shear procedure. First, the loading boundary conditions in this test resemble more directly the earthquake field conditions of vertically propagating seismic shear waves in level sites and, second, the pore pressure buildup at large cyclic shear strains can be consistently determined and modeled. On the other hand, the triaxial test does not strictly simulate the seismic field loading conditions characteristic of vertically propagating shear waves in level sites. The triaxial procedure is far more complex, and the pore pressures cannot sometimes be realistically modeled beyond cyclic shear strains of about 0.3%. Also, for sands coarser and cleaner than those tested here, a triaxial membrane compliance correction may be required for the measured pore pressures. A disadvantage of the NGI simple shear test, however, is that the pore pressures at very small shear strains around the threshold ($\gamma_{cy} \simeq 1 \times 10^{-2}\%$) cannot be exactly determined because the device has too much compliance for reliable small strain measurements.

Fortunately, the previous discussion on the relative merits of the simple shear and triaxial techniques turns out not to be critical in practice for fine sands and silty sands, because the authors verified here that the measured triaxial residual pore pressures can be easily transformed into those that would be measured in simple shear tests, despite the different loading conditions in the two tests. Either $\gamma_{cy} = 1.5\ \epsilon_{cy}$ or the similar expression $\gamma_{cy} = \sqrt{3}\ \epsilon_{cy} = 1.73\ \epsilon_{cy}$ can be employed for this transformation. In the case of medium and coarse clean sands, a membrane compliance correction may be necessary for the measured residual triaxial pore pressures before applying this transformation. Therefore, and as shown clearly by the Wildlife sand data, the pore pressure model obtained from triaxial tests on reconstituted silty sand specimens can be used with confidence for interpretation of level site seismic field conditions.

Acknowledgments

The tests presented were conducted in the Class of 1933 Earthquake Engineering and Cyclic Loading Laboratory of the Rensselaer Polytechnic Institute, Troy, NY, as a part of a joint project on liquefaction of sands in the Imperial Valley, CA, financially supported by the U. S. Geological Survey (USGS) through Contract Number 14-08-0001-21272. The joint project was carried out by several organizations: U. S. Geological Survey, Menlo Park, CA, under the supervision of T. Leslie Youd; University of Texas at Austin under the supervision of Kenneth H. Stokoe, II; Woodward-Clyde Consultants, Wayne, NJ under the supervision of Richard S. Ladd, and Rensselaer Polytechnic Institute. Work performed under NSF Grant No. CEE83-05653 was used to discard the need for membrane penetration correction during the cyclic triaxial test. The support of USGS and NSF, and the help and participation of all organizations and researchers involved are greatly appreciated.

References

[*1*]* Vucetic, M., "Pore Pressure Buildup and Liquefaction at Level Sandy Sites During Earthquakes," Ph.D. Thesis, Civil Engineering Department, Rensselaer Polytechnic Institute, Troy, NY, 1986, 611 pp. (available from University Microfilms International, Ann Arbor, MI 48106).

[*2*] National Research Council "Liquefaction of Soils during Earthquakes," National Research Council Special Publication, Committee on Earthquake Engineering, National Academy Press, Washington, DC, 1985, 240 pp.

[*3*] Dobry, R., Ladd, R. S., Yokel, F. Y., Chung, R. M., and Powell, D., "Prediction of Pore Water Pressure Buildup and Liquefaction of Sand During Earthquakes by the Cyclic Strain Method," National Bureau of Standards Building Science Series 138, Washington, DC, 1982, 154 pp.

[*4*] Dobry, R., Pierce, W. G., Dyvik, R., Thomas, G. E., and Ladd, R. S., "Pore Pressure Model for Cyclic Straining of Sand," *Journal of Geotechnical Engineering Division, American Society of Civil Engineers* (submitted).

[*5*] Dyvik, R., Dobry, R., Thomas, G. E., and Pierce, W. G., "Influence of Consolidation Shear Stresses and Relative Density on Threshold Strain and Pore Pressure During Cyclic Straining of Saturated Sands," Miscellaneous Paper GL-84-15, Department of the Army, U.S. Army Corps of Engineers, Washington, DC, 1984, 73 pp.

[*6*] Bennett, M. J., McLaughlin, P. V., Sarmiento, J. S., and Youd, T. L., "Geotechnical Investigation of Liquefaction Sites, Imperial Valley, California," Open-File Report 84-252, U.S. Geological Survey, Menlo Park, CA, 1984, 103 pp.

[*7*] Ladd, R. S., "Preparing Test Specimens Using Under Compaction," *Geotechnical Testing Journal, ASTM,* Vol. 1, No. 1, March 1978, pp. 16–23.

[*8*] Ladd, R. S., "Geotechnical Laboratory Testing Program for Study and Evaluation of Liquefaction Ground Failure Using Stress and Strain Approaches: Heber Road Site, 15 Oct. 1979, Imperial Valley Earthquake," Volumes I to III, Woodward-Clyde Consultants, Eastern Region, Wayne, NJ, 1982.

[*9*] Hammer, M. L., "The Membrane Penetration Effect on Pore Water Pressures Measured in Sands During Cyclic Triaxial Test," M.S. Thesis, Department of Civil Engineering, Rensselaer Polytechnic Institute, Dec. 1986.

[*10*] Prevost, J. H., "Mathematical Modelling of Monotonic and Cyclic Undrained Clay Behavior," *International Journal of Numerical and Analytical Methods in Geomechanics,* Vol. 1, 1977, pp. 195–216.

* This reference is identical to Vucetic, M., and Dobry, R., "Pore Pressure Buildup and Liquefaction at Level Sandy Sites During Earthquakes," Research Report No. CE-86-3, Civil Engineering Department, Rensselaer Polytechnic Institute, Troy, NY, prepared for the U.S. Geological Survey, Menlo Park, CA, 1986, 611 pp.

Hedi Dendani,[1] *Etienne Flavigny,*[1] *and Jean Jacques Fry*[2]

Triaxial Test for Embankment Dams: Interpretation and Validity

REFERENCE: Dendani, H., Flavigny, E., and Fry, J. J., "**Triaxial Test for Embankment Dams: Interpretation and Validity,**" *Advanced Triaxial Testing of Soil and Rock, ASTM STP 977,* Robert T. Donaghe, Ronald C. Chaney, and Marshall L. Silver, Eds., American Society for Testing and Materials, Philadelphia, 1988, pp. 486–500.

ABSTRACT: For the construction of two large dams, several triaxial test series were executed on the embankment materials. The first material is an altered sandstone and the second a filter material. Several stress paths of loading were tested: extension test, constant mean pressure test, constant stress ratio, and conventional tests. The various causes of error in the experiments were examined: end restraint, bedding error, and membrane penetration. For a good estimation of deformation modulus, direct measurements inside the triaxial cell were developed. The general results are presented and the methods produced high quality tests. The effects of the grain size distribution were also studied: on the same material, triaxial tests with different specimen diameters were conducted for various maximum grain sizes.

KEY WORDS: embankment dam, soil testing, triaxial test, lubricated ends, stress paths, membrane penetration, bedding effect, mechanical properties

Electricité de France has recently constructed the Grand-Maison (160-m high) and the Vieux-Pré (70-m high) earth dams. In both cases, the structures are zoned embankments with a vertical core. The monitoring of the construction has been compared with numerical simulation by finite element methods. The construction has been done by layers and the results of the monitoring give the real behavior of the materials. For the interpretation of the simulation results, the determination of the mechanical properties of the soils is very important.

At the Vieux-Pré dam, the monitoring results from field observations showed that the upstream and downstream zones were stiffer than the predicted values based on a preliminary laboratory test. This difference underestimated the risks of hydraulic fracturing and required a study to explain the causes of this fact.

At Grand-Maison, with the chosen computation parameters, similar results were obtained, especially for the stress distribution in the drains and filters.

To explain these differences between the results of the numerical simulation and the monitoring behavior of the dams, an extensive study of the mechanical properties of the materials was conducted: the objective of this study is to obtain realistic parameters of the constitutive equations used for the numerical simulation.

The different causes of error in the triaxial test are analyzed in detail: specimens with end restraint, membrane penetration effect, and bedding effect. The obtained results are then presented for the two construction materials: the Vieux-Pré altered sandstone and the Grand-Maison filter.

[1] Research assistant and assistant professor, respectively, Institut de Mécanique de Grenoble, BP 68, 38402 Saint Martin D'Heres, France.
[2] Geotechnical engineer, Electricité de France, BP 1034, 73010 Chambéry Cedex, France.

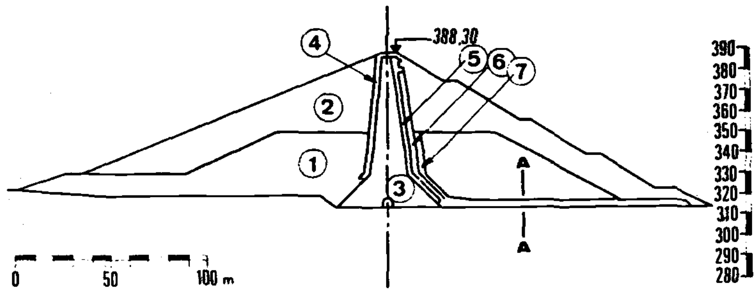

FIG. 1—*Vieux-Pré dam, typical cross section:* (1) *sandstone G1,* (2) *sandstone G2,* (3) *clay,* (4) *filter 0 to 5 mm,* (5) *filter 0 to 20 mm,* (6) *drain, and* (7) *filter 0 to 80 mm.*

Dams and Materials

The Vieux-Pré Dam

The Vieux-Pré dam [*1*] (Fig. 1) is an embankment dam, with a vertical core 79 m high above the foundations; the crest is 350 m wide for a total volume of 1.8 $10^6 \cdot m^3$. This water-resistant structure is made of two compacted rockfill zones surrounding the vertical clay core protected by filters and drains. The initial design study had been done using conventional methods (stability analysis, design filter criteria and so forth). To carry out the deformation analysis, the coarse material G1 had to be tested in laboratory.

The grain size distribution curve for the real material is presented in Fig. 2. For the laboratory experiments conducted by MECASOL (Paris), the material was limited at a maximum diameter of 63 mm (Curve 2, Fig. 2) for the specimens with a diameter of 300 mm; for the tests carried out at the Institut de Mécanique de Grenoble (I.M.G), only a small fraction of the material had been studied (Curve 3, Fig. 2) with a maximum grain size of 20 mm for the 100-mm specimens. To study the role of limited grain size, tests were conducted on a grain size distribution with more coarse sizes (Curve 4, Fig. 2).

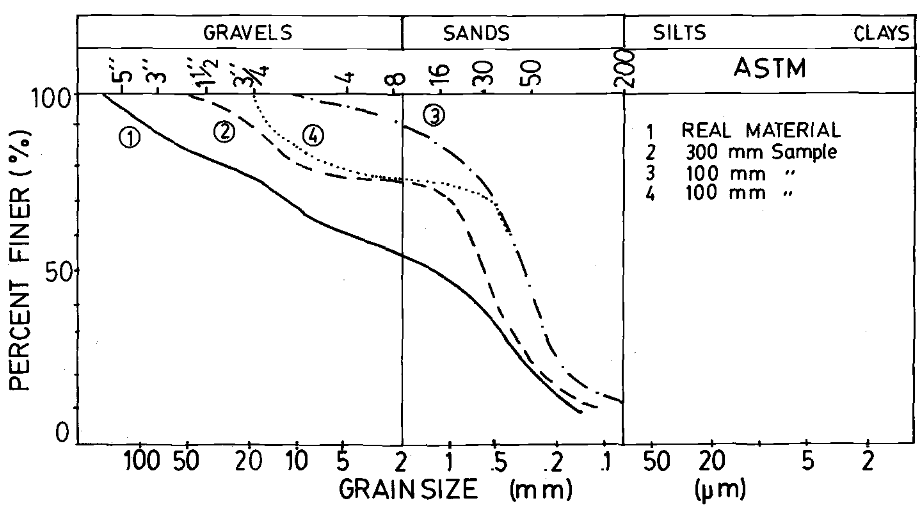

FIG. 2—*Grain size distribution curves for the Vieux-Pré material.*

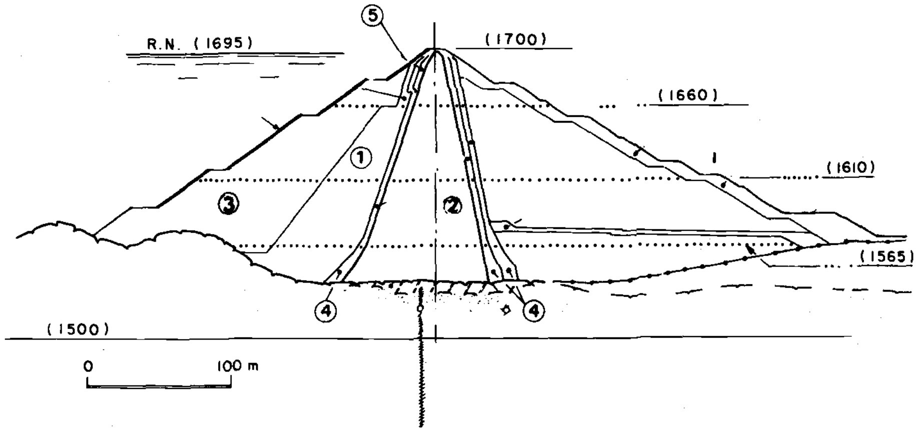

FIG. 3—*Grand-Maison Dam, typical cross section:* (1) *upstream scree shell,* (2) *earth core,* (3) *rockfill, and* (4) *filters.*

The Grand-Maison Dam

The Grand-Maison dam [*2*] is 160 m high, and is composed of 12 $10^6 \cdot m^3$ of compacted backfill. The cross section of the structure is shown in Fig. 3. The materials used for the embankments as well as the vertical core have a large range of grain size with a significant clay fraction. The filters used were made with crushed gneiss; the grain size distribution curve is given in Fig. 4. For the triaxial tests with a diameter of 100 mm, the size of the grains was limited to 20 mm (Curve 1, Fig. 4). Different grain size distributions were also tested at 10, 5, and 2 mm (Curves 2, 3, and 4, Fig. 4).

Experimental Tests

For the two materials, the experimental program consisted of:

- drained triaxial compression tests with constant lateral pressure,
- drained triaxial compression tests with constant mean pressure,
- drained triaxial compression tests with constant effective stress ratio, and
- drained triaxial extension tests with constant lateral pressure.

True triaxial tests were also conducted at the I.M.G. on the Grand-Maison filter [*3*].

Objectives of the Program

To determine the parameters of constitutive equations used in a numerical simulation by the finite elements method, an extensive experimental basis is necessary with several loading paths. Figure 5 shows the different effective stress paths in the plane of principal stresses for the Vieux-Pré material in a loose state (17.4 kN/m³). The values of the internal friction angle (at the peak of the stress-strain curve) are indicated in the figure; this angle decreases as the mean stress increases. For the extension tests, its values were higher than those obtained in the compression tests.

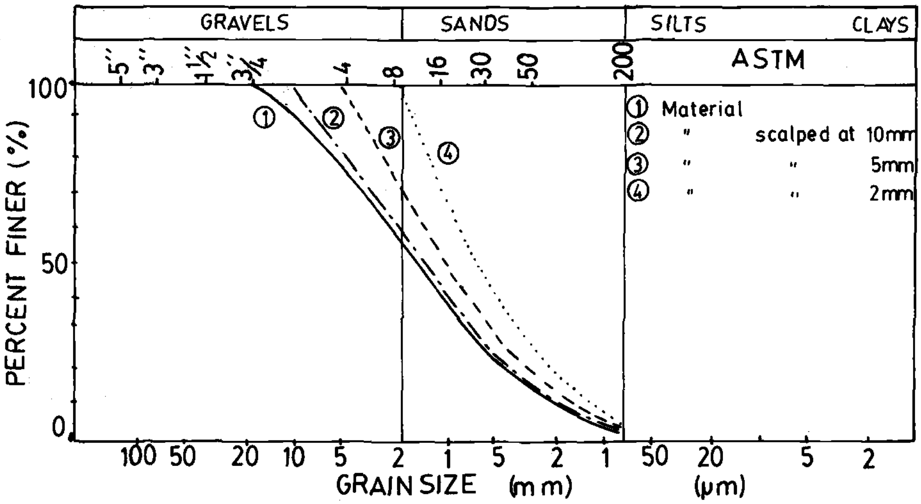

FIG. 4—*Granulometric curves for the Grand-Maison filter material.*

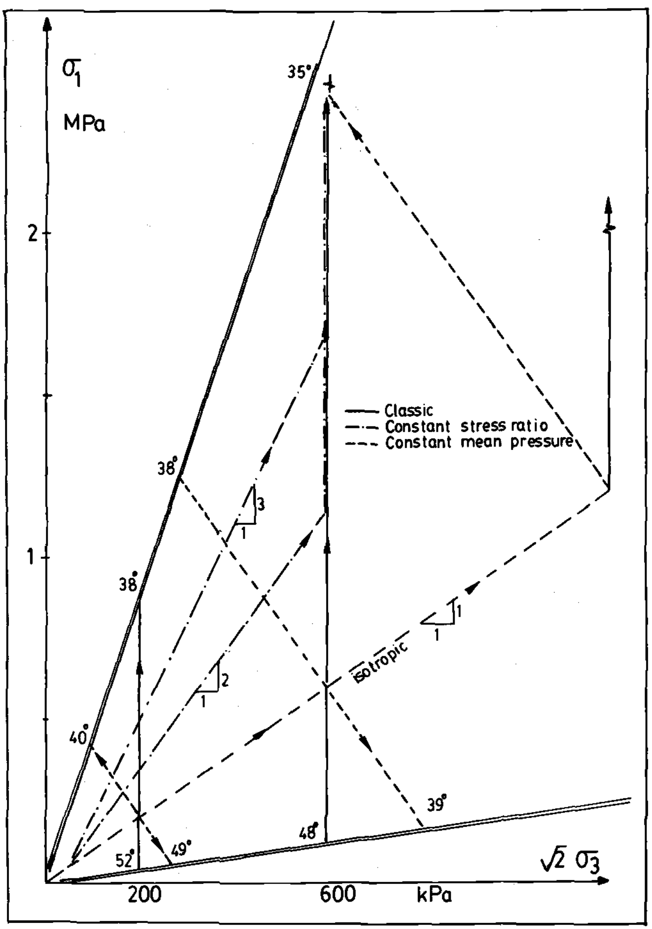

FIG. 5—*Stress paths tested for the Vieux-Pré material (initial dry weight: 17.4 kN/m³).*

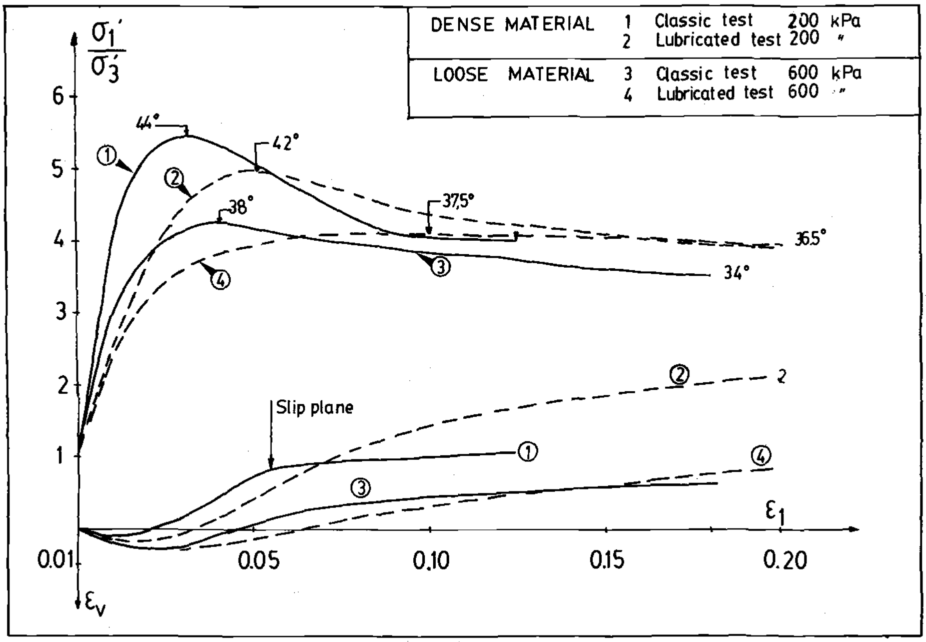

FIG. 6—*Stress-strain volume change curves: dense and loose Vieux-Pré material tested at constant lateral stress. Conventional tests and frictionless tests.*

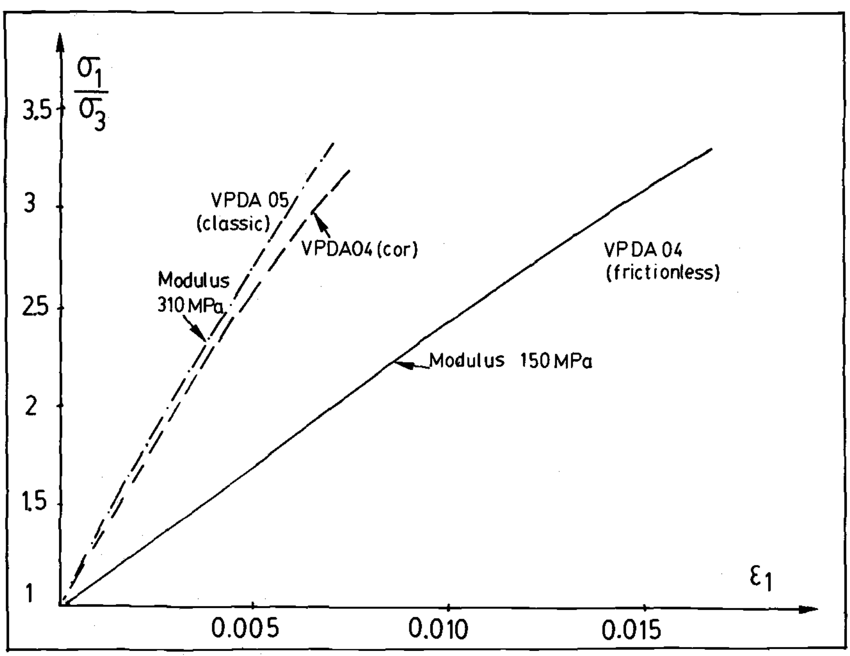

FIG. 7—*Deformation modulus: conventional test, corrected and uncorrected frictionless test.*

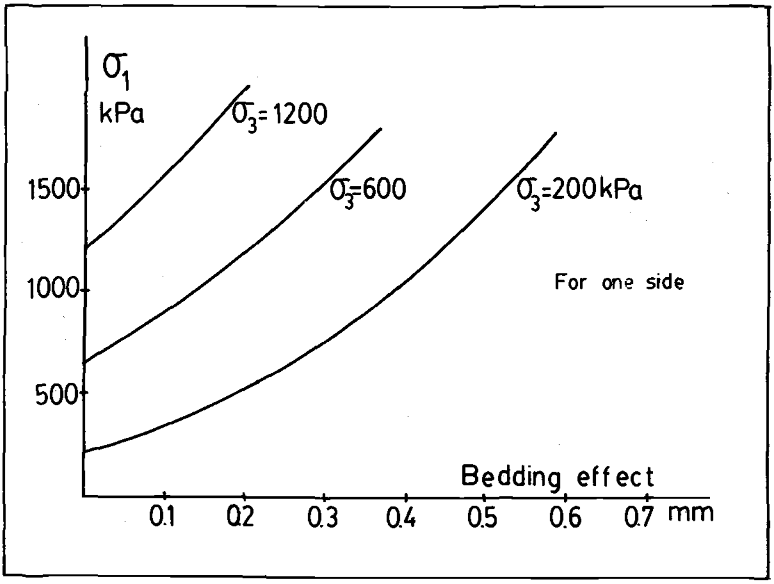

FIG. 8—*Abacus for bedding effect correction.*

These tests must be of very good quality for the different measurements; the various causes of error in the triaxial test were examined below with particular attention to:

- use of frictionless ends,
- bedding effect and direct measurement of axial strain,
- membrane penetration
- extension tests, and
- coarse particles effect.

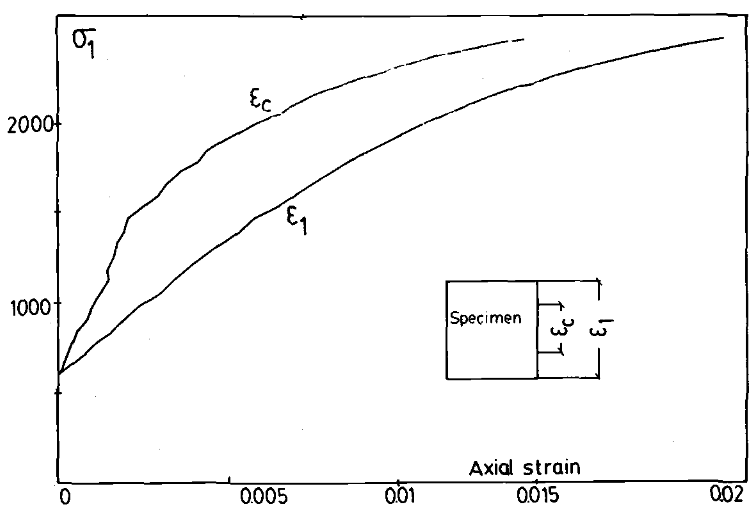

FIG. 9—*Axial stress versus conventional strain and local strain. Triaxial test at constant lateral pressure: 600 kPa. Vieux-Pré material.*

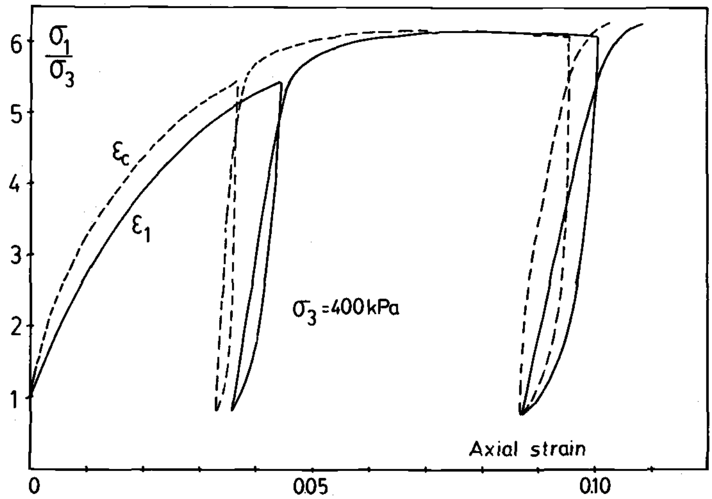

FIG. 10—*Bedding effect in cyclic triaxial test: Grand-Maison filter material tested at 400 kPa.*

Use of Frictionless Ends

For the triaxial tests, the conventional specimens have a slenderness ratio (height/diameter) of two. However, the use of such specimens often leads to barrelling with nonuniform deformations. Additionally, the localization of deformation along the failure plane transforms the specimen into rigid blocks which slip against each other. The volumetric strain then stabilizes, making interpretation of the test no longer possible, because the deformations are concentrated in the shear bands.

Short specimens with a slenderness ratio of one and a frictionless device are currently used in research laboratories: many articles have been published on the subject [*4–6*]. The device generally used is composed of polished and lubricated end platens, with one or more rubber disks, coated with silicon grease between the different layers. With this device, the loaded specimens retain a cylindrical shape and the strains are more homogeneous, without shear bands. The measurement of volume variations is possible up to large strains (20% or more for axial strain): the critical void ratio can be determined.

However, for coarse materials, like those studied here, tests with lubricated ends are rarely performed. The results of such tests are shown in Fig. 6 and compared with conventional triaxial tests for the Vieux-Pré material. These experiments consist of triaxial compression tests with a constant lateral pressure of 200 or 600 kPa. The volumetric weight is 19.4 kN/m^3 for dense and 17.4 kN/m^3 for loose material, the diameter of the specimens is 100 mm. EPS1 indicates the axial strain (logarithmic strains are used) and EPSV the volumetric strain (EPSV is positive for a contraction of the specimen).

The internal friction angle at peak strength is higher for the conventional specimen (with a slenderness ratio of two), especially at low lateral stress: this effect is due to specimen end restraint [*7*].

The major difference concerns the volume variations: the conventional specimens contract less at the beginning of test. The rates of dilatancy occurring after the minimum volume are achieved, but the dilatancy stops when a slip plane develops throughout the specimen (this point is indicated by an arrow in Fig. 6). For the frictionless tests, the dilatancy is continuous. At the end of the experiments, the dilatancy is twice as large for the frictionless specimen at 200 kPa.

One of the advantages of the frictionless test is the higher repeatability: for the conventional test, the premature occurrence of a slip surface reduces this repeatability.

When the experimental stress-strain curves are compared (Fig. 6), the initial tangent moduli of deformation are lower for the frictionless tests. This is the major disadvantage of the frictionless device: the so-called "bedding effect."

The Bedding Effect

Bedding error is caused by the penetration of soil grains into the latex disks and the compression of the grease layer. Many authors have studied this effect (see Refs 7–9). For coarse materials, this effect will be even more significant. However, for tested material with large grain size distribution, this effect has some limitation: after compaction, the top and the base of the specimen are smooth, the small particles surrounding the larger grains.

A simple calculation shows that Young's modulus can be reduced by more than 50%. Indeed, the axial compression of a "sandwich" composed of two layers of latex membrane and one soil specimen yields an apparent modulus reduced by 62%. This calculation is carried out with the following hypotheses:

- thickness of two latex disks: 0.04 mm
- latex modulus: 1100 kPa,
- real soil modulus: 110 MPa, and
- specimen length: 100 mm.

Figure 7 illustrates this fact by comparing the results of a conventional test (with end restraint, noted VPDA 05) with a frictionless specimen (VPDA 04). Only the beginning of the strain-stress curves is plotted for two tests shown completely in Fig. 6; the influence of experimental conditions on the modulus measurement is very significant. To check the possibility of a correction, several attempts were carried out leading to satisfying results.

The first method consisted in studying the compressibility of the latex disks in contact with a layer of soil: a dried Vieux-Pré specimen resting on two latex layers was tested in simple compression to determine the bedding effect (the dried material is sufficiently cohesive). The penetration of soil grains can then be measured. Another possibility is to glue soil grains onto a steel plate to conduct the same experiments.

The second method used was a comparative study between isotropic and odometric compression tests: in both cases, the results of the tests with or without a frictionless device were compared. In the isotropic test, a transducer inside the triaxial cell measures the axial strain. For the odometric test, a frictionless device layer is positioned in the mold base but the lateral expansion of the lower disk is then impossible. By assuming the specimens are identical, the bedding effect can be calculated.

These various attempts led to the calculation of the chart shown in Fig. 8 for different initial lateral pressures. For the higher stresses, a large part of the bedding takes place during the isotropic consolidation. The analytical equations of these curves were introduced into the data reduction programs to establish the new values of axial strains. An example is given in Fig. 7 where test VPDA 04 is corrected and transformed into test VPDA 04 (CORrected): the tests VPDA 05 and VPDA 04(COR) are then comparable. However, this satisfying result is produced by a large correction on the measured axial strain.

Direct Measurement of Axial Strain

The direct measurement of axial strain inside the triaxial cell is certainly a preferable method: the axial strain transducers (two linear variable differential transformers [LVDTs])

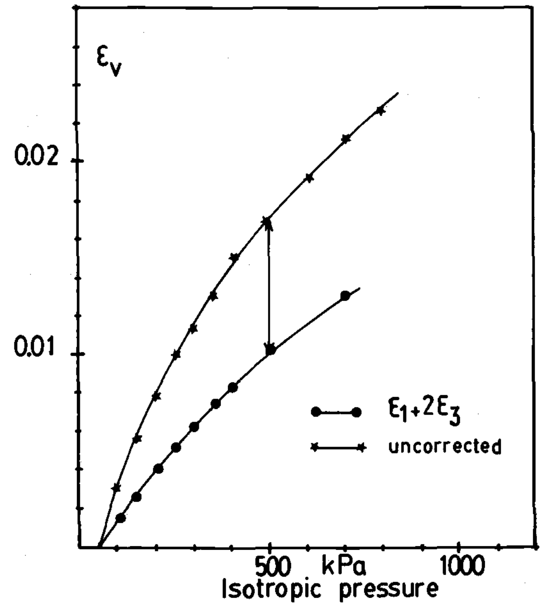

FIG. 11—*Isotropic test: Grand-Maison filter material: uncorrected and calculated results.*

are fixed directly on the specimen: the reliable axial strain is then measured. However, this strain is obtained locally and can be affected by nonuniformities.

Typical results of such tests are shown in Fig. 9 for the Vieux-Pré material; the axial strain (ϵ_1) is conventionally measured whereas the local strain (ϵ_c) is measured over the center portion equal to half of the specimen height: this figure demonstrates the bedding effect.

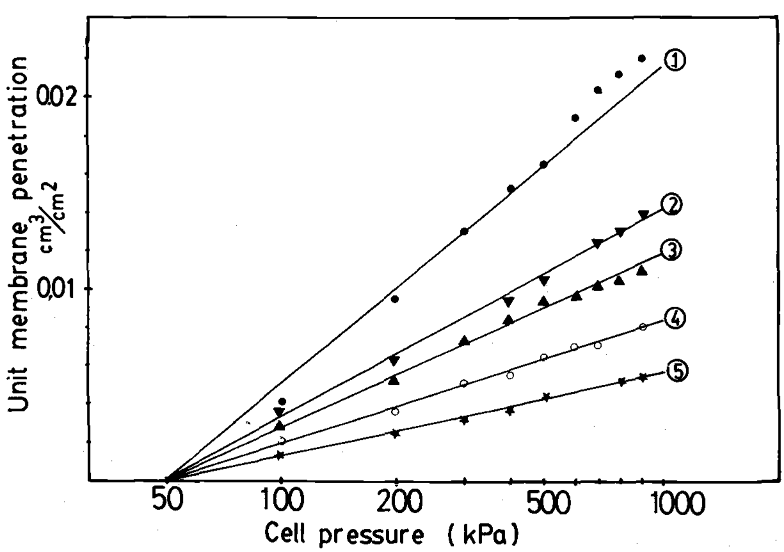

FIG. 12—*Unit membrane penetration* S (1) D_{max} = *16-mm Grand-Maison filter,* (2) D_{max} = *10-mm Grand-Maison filter,* (3) D_{max} = *5-mm Grand-Maison filter,* (4) D_{max} = *2-mm Grand-Maison filter, and* (5) *Vieux-Pré material (see Curve 3, Fig. 2).*

On the other hand, some irregularities in the curves illustrate the difficulties of such measurements.

The bedding effect is important as well for the loading-unloading cycles: this effect is irreversible and Fig. 10 gives such an example for the Grand-Maison filter.

A reliable measurement of deformation modulus is very difficult: the end restraint in the conventional test can also influence the obtained results. The direct measurement inside the triaxial cell is undoubtedly preferable but complicates the test.

Membrane Penetration

In the tests using stress paths with variable lateral pressure (that is, isotropic tests, constant stress ratio or mean pressure test), the directly measured volume change includes some part caused by membrane penetration [*10,11*]; as the lateral stress increases, an additional quantity of water is drained and the volumetric strain becomes too large. For comparison between conventional and constant mean pressure tests, or for isotropic tests, a reliable measurement of volumetric strain is necessary.

For coarse materials, this effect is more significant: generally, the volume change measurement is corrected by using the "unit normalized penetration" coefficient S: S is the slope of the curve in the axis of additional volume change caused by membrane penetration divided by the contact area versus the logarithm of the cell pressure [*12,13*].

To study the above correction, a special lateral strain indicator was designed. This transducer is similar to the one described in Ref *14*; the lateral strain is measured directly for one diameter. With the measurement of axial (ϵ_1), radial (ϵ_3), and volumetric (ϵ_v) strains,

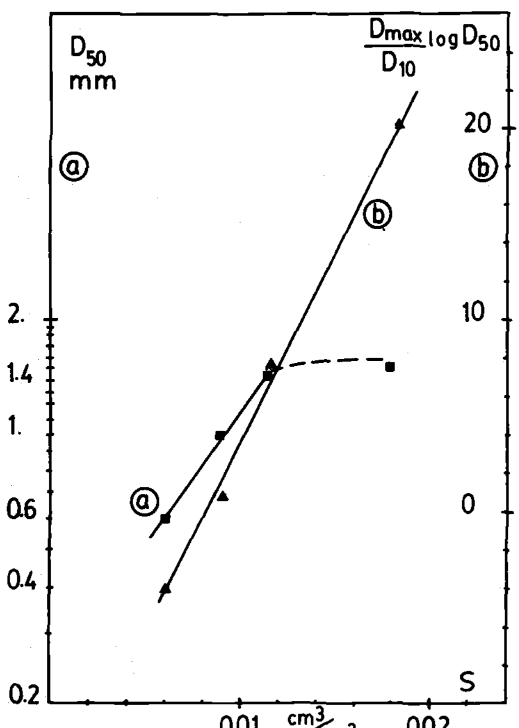

FIG. 13—*Grain size effect on the unit membrane penetration* S.

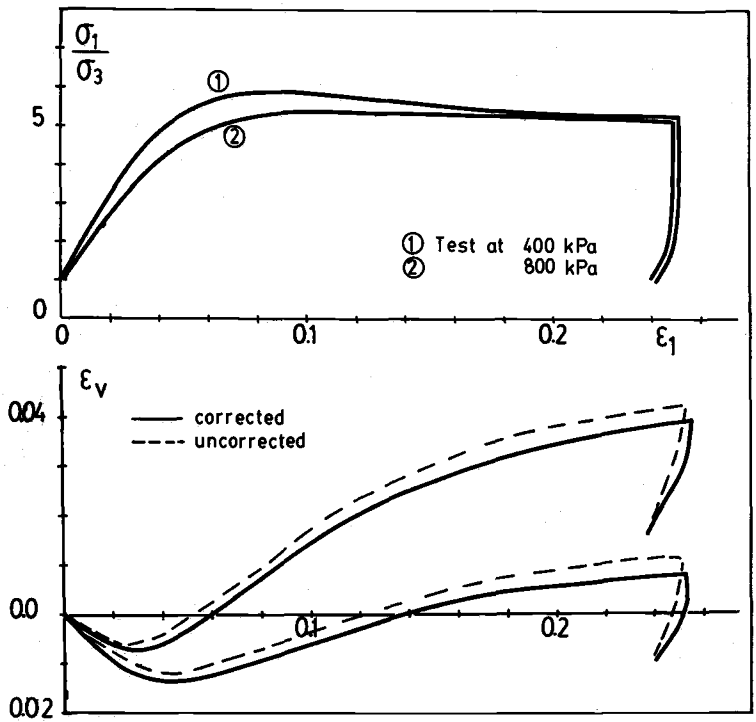

FIG. 14—*Uncorrected and corrected volume change. Grand-Maison filter material tested at constant mean pressure.*

the additional volume change caused by membrane penetration can be calculated. In Fig. 11, an isotropic test is shown; the uncorrected curve is obtained from direct measurement of expelled water. The true volumetric deformation is estimated from the direct measurements of axial and radial strain: the difference between the two curves allows the calculation of the additional volume change as a result of membrane penetration, and thus the calculation of S.

From different grain size distribution curves (Fig. 2, Fig. 4), it is possible to determine the curves in Fig. 12. The maximum grain size varies from 16 to 2 mm. Generally, the value of S is related to the mean grain diameter sizes: taking that into account, slope S was plotted in Fig. 13 using both scales:

(a) the value of mean grain diameter D_{50}: Curve a and

(b) the following value: $\dfrac{D_{max}}{D_{10}} \log D_{50}$ (mm): Curve b

where D_{10}: 10% diameter, D_{50} 50% diameter, and D_{max}: maximum grain diameter.

The relationship between the experimental values is better in the second case (b).

An example is shown in Fig. 14 for the Grand-Maison filter with an initial volumetric dry weight of 18.5 kN/m^3. These experiments were constant mean pressure tests conducted at 400 and 800 kPa. The membrane penetration effect is relatively limited for this example.

Extension Tests

The Grand-Maison filter material was the subject of a extensive experimental program for the determination of its mechanical properties:

- triaxial compression tests with four initial densities,
- triaxial compression tests with constant mean pressure (Fig. 14),
- true triaxial tests, and
- triaxial extension tests.

In this paper, only the triaxial extension tests using two different apparatus are discussed: a conventional triaxial cell and a true triaxial apparatus developed in Grenoble [3].

For extension test in a conventional cell, the specimen top is attached to the loading ram. The following points must be considered:

- The axial deviator stress is corrected because the axial extension of the lateral membrane produces additional strength.
- The slip plane appears at very low axial strain (0.03 to 0.05).
- The slip planes are often localized underneath the specimen top, leading to a very large decrease of the specimen area. The interpretation of the test results is then difficult because the calculation of the axial strain and stress is not reliable.

Two major causes can explain these facts: the specimen is less compacted near the top and the lateral membrane penetrates between the top plate and the specimen; consequently the effective area decreases.

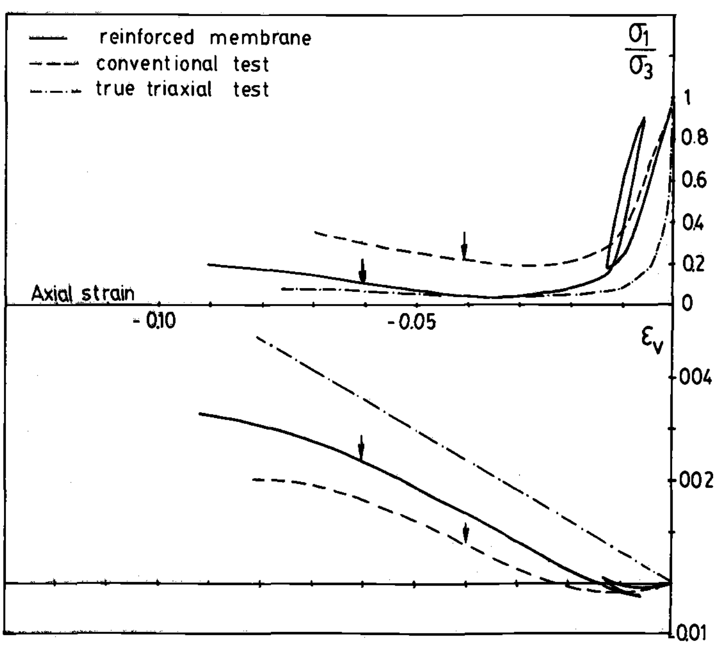

FIG. 15—*Grand-Maison filter material: extension triaxial tests.*

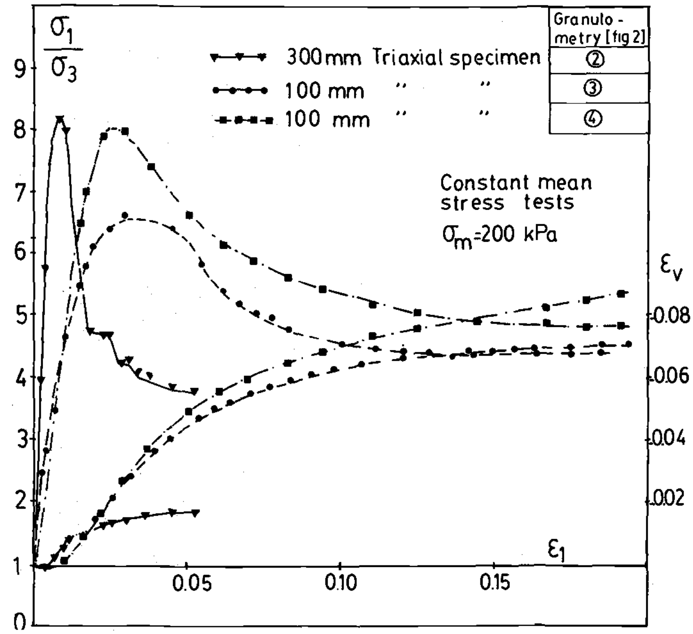

FIG. 16—*Constant mean pressure triaxial compression tests: 200 kPa.*

To avoid these problems, a reinforced membrane was designed consisting of a latex membrane to which brass plates are adhered in the axial direction. The rectangular plates are 30 mm long, 5 mm wide, and 0.02 mm thick. Thus, the membrane cannot penetrate underneath the top. The localization of deformation is delayed and the slip plane, when it appears, is located in the central zones of the specimen.

In Fig. 15, three triaxial extension tests at the same lateral pressure are compared. In the conventional test, a slip plane first occurs at 4% of axial strain, and with the reinforced membrane it occurs at 6% of axial strain, thus extending the limit of test validity. These points are marked by an arrow in Fig. 15.

A true triaxial with the same lateral stress is also plotted: the specimen is overconsolidated with a ratio of two: the initial modulus is higher but the angle of friction is the same as in the test with reinforced membrane. The volume change behavior in the true triaxial test is affected by overconsolidation. The dilatancy slopes are the same, but the true triaxial specimen dilates continuously.

The reinforced membrane is consequently useful in avoiding the frequent penetration of the membrane underneath the top of the specimen. The angle of friction is correctly evaluated.

Coarse Particles Effect

For embankment materials, it is often impossible to test a real material with its complete grain size distribution curve in a triaxial apparatus: even in the largest apparatus, a maximum grain size can be tested [*15*]. The effect of limiting grain size have been studied by several authors [*16,17*] with classical compression triaxial tests.

For the Vieux-Pré sandstone, different types of experiments were conducted to test the influence of coarse elements on the mechanical behavior of embankment materials.

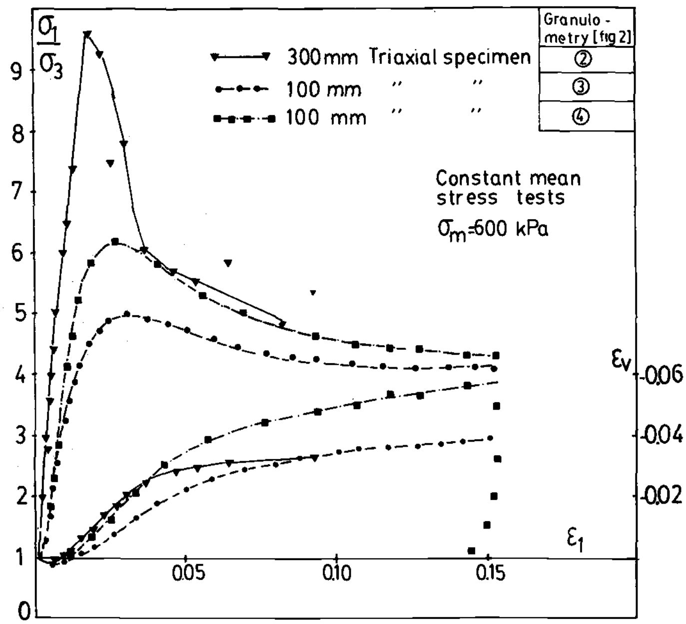

FIG. 17—*Constant mean pressure triaxial compression tests: 600 kPa.*

Two specimen diameters were used:

- 300 mm for the tests conducted by MECASOL (Paris), for a maximum grain size of 50 mm and
- 100 mm for the I.M.G. tests with grain sizes up to 20 mm.

The grain size distribution curves for the different specimens are given in Fig. 2. Triaxial tests at constant mean pressure of 200 and 600 kPa are compared in Figs. 16 and 17, which represent the stress and volume variations versus the axial strain.

The obtained results are very different: for the 300-mm specimen the stress ratio at failure is 8.2 and for the 100-mm specimen the stress ratio is only 6.4 for test at 200 kPa. The volume change behavior is also different: the 300-mm specimen dilates less than the 100-mm specimen.

With the objective of explaining these important differences, triaxial tests with 100-mm diameter were conducted on a coarser material: the initial grain fraction between 5 and 20 mm was replaced by a coarser fraction. The grain size distribution is given by Curve 4 in Fig. 2. These results showed the prominent part played by the coarser fraction on the peak behavior of the specimen; the obtained peak strength and angle of friction are higher.

For a good estimation of the real behavior of the material, the use of specimens with a large diameter appears to be necessary. With the use of the small diameter (100-mm) triaxial apparatus, only the finer fraction of the material is tested and a minimum value of friction angle is obtained for this material.

Conclusion

The triaxial test, with its versatility, is an appropriate tool for estimation of the mechanical properties of embankment materials. The use of different stress paths allows the validation of the constitutive law: the triaxial extension and the constant mean pressure tests were used to carry out this objective.

The study of the different causes of error or nonrepeatability requires particular attention. The use of frictionless devices is advantageous because the specimen deformation is much more homogeneous. However, the bedding effect requires a large correction to obtain the true deformation modulus.

A direct measurement of the axial strain by using transducers fastened to the specimen gives a reliable estimation of the deformation modulus.

The membrane penetration modifies the measurement of volume variations. For the tests presented here, technical solutions were successfully used and allowed a correction of the volumetric strain in constant mean pressure test.

The reinforced membrane eliminates the penetration underneath the top specimen and allows larger strain without slip plane in extension tests.

All these technical corrections or improvements have increased the reliability of the triaxial test, but the principal difficulty for the engineer concerns the problem of coarse particles. Only extensive series of tests with different specimen diameter can give a estimation of their influence.

Acknowledgments

The authors are grateful to MECASOL (PARIS, France) where the triaxial tests (diameter 300 mm) were conducted.

References

[1] "Auscultation de Barrages en remblai. . . ," 15ème Congrès des Grands Barrages, Lausanne, 1985, pp. 1439–1470.
[2] Clerdouet, D. and Post, G., *Revue Française de Geotechnique,* No. 27, April 1984, pp. 27–41.
[3] Lanier, J. and Stutz, P., in *Constitutive Relations for Soils,* Gudehus, Darve, and Vardoulakis, Eds., Balkema, 1984, pp. 67–70.
[4] Bishop, A. W. and Green, G. E., *Geotechnique,* Vol. 15, No. 3, Sept. 1965, pp. 243–266.
[5] Lee, K. L. and Seed, H. B., *Proceedings of the American Society of Civil Engineers, Journal of Soil Mechanics and Foundation Engineering,* Vol. 90, No. SM 6, June 1964, pp. 173–175.
[6] Sarsby, R. W., Kalteziotis, N. and Haddad, E. H., *Proceedings of the American Society of Civil Engineers, Journal of Geotechnical Engineering Division,* Vol. 104, No. GT6, June 1978, pp. 687–704.
[7] Colliat, J. L., Desrues, J., and Flavigny, E., *Revue Française de Geotechnique,* No. 34, 1986, pp. 41–55.
[8] Norris, G. M., in *Laboratory Shear Strength of Soil, ASTM STP 740,* R. N. Yong and F. C. Townsend, Eds., American Society for Testing and Materials, Philadelphia, 1981, pp. 303–314.
[9] Molenkamp, F., in *Constitutive Relations for Soils,* Gudehus, Darve, and Vardoulakis, Eds., Balkema, 1984, pp. 95–96.
[10] Costa Filho, L. de M., *Geotechnical Testing Journal,* Vol. 8, No. 1, March 1985, pp. 3–13.
[11] Baldi, G. and Nova, R., *Proceedings of the American Society of Civil Engineers, Journal of Geotechnical Engineering Division,* Vol. 110, No. 3, March 1984, pp. 403–420.
[12] Ramana, K. V. and Raju, V. S., *Proceedings of the American Society of Civil Engineers, Journal of Geotechnical Engineering Division,* Vol. 108, No. GT2, Feb. 1982, pp. 305–310.
[13] Vaid, Y. P. and Negussey, D., *Geotechnical Testing Journal,* Vol. 7, No. 2, June 1984, pp. 70–76.
[14] Darve, F., Flavigny, E., and Vuaillat, P., *7th European Congress of SM and FE,* Brighton, 1979, pp. 119–124.
[15] Leps, T. M., *Proceedings of the American Society of Civil Engineers, Journal of Geotechnical Engineering Division,* Vol. 96, No. SM4, July 1970, pp. 1159–1170.
[16] Marachi, N., Chan, C., and Seed, H. B., *Proceedings of the American Society of Civil Engineers, Journal of Geotechnical Engineering Division,* Vol. 98, No. SM1, Jan. 1972, pp. 95–114.
[17] Donaghe, R. T. and Torrey, V. H., *7th European Congress of SM and FE,* Vol. 2, Brighton, 1979, pp. 29–34.

Ryosuke Kitamura[1] *and Motohisa Haruyama*[1]

Compression and Shear Deformation of Soil Under Wide-Ranging Confining Pressure

REFERENCE: Kitamura, R. and Haruyama, M., "**Compression and Shear Deformation of Soil Under Wide-Ranging Confining Pressure,**" *Advanced Triaxial Testing of Soil and Rock, ASTM STP 977,* Robert T. Donaghe, Ronald C. Chaney, and Marshall L. Silver, Eds., American Society for Testing and Materials, Philadelphia, 1988, pp. 501–511.

ABSTRACT: The conventional triaxial drained compression test was conducted on specimens under wide-ranging confining pressure, 9.8 to 9.8 × 10^3 kN/m^2 (0.1 to 100 kgf/cm^2). Three kinds of soil were used for the test: clayey soil, Toyoura sand, and soft sedimentary rock ("Shirasu," derived from pyroclastic flows in the southern part of Kyushu Island in Japan). Confining pressure higher than 9.8 × 10^2 kN/m^2 (10 kgf/cm^2) was generated by a nitrogen gas cylinder; confining pressure lower than 9.8 × 10^2 kN/m^2 (10 kgf/cm^2) was supplied by a common air compressor. The compression curves (the *e*-log *p* relation) under wide-ranging pressure are shown for three kinds of soil. Stress–strain relations and stress–dilatancy relations in the shear deformation process are also shown. It is concluded that the mechanical behaviors of clayey soil and sandy soil are similar under wide-ranging confining pressure although these materials are often treated as different.

KEY WORDS: conventional triaxial test, clayey soil, sandy soil, low pressure, high pressure, compression, shear deformation, *e*-log *p* relation, stress–strain relation, stress–dilatancy relation

In soil mechanics clayey soil and sandy soil are often treated as different materials because of differences in grain size, permeability, compression and shear deformation characteristics, and so on. However, these differences are not intrinsic, but relative ones, taking account of the origin and the generation process of clay and sand. The recent development of computer science has brought rapid progress in the analysis of soil mechanics problems, for example, the finite element method. The accuracy of applying the finite element method to soil mechanics problems depends on the constitutive relation used in the analysis. Comprehensive constitutive laws that take the various mechanical behaviors of clayey soil and sandy soil into account must be established.

In this paper the mechanical characteristics of three kinds of soil in the compression and shear deformation processes are investigated. The soil tests are carried out under wide-ranging confining pressure to determine the similarities and the differences of clayey soil and sandy soil. The compression characteristic is discussed based on the compression curve (that is, the *e*-log *p* relation). The shear deformation characteristic is investigated based on the stress–strain relation and the stress–dilatancy relation.

[1] Professor and professor (deceased), respectively, Department of Ocean Civil Engineering, Kagoshima University, 1-21-40 Kourimoto, Kagoshima 890, Japan.

TABLE 1—*Physical properties of test materials.*

	Clay	Shirasu	Toyoura Sand
Specific gravity, G_s	2.60	2.41	2.65
Maximum void ratio, e_{max}	—	1.86	0.94
Minimum void ratio, e_{min}	—	0.94	0.58
Liquid limit (%), W_L	44.7	—	—
Plastic limit (%), W_P	23.0	—	—
Uniformity coefficient, U_c	3.59	4.27	1.48

Testing Material, Apparatus, and Procedure

Three kinds of soil are used for the test: clayey soil, Shirasu, and Toyoura sand. The physical properties of these materials are summarized in Table 1, and the grain size accumulation curves of these materials are shown in Fig. 1. The soft sedimentary rock, Shirasu, is a nonwelded part of pumice-tuff derived from the Pleistocene pyroclastic flow and distributed in the southern part of Kyushu Island in Japan. The particle of Shirasu is porous, and its specific gravity is small (see Table 1). The particle can be crushed much more easily than Toyoura sand.

The triaxial testing apparatus (Fig. 2) and the one-dimensional compression apparatus (Fig. 3) are used in the test. Confining pressure lower than 9.8×10^2 kN/m^2 (10 kgf/cm^2) is supplied by a common air compressor. Confining pressure higher than 9.8×10^2 kN/m^2

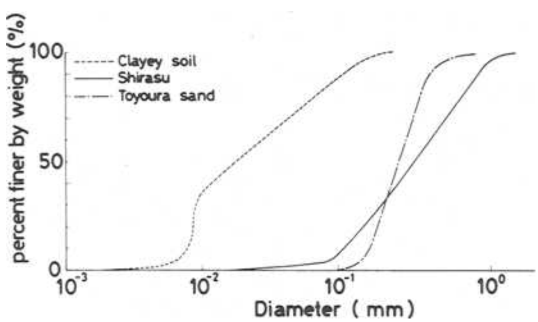

FIG. 1—*Grain size accumulation curves of clayey soil, Shirasu, and Toyoura sand.*

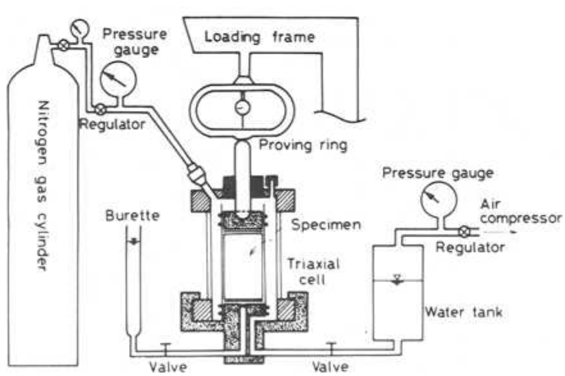

FIG. 2—*Schematic of triaxial testing apparatus.*

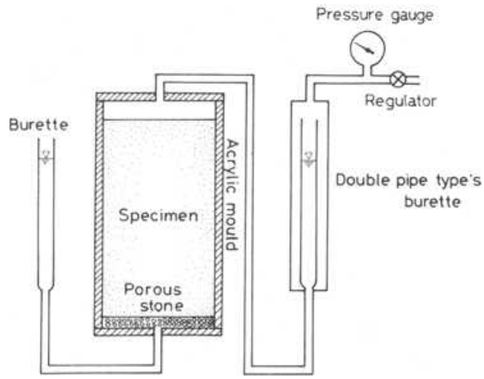

FIG. 3—*Schematic of one-dimensional compression apparatus.*

(10 kgf/cm^2) is supplied by a nitrogen gas cylinder with initial pressure and volume of 1.47 $\times$ 10^4 kN/m^2 (150 kgf/cm^2) and 7 m^3, respectively. Pressure in the nitrogen gas cylinder is controlled by the nonreleased type regulator and conveyed to the triaxial cell. This simple pressure generation system can supply steady confining pressure lower than 9.8 $\times$ 10^3 kN/m^2 (100 kgf/cm^2) for the triaxial compression test although pressures higher than 9.8 $\times$ 10^3 kN/m^2 (100 kgf/cm^2) cannot be controlled.

Three kinds of triaxial cells are used for the tests: the cell whose maximum allowable pressure is 9.8 $\times$ 10^2 kN/m^2 (10 kgf/cm^2) is used for the test of clay, and the cells whose maximum allowable pressures are 2.94 $\times$ 10^3 and 2.94 $\times$ 10^4 kN/m^2 (30 and 300 kgf/cm^2) are used for the test of Shirasu and Toyoura sand, respectively. The one-dimensional compression apparatus is also used for the test of the clayey soil under extremely low pressure. The specimen in the acrylic mold is consolidated by the vertical seepage force of the water. (For detailed explanation of the principle of this consolidation apparatus see Refs *1* and *2*.) After the clayey soil specimen is consolidated under about 9.8 kN/m^2 (0.1 kgf/cm^2) by the one-dimensional compression apparatus, the specimen is taken out of the mold and set in the triaxial cell. The specimen of Shirasu or Toyoura sand is prepared by freezing the saturated material. All the specimens in the triaxial cell are compressed under isotropic pressure and then sheared under a constant confining pressure. Two latex disks with lubricated layers are placed on the cap and the pedestal to reduce the friction between the specimen and the end surfaces at the cap and the pedestal. The strain-controlled shearing test is carried out under the drained condition, with strain rates of 2.5 $\times$ 10^{-2} mm/min for the clayey soil and 0.139 mm/min and 0.375 mm/min for Shirasu and Toyoura sand, respectively. The initial void ratio and other conditions of the specimens in this research are summarized in Tables 2 through 4.

TABLE 2—*Initial state of clayey soil specimen.*

Initial water content	75	140	200
Initial void ratio	1.90	3.75	4.83
Consolidation pressure at the final K_0-consolidation stage, kgf/cm^2	0.111	0.057	0.112
Confining pressure, kgf/cm^2	0.3	···	0.1

TABLE 3—*Initial void ratio of Shirasu.*

Initial Void Ratio	Confining Pressure, kgf/cm^2
1.34	2
1.64	6
1.36	10
1.34	30
1.32	50
1.44	100

TABLE 4—*Initial void ratio of Toyoura sand.*

Initial Void Ratio	Confining Pressure, kgf/cm^2
0.79	2
0.80	4
0.70	6
0.78	15
0.71	20
0.74	30
0.68	50
0.75	75
0.77	100

Results

Figures 4 and 5 show the compression curves (the *e*-log *p* relation) for clay, Shirasu, and Toyoura sand, where *e* denotes void ratio and *p* is the vertical compression pressure at the middle height of the specimen for the clayey soil and the isotropic pressure for Shirasu and Toyoura sand. The dotted line in Fig. 4 is the extrapolated line of the normal compression (consolidation) line for the clayey soil which is obtained under isotropic compression pressure, 9.8 to 2.94 × 10 kN/m^2 (0.1 to 0.3 kgf/cm^2) by the triaxial cell. The initial water content for each specimen is 75, 140, and 200% as shown in Fig. 4. The results for Shirasu and Toyoura sand are shown in Fig. 5, which also includes results obtained by Kitamura

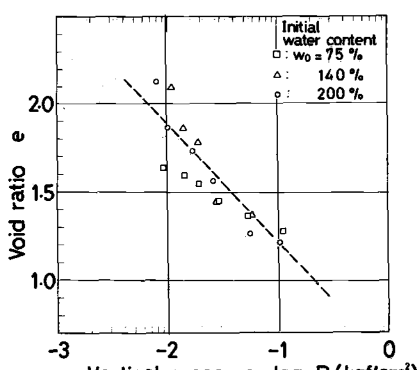

FIG. 4—e-*log* p *relation of clay.*

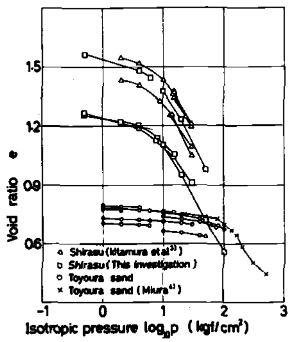

FIG. 5—e-*log* p *relation of Shirasu and Toyoura sand.*

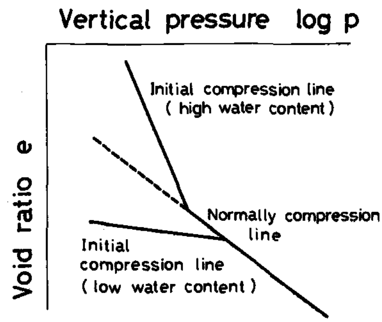

FIG. 6—*Schematic of* e-*log* p *relation of clay.*

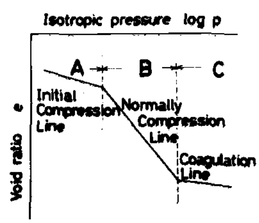

FIG. 7—*Schematic of* e-*log* p *relation of Shirasu and Toyoura sand.*

and coworkers [3] for Shirasu and by Miura [4] for Toyoura sand. The volume change due to the membrane penetration might occur when isotropic pressure changes, but correction for the membrane penetration was not done in this research. Figure 6 shows the schematic e-log p relation described based on the result in Fig. 4 (that is, under extremely low pressure the compression curve of the clayey soil deviates upwards for the high initial water content or downwards for the low initial water content from the normal compression line). Imai and coworkers [5] showed similar results for clayey soil with high water content (that is, the compression curve for clayey soil with high water content deviates upwards under extremely low pressure). In the following discussion this part of the compression curve is called the initial compression line as shown in Fig. 6. Figure 7 is the schematic e-log p relation described based on the result in Fig. 5 (that is, the e-log p relation for sandy soil is expressed by the initial compression line at low pressure, the normal compression line at

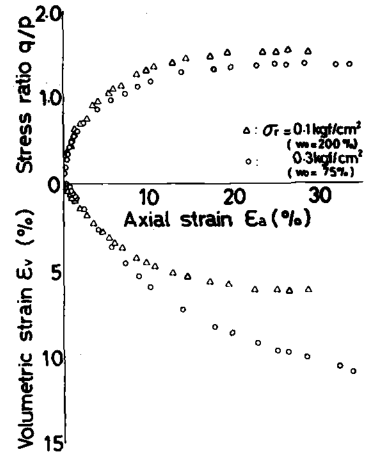

FIG. 8—*Stress-strain relation of clay.*

moderate pressure, and the coagulation line at high pressure where the coagulation line is tentatively named and means the process in which soil changes into rock). According to the result in Fig. 5, pressure at the intersection of the initial compression line with the normal compression line is about 1.96 × 10^3 kN/m^2 (20 kgf/cm^2) for Shirasu. The results obtained by Miura [*4*] and this research show that pressure at the intersection for Toyoura sand is about 9.8 × 10^3 kN/m^2 (100 kgf/cm^2). The coagulation line is supposed to come out at higher pressure although it does not appear in Fig. 5. It is suggested from Figs. 4 and 5 that the compression behavior of Shirasu under pressure, 4.9 × 10 to 9.8 × 10^2 kN/m^2 (0.5 to

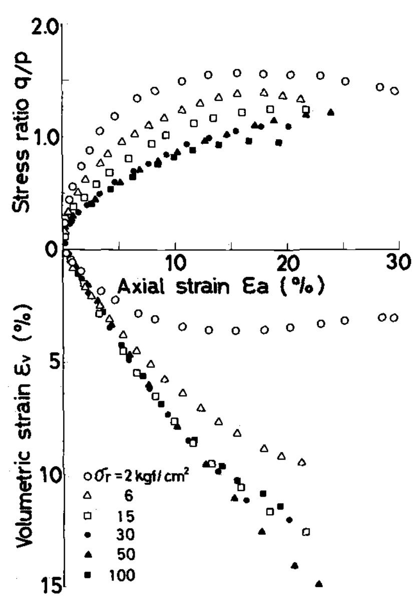

FIG. 9—*Stress-strain relation of Shirasu.*

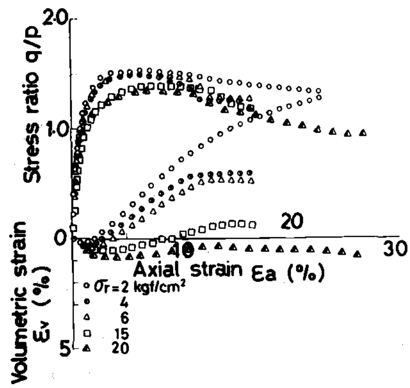

FIG. 10(*a*)—*Stress–strain relation of Toyoura sand (low confining pressure).*

10 kgf/cm²) and Toyoura sand under pressure, 9.8 × 10 to 9.8 × 10³ (1 to 100 kgf/cm²) corresponds to that of clayey soil under pressure lower than 4.9 kN/m² (0.05 kgf/cm²), and the compression behavior of the clayey soil under pressure higher than 4.9 kN/m² (0.05 kgf/cm²) corresponds to that of Shirasu under pressure higher than 9.8 × 10² kN/m² (10 kgf/cm²) and that of Toyoura sand under pressure higher than 9.8 × 10³ kN/m² (100 kgf/cm²). But more isotropic compression tests with various soils and states under wide-ranging pressure must be carried out to make this correspondence in the compression process of soil clearer.

Figures 8, 9, and 10 show the stress–strain relations of clayey soil, Shirasu, and Toyoura sand in the shear deformation process, where $q(= \sigma_a - \sigma_r)$ is the axial deviator stress, $p(= \sigma_a + 2\sigma_r)/3$ is the mean effective principal stress, ϵ_a is the axial strain, and ϵ_v is the volumetric strain. The specimen of clayey soil with an initial water content of 140% is taken out of the one-dimensional compression mold at consolidation pressure 5.6 kN/m² (0.057 kgf/cm²), but it is impossible to set it in the triaxial cell because the specimen cannot stand

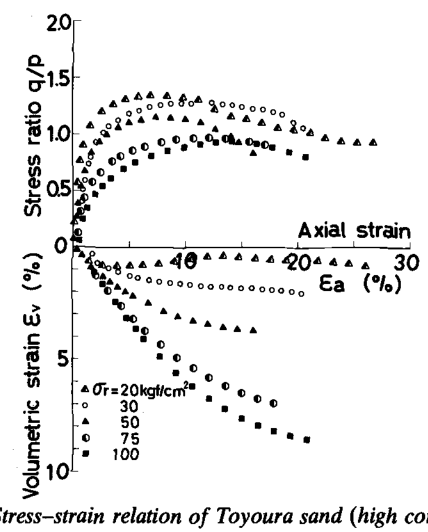

FIG. 10(*b*)—*Stress–strain relation of Toyoura sand (high confining pressure).*

by itself on the pedestal. So, only the results obtained from the specimens taken out of the mold at consolidation pressure, about 10 kN/m^2 (0.1 kgf/cm^2), are shown in Fig. 8. The stress–strain relation with confining pressure σ_r = 9.8 kN/m^2 (0.1 kgf/cm^2) is a little different from the one with σ_r = 2.94 × 10 kN/m^2 (0.3 kgf/cm^2). It is supposed that the specimen with σ_r = 9.8 kN/m^2 (0.1 kgf/cm^2) is in the slightly overconsolidated state and the one with σ_r = 2.94 × 10 kN/m^2 (0.3 kgf/cm^2) is in the normally consolidated state because final consolidation pressure in the one-dimensional compression mold is about 9.8 kN/m^2 (0.1 kgf/cm^2) as shown in Table 2. Figure 9 shows that the stress–strain relations of Shirasu at pressure higher than 2.94 × 10^3 kN/m^2 (30 kgf/cm^2) are almost unique although the ones at pressure lower than 2.94 × 10^3 kN/m^2 (30 kgf/cm^2) are not. Shibata has already pointed out that the deformation behavior of normally consolidated clayey soil under a constant mean effective principal stress condition is uniquely described on the q/p–ϵ_a-ϵ_v relation [*6*]. According to the *e*-log *p* relation of Shirasu in Fig. 5, the specimen whose stress condition is higher than 2.94 × 10^3 kN/m^2 (30 kgf/cm^2) before shearing is on the normal compression line defined in Fig. 7. Figure 10 shows that the stress–strain relation of Toyoura sand depends on the confining pressure although the stress–strain relation at higher confining pressure tends to come close. According to the *e*-log *p* relation of Toyoura sand in Fig. 5, the specimen whose stress condition is lower than 9.8 × 10^3 kN/m^2 (100 kgf/cm^2) before shearing is on the initial compression line defined in Fig. 7. Ponce and Bell [*7*] and Fukushima and Tatsuoka [*8*] carried out the shearing test on sandy soil under extremely low pressure. Fukushima and Tatsuoka showed that the stress–strain relation under extremely low pressure (lower than 1.96 × 10 kN/m^2 [0.2 kgf/cm^2]) tends to come close although the stress–strain relation under pressure between 1.96 × 10 and 3.92 × 10^2 kN/m^2 (0.2 and 4.0 kgf/cm^2) is different [*8*]. Murayama and coworkers defined the precompression stress of sandy soil on the *e*-log *p* relation under pressure of 41.2 to 83.3 kN/m^2 (0.42 to 0.85 kgf/cm^2), and they suggested the initial compression line in Fig. 7 is divided into two parts [*9*]. It is supposed from these experimental results that the stress–strain relation of the specimen whose stress condition before shearing is on the normal compression line or extremely low on the initial compression line can be uniquely expressed on the q/p–ϵ_a-ϵ_v relation.

Figures 11, 12, and 13 show the stress–dilatancy relation on the spatial mobilized plane (SMP) proposed by Matsuoka and Nakai [*10*]. The stress ratio τ/σ_N, the normal strain increment $d\epsilon_N$, and the shear strain increment $d\gamma$ on the SMP are defined by the following equations:

$$\frac{\tau}{\sigma_N} = \sqrt{\frac{J_1J_2 - 9J_3}{9J_3}}$$

$$d\epsilon_N = \frac{J_3}{J_2} \cdot \left(\frac{d\epsilon_1}{\sigma_1} + \frac{d\epsilon_2}{\sigma_2} + \frac{d\epsilon_3}{\sigma_3}\right)$$

$$\frac{d\gamma}{2} = \frac{J_3}{J_2} \cdot \sqrt{\frac{(d\epsilon_1 - d\epsilon_2)^2}{\sigma_1\sigma_2} + \frac{(d\epsilon_2 - d\epsilon_3)^2}{\sigma_2\sigma_3} + \frac{(d\epsilon_3 - d\epsilon_1)^2}{\sigma_3\sigma_1}}$$

where

$J_1 = \sigma_1 + \sigma_2 + \sigma_3$ = first stress invariant
$J_2 = \sigma_1\sigma_2 + \sigma_2\sigma_3 + \sigma_3\sigma_1$ = second stress invariant
$J_3 = \sigma_1\sigma_2\sigma_3$ = third stress invariant
σ_1, σ_2, and σ_3 = maximum, intermediate, and minimum effective principal stresses, respectively
$d\epsilon_1$, $d\epsilon_2$, and $d\epsilon_3$ = maximum, intermediate, and minimum principal strain increments, respectively

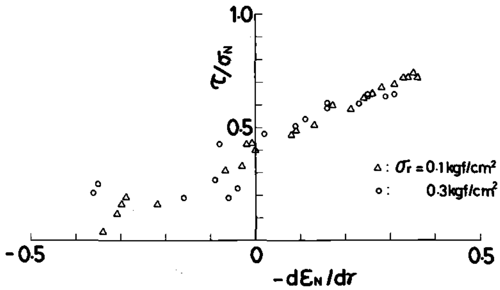

FIG. 11—*Stress–dilatancy relation of clay.*

The test results of Nakai and Matsuoka [*11*] and Shimizu [*12*] show that the stress–dilatancy relations for the normally and the overconsolidated clayey soil can be schematically described under a constant mean effective stress condition as shown in Fig. 14. The stress–dilatancy relation for the normally consolidated clayey soil is linear. The stress–dilatancy relation for the overconsolidated clayey soil is expressed by the dotted line at the initial stage of shearing and then the relation coincides with the normally consolidated line after the dotted line intersects with the solid line. The larger the overconsolidation ratio (OCR) is, the higher the stress ratio at the intersection is, as shown in Fig. 14. Comparing the result in Fig. 11 with the relation in Fig. 14, it is supposed that both the specimen with σ_r = 9.8 kN/m^2 (0.1 kgf/cm^2) and that with σ_r = 2.94 × 10 kN/m^2 (0.3 kgf/cm^2) are in the normally consolidated state although the specimen with σ_r = 9.8 kN/m^2 (0.1 kgf/cm^2) seems to be in the slightly overconsolidated state in Fig. 8. It might be found from Fig. 12 that the stress–dilatancy relation for Shirasu which is on the initial compression line before shearing is plotted on the dotted and then the solid lines in Fig. 14 and the one whose stress condition before shearing is on the normal compression line is expressed by the solid line in Fig. 14 although the data are scattered at the initial stage of shearing. It might be found from Fig. 13 that the stress–dilatancy relation for Toyoura sand is expressed by the dotted and the solid lines in Fig. 14, and the larger the confining pressure is, the closer the relation is to the one of the normally consolidated clayey soil. The stress–dilatancy relations are scattered at the initial stage of shearing because of errors due to the fit between the specimen and the cap or the pedestal and other mechanical errors of the measuring system. The more accurate triaxial test must be carried out to determine the stress–dilatancy characteristics, especially at the initial stage of shearing. The authors tried to carry out the shearing test of clayey soil

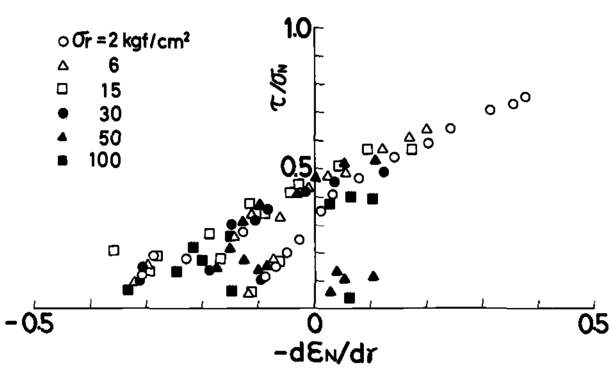

FIG. 12—*Stress–dilatancy relation of Shirasu.*

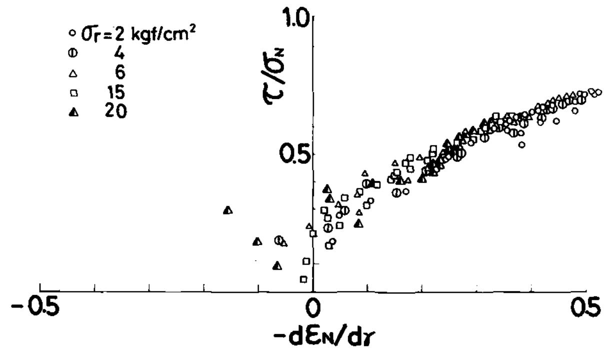

FIG. 13(*a*)—*Stress-dilatancy relation of Toyoura sand (low confining pressure).*

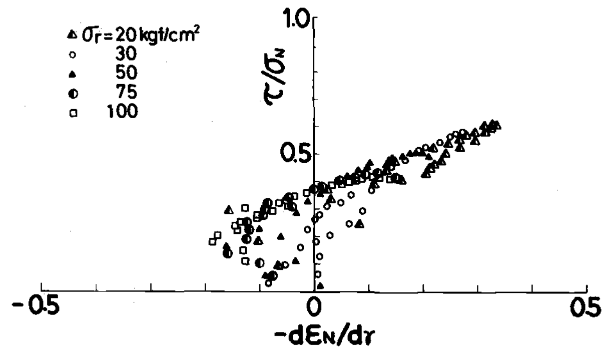

FIG. 13(*b*)—*Stress-dilatancy relation of Toyoura sand (high confining pressure).*

under confining pressure lower than 4.9 kN/m^2 (0.05 kgf/cm^2) to investigate the shear deformation characteristics of clayey soil whose stress condition is on the initial compression line, but it is impossible to do the triaxial test of the clayey soil under such extremely low confining pressure. An accurate testing method for the clayey soil under extremely low pressure must be established.

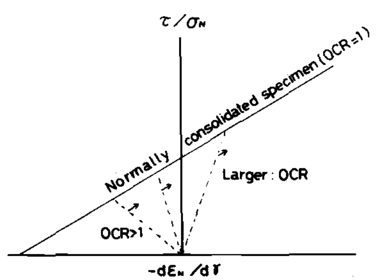

FIG. 14—*Schematic of stress-dilatancy relation.*

Conclusions

The results of this investigation of the compression and the shear deformation behaviors of three kinds of soil under wide-ranging confining pressure may be summarized as follows:

1. The normal compression line which is the same as the normally consolidated line exists for Shirasu and Toyoura sand at high pressure in the e-log p relation.
2. The initial compression line for clayey soil exists at extremely low pressure, and its slope might depend on the initial water content in the e-log p relation.
3. The shear deformation behavior of specimens on the normal compression line before shearing is supposed to be expressed by the unique curve on the q/p–ϵ_a-ϵ_v relation as well as the normal consolidated clayey soil.
4. The mechanical behavior of the clayey soil on the initial compression line should be investigated with greater accuracy and the method to test under extremely low pressure should be established.
5. The mechanical behavior of sandy soil on the normal compression line should be investigated with greater accuracy (that is, the testing apparatus should be improved to carry out the soil test under pressure higher than 9.8×10^3 kN/m^2 [100 kgf/cm^2]).

References

[1] Yoshimi, Y., Kuwabara, F., and Tokimatsu, K., *Soils and Foundations,* Vol. 15, No. 3, 1975, pp. 51–60.
[2] Imai, G., *Soils and Foundations,* Vol. 19, No. 3, 1979, pp. 45–60.
[3] Kitamura, R., Haruyama, M., and Misumi, K., *TSUCHI-TO-KISO JSSMFE,* Vol. 32, No. 2, 1984, pp. 17–21 (in Japanese).
[4] Miura, N., in *Proceedings,* Japan Society of Civil Engineering, No. 282, 1979, pp. 127–130 (in Japanese).
[5] Imai, G., Yano, K., and Aoki, S., *Soils and Foundations,* Vol. 24, No. 2, 1984, pp. 29–42.
[6] Shibata, T., Disaster Prevention Research Institute Annuals, Kyoto University, No. 6, 1963, pp. 128–134 (in Japanese).
[7] Ponce, V. M. and Bell, J. M., in *Proceedings, American Society of Civil Engineers,* Vol. 97, No. SM4, 1971, pp. 625–637.
[8] Fukushima, S. and Tatsuoka, F., *Soils and Foundations,* Vol. 24, No. 4, 1984, pp. 30–48.
[9] Murayama, S., Michihiro, K., and Sakagami, T., *Soils and Foundations,* Vol. 24, No. 2, 1984, pp. 1–15.
[10] Matsuoka, H. and Nakai, T., in *Proceedings,* Japan Society of Civil Engineering, No. 232, 1974, pp. 59–70.
[11] Nakai, T. and Matsuoka, H., *Soils and Foundations,* Vol. 23, No. 2, 1983, pp. 26–42.
[12] Shimizu, M., *Soils and Foundations,* Vol. 22, No. 4, 1982, pp. 121–135.

Richard W. Peterson[1]

Interpretation of Triaxial Compression Test Results on Partially Saturated Soils

REFERENCE: Peterson, R. W., "**Interpretation of Triaxial Compression Test Results on Partially Saturated Soils,**" *Advanced Triaxial Testing of Soil and Rock, ASTM STP 977,* Robert T. Donaghe, Ronald C. Chaney, and Marshall L. Silver, Eds., American Society for Testing and Materials, Philadelphia, 1988, pp. 512–538.

ABSTRACT: A laboratory investigation was conducted to assess the influence of density on the shear strength of unsaturated soil. To vary density, compacted specimens of an expansive clay soil were subjected to different stress histories prior to shear. Tests were performed at a constant water content. The Hvorslev "true friction–true cohesion" concept was used to normalize the effects of density differences on the shear strengths of both saturated and unsaturated specimens. It was determined that shear strengths of unsaturated soils were dependent on the stress state, density, and water content of specimens at failure. A modified Mohr-Coulomb failure model to predict the shear strength of unsaturated soils is proposed. The effect of suction is to increase the value of the cohesion intercept in this model. The actual measurement of soil suction is not required to apply the model.

KEY WORDS: unsaturated soils, expansive soils, clays, soil suction, laboratory tests, psychrometer, strength tests, consolidation tests, compaction tests

Numerous failures of compacted embankments, excavated and natural slopes, and foundations of unsaturated soils have been reported [*1–5*]. These failures are evidence that the geotechnical engineer does not possess an adequate understanding of the mechanical behavior of unsaturated soil. As a direct result of this technological inadequacy, designs of foundations and embankments of unsaturated soils may have been overly expensive, either due to extremely conservative design assumptions or in terms of aftermath failures. Realizing this inefficiency, a laboratory investigation was conducted to assess the influence of density on the shear strength of unsaturated soil.

Literature Review

Partially saturated soils, especially montmorillonitic clays, possess an affinity for water. Imbibing water often leads to changes in shear strength, differential heave, or collapse of these soils. A measure of the affinity for soil to retain water can be given by the magnitude of the negative pressure or suction in the pore water.

The apparent significance of negative pore water pressures in soils has stimulated many programs to develop techniques to measure suction and to evaluate its influence on soil behavior. Suction can be expressed quantitatively from the laws of thermodynamics [*6*]:

$$h_t = -\frac{RT}{v_w} \ln \frac{p}{p_o} \tag{1}$$

[1] Research civil engineer, U.S. Army Engineer Waterways Experiment Station, Vicksburg, MS 39180.

where

h_t = total suction
R = universal gas constant
T = absolute temperature
v_w = volume of a mole of liquid water
p/p_o = relative humidity
p = pressure of water vapor
p_o = pressure of saturated water vapor

Total suction is the algebraic sum of matrix and osmotic suction [6]:

$$h_t = h_m + h_s \tag{2}$$

where

h_m = matrix suction
h_s = osmotic or solute suction

Osmotic suction results from soluble salts in the pore water. Soluble salts influence the distance between clay particles [7,8], the interlayer spacings in the crystalline lattice [9], and the magnitude of swell and swell pressures [10,11]. The efficiency of osmotic suction to move external water into a soil depends on the type of dissolved salts in the pore water [12].

Matrix suction is related to the negative pore water pressure or capillary stress in soils [13–15]:

$$h_m = u_a - u_w \tag{3}$$

where

u_a = pore air pressure
u_w = pore water pressure

Pore air pressure is usually taken as zero for atmospheric pressure.

Hilf investigated pore water pressures in compacted cohesive soils [16]. He proposed a Mohr-Coulomb strength relationship of the form of Eq 4 to describe the shear strengths of unsaturated soils:

$$\tau = c' + \sigma' \tan \phi' \tag{4}$$

where

τ = shear strength
c' = apparent cohesion in terms of effective stress
ϕ' = angle of internal friction in terms of effective stress

and

$$\sigma' = (\sigma - u_a) - u_c \tag{5}$$

where

σ' = effective stress
σ = total normal stress
u_c = capillary stress = $-(u_a - u_w)$

Guided by the success of the effective stress equation for saturated soils, Bishop and his colleagues also suggested an effective stress relationship for partially saturated soils [*17*]:

$$\sigma' = (\sigma - u_a) + \chi(u_a - u_w) \tag{6}$$

where χ = a parameter which varies from 0 to 1 as saturation varies from 0 to 1
Unsaturated shear strengths were expressed in the form of a modified Mohr-Coulomb strength relationship [*17*] as

$$\tau = c' + [(\sigma - u_a) + \chi(u_a - u_w)] \tan \phi' \tag{7}$$

In practice, the χ factor for unsaturated soils did not work well. Jennings and Burland demonstrated that χ would have negative values for collapsing soils [*18*]. Blight reported two methods for evaluating the χ parameter; each method yielded different results [*19*]. Blight was unable to decide which method was correct. Furthermore, Blight reported that it was theoretically possible for values of χ to be greater than +1 in unsaturated soils close to saturation. Gulhati and Satija later presented test results where χ exceeded +1 for unsaturated specimens [*20*].

Fredlund postulated that unsaturated soil was a four-phase system consisting of solids, water, a continuous air phase, and contractile skin (or air–water interface) [*21*]. He suggested the air phase generally became continuous at degrees of saturation less than approximately 85% to 90%. Two independent stress tensors were proposed based on an analysis consistent with multiphase continuum mechanics. Conceptually, Fredlund suggested the shear strength of a partially saturated soil could be expressed in the form of an extended or three-dimensional, Mohr-Coulomb strength relationship:

$$\tau = c' + (\sigma - u_a) \tan \phi' + (u_a - u_w) \tan \phi^b \tag{8}$$

where

τ = shear strength
c' = cohesion intercept when the two stress state variables are zero
$(\sigma - u_a)$ = stress state variable, applied stress
$(u_a - u_w)$ = stress state variable, matrix suction
ϕ' = angle of friction with respect to applied stress
ϕ^b = angle of friction with respect to matrix suction

which is illustrated in Fig. 1. Furthermore, he stated there was a smooth transition from the unsaturated to the saturated case. As the degree of saturation approached 100% the pore water pressure would become equal to the pore air pressure and could be substituted for pore air pressure in the stress variable, $(\sigma - u_a)$. Matrix suction $(u_a - u_w)$ would go to zero. The c' and ϕ' strength parameters could be evaluated in the conventional manner used for saturated soils.

Ho and Fredlund [*22*] and Chantawarangul [*23*] reanalyzed test results of several soils reported in the literature using the unsaturated shear strength model, Eq 8. Typical values for the angle of friction, ϕ^b, ranged from 4° to 35°; ϕ^b was frequently one-third to two-thirds of the angle of friction, ϕ'.

Based on results of linear regression analyses for evaluating ϕ^b, the extended Mohr-Coulomb relationship for predicting the shear strengths of unsaturated soils appeared to be promising. However, because of the limited data base, uncertainty remained regarding variables that influence values of suction as well as the shear strengths of unsaturated soils.

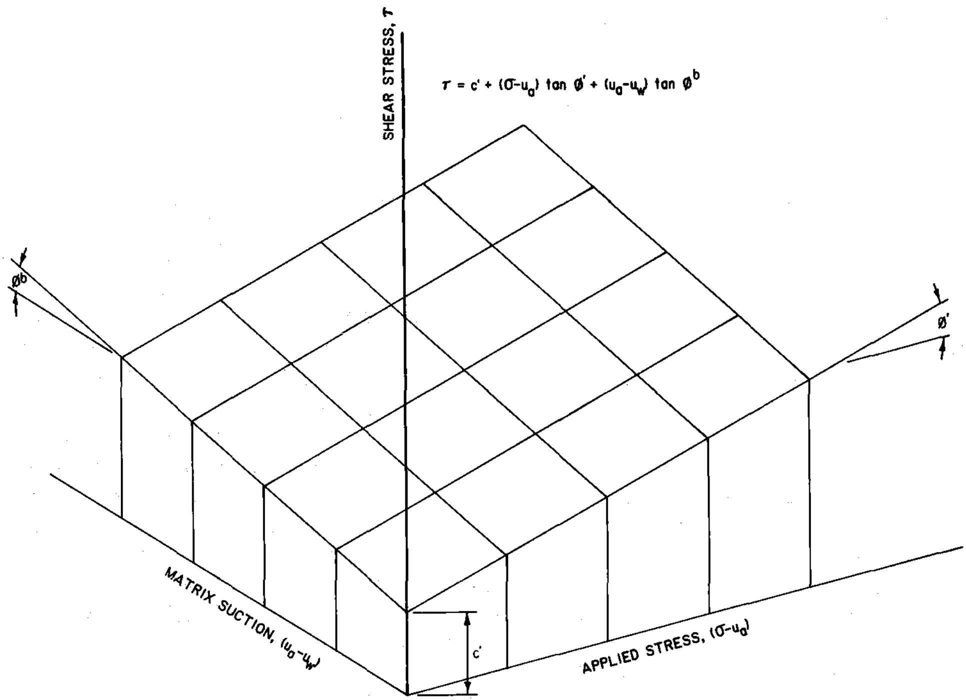

FIG. 1—*Extended Mohr-Coulomb strength relationship for unsaturated soils (after Fredlund [21]).*

Therefore, values for strength parameters, such as χ or ϕ^b, could not be anticipated with any degree of confidence. For example, Ho and Fredlund [*22*] reevaluated the shear strengths of compacted specimens of Dhanauri clay which had been previously reported by Gulhati and Satija [*20*], using the shear strength model given by Eq 8. Specimens were compacted to two initial densities and tested as constant water content ($\overline{CW}$) or consolidated drained (CD) triaxial compression tests. Values of ϕ^b appeared to be dependent on both the specimen density and the type of test (that is, $\overline{CW}$ or CD test). Similarly, other laboratory investigations have shown that shear strengths of unsaturated soils were affected by compaction water content and the method of compaction [*24–27*]. Specimens compacted dry of optimum were stronger, more brittle, and tended to swell, whereas specimens compacted wet of optimum were weaker, more ductile, and tended to consolidate. Specimens molded by dynamic or static compaction were more brittle and tended to swell as compared to those specimens molded by kneading compaction. However, soil suction was not measured and therefore unsaturated strength parameters could not be evaluated.

As a result of the observation that the strength parameter, ϕ^b, was apparently dependent on test type, a reexamination of the literature resulted in the identification of three types of triaxial tests routinely used to determine the shear strengths of unsaturated soils:

(a) *Constant water content* ($\overline{CW}$) *test* [17,20] The cell pressure, pore air pressure, and specimen water content are kept constant during shear. Volume changes and pore water pressures induced during shear are measured. Suction usually decreases as saturation increases due to volume decrease caused by increased normal stresses.

(b) *Consolidated-drained* (*CD*) *test* [20,22] Cell pressure, pore air pressure, and pore water pressure are kept constant during shear. Specimen volume changes and the volume of water entering or leaving the specimen during shear are measured. For these tests, suction remains constant because pore air and pore water pressures are kept constant.

(c) *Undrained* ($\overline{UU}$) *test* [28] The cell pressure and specimen water content are kept constant during shear. Pore air pressure, pore water pressure, and volume change induced during shear are measured. As with $\overline{CW}$ tests, suction usually decreases as saturation increases due to the decrease in specimen volume caused by increased normal stresses.

Laboratory Investigation

A laboratory investigation was conceived and executed to assess the influence of density variation on the shear strength of unsaturated soil. Constant water content ($\overline{CW}$) tests were conducted because the effects of density variation could be evaluated more easily than results of CD tests, in which both density and water content changes could occur. Soil suction was measured so that unsaturated strength parameters, such as χ or ϕ^b, could be evaluated.

Triaxial compression tests were conducted on unsaturated specimens that had been compacted at an initial water content of 20%. The compacted specimens were 2.8 in. (7.1 cm) in diameter by 6.0 in. (15.2 cm) high. Density was varied by applying different stress histories to replicate specimens. One group of specimens was isotropically consolidated to stress states of 0.7, 1.4, or 2.9 tsf (70, 140, or 280 kPa) prior to shear. A second group of specimens was consolidated to 2.9 tsf (280 kPa) and rebounded to 1.4 or 0.7 tsf (140 or 70 kPa) before shearing. A third group of specimens was consolidated to 11.5 tsf (1100 kPa), rebounded to 2.9, 1.4, or 0.7 tsf (280, 140, or 70 kPa), and then sheared.

To provide a reference for evaluating the shear strengths of unsaturated soil, 1.4-in. (3.6-cm) diameter by 3.0-in. (7.6-cm) high back-pressure saturated triaxial specimens were tested at various overconsolidation ratios (OCRs). Selected specimens were isotropically consolidated to stress states of 2.9 or 11.5 tsf (280 or 1100 kPa) prior to shear. A second group of specimens was consolidated to 2.9 tsf (280 kPa) and rebounded to 1.4, 0.7, or 0.4 tsf (140, 70, or 30 kPa) before shearing. A third series of specimens was consolidated to 11.5 tsf (1100 kPa), rebounded to 5.8, 2.8, 1.4, or 0.7 tsf (550, 280, 140, or 70 kPa), and then sheared.

Hvorslev's [*29,30*] concept of "true friction, ϕ_e–true cohesion, C_e" was selected to normalize the effects of density variation on the shear strengths of both saturated and unsaturated specimens. The Hvorslev strength parameters can be obtained by comparing the shear strengths of normally consolidated and overconsolidated specimens at the same void ratio at failure, as conceptually illustrated in Fig. 2*a* by points a and b, respectively. Due to the difficulty of performing tests on normally consolidated and overconsolidated specimens with identical void ratios at failure, Bishop and Henkel proposed a normalizing technique which consisted of dividing both the normal stress and the shear stress by an "equivalent consolidation stress," P_e [*31*]. For saturated specimens, P_e was defined as the consolidation pressure or stress that produced a particular water content (or void ratio) in a normally consolidated specimen. Bishop and Henkel's technique is presented in Fig. 2*b*.

To aid in the selection of a P_e-relationship, one-dimensional consolidation tests were conducted on specimens compacted at a water content of 20%. From each 2.8-in. (7.1-cm) diameter by 6.0-in. (15.2 cm) high compacted soil sample, three specimens, 2.5 in. (6.3 cm) diameter by 1.25 in. (3.2 cm) high, were prepared for consolidometer tests. For each test series, two specimens were inundated and one specimen was tested at the "as compacted" water content. Inundated specimens were subjected to initial boundary conditions imposed by the swell and swell pressure (constant volume) tests described in EM 1110-2-1906 [*32*]. The maximum stress applied to any specimen was 128 tsf (12.3 MPa), although several tests were terminated at lower stresses because soil was extruded around the top loading platen.

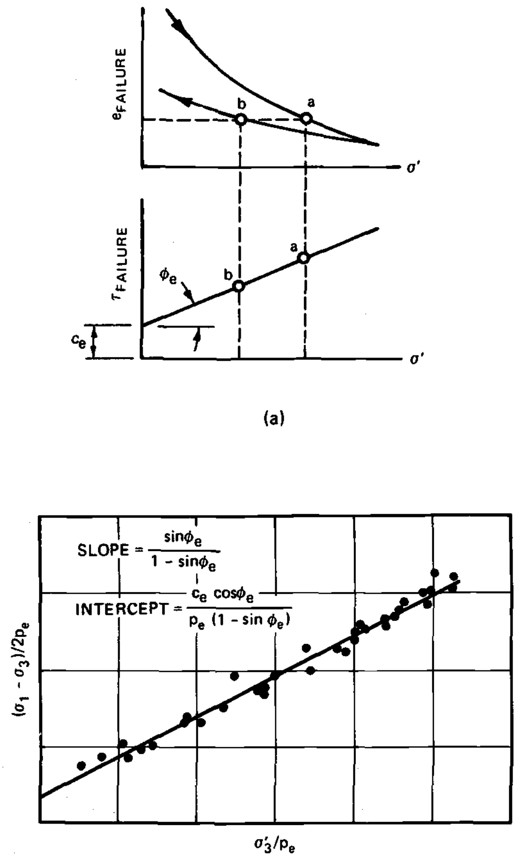

FIG. 2—*Determination of Hvorslev's "true friction–true cohesion" strength parameters.* (a) *Strength parameters determined using normally consolidated and overconsolidated specimens sheared with identical void ratios at failure.* (b) *Normalizing technique using an "equivalent consolidation pressure" (after Bishop and Henkel* [31]).

Laboratory Testing Equipment

The thermocouple psychrometer was selected to measure soil suction because initial values of suction in the unsaturated specimens were fairly large (for example, $h_t > 15$ tsf [1.4 MPa]). The principle of its operation consists of measuring the relative humidity of air in the voids of soil specimens; measurements are converted to total suction by Eq 1 [*6,33*].

Only minor modifications to conventional laboratory soils testing equipment were required for testing unsaturated soils:

1. One fixed ring consolidometer was modified to allow a psychrometer to be inserted into the top loading platen to measure suction in unsaturated specimens during the consolidation test. To minimize evaporation of water from the unsaturated soil specimen during the test, moist paper towels were placed within the inundation ring and a rubber membrane was stretched over the apparatus.

2. Two modifications to the triaxial apparatus were required. First, a thermocouple psychrometer was inserted into the soil specimen through the base platen of the device. Second, an internal cylindrical chamber was designed and constructed to permit the measurement

of volume changes of unsaturated soils in triaxial compression. During the test, the volume enclosed between the soil specimen and the internal chamber was saturated with water. The volume of water that flowed into or out of the internal chamber was related to the volume change of the unsaturated specimen.

During triaxial compression tests the assembled apparatus was submerged in a constant temperature (25 ± 0.02°C) water bath to minimize the influence of temperature fluctuations on the electromotive force (emf) output from the psychrometer. Preliminary analyses of one-dimensional consolidation test results had shown that emf values, when corrected to 25°C using Eq 9 [*34,35*], varied as a function of room temperature fluctuations; the variation of the corrected emf values was due likely to unbalanced temperatures between the soil and test apparatus.

$$E_{25} = \frac{E_t}{0.325 + 0.027t} \tag{9}$$

where

E_{25} = voltage at 25°C, μV
E_t = voltage at temperature t, μV
t = test temperature, °C

More repeatable results were also obtained when the volume change apparatus was calibrated at constant temperatures as compared to similar calibration results obtained at ambient temperatures.

To ensure thermal equilibrium between the water bath and triaxial apparatus, the assembled device was allowed to equilibrate thermally overnight before initiating any test or calibration; the time required to achieve thermal equilibrium within the triaxial apparatus was estimated to be 6 to 8 h using data published in Ref *36*.

Soil and Specimen Preparation

Vicksburg buckshot clay was selected for the investigation because it was available locally and a substantial amount of test data had been previously reported [*37–41*]. The soil is a brown clay (CH) with a trace of sand [*32,42*]. Ninety-seven percent of the soil by dry weight passes the No. 200 U.S. standard sieve (0.074 mm), and 43% is finer than 0.002 mm. The specific gravity is 2.72 and the Atterberg limits are

Liquid limit (LL) = 56%
Plastic limit (PL) = 21%
Plasticity index (PI) = 35%

The electrical conductivity of an extract of the pore fluid obtained by the saturation extract technique was 0.3 mmho/cm. From this value, solute suction was calculated as 0.1 tsf (10 kPa) [*43*].

Prior to the compaction of all specimens, the desired amount of air dry soil ($w \cong 5\%$ to 6%) was placed in a mixing bowl with sufficient distilled water to increase the water content of the soil–water mixture to approximately 20%. Both soil and water were thoroughly mixed using an electric mixer. After mixing, the moist soil was forced through a #4 wire screen (4.8 mm), placed in a plastic container, sealed, and allowed to equilibrate for 1 week prior to compaction.

All specimens were molded using kneading compaction. Compaction characteristics of Vicksburg buckshot clay are presented in Fig. 3. The optimum water content for the low compactive effort using kneading compaction was 23.2% with a corresponding maximum density of 99.3 lb/ft^3 (1590 kg/m^3). These values compare to the optimum water content–density relationships obtained by impact compaction using standard compactive effort of 12 375 ft-lb/ft^3 (5940 kJ/m^3) [*37,39*]. Compaction characteristics for other compactive efforts using both impact and kneading compaction are also presented in Fig. 3.

Consolidation Tests

Typical one-dimensional consolidation test results for specimens compacted at an initial water content of 20% are presented in Fig. 4. The data are expressed as void ratio, e, versus

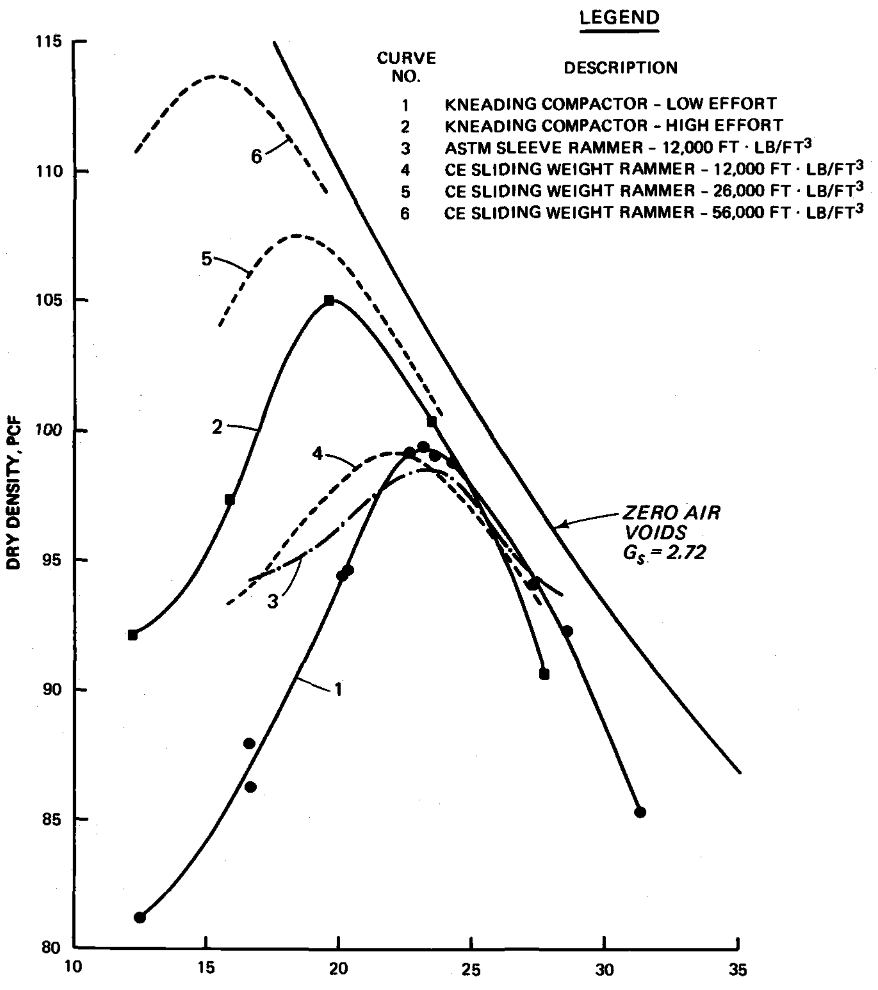

FIG. 3—*Compaction relationships for Vicksburg buckshot clay obtained by kneading compaction for this investigation and by impact compaction using the ASTM sleeve rammer (after Horz* [39]*) and the Corps of Engineers (CE) sliding weight rammer (after Brabston* [37]*) (1000 ft-lb/ft^3 = 480 kJ/m^3; 100 lb/ft^3 = 1600 kg/m^3).*

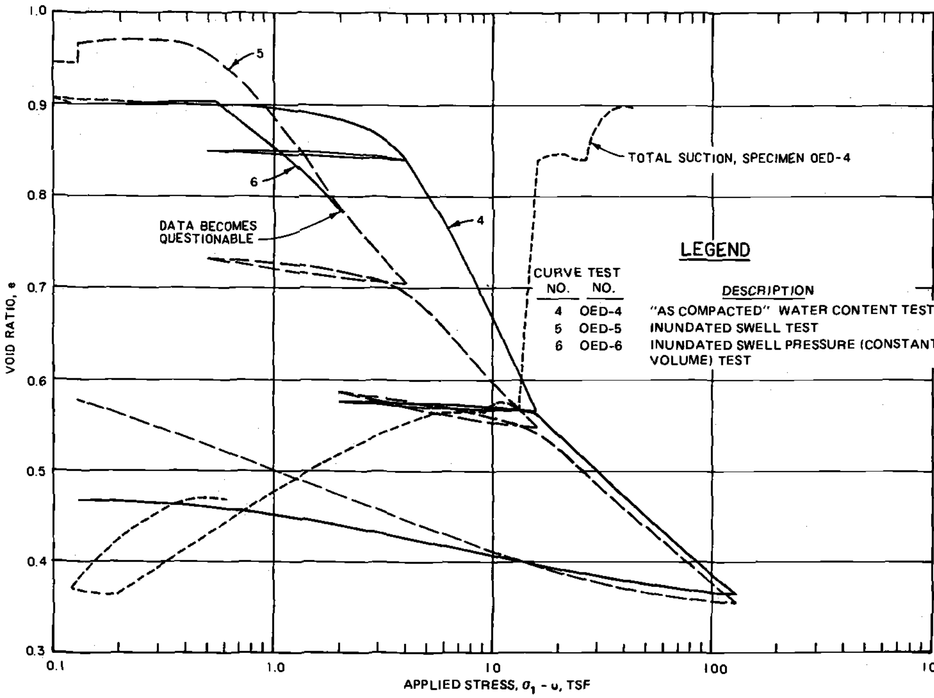

FIG. 4.—*Typical consolidation test results for specimens of Vicksburg buckshot clay compacted at an initial water content of 20% (1 tsf = 96 kPa).*

logarithm of applied stress, $\sigma - u$, where u is the pore air pressure for unsaturated specimens or pore water pressure for saturated specimens. Because these specimens were loaded slowly to allow pore pressures to dissipate, $u \cong 0$ for both unsaturated and saturated specimens. For inundated specimens identified as curves 5 and 6 for the swell and swell-pressure (constant volume) tests, respectively, the consolidation relationships converge at a vertical stress of approximately 2 tsf (190 kPa). Similar behavior was also observed for other tests on inundated specimens. Examination of curves 4 and 5 for unsaturated and inundated specimens, respectively, revealed that for stress levels less than 20 tsf (1.9 MPa) the compression index, C_c, is approximately 0.28 for the inundated specimen and 0.48 for the unsaturated specimen. At stress levels in excess of 20 tsf (1.9 MPa) the compression index for both inundated and natural water content specimens is approximately 0.22.

Total suction for the unsaturated specimen is superimposed on Fig. 4. Measured values of suction decreased as the specimen consolidated. At a void ratio of 0.84, suction was approximately 14 tsf (1.3 MPa). When the specimen had consolidated to a void ratio of 0.57, suction had decreased to 12 tsf (1.2 MPa). At a void ratio of 0.57, which corresponded to a degree of saturation of about 90%, suction decreased rapidly to a minimum value of 0.2 tsf (20 kPa) at a void ratio of 0.37. The compression index simultaneously reduced from 0.48 to 0.22 for the same range of void ratios. A possible explanation for this behavior is that pore air had become occluded and water was being forced from the moist soil as additional consolidation occurred.

At void ratios less than approximately 0.5, pore water was likely squeezed from the soil specimen as additional consolidation occurred. For this condition matrix suction would be approximately zero and the value of solute suction would be that measured using the thermocouple psychrometer. As can be seen from the void ratio–suction relationship given in Fig. 4, the measured value of (solute) suction decreased to less than 0.2 tsf (20 kPa) at a void ratio of 0.37. Although the accuracy of this measurement may be questionable because psychrometers are not reliable when measuring low values of suction, the value of 0.2 tsf (20 kPa) compares well with the value for solute suction of 0.1 tsf (10 kPa) determined by the saturation extract method [43]. One may conclude that for practical purposes matrix suction is equal to the measured value of total suction, as can be determined using Eq 2. Therefore, throughout the remainder of this study, measured values of (total) suction will be treated as matrix suction when evaluating unsaturated strength parameters, such as reported in Eq 7 and Eq 8.

The void ratio–applied stress relationships for the tests presented in Fig. 4 are presented in Fig. 5 along with several data points for slurry consolidated specimens of Vicksburg buckshot clay [38,40]. Using these data, a virgin compression relationship, or "equivalent consolidation stress," was constructed for this soil. Mathematically, the relationship is expressed as

$$P_e = \left[\frac{e}{a}\right]^b \tag{10}$$

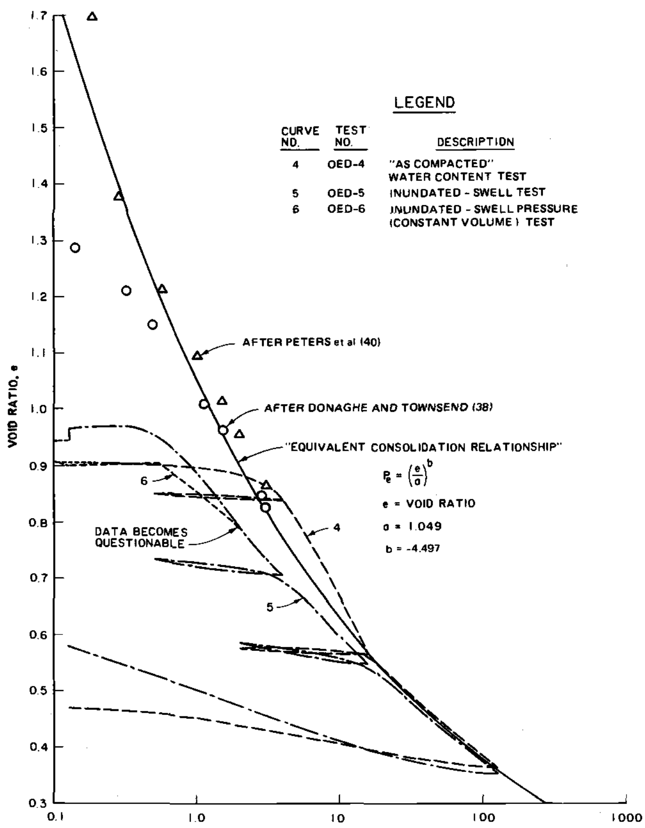

FIG. 5—*"Equivalent consolidation relationship" for Vicksburg buckshot clay (1 tsf = 96 kPa).*

where

P_e = equivalent consolidation stress, tsf
e = void ratio
a, b = coefficients
a = 1.049
b = −4.497

The equivalent consolidation relationship was used to normalize density variations for saturated and unsaturated triaxial compression test specimens. From volume change measurements obtained during triaxial tests, the void ratio at any time during the test could be calculated and expressed as an equivalent consolidation stress, P_e, by Eq 10.

Strength Tests

Saturated Tests

Curves presented in Fig. 6 are typical results of consolidated-undrained triaxial tests with pore water pressure measurements conducted on back pressure-saturated specimens expressed as shear stress versus normal stress, where

$$\text{shear stress} = \frac{(\sigma_1 - u) - (\sigma_3 - u)}{2} \tag{11}$$

and

$$\text{normal stress} = \frac{(\sigma_1 - u) + (\sigma_3 - u)}{2} \tag{12}$$

and u is the pore water pressure. The maximum and minimum principal stresses are $(\sigma_1 -$

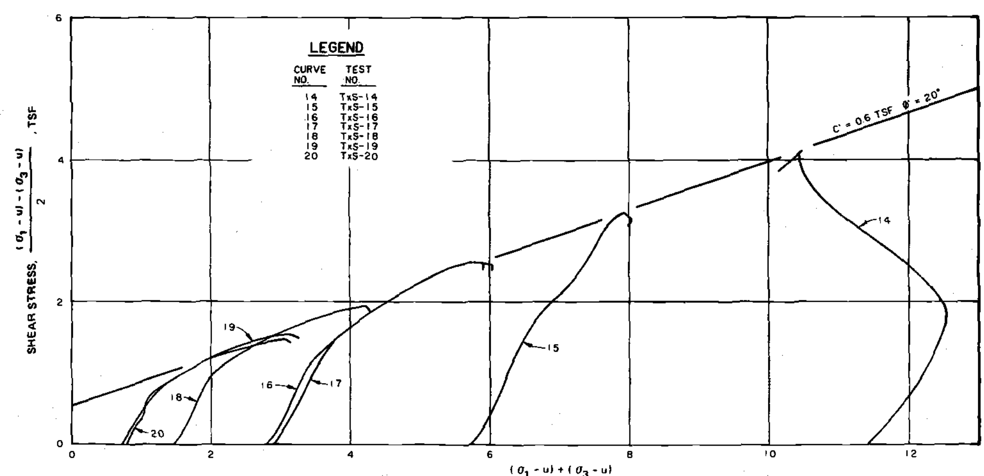

FIG. 6—*Stress path data for back pressure-saturated triaxial test specimens of Vicksburg buckshot clay (1 tsf = 96 kPa).*

u) and ($\sigma_3 - u$), respectively. The failure envelope can be expressed as

$$\frac{(\sigma_1 - u) - (\sigma_3 - u)}{2} = a + \frac{(\sigma_1 - u) + (\sigma_3 - u)}{2} \tan \alpha \tag{13}$$

The slope of the failure surface is tan α and the intercept is a. Apparent cohesion, c', and the angle of internal friction, ϕ', are related to a and α by the relationships

$$a = c' \cos \phi' \tag{14}$$

$$\tan \alpha = \sin \phi' \tag{15}$$

From the test results presented in Fig. 6, it was observed that the failure surface was curved concave downward. All specimens were overconsolidated and tended to dilate during shear. A linear "best fit" strength envelope of $c' = 0.6$ tsf (60 kPa) and $\phi' = 20°$ was determined for specimens rebounded from 11.5 tsf (1.1 MPa). Similarly, the strength envelope for specimens rebounded from 2.9 tsf (280 kPa) was determined to be $c' = 0.2$ tsf (20 kPa) and $\phi' = 27°$. The differences in strength parameters for specimens rebounded from 2.9 and 11.5 tsf (280 kPa and 1.1 MPa) were likely a result of specimen density variation. Void ratios ranged from 0.55 to 0.66 for specimens rebounded from 11.5 tsf (1.1 MPa) to void ratios of 0.67 to 0.75 for specimens rebounded from 2.9 tsf (280 kPa).

To minimize the effects of density differences, results of the strength tests were normalized by a Hvorslev technique similar to the procedure suggested by Bishop and Henkel [31]. Substituting Eq 14 and Eq 15 into Eq 13 and rearranging terms yields

$$\frac{(\sigma_1 - u) - (\sigma_3 - u)}{2} = c' \frac{\cos \phi'}{1 + \sin \phi'} + (\sigma_1 - u) \frac{\sin \phi'}{1 + \sin \phi'} \tag{16}$$

Each stress state in Eq 16 is then divided by an equivalent consolidation stress, P_e, to normalize differences caused by density variations. The normalized strength relationship becomes

$$\frac{(\sigma_1 - u) - (\sigma_3 - u)}{2P_e} = \frac{C_e}{P_e} \frac{\cos \phi_e}{1 + \sin \phi_e} + \frac{(\sigma_1 - u)}{P_e} \frac{\sin \phi_e}{1 + \sin \phi_e} \tag{17}$$

Data presented in Fig. 7 are typical of shear strength test results for saturated specimens that have been normalized for density variations.

For all back pressure-saturated triaxial tests, a least-squares regression analysis yielded the following normalized strength parameters:

$$\text{slope} = \frac{\sin \phi_e}{1 + \sin \phi_e} = 0.185 \tag{18}$$

$$\text{intercept} = \frac{C_e}{P_e} \frac{\cos \phi_e}{1 + \sin \phi_e} = 0.078 \tag{19}$$

$$\phi_e = 13.1° \tag{20}$$

$$C_e/P_e = 0.099 \tag{21}$$

$$\text{correlation coefficient, } r = 0.948 \tag{22}$$

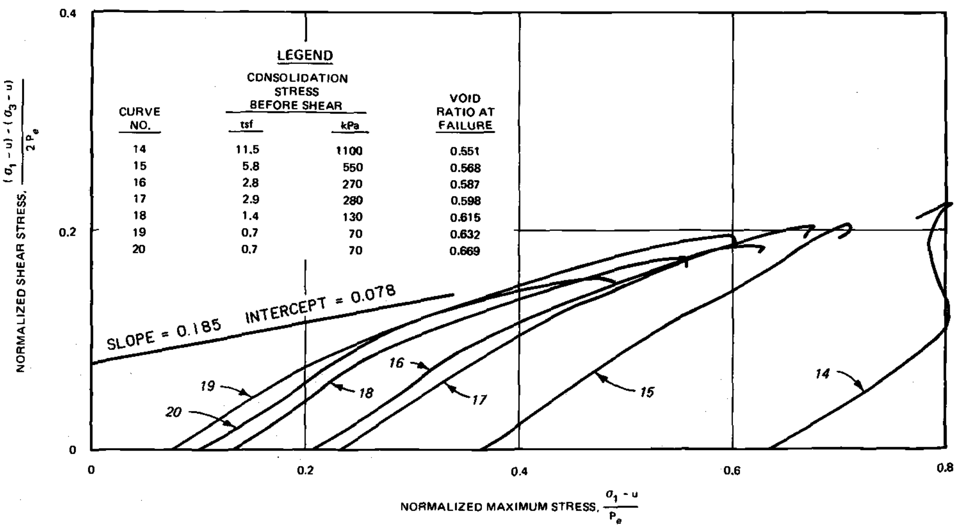

FIG. 7—*Normalized stress path data for back pressure-saturated triaxial test specimens of Vicksburg buckshot clay.*

These representative strength parameters provided a reference to evaluate the shear strengths of unsaturated soils.

Unsaturated Tests

Data presented in Fig. 8 are typical of the shear strengths of unsaturated triaxial test specimens expressed in a form amenable to Eq 13 as shear stress $[(\sigma_1 - u) - (\sigma_3 - u)]/2$, versus normal stress, $[(\sigma_1 - u) + (\sigma_3 - u)]/2$, where u is the pore air pressure. As can be seen from the test data presented in Fig. 8, unsaturated specimens exhibited a substantially larger shear strength at failure than companion saturated specimens. The magnitude of this strength difference was dependent on at least two variables: suction and density. However, the effects of each variable cannot be easily separated and evaluated when test results are expressed in the form of Eq 13.

Test results for eleven unsaturated specimens were normalized for density variations using the relationship given by Eq 17 where u is the pore air pressure. Typical normalized strength results for five specimens tested at a chamber pressure of 1.4 tsf (140 kPa) are presented in Fig. 9. Regression analyses were conducted to determine normalized strength parameters for unsaturated specimens. Strength data for each specimen were obtained at axial strains corresponding to the strains for Hvorslev failure of saturated specimens. Results are summarized in Table 1. Correlation coefficients were 0.998 or better. However, a fan of failure surfaces which appeared to be dependent on confining pressure was formed. The slopes of the failure surfaces increased from 0.33 to 0.37 as the confining stresses decreased from 2.9 to 0.7 tsf (280 to 70 kPa). Although much confidence was gained from the excellent values for the correlation coefficient, the meaning of different failure slopes as a function of confining stress was not immediately clear.

Because of the difficulty of using normalized strength parameters in geotechnical engineering practice, the added strength due to suction for unsaturated specimens was expressed in a form amenable to Mohr-Coulomb failure criteria. To accomplish this, normalized shear strengths for saturated specimens, calculated from the representative strength parameters given by Eq 18 and Eq 19, were subtracted from the normalized shear strengths of unsat-

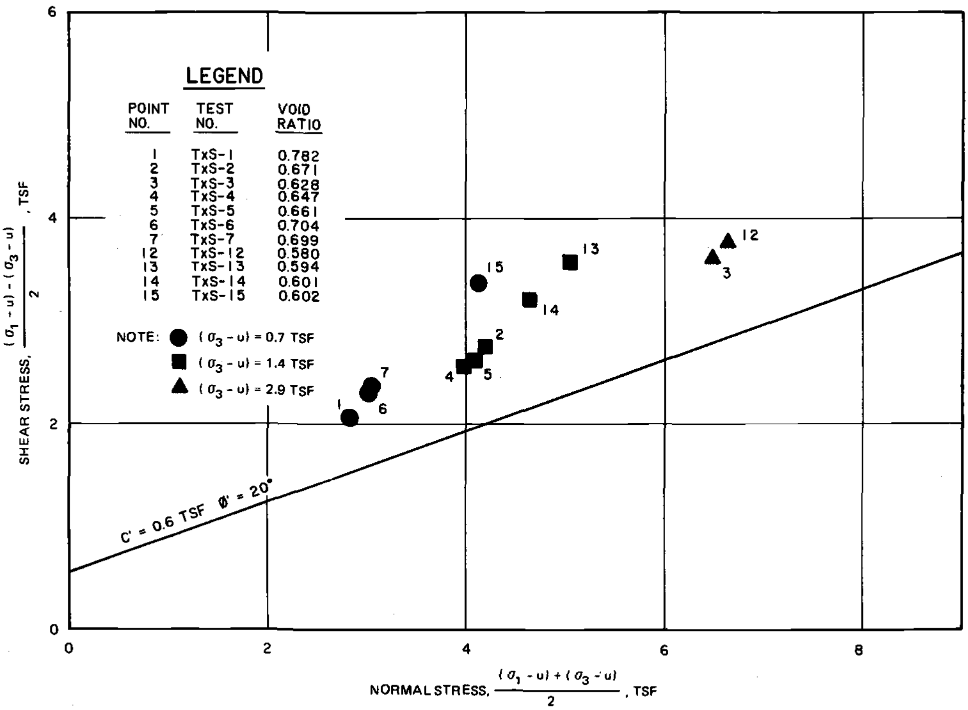

FIG. 8—*Shear strength data for unsaturated triaxial test specimens of Vicksburg buckshot clay (1 tsf = 96 kPa).*

urated specimens at identical normalized stress ratios, $(\sigma_1 - u)/P_e$. These differences were converted to apparent shear strength due to suction, q_ψ, by simply multiplying by P_e, as shown in Eq 23:

$$q_\psi = P_e \left\{ \left[\frac{(\sigma_1 - u) - (\sigma_3 - u)}{2P_e} \right]_{\text{unsaturated}} - \left[\frac{C_e}{P_e} \frac{\cos \phi_e}{1 + \sin \phi_e} + \frac{\sigma_1 - u}{P_e} \frac{\sin \phi_e}{1 + \sin \phi_e} \right]_{\text{saturated}} \right\} \quad (23)$$

where

P_e = equivalent consolidation stress for the unsaturated specimen at any instant during the test computed using Eq 10

$\frac{\sigma_1 - u}{P_e}$ = normalized stress state for the unsaturated specimen at any instant during the test

The slope and intercept of the normalized strength relationships for saturated specimens are

$$\text{slope} = \frac{\sin \phi_e}{1 + \sin \phi_e} = 0.185 \quad (18)$$

$$\text{intercept} = \frac{C_e}{P_e} \frac{\cos \phi_e}{1 + \sin \phi_e} = 0.078 \quad (19)$$

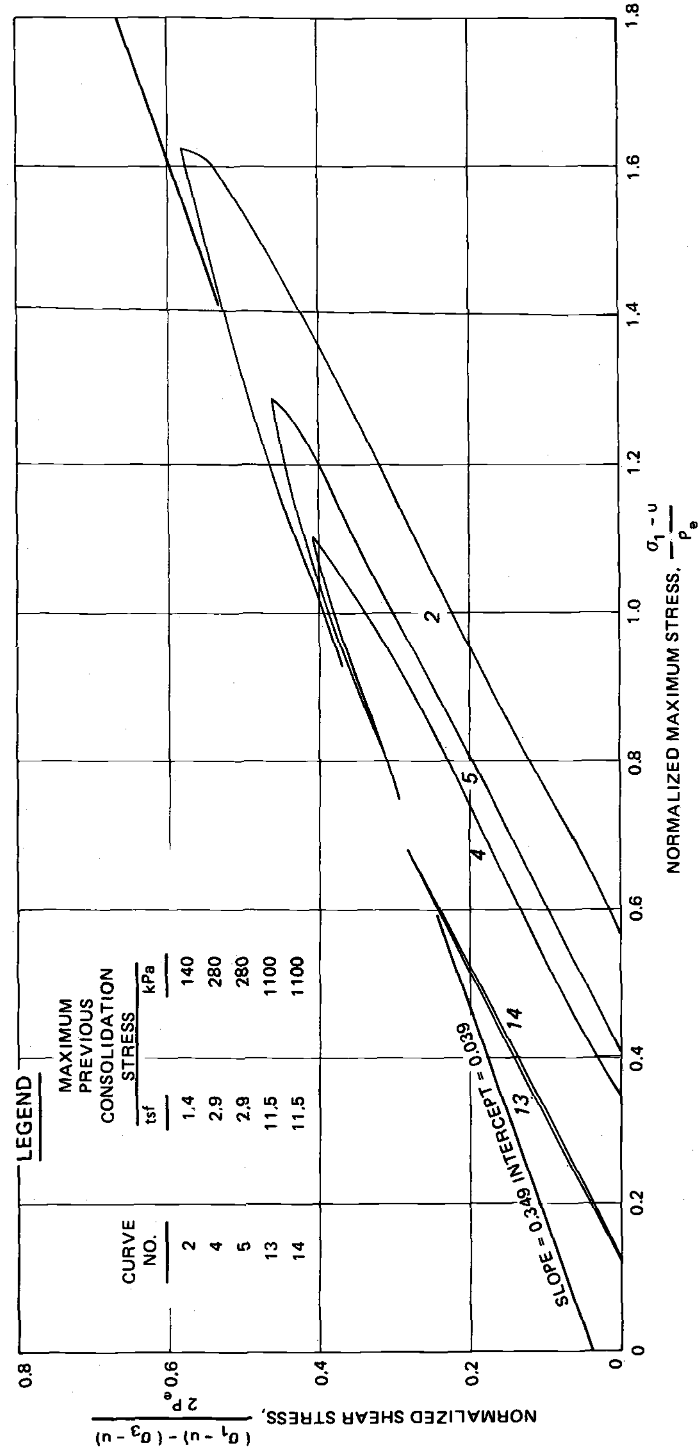

FIG. 9—*Normalized stress path data for unsaturated triaxial test specimens of Vicksburg buckshot clay tested at a confining stress of 1.4 tsf (140 kPa).*

TABLE 1—*Normalized strength parameters for unsaturated and saturated specimens of Vicksburg buckshot clay.*

Confining Stress ($\sigma_3 - u$)				
tsf	kPa	Correlation Coefficient, r	Intercept	Slope
0.7	70	0.999	0.050	0.375
1.4	130	0.998	0.039	0.349
2.9	280	0.999	0.025	0.329
——	——	0.948[a]	0.078[a]	0.185[a]

[a] Obtained from regression analysis of shear strengths of back pressure-saturated specimens for this investigation.

The results of this calculation disclosed that after density differences between saturated and unsaturated specimens had been negated by the normalizing technique, calculated values of apparent shear strength due to suction were nearly constant; values ranged from 0.7 to 1.0 tsf (70 to 95 kPa). Furthermore, the values of apparent shear strength due to suction were determined without using measured suction data.

Typical calculated values of apparent shear strength due to suction expressed as a function of axial strain for five specimens are presented in Fig. 10. These data show that the maximum strength increase occurred between 7 and 17% axial strain, which is consistent with the axial strain range for those data used in the regression analyses summarized in Table 1.

Table 2 summarizes the calculated values of apparent shear strength due to suction for eleven unsaturated specimens which vary from 0.7 to 1.0 tsf (70 to 95 kPa). Measured values of suction at failure and the strength parameter associated with suction, arctan $[q_\psi/h_t]$, are also tabulated. A linear regression analysis was conducted to evaluate the influence of suction on the apparent shear strength due to suction. The coefficient of correlation was poor ($r = -0.2$) which indicated the strengths that resulted from suction were not linearly related to measured suction values.

TABLE 2—*Influence of suction on the shear strength of unsaturated specimens of Vicksburg buckshot clay tested at a water content of 20%.*

Test No.	Saturation at Failure, S (%)	Apparent Shear Strength Due to Suction, q_ψ		Suction, h_t		Arctan, q_ψ/h_t (degrees)
		tsf	kPa	tsf	kPa	
TXS-1	67	0.79	76	9.5	900	4.5
TXS-2	74	0.88	84	9.0	850	5.5
TXS-3	77	0.98	94	4.0	400	13
TXS-4	78	0.74	71	...	...	...
TXS-5	74	0.78	75	3.0	300	15
TXS-6	73	0.85	81	4.0	400	13
TXS-7	72	0.89	85	3.5	350	13
TXS-12	90	0.74	71	3.0	300	13
TXS-13	88	0.98	94	4.0	400	14
TXS-14	88	0.79	76	...	...	...
TXS-15	86	1.04	100	3.5	350	16

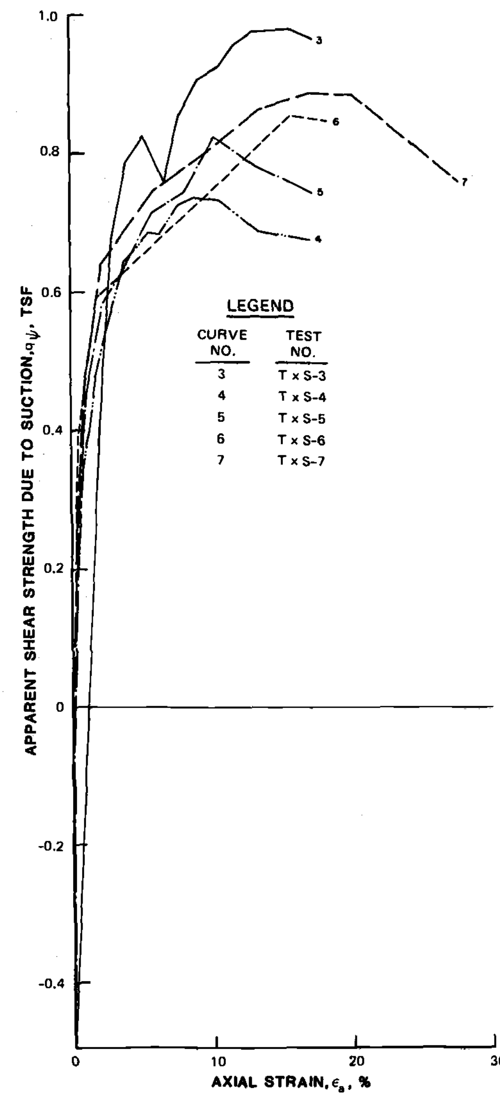

FIG. 10—*Calculated values of apparent shear strength due to suction as a function of axial strain (1 tsf = 96 kPa).*

Interpretation of Test Results

The data presented in Table 2 and Fig. 10 indicate that suction in unsaturated soil produced the same effect as increasing the value of cohesion in a Mohr-Coulomb strength relationship provided that density differences between saturated and unsaturated specimens were insignificant. This infers that shear strengths of unsaturated soils (for example, saturation less than approximately 85 to 90%) can be expressed by a modified Mohr-Coulomb failure criterion as

$$\tau = c' + (\sigma - u_a) \tan \phi' + C_\psi \qquad (24)$$

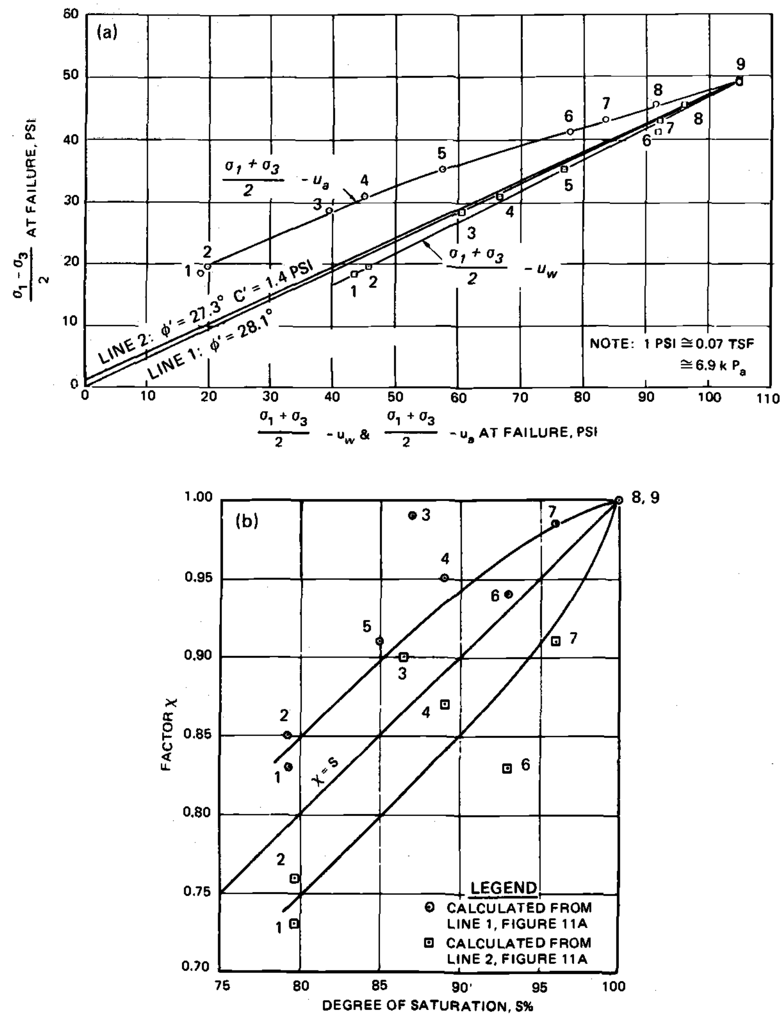

FIG. 11—(a) *Triaxial tests on a compacted boulder clay (clay fraction 18%) compacted at a water content of 11.6% and sheared at constant water content.* (b) *Relation between degree of saturation and factor* χ *for tests at constant water content on a compacted boulder clay (clay fraction 18%) (after Bishop et al.* [17]).

where

τ = shear strength
$(\sigma - u_a)$ = applied stress
c' = apparent cohesion evaluated in the conventional manner for saturated soils
ϕ' = angle of internal friction evaluated in the conventional manner for saturated soils
C_ψ = apparent cohesion due to suction

Preliminary assessment of the data reported in Table 2 and Fig. 10 appeared to be inconsistent with test results previously reported by Ho and Fredlund [22] and Chantawarangul

[23]. These researchers reported that shear strengths of unsaturated soils increased linearly as matrix suction increased whereas the strengths for the unsaturated soils reported herein were not linearly dependent on changes of suction. The most obvious explanation for these differences is test type. Ho and Fredlund [22] conducted CD tests on unsaturated specimens of decomposed granite and decomposed rhyolite; both the water contents and densities of these specimens could change during the test. $\overline{\text{CW}}$ tests were conducted for the investigation reported herein; the water content was held constant while the density could vary as the test was conducted.

To check the validity of the shear strength model proposed in Eq 24, constant water content test results from other studies of unsaturated soil behavior were reanalyzed. Bishop and his colleagues [17] presented $\overline{\text{CW}}$ test results for unsaturated specimens of compacted boulder clay which are illustrated in Fig. 11*a* and 11*b* and summarized in Table 3. From the curve identified as $(\sigma_1 + \sigma_3)/2 - u_a$ in Fig. 11*a*, the failure strength can be approximated as two linear segments for tests 1 through 4 and 5 through 9 with a curvilinear segment connecting tests 4 and 5. From the data presented in Fig. 11*b*, tests identified as 1 through 5 have degrees of saturation less than 90% while tests 6 through 9 have degrees of saturation greater than 90%.

Aided by Fredlund's guidance [21] that air becomes occluded at degrees of saturation greater than approximately 85 to 90% and by the shape of the failure envelope presented in Fig. 11*a*, the strength increase due to suction for tests 1 through 4 or tests 1 through 5 was examined and found to be nearly constant at a value of approximately 9 psi (0.6 tsf or 60 kPa). Linear regression analyses were conducted to evaluate the influence of suction on shear strength of unsaturated soil. Results are summarized in Table 3. For conditions when the degree of saturation at failure was less than approximately 90%, such as for tests 1 through 4 or tests 1 through 5, there was a poor correlation between the apparent shear strength due to suction and measured values of suction (for example, $-0.4 < r < 0.5$). A

TABLE 3—*Summary of shear strengths of unsaturated specimens of Boulder clay (after Bishop et al. [17]).*

	Shear Stress	Normal Stress	Normal Stress	Matrix[c] Suction	Calculated[d] Shear Stress	Apparent[e] Shear Strength Due to Suction	
Test[a] No.	$(\sigma_1 - \sigma_3)/2$, psi[b]	$(\sigma_1 + \sigma_3)/2 - u_a$, psi	$(\sigma_1 + \sigma_3)/2 - u_w$, psi	$u_a - u_w$, psi	$(\sigma_1 - \sigma_3)/2$, psi	$\Delta[(\sigma_1 - \sigma_3)/2]$, psi	Calculated[f] χ-Factor
1	18.5	18.7	43.6	24.9	9.8	8.7	0.76
2	19.6	19.9	45.8	25.9	10.4	9.2	0.78
3	28.6	39.6	60.6	21.0	19.4	9.2	0.95
4	31.1	45.0	66.7	21.7	21.9	9.2	0.93
5	35.3	57.5	76.7	19.4	27.6	7.7	0.87
6	41.4	77.8	91.8	14.0	36.9	4.5	0.70
7	43.3	83.3	92.1	8.8	39.5	3.8	0.95
8	45.8	91.5	96.1	4.6	43.2	2.6	1.22
9	49.2	104.8	104.8	0.0	49.3	−0.1	...

[a] For test numbers and test data refer to Fig. 11*a* and *b*.
[b] 1.0 psi ≅ 0.072 tsf ≅ 6.9 kPa.
[c] $u_a - u_w = [(\sigma_1 + \sigma_3)/2 - u_w] - [(\sigma_1 + \sigma_3)2 - u_a]$.
[d] The calculated value refers to the shear stress on the saturated failure envelop: $c' = 1.4$ psi, $\phi' = 27.3°$.
[e] The apparent shear strength due to suction is the difference between the shear stress of the unsaturated specimen and the calculated shear stress for a saturated specimen.
[f] $\chi_{\text{calculated}} = \Delta[(\sigma_1 - \sigma_3)/2]/[(u_a - u_w) \tan \phi' \cos \phi']$ based upon the saturated strength parameters: $c' = 1.4$ psi, $\phi' = 27.3°$.
[g] Obtained from Fig. 11*b* for saturated strength parameters: $c' = 1.4$ psi, $\phi' = 27.3°$.
[h] The calculated value is based upon saturated strength parameters: $c' = 0$ psi, $\phi' = 28.1°$.
[i] Obtained from Fig. 11*b* for saturated strength parameters: $c' = 0$ psi, $\phi = 28.1°$.

regression analysis was also conducted on tests 1 through 9. The coefficient of correlation, r, was 0.975 and $\phi^b = 22.4°$ which agree with the values reported by Ho and Fredlund [22] of $r = 0.974$ and $\phi^b = 21.7°$. However, tests 6 through 9 had degrees of saturation in excess of 90%, and probably should not be included in an analysis of the ϕ^b parameter.

The U.S. Bureau of Reclamation has conducted numerous studies of the shear strength of unsaturated soils. Results of two studies are summarized in Table 4. Richmond reported a study of the shear strengths of both saturated and unsaturated specimens of sandy clay [*44*]. The apparent shear strength due to suction was 0.5 tsf (50 kPa). The coefficient of correlation for the apparent shear strength due to suction as a function of suction was determined as −0.35. Prizio reported a similar study for compacted specimens of sandy silt [*45*]. The apparent shear strength due to suction was 0.4 tsf (40 kPa). A regression analysis to evaluate the influence of suction on the apparent shear strength due to suction was not appropriate because suction remained nearly constant for the range of test conditions to which the specimens had been subjected.

Casagrande and Hirschfeld reported a study of the shear strengths of compacted specimens of sandy clay [*46,47*]. Test results are summarized in Table 5. For specimens compacted to an initial dry density of 106 pcf (1700 kg/m^3) and tested at a water content of 16%, the apparent shear strength due to suction was approximately 0.2 tsf (20 kPa). The apparent shear strength due to suction increased to 0.5 tsf (50 kPa) when unsaturated specimens were tested at a water content of 14%. Similar behavior was observed for companion saturated and unsaturated specimens compacted to an initial dry density of 111 pcf (1780 kg/m^3). For unsaturated specimens compacted at initial water contents of 16 and 13%, the apparent shear strength due to suction was 0.2 and 0.4 tsf (20 and 40 kPa), respectively. Suction measurements were not obtained during these tests.

From the data reported by Casagrande and Hirschfeld it was evident that shear strengths of unsaturated specimens are dependent on both the water contents and densities of the

TABLE 3—*Continued*

				Regression Analyses for Apparent Shear Strength Due to Suction Versus Suction			
Measured[g] χ-Factor	Calculated[h] χ-Factor	Measured[i] χ-Factor	Saturation at Failure S, %	Test No.	Intercept, psi	Slope	Coefficient of Correlation r
0.73	0.83	0.83	79				
0.76	0.84	0.85	79				
0.90	1.00	0.99	87				
0.87	0.97	0.95	89				
...	0.90	0.91	85				
0.83	0.72	0.94	93				
0.91	0.98	0.98	96				
...	1.24	1.00	~100				
...	...	...	~100				
				1-4	10.1	−0.044	−0.425
				1-5	6.1	0.121	0.507
				1-9	0.4	0.366	0.975

TABLE 4—*Summary of shear strengths of saturated and unsaturated specimens of sandy clay and sandy silt (after Richmond* [44] *and Prizio* [45]).

Soil Type	Test Type[a]	Void Ratio at Failure e, %	Water Content at Failure w, %	Saturation at Failure S, %	Shear Stress[b] $[(\sigma_1 - u) - (\sigma_3 - u)]/2$		Normal Stress $[(\sigma_1 - u) + (\sigma_3 - u)]/2$		Matrix Suction $u_a - u_w$		Calculated Shear Stress[c] $[(\sigma_1 - u) - (\sigma_3 - u)]/2$		Apparent Shear Strength Due to Suction[d] $\Delta[(\sigma_1 - u) - (\sigma_3 - u)]/2$		Shear Values Corrected for Pore Pressure c'	ϕ'	Coefficient of Correlation r
					tsf	kPa	tsf	kPa	tsf	kPa	tsf	kPa	tsf	kPa	tsf (kPa)	deg	
Sandy clay	$\overline{CU}$	0.434	16.0	...	3.4	320	5.4	510	...	...	...	...	...	...			
		0.427	16.0	...	3.9	370	6.4	610	...	...	...	...	...	...			
		0.421	15.6	...	3.3	310	5.2	500	...	...	...	...	...	...			
		0.400	15.3	...	7.9	750	13.4	1280	...	...	...	...	...	...	0.4 (40)	34.4	0.9998
	$\overline{UU}$	0.443	14.1	81	4.1	390	5.8	560	0.5	50	3.6	340	0.5	50			
		0.420	14.0	81	4.1	390	6.2	600	0.9	90	3.8	370	0.3	30			
		0.433	14.0	83	8.0	770	13.1	1260	0.2	20	7.7	740	0.3	30			
		0.415	14.1	89	12.1	1160	19.6	1870	0.3	30	11.3	1090	0.8	70			
Sandy silt	$\overline{CU}$	0.496	18.4	...	3.7	360	6.2	600	...	...	...	...	...	...			
		0.503	18.3	...	3.8	370	6.5	630	...	...	...	...	...	...			
	CD	0.575	22.5	...	2.2	210	3.6	350	...	...	...	...	...	...			
		0.484	17.3	...	5.1	490	8.7	830	...	...	...	...	...	...			
		0.417	16.2	...	10.5	1010	17.7	1700	...	...	...	...	...	...	0.0 (0.0)	36.3	0.9999
	$\overline{UU}$	0.517	13.4	67	2.8	270	4.2	400	0.14	14	2.5	240	0.3	30			
		0.495	13.6	72	5.8	550	9.1	880	0.15	14	5.4	520	0.4	40			
		0.461	13.4	76	10.6	1020	17.1	1640	0.16	15	10.1	970	0.5	50			

[a] $\overline{CU}$ = Saturated, consolidated undrained with pore water pressure measurements.
CD = Saturated, consolidated drained.
$\overline{UU}$ = Unsaturated, unconsolidated undrained with pore air and pore water pressure measurements.
[b] u is the pore air pressure for unsaturated specimens and pore water pressure for saturated specimens.
[c] The calculated value refers to the shear stress on the saturation failure envelop.
[d] The apparent shear strength is the difference between the shear stress of the unsaturated specimen and the calculated shear stress.

specimens. The magnitude of the apparent shear strength due to suction is related to the water content of the specimen at failure and can be treated as a constant for a range of applied stresses provided the water content of the specimen remains constant. This observation provided the continuity for interpretation of $\overline{CW}$ and CD test results. Although Ho and Fredlund [22] reported a strong correlation between suction and apparent shear strength due to suction, the increased values for suction and apparent shear strength due to suction actually resulted from a decrease of the specimen's water content. Hence, Eq 24 can be used to analyze test results obtained by either $\overline{CW}$ or CD tests for unsaturated soils.

Summary

A modified Mohr-Coulomb strength relationship, given by Eq 24, has been proposed to describe the shear strengths of unsaturated soils. Apparent cohesion, c', and the angle of internal friction, ϕ', can be evaluated by conventional tests on saturated specimens. The magnitude of the apparent cohesion due to suction, C_ψ, is dependent on the water content of the specimen at failure. At full saturation the value of the apparent cohesion due to suction is zero, pore water pressure is equal to the pore air pressure, and Eq 24 reverts to the conventional saturated Mohr-Coulomb strength relationship. The measurement of suction is not required to apply this model.

Only two limitations of the strength model, given by Eq 24, have been identified.

1. Strengths of saturated and unsaturated specimens must be compared at similar void ratios and stress states. If this is not possible because of significant differences of consolidation characteristics of saturated and unsaturated specimens, a procedure to normalize density differences such as used for the investigation reported herein, must be employed to evaluate the apparent cohesion due to suction.
2. This model should not be used to analyze test results of unsaturated specimens when the air phase is discontinuous (for example, at high degrees of saturation). Although the data by Bishop and his colleagues [17] which is presented in Figure 11*a* (tests 6 to 9) indicated there was a smooth transition from unsaturated to saturated behavior, further comprehensive studies are needed to evaluate the shear strengths of unsaturated soils at high degrees of saturation and to assess existing models and/or to propose new models.

Other laboratory investigations should be undertaken to evaluate the unsaturated strength model, given by Eq 24, using low compressibility soils to minimize the effects caused by density differences between saturated and unsaturated specimens tested at similar stress states. Tests should be conducted on specimens at several void ratios and water contents to assess the influence of each variable. Suction measurements should be obtained such that other unsaturated strength models could be evaluated by conducting alternative analyses.

A comprehensive investigation also needs to be conducted to evaluate the influence of suction on the shear strengths of unsaturated soils at high degrees of saturation. Specimens should be subjected to both CD and $\overline{CW}$ test conditions at several initial water contents and densities.

Acknowledgments

The study described and the resulting data presented herein were obtained from research conducted at the U.S. Army Engineer Waterways Experiment Station, Vicksburg, MS under sponsorship of the Office, Chief of Engineers Research, Development, Test, and Evaluation Program. Valuable suggestions and assistance were provided by the staff of the Soil Mechanics Division. Permission was granted by the Chief of Engineers to publish this paper.

TABLE 5—*Summary of shear strengths of saturated and unsaturated specimens of sandy clay (after Casagrande and Hirschfeld* [46,47]).

Test No.	Test Type[a]	Water Content w, %	Dry Density[b] γ_d, pcf	Saturation S, %	Shear Stress[c] $[(\sigma_1 - u) - (\sigma_3 - u)]/2$		Normal Stress $[(\sigma_1 - u) + (\sigma_3 - u)]/2$		Calculated Shear Stress[d] $[(\sigma_1 - u) - (\sigma_3 - u)]/2$		Apparent Shear Strength Due to Suction[e] $\Delta[(\sigma_1 - u) - (\sigma_3 - u)]/2$		Shear Values Corrected for Pore Pressure		Coefficient of Correlation r
					tsf	kPa	tsf	kPa	tsf	kPa	tsf	kPa	c', tsf (kPa)	ϕ', deg	
R1	$\overline{CU}$	11.9	106.0	63.2	0.5	50	0.7	70	...	...	...	...			
R2		13.2	107.1	62.4	1.2	110	1.9	180	...	...	...	...			
R3		13.6	106.0	62.6	1.3	130	2.3	220	...	...	...	...			
R4		13.4	107.7	63.7	2.3	220	4.3	410	...	...	...	...			
R5		13.6	107.2	64.0	2.6	250	5.3	510	...	...	...	...			
R6		13.5	106.6	62.3	2.6	250	4.3	410	...	...	...	...			
R7		13.7	108.0	65.5	3.6	340	6.1	580	...	...	...	...			
R8		13.3	105.8	60.2	5.7	550	11.0	1050	...	...	...	...			
R9		16.4	108.0	78.8	1.0	90	1.4	140	...	...	...	...			
R10		16.7	105.5	75.0	1.2	120	2.1	200	...	...	...	...			
R11		16.6	106.1	76.0	1.6	150	2.6	250	...	...	...	...			
R12		15.5	107.9	74.2	2.3	220	3.7	240	...	...	...	...			
R13		16.7	107.2	78.8	3.7	350	5.9	560	...	...	...	...			
R14		16.2	107.7	76.6	5.9	560	11.2	1080	...	...	...	...	0.3 (30)	30.6	0.9930
Q1	$\overline{Q}$	13.8	105.5	62.5	2.0	190	2.6	250	1.6	150	0.38	36			

Q2		13.8	105.8	62.8	2.6	250	3.9	370	2.2	210	0.42	40			
Q3		13.8	106.4	63.9	4.6	450	7.1	680	3.9	370	0.79	76			
Q4		13.4	104.1	59.2	5.4	520	9.2	880	4.9	470	0.49	47			
Q5		13.2	104.6	57.7	7.1	680	12.2	1170	6.5	620	0.62	60			
Q9	$\overline{\text{Q}}$	16.1	105.5	73.3	1.3	120	1.7	160	1.1	110	0.15	15			
Q10		16.1	106.6	74.0	2.0	200	2.9	280	1.7	170	0.31	29			
Q11		16.4	106.6	76.7	2.5	240	3.9	370	2.2	210	0.28	26			
R40	$\overline{\text{CU}}$	13.3	112.9	72.1	1.2	110	1.8	170	...	...	...	...			
R41		14.3	112.7	77.5	2.6	250	4.4	420	...	...	...	...			
R42		13.4	113.3	74.0	2.6	250	4.2	400	...	...	...	...			
R43		13.1	110.8	67.2	2.0	190	3.4	330	...	...	...	...			
R44		13.1	111.2	68.3	2.8	270	4.4	430	...	...	...	...			
R45		12.5	111.9	65.9	4.1	390	6.7	640	...	...	...	...			
R46		13.2	110.0	66.4	5.8	550	10.1	970	...	...	...	...	0.2 (20)	33.7	0.9978
Q34	$\overline{\text{Q}}$	12.9	111.1	66.8	2.8	270	3.6	350	2.2	210	0.55	53			
Q35		12.8	110.9	66.1	3.8	360	5.6	530	3.3	320	0.49	47			
Q36		13.0	110.8	65.3	5.5	530	9.1	870	5.3	510	0.27	26			
Q37		13.1	111.6	69.0	7.4	710	12.1	1160	6.9	670	0.43	41			
Q40	$\overline{\text{Q}}$	16.3	110.7	83.8	1.3	130	1.8	170	1.2	110	0.14	14			
Q41		16.7	110.4	82.9	2.0	190	2.9	270	1.8	170	0.23	22			

[a] $\overline{\text{CU}}$ = Saturated, consolidated undrained with pore water pressure measurements.
$\overline{\text{Q}}$ = Unsaturated, unconsolidated undrained with pore air pressure measurements.

[b] 1 lb/ft^3 = 16.02 kg/m^3.

[c] u is the pore air pressure for unsaturated specimens and pore water pressure for saturated specimens.

[d] The calculated value refers to the shear stress on the saturation failure envelop.

[e] The apparent shear strength is the difference between the shear stress of the unsaturated specimen and the calculated shear stress.

References

[1] Adegoke-Anthony, C. W. and Agada, O. A., "Observed Slope and Road Failures in Some Nigerian Residual Soils," in *Proceedings,* Engineering and Construction in Tropical and Residual Soils, American Society of Civil Engineers, Honolulu, Hawaii, 11–15 Jan. 1982, pp. 519–536.

[2] Boonsinsuk, P. and Yong, R. N., "Analyses of Hong Kong Residual Soil Slopes," in *Proceedings,* Engineering and Construction in Tropical and Residual Soils, American Society of Civil Engineers, Honolulu, Hawaii, 11–15 Jan. 1982, pp. 463–482.

[3] Hale, G. P., "Report of Materials Testing, Borrow Source, Khashm Al An, Saudi Arabia for Saudi Arabian National Guard Headquarters Complex, Riyadh, Saudi Arabia," U.S. Army Engineer Waterways Experiment Station, Vicksburg, MS; transmittal of data to U.S. Army Engineer Division, Middle East (Rear), Winchester, VA, April 1982.

[4] Jones, D. E., Jr. and Holtz, W. G., "Expansive Soils—The Hidden Disaster," *Civil Engineering, American Society of Civil Engineers,* Vol. 43, No. 8, Aug. 1973, pp. 49–51.

[5] U.S. Army Corps of Engineers, Vicksburg District, "Long-Term Strength Reduction and Slough Slides in Mississippi River Levees," Feb. 1983.

[6] Review Panel, "Engineering Concepts of Moisture Equilibria and Moisture Changes in Soils," *Moisture Equilibria and Moisture Changes in Soils Beneath Covered Areas,* Australia, Butterworths, 1965, pp. 7–21.

[7] Richards, B. G., "Moisture Flow and Equilibria in Unsaturated Soils for Shallow Foundations," *Permeability and Capillarity of Soils, ASTM STP 417,* American Society for Testing and Materials, Philadelphia, Aug. 1967, pp. 4–34.

[8] Means, R. E., "Buildings on Expansive Clay, Theoretical and Practical Treatment of Expansive Soils," *Quarterly of the Colorado School of Mines,* Vol. 54, No. 4, Oct. 1959, pp. 1–31.

[9] Foster, W. R., Savins, J. G., and Waite, J. M., "Lattice Expansion and Rheological Behavior Relationships in Water-Montmorillonite Systems," in *Proceedings,* Third National Conference, Clay and Clay Minerals, National Academy of Sciences–National Research Council (NAS–NRC) Publication 395, 1955, pp. 296–316.

[10] Goris, J., "Pressures Associated with Swelling in Soils," M. S. thesis, Department of Civil Engineering, University of Alberta, Edmonton, Alberta, May 1955.

[11] Holt, J. H., "A Study of the Physico Chemical, Mineralogical and Engineering Properties of Fine-Grained Soil in Relation to Their Expansive Characteristics," Technical Report No. AFWL-TR-69-169, Air Force Weapons Laboratory, Kirtland Air Force Base, Albuquerque, NM, June 1970.

[12] Kemper, W. D. and Rollins, J. B., "Osmotic Efficiency Coefficients Across Compacted Clays," in *Proceedings,* Soil Science Society of America, Vol. 30, Sept.–Oct. 1966, pp. 529–534.

[13] Matyas, E. L. and Radhakrishna, H. S., "Volume Change Characteristics of Partly Saturated Soils," *Geotechnique,* Vol. 18, No. 12, Dec. 1968, pp. 432–448.

[14] Blight, G. E., "A Study of Effective Stresses for Volume Change," in *Concluding Proceedings of Moisture Equilibria and Moisture Changes in Soils Beneath Covered Areas,* Butterworths, Australia, 1965, pp. 259–269.

[15] Barden, L., Madedor, A. O., and Sides, G. R., "Volume Change Characteristics of Unsaturated Clay," *Journal of the Soil Mechanics and Foundations Division, American Society of Civil Engineers,* Vol. 95, No. SM1, Jan. 1969, pp. 33–51.

[16] Hilf, J. W., "An Investigation of Pore-Water Pressure in Compacted Cohesive Soils," Technical Memorandum 654, U.S. Department of the Interior Bureau of Reclamation, Denver, CO, Oct. 1956.

[17] Bishop, A. W., Alpan, I., Blight, G. E., and Donald, I. B., "Factors Controlling the Strength of Partly Saturated Cohesive Soils," in *Research Conference on Shear Strength of Cohesive Soils,* American Society of Civil Engineers, Boulder, CO, June 1960, pp. 503–532.

[18] Jennings, J. E. and Burland, J. B., "Limitations to the Use of Effective Stresses in Partially Saturated Soils," *Geotechnique,* Vol. 12, No. 2, Sept. 1962, pp. 125–144.

[19] Blight, G. E., "Effective Stress Evaluation for Unsaturated Soils," *Journal of the Soil Mechanics and Foundations Division, American Society of Civil Engineers,* Vol. 93, No. SM2, March 1967, pp. 125–148.

[20] Gulhati, S. K. and Satija, B. S., "Shear Strength of Partially Saturated Soils," in *Proceedings,* Tenth International Conference on Soil Mechanics and Foundation Engineering, Vol. 1, Stockholm, Sweden, 15–19 June 1981, pp. 609–612.

[21] Fredlund, D. G., "Appropriate Concepts and Technology for Unsaturated Soils," Second Canadian Geotechnical Colloquium, *Canadian Geotechnical Journal,* Vol. 16, No. 1, 1979, pp. 121–139.

[22] Ho, D. Y. F. and Fredlund, D. G., "Increase in Strength Due to Suction for Two Hong Kong Soils," in *Proceedings,* Engineering and Construction in Tropical and Residual Soils, American Society of Civil Engineers, Honolulu, Hawaii, 11–15 Jan. 1982, pp. 263–295.

[23] Chantawarangul, K., "Comparative Study of Different Procedures to Evaluate Effective Stress Strength Parameters for Partially Saturated Soils," Thesis No. GT-82-32, Asian Institute of Technology, Bangkok, Thailand, March 1983.
[24] Lee, K. L. and Haley, S. C., "Strength of Compacted Clay at High Pressure," *Journal of the Soil Mechanics and Foundation Division, American Society of Civil Engineers,* Vol. 94, No. SM6, Nov. 1968, pp. 1303–1332.
[25] Parcher, J. V. and Liu, P-C., "Some Swelling Characteristics of Compacted Clays," *Journal of the Soil Mechanics and Foundation Division, American Society of Civil Engineers,* Vol. 91, No. SM3, May 1965, pp. 1–17.
[26] Seed, H. B. and Chan, C. K., "Structure and Strength Characteristics of Compacted Clays," *Journal of the Soil Mechanics and Foundation Division, American Society of Civil Engineers,* Vol. 85, No. SM5, Oct. 1959, pp. 87–128.
[27] Seed, H. B., Mitchell, J. K., and Chan, C. K., "The Strength of Compacted Cohesive Soils," *Research Conference on Shear Strength of Cohesive Soils,* ASCE, Boulder, Colorado, June 1960, pp. 877–964.
[28] U.S. Department of the Interior Bureau of Reclamation, *Earth Manual,* 2nd Edition, Washington, D. C., 1974.
[29] Hvorslev, M. Juul, "Physical Components of the Shear Strength of Saturated Clays," in *Research Conference on Shear Strength of Cohesive Soils,* American Society of Civil Engineers, Boulder, CO, June 1960, pp. 169–273.
[30] Hvorslev, M. J., "Physical Properties of Remolded Cohesive Soils," Translation No. 69-5, U.S. Army Engineer Waterways Experiment Station, Vicksburg, MS, June 1969.
[31] Bishop, A. W. and Henkel, D. J., *The Measurement of Soil Properties in the Triaxial Test,* 2nd ed. Edward Arnold, London, 1962, pp. 164–166.
[32] Department of the Army, Office of the Chief of Engineers, "Laboratory Soils Testing," Engineer Manual EM 1110-2-1906, Washington, DC, 30 Nov. 1970.
[33] Daniel, D. E., Hamilton, J. M., and Olson, R. E., "Suitability of Thermocouple Psychrometers for Studying Moisture Movement in Unsaturated Soils," in *Permeability and Groundwater Contaminant Transport, ASTM STP 746,* Philadelphia, American Society for Testing and Materials, 1981, pp. 84–100.
[34] Brown, R. W., "Measurement of Water Potential with Thermocouple Psychrometers: Construction and Applications," USDA Forest Service Research Paper INT-80, Ogden, UT, 1970.
[35] Wiebe, H. H., Brown, R. W., Daniel, T. W., and Campbell, E., "Water Potential Measurement in Trees," *Bio Science,* Vol. 20, 1970, pp. 225–226.
[36] Hodgeman, C. D., Weast, R. C., and Selby, S. M., Eds., *Handbook of Chemistry and Physics,* 43rd ed., The Chemical Rubber Publishing Co., Cleveland, OH, 1961, pp. 2474–2476.
[37] Brabston, W. N., "Investigation of Compaction Criteria for Airport Pavement Subgrade Soils," Technical Report GL-81-11, U.S. Army Engineer Waterways Experiment Station, Vicksburg, MS, Oct. 1981.
[38] Donaghe, R. T. and Townsend, F. C., "Effects of Anisotropic Versus Isotropic Consolidation in Consolidated-Undrained Triaxial Compression Tests of Cohesive Soils," Technical Report S-75-13, U.S. Army Engineer Waterways Experiment Station, Vicksburg, MS, Oct. 1975.
[39] Horz, R. C., "Evaluation of Revised Manual Compaction Rammers and Laboratory Compaction Procedures," Miscellaneous Paper GL-83-20, U.S. Army Engineer Waterways Experiment Station, Vicksburg, MS, Sept. 1983.
[40] Peters, J. F., Leavell, D. A., and Johnson, L. D., "Analysis of Strain-Softening Behavior of Soil," Final Research Report, U.S. Army Engineer Waterways Experiment Station, Vicksburg, MS, Oct. 1982.
[41] Strohm, W. E., Jr., "Preliminary Analysis of Results of Division Laboratory Tests on Standard Soil Samples," Miscellaneous Paper No. 3-813, U.S. Army Engineer Waterways Experiment Station, Vicksburg, MS, April 1966.
[42] U.S. Army Engineer Waterways Experiment Station, "The Unified Soil Classification System," Technical Memorandum 3-357, Vicksburg, MS, April 1960.
[43] American Society of Agronomy, Inc., *Methods of Soil Analysis, Part 2, Chemical and Microbiological Properties,* C. A. Black, Ed., Madison, WI, 1965, pp. 933–940.
[44] Richmond, R. D., "Laboratory Studies of Proposed Borrow Materials for Choke Canyon Dam, Nueces River Project, Texas," Geotechnical Branch Memorandum 77-42-42, U.S. Bureau of Reclamation, Denver, CO, 14 May 1978.
[45] Prizio, J. V., "Results of Laboratory Tests on Soil from Hyrum Dam—Hyrum Project, Utah," Geotechnical Branch Memorandum 79-5, U.S. Bureau of Reclamation, Denver, CO, 7 Feb. 1979.
[46] Casagrande, A. and Hirschfeld, R. C., "First Progress Report on Investigation of Stress—De-

formation and Strength Characteristics of Compacted Clays," Harvard Soil Mechanics Series No. 61, Cambridge, MA, May 1960.

[47] Casagrande, A. and Hirschfeld, R. C., "Second Progress Report on Investigation of Stress—Deformation and Strength Characteristics of Compacted Clays," Harvard Soil Mechanics Series No. 65, Cambridge, MA, April 1962.

Daizo Karube[1]

New Concept of Effective Stress in Unsaturated Soil and Its Proving Test

REFERENCE: Karube, D., "**New Concept of Effective Stress in Unsaturated Soil and Its Proving Test,**" *Advanced Triaxial Testing of Soil and Rock, ASTM STP 977,* Robert T. Donaghe, Ronald C. Chaney, and Marshall L. Silver, Eds., American Society for Testing and Materials, Philadelphia, 1988, pp. 539–552.

ABSTRACT: Triaxial compression tests, including anisotropic consolidation tests, were performed on compacted kaolin clay by an automatically controlled apparatus. Test results were analyzed in terms of suction and $(\sigma - u_a)$, where σ is total normal stress and u_a is pore air pressure, recognizing that when soil is saturated, u_a becomes equal to u_w, pore water pressure.

When suction is kept constant, the relationships among the observed shear strength, stress–strain, and stress–water content change can be formulated in equations similar to those of saturated soil, in which suction can be regarded as a factor contributing to soil constants. When both suction and all-around pressure are varied, the plastic volumetric strain can be expressed by an equation in which $(\sigma - u_a)$ is multiplied by a function of suction. Therefore suction can be regarded as a factor contributing to soil constants in this case too. These facts mean that the suction need not be regarded as one of the principal stress components such as $(\sigma - u_a)$ in the stress–strain equations of unsaturated soil.

KEY WORDS: unsaturated soil, kaolin, suction, effective stress, triaxial compression test, stress–strain relationship

Bishop and coworkers proved that the factors controlling the shear strength and strains of unsaturated soil mass can be divided into two terms, $(\sigma - u_a)$ and $(u_a - u_w)$, where σ, u_a, and u_w denote the total normal stress, the pore air pressure, and the pore water pressure, respectively [*1*]. Based on this, they proposed an equation defining the effective stress of unsaturated soil, in which suction, $(u_a - u_w)$, was converted into $(\sigma - u_a)$ using a coefficient, χ. However, the equation is not valid when a soil mass collapses by soaking. Then Coleman proposed more fundamental equation (that is, an incremental equation in which suction was given equal weight to externally applied stress)

$$d\epsilon_j = C_{1j}\, d(\sigma_3 - u_a) + C_{2j} d(\sigma_1 - \sigma_3) + C_{3j} d(u_a - u_w) \quad (1)$$

where ϵ_j is arbitrary strain component, σ_1 and σ_3 are the principal stresses on triaxial compression test specimen, and C_{1j}, C_{2j}, and C_{3j} are the coefficients which are to be composed by some stress components, property indexes, and water content, w, or degree of saturation, S_r [*2*]. Barden and coworkers performed oedometer tests on unsaturated clays to evaluate these coefficients except for C_{2j}, however, they did not analyze the factors contributing to the coefficients [*3*]. Fredlund advanced Coleman's equation to a elasticity form of constitutive

[1] Associate professor, Department of Civil Engineering, Kobe University, Rokkodai-cho, Nada-ku, Kobe, Japan 657.

equation in which suction was regarded as one of the independent stress variables

$$\epsilon_x = \frac{\sigma_x - u_a}{E} - \frac{\mu}{E}(\sigma_y + \sigma_z - 2u_a) + \frac{(u_a - u_w)}{H}, \text{ etc.} \tag{2}$$

where H is the elastic modulus with respect to suction, $(u_a - u_w)$ [4].

Suction is essentially one of the internal stress components, such as Coulomb's force, and in the stress–strain equations for saturated soil, the internal stress components do not appear although they must affect the mechanical properties of saturated soil. It is believed that they contribute to the coefficients of equations. Therefore the effect of suction on unsaturated soil could be expressed by manipulating the coefficients of equations instead of adding a term of suction as an independent variable. If this is done, the equations for unsaturated soil would be in a form similar to ones for saturated soil, then existing advanced concepts for saturated soil such as the constitutive laws based on elastoplastic theory could become applicable to unsaturated soil. The results of triaxial compression tests are analyzed based on this point of view.

The following stress and strain components are defined and used hereafter: $p = ⅓ (\sigma_1 + 2\sigma_3) - u_a$, $q = (\sigma_1 - \sigma_3)$ = the deviator stress; $S = u_a - u_w$ = the suction; v = the volume strain $\doteqdot \epsilon_1 + 2\epsilon_3$, $\epsilon = ⅔ (\epsilon_1 - \epsilon_3)$ = the shear strain, where ϵ_1 is axial strain and ϵ_3 is lateral strain of triaxial specimen.

Test Apparatus

A conventional triaxial test apparatus was modified, as shown in Fig. 1, to perform stress-controlled, air- and water-drained tests on a 35-mm-diameter specimen. Two devices were added to the basic apparatus, one is a micropore disk of high air entry value which is buried on top of the support pedestal and leads pore water to a burette. Another device is for measuring volume change of the specimen, for which a pair of distortion sensors were attached to the side of specimen crossing the diameter. The volume of the specimen was calculated by averaging a column approximation and an approximation for a revoluted parabola body in which both ends keep their initial diameter. The test apparatus works

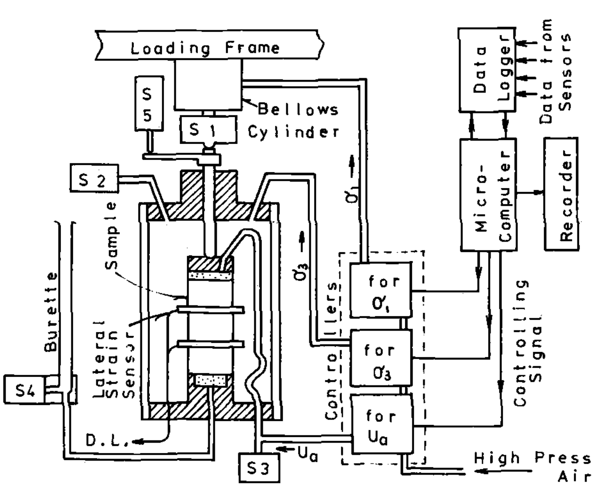

FIG. 1—*Layout of triaxial test apparatus for unsaturated soil.*

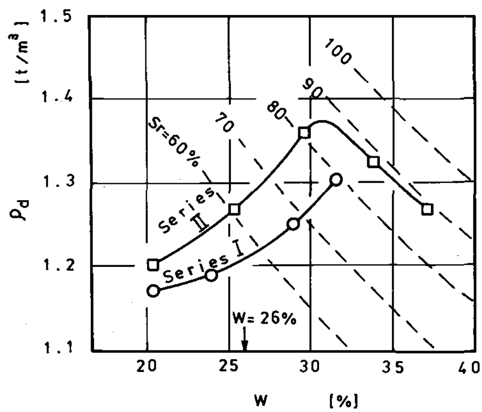

FIG. 2—*Compaction curves.*

automatically. Once the test program is keyed into the personal computer, the computer sends an electric pulse to electric-air pressure transducers at the proper time to control air pressure from an air compressor, and the specimen is loaded by these pressures. Applied air pressures and the force on the loading piston are detected by sensors, and the data are fed back to the computer by means of a data logger. The height of the water column in the burette is measured by a differential pressure sensor attached to the bottom of the burette.

Specimen Preparation and Tests Performed

Specimens were prepared from powdered kaolin clay having a specific gravity of soil grains of 2.70, maximum grain diameter of 0.04 mm, clay fraction (≦2 μm) of 22%, liquid limit of 37%, and plastic limit of 28%. After wetting by spray, the clay was put into a 35-mm-diameter mold in five layers and compacted by a California miniature compactor (15 times per layer with a force of 40 N). Figure 2 shows compaction curves of two series of triaxial test specimens. In series I, the optimum water content was not measured because clay lumps were formed at high water contents, so water content corresponding to 80% of saturation was assumed to be optimum. The water content of specimens for the triaxial tests was set at 26%, 6% dry of the assumed optimum. In series II, the spray was made finer and surfaces of soil layers in the mold were pressed lightly by a 34-mm-diameter plate before compaction. An optimum water content of 31% was obtained, and water content of the specimens was set again at 26%. Average values of void ratio, *e*, water content, *w*, and degree of saturation, S_r, of the triaxial specimens were 1.229, 26.1%, and 57.4% in series I and 1.114, 25.8%, and 62.7% in series II, respectively.

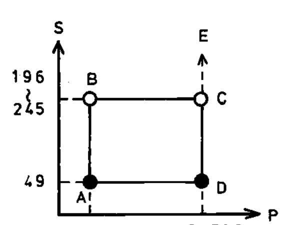

FIG. 3—*Symbols of stress points in the* p–S *plane, where* $p = (1/3)(\sigma_1 + 2\sigma_3) - u_a$ *and* $S = (u_a - u_w)$ *(unit: kPa).*

Tests were performed with air- and water-drained condition. Applied stresses were changed every 8 h. All specimens were held under an applied all-around pressure of 20 kPa in an undrained condition for a few hours, then the all-around pressure was raised to 69 kPa, pore air pressure of 49 kPa was applied, and the burette was opened simultaneously (that is, the stress state of the specimen became $[S, p, q] = [49, 20, \approx 0]$ kPa). This stress point is called "point A" hereafter. The average e, w, and S_r at the end of this stage were 1.219, 26.5%, and 58.8% in series I and 1.098, 26.2%, and 64.5% in series II, respectively. Strains and change in water content of specimen are defined hereafter based on the dimensions at that time.

Starting from point A, the following five tests were performed:

(a) Isotropic compression test, in which specimens were stressed along various stress paths on the p–S plane (Fig. 3)
(b) p-constant axial compression test, after consolidation along A → B or A → B → C on the p–S plane in Fig. 3, deviator stress was increased with constant suction and p. One specimen, however, was consolidated along A → D → C, which yielded different strains following axial compression from other specimens.
(c) σ_3-constant axial compression test, in which deviator stress was increased from A or B with constant suction and constant all-around pressure
(d) Anisotropic consolidation test, in which p was increased from A or B with constant suction and constant (q/q_f), where q_f is the failure stress at arbitrary p
(e) Stress-probe test, in which several specimens were stressed to the same stress point through the same stress path and then stressed for different directions in the S–p–q space. The test results are not described as "stress-probe test" in this paper, but as a datum for other tests if any part of the stress path is the same.

Test Results

Isotropic Compression Test

Figure 4*a* shows a looped stress path for two specimens starting from point A and going opposite to each other. Specimen II-1 traced the path twice. In Fig. 4*b*, void ratio changes on first cycle and second cycle are shown in thick and thin full lines, respectively. Specimen II-3 traced the path just once, and the void ratio change is indicated by the dotted line in Fig. 4*b*. At point C of the first cycle both specimens were loaded monotonically, but the specimen on which p was loaded first (dotted line) showed a larger compression, which coincides with the results by Barden and coworkers [3] and Karube [5]. Figure 4*c* shows the change in water content. Specimen II-3 (dotted line) showed little permanent change

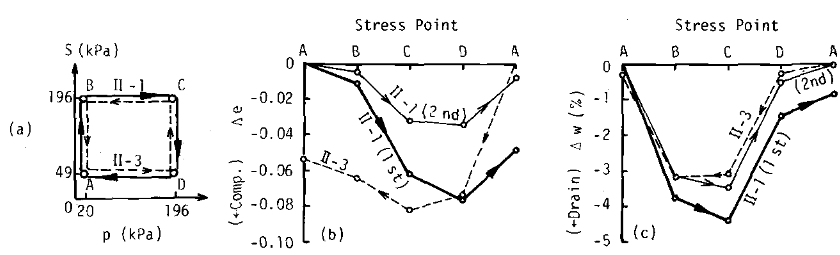

FIG. 4—*Strains along looped path:* (a) *stress paths,* (b) *void ratio change,* (c) *water content change.*

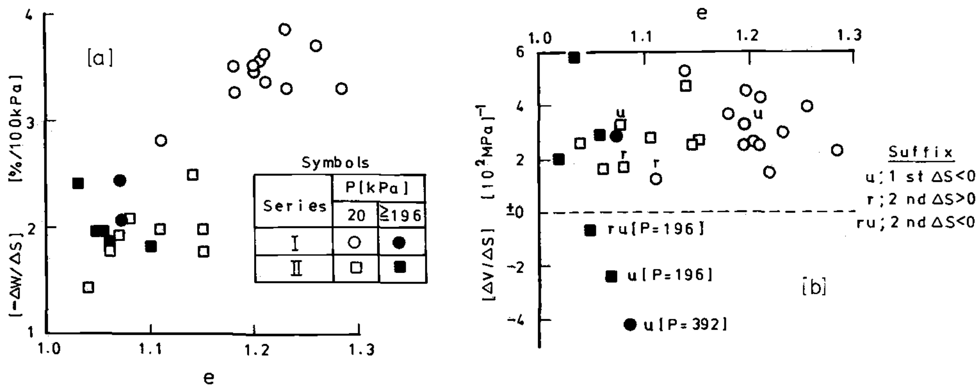

FIG. 5—*Influence of suction change on* (a) *water content and* (b) *void ratio.*

at the end of the cycle, caused by drainage during the unloading process C → B; specimen II-1 showed considerable permanent drainage on first cycle (thick full line), caused by permanent compression of the specimen as explained below.

Figure 5*a* shows the change in water content, and Fig. 5*b* shows the volume change with change in suction, both of which are plotted against their void ratios for all specimens. It seems that the ratio ($\Delta w/\Delta S$) is not affected by p, but increases with void ratio, e. On the other hand, Fig. 5*b* shows that void ratio has no effect on the ratio ($\Delta v/\Delta S$). In this figure suffix *u* means suction was reduced to 49 kPa, *r* means reloading of suction, and the number in parenthesis indicates current value of p in kPa. It is remarkable that solid symbols suffixed *u* or *ru* have negative value of ($\Delta v/\Delta S$), which means the volume of the specimen decreases when its suction is reduced under high all-around pressure. This phenomenon is known as collapse.

Coefficient of compressibility, m_v, is plotted against void ratio at p of 20 kPa in Fig. 6, where p was increased from 20 to 196 kPa (Fig. 6*a*) or to 392 kPa (Fig. 6*b*) with constant suction. It is obvious that a large m_v is obtained when p and suction are low and also that void ratio has little effect on m_v. Figure 7 shows some examples of drainage from increasing p under constant suction. It is seen that a specimen drains better under higher suction in spite of a lower water content and lower compressibility.

Failure Stresses

Failure stresses were measured on 17 specimens, but 2 of them had experienced too complex a stress history to be used for estimating failure criteria. Because of the stress-

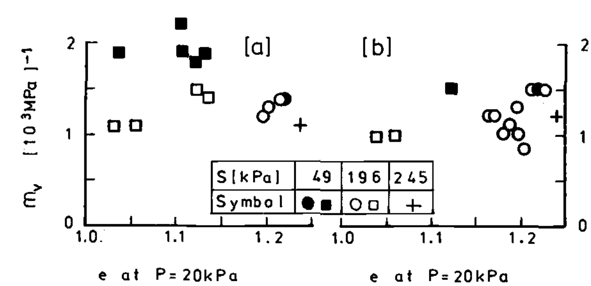

FIG. 6—m_v *versus void ratio* (a) *When* p *increases from 20 kPa to 196 kPa or* (b) *from 20 kPa to 392 kPa.*

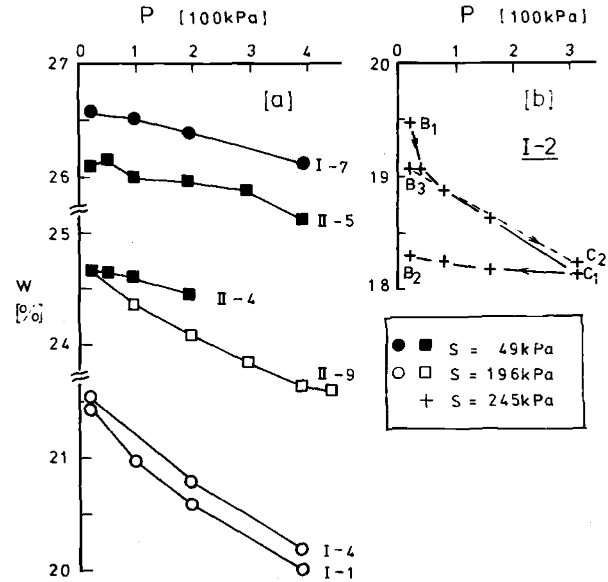

FIG. 7—*Water content change by* (a) *monotonic loading and* (b) *repeated loading along* $A \leftrightarrow B \leftrightarrow C$.

controlled nature of the tests, in which applied stresses were changed stepwise every 8 h, an exact condition of failure was seldom defined. Therefore, the failure stress was presumed equal to the applied stress when that stress was held out over 6 h, or, when failure occurred in less than 6 h, the failure stress was estimated by extrapolation of the preceding stress–strain plot. In Fig. 8*a*, failure lines through points of estimated failure stresses are drawn, but no failure line for a suction of 245 kPa is drawn because of insufficient data.

It seems that the failure line for the high suction has not only a larger cohesion but also a larger frictional angle. Because many of the specimens dilated at failure, an energy correction was made, as shown in Fig. 8*b*. Failure lines in this figure were drawn parallel to each other intentionally, but this seems allowable. Because the activity of tested kaolin clay is low ($A = 0.4$), cohesion can be assumed to be caused by suction in specimens [*6*]. Defining the absolute value of intercept of abscissa as $f(S)$, the equation of the failure line becomes

$$q_f' = M' [p + f(S)] = M' \left(\frac{1}{\alpha}\right) p \tag{3}$$

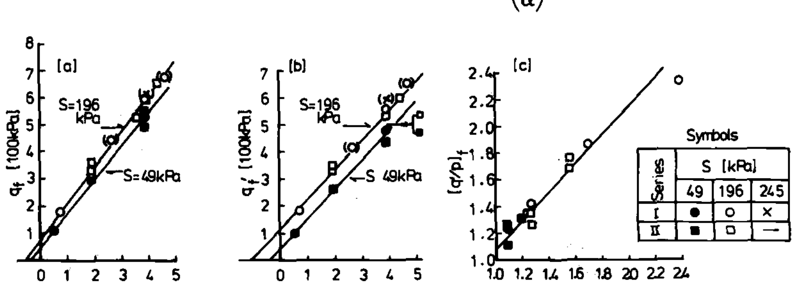

FIG. 8—*Failure stresses:* (a) *observed,* (b) *surface energy corrected,* (c) (q_f'/p) *versus* ($1/\alpha$).

where

$$q_f' = q_f - p\left(-\frac{\Delta v}{\Delta \epsilon}\right)_f \tag{4}$$

and q_f is deviator stress at failure, $(-\Delta v/\Delta\epsilon)_f$ is the dilatancy index, ϵ is shear strain defined by $\epsilon = \frac{2}{3}(\epsilon_1 - \epsilon_3)$, M' is the inclination of corrected failure lines, $f(S)$ is a function converting S into p at failure, which were evaluated from Fig. 8*b* as $M' = 1.08$, $f(S) = f(49\text{ kPa}) = 39$ kPa and $f(196\text{ kPa}) = 108$ kPa, and $(1/\alpha)$ is a parameter defined by

$$\left(\frac{1}{\alpha}\right) = \left[1 + \frac{f(S)}{p}\right] \tag{5}$$

If Eq 3 is correct, (q_f'/p) is directly proportional to $(1/\alpha)$ in spite of the values of suction and p. The straight line in Fig. 8*c* shows the theoretical relationship which has an inclination of 1.08 ($= M'$) and passes through the origin which is not shown on the figure, and the points are the experimental values. As the points distribute near the theoretical line, Eq 3 is confirmed. The strains during compression tests will be analyzed in the section entitled Case of Constant Suction.

Anisotropic Consolidation Test

Stress paths of anisotropic consolidation tests are shown with the failure lines in Fig. 9*a*. The lower half of Fig. 9*b* shows the resulting ratio (q/q_f), which was to be kept constant. The reason for fluctuation is that at the time of this test, failure lines had not been established. The upper half of the figure gives incremental strain ratio $(\Delta\epsilon/\Delta v)$. When a saturated clay is normally consolidated anisotropically, the ratio $(\Delta\epsilon/\Delta v)$ becomes a unique function of the stress ratio (q/q_f) regardless of the magnitude of p (see, for example, Ref 7). The behavior of unsaturated specimens is inconsistent with the behavior of saturated clay so that the ratio $(\Delta\epsilon/\Delta v)$ increases in spite of decreases of (q/q_f) in specimen 11 and specimen 12. In Fig. 9*c*, e–log p curves of anisotropic consolidation are shown with isotropic ones. Compression index, C_c, of the tests could be regarded as almost the same except for specimen 8.

Stress paths of anisotropic consolidation tests intersect those of p-constant compression tests in the S–p–q space. Figure 10*a* shows both stress paths with their intersections on the

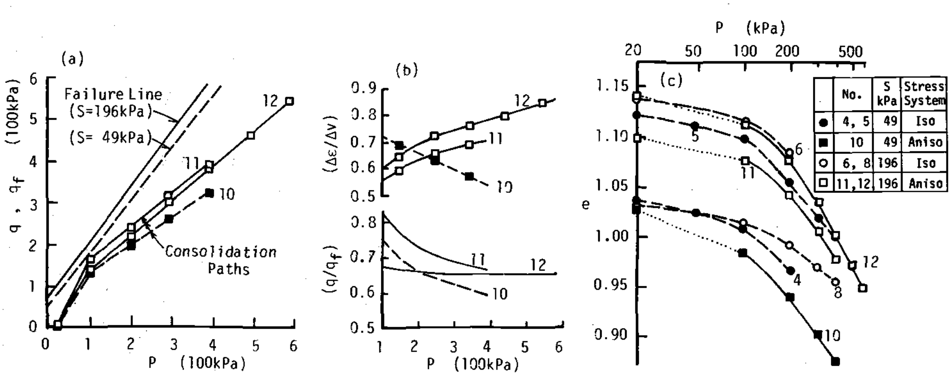

FIG. 9—*Results of anisotropic consolidation test:* (a) *loading paths,* (b) *strain rate corresponding to stress ratio, and* (c) e–*log* p *curves.*

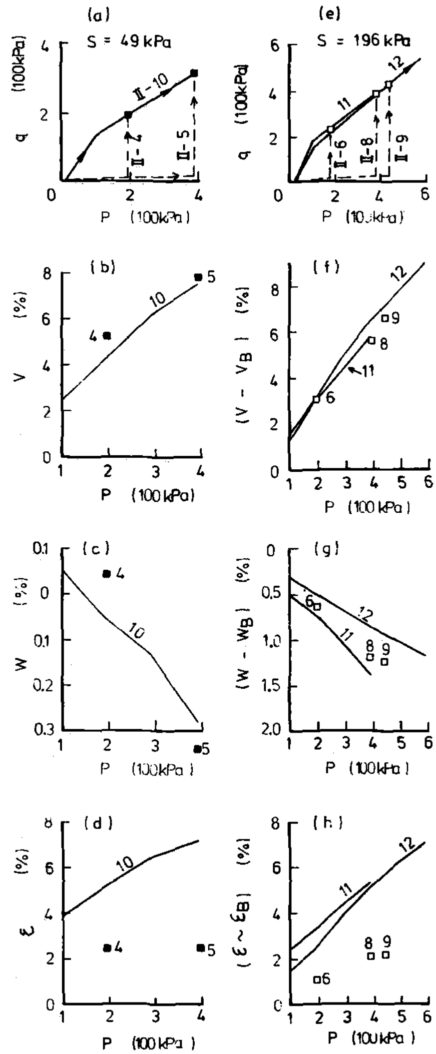

FIG. 10—*Examinations of stress path dependence of strains.*

plane of S = 49 kPa. Figure 10*e* shows similar paths on the plane of S = 196 kPa, however, p-constant paths of specimen II-6 and specimen II-8 intersect two anisotropic consolidation paths (II-11 and II-12, respectively). Therefore assumed intersection points were plotted midway between the two intersections. Broken lines in Fig. 10*b, c,* and *d* show volumetric strain, change in water content, and shear strain during anisotropic consolidation, respectively, and the points in the same figures represent the strains of p-constant tests at intersections on the plane of S = 49 kPa. Figure 10*f, g,* and *h* show the results of tests on S = 196 kPa, in which strains were measured from point B in Fig. 3, (p, S) = (20, 196) kPa. Volumetric strain and change in water content are not affected by stress path, and they are functions of current stress state (Fig. 10). On the other hand, the shear strain in anisotropic consolidation is larger than that of p-constant compression. These results coincide with the behavior of saturated soil.

Analysis and Discussion

Case of Constant Suction

It is obvious from the above test results that the failure condition and the relationship between stress and strain in terms of $(\sigma - u_a)$ are similar to those of saturated soil in terms of effective stress. It is also obvious that the change in water content does not depend on stress path. Therefore the only problem in this case is to evaluate the effect of suction on the soil parameters. Several soil parameters are analyzed as follows.

1. Shear strength parameter: Eliminate q_f' from Eqs 3 and 4, and the following equation is obtained:

$$q_f = \left[M'\left(\frac{1}{\alpha}\right) + \left(-\frac{\Delta v}{\Delta \epsilon}\right)_f\right] p \tag{6}$$

Because Eq 6 corresponds to Coulomb's shear strength equation with no cohesion component, the terms in brackets correspond to a frictional parameter, M, that is,

$$M = M'\left(\frac{1}{\alpha}\right) + \left(-\frac{\Delta v}{\Delta \epsilon}\right)_f \tag{7}$$

where α is defined by Eq 5. Generally, Eq 7 has no practical use without knowledge of the dilatancy factor, however this factor could be ignored if the specimen were shrinking or kept volume-constant at failure.

Bishop and coworkers introduced coefficient χ, which depends on the degree of saturation, in their effective stress equation and evaluated it by assuming the frictional angle, ϕ', is constant [*1*]. Blight obtained a failure line based on his advanced χ-theory [*8*]. Fredlund [*9*] proposed a simple failure criterion:

$$\tau = c' + (\sigma - u_a) \tan \phi' + (u_a - u_w) \tan \phi^b \tag{8}$$

where ϕ^b is the angle of shear strength increase with an increase in $(u_a - u_w)$.

Applying Bishop's χ to Eq 8, it becomes

$$\chi = \frac{\tan \phi^b}{\tan \phi'} \tag{9}$$

Therefore, if both ϕ' and ϕ^b are the material constants, χ should be uniquely defined regardless of the degree of saturation, and this is inconsistent with Bishop's experimental results [*1*]. The uniqueness of M defined by Eq 7 is that it contains a material constant, M', a characteristic factor, α, which is defined by Eq 5 and a dilatancy factor. Therefore it could be adapted to various conditions of material.

2. Coefficient of volume compressibility, m_v: In normally consolidated saturated clay, this can be defined as

$$m_v = \frac{0.434\ C_c}{1 + e}\frac{1}{\bar{p}}$$

where $\bar{p}$ is the average p when p is increased. This equation shows that the rigidity of soil skeleton increases in proportion to mean effective stress. If the rigidity of normally consolidated unsaturated soil is to vary as a function of $[p + f(S)]$, the following equation may be used in a similar analogy to the above equation:

$$m_v = \frac{0.434\, C_c}{1 + e} \frac{\alpha}{\bar{p}} \tag{10}$$

Figure 6 shows measured compressibility, m_v, which was obtained when p was increased from 20 to 196 kPa (Fig. 6*a*) or to 392 kPa (Fig. 6*b*). In these cases, the precompression pressure of specimens is 100 to 200 kPa as shown in Fig. 9*c*. Therefore, the compressibilities were measured covering both over- and normally consolidated ranges. Thus the applicability of Eq 10 is not guaranteed; however, it could be assumed that m_v would be in proportion to α if the value of p were fixed. The figures given in the upper and lower half of Table 1 correspond to Fig. 6*a* and Fig. 6*b*, respectively. The values of m_v and α in Table 1 are the averages of individual measured m_v and α, obtained by substituting the values of S and the average p into Eq 5. It is seen that the values of (m_v/α) are almost the same for the same $\bar{p}$, which justifies the above assumption.

3. Strains and the change in water content during p-constant compression process: In saturated soil, both shear and volumetric strain under p-constant compression are expressed by function of $\eta = (q/p)$ and overconsolidation ratio (OCR), irrespective of the current value of p. If $[p + f(S)]$ were assumed to take the place of p in unsaturated soil, strains would be defined as a function of

$$\frac{q}{[p + f(S)]} = \alpha\eta$$

The shear strain, ϵ, the volumetric strain, v, and the change in water content, Δw, during a p-constant test were plotted against the ratio $\alpha\eta$, but they showed significant scatter. This indicates that the value of α obtained from compressive strength is not valid for strains below failure condition. After trial and error, the following functions were found to minimize scatter (Fig. 11):

$$(\epsilon - \epsilon_c) = \alpha^2 G_1(\alpha\eta) \tag{11}$$

$$(v - v_c) = \alpha^2 G_2(\alpha\eta) \tag{12}$$

$$\Delta w = \alpha^2 H(S)\, G_3(\alpha\eta) \tag{13}$$

where ϵ_c and v_c are the strains at the start of axial compression, $H(S)$ is a function of suction

TABLE 1—*Correspondence of measured* m_v *and theoretical* α.[a]

p, kPa	S, kPa	m_v	α	$\frac{m_v}{\alpha}$
20 ⟶ 196	49	1.9	0.73	2.6
	196	1.3	0.50	2.6
20 ⟶ 392	49	1.5	0.84	1.8
	196	1.1	0.64	1.7

[a] $p = 1/3\,(\sigma_1 + 2\sigma_3) - u_a$; S = the suction; m_v = coefficient of compressibility; and α is defined by Eq 5.

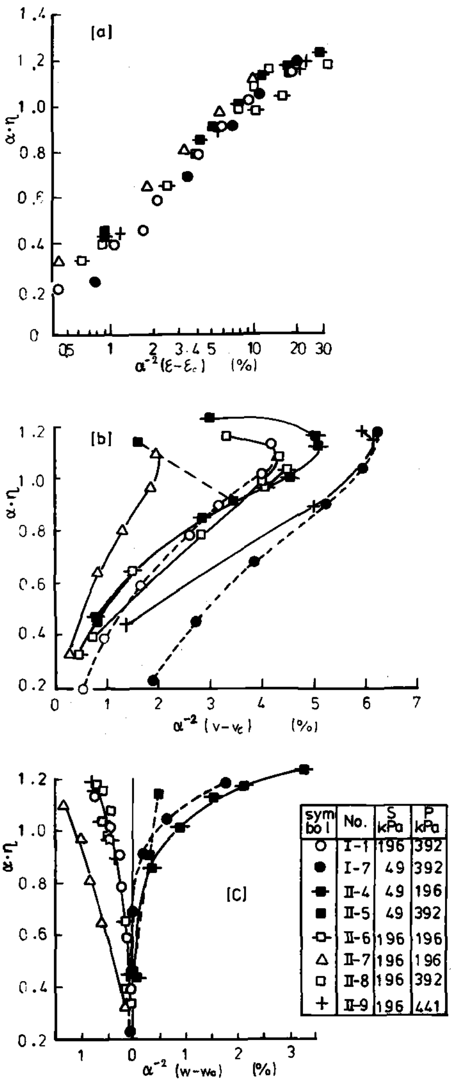

FIG. 11—*Unified stress–strain relationships during* p-*constant compression:* (a) *shear strain,* (b) *volumetric strain, and* (c) *water content change.*

which has positive or negative value when suction is low or high, respectively, and G_1, G_2, and G_3 are functions of $\alpha\eta$.

Specimen II-7 in Fig. 11 shows small strains and large drain. The specimen was consolidated along the path of A → D → C in Fig. 3, and therefore its void ratio was already small and the degree of saturation was high, which may explain its peculiar behavior.

Case of Variable Suction

In this paper the analysis of strains and water content change induced by varying suction is limited to isotropic stress condition.

Volumetric Strain—If unsaturated soil is an elastoplastic material, a yield locus must be defined on the p–S plane. By examining the void ratio changes along a looped stress path in Fig. 4*b*, the following equations can be proposed as yield functions (schematic views are shown in Fig. 12*a*):

$$\text{when } p_1 \leqq f(S_1), \quad p = f(S) \quad \text{or} \quad \left(\frac{1}{\alpha}\right) = 2 \tag{14}$$

$$\text{when } p_1 > f(S_1), \quad p = f(S) + p_1 - f(S_1) \tag{15}$$

$$\text{or} \quad \frac{p}{p_1} = \frac{(1/\alpha_1) - 2}{(1/\alpha) - 2} \tag{15a}$$

where (p_1,S_1) is a current stress point on loading path, and $(1/\alpha_1) = 1 + f(S_1)/p_1$.

At point D in Fig. 4*b*, specimen II-3 and the first cycle of specimen II-1 show almost the same void ratio change. If plastic strain function, F, is defined on the p–S plane, plastic strain increment, dv^p, would be given by

$$dv^p = \frac{\partial F}{\partial p}dp + \frac{\partial F}{\partial S}dS \tag{16}$$

From Eqs 10 and 5,

$$\frac{\partial F}{\partial p} = m_v - m_v' = \frac{\lambda - \kappa}{1 + e}\frac{1}{p + f(S)}$$

where

$\lambda = 0.434\ C_c$

$\kappa = 0.434\ C_s$

m_v' = the coefficient of rebound

Therefore

$$F = \frac{\lambda - \kappa}{1 + e}\ln\left[p + f(S)\right] - Q(S) \tag{17}$$

where $Q(S)$ is an arbitrary function of S.

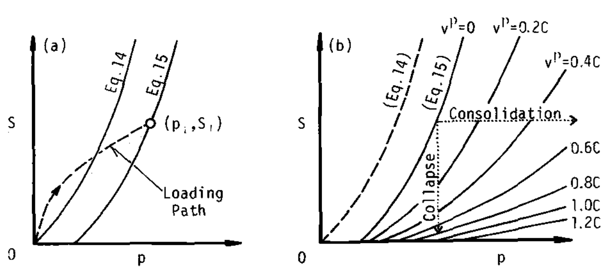

FIG. 12—*Elastoplastic behavior of unsaturated soil:* (a) *yield loci and* (b) *contours of plastic strain.*

Because the plastic strain must be zero in Eq 15, $Q(S)$ becomes

$$Q(S) = \frac{\lambda - \kappa}{1 + e} \ln [2f(S) + p_1 - f(S_1)] \tag{18}$$

Substituting Eq 18 into Eq 17, plastic strain function is obtained as

$$F = \frac{\lambda - \kappa}{1 + e} \ln \left[\frac{p + f(S)}{2f(S) + p_1 - f(S_1)}\right] \tag{19}$$

or

$$F = \frac{\lambda - \kappa}{1 + e} \ln \left[\frac{1}{2f(S) + p_1 + f(S_1)} \frac{1}{\alpha} p\right] \tag{19a}$$

Equation 19*a* means that the plastic strain function for unsaturated soil becomes a logarithmic function of p similar to the function for saturated soil, and suction, S, can be regarded as a factor contributing to the coefficient of p. Figure 12*b* shows contours of plastic strain calculated using Eq 19, in which $C = (\lambda - \kappa)/(1 + e)$. Therefore the volumetric strain increment in elastoplastic zone is given by

$$dv = dv^e + dv^p = \frac{\lambda}{1 + e} \cdot \frac{\alpha}{p} dp + \left[K - \frac{\partial F}{\partial f(S)} \frac{df(S)}{dS}\right] dS \tag{20}$$

where $K = \Delta v^e / \Delta S$.

Change in Water Content—The amount of drainage caused by p is affected by the magnitude of suction, as shown in Fig. 7, but the amount of drainage caused by suction seems independent of magnitude of p and dependent on void ratio, as shown in Fig. 5*a*. Therefore, the equation for the change of water content will become

$$\Delta(\Delta w) = R(S)\, \Delta p + T(e)\, \Delta S \tag{21}$$

where $R(S)$ and $T(e)$ are the functions of suction and void ratio, respectively, which increase as variables S and e increase. Suction must be treated as an independent stress component here.

Conclusions

Compacted unsaturated kaolin clay was treated in a triaxial compression apparatus.

When the suction is kept constant, the shear and the volumetric strain of unsaturated soil are expressed by equations similar to those for saturated soil, where effective stress is defined by $(\sigma - u_a)$ and suction is regarded as a factor contributing to soil constants. Water content changes are defined by characteristic equations whereby whether a specimen drains or sucks depends on the magnitude of the suction. However, the suction may be treated as a factor of soil constants. In this case, suction acts on soil constants with a function of α defined by Eq 5. Because pore air pressure is equal to pore water pressure when suction is absent, a conventional concept of effective stress for saturated soil is included in the more general concept above. Measured failure stresses indicate that the suction affects not only the cohesion but also the frictional parameter if dilatational energy is not corrected.

Volumetric strain and change in water content caused by the changes in both suction and p were analyzed on the p–S plane (isotropic stress condition). In the equation of plastic volumetric strain, suction can be regarded as a factor contributing to the coefficient of $(\sigma - u_a)$. On the other hand, in the equations of elastic volumetric strain and change in water content, suction acts as a independent variable.

Acknowledgments

Financial support for this experimental work was supplied by the Japanese Ministry of Education. The author wishes to express his thanks to Professor K. Tanimoto and Dr. Y. Tanaka for their encouragement and assistance throughout the work.

References

[*1*] Bishop, A. W. et al., "Factors Controlling the Strength of Partly Saturated Cohesive Soils," in *Proceedings*, Conference on Shear Strength of Cohesive Soils, American Society of Civil Engineers, Colorado, June 1960, pp. 503–532.
[*2*] Coleman, D. J., *Geotechnique*, Vol. 12, No. 4, 1962, pp. 348–350.
[*3*] Barden, L. et al., *Journal of the Soil Mechanics and Foundation Division, American Society of Civil Engineers*, Vol. 95, No. SM1, 1969, pp. 33–51.
[*4*] Fredlund, D. G., "Soil Mechanics Principles that Embrace Unsaturated Soils," in *Proceedings*, Eleventh International Conference on Soil Mechanics and Foundation Engineering, Vol. 2, San Francisco, August 1985, pp. 465–472.
[*5*] Karube, D., "Effect of Suction on Soil Behaviour," in *Proceedings*, Seventh Asian Regional Conference on Soil Mechanics and Foundation Engineering, Vol. 1, Haifa, August 1983, pp. 30–35.
[*6*] Gibson, R. E., "Experimental Determinaton of True Cohesion and True Angle of Internal Friction in Clays," in *Proceedings*, Third International Conference on Soil Mechanics and Foundation Engineering, Vol. 1, Zurich, August 1953, pp. 126–130.
[*7*] Roscoe, K. H. et al., *Geotechnique*, Vol. 13, No. 1, 1963, pp. 12–38.
[*8*] Blight, G. E., *Journal of the Soil Mechanics and Foundation Division, American Society of Civil Engineers*, Vol. 93, No. SM2, 1967, pp. 125–148.
[*9*] Fredlund, D. G. et al., *Canadian Geotechnical Journal*, Vol. 15, No. 3, 1978, pp. 313–321.

Pinnaduwa H. S. W. Kulatilake[1]

Probabilistic Characterization of Shear Strength Parameters Using Triaxial Test Data

REFERENCE: Kulatilake, P. H. S. W., "**Probabilistic Characterization of Shear Strength Parameters Using Triaxial Test Data,**" *Advanced Triaxial Testing of Soil and Rock, ASTM STP 977,* Robert T. Donaghe, Ronald C. Chaney, and Marshall L. Silver, Eds., American Society for Testing and Materials, Philadelphia, 1988, pp. 553–566.

ABSTRACT: The Mohr-Coulomb model is used as the strength criterion in this study to model shear strength. Thus, the procedure is applicable only for the soils and rocks whose deterministic strength follows the Mohr-Coulomb criterion. Available methods to obtain point estimates for the strength parameters from triaxial test data are discussed. Inaccuracy of the traditional method is pointed out. A method which requires weighted regression analysis and propagation of error technique is developed to obtain point estimates for the strength parameters. Chi-square tests for bivariate beta and bivariate normal distributions are performed on point estimates of strength parameters to check the applicability of the distributions in representing the distribution of the strength parameters. Both probability distributions seem to be useful in representing statistical distribution of strength parameters.

KEY WORDS: triaxial test, shear strength, probability and statistics, regression analysis, goodness-of-fit test, bivariate distributions

Shear failure of some soils and soft rocks in a triaxial test may be modeled by the Mohr-Coulomb strength criterion as given in Eq 1,

$$\bar{\sigma}_1 = A + B\bar{\sigma}_3 \tag{1a}$$

$$A = 2c\tan(\pi/4 + \phi/2) \tag{1b}$$

$$B = \tan^2(\pi/4 + \phi/2) \tag{1c}$$

where $\bar{\sigma}_1$ and $\bar{\sigma}_3$ are, respectively, the effective major principal stress and effective minor principal stress on a triaxial specimen at failure, c is the cohesion, and ϕ is the angle of internal friction. Earlier, it was believed that the strength parameters, (A,B) and (c,ϕ), were invariant properties for a given geologic material. Soon, however, researchers realized that similar shear strength tests on nearly identical samples of geologic material may result in a wide range of values for c and ϕ [*1,2*]. It is possible to include this variability by identifying the strength parameters as random variables and developing probabilistic models for their description. Probabilistic modeling of strength parameters is important in perform-

[1] Assistant professor, Department of Mining and Geological Engineering, University of Arizona, Tucson, AZ 85721.

ing reliability analysis of geotechnical structures. In this paper, the literature available on the topic is reviewed and procedures are suggested to improve the techniques in probabilistic description of shear strength parameters. An example is given to illustrate the application of the suggested procedures.

Literature Review

In probabilistic modeling of c and t, where t is tan ϕ, the task is to express the joint probability, $P(c,t)$, from the results of n pairs of values of c and t. First, it is necessary to discuss the methods of obtaining point estimates for c and t from triaxial test data. To obtain (c,t) sets, either the standard triaxial test or the multistage triaxial test could be performed. If heterogeneity of the geologic deposit is significant, the multistage triaxial test is recommended to reduce the variability. There are three methods to obtain point estimates for (c,t) using the Mohr-Coulomb strength criterion.

In the traditional method, simple linear regression anaylsis is performed between $(\bar{\sigma}_1 - \bar{\sigma}_3)/2$ and $(\bar{\sigma}_1 + \bar{\sigma}_3)/2$ to obtain point estimates for c and t. Theoretically, this method is not accurate because $(\bar{\sigma}_1 - \bar{\sigma}_3)/2$ and $(\bar{\sigma}_1 + \bar{\sigma}_3)/2$, respectively, are not the shear stress and normal stress on the failure plane.

Lisle and Strom have made a refinement in obtaining point estimates for c and t by implementing the criterion that the sum of squares of the radial distances from the Mohr circles perpendicular to the Mohr-Coulomb line be minimal [*3*]. However, for this method, expressions are not available to check the adequacy of the regression model. Also, equations are not available to calculate variances of estimated c and t.

In the third method, simple regression analysis is performed between $\bar{\sigma}_1$ and $\bar{\sigma}_3$ to estimate the regression coefficients A and B (see Eq 1a). Then, Eq 1b and Eq 1c can be used to estimate c and t. Franklin has used this method to estimate c and t for intact rock [*4*]. This method is theoretically correct and also simple. In this paper, the third method is used to obtain point estimates for c and t. Also, expressions are developed to calculate variances for estimates of c and t.

All the aforementioned regression analyses have assumed the variance of the regression line as a constant. However, strength data may show a variance that is not constant with the independent variable. Nonconstant variance can be included through a weighted regression analysis. A procedure to perform weighted regression is given in this paper.

Sets of point estimates of c and t obtained through any of the aforementioned procedures usually show scatter and negative correlation [*2*]. However, in estimating the joint probability of c and t, quite often c and t have been assumed to be independent. This assumption overestimates the variability of the shear strength. Therefore, to model strength parameters realistically, it is necessary to quantify the uncertainty, taking into account the correlation between c and t. Such modeling can be achieved by fitting bivariate probability distributions to c and t. Grivas and Williams have suggested a procedure to fit a bivariate beta distribution for (c,t) data [*5*]. In addition to fitting, it is important to look into how good the fit is. This can be done by goodness-of-fit tests. In this paper chi-square goodness-of-fit procedures are given for bivariate beta and bivariate normal distributions to test the applicability of these distributions to model the variability of (c,t), estimated from triaxial test data.

Suggested Procedure

Outline

Variability of a soil can be studied at different levels. It can be performed at low sampling ratios (that is, number of samples per cubic metre such as 75×10^{-6} or at high sampling ratios such as 500 [*2*]. If several sets of $\bar{\sigma}_1$ and $\bar{\sigma}_3$ are available and each set consists of at least four different $\bar{\sigma}_3$ values, then the suggested method is applicable. Data that belong to one set may come from just one specimen in the case of a multistage triaxial test or may come from almost identical specimens in the case of a standard triaxial test.

First, for each set, unweighted simple linear regression can be performed between $\bar{\sigma}_1$ and $\bar{\sigma}_3$ to obtain $\hat{A}$ and $\hat{B}$, which are estimates for A and B, respectively (see Eq 1a). Next, the residuals resulting from each regression analysis should be examined to check whether the residuals have a constant variance or not. If the variance shows a trend with $\bar{\sigma}_3$, then it is necessary to perform a weighted regression analysis between $\bar{\sigma}_1$ and $\bar{\sigma}_3$ to obtain $\hat{A}$ and $\hat{B}$; otherwise, the unweighted simple linear regression is appropriate to obtain $\hat{A}$ and $\hat{B}$. The computer program P5R of BMDP [*6*] can be used to perform both the unweighted and the weighted regression analyses mentioned above. The next section gives details related to carrying out the weighted regression analysis. These regression analyses also provide standard error of $\hat{A}$, S_A, standard error of $\hat{B}$, S_B, and covariance of $\hat{A}$ and $\hat{B}$, COV($\hat{A},\hat{B}$).

The corresponding estimates of (c,t), $(\hat{c},\hat{t})$, and variances of $(\hat{c},\hat{t})$, $(S_{\hat{c}}^2,S_{\hat{t}}^2)$, can now be found from $\hat{A}$, $\hat{B}$, $S_{\hat{A}}$, $S_{\hat{B}}$, and COV($\hat{A},\hat{B}$) using the "propagation of errors" approach [*7*]. The details of this approach are given in the section entitled Determination of $(\hat{c},\hat{t})$ and $(S_{\hat{c}}^2,S_{\hat{t}}^2)$.

Values of $(\hat{c},\hat{t})$ obtained for different sets of $\bar{\sigma}_1$ versus $\bar{\sigma}_3$ can be subjected to chi-square tests for bivariate beta and bivariate normal distributions to check the applicability of the distributions to describe the joint probability distribution of the strength parameters. This is dealt with in the sections entitled Chi-Square Goodness-of-Fit Test for Bivariate Beta Distribution and Chi-Square Goodness-of-Fit Test for Bivariate Normal Distribution.

Weighted Regression Analysis

For the theory of weighted regression analysis, the reader is referred to Ref *8*. To perform weighted regression analysis, it is necessary to find weight factors for each data set. The weighting function, which provides weight factors for each data set, is inversely proportional to the variance function of the residuals [*8*]. To obtain the relation between the variance of the residuals and $\bar{\sigma}_3$, it is possible to perform polynomial regression analysis between the square of the residuals and $\bar{\sigma}_3$ for different orders using P5R. The best polynomial to represent the variance of the residuals could be used to obtain the weighting function.

In general, the variance function for the residuals can be given as

$$S_i^2 = a_0 + a_1 x_i + a_2 x_i^2 + \cdots + a_n x_i^n \tag{2}$$

where x_i is the ith data value of the independent variable $\bar{\sigma}_3$, S_i^2 is the variance function value corresponding to ith data, and $a_0, \ldots, a_n$ are the coefficients of the best-fit polynomial. A weighting function corresponding to Eq 2 can be given as

$$W_i = \frac{1}{a_0 + a_1 x_i + a_2 x_i^2 + \cdots + a_n x_i^n} \tag{3}$$

Weight factors calculated according to Eq 3 can be used with original strength data to perform the weighted regression analysis [*6*].

Determination of $(\hat{c},\hat{t})$ *and* $(S_{\hat{c}}^2,S_{\hat{t}}^2)$

If $z = f(U,V)$ is some function of two random variables U, V, of means U_m, V_m, variances S_U^2, S_V^2, and covariance COV(U,V), then the first-order approximate mean and variance of z through the propagation of error approach [7] can be given by Eq 4 as follows:

$$E(z) \simeq f(U_m, V_m) \tag{4a}$$

$$\mathrm{Var}(z) \simeq S_U^2 \left[\frac{\partial f}{\partial U}\right]^2 + S_V^2 \left[\frac{\partial f}{\partial V}\right]^2 + 2\,\mathrm{COV}(U,V) \left[\frac{\partial f}{\partial U}\right]\left[\frac{\partial f}{\partial V}\right] \tag{4b}$$

Using Eq 1b and Eq 1c, it is possible to express c as a function of A and B as

$$c = A/(2B^{1/2}) \tag{5}$$

Application of Eq 4a and Eq 4b to Eq 5 gives

$$\hat{c} = \frac{\hat{A}}{2\hat{B}^{1/2}} \tag{6a}$$

and

$$S_{\hat{c}}^2 = \left[\frac{\hat{A}}{2\hat{B}^{1/2}}\right]^2 \left[\frac{S_{\hat{A}}^2}{\hat{A}^2} + \frac{S_{\hat{B}}^2}{4\hat{B}^2} - \frac{\mathrm{COV}(\hat{A},\hat{B})}{\hat{A}\hat{B}}\right] \tag{6b}$$

From Eq 1c and $t = \tan \phi$, t can be expressed as a function of B as

$$t = \tan\{2 \tan^{-1}(B^{1/2}) - \pi/2\} \tag{7}$$

Application of Eq 4a and Eq 4b to Eq 7 produces

$$\hat{t} = \tan\{2 \tan^{-1}(\hat{B}^{1/2}) - \pi/2\} \tag{8a}$$

and

$$S_{\hat{t}}^2 = S_{\hat{B}}^2 \frac{(1 + \hat{t}^2)^2}{\hat{B}(1 + \hat{B})^2} \tag{8b}$$

Chi-square Goodness-of-Fit Test for Bivariate Beta Distribution

If random variables X,Y are distributed according to a bivariate beta distribution, the joint density function of X,Y is given by [9]

$$f(x,y) = \frac{\Gamma(p_1 + p_2 + p_3)}{\Gamma(p_1)\Gamma(p_2)\Gamma(p_3)} x^{p_1-1} y^{p_2-1} (1 - x - y)^{p_3-1} \tag{9}$$

where $p_1, p_2, p_3 > 0$ and x, y take values within the whole triangular domain shown in Fig. 1. Notation Γ in Eq 9 is for the gamma function.

The chi-square statistic, $(\chi^2)_d$, for bivariate beta distribution can be computed by

$$(\chi^2)_d = N \sum_{i=1}^{I} \sum_{j=1}^{J_i} \frac{[(f_o)_{ij} - (f_e)_{ij}]^2}{(f_e)_{ij}} \tag{10}$$

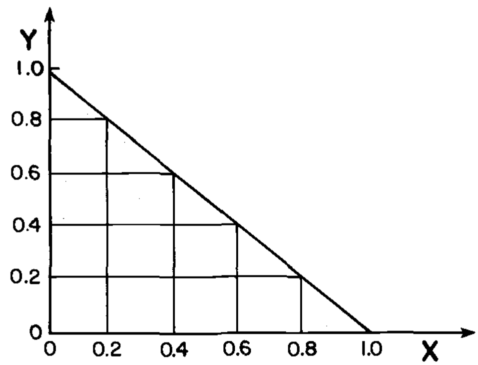

FIG. 1—*Discretized* X-Y *domain for bivariate beta distribution.*

where

$(f_o)_{ij}$ = observed relative frequency for ith interval of X and jth interval of Y
$(f_e)_{ij}$ = expected or theoretical relative frequency for ith interval of X and jth interval of Y
I = total number of intervals of X
J_i = total number of intervals of Y for ith X interval (see Fig. 1)
N = total number of data sets of (X,Y)

The (X,Y) domain can be discretized as shown in Fig. 1 and for each cell, $(f_o)_{ij}$ and $(f_e)_{ij}$ can be determined. To compute $(f_o)_{ij}$, it is necessary to transform $(\hat{c},\hat{t})$ *to* X, Y. If (Q,R) is picked to represent $(\hat{c},\hat{t})$, the required transformation can be given by

$$X = D\frac{Q - Q_{\min}}{Q_{\max} - Q_{\min}} \tag{11a}$$

$$Y = D\frac{R - R_{\min}}{R_{\max} - R_{\min}} \tag{11b}$$

where D is a constant and subscripts max and min represent the chosen maximum and minimum values, respectively. The possible values for D should satisfy $x \geqslant 0$, $y \geqslant 0$, and

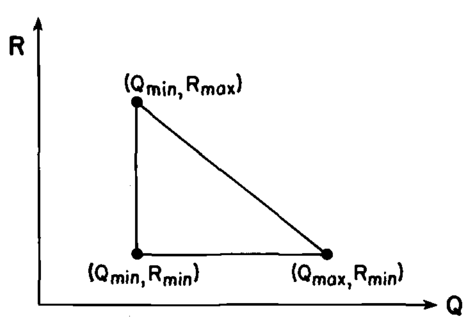

FIG. 2—Q-R *domain for bivariate beta distribution fitting.*

$x + y \leq 1$. This allows values between zero and one for D. It can be shown that the straight line joining (Q_{max}, R_{min}) and (Q_{min}, R_{max}) gets transformed into $X + Y = D$ under the transformation given by Eq 11. Thus, if one is interested in filling the whole domain available for X and Y, then the appropriate value for D is one. Figures 1 and 2 show the transformation in graphic form for $D = 1$. However, it seems other D values between zero and one are also theoretically correct for this transformation. Therefore, it may be worthwhile to pick different values for D to study the influence of D on the results of goodness-of-fit test. Also, it should be noted that (Q_{max}, R_{min}) and (Q_{min}, R_{max}) are not unique values for the transformation (see the section entitled Example). Equation 9 can be numerically integrated over each cell to obtain each $(f_e)_{ij}$. To perform this, it is necessary to know the values of p_1, p_2, and p_3. Parameters p_1, p_2, and p_3 can be estimated through [9]

$$\hat{p}_1 = -\frac{\overline{X}^2\overline{Y}}{r_{X,Y}S_XS_Y} - \overline{X} \tag{12a}$$

$$\hat{p}_2 = \hat{p}_1\frac{\overline{Y}}{\overline{X}} \tag{12b}$$

$$\hat{p}_3 = \frac{\hat{p}_1}{\overline{X}} - \hat{p}_1 - \hat{p}_2 \tag{12c}$$

where $\overline{X}, \overline{Y}, S_X, S_Y$, and $r_{X,Y}$ are, respectively, sample mean of X, sample mean of Y, sample standard deviation of X, sample standard deviation of Y, and sample coefficient of correlation of X and Y. Parameters of X and Y variables are related to parameters of Q and R through

$$\overline{X} = D\frac{\overline{Q} - Q_{min}}{Q_{max} - Q_{min}} \tag{13a}$$

$$\overline{Y} = D\frac{\overline{R} - R_{min}}{R_{max} - R_{min}} \tag{13b}$$

$$S_X = D\frac{S_Q}{Q_{max} - Q_{min}} \tag{13c}$$

$$S_Y = D\frac{S_R}{R_{max} - R_{min}} \tag{13d}$$

$$r_{X,Y} = r_{Q,R} \tag{13e}$$

where $\overline{Q}$, $\overline{R}$, S_Q, S_R, and $r_{Q,R}$ are, respectively, sample mean of Q, sample mean of R, sample standard deviation of Q, sample standard deviation of R, and sample coefficient of correlation of Q and R. To evaluate the theoretical chi-square value, $(\chi^2)_t$, the number of degrees of freedom for this distribution is

$$\left(\sum_{i=I}^{I} J_i\right) - 4$$

$(\chi^2)_t$ can be obtained from the chi-square table. The maximum significance level, P, up to which the tested distribution is considered to be a suitable representation of the data is known as the "P level" of the test [7]. This is the significance level at which $(\chi^2)_t$ equals $(\chi^2)_d$.

Chi-square Goodness-of-Fit Test for Bivariate Normal Distribution

Let (Q,R) represent $(\hat{c},\hat{t})$. $(\chi^2)_d$ can be computed from Eq 10 with J_i replaced by J. For this case, $(f_o)_{ij}$ and $(f_e)_{ij}$ are, respectively, observed and expected relative frequency for ith Q interval and jth R interval; I, J, and N are, respectively, total number of Q intervals, total number of R intervals, and total number of data sets of (Q,R).

To compute $(f_e)_{ij}$ and $(f_o)_{ij}$, it is necessary to estimate the means, (μ_Q,μ_R), the variances, $(\sigma_Q{}^2,\sigma_R{}^2)$, and the correlation coefficient, ρ, of the distribution using the strength parameter data. The required expressions to estimate parameters of the distribution are given in Ref *10*. Values of $\hat{\mu}_Q \pm 3\hat{\sigma}_Q$ and $\hat{\mu}_R \pm 3\hat{\sigma}_R$ can be used to cover the entire domain for bivariate normal distribution. Then suitable values can be selected for I and J to compute $(f_e)_{ij}$ and $(f_o)_{ij}$ for different cells. Obtained values for $\mu_Q,\mu_R,\sigma_Q,\sigma_R$, and ρ define the density function uniquely. This density function can be integrated over the cell domain of interest to compute each $(f_e)_{ij}$.

For details related to performing the χ^2 test, the reader is referred to Ref *10*. To evaluate $(\chi^2)_t$, the number of degrees of freedom for this distribution is $(I \times J - 6)$. The P value is computed as in the case of bivariate beta distribution fitting.

Example

Data

Data for the example, taken from Ref *11*, are for a highly weathered graywacke from the Wellington area in New Zealand. Reference *11* presents standard triaxial test data from five sites located within an area of approximately 0.25 km^2. From the point of view of visual classification, the materials at all the sites have been found to be similar. However, void ratios ranging between 0.25 and 0.8 have been observed for this material. A triple tube coring barrel has been used to recover continuous cores 100 mm in diameter. Consolidated undrained triaxial tests have been performed on 100-mm-diameter specimens with pore water pressure measurements.

For the example given in this paper, data from four sites for void ratios ranging between 0.5 and 0.8 were selected. To perform regression analysis between $\bar{\sigma}_1$ and $\bar{\sigma}_3$, data were grouped into eight sets as shown in Table 1. For the fifth site, there were not enough data under each void ratio range to perform regression analysis between $\bar{\sigma}_1$ and $\bar{\sigma}_3$. Data from Bolton Street bridge and Aurora Terrace bridge were considered together as in Ref *11*.

Regression Between $\bar{\sigma}_1$ and $\bar{\sigma}_3$

Effective principal stress data $(\bar{\sigma}_1,\bar{\sigma}_3)$ for each of the eight sets were subjected to unweighted first degree polynomial regression using program P5R of BMDP [*6*]. The plot between $\bar{\sigma}_1$ and $\bar{\sigma}_3$ for set 7 for both predicted and observed values is shown in Fig. 3*a*. It depicts that the Mohr-Coulomb criterion is suitable to model the trend of the strength data. This type of behavior was observed for all eight sets. The plot between the square of the residuals and $\bar{\sigma}_3$ for set 7 is shown in Figure 3*b*. This figure shows that the variance of the

TABLE 1—*Grouping of shear strength data.*

Data Set Number	Name of the Site	Void Ratio Range	Number of Specimens
1	Public Trust Office	0.5–0.6	17
2	Public Trust Office	0.6–0.7	24
3	Public Trust Office	0.7–0.8	21
4	Bolton Street and Aurora Terrace bridges	0.5–0.6	10
5	Bolton Street and Aurora Terrace bridges	0.6–0.7	12
6	Southern Portal Terrace Tunnel	0.5–0.6	6
7	Southern Portal Terrace Tunnel	0.6–0.7	9
8	Southern Portal Terrace Tunnel	0.7–0.8	6

residuals is nonconstant with $\overline{\sigma}_3$. This type of behavior was observed also for sets 1 and 5. Therefore, for each of these three sets, regression analysis was performed between the square of the residuals and $\overline{\sigma}_3$ up to the sixth degree polynomial using P5R to obtain a fit for the variance of the residuals. Table 2 shows the results for set 7. The polynomial that gave the lowest residual mean square was chosen as the best fit to represent the variance function of the residuals. One has to be careful using the residual mean square and the multiple R-square to decide the best fit when dealing with a set containing few data points or repetitive data points. Draper and Smith have discussed this issue [*8*]. For set 7, the fifth degree polynomial was chosen as the best fit, and the inverse of this function was used to calculate the weights to perform the first degree polynomial weighted regression analysis. Similarly, the weighted regression analysis was performed also for sets 1 and 5. The results for both unweighted and weighted regression analyses for the three sets are given in Table 3. For each of these three sets, weighted regression has resulted in a lower residual mean square value than for unweighted regression. For all three sets, multiple R-square has increased with weighted regression; the coefficients of variation of $\hat{A}$ and $\hat{B}$, respectively, $\delta_{\hat{A}}$ and $\delta_{\hat{B}}$, have decreased with weighted regression. These results show that the weighted regression estimates are better than unweighted regression estimates for these three data sets. However, the improvements on multiple R-square values are small (<7%). Therefore, even for data sets 1, 5, and 7, the point estimates based on unweighted regression may be satisfactory.

Variance of the residuals for each of the other five sets was found to be approximately constant with $\overline{\sigma}_3$. Due to this behavior, for these five sets, only unweighted regression results were used to obtain values for $\hat{A}$, $\hat{B}$, $S_{\hat{A}}$, $S_{\hat{B}}$, and COV($\hat{A}$,$\hat{B}$). The results, given in Table 3, show high multiple R-square values for all eight sets. This implies that the Mohr-Coulomb criterion is highly suitable to model the considered strength data.

Calculation of ($\hat{c}$,$\hat{t}$) *and* ($S_{\hat{c}}^2$,$S_{\hat{t}}^2$)

Obtained values for $\hat{A}$, $\hat{B}$, $S_{\hat{A}}$, $S_{\hat{B}}$, and COV($\hat{A}$,$\hat{B}$) were used in Eq 6 and Eq 8 to calculate values for $\hat{c}$, $\hat{t}$, $S_{\hat{c}}^2$, and $S_{\hat{t}}^2$ for each set. The results are shown in Table 4. This table also provides values for the coefficients of variation of $\hat{c}$ and $\hat{t}$, respectively, $\delta_{\hat{c}}$ and $\delta_{\hat{t}}$, to make comparisons about the uncertainty of $\hat{t}$ and $\hat{c}$ among different sets. For each set, $\delta_{\hat{t}}$ is smaller than $\delta_{\hat{c}}$. All the $\delta_{\hat{t}}$ values are less than 0.13. $\delta_{\hat{c}}$ values range from 0.19 to 0.41.

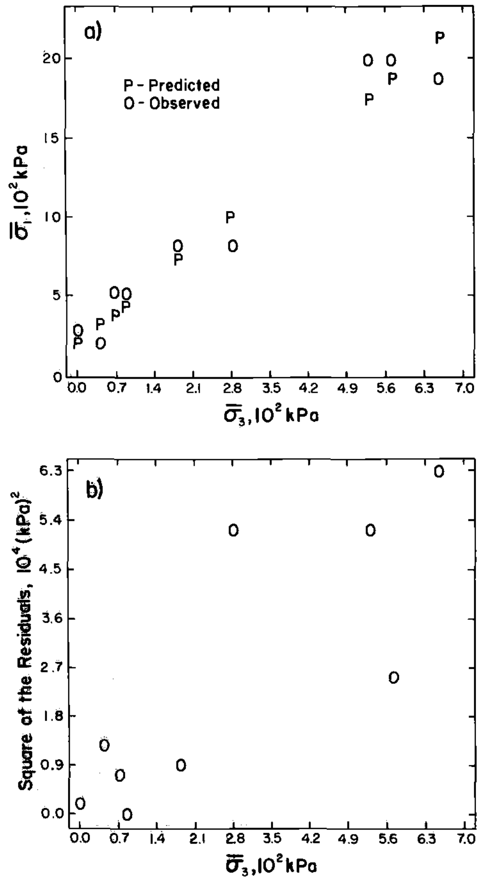

FIG. 3—*Typical results of unweighted linear regression for a data set that requires weighted regression analysis:* (a) *Predicted and observed* $\bar{\sigma}_1$ *versus* $\bar{\sigma}_3$ *for data set 7;* (b) *Square of the residuals versus* $\bar{\sigma}_3$ *for data set 7.*

Bivariate Beta Modeling of (c,t)

For convenience of presentation, $(\hat{c},\hat{t})$ is replaced by (Q,R). Figure 4 shows the values obtained for (Q,R) for all eight sets. Two different regions were chosen for Q versus R space as shown in Fig. 4 to investigate the effect of size of the region on fitting the distribution. For each case, (X,Y) and $(\overline{X},\overline{Y},S_X,S_Y,r_{XY})$ sets were calculated for six different D values,

TABLE 2—*Results of the polynomial regression between square of the residuals and* $\bar{\sigma}_3$ *for data set 7.*

Degree	Residual Mean Square	Multiple R-Square
1	2.11	0.69
2	2.37	0.70
3	2.81	0.70
4	1.84	0.84
5	0.08	0.99
6	0.12	0.99

TABLE 3—*Results of unweighted and weighted regression between* $\bar{\sigma}_1$ *and* $\bar{\sigma}_3$.

Data Set Number	Type of Regression	Residual Mean Square	Multiple R-Square	$\hat{A}$, hundreds of kPa	$\hat{B}$	$S_{\hat{A}}$, hundreds of kPa	$S_{\hat{B}}$	$\delta_{\hat{A}}$	$\delta_{\hat{B}}$	$r_{\hat{A}\hat{B}}$	COV($\hat{A}$,$\hat{B}$), hundreds of kPa
1	unweighted	4.70	0.90	2.135	3.270	1.049	0.279	0.491	0.085	−0.865	−0.253
1	weighted	0.99	0.96	1.882	3.216	0.615	0.159	0.327	0.049	−0.777	−0.076
2	unweighted	2.46	0.91	2.090	3.162	0.574	0.212	0.275	0.067	−0.830	−0.101
3	unweighted	2.39	0.83	2.705	2.323	0.639	0.238	0.236	0.102	−0.849	−0.129
4	unweighted	2.46	0.91	2.669	2.574	0.853	0.284	0.320	0.110	−0.814	−0.197
5	unweighted	1.35	0.96	1.408	2.981	0.526	0.187	0.374	0.063	−0.770	−0.076
5	weighted	1.21	0.99	1.560	2.939	0.311	0.095	0.199	0.032	−0.771	−0.023
6	unweighted	0.99	0.96	2.594	3.515	0.956	0.341	0.369	0.097	−0.905	−0.295
7	unweighted	3.17	0.95	2.134	2.904	0.889	0.247	0.417	0.085	−0.744	−0.163
7	weighted	1.11	0.96	2.284	2.979	0.389	0.222	0.170	0.075	−0.585	−0.051
8	unweighted	0.59	0.99	1.541	2.976	0.505	0.161	0.328	0.054	−0.782	−0.064

TABLE 4—*Estimates for parameters* c *and* t.

Data Set Number	$\hat{c} = Q$, hundreds of kPa	$\hat{t} = R$	$s_{\hat{c}}^2$, ten thousands of (kPa)^2	$s_{\hat{t}}^2$	$\delta_{\hat{c}}$	$\delta_{\hat{t}}$
1	0.525	0.618	0.0330	0.0008	0.346	0.047
2	0.588	0.608	0.0317	0.0015	0.303	0.064
3	0.887	0.434	0.0621	0.0031	0.281	0.129
4	0.832	0.491	0.0927	0.0038	0.366	0.125
5	0.455	0.565	0.0093	0.0003	0.212	0.033
6	0.692	0.671	0.0816	0.0034	0.413	0.087
7	0.662	0.573	0.0166	0.0019	0.195	0.075
8	0.447	0.573	0.0244	0.0010	0.349	0.055

using Eq 11 and Eq 13, respectively. Then Eq 12 was used to obtain $\hat{p}_1$, $\hat{p}_2$, and $\hat{p}_3$ values, which were used to find $(f_e)_{ij}$ for each of the grid cells shown in Fig. 1. Also, total expected probability, TEP, (that is, $\Sigma\ (f_e)_{ij}$) was calculated for each case. Values of $(f_o)_{ij}$ for each cell shown in Fig. 1 were calculated using the computed X,Y values. $(\chi^2)_d$ for each case was obtained through Eq 10. Table 5 shows the results of bivariate beta modeling. TEP values were found to be either one or very close to one for all the cases. This implies that both the regions of Q-R chosen for modeling are adequate for accurate $(\chi^2)_d$ calculations. For all cases, the number of degrees of freedom was 51. Table 5 shows that the $(\chi^2)_d$ value depends on D as well as on the size of the considered Q-R domain. In this particular case it may be due to small sample size and coarse grid cells. However, P values given in the table imply that a bivariate beta distribution is suitable to represent the distribution of (Q,R) at least up to a significance level of 99.5%.

Bivariate Normal Modeling of (c,t)

Again (Q,R) is used to represent $(\hat{c},\hat{t})$. Values of Q and R given in Table 4 were used to obtain estimates for μ_Q, μ_R, σ_Q, σ_R, and ρ through the moment estimation technique. The values obtained for $\hat{\mu}_Q$, $\hat{\mu}_R$, $\hat{\sigma}_Q$, $\hat{\sigma}_R$, and $\hat{\rho}$ were, respectively, 0.636, 0.567, 0.164, 0.074, and -0.594. These values led to coefficient of variation values of 0.26 and 0.13 for Q and R, respectively. The value obtained for $\hat{\rho}$ clearly shows that the correlation between Q and R is important for the considered strength data. For probability calculations, $\hat{\mu}_Q \pm 3\hat{\sigma}_Q$ and $\hat{\mu}_R \pm 3\hat{\sigma}_R$ were used to cover the (Q,R) domain. The whole domain was divided into 36 equal size grid cells to calculate $(f_o)_{ij}$ and $(f_e)_{ij}$ values and thus to find $(\chi^2)_d$. The total theoretical probability for the whole domain was found to be 0.9949. This value shows that the considered domain is highly adequate for accurate $(\chi^2)_d$ calculations. The number of degrees of freedom for this case was 30. $(\chi^2)_d$ was found to be 22.2, giving a P value of 83%. This implies that the bivariate normal distribution with the parameter values given above can be used to represent the (Q,R) distribution up to a significance level of 83%.

Conclusions

The suggested procedure for probabilistic description of shear strength parameters using triaxial test data requires either an unweighted regression analysis or a weighted regression analysis, the propagation of error technique, and the chi-square goodness-of-fit test. To decide whether a weighted regression analysis is required for a given set of data, it is important to perform a residual analysis. The suggested procedure was applied to eight sets

TABLE 5—*Results of bivariate beta modeling for* (Q,R).

	Region 1						Region 2					
D Value	TEP	$(\chi^2)_d$	P%	$\hat{p}_1$	$\hat{p}_2$	$\hat{p}_3$	TEP	$(\chi^2)_d$	P%	$\hat{p}_1$	$\hat{p}_2$	$\hat{p}_3$
1.0	1.000	6.5	>99.5	9.12	27.63	12.01	1.000	24.6	>99.5	3.35	8.29	6.42
0.8	1.000	4.3	>99.5	7.30	22.10	19.36	1.000	16.1	>99.5	2.69	6.63	8.75
0.6	1.000	3.5	>99.5	5.47	16.58	26.71	1.000	4.5	>99.5	2.01	4.97	11.08
0.5	1.000	1.4	>99.5	4.56	13.81	30.38	1.000	13.1	>99.5	1.68	4.14	12.24
0.4	1.000	4.4	>99.5	3.65	11.01	34.06	1.000	5.8	>99.5	1.34	3.31	13.41
0.2	1.000	1.9	>99.5	1.82	5.53	41.41	0.976	1.7	>99.5	0.67	1.66	15.73

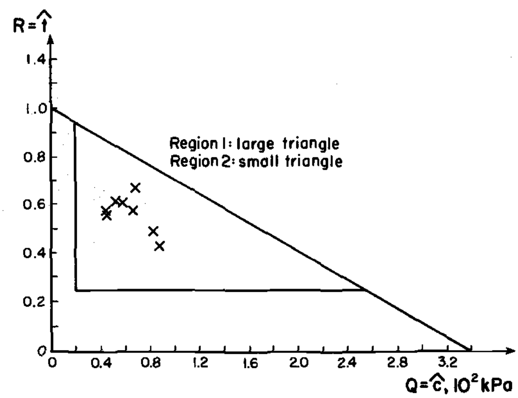

FIG. 4—*Domains and point estimates of* (c,t) *to perform bivariate beta fitting.*

of strength data belonging to one soil type. For three data sets, weighted regression estimates were found to be better than unweighted regression estimates. However, the difference between the weighted and unweighted fits were found to be small. The parameter c was found to have higher variability than t. This agrees with previous findings on the variability of c and t reported in geotechnical literature. In bivariate beta distribution modeling of c and t values, several factors were found to influence the $(\chi^2)_d$ value. Further research is recommended on this issue. In the example discussed, only eight points were available to perform a chi-square test. A sample size of about 30 to 40 may be considered as a lower limit to perform a proper chi-square test. In geotechnical literature it is difficult to find such a data set. This shows that careful planning of experiments is important if one is interested in analyzing strength data using probabilistic methods. Results of this investigation show that both bivariate beta and bivariate normal distributions are suitable to represent the distributions of strength parameters. For the tested data set, bivariate beta fits were found to be better than bivariate normal fit. However, it is important to note that carrying out a goodness-of-fit test for bivariate normal distribution is easier than for bivariate beta distribution.

Acknowledgments

Shoung Ouyang performed the computer runs for this study. The author acknowledges useful comments made by the ASTM reviewers.

References

[*1*] Schmertmann, J. H., and Osterberg, J. O., "An Experimental Study of the Development of Cohesion and Friction with Axial Strain in Saturated Cohesive Soils," Paper presented at American Society of Civil Engineers Conference on Shear Strength of Cohesive Soils, University of Colorado, Boulder, 1960.

[*2*] Lumb, P., *Canadian Geotechnical Journal,* Vol. 7, 1970, pp 225–242.

[*3*] Lisle, R. J., and Strom, C. S., *Quarterly Journal of Engineering Geology,* Vol. 15, No. 1, 1982, pp. 55–56.

[*4*] Franklin, J. A., *Rock Mechanics,* Vol. 3, 1971, pp. 86–98.

[*5*] Grivas, D. A., and Williams, K. H., "Joint Distribution of the Components of Soil Strength," *Proceedings,* Third International Conference on Application of Statistics and Probability to Soil and Structural Engineering, Sydney, Australia, 1979.

[*6*] *BMDP Statistical Software Manual,* University of California, 1985.

[7] Benjamin, J. R., and Cornell, C. A., *Probability, Statistics, and Decision for Civil Engineers,* McGraw-Hill, New York, 1970.
[8] Draper, N. R., and Smith, H., *Applied Regression Analysis,* Wiley, New York, 1981.
[9] Mardia, K. V., *Families of Bivariate Distributions,* Griffins Statistical Monographs and Courses, No. 27, Griffins, London, 1970.
[10] Kulatilake, P. H. S. W., *Journal of Mathematical Geology,* Vol. 18, No. 2, 1986, pp. 181–195.
[11] Pender, M. J., "Friction and Cohesion Parameters for Highly and Completely Weathered Wellington Greywacke," *Proceedings,* Third Australia-New Zealand Conference on Geomechanics, Wellington, New Zealand, Vol. 1, 1980.

Gilbert Y. Baladi[1] *and Thomas T. H. Wu*[2]

Interpretation of Triaxial Test Results of Cohesionless Soils: A New Model

REFERENCE: Baladi, G. Y. and Wu, T. T. H., "**Interpretation of Triaxial Test Results of Cohesionless Soils: A New Model,**" *Advanced Triaxial Testing of Soil and Rock, ASTM STP 977*, Robert T. Donaghe, Ronald C. Chaney, and Marshall L. Silver, Eds., American Society for Testing and Materials, Philadelphia, 1988, pp. 567–581.

ABSTRACT: The demand for more reliable methods of predicting the stress–strain relationship of large particle soils, and for more realistic assessment of the influence of grain characteristics on the shear behavior of cohesionless materials, makes it very important that the geotechnical profession develop a reliable modeling technique to accurately evaluate the effects of test and specimen variables. Large size particles in a soil matrix make it difficult to determine the strength parameters using conventional laboratory equipment. The relevant properties of the prototype materials (which contain large size particles) could be evaluated by using laboratory-reconstructed specimens with smaller particle sizes.

Traditionally, shear strengths of different types of cohesionless soils were compared using a constant relative density or void ratio. It was found that because of the differences in the range of limiting densities, soils with a constant relative density or void ratio but with different grain sizes would undergo different behavior during shear. At a constant void ratio or a constant relative density, some soils may experience volume increase; others may undergo a volume decrease; still others may experience no volume change during shear. Thus, comparing the shear strengths of different types of soils (that is, different grain size materials) based on the soils' relative densities or void ratios may led to inaccurate conclusions. The model should be based instead on the soils' response under the applied loads rather than their states of compaction.

This paper presents a new model (percent dilatation) whereby the shear strength of cohesionless soils, comprised of different particle sizes, can be compared and studied based on their behaviors during shear. The percent dilatation (PD) model was developed using data from 178 drained static triaxial tests, designed and conducted to study the effects of soil density, confining pressure, moisture content, and grain characteristics (size, gradation, shape, and particle angularity) on the shear strength of cohesionless soils.

KEY WORDS: cohesionless, sand, gravel, triaxial, shear strength, ultimate strength, grain size

The shear strength of *dry* cohesionless soils, described by their total angle of internal friction (ϕ), can be separated into two independent components:

(a) Ultimate angle of friction (ϕ_U), which is governed by microscopic interlocking of particles due to their surface roughness at contact points (grain-to-grain friction), and
(b) Interlocking angle of friction (ϕ_I), which consists of physical restraints to relative particle translation affected by adjacent particles.

[1] Associate professor of civil engineering, Department of Civil and Environmental Engineering, Michigan State University, East Lansing, MI, 48824-1212.
[2] Engineer, Jones, Kwong, Kishi Consulting Engineers, 235 15th Street, West Vancouver, British Columbia, Canada, V7T 2X1.

The interlocking angle of friction is affected by the sample dilatancy, which is a function of the state of compaction of the soil (that is, the denser the soil, the higher its dilatancy; the higher the degree of interlocking; and the higher the angle of interlocking friction [ϕ_I]).

The shear stress required to overcome particles interlocking and to bring the soils to a free-sliding position is greatly affected by the soil grain size [*1*]. This conclusion, however, is not consistent throughout the literature. Conflicting findings and opinions concerning the effects of grain size or percent gravel content on the shear strength of cohesionless soils [*2*] are summarized below.

1. The shear strength of cohesionless soils increases as the particle size increases [*1, 3–6*].
2. The shear strength of cohesionless soils decreases as the particle size increases [*7–13*].
3. The shear strength of cohesionless soils is not affected by the grain size [*14–17*].

TABLE 1—*Summary of the effect of grain size on the shear strength of cohesionless materials.*

Source	Maximum Particle Size, inch (mm)	Type of Test[a]	Conclusion[b]	Conclusion Based on a Constant Value of[c]	Uniformity of the Test Material
Bishop [*14*]	1.25 (31.8)	D	1*	*n*	Uniformly graded
Vallerga et al. [*16*]	0.20 (4.8)	T	1*	*e*	Uniformly graded
Zelasko [*17*]	0.03 (0.9)	T	1*	*e*	Varied
Kirkpatrick [*1*]	0.08 (2.0)	T	2*	*n*	Uniformly graded
Koerner [*8*]	0.10 (2.5)	T	2*	*e*	Uniformly graded
Leslie [*9*]	3.00 (76.2)	T	2*	*e*	Very well graded
Marachi [*10*]	6.00 (152.4)	T	2*	*e*	Well graded
Marshal [*11*]	8.00 (203.2)	T	2*	*n*	Varied
Rowe [*12*]	0.04 (1.0)	S	2*	*n*	Varied
Zeller & Williman [*13*]	3.94 (100.0)	T	2*	*n*	Very well graded
Donaghe & Torrey [*4*]	3.00 (838.2)	T	3*	*Dr*	Very well graded
Holtz & Gibbs [*5*]	3.00 (76.2)	T	3*	*Dr*	Varied
Lewis [*6*]	0.25 (6.4)	D	3*	*Dr*	Uniformly graded

[a] D = Direct shear test
T = Triaxial compression test
S = Sliding test (or angle of repose test)

[b] 1* = The shear strength is not affected by particle size.
2* = The shear strength decreases as the particle size increases.
3* = The shear strength increases as the particle size increases.

[c] *n* = Porosity
e = Void ratio
Dr = Relative density

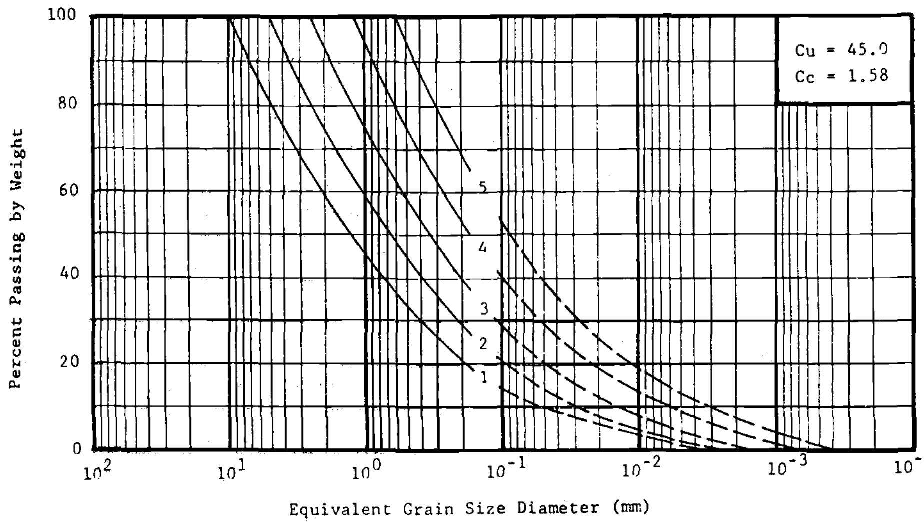

FIG. 1—*Parallel gradation curves.*

The differences between these findings are related mainly to the basis on which the shear strengths of different grain size soils were compared. Some researchers compared the shear strength of the soils using a constant relative density; others used a constant void ratio; still others did not separate variables that may affect shear strength. Table 1 summarizes past studies of the effects of grain size on the shear strength of cohesionless soils and the basis on which the analyses were conducted.

This paper presents a new analytical model, called the percent dilatation model (PD), whereby the effects of grain size on the shear strength of cohesionless soils can be studied. The model, based on the soil behavior during shear, was developed using drained triaxial test results.

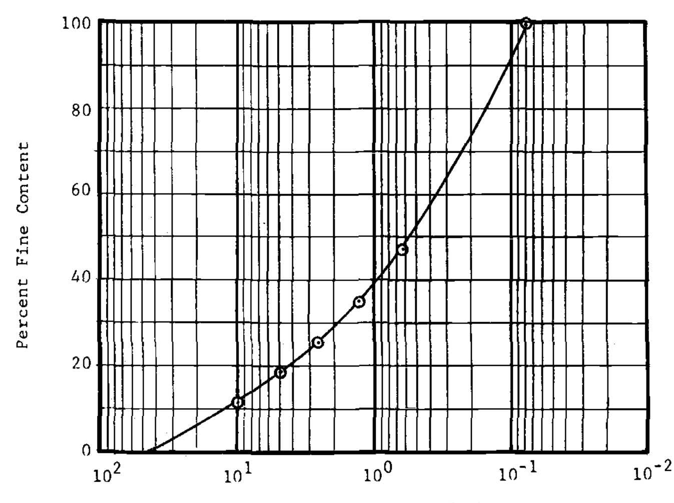

FIG. 2—*Relationship between the percent fine content and the maximum grain size of the series of samples.*

Test Material and Test Results

The original test material used in this investigation consisted of a natural deposit of rounded to subrounded aggregates. The aggregates consisted of the following percent mixture by weight: granite 39%, sandstone 20%, meta-quartzite 11%, dolomite 11%, limestone 11%, and chert 8%. The grain size of this material ranged from 1.5 to less than 0.003 in. (40 to 0.075 mm). A part of the original material was crushed and pulverized (C/P). The C/P material was then sieved and separated according to different fraction of grain sizes. The other parts of the natural aggregates were used to study the effects of particle angularity on the shear strength of the materials. The test results can be found in Ref *2*.

It should be noted that in this paper the term *soil sample* refers to a soil mixed according to any one of the five gradation curves (Curves 1 to 5 in Fig. 1). The term *soil or test specimen* indicates the physical test specimen made from a soil sample and tested under certain conditions. Thus, several test specimens could be made from one soil sample.

To study the effects of grain size on the shear strength of the C/P material, five soil samples from a series of five parallel gradation curves (Fig. 1) were used. Because the gradation curves are parallel, the soil samples possess the same coefficient of uniformity (C_u) of 45 and coefficient of curvature (C_c) of 1.58. The only difference between the five soil samples is the grain size or percent fine content (percent finer than the No. 200 sieve). For example, the soil of curve 1 (in Fig. 1) consists of the largest maximum grain size (0.375 in. or 9.5 mm), and the lowest percent fine content of 12%. For all curves, as the maximum

TABLE 2—*Percent gravel, sand, and fine content by weight, Atterberg limits, uniformity coefficient* (C_u) *coefficient of curvature,* (C_c) *and the Unified Soil Classification System* (*USCS*) *of the series of parallel graded samples.*

Soil Fraction or Component	Sample Number 1	2	3	4	5
Coarse-grained					
• Gravel					
Coarse	0.0	0.0	0.0	0.0	0.0
Fine	19.2	0.0	0.0	0.0	0.0
Total Gravel	19.2	0.0	0.0	0.0	0.0
• Sand					
Coarse	23.8	23.0	4.0	0.0	0.0
Medium	27.0	36.0	42.0	30.0	10.0
Fine	18.0	23.1	27.9	34.5	52.3
Total Sand	68.8	82.1	73.9	64.5	52.3
Fine-grained					
Silt	12.0	17.9	26.1	35.5	47.7
Uniformity coefficient (C_u)[a]	45.0	45.0	45.0	45.0	45.0
Coefficient of curvature (C_c)[a]	1.58	1.58	1.58	1.58	1.58
Atterberg Limits[b]					
Liquid Limit	21.9	21.9	21.9	21.9	21.9
Plastic Limit	21.62	21.62	21.62	21.62	21.62
Plasticity index	0.28	0.28	0.28	0.28	0.28
USCS symbol	SW-SM	SM	SM	SM	SM
Specific gravity	2.74	2.74	2.74	2.74	2.74

[a] C_u and C_c are presented here to indicate parallel graded samples.
[b] Tests were conducted on materials passing No. 200 sieve.

grain size decreases, the percent fine content increases. For any series of parallel graded soils, the value of the percent fine content of the soil is a function of its maximum grain size. The functional relationship for the series of curves of Fig. 1 is expressed in Eq 1 and shown in Fig. 2.

$$PF = -0.176\{1.0 - 3.187 \exp[-0.66(\log D_{max})]\} \tag{1}$$

where

PF = percent fine content (PF = 0.0 to 1.0)
exp = exponential function
log = logarithm to base 10
D_{max} = maximum particle size

In this paper, the percent fine content will be used to characterize the grain size of the soils.

As noted above, the C/P material was then blended in conformity with each of the parallel gradation curve of Fig. 1. This resulted in five different soil samples (different grain sizes) with the same coefficients of uniformity and curvature. The soil samples were then classified (see Table 2) in general accordance with the Unified Soil Classification System. Maximum and minimum dry density tests and angle of repose tests were conducted for all five soil samples. The test results, critical void ratio, and the ultimate angle of internal friction of the soil samples are summarized in Table 3.

From each soil sample, several 3-in. (76-mm) diameter triaxial test specimens were prepared at various densities and three levels of water content (dry, 5%, and 9%), and tested using confining pressures of 5, 25, and 50 psi (34.5, 172.5, and 345 kN/m^2). In this paper however, only the dry drained triaxial test results at the 5 psi (34.5 kN/m^2) confining pressure are presented (see Table 4) and discussed. Other data at different confining pressures and water contents, and the test procedures may be found in Ref 2.

Discussion

The characteristics of the stress–strain diagram of a cohesionless soil vary, and they depend on the density and moisture content of the soil specimen, and the test confining pressure.

TABLE 3—*Percent fine content; maximum particle size; maximum and minimum densities; maximum, minimum, and critical void ratios; ultimate angle of internal friction; and angle of repose of the series of parallel graded samples.*

Material Sample Number	Crushed and Pulverized					
	0[a]	1	2	3	4	5
Percent fine content	0.0	12.0	17.9	26.1	35.5	47.7
Maximum particle size, in.	1.5	0.38	0.19	0.09	0.05	0.02
Maximum density, pcf	134.4	131.0	129.5	126.5	123.0	118.0
Minimum density, pcf	111.0	103.5	99.5	94.0	88.5	80.0
Maximum void ratio	0.539	0.650	0.716	0.817	0.930	1.135
Minimum void ratio	0.271	0.304	0.319	0.350	0.388	0.447
Critical void ratio at 34.5 kN/m^2 (5 psi)	——	0.470	0.485	0.525	0.550	0.610
Ultimate angle of friction (ϕ_u) at 34.5 kN/m^2 (5 psi)	——	35.69	35.38	34.42	33.41	33.62
Angle of repose (ϕ_r)	37.75	33.67	31.61	28.50	27.75	26.76

[a] Sample number zero designates zero percent fine content.

TABLE 4—*Triaxial test results.*

σ_3[a]	D_r[b]	e[c]	ϕ_p[d]	ϵ_p[e]	PD[f]
		Sample 1, Crushed and Pulverized Material			
5	46.70	0.4882	35.69	20.0	−10.94
5	58.40	0.4477	37.34	6.0	13.40
5	62.70	0.4328	38.70	5.0	22.36
5	79.40	0.3750	47.53	3.5	57.09
5	91.30	0.3337	50.19	2.7	81.91
5	97.90	0.3109	55.88	2.5	95.61
		Sample 2, Crushed and Pulverized Material			
5	50.90	0.5139	35.38	20.0	−17.38
5	63.20	0.4650	*	*	12.03
5	67.10	0.4496	38.12	6.6	21.29
5	69.80	0.4388	39.69	5.5	27.78
5	90.10	0.3581	45.27	3.0	76.31
5	91.20	0.3537	47.04	3.5	78.95
5	96.30	0.3334	50.67	2.5	91.16
		Sample 3, Crushed and Pulverized Material			
5	55.70	0.5568	34.42	20.0	−18.17
5	64.60	0.5152	*[g]	*	5.60
5	71.90	0.4812	37.11	6.7	25.03
5	80.80	0.4396	39.27	4.5	48.80
5	90.20	0.3957	44.62	3.3	73.89
5	99.60	0.3519	51.33	2.2	98.91
		Sample 4, Crushed and Pulverized Material			
5	53.70	0.6390	33.41	20.0	−55.07
5	57.00	0.6212	33.41	20.0	−44.06
5	65.40	0.5757	33.41	20.0	−15.90
5	76.70	0.5148	35.69	4.8	21.78
5	80.70	0.4929	37.63	4.5	35.33
5	100.0	0.3884	52.40	2.4	100.00
		Sample 5, Crushed and Pulverized Material			
5	61.60	0.7113	33.62	20.0	−62.26
5	62.50	0.7051	33.62	20.0	−58.45
5	68.30	0.6652	33.62	20.0	−33.93
5	80.60	0.5807	35.08	4.0	18.01
5	80.70	0.5797	37.33	3.7	18.62
5	92.70	0.4975	47.27	2.5	69.15
5	95.50	0.4817	48.72	2.2	78.90
5	98.00	0.4609	49.89	2.1	91.60
		Sample 100, Crushed and Pulverized Material			
5	82.70	0.8100	34.69	4.9	25.65
5	95.30	0.7044	41.16	3.2	79.84
5	99.80	0.6672	43.71	2.9	98.92

[a] σ_3 = Confining pressure (psi).
[b] D_r = Relative density (after confining pressure).
[c] e = Void ratio (after confining pressure).
[d] ϕ_p = Peak angle of internal friction (degree).
[e] ϵ_p = Axial strain at peak strength.
[f] PD = Percent dilatation.
[g] * = No data.

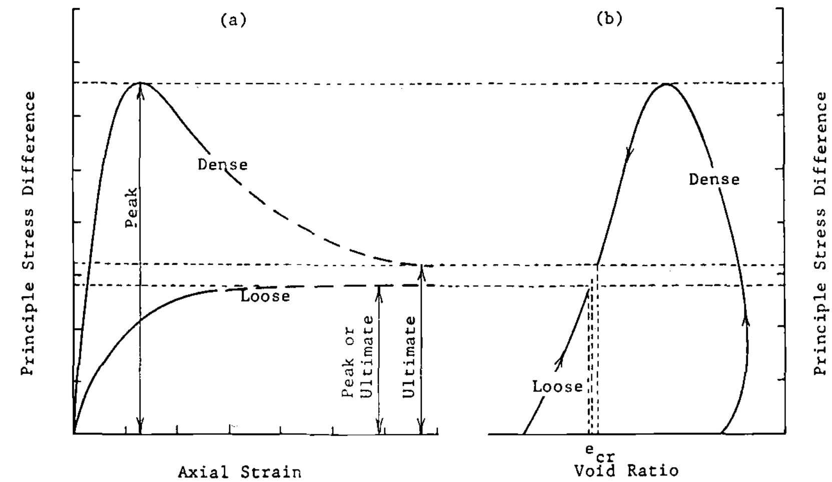

FIG. 3—*Typical stress–strain and stress–void ratio curves for loose and dense soil specimens.* (*From Holtz, R. D. and Kovacs, W. D.,* An Introduction to Geotechnical Engineering, *Prentice Hall, Englewood Cliffs, NJ, 1981.*)

Typical stress–strain curves of loose and dense soil specimens (Fig. 3*a*) show that dense soil possesses a peak strength (maximum principal stress difference) after which the stress drops to a constant value (ultimate strength) while the soil undergoes a continuous deformation (strain). On the other hand, the principal stress difference for loose soil increases with increasing strain until a constant stress level (ultimate strength) is reached. Figure 3*b* depicts the principal stress difference versus the void ratio of the same soil specimens. It can be seen from Fig. 3*b* that the dense specimen experiences an increase in the void ratio while the loose one undergoes a decrease in the void ratio as the stress increases. At ultimate strength, however, both samples would have approximately the same void ratio. This is called the *critical void ratio*—the void ratio at which cohesionless soils experience no volume change during shear. Any soil specimen with an initial void ratio of less than its critical void ratio is called a *dense specimen* and will undergo a volume dilatation (volume increase) during shear. If the void ratio of the soil specimen is higher than its critical void ratio, then the soil specimen is loose and will stand a volume decrease during shear. Further, the value of the critical void ratio depends on the soil in question and the test confining pressure [*18*].

Traditionally, the strength of soil specimens are compared, studied, and analyzed using the void ratio or the relative density of the soils. This method is useful when analyzing the strength variation of one type of soil (loose or dense) due to variations in the soil density or void ratio. If different types of soils or the same soil type but with different grain sizes are involved, however, the method may be inaccurate and may lead to conflicting conclusions concerning the effects of grain size on the shear strength of the soils. This point could be illustrated using the following examples:

Example 1

In this study, all soil samples possess the same type of gradation (coefficients of uniformity and curvature) but different percent fine content and maximum particle size. Several dry dense and loose soil specimens of each sample were tested using drained triaxial compression tests. Figure 4 shows plots of the peak angle of internal friction versus the relative density of the soil specimens. The ultimate angles of internal friction, and the critical relative densities

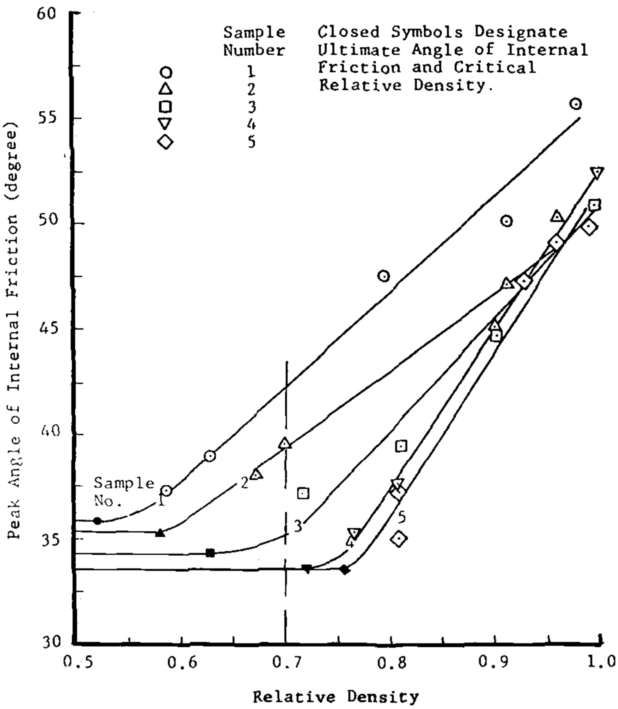

FIG. 4—*Peak angle of internal friction versus relative density of the series of samples for a confining pressure of 34.5 kN/m² (5 psi).*

(corresponding to the critical void ratios) of all samples are also shown in Fig. 4. It can be noted from the figure that for all soil specimens of any one sample of one gradation curve, the higher the relative density, the higher the angle of internal friction. If the peak angles of internal friction of all samples (different types of soils) are to be compared with one other using a constant relative density value (for example, 0.7), then samples 4 and 5 are on the loose side of the curves, sample 3 is in the vicinity of the critical void ratio, and samples 1 and 2 are on the dense side. Thus, the samples possess different behavior during shear and, consequently, their strengths cannot be compared. Nevertheless, if such comparison is to be made then the following conclusion can be drawn: *The larger the grain size (or the lower the percent fine content) of the soil, the higher the strength.* A similar conclusion was also reached by several other researchers [*1,3–6*].

Example 2

Figure 5 depicts the same data as Example 1, plotted against the void ratio of the soil specimens. It can be seen from the figure that for all test specimens of one soil sample, the lower the void ratio, the higher the angle of internal friction. If the data from all samples are to be compared at the same void ratio then the following conclusion can be made: *The larger the grain size (or the lower the percent fine content) of the soil, the lower the strength.* Again, a similar conclusion was reached by several other researchers [*7–13*].

It is clear that the conclusion of Example 1 is exactly the opposite of that of Example 2. The reason is that at a constant relative density or void ratio, soils with different grain sizes experience different behavior during shear.

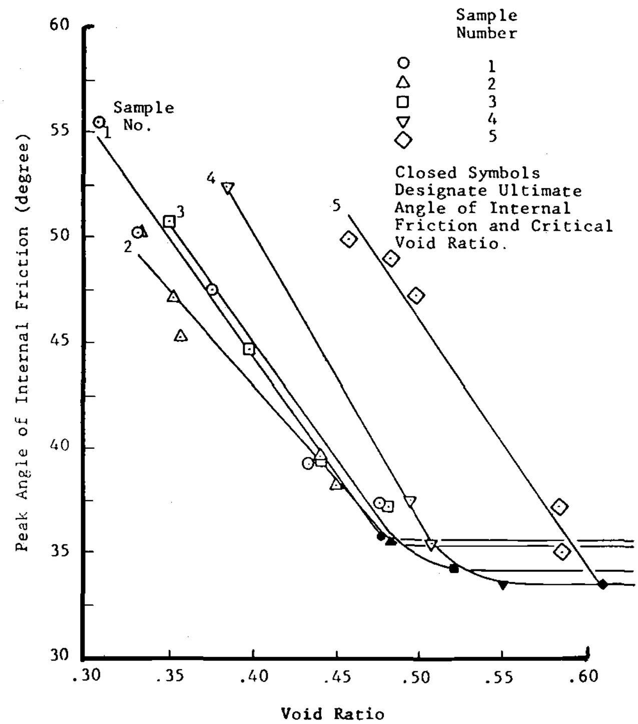

FIG. 5—*Peak angle of internal friction versus void ratio of the series of samples for a confining pressure of 34.5 kN/m² (5 psi).*

The above two examples illustrate, to some extent, the need to develop a new technique or analysis procedure to study the strengths of different types of soils.

To this end, a new model was developed based on the dilatant behavior of the soil during shear. The model can be expressed by the following equation:

$$PD = (e_{CR} - e)/(e_{CR} - e_{min}) \tag{2}$$

where

PD = percent dilatation of the soil specimen (percent volume change)
e_{CR} = critical void ratio of the soil (the void ratio at which the soil will not change volume during shear)
e = void ratio of the soil
e_{min} = minimum void ratio of the soil (it corresponds to the maximum dry density)

Irrespective of the type of soil and the grain size involved, the advantages of the percent dilatation model include

1. For zero percent dilatation, all cohesionless soils will experience no volume change during shear (that is, the void ratio of the soil will be the critical one).
2. For a positive value of the percent dilatation, all cohesionless soils will possess a void ratio less than the critical void ratio and will experience similar behavior (volume increase) during shear.
3. For a negative percent dilatation, all cohesionless soils will possess a void ratio higher than the critical void ratio, will undergo a volume decrease during shear, and will have a peak angle of internal friction equal to the ultimate angle of internal friction.

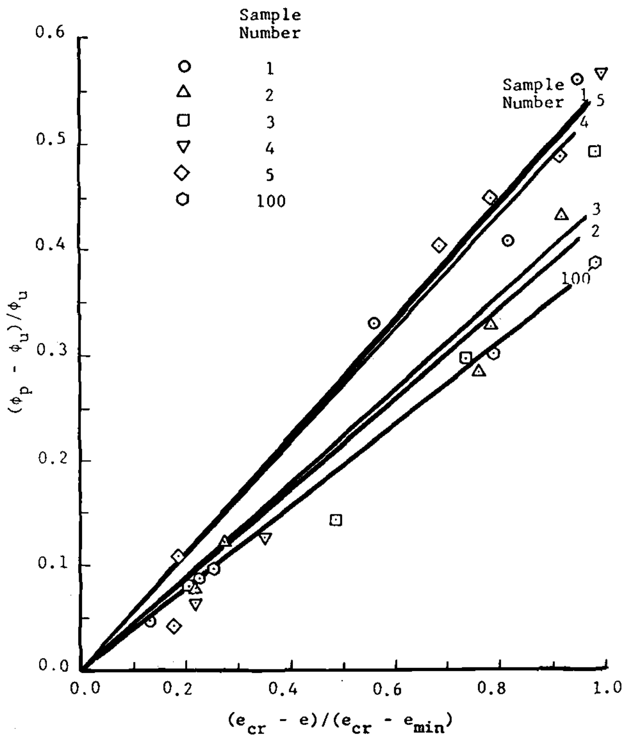

FIG. 6—*Normalized strength difference versus percent dilatation of the series of samples for a confining pressure of 34.5 kN/m² (5 psi).*

The same data of the two examples above were also analyzed using the percent dilatation model. The normalized strength difference (NSD) from each test was calculated using Eq 3. Then the NSD data were plotted against the percent dilatation (PD) of the test specimen (Fig. 6).

$$\text{NSD} = (\phi_P - \phi_U)/(\phi_U) \tag{3}$$

where

NSD = normalized stress ratio
ϕ_P = peak angle of internal friction (degree)
ϕ_U = ultimate angle of friction (degree)

The significance of the percent dilatation model can be realized by considering the characteristics of Fig. 6. These include

1. If the void ratio of the soil specimens is lower than the critical void ratio (that is, dense to relatively dense specimens), then the test data will be located in the first quarter of the axes system (as shown in Fig. 6).
2. If the soil specimens are loose (that is, the void ratio is higher than the critical), then the test data will be located along the negative part of the PD axis (the horizontal axis).
3. If the void ratio of the soil specimens is equal to the critical void ratio, then the data points will be located at the origin.

The benefit of the percent dilatation model is that the test data, as shown in Fig. 6, are separated into different regions whereby the soil specimens in any one region possess similar behavior during shear. For example, soil specimens with data points located in the first quadrant (24 data points are shown in Fig. 6) will undergo a volume dilatation (expansion) during shear; those with data points at the origin of the axes will theoretically experience no volume change during shear (no data points are available); and soil specimens with data points along the negative part of the PD axis will undergo volume decrease during shear (8 data points are available, see Table 4, but are not shown in Fig. 6 due to size restriction).

The test data of Fig. 6 were then used to obtain equations of the best fit lines using least square analysis. It should be noted here that the best fit lines (the solid lines in Fig. 6) were made to pass through the origin by adding several data points with zero coordinates to every set of data representing any one sample. The straight lines in Fig. 6 were modeled using the following general equation:

$$\text{NSD} = (\phi_P - \phi_U)/(\phi_U) = SP\,\frac{(e_{CR} - e)}{(e_{CR} - e_{\min})} \tag{4}$$

where

NSD = normalized stress ratio
ϕ_P = peak angle of internal friction in degrees
ϕ_U = ultimate angle of internal friction in degrees
e_{CR} = critical void ratio
$e_{\min}$ = minimum void ratio
e = void ratio of the soil specimen
SP = slope of the best fit line

Examination of Fig. 6 indicates that

1. The higher the percent dilatation of any soil sample, the higher the NSD and the higher the strength of the soil. This was expected because the higher the PD, the denser the soil and the higher the degree of particle interlocking.
2. There is no consistent (decreasing or increasing) order of the magnitude of the slopes of the best fit lines. Because the only difference between the parallel graded soil samples is grain size, the slopes of the straight lines of Fig. 6 are a function of the grain size of the samples or the percent fine content.

To study the effect of grain size on the peak strength of the soil samples, the slopes of the best fit lines of Fig. 6 are plotted against the percent fine content of the soils in Fig. 7. The values of the slope decrease as the percent fine content increases from zero to about 20; increase as the percent fine content increases from about 20 to about 45; and decrease thereafter. Nevertheless, the curve of Fig. 7 was modeled using Eq 5.

$$SP = \frac{0.41 + 3.16[\text{ABS}(\text{PF} - 0.205)]}{1.00 + 1.45[\text{ABS}(\text{PF} - 0.205)]}\exp[-1.26(\text{PF})^{1.35}] \tag{5}$$

where

SP = slope of the best fit lines of Fig. 6
ABS = absolute value
PF = percent fine content of the soil (PF = 0.0 to 1.0)
exp = exponential function

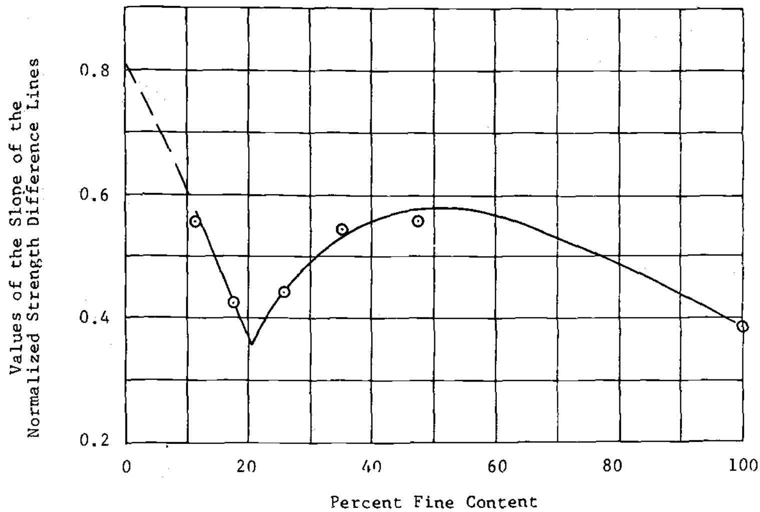

FIG. 7—*Values of the slope of the normalized strength difference lines versus percent fine content of the series of samples.*

By combining Eqs 4 and 5, the NSD of any soil specimen of the crushed and pulverized material could be calculated by using Eq 6:

$$NSD = \left\{ \left[\frac{(e_{CR} - e)}{(e_{CR} - e_{min})} \right] \left[\frac{0.41 + 3.16[ABS(PF - 0.205)]}{1.00 + 1.45[ABS(PF - 0.205)]} \right] \times \exp[-1.26(PF^{1.35}] + 1.0 \right\} \quad (6)$$

Equation 6 was found to be more than 95% accurate (that is, a comparison between the values of the NSD calculated by using Eq 6 and the measured data showed a maximum absolute difference of less than 5%).

Given the ultimate angle of internal friction of the soil samples, the effect of grain size on the peak strength of the soil can then be studied by using Eq 5 to calculate the peak angle of internal friction at constant levels of percent dilatation. Figure 8 depicts the calculated peak angle of internal friction plotted against the percent fine content of the soil for percent dilatation of 0.0, 0.25, 0.5, 0.75, and 1.00. Examination of the figures indicates that

1. For a constant percent fine content (particle size), the higher the percent dilatation of the soil specimen, the higher the value of the peak angle of internal friction (that is, the higher the density of the soil, the higher the shear resistance).
2. For a constant value of percent dilatation, the peak angle of internal friction decreases as the percent fine content increases from zero to 20.5%, then it increases as the percent fine content increases from 20.5 to about 40%, and finally it decreases once again as the percent fine increases above the 40% level.

The first observation was expected because the higher the percent dilatation, the lower the void ratio and the higher the density of the soil. The peak angle of internal friction of

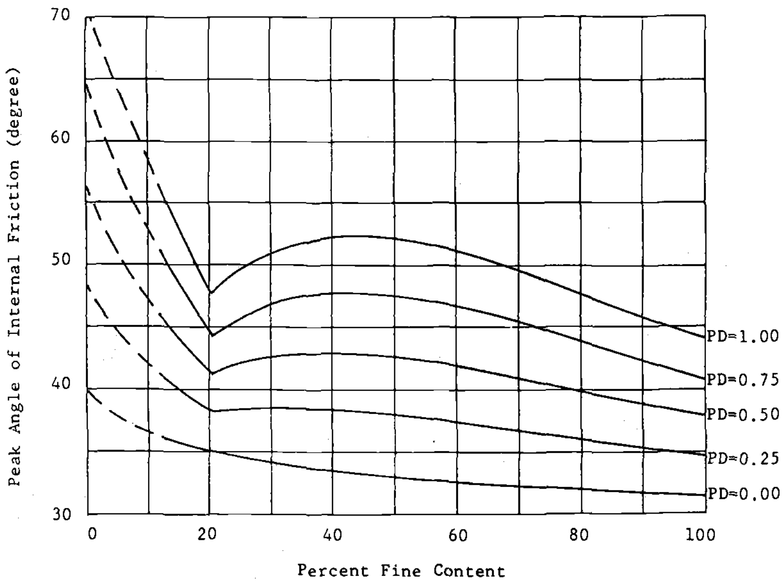

FIG. 8—*Peak angle of internal friction versus percent fine content of the series of samples for a confining pressure of 34.5 kN/m² (5 psi) and five values of the percent dilatation.*

the soil (also called the total angle of internal friction) is a function of the state of compaction of the soil (that is, the denser the soil, the higher the shearing resistance). The shearing resistance of cohesionless soils depends on the physical motion between particles which includes particles sliding and rolling relative to each other, and particle plucking and displacement from their interlocking seats. The former is being resisted by the sliding friction (ultimate friction), which is a function of the soil mineral and surface roughness of the grain. The latter consists of physical restraints to relative particle translation affected by adjacent particles. The resistance to this motion is offered by what is called interlocking friction. Particle interlocking is a function of the soil density and particle angularity. For a constant value of soil angularity, the denser the soil, the higher the particle packing and the higher the degree of interlocking. The peak angle of internal friction can be taken as the sum of the sliding (ultimate) and interlocking friction, and the ultimate friction is independent of the soil density, therefore, the higher the degree of interlocking, the higher the peak angle of internal friction.

The significance of the second observation is that two variables are affecting the peak angle of internal friction. The first is the percent gravel content of the sample, while the second is the percent fine content. As noted above, for parallel gradation curves, these two variables are dependent on each other. However, they possess independent influence on the shear strength of the soils. This observation is explained below.

Gravel Content

Figure 9 shows the percent gravel and sand contents plotted against the percent fine content of the five soil samples. First, the percent fine contents of all samples are known. To obtain the percent combination of gravel and sand, simply enter the percent fine content of the sample in question on the horizontal axis; draw a vertical line to intercept the gravel

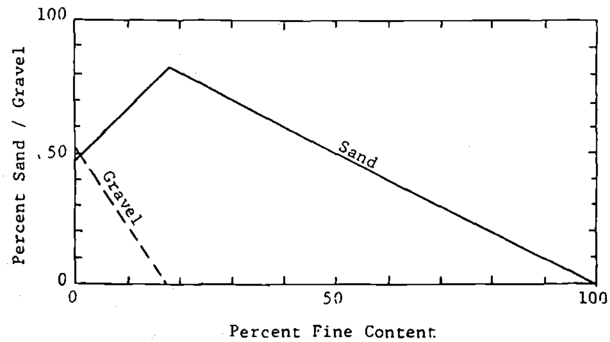

FIG. 9—*Percent combination of gravel and sand versus percent fine content for the series of samples.*

and sand lines; then read the percent gravel and sand contents on the vertical axis that correspond to the points of intersection. The percent gravel content decreases as the percent fine increases from zero to 17.9, and it is zero thereafter. Thus, for percent fine contents lower than 17.9%, gravel size particles reside in the soil matrix of the specimen. Large particles possess a relatively higher degree of interlocking than smaller particles (sand). Consequently, the interlocking friction is expected to increase, which causes an increase in the peak angle of internal friction.

Fine Content

Siddiqi concluded that the presence of oversized particles (larger than one sixth of the specimen diameter) in a soil matrix decreases its density due to less efficient packing around the oversized materials [*19*]. The presence of fine material around gravel and sand particles in a soil matrix offers a similar phenomenon (that is, they form localized loose soil pockets around denser and larger particles). These loose pockets possess lower shearing resistance than the rest of the soil. Consequently, the overall shearing resistance of the soil specimen will suffer. As the percent fine content increases and the gravel content decreases to zero percent, packing efficiency increases and the fine particles are forced closer together. Further increases in the percent fine content will cause fine materials to dominate the soil behavior which will result in a lower shearing resistance.

To summarize, the total effects of the grain size on the peak angle of internal friction can be separated into two components:

(a) their effect on the ultimate angle of internal friction, which is mainly (for the same mineral type) a function of the surface roughness of the particles. This in turn is a function of the percent fine content and the maximum particle size of the sample.
(b) their effect on the angle of interlocking friction, which is a function of the percent dilatation (sample density), the percent fine content, and the maximum grain size, and the percent combination of gravel, sand and fine materials of the sample.

Conclusions

The contradictory conclusions found in the literature concerning the effect of grain size on the shear strength of cohesionless soils were found to be related to the basis on which the analyses were conducted. This problem can be resolved by a new analytical model based on the dilatent behavior of the soil (percent dilatation model). It was found that this model is superior when compared to the traditional relative density and void ratio models. By using the percent dilatation model, the effects of grain size, gravel content, and percent fine of the soil can be separated and analyzed.

Based on constant percent dilatation, the shear strength of cohesionless soils was found to be dependent on the grain size and the percent fine content. In general, the shear strength of cohesionless soils increases with increasing grain size and gravel content.

References

[1] Hough, B. K., *Basic Soils Engineering*, Ronald Press, New York, 1957.
[2] Wu, T. T., "The Effects of Grain Characteristics on the Shear Strength of Cohesionless Soils," Ph.D. thesis, Michigan State University, East Lansing, MI, 1985.
[3] Donaghe, R. T., and Torrey, V. H., "Scalping and Replacement Effects on Strength Parameters of Earth Rockfill Mixtures," British Geotechnical Society, London, 1979.
[4] Donaghe, R. T., and Torrey, V. H., "Strength and Deformation Properties of Earth–Rock Mixtures," U.S. Army Engineer Waterways Experiment Station, Vicksburg, MS, Final Report on Project CWIS 31209, Sept. 1982.
[5] Holtz, W. G., and Gibbs, H. J., "Triaxial Shear Tests on Pervious Gravelly Soils," *Journal of the Soil Mechanics and Foundations Division, American Society of Civil Engineers*, Vol. 82, No. SM1, Jan. 1956.
[6] Lewis, J. G., "Shear Strength of Rockfill," in *Proceedings*, Second Australia-New Zealand Conference on Soil Mechanics and Foundation Engineering, 1965.
[7] Kirkpatrick, W. M., "Effects of Grain Size and Grading on the Shearing Behavior of Granular Materials," in *Proceedings*, Sixth International Conference on Soil Mechanics and Foundation Engineering, Montreal, Vol. 1, 1965.
[8] Koerner, R. M., "Effect of Particle Characteristics on Soil Strength," *Journal of the Soil Mechanics and Foundations Division, American Society of Civil Engineers*, Vol. 96, No. SM4, July 1970.
[9] Leslie, D. D., "Large Scale Triaxial Tests on Gravelly Soils," in *Proceedings*, Second Pan American Conference on Soil Mechanics and Foundation Engineering, 1963.
[10] Marachi, N. D., "Evaluation of Properties of Rockfill Materials," *Journal of the Soil Mechanics and Foundations Division, American Society of Civil Engineers*, Vol. 98, No. SM1, Jan. 1972.
[11] Marshal, R. J., "Large Scale Testing of Rockfill Materials," *Journal of the Soil Mechanics and Foundations Division, American Society of Civil Engineers*, Vol. 93, No. SM2, March 1967.
[12] Rowe, P. W., "The Stress–Dilatency Relation for Static Equilibrium of an Assembly of Particles in Concrete," in *Proceedings*, Royal Society, London, Series A, Vol. 269, 1962.
[13] Zeller, J., and Williman, R., "The Shear Strength of Shell Materials for the Goschenenalp Dam, Switzerland," in *Proceedings*, Fourth International Conference on Soil Mechanics and Foundation Engineering, London, Vol. 2, 1957.
[14] Bishop, A. W., "A Large Shear Box for Testing Sands and Gravels," in *Proceedings*, Second International Conference on Soil Mechanics and Foundation Engineering, Rotterdam, Vol. 1, 1948.
[15] Terzaghi, K., and Peck, R. B., *Soil Mechanics in Engineering Practice*, 2nd ed., Wiley, New York.
[16] Vallerga, B. A. et al., "Effect of Shape, Size and Surface Roughness of Aggregate Particles on the Strength of Granular Materials," in *ASTM STP 212*, American Society of Testing and Materials, Philadelphia, 1957.
[17] Zelasko, J. S., Kirzek, R. J., and Edil, T. B., "Shear Behavior of Sands as a Function of Grain Characteristics," in *Proceedings*, Istanbul Conference on Soil Mechanics and Foundation Engineering, Istanbul, 1975.
[18] Perloff, W. H., and Baron, W., *Soil Mechanics Principles and Applications*, Wiley, New York, 1976.
[19] Siddiqi, F. H., "Strength Evaluation of Cohesionless Soils with Oversize Particles," Ph.D. thesis, University of California, Davis, 1984.

William Z. Savage[1]

Pore-Pressure Distributions in Constant Strain-Rate Triaxial Tests

REFERENCE: Savage, W. Z., "**Pore-Pressure Distributions in Constant Strain-Rate Triaxial Tests,**" *Advanced Triaxial Testing of Soil and Rock, ASTM STP 977,* Robert T. Donaghe, Ronald C. Chaney, and Marshall L. Silver, Eds., American Society for Testing and Materials, Philadelphia, 1988, pp. 582–591.

ABSTRACT: A theoretical study of pore-pressure distributions in drained, constant strain-rate triaxial tests, an outgrowth and extension of earlier work by Gibson, Bishop, and Henkel, has been done to determine the experimental conditions under which pore-pressure gradients, and hence, effective stress differences throughout deforming triaxial test samples, are small.

It is concluded from the analysis of drained triaxial constant strain-rate tests that it is impossible to obtain a fully drained condition. In fact, in this test the long-term spatial pore-pressure distribution becomes parabolic. Unless strain rates are sufficiently low or permeabilities are sufficiently large to minimize the effect of this parabolic pore-pressure distribution, effective stresses in the deforming sample cannot approach uniformity and any property determinations based on the assumption of uniform effective stresses will be in error. A similar conclusion was reached by Gibson. It is also concluded that volumetric strains will be largest near the undrained end of a sample drained at one end, or largest in the middle of a sample drained at both ends. This strain distribution is a consequence of the parabolic pore-pressure distribution and suggests an explanation (apart from frictional end restraints) for any post-yield barreling observed in a drained triaxial test.

KEY WORDS: pore pressure, consolidation, triaxial, constant strain-rate tests, drained tests

Most triaxial tests done in rock and soil mechanics laboratories can be classified as drained, undrained, or pore-pressure-controlled. In drained tests, either one or both ends of a jacketed cylindrical sample are open to atmospheric pressure allowing drainage of pore fluid during deformation. In undrained tests, both ends of the sample are sealed, preventing any drainage during deformation. In the pore-pressure-controlled test, pore pressure is independent of confining pressure and maintained by external means. For each of these tests, it is necessary that pore-pressure gradients within the deforming test sample be small. If frictional effects near the ends of test samples can be minimized and pore-pressure gradients are small, then effective stresses across the material being tested will be reasonably uniform, and meaningful test results can be obtained.

In the following, Biot's theory of poro-elasticity [*1*] is applied to model pore-pressure distributions in drained constant strain-rate tests. Attention is focused on the conditions under which uniformity, or near-uniformity, in pore pressure is obtained in this type of triaxial test. However, no attempt is made to assess other effects, such as frictional end restraints, on the test sample.

Theoretical predictions of pore-pressure distributions in drained and undrained triaxial

[1] Geologist, United States Department of the Interior, Geological Survey, Box 25046, M.S. 966, Denver Federal Center, Denver, CO 80225.

tests have been presented previously. Gibson and Henkel [2] applied Biot's theory of poroelasticity [1] to find the time variation of spatially averaged pore pressure in a drained constant strain-rate triaxial test. Their interest was in determining the amount of time required for dissipation of at least 95% of the average excess pore pressure; a degree of dissipation sufficient to ensure negligible error in determining the drained strength. Because pore pressures were spatially averaged, no consideration was given to pore-pressure gradients, a factor considered below.

Gibson (quoted in Bishop and Henkel [3] also considered the time required for equalization of an initially nonuniform pore pressure in an undrained constant strain-rate triaxial test. The nonuniformity in pore pressure was attributed to nonuniformity in stress and strain due to end restraint in the test sample. This end restraint was thought to cause high pore pressures near the sample ends. Gibson treated the problem theoretically by assuming an initial parabolic nonuniformity in sample pore pressure, and found what strain rates were necessary to ensure nearly complete pore-pressure equalization at sample failure. This problem will not be considered here.

Gibson also considered theoretically the times required for equalization of pore pressures between a sample and a flexible pore-pressure measuring system [4]. No attempt is made here to analyze the effects of measuring system stiffness on the accuracy of pore-pressure measurements, and the reader is referred to Ref *4* for further details.

In the following, Biot's theory of consolidation [1] is specialized to the case of constant strain-rate deformation under fixed confining pressure. This leads to a diffusion equation for pore pressure, which in turn is solved for boundary and initial conditions appropriate for drained tests. The result of this analysis provides the experimentalist with an idea of pore pressure and volumetric strain distributions in drained constant strain-rate tests.

Biot's Theory of Consolidation

Biot considered the stress–strain response of a porous material having the following properties: (1) isotropy; (2) reversibility of stress–strain relations under final equilibrium conditions when all excess pore fluid pressures are dissipated; (3) linearity of stress–strain relations; (4) an incompressible pore fluid; (5) small strains; and (6) water flow through the porous skeleton according to Darcy's law [3]. (Discussions of Biot's theory and assumptions 1 through 6 can be found in Refs *5* to *7*.) These assumptions are fairly reasonable for porous rocks subjected to stress levels where strains remain small. However, for soils, the effects of finite strains must often be considered which complicates the analysis [8–10]. Such complications are avoided here because the intent is to explore the fundamental phenomenology of pore-pressure distribution in drained constant strain-rate tests.

The first of Biot's constitutive (stress–strain) relations are in standard tensor notation:

$$e_{ij} = \frac{1}{2\mu}\left(\sigma_{ij} - \frac{\lambda}{3\lambda + 2\mu}\delta_{ij}\,\sigma_{kk}\right) + \frac{P}{3H}\delta_{ij} \tag{1}$$

where e_{ij} represents strains; σ_{ij} represents stresses; δ_{ij} is the Kronecker delta; μ and λ are, respectively, the shear modulus and Lame's constant for the elastic skeleton; P is the pore pressure; and the coefficient $1/H$ is a measure of compressibility of the porous material for a given change in water pressure. As can be seen, Eqs 1 reduce to the usual elastic relations when the pore pressure, P, vanishes. Because consolidation involves removal of pore water, an additional variable specifying the change in the amount of pore fluid per unit volume of porous medium must be defined. For a saturated material containing an incompressible fluid, this variable, θ, is equal to $\eta - \eta_o$, where η and η_o are porosities in the strained and unstrained states. Biot assumed the relation between change in water content (porosity), pore pressure, and mean stress ($\sigma_{ii}/3$) to be

$$\theta = P/R + \frac{\sigma_{ii}}{3H} \tag{2}$$

where the coefficient $1/R$ measures the change in water content (porosity) for a given change in water pressure. This constitutive relation (Eq 2) predicts that an increase in pore-water pressure causes an increase in porosity, and an increase in compression causes a decrease in porosity in a water-saturated porous medium.

The constitutive Eqs 1 and 2 may be inverted for stress in terms of strain to give

$$\sigma_{ij} = \lambda\delta_{ij}\, e_{kk} + 2\mu e_{ij} - \alpha\delta_{ij}P \tag{3}$$

and

$$\theta = \alpha e_{ii} + P/Q \tag{4}$$

In Eq 3, $\alpha = 3\lambda + 2\mu/3H = K/H$, where K is the bulk modulus of the porous skeleton. In Eq 4, $1/Q = 1/R - \alpha/H$.

The stresses given by Eq 3 must satisfy equilibrium, or

$$\frac{\partial\sigma_{ij}}{\partial x_j} + \rho F_i = 0 \tag{5}$$

where F_i represents the components of body force per unit mass at the point x_i. Substitution of Eq 3 in Eq 5 and use of the strain displacement relation, $e_{ij} = ½\,[\partial u_i/\partial x_j + \partial u_j/\partial x_i]$, leads to the equations of equilibrium in terms of displacements:

$$(\lambda + \mu)\frac{\partial}{\partial x_j}\left(\frac{\partial u_i}{\partial x_i}\right) + \mu\frac{\partial}{\partial x_i}\left(\frac{\partial u_j}{\partial x_i}\right) - \alpha\frac{\partial P}{\partial x_j} + \rho F_j = 0 \tag{6}$$

We see that the pressure gradients $\partial P/\partial x_j$ affect the displacements like a body force.

An additional relation is needed to describe the flow of pore fluid in response to changes in pore pressure. According to Darcy's law, the rate of flow of fluid, V_i, at a point defined by the volume of fluid crossing a unit area per unit time, is proportional to the gradient of pore pressure at that point, or

$$V_i = -k\frac{\partial P}{\partial x_i} \tag{7}$$

where k is the permeability.

Assuming the pore fluid to be incompressible, continuity requires the increase of fluid content per unit time in a volume of porous solid, or $\int_v \partial\theta/\partial t\, dv$ to equal the volume of fluid entering per unit time through the surface, s, of the volume, or $-\int_s V_i\eta_i ds$, where η_i is an outward normal to s. We have, then

$$\int \frac{\partial\theta}{\partial t}\, dv = -\int_s V_i\eta_i ds$$

which, by the divergence theorem of Gauss, is

$$\int \frac{\partial \theta}{\partial t}\, dv = -\int \frac{\partial V_i}{\partial x_i}\, dv$$

or finally, the statement of continuity

$$\frac{\partial \theta}{\partial t} + \frac{\partial V_i}{\partial x_i} = 0 \tag{8}$$

Substituting Eqs 4 and 7 in Eq 8 leads to

$$k \frac{\partial^2 P}{\partial x_i \partial x_i} = \alpha \frac{\partial e_{kk}}{\partial t} + 1/Q \frac{\partial P}{\partial t} \tag{9}$$

Equations 6 through 9 in the four unknowns u_i and P constitute the basic equations in Biot's theory of consolidation [*3*].

Drained Constant Strain-Rate Test

As shown in Fig. 1, a sample of height h relative to an x_1, x_2, x_3 rectangular coordinate system is jacketed so that pore fluid moves in the axial direction only. The sample is subjected to a constant symmetric radial stress $\sigma_{11} = \sigma_{22} = -\sigma_c$. The upper boundary ($x_3 = h$) is open to atmospheric pressure and is subjected to a displacement $u_3 = -rth$ where r is a constant strain rate. The lower boundary of the sample is sealed against fluid flow and fixed so that $u_3 = 0$. The axial displacement would have the distribution $u_3 = -rx_3$ in the absence of pore pressure.

When pore fluid is present, some additional analysis is necessary. Because the pore fluid flow is axial, it is assumed that P is a function of the axial coordinate and time only. Also,

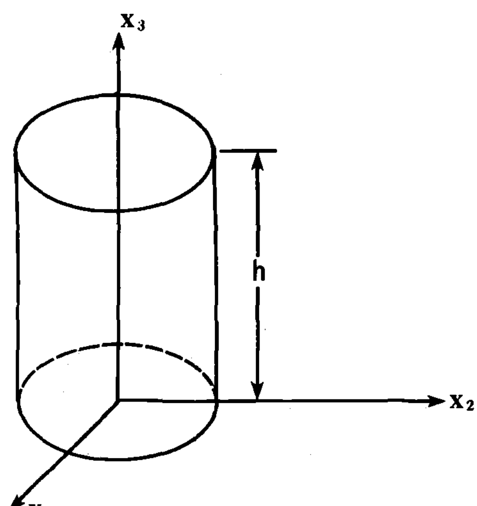

FIG. 1—*Triaxial test configuration referred to a Cartesian* x_1, x_2, x_3, *coordinate system. The sample, jacketed radially, is open to fluid flow at* x_3 = h, *and closed to fluid flow at* x_3 = *0.*

for the configuration shown in Fig. 1, the equations of equilibrium of total stresses and the fact that $\sigma_{11} = \sigma_{22} = -\sigma_c$ yields

$$\frac{\partial \sigma_{11}}{\partial x_3} = 0 \tag{10a}$$

$$\frac{\partial \sigma_{22}}{\partial x_3} = 0 \tag{10b}$$

$$\frac{\partial \sigma_{33}}{\partial x_3} = 0 \tag{10c}$$

and the constitutive equations (Eq 1) give

$$\frac{\partial e_{33}}{\partial x_3} = \frac{1}{3H}\frac{\partial P}{\partial x_3} = \frac{\alpha}{3\lambda + 2\mu}\frac{\partial P}{\partial x_3} \tag{11}$$

Integrating Eq 11 with respect to x_3 yields

$$e_{33} = \frac{\alpha P}{3\lambda + 2\mu} + f_o(t) \tag{12}$$

and a second integration yields

$$u_3 = \frac{\alpha}{3\lambda + 2\mu}\left[\int_o^{x_3} Pdz - \frac{x_3}{h}\int_o^h Pdz\right] - rtx_3 \tag{13}$$

which satisfies the boundary conditions on the displacement field.

The pore pressure distribution is governed by Eq 9 which reduces to

$$k\frac{\partial^2 P}{\partial x_3^2} = \alpha\frac{\partial e_{kk}}{\partial t} + 1/Q\frac{\partial P}{\partial t} \tag{14}$$

as P is a function of x_3 and t only. Also from Eq 1

$$e_{kk} = \frac{\sigma_{33} - 2\sigma_c}{3\lambda + 2\mu} + P/H \tag{15}$$

and from Eq 10

$$\frac{\partial e_{kk}}{\partial x_3} = \frac{1}{H}\frac{\partial P}{\partial x_3} \tag{16}$$

Taking derivatives with respect to x_3 of each term of Eq 14 and using Eq 16, one finds

$$k\frac{\partial^3 P}{\partial x_3^3} = \left[\frac{\alpha}{H} + \frac{1}{Q}\right]\frac{\partial^2 P}{\partial x_3 \partial t} \tag{17}$$

The initial ($t = 0$) condition for Eq 17 is obtained from Eq 2. When $t = 0$ the change in water content is zero and from Eq 2

$$P(x_3, 0) = P_o = \frac{R\sigma_c}{H} \tag{18}$$

Boundary conditions on the pore pressure are

$$P = 0 \text{ on } x_3 = h \text{ for } t > 0 \tag{19a}$$

$$\partial P / \partial x_3 = -rh/k \text{ on } x_3 = h \text{ for } t > 0 \tag{19b}$$

$$\partial P / \partial x_3 = 0 \text{ on } x_3 = 0 \text{ for } t > 0 \tag{19c}$$

Condition 19b is obtained from Darcy's law (Eq 7). That is, at the drained end the volume of fluid crossing unit area per unit time, V_i, can be considered the velocity of fluid relative to the velocity of the solid porous matrix (rh) or $V_3 = rh = -k\, \partial P / \partial x_3$.

The solution to Eq 17 satisfying the initial (Eq 18) and boundary conditions (Eq 19) is

$$P(x_3, t) = \frac{rh^2}{k}\left[\frac{1}{2}\left[1 - \frac{x_3^2}{h^2}\right] - \frac{2}{\pi^2}\sum_{n=1}^{\infty}\frac{[1 - (-1)^n \cos n\pi x_3/h]e^{-n^2\pi^2 Ct/h^2}}{n^2}\right]$$
$$- \frac{4P_o}{\pi}\sum_{n=1}^{\infty}\frac{(-1)^n e^{-(2n-1)^2\pi^2 Ct/4h^2}}{(2n-1)}\cos(2n-1)\frac{\pi x_3}{h} \tag{20}$$

where $C = kR$.

For $t = 0$, $P = P_o = R\sigma_c/H$. For large t, $P = rh^2(1 - x_3^2/h^2)/2k$—a final parabolic distribution of pore pressure which makes it impossible to obtain a fully drained condition in a drained constant strain-rate test. This effect is clearly shown in Fig. 2 where the dimensionless pore pressure kP/rh^2 is plotted for various dimensionless times, Ct/h^2, and positions x_3/h. Here, P_o, the initial pore pressure in the sample, is taken to be zero, as would be the case in an unconfined constant strain-rate test.

Figure 3 shows the spatial variation of pore pressure for various dimensionless times when

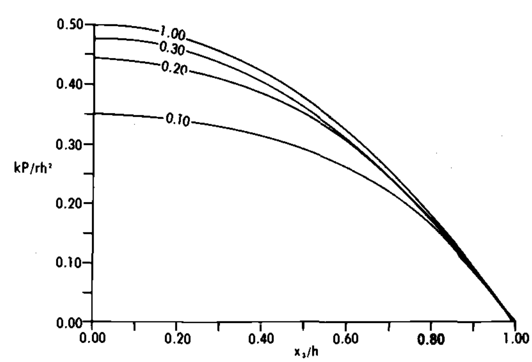

FIG. 2—*Variation of pore pressure with time and position for* $P_o = 0$. *Numbers on curves represent values of* Ct/h^2.

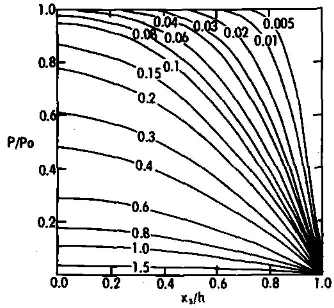

FIG. 3—*Variation of pore pressure with time and position for* $rh^2/k = 0$. *Numbers on curves represent values of* Ct/h^2.

rh^2/k vanishes and P_o is nonzero. This gives pore pressures for a consolidation process where axial strains vanish and radial stress is $-\sigma_c$. Note that pore pressures vanish in long time in this case.

The time variations of pore pressure at the closed end $x_3/h = 0$ are shown in Fig. 4 for various values of kP_o/rh^2 when rh^2/k and P_o are nonzero. From Eq 20 and Fig. 4, we see that pore pressure at the sealed end of the sample approaches, in long time, the final value $rh^2/2k$. Also, from Fig. 4 it can be seen that higher strain rates, lower permeabilities, or small initial pore pressures cause a continuous build-up of pore pressure at $x_3/h = 0$ to the long-term value. Conversely, lower strain rates, higher permeabilities, or large initial pore pressures lead to an initial additional pore pressure build-up at $x_3/h = 0$, followed by a slow decrease of pore pressure to the long-term value.

Axial displacements in the deforming test sample are (from Eq 13)

$$u_3 = \frac{\alpha}{3K}\left[\frac{rh^3}{k}\left[\frac{x_3}{6h}\left[1 - \frac{x_3^2}{h^2}\right] + \frac{2}{\pi^3}\sum_{n=1}^{\infty}\frac{(-1)^n}{n^3}e^{-n^2\pi^2Ct/h^2}\sin\frac{n\pi x_3}{h}\right]\right.$$
$$\left. + \frac{8P_o}{\pi^2}\sum_{n=1}^{\infty}(-1)^n\left[x_3\sin(2n-1)\pi/2 - h\sin(2n-1)\frac{\pi x_3}{2h}\right]e^{-(2n-1)^2\pi^2Ct/4h^2}\right] - rtz \quad (21)$$

For $t = 0$ axial displacements vanish and for large t axial displacements are given by the first and last terms on the right side of Eq 21.

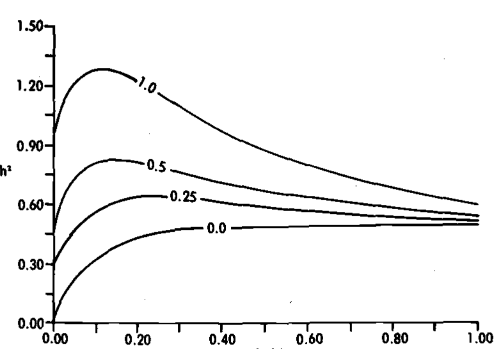

FIG. 4—*Variation of pore pressure at the closed end of a specimen* ($x_3/h = 0$) *in a singly drained constant strain-rate test. Numbers on curves represent values of* kP_o/rh^2.

Axial strains are given by

$$e_{33} = \frac{\alpha}{3K}\left[\frac{rh^2}{k}\left[\frac{1}{2}\left[\frac{1}{3} - \frac{x_3^2}{h_2}\right] + \frac{2}{\pi^2}\sum_{n=1}^{\infty}\frac{(-1)^n e^{-n^2\pi^2Ct/h^2}}{n^2}\cos\frac{n\pi x_3}{h}\right]\right.$$

$$+ \frac{8P_o}{\pi^2}\sum_{n=1}^{\infty}\frac{(-1)^n e^{-(2n-1)^2\pi^2Ct/4h^2}}{(2n-1)^2}$$

$$\left.\times \sin(2n-1)\pi/2 - \frac{4P_o}{\pi}\sum_{n=1}^{\infty}\frac{(-1)^n e^{-(2n-1)^2\pi^2Ct/4h^2}}{(2n-1)}\cos(2n-1)\frac{\pi x_3}{2h}\right] - rt \quad (22)$$

For $t = 0$, axial strains vanish and for large t axial strains are given by the first and last terms on the right side of Eq 22.

Total axial stresses, σ_{33}, are given by

$$\sigma_{33} = Ee_{33} - \frac{EP}{3H} - 2\upsilon\sigma_c = -\frac{\alpha E}{3K}\left[\frac{rh^2}{k}\left[\frac{1}{3} - \frac{2}{\pi^2}\sum_{n=1}^{\infty}\frac{e^{-n^2\pi^2Ct/h^2}}{n^2}\right]\right.$$

$$\left. - \frac{8P_o}{\pi^2}\sum_{n=1}^{\infty}\frac{(-1)^n e^{-(2n-1)^2\pi^2Ct/4h^2}}{(2n-1)^2}\sin(2n-1)\pi/2\right] - Ert - 2\upsilon\sigma_c \quad (23)$$

where E is Young's modulus and υ is Poisson's ratio. For $t = 0$, total axial stresses are given by

$$\sigma_{33} = -2\upsilon\sigma_c - \alpha(1 - 2\upsilon)P_o$$

For large t, total axial stresses reduce to

$$\sigma_{33} = \frac{\alpha(1 - 2\upsilon)}{3k}rh^2 - Ert - 2\upsilon\sigma_c$$

Equation 23 shows that total axial stress σ_{33} depends on time only. Hence, σ_{33} is unvarying with respect to position in the deforming sample. On the other hand, the effective axial stress is given by $\sigma_{33} = \sigma_{33} - \alpha P$, which clearly depends on position through $P(x_3, t)$. Note that effective axial stresses will alway be smallest near the undrained end ($x_3/h = 0$) where pore pressures are largest, and largest near the drained end where $P(h, t) = 0$. Finally, the volumetric strain (obtained from Eq 15) is

$$e_{kk} = -(1 - 2\upsilon)rt - \frac{2(1-2\upsilon)(1+\upsilon)\sigma_c}{E} + \frac{3\alpha(1-2\upsilon)}{E}\left[\frac{rh^2}{k}\left[\frac{1}{2}\left[1 - \frac{x_3^2}{h^2}\right]\right.\right.$$

$$\left. - \frac{2}{\pi^2}\sum_{n=1}^{\infty}\frac{[1 - (-1)^n \cos n\pi x_3/h]\, e^{-n^2\pi^2Ct/h^2}}{n^2}\right]$$

$$\left. - \frac{4P_o}{\pi}\sum_{n=1}^{\infty}\frac{(-1)^n e^{-(2n-1)^2\pi^2Ct/4h^2}}{(2n-1)}\cos(2n-1)\frac{\pi x_3}{h}\right]$$

$$- \frac{(1-2\upsilon)^2\alpha}{E}\left[\frac{rh^2}{k}\left[\frac{1}{3} - \frac{2}{\pi^2}\sum_{n=1}^{\infty}\frac{e^{-n^2\pi^2Ct/h^2}}{n^2}\right]\right.$$

$$\left. - \frac{8P_o}{\pi^2}\sum_{n=1}^{\infty}\frac{(-1)^n e^{-(2n-1)^2\pi^2Ct/4h^2}}{(2n-1)^2}\sin(2n-1)\pi/2\right] \quad (24)$$

For $t = 0$, the volumetric strain is given by

$$e_{kk} = \frac{2(1 - 2\upsilon)(1 + \upsilon)}{E} [\alpha P_o - \sigma_c]$$

and for large t, it is given by

$$e_{kk} = \frac{3\alpha(1 - 2\upsilon)}{2kE} rh^2[1 - x_3^2/h^2] - \frac{\alpha(1 - 2\upsilon)^2}{kE} rh^2 - (1 - 2\upsilon)rt - \frac{2(1 - 2\upsilon)(1 + \upsilon)\sigma_c}{E} \quad (25)$$

The first term on the right hand side of Eq 25 shows that a parabolic distribution of volumetric strain will persist at large time in the deformed sample. This a direct consequence of the final parabolic distribution of pore pressure (Eq 20) found earlier. This final strain distribution cannot be removed. However, if the strain rate or sample height is reduced or if Poisson's ratio is large, the effect can be reduced. This effect can also be minimized if permeability or Young's modulus is large.

Discussion

This theoretical study of pore-pressure distributions in drained constant strain-rate triaxial tests has been done to determine the conditions under which pore-pressure gradients in the deforming test sample are small. Such small gradients would yield reasonably uniform effective stresses in the deforming test sample. If effective stresses are uniform, and other problems, such as frictional end restraints, can be minimized, then reasonable effective-stress parameters can be obtained.

It has been determined from this and previous analyses of undrained triaxial constant strain-rate tests (see Refs *2* and *3*) that it is impossible to obtain a fully drained condition. In fact, in this test, the long-term spatial pore-pressure distribution becomes parabolic. Unless strain rates are sufficiently small or permeabilities are sufficiently large to minimize the effect of this parabolic pore-pressure distribution, effective stresses in the deforming sample cannot approach uniformity, and any property determinations based on the assumption of uniform effective stresses will be in error.

It is of interest that volumetric strains (Eq 24) will be largest near the undrained end of a sample drained at one end or largest in the middle of a sample drained at both ends. This strain distribution is a consequence of the parabolic pore-pressure distribution and suggests an explanation (apart from frictional end restraints) for any post-yield barreling observed in a drained triaxial test.

Acknowledgments

The writer thanks Harold W. Olsen, Robert L. Schiffman, and Henri S. Swolfs for thoughtful comments and suggestions.

References

[*1*] Biot, M. A., "General Theory of Three-Dimensional Consolidation," *Journal of Applied Physics,* Vol. 12, 1941, pp. 155–164.
[*2*] Gibson, R. B. and Henkel, D. J., "Influence of Duration of Tests at Constant Rate of Strain on Measured 'Drained' Strength," *Geotechnique,* Vol. 4, 1954, pp. 6–15.

[3] Bishop, A. W. and Henkel, P. J., *The Measurement of Soil Properties in the Triaxial Test,* 2nd ed., Edward Arnold, London, 1962.
[4] Gibson, R. E., "Analysis of System Flexibility and Its Effect on Time Lag in Pore Water Pressure Measurements," *Geotechnique,* Vol. 13, 1963, pp. 1–11.
[5] Schiffman, R. L., Chen, A. T-F., and Jordan, J. C., An Analysis of Consolidation Theories," *Journal of the Soil Mechanics and Foundations Division, Proceedings of the ASCE,* Vol. 95, No. SM1, 1969, pp. 285–312.
[6] Jaeger, J. C. and Cook, N. G. W., *Fundamentals of Rock Mechanics,* Methnen and Company Ltd., London, 1969, 513 p.
[7] Savage, W. Z., "A Model for Hydrostatic Consolidation of Pierre Shale," U.S. Geological Survey Open-File Report 82-1058, 1983, 21 p., 6 figs.
[8] Schiffman, R. L., "Finite and Infinitesinal Strain Consolidation," *Journal of the Geotechnical Engineering Division, Proceedings of the ASCE,* Vol. 106, No. GT2, 1980, pp. 203–207.
[9] Schiffman, R. L., Pane, V., and Gibson, R. E., "The Theory of One-Dimensional Consolidation of Saturated Clays; IV: An Overview of Nonlinear Finite Strain Sedimentation and Consolidation," in *Proceedings of the ASCE Symposium on Sedimentation and Consolidation Models; Predictions and Validations, San Francisco, California, October 1, 1984;* R. N. Yong and F. C. Townsend, Eds., ASCE, New York, 1985, pp. 1–29.
[10] Znidarcic, D., Croce, P., Pane, V., Ko, H. Y., Olsen, H. W., and Schiffman, R. L., The Theory of One Dimensional Consolidation of Saturated Days: III: Existing Testing Procedures and Analyses, *Geotechnical Testing Journal,* Vol. 7, No. 3, 1984, pp. 123–133.

John Anthony Little[1]

Pore Pressure Response of an Undisturbed and Reconstituted Anglian Till in Undrained Triaxial Compression

REFERENCE: Little, J. A., "**Pore Pressure Response of an Undisturbed and Reconstituted Anglian Till in Undrained Triaxial Compression,**" *Advanced Triaxial Testing of Soil and Rock, ASTM STP 977,* Robert T. Donaghe, Ronald C. Chaney, and Marshall L. Silver, Eds., American Society for Testing and Materials, Philadelphia, 1988, pp. 592–603.

ABSTRACT: Laboratory tests designed to expose fundamental mechanical behavior of very stiff, heavily overconsolidated soils can be difficult to interpret. Parallel testing of soil reconstituted from the matrix of the undisturbed soil therefore enables the observed behavior during testing to be assessed in a comparative way, and such effects as previous stress history, sampling, and soil fabric to be examined.

Undrained 38-mm-diameter triaxial compression testing of an Anglian till sampled undisturbed was carried out in conjunction with a soil reconstituted from its matrix. Analysis of pore pressure data showed that the critical state parameter A_{cs} gave good predictions of pore pressures generated in the normally and lightly overconsolidated specimens, but tended to overestimate pore pressure in the most heavily overconsolidated specimens. It is shown that this may be accounted for by the overconsolidated specimens not reaching ultimate failure at the critical state. Parry's (1958) method of presenting pore pressure data at failure is used to construct pore pressure paths for the tills during undrained compression.

KEY WORDS: till, overconsolidated soil, Pleistocene, pore pressure, undrained compression, critical state

Lodgement tills are soils formed within the basal traction zone of an ice sheet. The composition and texture of tills are extremely variable and will reflect both the nature of the original source material and the amount of particle comminution that has occurred over the distance of entrainment.

The growing bank of general engineering data reported in the literature relating to tills bears witness to the variability of these soils. Engineering parameters specific to the chalky Anglian tills found in the Vale of St. Albans, England, have been reported by Little [*1*] and Little and Atkinson [*2*]. This present paper describes the results of a series of conventional triaxial compression tests carried out on isotropically consolidated specimens of undisturbed Ware Till from the Vale of St. Albans and examines this natural till's pore pressure response during undrained loading.

The Vale of St. Albans lies very close to the southern limit of the inferred ice margin in the British Isles during the Anglian period [*3*]. The post-depositional history of the tills therein would therefore have been characterized by glacial overriding (inducing both consolidation and swelling), subsequent periglaciation, desiccation, carbonate cementation, and,

[1] Lecturer in soil mechanics, Department of Civil Engineering, Heriot-Watt University, Edinburgh, Scotland.

in part, decalcification. Because of these various factors, the interpretation of engineering tests designed to evaluate fundamental soil behavior becomes very difficult, and laboratory tests may usefully be carried out on soils that are reconstituted from the matrix of the undisturbed soil so as to facilitate analysis. The paper therefore also describes a parallel series of consolidated undrained triaxial tests carried out on a soil reconstituted from the screened matrix of the Ware Till so as to expose the combined but unknown effects of such things as sampling, soil fabric, previous stress history, freeze–thaw, and cementation.

Description of the Ware Till

Undisturbed and bulk samples of the till were obtained from Holwell Hyde quarry, Welwyn Garden City, approximately 25 miles (40 km) north of London. This locality lies within a part of the Vale of St. Albans associated with a pre-Anglian course of the proto-Thames. A detailed Pleistocene stratigraphy for the Vale of St. Albans has been described by Gibbard [*4*]. Generally, however, sedimentary sequences in the Vale are characterized by a lower (proto-Thames) fluviatile gravel (Westmill Lower Gravel) on chalk bedrock overlain by Ware Till. Above the till lie gravels of mainly glacial outwash origin (Westmill Upper Gravel) deposited on the proglacial fringe of the receding Ware Till ice front. Above this upper unit of gravel is occasionally seen a second lodgement till deposit referred to as Eastend Green Till by Gibbard and as Westmill Till by Cheshire[2].

In situ the Ware Till is a very dark (5Y 3/1)[3] stiff to very stiff and occasionally hard clay with fine, medium, and coarse (up to 100 mm), rounded to subrounded, fresh, white chalk clasts showing clearly marked glacial striations on their surfaces. Occasional angular fragments of medium to large flints are present. A derived Jurassic fauna is evident. A detailed description of the fabric of this till by Little [*1*] showed that whereas there was an identifiable clast fabric, there was relatively little fissuring, jointing, layering, or other fabric features normally recognized by engineers [*5,6*] and the occasional discontinuities found tended to reflect the structure of the underlying chalk.

The grading was approximately 10% by weight gravel, 10% sand, 40% silt, and 40% clay; in the gravel and sand sizes approximately 25% by weight was chalk. The mineralogy of the clay fraction determined by powder x-ray diffraction was approximately 20% illite, 10% Ca-montmorillonite, 10% kaolinite, and 60% amorphous iron and alumina hydrates. The Atterberg limits of the fraction passing a 0.425-mm sieve were LL = 40, PL = 18, and the natural water content of this fraction was 18%; thus, the liquidity index was zero. During determination of the grading and Atterberg limits, chalk clasts larger than about 0.5 mm were removed by hand before the residue was ground to avoid the inclusion of ground chalk in the finer fractions.

Laboratory Tests

A series of consolidated undrained triaxial tests was carried out on undisturbed and reconstituted specimens. The specimens were 76 mm in length and 38 mm in diameter, and the tests were carried out in commercially available triaxial testing equipment. The cells had internal axial load cells, electrical pore pressure transducers, and electrical axial and volumetric strain transducers. A diagrammatic layout of the equipment and instrumentation is shown in Fig. 1.

[2] D. A. Cheshire, Personal communication, 1985.
[3] Refers to hues in *Munsell Soil Color Charts* (1975 edition).

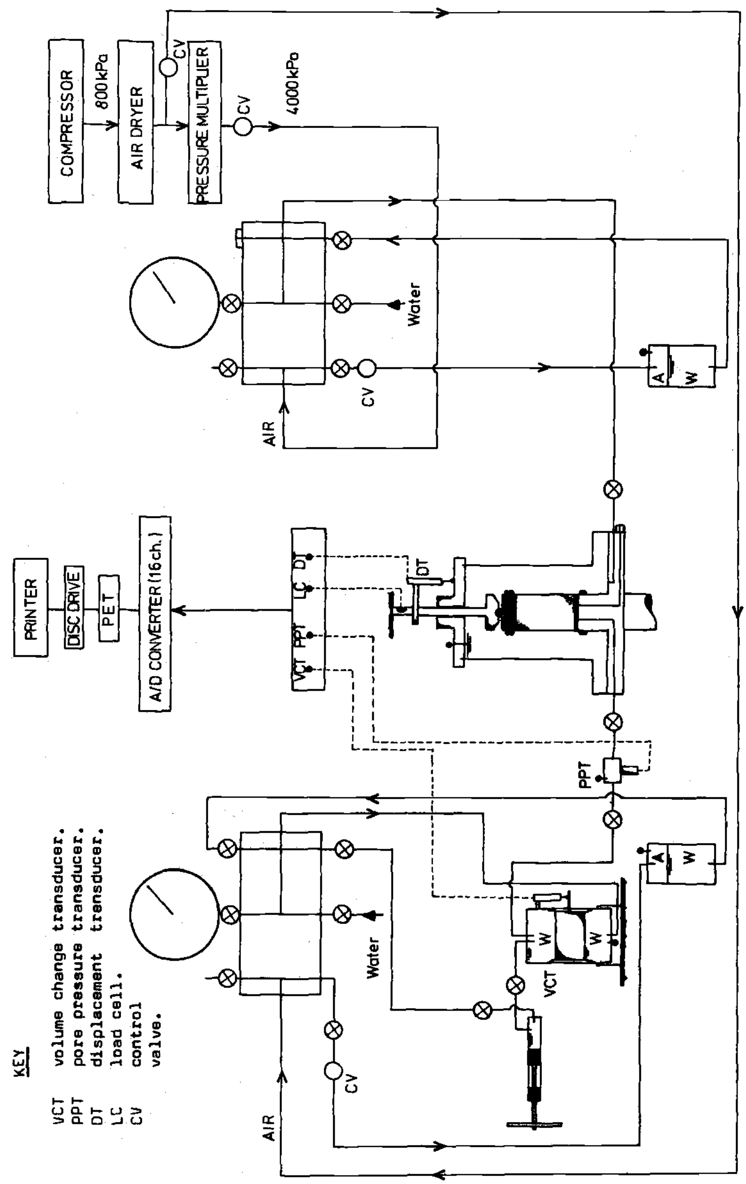

FIG. 1—*Layout of equipment and instrumentation.*

Undisturbed specimens of till were obtained by driving thin-walled 38-mm-diameter tubes vertically into soil freshly exposed in small trenches on the floor of the quarry. Specimens were extruded on site and carefully examined for flaws and signs of disturbance. By extruding all specimens from their sampling tubes while still on site and rejecting those that had been disturbed in the process of sampling, an important monitoring procedure was introduced at an early stage of the testing. All satisfactory specimens were wrapped in "clingfilm" (plastic wrap) placed in polyethylene bags, and, once in the laboratory, stored in a humidifier until required.

Reconstituted specimens were prepared by initially air drying a "crumbed" bulk sample of the till from which all chalk clasts had previously been removed by hand. The dried soil was then ground in a mortar with a rubber pestle before being transferred onto a 0.425-mm sieve. This screened fraction was then thoroughly mixed with distilled water to produce a homogeneous sample with a water content of 20%. At this stage the soil was wrapped in "clingfilm," bagged in polyethylene, placed in a humidifier, and allowed to equilibrate for about 48 hours. Cylindrical specimens of this soil were then produced by hand molding into a 38-mm-diameter tube, extruding, and cutting to length.

Both undisturbed and reconstituted till specimens were placed in the triaxial cells each with a saturated porous stone and with a slotted filter paper side drain. During initial isotropic consolidation of the till a back pressure acting through the pore fluid was applied incrementally to ensure saturation. Back pressure saturation techniques, which are now widely used in both consolidated undrained and consolidated drained tests have been described by several workers, and these have been summarized by Saada and Townsend [7]. The size of the pore pressure response during an undrained loading increment prior to isotropic consolidation is usually used to determine the degree of saturation of the specimen. This in turn can be used [8] to estimate the level of back pressure required to attain a desired degree of saturation. While the reconstituted soil examined in this way could be satisfactorily fully saturated with a back pressure of 200 kPa, the undisturbed soil required much larger pressures (this despite a theoretical degree of saturation = 0.94 calculated using measured values for the soil's natural water content, particle specific gravity, and bulk unit weight). In fact, with some of the undisturbed specimens satisfactory levels of saturation ($B \geq 0.95$; $B = \Delta u/\Delta\sigma_r$) were only achieved after a back pressure of 750 kPa was in operation. Similarly high back pressures (690 kPa) to ensure saturation greater than 95% have been reported by Soliman [9] for Sterling Till in Wisconsin.

The reconstituted and undisturbed specimens were then isotropically consolidated and overconsolidated to initial effective stresses in the range of 50 kPa to 1600 kPa producing a suite of soils with overconsolidation ratios in the range of 1 to 32. Shearing of the sample was carried out at nominal rates of axial strain of 0.06% per hour. While this rate of loading is slower than is normal for undrained tests, it was chosen to avoid the high rates of change of deviator stress that occur at the start of the test.

Analysis of Pore Pressure Data from the Tests

The response of the pore water pressure Δu to undrained compression may be expressed in terms of the two empirical parameters A and B [10,11] according to the equation:

$$\Delta u = B[\Delta\sigma_a + A(\Delta\sigma_a - \Delta\sigma_r)] \tag{1}$$

where σ_a, σ_r are the total axial and radial stresses acting on the boundary of the soil specimen.

Usually, the value of the pore pressure parameter at failure, A_f, is quoted (this corresponds to the observed pore pressure at maximum deviator stress), and a special interest has been

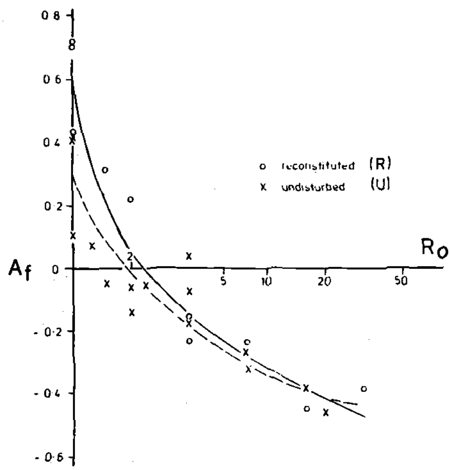

FIG. 2—*Pore pressure parameter* A_f *versus overconsolidation ratio.*

shown in the variation of A_f with overconsolidation ratio. Bishop and Henkel [*12*] quote values for A_f varying from $+1.3$ for normally consolidated undisturbed marine clay to -0.62 for undisturbed Weald (a region in southeastern England) clay; remolded Weald clay with an overconsolidation ratio $(R_o) = 8$ has $A_f = -0.22$, for example.

Values for A_f have been calculated from the pore pressure data for the reconstituted and undisturbed till, and these are shown plotted against overconsolidation ratio in Fig. 2. From this figure it can be seen that A_f varies from $+0.710$ at $R_o = 1$ to $A_f = -0.385$ at $R_o = 32$ (but note $A_f = -0.449$ at $R_o = 16$), for the reconstituted soil, while over the range of overconsolidation ratios $R_o = 1$ to 20 for the undisturbed soil A_f varies from $+0.423$ to -0.406.

Wroth [*13*] proposed an alternative pore pressure parameter, $A_{c.s}$, which is evaluated on the basis that the soil fails at the critical state:

$$A_{c.s} = \frac{1}{M}\left[\left(\frac{R_o}{r}\right)^{-\Lambda} + \frac{M}{3} - 1\right] \tag{2}$$

where

M = critical state frictional constant
Λ = $(\lambda - \kappa)/\lambda$,$(\lambda, \kappa$ are the slopes of the normal consolidation, swelling lines for the soil)
r = a parameter related to the spacing of the normal consolidation and critical state lines for the soil

At very large overconsolidation ratios the value of the term $(R_o/r)^{-\Lambda}$ becomes very small and, approximately,

$$A_{c.s} \rightarrow \left(\frac{1}{3} - \frac{1}{M}\right) \tag{3}$$

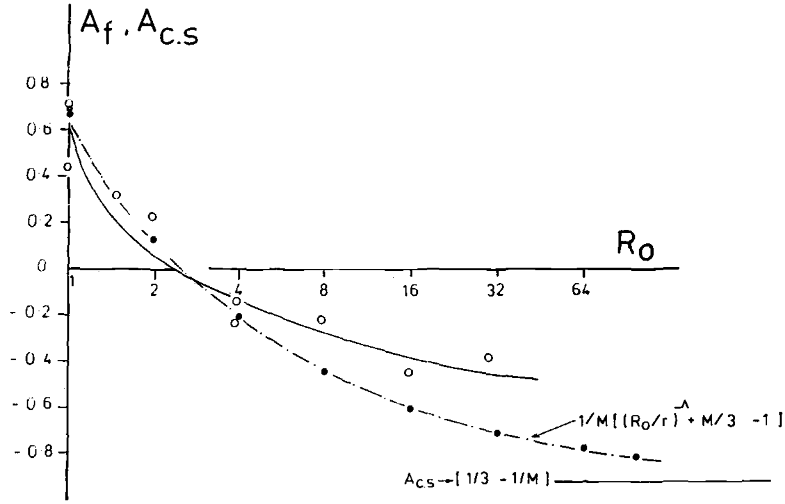

FIG. 3—*Pore pressure parameters* A_f, $A_{c.s}$ *versus overconsolidation ratio, reconstituted till.*

Values for $A_{c.s}$ calculated for the reconstituted and undisturbed tills are shown in Figs. 3 and 4; these are shown plotted against the corresponding overconsolidation ratio. Also included in these figures are the values for A_f from Fig. 2. It can be seen that the closest correspondence between A_f and $A_{c.s}$ exists between the normally consolidated and lightly overconsolidated samples. The reason why $A_{c.s}$ overpredicts the size of the (negative) pore pressures produced in the most heavily overconsolidated specimens at failure may be appreciated by examining the stress paths for the soil during compression.

Atkinson and Bransby [14] presented a method for normalizing stress paths based on a constant $p'(= \frac{1}{3}(\sigma_a' + 2\sigma_r'))$ section whereby a reference section of the state boundary surface for the soil at $p' = 1$ kPa is selected so that on this section the soil specific volume $V = V_o$ for the normal consolidation line and $V = \Gamma$ for the critical state line. Values for

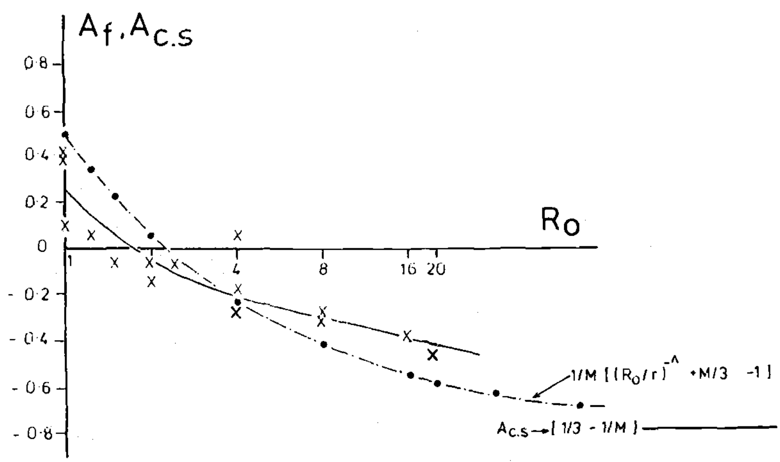

FIG. 4—*Pore pressure parameters* A_f, $A_{c.s}$ *versus overconsolidation ratio, undisturbed till.*

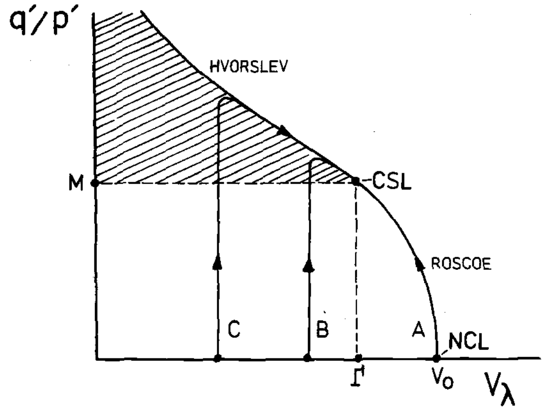

FIG. 5—*The reference section in* q'/p' : V_λ *space.*

specific volume V_λ on the reference section may be found from

$$V_\lambda = V + \lambda \ln p' \tag{4}$$

By plotting the deviator stress scaled in the ratio $1/p'$ against the corresponding V_λ the nature of the two sections of the state boundary surface are exposed (see Fig. 5). Therefore, all points on the critical state line (CSL) have $q'/p' = M(q' = (\sigma_a - \sigma_r))$ and all points on the normal consolidation line (NCL) have $q'/p' = 0$. Hence, all normally consolidated specimens (A) originate at $V_\lambda = V_o$, $q'/p' = 0$ and move along the Roscoe [*14*] surface to the critical state line whence $V_\lambda = \Gamma$, $q'/p' = M$. The more heavily overconsolidated samples (B,C) will have $V_\lambda < \Gamma$ and will be capable of sustaining $q'/p' > M$ (shaded portion) before reaching the Hvorslev [*14*] surface and proceeding down it toward the critical state line. Predictions of soil behavior for overconsolidated specimens on the Hvorslev surface may be obtained from an expression of the type shown in Eq 5 [*14*]:

$$q' = (M - h) \exp\left(\frac{\Gamma - V}{\lambda}\right) + hp' \tag{5}$$

where

h is a soil constant defining the Hvorslev surface

Figure 6 shows the relationship between V_λ and q'/p' for the reconstituted soil. The general pattern of behavior shown in this figure is consistent with that idealized in Fig. 5; stress paths for the normally consolidated specimens define a Roscoe state boundary surface for the soil, reaching ultimate failure at the critical state, while stress paths for the most heavily overconsolidated till extend into the region where $q'/p' > M$. Significantly, test paths for the most heavily overconsolidated specimens, although approaching the Hvorslev surface shortly after the maximum value for the principal effective stress ratio (σ_a'/σ_r') was attained, did not apparently reach ultimate failure at the critical state. Similar observations were made for the most heavily overconsolidated specimens of the undisturbed till (see Fig. 7; in this figure data for the reconstituted and undisturbed soils may be compared directly because the two reference sections have been matched at the point $V_\lambda = V_o$ for the reconstituted soil. It can be concluded therefore that the most heavily overconsolidated specimens of Ware Till failed in undrained compression furthest away from the critical state line, and

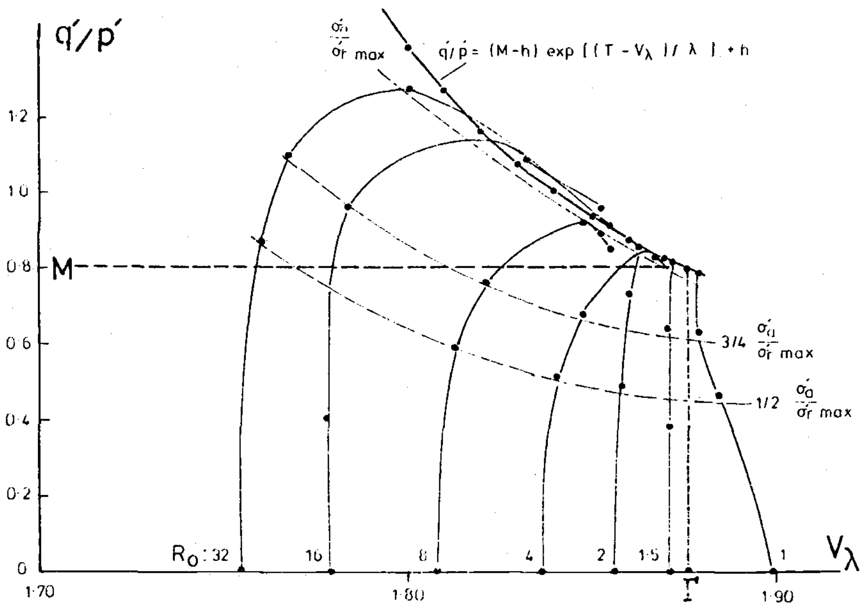

FIG. 6—*The reference section: reconstituted till.*

that predictions of undrained strength assuming ultimate failure at the critical state, should also be overestimated.

Parry [15] examined the rate and relative sign of the excess pore pressures generated during the undrained compression of London Clay and used these findings to infer the directions in which both normally consolidated and overconsolidated specimens were moving at failure. By plotting the rate of pore pressure change at failure

$$\left(\left(\frac{\Delta u}{p'}\right)\Big/\Delta\epsilon_s\right)_f$$

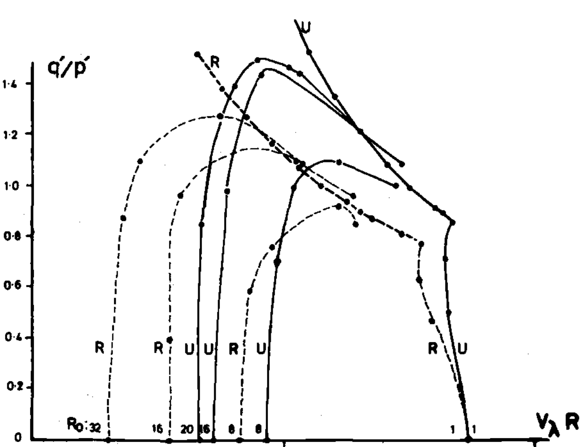

FIG. 7—*Reference sections for the reconstituted* (R) *and undisturbed* (U) *till matched at* $V_\lambda = V_o$ *for the reconstituted till.*

where

Δ = a large increment of . . .
ϵ_s = axial strain
f = at failure

against p_u'/p_f' for his tests, Parry was able to demonstrate that this rate of change was largest for those specimens failing (at p_f') furthest away from the critical state line (where the equivalent pressure = p_u'). In addition, the sign of the pore pressure change was such so as to move the specimen toward the critical state line. A more detailed interpretation of these results and their significance has been presented elsewhere [*14,16*].

A similar approach has been adopted for the pore pressure data from the tests on the Ware Till. Here, however, the rate of pore pressure change throughout each test

$$\left(\frac{\delta u}{\delta p'}\right) \Big/ \delta\epsilon_s$$

has been evaluated and plotted against p_u'/p'. Here, $\delta p'$ is the small increment in effective average pressure over the corresponding shear strain increment $\delta\epsilon_s$ in which the pore pressure increment δu is recorded. In this way, the complete pore pressure paths for the normally consolidated and overconsolidated specimens can be examined over the entire range of axial compression.

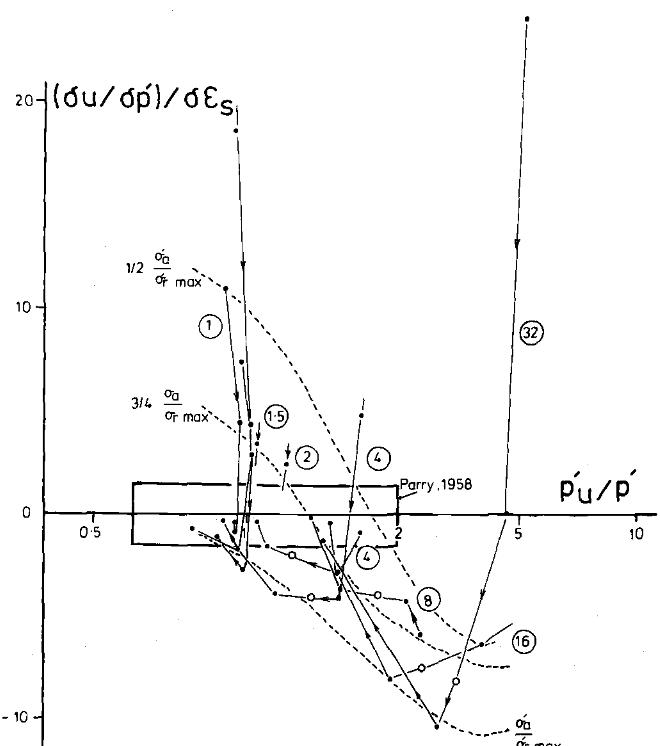

FIG. 8—*Rates of pore pressure change, reconstituted till.*

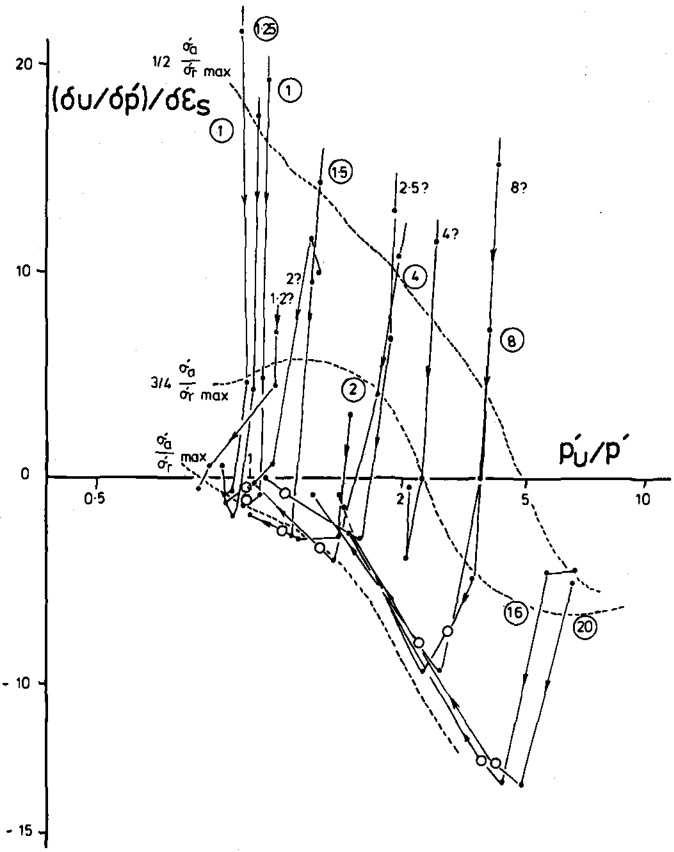

FIG. 9—*Rates of pore pressure change, undisturbed till.*

These results are presented in Figs. 8 and 9. Values for the overconsolidation ratios are shown (circled) against each pore pressure path; the estimated overconsolidation ratios for undisturbed tills isotropically consolidated and then overconsolidated to $p' < p_c'$ (p_c', the preconsolidation pressure for the Ware Till, has been estimated at ≈ 2000 kPa, [1]) are shown uncircled. The extent of Parry's data for the London Clay is also shown in Fig. 8.

Both reconstituted and undisturbed normally consolidated specimens showed reducing rates of positive pore pressure change over a narrow band either side of $p_u'/p' = 1.0$. Normally consolidated samples approached the critical state from within the top left-hand quadrant of the graph. With increasing overconsolidation ratio, the positions of the pore pressure paths shift further into the top right-hand quadrant to increasing positive values for the ratio p_u'/p'. This is entirely consistent with the expectation that overconsolidated soils should approach the critical state line during undrained compression with reducing pore pressures and therefore increasing effective stresses. Within each set of paths (reconstituted, undisturbed), increasing overconsolidation ratios are associated with larger negative values for the ratio $(\delta u/\delta p')/\delta\epsilon_s$. However, the undisturbed specimens showed larger negative rates of change. The minimum value of this ratio for the reconstituted till was -10.0 at $R_o = 32$; for the undisturbed till it was already -14.5 at $R_o = 20$. Comparing behavior at similar overconsolidation ratios also suggests that these minima occurred further away from the critical state line in the undisturbed soil. Compare, for example, the value of $p_u'/p' = 4.2$ for the undisturbed specimen, $R_o = 16$ with $p_u'/p' = 1.9$ for the reconstituted specimen with the same overconsolidation ratio at the points on their paths corresponding to the maximum rate of pore pressure reduction. The positions on each of these paths where the pore pressures first became negative (relative to the initial equilibrium pore pressure) are also indicated (by open circles). These show that negative pore pressures only occurred in the reconstituted tills when $R_o \geqslant 4.0$; however a negative pore pressure was recorded in the undisturbed till with $R_o = 1.5$. It is of interest to note that an extrapolation of these points produces an intersection of the p_u'/p' axis for both the reconstituted and the undisturbed till at small positive values, generally within the region where the pore pressure paths for the lightly overconsolidated specimens first traverse it.

Finally, the superimposition of the principal effective stress ratio contours at the arbitrary intervals $\times \frac{1}{2}$, $\times \frac{3}{4}$, $\times 1(\sigma_a'/\sigma_r')_{max}$ shows a similar contouring for the reconstituted and undisturbed till. These contours trace continuous lines across the mapped region over the entire range of overconsolidation ratios examined. The contour representing the maximum value for (σ_a'/σ_r') appears particularly significant in this respect: it apparently defines a surface beyond which the samples do not move, and along which the overconsolidated soils approach the critical state. The direction of movement of these paths parallel to this stress ratio contour in opposite directions either side of the vertical through $p_u'/p' = 1.0$ is, of course, a manifestation of the same effect observed by Parry [*15*].

Conclusions

1. A laboratory examination of the fundamental mechanical behavior of a stiff, overconsolidated, possibly cemented, natural till in undrained compression became more meaningful when a control sample of the soil was reconstituted from the natural soil's matrix and then tested in an identical manner.

2. The method of applying a back pressure through the pore fluid of the undisturbed till to ensure its saturation necessitated surprisingly large (750 kPa) pressures; saturated samples of the reconstituted till could be produced using back pressures of 200 kPa.

3. Values for the pore pressure parameter A_f showed a pattern consistent with expectations (that is, reducing A_f with increasing R_o). Predictions of pore pressures at ultimate failure using the equivalent critical state parameter $A_{c.s}$, while showing good agreement with A_f for the normally and lightly overconsolidated till, overestimated the size of the negative pore pressure response at the largest overconsolidation ratios.

4. An examination of $V_\lambda : q'/p'$ normalized stress paths for the reconstituted and undisturbed till showed that while the normally consolidated specimens reached ultimate failure at the critical state, the most heavily overconsolidated specimens apparently did not. It is not surprising, therefore, that overestimates of ultimate pore pressures made for these specimens on the assumption that the soil reaches ultimate failure at the critical state should result.

5. An examination of the measured rates of pore pressure change occurring during the undrained compression of the till indicated that the overconsolidated specimens were moving toward the critical state line at rates corresponding to their distance from it at failure. Testing that is carried out slowly enough will permit the plotting of complete pore pressure paths on which may be superimposed contours of the principal effective stress ratio $(\sigma_a'/\sigma_r')_{max}$ or any proportion of it.

References

[1] Little, J. A., "Engineering Properties of Glacial Tills in the Vale of St. Albans," Ph.D. thesis, The City University, London, England, 1984.

[2] Little, J. A. and Atkinson, J. H., "Some Engineering Properties of Anglian Tills in the Vale of St. Albans," *Proceedings of the International Conference on Construction in Areas of Glacial Tills,* Edinburgh, 1985, pp. 213–218.

[3] Bowen, D. Q., *Quaternary Geology: A Stratigraphic Framework for Multidisciplinary Work,* Pergamon Press, Oxford, 1981.

[4] Gibbard, P. L., *Phil. Trans. Royal Soc. London,* Vol. 280 (B975), 1977, pp. 445–483.

[5] McGown, A., Marsland, A., Radwan A. M., and Gabr, A. W. A., *Geotechnique,* Vol. 30, No. 4, 1980, pp. 417–447.

[6] Marsland, A., Prince, A., and Love, M. A., "The Role of Soil Fabric Studies in the Evaluation of the Engineering Parameters of Offshore Structures," *Proceedings of the International Conference on the Behavior of Offshore Structures,* Houston, June 1972.

[7] Saada, A. S. and Townsend, F. C., "State of the Art: Laboratory Strength Testing of Soils" in *Laboratory Shear Strength of Soil, ASTM STP 740,* R. N. Yong and F. C. Townsend, Eds., American Society for Testing and Materials, Philadelphia, 1981, pp. 7–77.

[8] Lowe, J. and Johnson, T. C., "Use of Back Pressure to Increase Degree of Saturation of Triaxial Test Specimens," *Proceedings of the American Society of Civil Engineers, Research Conference on Shear Strength of Cohesive Soils,* Boulder, Colorado, June 1960, pp. 819–836.

[9] Soliman, N., "Effect of Geologic History on the Design Parameters of Heavily Overconsolidated Till" in *Geological Environments and Soil Properties,* R. N. Yong, Ed., Special Publication of the American Society of Civil Engineers, Geotechnical Engineering Division, 1983.

[10] Skempton, A. W., *Geotechnique,* Vol. 4, 1964, pp. 77–101.

[11] Bishop, A. W., *Geotechnique,* Vol. 4, 1964, pp. 148–152.

[12] Bishop, A. W. and Henkel, D. J., *The Measurement of Soil Properties in the Triaxial Test,* Arnold, London, 1976.

[13] Wroth, C. P., "Critical State Soil Mechanics," lecture notes from a short course held at the Department of Engineering Science, University of Oxford, England, 28 Sept.–2 Oct., 1981.

[14] Atkinson, J. H. and Bransby, P. L., *The Mechanics of Soils,* McGraw-Hill, London, 1978.

[15] Parry, R. H. G., *Geotechnique,* Vol. 8, 1958, pp. 183–186.

[16] Schofield, A. N. and Wroth, C. P., *Critical State Soil Mechanics,* McGraw-Hill, London, 1968.

John F. Peters,[1] *Poul V. Lade,*[2] *and Anders Bro*[3]

Shear Band Formation in Triaxial and Plane Strain Tests

REFERENCE: Peters, J. F., Lade, P. V., and Bro, A., "**Shear Band Formation in Triaxial and Plane Strain Tests,**" *Advanced Triaxial Testing of Soil and Rock, ASTM STP 977,* Robert T. Donaghe, Ronald C. Chaney, and Marshall L. Silver, Eds., American Society for Testing and Materials, Philadelphia, 1988, pp. 604–627.

ABSTRACT: This paper presents the results of a combined theoretical and laboratory study of the formation of shear bands in triaxial compression, triaxial extension, and plane strain compression. The principal finding is that shear bands are initiated more easily under plane strain than under axially symmetric conditions of the triaxial test. The triaxial compression test is most resistant to shear banding, although the theory tends to overestimate the stability of this test. The lack of agreement between the theory and experiment requires a reassessment of the suitability of isotropic hardening laws even for monotonic loading.

KEY WORDS: triaxial test, plane strain test, instability, shear banding, bifurcation, failure

The phenomenon of shear banding is an important element in understanding the failure mechanisms of soil. The formation of shear bands in triaxial specimens is a common occurrence generally assumed to be associated with failure of the specimen. It is now understood that the formation of shear bands does not necessarily coincide with the peak of the stress–strain curve, and the tendency for shear banding may not be the same for all test configurations [*1,2*]. The recent availability of test devices capable of applying rather arbitrary stress paths requires particular attention to shear banding because comparisons of stress–strain response measured in different tests may be obscured by the device-dependent potential for shear band formation.

The problem is illustrated in Fig. 1 which shows the ideal stress–strain response of a soil and its relationship to the observed load deformation curve. It is assumed that the response for simple monotonic loading can be expressed in the form

$$f(\text{stress}) = g(\text{strain}) \tag{1}$$

so that the unique relationship describes the behavior for all stress states. Equation 1 may, for example, describe an elastoplastic model where f describes the shape of the yield surface and g describes the strain hardening. Thus, if the specimen deforms uniformly without formation of shear bands the stress–strain response shown by the solid line in Fig. 1 will be obtained. However, if shear banding occurs, the load-carrying capacity of the specimen will

[1] Research civil engineer, Geotechnical Laboratory (GL), U.S. Army Engineer Waterways Experiment Station (USAE WES), Vicksburg, MS 39180.

[2] Professor, Department of Civil Engineering, School of Engineering and Applied Science, University of California, Los Angeles, CA 90024.

[3] Graduate student, Civil Engineering Department, University of California, Berkeley, CA 94720.

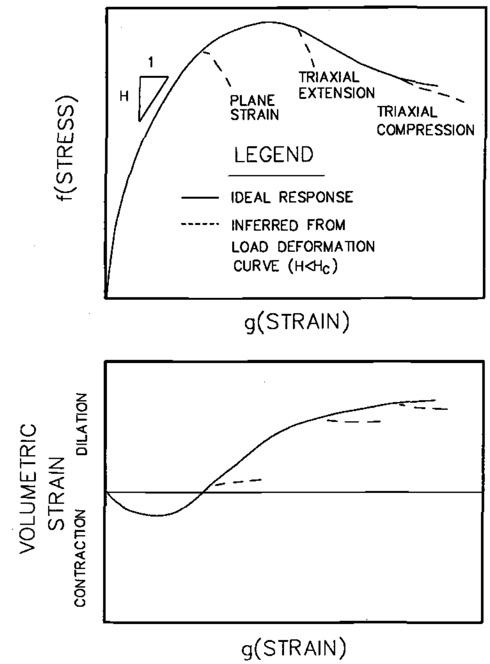

FIG. 1—*Relationship between stress–strain curve and observed load displacement.*

be reached rapidly, and the apparent stress–strain response depicted by the dashed line in Fig. 1 will be obtained. The important point to be made here is that the conditions for shear band formation depend on stress conditions and may occur at different points on the stress–strain curve depending on the test configuration. Therefore, while the stress–strain response can be expressed in a form that is independent of stress state (Eq 1), the load-deformation curve actually observed in the test is strongly dependent on stress conditions. To illustrate the problem, the impact of shear banding on sand behavior will be compared for triaxial compression, triaxial extension, and plane strain compression tests.

Theoretical Background

Formation of shear bands can be addressed theoretically by assuming that the physical appearance of the bands in a material is associated with a bifurcation in the solution of the corresponding boundary-value problem [*1–5*]. For example, an analysis of a plane strain test specimen with ideal boundary conditions should yield, as a solution, linearly varying displacements which correspond to uniform strain throughout the specimen (referred to as the trivial solution). Shear banding can occur when a second solution can be found that satisfies all equations of equilibrium and compatibility and gives rise to a displacement field that concentrates strains about a discrete surface. The existence of the second nontrivial solution is governed by the constitutive relationships.

To provide a basis to interpret the experimental results a computation was performed relating the stress–strain response to the critical condition for shear band formation. The computation to determine the critical condition where shear banding can occur has been well documented [*1–5*] with a particularly lucid account being presented by Vermeer [*5*]. The analysis that follows is similar to that presented by Molenkamp [*4*] except that terms related to the extra stress increments in the shear band that arise from rigid body rotations have been ignored. The result, which for plane strain conditions is identical to Vermeer's, has the advantage that the critical condition for shear banding can be expressed as explicit formulas for generalized stress conditions.

Critical Shear Band Condition

The condition associated with shear banding is shown in Fig. 2. The coordinate system x_1-x_2-x_3 is aligned such that the x_1 axis is parallel to the shear band, the x_2 axis is perpendicular to the shear band, and x_3 lies within the plane of the shear band but is perpendicular to the plane of sliding. It can be shown that x_3 corresponds to a principal stress direction [*1*] and, for the cases considered here, x_3 corresponds to the direction of the intermediate principal stress. Therefore, the x_1-x_2-x_3 direction can be related to the principal stress direction x-y-z by the angle θ. The increments of displacement due to shearing along the band are denoted, respectively, u_1, u_2, and u_3. The kinematic condition for shear banding can be expressed in terms of the incremental displacement gradients as follows [*1,2,4*]:

$$
\begin{aligned}
\frac{\partial u_1}{\partial x_2} &= g_1(x_2) \\
\frac{\partial u_2}{\partial x_2} &= g_2(x_2) \\
\frac{\partial u_1}{\partial x_1} &= 0 \\
\frac{\partial u_2}{\partial x_1} &= 0
\end{aligned}
\tag{2}
$$

where g_1 and g_2 are arbitrary functions that depend only on x_2. These relationships define the condition whereby all displacement gradients occur across the band (x_2-direction). Sep-

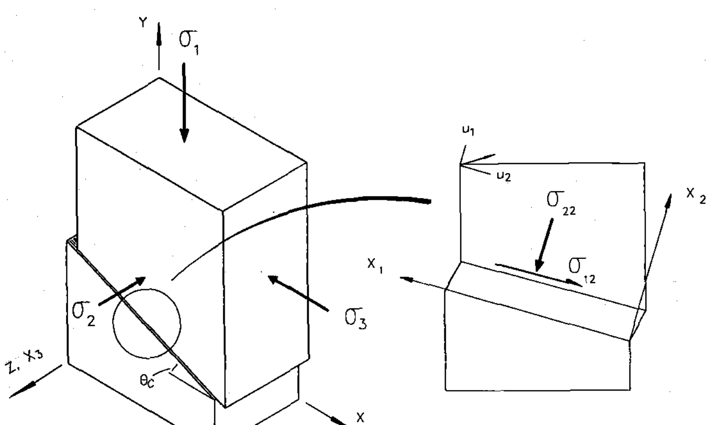

FIG. 2—*Conditions for shear banding.*

aration may occur as a result of dilation of the soil within the band, but there is no stretching along the band (x_1- and x_3-directions).

In addition to the kinematic conditions, equilibrium must be maintained as localization occurs. The stress change inside the band must be restricted as follows:

$$\begin{aligned} \Delta\sigma_{22} &= 0 \\ \Delta\sigma_{12} &= 0 \\ \Delta\sigma_{23} &= 0 \end{aligned} \qquad (3)$$

The change in stress within the band is related to the gradients in Eq 2 through an incremental constitutive relationship. For an elastoplastic material the quantities are related by the following:

$$\Delta\epsilon_{ij} = \left(C^e_{ijkl} + \frac{1}{H} Q_{kl} P_{ij}\right) \Delta\sigma_{kl} \qquad (4)$$

where

$\Delta\epsilon_{ij} = \dfrac{1}{2}\left(\dfrac{\partial u_i}{\partial x_j} + \dfrac{\partial u_j}{\partial x_i}\right)$

C^e_{ijkl} = elastic constants

H = plastic hardening modulus

Q_{ij} = direction of yield surface normal

= $\partial f/\partial\sigma_{ij}/(\partial f/\partial\sigma_{ij}\,\partial f/\partial\sigma_{ij})^{1/2}$

P_{ij} = direction of plastic strain increment

The directions Q_{ij} and P_{ij} are normalized such that $Q_{ij}Q_{ij} = 1$ and $P_{ij}P_{ij} = 1$. The direction P_{ij} is generally related to a plastic potential surface analogous to the relationship between Q_{ij} and the yield surface; for the analysis that follows, a plastic potential is not required.

Assuming an isotropic strain hardening model in which the yield surface expands in response to the total plastic strain, $d\bar{\epsilon} = (d\epsilon^p_{ij} d\epsilon^p_{ij})^{1/2}$, then the plastic hardening modulus can be defined as

$$H = \partial g/\partial\bar{\epsilon}/(\partial f/\partial\sigma_{ij}\,\partial f/\partial\sigma_{ij})^{1/2} \qquad (5)$$

By combining Eq 2, Eq 3, and Eq 4, the following relationship can be extracted for the nonzero stress increments:

$$\begin{aligned} C^{ep}_{1111}\,\Delta\sigma_{11} + C^{ep}_{1133}\,\Delta\sigma_{33} &= 0 \\ C^{ep}_{3311}\,\Delta\sigma_{11} + C^{ep}_{3333}\,\Delta\sigma_{33} &= 0 \end{aligned} \qquad (6)$$

where the coefficients C^{ep}_{ijkl} are the terms inside the parentheses in Eq 4. Equation 6 has a nontrivial (nonzero) solution for the stress increments only if the elastoplastic coefficients satisfy the following:

$$C^{ep}_{1111}\,C^{ep}_{3333} - C^{ep}_{1133}\,C^{ep}_{3311} = 0 \qquad (7)$$

Equation 7 can be solved for H which corresponds to the critical value of plastic hardening for which localization is possible. For an isotropic material, the critical value, H_c, is given by

$$H_c/E = -\frac{1}{1-\nu^2}(P_{33}Q_{33} + P_{11}Q_{11}) - \frac{\nu}{1-\nu^2}(P_{11}Q_{33} + P_{33}Q_{11}) \tag{8}$$

where E is the elastic Young modulus and ν is the elastic Poission ratio. The values of P_{11} and Q_{11} can be related to the principal values by the following transformation:

$$\begin{aligned} P_{11} &= P_n + P_d \cos 2\theta \\ Q_{11} &= Q_n + Q_d \cos 2\theta \end{aligned} \tag{9}$$

where

$$\begin{aligned} P_n &= \frac{1}{2}(P_1 + P_3) \\ P_d &= \frac{1}{2}(P_1 - P_3) \\ Q_n &= \frac{1}{2}(Q_1 + Q_3) \\ Q_d &= \frac{1}{2}(Q_1 - Q_3) \end{aligned}$$

and the subscripts 1 and 3 refer to the values in the directions of the major and minor principal stress, respectively. Equations 8 and 9 lead to a quadratic equation for cos2θ which has real solutions only if $H \leq H_c$. The value for $\cos 2\theta_c$ corresponding to H_c is the value that maximizes H_c in Eq 8 and thus can be readily determined as

$$\cos 2\theta_c = -\frac{1}{2}\left[\frac{Q_n + \nu\, Q_{33}}{Q_d} + \frac{P_n + \nu\, P_{33}}{P_d}\right] \tag{10}$$

Equations 9 and 10 define a necessary condition for which strains localize into distinct bands; their actual formation depends on the specific boundary conditions found in the test. Further, Eq 10 defines the orientation of the shear bands provided they form at the earliest possible instant in the test. If their formation is delayed and H falls below H_c, two orientations are possible. At the peak stress when $H = 0$, these two directions correspond to the plane of maximum obliquity (Coulomb direction) and direction of zero extension as predicted for a rigid plastic material.

Constitutive Model

The condition for shear banding is completely determined by P_{ij}, Q_{ij}, and ν. The critical modulus is a computed quantity, and E is needed only to relate H_c to experimental behavior. Both P_{ij} and ν can be measured directly by experiment, and the conditions of axisymmetry in the triaxial tests and the zero intermediate strain direction in the plain strain test limit the possible forms of P_{ij} and Q_{ij}. The possible constitutive response is further limited by the loading criterion which dictates $d\sigma_{ij}Q_{ij} \geq 0$. Therefore, a relatively simple constitutive law can be used as a basis to compare theory with experiment. Each experimental configuration will be treated as a separate case described by its own constitutive law. The constitutive relationship for each case has the following features in common which are believed to encompass a large number of constitutive models proposed in recent years:

1. The shear resistance should be proportional to the normal stress. Thus a Mohr-Coulomb yield law was used which can be written as

$$\sigma_1/\sigma_3 - g(\bar{\epsilon}) = 0 \tag{11}$$

where σ_1 and σ_3 are the maximum and minimum principal stresses (assumed to be compressive). Note that the function f defined previously is equal to the effective stress ratio σ_1/σ_3.

2. The volume change rate of the soil should be coupled to the shear strain rate by a function proportional to the effective stress ratio. Rowe's stress–dilatancy relationship [6] is suitable for this purpose because the analysis is restricted to the triaxial compression, extension, and plane strain tests. Rowe's relationship, which couples the rate of plastic volumetric strain, $d\epsilon_v^p/d\epsilon_1^p$ to the effective stress ratio, can be applied to each test configuration as follows:

$$\sigma_1/\sigma_3 = K(1 - d\epsilon_v^p/d\epsilon_1^p) \qquad \text{(triaxial and plane strain compression)} \tag{12a}$$

$$\sigma_1/\sigma_3 = K/(1 - d\epsilon_v^p/d\epsilon_3^p) \qquad \text{(triaxial extension)} \tag{12b}$$

where the major compressive stress and strain rates for the extension test, denoted by subscript 1, correspond to the radial direction. The parameter, K, is not necessarily the same for all test configurations but can be computed from experimental measurements for any point in the test using Eq 12a or Eq 12b.

The principal values of P_{ij} are given for each case in Table 1.

In Table 1 $R = \sigma_1/\sigma_3$. The relationships for Q_i can be obtained from Table 1 by replacing K with 1. The hardening modulus, H, is defined for each test configuration as follows:

Triaxial compression:

$$H = \frac{\sigma_3}{(4 + 2R^2)^{1/2}} \frac{\left|\dfrac{dR}{d\epsilon_1^p}\right|}{\left(1 + \dfrac{1}{2}(R/K)^2\right)^{1/2}} \tag{13a}$$

TABLE 1—*Relative components of principal plastic strain increments.*

Test Configuration	P_1	P_2	P_3
Triaxial compression	$\dfrac{2K}{(4K^2 + 2R^2)^{1/2}}$	$\dfrac{-R}{(4K^2 + 2R^2)^{1/2}}$	$\dfrac{-R}{(4K^2 + 2R^2)^{1/2}}$
Triaxial extension	$\dfrac{-2R}{(4R^2 + 2K^2)^{1/2}}$	$\dfrac{K}{(4R^2 + 2K^2)^{1/2}}$	$\dfrac{K}{(4R^2 + 2K^2)^{1/2}}$
Plane strain	$\dfrac{K}{(K^2 + R^2)^{1/2}}$	0	$\dfrac{-R}{(K^2 + R^2)^{1/2}}$

Triaxial extension:

$$H = \frac{\sigma_3}{(4R^2 + 2)^{1/2}} \frac{\left|\dfrac{dR}{d\epsilon_3^p}\right|}{\left(1 + \dfrac{1}{2}(K/R)^2\right)^{1/2}} \tag{13b}$$

Plane strain:

$$H = \frac{\sigma_3}{(1 + R^2)^{1/2}} \frac{\left|\dfrac{dR}{d\epsilon_1^p}\right|}{(1 + (R/K)^2)^{1/2}} \tag{13c}$$

In Fig. 3*a* the critical value of H is plotted as a function of critical stress ratio. For axisymmetric conditions, localization can occur only postpeak ($H < 0$) with the triaxial compression requiring a slope on the softening portion of the curve of over -40% of the elastic stiffness. Localization in the plane strain can occur in the prepeak portion of the curve ($H > 0$) at a value of H that is less than 5% of the elastic modulus. In Fig. 3*b* the critical angle θ is shown plotted as functions of stress ratio. Also shown are the directions predicted by classic Coulomb theory for maximum obliquity directions for stress and zero

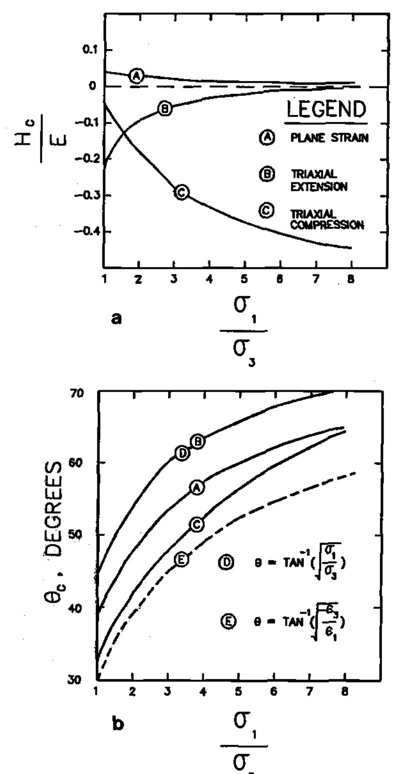

FIG. 3—*Shear banding predictions.*

TABLE 2—*Values of shear band orientation angle and normalized critical hardening modulus for* K = *2.50 and* ν = *0.15.*

	Compression		Extension		Plane Strain	
R	θ	H_c/E	θ	H_c/E	θ	H_c/E
1.0	32.4	−0.065	44.4	−0.229	38.8	0.022
1.5	38.0	−0.123	50.5	−0.142	44.3	0.025
2.0	42.2	−0.179	54.6	−0.094	48.2	0.024
2.5	45.6	−0.229	57.6	−0.065	51.2	0.022
3.0	48.5	−0.270	59.9	−0.048	53.6	0.019
3.5	50.9	−0.305	61.8	−0.036	55.6	0.017
4.0	53.1	−0.333	63.4	−0.028	57.3	0.015
4.5	55.0	−0.357	64.7	−0.022	58.7	0.013
5.0	56.7	−0.376	65.9	−0.018	60.0	0.011
5.5	58.2	−0.392	66.9	−0.015	61.1	0.010
6.0	59.7	−0.405	67.8	−0.013	62.1	0.009
6.5	61.0	−0.416	68.5	−0.011	63.0	0.008
7.0	62.2	−0.425	69.3	−0.009	63.9	0.007
7.5	63.4	−0.433	69.9	−0.008	64.6	0.006
8.0	64.4	−0.440	70.5	−0.007	65.3	0.006

extension direction for the plastic strain rate. The predicted values fall between the characteristic directions for stress and strain rate which agrees with the empirical relationship obtained by Arthur and coworkers [*7*] and is consistent with bifurcation computations made by Vardoulakis [*3*] and Molenkamp [*4*]. Values of critical hardening modulus and shear band orientation angle for K equal to 2.5, 3.0, and 3.5 are presented in Tables 2 to 4.

It is important to note that the peak stress condition for homogeneous deformation occurs at the point where the displacement increments can be arbitrarily large which is only possible when the elastoplastic matrix becomes singular as $H = 0$. The bifurcation condition can be satisfied by nonzero values of H and, as in the case of axisymmetric compression, may not

TABLE 3—*Values of shear band orientation angle and normalized critical hardening modulus for* K = *3.00 and* ν = *0.15.*

	Compression		Extension		Plane Strain	
R	θ	H_c/E	θ	H_c/E	θ	H_c/E
1.0	31.6	−0.049	42.9	−0.230	37.8	0.029
1.5	37.0	−0.096	49.0	−0.145	43.1	0.034
2.0	41.0	−0.145	53.0	−0.096	46.9	0.034
2.5	44.3	−0.190	56.1	−0.067	49.9	0.032
3.0	47.1	−0.230	58.4	−0.049	52.2	0.029
3.5	49.5	−0.264	60.4	−0.037	54.2	0.026
4.0	51.6	−0.294	62.0	−0.029	55.9	0.023
4.5	53.4	−0.320	63.3	−0.023	57.4	0.020
5.0	55.1	−0.341	64.5	−0.019	58.6	0.018
5.5	56.6	−0.359	65.6	−0.015	59.8	0.016
6.0	58.0	−0.375	66.5	−0.013	60.8	0.014
6.5	59.3	−0.388	67.3	−0.011	61.7	0.013
7.0	60.5	−0.400	68.0	−0.010	62.5	0.012
7.5	61.6	−0.410	68.7	−0.008	63.3	0.011
8.0	62.6	−0.418	69.3	−0.007	64.0	0.010

TABLE 4—*Values of shear band orientation angle and normalized critical hardening modulus for* K = *3.50 and* ν = *0.15.*

	Compression		Extension		Plane Strain	
R	θ	H_c/E	θ	H_c/E	θ	H_c/E
1.0	30.9	−0.037	41.7	−0.228	36.9	0.035
1.5	36.1	−0.076	47.7	−0.144	42.1	0.042
2.0	40.1	−0.117	51.7	−0.096	45.9	0.043
2.5	43.3	−0.157	54.8	−0.067	48.8	0.041
3.0	46.0	−0.195	57.2	−0.049	51.1	0.038
3.5	48.3	−0.228	59.1	−0.037	53.1	0.035
4.0	50.3	−0.258	60.7	−0.029	54.7	0.031
4.5	52.1	−0.285	62.1	−0.023	56.2	0.028
5.0	53.7	−0.308	63.3	−0.018	57.5	0.025
5.5	55.2	−0.327	64.4	−0.015	58.6	0.023
6.0	56.6	−0.345	65.3	−0.013	59.6	0.020
6.5	57.8	−0.360	66.2	−0.011	60.6	0.019
7.0	59.0	−0.373	66.9	−0.009	61.4	0.017
7.5	60.1	−0.385	67.6	−0.008	62.2	0.015
8.0	61.1	−0.395	68.3	−0.007	62.9	0.014

be possible even if the total response is singular. Localization represents a particular type of instability that does not coincide with the general instability that occurs at the peak stress condition [*2*]. Localization can control both the peak load observed in the test and the postpeak load-deformation behavior. Therefore, it is necessary to distinguish between behavior related to localization and the stress–strain response under homogeneous strain conditions.

The conclusions stated above are valid for a wide range of possible isotropic hardening plasticity models applicable to frictional materials, giving experimental verification of the theory importance that reaches beyond the prediction of instability by shear banding. For example, isotropic hardening models are simple and are justifiably popular for practical analysis because they can model many essential features of stress–strain behavior. Yet they are somewhat restrictive; it has been shown that shear banding occurs more readily when features such as vertices on the yield surface [*1*] and kinematic hardening [*8*] are incorporated into the model. Comparisons between theoretical modes of instability and experiments thus provide insight into the mechanical consistency of constitutive models that cannot be obtained from predictions of homogeneous behavior alone.

Experimental Investigation

Three series of tests were performed along different predetermined stress paths under conditions of triaxial compression (three tests), triaxial extension (three tests), and plane strain (three tests), and the similarities and differences in shear band formation characteristics were observed in these tests. The time of formation and the influence of formation of shear bands on the stress–strain and volume change behavior were also noted. All quantities necessary to define all stresses and all strains in each test were measured. These include direct measurements of the intermediate principal stress in the plane strain tests. Photographs were taken throughout each test to produce a record of the shear band locations and directions in the specimens.

Description of Sand Tested

All experiments included in this study were performed on specimens of sand obtained from the beach in Santa Monica, California. The sand was washed several times with fresh water to eliminate salt and impurities, and the portion passing the No. 40 U.S. sieve was used for testing.

The physical characteristics of Santa Monica beach sands are summarized in Table 5. The specific gravity was determined according to ASTM Test for Specific Gravity of Soils (D 854). The maximum void ratio was determined by the method proposed by Kolbuszewski [*9*] in which the loosest packing is obtained by tilting a graduated cylinder (2000 cm^3, 3.0 in. in diameter) containing dry sand (2000 g) through 180° from one vertical position to the other. This procedure was repeated several times, and the volume of the sand was measured for determination of the maximum void ratio. The minimum void ratio was determined by compacting the sand by vibration in a standard Proctor compaction test mold until no further densification was observed. The minimum void ratio was determined by weighing the sand and measuring the volume of the mold.

All tests were performed on dense specimens with relative densities of about 90%. Relatively high rates of dilation and consequently greater tendencies for development of shear planes are present for high relative densities [*10*]. Tests on dense sand are most useful, therefore, for studying formation of shear planes. The void ratio and the dry density used in the test specimens are also listed in Table 5.

Specimen Preparation and Testing Procedures

Triaxial Compression and Extension Tests—All triaxial tests were performed on cylindrical specimens with height of 7.4 in. (18.8 cm) and diameter of 2.80 in. (7.1 cm) corresponding to $H/D = 2.65$. This high H/D value was chosen to allow shear bands to develop freely and uninterrupted by the end plates. Lubricated end plates were used in all tests to avoid development of significant shear stresses at the cap and base.

The specimens were prepared by pluvial deposition through a No. 20 U.S. sieve placed on top of a cardboard tube approximately 70 cm above the forming jacket. A preweighed amount of dry sand was pluviated into the specimen cavity formed by the base and the

TABLE 5—*Properties of Santa Monica beach sand.*

D_{10}	0.18
D_{60}	0.28
$C_u = D_{60}/D_{10}$	1.58
D_{50}	0.265
Particle shapes	Angular to subangular
Mineral composition	45% quartz, 45% feldspar, 8% magnetite, 2% trace minerals
Specific gravity, G_s	2.659
Max. void ratio, e_{max}	0.87
Min. void ratio, e_{min}	0.58
Min. dry density (g/cm^3)	1.422
Max. dry density (g/cm^3)	1.683
Conditions in Tests	
Void ratio, e	0.609
Dry density, τ_d (g/cm^3)	1.653
Relative density, D_r (%)	90.0

membrane held by the forming jacket. After sealing the membrane to the cap, a small vacuum was applied and the specimen dimensions were measured.

Vertical lines were drawn with waterproof ink 1.0 cm apart on one side of the cylindrical specimen. This was done to enhance the detection and observation of developing shear planes during the test. To get an undistorted view and to take photographs of the developing shear planes, a rectangular Lucite compartment was attached and sealed on the outside of the Lucite cell wall. This compartment was filled with water as was the triaxial cell, thus providing an undistorted view of the specimen through this window.

After applying an initial confining pressure of 51 kPa, the dry specimen was saturated using the carbon dioxide method [*11*] combined with back pressure-assisted saturation to ensure a high degree of saturation. An indication of the degree of saturation of the specimens was obtained from *B*-value tests conducted immediately before the specimens were tested.

The deviator load, the confining pressure, the vertical deformation, and the volume changes were measured during each test. Constant or varying effective confining pressures in the range from 51 kPa to 406 kPa were employed in the testing program.

Corrections were applied to the measured deviator load for uplift force on the piston, piston friction, the load taken by the rubber membrane, and for the buoyed weight of the cap and the buoyed weight of the upper half of the specimen. The volumetric deformations were corrected for effects of membrane penetration which occurred in tests with varying effective confining pressure.

Plane Strain Tests—The plane strain tests were performed on specimens shaped as rectangular prisms 5.0 in. (12.7 cm) high, 1.75 in. (4.5 cm) wide, and 4.5 in. (11.4 cm) long. This shape corresponds to $H/D = 2.85$, thus allowing free development of shear planes. Lubricated ends were also used in these tests to avoid any influence of end restraint.

The specimens were prepared in the same manner as described above for the triaxial tests. Vertical lines were drawn on the membrane on one of the two sides that were to be restrained from deformation. The restraint was provided by two 1-in. (2.54-cm) thick clear Lucite plates which would allow observation of shear planes during the test. The two Lucite plates were placed on two opposite sides of the specimen and connected with four instrumented bars located in the far corners of the plates. Each of the two interfaces between the specimen and the Lucite plates were provided with extra lubricated rubber sheets to avoid development of significant shear stresses along these interfaces. The two plates were held in place by a small seating load applied by finger nuts on the ends of the four instrumented bars. The small buoyant weight of the two Lucite plates was supported on small blocks sitting on the bottom of the triaxial cell or by rubber bands hanging in small gallows.

The deviator load, the confining pressure, the vertical deformation, and the volume changes were measured in each plane strain test in addition to the horizontal deviator load determined from the four instrumented bars. Constant or varying effective confining pressures from 51 kPa to 406 kPa were used in the tests. Corrections similar to those employed in the triaxial tests were used for the measured quantities in the plane strain tests.

Stress Paths

Stress paths were chosen that would highlight deviations from the Mohr-Coulomb behavior assumed in the theoretical analysis. The stress paths used in the triaxial compression and extension tests are shown in Fig. 4; the stress path for the plane strain test is shown in Fig. 5.

Triaxial Compression and Extension Tests—The experiments consisted of three different stress paths in compression and three different stress paths in extension. The tests were initiated at an isotropic confining pressure of 51 kPa and then followed different stress paths to reach peak failure. Following peak failure and complete development of shear bands, the specimens were unloaded. The compression tests were then reloaded in extension to study the influence of compression shear bands on formation of extension shear bands. Following unloading in the extension tests the confining pressure was reduced to the initial isotropic state, and the specimens were reloaded in compression. This was done to study the effects of extension shear bands on development of compression shear bands.

Plane Strain Tests—The three different stress paths resemble those in triaxial compression in terms of the combination of variation of the stress difference ($\sigma_1 - \sigma_3$) and the confining pressure σ_3 excepting that extension loading was restricted by $\sigma_2 > 0$. The horizontal stress difference ($\sigma_2 - \sigma_3$) cannot be controlled, but basically is dictated by the condition that $\epsilon_2 = 0$. Following peak failure and shear banding, the specimens were unloaded at the confining pressure reached at failure.

Results

Formation of Shear Bands in Triaxial Compression

The stress–strain and volume change relationships obtained from the triaxial compression tests are shown in Fig. 6. The vertical stress difference and the volumetric strains are plotted against the vertical strain in these diagrams.

During the tests, the specimens were carefully observed for early detection of developing shear bands. The location on the stress–strain curves at which the first observation of shear bands was made is indicated on each figure for both compression and extension conditions. Considerable straining beyond the peak failure points occurs in all cases before shear bands develop in the compression tests. The stress–strain curves in Figs. 6 and 7 show only little sign of the formation of shear bands, whereas the rates of dilation diminish substantially immediately before the shear bands become visible. Thus, the reduced rates of dilation in all cases appear to be associated with the occurrence of shear bands. Once a shear band has developed fully, the stresses and the volume change curve tend to level off. It appears that the initiation of shear banding results in elastic unloading of the specimen outside the developing shear band which rapidly becomes weaker than the remaining major parts of the specimen.

The results of the extension tests following the compression tests on the same specimens are also shown in Fig. 6. Although very clear extension shear bands developed in each specimen, there does not appear to be any clear indication of these occurrences to be seen from the stress–strain and volume change curves. This may be because these two curves indicate very steady behavior before shear banding (that is, almost no change in stresses and only small volume dilation with continued straining). Therefore, the shear bands, which were rather slow to develop in these tests, did not cause any recognizable effects on the stress–strain and volume change curves. The new shear bands developing in the specimens seemed to initiate from one end of an old shear band where a loose zone was created.

Formation of Shear Bands in Triaxial Extension

Figure 7 shows the stress–strain and volume change relationships obtained from the triaxial extension tests. The vertical stress difference, which is negative during extension, and the

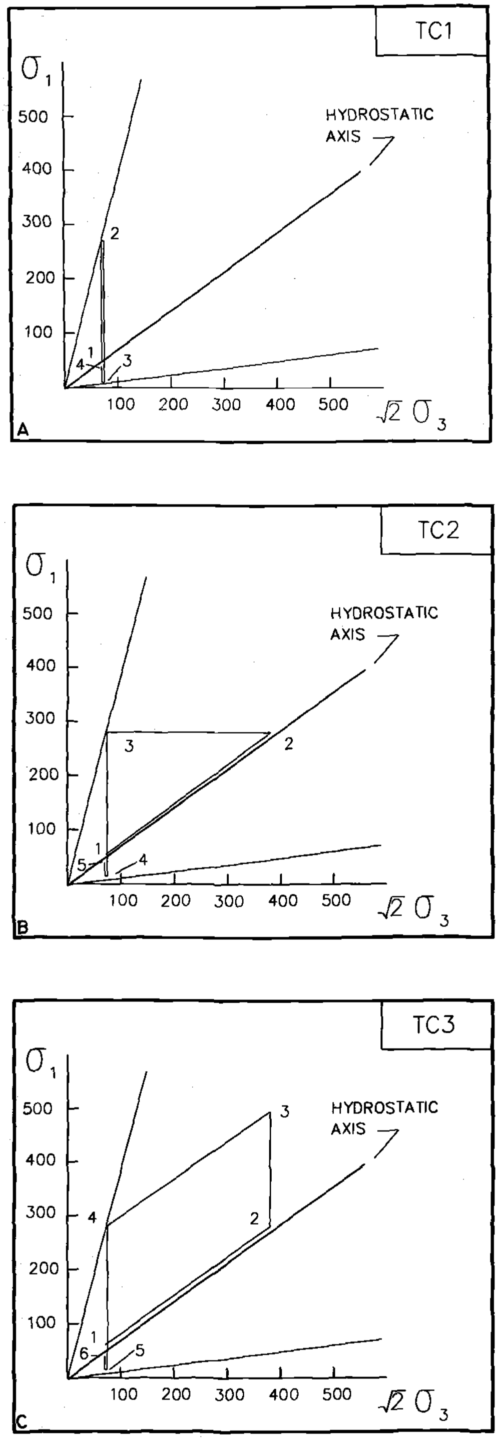

FIG. 4—*Stress paths for triaxial compression and extension.*

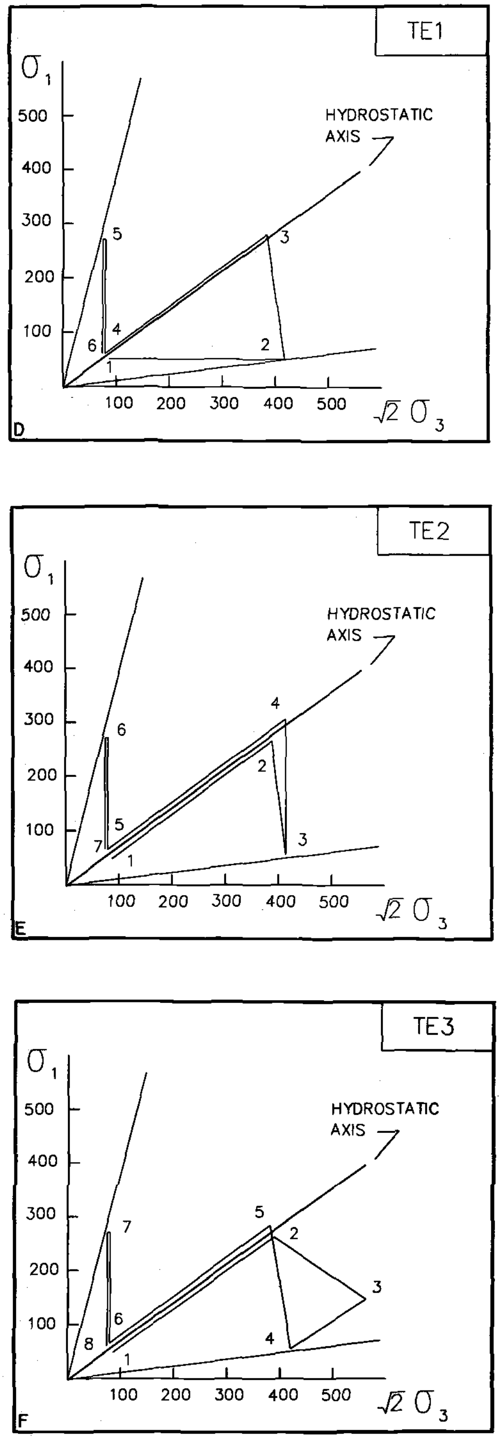

FIG. 4—*Continued.*

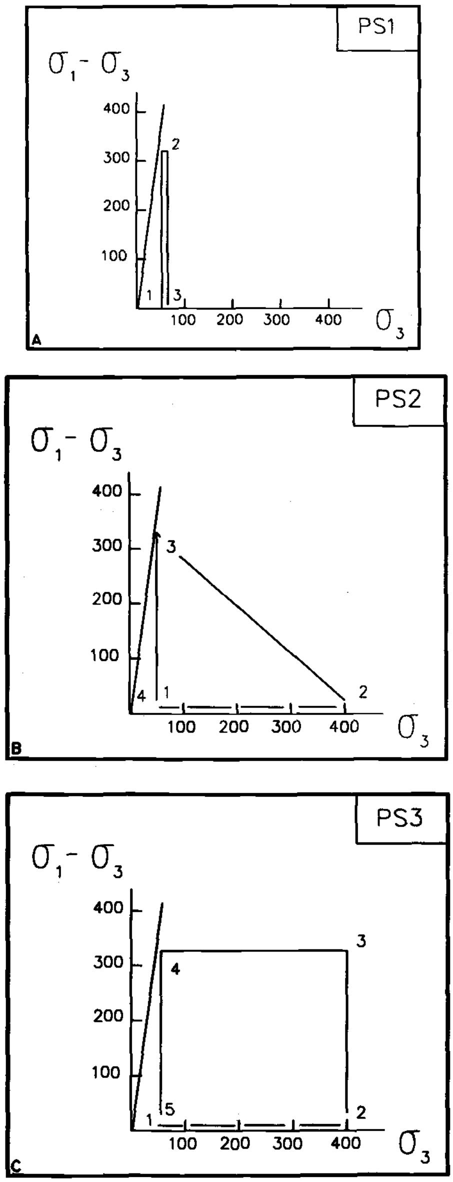

FIG. 5—*Stress paths for plane strain tests.*

volumetric strain are plotted against the vertical strain in these diagrams. The observations of developing shear bands are noted on all the diagrams. It may be seen from Fig. 7 that shear bands were observed closely after peak failure in all cases and they were accompanied by a sudden and considerable drop in sustained stress difference and almost complete termination of dilation. The rates of dilation observed in these tests were higher before shear banding than those measured in extension following the compression tests described above. The shear bands in these tests were also observed to develop abruptly and become very sharp and clear over a very small range of deformation.

The shear banding during the compression portion of the test is associated with drops in stress difference and in rate of dilation in all cases except one, in which several shear bands developed in the specimen. As in the compression tests, the development of new shear bands appeared to initiate from one end of an old shear plane where a loose zone was present.

Formation of Shear Bands in Plane Strain

Figure 8 shows the results of the three plane strain tests. Both the vertical stress difference and the horizontal stress difference ($\sigma_2 - \sigma_3$) as well as the volumetric strain are plotted against the vertical strain. The value of $b = (\sigma_2 - \sigma_3)/(\sigma_1 - \sigma_3)$ increases from zero to a value at failure indicated on the figure. Although both stress differences decrease after

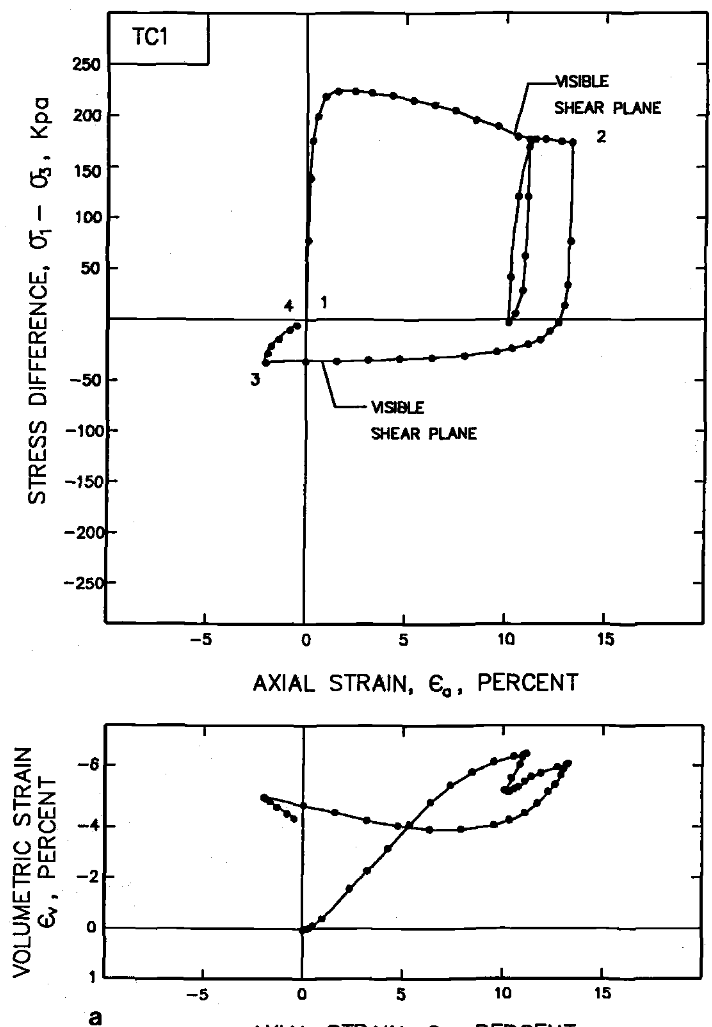

FIG. 6—*Stress–strain curves for triaxial compression. Test segments corresponding to stress paths in Fig. 4 are labeled.*

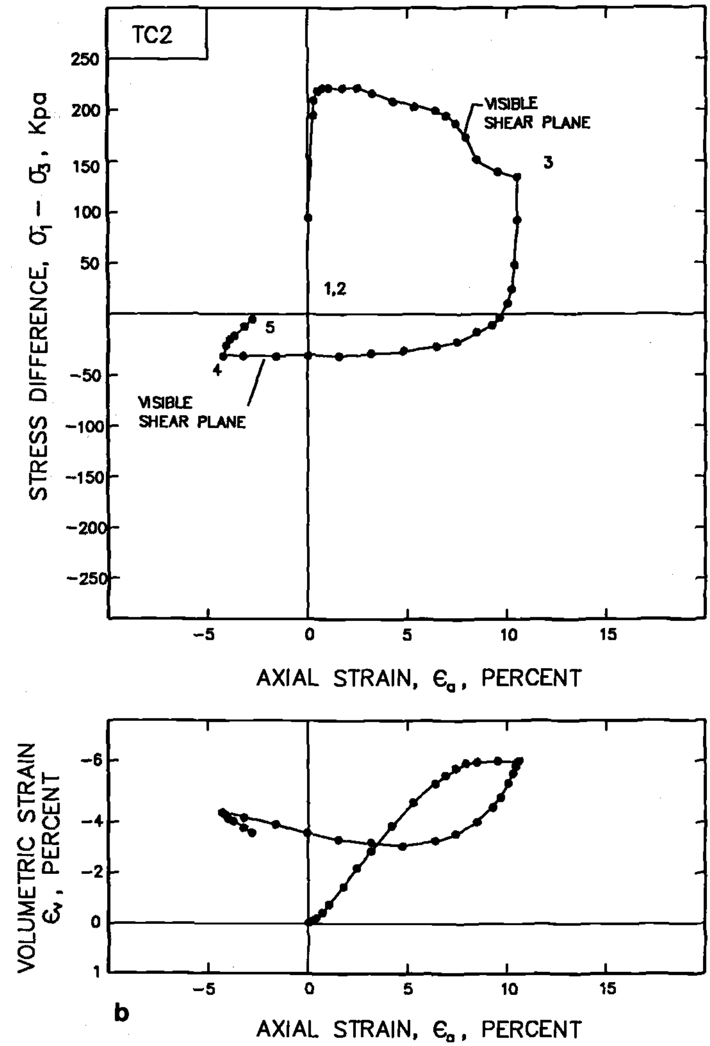

FIG. 6—*Continued.*

failure, their ratio, expressed in the *b* value, continues to increase indicating that the stress in the plane strain direction (σ_2) does not fall off rapidly in the postpeak portion of the test.

The strain to peak failure (or to maximum stress ratio) is very small in the plane strain tests (1.5 to 2.0%), and detection of visible shear bands was most difficult in these tests. In fact, it was necessary to compress the specimens to 3% to 4% vertical strain before the shear bands became recognizable in the specimens. The figures do not indicate when the shear bands became visible because they appeared to develop very gradually. However, the vertical stress difference was observed to suddenly drop off, whereas the decrease in rate of dilation occurred at a slightly later point in the tests. It is possible that the shear banding was similarly delayed (that is, the shear banding may be associated with the break in the volume change curve rather than the drop in the vertical stress difference).

Note that the sudden drops in vertical stress differences occur at points on the stress–strain curves where the specimens are apparently still being loaded (that is, the slopes of

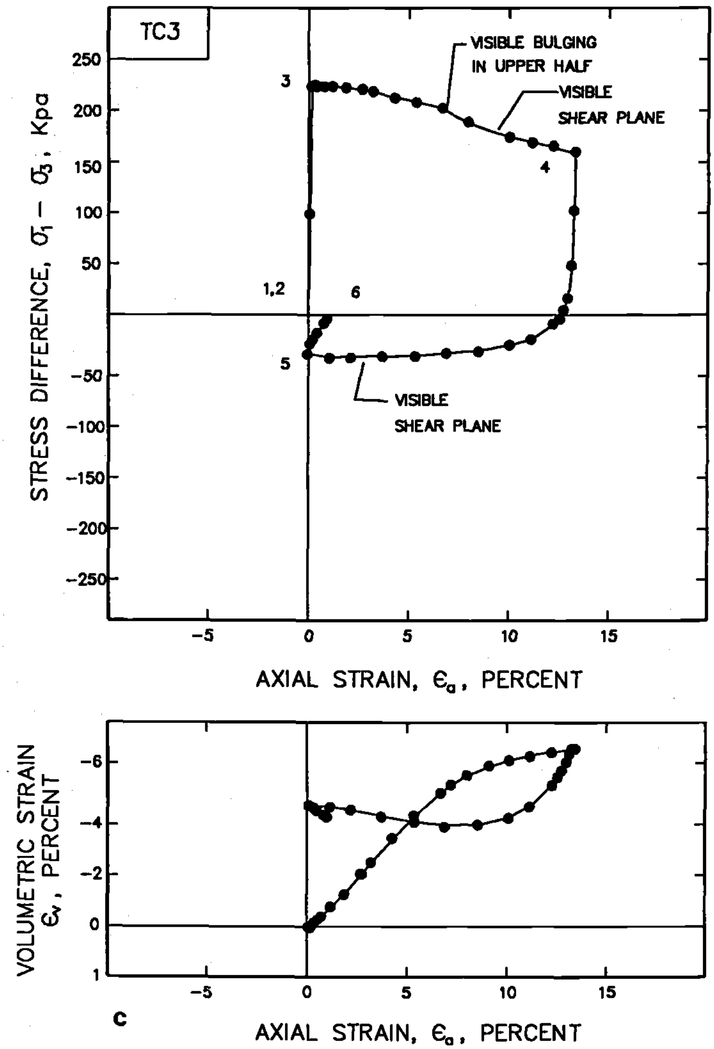

FIG. 6—*Continued.*

the stress–strain curves are still positive). Thus, the stress state does not continue smoothly over the peak point on the curves, and the peak point appears to represent a point of instability located before a smooth peak failure point can be obtained.

Following the drop-off, the vertical stress difference decreases to less than half of the maximum value before leveling off at 2.5 to 3.0% vertical strain. Thus, very little straining occurs under plane strain conditions before the residual strength is reached.

Variation of Friction Angles[4]

The friction angles observed in the triaxial compression tests and those obtained from compression of the extension specimens all correspond to confining pressures close to 51

[4] Averages reported here include replicate tests not shown in Figs. 6 and 7.

kPa. Their average (of eight tests), 43.5°, and standard deviation, 0.3°, indicate very little scatter of the experimental results. Thus, the influence of extension before compression testing on the strength is negligible. Similarly, the strengths obtained in the extension tests do not appear to be influenced by previous compression testing. The average friction angle and standard deviation for all eight extension tests are, respectively, 45.2 and 1.9°. However, if one outlying friction angle (40.6°) is removed, the result is 45.9 and 0.5°. The results of the plane strain tests show an average friction angle of 50.0° and a standard deviation of 0.6°.

Critical Strain Hardening Parameter

The hardening parameter H (Eq 13) and the theoretical critical hardening parameter H_c (Eq 8) were computed for each test at the point prior to observed shear banding as sum-

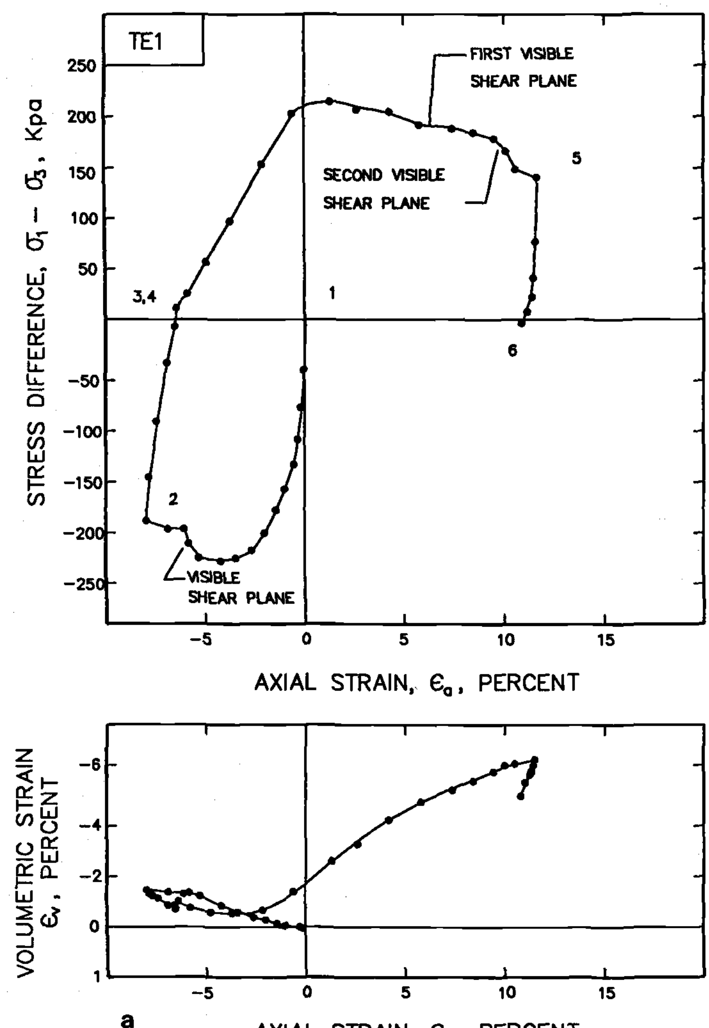

FIG. 7—*Stress–strain curves for triaxial extension. Test segments corresponding to stress paths in Fig. 4 are labeled.*

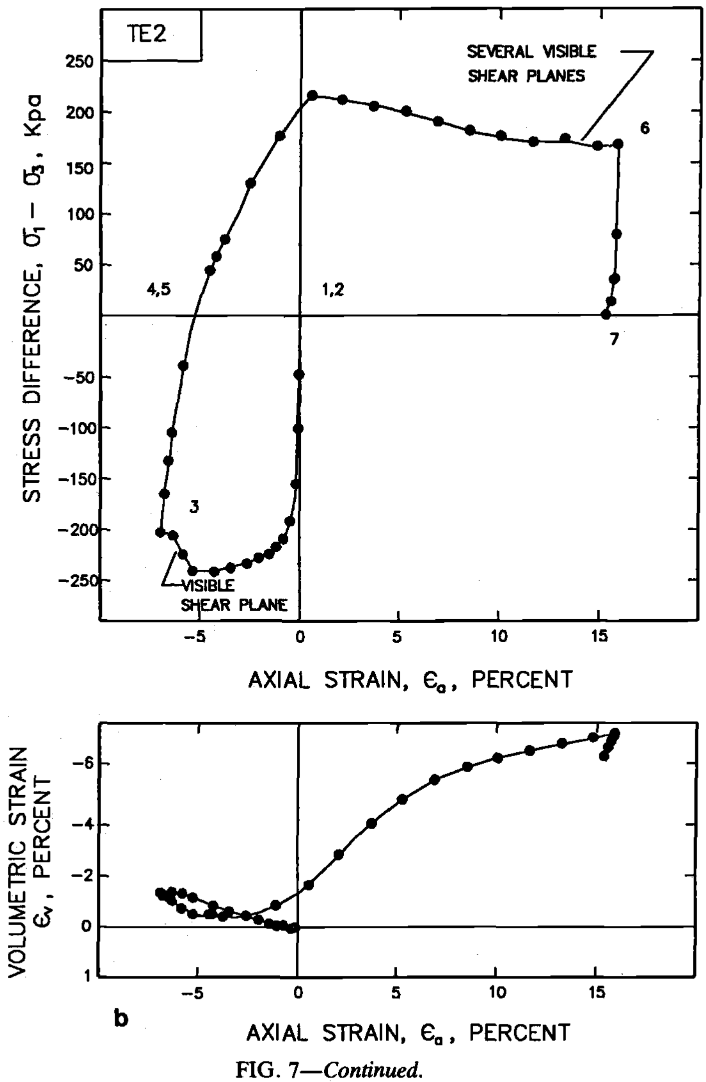

FIG. 7—*Continued.*

marized in Table 6. In comparing experimental and theoretical values, observe that the necessary condition for shear banding is $H < H_c$. The analysis involves four properties, two elastic constants, E and ν, hardening modulus, H, and the constant volume stress ratio, K. The values for E were computed from empirical relationships for Santa Monica beach sand given by Lade and Nelson [*12*]. All computations are based on $\nu = 0.15$. The value of K was computed from Eq 12 using the rate of dilatancy measured prior to the point of obvious localization. These values were consistently lowest in triaxial compression (average of six values, 2.81), highest in extension (average of six values, 4.18), and intermediate in plane strain (average of three values, 3.82).

A difficulty with the measurements is distinguishing between homogeneous behavior and that caused by shear band formation. In particular, it is difficult to determine whether the reduction in stiffness prior to failure in the plane strain test is the result of localization or part of the homogeneous behavior. The values shown in Table 6 for the plane strain test

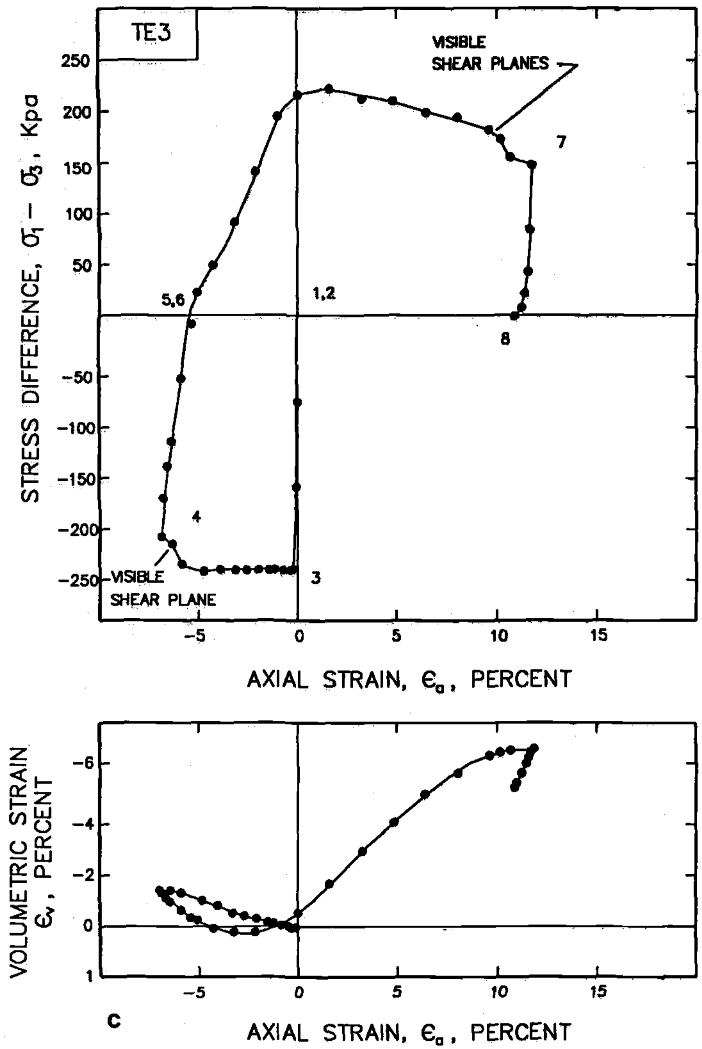

FIG. 7—*Continued.*

correspond to the rising portion of the stress–strain curve well before there is any evidence of instability. Even on the steeper portion of the curve the hardening modulus is less than the theoretical critical value indicating that localization is possible well before it actually occurs.

The critical condition for triaxial extension was influenced by the loading history. For the tests loaded directly into extension, shear banding appears to occur just after peak stress on the softening portion of the curve whereas shear banding clearly occurs in the hardening portion of the curve for the samples that were first loaded into compression. One possible explanation for this is that the axisymmetric condition is destroyed by the low density zone created in the initial compressive loading. If so, the triaxial compression test was not similarly influenced because shear banding was observed within the strain softening part of the test for all triaxial compression tests. In all cases the rate of softening for the axisymmetric tests

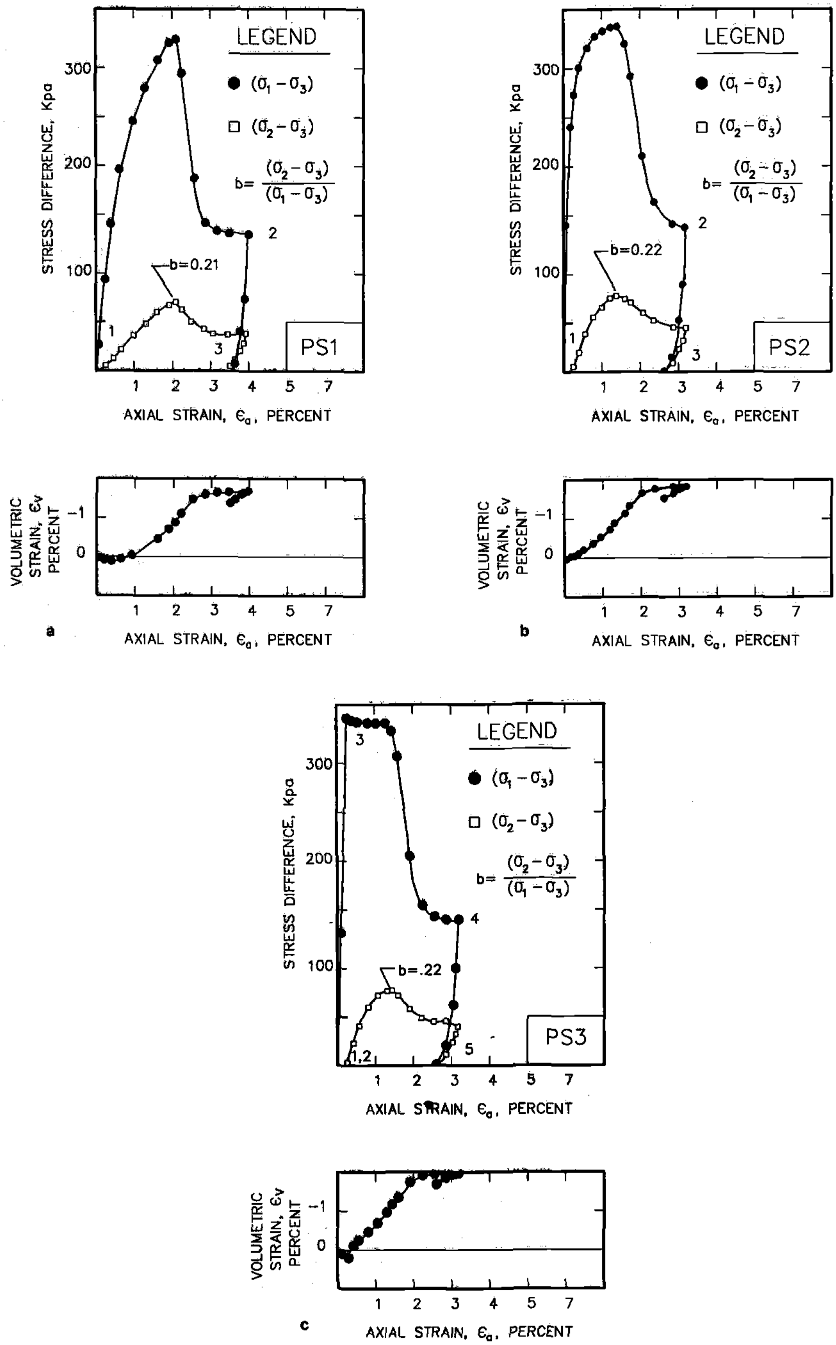

FIG. 8—*Stress-strain curves for plane strain. Test segments corresponding to stress paths in Fig. 5 are labeled.*

TABLE 6—*Summary of critical hardening modulus computation.*

Test[a]	R	$\frac{d\epsilon_v}{d\epsilon_a}$[b]	K[c]	$\frac{dR}{\lvert d\epsilon_a \rvert}$	σ_3, kPa	E[d], MPa	$\frac{H}{E}$[e]	$\frac{H_c}{E}$[f]
TC1								
Comp.	4.59	−0.283	3.58	−0.174	50.7	272.3	−0.0004	−0.279
Ext.	5.62	0.213	4.42	0.123	9.1	145.8	0.0001	−0.013
TC2								
Comp.	5.12	−1.079	2.46	−0.081	50.7	272.3	−0.0001	−0.380
Ext.	5.88	0.213	4.63	0.202	9.1	145.8	0.0001	−0.011
TC3								
Comp.	5.17	−1.018	2.56	−0.083	50.7	272.3	−0.0001	−0.374
Ext.	6.17	0.184	5.04	0.639	8.1	145.8	0.0003	−0.009
TE1								
Ext.	5.81	0.404	3.46	−0.136	50.2	327.6	−0.0006	−0.014
Comp.	5.06	−0.737	2.91	−0.068	50.7	272.3	−0.0001	−0.350
TE2								
Ext.	5.88	0.369	3.71	−0.032	52.2	327.6	−0.0000	−0.011
Comp.	5.12	−0.908	2.68	−0.060	50.7	272.3	−0.0001	−0.370
TE3								
Ext.	5.81	0.341	3.83	−0.396	51.9	327.6	−0.0005	−0.013
Comp.	5.01	−0.870	2.68	−0.138	50.7	272.3	−0.0002	−0.363
PS1	7.75	−0.845	4.20	2.984	50.7	340.8	0.0020	0.022
PS2	7.28	−0.883	3.87	2.783	57.1	340.8	0.0029	0.020
PS3	7.33	−1.143	3.42	1.929	61.1	340.8	0.0020	0.015

[a] Comp. and Ext. denote values measured in compression and extension portions of test, respectively.
[b] $d\epsilon_a$ is the axial strain in triaxial compression and extension test and the vertical strain in the plane strain test.
[c] Computed using Eq 12.
[d] From values given in Ref *12*.
[e] Computed using Eq 13.
[f] Computed from Eqs 8 and 10 using $\nu = 0.15$.

was less than the critical condition (that is, $H > H_c$), and localization was not theoretically possible.

Concluding Remarks

Comparison of the experiments with theoretical behavior clearly supports the theoretical conclusion that shear band formation is influenced by loading configuration. The triaxial compression test is the most resistant to shear banding whereas the plane strain test can display shear banding prior to reaching the peak of the stress–strain curve; the triaxial extension test appears to fall between these two extremes in terms of potential for shear banding. Comparison of behavior between different types of equipment should therefore include an assessment of the role that localization plays in each case.

The lack of quantitative agreement between experiment and theory for the triaxial compression test suggests that the theoretical requirements for bifurcation based on isotropic hardening may be too severe. There is, of course, the possibility that stress state in the triaxial compression test, when shear banding finally occurred, was approaching that of the plane strain test as a result of constraint at the sample ends. The relatively low value of b measured in the plane strain test indicates that only a small deviation from ideal end conditions could create a stress state close to plane strain where shear banding could readily occur. Yet, the axisymmetric configuration is clearly more stable than the plane strain configuration even when the specimen has undergone shear banding during previous loading and axisymmetry most certainly has been destroyed. The low density shear zones created during initial loading were observed to serve as points of initiation for shear bands but in no case did they cause the cylindrical specimens to display the degree of instability observed in the plane strain test. Thus, axisymmetry does not produce the degree of stability suggested by the analysis, nor does the loss of axisymmetry produce the degree of instability that might be expected from a comparison to plane strain conditions.

References

[1] Rudnicki, J. W. and Rice, J. R., "Conditions for the Localization of Deformation in Pressure-Sensitive Dilatant Materials," *Journal of the Mechanics and Physics of Solids,* Vol. 23, 1975, pp. 371–394.

[2] Rice, J. R., "The Localization of Plastic Deformation," in *Proceedings,* Fourteenth Conference on Theoretical and Applied Mechanics, W. T. Koiter, Ed., North-Holland Publishing Co., Amsterdam, 1976, pp. 207–229.

[3] Vardoulakis, I., "Shear Band Inclination and Shear Modulus of Sand in Biaxial Tests," *International Journal for Numerical and Analytical Methods in Geomechanics,* Vol. 4, 1980, pp. 103–119.

[4] Molenkamp, F., "Comparisons of Frictional Material Models with Respect to Shear Band Initiation," *Geotechnique,* Vol. 35, No. 2, 1985, pp. 127–143.

[5] Vermeer, P. A., "A Simple Shear-Band Analysis Using Compliances," in *Proceedings,* Symposium on Deformation and Failure of Granular Materials, International Union of Theoretical and Applied Mechanics, P. A. Vermeer and H. J. Luger, Eds., Delft, Holland, 1982, pp. 493–499.

[6] Rowe, P. W., "The Stress–Dilatancy Relation for Static Equilibrium of an Assembly of Particles in Contact," *Proceedings of the Royal Society,* Series A, London, Vol. 269, 1962, pp. 500–527.

[7] Arthur, J. R. F., Dunstan, T., Al-Ani, Q. A. J., and Assadi, A., "Plastic Deformation and Failure in Granular Media," *Geotechnique,* Vol. 27, 1977, pp. 54–74.

[8] Lemonds, J. and Needleman, A., "Finite Element Analysis of Shear Localization in Rate and Temperature Dependent Solids," *Mechanics of Materials,* Vol. 5, 1986, pp. 339–361.

[9] Kolbuszewski, J. J., "An Experimental Study of the Maximum and Minimum Porosities of Sand," in *Proceedings,* Second International Conference on Soil Mechanics and Foundation Engineering, Rotterdam, Vol. I, 1948, pp. 158–165.

[10] Lade, P. V., "Localization Effects in Triaxial Tests on Sand," in *Proceedings,* Symposium on Deformation and Failure of Granular Materials, International Union of Theoretical and Applied Mechanics, P. A. Vermeer and H. J. Luger, Eds., Delft, Holland, 1982, pp. 461–471.

[11] Lade, P. V. and Duncan, J. M., "Cubical Triaxial Tests on Cohesionless Soil," *Journal of the Soil Mechanics and Foundations Division, American Society of Civil Engineers,* Vol. 99, No. SM10, 1973, pp. 793–812.

[12] Lade, P. V. and Nelson, R. B., "Modeling the Elastic Behavior of Granular Materials," *International Journal of Numerical Methods in Geomechanics,* Vol. 11, No. 5, Sept.–Oct. 1987, pp. 521–542.

Daniel P. Dietzler[1], Devin A. Moose[1], and Jeffrey C. Schuh[1]

Effects of Sampling Disturbance on Shear Strength of Glacial Till and Compacted Fill

REFERENCE: Dietzler, D. P., Moose, D. A., and Schuh, J. C. **"Effects of Sampling Disturbance on Shear Strength of Glacial Till and Compacted Fill,"** *Advanced Triaxial Testing of Soil and Rock, ASTM STP 977*, Robert T. Donaghe, Ronald C. Chaney, and Marshall L. Silver, Eds., American Society for Testing and Materials, Philadelphia, 1988, pp. 628–641.

ABSTRACT: Shear strength tests employing back pressure saturation, isotropic consolidation, and pore pressure measurements in the triaxial chamber are routinely used in the evaluation of landfill sites, deep excavations, earth dams, and highway embankments. Continuous soil sampling using a 1.5-m (5-ft) long split-barrel sampler and hollow-stem augers has proved to be highly efficient in sampling predominantly cohesive soils and cohesive fills. Whereas sampling with thin-walled tubes, ASTM D 1587, has been recognized as providing essentially undisturbed samples, experience with the split-barrel continuous sampler system indicates that visually it will yield equally undisturbed samples and provide better recovery in cohesive fills and extremely hard soils.

A comparative laboratory testing program was undertaken to investigate the differences in shear strength between samples of a glacial till obtained in accordance with the ASTM Method for Thin-Walled Tube Sampling of Soils (D 1587), samples carved from blocks, and samples obtained with the continuous split-barrel sampler. These three sampling systems were used to obtain samples from the same strata of saturated glacial till. Zones of carefully monitored compacted clay fill were also sampled using the thin-walled tube sampler and the continuous split-barrel sampler. The factors affecting sample disturbance and the results of a limited testing program are discussed.

KEY WORDS: sample disturbances, sampling, samplers, shear strength (soils), soil properties, triaxial tests

Nomenclature

- A_r Area ratio
- $\overline{B}$ Terzaghi compression index for all-around triaxial pressure
- C_r Inside clearance ratio
- C' Cohesive intercept in terms of effective stress
- C_T Cohesive intercept in terms of total stress
- ϕ' Friction angle in terms of effective stress
- ϕ_T Friction angle in terms of total stress
- ψ' Slope of the K_F line on the p'-q' diagram

Introduction

Geotechnical investigations for landfills, flood control and highway projects, and structure foundations frequently require that "undisturbed" samples of cohesive soils be obtained to permit laboratory measurement of density, shear strength, compressibility, or hydraulic

[1] Principal, senior geotechnical engineer, and vice president, respectively, Patrick Engineering Inc., 346 Taft Avenue, Glen Ellyn, IL 60137.

conductivity. Continuous sampling to check for lenses of granular soils in these deposits is desirable or mandated by regulatory agencies when designing landfill or flood control projects.

Continuous sampling by conventional methods (for example, split-spoon sampling or thin-walled tube sampling) is relatively slow, and retrieval of thin sand lenses or very soft layers of cohesive soils can be difficult. Devices developed for the continuous sampling of cohesive soils more efficiently than the ASTM Method for Penetration Test and Split-Barrel Sampling of Soils (D 1586) or the ASTM Method for Thin-Walled Tube Sampling of Soils (D 1587) are commonly called continuous samplers.

The continuous split-barrel sampler operation is similar to conventional hollow-stem auger drilling except that, in lieu of a plug and string of drill rod, a 1.5-m (5-ft) long split-barrel sampler is fitted inside the lead auger and suspended on a string of hex rod with pinned joints. The hardened shoe for the split-barrel sampler can be adjusted from approximately 15 cm (6 in.) in front of the auger head to approximately flush with the auger head. The sampler tube is held from rotating with the auger by the hex rods which are fixed at the connection to the drill. As the hollow stem augers are turned, the split-barrel sampler is pushed into the soil, similar to thin-walled tube sampling techniques. An advantage to using the continuous sampler in hard cohesive soils is that the auger cuts away the soil around the sampler and reduces the side friction on the outside of the sampler barrel. The greater stiffness of the split-barrel and the reduction in side friction enables the sampling of hard cohesive soils which cannot be obtained with thin-walled tubes. Because the system does not require water, potential sample disturbance and moisture content changes as a result of washing are eliminated.

Samples of naturally overconsolidated cohesive soils and cohesive fills obtained in this manner visually appear to be relatively undisturbed. The continuous sampler system seems to have advantages over conventional sampling procedures, including (1) improved efficiency, (2) the ability to obtain samples of hard cohesive soils which cannot be sampled with thin-walled tubes, (3) occasionally the ability to obtain essentially "undisturbed" samples of compacted fills possessing stratified density resulting from compaction in lifts, and (4) the ability to visually inspect a continuous 1.5-m (5-ft) long sample of soil in the field without the extrusion process.

The two identified disadvantages of the continuous sampler also must be considered prior to using it instead of other conventional sampling methods. The sample is removed from the split-barrel sampler in the field where possible water content changes in the sample may occur due to uncontrolled climatic conditions. Also, field removal of the sample from the sample barrel allows for "unlimited" swell potential prior to testing unless the sample is immediately restrained.

The testing reported here was performed as an initial attempt to evaluate the difference, if any, in laboratory-measured properties of cohesive soils sampled with the continuous sampler and the same soils obtained in accordance with ASTM D 1587 and block samples carved from test excavations. It is recognized that the testing was limited and that the conclusions drawn from this comparative testing may not be applicable to all types of soils encountered.

Geotechnical Conditions

General

The samples were obtained from a site located within northeastern Illinois and more specifically within the Wheaton Morainal Division of the Central Lowlands Physiographic

Province [1]. The topography in the area is characterized as level to gently rolling. The entire area has been glaciated and has been covered with a thick mantle of glacial outwash and silty clayey till. The thickness of soil cover in the general geographic area is on the order of 18 to 30 m (60 to 100 ft) [2]. The soils generally consist of fine-grained glacial till and morainal deposits.

Soil Properties

The natural soil sampled for this study was gray silty clay till belonging to the Yorkville Member of the Wedron Formation [1]. Classification tests performed in accordance with ASTM standard procedures yielded average values of 22 and 14 for the liquid and plastic limits, respectively. The soil consists of, on the average, 1% gravel, 19% sand, 51% silt, and 29% clay based on the ASTM Classification of Soils for Engineering Purposes (D 2487), and defining clay particles as those smaller than 0.002 mm. The specific gravity, determined in accordance with the ASTM Test for Specific Gravity of Soils (D 854), was 2.67. The soil is classified as a lean clay in accordance with the Unified Soil Classification System, ASTM D 2487. The soil is slightly overconsolidated with an estimated maximum past vertical effective stress (preconsolidation pressure) of 220 kPa (31.9 psi).

The compacted fill sampled for this study was pinkish-brown silty clay till belonging to the Tiskilwa Member of the Wedron Formation [1]. The average liquid and plastic limits of the soil are 24 and 12, respectively. The particle size distribution analysis yielded average values of 2% gravel, 32% sand, 40% silt, and 26% clay. The soil is classified as a lean clay in accordance with the Unified Soil Classification System. The soil was placed and compacted in lifts using a Caterpillar® 825C sheepsfoot roller. The final compacted lift thickness was typically less than 8 in. (20 cm). Approximately three to four passes with the sheepsfoot roller were required to achieve a minimum compaction of 95% of maximum density as determined in accordance with ASTM Tests for Moisture-Density Relations of Soils and Soil-Aggregate Mixtures, Using 5.5-lb (2.49-kg) Rammer and 12-in. (304.8-mm) Drop (D 698, Method A). Typically, the soil was compacted within two percentage points of the laboratory-determined optimum moisture content.

Sampling Procedures

Block Samples

Block samples [3] of the gray silty clay till were obtained by excavating a 1.3-m (4-ft) deep trench adjacent to the proposed sample location. The sample was isolated roughly using shovels and then trimmed to the desired shape using soil knives. Before cutting the soil column free, the sample was wrapped with plastic wrap, then cheesecloth, and a circular rigid plastic tube was placed over the sample with approximately a 1.3-cm (0.5-in.) space between the sample and tube. The annular space between the sample and rigid plastic tube was then filled with beeswax to obtain a moistureproof seal. The sample was transported in a vertical position to the laboratory and was placed in a humidity-controlled environment.

Thin-Walled Tube

The thin-walled tubes were 7.6 cm (3 in.) in diameter with an inside clearance ratio [4] of 1% and an area ratio [4] of 12%. The tubes were butt welded and galvanized. The dimensions and construction of the tubes were in conformance with ASTM D 1587.

The borehole was advanced to a depth of 0.3 m (1 ft) using hollow stem augers with a central plug. The central plug was removed, and the thin-walled tube with coupling head having a suitable check valve and venting area was lowered to the bottom of the hole. The tube was then hydraulically pushed into the soil using a continuous and rapid motion.

Upon removal of the sample from the hole, the tube ends were sealed in accordance with ASTM D 1587. The tubes were labeled and transported to the laboratory in a vertical position. Samples were stored in a humidity-controlled environment until they were extruded for logging and shear strength testing.

Continuous Sampler

The continuous sampling device, manufactured by the Central Mine Equipment Company, St. Louis, MO, is capable of obtaining a sample 1.5 m (5 ft) in length and 5.8 cm (2.3 in.) in diameter. The inside clearance ratio [*4*] of the cutting head is 14% and the area ratio [*4*] is 89%. Continuous samples of both the natural soil and compacted fill, using the thin-walled tube sampling technique and the continuous sampler, were obtained within a horizontal distance of 1 m (3 ft) of one another. The continuous sampler penetrated the soils 1 m (3 ft).

After removal of the continuous sampler from the soil deposit, the shoe and sampler head were removed and the split barrel was opened. The sample was expeditiously and carefully transferred to a rigid, flat surface and wrapped in plastic wrap. Cheesecloth was then placed around the sample, and the sample was wrapped with aluminum foil. Beeswax was placed along any exposed seams in the foil. The sample was wrapped with adhesive tape and placed into a rigid cardboard tube to facilitate transport to the laboratory for humid storage.

Specimen Preparation

Block samples were carefully exposed using soil knives to remove the rigid plastic tube, beeswax, cheesecloth, and plastic wrap. The block sample, which was approximately 0.3 m (12 in.) in diameter and 0.5 m (18 in.) long, was quartered to provide a sufficient number of specimens for initial testing. Specimens were trimmed using a manual soil lathe with the specimens oriented in the same direction as obtained from the field. The specimen was trimmed to a diameter of approximately 7.4 cm (2.9 in.).

Thin-walled tube samples were extruded in a horizontal direction using a hydraulically operated extruder. Tubes were extruded in the same direction as they were filled. The average diameter of the thin-walled tube samples was 7.4 cm (2.9 in.).

The samples obtained from the continuous sampler were carefully placed on a rigid surface, and the wrappings were removed. The samples were generally 5.8 cm (2.3 in.) in diameter.

All soil samples were visually inspected for desiccation or possible disturbance during transport. The specimen used for testing was typically taken from within the middle third of the sample with care taken to avoid including gravel size particles. The specimen was then placed in a mitre box, and the ends were trimmed square. The height-to-diameter ratio used for testing was between two and three, in accordance with the ASTM Test for Unconsolidated, Undrained Strength of Cohesive Soils in Triaxial Compression (D 2850). The time between sampling and testing ranged from one week to two months. The influence of length of time between sampling and testing on shear strength was not determined as part of this initial study.

Testing Equipment

The triaxial cell, manufactured by Wykeham Farrance, Raleigh, NC, has bonded perspex chambers for working pressures up to 1725 kPa (250 psi). The cell has four valve ports for cell pressure, bottom and top back pressure, and pore water pressure. An O-ring is fitted inside the bushing bore to reduce the loss of fluid along, and friction on, the stainless steel ram.

Triaxial test membranes, formulated from pure latex rubber, were seamless, pinhole free, uniform in elongation, and transparent. The wall thickness was 2 mm (0.08 in.). Filter paper disks and strips were made from Whatman's No. 54 filter paper.

The load cell, pore pressure transducers, and digital indicators were manufactured by Sensotec, Inc., Columbus, OH. The load cell used was Model No. 53 with a capacity of 4536 kg (10 000 lb) with an accuracy within 4% of the indicated load. The pore pressure transducer, Model A205/281-07, has a capacity of 1725 kPa (250 psi) and is accurate to 0.7 kPa (0.1 psi). The digital readout, Model No. 450D, is a 4.5-digit instrument with fine zero adjust, fine gain adjust, and shunt calibration controls.

Testing Procedure

The isotropically consolidated undrained triaxial tests with pore pressure measurements were performed on specimens saturated by back pressure. To reduce the time required for saturation and consolidation of the specimens, saturated strips of filter paper were placed beneath the rubber membrane in accordance with U.S. Army Corps of Engineers standard procedures *[5]*. Saturated filter paper disks were placed at the top and bottom of all specimens tested. Corundum stones with a porosity of approximately 50% were also placed on the base pedestal and below the top platen. Prior to back pressure saturation, a small confining pressure was placed on the specimen, generally 14 kPa (2 psi), and the specimen was allowed to equilibrate. Any change in volume, as measured by a calibrated manometer system *[6]*, was recorded for future use in determining the change in specimen size due to confinement. After equilibrium, the specimen was saturated using 69-kPa (10-psi) increments of cell and back pressure until $\overline{B}$ was measured to be about 1.0. Changes in pore water pressure were taken immediately after application of the increased confining pressure and were measured using a pore pressure transducer connected to the bottom platen. Upon verification of 100% saturation, the specimen was consolidated under the preselected confining pressure. Confining pressures were selected to encompass the preconsolidation pressure of 220 kPa (31.9 psi) for the natural soil specimens and were selected based on experience for the compacted fill. Readings of change in volume of the specimen versus time were taken and plotted for both the top and bottom manometers to ensure 100% primary consolidation was reached prior to shearing. Upon verification of 100% primary consolidation, the change in specimen height was obtained by seating the piston and recording the distance moved.

The piston was seated using the same rate of vertical movement as for the specimen loading. The load registered by the load cell was recorded and used as the zero "differential" load applied to the soil specimen. This zero load takes into account bushing friction along the load rod.

Pore pressure, axial load, and strain measurements were made prior to and during shearing. Generally, the specimens were loaded at a strain rate of 5% per hour and tested to 20% strain.

Results

General

Failure of the soil specimens is defined according to the maximum principal stress difference, more commonly known as the deviator stress. In accordance with U.S. Army Corps of Engineers standards, failure was defined as the deviator stress at 15% axial strain when the deviator stress continually increased during the test [5]. When the deviator stress decreased after reaching a maximum value, the minimum deviator stress obtained after the maximum value but before 15% axial strain was considered the ultimate deviator stress [5]. Nearly all specimens tested reached their peak stress near 15% strain.

Natural Soil

The test results for the natural soil are presented in Figs. 1 and 2. The shear strength values for the block sample determined using the Mohr failure envelopes are ϕ_T = 11.5°, C_T = 76 kPa (11 psi), and ϕ' = 27.2°, C' = 0 kPa (0 psi). The plot of effective stress paths indicates that the specimens were overconsolidated within the lower range of confining pressures; however, this change in strength was not indicated in the effective Mohr failure envelope.

The total strength parameters for the 7.6-cm (3-in.) thin-walled tube samples were ϕ_T = 11°, C_T = 90 kPa (13 psi) below a normal stress of 480 kPa (70 psi), and ϕ_T = 21°, C_T = 0 kPa (0 psi) above a normal stress of 480 kPa (70 psi). The break in strength occurred at approximately twice the estimated preconsolidation pressure. The effective strength was ϕ' = 28.7°, C' = 0 kPa (0 psi) for all normal stresses. The K_F line plotted using the effective stress paths is linear suggesting that the specimens were not overconsolidated, even at low confining pressures. However, individual stress paths at low confining pressures are indicative of overconsolidated soil.

The total strength parameters for the soil samples obtained using the continuous sampler were ϕ_T = 10°, C_T = 69 kPa (10 psi) below 275 kPa (40 psi) normal stress, and ϕ_T = 22°, C_T = 0 kPa (0 psi) above 275 kPa (40 psi) normal stress. The effective strength of ϕ' = 29.3°, C' = 0 kPa (0 psi) was obtained for all normal stresses. The plotted K_F line also suggests that the specimens were not overconsolidated, even under low confining pressures.

The dry density and change in volume for the natural soil specimens after isotropic consolidation and prior to shear are presented in Table 1. The moisture contents were physically determined on the entire soil specimen after shearing in accordance with ASTM D 2216. The dry density values were calculated using the volume change during isotropic consolidation as measured on the calibrated manometer system.

Compacted Fill

Test results for the compacted fill are presented in Fig. 3. The results for the 7.6-cm (3-in.) thin-walled tube samples yielded effective strength parameters of ϕ' = 29.1°, C' = 0 kPa (0 psi), and total strength parameters of ϕ_T = 18.5°, C_T = 34 kPa (5 psi). The effective stress Mohr failure envelope did indicate a change in strength due to overconsolidation by compaction. The effective stress paths indicate that the compacted fill is slightly overconsolidated with the break in strength occurring below a normal stress of 275 kPa (40 psi).

The effective strengths determined from soil samples obtained using the continuous sampler were ϕ' = 27.2°, C' = 0 kPa (0 psi). Total strength parameters are ϕ_T = 18°, C_T = 34 kPa (5 psi). The plotted effective stress paths also indicate that the material has been overconsolidated with a change in strength occurring below a normal stress of 275 kPa (40 psi).

The dry density and change in volume for the compacted fill specimens after isotropic consolidation and prior to shear are presented in Table 2. The moisture contents were physically determined on the entire soil specimen after shearing in accordance with the ASTM Method for Laboratory Determination of Water (Moisture) Content of Soil, Rock, and Soil-Aggregate Mixtures (D 2216). The dry density values were calculated using the

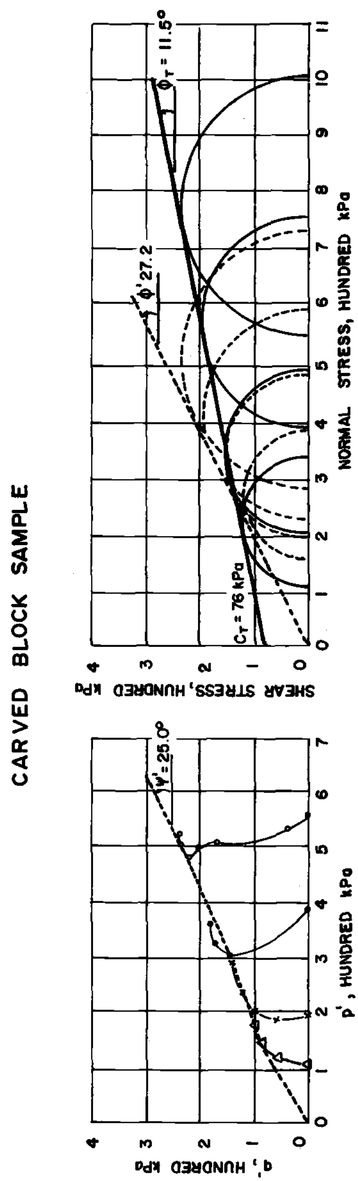

FIG. 1—*Natural soil effective stress paths with Mohr failure envelopes.*

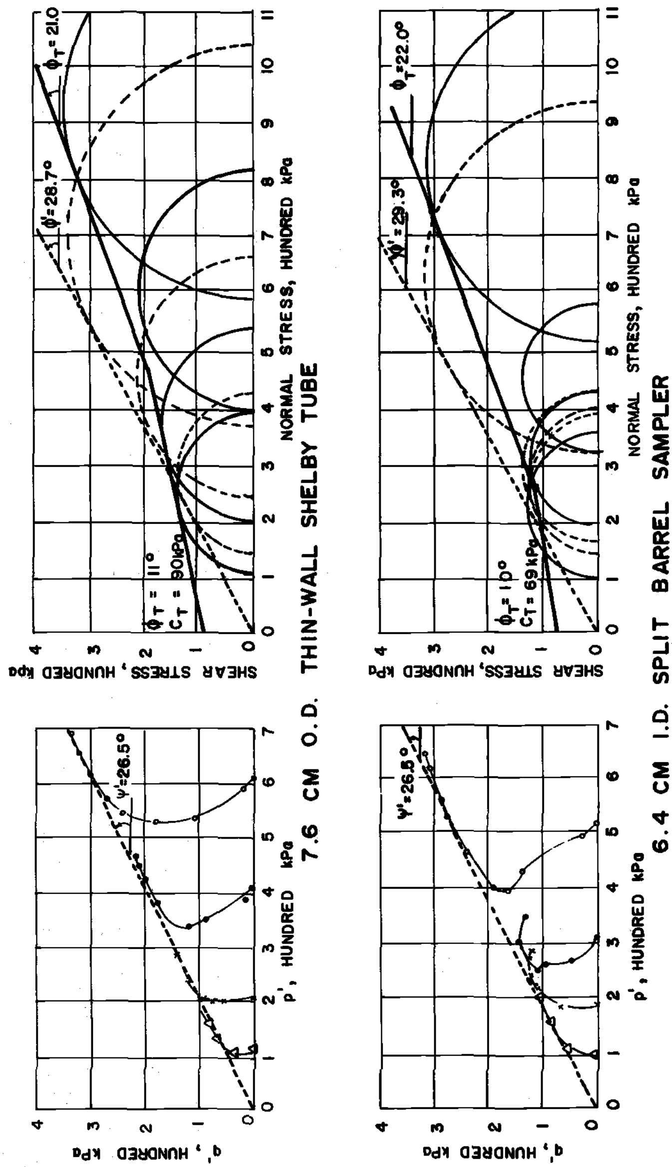

FIG. 2—Natural soil effective stress paths with Mohr failure envelopes.

TABLE 1—*Physical characteristics of natural soil samples before shearing.*

BLOCK SAMPLE				
Confining Pressure, kPa	100	195	385	550
Density, Kg / m³	1980	1930	2000	1920
Moisture Content, %	13.7	13.7	13.5	16.6
Volume Change, %	-0.6	-1.6	-2.0	-1.5
7.6 CM THIN-WALL TUBE SAMPLE				
Confining Pressure, kPa	110	200	400	590
Density, Kg/m³	2080	1940	2090	1950
Moisture Content, %	12.6	16.3	11.7	15.4
Volume Change, %	-1.5	-2.9	-3.8	-4.1
CONTINUOUS SAMPLER				
Confining Pressure, kPa	100	190	320	520
Density, Kg/m³	1930	1720	1710	2080
Moisture Content, %	16.4	21.9	20.2	10.2
Volume Change, %	-1.9	-3.4	-4.8	-3.7

volume change during isotropic consolidation as measured on the calibrated manometer system.

Discussion

General

The process of soil sampling necessarily results in some sample disturbance. The degree of disturbance is dependent on the method and care during and subsequent to sampling. Sampling disturbance occurs as a result of compression of the soil and removal of in situ confining stresses during drilling and sampling, moisture content change due to uncontrolled climate conditions, jostling during transportation, compression during extrusion, and desiccation while trimming and placing the specimen within the triaxial cell. The results of the initial testing program indicate that sample disturbance of various degrees has occurred for each type of sample obtained, thus affecting the laboratory measured strengths.

Ladd and Foott have indicated that a major source of sample disturbance is caused by stress relief which allows negative pore pressures to develop in the sample [7]. Density and shear strength would be expected to vary in the range of confining stress up to the preconsolidation stress depending on the sample type and the time and degree to which the sample has been allowed to rebound. In particular, the tendency for microfissures to develop in the soil after it is removed from its natural confinement may affect the measured hydraulic conductivity, density, and shear strength.

Continuous samplers afford the only practical opportunity to obtain "undisturbed" deep samples in hard soil deposits without introducing wash water. Where block samples can be

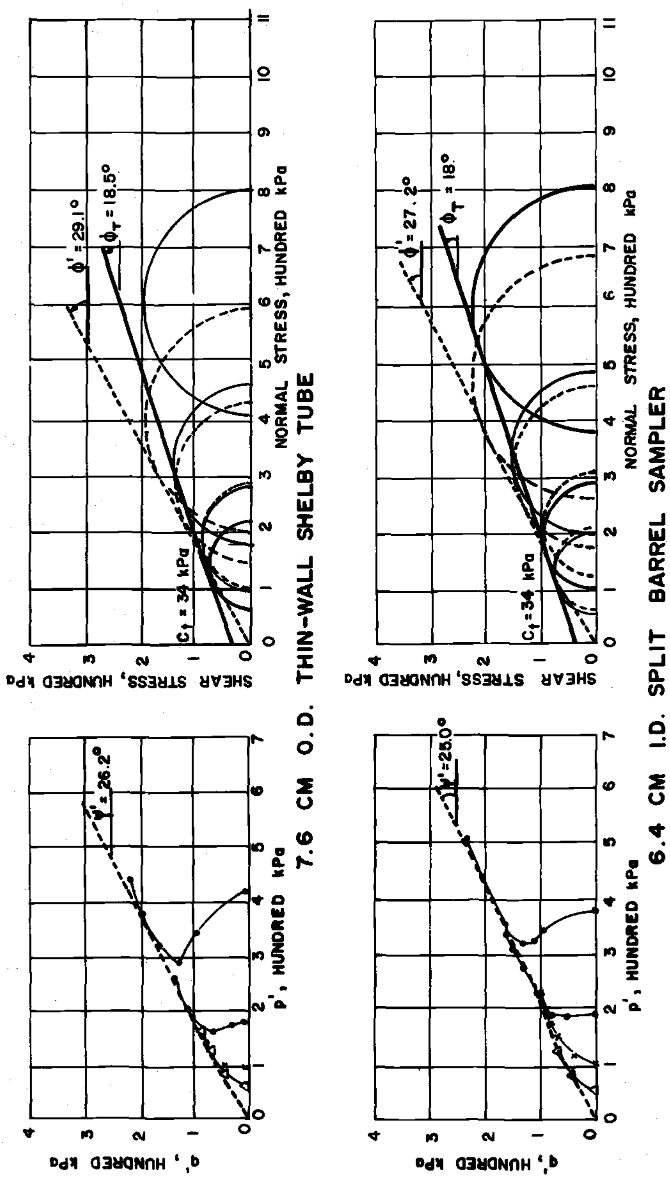

FIG. 3—*Compacted fill effective stress paths with Mohr failure envelopes.*

TABLE 2—*Physical characteristics of compacted fill samples before shearing.*

7.6 CM THIN-WALL TUBE SAMPLE				
Confining Pressure, kPa	60	100	180	410
Density, Kg / m^3	1890	2050	2000	2000
Moisture Content, %	17.6	13.1	12.7	12.4
Volume Change, %	− 1.2	−2.9	− 2.4	−4.4
CONTINUOUS SAMPLER				
Confining Pressure, kPa	55	100	190	380
Density, Kg/ m^3	1950	1960	2000	2040
Moisture Content, %	13.8	13.3	12.4	11.8
Volume Change, %	-0.3	- 0.5	- 2.3	- 4.6

obtained, the amount of stress relief and sample expansion depends on the length of time the sample has been unloaded, the size of the block, and the time between laboratory specimen preparation and insertion into the confining cell.

Thin-walled tube samples typically experience expansion related to the difference between the inside diameter of the tube cutting edge and the inside diameter in the body of the tube. The inside clearance ratio, C_r, which is a function of these two dimensions, should not exceed 1% for high quality "undisturbed" samples [*8*]. The inside clearance ratio for thin-walled tubes must be between 0.5% and 3% by specification, ASTM D 1587.

Limited expansion of thin-walled tube samples occurs through rebound while the samples are stored in the tube. Tubes having a higher inside clearance ratio will have greater capacity for sample expansion due to stress relief. A portion of the rebound is almost instantaneous. This enables thin-walled tube samples to be retrieved in stiff clay soils. Rebound is, however, time dependent and thus the time interval between sample extrusion and application of confinement stress by the cell pressure is important. By contrast, expansion of the samples obtained using the continuous sampler is, for practical purposes, unlimited because the inside clearance ratio for the continuous sampler used is on the order of 14%. The amount of stress relief may be reduced if the samples are held in a confining mechanism immediately after opening the split-barrel sampler.

Disturbance during the sampling operation is dependent not only on the inside clearance ratio but also on the disturbance incurred while physically trimming the sample. This disturbance is directly related to the outside diameter of the sampler as it compares to the inside diameter of the cutting edge. The area ratio, A_r, which is a function of these two values, reportedly should be below about 13 to 15% to obtain "undisturbed" samples [*8*]. The thin-walled tubes and the continuous sampler used for this investigation had area ratios of 12 and 89%, respectively.

Natural Soil

The results indicate that the shear strengths within the overconsolidated zone were similar for all three soil sample types considering the degree of accuracy inherent in triaxial tests routinely used for real projects having limited testing budgets. The effective strength failure envelope had a cohesion intercept of 0 kPa (0 psi) for all three sampler types with the value of ϕ' increasing from 27.2° for the block samples to 29.3° for the continuous samples. The total strength envelope for the block samples was independent of confining pressures having a friction angle of ϕ_T = 11.5° and a cohesion intercept of C_T = 76 kPa (11 psi). The total strength envelope for both the thin-walled tube samples and continuous samples was ϕ_T = 11°, C_T = 90 kPa (13 psi), and ϕ_T = 10°, C_T = 69 kPa (10 psi), respectively, for low confining pressures. For high confining pressures the total strengths for the thin-walled tube samples and continuous samples increased substantially to ϕ_T = 21°, C_T = 0 kPa (0 psi), and ϕ_T = 22°, C_T = 0 kPa (0 psi), respectively.

A review of the consolidation data indicates that the block sample specimens yielded considerably smaller volume changes as a result of increased confining pressures than samples obtained from thin-walled tubes or the continuous sampler. The volume changes for both the thin-walled tube specimens and continuous sampler specimens were similar, with the continuous sampler specimens generally having a greater decrease in volume. This greater volume change for the continuous sampler specimens indicates that more rebound occurred during or subsequent to the sampling operations, and is most likely due to the greater inside clearance ratio.

The lack of sufficient strength data and the minor inconsistencies in dry density and moisture content data suggest a statistical evaluation of the data should not be attempted. The results do indicate that the continuous sampler and thin-walled tubes provided soil samples which, when tested in the laboratory, provided effective shear strength values which appear accurate and consistent enough for feasibility studies, preliminary analyses, and for final design when the range of applied stresses will be above the maximum past pressure. Total strength parameters as determined from this preliminary study suggest that sample disturbance produced by each of the three methods will affect the laboratory strength data.

Compacted Fill

The data obtained from samples of the compacted fill were similar for both sampling methods. The dry density values for the continuous sampler specimens increased with confining stress as the moisture contents decreased. The moisture contents for the thin-walled tube sample specimens also decreased as expected; however, there was not a definite increase in dry density.

The change in specimen volume with increased confining pressure was considerably less for the continuous sampler specimens within the area of specimen reloading. When the confining pressures exceeded the estimated past pressure induced during compaction, both the continuous sampler specimens and the thin-walled tube specimens behaved similarly with a marked increase in volume change. These results were expected and indicate that at high pressures the specimens will behave as normally consolidated soils.

The data, while limited, indicate that the continuous sampler can be used to obtain compacted clay fill samples that are equivalent, if not better, than those obtained using 7.6-cm (3-in.) diameter thin-walled tubes. The relationship between laboratory measured strengths from block samples and those from continuous samples was not determined and therefore the quantitative effect of using the continuous sampler within fills cannot be determined from the limited testing.

Additional Factors Affecting Strength

The sample disturbance produced during drilling and sampling operations affects the shear strength by altering the soil structure through remolding and relaxation of in situ confining pressures. Additional factors will affect the measured shear strength of soil samples and must be taken into account when selecting the sampler type and testing procedures used for geotechnical investigations.

Results of this study and previous work by others suggest that selection of the sampler type should be based on the following considerations:

1. *Sample Diameter*—Samples having large-diameter particles or secondary structure will be affected by sample size. The smaller sized samples may yield falsely higher strengths due to failure plane restrictions or exclusion of natural weak seams or layers.
2. *Thixotropic Regain*—The increase in strength after sampling, during sample preparation, sample saturation and consolidation, and the length of time between sampling and shearing will to some degree influence laboratory test results and should be considered when analyzing test data.
3. *Rate of Back Pressure Saturation*—Increased rates and magnitudes of back pressure saturation may change the structure of the soils depending on the compressibility of the soil skeleton.
4. *Confining Pressure*—The application of confining pressures and previous stress history of the soil will have a direct influence on measured shear strength. The use of normalized testing methods should be considered to reduce the effect of sample disturbance on measured shear parameters.
5. *Rate of Load Application*—The measured strength of cohesive soil generally increases as the rate of shear is increased.
6. *Accuracy of Measuring Devices*.

Conclusions

The effective shear strength of an overconsolidated clayey till soil in the range of confining stress above the preconsolidation stress appears to be unaffected by whether the sample was carved from a block sample, obtained with a thin-walled tube, or obtained using a continuous sampler. In the range of confining stresses above which the soils will behave as though normally consolidated, shear strength would be expected to be relatively unaffected by any of the three sampling techniques described above. Therefore, in those higher stress ranges, samples obtained using the continuous sampler would be considered to yield representative "undisturbed" samples.

In the range of confining stress below the preconsolidation stress, constraint of the sample will to some degree affect the density and the shear strength even though the moisture content may not change. Similarly the laboratory-measured hydraulic conductivity of samples may be affected by the potential for rebound and the development of microfissures. Conventional thin-walled tube samples obtained in accordance with ASTM D 1587 allow for limited rebound and expansion and thus may have limited sample disturbance for recovery ratios of 100%. Samples obtained with the continuous sampler have the potential for unlimited rebound and expansion unless restrained by some type of mechanical device such as the walls of a thin-walled tube.

The selection of which sampler to use for securing "undisturbed" samples should consider the confinement afforded to the soil in the prototype at the time the shear strength or other parameters are desired.

The results of this initial comparative testing program indicate that:

1. The continuous sampler may be used, under limited conditions, to provide soil samples of cohesive fills which are equivalent to those obtained using thin-walled tubes.

2. Samples of the slightly overconsolidated glacial till obtained with the continuous sampler visually appeared to be more disturbed than those obtained with the thin-walled tubes.
3. Effective shear strength parameters determined using samples obtained by any of the three methods are considered accurate for use in feasibility or preliminary investigations, especially where the future loading conditions and testing pressures exceed the maximum past confinement.
4. The continuous sampler can be used to obtain samples of hard cohesive soils where thin-walled tubes may be impossible to push. This testing indicates the continuous sampler affords the opportunity to obtain a relatively undisturbed soil sample below the practical depth limits for test pits without the introduction of wash water.

Recommendations

Additional work is required to determine the effectiveness of using the continuous sampler within various soil deposits having different depositional characteristics. This work should include:

(1) effect of sampling rate,
(2) effect of sample size,
(3) effect of storage time,
(4) effect of confining stresses placed on the sample during storage,
(5) effect of hardened shoe dimensions and sample retainer shape on soil samples, and
(6) effect of sample sensitivity.

References

[1] Willman, H. B., *Summary of the Geology of the Chicago Area*, Circular 460, Illinois State Geological Survey, Urbana, IL, 1975.

[2] Willman, H. B. et al., *Handbook of Illinois Stratigraphy*, Bulletin 95, Illinois State Geological Survey, Urbana, IL, 1975.

[3] Hvorslev, M. J., *Subsurface Exploration and Sampling of Soils for Civil Engineering Purposes*, Waterways Experiment Station, Vicksburg, MI, Nov. 1949 (Reprint, 1962 and 1965).

[4] Peck, R. B., Hanson, W. E., and Thornburn, T. H., *Foundation Engineering*, 2nd ed., Wiley, New York, June 1973.

[5] U.S. Army Corps of Engineers, *Triaxial Compression Tests*, Appendix X, Laboratory Soil Testing, Engineering Manual EM 110-2-1906, Department of the Army, Washington, DC, May 1980.

[6] Bishop, A. W., and Henkel, D. J., *The Measurement of Soil Properties in the Triaxial Test*, 2nd ed., Edward Arnold, London, 1962.

[7] Ladd, C. C., and Foott, R., "New Design Procedure for Stability of Soft Clays," *Journal of the Geotechnical Engineering Division, American Society of Civil Engineers*, Vol. 100, No. GT7, July 1974, pp. 703–786.

[8] The Sub-Committee on Soil Sampling, International Society for Soil Mechanics and Foundation Engineering, *International Manual for the Sampling of Soft Cohesive Soils*, Tokai University Press, Tokyo, Japan, 1981.

Norman D. Dennis[1]

Influence of Specimen Preparation Techniques and Testing Procedures on Undrained Steady State Shear Strength

REFERENCE: Dennis, N. D., "**Influence of Specimen Preparation Techniques and Testing Procedures on Undrained Steady State Shear Strength,**" *Advanced Triaxial Testing of Soil and Rock, ASTM STP 977,* Robert T. Donaghe, Ronald C. Chaney, and Marshall L. Silver, Eds., American Society for Testing and Materials, Philadelphia, 1988, pp. 642–654.

ABSTRACT: Results are presented for four series of isotropically consolidated undrained triaxial shear tests conducted on recompacted specimens of Banding Sand. Specimen preparation procedures and the method of loading were varied to determine their effect on the undrained steady state strength of the sand and on the position of the steady state void ratio curve. Comparison of test results indicates that both sample preparation technique and method of loading affect the undrained steady-state strength.

KEY WORDS: triaxial test, liquefaction, steady state strength, critical void ratio, compaction, specimen preparation

The undrained steady state shear strength of sandy soils has been used for evaluating stability against flow slides or liquefaction failures for nearly 50 years, since Casagrande first proposed the concept of critical void ratio [*1*]. Within the past two decades considerable effort has been devoted to the study of liquefaction phenomena. Laboratory and in situ testing procedures have been improved, and theoretical models have been developed to aid the engineer in predicting the physical behavior of soil. Yet, many uncertainties remain in determining the effects of various laboratory testing procedures on measured properties and in the ability to correlate laboratory test results to field conditions.

The procedures in use today for analyzing the safety of slopes and embankments against liquefaction failure may be broadly categorized into two general approaches. One approach focuses on the buildup of pore pressure which may trigger liquefaction. The susceptibility of soils to such buildups is inferred from in situ penetration tests and cyclic load testing of undisturbed samples in the laboratory. The other approach focuses on the potential for a flow failure to occur through the determination of the in situ steady state strength of the soil by means of laboratory tests. Uncertainties exist in both procedures. The ability to predict pore pressure buildup accurately in the field from cyclic load tests has been questioned, as has the ability to correlate the undrained steady state shear strength measured in the laboratory to in situ strength.

Undrained steady state shear strength is known to be sensitive to minor changes in void ratio which occur during sampling and testing. This sensitivity requires that the strength, measured in the laboratory, be corrected to reflect the actual in situ void ratio of the soil. One procedure for accomplishing this correction first establishes the steady state void ratio

[1] Executive officer, 92nd Engineering Branch, Fort Stewart, GA 31314.

as a function of the minor principal effective stress at failure ($\bar{\sigma}_{3f}$), using consolidated undrained triaxial compression tests ($\bar{R}$-type) on a series of reconstituted test specimens [2]. The slope of the resulting steady state line is then used as a reference to adjust the value of $\bar{\sigma}_{3f}$, obtained from a test on an undisturbed specimen, to a new value at the in situ void ratio. The basis for this correction procedure is the presumption that the steady state void ratio (by extension, the slope of the steady state line) is independent of sample preparation techniques and testing procedures. Presumably, at the large strains necessary to reach steady state the specimen becomes completely remolded.

While the $\bar{R}$-type triaxial test is used frequently in practice, only a limited number of studies have been conducted to determine the effects of testing procedures on the measured steady state strength [3–5]. In contrast, numerous studies have addressed procedural effects on cyclic triaxial testing and have established guidelines for the conduct of that test [6–12]. Some of the procedural aspects found to affect cyclic triaxial testing may also affect monotonic triaxial testing. Hence, the purpose of this investigation was to isolate two readily controllable testing variables and determine their effects on undrained steady state strength, measured using the $\bar{R}$-type triaxial compression test.

Scope

Four series of isotropically consolidated undrained triaxial compression tests were performed with the test variants being the method of loading and the specimen preparation technique. The results of Castro were used as a reference for the comparison of the steady state lines [3]. The principal objective was to determine if stress-controlled versus strain-controlled loading and equal-energy versus equal-volume compaction produced significant differences in the slope of the associated steady state lines. A secondary objective was to determine if Castro's results could be reproduced with a different triaxial test device.

Laboratory Procedures

Specimen Material

All test specimens were prepared from a uniform, clean, fine quartz sand, sold by the Ottawa Silica Company under the brand name of Banding Sand. The grain size and grain shape characteristics of this sand were nearly identical to those of the Banding Sand tested by Castro, which provided a basis for the direct comparison of the results of this investigation with those of Castro [3]. A summary of the physical characteristics of the sand used in this investigation and those reported by Castro [3] are illustrated in Fig. 1.

Equipment

The triaxial test chamber employed a 19-mm-diameter loading piston guided through the head plate by a linear ball bushing with an O-ring seal. The loading piston was rigidly attached to the specimen top cap with a threaded connection. This arrangement facilitated vertical alignment and prevented tilting which would allow the specimen to slide out from under the loading platen at large strains. The specimen end platens were 73.6 mm (2.9 in.) in diameter with 71.2-mm (2.8-in.) diameter, recessed, porous stones.

The use of nonlubricated end platens is a significant variation from the triaxial chamber used by Castro [3], although, it is similar to many used by commercial laboratories today. Even though the work of Johnson [4], Olsen and Campbell [13], and Bishop and Green [14] indicates that the use of nonlubricated end platens has a small effect on strength, when specimens have a length-to-diameter ratio greater than 2.0, it is conceded that the end platen

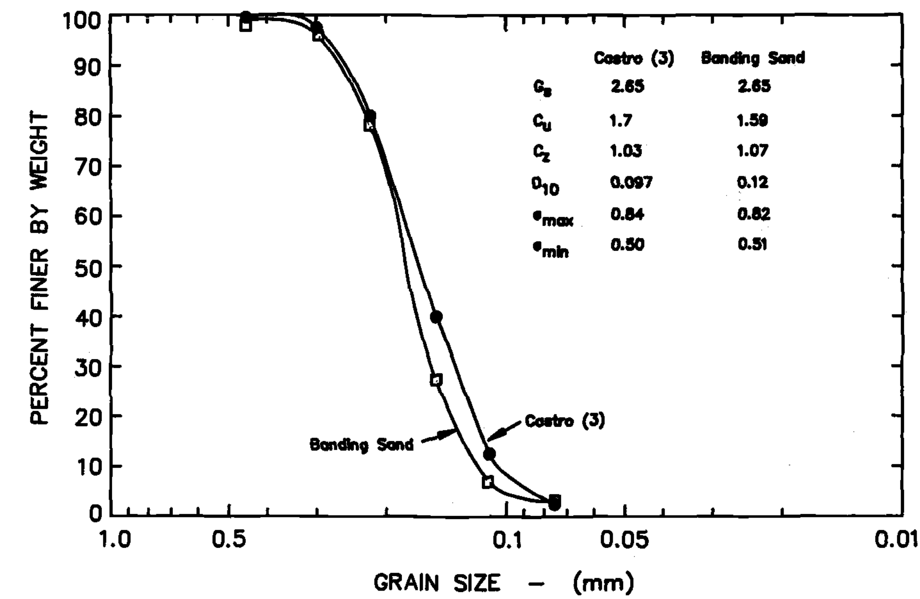

FIG. 1—*Comparison of physical characteristics of the Banding Sand used in this study with the sand used by Castro* [3].

arrangement probably results in higher measured strengths. However, the purpose of this investigation was to measure strength in comparative rather than absolute terms, so the potential for obtaining inferior quality data is less important.

Electrical transducers were used to measure load, pore pressure, chamber pressure, and specimen deflection. Axial load and deflection were measured externally. For strain-controlled tests these parameters were recorded using a multichannel digital voltmeter with a pushbutton-initiated printer. For stress-controlled tests, a light-recording oscillograph, operating at speeds ranging from 2.5 to 40 cm/s, was used to provide a continuous record of the transducer output.

Specimen Preparation

Both specimen preparation procedures used in this investigation are moist tamping techniques. The only variation in the two procedures is the method of compaction. The initial dimensions of all test specimens were 71.2 mm in diameter and 155 mm in height.

All test specimens consisted of ten layers, compacted in a rubber membrane confined by an airtight split mold securely positioned around the base pedestal of the triaxial cell. A predetermined weight of oven-dried sand, sufficient to obtain the prescribed density for one layer, was mixed with enough water to achieve a molding water content of 8% prior to placement in the mold. This water content produced the greatest bulking of the sand and allowed very loose test specimens to be prepared.

The compaction procedure, referred to here as the equal-volume method, employed undercompaction to account for the densification of lower layers due to the placement of succeeding layers. While the height of each layer was maintained constant, the weight of the sand placed in the lowest layer was 2% less than the weight of the sand placed in the top layer. The tamping device, illustrated in Fig. 2, was adjusted to produce the correct layer height and then lowered repeatedly into the mold to compact the specimen. Tamping

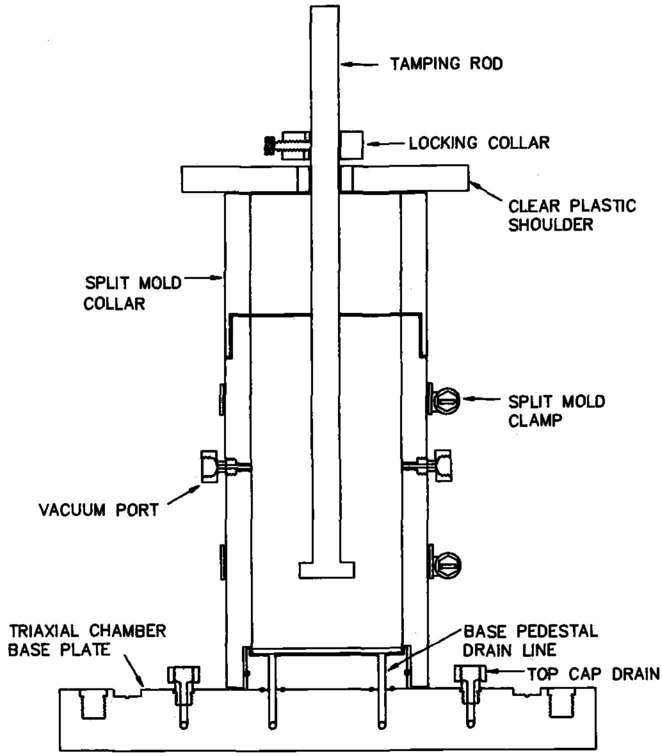

FIG. 2—*Schematic diagram of tamping device for equal-volume compaction.*

started in the center of the specimen and proceeded in a radial fashion to the perimeter of the mold until no further compactive effort could be imparted by the tamper. The surface of each compacted layer was scarified lightly, and the procedure was repeated until all ten layers were in place. Following compaction, the mold collar was removed, and the specimen top cap was placed. The rubber membrane was securely fastened to the top cap with an O-ring.

The compaction procedure referred to as the equal-energy method was modeled after the technique reported by Castro [*3*]. Ten layers of equal weight were placed in the mold using a constant compactive effort of twelve static applications of a weighted tamping foot. A trial and error procedure was necessary to determine the correct tamper weight to use for a given target density. The target height for specimens prepared in this manner was slightly higher than 155 mm to allow for subsequent screeding of the top surface. Once the specimen surface was smooth and level, the top cap was placed as described earlier. The remainder of the testing procedure was the same for each specimen regardless of preparation technique.

Saturation

After a vacuum of 34.5 kPa was applied to the top and bottom drainage lines, the split mold was removed. The specimen was then measured at five locations using a circumferential tape for the diameter and at three locations using a vernier caliper for the height. The average of the measurements, combined with the total dry weight of the material, was used to calculate the initial void ratio of the test specimen. The triaxial cell was then assembled and filled to within 10 mm of the head plate with deaired water.

To facilitate saturation, a differential vacuum was applied to both the specimen drainage lines and the triaxial chamber. The two vacuum sources were controlled in such a manner that the specimen vacuum was increased to 96 kPa while the effective confining pressure was maintained at 34.5 kPa. Deaired water, held under a vacuum of 85 kPa, was slowly introduced through the bottom drainage line and allowed to flow through the specimen under a small gradient of 11 kPa into a collection burette. Typically, 10 to 20 mL of water were collected in the burette before minute air bubbles ceased to appear. At this point the bottom drainage line was closed and vacuum was incrementally removed from both the chamber and the specimen until the chamber pressure was a positive 34.5 kPa and the specimen pore pressure was zero. Back pressure was applied in increments of 69 kPa until a B value exceeding 0.99 was obtained. Using this technique, the maximum back pressure required for saturation was only 207 kPa and there was no need for subsequent flushing of the specimen. Volume change during the saturation process was calculated based on movement of the loading piston and the assumption that the specimen deformed as a right cylinder. Piston movements during this phase were less than 0.03 mm which suggests the volume change was small.

Consolidation

Test specimens were consolidated by increasing the chamber pressure and simultaneously applying a small axial load to maintain an isotropic state of stress. During this phase changes in both axial height and volume were measured. The measured change in volume was used to compute the final void ratio of the specimen after consolidation. The measured volume change was in close agreement with the volume change calculated using the change in axial height and the right cylindrical deformation assumption.

Loading

Specimens tested in the strain-controlled mode were loaded by a gear-driven press operating at a constant velocity of 0.95 mm/min. The specimen was loaded until a strain in excess of 25% was attained, or until the specimen evidenced strong dilation and the applied force approached the safe limit of the load cell.

Stress-controlled loading was accomplished using a pneumatic cylinder with a 92-mm "Bellofram type" diaphragm capable of providing an axial force of 1500 N from a high-volume air supply. Specimens were step loaded at 1-minute intervals by initially increasing the applied force in increments of 10% of the expected failure load. As the specimen approached failure, the loading increment was reduced to 2% of the expected failure load. Specimens loaded in this fashion typically reached peak strength in 14 to 16 min with subsequent failure occurring in less than two tenths of a second.

Results and Discussion

With two exceptions, the test results reported here are for specimens that exhibited contractive behavior and approached what is believed to be steady state conditions. The two exceptions were tested under strain-controlled loading and dilated early in the test. No clearly defined failure surfaces were observed for these tests before they were terminated at an axial load near the rated limit of the load cell. The failure mode for the remainder of the strain-controlled tests was by progressive bulging in the middle third of the specimen.

The bulging of specimens prepared using the equal-volume technique progressed toward the end caps at large strains. The bulging of specimens prepared with the equal-energy technique remained within the middle third of the sample.

For stress-controlled tests the failure mode was less obvious because of the rapidity of the failure. The loading piston was fitted with a load stop to prevent travel beyond 35% strain so a true flow failure was interrupted at this point. At the point of peak strength, strains were small and there was no evidence of bulging in the sample. At the conclusion of the test the bulging appeared to be uniform throughout the entire height of the sample. In several tests the bulging was slightly more pronounced in the lower third of the sample. However, this was not related to the sample preparation technique, because samples prepared using both techniques failed in a similar manner.

The stress–strain responses for all tests were similar in that peak strength was reached at strains of less than 1%, and ultimate strength was reached by 8% strain. Three general stress–strain responses were observed and are illustrated in Fig. 3. The stresses illustrated

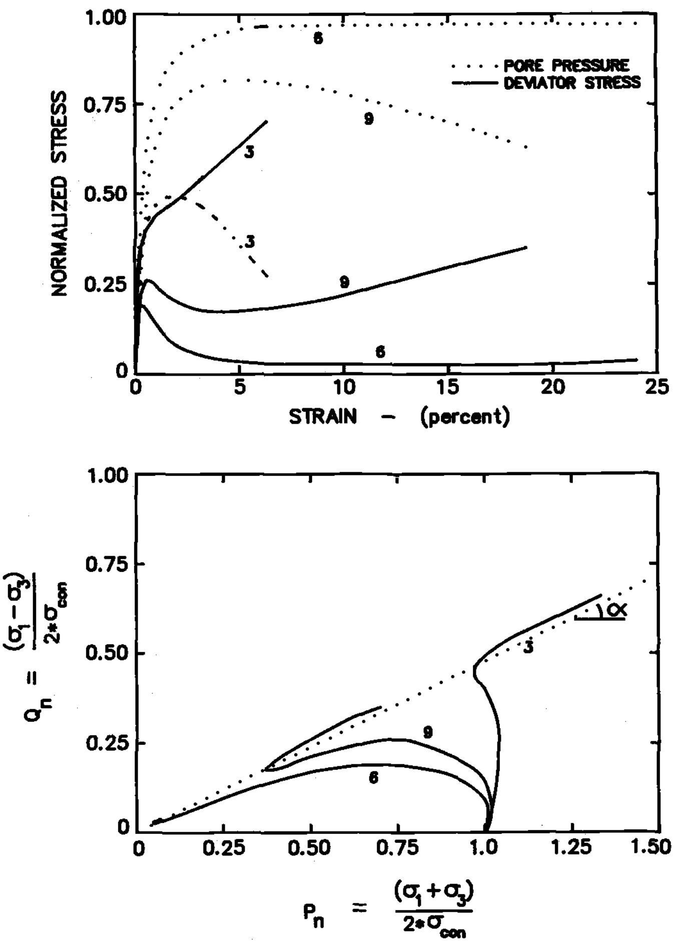

FIG. 3—*Stress–strain curves and stress paths for liquefaction, limited liquefaction, and dilative response.*

in Fig. 3 have been normalized by dividing the shear stress and normal stress by the consolidation pressure to allow all of the data to be presented on the same axes.

Both the stress–strain curve and the stress path for test number 6 are representative of a liquefaction-type failure. With this type of failure the steady state strength of the specimen is achieved at a relatively small strain and remains constant to very large strains. This type of failure is also evidenced by a stress path that exhibits no reversal in curvature at the α-line, which is analogous to the failure envelope, or strength envelope, at steady state. The parameter α is defined as

$$\alpha = \tan \frac{(\bar{\sigma}_{1s} - \bar{\sigma}_{3s})}{(\bar{\sigma}_{1s} + \bar{\sigma}_{3s})} \tag{1}$$

and

$$\sin \phi = \tan \alpha \tag{2}$$

where

$\bar{\sigma}_{1s} - \bar{\sigma}_{3s}$ = Principal stress difference at steady state
$\bar{\sigma}_{1s} + \bar{\sigma}_{3s}$ = Normal stress at steady state
ϕ = Steady state friction angle (in terms of effective stress)

The stress–strain curve and stress path for test number 9 illustrates a limited liquefaction failure. The specimen initially exhibited contractive behavior, indicated by a decrease in strength and the stress path curving toward the origin. However, at larger strains the specimen began to dilate, which is indicated by the reversal in curvature of the stress path and by the increase in strength. While the stress–strain response for test number 9 is less desirable than that of test number 6 for this testing program, it is believed that the measured effective stress and strength at the point of stress path reversal were very close to steady state values.

The stress–strain curve and the stress path for test number 3 characterize a dilative response. Specimen strength continues to increase with increasing strain and the stress path moves up, rather than down, the α-line. Without a well-defined reversal in curvature of the stress path even estimation of steady state conditions is questionable.

Steady State Strength

A summary of all test results are presented in Table 1. Tests are grouped by compaction technique and method of loading and are ordered by decreasing void ratio within each category. The values for α, presented in the final column, are for a linear regression line which was forced through the origin. Thus, they are not actually average values for the series and the importance of the high values of α for samples with stress paths terminating near the origin is reduced. These values for α, in combination with the deviator stress at steady state, provide an indication of the specimen strength over a relatively narrow range in void ratios. The strain-controlled series both had very similar strength envelopes, as defined by the value for α, even including the two tests where dilation occurred. However, the strength envelopes for the stress-controlled series were significantly different.

This difference in the strength envelopes, as well as the observed differences in the deviator stress for the stress-controlled series, indicates that the specimens prepared using the equal-volume technique were stronger than those prepared using the equal-energy procedure. Although it has not been proven in this investigation, by extension of the work by Gilbert

[7], it may be inferred that the increase in strength is a result of a more uniform void ratio distribution within the test specimen at steady state.

Another indication of specimen strength was the resistance to volume change when the compacted specimens were initially subjected to a small vacuum prior to removal of the mold. The equal-volume compaction series of tests was conducted first, and the target densities for the equal-energy compaction tests were based on the results of the first series. In every case, save one, the void ratios for the equal-energy compacted specimens were lower after application of the initial vacuum than those for the equal-volume compacted specimens. Numerous attempts were made, using the equal-energy procedure, to create specimens with a void ratio greater than eight, after consolidation. The target densities for the equal-energy specimens were reduced well below those of the equal-volume specimens, but when the initial confining vacuum was applied the soil contracted to produce a void ratio at or below eight prior to consolidation. Thus, the disparity of the void ratios for the strain-controlled series was not deliberate, but a result of an inability to create specimens of similar void ratios using the two different compaction procedures.

The similarity in the strength envelopes for the strain-controlled tests is believed to have resulted from a redistribution of void ratios within the test specimen during loading. Unlike the stress-controlled test, where the transition from peak strength to ultimate strength is virtually instantaneous (< 0.2 s) and is initiated at small strains, the strain-controlled test allows a sufficient period of time for internal readjustment of particles [15]. Thus, the zone of failure may be at a void ratio significantly different than that at which the specimen was prepared. Under stress-controlled loading conditions the measured test parameters are much more likely to reflect the strength of the localized zones of loose material within the specimen that were created during its preparation. Therefore, the preparation technique should ensure a uniform density distribution throughout the test specimen.

Steady State Line

The relative vertical and horizontal position of the steady state line is not considered important when employing the procedure recommended by Poulos and coworkers [2] to correct the undrained steady state strength, measured in the laboratory, to its in situ value. Relatively minor differences in grain size distribution may greatly affect the vertical position of this line [16]. However, the slope of the steady state line is critical to the correction procedure and should be affected only by the soil properties and not the testing procedures.

The steady state line reported by Castro [3] was used initially as a guide to achieve a target void ratio, after consolidation, which would result in a contractive specimen. After several unsuccessful attempts at creating a specimen with a contractive response in the range of void ratios used by Castro it was concluded that his results could not be reproduced precisely. All specimens tested in this investigation resulted in a steady state line well above that reported by Castro [3]. This discrepancy may have been the result of minor differences in the grain size distribution between the two sands but is more likely a result of differences in the triaxial devices. The use of nonlubricated end platens in this investigation likely produced more resistance to a flow failure than the lubricated end platens used by Castro. Another probable cause for the discrepancy was the difference in tracking the specimen volume change from preparation through consolidation. Volume changes reported by Castro [3] were calculated based on the one-dimensional consolidation characteristics of the sand, rather than physically measured, as in this investigation.

Stress-Controlled Loading

Figure 4 illustrates a comparison of the steady state lines obtained from this study and the line reported by Castro [3]. Two points may be inferred from the comparison. First,

TABLE 1—*Summary of test results.*

Test Number	σ_c, kPa	e_c	ϵ_p, %	$(\bar{\sigma}_1 - \bar{\sigma}_3)_p$, kPa	ϵ_u, %	$(\bar{\sigma}_1 - \bar{\sigma}_3)_u$, kPa	Stress–Strain Response[a]	σ_{3min} kPa[b]	α, degrees[c]	Average α, degrees[c]
				Strain Control, Equal Energy						
1	207	0.861	0.48	72.3	4.0	4.9	L	3.5	22.5	
2	483	0.749	0.67	380	3.0	345	L-D	187	25.5	25
3	1035	0.717	—	—	—	—	D	438	25.2	
4	1035	0.705	—	—	—	—	D	525	24.4	
				Strain Control, Equal Volume						
5	207	0.833	0.23	73.5	6.0	6.5	L	2.0	30.4	
6	207	0.826	0.38	78.5	6.0	10.3	L	5.5	25.3	
7	345	0.805	0.33	159	6.0	39.7	L	20.0	26.5	26
8	345	0.787	0.55	168	4.0	73.8	L	36	26.9	
9	483	0.772	0.57	251.8	4.0	167.7	L-D	89	25.9	
				Stress Control, Equal Energy						
10	207	0.844	0.40	86.9	6.0	6.7	L	1.4	35.4	
11	207	0.775	0.60	118.3	6.5	50	L	33.1	23.3	
12	345	0.772	0.40	180.4	7.5	66.2	L	40.7	24.1	22.5

13	345	0.761	0.50	265.1	8.0	125.6	L	103.5	20.5	
14	483	0.755	0.76	353.9	8.0	144.9	L	125.5	20.0	
Stress Control, Equal Volume										
15	345	0.799	0.60	189	6.0	12.4	L	0.34	43.5	
16	207	0.787	0.67	120.8	4.0	27.9	L	0.69	43.7	
17	207	0.760	0.35	132.5	4.0	53.8	L	20.7	29.5	31
18	207	0.758	0.50	180.6	4.0	122.0	L	27.6	24.5	
19	345	0.751	0.80	292	3.0	221.5	L	97.5	28.0	

[a] L = Contractive behavior, steady state achieved
L-D = Contractive behavior followed by dilation
D = Dilative behavior
[b] Effective confining pressure at maximum pore pressure response.
[c] Taken at maximum stress ratio, $\alpha = \bar{\sigma}_1 - \bar{\sigma}_3/\bar{\sigma}_1 + \bar{\sigma}_3$.
[d] Linear regression forced through the origin
σ_c = Consolidation pressure
ϵ_c = Void ratio after consolidation
ϵ_p = Strain at peak strength
$(\bar{\sigma}_1 - \bar{\sigma}_3)_p$ = Deviator stress at peak strength
ϵ_u = Strain at ultimate strength
$(\bar{\sigma}_1 - \bar{\sigma}_3)_u$ = Deviator stress at ultimate strength

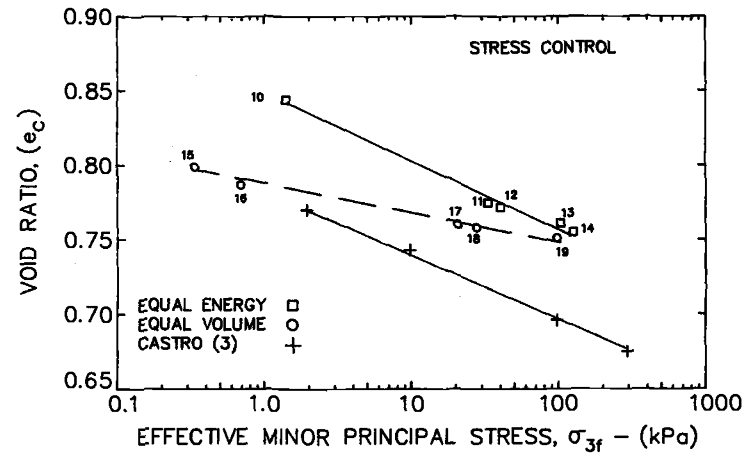

FIG. 4—*Comparison of steady state lines achieved with stress-controlled loading and steady state line after Castro* [3].

the difference in slope of the steady state lines for the two series of tests conducted during this investigation indicates that sample preparation technique does affect the slope of the steady state line. Second, the slope of the steady state line for the equal-energy series is virtually parallel to the steady state line reported by Castro [3]. Because the sample preparation technique and method of loading for this series were the same as those used by Castro in his investigation, it would appear that differences in the triaxial apparatus are not important in the determination of the slope of the steady state line.

The value of the effective confining stress at failure for test number 15 is reported in Table 1 as 0.34 kPa, and it was interpolated from the oscillograph recording as that value. However, the expanded scale of the recording allowed interpolation of stresses somewhat below the manufacturer's advertised repeatable accuracy for the pore pressure transducer of 0.625 kPa. In light of this fact, that value might be more properly reported as the limiting

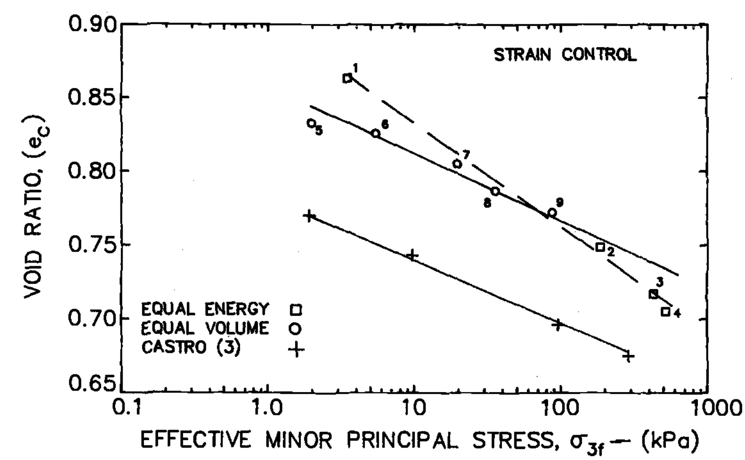

FIG. 5—*Comparison of steady state lines achieved with strain-controlled loading and the steady state line after Castro* [3].

accuracy of the transducer, or 0.625 kPa. This change would alter the slope of the steady state line for the equal-volume series only slightly, and would not alter any conclusions drawn from Fig. 4.

Strain-Controlled Loading

The results of strain-controlled tests, illustrated in Fig. 5, indicate that differences in sample preparation technique had a very small influence, if any, on the slope of the steady state line. While the data could be interpreted to represent two steady state lines, as illustrated in Fig. 5, a more reasonable interpretation would be one line which best fits all the data except tests 3 and 4. The resulting steady state line would then agree favorably with that reported by Castro [*3*]. In addition, the average strength parameter α, determined in this investigation, is also in close agreement with that of Castro (25 and 26° versus 26.5°).

Data for Tests 3 and 4 are included in Fig. 5 even though a dilative response was obtained in those tests. The data presented represent the point of maximum induced pore pressure and serve to illustrate that data from dilative tests may be useful in establishing the steady state line. Necessary conditions would be that the pore pressure response be a significant fraction of the applied confining pressure, and a reasonably well-defined reversal in curvature of the stress path at the α-line.

Comparison of Testing Procedures

The range of void ratios over which a liquefaction type failure will occur is very small for strain-controlled loading unless extremely high confining pressures are used (higher than those normally available in most laboratories) or extremely loose samples can be prepared. By contrast, liquefaction failures were induced through stress-controlled loading over a much broader range in void ratios, and at lower confining pressures. One major disadvantage of stress-controlled loading has been the need for more complicated data recording equipment. However, with the availability of relatively inexpensive high-speed data acquisition systems, this disadvantage is no longer as significant. Of the two compaction methods used in this investigation, the equal-volume technique was easier to employ. There was no need for trial and error determinations for the correct tamper weight, and the resulting specimens were more resistant to volume change when a confining vacuum was applied. For strain-controlled loading the equal-volume procedure would be the method of choice because looser specimens could be prepared. This, in turn, would reduce the required confining pressure necessary to produce a contractive response.

Conclusions

- Specimens prepared using the equal-volume technique were more resistant to volume change when subjected to a confining vacuum than those prepared using the equal-energy technique.
- Specimen preparation technique affected the slope of the steady state line for stress-controlled loading.
- The effect of specimen preparation technique was insignificant for strain-controlled loading.
- Liquefaction type failures could be induced at much lower void ratios for stress-controlled loading than for strain-controlled loading when confining pressures were equal.
- Specimens tested using strain control had significantly higher strengths at steady state than specimens tested using stress control when void ratios were similar.

Acknowledgment

The work described was performed at the U.S. Army Engineer Waterways Experiment Station, Geotechnical Laboratory, Vicksburg, Mississippi. Sincere appreciation is extended to the staff for providing equipment and instrumentation support.

References

[1] Casagrande, A., "Characteristics of Cohesionless Soils Affecting the Stability of Slopes and Earth Fills," *Journal of the Boston Society of Civil Engineers,* Jan. 1936. (Reprinted in "Contributions to Soil Mechanics 1925–1940," *Journal of the Boston Society of Civil Engineers,* Oct. 1940.)
[2] Poulos, S. J., Castro, G., and France, J. W., "Liquefaction Evaluation Procedure," *Journal, Geotechnical Engineering Division, American Society of Civl Engineers,* Vol. III, No. 6, June 1985.
[3] Castro, G., "Liquefaction of Sands," Ph.D. thesis, *Harvard Soil Mechanics Series,* No. 81, 1969.
[4] Johnson, H. V., "The Effects of End Platens, Method of Loading and Specimen Size in Monotonic Triaxial R Tests," Misc. Paper GL-82-10, U.S. Army Engineer Waterways Experiment Station, Vicksburg, MS, Sept. 1982.
[5] Torrey, V. H., "Some Effects of Rate of Loading, Method of Loading, and Applied Total Stress Path on the Critical Void Ratio of Fine Uniform Sand," Ph.D. Dissertation, Texas A&M University, College Station, 1981.
[6] Mulius, J. P., Chan, C. K., and Seed, H. B., "The Effects of Method of Preparation on Cyclic Stress–Strain Behavior of Sands," Report No. EERC 75-18, University of California, Berkeley, 1975.
[7] Gilbert, P. A., "Investigation of Density Variation in Triaxial Test Specimens of Cohesionless Soil Subjected to Cyclic and Monotonic Loading," Technical Report No. GL-84-10, U.S. Army Engineer Waterways Experiment Station, Sept. 1984.
[8] Ladd, R. S., "Specimen Preparation and Liquefaction of Sands," *Journal, Geotechnical Engineering Division, American Society of Civil Engineers,* Vol. 100, No. 10, Oct. 1974, pp. 1180–1184.
[9] Vernese, F. J., and Lee K. L., "Effects of Frictionless Caps and Bases in the Cyclic Triaxial Test," Contract Report, S-77-1, U.S. Army Engineer Waterways Experiment Station, Vicksburg, MS, 1977.
[10] Castro, G., "Liquefaction and Cyclic Mobility of Sands," *Journal, Geotechnical Engineering Division, American Society of Civil Engineers,* Vol. 101, No. 6, June 1975, pp. 551–569.
[11] Lee, K. L., and Fitton, J. S., "Factors Affecting the Dynamic Strength of Soil," *Vibration Effects on Soils and Foundations, ASTM STP 450,* American Society for Testing and Materials, Philadelphia, 1969.
[12] Seed, H. B., and Peacock, W. H., "Test Procedures for Measuring Soil Liquefaction Characteristics," *Journal, Soil Mechanics and Foundations Division, American Society of Civil Engineers,* Vol. 97, No. 8, Aug. 1971, pp. 1099–1199.
[13] Olsen, R. E., and Campbell, L. M., Discussion on "Importance of Free Ends in Triaxial Testing," *Journal, Soil Mechanics and Foundations Division, American Society of Civil Engineers,* Vol. 90, No. 6, June 1964, pp. 167–173.
[14] Bishop, A. W., and Green, G. E., "The Influence of End Restraint on the Compression Strength of a Cohesionless Soil," *Geotechnique,* Vol. 15, No. 3, 1965, pp. 143–265.
[15] Casagrande, A., "Liquefaction and Cyclic Deformation of Sands: A Critical Review," Harvard Soil Mechanics Series No. 88, Pierce Hall, Cambridge, MA, Jan. 1976. (Presented at Fifth Panamerican Conference on Soil Mechanics and Foundation Engineering, Buenos Aires, Argentina, Nov. 1975.)
[16] Castro, G., and Poulos, S. J., "Factors Affecting Liquefaction and Cyclic Mobility," *Journal, Geotechnical Engineering Division, American Society of Civil Engineers,* Vol. 103, No. 6, 1977, pp. 501–516.

Woon-Kwan Lam[1] *and Fumio Tatsuoka*[2]

Triaxial Compressive and Extension Strength of Sand Affected by Strength Anisotropy and Sample Slenderness

REFERENCE: Lam, W.-K. and Tatsuoka, F., **"Triaxial Compressive and Extension Strength of Sand Affected by Strength Anisotropy and Sample Slenderness,"** *Advanced Triaxial Testing of Soil and Rock, ASTM STP 977,* Robert T. Donaghe, Ronald C. Chaney, and Marshall L. Silver, Eds., American Society for Testing and Materials, Philadelphia, 1988, pp. 655–666.

ABSTRACT: Drained triaxial compressive and extension strengths of air-pluviated sand were evaluated by means of a conventional triaxial apparatus taking into account both strength anisotropy and the effects of sample slenderness, that is, height/width or diameter ratio (H/D). The initial values of H/D employed were 2.0, 1.0, 0.5, and 0.25. The direction of the major principal stress σ_1' was either normal to or parallel to the bedding plane. It was found that the triaxial extension strength is greatly influenced by H/D. Strengths in the following four stress conditions were compared: (1) triaxial compression where the σ_1' direction is normal to the bedding plane, (2) triaxial extension where one of two σ_1' directions is normal to the bedding plane while the other is parallel to the bedding plane, (3) triaxial compression where the σ_1' direction is parallel to the bedding plane, and (4) triaxial extension where both σ_1' directions are parallel to the bedding plane. It was found that while the relative strength is a complicated function of H/D, generally the strength is the largest for the second case, intermediate for the first and fourth cases, and the smallest for the third case. This result suggests that ϕ is not a simple function of $b = (\sigma_2' - \sigma_3')/(\sigma_1' - \sigma_3')$, which represents the relative magnitude of σ_2' against σ_1' and σ_3', but the strength anisotropy and failure mode, especially in triaxial extension, should be taken into account in a combined manner.

KEY WORDS: triaxial compression test, triaxial extension test, sandy soil, angle of internal friction, strength anisotropy, sample slenderness

The angle of internal friction of $\phi = \arcsin\{(\sigma_1' - \sigma_3')/(\sigma_1' + \sigma_3')\}_{max}$ of sand is a function of both $b = (\sigma_2' - \sigma_3')/(\sigma_1' - \sigma_3')$ and strength anisotropy among other parameters. The large strength anisotropy has been observed for water-pluviated or air-pluviated sands by many investigators [*1–6*]. However, Yamada and Ishihara [*7*] reported that no pronounced strength anisotropy appeared in loose samples. Ochiai and Lade [*8*] also reported that this anisotropic behavior diminished at large strains in both loose and dense samples.

On the other hand, many inconsistent results as to the effects of b on ϕ have been reported by Ladd et al. [*9*]. Note that in some previous studies the strength anisotropy was not accounted for in discussing the effect of b on ϕ.

[1] Formerly, graduate student, University of Tokyo, now, research engineer, OYO Corporation, 13-12 Honkomagome 2, Bunkyo-ku, Tokyo 113, Japan.

[2] Associate Professor, Institute of Industrial Science, University of Tokyo, 22-1, Roppongi 7-chome, Minato-ku, Tokyo 106, Japan.

These inconsistencies as to the strength anisotropy and the effect of b on ϕ may be due partly to differences in several test conditions among these previous studies, for example, sample slenderness, boundary condition (rigid or flexible), void ratio, sample size, and sample shape, among others. In particular, it has been suggested by Lade [4] and Barden et al. [10,11] that triaxial extension strength is strongly influenced by the failure mode of the sample, which is a function of some, if not all, of the above test conditions.

In this study, to get better insight into ϕ of sand as a function of b, the strength anisotropy and the failure mode, a series of drained triaxial compression and extension tests was performed with careful control of the above test conditions. However, the stress conditions employed are rather limited, that is, b = 0.0 and 1.0, and the angle of σ_1' direction from the bedding plane δ = 0 and 90°. The strength of air-pluviated Toyoura sand, which is the test material in this study, as a function of b = 0.0 to 1.0 and δ = 0 to 90° has been presented elsewhere [6,12].

Testing Method

The test material was Toyoura sand, a uniform sand with a high content of feldspar, consisting of subangular particles. The mean diameter d_{50} is 0.16 mm, the uniformity coefficient is 1.46, the specific gravity is 2.64, and the maximum and minimum void ratios are 0.977 and 0.605, which have been determined by the method specified by the Japanese Society of Soil Mechanics and Foundation Engineering [13].

Prismatic samples having square cross sections and cylindrical samples listed in Table 1 were used. These were prepared by pluviating air-dried sand through air from a nozzle having an inner cross section of 1.5 by 15.0 mm at a constant fall height for each specimen. The stress conditions for these samples are illustrated in Fig. 1. Four stress states of samples employed in this study are represented by four angles α defined on a π-plane (constant mean principal stress plane, that is, $\sigma_X + \sigma_Y + \sigma_Z$ = constant) (Fig. 1*a*). Two kinds of triaxial compression test were performed; these are α = 0° tests for which the angle α is equal to 0° and the σ_1' direction is normal to the bedding plane (see Fig. 1*b*), and α = 120° tests for which the angle α is equal to 120° and the σ_1' direction is parallel to the bedding plane. Two kinds of triaxial extension test were performed; these are α = 60° tests for which one of two σ_1' directions is normal to the bedding plane while the other is parallel to the bedding plane, and α = 180° tests for which both σ_1' directions are parallel to the bedding plane. In the triaxial compression tests, the σ_1' planes were rigid and the σ_3' planes were flexible, whereas in the triaxial extension tests, the σ_1' planes were flexible and the σ_3' planes were rigid.

The height, H, and width, D, for prismatic samples are the distances between the cap and the pedestal and between the lateral membranes, respectively, as shown in Fig. 1*b*. The ratios H/D were selected as 2.0, 1.0, 0.5, and 0.25 to produce possible different failure modes. Only the cylindrical samples for α = 0° tests (that is, conventional triaxial compression tests) were produced directly on the pedestal of the triaxial cell. The cylindrical samples for α = 180° tests (that is, conventional triaxial extension tests) and the other prismatic samples were frozen, either because the mold did not fit the pedestal or because the sample was subsequently rotated 90° in the testing equipment for α = 60° tests and 120° tests (see Fig. 1*b*). The samples were frozen as follows: A sample was moistened by allowing water to seep through the 10-mm-diameter drainage hole at the bottom of the duralumin mold with the water level outside the sample maintained at 5 mm above the drainage hole. After having been well moistened, the specimen was left for 2 h in a humidity controlled (60% humidity) room to remove excess water from the sample. The top surface of the sample was then covered with eight pieces of filter paper for additional free water removal and a

TABLE 1—*Sample size and testing condition.*

Test Type	Sample size, mm $L \times D \times H$ or $D \times H$	H/D[a] Slenderness	σ_c'	Type of Lubrication [18]	Sample Preparation Method	
Triaxial compression	ϕ70 × 150[b]	2.1	1.0 kgf/cm²			nonfreezing
α = 0 and α = 120°	78 × 78 × 160	2.0				
b = 0.0	78 × 78 × 78	1.0	(98 kN/m²)	Type 4	air-pluviation	freezing-thawing
	78 × 78 × 40	0.5				
	78 × 78 × 20	0.25				
Triaxial extension	ϕ95 × 196[c]	2.0	4.0 kgf/cm²			
α = 60 and α = 180°	78 × 78 × 160	2.0		Type 1	air-pluviation	freezing-thawing
b = 1.0	78 × 78 × 78	1.0	(392 kN/m²)			
	78 × 78 × 20	0.25				

[a] H and D are defined in Fig. 1*b*.
[b] Only for α = 0°.
[c] Only for α = 180°.

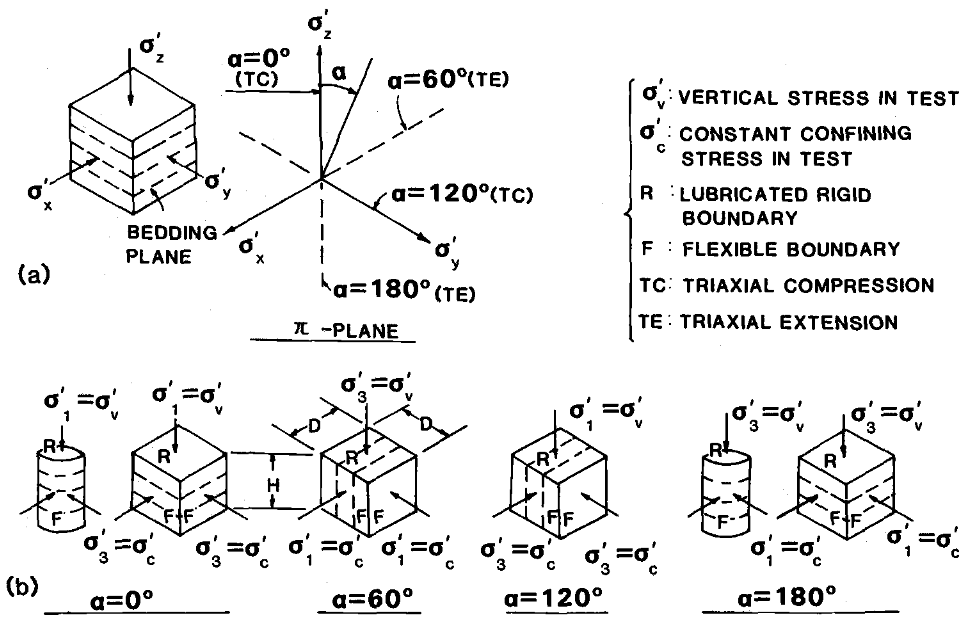

FIG. 1—(a) *Stress states on* π*-plane (constant mean principal stress plane) in the principal stress space* (σ_x', σ_y', σ_z'), *and* (b) *boundary conditions and sample shapes.*

vertical stress of 0.1 kgf/cm^2 (9.8 kN/m^2) was then applied. This sample was frozen inside a refrigerator at -20°C (-4°F) for 6 h. It has been reported that the stress–strain relationships between frozen–thawed and unfrozen samples of Toyoura sand in drained triaxial compression tests are almost the same [*14,15*].

After a frozen sample was set on the pedestal and sealed with latex membrane having a thickness of 0.3 mm, the sample was allowed to thaw under a suction of -0.3 kgf/cm^2 (-29.4 kN/m^2) for about 12 h at a controlled room temperature of 20°C (68°F). To saturate the sample well, carbon dioxide and deaired water were circulated through the sample and then a back pressure of either 2.0 kgf/cm^2 (196 kN/m^2) for a triaxial compression test or 1.0 kgf/cm^2 (98 kN/m^2) for a triaxial extension test was applied. Effective confining pressure σ_c' was either σ_3' in triaxial compression or σ_1' in triaxial extension. In this study, σ_c' was either 1.0 kgf/cm^2 in the triaxial compression tests or 4.0 kgf/cm^2 in the triaxial extension tests. Thus in the triaxial extension tests, σ_3', which is equal to $\sigma_c'/(\sigma_1'/\sigma_3')_{max}$ at the failure of sample, was around 1.0 kgf/cm^2 as in the triaxial compression tests.

For all the tests, enlarged, lubricated ends were used and a cap was guided against tilting. While the axial load was measured by means of an outer load cell for the triaxial compression tests, an internal load cell was used for the triaxial extension tests to measure precisely the axial stress (σ_3'). This point is discussed in detail elsewhere [*16*]. The effective confining pressure σ_c' was measured by means of a high capacity differential pressure transducer [*16*]. The water level in a burette, which was connected to a saturated sample, was measured by means of a low capacity differential pressure transducer [*16,17*].

To minimize the shear stresses between the loading platens and samples, Dow grease (thickness of 50 μm) was smeared between two 300-μm-thick latex rubber disks, and these all together were placed at the end surface of cap and pedestal for the triaxial compression tests. This lubrication layer has been classified as type 4 by Tatsuoka et al. [*18*] and has shown minimum shear stresses developed at a high stress level. For the triaxial extension tests, 50-μm-thick Dow grease was smeared between the loading platen and one 300-μm-thick latex rubber disk at each sample end. This lubrication layer has been classified as type 1 and has shown minimum shear stresses developed at a relatively low stress level [18]. These lubrication methods are fully described elsewhere [18].

Test Results

Triaxial Compression

Figure 2 shows the relationships between ϕ and void ratio measured at $\sigma_c' = 0.3$ kgf/cm² (29.4 kN/m²), $e_{0.3}$, by the triaxial compression tests on $\alpha = 0$ and 120° samples. The following points may be seen.

1. For $\alpha = 0°$ samples of $H/D = 2.1$ or 2.0, no pronounced shape effect on ϕ can be seen. A similar result has been reported by Green and Reades [19].

2. For both $\alpha = 0$ and 120°, ϕ for dense samples is similar for $H/D = 0.25$ to 2.1, whereas for looser samples ϕ increases with decreasing H/D from 2.0. This tendency has also been observed for air-pluviated Toyoura sand by Goto and Tatsuoka [20], but at a lesser degree; for $e = 0.63$ to 0.85, ϕ changed not more than 1° for a range of H/D between 0.3 and 2.1. The differences in test conditions between these two studies are as follows: in this study the samples of $H/D \leqq 2.0$ had square cross sections and the sample ends were lubricated by means of the type-4 method [18], whereas Goto and Tatsuoka [20] used cylindrical samples having ends lubricated by means of the type-1 method [18]. It is not

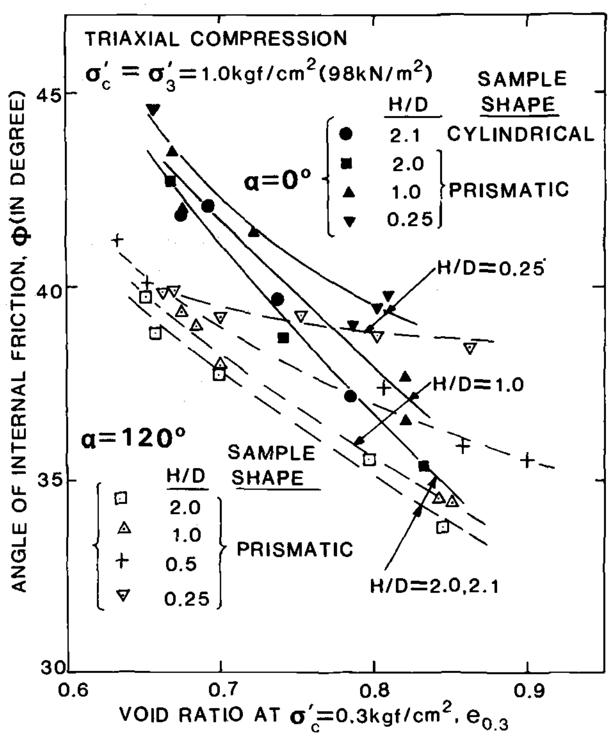

FIG. 2—*Results of triaxial compression tests* (α = *0 and 120°*).

known yet which of the above two factors or both or others are reasons for the different tendency in the effects of H/D on ϕ of looser samples in these two studies. On the other hand, it has been shown by both studies that ϕ for $H/D = 2.0$ and 2.1 is rather stable; ϕ is rather independent of both possible slight end restraint and the shape of sample cross section. Therefore, only ϕ for $H/D = 2.0$ to 2.1 will be used as ϕ in triaxial compression in comparing with ϕ by plane strain compression tests and triaxial extension tests as shown in the following part.

3. For any H/D, the strength anisotropy is very pronounced in dense samples, whereas this decreases with increasing void ratio. A lesser degree of strength anisotropy for looser samples obtained by this study is consistent with results obtained by Yamada and Ishihara [7]. It was considered that even the results for $H/D = 0.25$ reflect precisely the comparative variation which has been created in the $\alpha = 0$ and 120° samples. In Fig. 3, the triaxial compressive strengths for $H/D = 2.0$ to 2.1 are compared with the plane strain compressive strengths obtained at $\sigma_3' = 1.0$ kgf/cm² (98 kN/m²) by Tatsuoka et al. [6]. In these plane strain compression tests, samples were $H = 10.5$ cm, $W = 4$ cm, and L (in σ_2' direction) = 8 cm having lubricated ends, and the angles of σ_1' direction from the bedding plane δ were 0, 11, 23, 34, 45, 67, or 90°. At $\sigma_3' = 1.0$ kgf/cm², the largest and smallest ϕ were observed at $\delta = 90$ and 34°. In Fig. 3 only the data for $\delta = 0$, 34, and 90° are shown for

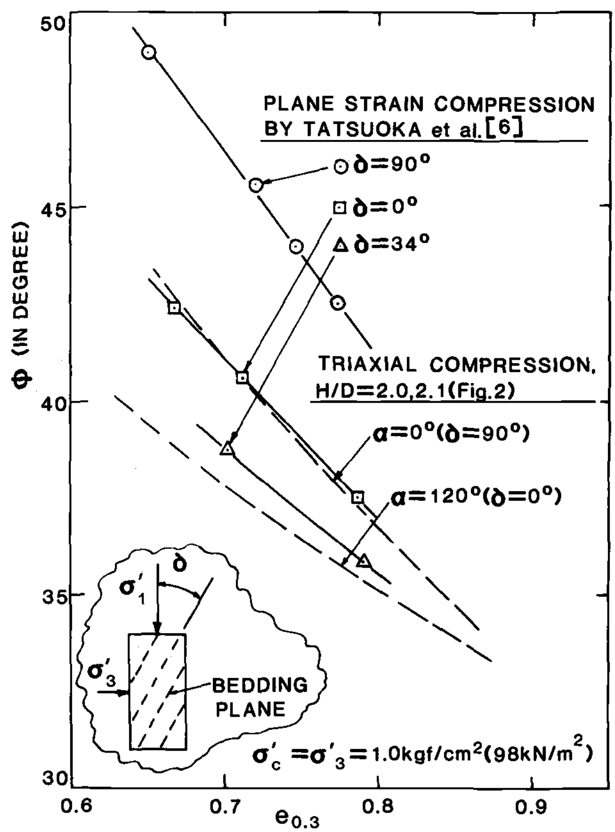

FIG. 3—*Comparison of triaxial compressive strength with plane strain compressive strength* [6] *for the same angle of σ_1'-direction from the bedding plane $\delta = 0$ and 90°.*

brevity. On the other hand, it has been observed that in triaxial compression the largest and smallest ϕ are obtained at $\delta = 90$ and $0°$ [1,2,3,12]. Note that $\delta = 90°$ in the $\alpha = 0°$ samples and $\delta = 0°$ in the $\alpha = 120°$ samples. Therefore, the values of ϕ for both the triaxial and plane strain compression tests shown in Fig. 3 show the upper and lower bounds of ϕ for $\delta = 0$ to $90°$ in each testing method. It may be seen that the range of ϕ is much larger in the plane strain compression tests than in the triaxial compression tests. In particular, for loose samples the strength anisotropy in terms of the range in ϕ as seen in Fig. 3 is still very large in the plane strain compression tests.

Triaxial Extension

Figure 4 shows the relationships between ϕ and $e_{0.3}$ for $\alpha = 60$ and $120°$ samples in triaxial extension. All the results presented here have been corrected for the local area reduction as a result of the necking effect which is inevitable in the triaxial extension tests with flexible σ_1' planes. The local cross-sectional area was carefully evaluated by means of the photo-

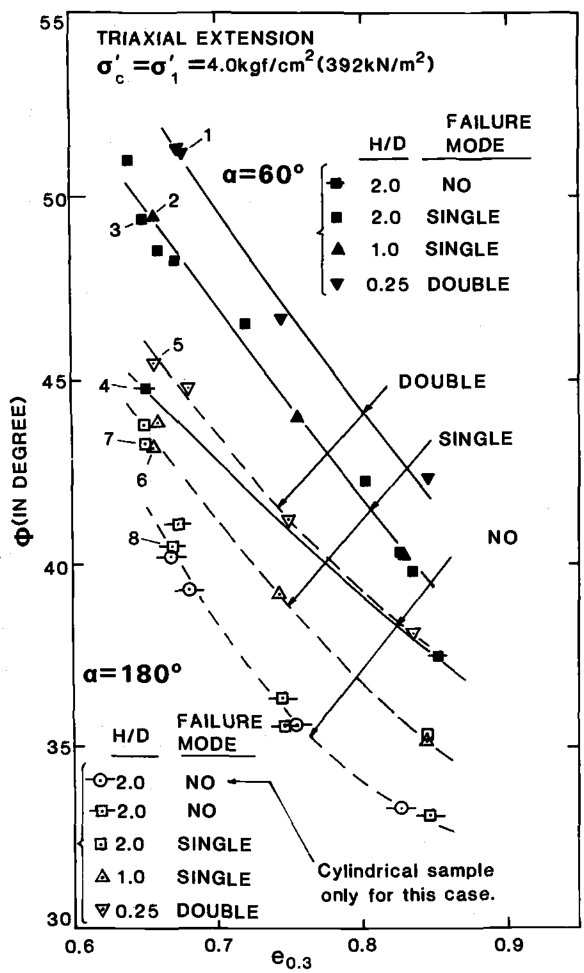

FIG. 4—*Results of triaxial extension tests* (α = *60 and 180°*).

grammetric method. The values of ϕ were not corrected for different σ_3' levels at the failure of specimen other than 1.0 kgf/cm^2 (98 kN/m^2).

The following three patterns of shear band formation were observed.

1. A shear band develops through two opposite flexible boundaries (σ_1' planes) without intersecting with the rigid end boundaries (σ_3' planes); this first mode was defined as the "no intersection" failure mode.
2. A shear band intersects with either the top or the bottom rigid loading platens (σ_3' plane); this second mode was defined as the "single intersection" failure mode.
3. A shear band intersects simultaneously with the top and bottom rigid loading platens (σ_3' planes); this third mode was defined as the "double intersection" failure mode.

For the prismatic $\alpha = 60$ and 180° samples with $H/D = 2.0$, either the first "no intersection" failure mode or the second "single intersection" failure mode appeared, while for the cylindrical $\alpha = 180°$ samples with $H/D = 2.0$, only the first failure mode was observed. For the $\alpha = 180°$ samples with $H/D = 2.0$ which exhibited the first failure mode, no clear shape effect was found. For $H/D = 1.0$, only the second "single intersection" failure mode appeared, and for $H/D = 0.25$, only the third "double intersection" failure mode appeared. As may be seen in Fig. 4, a clear relationship between ϕ and $e_{0.3}$ can be defined for each failure mode. Note that for both the $\alpha = 60$ and 180° samples the strength for the second "single intersection" failure mode is similar for $H/D = 1.0$ and 2.0. This means that ϕ in triaxial extension is controlled by the failure mode, but not directly by H/D. It also follows that large scatter in ϕ by conventional triaxial extension tests with use of long cylindrical samples as reported often in the literature is due largely to different failure modes. Such a strong dependency of ϕ in triaxial extension on the failure mode as shown above has been observed already [*4,10,11*], but only in more limited test conditions.

The lubrication layer employed in the triaxial extension tests was so-called type 1 [*18*]. The apparent angle of friction which develops at 1.0 kgf/cm^2 (98 kN/m^2) has been found to be around 0.2° [*18*]. It has been shown by Drescher and Vardoulakis [*21*] that the effects of the end friction of this order on the triaxial extension strength even for H/D less than 0.25 is negligible. This point is supported by the results obtained by Takano [*22*] that for any H/D ratio among 2.0, 1.0, 0.5, and 0.25 the triaxial extension strengths are virtually identical for lubricated and regular (nonlubricated) ends. Consequently, it can be considered that the increase in ϕ with decreasing H/D seen in Fig. 4 may not be due to the end friction.

The stress–strain relationships for the data points denoted by the numbers 1 to 4 for $\alpha = 60°$ and 5 to 8 for $\alpha = 180°$ shown in Fig. 4 are compared in Fig. 5*a* and *b*. Obviously a sort of premature failure occurred for the $\alpha = 60°$ samples 2 to 4 and the $\alpha = 180°$ samples 6 to 8. This tendency is most obvious for the first "no intersection" failure mode (samples 4 and 8). Therefore, it seems that ϕ in triaxial extension for the first and second (no and single intersection) failure modes may not be comparable with ϕ by the triaxial compression tests with use of rigid σ_1' planes in which such a premature failure as above does not occur.

It may be seen by comparing ϕ for $\alpha = 60$ and 180° shown in Fig. 4 that for each failure mode ϕ is larger by about 4 to 6° for $\alpha = 60°$ than for $\alpha = 180°$. Note that this difference in ϕ is still very large for loose samples; this tendency is similar to that in plane strain compression but is different from that in triaxial compression (see Fig. 3). Further research work is required to clarify this point.

Discussion

Figure 6 shows the relationship between ϕ and α for $e_{0.3} = 0.7$ and 0.8. Because the parameter b is a function of the angle α, this also shows the relationship between ϕ and b.

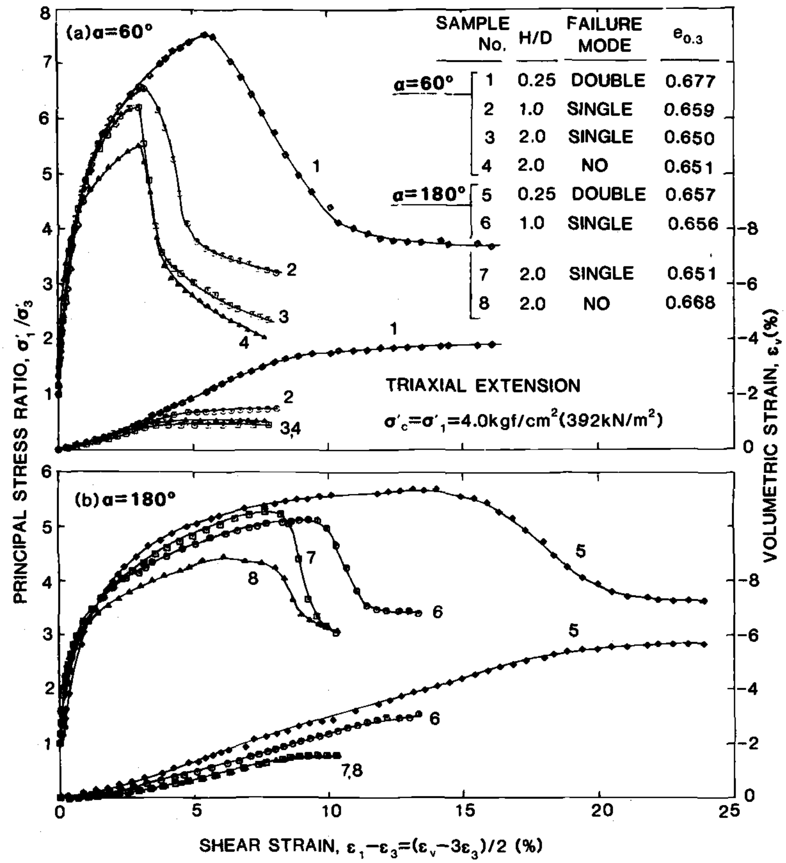

FIG. 5—*Stress-strain relations for three failure modes at* (a) $\alpha = 60°$ *and* (b) $\alpha = 180°$ *in triaxial extension (dense samples).* σ_1'/σ_3' *in this figure is not corrected for area reduction.*

In Fig. 6, the data points denoted as PSC were obtained from the plane strain compressive strengths at $\delta = 0$ and 90° [6] shown in Fig. 3. These are plotted against the α axis. Note that for the ranges $\alpha = 0$ to 60° and $\alpha = 120$ to 180°, δ as defined in the figure inset in Fig. 3 is 90 and 0°, respectively. Because the other parameters including δ are kept constant in each range of $\alpha = 0$ to 60, 60 to 120, or 120 to 180°, the change in ϕ by the change in α is due to the change in b together with the change in the failure mode, which is associated with the change in b in this study.

The following points may be seen in Fig. 6:

1. The largest change in ϕ by the change in α is seen for the range $\alpha = 60$ to 120°.
2. In each range, greatly different conclusions as to the effect of b on ϕ may be obtained depending on which of ϕ in triaxial extension is employed. In particular, in both ranges $\alpha = 0$ to 60° and $\alpha = 120$ to 180°, ϕ increases continuously with increasing b when ϕ for the double intersection failure mode in triaxial extension is employed.

On the other hand, all three principal stresses (that is, σ_1' and σ_3') are interchanged between the conventional triaxial compression test ($\alpha = 0°$) and the conventional triaxial extension test ($\alpha = 180°$). In this case, ϕ in the triaxial compression test is very similar to

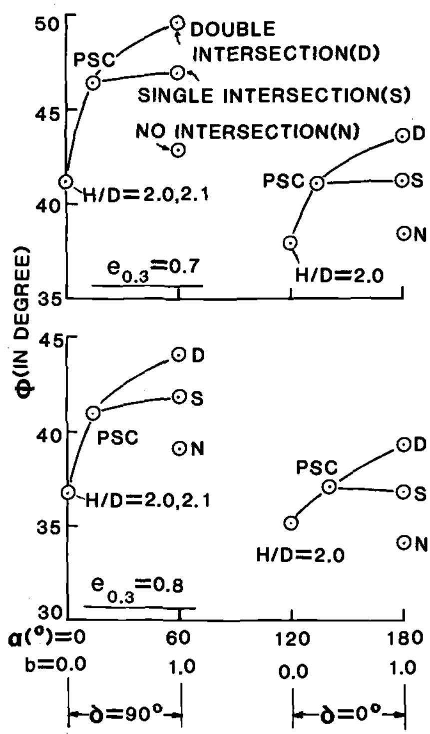

FIG. 6—*ϕ as a function of α.*

ϕ for the second "single intersection" failure mode in the triaxial extension test. Therefore, it is misleading to conclude based on such results as above that generally ϕ for $b = 0.0$ and $b = 1.0$ are similar.

It is not fully understood yet why ϕ in triaxial extension is so different among these three failure modes as shown by this study. Furthermore, it is not well known whether such failure modes as the no and single intersection failure modes may also occur in triaxial compression and plane strain compression by employing flexible σ_1' planes and whether in this case ϕ is also a strong function of different failure modes.

In view of the above, it seems that inconsistencies as to the effects of b on ϕ, as seen in the literature, are due largely to the fact that the strength anisotropy together with the effects of failure mode on ϕ were not fully taken into account in a combined manner. And it is also not well known how these results for different failure modes are used in the analyses of boundary value problems. Therefore, it is very desirable at present to examine and identify the failure mode in each laboratory test, as suggested by Lade [*4*].

Conclusions

Within the limits of the results on air-pluviated sand obtained by this study, the following can be concluded:

1. In the triaxial compression tests, strong strength anisotropy was observed in dense samples, whereas this was less significant in looser samples. This tendency was rather similar for a wide range of sample slenderness, H/D = 0.25 to 2.0.

2. In the triaxial extension tests, the strength was a function of failure mode, which was controlled by the sample slenderness H/D, boundary condition (rigid or flexible), and other unknown factors. For each of three failure modes observed in this study, a similar degree of strength anisotropy was observed, and this was rather independent of void ratio.

3. When b increases from 0.0 to 1.0 by replacing one of two σ_3's in triaxial compression with σ_1', α changes from 0 to 60°, from 120 to 60°, or from 120 to 180°. In this study, in each of these cases ϕ did not decrease, but ϕ increased in most cases, or in the other cases ϕ at b = 0.0 and 1.0 was similar. In this study, the manner in which ϕ changed by the change in b depended on both the angles of principal stress directions from the bedding plane (δ = 0 or 90°) and the failure mode in triaxial extension.

4. In summary, ϕ is not a simple function of b, but the strength anisotropy and the effects of failure mode should be equally taken into account when the effects of b on ϕ are discussed.

Acknowledgments

The first author wishes to express his appreciation and gratitude to the Japanese government for providing the Monbusho scholarship grant for his Doctor of Engineering study at University of Tokyo. Moreover, the authors would like to acknowledge the cooperation provided by the colleagues at Geotechnical Laboratory, Institute of Industrial Science, University of Tokyo.

References

[1] Arthur, J. R. F. and Menzies, B. K., "Inherent Anisotropy in a Sand," *Geotechnique*, Vol. 22, No. 1, 1972, pp. 115–128.
[2] Oda, M., "Initial Fabrics and Their Relations to Mechanical Properties of Granular Material," *Soils and Foundations*, Vol. 12, No. 1, 1972, pp. 17–36.
[3] Oda, M., "Anisotropic Strength of Cohesionless Sands," *Journal of Geotechnical Engineering Division, American Society of Civil Engineers*, Vol. 107, 1981, pp. 1219–1231.
[4] Lade, P. V., "Localization Effects in Triaxial Tests on Sand," in *Proceedings of International Union of Theoretical and Applied Mechanics, Conference on Deformation and Failure of Granular Materials*, Delft, 1982, pp. 461–471.
[5] Ricceri, G. and Soranzo, M., "Anisotropic Behavior of a Saturated Uniform Sand," *Proceedings of Tenth International Conference on Soil Mechanics and Foundation Engineering*, Vol. 1, Stockholm, 1981, pp. 759–764.
[6] Tatsuoka, F., Sakamoto, M., Kawamura, T. and Fukushima, S., "Strength and Deformation Characteristics of Sand in Plane Strain Compression at Extremely Low Pressures," *Soils and Foundations*, Vol. 26, No. 1, 1986, pp. 65–84.
[7] Yamada, Y. and Ishihara, K., "Anisotropic Deformation Characteristics of Sand under Three Dimensional Stress Conditions." *Soils and Foundations*, Vol. 19, No. 2, 1979, pp. 79–94.
[8] Ochiai, H. and Lade, P. V., "Three-dimensional Behavior of Sand with Anisotropic Fabric," *Journal of Geotechnical Engineering Division, American Society of Civil Engineers*, Vol. 109, 1983, pp. 1313–1328.
[9] Ladd, C. C., Foott, R., Ishihara, K., Schlosser, F. and Poulos, H. G., "Stress-Deformation and Strength Characteristics," S-O-A Report, *Proceedings Ninth International Conference on Soil Mechanics and Foundation Engineering*, Tokyo, Vol. 2, 1977, pp. 421–494.
[10] Barden, L. and Khayatt, A. J., "Incremental Strain Rate Ratios and Strength of Sand in the Triaxial Test," *Geotechnique*, Vol. 16, 1966, pp. 338–357.
[11] Barden, L. and Proctor, D. C., "The Drained Strength of Granular Material," *Canadian Geotechnical Journal*, Vol. 8, No. 8, 1971, pp. 372–383.
[12] Lam, W. K., and Tatsuoka, F., "Effects of Initial Anisotropic Fabric and σ_2 on Strength and Deformation Characteristics of Sand," *Soils and Foundations*, Vol. 28, No. 1, 1988, pp. 89–106.
[13] Japanese Society of Soil Mechanics and Foundation Engineering, "Soil Testing Method," Chap. 9, Maximum and Minimum Densities Test for Sand, 1979, pp. 172–188 (in Japanese).
[14] Yoshimi, Y., Hatanaka, M. and Oh-Oka, H., "Undisturbed Sampling of Saturated Sand by Freezing," *Soils and Foundations*, Vol. 18, No. 3, 1978, pp. 59–73.

[15] Tatsuoka, F., Goto, S. and Sakamoto, M., "Effects of Some Factors on Strength and Deformation Characteristics of Sand at Low Pressures," *Soils and Foundations*, Vol. 26, No. 1, 1986, pp. 105–114.
[16] Tatsuoka, F., "Some Recent Developments in Triaxial Testing Systems for Cohesionless Soils," in this volume, pp, 7–67.
[17] Tatsuoka, F., "A Simple Method for Automated Measurement of Volume Change in Laboratory Tests," *Soils and Foundations*, Vol. 21, No. 3, 1981, pp. 104–105.
[18] Tatsuoka, F., Molenkamp, F., Torii, T. and Hino, T., "Behavior of Lubrication Layers of Platens in Element Tests," *Soils and Foundations*, Vol. 24, No. 1, 1984, pp. 113–128.
[19] Green, G. E. and Reades, D. W., "Boundary Conditions, Anisotropic and Sample Shape Effects on the Stress–Strain Behavior of Sand in Triaxial Compression and Plane Strain," *Geotechnique*, Vol. 25, No. 2, 1975, pp. 233–256.
[20] Goto, S. and Tatsuoka, F., "Effects of End Conditions on Triaxial Compression Strength for Cohesionless Soil," in this volume, pp. 692–705.
[21] Drescher, A. and Vardoulakis, I., "Geometric Softening in Tests on Granular Material," *Geotechnique*, Vol. 32, No. 4, 1982, pp. 291–303.
[22] Takano, K., "Influence of Boundary Conditions in Triaxial Tests," Master's thesis, University of Tokyo, 1982 (in Japanese).

Toshiyuki Mitachi,[1] Yukihiro Kohata,[1] and Yutaka Kudoh[1]

The Influence of Filter Strip Shape on Consolidated Undrained Triaxial Extension Test Results

REFERENCE: Mitachi, T., Kohata, Y., and Kudoh Y., **"The Influence of Filter Strip Shape on Consolidated Undrained Triaxial Extension Test Results,"** *Advanced Triaxial Testing of Soil and Rock, ASTM STP 977,* Robert T. Donaghe, Ronald C. Chaney, and Marshall L. Silver, Eds., American Society for Testing and Materials, Philadelphia, 1988, pp. 667–678.

ABSTRACT: A series of consolidated undrained triaxial extension tests was performed to investigate the influence of shape of filter strips on the required time of consolidation and undrained shear behavior of clay. Remolded saturated specimens of clay with five different filter strip shapes were consolidated isotropically in the triaxial apparatus and then sheared under undrained extension by decreasing axial stress, while lateral stress was maintained constant. Based on the test results, the filter strip with spiral slit is recommended for practical use in a consolidated undrained extension test because of fast consolidation and low tensile strength.

KEY WORDS: angle of shear resistance, clay, consolidated undrained shear, pore pressure, shear strength, stress–strain curve, test procedure, triaxial test

In consolidated undrained triaxial tests on cohesive soils, filter strips are usually used as side drains to accelerate consolidation. Filter strip spirals have been recommended [*1,2*] for triaxial extension tests. Some experimental results concerning the influence of the shape of the side drain on the triaxial test results have been reported [*3–6*] in which ordinary type and spiral type filter strips are used for compression and extension tests, respectively. These studies, however, scarcely discuss the influence of filter strip shape on the stress–strain–strength behavior of clay in consolidated undrained extension tests.

The purpose of this paper is to evaluate the effect of the shape of filter strips on the required time of consolidation and undrained stress–strain–strength behavior of clay, based on a series of isotropically consolidated undrained triaxial extension tests on a remolded saturated clay with five different shapes of filter strips.

Sample Preparation

A remolded natural clay sampled in the suburbs of Sapporo, Japan, was used. The sample was thoroughly mixed with distilled water, sieved through a 0.42-mm size sieve, and stored in the state of slurry. Liquid and plastic limits of this slurry sample were 63 and 33%, respectively, and particle size analyses indicated that 60% of the sample was smaller than 0.005 mm. Before making the test specimen, the slurry was stirred again in a soil mixer for

[1] Professor, graduate student, and research engineer, respectively, Department of Civil Engineering, Hokkaido University, North 13, West 8, Kita-ku, Sapporo, 060 Japan.

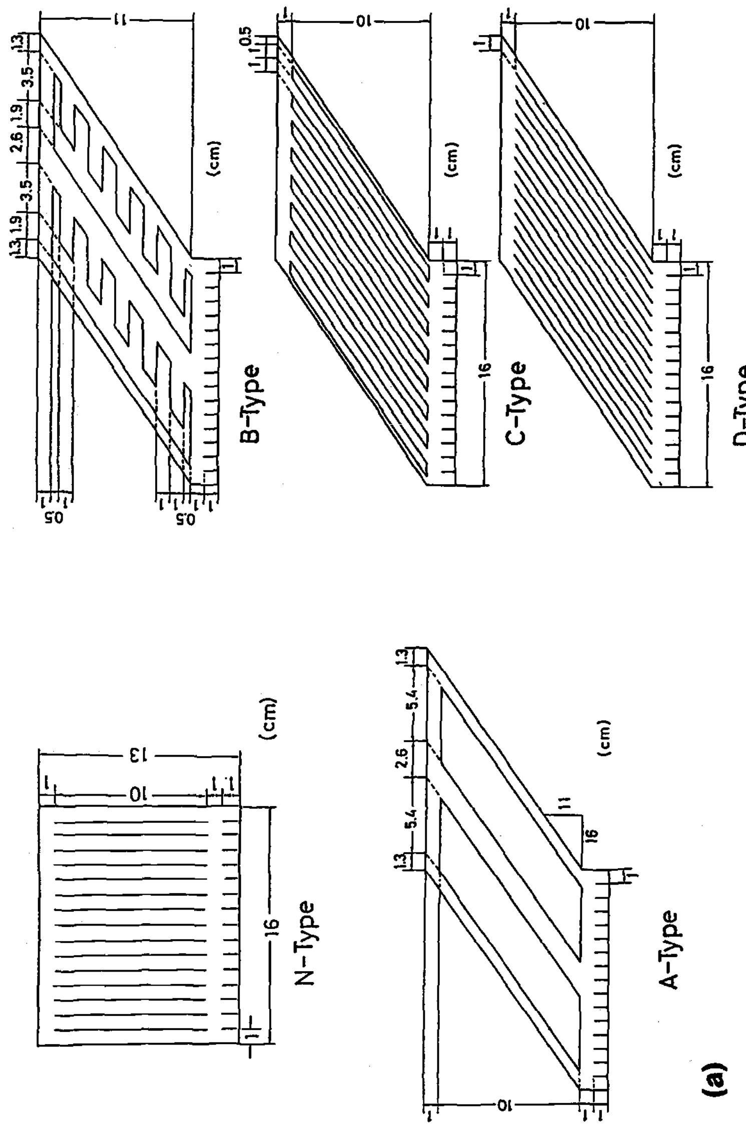

FIG. 1—*Five types of side drain paper used and schematic representation of triaxial test apparatus.*

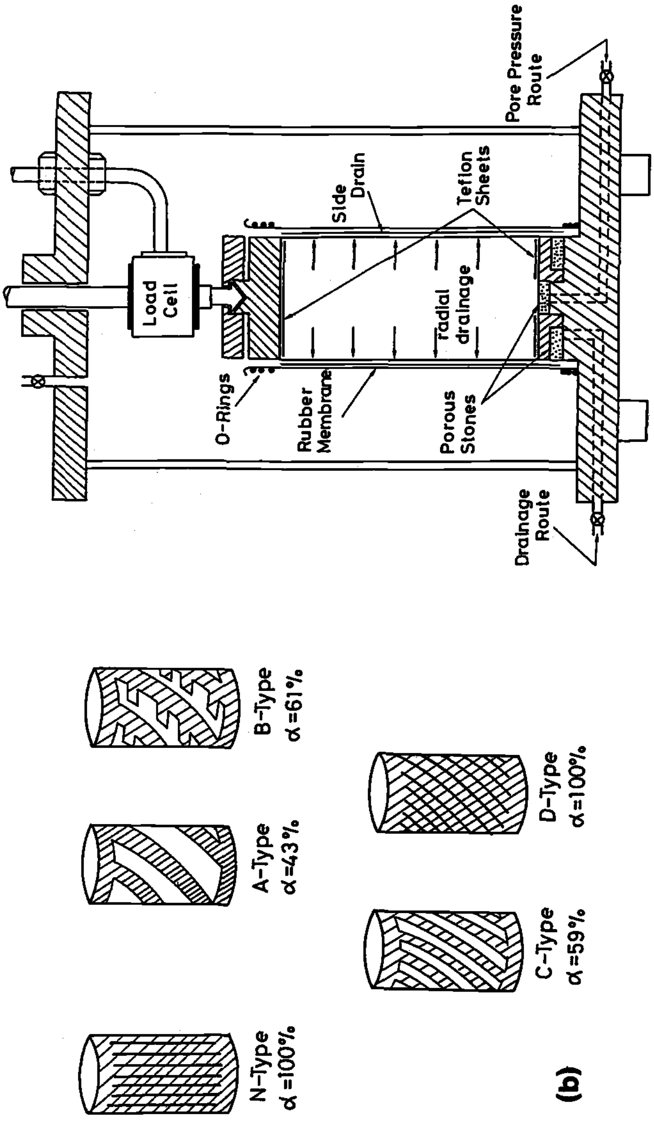

FIG. 1—*Continued.*

about 2 h and then transferred under a vacuum to a preconsolidation cell, 200 mm in diameter and 400 mm in height. The slurry was initially consolidated one dimensionally under vertical consolidation pressure of 80 kPa. Variation in water content throughout the preconsolidated sample after two weeks consolidation was less than 1%. Cylindrical specimens for triaxial tests, 50 mm in diameter and 120 mm in height, were trimmed from the preconsolidated sample. The specimen was set up on the triaxial cell base under water to avoid air entraining. Drainage during consolidation was forced in the radial direction through the side drain paper (Toyo No. 2) wrapped in the following manner. A side drain (one of those shown in Fig. 1) cut from a piece of filter paper was overlaid on a paper towel slightly larger than the side drain. The filter paper and the paper towel were then soaked together in water. After they were wrapped together around the specimen, the paper towel was stripped off. Then, the specimen and side drain were enclosed in a 0.2-mm-thick rubber membrane which was sealed against the cap and pedestal by O-rings. Lubrication by Teflon® sheet with silicone grease was applied to top and bottom of the specimen.

Testing Procedure

A series of isotropically consolidated undrained triaxial extension tests with five different shapes of side drain papers as shown in Fig. 1 was performed. Parameter α in Fig. 1*b* denotes the ratio of the surface area of the sample covered by the drain to the total side area of the sample, and it is called the area ratio in this paper.

N-type drains have been used in the authors' laboratory for consolidated undrained triaxial compression tests for the acceleration of radial drainage. Side drains similar to the A type have been frequently used in triaxial extension tests [*1,2,5*] to reduce the effect of tensile strength of the drain paper itself when the specimen is loaded in extension, but the rate of pore water pressure dissipation during consolidation is also reduced. B- and C-type drains, which have similar area ratios, are designed to extend the part of the side area of the samples covered by the drains. The D-type drain combines the advantage of the N-type drain with those of A-, B-, and C-type drains.

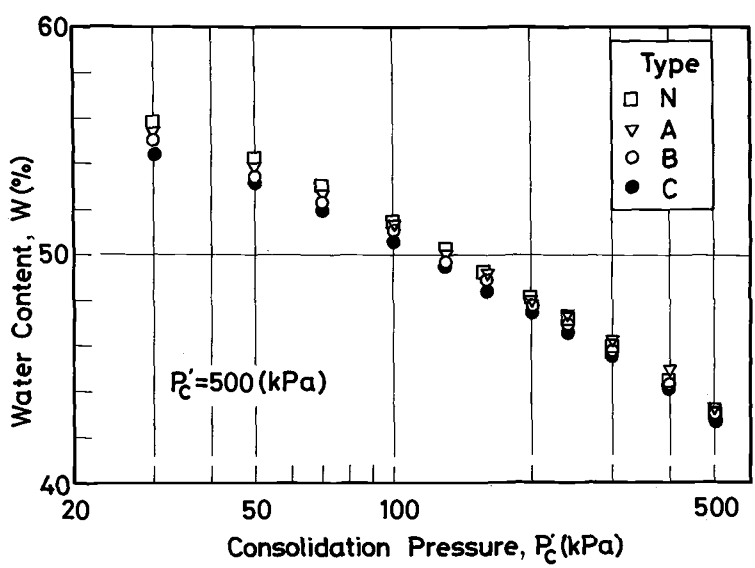

FIG. 2—*Water content versus effective consolidation pressure.*

Specimens with the five different side drains mentioned above were consolidated under isotropic stress of 200, 300, 400, and 500 kPa. Consolidation pressure was increased step by step with a time interval of 12 h between steps. Four, five, six, and seven days were required before undrained shear, respectively, for 200-, 300-, 400-, and 500-kPa consolidation pressure. Initial back pressure of 100 kPa was applied to all specimens. Pore pressure was measured at the bottom of the specimen by pressure transducer, and axial load was measured by load cell set up inside the triaxial cell. The undrained extension test was performed by decreasing axial stress at a constant rate of strain while lateral stress was maintained constant. The rate of axial strain in the undrained test was 0.04%/min for all specimens. The temperature of the laboratory during the test was controlled at 20 ± 0.5°C.

In addition to the tests mentioned above, a series of consolidated undrained triaxial compression tests with a D-type drain was performed under entirely the same conditions.

Test Results and Discussion

Consolidation

Figure 2 shows an example of the water content w calculated from the volume change during consolidation versus effective consolidation pressure p_c' relationship for final effective

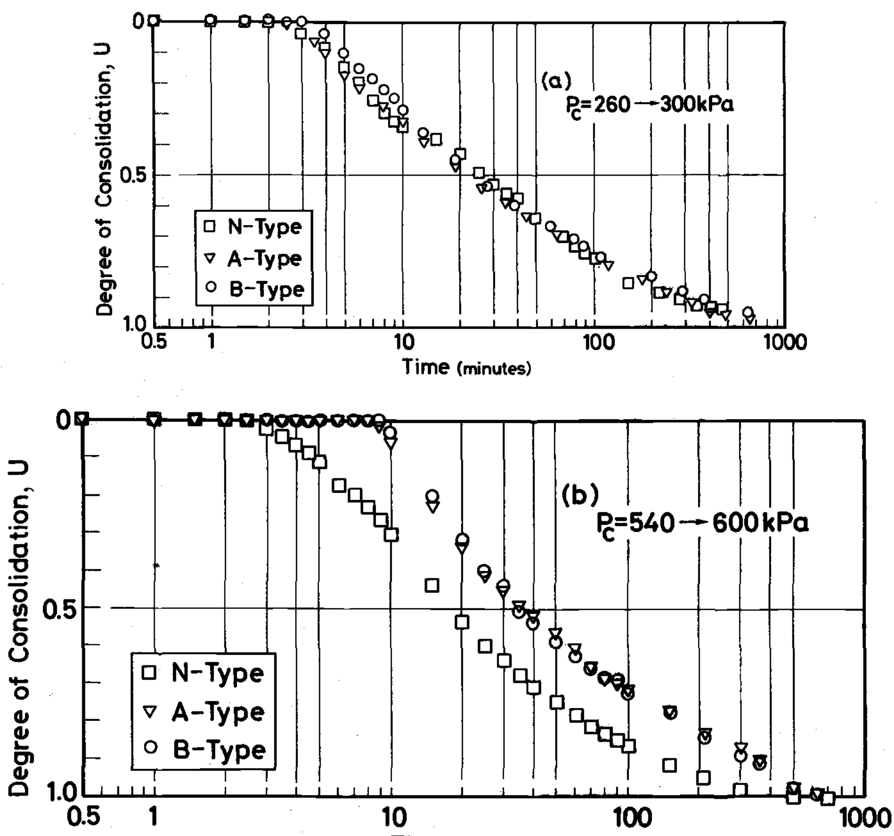

FIG. 3—*Typical rate of pore pressure dissipation during consolidation.*

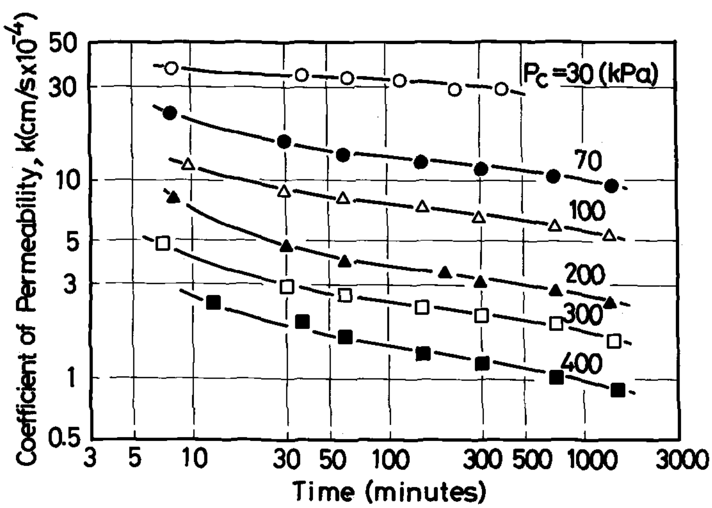

FIG. 4—*Change in the coefficient of permeability of filter drains measured with a dummy specimen during consolidation.*

consolidation pressure of 500 kPa. Although there is some scattering in the initial part of the curves as a result of the variation of initial water content, the differences of ordinate among each w-log p_c' curves almost disappear with the increase in consolidation pressure. Based on the test results shown above, it is concluded that the shape of side drain does not affect the water content versus effective consolidation pressure relationship after completion of consolidation.

Figure 3*a* and *b* show typical examples of the change in degree of consolidation U with time for N-, A-, and B-type side drains for low and high consolidation pressure, respectively, where U is defined by the increment of consolidation pressure $\Delta p'$, and that of excess pore water pressure Δu as follows:

$$U = 1 - \Delta u / \Delta p'$$

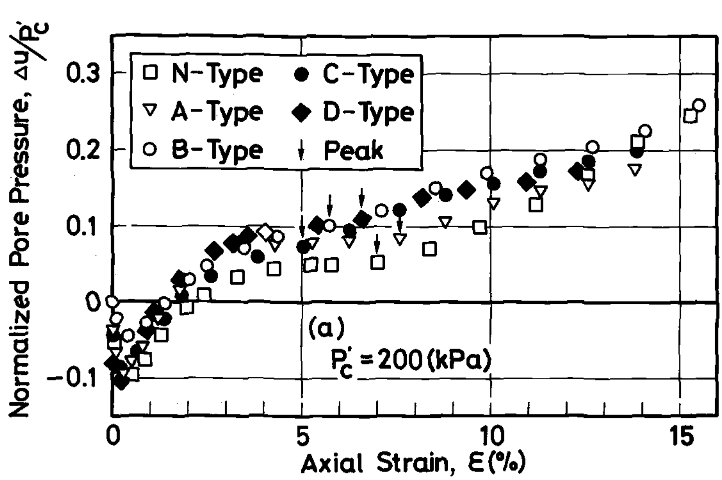

FIG. 5—*Normalized pore water pressure versus axial strain relationships for undrained extension test.*

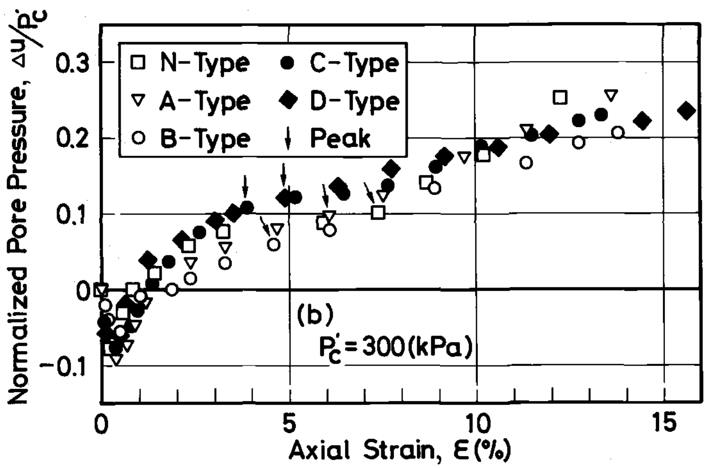

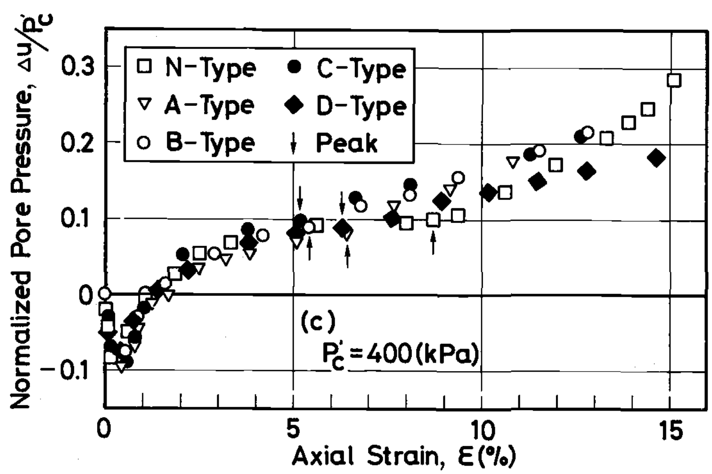

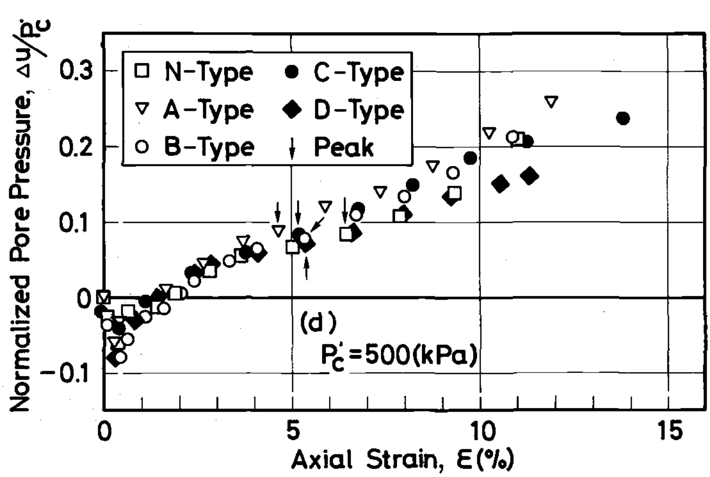

FIG. 5—*Continued.*

Any difference in the rate of pore pressure dissipation as a result of the difference in the shape of side drain cannot be found in Fig. 3*a*. On the other hand, there is a significant difference among A-, B-, and N-type drains in Fig. 3*b*. Although the *U–t* curve of a D-type drain is not shown in Fig. 3, it is essentially the same as that of an N-type drain. As shown in Fig. 4, permeability of filter paper measured with a dummy specimen made of Plexiglas decreases with an increase in consolidation pressure. At low consolidation pressure, the permeability of filter paper is about a hundred times that of clay used in this study, and the difference in the area ratio does not influence the rate of pore pressure dissipation. On the other hand, the decreased permeability of filter paper under high consolidation pressure reduces the rate of pore pressure dissipation in the specimen with side drains of low area ratio. Therefore, an N- or D-type drain is best in terms of accelerating rate of consolidation.

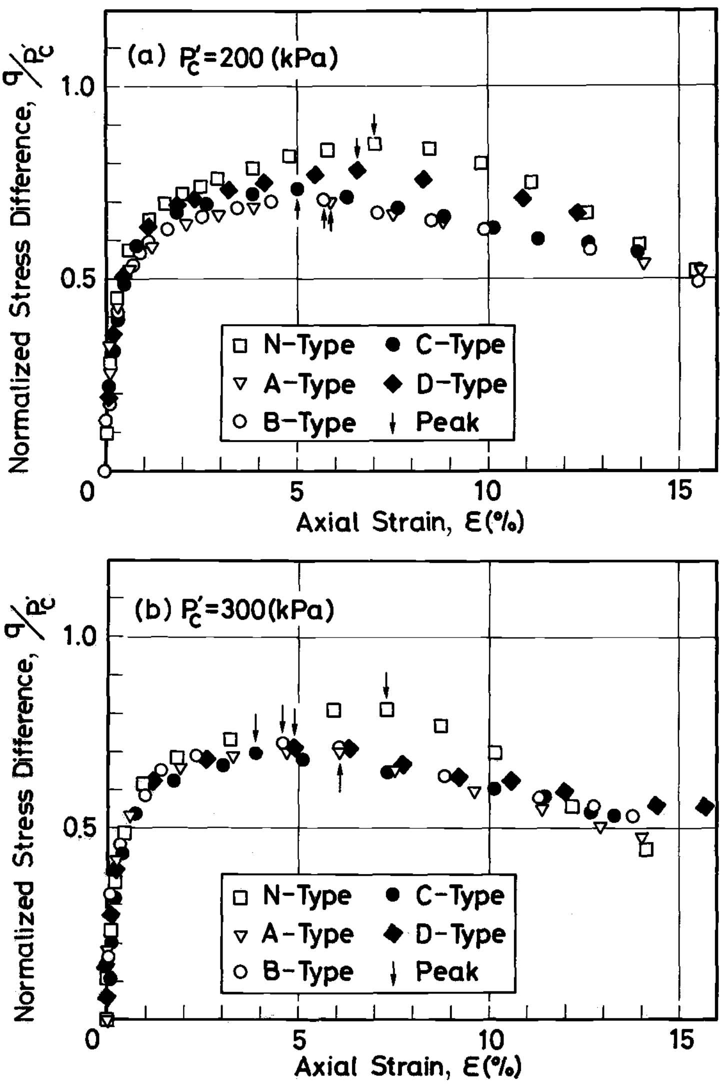

FIG. 6—*Normalized stress–strain relationships for undrained extension test.*

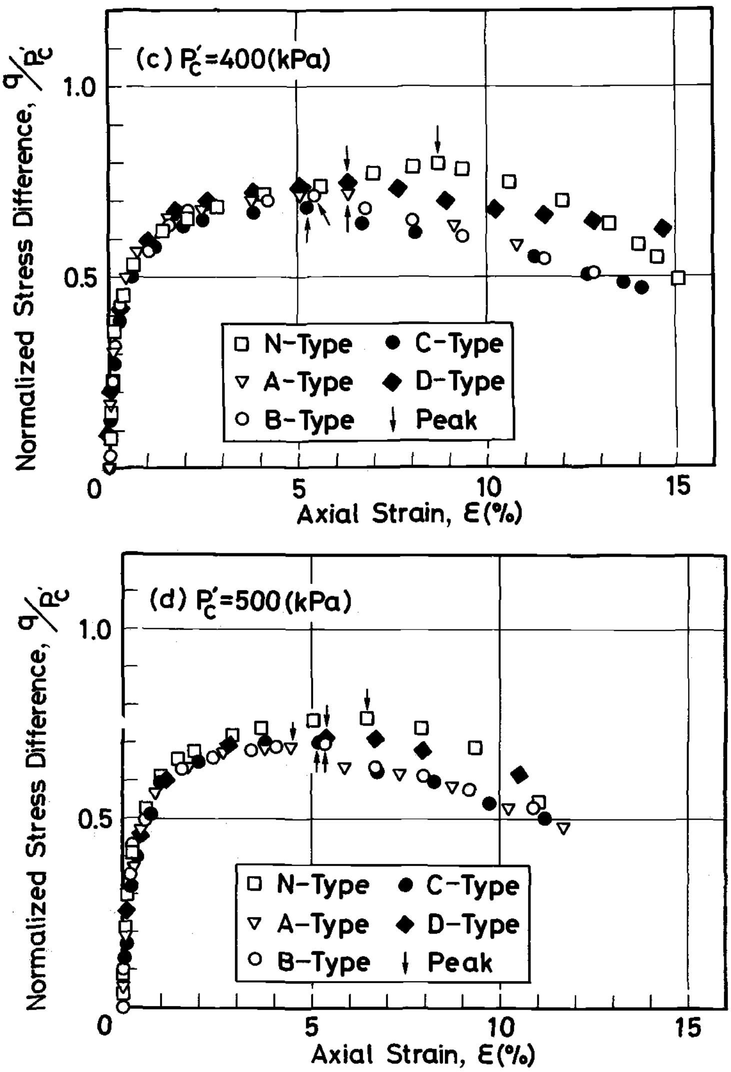

FIG. 6—*Continued.*

Undrained Shear Behavior

Pore pressure developed during shear Δu normalized by effective consolidation pressure p_c' versus axial strain ϵ relationships are shown in Fig. 5. As can be seen from these figures, the curves of the different type of drain almost coincide with each other, although the scattering after peak stress difference is relatively large.

Principal stress difference $q = (\sigma_1 - \sigma_3)$ normalized by effective consolidation pressure p_c' versus axial strain ϵ relationships are illustrated in Fig. 6. Normalized stress–strain curves for A-, B-, and C-type drains are almost the same irrespective of the magnitude of consolidation pressure, while the stress difference of an N-type drain is always greater than other types for the same axial strain. The stress–strain curve for a D-type drain locates midway among the N type and others. Almost all the curves coincide with each other for prepeak

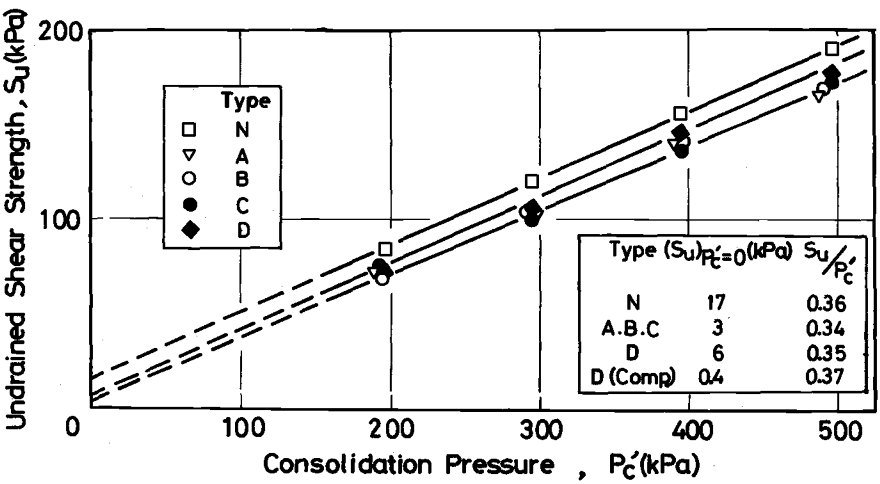

FIG. 7—*Undrained shear strength versus effective consolidation pressure.*

behavior within 4% axial strain, but stress differences of N- and D-type drains increase for greater strains. It can be concluded that the peak stress difference for specimens completely covered by side drain is higher than those covered by spiral drains, and the peak stress difference of the D-type drain with spiral slit is lower than that of N-type drain in spite of the same area ratio.

Undrained shear strength S_u, defined by one half of maximum principal stress difference, versus consolidation stress p_c' relationships are shown in Fig. 7. For comparison, the intercepts and slopes of S_u versus p_c' curves are shown in the figure, including those of compression tests with a D-type drain. It is seen that the undrained strength of N type is about 15 kPa higher than those of A, B, and C type for the range of consolidation pressure up to 500 kPa. Specimens with a D-type drain and failed in extension show intermediate strength between N type and the group of A to C type.

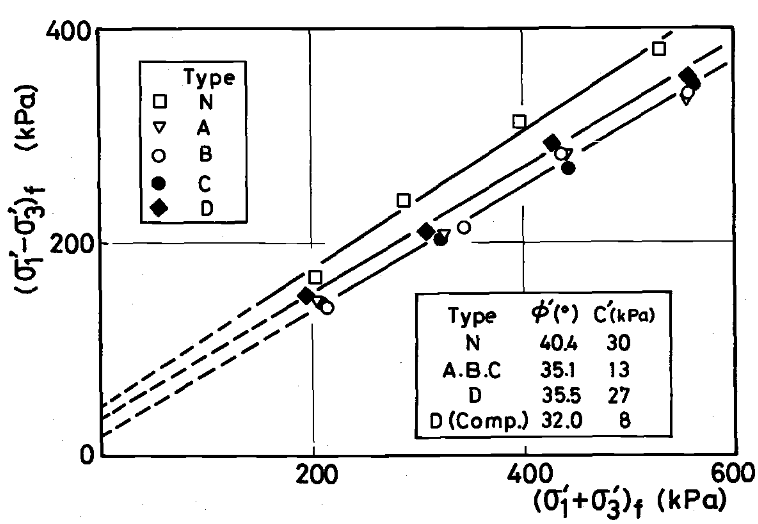

FIG. 8—*Effective stress failure envelopes.*

Tensile strength of the filter strips used in this study was obtained as follows. The filter strip put on a dummy specimen is bound by O-rings to the top cap and pedestal, damped by a sprayer, and then tested in the same way as in the extension test for clay specimens. Tensile strength of 2 kPa was obtained for A-, B-, and C-type drains, and 5 and 9 kPa were obtained for D- and N-type drains, respectively. Extension modulus of membrane was measured by the same method proposed by Henkel and Gilbert [*6*], and the tensile strengths of 1.5 and 3 kPa were calculated for 4 and 8% axial strain, respectively, because the peak extensive strength of the clay in the present study is obtained at 4 to 8% strain. It is seen that the intercepts in Fig. 7 almost coincide with the sum of the tensile strengths of filter strip and membrane.

Figure 8 illustrates the relationship between $(\sigma_1' - \sigma_3')$ and $(\sigma_1' + \sigma_3')$ at failure defined by the maximum principal stress difference criterion. Effective strength parameters c' and ϕ' are shown in the figure with those obtained from compression test with a D-type drain. The same trend as S_u versus p_c' is seen.

As shown above, it is concluded that the shape of the filter strip has appreciable influence on the stress–strain–strength behavior of clay in consolidated undrained extension test.

Figure 9 shows the typical pattern of constriction that occurs after peak stress in the test specimen with each type of side drain. For A- to C-type test, constriction occurred in the part close to the midheight of the specimen. On the other hand, for N-type side drain, constriction was observed near the top end of the specimen. For D-type side drain, constriction was observed at the top end in one test, midheight in two tests, and at the bottom in another test. As it is considered that constriction occurs around the weak point of the specimen resulting from the concentration of strain, occurrence of midheight constriction in A- to C-type specimens can be explained by the fact that the part not covered by filter paper is the weak point of those specimens. In contrast to this, the weak point of N-type specimens is inferred to be the top end because of the disturbance at the time of specimen set-up. In D-type specimens, it is inferred that the probability of occurrence of constriction at the top end is almost the same as that at midheight, because the top end is completely covered by filter paper and the confinement of the midheight of the specimen by the spiral type filter is weaker than that by an N-type drain.

Based on the above discussion, a D-type side drain is recommended for practical use in

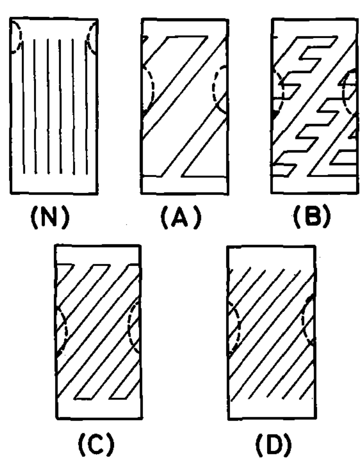

FIG. 9—*Location of occurrence of constriction in the triaxial test specimen for five types of side drain.*

consolidated undrained extension tests, because the rate of consolidation is about two times faster than that with A-, B-, and C-type drains, principal stress difference at failure is only slightly higher than that obtained by correcting the effect of tensile strength of membrane, and the probability of occurrence of constriction is almost equal throughout the specimen.

Conclusions

1. Rate of pore pressure dissipation during consolidation depends on the area ratio of side drain papers and the magnitude of consolidation pressure, although unique relation between water content and consolidation pressure is found irrespective of shape of side drain.
2. Pore pressure development during undrained extension tests is not affected by the shape of the side drain.
3. The influence of the shape of side drain on the undrained stress–strain–strength behavior is large.
4. From the practical point of view, a D-type side drain is recommended to evaluate proper stress–strain–strength behavior of clay by consolidated undrained extension test.

Acknowledgments

The authors gratefully acknowledge the helpful cooperation provided by R. Aramaki, K. Ikeda, and M. Sugawara.

References

[1] Bishop, A. W. and Henkel, D. J., *The Measurement of Soil Properties in the Triaxial Test*, Edward Arnold Ltd., London, 1957, p. 82.
[2] Berre, T., "Triaxial Testing at the Norwegian Geotechnical Institute," N.G.I. Publication 134, 1981, pp. 1–17.
[3] Olson, R. E. and Kiefer, M. L., in *Laboratory Shear Testing of Soils, ASTM STP 361*, American Society for Testing and Materials, Philadelphia, 1963, pp. 482–491.
[4] Yoshikuni, H. and Nakanodoh, H., "The Influence of the Permeability of Filter Paper on the Triaxial Consolidation Behavior of Cylindrical Clay Specimen," *Proceedings*, Twentieth Symposium on Soil Mechanics and Foundation Engineering, *Japanese Society of Soil Mechanics and Foundation Engineering*, 1975, pp. 121–124 (in Japanese).
[5] Nakai, T., "Effect of Tensile Strength of Filter Paper on the Triaxial Extension Test for Clay," TSUCHI-TO-KISO, *Japanese Society of Soil Mechanics and Foundation Engineering*, Vol. 31, No. 7, 1983, p. 68 (in Japanese).
[6] Henkel, D. J. and Gilbert, G. D., *Geotechnique*, Vol. 3, No. 1, 1952, pp. 20–29.

Tzou-Shin Ueng,[1] Yeong-Ming Tzou,[2] and Chung-Jung Lee[3]

The Effect of End Restraint on Volume Change and Particle Breakage of Sands in Triaxial Tests

REFERENCE: Ueng, T-S., Tzou, Y-M., and Lee, C-J., **"The Effect of End Restraint on Volume Change and Particle Breakage of Sands in Triaxial Tests,"** *Advanced Triaxial Testing of Soil and Rock, ASTM STP 977,* Robert T. Donaghe, Ronald C. Chaney, and Marshall L. Silver, Eds., American Society for Testing and Materials, Philadelphia, 1988, pp. 679–691.

ABSTRACT: The distributions of volume change and particle breakage within specimens were compared for uniform sands in drained triaxial tests with and without lubricated end platens. The results showed that the volume change at failure, either dilation or compression, of the sands was slightly higher for lubricated specimens at a higher failure strain than for unlubricated specimens, and the difference was proportional to the total volume change at failure. The sands exhibited insignificant differences in uniformity of volume change for specimens with and without lubricated ends under loading before the peak strength. However, a distinctly larger volume change at the middle portion of unlubricated specimens was observed after the loading reached the peak strength. Similar results were obtained for the particle breakage within the specimens in triaxial tests. End lubrication induced more uniform particle breakage of sands after the peak strength was reached. Finally, Rowe's stress-dilatancy theory was evaluated with considerations of dilatancy factor and particle breakage. Particle breakage was found very important in considering strength and volume change of sands.

KEY WORDS: triaxial testing, end restraint, volume change, particle breakage, dilatancy, shear strength, sands

The effect of end restraint on triaxial test results has been investigated by many researchers. End restraint prevents the soil from moving outwards freely and induces a shear stress on the ends of the specimen. Thus, the stress conditions and deformations within the specimen are no longer uniform. This causes difficulty and errors in the interpretation of test results.

Most studies emphasize the influence of end restraint on the shear strength of soils. The difference between the shear strength of a soil specimen with and without lubricated end platens generally is considered insignificant, provided that the specimen's height-to-diameter ratio (H/D) is larger than 2 [*1,2*]. However, the volume change of a soil under loading is also essential for obtaining values of the parameters in the constitutive relation of soil. Therefore, the effect of end restraint on volume change of soils in triaxial tests deserves a close look to assure the representative test data for constitutive relations of soils.

Some studies have indicated that the axial strains at failure are generally higher for specimens with lubricated ends than those without lubricated ends [*1,3,4*]. The difference

[1] Formerly, professor, National Taiwan University, Taipei, Taiwan, Republic of China; now, geotechnical engineer, Lawrence Livermore National Laboratory, Livermore, CA 94550.
[2] Engineer, United Geotech, Inc., Taipei, Taiwan, Republic of China.
[3] Lecturer, National Central University, Taiwan, Republic of China.

may be as high as 3% for dense sands, but for loose sands the difference is negligible. Norris [4], Lee [5], Lade [6], and Rowe and Barden [7] found that, for the samples with a height-to-diameter ratio of 2 to 1, the volume change at failure for the samples with lubricated ends is higher than that without lubricated ends by about 1.0 to 1.5%, while Bishop and Green [1] indicated that the dilations of soils in both end conditions are practically the same. On the other hand, the test results obtained by Raju and coworkers [3] showed less volume change at failure for tests with lubricated ends. These discrepancies may be due to the differences of axial strains at failure.

Controversial data were also found in previous studies for dilation rate, $d\epsilon_v/d\epsilon_1$, at failure, where $d\epsilon_1$ is the change of axial strain and $d\epsilon_v$ is the change of volumetric strain. Some studies showed that the dilation rate is higher for the samples without end lubrication [1,7], while others found the contrary [4,5]. Raju and coworkers [3] gave the following plausible explanation for the discrepancy: For the specimens without end lubrication, most of the axial strain and volume change occur at the middle portion of the specimen, but the volume change and axial strain are computed based on the volume and deformation of the whole specimen, whose values are both lower than the actual ones at the middle part. Hence, the dilation rate, the ratio between the change of volumetric strain to that of axial strain, of specimens without lubrication may be similar to that with lubricated ends due to the compensating effect.

Only a few studies have been conducted on particle breakage in triaxial tests [8–11]. Most have dealt with soils under very high confining pressure or rockfill materials. Little attention has been given to the effect of end restraint on particle breakage, and there is very limited information available. Due to the importance of particle breakage to the strength and volume change of soils, a careful study of particle breakage and how it is affected by end restraint is needed.

In this investigation the effect of the end restraint on the volume change and particle breakage within the specimen in triaxial testing was closely examined, and the role of particle breakage in the strength of sands was also studied.

Lubrication of End Platens

Lubrication of end platens by rubber (latex) membranes with silicone grease in between was one of the most commonly used methods of eliminating end restraint in previous studies [1,2,3,11]. Tatsuoka and his associates, in their excellent investigation on methods of lubrication of end platens, found that latex membranes with silicone grease in between showed the best result with a friction angle less than 1.0° [12,13]. Other lubrication methods, such as Teflon sheet, glass plate, polished stainless steel plate, exhibited rather unsatisfactory results.

Additional tests and evaluation of lubrication methods were also performed by the authors

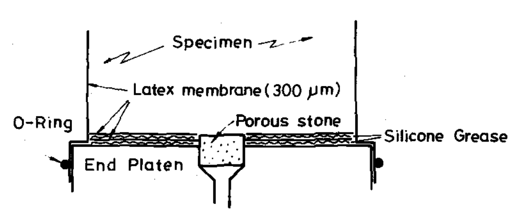

FIG. 1—*Lubrication of end platen.*

in this investigation. The friction angles between Fulung sand and platens lubricated with various methods were obtained in direct shear tests. The results also confirmed that latex membranes with silicone grease is one of the best lubrication methods for the end platens. In this investigation, the end lubrication method was two 0.3-mm-thick latex membranes and one thin layer of Dow Corning high vacuum silicone grease between the two membranes and another layer between the membranes and the platen. The apparent friction angle between Fulung sand and this kind of lubrication was 1.6° based on the results of the direct shear tests. For those platens without lubrication, the friction angle was about 28°. Before triaxial testing, both the top and bottom end platens lubricated with latex membranes and silicone grease were pressed together under a pressure of 400 kPa for about 2 h to remove the excessive grease and to make the lubricated ends more uniform and smooth. A porous stone about 12 mm in diameter was placed at the center of the membrane disks for drainage in drained tests. Figure 1 shows the lubrication of the end platen in this investigation.

Testing Program

Three types of sands were used:

(1) Fulung sand—a fine beach sand composed mainly of subangular quartz grains
(2) Ottawa sand—a commercially available sand of rounded hard quartz particles
(3) Tamsui River sand—a black river sand composed of about 40 to 50% slate particles and about 30 to 40% quartz and a small amount of other minerals. The particles were mostly flaky and friable. This type of sand is one of the very common subsoils in the Taipei basin and other locations in Taiwan.

These sands were sieved before testing that they passed the No. 40 (425-μm) sieve and were retained on the No. 60 (250-μm) sieve. The specimens of these sands were prepared by the moist tamping method [*14,15*]. The sands, with a water content of 8%, were placed in six layers, each compacted to a predetermined height to obtain the desired density. The specimen dimensions were 152 mm in height and 71 mm in diameter. The relative density, D_r, ranged from 30 to 80%. All the specimens were saturated with a back pressure of 400 kPa before shearing.

Triaxial drained tests with and without lubricated ends were conducted for each sand of various relative densities under confining pressures from 50 to 400 kPa. The tests were stopped at various stages of loading, and the volume change and particle breakage of different portions within the specimens were compared for the specimens with and without the end lubrication.

At the end of each loading stage the volume change of the specimen was measured and the volume of the specimen at every loading stage before unloading was obtained. For the measurement of volume in the different portions of the specimen, a small confining pressure was applied with a vacuum inside the specimen when the axial load and chamber pressure were released. The specimen, with its shape maintained by this confining pressure, was then put under a temperature of −15°C for 8 h before it was cut into five sections along the axis. The volume of each frozen section was measured by submerging each section in a container of kerosene at −15°C and measuring the volume of kerosene displaced by the frozen soil. The total volume of these five frozen sections was compared with the whole specimen volume at the end of the loading stage to consider the expansion of the water within the specimen as a result of freezing. The volume of each section was corrected by multiplying by the ratio of the total volume of the specimen before freezing to that after freezing. The soil of each section was dried and weighed. The dry density and void ratio of each portion within the

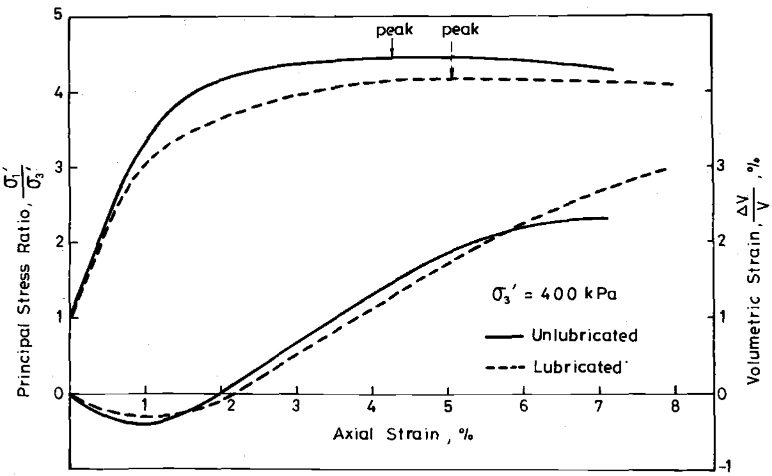

FIG. 2—*Stress–strain–volume change relationships for Fulung sand,* D$_r$ = *70%.*

specimen were then obtained. The volume change of each section was computed by comparing the void ratio of each section with the initial void ratio of the specimen.

Sieve analysis was also performed to get the grain sizes of the sands of each section. Great pains were taken in the sieve analysis to secure results as accurate as possible. The sieving time was 5 min, and the amount of sand in each sieving was approximately 200 g. The sand grains plugging the sieve openings were removed before every sieving. The particle breakage was defined as the percentage by weight of the particles passing the No. 60 sieve.

Stress–Strain–Volume Change Relationship

Figure 2 shows a typical relation between stress, strain, and volume change in a triaxial test for Fulung sand. The peak strength was higher at a lower failure strain for the sample without end lubrication than that with lubricated ends at a higher failure strain. The volume change of the sand under the same stress was higher for the lubricated specimen than the

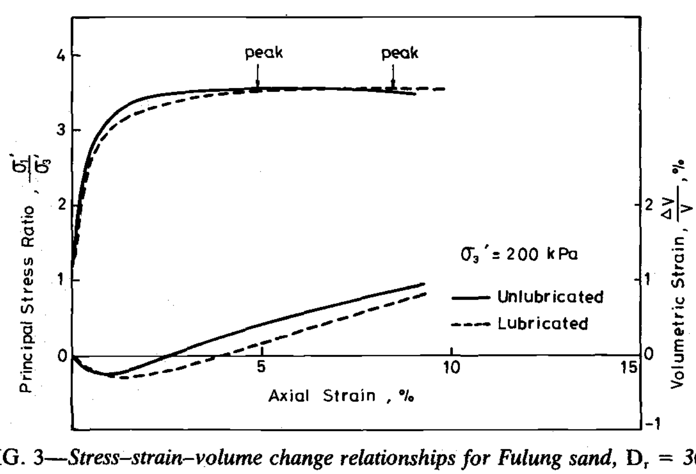

FIG. 3—*Stress–strain–volume change relationships for Fulung sand,* D$_r$ = *30%.*

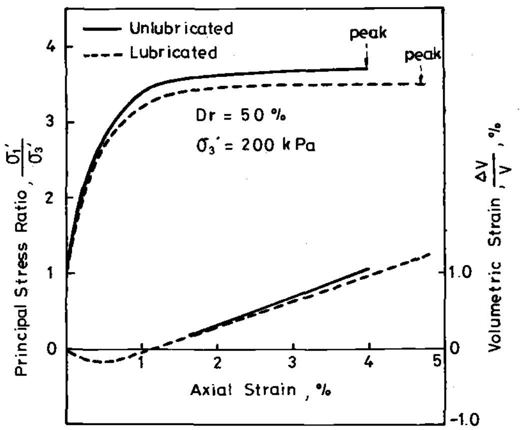

FIG. 4—*Stress–strain–volume change relationships for Ottawa sand.*

unlubricated one, but the dilation at the same axial strain was higher for the unlubricated specimen. Lee also indicated similar findings [5]. For the loose Fulung sand of a relative density of 30% under 200 kPa confining pressure, similar results of volume change were obtained as shown in Fig. 3, although the peak strength and total volume change at failure are approximately the same for the lubricated and unlubricated samples.

Figures 4 and 5 show the typical stress–strain–volume change relationship for Ottawa sand and Tamsui River sand. The relationship was similar to that for Fulung sand, except the volume change of Tamsui River sand is mostly compression even under a relative low confining pressure (that is, 100 kPa).

Density and confining pressure are two main factors affecting the effect of end restraint

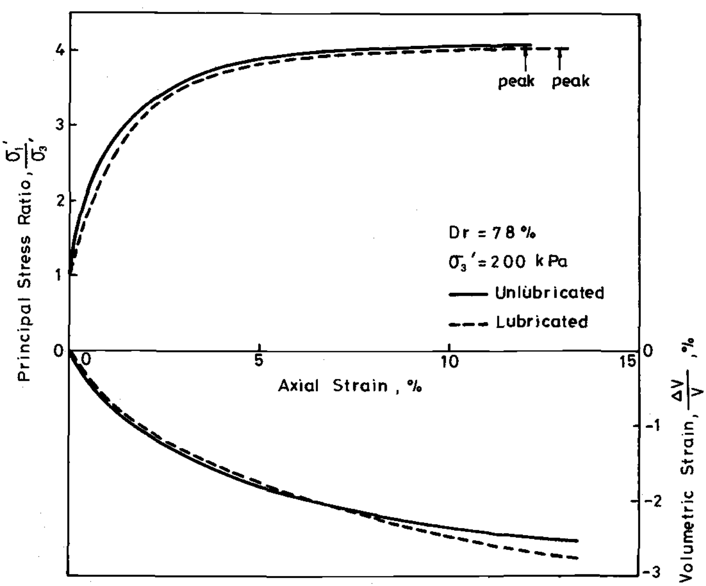

FIG. 5—*Stress–strain–volume change relationships for Tamsui River sand.*

on the peak effective stress ratio, $(\sigma_1'/\sigma_3')_{max}$. High density and low confining pressure will induce a higher peak strength in terms of peak effective stress ratio for the specimens without lubricated ends by up to about 0.25, which is equivalent to a difference in friction angle of about 1.0°. The peak strength always occurred at a higher axial strain for the lubricated specimens. Similar findings were also obtained in other investigations [*3–5*]. It is interesting to note that regardless of dilation or compression during tests, the total volume change at failure of the sands is always higher for the specimens with lubricated end platens even though outward radial displacements were observed in the condition of volume compression. The differences of the volume change at failure between the specimens with and without lubrication were found approximately proportional to the total volume changes of the sands as depicted in Fig. 6.

The dilation rate at the peak strength in the triaxial tests without lubricated end platens showed slightly higher values by about 0.03 to 0.05 than those with lubricated ends for dense sands under low confining pressures. No significant difference of dilation rate was found for loose sands under high confining pressures. This is similar to the findings of Bishop and Green [*1*], Raju and coworkers [*3*], and Rowe and Barden [*7*].

Volume changes were also measured for the triaxial tests of Ottawa sand (D_r = 30%) under static cyclic loading with the same strain rate as in the compression drained tests (Fig. 7). A comparison of the volume change of these specimens also showed a higher compressive volume change for specimens with lubricated ends than those without lubrication under the cyclic loading condition.

Volume Change Distributions Within Specimens

Regarding the triaxial tests of Fulung sand of a relative density of 50% under a 400-kPa confining pressure (Fig. 2), the distribution of the volume change of different portions within the specimen at various loading stages are shown in Fig. 8. It indicates that before the peak strength there is no significant difference in the uniformity of volume change within the specimen regardless of the end lubrication. When the loading reached and passed the peak strength, the middle portion of the specimen without lubricated end platens exhibited a distinctly higher volume change than that at both ends, while the specimen with lubricated ends still showed a rather uniform volume change within the specimen throughout the test.

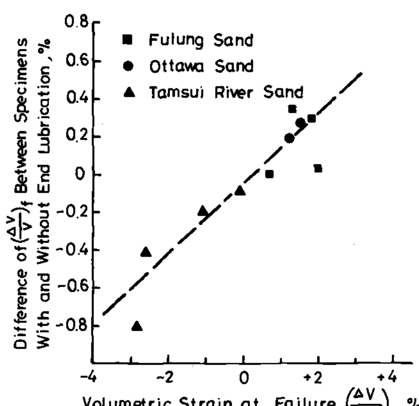

FIG. 6—*Relation of difference of volumetric strains at failure between specimens with and without lubricated ends.*

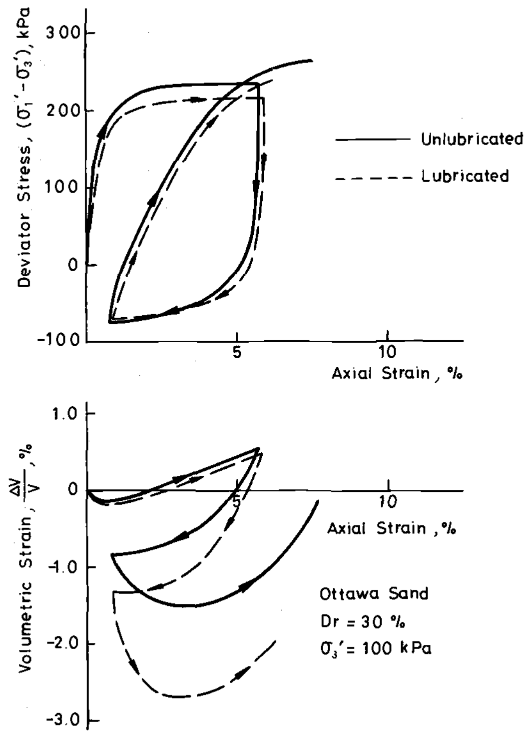

FIG. 7—*Stress-strain-volume change relationships under static cyclic loading.*

It appears that the end lubrication did not give the perfect uniformity of volume change distribution within the specimen, although no bulging or slip surfaces were observed in most tests. The reasons may be that (1) the end lubrication was not absolutely frictionless, (2) the sample was not prepared perfectly uniform, and/or (3) unavoidable errors in testing and measurement existed.

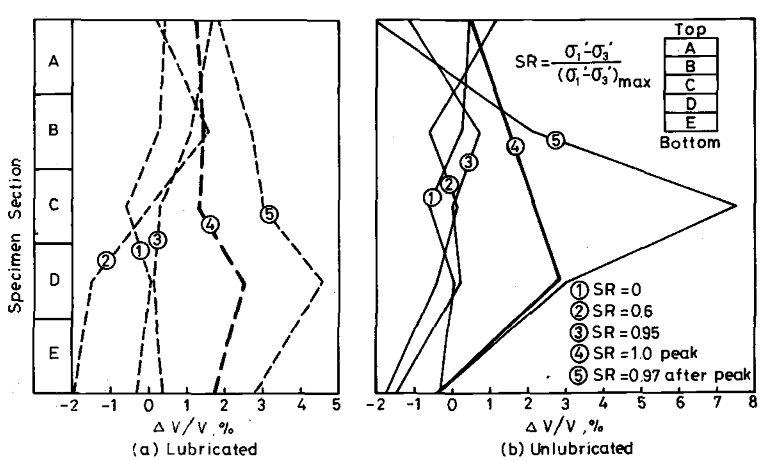

FIG. 8—*Volume change distributions for Fulung sand,* D_r *= 70%,* σ_3' *= 400 kPa.*

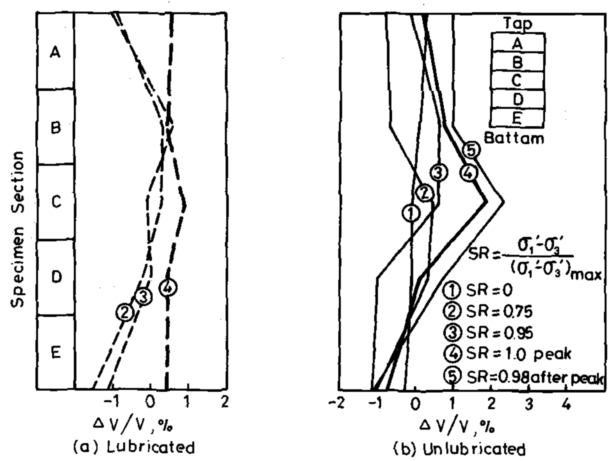

FIG. 9—*Volume change distributions for Fulung sand,* D_r *= 30%,* σ_3' *= 200 kPa.*

Figures 8 to 11 show the distributions of volume change within the specimens for Fulung sand, Ottawa sand, and Tamsui River sand under various testing conditions. The lubricated ends in the triaxial tests clearly induced more uniform volume changes within the specimens at and past the peak strength.

Particle Breakage Within Specimens

The amount of particle breakage of sands depends on many factors including particle shape and hardness, void ratio, effective stress, stress path, and particle size distribution [*16*]. In this investigation, the percentage of particle breakage under deviator stresses ranged from 0.05% for the hard Fulung sand (D_r = 70%) under a low confining pressure of 50 kPa to 23.6% for the friable Tamsui River sand (D_r = 78%) under a high confining pressure of 400 kPa. Generally, the total amount of particle breakage was less for the specimens without than with the end lubrication.

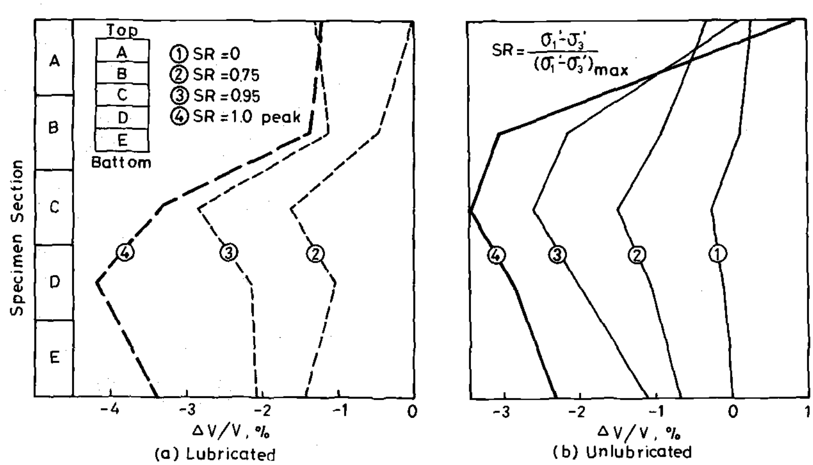

FIG. 10—*Volume change distributions for Tamsui River sand,* D_r *= 78%,* σ_3' *= 200 kPa.*

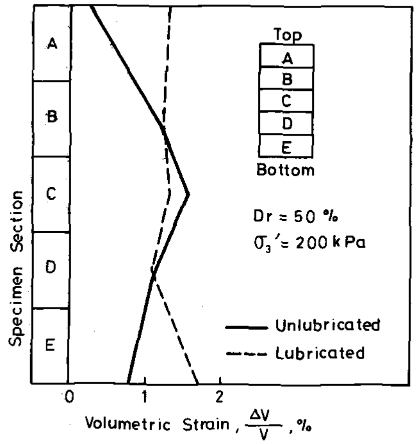

FIG. 11—*Volume change distributions at failure for Ottawa sand.*

The distributions of particle breakage within the specimens for Fulung sand and Tamsui River sand at different loading stages under various testing conditions are shown in Figs. 12 to 14. For the tests without end lubrication, there was obviously much higher particle breakage at the midportion of the specimens when the loading approached the peak strength. The amount of particle breakage for specimens with lubricated end platens showed quite uniform distributions within the specimens even after the peak strength was reached.

Particle Breakage and Strength

Particle breakage will cause more volume compression or less dilation under shearing and result in a lower shear strength. However, according to Lee and Seed, the energy consumption for particle breakage will induce some shear strength increase for the sands [8]. Hence, the role of particle breakage in volume change and shear strength of sands was examined based on the test results in this investigation.

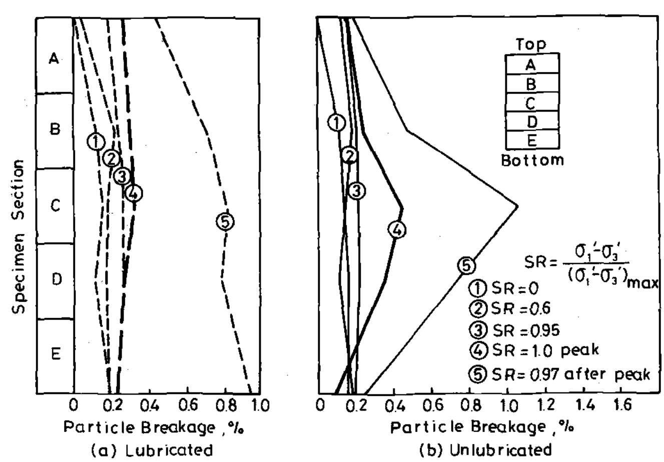

FIG. 12—*Particle breakage distributions for Fulung sand,* D_r = *70%,* σ_3' = *400 kPa.*

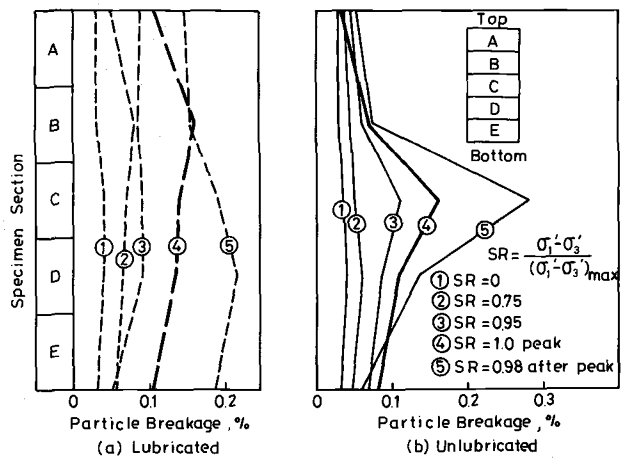

FIG. 13—*Particle breakage distributions for Fulung sand,* D$_r$ = *30%,* σ_3' = *200 kPa.*

Rowe [17] proposed the following stress–dilatancy relationship:

$$\frac{\sigma_1'}{\sigma_3'} = \left(1 + \frac{d\epsilon_v}{d\epsilon_1}\right) \tan^2\left(45° + \frac{\phi_\mu}{2}\right)$$

where

σ_1' = effective major principal stress
σ_3' = effective minor principal stress
$d\epsilon_v$ = change of volumetric strain, dilation positive
$d\epsilon_1$ = change of axial strain, compression positive
ϕ_μ = friction angle between the sand grain

In addition to the pure friction between soil grains and volume change, Rowe found that

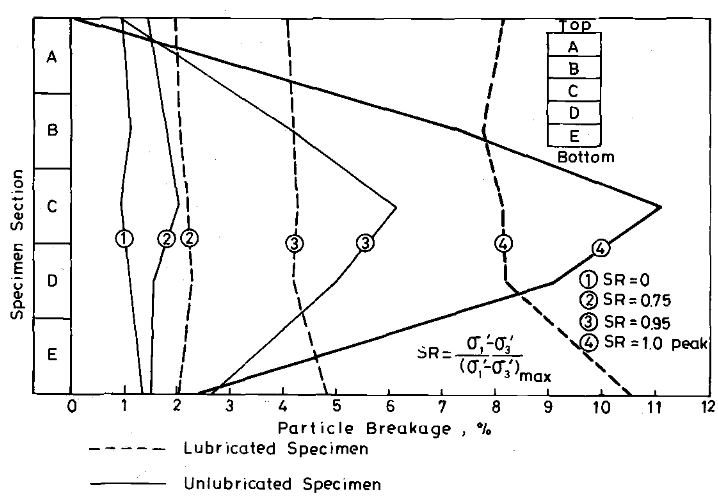

FIG. 14—*Particle breakage distributions for Tamsui River sand,* D$_r$ = *78%,* σ_3' = *200 kPa.*

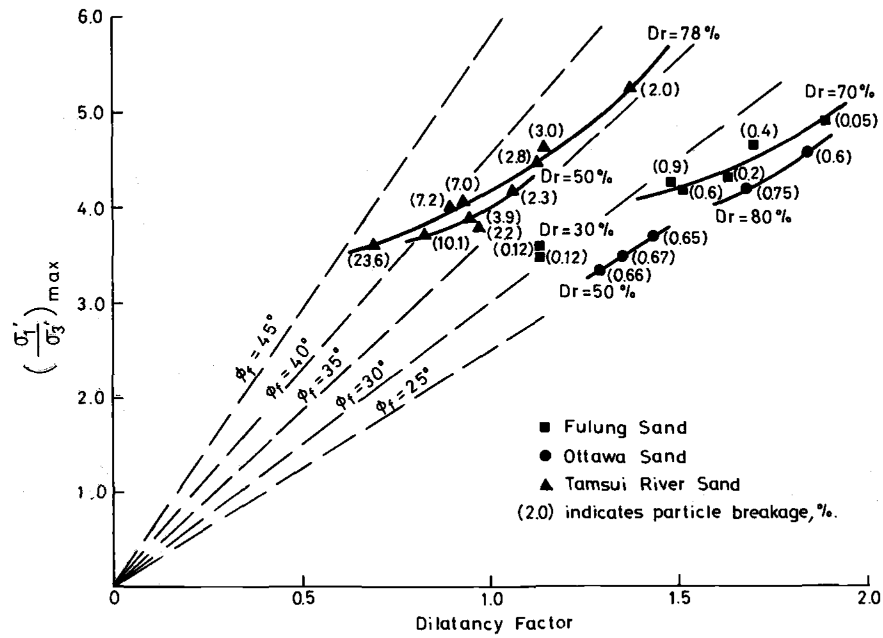

FIG. 15—*Relationship between stress ratio, dilatancy, and particle breakage.*

particle rearrangement also contributed to the strength of sands. Later studies indicated that particle crushing and particle shape also affected the strength of sands [*8,18,19*]. Therefore, ϕ_μ is usually replaced by ϕ_f to include all these effects in addition to pure friction.

Previous studies indicated a linear relationship between the peak stress ratio, $(\sigma_1'/\sigma_3')_{max}$, and the dilatancy factor, $(1 + d\epsilon_v/d\epsilon_1)$, at failure for a sand [*17–19*]. In this investigation, the peak stress ratio, $(\sigma_1'/\sigma_3')_{max}$, of each sand under various testing conditions was plotted against the dilatancy factor at failure in Fig. 15. Particle breakage during shearing was also indicated for each sample. The relations between the peak stress ratio and the dilatancy

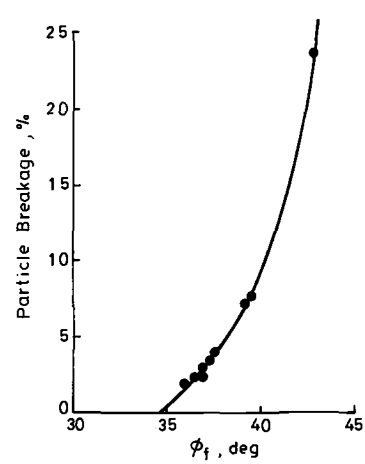

FIG. 16—*Relationship between ϕ_f and particle breakage for Tamsui River sand.*

factor were not linear, especially for Tamsui River sand with a large amount of particle breakage. Straight lines representing various ϕ_fs were drawn on the same plot. Based on the available data, the relation between $(\sigma_1'/\sigma_3')_{max}$ and the dilatancy factor of a sand of the same density with the same amount of particle breakage was a straight line passing through the origin. This showed that Rowe's stress–dilatancy theory was applicable for the sands of the same amount of particle breakage at failure. The ϕ_f values of Tamsui River sand seemed unaffected by the densities. Figure 16 shows the relationship between ϕ_f and the amount of particle breakage for Tamsui River sand.

Conclusions

The lubrication method of silicone grease between two latex membranes was found quite satisfactory for eliminating end restraint in triaxial tests. The effects of end restraint in triaxial testing were investigated based on the results of triaxial tests on Fulung sand, Ottawa sand, and Tamsui River sand specimens 71 mm in diameter and 152 mm in height. Lower peak strengths at higher axial strains with slightly higher volume changes at failure were usually obtained for the specimens with lubricated end platens. The volume changes at failure of the sands, either dilation or compression, were higher for the specimens with lubricated ends. The specimens with and without end lubrication in triaxial testing showed insignificant differences in uniformity of volume changes within the specimens prior to the peak strength, while in the middle portion of the specimens without end lubrication the soils underwent a distinctly higher volume change at and past the peak strength. The particle breakage within the specimens with lubricated end platens was quite uniform throughout the tests, whereas that of the specimens without end lubrication was higher at the midportion of the specimen when the loading approached peak strength and afterwards. Particle breakage played an important role in the volume change and strength of sands.

End lubrication in triaxial testing offers a more uniform and better loading condition on the specimen and should result in better testing data. Although some results in the triaxial tests on specimens with H/D ratios larger than two will not be significantly affected by end restraint, it is still recommended that lubricated end platens be used in triaxial testing for obtaining the values of parameters in constitutive relations, especially when the particle breakage is involved.

References

[1] Bishop, A. W. and Green, G. E., *Geotechnique,* Vol. 15, No. 3, 1965, pp. 243–265.

[2] Duncan, J. M. and Dunlop, P., *Journal of the Soil Mechanics and Foundations Division, American Society of Civil Engineers,* Vol. 94, SM1, 1968, pp. 271–290.

[3] Raju, V. S., Sadasivan, S. K., and Venkataraman, M., *Soils and Foundations,* Vol. 12, No. 4, 1972, pp. 35–43.

[4] Norris, G. M., in *Laboratory Shear Strength of Soil, ASTM STP 740,* American Society for Testing and Materials, Philadelphia, 1981, pp. 303–314.

[5] Lee, K. L., *Journal of the Geotechnical Engineering Division, American Society of Civil Engineers,* Vol. 104, GT6, 1978, pp. 687–703.

[6] Lade, P. V., in *Proceedings,* Conference on Deformation and Failure of Granular Materials, International Union of Theoretical and Applied Mechanics, Delft, 1982, pp. 461–471.

[7] Rowe, P. W. and Barden, L., *Journal of the Soil Mechanics and Foundations Division, American Society of Civil Engineers,* Vol. 90, SM1, 1964, pp. 1–27.

[8] Lee, K. L. and Seed, H. B., *Journal of the Soil Mechanics and Foundations Division, American Society of Civil Engineers,* Vol. 93, SM6, 1967, pp. 117–141.

[9] Marsal, R. J., in *Embankment-Dam Engineering,* Casagrande Volume, R. C. Hirschfeld and S. J. Poulos, Eds., Wiley, New York, 1973, pp. 109–200.

[10] Miura, N. and Ohara, S., *Soils and Foundations,* Vol. 19, No. 3, 1979, pp. 1–14.

[11] Roy, M. and Lo, K. Y., *Canadian Geotechnical Journal,* Vol. 8, 1971, pp. 579–588.
[12] Tatsuoka, F., Molenkamp, F., Torii, T. and Hino, T., *Soils and Foundations,* Vol. 24, No. 1, 1984, pp. 113–128.
[13] Tatsuoka, F. and Haibara, O., *Soils and Foundations,* Vol. 25, No. 1, 1985, pp. 89–98.
[14] Ladd, R. S., *Journal of the Geotechnical Engineering Division, American Society of Civil Engineers,* Vol. 100, GT10, 1974, pp. 1180–1184.
[15] Silver, M. L., Chan, C. K., Ladd, R. S., Lee, K. L., Tiedmann, D. A., et al., *Journal of the Geotechnical Engineering Division, American Society of Civil Engineers,* Vol. 102, GT5, 1976, pp. 511–523.
[16] Hardin, B. O., *Journal of Geotechnical Engineering, American Society of Civil Engineers,* Vol. 111, No. 10, 1985, pp. 1177–1192.
[17] Rowe, P. W., in *Proceedings,* Royal Society, London, Series A, Vol. 269, 1962, pp. 500–527.
[18] Miura, N., Murata, H. and Harada, A., *Transaction, Japanese Society of Civil Engineering,* Vol. 15, 1983, pp. 377–380.
[19] Frossard, E., *Geotechnique,* Vol. 29, No. 3, 1979, pp. 341–350.

Satoshi Goto[1] *and Fumio Tatsuoka*[2]

Effects of End Conditions on Triaxial Compressive Strength for Cohesionless Soil

REFERENCE: Goto, S. and Tatsuoka, F., "**Effects of End Conditions on Triaxial Compressive Strength for Cohesionless Soil,**" *Advanced Triaxial Testing of Soil and Rock, ASTM STP 977,* Robert T. Donaghe, Ronald C. Chaney, and Marshall L. Silver, Eds., American Society for Testing and Materials, Philadelphia, 1988, pp. 692–705.

ABSTRACT: Drained triaxial compression tests of Toyoura sand were carried out with conventional triaxial apparatus to evaluate the effects of sample slenderness and end conditions on triaxial compression strength. It was found that the maximum difference in the angle of internal friction ϕ_d for different test conditions employed was about $\pm 1°$. At the same time, the effects of the sample slenderness and each end condition on the strength value could be clearly identified.

KEY WORDS: triaxial compression test, sandy soil, angle of internal friction, boundary conditions

It is one of the classic problems of laboratory soil testing to evaluate the effects of the slenderness and the end conditions of the sample on the deformation and strength characteristics of sand in triaxial compression. While it has been shown by many researchers that when well lubricated ends are used the triaxial compressive strength is similar for $H_0/D_0 = 2.0$ and 1.0 (H_0 and D_0 are initial height and diameter of sample), some contradicting results of the effects of end surface friction on the triaxial compression strength have been reported. Bishop and Green [*1*] showed that for $H_0/D_0 = 2.0$ the angle of internal friction ϕ_d for nonlubricated (regular) fixed ends is similar to that for well lubricated fixed ends. On the other hand, Rowe and Barden [*2*], Raju et al. [*3*], Lee [*4*], and Lade [*5*] have shown that ϕ_d for a sample of $H_0/D_0 = 1.0$ or 2.0 with lubricated ends is slightly lower by 1 to 3° than that for a sample of $H_0/D_0 = 2.0$ to 2.7 with regular ends, the difference being larger for denser samples.

The importance of end lubrication in obtaining a homogeneous strain state within a sand sample in triaxial compression has been demonstrated by measuring the strain state by Kirkpatrick and Belshaw [*6*] and Kirkpatrick and Younger [*7*]. Thus, owing to the effects of end restraint of regular ends on measured average values of both stresses and strains, the relationship between average stress and average strain becomes different between regular and lubricated ends.

Furthermore, note that for shorter samples the degree of kinematic restraint by lubricated rigid ends against the development of single or multiple shear band(s) is larger, resulting in a larger degree of deformation uniformity. Thus, to obtain a larger degree of uniformity in

[1] Formerly, graduate student, University of Tokyo; now research engineer, Technical Research Institute of Taisei Corp., 344-1, Nagemachi, Totsuka-ku, Yokohama, 245, Japan.

[2] Associate professor, Institute of Industrial Science, University of Tokyo, 22-1, Roppongi 7-chome, Minato-ku, Tokyo 106, Japan.

strain distribution it would be preferable to perform triaxial compression tests on samples as short as possible. In fact, it will be shown later in this paper that for well lubricated ends even before the peak stress condition the relationship between average stress and average strain is a strong function of the sample slenderness H_0/D_0. However, only a very limited number of triaxial compression tests on very short samples, say $H_0/D_0 = 0.3$, with well lubricated ends have been reported [*8,9*].

Concerning the effects of the kinematic condition of the cap, Hettler and Vardoulakis [*9*] reported that ϕ_d of dense Karlsruhe sand by triaxial compression testing on large and short samples (H_0/D_0 = 28 cm/78 cm) with a lubricated guided cap was larger than that for small and short samples (H_0/D_0 = 2.5 cm/10 cm) with a lubricated nonguided cap by as large as about 6°. Furthermore, Hettler and Gudehus [*10*] reported that ϕ_d by the conventional triaxial compression test (that is, H_0/D_0 = 21.1 cm/10 cm with a nonguided cap and with non lubricated ends) was about 5° less than that by the large triaxial compression test (that is, H_0/D_0 = 28 cm/78 cm). Because in each case they changed multiple test variables (that is, sample size, kinematic and surface conditions of cap) at the same time, the true reason for this difference is still not clear.

It is apparent from the above that an overall picture of the effects of the end condition and the sample slenderness on the triaxial compression strength has not been obtained because so far no systematic study has been performed; one or only a limited number of test variables were changed arbitrarily. In some cases, results are even contradictory.

In this study, a series of triaxial compression tests of saturated Toyoura sand as listed in Table 1 (see also Fig. 1) was performed at a confining pressure σ_3' = 98.1 kN/m² (1.0 kgf/cm²). This kind of research is also needed from a practical point of view because the sample slenderness and end conditions employed in different laboratories have a very large variety and the effects of these different test conditions, which are being actually used, on test

TABLE 1—*List of test conditions.*

Type	Sample Dimension: Diameter, D_0 (cm)	Sample Dimension: H_0/D_0	End Surface Condition	End Kinematic Condition
A	7	2.6 2.1 1.0 0.6 0.3~ 0.35	lubricated; one-layer, Dow (except for H_0/D_0 = 2.6) or two-layer, KS63G (only for H_0/D_0 = 2.1 and H_0/D_0 = 2.6)	fixed to rotation (fixed)
B	7.5	2.7 2.4 2.0	regular (nonlubricated)	fixed
C	7.5	2.0	regular	rotating, radius of rotating = 13, 22, 38, or 58 mm
		2.4	regular	rotating; radius of rotating = 13 mm
D	7	2.1	lubricated; two-layer, KS63G	free horizontal movement

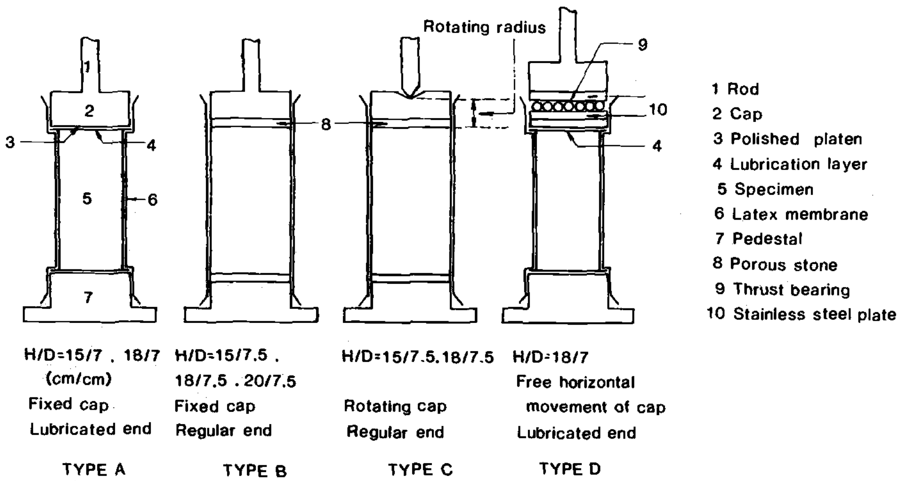

FIG. 1—*End conditions: types A, B, C, and D.*

results are still not well understood. In this paper, only test results concerning strength will be reported in detail.

Test Program

Fresh Toyoura sand (mean diameter d_{50} = 0.16 mm, uniformity coefficient = 1.46, specific gravity = 2.64, and particle shape = subangular) was used throughout this study. The details of the triaxial apparatus and the testing method are described elsewhere [*8,11–13*].

In the type A tests (see Fig. 1 and Table 1), two types of lubrication methods were used (described in detail by Tatsuoka et al. [*8*]). The type B tests are rather conventional ones. In the type C tests, the rotating radius is defined as the distance between the center of rotation and the nearest point on the top surface of the sample. In the type D tests, ends were lubricated and a cap was allowed to move in the horizontal direction while being fixed against the rotation in a vertical plane.

The samples were prepared by pluviating air-dry sand through air from a nozzle having an inner cross section of 1.5 by 15.0 mm. Then, samples were saturated at a confining pressure. Lubricated enlarged ends with a diameter of 7.5 cm were used, while regular ends had a diameter of 7.5 cm which equaled a sample's initial diameter D_0 of 7.5 cm.

Effects of End Surface Conditions

First of all, the angles of internal friction, $\phi_d = \arcsin\{(\sigma_1' - \sigma_3')/(\sigma_1' + \sigma_3')\}_{max}$, for lubricated fixed ends with $H_0/D_0 \fallingdotseq 2.1$ to 2.6 (type A) were obtained as a function of initial density (Fig. 2). These values will be used as reference values for the other test conditions. The initial void ratio, $e_{0.3}$, is the one measured at σ_3' = 29.4 kN/m^2 (0.3 kgf/cm^2) where sample dimensions were measured. It may be seen from Fig. 2 that when the cap is fixed and lubricated (type A), the difference in ϕ_d either between two kinds of lubrication methods or between H_0/D_0 = 15 cm/7 cm (2.1) and 18 cm/7 cm (2.6) is negligible. An average line for these data points A–A′ was determined by visual observation. Figure 2 also shows the values of ϕ_d for fixed regular ends (type B) with H_0/D_0 = 15 cm/7.5 cm (2.0), 18 cm/7.5 cm (2.4), and 20.3 cm/17.5 cm (2.7). It may be clearly seen from this figure that when the

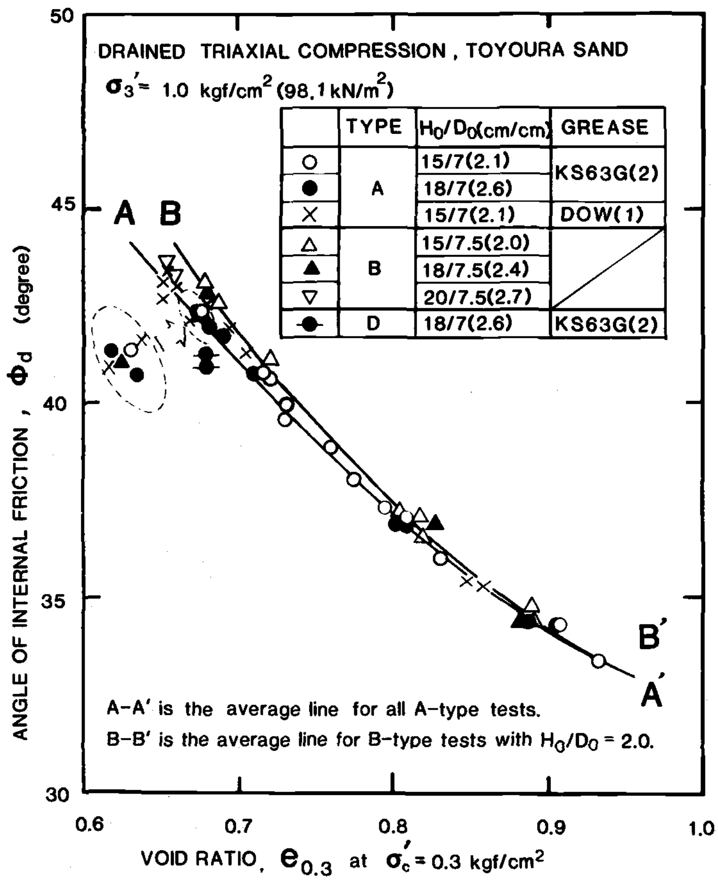

FIG. 2—*Friction angle versus void ratio from test types A, B, and D.*

cap is fixed and $H_0/D_0 \fallingdotseq 2.0$, ϕ_d of dense samples is larger for regular ends than for lubricated ends by about 1°, while ϕ_d for loose samples is similar in both regular and lubricated ends. An average line B–B′ was also determined by visual observation for the data points of regular ends with $H_0/D_0 = 2.0$. It may be noted that for dense samples with regular ends, ϕ_d decreases with increasing H_0/D_0 from 2.0 to 2.7, and at $H_0/D_0 = 2.7$, ϕ_d becomes essentially the same with that for lubricated ends (the line A–A′).

Overall stress–strain behaviors between lubricated end (type A) and regular end (type B) are compared in Figs. 3 and 4. Note that the precise comparison of strength cannot be made in these figures because the void ratio values are slightly different in each figure. It may be seen that the overall behaviors of types A and B are different to some extent.

For lubricated ends, measured boundary axial strain involves a so-called bedding error caused by the lateral squeezing out of grease, the lateral spreading of latex membrane sheets in lubrication layers, the indentation of sand particles in the lubrication layer, and the rearrangement in the looser surface particles [*14*]. The correction method for the bedding error will be reported in detail elsewhere by the authors. As shown later more in detail (see Fig. 12), differences in stress–strain behavior between regular and lubricated fixed ends seen in Figs. 3 and 4 do not disappear even after the axial strain is corrected for bedding error at lubricated ends. It seems that these differences are due to the effects of end restraint on

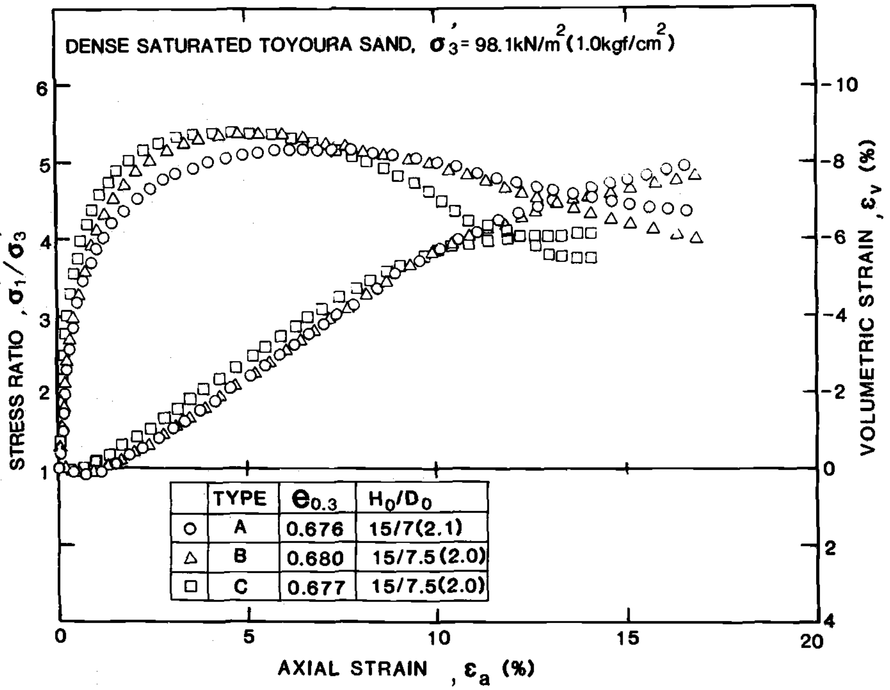

FIG. 3—*Comparisons of stress–strain curves among different boundary conditions for dense samples.*

measured average values of both stresses and strains for regular ends. For regular ends, the axial stress is overestimated because of the end friction, and the axial strain is underestimated by the nonuniform deformation.

In summary, when H_0/D_0 is about 2.0 and a sample is dense, ϕ_d for regular fixed ends is slightly larger than that for lubricated ends; for ϕ_d = 40 to 45°, the difference is about 1°. It can be suggested to employ a large H_0/D_0, say more than 2.5, for the purpose of obtaining ϕ_d of a dense sand which is free from the effects of end restraint; however, the overall stress–strain behaviors may still be affected by the restraint at end surfaces.

Effects of End Kinematic Conditions

Rotation of Cap

The values of ϕ_d for rotating regular (nonlubricated) caps with H_0/D_0 = 2.1 or 2.4 (type C) are plotted in Fig. 5 in comparison to the two average lines from Fig. 2. It may be seen that the data points for dense samples of H_0/D_0 = 2.0 with rotating regular ends are located well above the line A–A′ and close to the line B–B′. Furthermore, it may be seen by comparing Fig. 2 and Fig. 5 that when H_0/D_0 = 2.4, the value of ϕ_d of dense samples for regular ends is similar with both fixed (type B) and rotating caps (type C) as well as when H_0/D_0 = 2.0. These results indicate that for dense samples with rotating regular ends ϕ_d increases as a result of the end restraint by end friction but does not decrease because of the rotation of cap. Because of the cap rotation, concentration of deformation occurs more easily, resulting in easier formation of single shear band. However, it seems that the effects of cap rotation on ϕ_d are negligible when a sample is dense. On the other hand, it may be

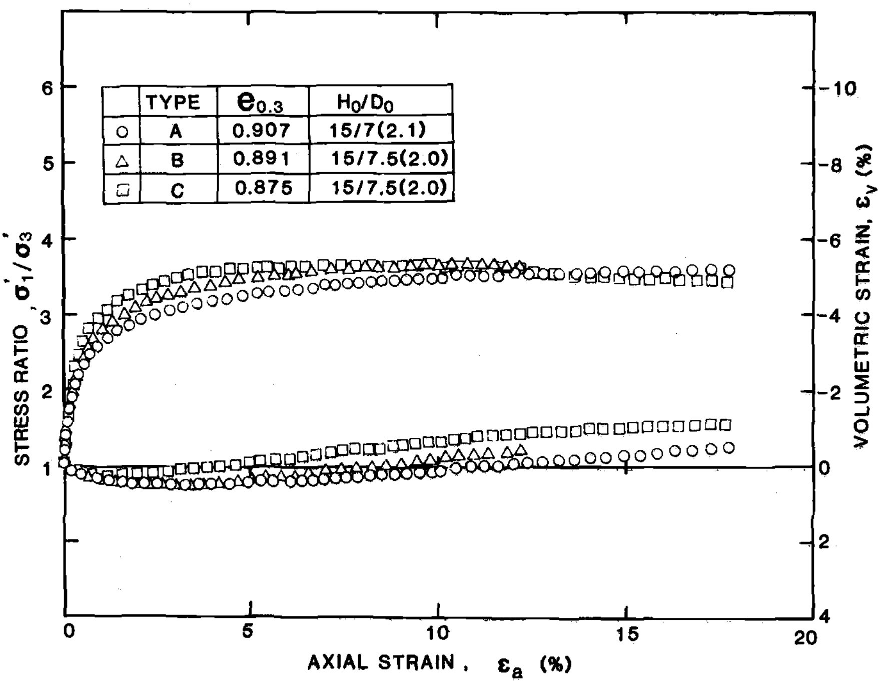

FIG. 4—*Comparisons of stress–strain curves among different boundary conditions for loose samples.*

seen from Fig. 5 that the data points for loose samples of $H_0/D_0 = 2.0$ with rotating regular ends are located below both the lines of A–A′ and B–B′. This suggests that because the effect of end friction on ϕ_d is negligible for loose samples of $H_0/D_0 \geqq 2$, ϕ_d for loose samples decreases due to the cap rotation. The effect of the rotation radius r on ϕ_d is not clear within the range of r examined.

To see why the effect of cap rotation on ϕ_d is negligible for dense samples whereas it is not the case for loose samples, the rotation of cap during triaxial compression test was measured by means of two small potentiometer-type inclinometers fixed on the cap. Because each inclinometer can measure only a rotation in one vertical plane, two inclinometers were used to measure the rotation in two perpendicular vertical planes. The angle of rotation θ is defined as arctan $\sqrt{(\tan\alpha)^2 + (\tan\beta)^2}$ where α and β are the angles of rotation measured by two inclinometers (Fig. 6*b*). Typical results for dense and loose samples are shown in Figs. 6*a* and 7. It may be seen that the cap started rotating from the very beginning stage of test even though the top surface of sample was prepared very carefully to be perpendicular to the axis of both the loading ram and the sample. It may also be seen that the relationship between θ and the measured average axial strain ϵ_a is similar in both loose and dense samples. Hence the value of θ at the maximum stress condition is very small for the dense sample and much larger for the loose sample. This phenomenon may explain why the effect of the cap rotation on ϕ_d is negligible for dense samples, but not for loose samples. It may also be seen from Figs. 6*a* and 7 that the rate of the increase in θ increases with increasing axial deformation up to $\epsilon_a \fallingdotseq 10$ to 12%, then θ increases at a constant rate thereafter. The authors cannot explain these phenomena in physical terms at present.

In Figs. 3 and 4, the stress–strain relationships for the rotating regular cap (type C) are compared with those for fixed regular ends (type B) and those for fixed lubricated ends

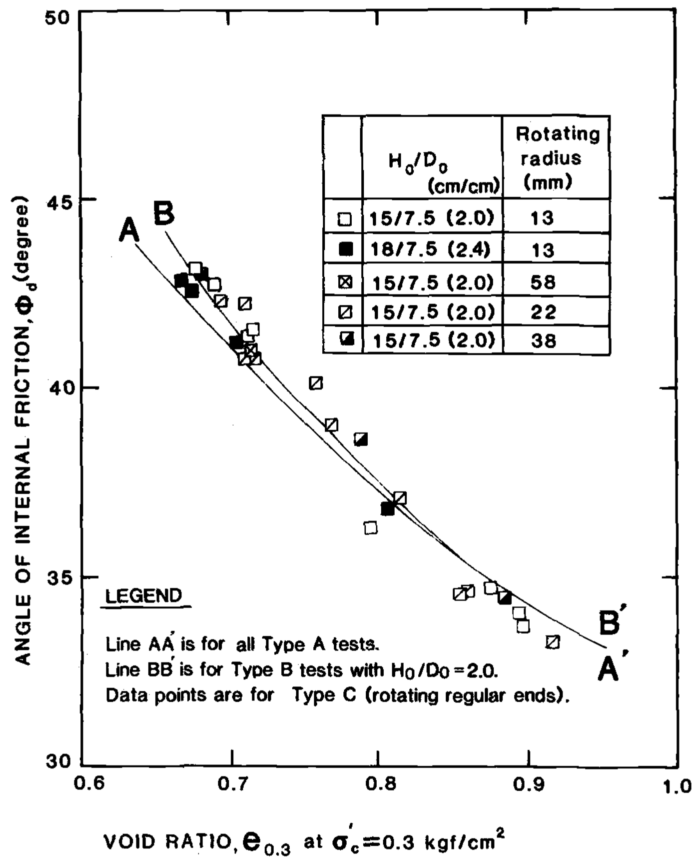

FIG. 5—*Friction angle versus void ratio from test type C.*

(type A). It may be seen that when samples are dense, the reduction in stress after peak for the rotating regular cap is larger than those for the other two cases. Furthermore, it may also be seen that for both loose and dense samples even before the peak stress condition the samples showed stiffer responses for type C than for type B. It is apparent that sample deformations become less uniform as a result of cap rotation. Therefore, the difference in the relationship between average stress and average strain between fixed and rotating caps as seen in Figs. 3 and 4 may be primarily due to a higher degree of nonuniform deformation caused by cap rotation.

Free Horizontal Movement of Cap

When a cap rotates at a certain rotating radius, this rotation can be separated into two components: a pure rotation without horizontal movement at the center of the top surface of sample and a horizontal movement without rotation. It is clear that both kinds of movement induce nonuniform deformation within a sample. To separate the effects of each movement component on the measured deformation and strength characteristics of sand, both kinds of tests should be performed: the one in which a cap is allowed to move horizontally without any rotation and the other one in which a cap is allowed to rotate at zero rotating radius.

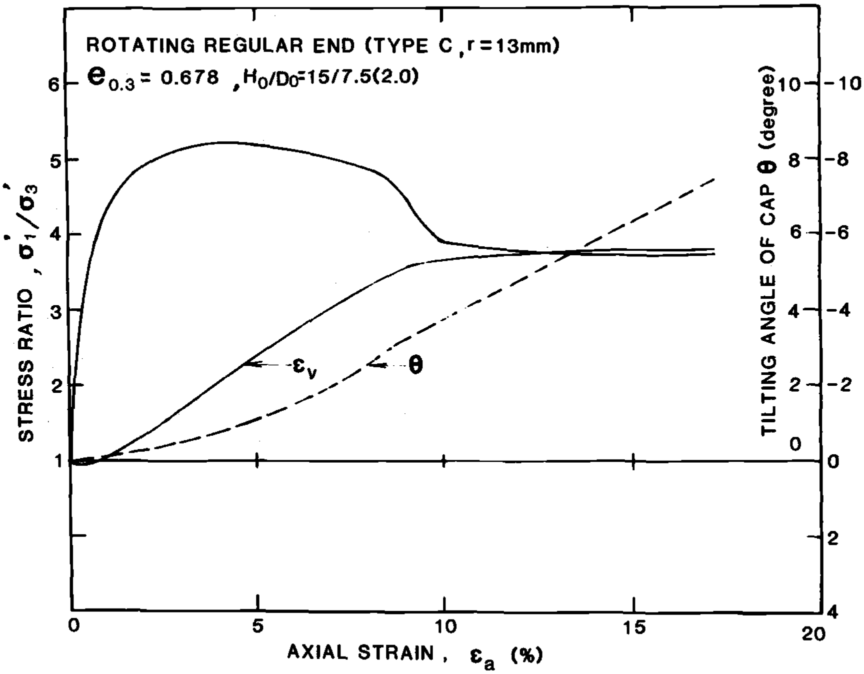

FIG. 6a—*Measured rotation of cap for dense sample (type C).*

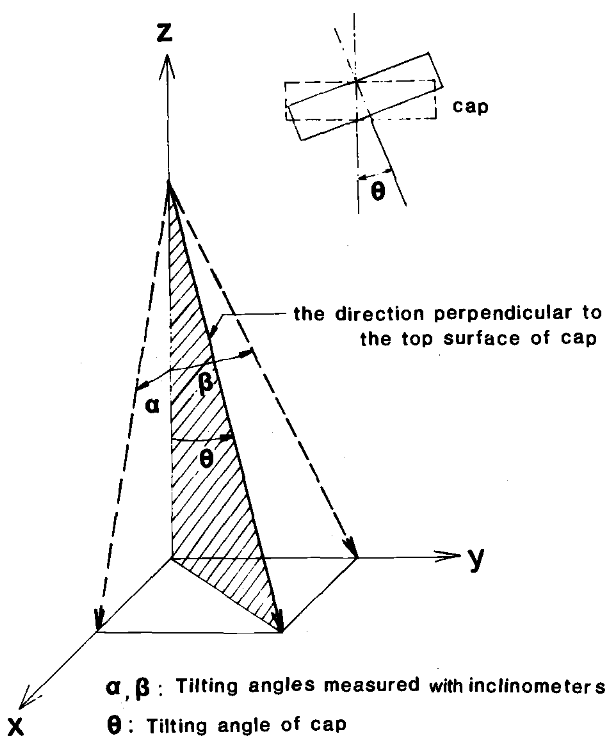

FIG. 6b—*Definition of the tilting angle of cap.*

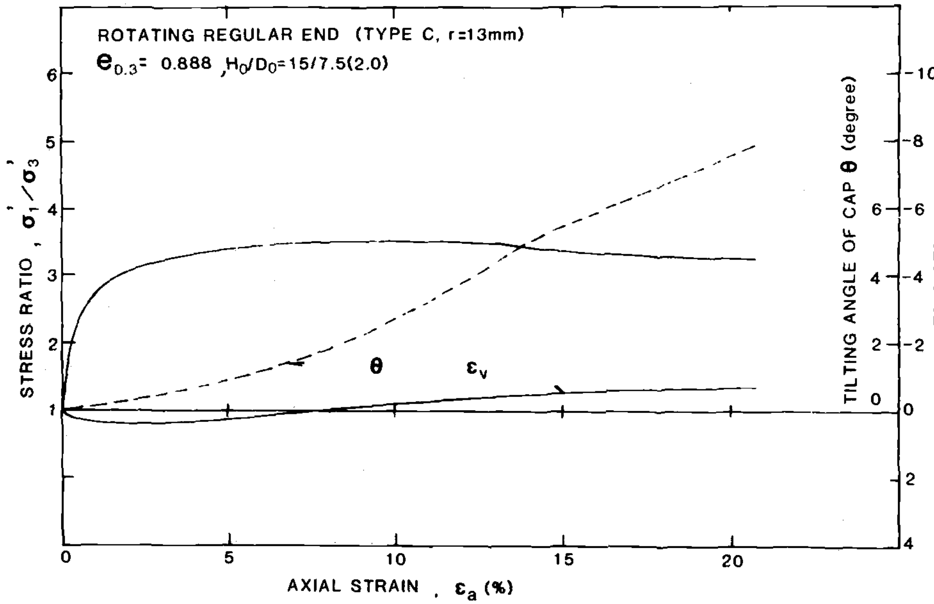

FIG. 7—*Measured rotation of cap for loose sample (type C).*

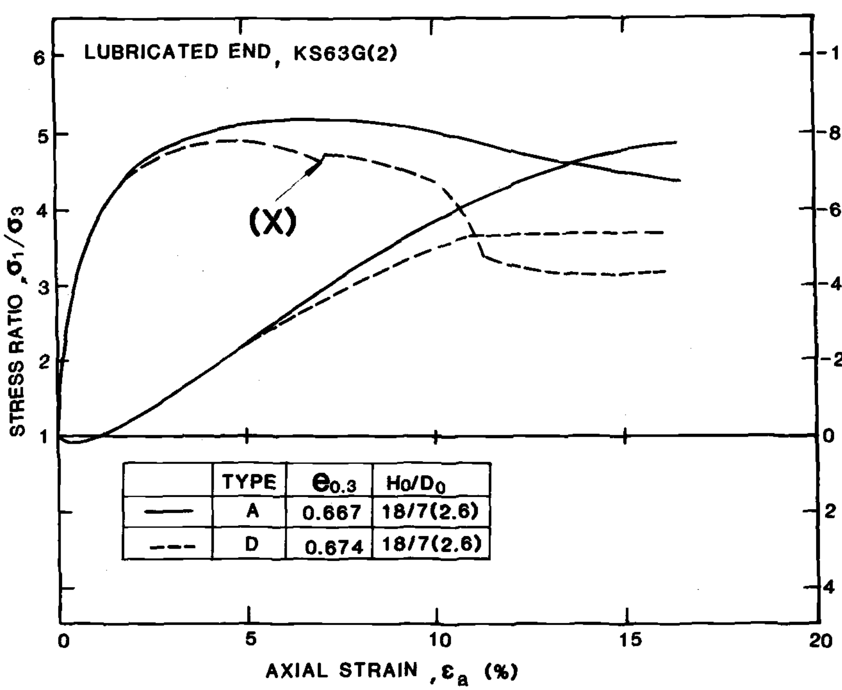

FIG. 8—*Comparisons of stress–strain curves between samples with and without free horizontal movement of cap.*

In this study, the first kind of test (type D) was performed on dense samples as follows. Both ends were lubricated with two-layer-type lubrication with silicone grease KS63G (KS63G(2)). The cap was loaded through a thrust bearing placed horizontally as shown in Fig. 1. It may be seen from Fig. 8 that the average stress is reduced due to the free horizontal cap movement even before the peak stress condition. While the horizontal movement of cap was not measured in this test, it was confirmed by visual observation that the cap started to move horizontally long before the peak stress condition. It was also observed that the cap had moved 8 mm at the point designated by the letter X in Fig. 8 which is the horizontal stroke of cap movement. Thereafter, no further horizontal movement of the cap occurred, but the top and bottom surfaces of the sample started to move horizontally at lubrication layers.

The values of ϕ_d from type D tests are compared to those for fixed cap tests (type A) in Fig. 2. It may be seen that the reduction caused by the free horizontal movement at sample ends is about 1° for dense sand. This may be due partly to the fact that the horizontal movement of the sample end induces the nonuniform stress distribution because of the noncoaxiality between the piston and the sample.

One of the practical meanings of the results shown above may be as follows: In most conventional triaxial tests, the cap is not lubricated and H_0/D_0 is between 2.0 and 2.5 and either the cap is fixed or it can rotate at a certain rotating radius. On the other hand, the ends may be lubricated in tests for research purposes and the cap is usually fixed. The results show that when nonlubricated ends are used for a range of H_0/D_0 between 2.0 and 2.4, the combined effects of end friction and cap rotation on the measured values of ϕ_d may not be larger than around ± 1°. Note, however, that when the cap is allowed to rotate, the scattering in data will become larger when compared to that when the cap does not rotate. Consequently, for nonlubricated ends it can be suggested to employ a fixed cap together with a

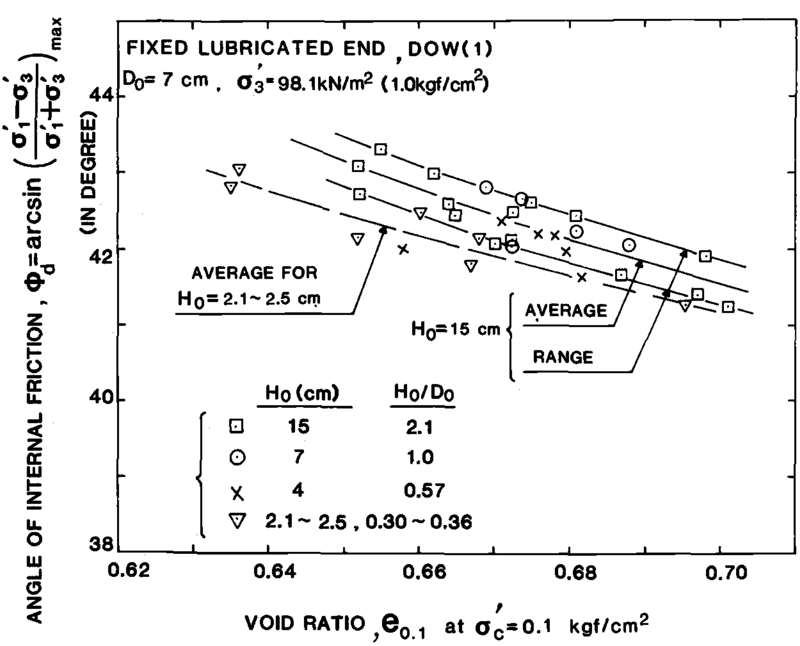

FIG. 9—ϕ_d *versus void ratio at* $\sigma_c' = 9.81\ kN/m^2$ *(0.1* kgf/cm^2*) for dense samples with fixed lubricated ends (type A) having* H_0/D_0 *= 15/7, 7/7, 4/7, 2.1 to 2.5/7.*

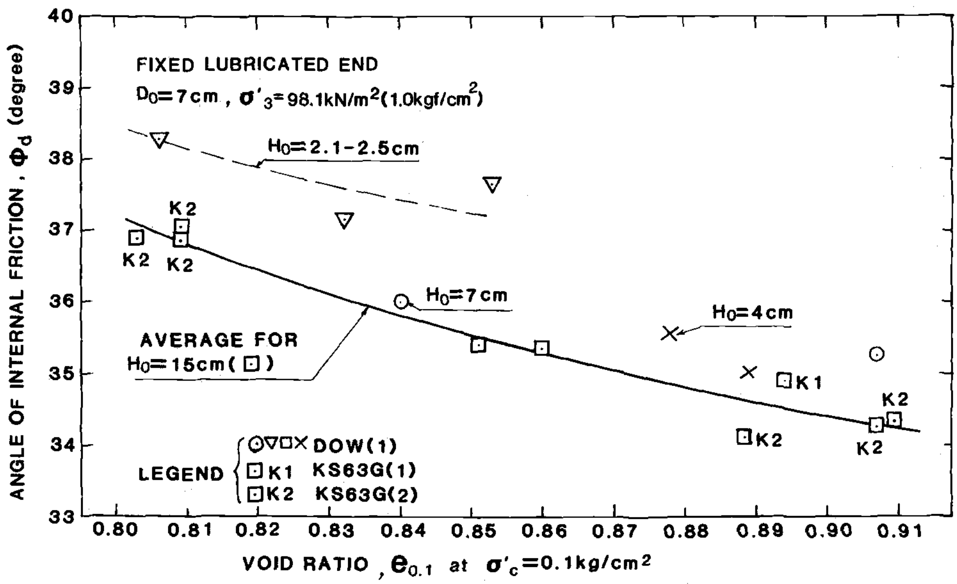

FIG. 10—ϕ_d *versus void ratio at* $\sigma_c' = 9.81\ kN/m^2$ $(0.1\ kgf/cm^2)$ *for loose samples with fixed lubricated ends (type A) having* H_0/D_0 = *15/7, 7/7, 4/7, 2.1 to 2.5/7.*

sufficiently high H_0/D_0, say 2.5 to 2.7, to obtain the value of ϕ_d which is free from the effects of both the end surface friction and the cap rotation. On the other hand, for lubricated ends it can be suggested to use a fixed cap because a clear strength reduction as a result of the horizontal cap movement may be observed as seen in this study.

Effects of Sample Slenderness for Lubricated Ends

Figures 9 and 10 show the values of ϕ_d for lubricated fixed ends of dense and loose samples with H_0/D_0 being 2.1 to 2.5 cm/7 cm, 4 cm/7 cm, 7cm/7 cm, or 15 cm/7 cm. In most tests,

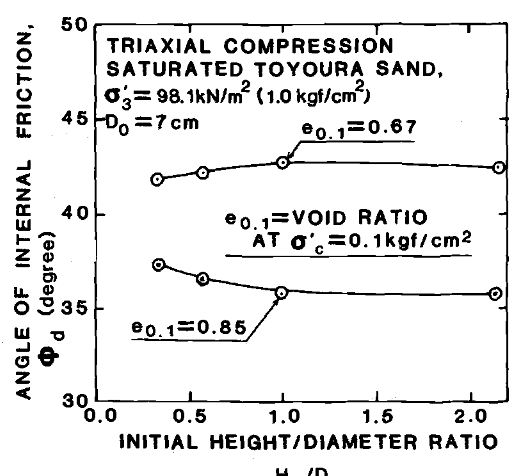

FIG. 11—ϕ_d *versus* H_0/D_0 *at* $e_{0.1}$ = *0.67 and 0.85 for fixed lubricated ends (type A).*

one-layer-type lubrication with Dow grease (Dow(1)) was used, while two-layer-type lubrication with silicone grease KS63G (KS63G(2)) was also used for loose samples with $H_0/D_0 = 2.0$. The sample dimensions were measured at $\sigma_3' = 9.8$ kN/m^2 (0.1 kgf/cm^2) to minimize the effects of bedding error and membrane penetration on measured sample density. In Fig. 10 additional data (KS63G(1) from Tatsuoka et al. [8]) are included. The angle of friction at end surfaces for the lubrication type Dow(1) was measured by the direct shear tests [8] and was found to be 0.14 to 0.16° at normal stresses ≒200 to 600 kN/m^2 (≒2 to 6 kgf/cm^2) for a wide range of void ratio (e = 0.65 to 0.85). The effect of this friction on ϕ_d is not more than 0.2° even for a very short sample with a H_0/D_0 of 0.2 based on the correction method by Drescher and Vardoulakis [15]. Therefore, ϕ_d was not corrected for the data shown in Figs. 9 and 10.

It may be seen from Fig. 9 that for dense samples, while the difference in ϕ_d between H_0 = 15 cm and 7 cm is negligible, ϕ_d decreases slightly when H_0 decreases from 7 cm down to 2.1 to 2.5 cm; however, this reduction is not larger than 0.5°. On the other hand, it may be seen from Fig. 10 that for loose samples, the value of ϕ_d increases with decreasing H_0

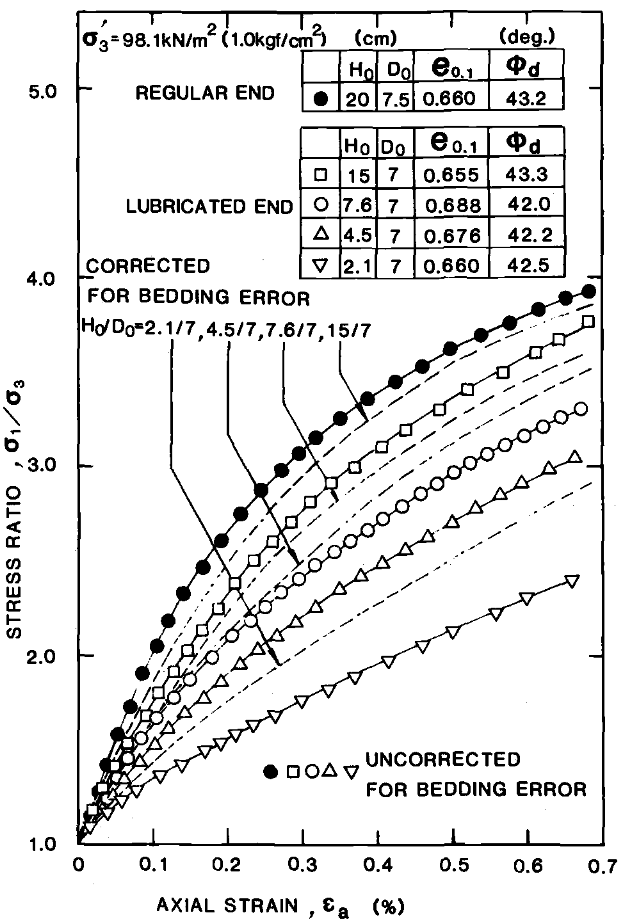

FIG. 12—σ_1'/σ_3' *versus axial strain of dense samples at small strains for lubricated and regular fixed ends.*

from 15 cm to 2.1 to 2.5 cm. Figure 11 shows the relationship between ϕ_d and H_0/D_0 for $e_{0.1} = 0.67$ and 0.85 obtained from the data shown in Figs. 9 and 10.

The reason for this change of ϕ_d by the change in H_0/D_0 seen in Figs. 9, 10, and 11 is not known yet. In Fig. 12 the stress–strain relations at small strains of dense samples with lubricated and regular ends are compared. For lubricated ends, the curves after the bedding error correction are shown too. It may be seen that for the same $H_0/D_0 = 2.0$, the stress–strain curves are different for lubricated and regular ends as may also be seen in Figs. 3 and 4. Also note that for lubricated ends the stress–strain curves are very different among these different H_0/D_0 ratios. These results suggest that the degree of deformation uniformity increases when the H_0/D_0 ratio decreases from 2.0 to 0.3. Therefore, for the purpose of achieving a very uniform strain condition, tests on very short samples with well lubricated ends may be needed as has been suggested by Hettler and Vardoulakis [9]. However, such a large difference as 4 to 6° in ϕ_d among different test conditions as reported by Hettler and Vardoulakis [9] and Hettler and Gudehus [10] was not obtained in this study.

Conclusions

From the results of a series of triaxial compression tests on samples of saturated Toyoura sand at $\sigma_3' = 98.1$ kN/m^2 (1.0 kgf/cm^2), the following conclusions may be drawn.

1. At $H_0/D_0 \fallingdotseq 2.0$ with fixed caps, the value of ϕ_d with regular (nonlubricated) ends was larger than that with lubricated ends by around 1° in dense samples, and the difference in ϕ_d was negligible in loose samples. ϕ_d for dense samples of $H_0/D_0 = 2.7$ with fixed regular ends was very similar to the value for lubricated ends at $H_0/D_0 = 2.1$ to 2.6.
2. For $H_0/D_0 = 2.0$ to 2.4 with regular ends, the effects of cap rotation on the value of ϕ_d were negligible in dense samples and ϕ_d decreased because of the cap rotation by about 1° in loose samples.
3. For lubricated ends, horizontal cap movement reduced ϕ_d for dense samples by about 1°.
4. For samples of a diameter of 7 cm with lubricated ends, with decreasing the sample height from 15 cm to 2.1 to 2.5 cm, ϕ_d decreased in dense samples, whereas ϕ_d increased in loose samples; however, the variation in ϕ_d was not more than ± 1°.
5. Only for the purpose of evaluating ϕ_d, a fixed cap with a nonlubricated surface may be used if a sample has a large H_0/D_0 ratio, say 2.5 to 2.7 for dense samples and 2.0 to 2.5 for loose samples. To obtain an overall stress–strain behavior for a homogeneous deformation, a short sample with well lubricated fixed ends should be used.

Acknowledgments

This study was performed at Institute of Industrial Science, University of Tokyo. The cooperations provided by T. Sato, K. Enokido, T. Takizawa, and M. Torimitsu are sincerely acknowledged.

References

[1] Bishop, A. W. and Green, G. E., "The Influences of End Restraint on the Compression Strength of a Cohesionless Soil," *Geotechnique*, Vol. 15, No. 3, 1965, pp. 243–266.

[2] Rowe, P. W. and Barden, L., "Importance of Free Ends in Triaxial Testing," *Journal of Soil Mechanics and Foundations Division, American Society of Civil Engineers*, Vol. 90, No. SM1, Jan. 1964, pp. 1–27.

[3] Raju, V. S., Sadasivan, S. K. and Venkataraman, M., "Use of Lubricated and Conventional End Platens in Triaxial Tests on Sands," *Soils and Foundations*, Vol. 12, No. 4, 1972, pp. 35–43.
[4] Lee, K. L., "End Restraint Effects on Undrained Static Triaxial Strength of Sand," *Journal of Geotechnical Engineering Division, American Society of Civil Engineers*, Vol. 104, No. GT6, June 1978, pp. 687–703.
[5] Lade, P. V., "Localization Effects in Triaxial Tests on Sand," *Proceedings of International Union of Theoretical and Applied Mechanics, Symposium on Deformation and Failure of Granular Materials*, Delft, 1982, pp. 461–472.
[6] Kirkpatrick, W. M. and Belshaw, D. J., "On the Interpretation of the Triaxial Test," *Geotechnique*, Vol. 18, No. 3, 1968, pp. 336–350.
[7] Kirkpatrick, W. M. and Younger, J. S., "Strain Conditions in Compression Cylinder," *Journal of Soil Mechanics and Foundations Division, American Society of Civil Engineers*, Vol. 96, No. SM5, Sept. 1970, pp. 1683–1695.
[8] Tatsuoka, F., Molenkamp, F., Torii, T. and Hino, T., "Behavior of Lubrication Layers of Platens in Element Tests," *Soils and Foundations*, Vol. 24, No. 1, 1984, pp. 113–128.
[9] Hettler, A. and Vardoulakis, I., "Behavior of Dry Sand Tested in a Large Triaxial Apparatus," *Geotechnique*, Vol. 34, No. 2, 1984, pp. 183–198.
[10] Hettler, A. and Gudehus, G., Discussion, *Soils and Foundations*, Vol. 25, No. 3, 1985, p. 140.
[11] Fukushima, S. and Tatsuoka, F., "Strength and Deformation Characteristics of Saturated Sand at Extremely Low Pressures," *Soils and Foundations*, Vol. 24, No. 4, 1984, pp. 30–48.
[12] Tatsuoka, F., Goto, S. and Sakamoto, M., "Effects of Some Factors on Strength and Deformation Characteristics of Sand at Low Pressures," *Soils and Foundations*, Vol. 26, No. 1, 1986, pp. 105–114.
[13] Tatsuoka, F., Sakamoto, M., Kawamura, T. and Fukushima, S., "Strength and Deformation Characteristics of Sand in Plane Strain Compression at Extremely Low Pressures," *Soils and Foundations*, Vol. 26, No. 1, 1986, pp. 65–84.
[14] Molenkamp, F. and Tatsuoka, F., Discussion on "Compression of 'Free-Ends' During Triaxial Testing," *American Society of Civil Engineers, Newsletter*, Vol. 109, No. 5, May 1983, pp. 766–773.
[15] Drescher, A. and Vardoulakis, I., "Geometric Softening in Triaxial Tests on Granular Material," *Geotechnique*, Vol. 32, No. 4, 1982, pp. 291–303.

Poul V. Lade[1] *and Uzair Wasif*[1]

Effects of Height-to-Diameter Ratio in Triaxial Specimens on the Behavior of Cross-Anisotropic Sand

REFERENCE: Lade, P. V. and Wasif, U., "**Effects of Height-to-Diameter Ratio in Triaxial Specimens on the Behavior of Cross-Anisotropic Sand,**" *Advanced Triaxial Testing of Soil and Rock, ASTM STP 977,* Robert T. Donaghe, Ronald C. Chaney, and Marshall L. Silver, Eds., American Society for Testing and Materials, Philadelphia, 1988, pp. 706–714.

ABSTRACT: The drained stress–strain, volume change, and strength behaviors of sand with cross-anisotropic fabric were studied in triaxial compression tests. Dense specimens with square cross-sections, height-to-diameter (H/D) ratios of 1.0 and 2.5, and lubricated ends were employed. Specimens consisting of relatively long, flat sand grains were prepared with cross-anisotropic grain structure, whose axis of rotation was inclined at various orientations from vertical to horizontal. The specimen boundary conditions (flexible membrane and lubricated, rigid end plates) had different effects on the results for specimens with H/D = 1.0 and 2.5. The specimens with H/D = 2.5 exhibited distinct, but temporary drops in their prefailure stress–strain curves, and the friction angles changed in a consistent pattern over a range of 5.5°. In comparison, the specimens with H/D = 1.0 showed more smooth stress–strain behavior, and their friction angles were essentially constant with very little effect of orientation.

KEY WORDS: anisotropic, boundary condition, dilation, failure, laboratory test, mechanical properties, sands, shear strength, soil mechanics, stress–strain curve, triaxial test

Virtually all natural in situ sand deposits display fabric anisotropy due to parallel alignment of particles [*1*]. Several experimental studies have shown that fabric anisotropy may have considerable influence on the stress–strain and strength behaviors of sand obtained in triaxial compression, plane strain, and cubical triaxial tests [*1–14*]. Some of these investigations have been performed on specimens with cross-anisotropic grain structure, whose initial axis of rotation was inclined at various constant angles with the direction of the major principal stress [*1–3,9–13*]. The results of some of these studies have indicated that the maximum strength of homogeneous specimens was mobilized in the drained triaxial compression tests when the major principal stress, σ_1, was applied perpendicular to the bedding planes, and the minimum strength was obtained when σ_1 was applied parallel to the bedding planes. However, recent studies have indicated that the experimental conditions used in the previous studies may be particularly susceptible to development of localized plastic deformations, a condition which may lead to low strength of soils that dilate [*15*]. It is possible, therefore, that the low strength observed in tests with σ_1 parallel to the bedding planes is a result of the experimental technique employed in the previous investigations.

[1] Professor and former graduate student, respectively, Department of Civil Engineering, School of Engineering and Applied Science, University of California, Los Angeles, CA 90024.

Presented herein is an experimental study of the influence of boundary conditions in triaxial compression tests on the stress–strain and strength characteristics of sand with cross-anisotropic fabric, whose initial axis of rotation was inclined at various constant angles with vertical. Each specimen consisted of sand grains deposited under water in a mold tilted at the desired angle, then frozen, removed from the mold, and placed upright (that is, with inclined bedding planes) in the triaxial apparatus, thawed, and tested in compression.

Characterization of Sand, Specimen Preparation, and Fabric

Sand Composition

All tests in this study were performed on uniformly graded Cambria sand with particle sizes between No. 10 and No. 20 U.S. sieves (2.00 to 0.84 mm). The specific gravity of grains was 2.708, and the maximum and minimum void ratios were 0.80 and 0.51, respectively.

The three principal dimensions of the sand particles (that is, length, width, and height) were studied using two microscopes. A grain was placed in its most stable position at the edge of a table and measured in vertical and horizontal directions through the two microscopes. Results based on the study of 250 particles are shown in Fig. 1*a*. As in Ref *16*, the results are presented as length-to-height ratios (L/H) and length-to-width ratios (L/W) and they indicate that the sand grains are somewhat long and flat. According to previous studies of several natural sands [*11,12*], typical values of axial ratio, which may include both W/L and H/L (no distinction was made between the two ratios), range from 0.5 to 0.7 corresponding to L/W and/or L/H ratios from 2.0 to 1.4. The sand selected for the present study is representative, therefore, of common natural sands, possibly with axial ratios in the upper end of the range. (This sand was also used in a previous study of the three-dimensional behavior of sand with cross-anisotropic fabric under conditions of principal stress directions fixed and aligned with directions of material axes [*8*].)

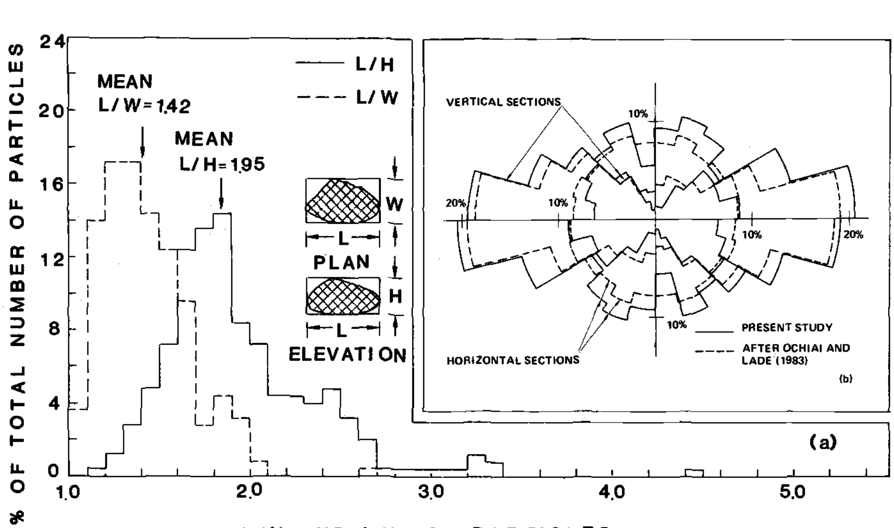

FIG. 1—(a) *Grain shape distribution and* (b) *Rose diagrams of particle long axis orientations for specimens of Cambria sand.*

Specimen Preparation

Dense specimens with square cross-sections and with height-to-diameter (H/D) ratios of 1.0 and 2.5 were prepared in specially designed molds by pouring and shaking sand grains in several layers. The specimens were then frozen in molds designed to avoid expansion or disturbance of the sand structure during freezing.

The four sides and the top of each mold were made of polyvinyl chloride (PVC), and the bottom plate was made of copper. So the sand could be poured vertically into an inclined mold, one side and the top were cut into sections (Fig. 2). These sections could then be added as the sand was deposited in the mold. Silicone grease was smeared on the faces of the PVC sections to seal the mold and to avoid adherence between the mold and the frozen specimen. The molds were held together by threaded rods attached to the copper base plates, and they could be completely disassembled to remove the frozen specimen. The side length of the square specimens were 76 mm, and their heights were 76 and 190 mm, respectively.

To prepare a specimen, the mold was placed in a bucket with deaired water. A cradle was employed to hold the mold at the desired tilt angle. Sand was poured into the mold in 10 to 25 evenly thick layers. The bucket was placed on a vibrator, and after deposition of each sand layer the bucket was shaken for 1 min by horizontal, gyrating movements.

Following deposition of a specimen, the mold was placed upright in a freezer. Because copper has a much higher heat conductivity than PVC, freezing of the specimen proceeded upwards from the bottom plate, thereby pushing excess water out through holes in the top plates. To further enhance the process of freezing from the bottom, the mold was placed on a large, solid piece of aluminum (which also has high heat conductivity) inside the freezer.

Specimens prepared for this study had void ratios from 0.52 to 0.57.

Fabric Characterization

In order to examine the fabric of a specimen, photographs were taken of horizontal and vertical sections through central regions of the specimen. This could be accomplished by melting part of a frozen specimen. The central region (that is, the region within one to two

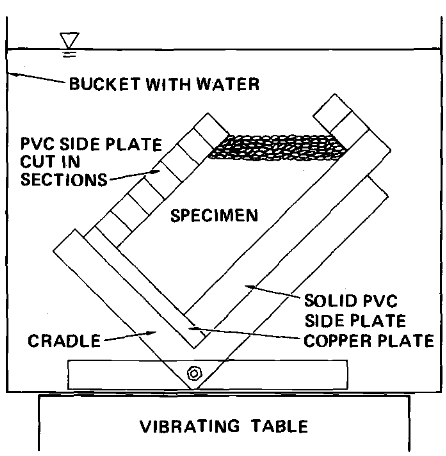

FIG. 2—*Mold for preparation of specimens with inclined bedding planes.*

grain diameters from the side walls) was used to avoid effects of the side walls which may locally have influenced the fabric. Measurements of orientation were made on photographic enlargements. The orientations of apparent long axes in one horizontal and two vertical sections of a specimen with horizontal bedding planes are shown on the rose diagram in Fig. 1*b*. In this study the orientations of 280 particles were measured for each section, and the orientation of each particle was assigned to one of the 15° intervals between 0 and 180°. Figure 1*b* shows that the particles in the specimens prepared by the method described above had strong preferred orientations in the vertical sections, but almost completely random orientations in the horizontal section. Results of similar analysis from a previous study [*8*] are shown in Fig. 1*b* for comparison.

To compare the intensity of fabric anisotropy with previously obtained intensities, the mean vector direction, $\bar{\alpha}$, and vector length, L, defined by Curry [*17*] and used in several previous studies [*7,9,11,12*], were calculated according to:

$$\bar{\alpha} = \frac{1}{2} \cdot \arctan \frac{\sum n \cdot \sin 2\alpha}{\sum n \cdot \cos 2\alpha} \; (°) \tag{1}$$

$$L = \frac{100}{\sum n} \cdot \sqrt{(\sum n \sin 2\alpha)^2 + (\sum n \cdot \cos 2\alpha)^2} \; (\%) \tag{2}$$

where α is the orientation of the apparent long axis relative to a reference axis, and n is the number of particles oriented at α. The value of L varies from 0 to 100%. $L = 0\%$ corresponds to completely random orientation of particle long axes, whereas $L = 100\%$ corresponds to all long axes having exactly the same direction.

For the vertical sections of a specimen of Cambria sand with horizontal bedding planes, $\bar{\alpha} = 2.1°$. This means that the apparent long axes in the specimen were preferably parallel to horizontal, which was used as a reference axis. The vector length was calculated to be $L = 55.5\%$ for the vertical sections. Compared to values of L obtained in previous studies of natural sand deposits [*11,12*], this value of vector length corresponds to a high degree of preferred particle orientation. Corresponding values of $\bar{\alpha}$ and L for the horizontal section of the Cambria sand specimen were 7.8° and 5.8%, respectively. Thus, an almost completely random orientation of particles in the horizontal plane was obtained. The specimen fabric is therefore of the cross-anisotropic type with a vertical axis of rotational symmetry and horizontal planes of isotropy.

Testing Equipment

Triaxial Apparatus—The drained tests were performed in a conventional triaxial apparatus. Enlarged, square end plates with central drainage were employed. A clip gauge was attached to the middle of the specimen, measuring one of the horizontal strains. The other horizontal strain was calculated from the measured volume change and the vertical deformation.

Lubricated End Plates—To avoid development of significant shear stresses between the end plates and the specimen, and to reduce nonuniformities in strains, lubricated ends were provided on the cap and base. Each of the two lubricated ends consisted of two rubber sheets coated with silicone grease. Tests with regular end plates were not performed in this study.

Measurements and Corrections

Corrections to measured loads and pressures were found to be negligible. All measured strains presented herein have been corrected as appropriate for sand grain penetration into the lubricating rubber sheets.

Representation of Stress and Material Axes

To present results of tests on anisotropic materials, it is important to indicate clearly the directions of stress relative to the principal axes of the material. For this purpose two Cartesian coordinate systems are employed, as indicated in Fig. 3. One coordinate system (123) indicates the principal stress directions (vertical and horizontal), and the other coordinate system (XYZ) is located such that the X-axis coincides with the axis of initial rotational symmetry of the cross-anisotropic specimens. The angle β between the vertical σ_1-direction and the X-axis indicates the inclination of the bedding planes.

Testing Program and Procedures

Drained triaxial compression tests were performed with constant effective confining pressures of 1.00 kgf/cm^2 (98 KN/m^2) and with back pressures of 2.0 kgf/cm^2 (196 KN/m^2). Tests were performed with inclination angles β of 0, 45, 60, and 90°.

Stress–Strain and Volume Change Characteristics

Figure 4 shows stress–strain and volume change relations obtained from triaxial compression tests with β = 0, 45, 60, and 90°. The results for specimens with H/D = 2.5 are shown in Fig. 4*a*, and the results for specimens with H/D = 1.0 are shown in Fig. 4*b*.

The steepest stress–strain curve obtained for the tall specimens (Fig. 4*a*) corresponds to β = 0°, which represents a conventional specimen with horizontal bedding planes. The stress–strain relation is smoothly curved well beyond failure at which time the stress drops off abruptly. Additional straining results in increasing stresses, but the peak strength is not reached again. The abrupt drop-off is associated with development of a shear band, which is allowed by the flexible rubber membrane to progress through the specimen. The volume change curve for this specimen exhibits a temporary decrease in rate of dilation at the time of the shear band development.

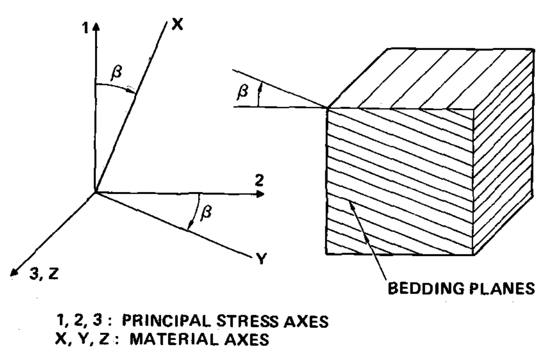

FIG. 3—*Coordinate systems for indication of initial bedding plane inclination of cross-anisotropic specimens.*

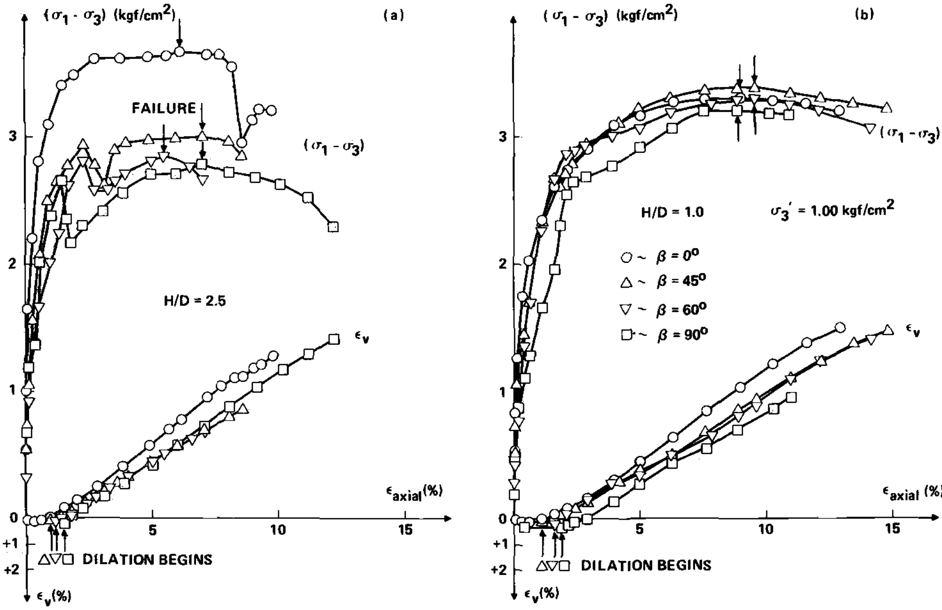

FIG. 4—*Stress–strain and volume change characteristics obtained in triaxial compression tests on Cambria sand with cross-anisotropic fabric ($1.00\ kgf/cm^2 = 98.1\ KN/m^2$).*

All tests with inclined and vertical bedding planes shown in Fig. 4*a* indicate clear effects of the inherent cross-anisotropic fabric in the sand specimens. In specimens with initially isotropic material, shear planes initiate in triaxial compression after the peak failure point has been exceeded [*18*]. Thus, the prefailure observations presented here are related to the anisotropic nature of the soil fabric. The possible lack of correct grain orientation near the cap and base caused by the side walls during specimen preparation is believed to have had only small, if any, effect on the overall behavior of the anisotropic sand. The prefailure stress–strain and volume change behaviors appear to show that the grain structure temporarily locks up. This is indicated by the stress–strain curves which begin to steepen about halfway up to failure. The corresponding volume change curves show zero rates of dilation until the stress–strain curves begin to flatten again. Then dilation begins and almost immediately reaches the maximum rate. As the tests progress, sudden drop-offs in stress occur before the peak strengths are obtained at larger strains. The drop-offs occur after dilation begins in the specimens with inclined bedding planes, whereas the stress drop-off is observed simultaneously with initiation of dilation in the specimen with vertical bedding planes ($\beta = 90°$). Shear bands were not visible at the time of the stress drop-offs, and the volume change curves do not indicate any temporary decrease in rates of dilation. The axial strains-to-failure range from 5 to 7%.

The tests performed on specimens with $H/D = 1.0$ (Fig. 4*b*) show similar trends, but not nearly as pronounced as obtained for specimens with $H/D = 2.5$. Thus, the stress–strain curves are more smooth, and the axial strains-to-failure range from 9 to 10% (that is, larger values than obtained for the tall specimens). This strain-to-failure pattern often is observed when comparisons of results are made for specimens with $H/D = 1.0$ and 2.5 (see, for example, Ref *15*). The prefailure stress–strain and volume change behaviors also indicate that the grain structure temporarily locks up for the short specimens with $\beta = 45$, 60, and 90°. Only the stress–strain curve for $\beta = 45°$ exhibits a small drop-off in stress, but the curves for β = 60 and 90° show clear evidence of the cross-anisotropic sand fabric. As in the tall specimens, the volume change curves indicate zero rates of dilation over extended ranges of axial strains before dilation is initiated at almost constant rates. Thus, the lock-up phenomenon is also present in the short specimens with the most pronounced effect for the specimen with vertical bedding planes (β = 90°). Although shear bands were not visible in the short specimens, the volume change curves do indicate several ranges of temporary diminished rates of dilation near and beyond peak failure.

It should be noted that the shape of the stress–strain curve obtained in the present study for the specimen with β = 90° (Fig. 4*b*) is quite different from that obtained in a previous study [*8*] for a similar specimen. The previous study produced a smoothly curved stress–strain relation, but the same strengths were obtained in the two studies. The reason for the different shapes of the stress–strain curves has not been identified.

Strength Characteristics

The results in Fig. 4 show that the strength of the tall specimens decreases with increasing bedding plane inclination β, whereas the short specimens exhibit very little variation in strength.

The friction angles from all the triaxial compression tests are compared in Fig. 5. The friction angles from the tests on specimens with H/D = 2.5 decrease consistently over a range of 5.5° with increasing value of β. Thus, the highest friction angle is obtained when the major principal stress, σ_1, is applied perpendicular to the bedding planes, and the lowest friction angle is obtained when σ_1 is applied parallel to the bedding planes. Similar results have been obtained in previous studies [*1–3,11–13*] in which the boundary conditions were similar to those in the specimens with H/D = 2.5.

The specimens with H/D = 1.0 show very little effect of the bedding plane inclination on the measured friction angles, although a small decrease in friction angle with increasing value of β may be detected. The results of two triaxial compression tests performed on specimens with H/D = 1.0 and with β = 0 and 90° from the previous study of dense Cambria sand [*8*] are also shown in Fig. 5. These two friction angles correspond very well with those obtained in the present study. Further, these two values are consistent with the three-

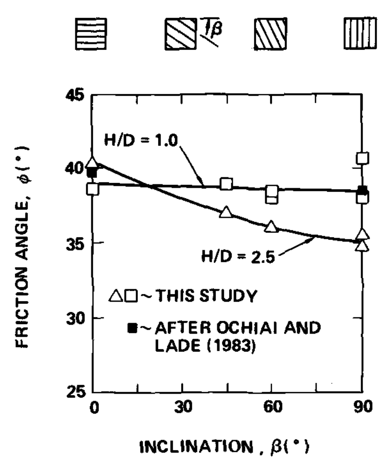

FIG. 5—*Variation of friction angles with bedding plane inclination in triaxial compression tests on Cambria sand with cross-anisotropic fabric.*

dimensional strength pattern obtained from cubical triaxial tests [8]. However, they do not fit the pattern shown in Fig. 5 for specimens with $H/D = 2.5$.

From these and previously published results of triaxial compression tests on cross-anisotropic soil it appears that the specimen boundary conditions (flexible membrane and lubricated, rigid end plates) have different effects on the results for specimens with H/D ratios of 1.0 and 2.5. The flexible membrane allows development of nonuniform deformations in the tall specimens, whereas the rigid, lubricated end plates inhibit propagation of temporarily developing nonuniform deformations within the short specimens. Thus, macroscopically uniform strains are obtained in the short specimens. Consequently, different conclusions can be reached regarding the behavior at cross-anisotropic soils depending on the boundary conditions or, nominally, the H/D ratio of the triaxial specimens.

Summary and Conclusions

The stress–strain, volume change, and strength characteristics of dense Cambria sand prepared with cross-anisotropic fabric in specimens with height-to-diameter ratios of 1.0 and 2.5 were studied in drained triaxial compression tests. The bedding planes of the cross-anisotropic specimens were inclined at different angles with the vertical, major principal stress to investigate the effects of boundary conditions in the two different specimen types.

Specimens consisting of relatively long, flat sand grains were prepared with strong preferred grain orientations in sections perpendicular to the bedding planes and almost completely random orientations in sections parallel to the bedding planes. The specimen preparation technique is reviewed, and the resulting grain structure is characterized by appropriate parameters.

The tests show that the specimen boundary conditions (flexible membrane and lubricated, rigid end plates) had different effects on the results for specimens with H/D ratios of 1.0 and 2.5. The stress–strain, volume change, and strength relationships were quite different for comparable tests, although the only nominal difference was the H/D ratios of the specimens. Notably, the specimens with $H/D = 2.5$ and with inclined or vertical bedding planes exhibited distinct, but temporary drops in their prefailure stress–strain curves, and the friction angles decreased consistently over a range of 5.5° with increasing inclination of the bedding planes. In comparison, the specimens with $H/D = 1.0$ exhibited more smooth stress–strain behavior, although definite effects of the cross-anisotropic fabric were present. The friction angles were not affected much by the bedding plane inclination.

In view of these results, different conclusions can be reached regarding the behavior of cross-anisotropic soils depending on the boundary conditions or nominally, the H/D ratio of the triaxial specimens. The most consistent results appear to be obtained from specimens with $H/D = 1.0$ in which macroscopically uniform deformations are obtained.

Acknowledgment

This study was supported by a research grant from the Academic Senate, University of California, Los Angeles, CA.

References

[1] Oda, M., "Initial Fabrics and Their Relations to Mechanical Properties of Granular Materials," *Soils and Foundations*, Vol. 12, No. 1, March 1972, pp. 17–36.

[2] Arthur, J. R. F. and Menzies, B. K., "Inherent Anisotropy in a Sand," *Geotechnique*, Vol. 22, No. 1, March 1972, pp. 115–128.

[3] Arthur, J. R. F. and Phillips, A. B., "Homogeneous and Layered Sand in Triaxial Compression," *Geotechnique*, Vol. 25, No. 4, Dec. 1975, pp. 799–815.
[4] Haruyama, M., "Anisotropic Deformation-Strength Characteristics of an Assembly of Spherical Particles under Three-Dimensional Stresses," *Soils and Foundations*, Vol. 21, No. 4, Dec. 1981, pp. 41–55.
[5] Mahmood, A. and Mitchell, J. K., "Fabric-Property Relationship in Fine Granular Materials," *Clay and Clay Minerals*, Vol. 22, No. 516, 1974, pp. 397–408.
[6] Matsuoka, H. and Ishizaki, H., "Deformation and Strength of Anisotropic Soil," in *Proceedings*, Tenth International Conference on Soil Mechanics and Foundations Engineering, Stockholm, Sweden, Vol. 1, 1981, pp. 699–702.
[7] Mitchell, J. K., Chatoian, J. M., and Carpenter, G. C., "The Influences of Sand Fabric on Liquefaction Behavior," Report No. TE76-1, College of Engineering, Office of Research Services, University of California, Berkeley, CA, June 1976.
[8] Ochiai, H. and Lade, P. V., "Three-Dimensional Behavior of Sand with Anisotropic Fabric," *Journal of Geotechnical Engineering, American Society of Civil Engineers*, Vol. 109, No. 10, Oct. 1983, pp. 1313–1328.
[9] Oda, M., "The Mechanism of Fabric Changes during Compressional Deformation of Sand," *Soils and Foundations*, Vol. 12, No. 2, June 1972, pp. 1–18.
[10] Oda, M., "Anisotropic Strength of Cohesionless Sands," *Journal of the Geotechnical Engineering Division, American Society of Civil Engineers*, Vol. 107, No. GT9, Sept. 1981, pp. 1219–1231.
[11] Oda, M. and Koishikawa, I., "Anisotropic Fabric in Sands," in *Proceedings*, Ninth International Conference on Soils Mechanics and Foundation Engineering, Tokyo, Japan, Vol. 1, 1977, pp. 235–238.
[12] Oda, M., Koishikawa, I., and Higuchi, T., "Experimental Study of Anisotropic Shear Strength of Sand by Plane Strain Test," *Soils and Foundations*, Vol. 18, No. 1, March 1978, pp. 25–38.
[13] Tatsuoka, F., Sakamoto, M., Kawamura, T., and Fukushima, S., "Strength and Deformation Characteristics of Sand in Plane Strain Compression at Extremely Low Pressures," *Soils and Foundations*, Vol. 26, No. 1, March 1986, pp. 65–84.
[14] Yamada, Y. and Ishihara, K., "Anisotropic Deformation Characteristics of Sand Under Three Dimensional Stress Conditions," *Soils and Foundations*, Vol. 19, No. 2, June 1979, pp. 79–94.
[15] Lade, P. V., "Localization Effects in Triaxial Tests on Sand," in *International Union of Theoretical and Applied Mechanics Conference on Deformation and Failure of Granular Materials*, P. A. Vermeer and H. J. Luger, Eds., A. A. Balkema, Rotterdam, The Netherlands, 1982, pp. 461–471.
[16] Mitchell, J. K., *Fundamentals of Soils Behavior*, Wiley, New York, 1976.
[17] Curry, J. R., "The Analysis of Two-Dimensional Orientation Data," *Journal of Geology*, Vol. 64, 1956, pp. 117–131.
[18] Peters, J. F., Lade, P. V., and Bro, A., "Shear Band Formation in Triaxial and Plane Strain Tests," in this volume, pp. 604–627.

Pierre La Rochelle,[1] S. Leroueil,[1] B. Trak,[1] L. Blais-Leroux,[1] and F. Tavenas[1]

Observational Approach to Membrane and Area Corrections in Triaxial Tests

REFERENCE: La Rochelle, P., Leroueil, S., Trak, B., Blais-Leroux, L., and Tavenas, F., **"Observational Approach to Membrane and Area Corrections in Triaxial Tests,"** *Advanced Triaxial Testing of Soil and Rock, ASTM STP 977,* Robert T. Donaghe, Ronald C. Chaney, and Marshall L. Silver, Eds., American Society for Testing and Materials, Philadelphia, 1988, pp. 715–731.

ABSTRACT: The corrections to account for the changes in the cross-sectional area and for the restraint of the membrane during a triaxial test may vary considerably depending on the actual behavior of the soil specimen. This paper shows how observations and measures can lead to a choice of corrections which are in good agreement with the true behavior of the soil–membrane system both for bulging failures and for failures along a shear plane. The data obtained by compression tests on rubber and rigid dummies offer a valuable basis for quantifying the required area and membrane corrections. An example illustrates the merits of the proposed corrections and shows that different interpretations of the membrane correction may have an important implication on the effective stress cohesion intercept.

KEY WORDS: triaxial test, membrane correction, cross-sectional area correction, bulging failure, shear plane failure, stress–strain curves, soft clays, cohesion intercept

The standard triaxial equipment and test procedure involve many sources of errors which often are completely ignored. In a companion paper presented in this volume, Leroueil and coworkers deal with problems of leakage through fittings, diffusion through the membrane, and permeability and strength of filter drains [*1*].

In the present paper, the problems of membrane restraint and of change in the cross-sectional area of the specimens in triaxial tests will be considered; they are two sources of error still not properly resolved. Although the currently used corrections are small or even negligible when applied to the failure stress of brittle specimens failing at small strains, they may become quite important at large strains, depending on the geometry of the failure. As geotechnical practice becomes more and more concerned with the strength measured at large strains in laboratory tests or at the critical state, more attention must be paid to the choice of adequate membrane and area corrections for the triaxial test.

The corrections that are currently applied are based on some idealized geometries of failure assumed to occur in triaxial tests: the specimens are expected to fail either along multiple shear zones resulting in a bulging deformation, or along a well-defined shear plane with sharp edges cutting into the membrane. The corresponding suggested corrections, both for the membrane and the cross-sectional area, are greatly influenced by these geometries: in the plastic bulging failure, the membrane correction is moderate and the average cross-

[1] Professor, associate professor, former graduate students, and dean, respectively, Laval University, Department of Civil Engineering, Pavillon Pouliot, Quebec, G1K 7P4 Canada.

sectional area of the specimen increases with strain; in the brittle shear plane failure, the membrane correction can be quite high and the effective cross-sectional area of the specimen is assumed to decrease [2,3]. However, in most natural soil specimens, the actual geometry at failure and at large strains usually lies between these two extreme idealized shapes. As a result, the indiscriminate use of the existing corrections may lead to significant errors.

The deformation of the specimen and the resulting interaction between the soil and the rubber membrane are so unpredictable and complex that they cannot be analyzed thoroughly. The empirical approach seems to offer the only practical means to arrive at realistic corrections. Previous studies, based on results of tests made on different types of specimens: on remolded clay samples [4], on rigid dummies [2,5,6], and on plasticine dummies with a precut lubricated shear plane [3], have generated a number of suggestions for the membrane and area corrections. However, to apply a realistic correction, the specimen must be observed during and after the test to judge the mechanism of membrane mobilization and of the changes in the cross-sectional area, and to adjust the correction to the observed behavior.

After a reevaluation of test results on dummies, it will be shown how the observation of the specimen during and after the test can lead to a better assessment of the corrections. The two different geometries of failure commonly encountered, that is, bulging and shear plane failures, will be considered separately, both for the area and for the membrane corrections.

Area Correction

Bulging Failure

When the specimen fails or deforms by bulging with no apparent shear plane, it is generally agreed that the corrected cross-sectional area a_c is given by

$$a_c = a_o \frac{1 + \Delta V/V_o}{1 - \epsilon} \tag{1}$$

where

a_o = initial cross-sectional area at the beginning of the triaxial shear test (that is, after consolidation)
$\Delta V/V_o$ = unit change of volume during shear test
ϵ = axial strain

This formula is based on the assumption that the specimen deforms as a cylinder with a constant diameter through its height (Fig. 1*a*). Because this condition is seldom met in actual soil specimens, the formula is approximate. However, other expressions considered to be more accurate [7] give a difference of only 2 to 3% relative to Eq 1 and are not necessarily based on more realistic assumptions. Equation 1 can be considered satisfactory for the case in which the specimen deforms by bulging only.

Shear Plane Failure

Area correction when a shear plane is formed across the sample is much more problematic. In theory, for example in the case of a presheared rigid dummy, the decrease in the cross-sectional area can be calculated by the expressions given in Fig. 1*b* [6]; it is a function of the movement along the shear plane and of its angle of inclination. The idealized condition corresponding to Fig. 1*b* may be met in very stiff clays and clay shales, but certainly not in softer clays. In such cases, bulging is also observed around the edge of the shear plane so

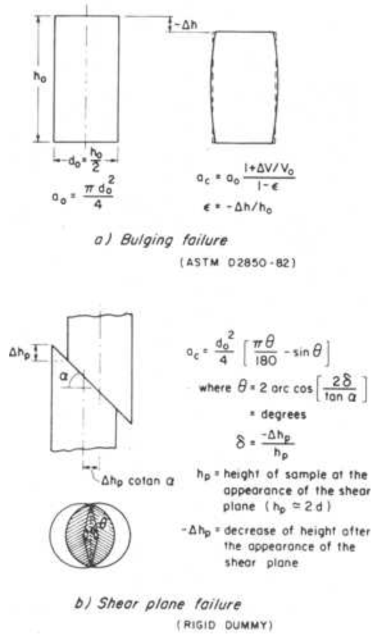

FIG. 1—*Illustration of the correction for the cross-sectional areas:* (a) *bulging failure and* (b) *shear plane failure* [6].

that there is a mixture of failure patterns which implies both a decrease of area due to the movement along the shear plane and an increase due to the localized bulging; the relative contribution of these two phenomena varies from one specimen to the other and cannot be evaluated without observing the specimen during or after the test. Figure 2*a* illustrates the typical shape of a specimen of an overconsolidated sensitive clay strained at 15% deformation in an isotropically consolidated undrained (CIU) triaxial test, viewed across the plane and at 90° rotation; the shear plane has appeared after the peak of the stress–strain curve, but the deformation at larger strain has developed both by bulging and by movement along the shear plane. In such cases, the variation of the cross-sectional area of the specimen can be estimated by the measurements given in Fig. 2*b*. To preserve the shape of the specimen when removing the top of the triaxial cell to measure, the piston should be kept fixed while the cell pressure is lowered and the cell emptied; this procedure prevents the relative movement of the two parts of the specimen following the removal of the axial load. Then the top of the cell can be removed without noticeable change in the geometry of the specimen.

The corrected cross-sectional a_c area corresponding to the contact area on the shear plane between the two parts of the specimen at the end of the test is given by the surface of the ellipse (Fig. 2*b*).

$$a_c = \frac{\pi}{4} d_a \cdot d_b \tag{2}$$

This approach is thought to give a realistic value of the effective cross-sectional area when a shear plane is formed. For the specimen illustrated in Fig. 2*a*, the corrected area at 15% strain is 11.03 cm^2 which represents a reduction of 4.0% relative to the initial cross-sectional area of 11.40 cm^2. In some tests in which the bulging around the contour of the shear plane is important, the measurement may lead to an increase of area, which is not unreasonable.

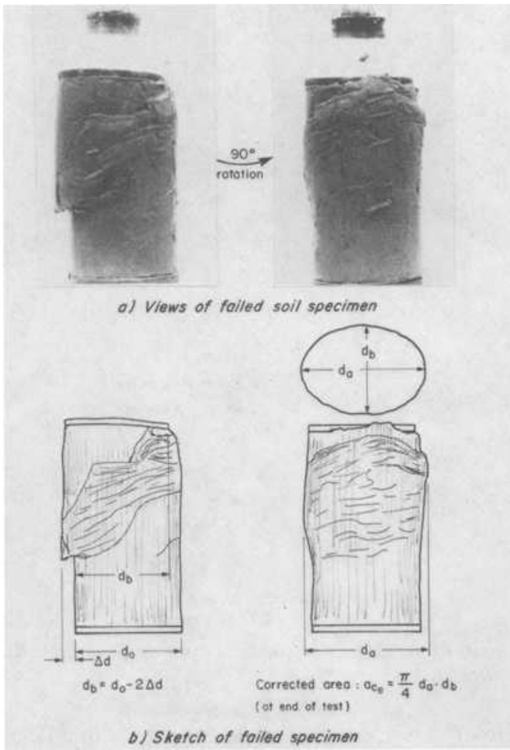

FIG. 2—*Correction of the cross-sectional area for a shear plane failure in a soil specimen.*

Hence, the authors recommend that in triaxial tests in which the specimen fails along a shear plane, the correction given by Eq 1 be applied until the shear plane forms, which is usually at the peak of the stress–strain curve although it becomes visible at a slightly larger strain; for the remainder of the test, the reduction or increase of the cross-sectional area, as measured at the end of the test according to the rules given above, should be applied proportionally with strain from the peak to the end of the test as follows:

$$a_c = a_f + (a_{ce} - a_f)\left(\frac{\epsilon - \epsilon_f}{\epsilon_e - \epsilon_f}\right) \tag{3}$$

where

a_f = cross-sectional area at peak strength
a_{ce} = cross-sectional area at end of test (Eq 2)
ϵ_e = axial strain at end of test
ϵ_f = axial strain at peak strength

Membrane Corrections

Properties of the Membranes

The contribution of the membrane to the measured strength of the triaxial specimen depends not only on its elastic properties but also on its initial diameter; both these characteristics need to be measured to apply a realistic correction.

The modulus can be measured by a simple method described by Henkel and Gilbert [*4*] or Bishop and Henkel [*8*]; the extension of a circumferential strip suspended between two glass rods covered with talc is measured for different loads. The thicker membranes used are commercially available latex rubber membranes. The measured values given in Fig. 3 indicate that the modulus increases with the thickness of the membrane, and suggest also a variation with strain. Indeed it is observed that the modulus has a maximum value at low strain and decreases with increasing strain; this variation is more important for thicker membranes and negligible in the case of the thin Ramses prophylactic membranes which have a very low modulus.

The secant modulus measured at 20% extension corresponds to the maximum strain the membrane undergoes during a test; consequently, an average modulus secant at 10% extension should be used for calculating the corrections, except for calculating the initial confining pressure at the beginning of the compression test for which the secant 1% modulus should be used, because the strain in the membrane is very small.

Initial Confining Pressure

When the membrane is placed around the specimen, it applies a lateral confining pressure which is a function of the modulus and of the initial diameters of the membrane and of the specimen. Although negligible at high cell pressures, it may become quite significant at low cell pressures on soft soils. The initial confining pressure can easily be calculated as follows:

$$p_{om} = 2\,M_i\,\frac{d_o - d_{im}}{d_o \cdot d_{im}} \tag{4}$$

where

d_o = diameter of specimen at the end of consolidation
d_{im} = initial diameter of the membrane
M_i = initial tangent modulus (1% modulus)

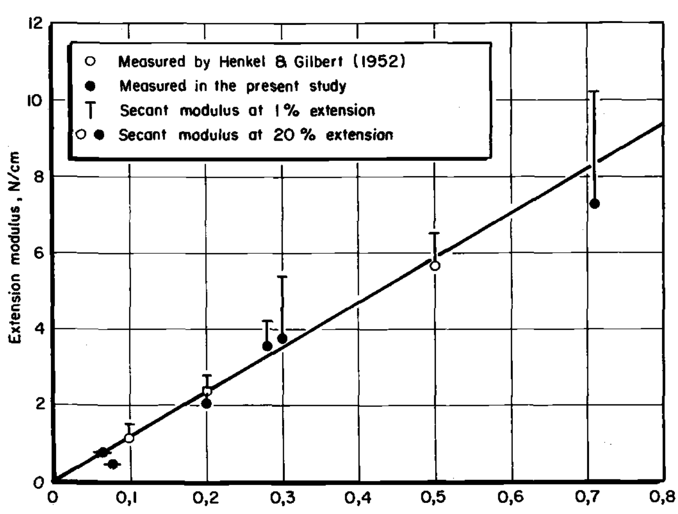

FIG. 3—*Extension moduli for membranes of different thicknesses.*

The magnitude of the confining pressure calculated by Eq 4 has been checked experimentally in the authors' laboratory by mounting membranes on solid dummies and measuring the air pressure required to infiltrate the contact between the membrane and the dummy (Fig. 4). For contact pressures larger than 1 kPa, the calculated and measured values were in fairly good agreement, but for pressures lower than 1 kPa, the measures were not meaningful.

Although a certain contact pressure between the membrane and the specimen is required for mounting and saturating the specimen, this pressure should be kept to a minimum. Therefore, a membrane of appropriate diameter and thickness must be used. The ASTM Test for Unconsolidated, Undrained Strength of Cohesive Soils in Triaxial Compression (D2850) specifies that the unstretched diameter of the membrane should be between 75 and 90% of that of the specimen and its thickness shall not exceed 1% of the diameter of the specimen. The implication of the most unfavorable conditions of this specification can be evaluated: for a specimen of 38.1 mm diameter, the thickness of the membrane could be up to 0.38 mm, which gives a secant 1% modulus of approximately 5.5 N/cm (Fig. 3). With a diameter of the membrane at 75% that of the specimen, the initial confining pressure would be p_{om} = 9.6 kPa. This pressure, which has to be added to the cell pressure, is far from being negligible for most tests on clay specimens. In terms of stress path, it has a direct influence on the cohesion intercept as will be discussed later. It is fortunate, however, that commercially available membranes are usually manufactured with diameters of 90 to 95% and with thicknesses of less than about 0.5% of the diameter of the specimen; in which case, the calculated initial confining pressure would be on the order of 1 kPa—the same value as measured on a specimen in the laboratory. When a prophylactic membrane with a modulus of 0.45 N/cm is used, the initial lateral pressure is 0.23 kPa on a 38.1-mm-diameter specimen, which is very small indeed and truly negligible in most cases.

For thicker membranes, the value of p_{om} should then be calculated and taken into account in the determination of the cell pressure applied during the test. In such a case, if no vertical load is applied by the piston on the specimen, the stress state is not isotropic.

Bulging Failure

The restraint of the membrane in a bulging type of failure was first studied by Henkel and Gilbert [4] who made a series of tests on remolded London clay with membranes of three different thicknesses. They observed that the strength contributed by the membrane is proportional to the stiffness of the membrane and is independent of the cell pressure. However, when they used only the membrane to confine the specimen (that is, with zero cell pressure) the load taken by the membrane was appreciably lower (Fig. 5). From these observations, they proposed two theories to determine the membrane correction. In the case in which the cell pressure is high enough to hold the membrane firmly against the specimen, no buckling of the membrane is likely to occur and the membrane is assumed to act as a reinforcing compression cell around the specimen; this correction, given in Eq 5 and based on the "compression theory" (Fig. 5), should be applied on the major principal stress:

$$\sigma_{1m} = \frac{\pi\, d_o\, M\epsilon}{a_c} \tag{5}$$

If the rubber membrane is not held firmly against the specimen, as in the test with zero cell pressure, it will buckle and act as a rubber belt around the lateral faces of the cylinder restraining the circumferential strain of the specimen. As in the case of the initial confining effect of the membrane, this restraint influences directly the lateral confining stresses so

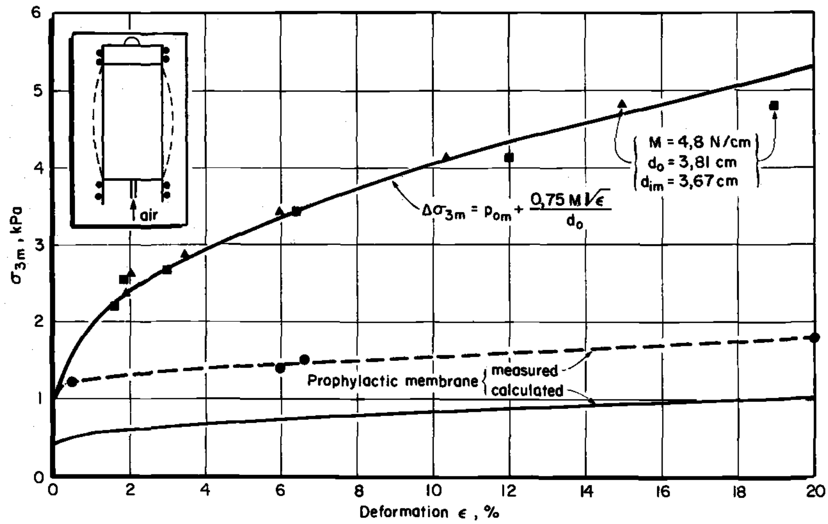

FIG. 4—*Lateral restraint of membrane determined by air inflation tests.*

that this contribution of the membrane results in an increase of the minor principal stress and should be applied accordingly, although Henkel and Gilbert recommend that it be applied as a decrease of the major principal stress [4]. The ensuing correction can be estimated by Eq 6 based on the "hoop stress theory" (Fig. 5):

$$\sigma_{3m} = \frac{2M}{d_o}(1 - \sqrt{1 - \epsilon}) \simeq \frac{M\epsilon}{d_o} \tag{6}$$

When comparing the values of correction given by Eq 5 and Eq 6 to the experimental values obtained by Henkel and Gilbert [4] (Fig. 5), it is seen that they underestimate the

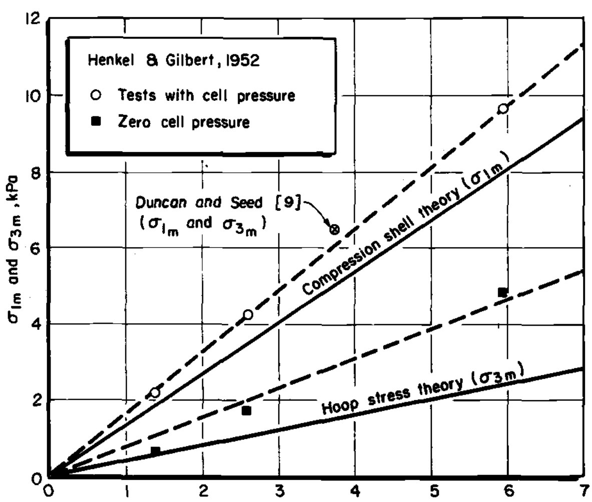

FIG. 5—*Experimental results obtained at 15% strain on specimens of remolded clay* [4].

required corrections by 17.5 and 49%, respectively. It is interesting to note, however, that if the initial confining stress of the membrane is taken into account, Eq 5 agrees fairly well with the experimental results; for example, the confining stress of a commercial membrane with an extension modulus of 4 N/cm would be on the order of 1 kPa.

This problem of rubber membrane correction in bulging failure was also studied analytically by Duncan and Seed [9] who took into account volumetric and axial strains, and proposed corrections to be applied both to the axial and lateral stresses. The value of these corrections was calculated for a membrane 0.3 mm thick (Fig. 3) having an extension modulus of 3.8 N/cm and was plotted on Fig. 5 giving Henkel and Gilbert's results. The calculated value agrees well with the experimental results of Henkel and Gilbert. The expression proposed by Duncan and Seed incorporates the influence of the confining stress of the membrane. When triaxial tests are made at low cell pressures with thin membranes, some buckling of the membrane will usually occur if the specimen fails by bulging, and the use of Eq 5, as recommended by ASTM Standard D2850, or the use of Duncan and Seed's correction [9] may grossly overestimate the correction at large strains.

Tests on Dummies

In view of the observed variation of the extension modulus with strain, the assumed linearity with strain of the corrections given by Eq 5 and Eq 6 can be questioned. To check this point, two series of tests were made on dummies. In the first series, membranes were mounted on a specimen and air pressure was used to inflate the membrane; one test was carried out with a 0.33-mm-thick membrane, and one with a prophylactic membrane with a modulus of 0.7 N/cm. The deformation of the membranes was very similar to a bulging failure of a normally consolidated or remolded clay sample. The variation of the maximum diameter of the membrane was measured at different air pressures, and the results are plotted in Fig. 4 in terms of axial strain.

The results show clearly that there is an initial contact pressure followed by a rapid increase of pressure at small strain. As the "hoop stress theory" ignores the variation of the extension modulus of the membrane with strain, and possibly some other unknown factors, some adjustments had to be made to Eq 6 to obtain a working formula to calculate the required correction. Hence, the modified formula becomes

$$\sigma_{3m} = p_{om} + 0.75 \frac{M\sqrt{\epsilon}}{d_o} \tag{7}$$

This equation, which fits the results of the test on the thick membrane (Fig. 4), was used to calculate the restraint of a Ramses prophylactic membrane on which inflating pressures were measured. Except for a small difference in the initial contact pressure, the calculated curve is the same as the experimental one. With the experimental set up used to make this test, pressures lower than 1 kPa were hardly measurable. It should also be noted that the restraint pressure of the prophylactic membrane remains below 2 kPa at more than 20% strain. The corrections calculated with Eq 7 agree very well with the experimental values obtained at 15% strain with zero cell pressures on specimens of remolded London clay [4] given in Fig. 5. For example, disregarding the initial contact pressure, p_{om}, the calculated correction for a thick membrane having an extension modulus of 5.95 N/cm is 4.6 kPa, compared to 4.8 kPa measured. The piston of the cell, which is not supported at zero cell pressure, has an equivalent weight of over 1 kPa of axial pressure on the specimen. This compensates for the initial contact pressure of the membrane, and p_{om} should not be taken into account.

To substantiate the process of rapid mobilization of the membrane strength at the beginning of the test as observed in the air-inflated membrane, a second series of tests on a rubber dummy was carried out. Unconfined tests were made on the dummy as a reference, followed by tests with membranes of different thicknesses and at cell pressures of 0 and 100 kPa. Due care was taken to repeat the tests in the same conditions. Some typical differences between the strength measured with and without membrane are plotted in Fig. 6. The following observations are made:

- At zero cell pressure, some buckling of the membrane occurred (except for thick membranes which did not buckle).
- With a cell pressure of 100 kPa, no buckling was observed in any of the membranes.

The corresponding calculated correction curves are plotted in Fig. 6 and compared with the measures on the dummy for a 0.30-mm-thick membrane. The correction corresponding to the zero cell pressure with buckling condition (Eq 7) fits very well the measured strength; however, the correction curve for the case of "no buckling" given by Eq 5 to which is added the influence of the initial restraint (Eq 4) is lower than the values measured on the dummies. Both of these calculated corrections are in good agreement with the experimental data obtained for 15% strain by Henkel and Gilbert [*4*], given in Fig. 5 and plotted in Fig. 6 for the membrane with a modulus of 4.8 N/cm.

In the "no buckling" condition, the correction proposed by Duncan and Seed [*9*] and plotted in Fig. 6 for the membrane used in the test underestimates the contribution of the membrane relative to all experimental results. However, as Duncan and Seed's analysis [*9*] is the only one considered in this paper which takes into account the volumetric strain of

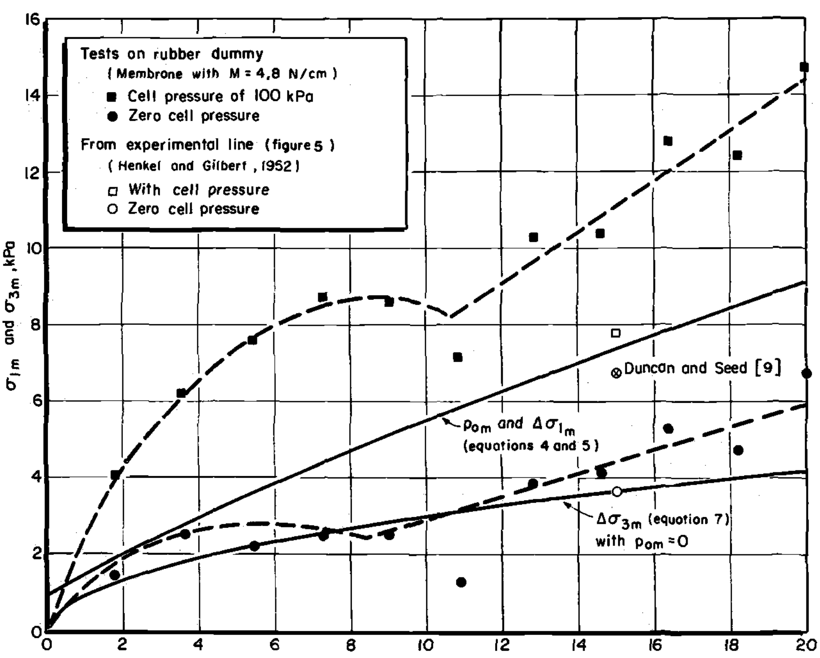

FIG. 6—*Axial load and lateral restraint of membrane determined by tests on rubber dummy.*

the soil specimen, their proposed correction should probably be preferred in the tests in which large volumetric strains occur during the shearing deformation. With thicker membranes, no buckling has been observed during the test even at zero cell pressure, and the strength taken by the membranes was also underestimated by the combined use of Eq 5 and Eq 6. The prophylactic membranes gave no measurable restraint under zero cell pressure, and a maximum strength value of the order of 4.0 kPa was obtained at 20% strain under a cell pressure of 100 kPa.

Discussion on Bulging Failure

From the observations made during the study on dummies (which confirm and add to some conclusions of previous studies on bulging failures), it has become apparent that the mechanism of mobilization of the strength of the membrane is quite different depending on whether the membrane is buckling or not. In the absence of observable buckling, the membrane acts like a compression shell and its contribution to the strength of the specimen, which translates into an increase of the axial stress σ_1 is far from being negligible. Even when the initial confining stress of the membrane is taken into account, the correction formula (Eq 5), proposed by Henkel and Gilbert [*4*] and recommended in practice (ASTM D2850), underestimates the required correction for the results obtained with the rubber dummy, especially at small strains. To simulate the correction determined by the experimental results on London clay [*4*] (Fig. 6), the correction for the initial confining stress given by Eq 4 must be added to that of Eq 5. If buckling occurs, the membrane cannot support an axial load, and its circumferential stretching contributes to increasing the lateral stress on the specimen; the contribution of the membrane in this latter case, although less important than in the previous case, is not negligible at large strains especially on soft clays and can be estimated by Eq 7. In all cases the initial confining stress of the membrane should be taken into account when calculating the cell pressure to be applied.

The important differences in the magnitude of the two corrections "with" and "without buckling" accentuate the need for careful observation of the specimen during and after the test to select the type of correction to be applied. The increased use of data acquisition and processing systems in the soils laboratories increases the danger that such important observations will be neglected.

Shear Plane Failure

The failure along a shear plane of a soil specimen in a triaxial test is the most frequently encountered mode of failure in overconsolidated clays. The movement along the plane which usually appears at the peak strength or at a slightly larger strain mobilizes rapidly the strength of the membrane, and, at large strain, the load on the membrane becomes important.

It might be worth mentioning that, at large strains, the lateral thrust on the ram during failure along an inclined shearing plane in the triaxial test can also be a source of error; it may be prevented by using either longitudinal cylindrical ball bearings to support the ram, or load cells located inside the triaxial cell provided that these cells are proven to be independent of lateral thrust, which is not the case for most commercial models available. The mobilization of the membrane in such a case is complex because it is influenced by such factors as the stiffness of the membrane and of the soil, the friction between the soil and the membrane which itself depends on the normal effective stress at the soil–membrane contact, the angle of inclination, and the overall geometry of the shear plane. The complexity is such that most authors who have studied this problem have resorted to tests on dummies; indeed this approach seems to offer the most reliable way to evaluate the contribution of the many factors involved.

Dummies are usually made of Plexiglas or softer materials such as plasticine and are precut at a chosen angle. The two main problems with dummies are the elimination of the friction on the shear plane, and the difficulty in quantitatively comparing the deformations in the dummy and in the soil specimen to make the analogy valuable. Some tentative solutions to these problems are suggested below.

Tests with Rigid Dummies

The two Plexiglas dummies used in this study were cut at two different angles of inclination of the shear plane; they are refined versions of a dummy with a steel ball bearing plane developed by La Rochelle [*2,6*], and used later by Symons [*10*]; the principle of the dummy is illustrated in Fig. 7 together with the general testing arrangement. The dummies incorporate a shear plane bearing on steel balls dropping into a cage as the movement progresses along the plane; this system allows a frictionless movement large enough to accommodate an equivalent axial strain of over 20%. Some steel balls are also placed on the top cap to allow free lateral movement of the upper part of the dummy.

To evaluate the influence of the angle of inclination of the plane in the range of the angles

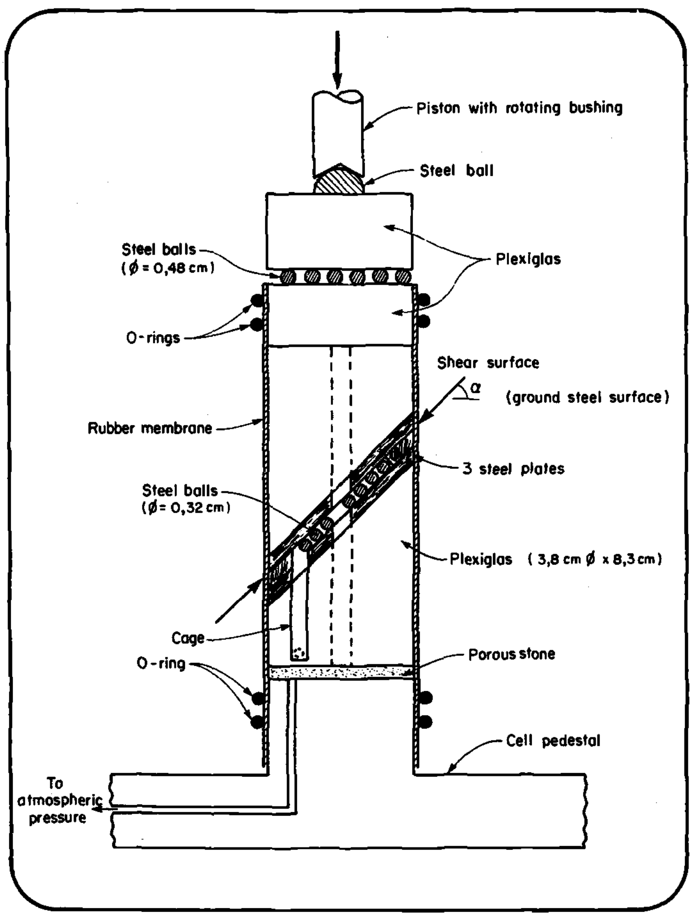

FIG. 7—*Rigid dummy with testing arrangement.*

usually observed in soil specimens, 45 and 60° angles were chosen. Tests were made with the two dummies using membranes of different thicknesses and at different cell pressures. The results of these tests are given in Figs. 8 and 9. From these experimental curves, the following observations can be made:

- There is a rapid increase of the membrane load at low strain which cannot be attributed to the friction resistance on the plane because this effect is a function of the modulus and is far smaller in the case of prophylactic membrane of low moduli.
- In all cases, the load taken by the membrane at large strain is important and needs to be taken into account.
- The effect of lateral effective stress variation is similar to the variation of the modulus of the membrane (that is, doubling the effective stress is equivalent to doubling the membrane modulus).
- The angle of inclination of the plane has a negligible influence on the load taken by the membrane.
- The load taken by the Ramses prophylactic membrane, although not negligible, is much smaller than with thicker triaxial membranes.

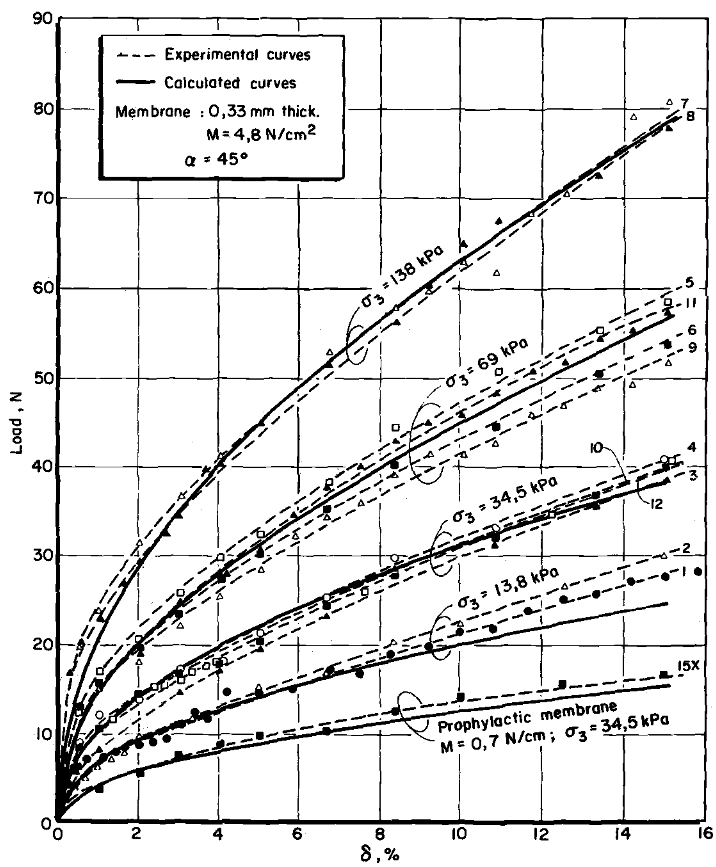

FIG. 8—*Experimental results on 45° dummy.*

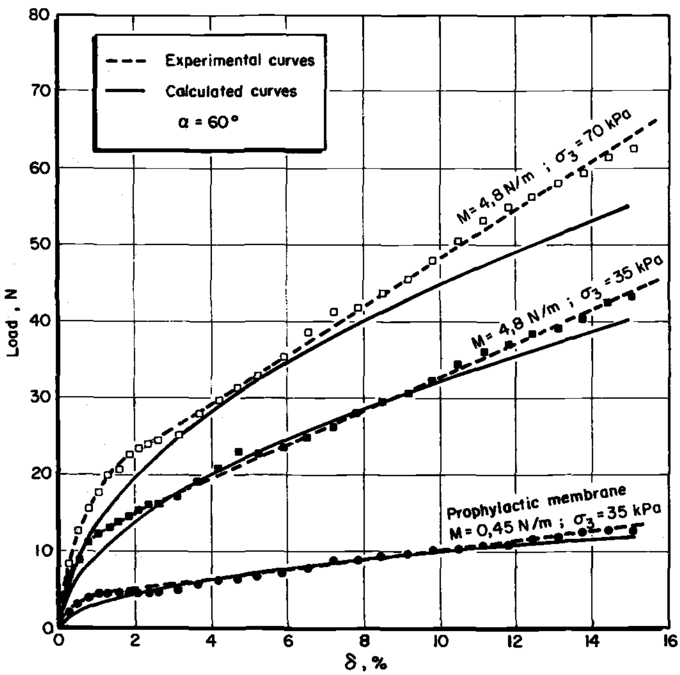

FIG. 9—*Experimental results on 60° dummy.*

Correction Formula

To transpose these experimental results to actual triaxial tests on soil specimens, it is useful to try and simulate the experiments by a simple formula taking into account the different factors involved. From La Rochelle [*6*], it can be shown that the buildup of load in a membrane as it deforms in a shear plane failure in a triaxial test can be represented by the following equation [*10*]:

$$(\sigma_1 - \sigma_3)_m \, a_c = 1.5 \, \pi \, d_o \sqrt{M f d_o \delta} \tag{8}$$

where

$(\sigma_1 - \sigma_3)_m$ = deviator stress taken by the membrane
f = unit friction between the membrane and the dummy
δ = axial strain due to the movement along the plane

As confirmed by the experimental results on the dummies, the angle of inclination α of the shear plane has a negligible effect on the membrane load.

The unit friction f between the membrane and the dummy depends on the normal pressure at the interface given by the cell pressure. For the case of a rubber membrane on Plexiglas, the unit friction was measured in a shear box and found approximately equal to half the normal pressure, which is the cell pressure in the triaxial tests on dummies.

The curves plotted on Figs. 8 and 9 show fairly good agreement between Eq 8 and the experimental results for the different testing conditions studied. Variations of cell pressure and of the extension modulus of the membrane are simulated with reasonable accuracy; hence, the above formula can be used as a tool to evaluate the correction to be applied in a triaxial test on a soil specimen.

Observation of Soil Specimens

If the soil specimens behaved like a perfectly rigid dummy, the above correction should be applied from the strain at which the shear plane forms. Because the plane usually appears immediately after the peak strength, it probably forms at the failure strain ϵ_f and the membrane correction calculated at strains $\delta = \epsilon - \epsilon_f$ due to movement along the plane should then be applied starting from the strain ϵ_f.

However, when comparing the rigid dummy deformed at 15% strain with specimens of overconsolidated soft clays at similar strains, it is obvious that the deformation of the membrane under the protruding edges of the dummy looks much more severe than in the case of the clay specimen. In soft clays, a certain amount of bulging accounts for part of the measured strain and the protruding edges of the failure plane are often partly crushed under the pressure of the membrane especially when the edge moves out near the top cap or the pedestal.

The amount of movement which occurs on the shear plane in the soil specimen governs the membrane correction and can be evaluated by observing and measuring the geometry of the specimen after the test. In Fig. 2*b*, a schematic view of a failed specimen, the distance Δd by which the edge of the plane is protruding from the lateral surface is indicative of the magnitude of movement that has occurred along the plane. This value Δd corresponds to Δh_p cotan α of Fig. 1*b*. Hence the strain due to the movement along the plane as measured at the end of the test on the soil specimen is given by

$$\delta_e = \frac{\Delta h_p}{h_o} = \frac{\Delta d \tan \alpha}{h_o} \tag{9}$$

where α and Δd are measured on the soil specimen at the end of the test. The values of δ_e measured on overconsolidated soft clay specimens at 15% strain usually lie in the range of 6 to 12%.

The strain δ to be introduced in Eq 8 to calculate the membrane correction for any strain ϵ of the soil specimen larger than ϵ_f is given by

$$\delta = \delta_e \frac{\epsilon - \epsilon_f}{\epsilon_e - \epsilon_f} \tag{10}$$

The unit friction f between the soil and the membrane (Eq 8) was measured in a shear box on samples of different clays [*6,10*]; it was found to be proportional to the effective stress normal to surface of contact, and to be related to the angle of friction of the soil ϕ' as follows

$$f = \sigma_3' \tan \phi' \tag{11}$$

where ϕ' is usually determined at large strains in isotropically consolidated undrained CIU or drained (CID) triaxial tests; a first approximation value is sufficient for the purpose of Eq 11.

Discussion

Taking into account the magnitude of the membrane loads given by the tests on dummies for shear plane failures (Figs. 8 and 9), the membrane correction may be anticipated to be excessive for soft clays. However, because the effective stress at large strain is usually small in tests on overconsolidated clays failing along a shear plane, and the cross-sectional area often decreases after peak, the combined effect of both corrections gives a final result that is quite reasonable.

An example of the effect on the stress–strain curve of the corrections in the case of a shear plane failure is given in Fig. 10. This graph presents the results of a consolidated undrained triaxial test with pore pressure measurement carried out on a sample of soft clay from the well-known site of Saint-Alban located 50 km west of Quebec city in the Saint-Laurent lowlands [*11*]. The failure occurred along a well-defined shear plane and, at 15% strain, the specimen looked similar to the specimen illustrated in Fig. 2*a*; the measured reduction of the cross-sectional area was 12.3% relative to peak condition, and the strain δ_e = 11%. The effects of the reduction in the cross-sectional area and of the membrane load partly cancel each other and the resulting combined correction at 14% strain is 10.1 kPa (that is, 27% of the measured deviator stress at large strain).

It is interesting to consider the implication of this correction on the effective stress path

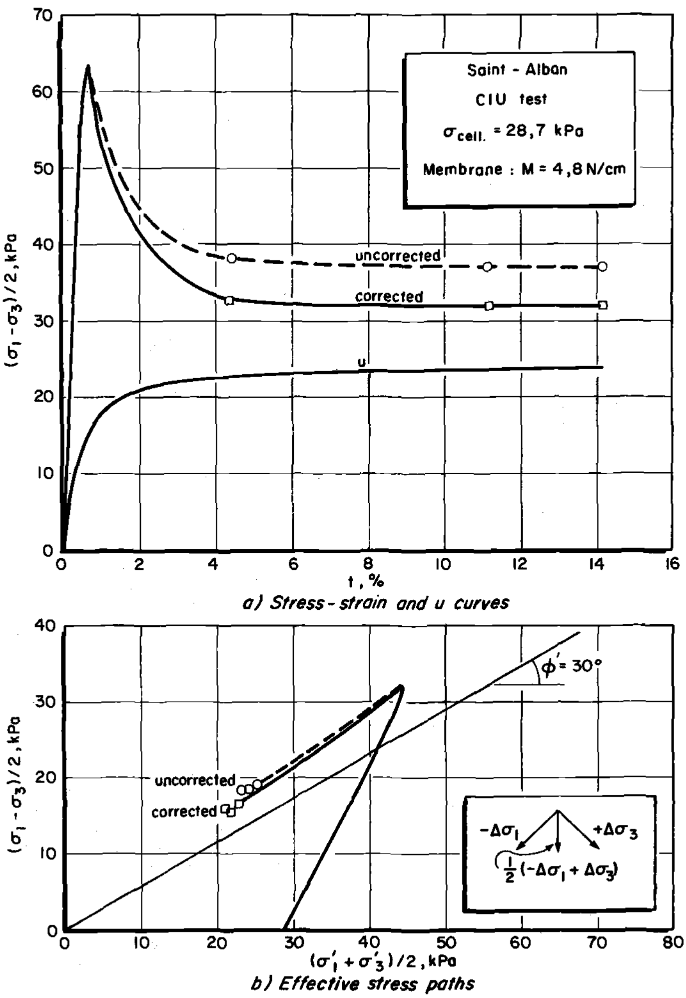

FIG. 10—*Example of the effect of the area and membrane corrections for the shear plane failure in a soft clay specimen.*

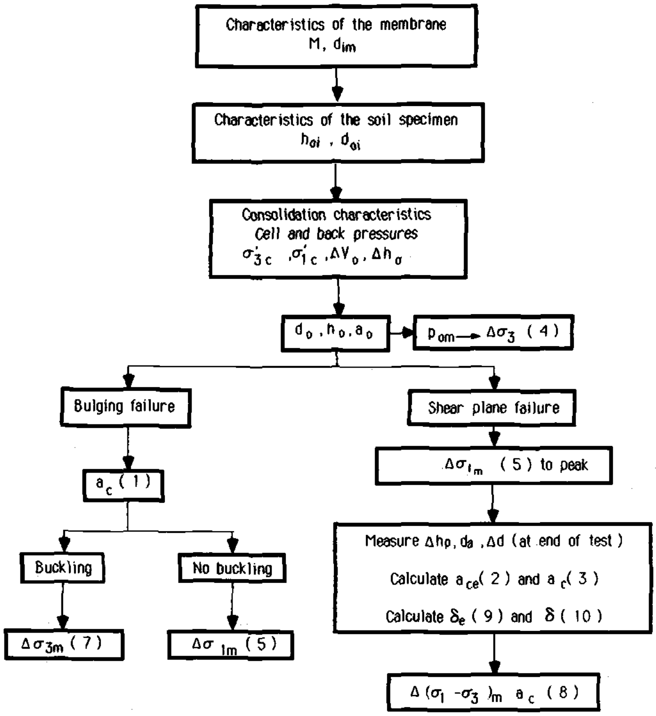

FIG. 11—*General procedure for area and membrane corrections.*

as given in Fig. 10*b*. Although the magnitude of the correction is important, when it is applied as a decrease of the major principal stress $-\Delta\sigma_1$, the correction vector at 45° is more or less parallel to the strength envelope at an angle of 30° and has a limited influence on the cohesion intercept. However, if it were applied as an increase of the minor principal stress $+\Delta\sigma_3$, it would result in an important reduction of the cohesion intercept (Fig. 10*b*). The membrane correction has traditionally been applied as a decrease of σ_1; however, when looking at the orientation of the crinklings in the membrane, it is evident that part of the membrane load is due to a circumferential strain which in the dummy results in an increase of σ_3. It is thus probable that in triaxial tests on soil specimens, the correction should be divided in equal parts on both principal stresses; this would give a vertical correction vector as indicated on Fig. 10*b*, resulting in a moderate but significant reduction of the cohesion intercept. This question remains open and needs further research.

The authors have no doubt that the corrections for the initial restraint of the membrane p_{om} and for the bulging failure with buckling of the membrane (Eq 7) should be applied as an increase of σ_3.

The calculation of the corrections suggested in this paper can be programmed according to the procedure given in Fig. 11 and requires only a minimum of observation and measurement of the soil specimen at the end of the test.

Conclusion

The observational approach presented in this paper allows the experimenter to apply a correction for the changes in the cross-sectional area of the soil specimen in the triaxial test and for the contribution of the membrane to the applied stress. Considering that both phenomena may result in major errors at large strains if they are not properly taken into account, it is worthwhile to invest a supplementary effort in the observation of the soil specimen to apply corrections which are in agreement with the true behavior. It is thought that the data and method given in this paper offer valuable guidelines leading to realistic evaluation of the membrane and area corrections for triaxial tests.

Acknowledgments

The research presented in this paper has been supported partly by grant No. A1503 from the National Science and Engineering Research Council of Canada (NSERC) and grant No. EQ-1016 from the Ministry of Education of Québec. The authors are indebted to J. P. Dussault, senior technician, who very competently carried out all the experimental work.

References

[*1*] Leroueil, S., Tavenas, F., La Rochelle, P., and Tremblay, M., "Influence of Filter Paper and Leakage on Triaxial Testing," in this volume, pp. 189–201.
[*2*] La Rochelle, P., "The Short-Term Stability of Slopes in London Clay," Ph.D. thesis, University of London, England, 1960.
[*3*] Chandler, R. J., "The Measurement of Residual Strength in Triaxial Compression," *Geotechnique*, Vol. 16, 1966, pp. 181–186.
[*4*] Henkel, D. J. and Gilbert, C. D., "The Effect of the Rubber Membrane on the Measured Triaxial Compression Strength of Clay Samples," *Geotechnique*, Vol. 3, 1952, pp. 20–29.
[*5*] De Lory, F. A., "Long-Term Stability of Slopes in Over-consolidated Clays," Ph.D. thesis, University of London, England, 1957.
[*6*] La Rochelle, P., "Membrane, Drain and Area Correction in Triaxial Test on Soil Samples Failing Along a Single Shear Plane," Third Pan-American Conference of Soil Mechanics and Foundation Engineering, Caracas, Venezuela, 1967, pp. 273–293.
[*7*] Waterway Experiment Station, "Triaxial Shear Research and Pressure Distribution Studies on Soils," Progress Report, Soil Mechanics Fact Finding Survey, Vicksburg, MS, April 1947.
[*8*] Bishop, A. W. and Henkel, D. J., *The Measurement of Soil Properties in the Triaxial Test*, Edward Arnold, London, 1957, 191 pp.
[*9*] Duncan, J. M. and Seed, H. B., "Correction for Strength Test Data," *Journal of the Soil Mechanics and Foundation Division, American Society of Civil Engineers*, Vol. 93, No. SM5, 1967, pp. 121–137.
[*10*] Symons, I. F., Discussion, in *Proceedings*, Geotechnical Conference, Oslo, Norwegian Geotechnical Institute, Vol. II, 1967, pp. 175–177.
[*11*] La Rochelle, P., Trak, B., Tavenas, F., and Roy, M., "Failure of a Test Embankment on a Sensitive Champlain Clay," *Canadian Geotechnical Journal*, Vol. 11, 1973, pp. 142–164.

Mark R. Schoenemann[1] *and Marvin R. Pyles*[1]

Stress Path Considerations in Multistage Triaxial Testing

REFERENCE: Schoenemann, M. R. and Pyles, M. R., "**Stress Path Considerations in Multistage Triaxial Testing,**" *Advanced Triaxial Testing of Soil and Rock, ASTM STP 977,* Robert T. Donaghe, Ronald C. Chaney, and Marshall L. Silver, Eds., American Society for Testing and Materials, Philadelphia, 1988, pp. 732–739.

ABSTRACT: The particular sequence of axial load and confining-stress change employed in a multistage triaxial test can dramatically influence the stress paths imposed on triaxial specimens, as can isotropic and anisotropic consolidation. The cumulative radial strain in isotropically consolidated specimens can be as much as three times greater than that in anisotropically consolidated specimens at the end of the third stage of a test. Cumulative axial strain was about equal in isotropically and anisotropically consolidated specimens, even though the isotropically consolidated specimens apparently experienced less total compressive strain by the end of a test. While increased strain did not appear to influence the results from multistage triaxial tests on relatively insensitive residual soils, the influence on tests results for more sensitive soils may be significant.

KEY WORDS: soil test, triaxial test, isotropic consolidation, anisotropic consolidation, stress path, multistage triaxial test

Multistage triaxial (MST) testing permits determination of a Mohr strength envelope by testing a single soil specimen in a series of consolidation and shearing stages. In appropriate soils, the technique allows the determination of strength parameters from many fewer specimens than does conventional triaxial (CT) testing, which requires three or more specimens to determine one Mohr envelope. Additionally, use of MST testing may allow a more accurate representation of the spatial variability of soil strength, because all between-sample variation can be fully reflected, rather than partially hidden by deducing strength envelopes from separate CT tests [*1,2*].

Although MST testing is approximately 35 years old, several MST procedures have not been standardized and, in fact, have not always been well documented. In particular, the sequence of events taking place between test stages is often poorly reported. Establishment of a rigidly standardized procedure for MST tests would probably be unwise, because one of the virtues of triaxial testing is the ease of adjusting the test procedure to match or simulate special conditions. However, certain portions of CT test procedure are rather standardized. For example, when elevated back pressures are used to saturate the specimen, the back pressure commonly is raised in increments no larger than the effective confining pressure under which the specimen is to be consolidated [*3*]; ample time is allowed between increments for equilibration. This procedure is followed to avoid producing an artificially overconsolidated specimen.

[1] Doctoral candidate and associate professor, respectively, Department of Forest Engineering, College of Forestry, Oregon State University, Corvallis, OR 97331.

Certain MST testing procedures also may affect test results. Different researchers have employed a variety of techniques during MST tests, and no standard procedure exists for controlling stresses between shearing stages. The effects of test procedure on the states of stress imposed on the specimen have not been discussed fully in the literature. Of particular concern here is the effect on the test specimen of the handling of the deviator stress of a given stage before the consolidation phase of the next stage. For example, in their pioneering work, Taylor [*4*] and Fleming [*5*] conducted MST tests on partially saturated soils of low plasticity, carrying each specimen to failure three or four times under progressively larger confining pressures. In both works, the data suggest that each ending deviator stress was maintained during the subsequent consolidation phase, but the exact procedures were not stated.

Kenney and Watson compared the results of MST tests with those of conventional single-stage tests [*6*]. They removed the deviator stress and allowed specimen pore pressures to equalize before the beginning of the next consolidation phase.

In their MST testing of lightly overconsolidated clays, Parry and Nadarajah removed the deviator stress after the end of each shearing phase, before the consolidation phase of the next stage [*7*]. Most specimens were consolidated isotropically, but some were consolidated anisotropically, with a small σ_1'/σ_3' ratio of 1.08. Parry also removed the deviator stress between stages [*8*]. In Parry's earlier work, it appeared that the deviator stress at the end of each shearing stage was maintained through the subsequent consolidation stage, but the procedure followed was not given [*9*].

Stress States Imposed by Test Procedures

During research to characterize the strength behavior of relatively undisturbed residual soils at low confining stresses, the authors have made several potentially valuable observations [*2*].

An extensive series of MST tests was conducted on relatively undisturbed samples of residual/colluvial soils developed from marine basalt. Samples were obtained by hand advance of a thin-walled sampling tube aided by hand excavation and trimming just ahead of the cutting edge. Soil profiles sampled were shallow [<1.5 m (5 ft) to weathered bedrock]. Unified classifications (ASTM D2487) ranged from silty sand (SM) to silt of medium to high plasticity (MH), with most falling into the MH class. Plasticity indexes ranged from 6 to 23. Consolidation specimens exhibited apparent preconsolidation stresses of 100 to 200 kPa. These values are quite reasonable, considering the desiccation to which the profiles are subjected during most summers. Because the overburden stresses in these shallow profiles are small, overconsolidation ratios computed for the specimens ranged from 15 to 30, abnormally high compared to the ratios encountered in typical engineering practice.

All triaxial tests were consolidated undrained (CU) tests, with pore pressures measured by a Validyne DP15 electronic pressure transducer. This differential pressure transducer was arranged to measure the effective confining stress (σ_3') directly. Test specimens were 7.1 cm (2.8 in.) in diameter and at least 14.2 cm (5.6 in.) long. Confining stress was delivered by a special pressure-regulator network which allowed accurate testing at stresses as low as 5.5 kPa (0.8 psi). All test specimens were saturated by back pressure [*3*]; pressures of 275 to 450 kPa (40 to 65 psi) were required to obtain *B* values between 0.96 and 0.98 for the 15 specimens tested. Axial strain rates were about 0.04% per minute.

In general, maximum principal stress ratio and maximum principal stress difference yield inconsistent effective stress failure points in CU tests, depending on where the effective confining stress falls in relation to the apparent preconsolidation stress [*6*]. To determine consistent failure points in this study, failure was determined for each shearing phase by the stress-path method [10]. Failure was most difficult to judge during first-stage shear, because a stress-path failure line (K_f line, or tangent) had not been established yet. First-stage shear generally was stopped when the stress path appeared to have established a tangent. During subsequent shearing phases, shear was stopped when the stress path appeared to have reached an envelope consistent with the first-stage tangent. In general, these stress-paths either displayed a marked direction change at these points or terminated (Fig. 1).

Axial load was measured by a special, "diaphragm-type" strain-gage load cell mounted on the lower end of the loading ram, inside the triaxial chamber. This equipment eliminated loading-ram friction effects from the load measurement, and load on the specimen could be determined at any time during a test.

Initial testing followed the procedures given by Kenney and Watson [6]. At the end of first-stage shear, the deviator stress was removed entirely, while the total confining stress was maintained and the drainage line was kept closed. Time was allowed for the specimen pore pressures to equalize, although, in the soils tested, measured pore pressure response coincided with deviator stress removal and no further change was noted. The next consolidation (total) stress was then imposed on the specimen and the drainage line was opened. Following consolidation, the sample was sheared undrained. This entire process was repeated until the specimen had been sheared three or four times.

The complete stress paths observed during these tests (Fig. 1) caused some concern. At each stage, removal of the deviator stress generated a substantial positive excess pore pressure; the pressure drove the effective confining stress to values considerably smaller than those exerted on the specimen at any time during the preceding consolidation and shear. Such behavior was also strikingly evident in the data presented by Kenney and Watson [6]. During the removal of deviator stress, the specimens also experienced considerable axial rebound, such that each subsequent shear phase began at a strain 1 to 3% less than the ending strain of the previous stage (Fig. 2). Because of this, the total strain experienced by the specimen in all shearing stages was several percent more (absolute values) than that implied by the strain value at the end of the last stage. The extra work performed on the specimen during this additional strain may be significant when testing certain soils.

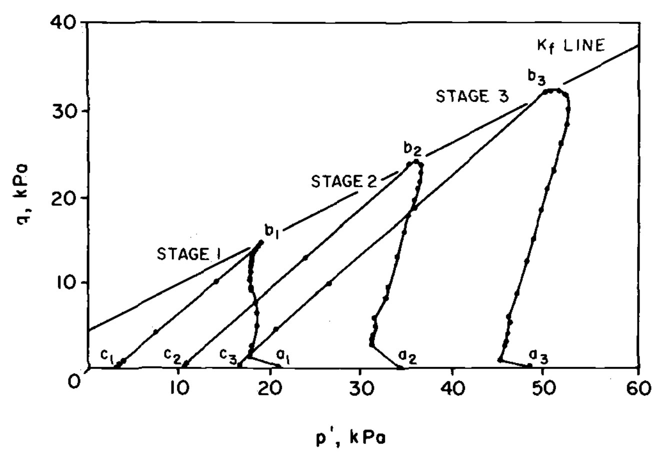

FIG. 1—*Typical stress paths for an ICU multiple-stage triaxial test.* a_nb_n *denotes stress path during undrained shear;* b_nc_n *denotes stress path on removal of deviator stress;* c_na_{n+1} *denotes stress path during consolidation between stages.* $p' = (\sigma_1' + \sigma_3')/2$, $q' = (\sigma_1' - \sigma_3')/2$, *where* σ_1' = *effective major principal stress and* σ_3' = *effective minor principal stress.*

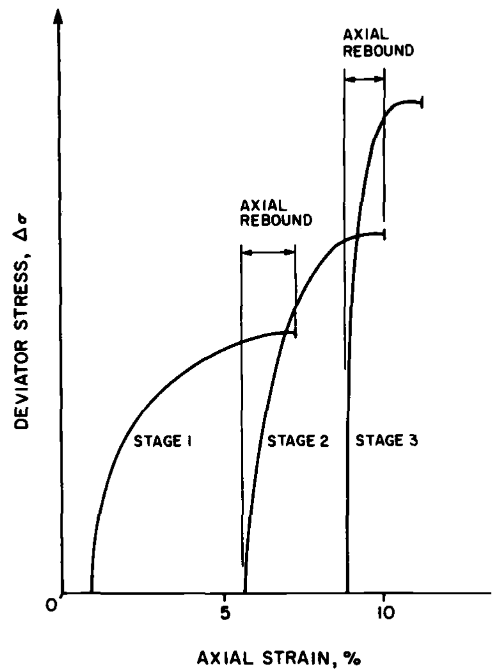

FIG. 2—*Typical stress–strain behavior in an ICU test.* $\Delta\sigma = \sigma_1' - \sigma_3'$.

Because deviator stress removal and axial rebound occurred while the specimen drainage line was closed, it follows that the rebound was accompanied by substantial radial compression. The cyclic nature of the stresses imposed by the procedure is well illustrated by the example shown in Fig. 1. Over the course of a multistage test on a specimen, the stress paths typically describe broad loops. It was felt that eliminating axial rebound and "hidden" excess axial strain and reducing the size of the stress path loops described by an MST specimen would be desirable. These objectives could be accomplished by maintaining the axial stress at the conclusion of a shearing phase throughout the following consolidation phase.

Because stress relaxation could cause significant decay of the axial stress in a stationary, strain-controlled loading frame, a stress-controlled frame was required during the consolidation phase. With such a frame, anisotropic consolidation seemed a logical procedure for these tests (that is, anisotropically consolidated undrained—ACU).

Modified Test Procedure

Accordingly, the remaining specimens (ACU specimens) were tested using the following procedural modifications.

1. All consolidation was under anisotropic conditions. For most specimens, consolidation to an effective principal stress ratio $(\sigma_1'/\sigma_3')_c$ of 3.0 approximated the presumed in situ stress field, and also yielded zero radial strain during consolidation.
2. At the end of each consolidation phase, the loading ram was locked in place, and the triaxial assembly was removed from the consolidation loading frame and placed in the shear loading frame. The loading platen was advanced by hand until solid contact was achieved between loading ram and load frame. The loading ram was unlocked and strain-controlled

shearing began. Some stress relaxation occurred in all specimens during the short period (<5 min) when the loading ram was locked in place.

3. At the end of any shearing phase that was to be followed by further consolidation, the loading ram was locked in place, and the triaxial assembly was removed from the shear loading frame and placed in the consolidation loading frame. Hanging weights were placed to deliver an axial load such that axial stress would equal the peak axial stress attained during the immediately preceding shearing phase, and the axial and radial stresses would be in the desired ratio. Chamber pressure was then increased to deliver the necessary radial stress. Consolidation began with the simultaneous opening of the drainage valve and unlocking of the loading ram. Some stress relaxation occurred in all specimens during the period (<15 min) when the loading ram was locked in place.

These procedural modifications reduced the magnitude of the loops in the stress paths over the course of each test (Fig. 3). More importantly, axial extension was prevented, and total strain experienced by the specimen equaled the ending strain value.

A more striking display of the differences in strain behavior of the two groups of specimens is provided by Figs. 4 and 5, which depict both the axial and the radial strain experienced by one typical specimen from each group. The stress-maintenance group (ACU) displayed a relatively uniform and constant trend of compressive axial strain and radial extension strain (Fig. 4). In contrast, the stress-removal specimens (that is, isotropically consolidated undrained—ICU) show a complicated pattern of strain behavior resulting from the various phases of the multistage test (Fig. 4). The ICU example displays a rather modest final axial strain value. However, when the absolute values of all strains are used, a more complete picture of this strain behavior emerges (Fig. 5). The rationale for this approach is that strain of any kind, either compressive or extensive, may cause structural changes affecting strength. Considerable axial strain is evident during the rebound of the ICU specimens, strain which is not reflected in the final strain value. The difference in cumulative radial strain experienced by the two groups of specimens is even more striking. The typical ICU specimen experienced three times the radial strain of the typical ACU specimen.

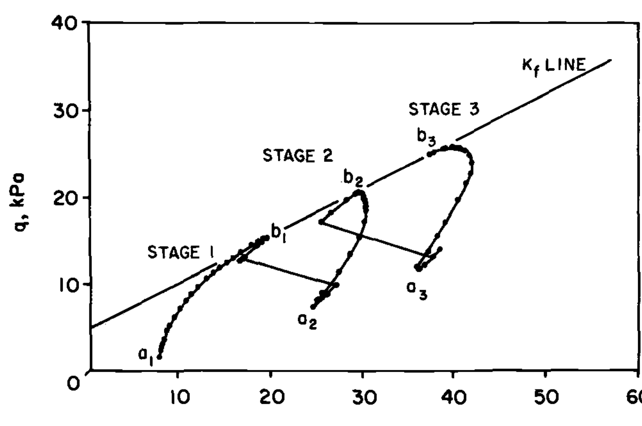

FIG. 3—*Typical stress paths for an ACU multiple-stage triaxial test. Consolidation stress ratio of 2:1 used for this specimen more clearly displays stress path patterns common to entire group of ACU specimens, most of which were consolidated at a 3:1 ratio.* a_nb_n *denotes stress path during undrained shear;* b_na_{n+1} *denotes stress path between end of stage* n *and beginning of shear for stage* n + *1 including anisotropic consolidation.* $p' = (\sigma_1' + \sigma_3')/2$, $q' = (\sigma_1' - \sigma_3')/2$, *where* σ_1' = *effective major principal stress and* σ_3' = *effective minor principal stress.*

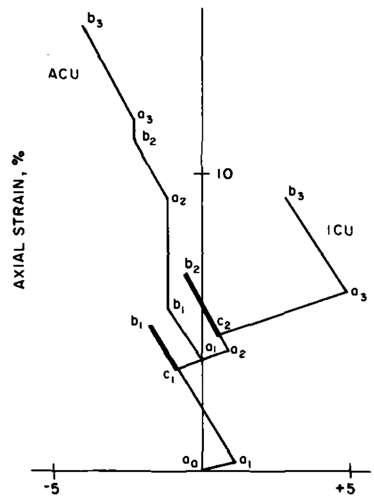

FIG. 4—*Idealized plot of axial strain versus radial strain for ICU and ACU multiple-stage triaxial tests.* a_nb_n *denotes strain path during undrained shearing;* b_na_{n+1} *denotes strain path between stages of ACU test;* b_nc_n *denotes strain path on removal of the deviator stress in the ICU test;* c_na_{n+1} *denotes strain path during consolidation between stages in the ICU test.*

Significance of Changes in Test Procedure

The average values of slope angle (α) and intercept (a) of the K_f lines from the stress-removal (ICU) and the stress-maintenance (ACU) group of tests (Table 1) are not significantly different at the 90% confidence level. We thus conclude that, for these soils, the procedures provide equivalent results.

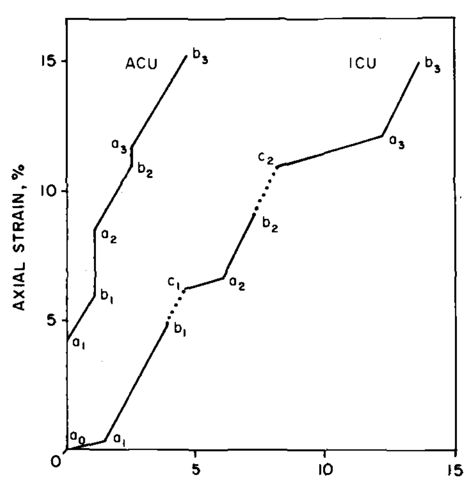

FIG. 5—*Cumulative absolute axial strain versus cumulative absolute radial strain for ICU and ACU multiple-stage triaxial tests.* a_nb_n *denotes strain path during undrained shearing;* b_na_{n+1} *denotes strain path between stages of ACU tests;* b_nc_n (····) *denotes strain path on removal of the deviator stress in the ICU test;* c_na_{n+1} *denotes strain path during consolidation between stages in the ICU test.*

TABLE 1—*Average values of parameters from* K_f *lines.*

Test type	n^a	α,[b] degrees	a,[b] kPa
ICU	3	28.6	5.48
ACU	12	30.0	4.70

[a] n = number of specimens.
[b] Transformation equations: $\sin \sigma' = \tan \alpha$

$$c' = \frac{a}{\cos \sigma'}$$

We speculate, however, that this equivalence does not extend to all soils. Sensitive clay soils probably would be less tolerant of the stress-removal procedure, with its attendant stress path loops, shear-generated excess pore pressures during axial rebound, and wide cyclic fluctuations in stress ratio. Indeed, use of this procedure may be responsible for the reputed unsuitability of MST testing for many sensitive soils. Parry [9] and Taylor [4] indicated that MST testing may not be suitable for testing sensitive clays but offered no data or particulars. Strength parameters derived from consolidated undrained MST tests on soils with sensitivities of 10 and 20 agreed closely with the results of consolidated undrained CT tests [6]. In consolidated drained (CD) testing, however, the large volumetric and axial strains experienced by these soils precluded MST testing. Kenney and Watson [6] concluded that CU MST testing was appropriate on these sensitive soils; however, in CD testing, ϕ' and c' could not reliably be mobilized completely at axial strains small enough to permit MST testing within reasonable limits of total strain.

Hard, brittle, desiccated soils may also be unsuitable for MST testing, although Parry's data indicate that many such soils may be candidates for MST testing [9]. However, his generally good results came from tests in which the deviator stress apparently was maintained between stages. Few other workers have commented on the suitability of such soils. Such soils probably would be more amenable to MST testing if they were not subjected to large cyclic variations in stress.

The details of testing procedures reviewed here appear to have major effects on the stress states imposed on MST test specimens. Until the importance of these effects is demonstrated, these details should not be ignored during MST testing.

Acknowledgments

This is Paper FRL-2122 of the Forest Research Laboratory, Oregon State University, Corvallis, OR 97331. Mention of a trademark or commercial product does not constitute endorsement by Oregon State University.

References

[1] Handy, R. L., in *Proceedings*, Conference on In-Situ Measurement of Soil Properties, Raleigh, NC, American Society of Civil Engineers, Vol. 2, June 1975, pp. 143–149.

[2] Schoenemann, M. R. and Pyles, M. R., in *Proceedings*, Symposium on Effects of Forest Land Use on Erosion and Slope Stability, Honolulu, Hawaii, International Union of Forestry Research Organizations, May 1984, pp. 73–82.

[3] Lowe, J. and Johnson, T. C., in *Proceedings*, Research Conference on Shear Strength of Cohesive Soils, Boulder, CO, American Society of Civil Engineers, June 1960, pp. 819–836.

[4] Taylor, D. W., *Triaxial Testing of Soils and Bituminous Mixtures, ASTM STP 106*, American Society for Testing and Materials, Philadelphia, 1950, pp. 180–191.

[5] Fleming, H. D., in *Proceedings*, First Australia-New Zealand Conference on Soil Mechanics and Foundation Engineering, Melbourne, Victoria, Australia, June 1952, pp. 112–122.
[6] Kenney, T. C. and Watson, G. H., in *Proceedings*, Fifth International Conference on Soil Mechanics and Foundation Engineering, Paris, France, Vol. 1, July 1961, pp. 191–195.
[7] Parry, R. H. G. and Nadarajah, V., *Journal of Testing and Evaluation*, Vol. 1, No. 5, 1973, pp. 374–381.
[8] Parry, R. H. G., *Geotechnique*, Vol. 18, 1968, pp. 151–171.
[9] Parry, R. H. G., in *Proceedings*, Fourth Australia-New Zealand Conference on Soil Mechanics and Foundation Engineering, Adelaide, South Australia, Aug. 1963, pp. 61–68.
[10] Lambe, T. W., *Journal of Soil Mechanics and Foundation Division, American Society of Civil Engineers*, Vol. 93 (SM6), 1967, pp. 309–330.

New Test Varieties

J. R. F. Arthur[1]

STATE-OF-THE-ART PAPER

Cubical Devices: Versatility and Constraints

REFERENCE: Arthur, J. R. F., **"Cubical Devices: Versatility and Constraints,"** *Advanced Triaxial Testing of Soil and Rock, ASTM STP 977*, Robert T. Donaghe, Ronald C. Chaney, and Marshall L. Silver, Eds., American Society for Testing and Materials, Philadelphia, 1988, pp. 743–765.

ABSTRACT: The main types of cubical shear devices are described and classified according to the applied boundary conditions. There is no attempt to include all or even a large selection of individual designs; examples are used to develop a critical review of the types used presently and the way in which these are evaluated. The need to consider the material and specimen to be tested when deciding on the appropriate shear device is emphasized. The chosen examples amply illustrate the wide range of uses of the devices; special attention is given to the application of controlled rotation of principal stress directions. The capability of cubical devices to accept undisturbed samples after straightforward trimming is seen as enough to ensure future developments. A major theme is constraint unintentionally imposed through the boundaries; recognition, assessment, and reduction or elimination of boundary constraint are extensively considered. Classification of stress–strain data as true, comparative, or corrected is advocated as a means of ensuring proper data quality. An example is given from current work at the author's laboratory.

KEY WORDS: apparatus, evaluation, boundary–material interactions, stress–strain, strength, principal stress rotation

Testing cubical specimens in advanced shear apparatus became fashionable in the 1960s. General models of failure and stress–strain behavior required the independent variation of the principal stresses, and the cube was the obvious shape to use. The impetus came from research workers rather than geotechnical engineers and perhaps from theoreticians rather than experimentalists.

The cubical shape is deceptively simple; the underlying difficulty is in eliminating or controlling unwanted sample–boundary interactions. If either of these aims can be achieved, the shape of the specimen has potential for practical geotechnical engineers because trimming undisturbed cores is straightforward. Versatility is another advantage: effectively uniform shear stresses as well as the expected normal stresses can be applied to the cube faces.

The aim of this paper is to discuss and evaluate apparatus and experiment design choices. No attempt will be made to review existing apparatus, instead examples based on work done in the author's laboratory at University College London will illustrate this theme. Six largely different cubical apparatus have been in use in the author's laboratory over varying periods since 1969, all of which employed flexible boundaries. Devices with all rigid, and mixed rigid and flexible, boundaries will be evaluated to complete the picture.

It may not be sufficiently appreciated that shear apparatus performance cannot be evaluated without considering the material being tested. Stiff brittle materials, which reach an

[1] Professor of soil mechanics, Department of Civil Engineering, University College, Gower Street, London, England WC1E 6BT.

unstable state in which bifurcation occurs after a strain-hardening phase, are by far the most sensitive to apparatus imperfections. Dense sand is a good example and will be the specimen material in most subsequent illustrations.

The need to consider changes in stress level and principal stress directions will be given some prominence because these are topical issues for engineers.

Boundary and Specimen Material Interaction

The fixed geometry ensures that imperfections in the applied boundary conditions, as opposed to the intended ideal boundary conditions, will affect the behavior of the specimen and may easily produce misleading stress–strain and strength data. This may be a disadvantage in comparison with the hollow cylinder in which geometric proportions can and should be carefully chosen to minimize undersirable nonuniformities [*1*]. The designer of a cubical device must pay exceptional attention to the parts that impose the boundary conditions. A suitable extensive series of experiments must be done to prove the performance of the new device. Ways of proving performance will be outlined later.

Early work by Rowe and Barden [*2*], Bishop and Green [*3*], and Kirkpatrick and Belshaw [*4*] clearly indicated the importance of eliminating surface friction at a boundary that was intended only to apply a normal stress to the specimen face. Lubricated end platens are widely employed in axisymmetric and cubical apparatus as a result of their work.

Boundary and specimen material interaction is not limited to surface friction effects. Recent two-dimensional disk models and similar computer models have demonstrated that in granular materials contact forces are usually concentrated in strong force paths [*5–7*]. This indicates the probability of very irregular load distributions across boundary to specimen interfaces, and even poses questions about the limits of the concept of stress in granular materials. It is possible, but perhaps not productive, to question the relevance of the application of uniform boundary stress on these grounds. At a somewhat larger scale, engineers are well aware of the stress-arching effects that occur in soils. We must not suppose that these complex phenomena will be absent from cubical shear specimens which are usually thought of as behaving as homogeneous elements subjected to uniform stresses.

Specimen Homogeneity

In granular materials, the ideal of homogeneity cannot be achieved at the scale of individual particles. The uncertainty of the scale at which homogeneity can be achieved poses an interesting challenge for the experimenter, perhaps especially if he or she wishes to use a cubical apparatus. Geotechnical engineers have long been aware of the problems posed by inhomogeneity of undisturbed specimens of natural soils; for example, fissures in overconsolidated clays have received considerable attention [*8*]. Choice of specimen size is rarely discussed; in reality, evidence is needed to establish that the chosen size is suitable.

Uses of Cubical Shear Device Data

Considering the uses to which cubical shear device data might be put will demonstrate the versatility of these devices. All are related to understanding material behavior under generalized stresses.

First, it must be possible to vary the principal stresses independently; the cubical shape is extremely practical for this. Varying the directions of the principal stresses is more difficult, but this has been achieved without restriction for the major and minor principal stresses, provided these remain in one plane.

Shear strength measurement is a common use which appears easy but may in fact be difficult because boundary constraints can seriously inflate the measurement. There are interests in both strain-hardening and strain-softening deformation; studying strain softening in which rupture layers have formed may be difficult although there are examples [*9*]. Frequently it may be better to use a ring shear apparatus in which the position and orientation of the rupture layer are set. Otherwise studying bifurcation and the formation of rupture layers requires x-rays for "whole specimen" data; photogrammetry using boundary plane strain measurements may be an attractive alternative [*10*] provided that boundary–surface interaction does not affect the observation of rupture layer formation. When geotechnical engineers test undrained, constant-volume specimens with no pore fluid flow in or out of the specimen, special treatment may be necessary if the boundary stresses are applied through flexible boundaries [*11,12*]. There are no difficulties for the corresponding drained tests in which volume change is allowed. Extremes of stress level are of interest to geotechnical engineers and will require special consideration. In view of this great range of potential uses it is good that there are alternative methods for stressing the surfaces of cubical specimens.

Alternative Perfect Surface Conditions

Two idealized alternative boundary faces can be used for cubical specimens—rigid and flexible. The former can impose uniform boundary displacement and, simultaneously, sustain stress concentrations which may go undetected unless the surface is made up of pressure or stress cells. The imposition of boundary displacement is often called "strain control"—a misnomer because there must be perfectly applied stresses and a homogeneous strain-hardening specimen before it is possible to assume uniformity and compute strain [*13*]. This error flawed the conventional triaxial cell measurements of modulus for many years and discredited the method with geotechnical engineers. Very sensitive sensors which avoid end platen effects have now been developed [*14*].

Perfectly flexible boundary surfaces (usually pressurized rubber membranes) apply uniform boundary stresses to the specimen surfaces so that the claim of stress control is sustainable provided there is high flexibility in the membranes and the specimen is sufficiently homogeneous. Boundary stress concentrations are eliminated even if such concentrations are a normal aspect of granular soil behavior.

Cubical specimens can be stressed, of course, through a mixture of rigid and flexible boundaries, and probably the majority of existing devices fall into this category (see, for example, Refs *15* and *16*). There are certain design simplifications to be gained and there is a wealth of inventive ingenuity to be tapped in previous generations of work on conventional cell systems.

Table 1 takes these three categories of applied boundary conditions and examines the resulting capabilities of the devices together with appropriateness for specified specimen characteristics such as degree of homogeneity and intended study application. A similar classification was used by Mould and Sture in 1979 [*17*]. This table assumes that for certain study aims the determination of strain distributions by radiography will be standard practice; the symbol R in Table 1 denotes this assumption. Frequently, it will be difficult or impossible to use radiography for rigid boundary true triaxial apparatus because of the radiation absorption of the boundary platens and mechanisms. This difficulty does not arise in apparatus with some flexible boundaries or those shearing in plane strain.

Table 1 is a largely self-explanatory summary of points already made in the text, but some of the rows under the heading "Study Applications" need further explanation here. Principal stress rotation is the first of these. Two types of these rotations can be achieved in the true triaxial and plane strain devices—orthogonal jump and axisymmetric. In the first, a shear

TABLE 1—*Capabilities of cubical sample apparatus.*

Cubical Sample Apparatus		Boundary Surfaces Condition	All Rigid	All Flexible	Mixed Surfaces
Boundary control capabilities	Stress	Average normal stress	Yes	Yes	Yes
		Average shear stress	Yes	Yes	Yes
		Uniform normal stress	Restricted	Yes	Yes/no according to surfaces concerned
		Uniform shear stress	No	Yes	
	Deformation	Uniform boundary displacement	Yes	Restricted	
		Uniform sample strain	Cannot be assumed	Cannot be assumed	Cannot be assumed
Study applications	Material type	Homogeneous strain hardening	Yes	Yes	Yes
		Homogeneous strain hardening (→softening)	Yes	Yes	Yes
		Inhomogeneous sample or material	Restricted R[a]	Yes R	Restricted R
	Stress–strain behavior	Drained or undrained shear	Either	Either	Either
		Independent variation of principal stresses	Yes	Yes	Yes
		Principal stress direction rotation	Very restricted	Planar restriction only	According to surface
		Post peak strain (after rupture layer formed)	Restricted R	Restricted R	Restricted R
		Exceptional stress levels High	Yes	Yes	Yes
		Exceptional stress levels Low	Difficult	Yes	Difficult
	Failure	Shear strength measurement	R Yes	R Yes	R Yes
		Rupture layer formation (bifurcation phenomena)	Restricted R	Yes R	Yes R

[a] R = Radiography needed.

stress is applied with fixed directions, $\sigma_1 > \sigma_2 \geq \sigma_3$, and then removed so that $\sigma_1' = \sigma_2' = \sigma_3'$ (or $\sigma_1' = \sigma_3'$ in plane strain devices). Then shear stress is reimposed with different fixed directions (stage 1: $\sigma_1' = \sigma_x'$, for example, and stage 2: $\sigma_1' = \sigma_y'$). In the axisymmetric type, while shear is imposed with fixed directions, σ_2' is increased until $\sigma_1' = \sigma_2'$ and the subsequent stress increment makes the former intermediate principal stress the major. Rigid boundary devices are restricted to these rotations only. Flexible boundaries allow any type of controlled rotation in the plane of maximum shear stress; this restriction is similar to the one that applies to hollow cylinder apparatus. The cubical devices designed for this purpose are called directional shear cells; there is, in fact, no requirement that the specimens in these devices be cubes.

Two rows in Table 1 deal with post-peak strain-softening behavior in which rupture layers will usually be present in the samples. In both cases radiography is essential for all apparatus to ensure that the inhomogeneities are clearly defined.

Another row in Table 1 is concerned with exceptional stress levels. While there may be no unusual difficulties at high levels, there will be problems when the minor principal stress is low (0 to 25 kPa). Some careful evaluations of corrections for conventional triaxial data at these low levels have been provided by Fukushima and Tatsuoka [*18*]. Flexible boundary devices with direct and simple application of uniform stress to the sample are more likely to succeed here, but special techniques and radiography are needed to confirm success.

Representative Design Examples

There will be no attempt at an overall review of the very wide range of designs developed over the last 25 years. Historical interest demands mentioning the pioneer designs of Hambly [*19*] for the rigid boundary type, Ko and Scott [*20*] and Lomize and Kryzhanovsky [*21*] for the flexible type, and Green [*16*] and Lade [*15*] for the mixed boundary type. Representative examples are briefly described in the following paragraphs. As wide a range of study application as possible has been covered.

True Triaxial (*All Rigid*)

Hambly's design concept for the all rigid device is outstanding and has been imitated (for example, Gudehus [*22*]). Pearce reported the development of this design in 1971 [*23*], and Fig. 1 is his illustration of the concept. The great attraction is the unlimited boundary displacement available in any of the three axes. The complexity of the mechanism limits the practical stress range and implies inevitable high cost.

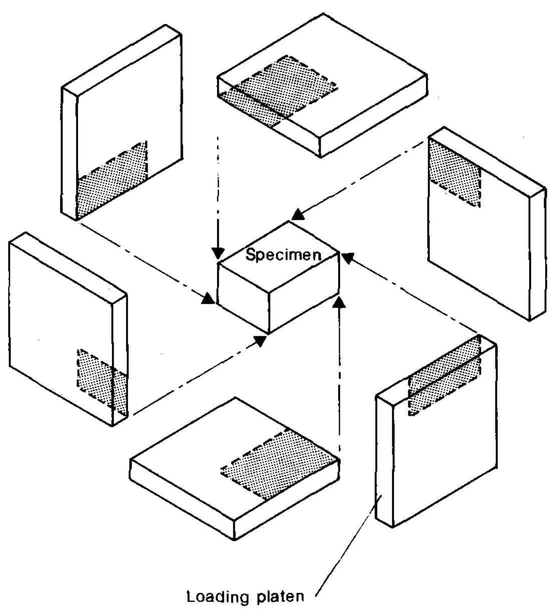

FIG. 1—*Hambly's rigid boundary true triaxial concept as depicted by Pearce* [23].

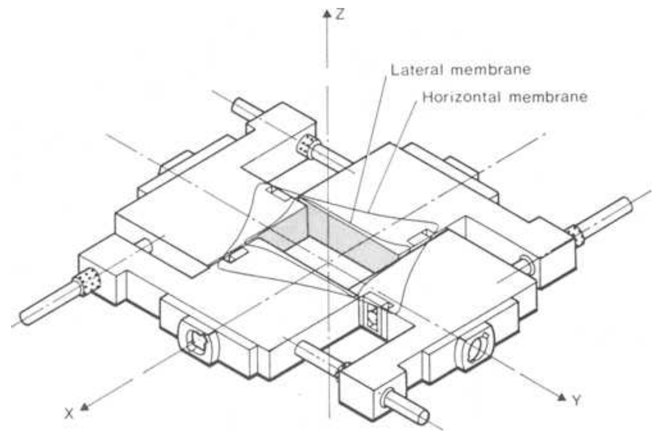

FIG. 2—*Rigid boundary biaxial tester by Harder and Schwedes* [24].

Plane Strain (All Rigid)

Again Hambly's concept leads to an interesting design developed by Harder and Schwedes [*24*] with low stress levels in mind (Fig. 2). Stretched lateral and horizontal rubber membranes are used to reduce unwanted surface shear. The action of the lateral membranes is especially satisfactory because there is no movement between specimen face and membrane when the latter is straining uniformly. The top and bottom horizontal membranes do not achieve this ideal. Figure 3 shows how four boundary cells measuring normal and shear stresses were incorporated into one lateral platen to check on performance (a similar approach was adopted by Pearce in 1971). Harder and Schwedes report normal stress variations of ±3% of the mean for the whole platen and friction coefficients of up to 0.05 at very low stress levels of 2 kPa. At higher stress levels the coefficient dropped to 0.01. The material sheared in these tests was crushed limestone with particle sizes less than 15 μm. The device is aimed at the low-stress range suitable for material handling.

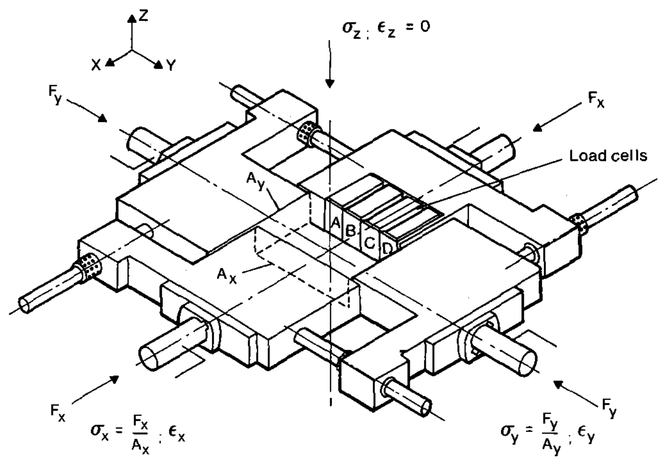

FIG. 3—*Rigid boundary biaxial tester by Harder and Schwedes, showing load cells* [24].

True Triaxial (Mixed Rigid and Flexible)

These devices are the most direct developments from conventional triaxial cells; Green [*16*] presents a sophisticated version developed with Bishop at Imperial College which draws on immense conventional cell experience. Platen interference, a difficulty in these devices, was solved brilliantly for research purposes by Lade and Duncan [*15*]. One pair of platens, made of alternate strips of stainless steel and balsa wood, could be compressed by the other rigid pair when moving inwards (Fig. 4). The price of this solution is in the loss of ability to rotate principal stress directions in jumps of 90°.

True Triaxial (All Flexible)

High Stress Level—Meier, Ko, and Sture provide the example [*25*]. This is perhaps only a relatively flexible device because the stresses are transmitted through a vinyl membrane, and then through a substantial pad of polyurethane, followed by a thinner pad of a material dependent on the sample material. (For example, leather was used for rock and concrete samples.) Figure 5 illustrates this simple design which can apply stresses up to 138 MPa.

Intermediate Stress Level—Yamada and Ishihara [*26*] have developed another simple design derived from the original Ko and Scott [*20*] design (Fig. 6). This apparatus has been used successfully to investigate the anisotropic stress–strain behavior of sand, that is in the comparative sense; the authors themselves have noted the possibility of restraint by the space frame on the same lines as that reported by Arthur and Menzies [*27*]. The likelihood

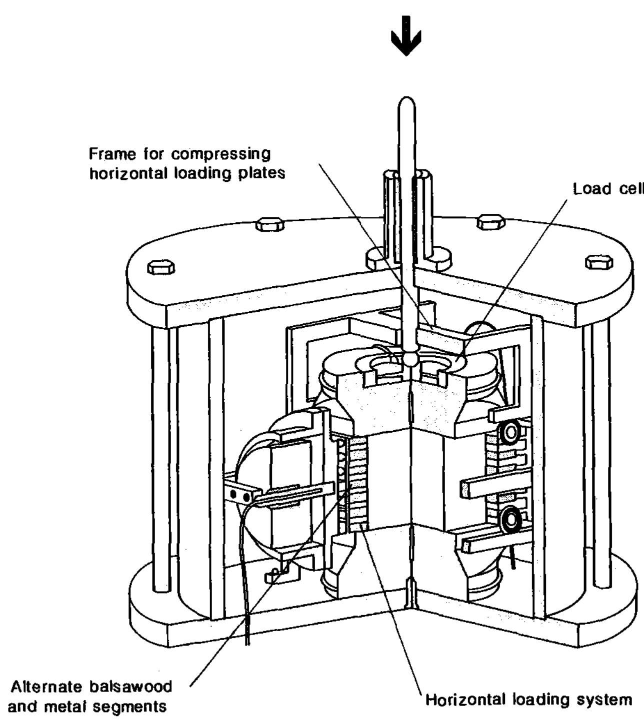

FIG. 4—*Mixed boundary true triaxial by Lade and Duncan* [15].

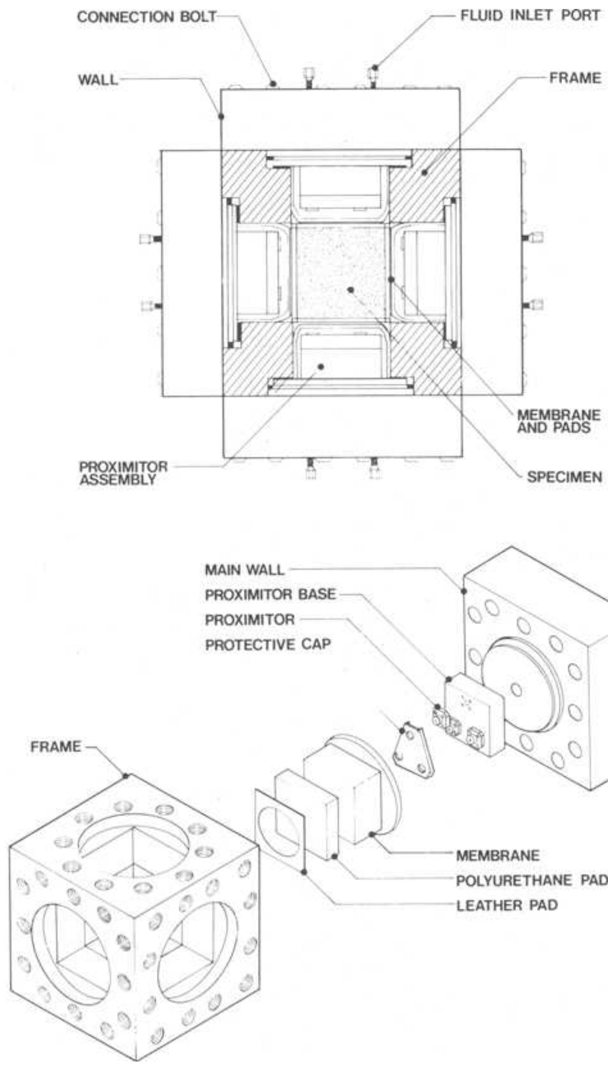

FIG.5—*High stress flexible boundary true triaxial by Meier et al.* [25].

of this restraint was established by comparing stress–strain curves measured in the new apparatus and a conventional axisymmetric triaxial cell applying nominally identical stress paths [*26*]. This is an important comparative technique for establishing the reliability of data from new apparatus; of course in applying it, due regard must be paid to the known shortcomings of the old device.

Dunstan has suggested an arrangement that avoids contact between any rigid part of the apparatus and the specimen; Fig. 7 shows a cross-section of this approach as developed by Davoudzadeh [*28*]. A major principal strain of over 10% can be achieved provided the specimen is held centrally by controlling the flow in and out of the pressure bags.

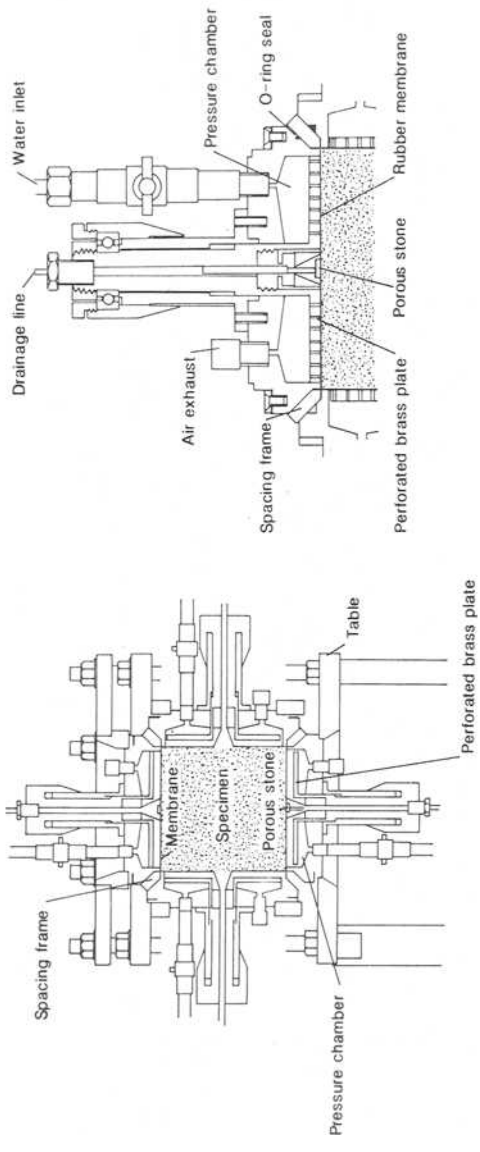

FIG. 6—*Flexible boundary true triaxial by Yamada and Ishihara* [26].

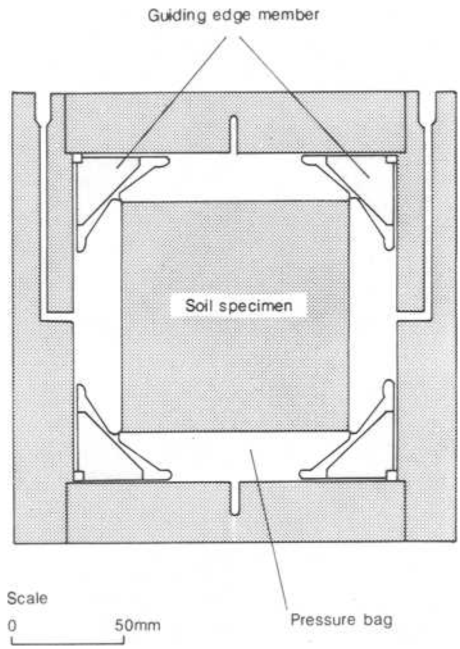

FIG. 7—*Flexible boundary true triaxial by Dunstan and Davoudzadeh* [28].

Plane Strain (All Flexible)

Arthur, Dunstan, and Enstad [*29*] are developing a cubic device especially for the low stresses applicable to materials handling. There are several novel features which should eliminate all boundary restraints while maintaining uniform boundary stresses when testing initially homogeneous specimens. The device makes use of the proposition that perfectly uniform boundary stresses applied to a homogeneous specimen must result in a uniform strain distribution through it. Figure 8 illustrates the operation for the plane of strain; any very small deviation of the stretched membranes from a true plane is detected and corrected by movements of the four corner pieces. These corner pieces also control stretched rubber membranes on the top and bottom faces so that these membranes strain exactly with the adjacent surfaces of the specimen; the forces to stretch all six rubber membranes are supplied through the corner pieces entirely independently of the specimen.

Directional Shear Cell (DSC) (All Flexible in the Plane of Strain)

The three designs of these essentially plane strain devices all aim to apply uniform normal and shear stresses to opposing sample faces normal to the plane of strain. Figure 9 shows the cross-section of the original device [*30*]. Varying σ_a, σ_b, τ_a, and τ_b controls the directions of the principal stresses in the plane of strain. The soil sample in its rubber membrane is in direct contact with the shear sheets inner rubber membrane, and, when degreased, these membranes bond together completely as the normal stress is applied across the pair. Fifteen stretchable rubber pulling strips are attached to the outer surface of each face of this inner membrane. These strips stretch up to 300% their original length and distribute the shear stress evenly onto the specimen. A layer of sand glued onto the inner surface of the specimen membrane is used in the final shear stress transfer into the specimen. An alternative shear

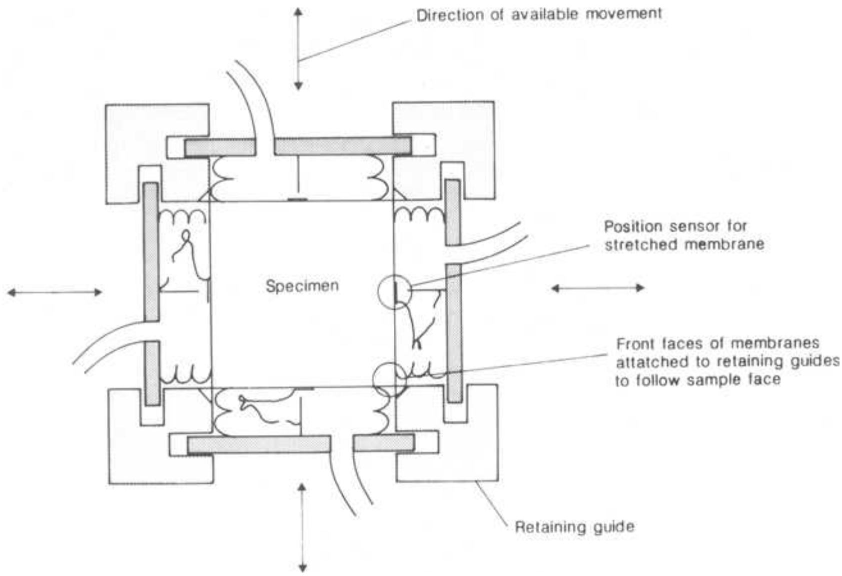

FIG. 8—*Flexible boundary biaxial tester by Arthur et al.* [29].

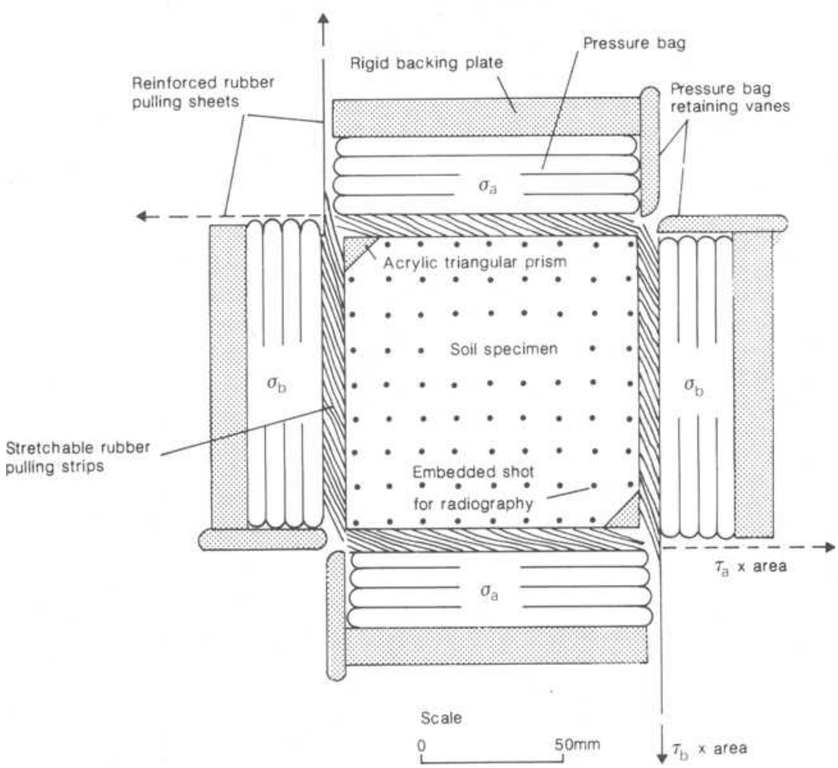

FIG. 9—*Directional shear cell by Arthur et al.* [30].

sheet design developed by Sture et al. uses molded silicon rubber as opposed to natural rubber [*31*]. Silicon rubber does not self-adhere under normal stress (or adhere to natural rubber), so shear transfer is affected by short silicon "rubber teeth." In this version only seven stretching strips are used on a larger cube side of 170 mm. The main advantage of this alternative is probably ease of manufacture, but there may be a penalty in the degree of uniformity of the applied shear stress. Although hard to make, the original type of sheets usually last two years in normal use. Figure 10 shows a new daisy chain version of the shear sheets in use at University College London; the principle is the same as in the original, but the stress range can be increased enormously because each strip can incorporate a succession

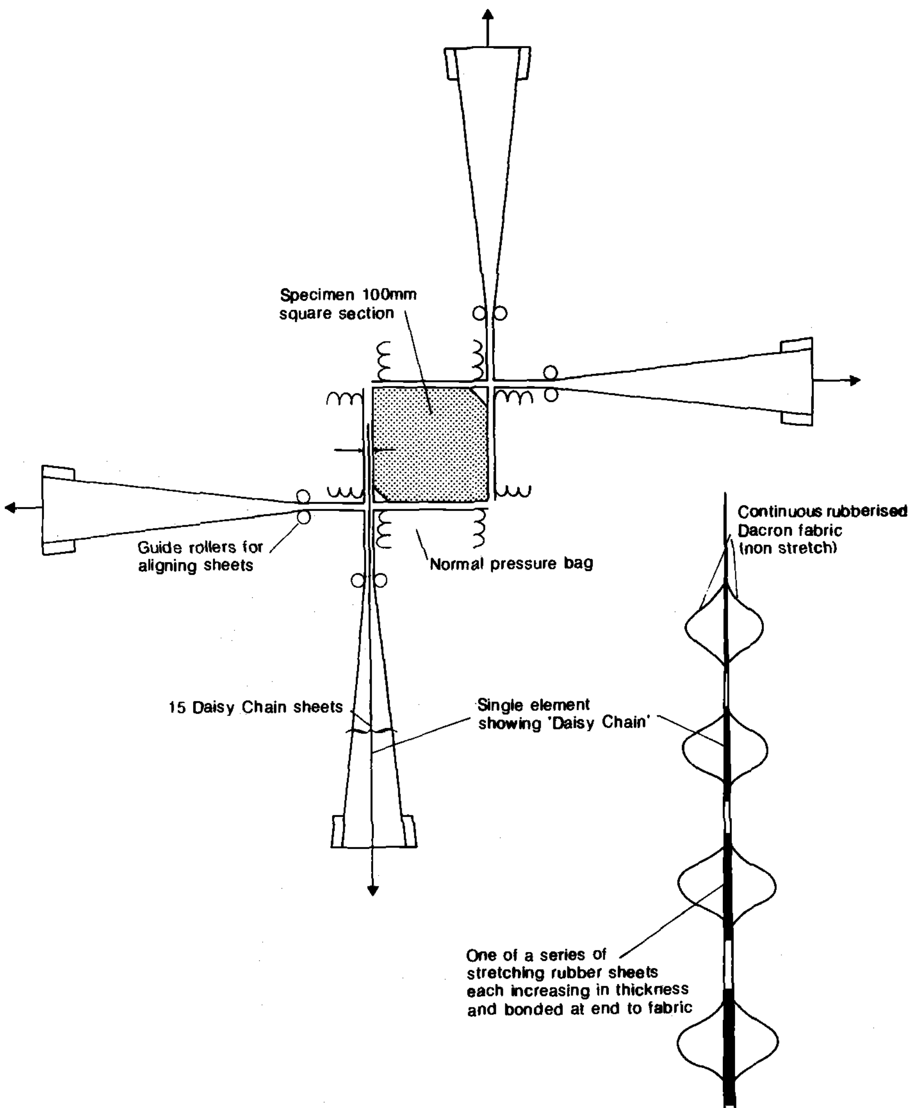

FIG. 10—*DSC daisy chain shear sheets to increase range of applied shear stresses.*

of stretching elements of increasing stiffness which come into play one after the other as the stress level rises. When each element has stretched 25 mm, the strong sailcloth in series with it takes any further increase in load. A further advantage of the new design is the elimination of hysteresis in the shear sheets while imposing cyclic variations in shear stress.

Proving Apparatus Performance

As already stated, the decision to shear a cubical specimen implies that unintentional boundary restraints must be investigated. True material stress–strain data will only be gained if these restraints either can be held at acceptably low levels or estimated sufficiently well to apply appropriate corrections. The inhomogeneous contact force distributions common in particulate materials indicate the potential for serious problems. The effects of any consistent inhomogeneity in applied boundary conditions will be especially severe in materials initially strain hardening and subsequently strain softening. All densely packed granular materials fall into this category.

All cubical devices are intended to be element testers which yield a single complete stress–strain relationship with a measurement of shear strength achieved at some time in the test. This simple aim provides the initial criteria for proving and evaluating performance:

1. The boundary stresses should be uniform over all faces of the sample with no unintentional shear components.
2. The strain distribution must be uniform through the sample if the sample was in every sense homogeneous before shear commenced.
3. If the sample was initially isotropic in the plane of strain, then when constant principal stress directions are applied at the boundaries, principal strain and strain increment directions must coincide with these directions.

Both Pearce [*23*] and Harder and Schwedes [*24*] used boundary load cells to establish that the actual boundary stresses on the sample were nearly uniform and that unintentional shear components were small. These favorable results may be due at least in part to the small particle sizes used.

Flexible boundary devices require measurements of uniform internal strain distribution to establish proper performance. Radiography provides these measurements using embedded shot as markers as shown in Fig. 9. Wong and Arthur [*32,33*] provide an example of this type of evaluation, which unfortunately omitted item 3 above. This omission is repaired in Fig. 11 which compares the applied boundary major principal stress direction with the local major principal strain direction within an initially isotropic sample and also provides a mean and standard deviation for the strain direction.

Further criteria must be sought before accepting strength and stress–strain data as true. Uniformity of distribution will never be perfect; relative performance among apparatus can be checked objectively by comparing coefficients of variation (standard/mean) obtained for similar samples and stress paths. The possibility of uniform restraint must be considered also, and a comparison made with a device in which the restraint is known to be absent is the ideal and final verification (an example will be given later).

Actual Boundary Surface Conditions

Previous sections and Table 1 make very limited reference to the limitations and practical problems of achievable boundary surface conditions. Both will be considered in this section.

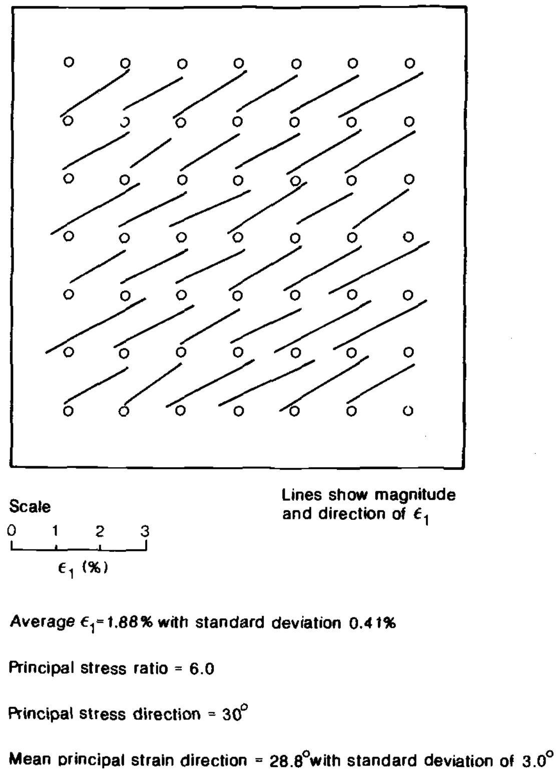

FIG. 11—*DSC distribution of principal strain magnitudes and directions for an initally isotropic specimen monotonically stressed.*

Boundary Surface Friction

Relative lateral movement at faces only intended to transmit normal stress causes surface shear which restrains the lateral strain of the specimen. Both rigid and flexible boundaries suffer; mitigation is usually provided by three layers of a silicon grease separated by two thin rubber sheets [*34–36*]. Most greases used are now filled with a small quantity of some powder such as polytetra fluorethylene. The aim is to achieve as low a coefficient of friction as possible and continued good performance through time and cyclic variations in stress. Both stress level and particle size must be taken into account in designing the lubrication.

Rigid Boundaries

Hambly's design concept leads to almost unlimited boundary displacement, but in the true triaxial form this is paid for in the expense of the mechanism. This mechanism also eliminates the possibility of using radiography to check whether uniform strain is being imposed during a test. Postmortems cannot indicate when rupture layers are formed. Desrues and co-workers report complex rupture layer patterns formed in an all-rigid true triaxial apparatus while also reporting exceptionally detailed measurements using a plane strain device which showed rupture layers forming before peak shear resistance was attained [*10*]. These experiments were made on dense sand specimens.

Boundary stress cells measuring shear as well as normal stress are needed over appreciable areas of the boundaries to check that there are no stress concentrations and that unwanted shear stress is absent. These are not necessarily once-and-for-all checks because changes in particle size and initial sample homogeneity may affect the results.

As already indicated, boundary shear must be controlled by lubrication with thin rubber membranes. Because the platens must slide closely, there is a risk of damaging the membranes or even jamming the mechanism. Nevertheless, very good results can be obtained as shown recently by Harder and Schwedes [*24*].

Mixed Rigid and Flexible Boundaries

These devices do not use the Hambly platen configuration, and this leads to problems of platen interference which are difficult to overcome. (The best solution, offered by Lade and Duncan [*15*], has already been mentioned.) Other boundary effects are covered in the sections on rigid and flexible types.

Flexible Boundaries

Normal Stresses Acting Alone—The ideal of uniformly applied normal stress through a perfectly flexible membrane comes up against the practical difficulty of maintaining this stress to the absolute edge of the sample. There are, of course, two possible conditions:

1. Stresses too high along edge—This is the effect of the type that uses a fixed edge space frame such as that of Yamada and Ishihara [*26*] (Fig. 6) when the strain of the sample drives its edge into that of the frame. Although the area of contact will usually be small, the rigidity of the frame makes unlimited stress concentrations possible. Those that actually develop will depend on the stress path applied and specimen characteristics. Dense sand might be expected to produce a severe concentration in comparison with a loose sand. Departures from true material stress–strain relationships in the data obtained will vary accordingly. An apparent advantage of this condition is that the undrained constant volume condition can be maintained for a fully saturated sample even when there is a positive pore water pressure.
2. Stresses too low along edge—This is the effect of a pressure membrane that does not exert the correct pressure to the sample edge, usually after some sample strain; the magnitude of the error is related to the pressure deficiency and the area over which it occurs. There will usually be no compensating contact with a fixed space frame and, however small this

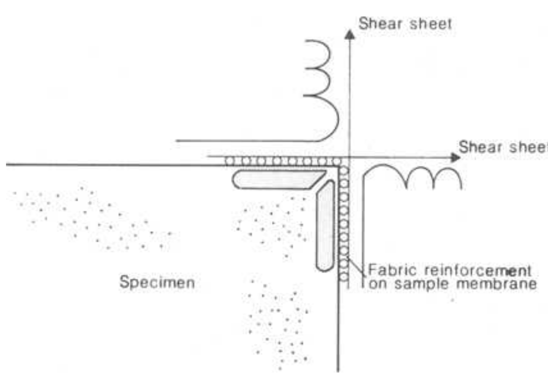

FIG. 12—*New type of DSC specimen corner.*

stress deficiency is, it will make it impossible to reliably maintain undrained constant volume conditions when there is a positive pore water pressure in the sample. Undrained tests can be carried out by controlling the total stresses so that the pore water pressure is held constant at zero. This requires a good pore pressure sensor and computer control.

A successful design is one that minimizes these edge stress errors over as large a range of sample strain as possible. Change from condition 1 to condition 2 during a stress path may pose a problem for undrained testing. Radiography of this type of device is usually relatively easy; determination of strain distributions is essential to prove performance for each device.

Shear Stresses Acting with Normal Stresses—Incorrect edge stresses, in addition to having the effects already described in relation to normal stresses, can easily induce progressive extensive failure at the corners where the shear sheets emerge in the DSC (Fig. 9); this

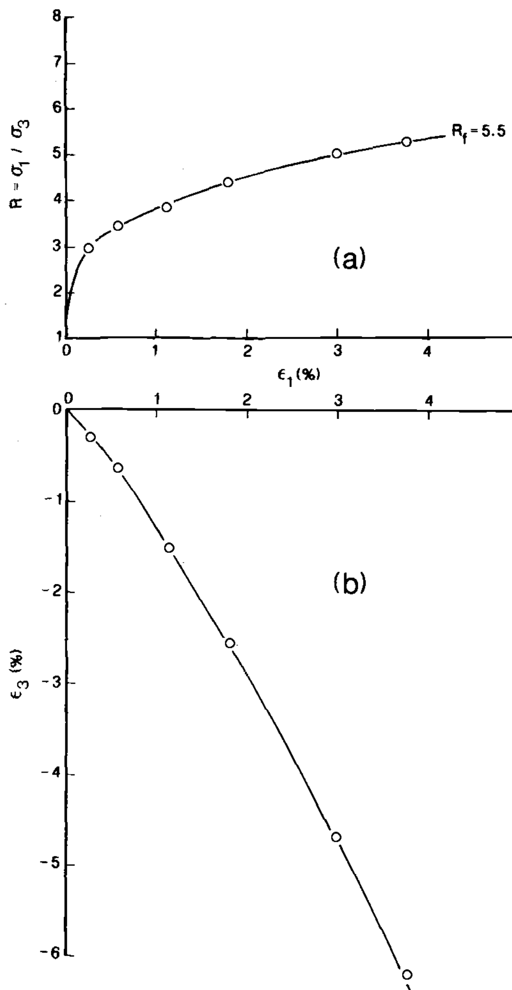

FIG. 13—*Data from flexible boundary biaxial test on dense Leighton Buzzard sand.*

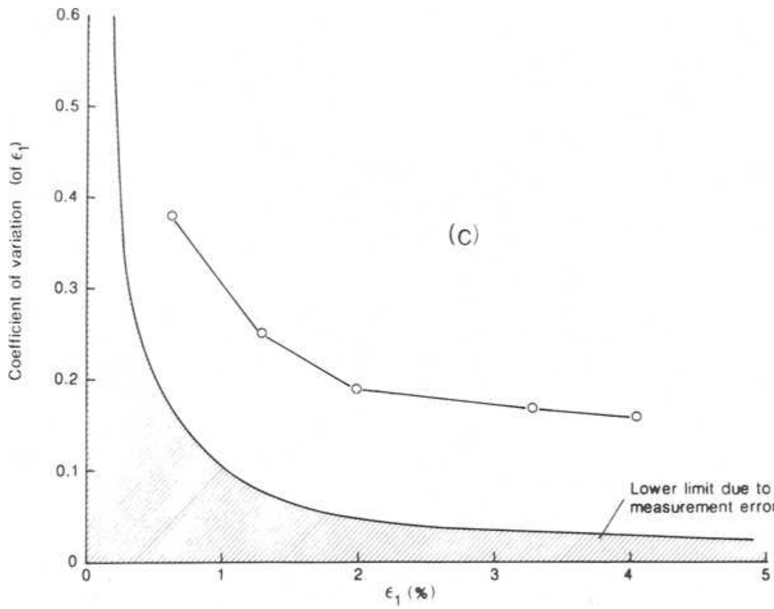

FIG. 13—*Continued.*

problem was solved by not attaching a shear strip within 5 mm of the edge and replacing the sample material within these corners with unfailable acrylic prisms. An improved solution has been used recently: the sample membrane is reinforced with fabric around the corner, and within the membrane two aluminum strips are glued to the orthogonal inside faces close to the corner (Fig. 12). The angle of these corners can now change with the distortion of the whole sample; the aluminum strips are needed to distribute the residual end restraint of the lubricated top and bottom surfaces uniformly through the sample.

The DSC generally fails to apply the boundary stresses to the sample edge limits and accordingly undrained tests must be done at zero pore water pressure under computer control. To achieve virtually the correct normal stresses the concertina bags shown in Fig. 9 must be kept within ±5 mm of optimum thickness [*11*]. For correct shear stresses, the shear pulling sheets must be aligned continually with the specimen faces. Lubrication is needed between the stretching strips, immediately in front of the pressure bags, and on the top and bottom specimen surfaces.

Toward True Stress–Strain Data

The original and perhaps naive aim of cubical testing was to obtain true stress–strain data; time has revealed the difficulties. Verification of apparatus performance is essential and probably impossible without radiography. However, the essence of the problem of obtaining true stress–strain data goes deeper; it is not enough to use radiography to show uniform strain response from a homogeneous specimen subjected to uniform boundary stresses. There must be no unintentional uniform restraint imposed through the specimen boundaries; the biaxial shear tester shown in Fig. 8 should fulfill this condition. Uniform stresses are applied to the full area of each specimen face throughout any stress path, and the deformation of the specimen dictates an exactly matching uniform boundary strain without imposing any restraint on the specimen. Radiographic determinations of the strain distribution have shown coefficients of variation as low as any known to be obtained in any device shearing granular material. The strains used to define the stress–strain relationship are the mean values of these distributions. Ogunbekun is using the tester to define the stress–strain relationship for dense Leighton Buzzard sand. Data plotted in Fig. 13 indicate a 33% overestimate of the drained shearing resistance of the sand as measured in the DSC [*33*] and in the Cambridge simple shear apparatus [*37*]. This apparent error is large, and a very full investigation of the biaxial tester results is in progress, but for the purposes of illustration it is assumed that this error is established.

Comparative Stress–Strain Data

Must we throw away all our previous data? Fortunately the pain need not be so great even if the error is established. The data may remain valuable for comparative purposes provided we can satisfy ourselves that the unintentional restraint affecting the results did so equally while we changed the other variables we were interested in. Wong and Arthur describe tests in the DSC in which the same stress path was applied to identical isotropic specimens of dense sand with different proportions of normal and shear stress applied to the boundaries [*32,33*]. The tests span the full range from zero boundary shear stress to maximum boundary shear stress ($\psi = 0°$, $\psi = 45°$) and the satisfactory performance is presented in Fig. 14. This testing program established that directional effects could be investigated without bias. Thus the value of comparative tests in the DSC is vindicated. There are doubtless many data sets obtained from cubical devices which are valid for similar comparative purposes, but perhaps fewer providing true stress–strain data.

Corrected Stress–Strain Data

In the biaxial tester we changed the conditions on the top and bottom boundaries to correspond to those of the DSC; preliminary results indicate that the discrepancies between the results from the two apparatus are entirely due to the different restraints imposed through the plane strain boundaries of the DSC. This leads to a simple correction, namely, proportionally reducing all stress ratios greater than one measured in the DSC so that the stress ratio at failure equals that found in the biaxial tester. Figure 15*a* compares the DSC data corrected in this way with that from the biaxial tester for tests with identical specimens and stress paths. Of course, a reversal with corrected biaxial data fitted to as-measured DSC data is possible and may be appropriate. No correction is required for the comparisons in Figs. 15*b* and 15*c*; the close agreements on dilation rates and coefficients of variation are encouraging. For the moment, the results in Fig. 15 can be treated as an unverified example of true and corrected stress–strain data.

Needed Developments

The following developments are needed:

In laboratory testing

(a) Proper proving of apparatus using radiography and comparison of data from different devices
(b) Classification of stress–strain data quality (true, comparative, or corrected)

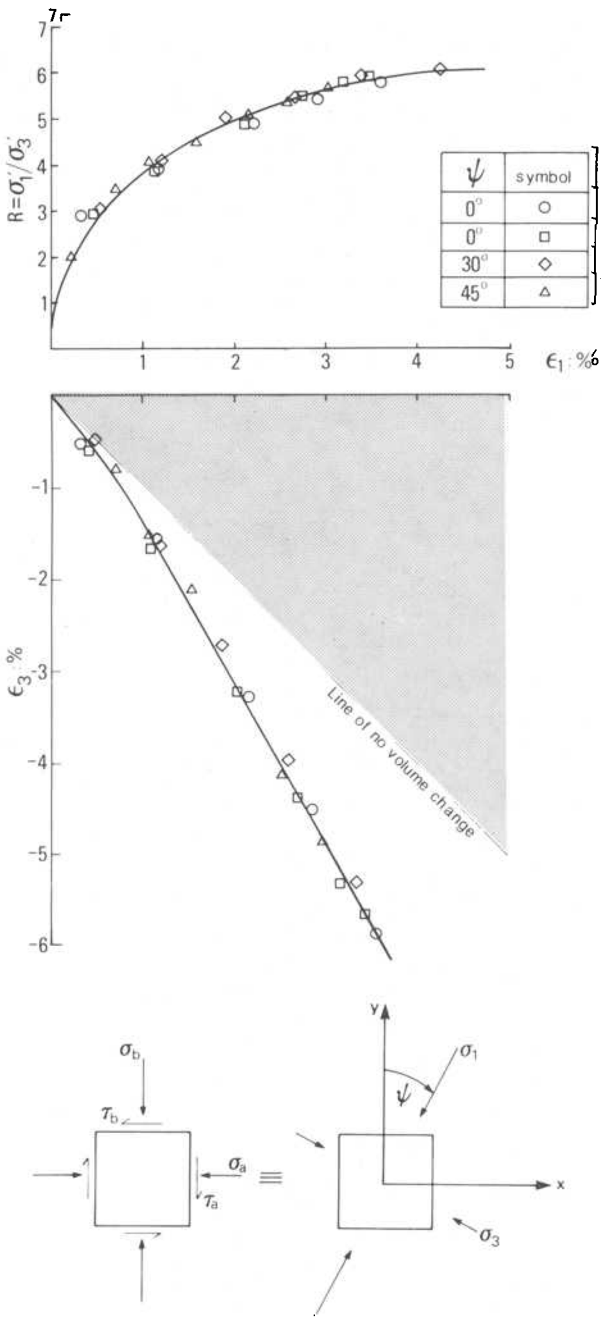

FIG. 14—*Directional verification of the DSC.*

Material behavior studies in:

(a) Low stress level effects
(b) Low strain level response
(c) Inhomogeneity
(d) Rotation of principal axes
(e) Cyclic stress paths embodying a, b, c, and d above

Testing undisturbed field samples

Conclusion

Cubical devices are far too versatile to be discarded because of the unintentional constraints that often occur. There are equivalent disadvantages in other types of shear appa-

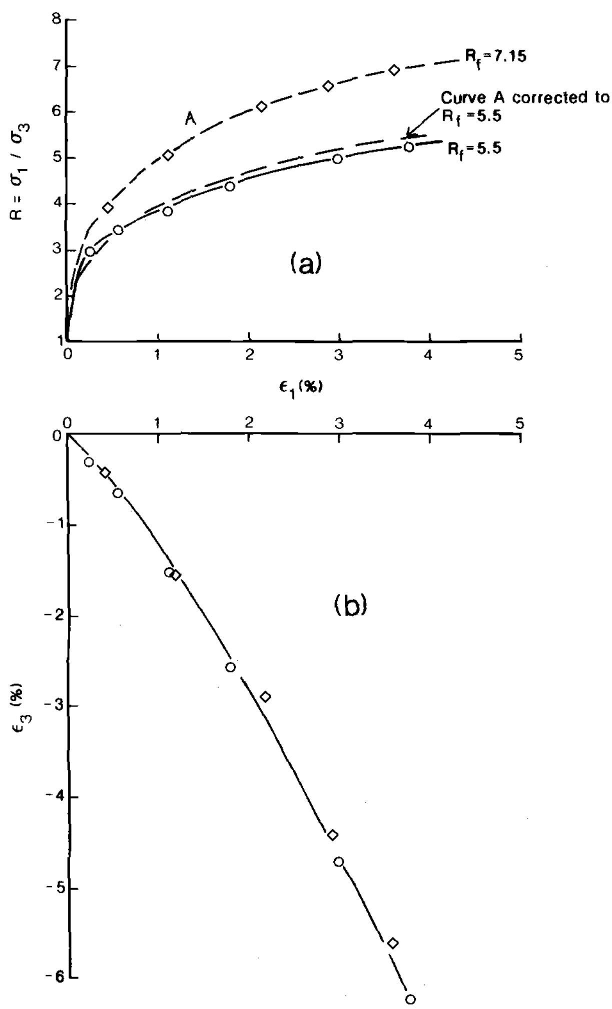

FIG. 15—*DSC data compared with data in Fig. 13 for the same stress path applied to an exactly similar specimen, also the same DSC data corrected.*

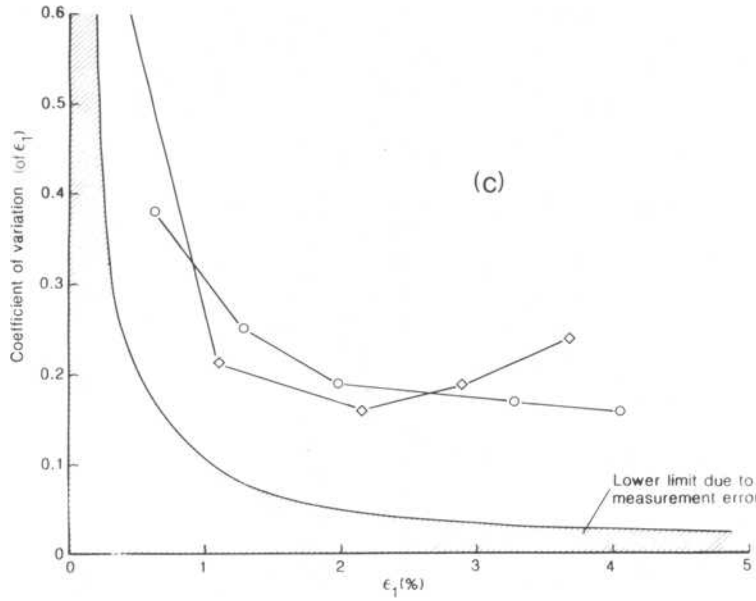

FIG. 15—*Continued.*

ratus. All apparatus must be thoroughly proved, and measuring internal strain distributions using radiography is an important part of the proving process. Much valuable research time can be saved by adopting this approach. Often comparative measurements of material properties are all that are needed and all we will get, but we must always evaluate the quality of data by adequately assessing the performance of the shear apparatus.

Acknowledgments

I thank the Organizing Committee for giving me the opportunity to review this topic. The biaxial shear tester (Fig. 8) is being developed in enjoyable cooperation with the Christian Michelsen Institute of Bergen, Norway. I am very grateful to colleagues and students in the research group at University College London whose efforts made the whole enterprise possible.

References

[1] Saada, A. S. and Townsend, F. H., "Shear Strength Laboratory Testing of Soils," in *Proceedings, ASTM Symposium, STP 740,* American Society for Testing and Materials, Philadelphia, 1982, pp. 7–77.
[2] Rowe, P. W. and Barden, L., *Proceedings, American Society of Civil Engineers,* Vol. 90, No. SM1, 1964, pp. 1–27.
[3] Bishop, A. W. and Green, G. E., "The Influence of End Restraint on the Compression Strength of a Cohesionless Soil," *Geotechnique,* Vol. 15, No. 3, 1965, pp. 243–266.
[4] Kirkpatrick, W. M. and Belshaw, D. J., "On the Interpretation of the Triaxial Test," *Geotechnique,* Vol. 18, No. 3, 1968, pp. 336–350.
[5] Biarez, J. and Wiendieck, K., "La Comparaison Qualitative entre l'Anisotropie Mechanique et l'Anisotropie de Structure des Milieux Pulverulent," *Compres Rendus Hebdomadairs des Seánces de l'Academie des Sciences, Paris,* Vol. 256, 1963, pp. 1217–1220.
[6] Cundall, P. and Strack, O. D. L., "A Discrete Numerical Model for Granular Assemblies," *Geotechnique,* Vol. 29, No. 1, 1979, pp. 47–65.

[7] Arthur, J. R. F., Koenders, M. A., and Wong, R. K. S., "Anisotropy in Particle Contacts Associated with Shearing in Granular Media," *Acta Mechanica*, Vol. 64, 1986, pp. 19–29.
[8] Marsland, A., "Laboratory and Insitu Measurements of the Deformation Moduli of London Clay," in *Proceedings*, International Symposium on Structures and Foundations, Birmingham, U.K., 1971, pp. 1–17.
[9] Arthur, J. R. F. and Assadi, A., "Ruptured Sand Sheared in Plane Strain," in *Proceedings*, Ninth International Conference on Soil Mechanics and Foundation Engineering, Tokyo, Vol. 1, 1977, pp. 19–22.
[10] Desrues, J., Lanier, J. and Stutz, P., "Localisation of the Deformation in Tests on Sand Sample," *Eng. Fracture Mech.*, Vol. 21, No. 4, 1985, pp. 909–920.
[11] Germaine, J. T., "Development of the Directional Shear Cell for Measuring Cross Anisotropic Clay Properties," Sc.D. thesis, Massachusetts Institute of Technology, Cambridge, 1980.
[12] Jamiolkowski, M., Ladd, C. C., Germaine, J. T., and Lancellotta, R., "New Developments in Field and Laboratory Testing of Soils," in *Proceedings*, Eleventh International Conference on Soil Mechanics and Foundation Engineering, San Francisco, Vol. 1, 1985, pp. 57–153.
[13] Arthur, J. R. F. and Phillips, A. B., "Homogeneous and Layered Sand in Triaxial Compression," *Geotechnique*, Vol. 25, No. 4, 1975, pp. 799–815.
[14] Burland, J. B. and Symes, M. J. P. R., "A Simple Axial Displacement Gage for Use in the Triaxial Apparatus," *Geotechnique*, Vol. 32, No. 1, 1982, pp. 62–65.
[15] Lade, P. V. and Duncan, J. M., "Cubical Triaxial Tests on Cohesionless Soil," *Journal of the Soil Mechanics and Foundation Division, American Society of Civil Engineers*, Vol. 99, No. SM10, 1973, pp. 793–812.
[16] Green, G. E., "Stress Strain Behaviour of Soils," in *Proceedings*, Roscoe Memorial Symposium, G. T. Foulis, Henley on Thames, 1972, pp. 285–324.
[17] Mould, J. C. and Sture, S., "Constitutive Characterisation of Granular Materials at Low Stress Levels," Report No. VPI E 79 39, Virginia Polytechnic Institute and State University, Blacksburg, 1979.
[18] Fukushima, S. and Tatsuoka, F., "Strength and Deformation Characteristics of Saturated Sand at Extremely Low Pressures," *Soils and Foundations*, Vol. 24, No. 4, 1984, pp. 30–48.
[19] Hambly, E. C., "A New Triaxial Apparatus," *Geotechnique*, Vol. 19, No. 2, 1969, pp. 307–309.
[20] Ko, H-Y. and Scott, R. F., "A New Soil Testing Apparatus," *Geotechnique*, Vol. 17, No. 1, 1967, pp. 40–57.
[21] Lomize, G. M. and Kryzhanovsky, A. L., "On the Strength of Sand," in *Proceedings*, Geotechnical Conference, Norwegian Geotechnical Institute, Oslo, Vol. 1, 1967, pp. 215–219.
[22] Gudehus, G., "Discussion," in *Proceedings*, Roscoe Memorial Symposium, G. T. Foulis, Henley on Thames, 1972, pp. 373–375.
[23] Pearce, J. A., "A New Triaxial Apparatus, " in *Proceedings*, Roscoe Memorial Symposium, G. T. Foulis, Henley on Thames, 1972, pp. 330–339.
[24] Harder, J. and Schwedes, J., "The Development of a True Biaxial Tester," in *Proceedings*, International Symposium on Reliable Flow of Particulate Solids, Christian Michelsen Institute, Bergen, Norway, 1985.
[25] Meier, R. W., Ko, H.-Y., and Sture, S., "A Direct Tensile Loading Apparatus Combined with a Cubical Test Cell for Testing Rocks and Concrete," *Geotechnical Testing Journal*, GTJODJ, Vol. 8, No. 2, June 1985, pp. 71–78.
[26] Yamada, Y. and Ishihara, K., "Anisotropic Deformation Characteristics of Sand under Three Dimensional Stress Conditions," *Soils and Foundations*, Vol. 19, No. 2, 1979, pp. 79–94.
[27] Arthur, J. R. F. and Menzies, B. K., "Inherent Anisotropy in a Sand," *Geotechnique*, Vol. 22, No. 1, 1972, pp. 115–128.
[28] Davoudzadeh, F., "Response of Sand to Three Independently Controlled Principal Stresses," Ph.D. thesis, London University, 1982.
[29] Arthur, J. R. F., Dunstan, T., and Enstad, G. G., "Determination of the Flow Function by Means of a Cubic Plane Strain Tester," *International Journal of Bulk Storage in Silos*, Vol. 1, No. 2, 1985, pp. 7–10.
[30] Arthur, J. R. F., Chua, K. S., and Dunstan, T., "Induced Anisotropy in a Sand," *Geotechnique*, Vol. 22, No. 1, 1977, pp. 13–30.
[31] Sture, S., Ko, H-Y., Budiman, J., and Ontuna, A., "Constitutive Behaviour of Cohesive and Cohesionless Soils during Continuous and Discrete Jump Rotations of Principal Stress Directions in a Directional Shear Cell," in *Proceedings*, Eleventh International Conference on Soil Mechanics and Foundation Engineering, San Francisco, Vol. 2, 1985, pp. 1061–1064.
[32] Wong, R. K. S. and Arthur, J. R. F., "Determinations and Uses of Strain Distributions in Sand Samples," ASTM *Geotechnical Testing Journal*, Vol. 8, No. 3, 1985, pp. 101–110.

[33] Wong, R. K. S. and Arthur, J. R. F., "Induced and Inherent Anisotropy in a Sand," *Geotechnique*, Vol. 35, No. 4, 1985, pp. 471–481.
[34] Arthur, J. R. F. and Dalili, A., "On the Lubrication of Rubber Surfaces," *Geotechnique*, Vol. 29, No. 1, 1979, pp. 98–99.
[35] Tatsuoka, F., Molenkamp, F., Toril, T., and Hino, T., "Behaviour of Lubricated Layers in Element Tests," *Soils and Foundations*, Vol. 24, No. 1, 1984, pp. 113–128.
[36] Tatsuoka, F. and Haibara, O., "Shear Resistance Between Sand and Smooth or Lubricated Surfaces," *Soils and Foundations*, Vol. 25, No. 1, 1985, pp. 89–98.
[37] Stroud, M. A., "The Behaviour of Sand at Low Stress Level in the Simple Shear Apparatus," Ph.D. thesis, Cambridge University, 1971.

Adel S. Saada[1]

STATE-OF-THE-ART PAPER

Hollow Cylinder Torsional Devices: Their Advantages and Limitations

REFERENCE: Saada, A. S., "**Hollow Cylinder Torsional Devices: Their Advantages and Limitations,**" *Advanced Triaxial Testing of Soil and Rock, ASTM STP 977,* Robert T. Donaghe, Ronald C. Chaney, and Marshall L. Silver, Eds., American Society for Testing and Materials, Philadelphia, 1988, pp. 766–795.

ABSTRACT: Hollow cylinder torsional devices have recently attracted the attention of both researchers and practitioners as tools of great promise to be used in the development of constitutive relations as well as in the determination of strength parameters of both isotropic and anisotropic soils. They are a natural extension of the standard triaxial devices and provide a much wider variety of stress paths to be investigated or to simulate. This state-of-the-art paper reviews the relevant literature, examines the advantages and limitations of these devices, and discusses some of the difficulties encountered in their use. Their versatility is pointed out, and the role they play in the development of constitutive relations is evaluated. Examples, drawn from both static and dynamic conditions, help illustrate the wide variety of stress paths these devices are capable of producing.

KEY WORDS: hollow cylinders, torsional shear, stress paths, constitutive equations, anisotropy

The solution of complicated soil engineering and soil–structure interaction problems requires the use of realistic constitutive equations and failure criteria. Once such equations and criteria are established the finite elements as well as other numerical methods become valuable tools in guiding the engineer in his design. Laboratory investigations of the highest technical caliber are needed to establish the validity of mathematical models. Such models often emerge as an assumption based on observations made by researchers in the area of soils or other materials. In recent years emphasis has been placed on obtaining a wider variety of stress paths than that possible in the standard triaxial test. In addition, anisotropy has finally been acknowledged as an important reality to be reckoned with both in analysis and design.

True triaxial apparatus using a cubic or a parallelepipedic sample configuration are used extensively to generate a wide variety of stress paths. Stresses can be applied with rigid platens, flexible membranes, or a mixture of both. The advantages and limitations of each type have been described in detail by Saada and Townsend [*1*] in their state-of-the-art paper on the strength testing of soils. While each of the faces of the cube can become a major, intermediate, or minor principal plane, the true triaxial apparatus does not allow for a continuous rotation of principal stresses. It is ideal for conducting plane strain tests and

[1] Frank H. Neff professor and chairman, Department of Civil Engineering, Case Western Reserve University, Cleveland, OH 44106.

varying independently three principal stresses along the axes of symmetry of the material. Thus, anisotropy cannot be fully investigated with this type of apparatus alone.

Natural sand deposits are not isotropic. Nonspherical particles have a strong tendency to align themselves in a direction normal to the direction of deposition. This endows the material with anisotropic mechanical properties. Even spherical particles deposited in the gravity field exhibit a response that varies with the direction of the applied stresses. For clays, the process of sedimentation followed by one-dimensional consolidation results in a fabric that is strongly anisotropic. The material's response to stress is, of course, anisotropic too, reflecting the geometrical arrangement of the clay particles and their contacts. Structure anisotropy in clays may also arise due to anisotropic electro-chemical interparticle bonds, in addition to anisotropic fabric.

The influence of anisotropy has largely been neglected in engineering practice, primarily because it was thought to be unimportant, but also because the tools to investigate it were lacking. In the last 15 years two approaches to study anisotropy emerged: A traditional one based on testing specimens inclined to the direction of deposition in classical triaxial or plane strain devices; and a second one based on inclining the principal stresses on the direction of deposition, through a combination of axial and shearing stresses applied to faces of test specimens. The first approach results in very undesirable end shears and bending moments [2]. The second approach can be achieved in the thin long hollow cylinder subjected to the same internal and external pressure and to combinations of axial and torsional stresses.

In addition to the validation of constitutive equations and the study of anisotropy, there is a need to duplicate stress conditions that occur in the field. Combinations of normal and shear stresses are ever present under structures subjected to both static and dynamic effects. Whether dealing with a tall building under wind loads, a power plant, or an offshore structure, the designer often needs to have some numerical idea about the reaction of the soil within the range of stresses.

Historical Background and Brief Review of Earlier Uses of the Hollow Cylinder

The idea of combining axial and torsional stresses in thin long hollow cylinders goes back many years. In 1931 Taylor and Quinney [3] used it to study the plastic yielding of metals, and in 1932 Schmidt [4] used it to vary the principal stresses and maintain a constant ratio between them. In 1936, Cooling and Smith [5] used a hollow cylinder laterally unconfined and subjected to torque to obtain the resistance of soils in pure shear. In 1952 Geuze and Tan [6] studied the rheology of clays on thin long hollow cylinders subjected to torque. Later, hollow cylinders were placed in cells and pressurized in order to generate a wide variety of stress paths. Two approaches were used. In the first the inner and outer pressures are different, and in the second they are identical. Both approaches may or may not involve torsion. We are reviewing here only those devices where torsion was applied to the specimens during various investigations. The others are described in Ref *1* and listed in Ref *7*.

Even though their introduction goes back to 1936, it is only relatively recently that hollow cylinders have been used to simulate a wide variety of stress paths loading to failure. The aim was and often still is to study the validity of Coulomb's failure criterion when the testing conditions differ from those in the standard triaxial cell. For example, in 1965, Broms and Casbarian [8] and Haythornthwaite [9] used hollow cylinders under torsion to study the effects of σ_2 and the rotation of the principal stresses on the strength.

In 1965 the author received a grant to study the properties of anisotropic clays using hollow cylinders subjected to axial and torsional stresses. It was the first investigation in soil mechanics in which the inclination of the principal stresses created by torsion was thought of as a means of studying the effects of anisotropy on the mechanical response of soils.

Driving systems that could keep the ratio of the torsional to the axial stress constant were devised and fixed the directions of the principal stresses while other parameters were varied. The results, published in 1967 [*10*], emphasized the influence of anisotropy on the behavior of clays. In 1969 Saada and Zamani [*11*] used results from hollow cylinder testing to validate one of the first constitutive models for anisotropic clays. This model was refined in 1973 [*12*] and 1975 [*13*], and a failure criterion inspired by the work of Gol'denblat and Kopnov [*13a*] was shown to be acceptable. Lomize et al. [*14*] described a hollow cylinder device without indicating the kind of investigation they conducted with it. A special geometry was used by Yoshinu and Ohoka [*15*] and Sherif and Ishibashi [*16*] to obtain a uniform distribution of shearing strain under torque. While the uniformity of the torsional shearing strain was achieved by keeping the ratio of the height to the distance from the center constant, the resulting stress distribution was not [*1*]. In 1975, Lade [*17*] used a hollow cylinder with outer and inner diameters of 22 and 18 cm, respectively, and a height of 5 cm to study the properties of sand. Such dimensions were judged inadequate [*1*] and, in a later study [*18*], Lade increased the height and showed experimentally that beyond a certain dimension little would be gained in increasing accuracy.

The advantages of a hollow cylinder configuration were realized in the early 1970s by workers in soil dynamics, in particular by Richart and his co-workers. Hollow cylinders were used in resonant column devices by Drnevich and Richart [*19*], Drnevich [*20*], and Hardin and Drnevich [*21*] to study shear moduli and damping ratios of sands, clays, and other materials. Researchers in Japan used hollow cylinders to study liquefaction. Ishihara and Yasuda [*22*] applied irregular excitations to sand samples and compared the results to those obtained in dynamic triaxial compression.

In 1977 the state-of-the-art paper presented at the International Conference on Soil Mechanics and Foundation Engineering [*23*] drew attention to the fact that anisotropy should be taken into account during both analysis and design of earth structure. Anisotropy became fashionable overnight, and many felt the recognition of this important property would help explain much of the unexplainable in soil behavior. It is this recognition that brought hollow cylinder devices to the public's mind and gave them the important place they hold today in the arsenal of soil testing.

With anisotropy, both inherent and induced, moving to the forefront of the profession's consciousness, hollow cylinder attracted the attention of more investigators. Iwasaki, Tatsuoka, and Takagi [*24*] combined the resonant column and a slower cyclic torsional device to cover a broad range of shear strain amplitudes and study their effects on the moduli. Saada, et al. [*25*] conducted an extensive series of tests in the resonant column and determined and compared the moduli of isotropic and K_o consolidated anisotropic kaolinite. In 1980 Ishihara et al. [*26*] used hollow cylinders to study the effects of rotation of the principal stress axes on sand liquefaction. In 1981 Saada and Shook [*27*] showed through testing both laboratory-prepared samples and undisturbed samples from the Gulf of Mexico that the Ramberg-Osgood Masing Model was not satisfactory in representing the behavior of clays under cyclic loading. Bianchini and Saada [*28*] studied layered clay systems in the resonant column and demonstrated the existence of dynamic instability due to the nonlinearities of the material even at very small strains. In 1982 Bianchini [*29*] analyzed in great detail the behavior of hollow cylinders in fixed-free conditions in the resonant column and studied the nonlinear behavior of clays and clay-layered systems. Tatsuoka, Muramatsu, and Sasaki [*30*] studied the undrained behavior of sand with a hollow cylinder device and a driving system bearing very close resemblance to the one designed and perfected at Case Western Reserve University. They found that many of the variables that have only slight effect on the strength of loose sands become quite significant when dealing with dense sands. Ray [*31*] used a computer-controlled resonant column type of device to study moduli and damping ratios of the order of 2×10^{-3}.

In 1983 Hight et al. [7,32] developed a large hollow cylinder device and used it to study anisotropy and the influence of the principal stress rotation on the behavior of saturated sands. They used finite elements to determine the optimum dimensions to be given to the specimen. A wide variety of measuring devices aimed at ensuring proper data acquisition are described in their paper. Large diameter samples are needed to accommodate the proper instrumentation, thus limiting the use of the device to laboratory-prepared specimens. Saada and Macky [33,34] studied the dynamic behavior of both laboratory-prepared and natural clays. Resonant column tests as well as slow cyclic tests on hollow cylinders led to a coverage of moduli and damping over the complete range of strains possible, both axially and torsionally. Ishibashi, Kawamura, and Bhatia [35] conducted a series of experiments to investigate the effects of initial static shear applications on volumetric and liquefaction characteristics of loose and dense sand; such effects were found to be minimal.

More recently, Miura, et al. [36] used ideas similar to those of Hight's et al. [7] to rotate principal stresses and change values of *b*. Tatsuoka et al. [37] stressed the importance of accurate measurements in hollow cylinder devices especially under low confining effective stresses where membrane effects seem to be quite noticeable. They observed shear bands which appear under torsion at values of shearing strains that vary with the confining stress.

It was only a matter of time before a device was constructed that could serve both as a resonant column and a slow cyclic large strain testing apparatus. Such a device was used by Alarcon, Chameau, and Leonards [38] to study the moduli of sand on the same specimen for shearing strains varying between 10^{-4} and 10%.

While many institutions were conducting limited numbers of tests aimed at investigating a specific topic, it became clear that a broad database covering a large spectrum of stress paths was needed for generators and users of constitutive equations to calibrate and test their models. A database of results of tests conducted in cubical and hollow cylinder devices has been built at Case Western Reserve University with the cooperation of the University of Grenoble, France. Over 200 hollow cylinder test results on granular materials are already part of this data base. All tests were conducted by one small group of researchers with the same state-of-the-art equipment and the same methods of preparation. Test results are available to the scientific community in the proceedings of a workshop on constitutive equations for granular noncohesive soils [39].

The brief historical background given above relates only to research. There are limited published cases indicating the uses of the hollow cylinder device for engineering design purposes [40]. Such work is proprietary in nature. However, many large firms have had hollow cylinder tests conducted for specific projects. Their use will spread as more laboratories acquire the necessary hardware to conduct them. The design information they yield has proven to be extremely valuable to practicing engineers.

The Cell and Its Measuring Devices

Triaxial cells for the application of axial, torsional, internal, and external stresses vary in size and complexity. Most allow the control of the internal and external pressures independently; axial and torsional stresses can also be varied at will. Early cells such as Haythornthwaite's [9] used short and relatively thick samples where the end effects were quite prominent. In others such effects were reduced to a minimum. In general a cell allowing relatively large outside diameter, thin walls, and sample height one and a half to two times this outside diameter will be satisfactory. More details on sample sizes will be given in the following sections.

Practically all of the papers cited in the historical background give a schematic of the cell used by its author. Some are more elaborate than others, but all aim at measuring the variables inside the cell rather than outside. Figure 1 shows a schematic of the cell used at Case Western Reserve University. Most of the refinements in cell design have occurred in

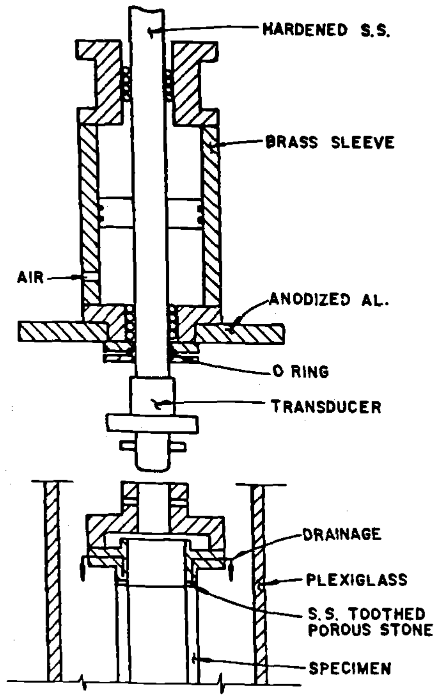

FIG. 1—*Cell for axial and torsional stresses.*

the design of the piston and the minimization of the friction between piston and bushing. The fact that the piston has to rotate relative to the cell introduces additional difficulties. Air bearings, ball and roller bearings with special greases, bellofram, and above all precise machining have improved cell quality. In Fig. 1 the piston assembly is also an actuator and can be used to apply extension to the sample using air pressure. It also rotates, which precludes the use of a bellofram in this part of the machine.

The quantities that are usually measured are the axial force, the torque, the pressures inside and outside the hollow cylinder, the pore water pressure for undrained tests and volume changes for drained tests, the axial deformation, the relative rotation of two sections along the length of the sample, and the changes in inner and outer radii. Here, too, each laboratory has its own set of refined gages. Forces and torques are measured with four arms transducers or load cells; displacements and rotations are measured with linear or rotational differential transformers. Proximity transducers are also being used in pressurized cells to measure displacements. Figure 2 shows an arrangement adopted by Hight et al. [7] to record changes in thickness of the cylinder's walls. Such transducers are not easy to use under the conditions present in a triaxial cell. The target's size, its material, and the curvature of the surface on which it is mounted all have an effect on the readings. Duplication of data from identically conducted tests are hard to achieve. Sometimes the errors involved in accuracy and linearity are of the same order as the deformations to be measured. Bedding errors are very difficult to avoid.

Local axial and shearing strains can be measured on specific parts of the sample. Figure 3 shows electrolevels being used to measure vertical and circumferential displacements [7]. Volume changes are measured by water expulsion in saturated samples and also by noting the height of the cell's fluid inside and outside the cylinder and calculating the changes in

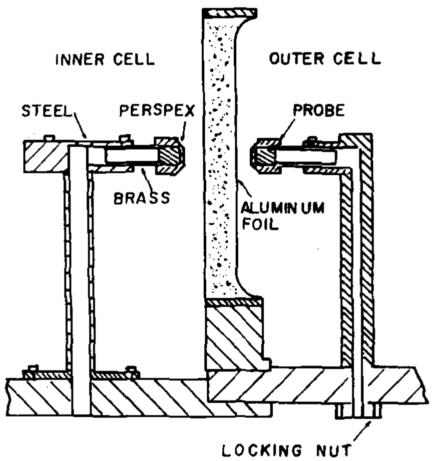

FIG. 2—*Proximity gages for thickness measurements* [7].

the radii. But then the assumption of uniform deformation has to be made and the accuracies of 1 μm claimed by many authors become meaningless. Tatsuoka [*41*] in his state-of-the-art paper touches on some of these points in slightly more detail. Measuring gages and probes may have high resolution, but within the context of triaxial tests where membranes are being used, the publication of such resolutions may lead to a false sense of accuracy.

Practicality and convenience affect cell design. A large size allows one to install a wide variety of gages and sensors. A large internal diameter is needed to place proximity gages inside the cylinder [7]. This in turn necessitates a tall sample to avoid undesirable end effects. Such sizes may be used for sand specimens but are impossible to use for disturbed or undisturbed clay specimens. The author has adopted in his laboratory a size of cell that can accommodate a standard Shelby tube. In this case the use of proximity gages inside the cylinder is impossible, but an integrated approach in testing soils under static and dynamic conditions can be accomplished easily [*34*].

The soil specimen is usually fixed to the top and bottom caps by radial thin teeth about 3 to 5 mm high, fixed to the porous stones. These stones are themselves fastened to the

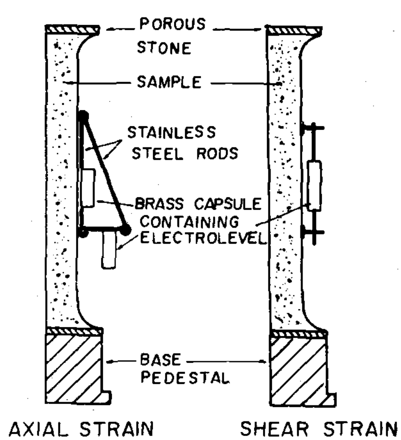

FIG. 3—*Axial and shear strain measurements* [7].

heads. Experience of the author and many others has shown that under hydrostatic stress this system provides positive, no-slip contact. To avoid failure from being initiated at the teeth, some authors have enlarged their specimens at the ends [*7*]. Coarse sand particles have also been glued to the annular porous stones to improve frictional characteristics at the interface.

The cells are placed in loading frames where mechanical or fluidic elements provide the driving forces and torques or the induced deformations and rotations. Each of the authors mentioned in the historical review describes his own set-up with its elaborate data acquisition system. In resonant columns electromagnets induce the necessary vibrations [*1,25,34*].

Sample Preparation

Various techniques have been developed to prepare clay hollow cylinders from both disturbed and undisturbed materials. Hvorslev [*42*] shows schematically a simple mold he used to cut short hollow disks. The idea was extended by Saada [*10*]. Figure 4 shows the succession of steps used to prepare a hollow cylinder from a block of clay obtained by one-

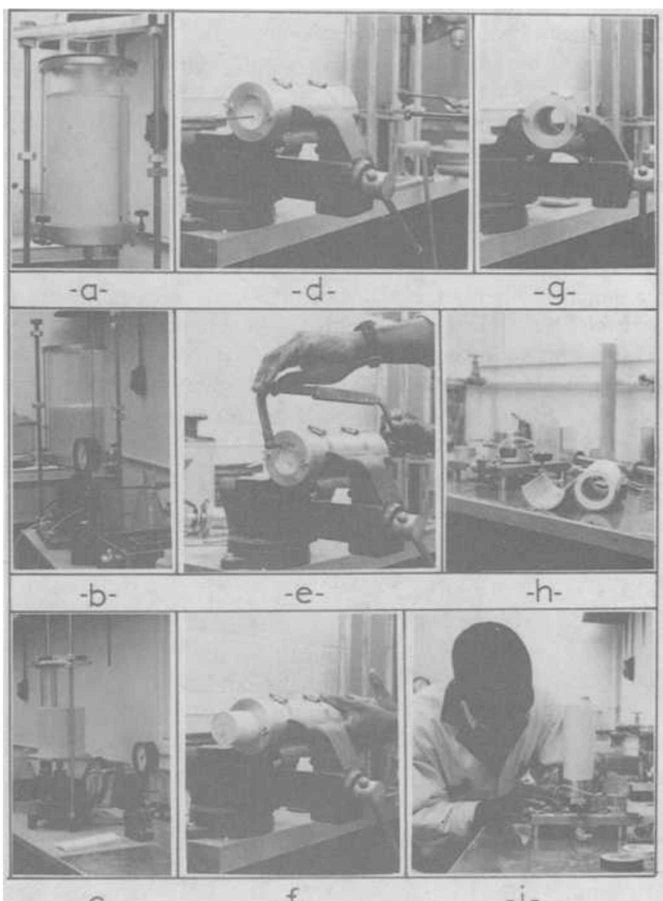

FIG. 4—*Preparation of clay hollow cylindrical specimens* [10].

dimensional consolidation of a slurry. The same technique has been applied to undisturbed clay cylinders. It is valid for any material that one can cut with a piano wire. If the clay is sensitive, the templates at the ends of the split mold in Fig. 4*d* are made with an internal diameter smaller than the required one. Thus, after the core is pushed out (Fig. 4*f*), the local disturbed zone can be removed by having the piano wire follow a larger template. This larger template is made to the required size of the core to be cut out of the solid cylinder. This technique of successive coring has been quite successful with clayey silts. Samples can even be drilled initially with a bit half the size of the required hole—the final size being achieved by successive "peeling" with blades following larger and larger end templates.

Sand specimens are prepared by pluviation or tamping. Pluviation is often followed by vertical or horizontal vibration to reach a certain density. Generally, pluviation will result in a material with cross anisotropic properties. Vertical vibration at less than 1 g will not change the density much; above 1 g the density will increase and the material will keep its cross anisotropic properties. Tamping will destroy most of the anisotropy produced during pluviation and result in a material that responds isotropically to a hydrostatic state of stress. Sample preparation has been studied by Mulilis et al. [*43*], and their remarks apply to hollow cylinders. However, there seems to be a difference resulting from pouring sands between two close walls and pouring them in a large open container like a solid cylinder or a cube. Recent experience in trying to duplicate samples in a cubical specimen and in a hollow cylinder showed that during pouring, the freedom in the third dimension resulted in specimens with more tendency to react isotropically. Figures 5*a* and 5*e* show the successive steps

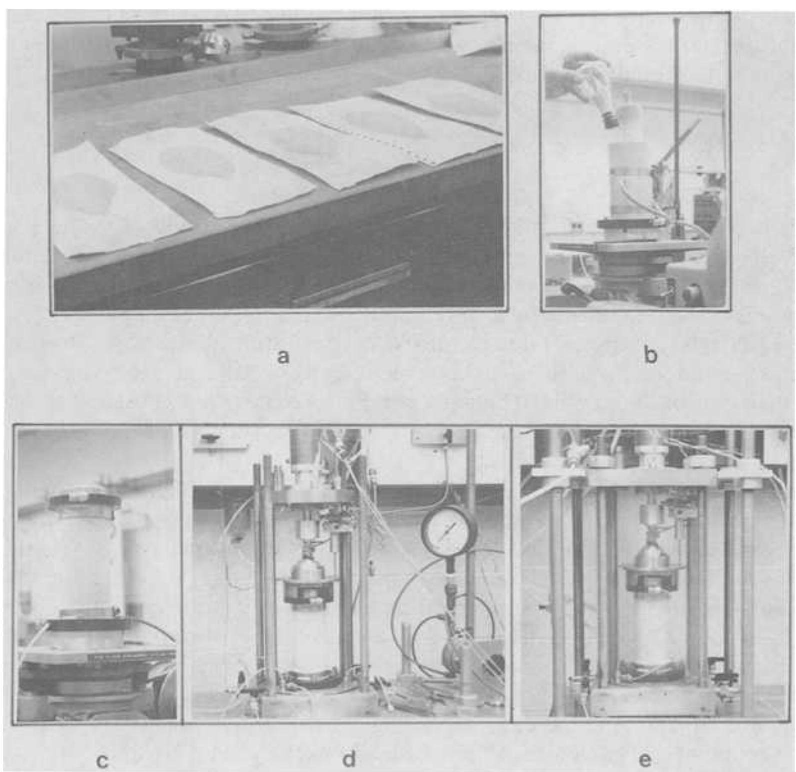

FIG. 5—*Preparation of sand hollow cylindrical specimens* [39].

in preparing sand samples at Case Western Reserve University: The total weight of the sand entering in a specimen is divided in several parts to be poured and vibrated (or poured and tamped) in succession. Vacuum is used, first to hold the membranes against the inner and outer molds and then to keep the sample from collapsing during placement in the cell and saturation.

Specimen Dimensions and Boundary Effects

In the hollow cylinder, geometry affects the uniformity of the stress distribution. Radial frictional forces are developed at the ends of the specimen if it has a tendency to expand or contract. This tendency is always present when there is volume change or a change in length at constant volume. The radial frictional forces are self-equilibrating and their influence vanishes as one moves away from the end platens. St. Venant's principle, which is often invoked to dismiss the effects of end platens, requires a certain minimum distance from the end platens to become operative. In the triaxial test on solid circular cylinders, it is customary to consider that a length-to-diameter ratio of 2.5 to 1 is adequate for routine testing. For hollow cylinders, in addition to the thickness, the mean radius plays an extremely important part in the determination of the proper dimensions. The radial frictional forces imposed upon the specimen by the platens cause circumferential normal forces (hoop forces), shearing forces, and bending moments whose magnitude decreases rapidly as one moves away from the ends. Using the equations of the theory of thin elastic cylindrical shells, it is possible to gain insight concerning the relative magnitude of the stresses and their relation to the generating frictional force [*44*]. The author did just that in 1981 [*1*] and reached the conclusion that to have, in a sample, a reasonable central zone free from end effects the following criteria should be satisfied:

$$H \geqslant 5.44\sqrt{R_o - R_i} \quad \text{and} \quad n = \frac{R_i}{R_o} \geqslant 0.65 \tag{1}$$

where H is the height and R_o and R_i are the outer and inner radii of the test specimen, respectively. Lade [*18*] showed experimentally, however, that the above criterion is conservative and that beyond a height equal to about 1.5 times the mean radius not much accuracy was gained. Similar results were found by Hight, Gens, and Symes [*7*] and Gens and Potts [*45*] who conducted finite elements analyses, using elastic as well as elastoplastic constitutive equations. In their case, however, they adopted a height nearly equal to the outside diameter of the sample. The author in his laboratory has chosen H to be close to or higher than 1.5 R_o and a ratio $n = 0.71$. Table 1 gives the dimensions used by many of the investigators referred to in this paper.

There are two ways in which the membranes affect test results. The first is related to the torsional resistance of the inner and outer membranes. This resistance is calculated using the theory of elasticity with a Poisson ratio for the membrane equal to 0.5. While Tatsuoka et al. [*37*] list the equations they used with their own notation, it is more appropriate to refer to any text on elasticity or strength of material [*44*] for such equations. The second is related to membrane penetration. This penetration is estimated with various equations and affects volume change measurements and pore water pressures in drained and undrained tests, respectively. This influence increases with the particles size for granular material, especially if the pressure in the cell rises during a test. Various equations to estimate those effects in terms of the grain size are available. Tatsuoka et al. [*37*] found the corrections suggested by Raju and Sadaswan [*46*] quite satisfactory, and Kiekbusch and Schuppener [*47*] confirmed the relation of Frydman et al. [*48*]. In the hollow cylinder the area exposed

TABLE 1—*Summary of dimensions of hollow cylinders.*

Reference	Dimensions, mm		
	I.D.	O.D.	*H*
Broms and Casbarian [*8*]	76	127	254
Saada and co-workers [*10,13,25,34,40*]	51	71	127 to 177
Lomize et al. [*14*]	250	310	180
Lade [*17*]	180	220	50
Lade [*18*]	180	220	100 to 400
Ishihara and Yasuda [*22*]	60	100	70
Ishihara et al. [*26*]	60	100	106
Tatsuoka, Muramatsu, and Sasaki [*30*]	60	100	100
Hight, Gens, and Symes [*7*]	203	254	254
Miura, Miura, and Toki [*36*]	30	50	200
Tatsuoka et al. [*37*]	30	50	200
Alarcon, Chameau, and Leonards [*38*]	38	71	200
	71	100	200

to the membrane is large, and some sort of correction is needed for coarse sands. There does not seem to be a general agreement on which equation is the most suitable; for some time this will depend on the mood of the researcher.

Stress Distribution, Measured and Calculated Stresses and Strains

The combination of axial and torsional stresses leads to principal stresses that are inclined on the axes of symmetry of the material (Fig. 6). The interpretation of test results is made in terms of averages. Average values of stresses and strains have generally been calculated with the assumption that the work done by the applied forces and torques is equal to the sum of the work done by the stresses and strains involved. They are as follows (see Fig. 7):

$$\text{Average axial stress } \sigma_z = \frac{F_{ax}}{\pi(R_o^2 - R_i^2)} + \frac{P_o R_o^2 - P_i R_i^2}{R_o^2 - R_i^2} \tag{2}$$

$$\text{Average } \sigma_r = \left.\frac{P_o R_o + P_i R_i}{R_o + R_i}\right\} = P \text{ for } P_i = P_o \tag{3}$$

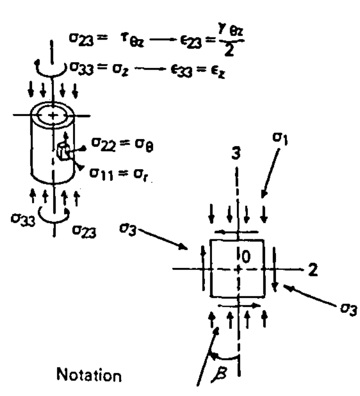

FIG. 6—*System of stresses and reference axes* [1].

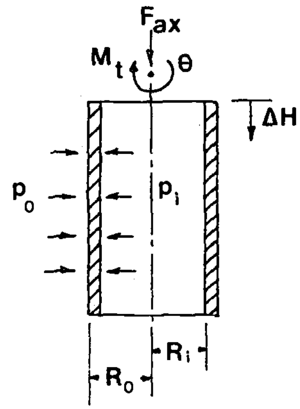

FIG. 7—*Notation.*

$$\text{Average } \sigma_\theta = \frac{P_oR_o - P_iR_i}{R_o - R_i} \tag{4}$$

$$\text{Average } \tau_{\theta z} = \frac{3M_t}{2\pi(R_o^3 - R_i^3)} \tag{5}$$

$$\text{Average } \epsilon_z = \frac{\Delta H}{H} \tag{6}$$

$$\text{Average } \epsilon_r = -\frac{u_o - u_i}{R_o - R_i} \tag{7}$$

$$\text{Average } \epsilon_\theta = -\frac{u_o + u_i}{R_o - R_i} \tag{8}$$

$$\text{Average } \gamma_{\theta z} = \frac{2\theta(R_o^3 - R_i^3)}{3H(R_o^2 - R_i^2)} \tag{9}$$

These values appear in many of the manuals on strength of materials. It must be noted that average values of σ_z and σ_θ are based on equilibrium equations only, and average values of ϵ_z and $\gamma_{\theta z}$ are based on strain compatibility only; all are therefore independent of the constitutive laws of the material being tested. The expression for the average value of σ_r is based on a linear elastic stress distribution; the average σ_z is based on a uniform stress distribution; the average ϵ_r and ϵ_θ are based on a linear variation of radial displacement across the wall.

It must be noted that the equation of equilibrium in the radial direction yields

$$\frac{d\sigma_r}{dr} + \frac{\sigma_r - \sigma_\theta}{r} = 0 \tag{10}$$

and if the same pressure acts inside and outside the cylinder, that is $P_i = P_o = P$, then it is quite proper to assume that there is no variation in the value of the normal radial stress

σ_r across the thickness. Thus $d\sigma_r/dr = 0$ and $\sigma_r = \sigma_\theta = P$. Also the compatibility equation in the $[r,\theta]$ plane yields

$$\frac{d\epsilon_\theta}{dr} + \frac{1}{r}(\epsilon_\theta - \epsilon_r) = 0 \tag{11}$$

and if one assumes that ϵ_θ is uniform across the thickness, then $\epsilon_\theta = \epsilon_r$. This leads to a linear variation of the radial displacement across the wall.

There are implications connected to $\epsilon_r = \epsilon_\theta$ if one uses classical plasticity theory in expressing stress–strain relations. It places restrictions on the shape of the potential functions. A detailed study of those implications can be found in a discussion written by Lade and in the closure of the author at the end of this paper.

The author is not in favor of using different inner and outer pressures P_i and P_o because this necessarily leads to nonuniform normal stresses across the sample which result in different axial strains due to Poisson's effects. Because the end platens are rigid, the result is nonuniform axial stresses. Unfortunately, these nonuniformities are to be added to those caused by the nonuniform torsional stresses which will induce nonuniform volume changes, and as such, nonuniform normal strains ϵ_r, ϵ_θ, and ϵ_z.

In their rebuttal to the author's discussion, Symes et al. [*49*] justify the use of different internal and external pressures through the need for separating the effects of σ_2 from those of the inclination of the principal stresses. We believe that this is done at too high a price in accuracy. For anisotropic materials the effects of σ_2 can be studied with cubical devices if one insists on keeping the mean stress constant. The coefficient $b = \sigma_2 - \sigma_3/\sigma_1 - \sigma_3 =$

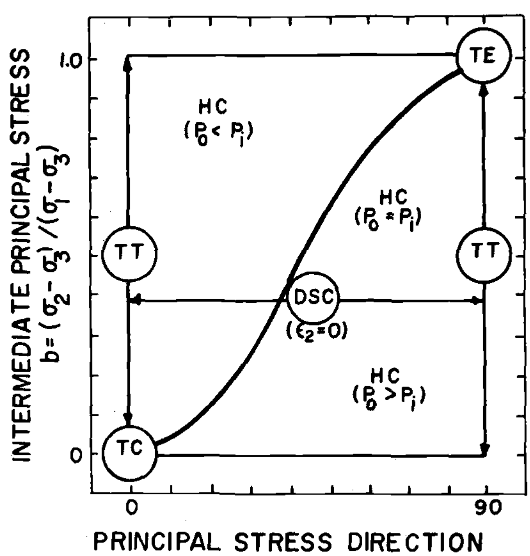

DSC = DIRECTIONAL SHEAR CELL
HC = HOLLOW CYLINDER (VARYING σ_3, $\tau_{r\theta}$, P_o & P_i)
TC = TRIAXIAL COMPRESSION
TE = TRIAXIAL EXTENSION
TT = TRUE TRIAXIAL

FIG. 8— *Combination of* b *and* β *achieved in various devices* [50].

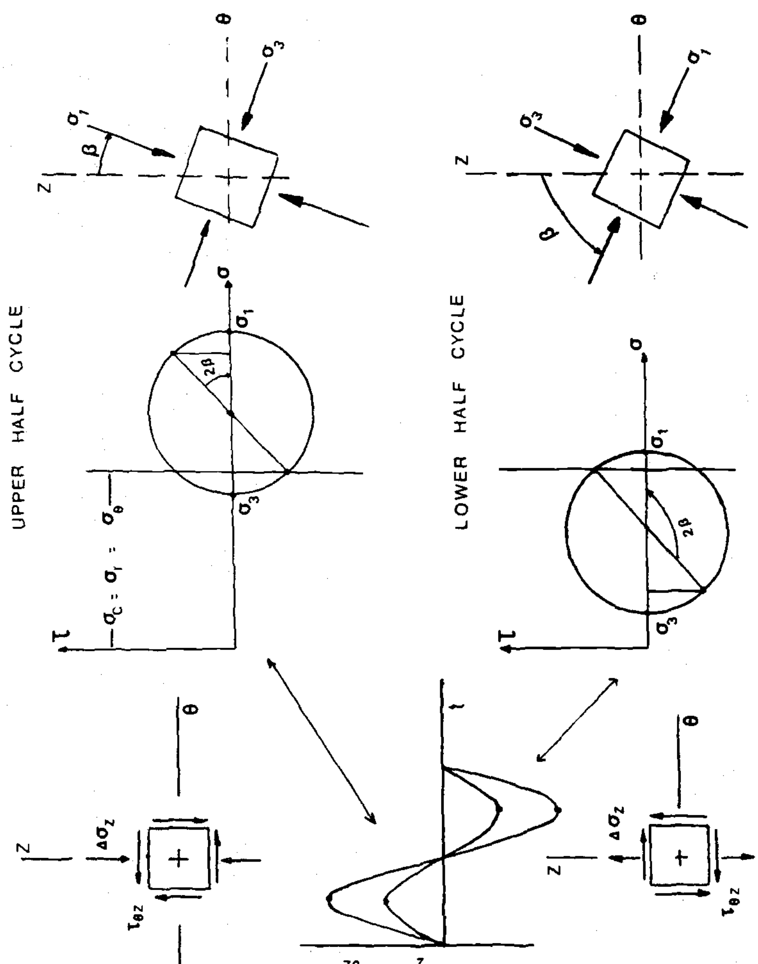

FIG. 9—*Mohr circles for continuously rotating principal stresses.*

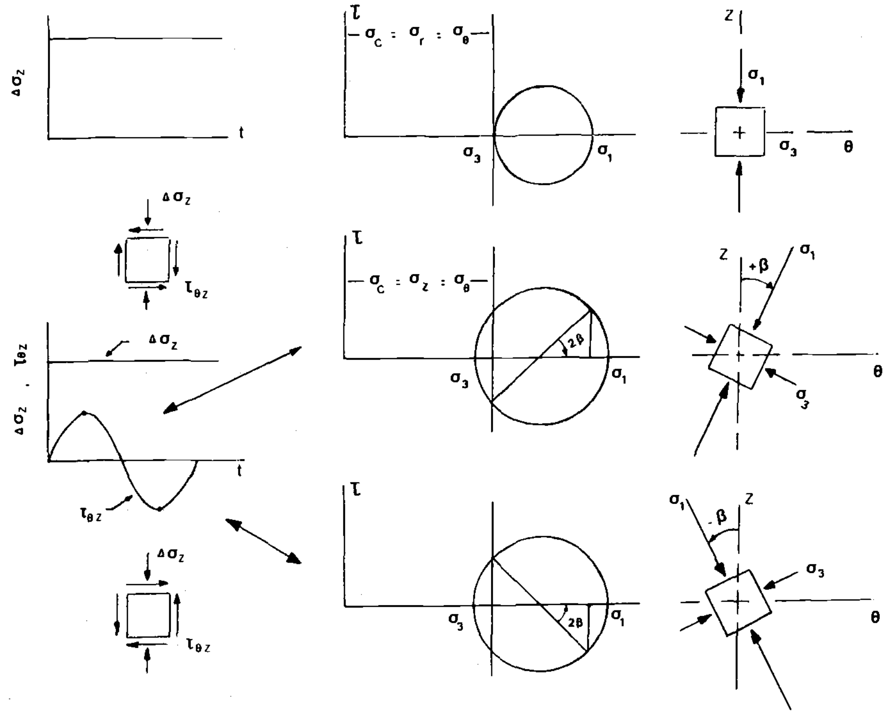

FIG. 10—*Mohr circles for synchronized proportional loading.*

$\sin^2 \beta$ is often used to place the relative magnitude of σ_2 with respect to σ_1 and σ_3. In the hollow cylinder with the same P_o and P_i it can only be changed by changing the inclination of the principal stresses. Figure 8 shows the relation between b and β with an eye on P_o and P_i [*50*].

Stress Paths and Constitutive Equations

The search for a set of constitutive equations that would be applicable to all soils has been going on for years. At the heart of the search are the calibration of the model through the use of some simple triaxial experiments, the prediction of results for complicated stress paths, and the comparison of those predictions to the actual results obtained in controlled

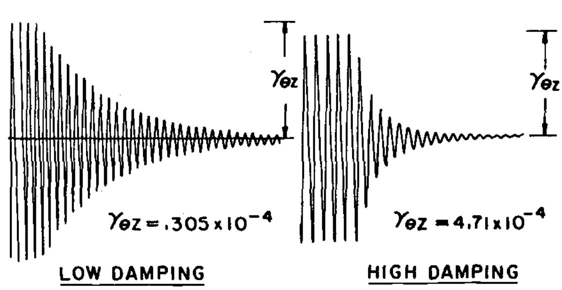

FIG. 11—*Amplitude decay in resonant column tests* [51].

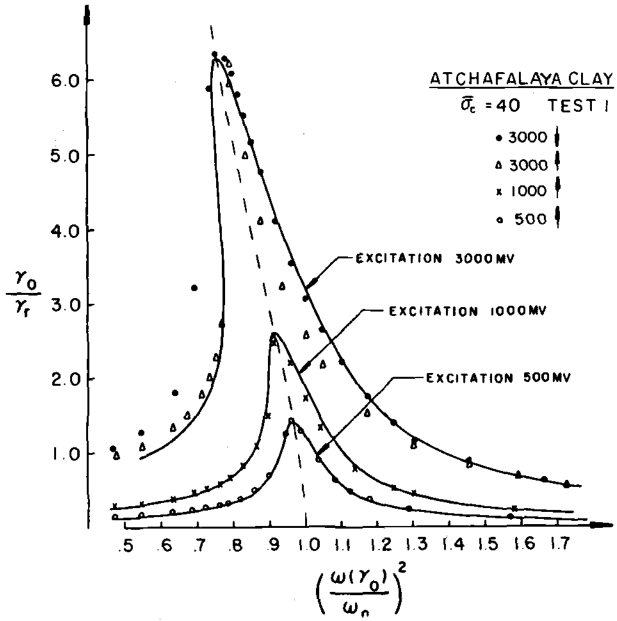

FIG. 12—*Frequency response of Atchafalaya clay showing potential instabilities in the behavior* [52].

laboratory environments. Whether the material studied is isotropic or anisotropic, the hollow cylinder can provide as complicated a path as necessary to test the validity of any model. Paths that often occur in the field involve combinations of vertical normal and horizontal shearing stresses; both stresses can be fixed or variable: The hollow cylinder can duplicate those conditions very well. In dynamic behavior, the normal and shearing stresses can be in or out of phase, and the spectrum that occurs during earthquakes is unpredictable. With proper computer-regulated drives, measured intensities and modes can be applied easily to a specimen.

One usually starts with a state of hydrostatic stress in hollow cylinder testing. At this stage $\sigma_r = \sigma_\theta = \sigma_z$. The addition of axial and torsional stresses will cause a rotation of the major and minor principal stresses as shown in Fig. 6. If the ratio $\Delta\tau_{\theta z}/\Delta\sigma_z$ remains constant, the inclination β remains constant, and one has a case of proportional stressing; if not, σ_1 and σ_3 rotate. $\sigma_2 = \sigma_r = \sigma_c$, the pressure in the cell. Changing the cell pressure will change σ_2. If the test is undrained the effective value of σ_2 will not change when the cell pressure is changed. If one starts by consolidating a specimen anisotropically, such as under K_o

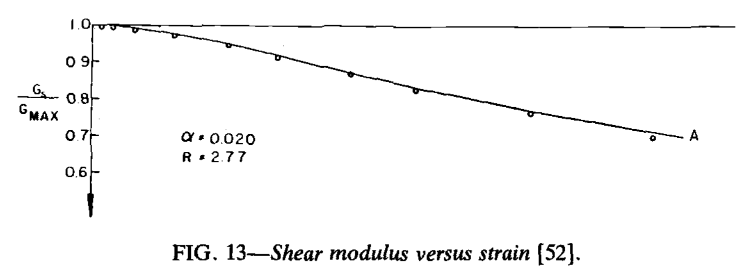

FIG. 13—*Shear modulus versus strain* [52].

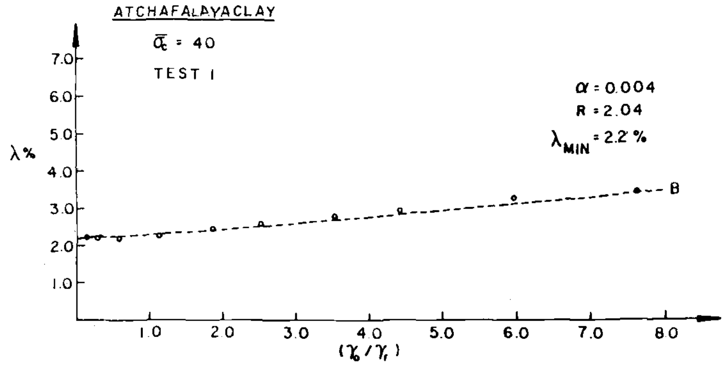

FIG. 14—*Damping ratio versus strain* [52].

conditions, any additional torsion will cause changes in β. In research work it is often necessary to fix the directions of the principal stresses with respect to the axes of symmetry of the material and study the directions of the principal strains or their increments. This is achieved by keeping the ratio of axial to torsional stresses constant during a test. Indeed for a thin long hollow cylinder subjected to the same inner and outer pressure in the triaxial cell, as well as to additional axial and torsional stresses, the change in principal stresses and their directions are given by (see Fig. 6):

$$\Delta\sigma_1 = \frac{\Delta\sigma_z + \Delta\sigma_\theta}{2} + \sqrt{\left(\frac{\Delta\sigma_z - \Delta\sigma_\theta}{2}\right)^2 + \Delta\tau_{\theta z}{}^2} \tag{12}$$

$$\Delta\sigma_3 = \frac{\Delta\sigma_z + \Delta\sigma_\theta}{2} - \sqrt{\left(\frac{\Delta\sigma_z - \Delta\sigma_\theta}{2}\right)^2 + \Delta\tau_{\theta z}{}^2} \tag{13}$$

$$\frac{1}{2}\tan 2\beta = \frac{\Delta\tau_{\theta z}}{\Delta\sigma_z - \Delta\sigma_\theta} \tag{14}$$

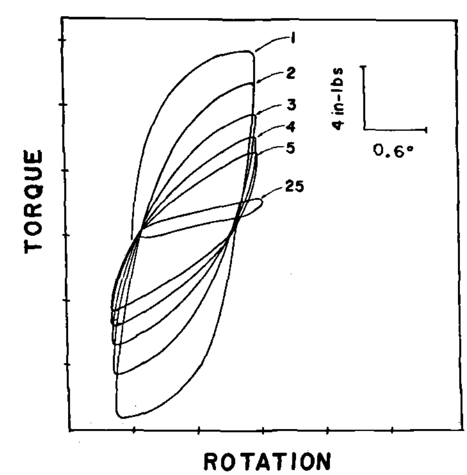

FIG. 15—*Degradation of shear modulus during liquefaction test* [40].

The major and minor principal stresses are always in the vertical plane and equal to the values of Eq 12 and Eq 13 plus the cell pressure. The intermediate principal stress, $\sigma_2 = \sigma_r$, is always radial, never changes direction, and is equal to σ_θ, both being equal to the pressure in the cell. If the pressure in the cell changes, so will σ_2, σ_r, and σ_θ, in addition, of course, to σ_z. If the pressure in the cell remains constant and the axial and torsional stresses are changed so that their ratio remains constant, Eq 14 gives

$$\frac{1}{2}\tan 2\beta = \frac{\Delta\tau_{\theta z}}{\Delta\sigma_z} = K \tag{15}$$

showing that β remains constant; the cell pressure acting equally in all directions has no effect on the direction. Equations 12 and 13 become

$$\Delta\sigma_1 = \frac{\Delta\sigma_z}{2}(1 + \sqrt{1 + 4K^2}) \tag{16}$$

$$\Delta\sigma_3 = \frac{\Delta\sigma_z}{2}(1 - \sqrt{1 + 4K^2}) \tag{17}$$

$$\Delta\sigma_2 = 0 \tag{18}$$

Under these conditions, the tests would not only proceed at a constant inclination of σ_1, σ_2, σ_3, but also at a constant ratio $\Delta\sigma_1$: $\Delta\sigma_2$: $\Delta\sigma_3$, all fixed by choice of K.

If the pressure in the cell changes by an amount that is also proportional to the change in the axial stress, the properties stated earlier still hold. Consider, for example, a test in which the mean stress is to remain constant. In this case the cell pressure is decreased, say, and the axial pressure is increased in the ratio of 2 to 1. Equation 14 gives

$$\frac{1}{2}\tan 2\beta = \frac{\Delta\tau_{\theta z}}{\Delta\sigma_z + \dfrac{\Delta\sigma_z}{2}} = \frac{\Delta\tau_{\theta z}}{\dfrac{3}{2}\Delta\sigma_z} = K \tag{19}$$

Equations 12 and 13 become

$$\Delta\sigma_1 = \frac{\Delta\sigma_z}{2}\left(\frac{1}{2} + \frac{3}{2}\sqrt{1 + 4K^2}\right) \tag{20}$$

$$\Delta\sigma_3 = \frac{\Delta\sigma_z}{2}\left(\frac{1}{2} - \frac{3}{2}\sqrt{1 + 4K^2}\right) \tag{21}$$

$$\Delta\sigma_2 = -\frac{\Delta\sigma_z}{2} \tag{22}$$

Here again, the test will proceed at a constant inclination of σ_1, σ_2, σ_3 and at a constant ratio $\Delta\sigma_1$: $\Delta\sigma_2$; $\Delta\sigma_3$, all fixed by the value of K.

The possibilities offered by the use of a thin hollow cylinder subjected to combinations of axial, torsional, and spherical stresses are practically unlimited. For example, two identical tests with the same inclination of principal stresses on the axis of symmetry can be conducted, one at a constant σ_2 and the other with a variable one, to study the effects of the intermediate

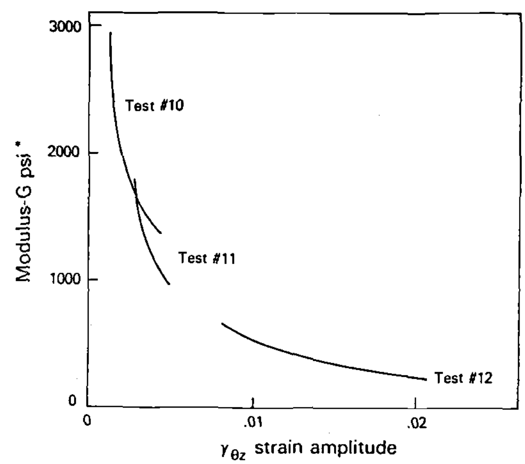

FIG. 16—*Degradation of shear modulus with strain for different frequencies and axial load* [33].

principal stress. An examination of Eqs 16 to 22 shows that the two tests would have the same $b = (\sigma_2 - \sigma_3)/(\sigma_1 - \sigma_3)$ in spite of the fact that in one σ_2 is constant and in the other σ_2 varies continuously [*13*].

It is traditional in soil mechanics to represent the state of stress at a point by means of Mohr's construction. Ideally a test specimen is a point, if one assumes a uniform distribution of the state of stress in it and on its boundaries. Figure 9 shows Mohr circles for synchronized sinusoidal cyclic loading. During each half cycle the directions of the principal stresses remain constant. Figure 10 shows Mohr circles, first for an initial increase of axial stress, then for a superimposed cyclic torsional stress at points of maximum and minimum shearing stresses. The direction of σ_1 fluctuates between $+\beta$ and $-\beta$.

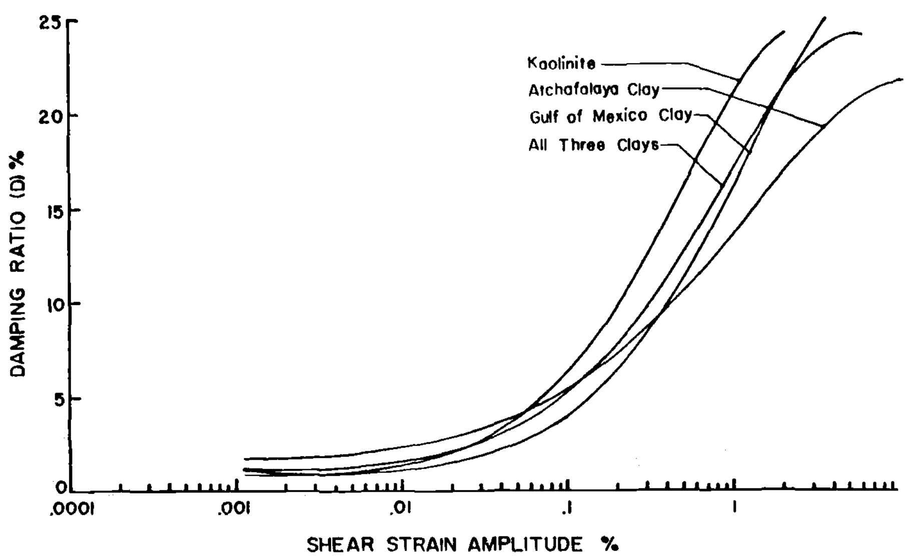

FIG. 17—*Damping ratios at large strain.*

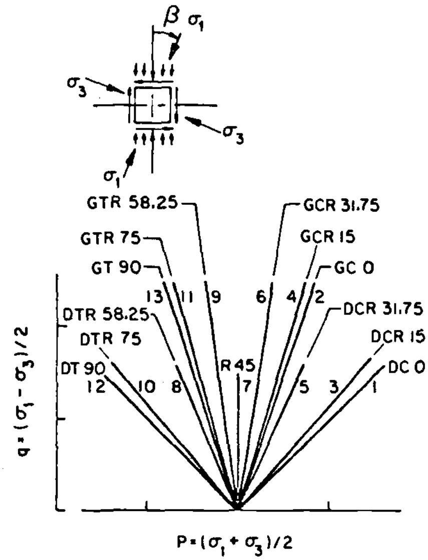

FIG. 18—*Total stress paths under proportional stressing in the hollow cylinder.*

It is worth mentioning that the material's anisotropy can be detected by subjecting the specimen to a change in hydrostatic stress and measuring the deformations. If the three principal strains are unequal ($\sigma_z \neq \sigma_r = \sigma_\theta$), then the material is anisotropic. For a linearly elastic isotropic material the directions of the principal stresses and principal strains coincide. This, however, is not true for plastic materials where the directions of the principal strains do not necessarily coincide with the directions of the principal stresses.

Some Examples of Stress Paths and Failure Patterns Obtained with Hollow Cylinders

This section is included for the sake of completeness and was requested by the reviewers of this paper. Like the rest of this state-of-the-art paper, its contents can be found in papers previously referred to by the author. There is merit, however, in having typical graphs representing test results under various conditions, if only to give the reader an idea of what "in general" one should expect from a test.

Resonant Column Tests

Figures 11 to 14 show the form of the decay curves for low and high strain, the frequency response with the instability due to nonlinearity, the shearing modulus variation with strain, and the damping ratio variation with strain [*51,52*]. While these curves relate to clays, sands give similar shapes.

Slow Cyclic Loading

These tests are used to study moduli and damping under large strains as well as to simulate conditions during earthquakes or under offshore structures. Figure 15 shows the degradation

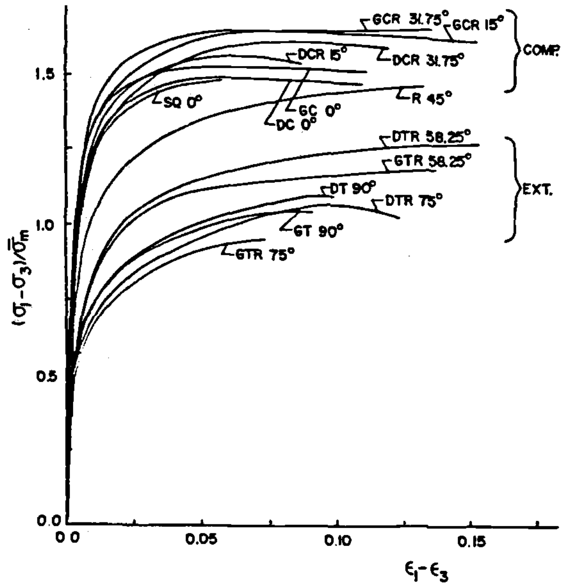

FIG. 19—*Normalized stress-strain relations for anisotropic sand* [49].

of the shear modulus during the undrained torsional cyclic testing of a loose Latin American sand under controlled strained conditions; the pore water pressure generated reached the cell pressure after 20 cycles. Figure 16 shows the degradation of the shear modulus with strain for three tests on a Beaufort Sea (in Alaska) clay [*40*]. For the test marked #10 in Fig. 16 the frequency of the pure torsional stresses was 1 cpm; for test #11, the frequency was 0.2 cpm; for test #12 the cyclic torsion was coupled synchronously with a cyclic axial load at 1 cpm. Figure 17 shows damping versus strain for two undisturbed and one disturbed clay.

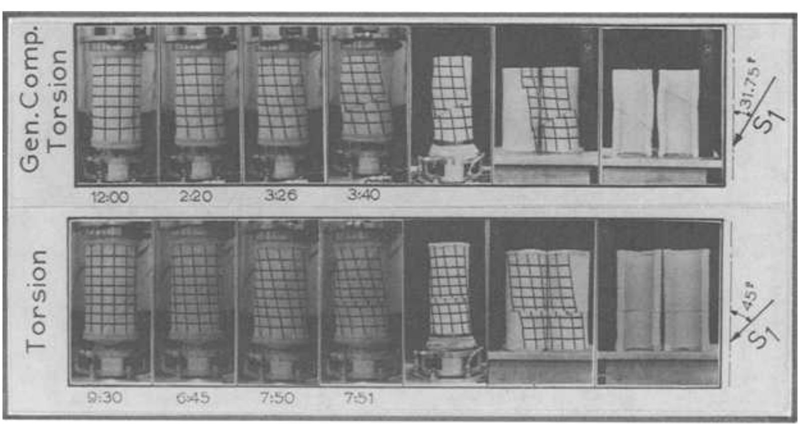

FIG. 20—*Deformation and failure patterns of kaolinite hollow cylinder for* β *=* 31.75° *and* β *=* 45°.

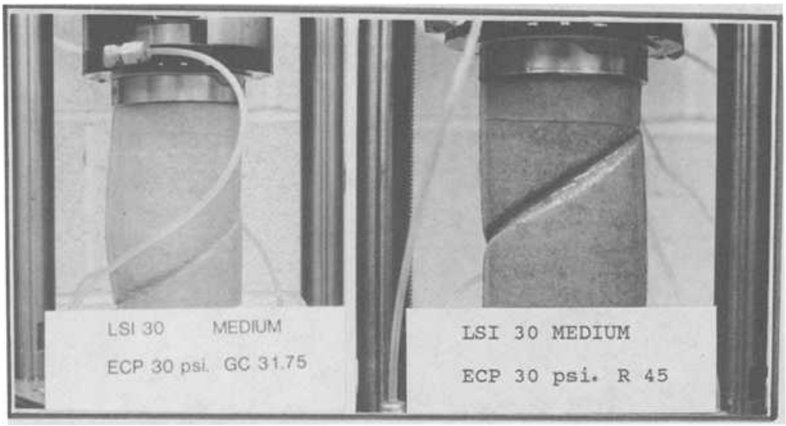

FIG. 21—*Failure patterns of sand hollow cylinder for* β = *31.75°* *and* β = *45°*.

Static Tests

As mentioned previously, the number of stress paths that one can get through combinations of axial and torsional stress is practically unlimited. Figures 18 and 19 show the effective stress paths and the stress–strain curves of a sand subjected to fixed ratios of torsional to normal stress differences [*49*]. Each ratio corresponds to a fixed inclination of the principal stresses on the vertical axis of symmetry. The angles β are shown at the end of the lettered denominations.

To get a good picture of the patterns of deformation and failure, grids have often been drawn either on the membranes surrounding samples or on the filter paper under the membranes. Figure 20 shows a succession of photographs for tests on clays. The first set corresponds to a combination of equal compression and torsional stresses (β = 31.75°) and the second set corresponds to pure torsion (β = 45°). Notice the inclination of the failure

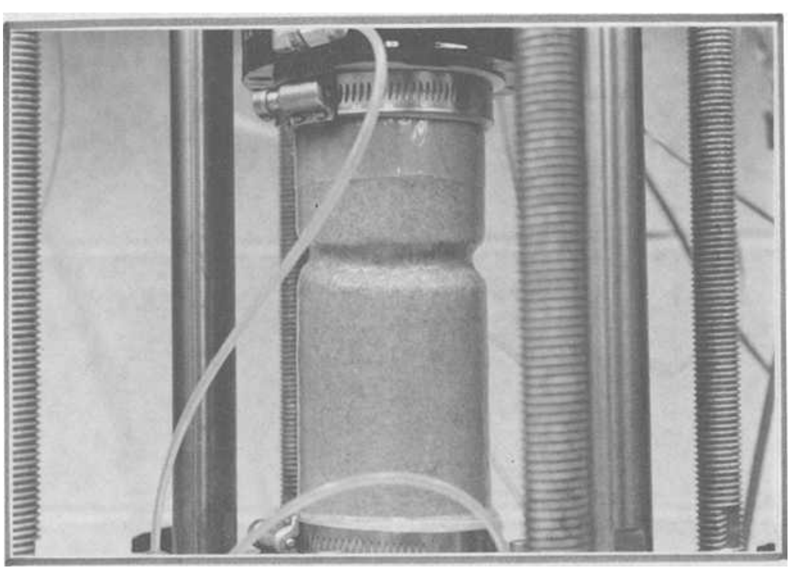

FIG. 22—*Hollow cylinder instability in tension.*

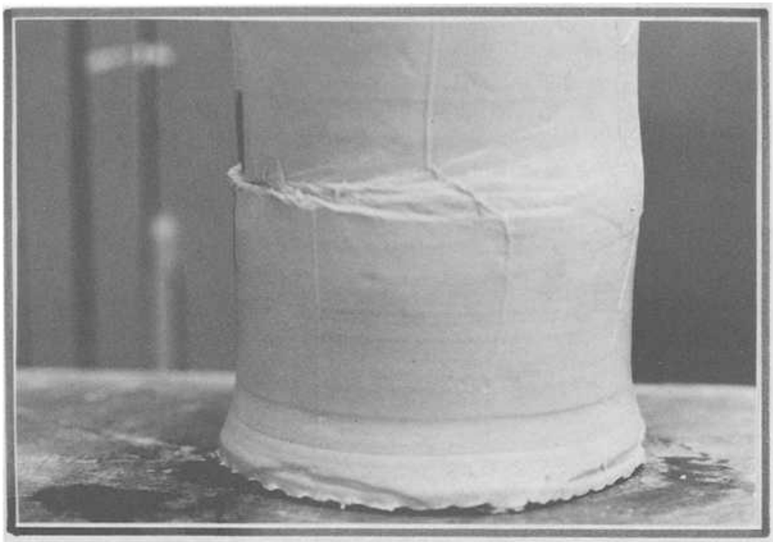

FIG. 23—*Crack and damage propagation in mode II.*

surfaces in both cases. Figure 21 shows the failure surfaces for sand for the same previous inclinations. A comparison of the inclinations of the failure surfaces between sand and clay is worth pointing out especially for $\beta = 45°$.

Finally, as is the case in the traditional triaxial cell, instabilities occur during tests where extension is the main mode of failure. Up to an inclination of $\beta = 58°$ where the magnitude of the shearing stress is equal to that of the tensile stress, the torsional mode is often dominant. Beyond that, and of course for the pure extension test corresponding to $\beta = 90°$, necking takes place. The tensile strength as measured by this test is noticeably decreased. Tests conducted in cubical devices with solid faces have shown that the strengths obtained in the cube are generally higher; however, they have their own instabilities which occur under the form of bifurcations. Figure 22 shows the instability in an extension mode.

While it is not suggested that the hollow cylinder device be used for routine testing, it can become an invaluable tool in studying the behavior of special materials under delicate conditions. Recently, undisturbed samples from the Beaufort Sea [*40*] were subjected to a variety of stress systems expected to take place under an offshore platform. The results showed that the shear strength from pure torsion (simple shear) was twice as high as that obtained from conventional triaxial compression, and the degradation of the shear modulus was found to be very highly influenced by a small cyclic axial load. Both those results have a profound influence on the recommended design values.

It is not easy to cut hollow cylinders from blocks of very stiff clays, but it is not impossible either. By using the proper tools and appropriate care the author and his co-workers have even cut "undisturbed" samples of cemented silt.

Finally it must be mentioned that some new areas in soil mechanics are presently being investigated using the hollow cylinder. Crack and damage zone propagation in stiff clays is being studied at Case Western Reserve University [*53*] and the rules of thermodynamics of irreversible processes are being applied. Because of the possibility of applying hydrostatic stresses, pure mode II fracture has been obtained using pure torsion. This is rather unique because it is practically impossible to obtain such a mode by itself in other engineering materials. Figure 23 shows photographs of damage propagation in front of a crack in a hollow cylinder under mode II condition.

Conclusions

This state-of-the-art paper has focused on the advantages and limitations of the long hollow cylinder device. Its potential for both research and industry applications is enormous. It is in the same position the conventional triaxial test was 25 years ago. Then, only universities were supposed to be able to conduct this test. Many reasons were put forth to perpetuate the use of the shear box: Engineering practice, the need for a ball-park value, the lack of education of laboratory technicians, and so forth, all causing only a slight delay in the triaxial test replacing the shear box. Today we hear the same reasons for not using the hollow cylinder device from many of the present users of triaxial and simple shear tests. In the end, researchers and engineers slowly but surely adapt to new devices which invariably find their proper place in our design arsenal.

References

[1] Saada, A. S. and Townsend, F. C., in *Laboratory Shear Strength of Soil, ASTM STP 740,* American Society for Testing and Materials, Philadelphia, 1981, pp.7–77.

[2] Saada, A. S., *Journal of the Soil Mechanics and Foundations Division, ASCE,* Vol. 96, No. SMS, 1970, pp. 1847–1852.

[3] Taylor, G. I. and Quinney, H., *Philosophical Transactions, Royal Society, London,* A 230, pp. 323–363.

[4] Schmidt, R., "Dissertation Gottingen," 1932.

[5] Cooling, L. F. and Smith, D. B., *Journal of the Institution of Civil Engineers,* Vol. 3, 1935, pp. 333–343.

[6] Geuze, E. C. W. A. and Tan, T. T., in *Proceedings,* Second International Congress on Rheology, V. G. W. Harrison, Ed., Oxford, 1953.

[7] Hight, D. W., Gens, A., and Symes, M. J., *Geotechnique,* Vol. 33, 1983, pp. 355–383.

[8] Broms, B. B. and Casbarian, A. O., in *Proceedings,* Sixth International Conference on Soil Mechanics and Foundation Engineering, Montreal, Vol. 1, 1965, pp. 179–183.

[9] Haythornthwaite, R. M., in *Plasticity,* Pergamon Press, London, 1960, pp. 185–193.

[10] Saada, A. S. and Baah, A. K., in *Proceedings,* Third Pan-American Conference on Soil Mechanics and Foundations Engineering, Caracas, Vol. 1, 1967, pp. 67–88.

[11] Saada, A. S. and Zamani, K. K., in *Proceedings,* Seventh International Conference on Soil Mechanics and Foundation Engineering, Mexico, Vol. 1969, pp. 351–359.

[12] Saada, A. S. and Ou, C. C., *Journal of the Soil Mechanics and Foundations Division, ASCE,* Vol. 99, No. SM12, 1973, pp. 1091, 1111.

[13] Saada, A. S. and Bianchini, G. B. *Journal of the Soil Mechanics Division, ASCE,* Vol. 101, No. GT11, 1975, pp. 1151–1164.

[13a] Gol'denblat, I. I., and Kopnov, V. A., Criteria of Strength and Plasticity of Construction Materials, (in Russian) Mashinostroenie, Moscow, U.S.S.R., 1968.

[14] Lomize, G. M. et al., in *Proceedings,* Seventh International Conference on Soil Mechanics and Foundation Engineering, Mexico, Vol. 1, 1969, pp. 257–265.

[15] Yoshinu, Y. and Ohoka, H., in *Proceedings,* Eighth International Conference on Soil Mechanics and Foundation Engineering, Moscow, Vol. 1.2, 1973, pp. 501–506.

[16] Sherif, M. A. and Ishibashi, I., *Journal of the Geotechnical Engineering Division, ASCE,* Vol. 100, No. GT8, 1974, pp. 871–888.

[17] Lade, P. V., "Torsion Shear Test on Cohesionless Soil," in *Proceedings,* Fifth Pan-American Conference on Soil Mechanics and Foundations Engineering, Buenos Aires, 1975.

[18] Lade, P. V., in *Laboratory Shear Strength of Soil, ASTM STP 740,* American Society for Testing and Materials, Philadelphia, 1981, pp. 145–163.

[19] Drnevich, V. P. and Richart, F. E., *Journal of the Soil Mechanics and Foundations Division, ASCE,* Vol. 96, No. SM2, 1970, pp. 453–469.

[20] Drnevich, V. P., *Journal of the Soil Mechanics and Foundations Division, ASCE,* Vol. 98, NO. SM8, 1972, pp. 807–825.

[21] Hardin, B. O. and Drnevich, V. P., *Journal of the Soil Mechanics and Foundations Division, Proceedings of the American Society of Civil Engineers,* Vol. 98, No. SM6, 1972, pp. 603–624.

[22] Ishihara, K. and Yasuda, S., *Soils and Foundations,* Vol. 15, No. 1, 1975, pp. 45–59.

[23] Ladd, C. C., "State-of-the-Art Report," in *Proceedings,* Ninth International Conference on Soil Mechanics and Foundation Engineering, Japan, Vol. 2, 1977, pp. 421–494.
[24] Iwasaki, T., Tatsuoka, F., and Takagi, Y., *Soils and Foundations,* Vol. 18, No. 1, 1978, pp. 39–56.
[25] Saada, A. S., Bianchini, G., and Shook, L. P., in *Proceedings,* Geotechnical Engineering Division Specialty Conference on Earthquake Engineering and Soil Dynamics, ASCE, Vol. 2, 1978, pp. 777–801.
[26] Ishihara, K. et al., Reprint of Annual Meeting of Japanese Society of Soil Mechanics and Foundation Engineering, 1980 (in Japanese).
[27] Saada, A. S. and Shook, L. P., in *Proceedings,* International Conference on Recent Advances in Geotechnical Earthquake Engineering and Soil Dynamics, Vol. 1, 1981, pp. 369–376.
[28] Bianchini, G. F. and Saada, A. S., in *Proceedings,* Tenth International Conference on Soil Mechanics and Foundation Engineering, Stockholm, Vol. 3, pp. 189–192.
[29] Bianchini, G. F., Thesis presented to Case Western Reserve University in partial fulfillment of the requirements for the degree of Doctor of Philosophy, 1982.
[30] Tatsuoka, F., Muramatsu, M., and Sasaki, T., *Soils and Foundations,* Vol. 22, No. 2, 1982, pp. 55–70.
[31] Ray, R. P., "Changes in Shear Modulus and Damping in Cohesionless Soils due to Repeated Loading," thesis presented to the University of Michigan in partial fulfillment of the requirements for the degree of Doctor of Philosophy, 1983.
[32] Symes, M. J. P. R., Gens, A., and Hight, D. W., *Geotechnique,* Vol. 34, No. 1, 1984, pp. 11–27.
[33] Macky, T. A. and Saada, A. S., "Dynamics of Anisotropic Clays Under Large Strains," *Journal of Geotechnical Engineering, Proceedings of the American Society of Civil Engineers,* Vol. 110, No. 4, April 1984, pp. 487–504.
[34] Saada, A. S. and Macky, T. A., *Strength Testing of Marine Sediments, ASTM STP 883,* American Society for Testing and Materials, Philadelphia, 1985, pp. 363–380.
[35] Ishibashi, I., Kawamura, M., and Bhatia, A. M., "Advances in the Art of Testing Soils Under Cyclic Conditions," in *Proceedings,* ASCE Convention, Detroit, 1985, pp. 51–73.
[36] Miura, K., Miura, S., and Toki, S., *Soils and Foundations,* Vol. 26, No. 1, 1986, pp. 36–52.
[37] Tatsuoka, F. et al., *Soils and Foundations,* Vol. 26, No. 4, 1986, pp. 79–97.
[38] Alarcon, A., Chameau, J. L., and Leonards, G. A., *Geotechnical Testing Journal, GTJODJ,* Vol. 9, No. 4, 1986, pp. 204–212.
[39] Saada, A. S. and Bianchini, G. F., in *Proceedings,* International Workshop on Constitutive Equations for Granular Non-Cohesive Soils, Saada and Bianchini, Eds., Balkema, 1988.
[40] Saada, A. S. and Funegard, E., *Proceedings,* First Offshore Mechanics and Arctic Engineering Specialty Symposium on Offshore and Artic Frontiers, ASME, 1986, pp. 137–149.
[41] Tatsuoka, F., "Some Recent Developments in Triaxial Testing Systems for Cohesionless Soils," in this volume, pp. 7–67.
[42] Hvorslev, M. J. and Kaufman, R. I., "Torsion Shear Apparatus and Testing Procedures," Bulletin No. 38, USAE, Waterways Experiment Station, Vicksburg, MS, 1952.
[43] Mulilis, J. P., Chan, C. K., and Seed, H. B., Earthquake Engineering Research Center Report No. 75–18, University of California, Berkeley, 1975.
[44] Saada, A. S., *Elasticity, Theory and Application,* Krieger, Malabar, FL, 1983.
[45] Gens, A. and Potts, D. M., *Engineering Computation,* Vol. 1, No. 2, 1984.
[46] Raju, V. S. and Sadaswan, S. K., *Journal of the Geotechnical Engineering Division, ASCE,* Vol. 100, No. GTA, 1974, pp. 482–489.
[47] Kiekbusch, M. and Schuppener, B., *Journal of the Geotechnical Engineering Division, ASCE,* Vol. 103, No. GT11, 1977, pp. 1267–1279.
[48] Frydman, S., Zeitlin, I. G., and Alpan, I., *Journal of Testing and Evaluation,* Vol. 1, No. 1, 1973, pp. 37–41.
[49] Symes, M. J. P. R., Gens, A., and Hight, D. W., *Geotechnique,* Vol. 35, No. 1, 1985, pp. 78–85.
[50] Jamiolkowksi, M., et al., "Theme Lecture 2," in *Proceedings,* Eleventh International Conference on Soil Mechanics and Foundation Engineering, San Francisco, Vol. 1, 1985, pp. 57–151.
[51] Saada, A. S., and Shook, L. P., in *Proceedings,* Euromech Colloquium 115, Villard-de-Lans, France, 1979, pp. 833–851.
[52] Bianchini, G. F., "Advances in the Art of Testing Soils under Cyclic Conditions," in *Proceedings,* ASCE, Detroit, 1985, pp. 197–231.
[53] Saada, A. S. and Chudnovsky, A., in *Proceedings,* Eleventh International Conference on Soil Mechanics and Foundation Engineering, San Francisco, Vol. 1, 1985, pp. 637–640.

STP977-EB/Nov. 1988

DISCUSSION

P. V. Lade[1] (*written discussion*)—The author has presented a comprehensive review of torsion shear testing of soils. Experimental observations discussed by the author suggest that the two horizontal, normal strains in a hollow cylinder exposed to torsional shear stresses may be equal in magnitude. It may, however, be inappropriate to set these strains equal a priori. This is demonstrated by the following theoretical derivations.

The stresses acting in the hollow cylinder specimen employed in torsion shear tests are shown in Fig. A. Equilibrium in the radial direction expressed in polar coordinates for an element of the specimen requires:

$$\frac{\partial \sigma_r}{\partial r} + \frac{\sigma_r - \sigma_\theta}{r} = 0 \quad (1)$$

in which r = radial distance to a point in the hollow cylinder, σ_r = radial normal stress, and σ_θ = tangential normal stress. The horizontal strain–displacement equations are:

$$\epsilon_r = -\frac{\partial u_r}{\partial r} \quad (2)$$

$$\epsilon_\theta = -\frac{u_r}{r} \quad (3)$$

in which u_r = radial displacement.

Elastic Behavior

For isotropic elastic behavior of soils, Hooke's law provides the following expressions for the horizontal normal stresses:

$$\sigma_r = (\lambda + 2G) \cdot \epsilon_r + \lambda \cdot \epsilon_\theta + \lambda \cdot \epsilon_z \quad (4)$$

$$\sigma_\theta = \lambda \cdot \epsilon_r + (\lambda + 2G) \cdot \epsilon_\theta + \lambda \cdot \epsilon_z \quad (5)$$

in which λ = Lame's constant and G = shear modulus. Since ϵ_z is not a function of the

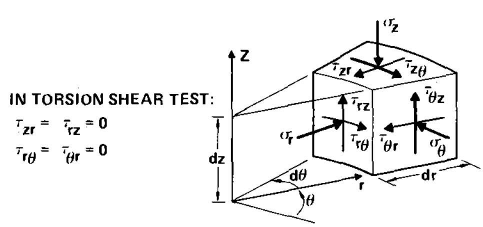

FIG. A—*Stresses acting in hollow cylinder specimen employed in torsion shear tests.*

[1] Professor, Department of Civil Engineering, School of Engineering and Applied Science, University of California, Los Angeles, CA 90024.

radius in a torsion shear tests, Eq 4 yields:

$$\frac{\partial \sigma_r}{\partial r} = (\lambda + 2G) \cdot \frac{\partial \epsilon_r}{\partial r} + \lambda \cdot \frac{\partial \epsilon_\theta}{\partial r} \tag{6}$$

Substitution of Eqs 2 to 6 into Eq 1 produces

$$\frac{\partial^2 u_r}{\partial r^2} + \frac{1}{r} \cdot \frac{\partial u_r}{\partial r} - \frac{u_r}{r^2} = 0 \tag{7}$$

in which substitution of Eqs 2 and 3 yields:

$$-\frac{\partial \epsilon_r}{\partial r} - \frac{\epsilon_r - \epsilon_\theta}{r} = 0 \tag{8}$$

This equation is fulfilled by an elastic hollow cylinder exposed to inside and outside pressures as well as torsional shear stresses. For a thin-walled hollow cylinder the variation in radial strain over the wall thickness is negligible. Equation 8 shows that in this case of elastic behavior the two horizontal normal strains are equal.

Plastic Behavior

Since the relative magnitudes of the horizontal, normal strains are being considered, only the plastic potential function and its derivatives need be considered. For an isotropic material the plastic potential function may be expressed in terms of stress invariants:

$$g = g(I_1, I_2, I_3) \tag{9}$$

in which I_1, I_2, and I_3 are the invariants of the stress tensor:

$$I_1 = \sigma_r + \sigma_\theta + \sigma_z \tag{10}$$

$$I_2 = \tau_{r\theta} \cdot \tau_{\theta r} + \tau_{\theta z} \cdot \tau_{z\theta} + \tau_{zr} \cdot \tau_{rz} - (\sigma_r \cdot \sigma_\theta + \sigma_\theta \cdot \sigma_z + \sigma_z \cdot \sigma_r) \tag{11}$$

$$\begin{aligned} I_3 = {} & \sigma_r \cdot \sigma_\theta \cdot \sigma_z + \tau_{r\theta} \cdot \tau_{\theta z} \cdot \tau_{zr} + \tau_{\theta r} \cdot \tau_{z\theta} \cdot \tau_{rz} \\ & - (\sigma_r \cdot \tau_{\theta z} \cdot \tau_{z\theta} + \sigma_\theta \cdot \tau_{zr} \cdot \tau_{rz} + \sigma_z \cdot \tau_{r\theta} \cdot \tau_{\theta r} \end{aligned} \tag{12}$$

Other stress invariants which encompass similar effects as those in Eqs 10–12 may also be employed.

According to St. Venant's observations the plastic strain increments in the horizontal directions may be written as:

$$\dot{\epsilon}_r^p = \dot{\lambda} \cdot \frac{\partial g}{\partial \sigma_r} \tag{13}$$

$$\dot{\epsilon}_\theta^p = \dot{\lambda} \cdot \frac{\partial g}{\partial \sigma_\theta} \tag{14}$$

in which $\dot{\lambda}$ is a scalar and

$$\frac{\partial g}{\partial \sigma_r} = \frac{\partial g}{\partial I_1} \cdot \frac{\partial I_1}{\partial \sigma_r} + \frac{\partial g}{\partial I_2} \cdot \frac{\partial I_2}{\partial \sigma_r} + \frac{\partial g}{\partial I_3} \cdot \frac{\partial I_3}{\partial \sigma_r} \tag{15}$$

$$\frac{\partial g}{\partial \sigma_\theta} = \frac{\partial g}{\partial I_1} \cdot \frac{\partial I_1}{\partial \sigma_\theta} + \frac{\partial g}{\partial I_2} \cdot \frac{\partial I_2}{\partial \sigma_\theta} + \frac{\partial g}{\partial I_3} \cdot \frac{\partial I_3}{\partial \sigma_\theta} \tag{16}$$

The derivatives of the three stress invariants with regard to the normal stresses σ_r and σ_θ are:

$$\frac{\partial I_1}{\partial \sigma_r} = 1 \tag{17}$$

$$\frac{\partial I_1}{\partial \sigma_\theta} = 1 \tag{18}$$

$$\frac{\partial I_2}{\partial \sigma_r} = -(\sigma_\theta + \sigma_z) = \sigma_r - I_1 \tag{19}$$

$$\frac{\partial I_2}{\partial \sigma_\theta} = -(\sigma_r + \sigma_z) = \sigma_\theta - I_1 \tag{20}$$

$$\frac{\partial I_3}{\partial \sigma_r} = \sigma_\theta \cdot \sigma_z - \tau_{\theta z} \cdot \tau_{z\theta} \tag{21}$$

$$\frac{\partial I_3}{\partial \sigma_\theta} = \sigma_r \cdot \sigma_z - \tau_{zr} \cdot \tau_{rz} \tag{22}$$

The coefficients $\partial g/\partial I_1$, $\partial g/\partial I_2$, and $\partial g/\partial I_3$ are the same in Eqs 15 and 16. The coefficients $\partial I_1/\partial \sigma_r$ and $\partial I_1/\partial \sigma_\theta$ in these two equations are also the same (Eqs 17 and 18). For a test on a thin-walled hollow cylinder in which the inside and outside pressures are equal, equilibrium requires that $\sigma_r = \sigma_\theta$. For this case the coefficients $\partial I_2/\partial \sigma_r$ and $\partial I_2/\partial \sigma_\theta$ also have equal values (Eqs 19 and 20). Thus, if the plastic potential function g (Eq 9) is a function of I_1 and I_2 only, then the two strain increments $\dot{\epsilon}_r^p$ and $\dot{\epsilon}_\theta^p$ would be equal for the isotropic plastic material. Since the elastic and plastic strains are usually considered to be additive, an isotropic elasto-platic material for which $g = g(I_1, I_2)$ would always produce equal horizontal normal strains, $\epsilon_r = \epsilon_\theta$. For such a material it would not be necessary to measure the horizontal strains, since they could be calculated from the vertical and the volumetric strains, as in the triaxial test: $\epsilon_r = \epsilon_\theta = \frac{1}{2} \cdot (\epsilon_v - \epsilon_1)$.

In the general case the plastic potential function may depend on all three stress invariants. If torsional shear stress were not applied to the hollow cylinder, the coefficients $\partial I_3/\partial \sigma_r$ and $\partial I_3/\partial \sigma_\theta$ would also be the same, as long as the inside and outside pressures were equal, resulting in $\sigma_r = \sigma_\theta$. This is the case for isotropic compression and triaxial compression (that is, vertical loading) of the hollow cylinder specimen in which $\epsilon_r = \epsilon_\theta$. However, Eqs 21 and 22 show that if torsion shear stress, $\tau_{\theta z} = \tau_{z\theta}$ (see Fig. A), are applied to the hollow cylinder specimen in which $\sigma_r = \sigma_\theta$, then $\partial I_3/\partial\sigma_r$ and $\partial I_3/\partial\sigma_\theta$ would be different, because $\tau_{\theta z} = \tau_{z\theta} \neq 0$ and $\tau_{zr} = \tau_{rz} = 0$. Consequently, the values of $\dot{\epsilon}_x{}^p$ and $\dot{\epsilon}_\theta{}^p$ would be different for a material whose description requires the presence of the third stress invariant I_3 (or similar) in the plastic potential function.

In general, and from an objective experimental point of view, it would not be reasonable for deny the occurrence of I_3 in the plastic potential function. In particular, experimental evidence for frictional materials has clearly shown that I_3 (or similar) plays a key role in the description of these types of materials. The presence of I_3 in failure criteria, yield criteria, and plastic potential functions accounts for the smooth triangular cross sections in octahedral planes which are so characteristic of frictional materials such as sand, clay, concrete, rock, and ceramic.

In conclusion, it does not appear to be appropriate to set $\epsilon_r = \epsilon_\theta$ a priori for torsion shear tests on soil. These two horizontal normal strains should clearly be different for any frictional material tested in a hollow cylinder specimen under usual torsion shear conditions, especially near failure where the plastic behavior dominates the elastic behavior.

A. S. Saada (*author's closure*)—Professor Lade is quite correct in trying to put an emphasis on the fact that assuming $\epsilon_r = \epsilon_\theta$ results in restrictions being placed on the potential function of classical plasticity theory, when such a theory is used. Indeed the author himself makes such a statement in his presentation. In the elastic stage, Eqs 1 to 8 of the discussion are quite appropriate. However, for the case of a linearly elastic hollow cylinder subjected to the same inner and outer pressure, with or without torsion, $\epsilon_r = \epsilon_\theta$. The cylinder does not have to be thin walled, and no assumption has to be made on whether the variation of ϵ_r across the thickness is negligible or not. This can be directly seen from the expression of u_r which can be found in any elasticity book (see Ref *1* for example). Indeed, ϵ_r is simply a constant! So is ϵ_θ. Let us not forget however that $\tau_{\theta z}$ and $\gamma_{\theta z}$ vary linearly across the thickness, and that there is an approximation involved in assuming their uniform distribution. This assumption decreases in importance as one proceeds into the plastic stage.

In the plastic stage, the author would like to write the equations in a way slightly more general than that of the discusser. Using classical plasticity,

$$\dot{\epsilon}_{ij}{}^p = \dot{\lambda}\,\frac{\partial g}{\partial \sigma_{ij}}$$

If we assume that the potential g is an isotropic function of the state of stress, this function must depend only on the invariants, so that

$$g = g\,(I_1, I_2, I_3)$$

and

$$\dot{\epsilon}_{ij}{}^p = \dot{\lambda}\left(\frac{\partial g}{\partial I_k}\,\frac{\partial I_k}{\partial \sigma_{ij}}\right)$$

where

$$\frac{\partial I_1}{\partial \sigma_{ij}} = \delta_{ij},\ \frac{\partial I_2}{\partial \sigma_{ij}} = 2\sigma_{ij},\ \frac{\partial I_3}{\partial \sigma_{ij}} = 3\sigma_{it}\,\sigma_{tj}$$

The flow rule is of the form,

$$\dot{\underset{\sim}{\epsilon}}^p = \dot{\lambda}\,(A\,\underline{\delta} + B\,\underset{\sim}{\sigma} + C\underset{\sim}{\sigma}^2) \tag{1}$$

where A, B, and C are constants.

If on the other hand $\partial g/\partial I_3 = 0$, $g = g\,(I_1, I_2)$ and

$$\dot{\underset{\sim}{\epsilon}}^p = \dot{\lambda}\,(A\,\underset{\sim}{\delta} + B\,\underset{\sim}{\sigma}) \tag{2}$$

It is the derivative of the third invariant that brings in the square of the stress tensor $\underset{\sim}{\sigma}^2$. If $\sigma_r = \sigma_\theta = p$, the pressure in cell, Eq 2 gives

$$\dot{\epsilon}_r^p = \dot{\epsilon}_\theta^p = \dot{\lambda}\,(A + Bp) \tag{3}$$

This equality only takes place if $\partial g/\partial I_3 = 0$, that is, if the cross section of the yield function by the π plane is circular (similar to Von Mises or Prager-Drucker). On the other hand, Eq 1 gives

$$\dot{\epsilon}_r^p = \dot{\lambda}\,(A + Bp + Cp^2) \tag{4}$$

$$\dot{\epsilon}_\theta^p = \dot{\lambda}\,[A + Bp + C\,(p^2 + \tau_{\theta z}^2)] \tag{5}$$

As one can see $\dot{\epsilon}_r^p \neq \dot{\epsilon}_\theta^p$ when the torsional stresses are applied to the sample, and g is also a function of the third invariant.

There also is another equation that does not depend on the law of behavior of the material and that is the compatibility equation:

$$\frac{\partial \epsilon_\theta}{\partial r} + \frac{\epsilon_\theta - \epsilon_r}{r} = 0 \tag{6}$$

If one assumes that ϵ_θ does not vary with the radius then $\epsilon_r = \epsilon_\theta$. Is that assumption better or worse than assuming that $\tau_{\theta z}$ is uniform and does not vary with the radius? After all, in both cases we chose some uniform value which is obtained, at least in theory, by an averaging procedure and assume that it is constant across the thickness.

Experiments seem to show that at "failure" the trace of the failure surface on the π plane is not exactly circular and is closer to the shape of the coulomb criterion, but with curved segments. In fitting the data by plotting increments of strain, how accurate can one be in distinguishing between a perfectly circular segment of the yield surface or just a curved one? To simplify their calculation some modellers keep two invariants only; are they farther from reality than those who use the three invariants? Moreover, let us not forget that the assumption that g can be expressed in terms of the invariants implies an isotropic material which, more often than not, is far from being the case.

Finally, the above discussion is aimed at the situation where classical plasticity is used. There are other theories that do not use plastic potentials and where the assumption that $\epsilon_r = \epsilon_\theta$ does not create particular hardships: elasto-plastic rules are not the only ones in use today.

When it comes to comparing predicted and measured strains, one may accept as a temporary compromise to compare the measured and predicted values of $(\epsilon_r + \epsilon_\theta)$ which can be obtained without difficulty and quite accurately in most tests.

Bibliography

Saada, A. S., *Elasticity, Theory and Applications* Krieger, Malabar, FL, 1983.

David W. Airey[1] *and David M. Wood*[2]

The Cambridge True Triaxial Apparatus

REFERENCE: Airey, D. W. and Wood, D. M., **"The Cambridge True Triaxial Apparatus,"** *Advanced Triaxial Testing of Soil and Rock, ASTM STP 977*, Robert T. Donaghe, Ronald C. Chaney, and Marshall L. Silver, Eds., American Society for Testing and Materials, Philadelphia, 1988, pp. 796–805.

ABSTRACT: In true triaxial apparatus, samples of soil are subjected to three independent principal stresses and strains. Such apparatus can readily be used for controlled exploration of principal stress or principal strain space to provide information concerning the anisotropic response of the soil to aid the development of constitutive relations.

The Cambridge true triaxial apparatus has recently been reconstructed and is described in its new form. Some experimental data from a stress controlled test on kaolin are presented as an illustration of the capabilities of the apparatus and as an illustration of alternative ways in which such data may be presented while maintaining maximum objectivity.

KEY WORDS: soil mechanics, research, shear testing, true triaxial, stress path, strain path, clay, anisotropy

True triaxial apparatus provide the capability of applying three independent principal stresses or strains to cuboidal samples of soil and, thus, provide one more degree of freedom than the conventional triaxial apparatus. Principal axes remain fixed in true triaxial apparatus, so that they cannot attempt to apply the continuous rotations of principal stress that are possible in hollow cylinder apparatus and directional shear cells. Nevertheless, the freedom that is provided to explore three-dimensional principal stress space and principal strain space represents a significant advance. Rotations of the directions of the major principal stress are confined to 90° jumps. These 90° jumps can occur at any combination of principal stresses, and they are not necessarily associated with passage through a purely hydrostatic stress state, as is the case with a triaxial test path passing from compression to extension.

There have been many approaches to the development of true triaxial apparatus, using a variety of different devices to provide the three degrees of freedom. Apparatus have been built with rigid, deformation controlled boundaries [*1*]; flexible, stress controlled boundaries [*2*]; and combinations of rigid and flexible boundaries [*3,4*]. It is evident that use of a rigid boundary cannot guarantee uniformity of applied stress, and use of a flexible boundary cannot guarantee uniformity of applied deformation. There is some advantage to be gained from maintaining an "isotropy" of boundary conditions. Where true triaxial apparatus have been constructed with a mixture of rigid and flexible boundaries and the soil wishes to form a failure plane, the flexible boundary provides no restraint against such a plane forming and deformations may tend to occur preferentially toward the flexible boundary [*5*]. Where the

[1] Research fellow, Department of Civil Engineering, The University of Western Australia, Nedlands, Western Australia 6009; formerly, Cambridge University Engineering Department.

[2] Professor, Department of Civil Engineering, Rankine Bldg., The University, Glasgow G12 8LT Scotland; formerly, Cambridge University Engineering Department.

boundaries are either all rigid or all flexible, the isotropy of the boundary conditions gives no preferred direction of failure. It may also be noted that most of the true triaxial apparatus that use mixtures of rigid and flexible boundaries have been constructed as modifications of conventional triaxial apparatus. In such apparatus the cell pressure in the triaxial cell provides the minor principal stress, and the direction of this minor principal stress cannot be varied, thus limiting the possibilities for exploration of principal stress space.

The most suitable true triaxial apparatus to be used for research purposes are thus those in which the sample is contained between six flexible boundaries or between six rigid boundaries. The Cambridge true triaxial apparatus falls into this latter category.

Description of the Apparatus

The central part of the Cambridge true triaxial apparatus is formed of six blocks or platens which are nested together (Fig. 1) in such a way that any dimension of the cuboidal space that they enclose can be varied independently between 70 and 130 mm, giving a nominal strain capability of ±30% from the mean sample size of 100 mm. Four of the blocks are fitted with arrays of four contact stress transducers (Fig. 2) which can measure the distribution of stresses on the boundaries of the sample—on each face two of these transducers measure only the normal stress while the other two measure normal stress, shear stress, and gradient of normal stress so that nonuniformities of the stress distribution which develop in spite of the imposed uniform deformations can be detected. The stress transducers have a normal stress capacity of about 1000 kPa, and the resolution of stress measurement provided by the data logging equipment is ±1 kPa.

Each platen surrounding the sample in the true triaxial apparatus is loaded through a ram which bears on it through roller bearings; deformations of the sample are produced by movements of these rams. As originally designed and constructed by Pearce [*1*] and operated by Wood [*6*], movements of pairs of opposite rams were produced by chains (Fig. 3) running over a number of pulleys, and pulled by a small DC motor driving through a series of gears. With this arrangement, the ability of the apparatus to turn sharp corners accurately in strain space was restricted because of the flexibility of the chains and because the maximum motor speed was limited. Recently the whole drive system of the apparatus has been redesigned and rebuilt to make it much stiffer. Now movements of the rams are produced by stepper

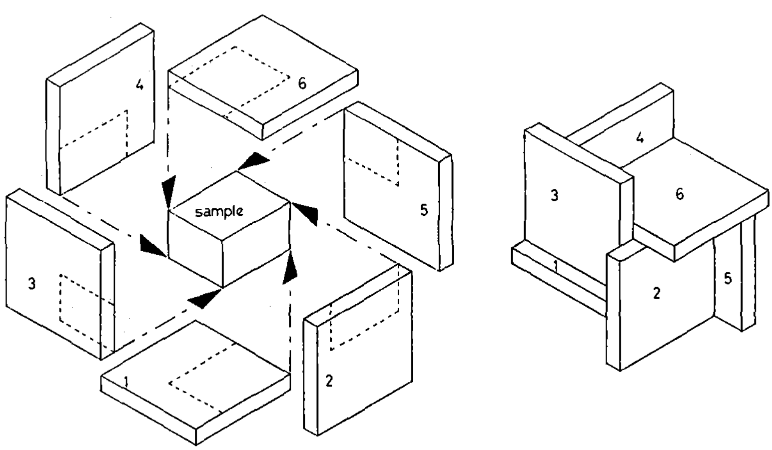

FIG. 1—*Arrangement of platens in Cambridge true triaxial apparatus.*

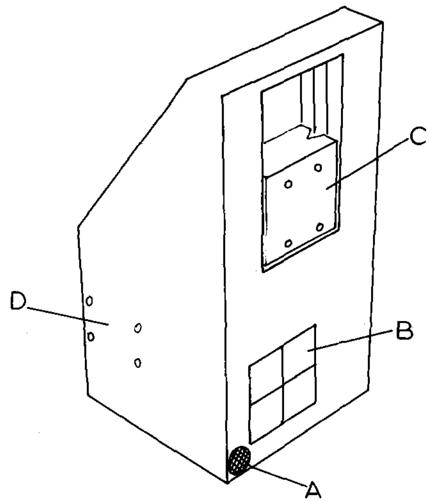

FIG. 2—*Typical platen of true triaxial apparatus*—A: *porous stone/drainage plug;* B: *array of contact stress transducers;* C: *slider for connection to adjacent platen;* D: *connection to adjacent platen.*

motors driving each ram directly (Fig. 4) through a "no backlash" gear box and worm gear "jactuator" which has been modified to take a linear ballscrew, thus reducing friction in the drive and allowing preloading to be introduced so that slack in the drive can be almost eliminated. The stepper motors on each axis are controlled together so that opposite rams always move by equal and opposite amounts and the center of the sample does not move

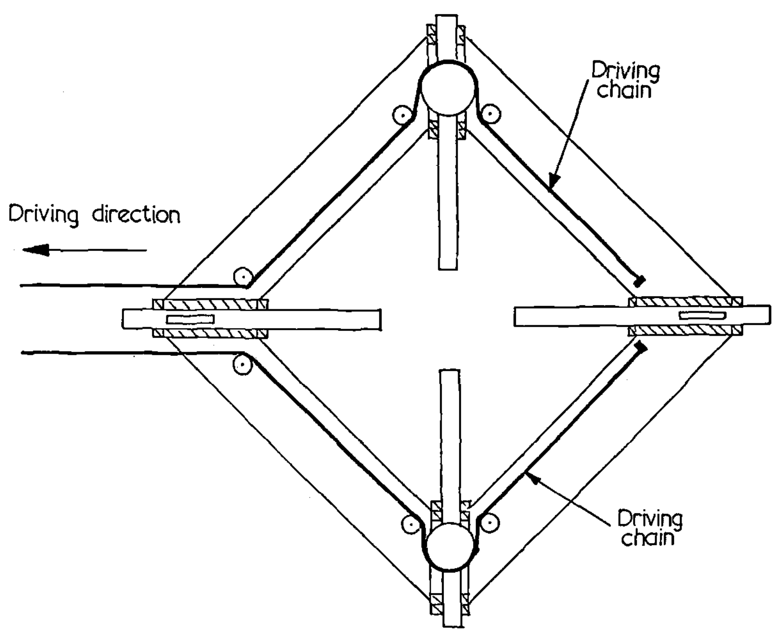

FIG. 3—*Schematic section through true triaxial apparatus showing chains formerly used to control movement of pair of platens.*

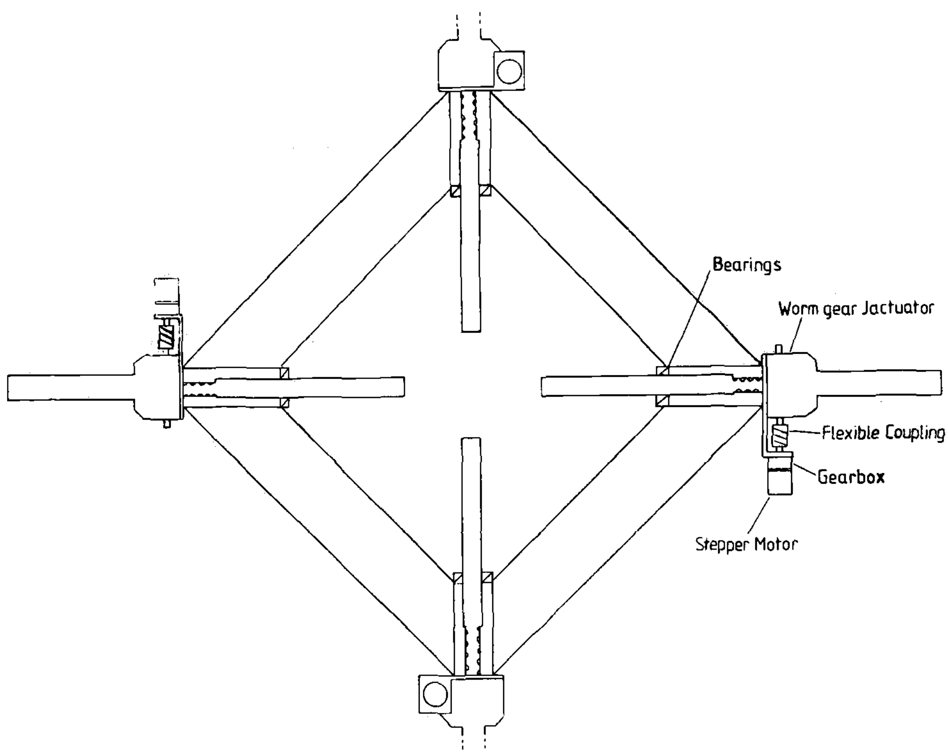

FIG. 4—*Schematic section through true triaxial apparatus showing stepper motors now used to provide direct control of movements of rams.*

but remains at the point defined by the intersection of the axes of the six rams. The maximum rate of change of sample dimensions with these motors is about 100 mm/h, which corresponds to a nominal strain rate of 100%/h for a sample dimension of 100 mm.

Relative movements of the pairs of opposite platens are measured by means of three linear variable differential transducers (LVDTs) which have essentially infinite resolution—the actual resolution is governed by the data logging equipment, and at present is 0.01 mm. Although, of course, part of the face of each platen may disappear behind the adjacent platens as the dimensions of the cuboidal sample change, there is one corner of each platen that is never covered. At these points in the four faces forming the vertical sides of the cuboid, a porous stone is placed to provide drainage (Fig. 2), and at this point in the bottom platen a pore pressure transducer is placed. A further pressure transducer measures the back pressure applied to the drainage system.

Data from all the transducers are received by a Solartron Orion data logger, which also provides a constant voltage source to energize each stress transducer circuit as it is selected and read. This data logger and the drive units for the six stepper motors (connected in three pairs) are controlled by an ACT Sirius microcomputer through an IEEE 488 parallel interface. This microcomputer is able to monitor the stress transducers and linear transducers and control the stepper motors in such a way as to cause the sample to follow any specified stress path or strain path in three-dimensional principal stress space or strain space, with fixed directions of principal axes. Hybrid paths are also possible, such as plane strain tests with controlled stress paths. Of course the paths that are specified must lie within the mechanical capabilities of the apparatus—it is not difficult to conceive of strain paths that would cause the stress capacity of the stress transducers to be exceeded. The rate at which changes of total or effective stress can be imposed will be limited by the maximum rate at which the sample may be deformed, and effective stress paths will only be accurately applied if the rates of deformation of the sample are sufficiently low that it is able to be fully drained, with no significant internal gradients of pore pressure.

The rigid platens enclose a sample space which is always cuboidal; principal directions of imposed boundary deformations cannot rotate. The contact stress transducers record normal stresses, gradients of normal stresses, and shear stresses on the platens. There are two reasons why shear stresses and gradients of normal stresses may be observed. As the size of the cuboidal sample changes so the platens must slide relative to the soil—frictional shear stresses can be generated as a result of this sliding. To minimize friction, the sample is contained in two membranes, with silicon grease between the membranes and between the outer membrane and the rigid platens. The platens are sprayed with polytetrafluoroethylene (PTFE) in a further attempt to keep friction to a minimum. In practice, measured shear stresses have typically not exceeded about 5% of the normal stresses, eccentricities of normal stress over any individual contact stress transducer have typically not exceeded 1 or 2 mm, and variations of normal stress over the surface of a platen have typically not exceeded about 5% of the corresponding average measured normal stress.

If the soil sample has been taken from the ground, rather than being compressed from a slurry in the true triaxial apparatus itself, then it may not want to respond to a cuboidal deformation by developing only uniform normal stresses on the six faces of the cuboid. The lubrication may prevent shear stresses from developing, but gradients of normal stresses can be interpreted as an indication that the principal axes of the average stress tensor that the soil is generating are not aligned with the principal axes of the imposed deformations. The contact stress transducer information could be used to quantify the anisotropy of the soil in small excursions of deformation. This would be analogous to the subsectioning technique used by Mould [7] (but complementary to his procedure because he was using a flexible boundary true triaxial device and applying uniform normal stresses and measuring the possibly nonuniform boundary deformations).

Sample Preparation

The Cambridge true triaxial apparatus has been used so far exclusively for testing clay samples. There are two methods by which the clay sample can be prepared and placed in the apparatus. All the tests reported by Pearce [1] and by Wood [6] were performed on samples of kaolin which had been consolidated from a slurry in the apparatus itself, making use of part of the large deformation range of the apparatus for this consolidation process. The clay was mixed as a slurry at twice its liquid limit (at a water content of 160%) and then pumped into a membrane in the apparatus. The membrane, restrained at the drainage points mentioned before, had a natural size of about 95 by 95 by 95 mm, but it was expanded to 125 by 125 by 125 mm by the slurry. Isotropic compression to a mean stress level of about 150 kPa brought the sample size down to about 95 by 95 by 95 mm, and shearing could continue from there without interruption.

A similarly reasonable stress level could not be reached in one-dimensional compression from a slurry. The alternative procedure typically adopted then was to start as before with a sample of slurry of size 125 by 125 by 125 mm and to compress this sample initially two-dimensionally to a size 125 by 100 by 100 mm which expelled a large amount of water without raising the stress level significantly, but which retained the symmetry of the subsequent one-dimensional compression to a size of, say 95 by 100 by 100 mm. The strain path followed during such a two-stage consolidation procedure is shown in Fig. 5 in two

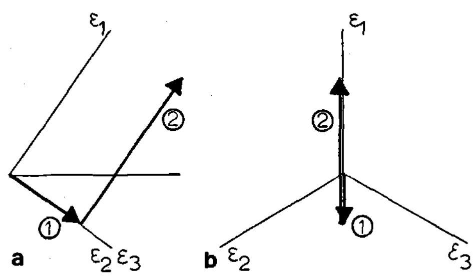

FIG. 5—*Strain path used to prepare one-dimensionally compressed samples, shown in two orthogonal views of principal strain space.*

orthogonal views of principal strain space—one, Fig. 5*b*, being a deviatoric view, and the other, Fig. 5*a*, being an orthogonal view in which the principal axis 1 appears at its true length, whereas the other two principal axes 2 and 3 appear foreshortened. The two views are shown in relationship to each other according to the rule of third-angle projection, so that the two diagrams of Fig. 5 provide a proper pair of two-dimensional views of a three-dimensional object—a path in principal strain space.

Provision is now also made for inserting precut samples into the true triaxial apparatus. With the top platen removed, a latex membrane is held back against the side platens while the sample is extruded from a special 100- by 100-mm-square sampling tube. A square piece of latex is then fixed to the top of the membrane by painting both it and lateral flaps with latex solution, so that the sample is sealed, the top platen can then be replaced, and testing can proceed.

Presentation of Test Results

Test results presented by Wood [*6*] were discussed in relation to the predictive capabilities of simple models such as Cam clay [*8*] based on isotropic elasticity and plasticity. Now it is more fashionable to interpret results of true triaxial and other sophisticated tests in terms of the clues they present concerning the anisotropic properties of soils, and many constitutive models, more elaborate than the Cam clay models, are now available for comparison and evaluation.

One set of results will be presented here, but first it is important to understand that with complex testing apparatus such as the true triaxial apparatus, and even more so with the

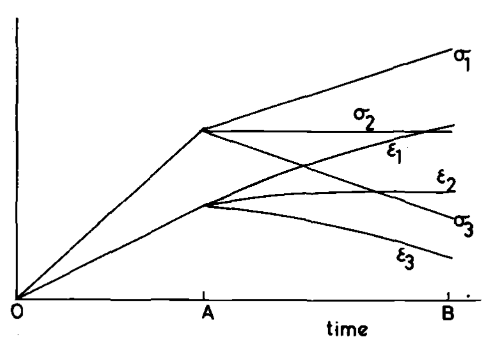

FIG. 6—*Variations with time of three principal stresses and three principal strains.*

hollow cylinder apparatus and directional shear cell, it is difficult to present test results in an entirely objective way without interposing some subjective interpretation between the data and the unfamiliar reader. The most objective way of presenting test data is in terms of plots of variation with time of individual stress and strain variables (Fig. 6). However, although this is objective it is not particularly helpful because it gives the unfamiliar reader no information as to the nature of the stress or strain path that was followed. At least, because the true triaxial apparatus provides only three degrees of freedom, it is possible to represent stress and strain paths in orthogonal two-dimensional views of three-dimensional stress or strain space—engineers are familiar with looking at views of three-dimensional objects. The choice of these views involves a small element of subjectivity: to choose a deviatoric view and the orthogonal view (Fig. 7) (which, as in Fig. 5, are displayed in third-angle relation to each other) already suggests some assumption concerning the division of response into volumetric and distortional or deviatoric parts. (Where an apparatus provides four degrees of freedom, the paths followed must be displayed in two-dimensional views of three-dimensional views of a four-dimensional stress or strain space—and this idea is less familiar to most engineers.)

Figures 8, 9, and 10 show data from an actual true triaxial test. (Figures 6 and 7 relate to a schematic test.) In this test a sample of spestone kaolin was prepared by consolidation from a slurry in the true triaxial apparatus. The clay was isotropically compressed to a mean effective stress of 150 kPa and then sheared at constant mean effective stress. Figure 8*a* shows the imposed deviatoric stress path ABC containing a corner at B. On section AB the stress σ_1 is increased, while the stress σ_2 is decreased by an equal amount and the stress σ_3 is held constant. On section BC the stress σ_2 is increased, while the stresses σ_1 and σ_3 are both decreased by half this amount, so that the mean stress remains constant. This test was one of a series of tests performed to study the response of the clay to stress paths involving corners of different sharpness in principal stress space.

One way in which data of stresses and strains can be conveniently shown in a single diagram is illustrated in Fig. 8. Whereas the imposed deviatoric stress path ABC is shown in Fig. 8*a*, the corresponding deviatoric strain path for the section BC is shown in Fig. 8*b*. In this figure, at each point of the strain path a line has been drawn proportional in length

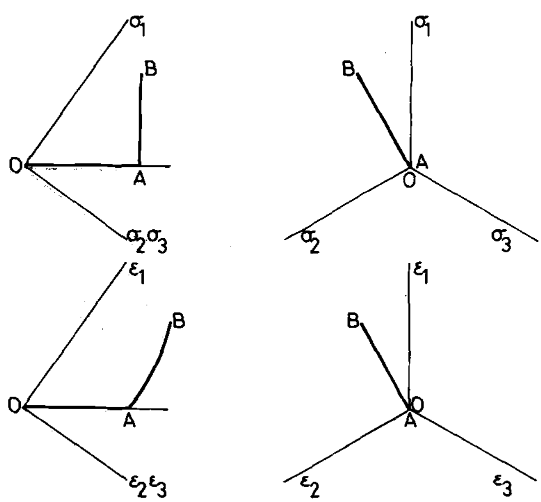

FIG. 7—*Stress and strain paths shown in two orthogonal pairs of views of principal stress space and principal strain space.*

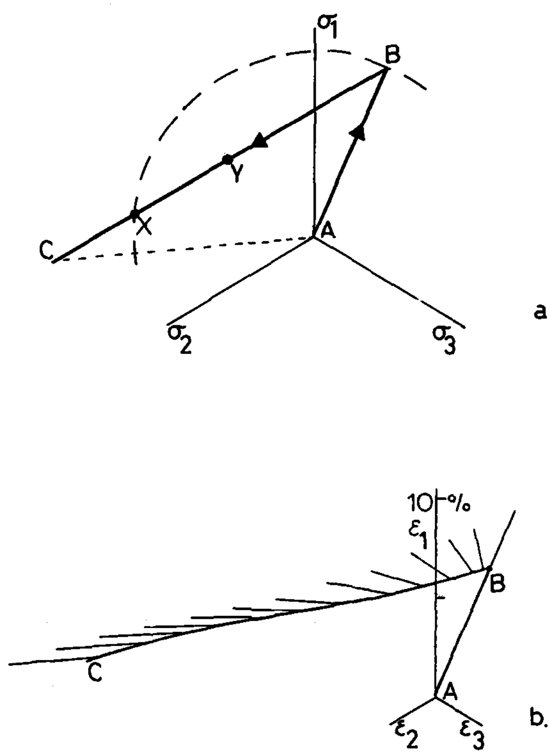

FIG. 8—(a) *Deviatoric stress path ABC containing a corner, and* (b) *corresponding deviatoric strain path.*

to and parallel to the current deviatoric stress vector. Thus, at B in Fig. 8*b* the line drawn is equivalent to the line AB in Fig. 8*a*, and at C in Fig. 8*b* the line drawn is equivalent to the line AC in Fig. 8*a*. Apart from the selection of the deviatoric response as one part of the response of the soil, this plot is entirely objective and proposes no specific relationship between stresses and strains, but shows all the deviatoric data in a single figure. There is no reason why such combined plots should not be used for displaying two-dimensional views of data from other tests with three or four degrees of freedom, provided that the stress and strain quantities are correctly linked.

When graphs are drawn to show stress–strain response, objectivity begins to be lost. The response of the soil to the stress path ABC of Fig. 8*a* could be shown in terms of the variation of volumetric strain

$$v = \epsilon_1 + \epsilon_2 + \epsilon_3$$

and a deviatoric strain

$$\epsilon = \{2[(\epsilon_2 - \epsilon_3)^2 + (\epsilon_3 - \epsilon_1)^2 + (\epsilon_1 - \epsilon_2)^2]\}^{1/2}/3$$

with the length of deviatoric stress path

$$s_\sigma = \Sigma\{[(\delta\sigma_2 - \delta\sigma_3)^2 + (\delta\sigma_3 - \delta\sigma_1)^2 + (\delta\sigma_1 - \delta\sigma_2)^2]/2\}^{1/2}$$

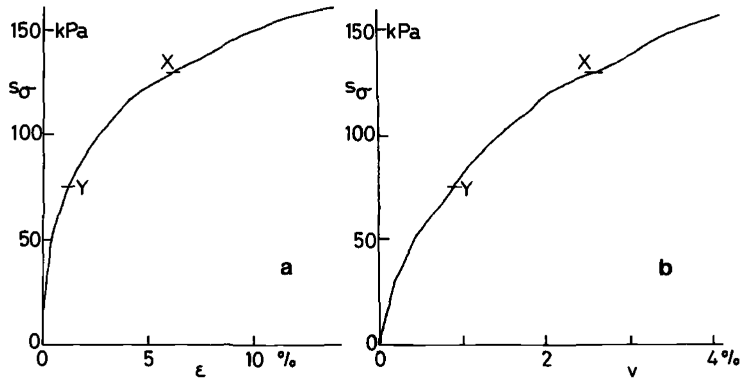

FIG. 9—*Variations of* (a) *deviatoric and* (b) *volumetric strain with length of stress path, for stage BC of path ABC shown in Fig. 8.*

for the section BC (Figs. 9*a*,*b*). (The meaning of s_σ is the distance from B along the stress path in Fig. 8*a*.) But this involves a loss of information about part of the deviatoric response because the deviatoric strain path is not actually straight. A more complete picture of the deviatoric response is shown in Figs. 10*a*, *b* where the deviatoric strain increment $\delta\epsilon$ is divided into components along and orthogonal to the straight deviatoric stress path BC, and these increments are summed to give strains ϵ_t and ϵ_n, respectively. This might not be the particular division that would have been preferred by the impartial reader, but there is a logic behind this choice.

If the soil were behaving isotropically and elastically throughout this path BC, then it would be expected that only deviatoric strain increments in the direction of the stress path would be observed, in other words, $\delta\epsilon_n = 0$. According to the Cam clay model [*8*], isotropic elastic response should be expected over the section BX of the path (Fig. 8*a*), that is, until the stress path reaches the circular constant mean stress section of the yield surface created by the shearing from A to B. (This circular section is shown dashed in Fig. 8*a*.) In fact, nonzero strains, ϵ_n, occur well before X (Fig. 10*b*), and their occurrence might be interpreted as an indication of the onset of yielding and plastic deformations, at some point such as Y in Figs. 8*a* and 10*b*. However, looking at these stress–strain plots, there is no evidence of

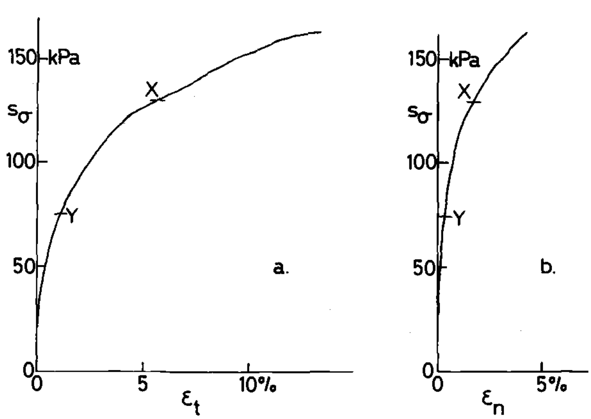

FIG. 10—*Division of deviatoric strain into orthogonal components for stage BC of path ABC shown in Fig. 8.*

a sharp drop in stiffness at this or any other point—the stiffness drops steadily as the stress path proceeds.

Consequently, it would appear that models that describe soils as elastic-plastic, with a yield surface marking the sharp transition from elastic to plastic response, are not going to be particularly satisfactory in matching the response of this clay, after a corner, on a path such as BC in Fig. 8*a*. However, it has been shown [*6*] that once the clay is supporting stresses such that even the Cam clay model expects it to be behaving plastically (section XC of the path in Fig. 8*a*), then that model is actually quite successful in matching the response.

Conclusion

It has been the intention of this paper to give an indication of the mode of operation and the capabilities of the Cambridge true triaxial apparatus. True triaxial testing can provide much information to guide the generation of realistic constitutive relations for soils which are applicable in regions of stress and strain space which are inaccessible in conventional triaxial testing. True triaxial apparatus have the advantages of simplicity and uniformity of imposed deformations or stresses, which are absent in testing devices that permit controlled gradual rotations of principal axes of stress and strain.

A program of tests is continuing to probe the anisotropic response of clays under conditions of three independent principal stresses and strains. Careful thought is necessary in presenting results of true triaxial and other sophisticated tests to avoid giving a biased interpretation which may obscure important aspects of real material response.

Acknowledgment

The reconstruction of the Cambridge true triaxial apparatus has been made possible through a grant from the Science and Engineering Research Council.

References

[*1*] Pearce, J. A., "A New True Triaxial Apparatus" in *Stress–Strain Behaviour of Soils* (Proceedings, Roscoe Memorial Symposium, Cambridge), R. H. G. Parry, Ed., G. T. Foulis & Co., Henley-on-Thames, 1971, pp. 330–339.

[*2*] Ko, H. Y. and Scott, R. F., "A New Soil Testing Apparatus," *Géotechnique*, Vol. 17, No. 1, 1967, pp. 40–57.

[*3*] Shibata, T. and Karube, D., "Influence of the Variation of the Intermediate Principal Stress on the Mechanical Properties of Normally Consolidated Clays," *Proceedings of the Sixth International Conference on Soil Mechanics and Foundation Engineering*, Montreal, University of Toronto Press, Vol. 1, 1965, pp. 359–363.

[*4*] Green, G. E., "Strength and Deformation of Sand Measured in an Independent Stress Control Cell" in *Stress–Strain Behaviour of Soils* (Proceedings, Roscoe Memorial Symposium, Cambridge), R. H. G. Parry, Ed., G. T. Foulis & Co., Henley-on-Thames, 1971, pp. 285–323.

[*5*] Yong, R. N. and McKyes, E., "Yield and Failure of a Clay under Triaxial Stresses," *Proceedings of ASCE, Journal of the Soil Mechanics and Foundations Division*, Vol. 97, No. SM1, 1971, pp. 159–176.

[*6*] Wood, D. M., "Explorations of Principal Stress Space with Kaolin in a True Triaxial Apparatus," *Géotechnique*, Vol. 25, No. 4, 1975, pp. 783–797.

[*7*] Mould, J. C., "Stress Induced Anisotropy in Sand and the Evaluation of a Multi-Surface Elasto-Plastic Material Model," Ph.D. thesis, University of Colorado, Boulder, 1983.

[*8*] Roscoe, K. H. and Burland, J. B., "On the Generalised Stress–Strain Behaviour of 'Wet' Clay," in *Engineering Plasticity*, J. Heyman and F. A. Leckie, Eds., Cambridge University Press, Cambridge, England, 1968, pp. 535–609.

Paul Michelis[1]

A True Triaxial Cell for Soil and Rock

REFERENCE: Michelis, P., "**A True Triaxial Cell for Soil and Rock,**" *Advanced Triaxial Testing of Soil and Rock, ASTM STP 977*, Robert T. Donaghe, Ronald C. Chaney, and Marshall L. Silver, Eds., American Society for Testing and Materials, Philadelphia, 1988, pp. 806–818.

ABSTRACT: The design and performance of a membrane-piston, high-pressure ($\sigma_2 - \sigma_3 \leqq 300$ MN/m^2) cell are presented. This device is similar to the one used for standard triaxial tests differing only in the stresses, σ_2 and σ_3, which are independently applied through flexible polyvinyl chloride (PVC) fluid cushions on prismatic specimens. The cell has been used extensively for monotonic-cyclic, compression-tension, plane strain-plane stress tests on a variety of materials.

The design and construction of a similar cell, which fulfills different requirements, are also presented. It uses flexible fluid cushions to transmit pressures up to 250 MN/m^2 for σ_1, and fluid cushions and fluid chamber pressure for stresses σ_2 and σ_3, respectively. It transmits uniform boundary loading to large specimen surfaces (19 by 19 by 19 cm), allowing both the development of unrestrained large deformation and its reliable measurement at several locations. The cell possesses a substantial degree of experimental flexibility for testing isotropic and anisotropic materials under drained and undrained conditions as well as ease of assembly and dismantling.

KEY WORDS: multiaxial test cell, direct tensile apparatus, triaxial test, soil test, combined tension compession, stress–strain curves, mechanical properties

Stress analyses of geotechnical engineering problems require constitutive relations for the materials involved. The determination of material parameters for a constitutive law makes use of laboratory or field test data. The standard triaxial test provides the most information, but its main limitation is that two principal stresses must always be equal. Therefore, stress conditions imposed on a triaxially tested specimen are directly relevant to practice only in rare cases, such as those with axisymmetric stress conditions. Meanwhile, numerical techniques applied to civil engineering practice require laboratory data pertaining to the more general stress conditions.

To deal with this problem, a number of true triaxial cells have been proposed to apply to a variety of practical problems [*1–4*]. These devices apply independent principal stresses σ_1, σ_2, and σ_3 through rigid platens (pistons) and/or flexible membranes. The imposed boundary conditions are strain- and stress-controlled, respectively. The resulting boundary effects from the use of rigid platens are normal and lateral strain constraints arising from the differences in the elastic moduli and Poisson's ratios of the loading platen and specimen. The flexible membranes can transmit very small shear stresses and, therefore, they impose the minimum constraints.

This paper has two objectives: to present an improved version of a true triaxial cell used presently [*5*] and to propose a new triaxial cell which applies all independent principal

[1] Director, Institute of Mechanics and Geostructures S.A., 114, Perikleous St., 152 31 Chalandri, Greece.

stresses through flexible fluid cushions, accommodates a large specimen, reliably determines small and large strains, and operates well at low- and high-stress levels.

Description and Operation of Membrane-Piston Cell

The improved membrane-piston cell (Figs. 1 and 2) is similar to standard triaxial devices and develops mixed boundary conditions of rigid and flexible boundaries on a prismatic specimen 10 by 5.2 by 5.2 cm in size. Its body consists of two cylindrical parts acting as the reaction frame for stresses σ_2 and σ_3. The cylindrical parts are locked together by locking segments and a retaining ring. The cell also consists of two pistons of a square cross-section with two spherical seats and a load cell. Two pairs of opposing prismatic PVC fluid cushions, filled and pressurized by hydraulic oil, apply the stresses σ_2 and σ_3 to the sides of the specimen. The cell has two symmetries, one each along two perpendicular planes intersecting along the longitudinal axis of the specimen and another symmetry along a perpendicular plane cross-section passing through the center of the specimen. It is manufactured from Orvar steel with a yield point of 1800 MN/m^2, Young's modulus of 206 GN/m^2, and Poisson's ratio of 0.30. The dimensions of the body were defined by the use of a finite element method (FEM) analysis such that it may sustain differential stress $\sigma_2 - \sigma_3$ of 250 MN/m^2 when $\sigma_3 = 0$ or stresses generated by standard triaxial tests when $\sigma_2 = \sigma_3 = 400$ MN/m^2 and where the safety factor is greater than 1.5. The permissible maximum axial loading is 1500 MN/m^2.

Boundary effects generated by the use of steel prisms, which applied the stress σ_2 in the earlier cell [5], were eliminated. Screw threads, which are liable to distortion and subsequent seizure, were replaced by a locking system to ensure ease of assembly and dismantling and to improve safety.

The PVC fluid cushions expand easily as flexible fluid-filled membranes in the space between the deforming sample and the body of the cell. Their important property is that they transmit normal stress through fluid pressure and allow for large specimen strains without boundary interference. In addition they allow thin rods, which record the sample deformation, to pass through them. The manufacturing technique involves rotational casting of a mixture of PVC emulsion, dioctyl phthalate as plasticizer, and fatty alcohols as stabilizer. During heating and rotation of the mixture in a mold, stereo cross-linking is obtained at elevated temperatures which greatly increases the strength of the polymer. The corners of the two cushions applying the intermediate stress, σ_2, are made stiffer and thicker to protect against extrusion, particularly when high values of σ_2 are to be applied.

The strains ϵ_2 and ϵ_3 are calculated by boundary measurements of specimen displacements transmitted to thin rods through cushions and recorded by linear variable differential transformers (LVDTs) or displacement dial gauges. The surface of the specimen may be porous, rough, or damp, but this technique remains accurate and simple. The strain ϵ_1 is calculated by measuring the displacement of the ends of the specimen as well as inside the specimen, at the upper boundary of its central (cubical) part [5]. Then the axial strain of the central part is calculated. For proper cell operation the maximum permissible value of ϵ_2 is $\pm 10\%$. Nonuniform strain is developed due to the application of axial stress σ_1 by rigid pistons (end effects), similar to the one developed under standard triaxial testing [6]. However, at small axial strains and particularly in the pre-peak region, the apparent strain nonuniformity effect seems limited in the central region of the specimen, where all measurements are made.

Performance

The described cell and its earlier version were extensively used for monotonic and cyclic standard triaxial tests on marble and granular materials [7], biaxial and polyaxial tests on

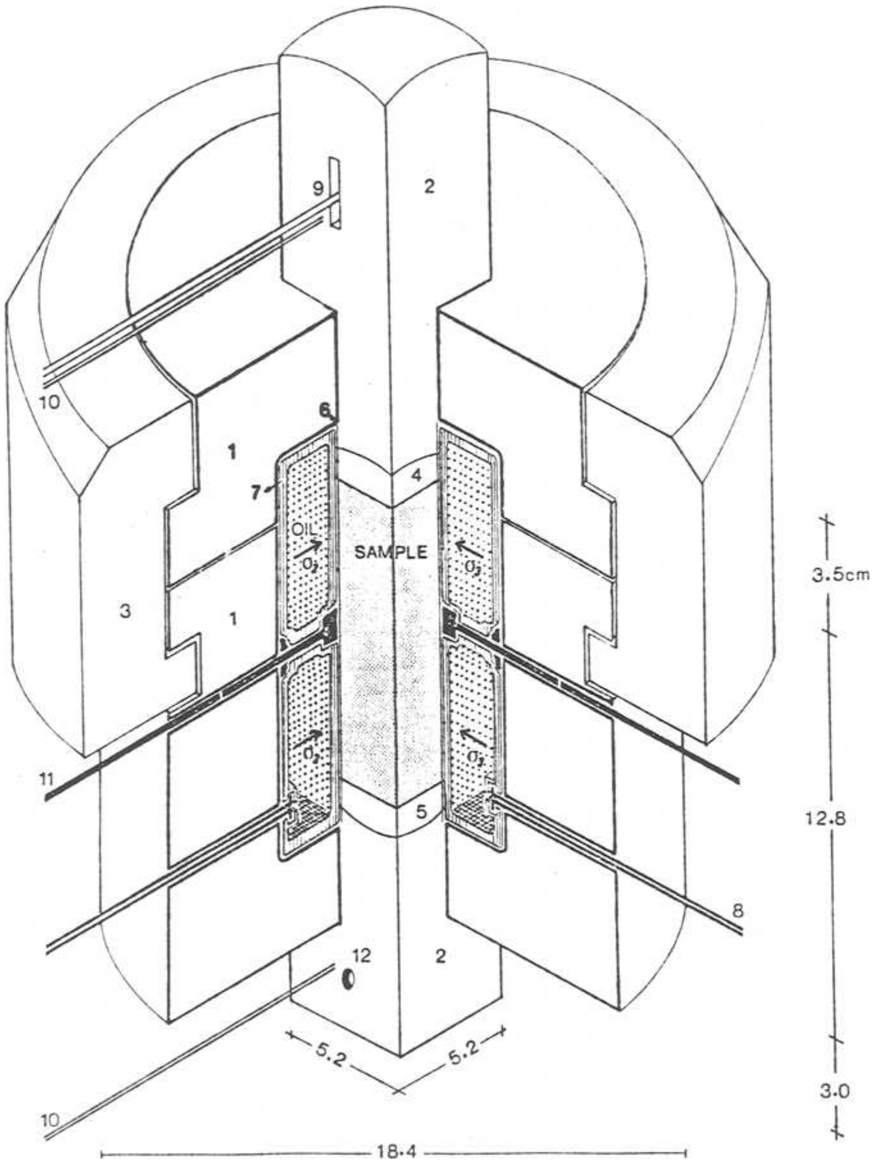

FIG. 1—*Three-dimensional cutaway view of membrane-piston cell:* 1 = *cylindrical body;* 2 = *piston;* 3 = *locking segment;* 4 = *spherical seat and load cell;* 5 = *spherical seat;* 6 = *very thin copper sheet;* 7 = *PVC fluid cushion;* 8 = *high pressure tube for filling and pressurizing cushion with oil;* 9 = *partial axial deformation measuring rod;* 10 (*upper and lower*) = *total axial deformation measuring rod;* 11 = *lateral deformation measuring rod;* 12 = *exit for pore water and strain gauge cables.*

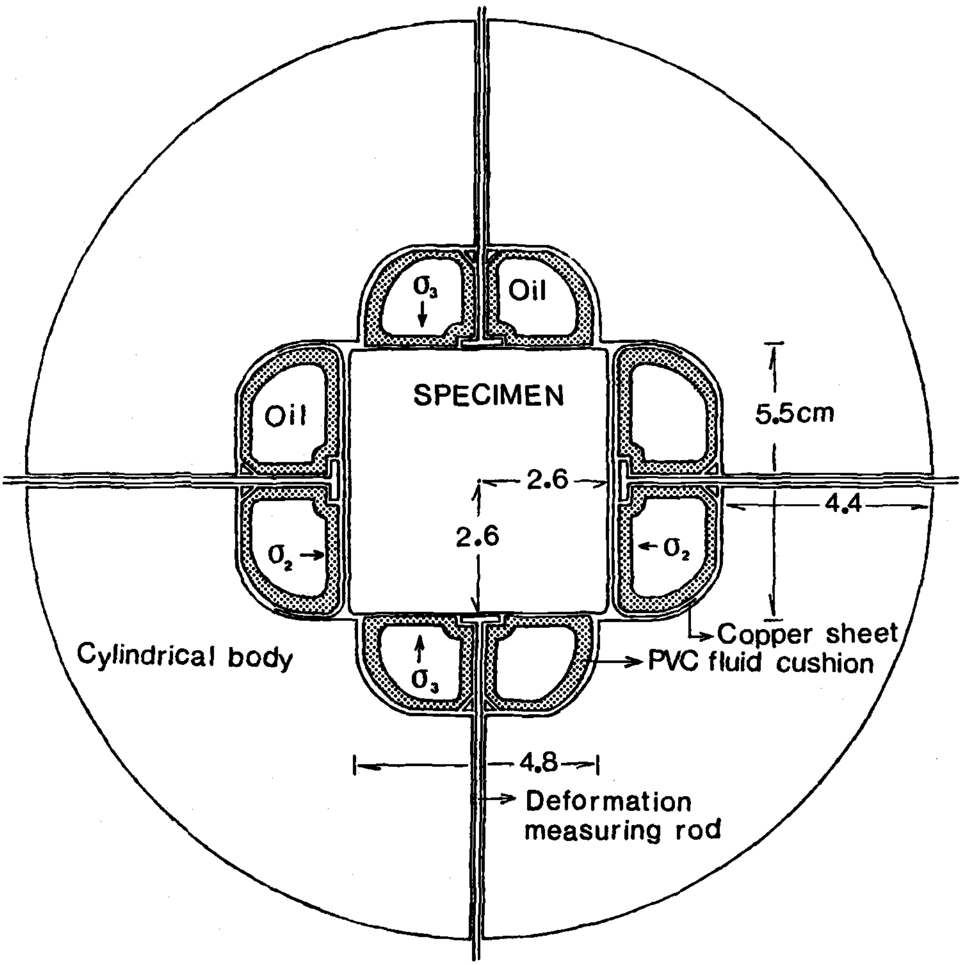

FIG. 2—Cross-sectional drawing of membrane-piston cell.

marbles [*8,9*], cyclic polyaxial tests on concrete [*10*], compression–tension biaxial tests on concrete [*11*], cyclic compression–tension polyaxial tests on concrete, and plane-strain tests on marbles. Tension–compression tests were successfully performed by axial tensioning of a "dog-bone"-shaped specimen, reduced in length in one direction (Fig. 3).

The stresses were applied by means of a high-pressure hydraulic system consisting of one pressure vessel loaded by a servo-controlled testing machine and two servo-controlled pumps. The pressurized fluid of the vessel generated the major stress σ_1, and the pumps generated the stresses σ_2 and σ_3. The experimental process was axially strain servo-controlled up to peak strength, on any preselected stress path, while stress and deformation were recorded. The displacement transducers were calibrated by means of a micrometer to an accuracy of 0.001 mm. The cumulative deformation was magnified by a simple technique in which deformation was transmitted through rods to two pistons and then through tubes filled with mercury to one piston (Fig. 3). This technique minimizes the measuring devices necessary [*5*].

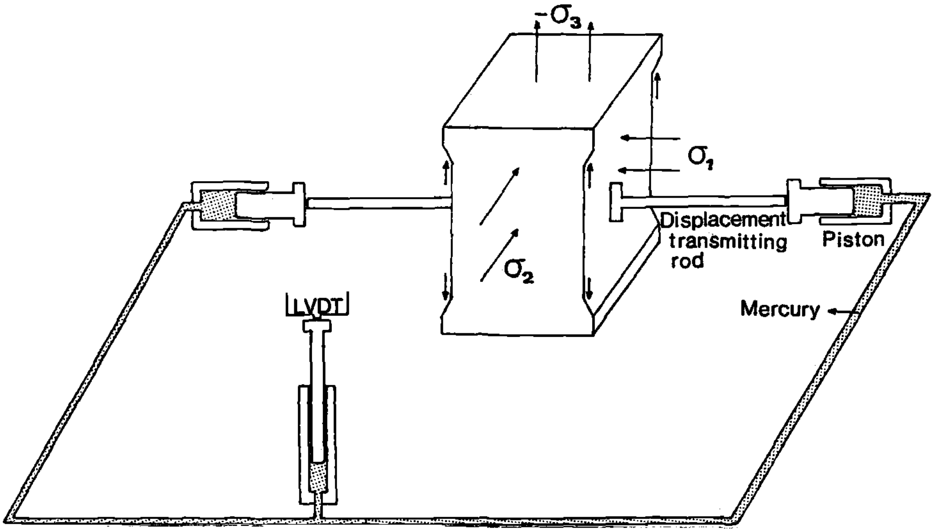

FIG. 3—*Schematic presentation of deformation measuring device and a properly shaped specimen for direct tension test.*

The uniformity of small deformations in the surfaces of plasticized epoxy resin specimens at the end of true triaxial tests demonstrated strain uniformity. Reproducibility of results was checked for different loading paths and materials, and a comparison was made for results obtained under standard triaxial conditions with those obtained from standard triaxial devices [6]. The PVC cushion proved to be sufficiently oil-resistant.

Figure 4 presents results of four true triaxial tests performed with the same σ_3 and increasing σ_2 for Naxos marble [8], Fig. 5 shows results for cyclic tests on concrete, and Fig. 6 presents cyclic compression–tension test results for concrete. Creep is intense during straining of concrete, as evidenced by the negative slopes of the unloading curves at and immediately after the initial point of unloading.

On the basis of the observed performance and particularly from the observed physical condition of specimens at the end of the tests it can be concluded that the cell operates well for various loading paths and strain conditions under small and very high pressures. Its main drawbacks are related to the strain constraints imposed by the mixed loading conditions which apparently affect behavior of the materials at large strains as with standard triaxial cells, and also to the relatively small specimen size for testing rock mass and concrete.

Membrane-Fluid Cell

In this section a new true triaxial cell is proposed which accommodates large prismatic specimens (19 by 19 by 19 cm) and applies the stresses σ_1 and σ_2 by fluid cushions and the stress σ_3 by fluid chamber pressure.

Its body consists of two cylindrical parts (Figs. 7, 8, and 9) acting as the reaction frame for application of all principal stresses and two locking segments held in place by a ring. The pistons were replaced for the application of σ_1 by a pair of opposing PVC fluid cushions while σ_2 is applied by another pair of cushions. Minor stress, σ_3, is generated by pressurizing fluid in the chamber after sealing the two cylindrical body parts with an O-ring seal. In this way, by applying equal pressures to opposite sides of the specimen, it effectively "floats"

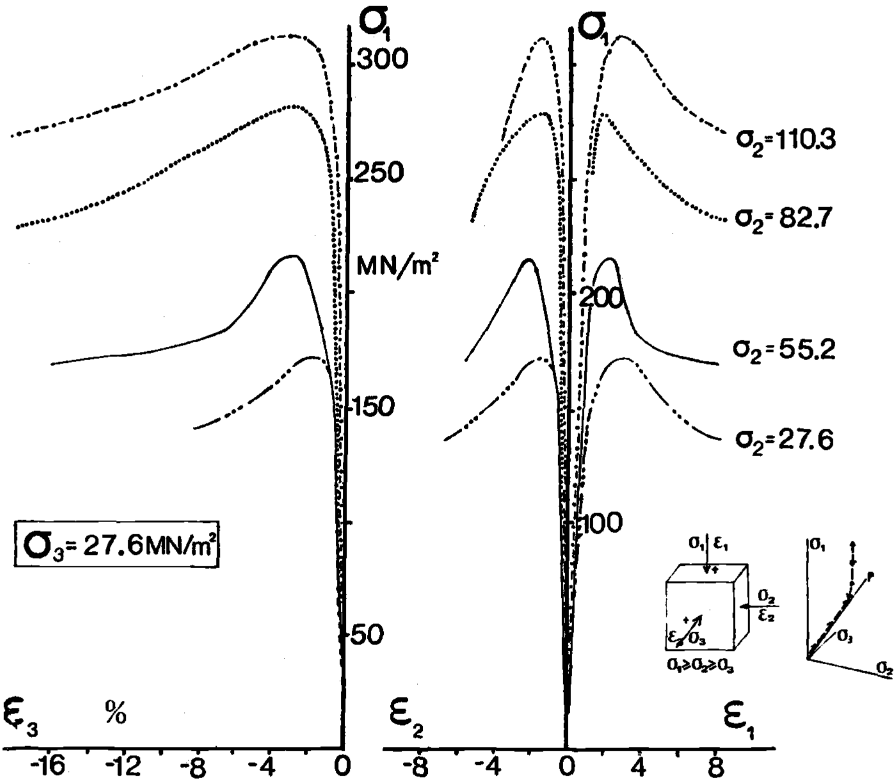

FIG. 4—*Results of four tests performed under same minor stress and increasing intermediate for Naxos marble* [8].

and does not touch the body. The cell is symmetrical along vertical and horizontal planes. The dimensions were defined by the use of finite element method analysis to apply major stress $\sigma_1 \leqq 250$ MN/m^2, differential stress $\sigma_2 - \sigma_3 \lesseqgtr 70$ MN/m^2 when $\sigma_3 = 0$, and isotropic $\sigma_1 = \sigma_2 = \sigma_3 \leqq 150$ MN/m^2 (safety factor greater than 1.5).

As is evident, the stresses are applied to the specimen in such a way that interference between the stress application mechanisms is minimal for small and large deformation. Indeed the major stress, σ_1, is uniformly applied on the specimen's sides by the cushions and also by two steel rings along the expanding or contracting edges of the specimen (Fig. 7). The steel rings slide easily, forced by the major stress cushions, compressing the ends of the thinner and more flexible cushions generating the intermediate stress. The chamber pressure, generating the minor stress, acts uniformly upon the rings. Their dimensions and particularly the width, d, are chosen for each loading path in order to contribute to the application of uniform σ_1 on the edges of specimens, along the critical path of loading. Therefore, a series of steel rings of varying dimensions must be available. The intermediate and minor stresses are uniformly applied along the sides and edges of a specimen during its deformation. The seal between the cylindrical body and the specimen is critical. A flexible fluid cushion, 2 to 3 mm thick, can bridge gaps up to 2 mm for a maximum pressure of 70 MN/m^2, without excessive extrusion. If the specimen contracts, steel platens can be fixed on the body of the cell leaving a small gap of less than 1 mm between the cell and the specimen for the application of fluid pressure σ_3 (Fig. 9: ABC, DEF).

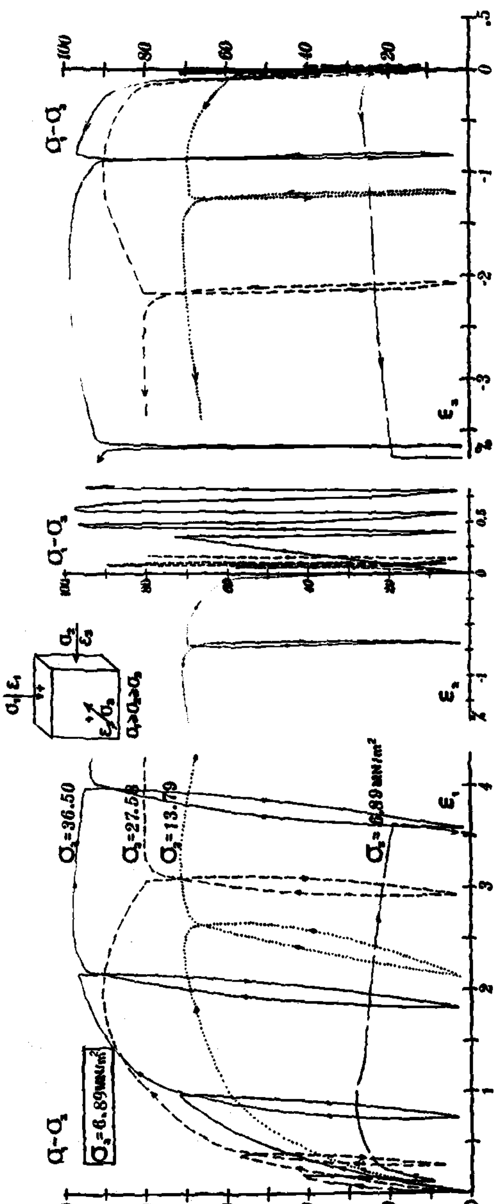

FIG. 5—*Results of four cyclic tests performed under same minor stress on concrete.*

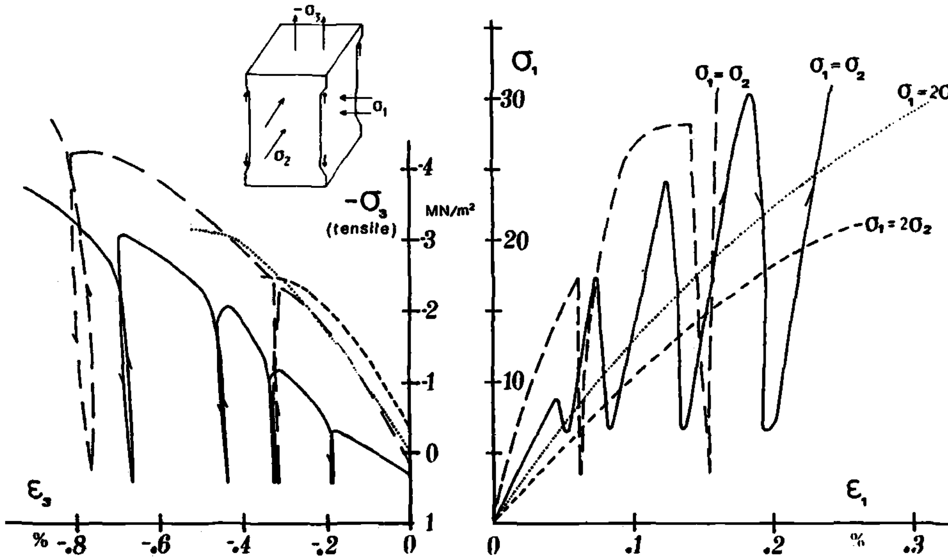

FIG. 6—*Results of cyclic compression-tension tests on concrete.*

Figure 10 shows details of the specimen–PVC drainage sheet–thin copper sheet–cushion arrangement at an edge for a specimen, which will be loaded under drained conditions. The PVC drainage sheet expands and contracts easily as a flexible membrane and acts as an isolated drainage blanket, collecting pore water seeping from the covered side of the prismatic specimen and leading the pore water to the water exit tube.

The cell allows values of strain ϵ_1 to range between $\pm 15\%$ and ϵ_2, ϵ_3 between $+15$ and -5%. The relative deformations can be accurately measured integrally, locally, or pointwise by a system containing deformation rods (Fig. 7), by the device presented in Fig. 3, and by LVDTs.

Deformation can be easily measured at several locations on each face of a specimen. Therefore, angular deformation and shear strain can be defined for anisotropic materials including rock masses. Pore water pressure measurements can be taken by measuring water pressure at one or more locations of a specimen (Figs. 7 and 10).

The fluid cushions vary in thickness depending on the maximum level of pressure to be applied. Particularly for testing soils, thin cushions (<1 mm) are used.

Standard triaxial and biaxial stress paths can be easily followed due to the independent control of the three principal stresses.

Tension–compression tests can be performed under satisfactory boundary conditions on "dog-bone"-shaped specimens.

Plane-strain tests can be performed by preventing one lateral expansion, adding steel platens (Fig. 9: ABC, DEF). A small diameter load cell, built in each platen, can measure the developing stress.

Further research will aid in the development of a suitable technique, which will superimpose, in the above cell, shear stress fields on the boundaries of the specimen, loaded by normal stresses.

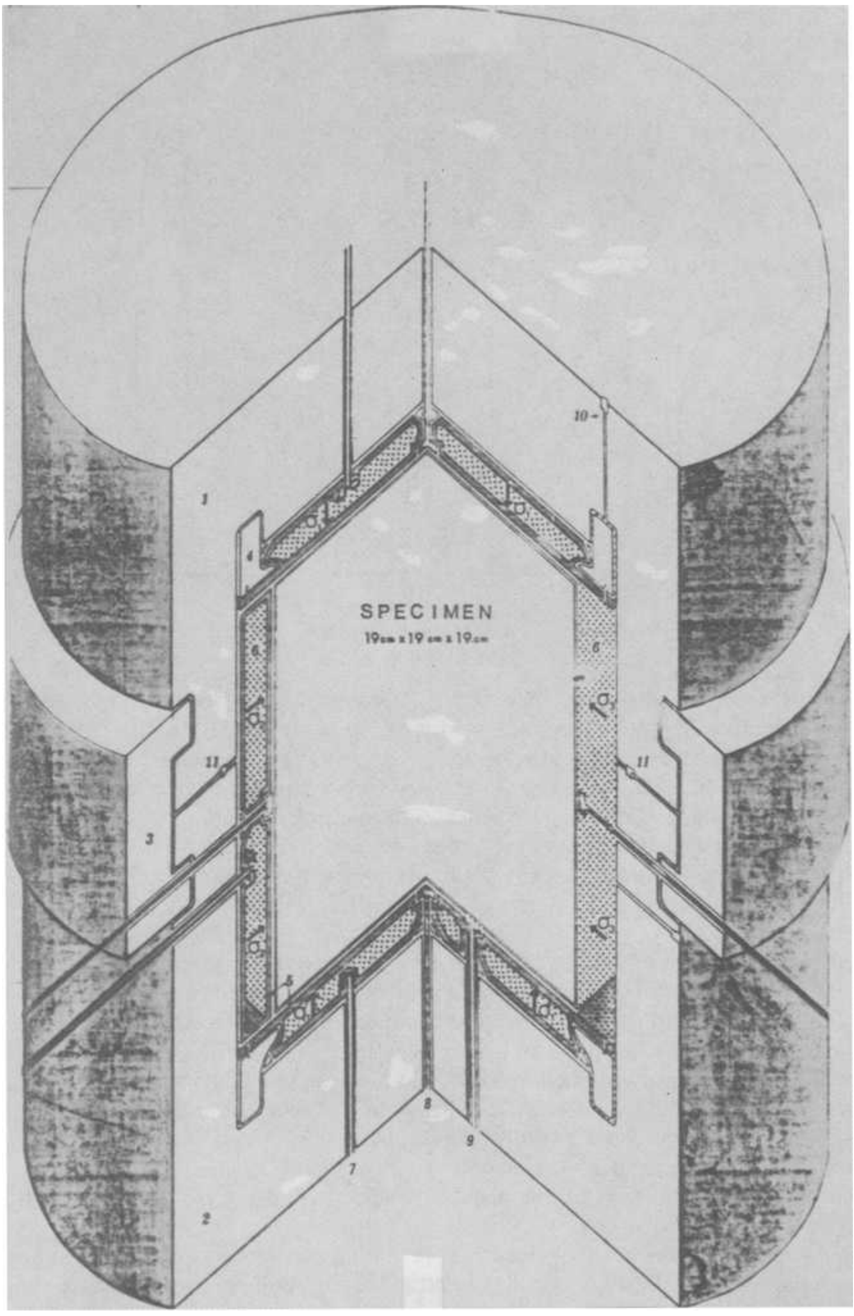

FIG. 7—*Three-dimensional cutaway view of membrane-fluid cell:* 1 = *upper cylindrical reaction frame;* 2 = *lower cylindrical reaction frame;* 3 = *locking segment;* 4 = *steel ring;* 5 = *PVC fluid cushions;* 6 = *pressurizing fluid;* 7 = *high pressure tube for filling and pressurizing cushion with fluid;* 8 = *deformation measuring rod;* 9 = *pore water tube;* 10 = *de-airing value;* 11 = *O-ring seal.*

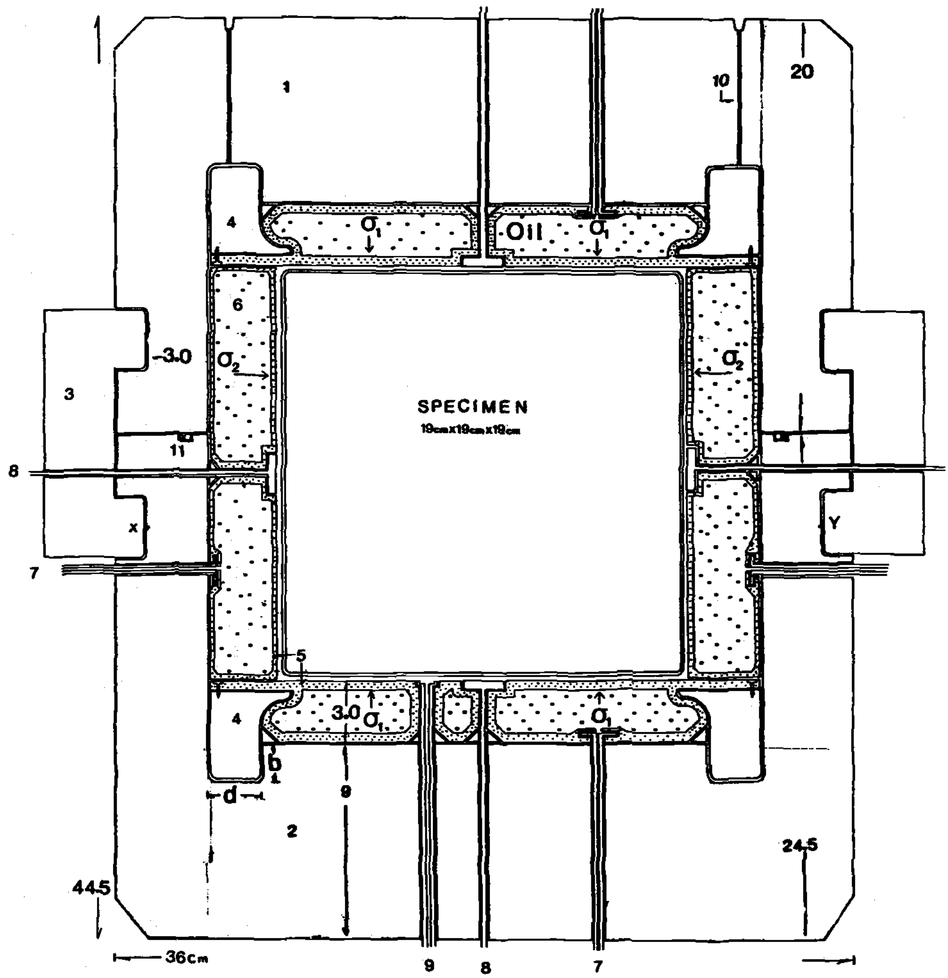

FIG. 8—*Longitudinal drawing of membrane-fluid cell.*

Conclusions

The cells presented in this paper combine a fair degree of versatility of stress and strain path applications with stress–strain uniformity in distribution and accuracy in measurement.

The main characteristics are

The membrane-piston cell

1. Independent application of the three principal stresses. The axial load is applied by two pistons while the stresses σ_2 and σ_3 are applied by flexible fluid-filled membranes.
2. Specimen dimensions are 10 by 5.2 by 5.2 cm.
3. Application of small and very high stresses. The possibility of testing materials of relatively high strength where the operational differential stress $\sigma_2 - \sigma_3$ is limited to 250 MN/m^2.
4. Accurate and direct measurement of strains and stresses.
5. Ease of assembly and dismantling. Similar to the standard triaxial cells.

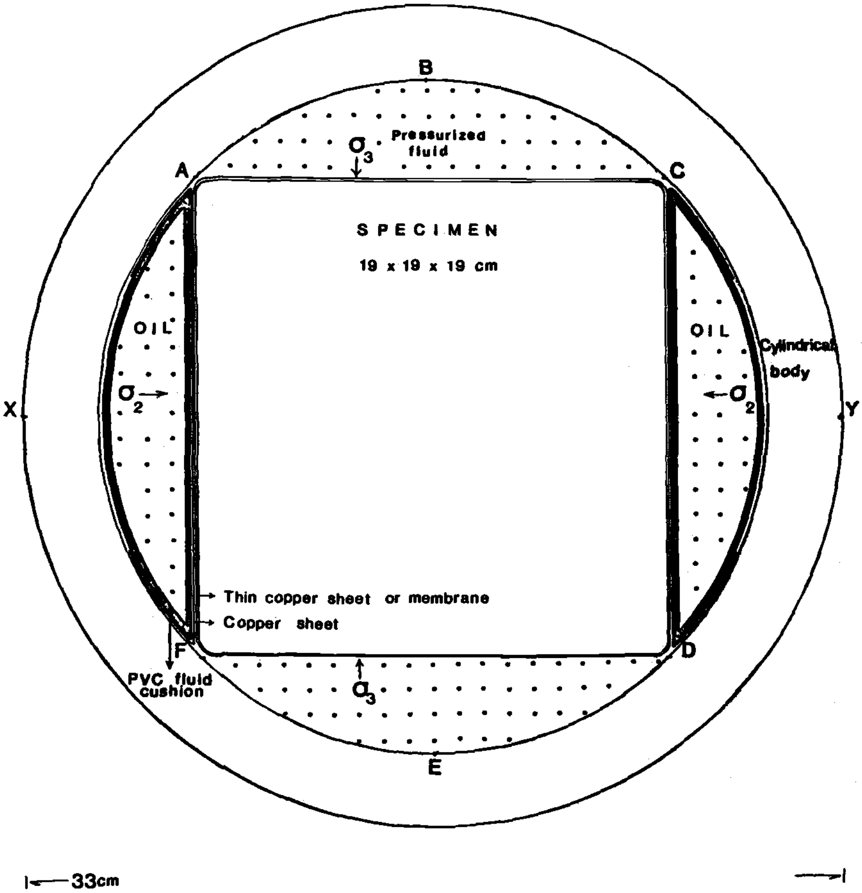

FIG. 9—*Cross-sectional drawing at* xy *of membrane-fluid cell.*

6. Satisfactory performance for biaxial, triaxial, polyaxial, combined compression–tension tests for a wide variety of materials.
7. Nonuniformity in stress–strain distribution, apparent at large lateral deformations, as a result of application of mixed loading conditions.
8. Inability of continuous rotation of the axes of principal stresses and strains and ability to provide a 90° jump rotation.
9. Small specimen size for testing rock mass and concrete.

The membrane-fluid cell:

1. Independent application of the three principal stresses. The stresses σ_1 and σ_2 are applied by flexible fluid cushions while σ_3 is generated by cushions or fluid pressure. Maximum operational stress, σ_1, is 250 MN/m^2.
2. Specimen dimensions are 19 by 19 by 19 cm.
3. Application of small and high stresses is uniformly distributed.

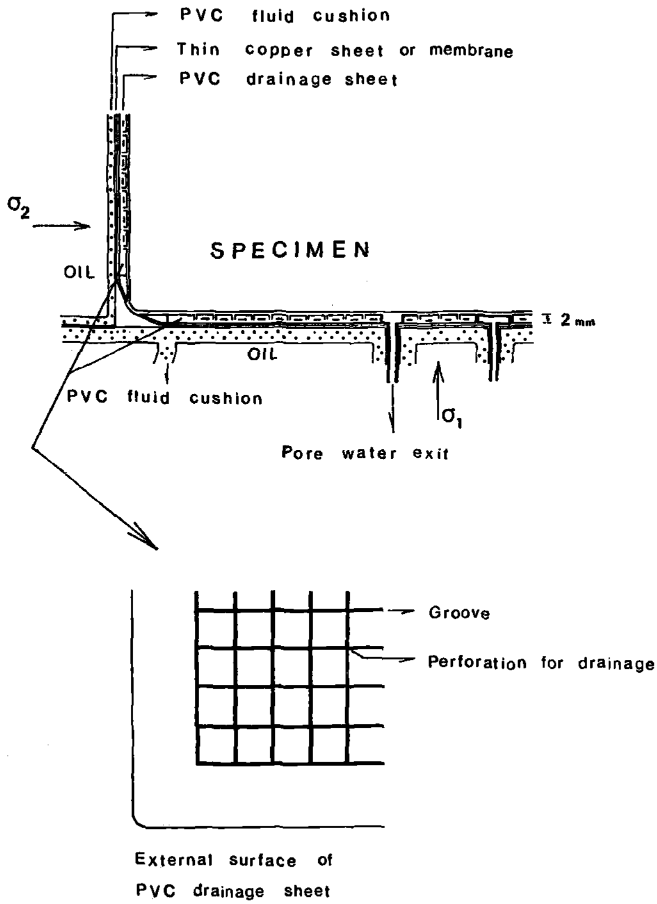

FIG. 10—*Details of Fig. 9 at the edge of a specimen for the case of a drained test.*

4. Accurate and direct measurement of strains at one or several locations on each specimen face. The possibility of defining angular deformation and shear strain for testing anisotropic materials.
5. Ease of assembly and dismantling.
6. Ability to perform monotonic and cyclic biaxial, triaxial, polyaxial, combined compression–tension, and plane-strain tests on a great variety of isotropic and anisotropic materials including concrete and rock mass as well as the further possibility of performing undrained and drained tests with pore water pressure measurements.
7. Ability of rotation of directions of the principal stress axes with a 90° jump.

Acknowledgments

The membrane-fluid cell was designed and constructed in an ongoing research program investigating dynamic rock behavior. The author wishes to thank Dr. D. Mameletzis for several suggestions on polymer chemical behavior, and S. Kakarinos, J. Semboglou, and A. Samios for constructing the cell.

References

[1] Pearce, J. A., "A New True Triaxial Apparatus," in *Stress–Strain Behaviour of Soils*, Proceedings, Roscoe Memorial Symposium, G. T. Foulis, London, 1971, pp. 330–339.
[2] Atkinson, R. H., and Ko, H.-Y., "A Fluid Cushion, Multiaxial Cell for Testing Cubical Rock Specimens," *International Journal of Rock Mechanics and Mining Sciences and Geomechanics Abstracts*, Vol. 10, 1973, pp. 351–361.
[3] Desai, C. S. Janardahanam, R., and Sture, S., "High Capacity Multiaxial Testing Device," *Geotechnical Testing Journal*, Vol. 5, No. 1, 1982, pp. 26–33.
[4] Michelis, P. N. and Demiris, C. A., "Conception et construction d'une vraie cellule triaxiale (cellule De-Mi)," in *Proceedings*, French Academy of Sciences, Paris, November 1983.
[5] Michelis, P. N., "A True Triaxial Cell for Low and High Pressure Experiments," *International Journal of Rock Mechanics and Mining Sciences and Geomechanics Abstracts*, Vol. 22, No. 3, 1985, pp. 183–188.
[6] Michelis, P. N., "Work-Softening and Hardening Behaviour of Granular Rocks," *Journal of Rock Mechanics*, Vol. 14, 1981, pp. 187–200.
[7] Michelis, P. N., and Brown, E. T., "A Yield Equation for Rock," *Canadian Geotechnical Journal*, Vol. 23, No. 1, 1986, pp. 9–17.
[8] Michelis, P. N., "Polyaxial Yielding of Granular Rock," *Journal of Engineering Mechanics, American Society of Civil Engineers*, Vol. 111, No. 8, 1985, pp. 1049–1066.
[9] Michelis, P. N., "True Triaxial Yielding and Hardening of Rock," *Journal of Geotechnical Engineering Division, American Society of Civil Engineers*, Vol. 113, 1987, pp. 616–635.
[10] Michelis, P. N., "True Triaxial Cyclic Behavior of Concrete and Rock in Compression," International Journal of Plasticity, Vol. 3, 1987, pp. 249–270.
[11] Katsaragakis, E., "Biaxial Tension-Compression Tests on Concrete," Ph.D. thesis, National Technical University of Athens, 1988.

Vincent Silvestri,[1] *Raymond N. Yong,*[2] *and Abdel Moshen Onsy Mohamed*[3]

A True Triaxial Testing Cell

REFERENCE: Silvestri, V., Yong, R. N., and Mohamed, A. M. O., "**A True Triaxial Testing Cell,**" *Advanced Triaxial Testing of Soil and Rock, ASTM STP 977,* Robert T. Donaghe, Ronald C. Chaney, and Marshall L. Silver, Eds., American Society for Testing and Materials, Philadelphia, 1988, pp. 819–833.

ABSTRACT: Results of both drained and undrained triaxial tests performed with a true triaxial cell on both natural and artificial clays are presented and discussed. The true triaxial apparatus, which has been used for about 20 years, is fully described. The apparatus has recently been modified to improve the measurement of lateral deformations. Tests were performed on both isotropic and anisotropic materials.

KEY WORDS: true triaxial cell, isotropic and anisotropic clays, sensitive clay, principal stress and strain spaces, drained and undrained tests

Nomenclature

- b_n Stress ratio
- c' Effective cohesion
- p' Mean effective stress
- u Pore pressure
- W Water content
- W_L Liquid limit
- W_N Natural water content
- W_P Plastic limit
- Δ Increment
- ϵ Strain
- $\epsilon_1, \epsilon_2, \epsilon_3$ Principal strains
- ϵ_v Volumetric strain
- ϵ_{oct} Octahedral normal strain
- γ_{oct} octahedral shear strain

[1] Professor, Department of Civil Engineering, École Polytechnique, Montreal, Quebec, Canada H3C 3A7.

[2] William Scott professor of civil engineering and applied mechanics, and director, Geotechnical Research Centre, McGill University, Montreal, Quebec, Canada H2A 2K6.

[3] Graduate research assistant, Soil Mechanics Laboratory, McGill University, Montreal, Quebec, Canada H2A 2K6.

σ Total normal stress

σ' Effective normal stress

$\sigma_1, \sigma_2, \sigma_3$ Total principal stresses

$\sigma_1', \sigma_2', \sigma_3'$ Effective principal stresses

σ_c' Effective consolidation pressure

σ_{oct} Octahedral normal stress

τ_{oct} Octahedral shear stress

φ' Effective angle of friction

Introduction

In soil mechanics and geotechnical engineering, constitutive relationships are usually obtained from the conventional triaxial test. However, because the lateral stress conditions imposed on a conventional triaxial sample are equal ($\sigma_2 = \sigma_3$) and therefore directly relevant only in certain cases, the limitations of the conventional tests, when applied to problems where non-axisymmetric or generalized stress conditions ($\sigma_1 = \sigma_2 = \sigma_3$) prevail, are a major disadvantage [*1*]. These limitations inhibit improvement of procedures for predicting the response behavior of soils from the results obtained in the conventional triaxial test.

For example, professional practice largely ignores soil anisotropy, even though it may be of fundamental importance in some soils, because (1) it is very difficult to measure in the conventional triaxial cell; (2) most models used for predicting soil response ignore anisotropic behavior; and (3) little information exists on its importance relative to that of other factors known to influence soil response [*2*].

If progress is to be made in developing more adequate constitutive relationships and in realistically simulating the stress path conditions encountered in the field, a triaxial test device capable of controlling both the magnitude and direction of the principal stresses must be used. The main factors that influence stress–strain response can be identified and used to evaluate the limitations of the existing soil models. The information obtained also may be used to develop new and more adequate constitutive relationships which better represent soil response under generalized states of stress. In addition, it is believed that, as more refinements are added to numerical methods of analysis used in geotechnical engineering problems, good use may be made of generalized stress–strain data pertaining to the more general conditions likely to exist in most regions of a soil mass.

This paper describes a true triaxial cell developed and in use for about 20 years at the Geotechnical Research Centre of McGill University for investigating the constitutive relationships of both granular and cohesive soils. Experimental data obtained on a variety of soils using the true triaxial cell are presented for the purpose of evaluating its reliability and versatility. The cell permits study of both the stress and strain response of soils under complex states of stress, under either drained or undrained conditions, with and without back pressure.

Description of the Test Facility

True Triaxial Cell

Ideally, to test a given theory or to develop stress–strain–failure relationships for comparison with a theory, a soil test should subject the soil specimens to homogeneous stress and strain conditions [*3*]. In addition, to represent the conditions imposed on real soils by real structures, it should be able to place the soil specimen in a general three-dimensional stress (or strain) space. The apparatus described in this section has been found to satisfy the homogeneity conditions and has undergone several stages of updating [*4–9*].

A schematic diagram of the true triaxial cell in present use is shown in Fig. 1. The principal feature of the apparatus is a set of brass pressure boxes for the application of the intermediate principal stress, σ_2. The brass boxes which contain deaired water may be pressurized to different levels to permit variations in applied σ_2 values. The desired value of the intermediate principal stress, σ_2, is applied to the soil through flexible but inextensible polyethylene membranes across openings congruent with the intermediate faces of the test samples. The application of the intermediate principal stress by means of the flexible membranes is believed to result in a quite uniform pressure distribution, as discussed also by Saada and Townsend [*3*].

The major principal stress, σ_1, is applied vertically through the ram by means of top and bottom Lucite platens. A porous stone embedded in the bottom platen allows drainage of the pore fluid. After the specimen was mounted on the pedestal and the lower part of the rubber membrane was sealed to the soil with two O-rings, distilled deaired water was allowed to run from the burette up between the specimen and the membrane to remove the air before sealing the top loading cap.

The minor principal stress, σ_3, or the cell pressure, results from a separate control system. Also, the triaxial cell is equipped with a rotating bushing for reducing piston friction.

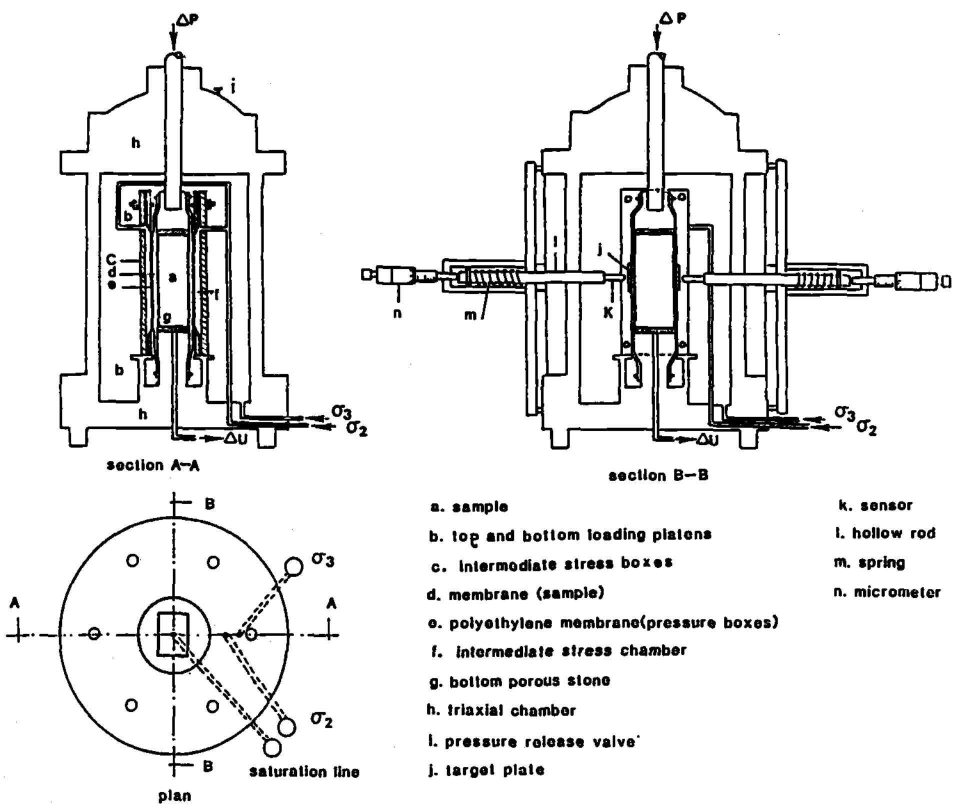

FIG. 1—*True triaxial apparatus.*

Vertical movements are measured by both a dial gauge and a linear variable differential transformer (LVDT) connected to the loading ram. In earlier versions of the cell, lateral deformations of the samples, in the direction of the minor principal stress σ_3, were recorded by a pair of dial gauges mounted on the pressure boxes, and connected by two lever mechanisms to the vertical faces of the specimen. In the most recent version of the cell, lateral deformations are measured by two micrometers mounted on the exterior of the cell chamber. The tests conducted with the pressure boxes showed that the faces of the clay specimens remained essentially planar during yielding. This was verified by stopping some of the tests at different strain levels and by observing the shapes of the deformed specimens. However, for the specimens brought to failure, it was observed that some bulging occurred; this was particularly true for those specimens in which plunging failure was not prevented. It is believed that bulging occurred because of the restriction caused by both the top and bottom loading caps.

In drained tests, volume changes are usually measured by means of graduated burettes. These changes may also be automatically recorded by using a differential pressure transformer. In undrained tests, the pore water pressure is measured by means of pore pressure transducers. In all the tests, back pressure may be used to ensure full saturation. Specifically, back pressure was used in the last series of tests reported in the paper, and saturation checks were made by calculating the value of the pore pressure coefficient B, at the beginning of the consolidation phases of the tests.

Because the test facility does not allow direct measurement of the deformation in the direction of the intermediate principal stress, σ_2, the strain in this direction is calculated by the following equation:

$$\epsilon_2 = \epsilon_v - (\epsilon_1 + \epsilon_3) = 3\,\epsilon_{oct} - (\epsilon_1 + \epsilon_3) \tag{1}$$

where

$\epsilon_1, \epsilon_2, \epsilon_3$ = strains in the major, intermediate, and minor principal stress directions
ϵ_v = volumetric strain
ϵ_{oct} = octahedral strain

For small strains, Eq 1 may be written

$$\frac{dL_2}{L_2} = \frac{dV}{V} - \left(\frac{dL_1}{L_1} + \frac{dL_3}{L_3}\right) \tag{2}$$

where

dL_1, dL_2, dL_3 = deformations in the major, intermediate, and minor principal stress directions
L_1, L_2, L_3 = original (before shearing) dimensions of the specimen in the direction of the major, intermediate, and minor principal stresses
dV = volume change
V = original (before shearing) volume of the specimen

When applying either Eq 1 or Eq 2, compressive strains are considered positive.

Sample Preparation

Soil specimens are prepared as for conventional triaxial tests. However, the specimens have a prismatic shape, as shown in Fig. 2, and measure 100.0 mm long by 50.8 mm wide by 38.1 mm thick.

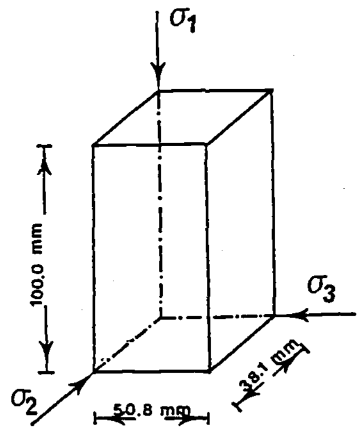

FIG. 2—*Specimen dimensions.*

For clay soils, following the trimming operations, each specimen is placed on the bottom platen, and side filter paper drains, measuring 2.5 to 5.0 mm wide, are added to reduce the time for consolidation. Detailed sample preparation techniques are described later in this paper.

The specimen is then enclosed in a thin rubber membrane sealed against the smooth surface of the loading cap and of the pedestal by rubber O-rings under tension, sprung into place from the end of a metal tube. Hose clamps fastened around the rubber O-rings were found to prevent the chamber fluid from leaking into the specimen.

The faces of the sealed specimen in contact with the flexible polyethylene membranes which apply the intermediate principal stress are covered with a thin film of petroleum jelly to reduce the friction between the deforming specimen and the flexible membranes.

Test Procedure

Following installation in the triaxial cell, each specimen is consolidated to a predetermined stress level. Once the consolidation phase is over, the specimen is sheared following a prescribed stress path. The direction of the stress path in principal stress space is a function of the values of the three principal stresses. The specimens are brought to failure by adding stress increments in the three principal stress directions. For the drained tests, volume change equilibrium is allowed to occur after each stress increment. For the undrained tests, the required degree of mobilization of both the deformations and excess pore water pressure determines the time for application of the next stress increment.

The method of loading is achieved through hydraulic controlled pressures providing the necessary stress increments. The manner of prescribing these stress increments is in the form of finite constant ratios established among the principal stresses. The intent here is to provide sufficient test information to allow for the examination of the experimental data in principal stress and strain space. As the true triaxial cell permits variations of the three principal stresses, it is possible to study the soil response in any chosen quadrant of the principal stress space shown in Fig. 3. However, it is easier to visualize the stress path followed in a particular test on a projection of the stress path on a octahedral plane, as shown in Fig. 4, than on the three-dimensional plot of Fig. 3.

To maintain linear stress paths in any chosen sector of the octahedral plane, increments in principal stresses need to be adjusted according to a stress ratio b_n^- where n varies from

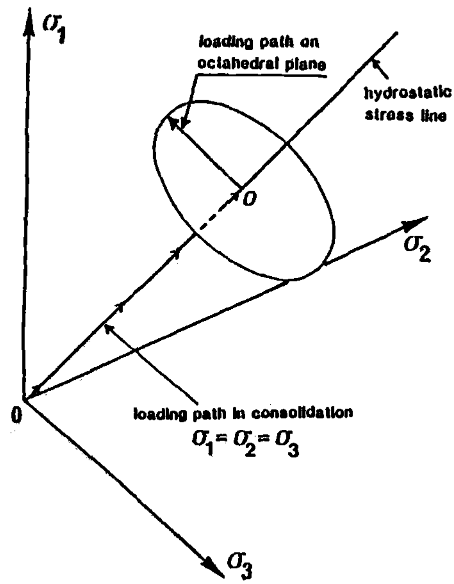

FIG. 3—*Principal stress space.*

1 to 6, as shown in Fig. 4. For example, if one chooses sector 6, adjustments in the stress increments are made in such a way that $b_6 = (\sigma_2 - \sigma_3)/(\sigma_1 - \sigma_3)$. For $b_6 = 0$, the test reduces to a conventional triaxial compression test in which $\sigma_1 > \sigma_2 = \sigma_3$, and the projection of the stress path is along the positive σ_1-axis. For $b_6 = 1.0$, the test conditions are $\sigma_1 = \sigma_2 > \sigma_3$ and the projection of the stress path is along the negative σ_3 axis. For loading along

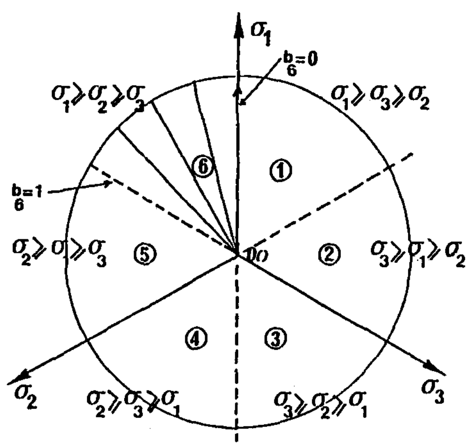

$b_1 = \sigma_3 - \sigma_2 / \sigma_1 - \sigma_2$	$b_4 = \sigma_3 - \sigma_1 / \sigma_2 - \sigma_1$
$b_2 = \sigma_1 - \sigma_2 / \sigma_3 - \sigma_2$	$b_5 = \sigma_1 - \sigma_3 / \sigma_2 - \sigma_3$
$b_3 = \sigma_2 - \sigma_1 / \sigma_3 - \sigma_1$	$b_6 = \sigma_2 - \sigma_3 / \sigma_1 - \sigma_3$

FIG. 4—*Front view of octahedral plane.*

other linear stress paths in sector 6, the ratios established for b_6 are chosen to vary between 0 and 1. In addition, a conventional triaxial extension test in which $\sigma_3 = \sigma_2 > \sigma_1$ has the projection of its stress path along the negative σ_1 axis.

Test Results

Undrained Tests on a Normally Consolidated Kaolinite

The first series of tests with the true triaxial cell was carried out on specimens of normally consolidated remolded kaolinite, under undrained conditions and without back pressure [*4–6*]. The clay used in this study was a kaolinite, identified as S187 English clay, with the following properties: $W_L = 54\%$; $W_P = 37.5\%$; specific gravity = 2.62; and grain sizes by weight = 99.5% finer than 10 μm and 77.8% finer than 2 μm.

Samples of the clay were prepared initially in slurry form ($W = 120\%$) with deaired, distilled water. Each sample was vacuum deaired and mixed in a 78.0-mm-diameter Lucite cylinder. Once the cylinder was filled with slurry, the vacuum system was dismantled and the soil was one-dimensionally consolidated in steps under static loads, up to a maximum pressure of about 100 kPa. Following consolidation the sample was extruded and cut in several pieces. Each piece was then trimmed to the final dimensions of the prismatic specimen shown in Fig. 2. The specimen was isotropically consolidated under a predetermined confining pressure, σ_c', which varied from 207.0 to 414.0 kPa for all the tests.

After consolidation, loading combinations were applied to the clay specimen in small equal increments. The specimens were brought to failure by keeping the cell pressure, σ_3, constant and equal to the consolidation pressure, σ_c', and by increasing the values of both σ_1 and σ_2. The major principal stress, σ_1, was increased by adding dead load increment on the top loading ram. The intermediate principal stress, σ_2, was increased by increasing the water pressure in the flexible polyethylene membranes. These two operations were performed manually and simultaneously. During each increment of loading, deformations and pore water pressures were continuously monitored and recorded. Additional load increments were applied only after equilibrium in both the deformations and pore water pressures was achieved for the previous loads. Because these experiments allowed full variation of the intermediate principal stress between the major and minor principal stresses, the entire range of stress combinations in principal stress space ($\sigma_1 \geq \sigma_2 \geq \sigma_3$) could be investigated.

In the authors' opinion, the most important results obtained in this study are the following:

1. The clay obeys Prandtl-Reuss plastic strain increment–deviator stress proportionality relations, for octahedral shear strains, γ_{oct}, where

$$\gamma_{oct} = \frac{1}{3}[(\epsilon_1 - \epsilon_2)^2 + (\epsilon_2 - \epsilon_3) + (\epsilon_3 - \epsilon_1)^2]^{1/2} \tag{3}$$

   not exceeding 0.5%. This result allows the use of analytical concepts of normality of plastic strain increments to the yield surface in stress space and coincidence of the plastic potential and yield surface.
2. When the deviator stresses are increased to more than one half of the ultimate shear strength of the clay, the deformation behavior deviates from that of an isotropic plastic material and approaches that of a purely frictional medium. The ultimate stresses the clay can resist obey a linear Mohr-Coulomb criterion having $c' = 34.5$ kPa and $\varphi' = 19°$. Some of the results obtained at failure are shown in Figs. 5 and 6.

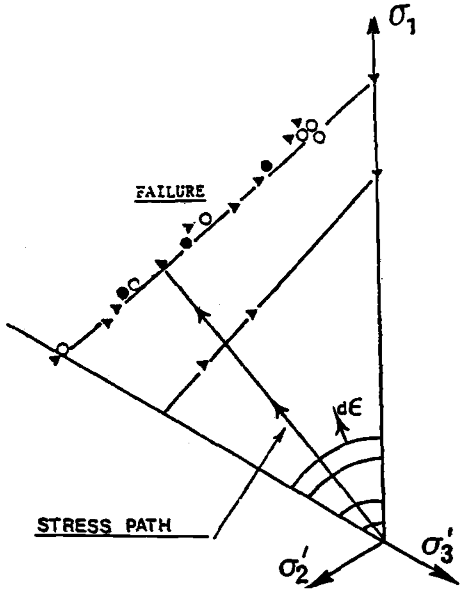

FIG. 5—*Failure stress combinations in octahedral plane in principal stress space (adapted from Ref 5).*

Drained Response of a Sensitive Clay

The second series of tests was carried out on undisturbed samples of a sensitive clay from St-Louis de Bonsecours, Quebec. These tests were performed to determine the drained stress–strain–failure response of this cemented clay having the following properties: W_N = 64%; W_L = 48%; W_P = 28%; clay content = 79%; silt content = 20%; sand content = 1%; sensitivity = 50; vertical preconsolidation pressure = 160 kPa; overconsolidation ratio = 2.2.

Following isotropic consolidation, two types of true triaxial tests were performed in this study. These were

(a) Constant p' tests in which the effective mean stress p' or σ_{oct}', defined by

$$\sigma_{oct}' = \frac{\sigma_1' + \sigma_2' + \sigma_3'}{3} \tag{4}$$

was kept constant throughout each test

(b) Variable (increasing) p' tests in which the effective mean stress p' increased throughout the shearing process

The confining pressure, σ_c', used in these tests varied between 17.3 and 276.0 kPa, and the stress boundary conditions were such as to result in stress paths again contained in sector 6 of Fig. 4.

Some of the results obtained in the course of this study have already been reported [*5*,*7*,*8*,*10*,*11*].

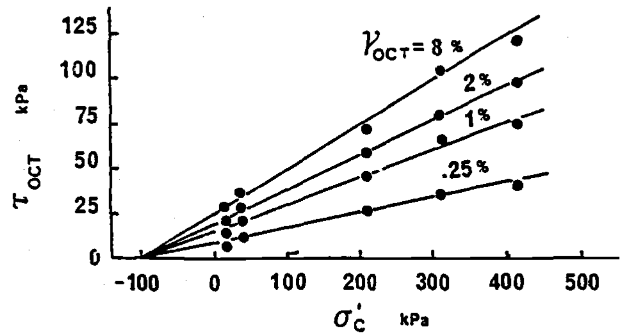

FIG. 6—*Octahedral shear stress levels versus consolidation pressures at various octahedral shear strain levels (adapted from Ref 5).*

The experimental data obtained in this study permitted the following observations:

1. The stress–strain curves for samples consolidated at confining pressures less than about 60 to 70% of the vertical preconsolidation pressure of the clay were linear up to the failure strength.

   Different stress ratios b_6 resulted in different stress–strain curves. In addition, it was possible to predict, within certain limits, the soil response by using the theory of anisotropic elasticity, thus reinforcing the evidence that some of the cemented sensitive clays of Eastern Canada may be considered as anisotropic elastic materials at working stress levels. It was also observed that as yielding of the soil approached, deviations between predicted and measured results became more pronounced. Such a behavior was as expected because the relationships used depended on the constancy of the values of the elastic parameters retained and were therefore viable as predictions as long as the clay structure remained intact.

   Further, when considering the failure stresses, it was found that the intermediate principal stress, σ_2', influenced the response of the clay to a large extent. It was determined that Hill's failure criterion of anisotropic plasticity [*12*] best represented the observed behavior. It was concluded that, at low confining pressures, because the consolidation pressures are not sufficient to cause a breakdown of the cementation bonds and the soil structure, the clay failed at stresses dictated by the strength of the cementation bonds and the anisotropy of the soil. Such a response was compatible with the fact that both axial deformations and volumetric strains were very low at failure, suggesting that the bonds provided most of the strength and resulted in a minimum amount of relative movement between the soil particles.
2. It was found that for consolidation pressures in excess of about 60 to 70% of the vertical preconsolidation pressure of the clay, there appeared to be a progressive breakdown of the cementation bonds following initial yield and the post-yield might be identified with an insensitive, normally consolidated clay. When considering the stress–strain curves obtained, for example, in the constant p' tests, it is observed again that there is not a unique relationship for the various values of the stress ratio b_6 used. In addition, for the same value of the octahedral shear stress, τ_{oct}, defined by

$$\tau_{oct} = \frac{1}{3}\left[(\sigma_1 - \sigma_2)^2 + (\sigma_2 - \sigma_3)^2 + (\sigma_3 - \sigma_1)^2\right]^{1/2} \tag{5}$$

the volumetric strain, ϵ_v, obtained in the case of the lower values of b_6 was larger than that obtained for higher stress ratios. Such a behavior resulted from the fact that for high values of b_6, there is a very important expansion in the direction of σ_3', which is compensated by the compressions in the direction of both σ_1' and σ_2'.

The stress–strain curves also indicated a pronounced nonlinear behavior and a stiffness increasing with the consolidation pressure, as is usually observed in the case of remolded insensitive clays. The mobilization of large volumetric strains in the constant p' tests indicated that the destructured clay may not be considered as an isotropic workhardening plastic material because, in this type of test, no volumetric strains should occur. In addition, when considering the failure stresses, it was found that the intermediate principal stress was of no influence and that a linear Mohr-Coulomb criterion having $c' = 0$ and $\varphi' = 27$ to $30°$ was adequate in representing its response. Among the various results obtained in this study, there are two diagrams which, in the authors' opinion, are of utmost importance for the understanding of clay behavior. The first, shown in Fig. 7, presents in principal stress space the successive yield surfaces observed for the tests performed at $p' = 207.0$ kPa. The stress contours have been drawn at increasing values of the octahedral shearing strain, γ_{oct}. On the same diagram the projections of the strain increment vectors have been superimposed. The results show that there is a gradual change of shape of the yield surfaces and that, at failure, the clay obeys a Mohr-Coulomb criterion because the experimental points plot on an irregular hexagon as required by the Mohr-Coulomb theory. In addition, at failure, the strain increment vectors appear to be normal to the Mohr-Coulomb failure surface. However, when one superimposes a γ_{oct}–ϵ_{oct} diagram on the failure envelopes of the normally consolidated clay, as shown in Fig. 8, it appears then that it is not the strain increment vectors themselves that are normal to the failure surface but it is their

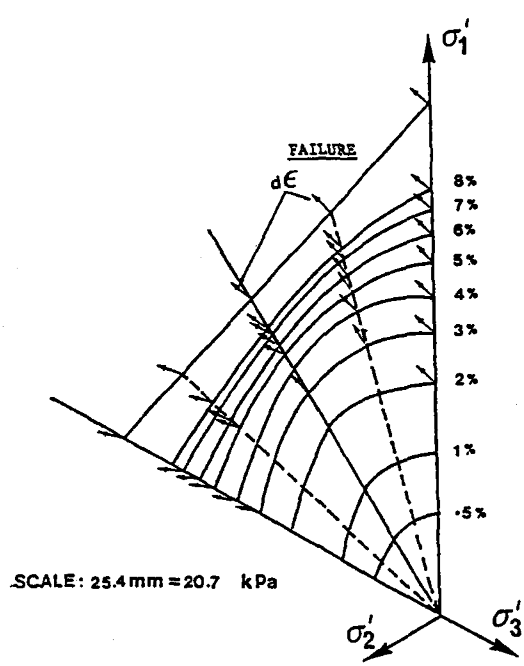

FIG. 7—*Loading and failure surface in octahedral plane.*

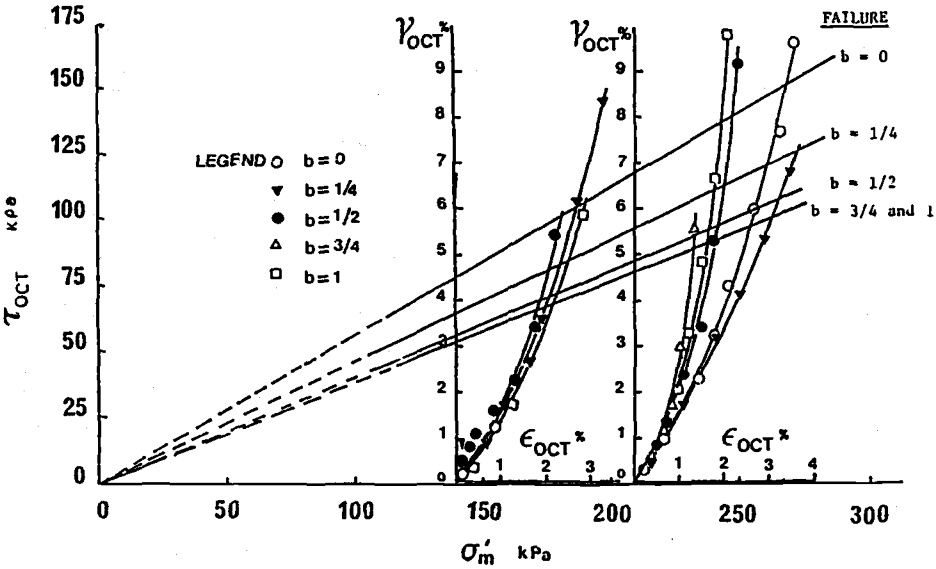

FIG. 8—*Failure envelopes and octahedral shear strain–normal strain relationships.*

projections, as already shown in Fig. 7. Had the strain increment vectors been normal to the failure envelopes, the slopes of the γ_{oct}–ϵ_{oct} curves would have been perpendicular to the corresponding failure lines.

Undrained Response of an Anisotropic Remolded Clay

The latest series of tests with the true triaxial cell was carried out on specimens of normally consolidated anisotropic remolded clay, under undrained conditions and with back pressure saturation [*9,13*]. The clay used in this study was a kaolinite clay identified as Hydrite 121 from Georgia Kaolin Co. Some of its engineering properties are as follows: W_L = 49.6%; W_P = 37.90%; specific gravity = 2.61; and grain sizes by weight = 100% finer than 30 μm and 10% finer than 0.2 μm.

The dry powdered kaolinite was mixed with distilled water to a slurry of about 120% water content, and subsequently drawn by vacuum through distilled deaired water and allowed to settle in a 203-mm-diameter consolidation apparatus. Each sample was consolidated one-dimensionally under increasing loads to a final vertical consolidation pressure of 207 kPa. The cylindrical block samples obtained were 203 mm in diameter and approximately 177.8 mm in height.

Four series of unconsolidated undrained true triaxial tests with pore pressure measurements were performed on prismatic specimens shown in Fig. 2. In the first series, the major principal stress axis was applied coincident with the direction of the one-dimensional consolidation load application, that is, "perpendicular" to the bedding plane of the soil particles. In the other series of tests, the directions of major principal stress relative to the bedding plane were 60, 30, and 0°.

In the testing procedure, specimens were first consolidated under application of equal principal stresses (that is, $\sigma_1 = \sigma_2 = \sigma_3$) to a predetermined stress level. Following consolidation, increments in principal stresses were made to provide loading along a prescribed stress path on the octahedral plane as shown in Fig. 3. To maintain linear stress paths in any chosen segment on the octahedral plane shown in Fig. 4, increments in principal stresses (that is, $\Delta\sigma_1$, $\Delta\sigma_2$, and $\Delta\sigma_3$) need to be adjusted according to a set of stress ratio b_n^- where n varies from 1 to 6 as shown in the figure. For the test series in this study, segment 6 was chosen, and adjustments were made in the increments of principal stresses such that $b_6 = (\sigma_2 - \sigma_3)/(\sigma_1 - \sigma_3)$ remained constant. During the process of loading the mean stress $(\sigma_1 + \sigma_2 + \sigma_3)/3$ was constant.

The experimental data obtained in this study permitted the following observations:

1. It is apparent from Fig. 9 that the deviation between the stress and strain increment

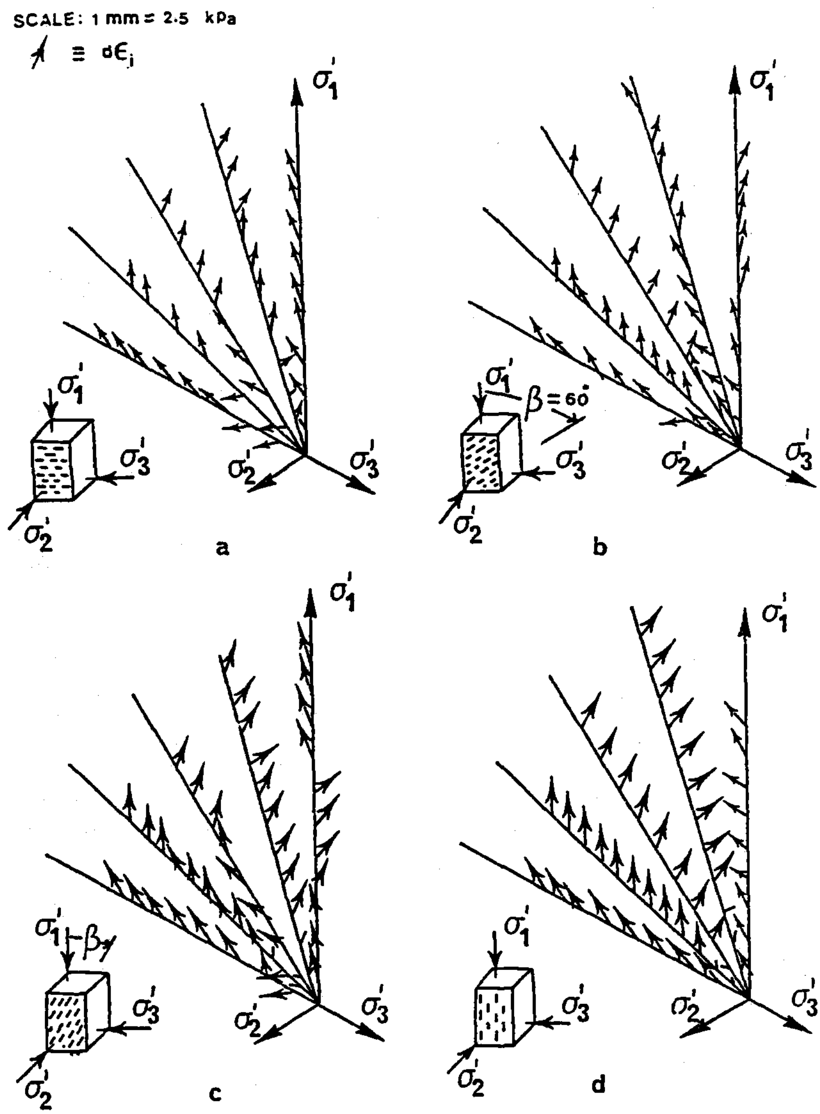

FIG. 9—*Deviatoric stress vectors and strain increment vectors in octahedral plane.* (a) *90° orientation angle.* (b) *60° orientation angle.* (c) *30° orientation angle.* (d) *0° orientation angle.*

vectors is a consequence of material structure anisotropy which is associated with the procedure used in preparing the anisotropic specimens. For the test results, the effect of initial and induced anisotropies on the resultant deformation anisotropy is evident. The former effect can be explained by choosing a test series, loaded at a particular value of stress ratio b_6, using specimens with varying initial degrees of particle bedding orientation. The disassociation angle between the strain increment vectors and the stress increments along the prescribed stress path is seen to vary with the initial degree of orientation of bedding planes. These variations appear to be a function of the structure and rigidity of the soil under consideration.

The effect of stress-induced anisotropy on the resultant strain increment vectors is characterized by the effect of the intermediate principal stress. The variation of the disassociation angle from one state of stress to another is a function of the degree of reorientation of clay particles in the process of loading. (This is discussed in Ref 9.) The experimental results clearly show that the initial and induced anisotropies exercise significant control on the characteristics of the resultant strain increment vectors.

2. Figure 10 shows the stress surface results from tests conducted at σ_{oct} = 207 kPa for 90, 60, 30, and 0° inclinations of bedding planes. The solid lines connecting the points for each stress ratio represent the failure surface in the octahedral plane. The dashed lines represent the successive stress "surfaces" for different octahedral shear strains. These successive surfaces show convexity and concavity at various stages of straining. Concavity appears to vanish when the specimens approach failure, ending with a convex failure surface in each stress sector. This behavior can be attributed to the effect of initial and stress-induced anisotropies.

From these observations one concludes that the degree of disassociation depends on initial fabric anisotropy and stress-induced anisotropy. Nevertheless, for the inherently anisotropic material, there is no particular requirement (1) for the yield and plastic potential to coincide, and (2) for an associated flow rule to hold.

Conclusions

A true triaxial apparatus, in which a prismatic specimen is confined between cap and base rings and outside membrane, offers the advantage of individual control of major, intermediate, and minor principal stresses. This advantage helps in realistically simulating the stress path conditions encountered in the field and in adequately developing a more rigorous constitutive relationship which better represents soil response under generalized states of stress. It is shown that the true triaxial cell permits study of both the stress and strain response of soils under complex states of stress, under either drained or undrained conditions, with or without back pressure.

In the first series of tests, the true triaxial cell permits evaluation of the analytical concepts of normality of plastic strain increments to the yield surface in stress space and coincidence of the plastic potential and yield surface for initially isotropic clays; while, in the second series of tests, the cell permits evaluation of the effect of the cementation bonds and the anisotropy of the soil at low and high confining pressures.

In the last series of tests, the true triaxial cell permits evaluation of the effect of initial and stress-induced anisotropies on the yielding and failure of anisotropic clay. Nevertheless, the specification of both the magnitudes and directions of stress and strain increment vectors, which are important in developing a more adequate constitutive relationship, is also provided.

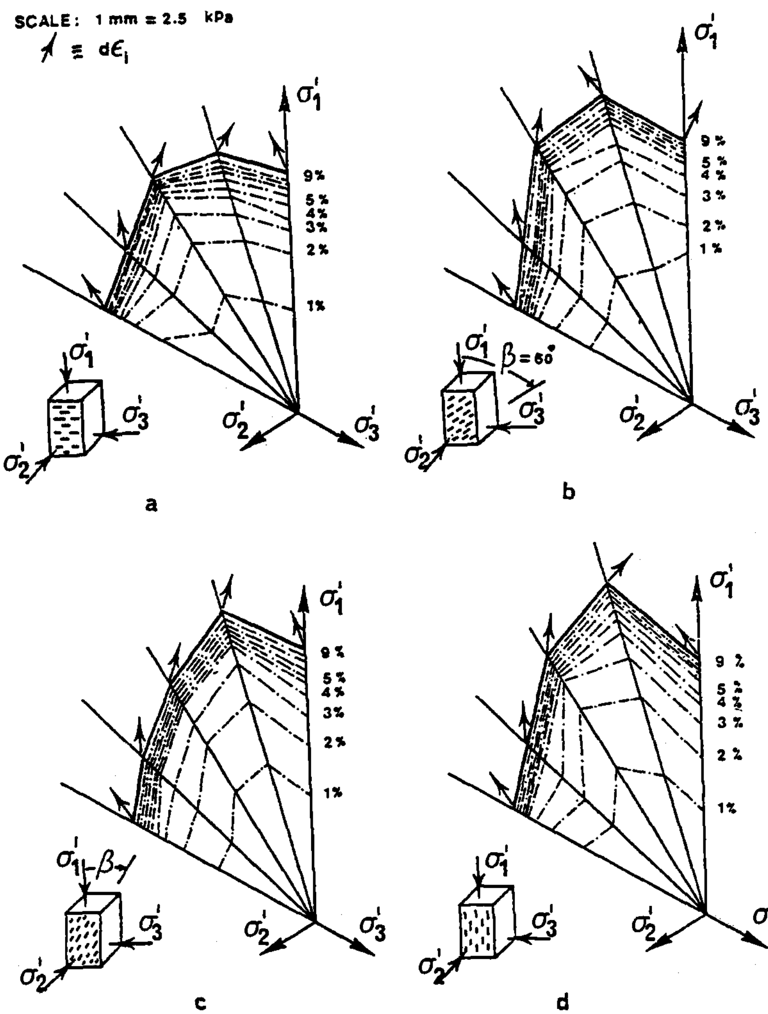

FIG. 10—*Loading and failure surface in octahedral plane.* (a) *90° orientation angle.* (b) *60° orientation angle.* (c) *30° orientation angle.* (d) *0° orientation angle.*

Acknowledgments

These studies were conducted under funding support from the Natural Sciences and Engineering Research Council of Canada (NSERC), Grant No. A-882 to the second named author. General support for all the authors from NSERC is gratefully acknowledged.

References

[*1*] Pearce, J. A., in *Stress-Strain Behaviour of Soils*, R. H. G. Parry, Ed., Cambridge University, Cambridge, England, 1972, pp. 330–339.

[*2*] Arthur, J. R. F., Bekenstein, S., Germaine, J. T., and Ladd, C. C., in *Laboratory Shear Strength of Soil, ASTM STP 740*, American Society for Testing and Materials, Philadelphia, 1981, pp. 516–540.

[3] Saada, A. S. and Townsend, F. C., in *Laboratory Shear Strength of Soil, ASTM STP 740*, American Society for Testing and Materials, Philadelphia, 1981, pp. 7–77.
[4] Yong, R. N. and McKyes, E., in *Proceedings*, Third Pan-American Conference on Soil Mechanics and Foundation Engineering, Caracas, Vol. 1, 1967, pp. 131–143.
[5] Yong, R. N. and McKyes, E., *Journal of Soil Mechanics and Foundation Engineering Division, American Society of Civil Engineers*, Vol. 97, No. SM1, 1971, pp. 159–176.
[6] Yong, R. N., McKyes, E., and Silvestri, V., *Archives of Mechanics*, Vol. 14, No. 3, 1972, pp. 511–528.
[7] Yong, R. N. and Silvestri, V., in *Proceedings*, Ninth International Conference on Soil Mechanics and Foundation Engineering, Specialty Session No. 9, Tokyo, 1977, pp. 271–277.
[8] Yong, R. N. and Silvestri, V., *Canadian Geotechnical Journal*, Vol. 16, No. 2, 1979, pp. 335–350.
[9] Yong, R. N. and Mohamed, A. M. O., *International Journal of Mechanics of Materials*, Vol. 3, No. 4, 1984, pp. 301–310.
[10] Silvestri, V., in *Proceedings*, International Symposium on the Mechanical Behaviour of Structured Media, Ottawa, Vol. 5B, 1981, pp. 357–372.
[11] Yong, R. N. and Ko, H.-Y., in *Limit Equilibrium, Plasticity and Generalized Stress–Strain in Geotechnical Engineering*, American Society of Civil Engineers, Montreal, 1981, pp. 1–48.
[12] Hill, R., *The Mathematical Theory of Plasticity*, Oxford University Press, London, 1950, p. 355.
[13] Mohamed, A. M. O., *The Behaviour of Anisotropic Clay Under a Complex State of Stress*, M. Eng. thesis, McGill University, Montreal, Quebec, Canada, 1983, p. 230.

Tetsuro Esaki,[1] Tsuyoshi Kimura,[2] Kazuo Aoki,[3] and Tadashi Nishida[1]

True Triaxial Test of Rock Under Stress and Strain Rate Control

REFERENCE: Esaki, T., Kimura, T., Aoki, K., and Nishida, T., **"True Triaxial Test of Rock Under Stress and Strain Rate Control,"** *Advanced Triaxial Testing of Soil and Rock, ASTM STP 977,* Robert T. Donaghe, Ronald C. Chaney, and Marshall L. Silver, Eds., American Society for Testing and Materials, Philadelphia, 1988, pp. 834–843.

ABSTRACT: The significance of true triaxial tests instead of conventional tests has been enhanced because of the need for generalized constitutive laws for geomaterials. To investigate the behavior of rock masses having restricted conditions for strains, tests of marble under strain rate control as well as stress rate control were performed using a specially designed true triaxial apparatus with rigid platens. As an example of a set of restricted conditions, the condition of the mean principal strain being constant was adopted when the octahedral shear strain was increased. The direction of stress paths obtained under these conditions is discussed, along with the elastic, dilatant, and contractile behavior of marble as clarified by stress controlled tests.

KEY WORDS: true triaxial tests, rock, stress rate control, strain rate control, mean principal strain, mean principal stress, octahedral shear strain, octahedral shear stress, stress path, constitutive laws, rigid platens, flexible membranes

Characteristics of strength and deformation of rocks have usually been investigated by triaxial compression tests because of the simplicity of the testing apparatus. However, considering that stress distributions are inherently three-dimensional and that the development of numerical methods and constitutive laws enables structural analyses of complex three-dimensional problems, the need for true triaxial tests (often called multiaxial tests) is reinforced. Handin et al. [*1*] applied a torsion to the hollow cylindrical specimen under confining pressure with axial loading to obtain three different principal stresses. This experimental procedure, however, is unsuitable because of the difficulty of preparing the specimen. The alternative is compressive loading on three opposite pairs of faces of the prismatically (cubically) shaped specimen [*2–6*]. Whether forces are applied on the specimen through flexible membranes or rigid platens has a great influence on the distribution of stresses and strains within the specimen as pointed out by Sture and Desai [*3*]. In using flexible membranes, normal principal stresses can be assured on the loading faces and a uniform stress distribution overall is possible. On the contrary, strains can be measured accurately and higher stress fields are reproducible in rigid platens, although the uniformity of induced stresses is difficult to verify.

[1] Associate professor and professor of Faculty of Engineering, respectively, Kyushu University, Fukuoka 812, Japan.

[2] Research associate of Department of Mining, Kyushu University, Fukuoka, 812, Japan.

[3] Senior research officer of National Research Institute for Pollution and Resources, MITI, Tsukuba 305, Japan.

Stress paths in the above mentioned true triaxial tests are generally as follows:

1. After increasing the hydrostatic stress (corresponding to the minimum principal stress) to a specified level, the intermediate and maximum principal stresses are raised to another specified level while holding the minimum principal stress constant. Finally, the maximum principal stress is varied while holding the minimum and intermediate principal stresses constant. If the intermediate principal stress equals the minimum principal stress, these tests correspond to conventional triaxial tests under constant confining pressure.
2. After increasing the mean principal stress along the hydrostatic axis up to a specified level, the octahedral shear stress is increased while holding the mean principal stress constant.

The tests with stress paths 1 and 2 can show the influence of the intermediate principal stress on characteristics of materials, and the latter tests can also give the failure surface on the octahedral plane. In both the tests, however, all principal stresses may be controlled at given rates (including no increment). Therefore, stress states change on specified paths only.

It is not assumed that these test conditions replicate natural loading conditions. The actual behavior of rock masses with free surfaces is restricted to various conditions for stresses or strains. To investigate the behavior of rock masses, it is necessary to perform the tests as simulations of natural restricted conditions. For example, the phenomenon of slope sliding near the ground surface demonstrates that the displacement in the sliding direction increases under the condition that the normal stress on the sliding plane is constant. This is treated by direct shear tests under constant normal stress which are a reasonable simulation of reality. On the other hand, the rock masses surrounding underground openings at great depth move to their free surface when the displacement perpendicular to the direction of their movements is restricted. The laboratory tests corresponding to such strain paths, that is, ones in which two or three principal strains are controlled at given rates, have not been performed until now.

For the purpose of simulating the fundamental behavior of rock masses that have restricted strain paths, in this study, strain controlled true triaxial tests of rock were performed by using a specially constructed testing apparatus with rigid platens. The rigid platens allow more accurate measurement of strains and the reproduction of higher stress fields than when using flexible membranes. The direction of the stress paths obtained by the increase of the octahedral shear strain under the constant mean principal strain condition were investigated, along with the results of the constant mean principal stress tests.

Experimental Procedure

Apparatus

The true triaxial testing apparatus used in the present experiment has one jack with a capacity of 2 MN in the vertical direction and four jacks of 1-MN capacity in the horizontal directions. The value of stress is calculated by dividing the load, measured with a load cell, by the area of the rigid platens, 36 by 36 mm, so that the magnitude of stress in the vertical direction can be increased up to about 1.5 GPa. The triaxial box (Figs. 1, 2, and 3), specially designed to produce more uniform stress distribution and prevent eccentric loading, has six guide holes through which the piston rods are applied. Relative displacements between two opposite rings set up on the piston rods are measured by two displacement transducers of strain-gauge-type in each direction. At that time, by connecting the cables of the two transducers in parallel, the average value of the two is detected. The value detected is divided by the distance between the two rings to calculate the magnitude of strain. The strain obtained in this way includes also an elastic component of the piston rods. The elastic

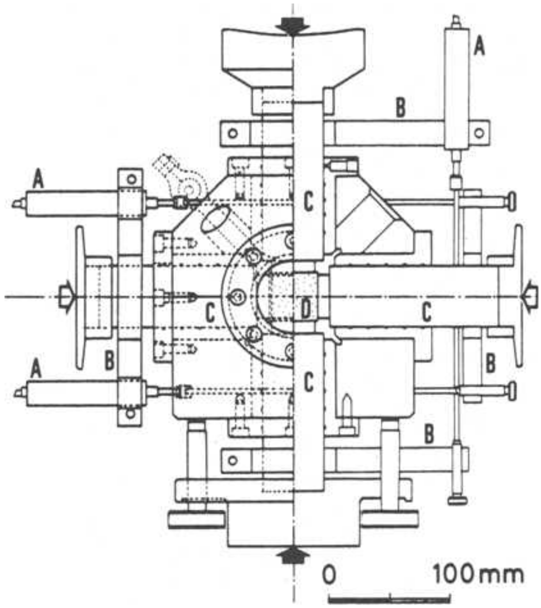

FIG. 1—*Side view of triaxial box:* (a) *displacement transducer,* (b) *ring,* (c) *piston rod, and* (d) *specimen.*

strain can be calculated by microcomputer considering the value of stress at that time and the deformation of the piston rods. The strain, from which the elastic component of the piston rods is excluded, or stress is used as a feedback signal of a closed-loop servo system with process controller. Three sets of that system give exact stress rates or strain rates independently in the three directions.

Specimen

All of the experimental work was performed using Akiyoshi marble. Cubic 40-mm specimens were cut from one large block and their surfaces were ground flat to within ±0.05

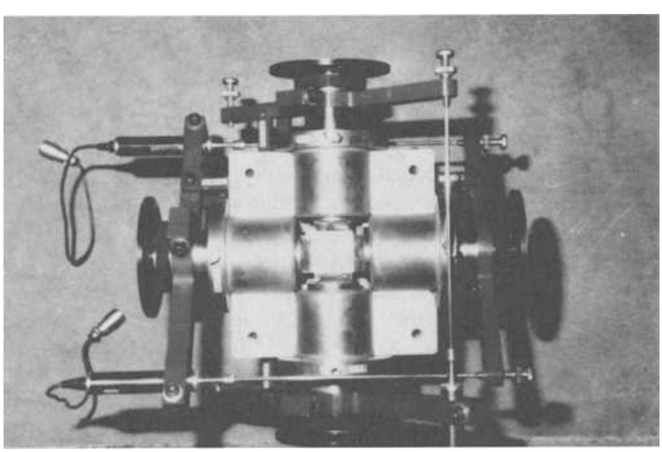

FIG. 2—*Top view of triaxial box.*

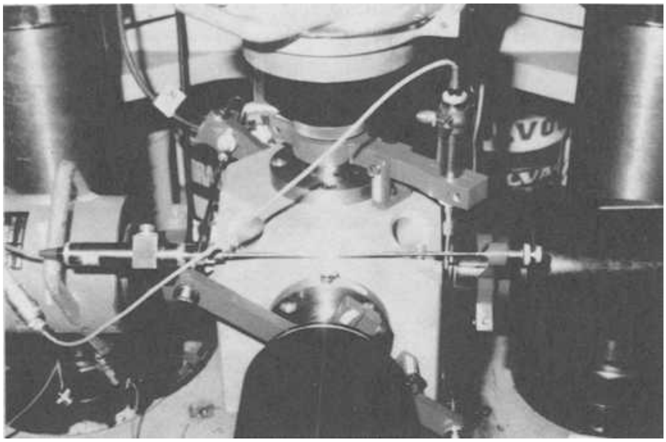

FIG. 3—*Triaxial box set up in loading apparatus.*

mm. Because the strength (uniaxial compressive strength σ_c = 71.6 MPa) and the deformability (Young's modulus E = 60.0 GPa) of Akiyoshi marble are nearly constant in three mutually perpendicular directions, it is considered to be homogeneous and isotropic.

Procedure

In the present experiment, first, the mean principal stress σ_m was increased to given values along the hydrostatic axis. We term the values the initial hydrostatic pressure, σ_{m0}. After that, tests were carried out under two conditions:

(A) mean principal stress σ_m is constant and
(B) mean principal strain ϵ_m is constant.

Under Condition A, the octahedral shear stress τ_{oct} was increased up to failure states of the specimen with various values of μ which is called Lode's parameter and given by the expression [7]

$$\mu = (2\sigma_2 - \sigma_1 - \sigma_3)/(\sigma_1 - \sigma_3) \tag{1}$$

where σ_1, σ_2, and σ_3 are the maximum, intermediate, and minimum principal stresses, respectively. This parameter ranges between -1 and 1, which represent the states of triaxial compression ($\sigma_2 = \sigma_3$) and triaxial extension, ($\sigma_1 = \sigma_2$), respectively. Under Condition *B*, the octahedral shear strain γ_{oct} was increased with various values of μ' given by the expression

$$\mu' = (2\epsilon_2 - \epsilon_1 - \epsilon_3)/(\epsilon_1 - \epsilon_3) \tag{2}$$

TABLE 1—*The values of* μ' *and three principal strain rates used under Condition B.*[a]

μ'	$\dot{\epsilon}_1$	$\dot{\epsilon}_2$	$\dot{\epsilon}_3$
−1	1600	−800	−800
−1/3	2750	−550	−2200
1/3	2200	550	−2750
1	800	800	−1600

[a]Unit : $\times 10^{-6}$/min.

where ϵ_1, ϵ_2, and ϵ_3 are the maximum, intermediate, and minimum principal strains, respectively. The value of μ' in perfectly homogeneous and isotropic materials equals that of μ. The tests with $\mu' = -1$ correspond to conventional triaxial undrained tests of soils. The values of μ' and the three strain rates used are shown in Table 1. No lubricant was usually inserted between the specimen and the rigid platens in both Conditions A and B, for the reason that the lubricants prevent accurately measuring the relative displacement between two opposite platens.

Results and Discussion

Tests Under Condition A

The relationship between the octahedral shear stress and the octahedral shear strain for $\mu = -1$ is shown in Fig. 4. The slope of the stress-strain curves which represent a shear modulus, decreases progressively to zero with increasing the octahedral shear stress. This final behavior is a perfectly plastic flow in appearance. We define the yield stress at the inflection point of the stress-strain curve expressed in logarithms, and the failure stress at the stress level of the perfectly plastic flow. The slope of the stress-strain curves does not depend on the initial hydrostatic pressure but on the failure stress. Figure 5 shows the relationship between the octahedral shear stress and the mean principal strain for $\mu = -1$. The curve of $\sigma_{m0} = 50$ MPa rises perpendicularly to the axis of the mean principal strain up to $\tau_{oct} = 30$ MPa and thereafter turns to the negative strain. The perpendicularity and the nonlinearity show the elastic and dilatant behaviors of Akiyoshi marble, respectively. At more than 250 MPa in the initial hydrostatic pressure, the mean principal strain changes with positive increments only. This deformation suggests the contractile behavior. The boundary which distinguishes between the dilatant and contractile behaviors at failure is in $\sigma_m = 200$ to 300 MPa. The stress of this boundary agrees with that of the brittle-ductile transition, obtained from conventional triaxial tests, as described by Gowd and Rummel [8].

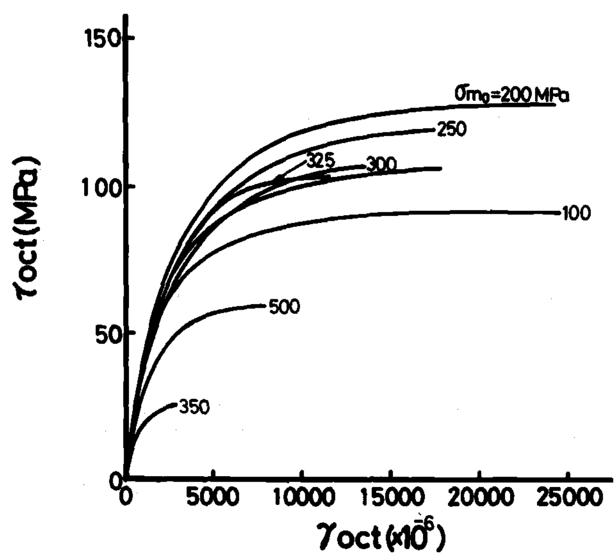

FIG. 4—*The octahedral shear stress-octahedral shear strain curves for* $\mu = -1$ *under Condition A.*

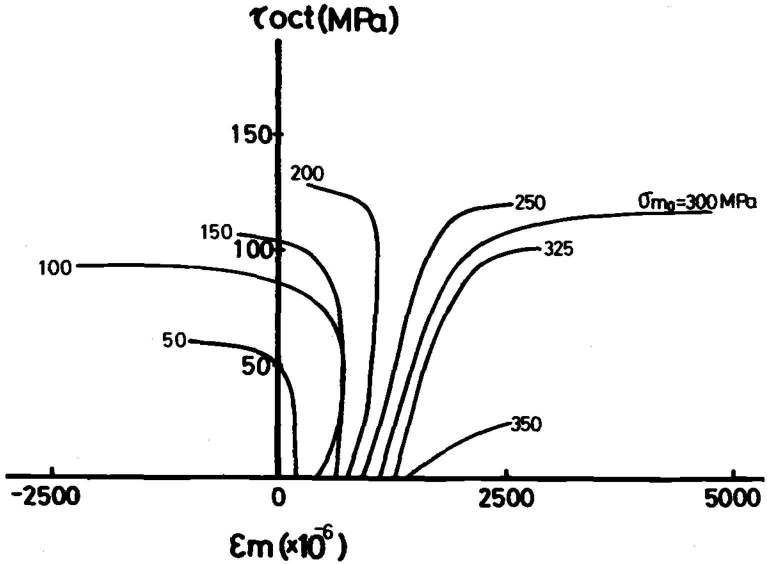

FIG. 5—*The octahedral shear stress-mean principal strain curves for* $\mu = -1$ *under the Condition A.*

Figure 6 shows the yield and failure surfaces on the Rendulic stress plane. The yield surface is closed on the hydrostatic axis as treated as Cap Model [*9*] in soil mechanics and as also found in some rocks [*10*]. The failure surface obtained by using Teflon® sheets to eliminate the friction between the platens and the specimen is also shown in Fig. 6. The magnitude of the failure stresses depends on whether the Teflon sheets are used or not.

In lower mean principal stresses, the failure stresses of the specimen without the Teflon

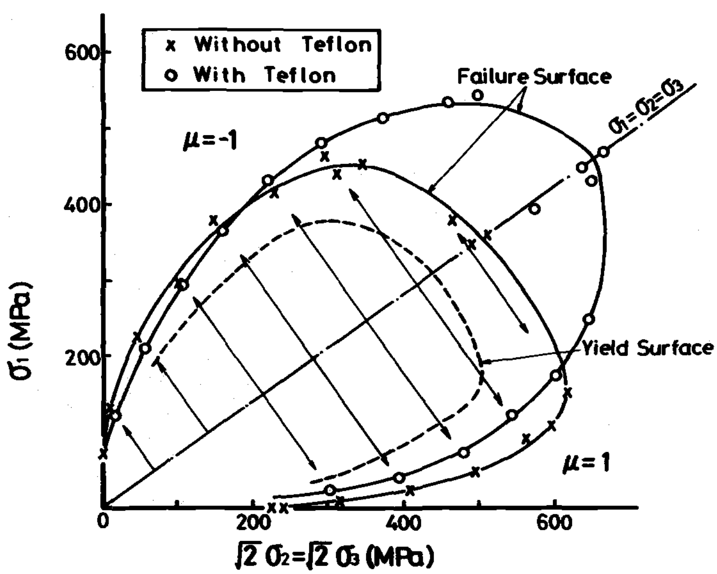

FIG. 6—*The yield and failure surfaces on the Rendulic stress plane.*

sheets are greater than those with the Teflon sheets. This difference can be explained by the friction on the surface of the specimen without the Teflon sheets. The friction that results from the strain incompatibility between rock and steel acts against the maximum stress applied along an axis of the specimen, and is added to the minimum stress along another axis. The effect of this friction requires greater octahedral shear stress to fail the specimen than the intrinsic strength of rock which, if the Teflon sheets entirely play their part, could be identical with the failure stress of the specimen with the Teflon sheets.

In higher mean principal stresses, on the other hand, the failure stresses of the specimen without the Teflon sheets are less than those with the Teflon sheets, and the two failure surfaces are closed on the hydrostatic axis as well as the yield surface. In very high stress levels, intense damages were observed at the edges of the specimen, especially without the Teflon sheets (while only macroscopic fractures were visible in lower mean principal stresses). Since the steel platens are somewhat smaller than the surface of the specimen, no normal stress can be applied to its edges. This geometrical condition and the friction on the surface of the specimen produce enormously nonuniform stress distributions at the edges and result in localized damages before the whole specimen fails. Therefore, it is considered that the apparent failure under hydrostatic stress might be caused by significant shear stress; the closed failure surfaces as shown in Fig. 6 do not adequately represent the intrinsic strength of rock. It is appropriate to say that the yield surface having an end cap enlarges with strain hardening in higher stresses. Since there are problems in the vicinity of the end cap of the failure surface as mentioned above and the use of the Teflon sheets is undesirable for the strain control tests under Condition B, what we will mainly discuss is based on the failure surface obtained by using no Teflon sheet in lower stress levels. In such lower stresses, the stress states in the specimen are expected to be better to some extent than in higher stresses, considering that no damage at the edges is observed.

Contour lines of the plastic mean principal strain are shown in Fig. 7. The region enclosed by the failure surface is divided into three, considering whether the plastic strain is positive or negative: the elastic, dilatant, and contractile regions. Although the boundaries between them are much the same as those by Schock et al. [11], it can be pointed out that the elastic region in $\mu = -1$ (compression) is larger than in $\mu = 1$ (extension). Furthermore, the region is much smaller than that enclosed by the yield surface in Fig. 6. This indicates the

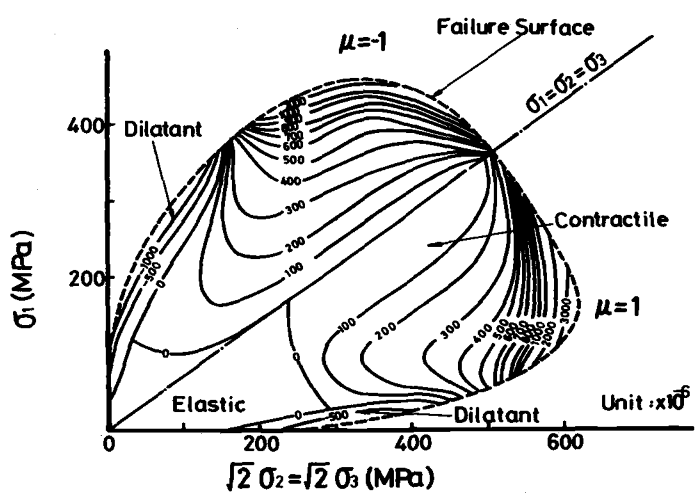

FIG. 7—*The contour lines of plastic mean principal strain.*

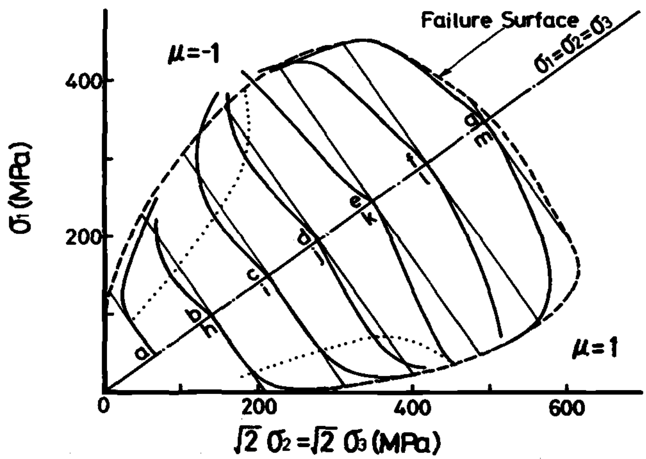

FIG. 8—*The stress paths on the Rendulic stress plane for* $\mu' = -1$ *and 1 under Condition B.*

difficulty of the determination of yield points using stress-strain curves. The higher mean principal stress is with greater plastic strains and denser contour lines. The phenomena show the behavior that the yield surface enlarges with strain hardening.

Tests Under Condition B

The stress paths for $\mu' = -1$ and 1 under Condition B are shown on the Rendulic stress plane in Fig. 8, although the situation of these values of μ' does not exactly result in that of $\mu = -1$ and 1. The broken line shows the failure surface obtained under Condition A. With increasing the octahedral shear strain, the stress states deviate from the lines which are perpendicular to the hydrostatic axis and correspond to the stress paths under Condition A, which we term the constant mean principal stress lines. Then these stress states asymptotically approach the failure surface and all tend to be directed to certain points thereafter. Their deviation indicates different directions depending on the value of the mean principal stress; at higher mean principal stresses, the stress states deviate from the constant mean principal stress lines to the origin of the stress space as the stress paths e, f, g, k, l, and m in Fig. 8. This behavior is similar to that of overconsolidated clays in undrained tests [*12*].

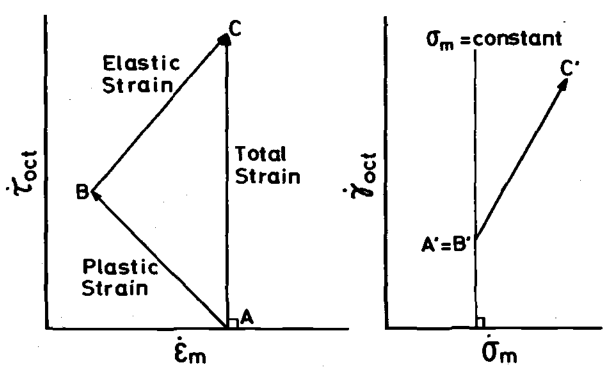

FIG. 9—*The relationship between the increments of plastic strain and stress in the dilatant region.*

Figure 9 shows each increment of stress and strain in the dilatant region, as an example, to explain the deviation from the constant mean principal stress lines. The increment of a total strain can be expressed as the vector AC in Fig. 9 which is perpendicular to the axis of the increment of the mean principal strain, while the plastic component of it is expressed as the vector AB directed to the negative axis because of dilatant behavior. In the result, the elastic strain increment expressed as the vector BC gives the stress increment of the vector B′C′ which is directed against the origin from the constant mean principal stress line. This explanation is applicable to the stress paths in the contractile region also. This consideration of the stress paths parallel to the constant mean principal stress lines gives the dotted lines shown in Fig. 8 as the boundary between the dilatant and contractile regions. This boundary represents the critical state in soil mechanics and is similar to that in Fig. 7 obtained under Condition A.

The stress paths for $\mu' = -1/3$ and $1/3$ are shown in the mean principal stress-octahedral shear stress space of Fig. 10. Characteristics of the stress paths are similar to that of $\mu' = -1$ and 1. The envelopes of the stress paths in the region of the mean principal stress from 100 to 300 MPa may suggest the failure surfaces for $\mu = -1/3$ and $1/3$, as those for $\mu' = -1$ and 1 on the Rendulic stress plane shown in Fig. 8; then the former envelopes are between the latter envelopes.

Conclusions

Stress and strain controlled tests of Akiyoshi marble were performed to investigate the fundamental behavior of rock masses under restricted strain conditions. The specially designed true triaxial testing apparatus with rigid platens was used for that purpose. The rigid platens as the boundary condition give more accurate measurement of strains and higher stress fields than flexible membranes. The following properties of marble were revealed

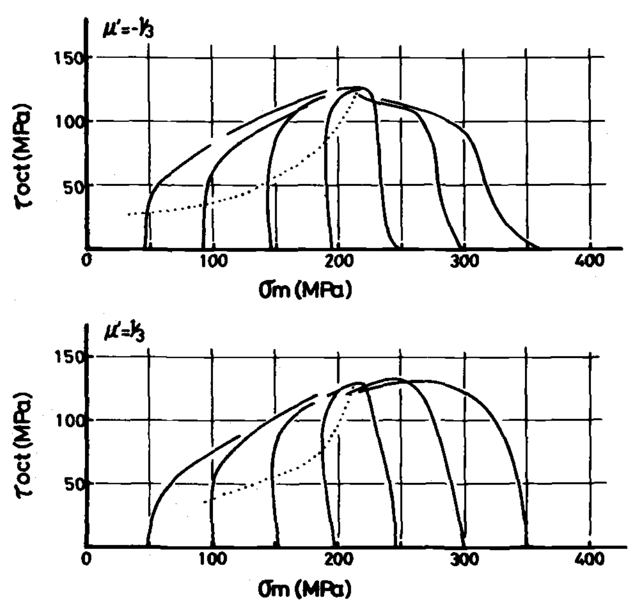

FIG. 10—*The stress paths on the mean principal stress-octahedral shear stress plane for* $\mu' = -1/3$ *and 1/3 under Condition B.*

from the experiment. The yield surface is closed on the hydrostatic axis, and it enlarges with strain hardening. The failure at higher mean principal stresses does not imply that of the whole specimen but results from the damages at its edges because of stress concentration. The region enclosed by the failure surface is divided in three: the elastic, dilatant, and contractile regions. With increasing the octahedral shear strain under the condition of constant mean principal strain, the stress states deviate from the lines perpendicular to the hydrostatic axis and approach the failure surface asymptotically. The direction of their deviation from the lines is related to the above three regions. Consideration of these characteristics would be the first step for the derivation of constitutive laws.

References

[1] Handin, J., Heard, H. C., and Magouirk, J. N., "Effects of the Intermediate Principal Stress on the Failure of Limestone, Dolomite and Glass at Different Temperatures and Strain Rates," *Journal of Geophysical Research,* Vol. 72, 1967, pp. 611–640

[2] Atkinson, R. H. and Ko, H. Y., "A Fluid Cushion, Multiaxial Cell for Testing Cubical Rock Specimens," *International Journal of Rock Mechanics and Mining Science,* Vol. 10, 1973, pp. 351–361

[3] Sture, S. and Desai, C. S., "Fluid Cushion Truly Triaxial or Multiaxial Testing Device," *Geotechnical Testing Journal,* Vol. 2, 1979, pp. 20–33.

[4] Mogi, K., "Flow and Fracture of Rocks Under General Triaxial Compression," in *Proceedings of 4th Congress of International Society for Rock Mechanics,* Montreux, Vol. 3, 1979, pp. 123–130.

[5] Gau, Q. Q, Cheng, H. T., and Zhuo, D. P., "The Strength Deformation and Rupture Characteristics of Red Sandstone Under Polyaxial Compression," in *Proceedings of 5th Congress of International Society for Rock Mechanics,* Melbourne, 1983, pp. A157–160.

[6] Michelis, P., "True Triaxial Cell for Low and High Pressure Experiments," *International Journal of Rock Mechanics and Mining Science,* Vol. 22, 1985, pp. 183–188.

[7] Hill, R., *The Mechanical Theory of Plasticity,* Oxford University Press, London, 1950.

[8] Gowd, T. N. and Rummel, F., "Effect on Confining Pressure on the Fracture Behavior of a Porous Rock," *International Journal of Rock Mechanics and Mining Science,* Vol. 17, 1980, pp. 225–229.

[9] Sandler, I. S., DiMaggio, F. L., and Baladi, G. Y., "Generalized Cap Model for Geological Materials," *Journal of the Geotechnical Engineering Division, American Society of Civil Engineers,* Vol. 102, 1976, pp. 683–699.

[10] Miller, T. W. and Cheatham, J. B., "A New Yield Condition and Hardening Rule for Rocks," *International Journal of Rock Mechanics and Mining Science,* Vol. 9, 1972, pp. 453–474.

[11] Schock, R. N., Heard, H. C., and Stephens, D. R., "Stress-Strain Behavior of a Granodiolite and Two Graywackes on Compression to 20 Kilobars," *Journal of Geophysical Research,* Vol. 78, 1973, p. 5922–5941.

[12] Henkel, D. J., and Sowa, V. A., "The Influence of Stress History on Stress Path in Undrained Triaxial Test on Clay," *Laboratory Shear Testing of Soils, ASTM STP 361,* American Society for Testing and Materials, Philadelphia, 1964, pp. 280–291.

Akitoshi Mochizuki,[1] Masato Mikasa,[2] and Shinichi Takahashi[3]

A New Independent Principal Stress Control Apparatus

REFERENCE: Mochizuki, A., Mikasa, M., and Takahashi, S., "**A New Independent Principal Stress Control Apparatus,**" *Advanced Triaxial Testing of Soil and Rock, ASTM STP 977,* Robert T. Donaghe, Ronald C. Chaney, and Marshall L. Silver, Eds., American Society for Testing and Materials, Philadelphia, 1988, pp. 844–858.

ABSTRACT: A newly designed independent principal stress control apparatus is presented together with some typical test results obtained by the apparatus. The minor principal stress on a cuboidal specimen, σ_x, is loaded by air pressure in the triaxial cell, and two couples of rigid platens are used to load the major and intermediate principal stresses, σ_z and σ_y.

This apparatus has the following features:

1. The axial stress, σ_z, is applied from the underside of the specimen, the reaction being supported by a frame in the cell. It makes both the anisotropic consolidation and extension test possible; it also makes the preparation of sand or soft clay specimens very easy.
2. A new device to load intermediate stress, σ_y, was developed to minimize the friction between lateral loading platens and the specimen.
3. A new system to measure the specimen deformation is also developed with a no-contact gap sensor which moves up and down during the test. It can measure the total volume change and also the change of the shape of the specimen.

Some typical results of triaxial test, plane strain test, and independent stress control test on two sands are presented. Deformation or distribution of strain of the specimen observed by no-contact gap sensor is also discussed.

KEY WORDS: test equipment, triaxial compression test, plane strain test, true triaxial test, shear strength of soil

Since Kjellman reported the first independent stress control (ISC) apparatus in 1936, many types of ISC testing apparatus have been developed [*1*]. These apparatus are grouped roughly into six types based on their loading mechanisms. The first group consists of apparatus with rigid loading platens for three principal stresses [*2–4*]. The second group uses three pairs of rubber bags to apply principal stresses [*5,6*]. The third, fourth, and fifth groups have ordinary triaxial cells and rigid loading platens to apply the minor and major principal stresses, σ_x and σ_z, respectively. The intermediate principal stress, σ_y, is applied by three different loading devices: a pair of (1) rubber bags [*7,8*], (2) rigid platens [*9,10*], and (3) platens composed of solid blocks with springs [*11*] or of steel and balsa wood [*12*], which are compressed vertically with small interference. In contrast to all of these with cuboidal specimens, the apparatus of the sixth group uses cylindrical specimens [*13,14*].

[1] Associate professor of civil engineering, Osaka City University, Sugimoto, Sumiyoshi-ku, Osaka, Japan 558.
[2] Professor of civil engineering, Setsunan University, Ikedanaka, Neyagawa, Osaka, Japan 572.
[3] Researcher, Ohbayashi Corporation, Technical Research Institute, Shimokiyoto, Kiyose, Tokyo, Japan 204.

In 1981, the authors developed an apparatus that applies the minor principal stress, σ_x, on a cuboidal specimen by air pressure in a triaxial cell, and the major and intermediate principal stresses, σ_z and σ_y, by rigid platens. The apparatus has a unique loading system of axial stress, σ_z, which has been used in the triaxial testing apparatus in our laboratory because of its convenience in specimen preparation and testing. In addition, it has several new features such as (1) applying compressed air for loading cell pressure, σ_x, with the help of a newly developed impermeable rubber sleeve, (2) a special device for loading σ_y to minimize the effect of the friction of the lateral loading platens, and (3) a new system to measure lateral deformation of the specimen. This paper will present these main features of the new ISC apparatus and some examples of test results.

A New Independent Stress Control Apparatus

Figure 1 is a general view of the apparatus. The pressure cell is hoisted up for specimen setting, showing a supporting frame, composed of four posts and a plate, together with a lateral loading frame. This apparatus has four independent systems to control σ_x, σ_y, σ_z, and back pressure.

Figure 2 shows the cross section of the pressure cell with a prismatic specimen 64 mm long, 41 mm wide, and 80 mm high. The significant features of this apparatus include:

1. The axial load, σ_z, is applied from the underside of the specimen, the reaction being supported by a frame in the cell. This loading system makes σ_z independent of the cell pressure, σ_x, making anisotropic consolidation and extension testing very easy. The setting of a specimen of soft clay or loose sand is also easily done with the least disturbance. A

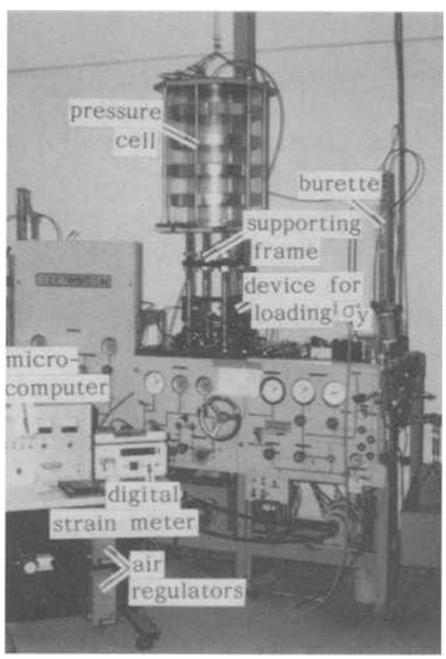

FIG. 1—*General view of ISC apparatus.*

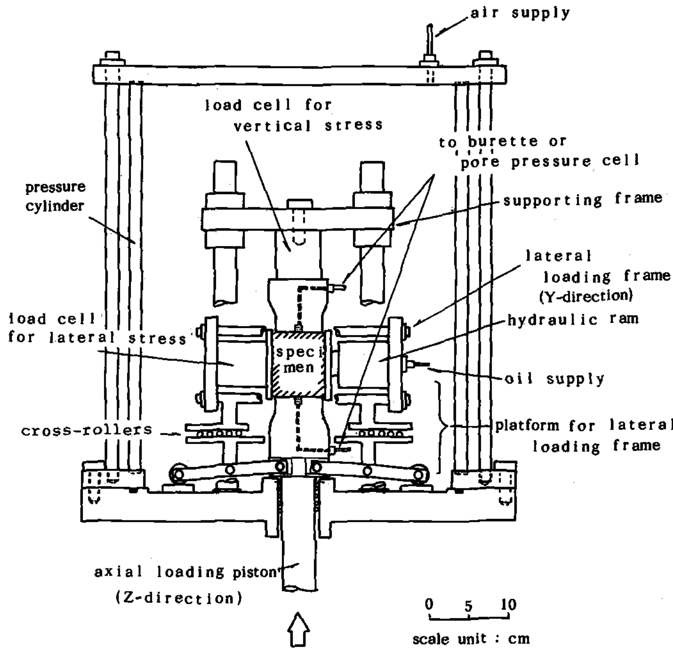

FIG. 2—*Independent principal stress control apparatus.*

large cylindrical specimen, 40 cm high and with $\phi = 20$ cm, can be tested by using a larger supporting frame.

2. The apparatus has two axial loading systems: a stress-controlled system with a continuously increasing water load in a bucket hung at the end of the loading lever, and a strain-controlled system with a screw jack. The system is switched from the former to the latter when the stress–strain curve approaches its peak point to get precise stress–strain curves.

(The basic idea for these two features was developed by Mikasa for a triaxial apparatus [*15*].)

3. Air pressure is used in the cell to apply the minor principal stress, σ_x, on the specimen. This makes the design of both the loading and measuring systems in the pressure cell much easier than when water pressure is used. However, the permeation of air through the rubber sleeve becomes a serious problem, and a new rubber sleeve with very low permeability had to be developed.

4. A device for loading intermediate principal stress, σ_y, to minimize the friction between the lateral loading platens and the specimen by keeping their centers at the same level in axial compression, greatly improves the accuracy in measuring the vertical stress, σ_z.

5. A new measurement system of specimen deformation uses no-contact type gap sensors. This allows tracing of not only the total volume change but also the deformation of the specimen. It also eliminates the "membrane penetration" problem of coarse-grained soils, which is inevitable when the volume change is measured by the amount of drained water or by using a double cell.

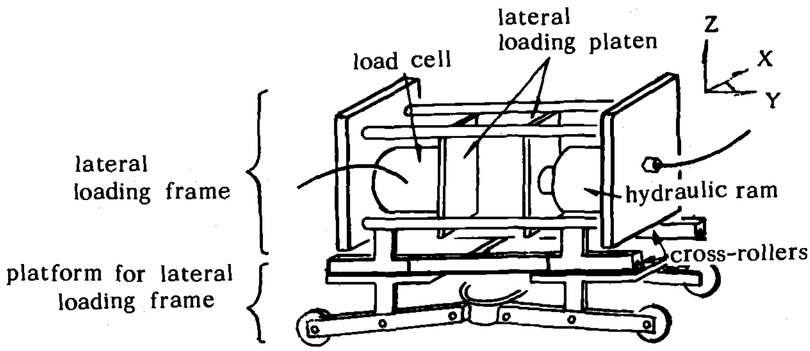

FIG. 3—*Device for loading* σ_y.

Device for σ_y *Loading*

The device for loading σ_y shown in Figs. 2 and 3 consists of a lateral loading frame and a movable platform to support it.

The lateral loading frame has a hydraulic ram and a load cell on its opposite sides to compress the specimen between them in a Y-direction through rigid platens. The platens' surfaces were coated with Teflon to reduce the friction of the rubber membrane on the specimen. The lateral loading frame is placed on a platform and can move on it in the Y-direction, without any resistance, with the help of cross-rollers. The platform moves up and down by exactly one-half the displacement of the axial loading piston (Z-direction) by the mechanism shown in Figs. 2 and 3. When the specimen is compressed uniformly in a vertical direction, the midheight of the lateral loading platens will always be at the same level as the midheight of the specimen. This reduces the error in measuring the axial stress, σ_z, by producing a symmetric distribution of friction between the platen and the specimen with respect to the midheight of the specimen. Silicon grease also was used on the specimen–platen interface to reduce the friction even further.

The results of an experiment conducted to confirm the effectiveness of the new device in a plane strain test under $\sigma_x = 2$ kgf/cm^2 are shown in Fig. 4. Load cells were placed at both the top and bottom of the specimen so that the difference of the two axial stresses could be kept within $\pm 1\%$ of the measured stress.

The two pairs of rigid platens used in this system cannot be free of the junction problem

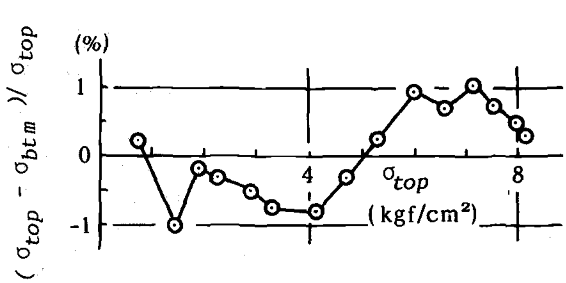

σ_{top} : stress measured at the top of the specimen
σ_{btm} : stress measured at the bottom of the specimen

FIG. 4—*Precision test of* σ_y *loading system.*

at the four corners of the specimen, just as in other types of ISC testing apparatus that use two pairs of rigid platens [10]. Initial gaps of 2 mm were given at the junctions as a provision for jamming, which was sufficient in most cases.

A New Specimen Sleeve

Air permeates through a rubber membrane 10 to 20 times as much in volume as water, which is a serious problem in cases where pore water pressure or the quantity of drained water is to be measured. Preliminary tests revealed that a natural rubber membrane 0.9 mm thick cannot be used under air pressure for an ordinary triaxial test. Therefore we had to develop a new 0.35-mm-thick rubber membrane, composed of two thin layers of natural rubber sandwiching five thin synthetic rubber layers of epi-chlorohydrin. The results of an air permeation test of both a 0.35-mm-thick rubber membrane and a 0.9-mm-thick natural rubber membrane under pressure differences of 3 to 5 kgf/cm^2 are shown in Fig. 5. The permeability of the sleeves is shown as the rise in pore pressure in an undrained condition, which is very sensitive to air permeation through the membrane. The new membrane, when used singly, did not satisfactorily reduce the permeation of air under both 3 and 5 kgf/cm^2. However, when the new rubber sleeve was doubled with silicon oil in between, the rise in pore pressure was kept less than 0.04 kgf/cm^2 under a confining air pressure of σ_3 = 5 kgf/cm^2, which can be evaluated as a satisfactory performance under air pressure. In practice a rubber sleeve of a slightly larger diameter was used as the outer sleeve without affixing its top end to the pedestal, which would increase constraint on the specimen.

The natural rubber sleeve doubled in the same way as described above did not show any satisfactory results.

Deformation Measurement Using No-Contact Gap Sensors

In a triaxial test, volume change of a specimen is usually measured either by the quantity of drained water from a burette or directly by the water level change in a double cell.

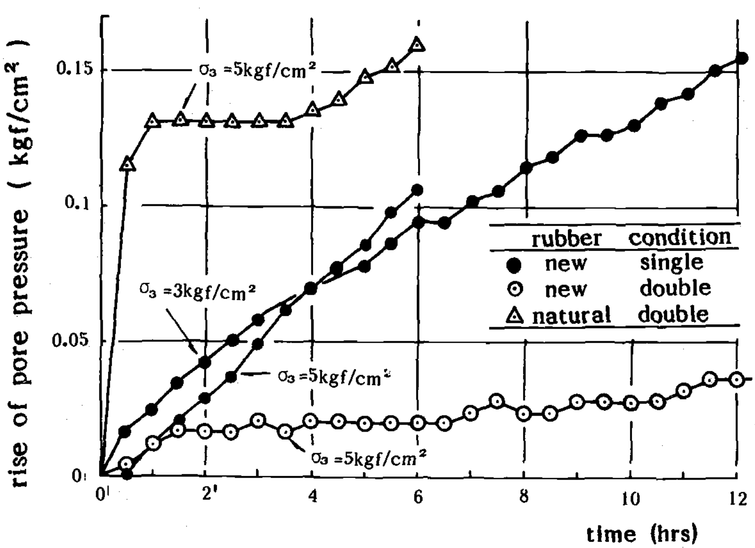

FIG. 5—*Air permeation test of sleeves.*

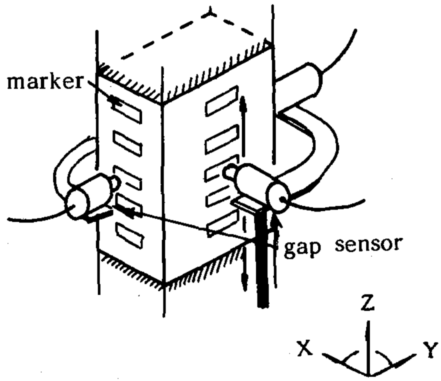

FIG. 6—*No-contact gap sensors and markers.*

However, when the deviation between the confining pressure and the pore pressure varies, the degree of penetration of a rubber membrane into the hollows of an uneven surface of a coarse-grained sample varies during testing resulting in an erroneous measurement. To avoid this difficulty, and to measure not only the total volume change but also the shape of the specimen, the authors developed a new deformation measuring method that uses no-contact gap sensors. Figure 6 illustrates the specimen with markers of aluminum foil of 10 by 20 by 0.1 mm on its sides together with gap sensors set in position for a triaxial compression test. Five markers were attached to each face of the rubber sleeve of the specimen. The no-contact gap sensors induce the variation of outlet voltage when conductors such as iron or aluminum change the distance to the markers on the specimen sides; a clearance of less than 8 mm can be measured to an accuracy of 1/100 mm.

In both an ISC test and a plane strain test, only a couple of sensors facing the free sides of the specimen are used. The measurement is done by moving the gap sensors in a *Z*-

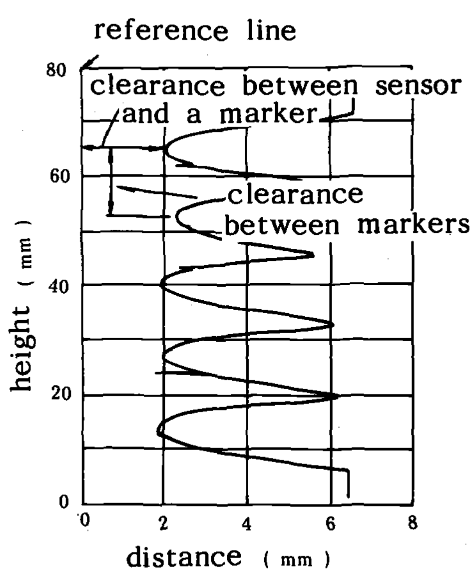

FIG. 7—*Output record by gap sensor method.*

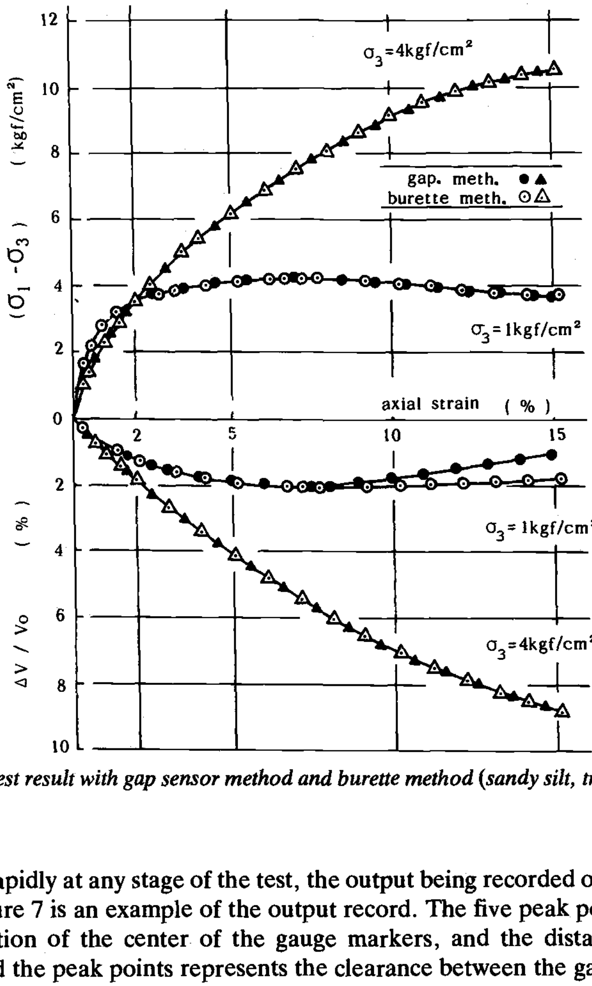

FIG. 8—*Test result with gap sensor method and burette method (sandy silt, triaxial compression test).*

direction rather rapidly at any stage of the test, the output being recorded on a direct-writing oscillograph. Figure 7 is an example of the output record. The five peak points of the curve indicate the location of the center of the gauge markers, and the distance between the reference line and the peak points represents the clearance between the gauge markers and

TABLE 1—*Properties of sand specimens.*[a]

		Seto Sand	Toyoura Sand
Primary Properties	G_s	2.557	2.652
	d_{max}	2.0 mm	0.42 mm
	d_{min}	0.05 mm	0.072 mm
	U_c	3.1	1.6
Secondary Properties	ρ_d	1.633 g/cm^3	1.516 g/cm^3
	ρ_t	1.755 g/cm^3	1.517 g/cm^3
	e	0.566	0.75
	D_r	90%	58.4%
	w	7.5%	0.1%

[a] G_s = specific gravity; d_{max} = maximum grain size; d_{min} = minimum grain size; U_c = uniformity coefficient (= D_{60}/D_{10}); ρ_d = dry density; ρ_t = wet density; e = void ratio; D_r = relative density; w = water content.

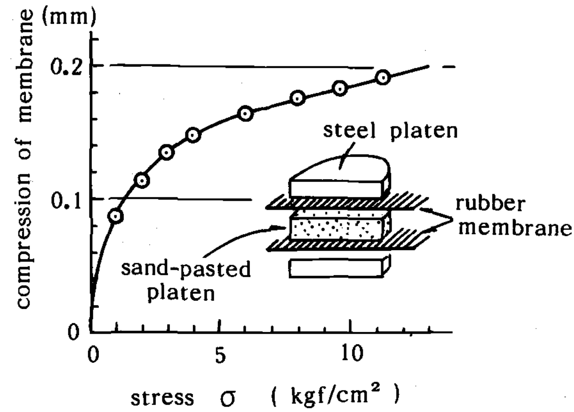

FIG. 9—*A test for compressibility of rubber membranes.*

the gap sensors. The *X-Y* coordinates of the peaks are read by a digitizer, and through data processing by a computer, graphical presentation of specimen deformation is obtained. In the case of Fig. 6, the volume of the specimen is calculated as the summation of the volumes of six three-dimensional trapezoidal bodies sectioned at the level of the center of the gauge marks.

Figure 8 shows the results of two CD tests on a sandy silt under σ_3 = 1 and 4 kgf/cm^2, the volume change being measured by both the burette method and the gap sensor method.

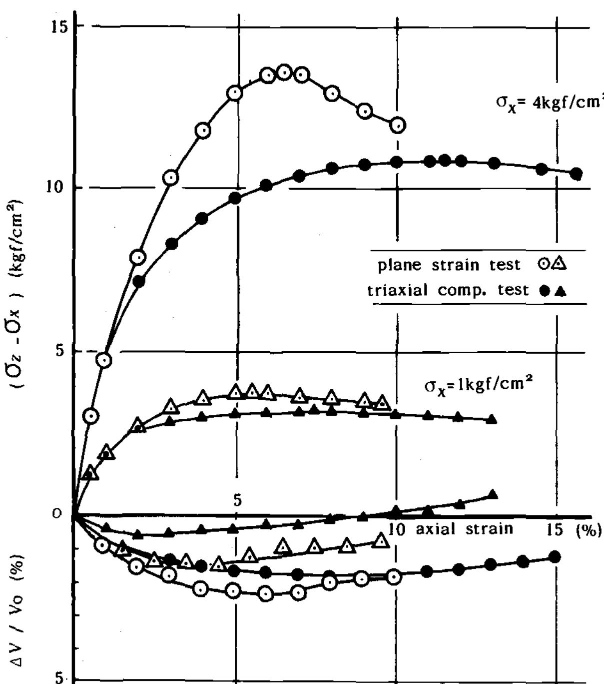

FIG. 10—*Comparison of plane strain test and triaxial compression test (Seto sand).*

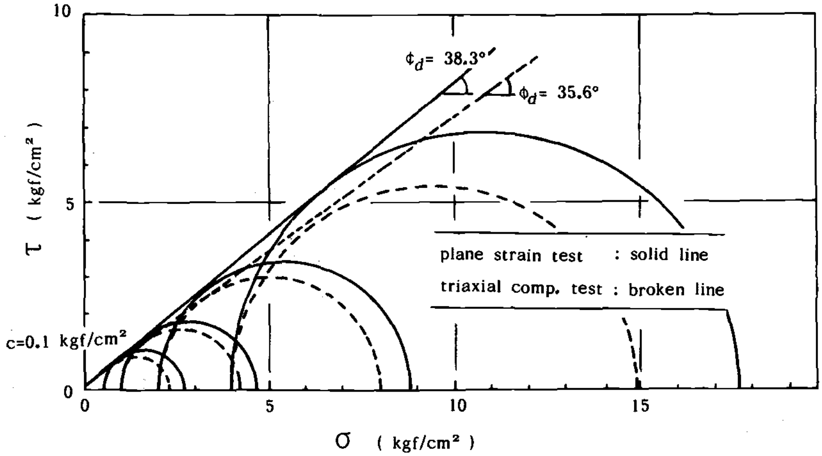

FIG. 11—*Mohr's stress circle and strength lines (Seto sand).*

The two measuring methods yielded quite the same volume change except after the peak stress of the test under $\sigma_3 = 1$ kgf/cm². Here the burette method is considered to have shown a slightly too small volume increase of the specimen owing to an insufficient water intake into the voids of the expanding specimen. The stress–strain curves were obtained in accordance with the routine correction that uses the average section area of the specimen. The two stress–strain curves, however, did not show any appreciable difference, even in the case of $\sigma_3 = 1$ kgf/cm². In a CD test on a fine sand sample (data omitted here), error of 1% due to membrane penetration was seen in the burette method.

Microcomputer Control of the Principal Stresses

Electrical sensors were used for all measurements except in the burette reading. In ISC tests under a condition of constant mean pressure, σ_m, outputs of sensors are put into a microprocessor by means of a general purpose interface bus (GPIB), and after calculations, electrical signals are sent to two air valves for the control of σ_x and σ_y, respectively. The measurement frequency of 38 times/min was sufficient to control the stresses smoothly and precisely, the error not exceeding 0.05% of the programmed stress value. In extension tests, however, shear rate was lowered from one-half to one-fourth of the standard rate of the compression test, because the above stated stress control could not follow exactly the rapid variation of the stresses near the failure.

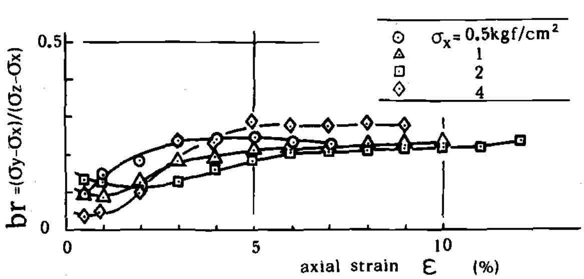

FIG. 12—*Progress of intermediate principal stress coefficient (Seto sand).*

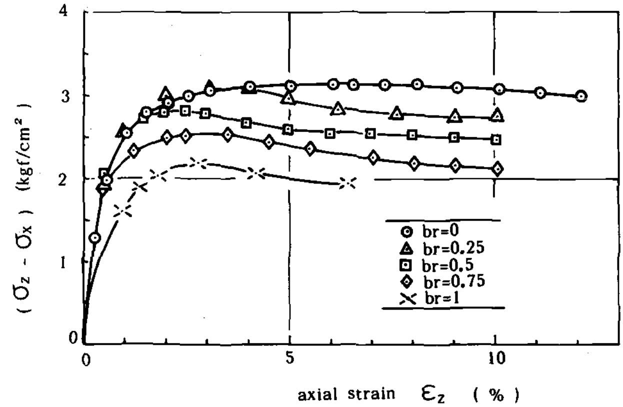

FIG. 13—$(\sigma_z - \sigma_x) - \epsilon_z$ *of ISC test (Seto sand).*

Test Results

Plane strain and ISC tests were carried out on two types of sand whose properties are shown in Table 1. The specimens were prepared cautiously to give the specimen a uniform and isotropic structure. Some typical results will be presented in this section.

Plane Strain Test

A test for the compressibility of rubber membranes yielded the result shown in Fig. 9, which was used to keep rigorous "zero" lateral deformation of the specimen in a plane strain test.

The deviator stress of plane strain tests of Seto sand under $\sigma_x = 1$ and 4 kgf/cm^2 and the results of the triaxial tests for the same sand of the same specimen size are shown in Fig. 10. The plane strain tests show higher strengths at earlier peak points compared to the triaxial compression tests. Mohr's stress circles at failure and their envelopes are shown in Fig. 11. The strengths of the plane strain tests are 2.7° higher than the triaxial test in terms of internal friction angle ϕ.

The change of the intermediate principal stress coefficients, $br = (\sigma_y - \sigma_x)/(\sigma_z - \sigma_x)$, against an axial strain is shown in Fig. 12. The *br*-value becomes larger for a larger strain gathering in a range from 0.2 to 0.3 at failure in all cases.

Independent Stress-Controlled Test

Figure 13 shows the $(\sigma_z - \sigma_x) \sim \epsilon_z$ relationships of the tests on Seto sand where $br = 0$, 0.25, 0.5, 0.75, and 1 under $\sigma_m = 2$ kgf/cm^2. The smaller the value of *br*, the higher the peak strength. The axial strain at the peak strength does not exceed 3% except when $br = 0$.

Figure 14 shows the incremental strain vectors superimposed on the stress paths, which are expressed as radiating lines from the origin on the octahedral plane of $\sigma_m = 2$ kgf/cm^2. The incremental strains increased remarkably when approaching failure, showing deviations from the stress paths in the direction of the strains in all cases except when $br = 0$ [*12*]. The failure criterion shown in the figure by a solid line is obtained in conformity to the normality rule and expressed as follows:

$$f = I_1 \times I_2 - A \times I_3 \tag{1}$$

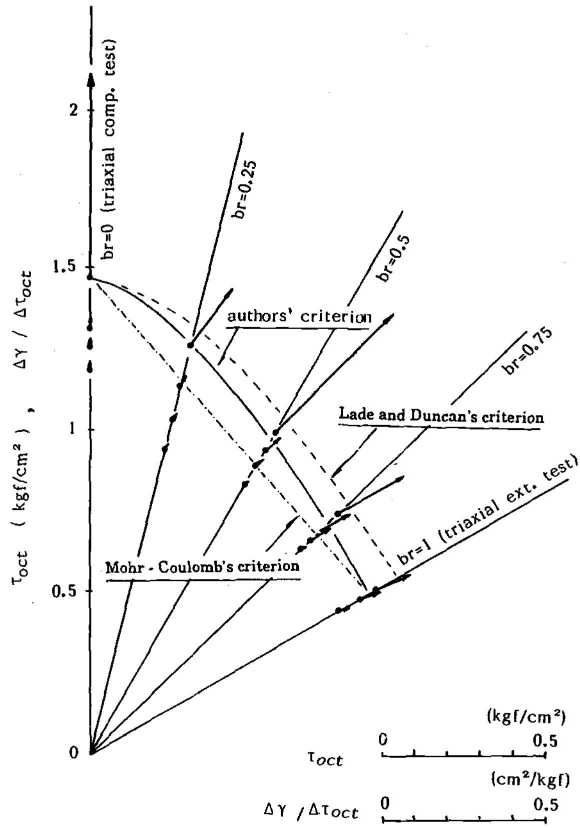

FIG. 14—*Incremental strain vectors on the octahedral plane (Seto sand,* σ_m *= 2 kgf/cm²).*

where

I_1, I_2, I_3 = invariant of the stress tensors
A = a coefficient that depends on the work done by plastic strain (in this case, A = 13.7)

This criterion coincides with Matsuoka and Nakai's criterion when the *k*-value in their equation is 0.722 [*16*]. However the difference betwen Lade and Duncan's criterion, shown by a dashed line, and the authors' criterion increases with an increasing *br*-value. The Mohr-Coulomb criterion is also shown by a dash-dotted line.

A Deformation Measurement by a Gap Sensor Method

Restraint from σ_z Loading Platen

Figure 15 shows the deformation of the specimens measured by a gap sensor method for three different end conditions of a σ_z loading platen: (1) a maximum porous stone area of 95% of the loading surface, (2) a well-polished stainless steel surface with only a 1-cm-diameter porous stone at its center, and (3) two thin rubber membranes coated with silicon grease and placed on platen (2).

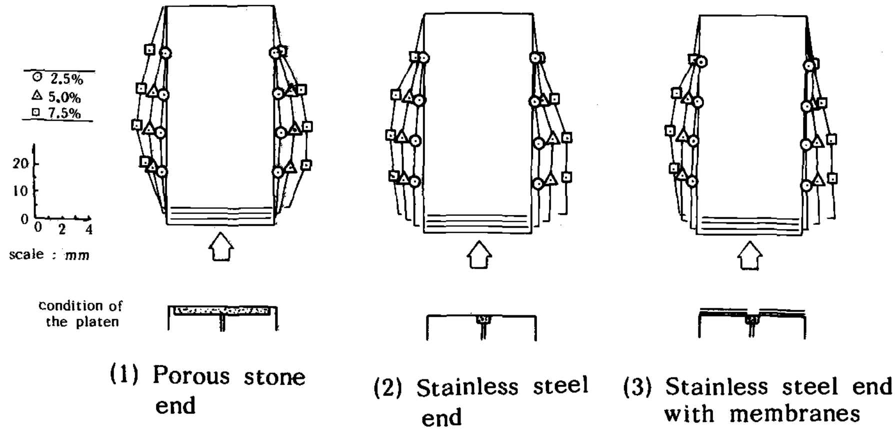

FIG. 15—*Deformation of specimens with different end platens (Seto sand, plane strain test,* $\sigma_x = 1$ *kgf/cm²).*

The deformation of the specimens shown in Fig. 15 are those at axial strains of 2.5, 5.0, and 7.5%. There was little difference between case (2) and (3) both in the deformation of the specimens and in the stress–strain curves (not shown here), while case (1) yielded a different behavior of the specimen owing to the end surface restraint.

Strain Distribution in the Specimen

Figure 16 shows the distribution of the principal strains and the maximum shear strains at axial strains of 5 and 8% in a plane strain test on Toyoura sand under 4 kgf/cm². The lines of shear strains were drawn selecting the direction of shear that would constitute a continuous slip plane or slip zone in the specimen from a pair of maximum shear strains that cross each other at each of the triangle-shaped elements.[4] When $\epsilon_z = 5\%$, the principal strains are comparatively uniform in the specimen. When $\epsilon_z = 8\%$, the principal strains grew larger except in the two triangle elements in the upper left and lower right corners, and a shear band formed in the specimen through the other two corners. Figure 17 is a picture of a specimen of Seto sand after a plane strain test in which a slip surface is clearly observed. The direction and location of this slip surface are very similar to the shear band shown in Fig. 16 (2).

Conclusions

The features of this new independent principal stress control apparatus are summarized as follows:

1. The loading of σ_z from under the specimen through the cell base with a supporting frame in the cell is the basic structure of this apparatus.
2. Cell pressure is applied by air with the help of a newly developed impermeable rubber sleeve.

[4] The triangle net was constructed from the measured specimen deformation assuming that each horizontal section is kept plain and that lateral deformation along it is uniform.

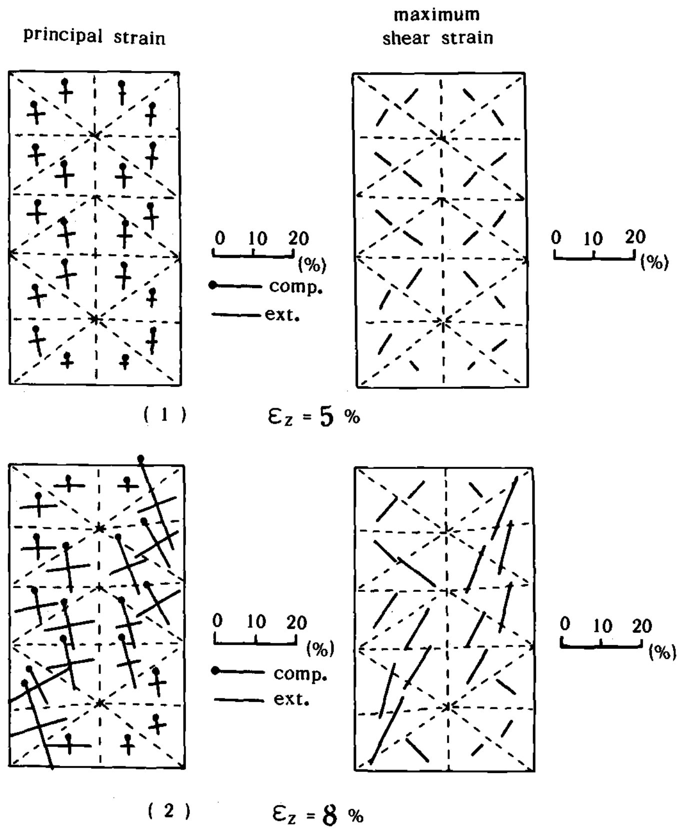

FIG. 16—*Distribution of strains (Toyoura sand, plane strain test, σ_x = 4 kgf/cm², platen (3) in Fig. 16 was used).*

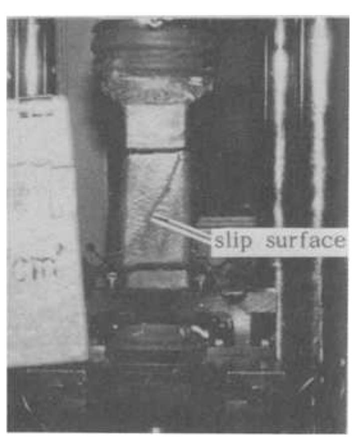

FIG. 17—*Specimen after plane strain test (Seto sand, σ_x = 4 kgf/cm²).*

The above two devices provided an ideal condition for the design of the equipment in the cell, and the following new systems were developed:

3. The lateral loading system was placed on a platform that moves exactly half of the axial piston movement, thus eliminating harmful friction on the specimen sides.
4. A new measurement method using gap sensors enabled us to trace not only the volume change but also the deformation of the specimen correctly during the test.
5. σ_x and σ_y are controlled accurately using a commercially available eight-bit microcomputer.

Examples of triaxial testing, plane strain testing, and ISC testing shown in this paper will serve as evidence of the effectiveness of the new apparatus.

Acknowledgments

The authors gratefully acknowledge the cooperation given by Yoshihiro Yamane, Takuji Shibata, and Morifumi Katsuda, postgraduate students of Osaka City University. The authors would also like to thank Shigeo Kishi, chief director of Higashi Chemical Co., Ltd., for his helpful cooperation in developing the new rubber sleeve.

References

[*1*] Saada, A. S., and Townsend, F. C., "Laboratory Strength Testing of Soil (State of Art)," in *Laboratory Shear Strength of Soil, ASTM STP 740,* American Society for Testing and Materials, Philadelphia, 1981, pp. 7–77.
[*2*] Hambley, E. C., and Roscoe, K. H., "Observations and Predictions of Stresses and Strains during Plane Strain of 'Wet' Clays," in *Proceedings,* Seventh International Conference on Soil Mechanics and Foundation Engineering, Mexico, Vol. 2, 1969, pp. 173–181.
[*3*] Roscoe, K. H., "The Influence of Strains in Soil Mechanics," *Geotechnique,* Vol. 20, No. 2, 1970, pp. 129–170.
[*4*] Goldscheider, M., and Gudehus, G., "Rectilinear Extension of Dry Sand-Testing Apparatus and Experimental Results," in *Proceedings,* Eighth International Conference on Soil Mechanics and Foundation Engineering, Moscow, Vol. 1, 1973, pp. 143–149.
[*5*] Ko, H-Y., and Scott, R. F., "A New Soil Testing Apparatus," *Geotechnique,* Vol. 17, No. 1, 1967, pp. 40–57.
[*6*] Arthur, J. R. E., and Menzies, B. K., Correspondence to "A New Soil Testing Apparatus, by Ko, H., and Scott, R. F.," *Geotechnique,* Vol. 18, No. 2, 1968, pp. 271–272.
[*7*] Shibata, T., and Karube, D., "Influence of the Variation of the Intermediate Principal Stress on the Mechanical Properties of Normally Consolidated Clays," in *Proceedings,* Sixth International Conference on Soil Mechanics and Foundation Engineering, Canada, Vol. 1, 1965, pp. 359–363.
[*8*] Sutherland, H. B., "The Influence of the Intermediate Principal Stress on the Strength of Sand," in *Proceedings,* Seventh International Conference on Soil Mechanics and Foundation Engineering, Mexico, Vol. 1, 1969, pp. 391–399.
[*9*] Green, G. E., and Bishop, A. W., "A Note on the Drained Strength of Sand under Generalized Strain Conditions," *Geotechnique,* Technical Note, Vol. 19, No. 1, 1969, pp. 144–149.
[*10*] Green, G. E., "Strength and Deformation of Sand Measured in an Independent Stress Control Cell," in *Proceedings,* Roscoe Memorial Symposium, Cambridge, England, G. T. Foulis & Co. Ltd., 1971, pp. 285–323.
[*11*] Mitchel, R. J., "An Apparatus for Plane and True Triaxial Testing of Undisturbed Soil Samples," *Canadian Geotechnical Journal,* Vol. 10, 1973, pp. 520–527.
[*12*] Lade, P. V., and Duncan, J. M., "Cubical Triaxial Tests on Cohesionless Soil," *Journal of the Soil Mechanics and Foundations Division, American Society of Civil Engineers,* Vol. 99, No. 10, 1973, pp. 793–812.
[*13*] Kirkpatrick, W., "The Condition of Failure for Sands," in *Proceedings,* Fourth International Conference on Soil Mechanics and Foundation Engineering, London, Vol. 1, 1957, pp. 172–178.

[14] Wu, T. H., Loh, A. K., and Malvern, L. E., "Study of Failure Envelope of Soils," *Journal of the Soil Mechanics and Foundations Division, American Society of Civil Engineers,* Vol. 89, No. 1, 1963, pp. 145–181.
[15] Mikasa, M., "On the New Type Triaxial Compression Apparatus," presented at the First Asian Regional Conference on Soil Mechanics and Foundation Engineering, Division I, New Delhi, 1960.
[16] Matsuoka, H., and Nakai, T., "Stress–Strain Relationship of Soil Based on the 'SMP', Constitutive Equation of Soils," Preprint of Specialty Session 9, Ninth International Conference on Soil Mechanics and Foundation Engineering, Tokyo, 1977, pp. 153–162.

Jack Lanier[1]

Special Stress Paths Along the Limit Surface of a Sand Specimen with the Use of a True Triaxial Apparatus

REFERENCE: Lanier, J., "**Special Stress Paths Along the Limit Surface of a Sand Specimen with the Use of a True Triaxial Apparatus,**" *Advanced Triaxial Testing of Soil and Rock, ASTM STP 977,* Robert T. Donaghe, Ronald C. Chaney, and Marshall L. Silver, Eds., American Society for Testing and Materials, Philadelphia, 1988, pp. 859–869.

ABSTRACT: This paper presents a true triaxial apparatus with rigid platens and its means of measurement and regulation. For tests performed on dry sand specimens, the loss of homogeneity by localization of deformation along shear bands is first analyzed. Then special circular paths in deviatoric stress plane are obtained. If the radius of this path is large enough, the author shows that the actual stress point moves on the limit surface which is well approximated experimentally. The more surprising result is that the volume of the specimen, on such cyclic paths, decreases. This result outlines the danger of liquefaction even for dense sand under complex stress path.

KEY WORDS: dry sand, limit surface, cyclic behavior, liquefaction, true triaxial, localization, shear bands

During the past 15 years, many true triaxial apparatus have been developed for studying the behavior of materials under three-dimensional state of stress ($\sigma_1 > \sigma_2 > \sigma_3$) and especially the influence of intermediate stress, σ_2. Designs of these apparatus can be classified in three types according to the boundary conditions:

- Apparatus with six rigid boundaries. The test is strain-controlled.
- Apparatus with six flexible boundaries. The test is stress-controlled.
- Apparatus with mixed boundary conditions.

(See Saada and Townsend [*1*] for advantages and disadvantages of each type.)

The apparatus used in this study is of the first type and will be described below.

Whatever the type, the two following hypotheses are necessary to have a correct interpretation of the measures in terms of element test:

1. Deformation and stress are homogeneous inside the specimen.
2. Principal axes of strain and stress coincide.

Theoretically the second hypothesis is verified if the specimen is isotropic in its initial state, but during the test, induced orthotropic anisotropy can occur with the same axes as stress

[1] Maitre de Conférences, Institut de Mécanique de Grenoble, BP 53X, 38041 Grenoble, Cedex, France.

and strain [2]. Experimentally, for rigid platens apparatus, shear stresses can appear at the boundaries because of the relative motion of platens and specimen. So the friction must be reduced by greasing the boundary of the sample and by means of well-polished platens. The author used a silicon grease on the inner platens and on the membrane. The value of the coefficient of friction is 0.5 to 2%.

The first hypothesis is difficult to control. The loss of homogeneity can be diffuse (as a result of nonhomogeneous initial specimen and shear stress at the boundaries) or localized when shear bands are developed. This last point will be illustrated.

Despite difficulties in obtaining a perfect homogeneity (these difficulties occur in all experimental studies), the true triaxial is the only apparatus that allows control of the three principal values of stress or strain. So, the behavior of the specimen under complex stress or strain paths can be tested. Some original results, obtained along cyclic circular paths in the deviatoric stress plane, will be presented. Similar tests have been performed earlier by Lewin [3] and Matsuoka and co-workers [4], but the novelty of the tests discussed in this paper is related to the fact that, for large radius, the expected state of stress cannot be reached and the actual stress slips on the limit surface. In this case, the kinematic response is analyzed.

Equipment and Testing Procedure

Equipment

The sand specimen is deformed by a system of six rigid platens. The movement of compression or extension is controlled by six electric motors; 12 hydraulic jacks keep the testing box closed during the test (Fig. 1) so there is no gap between the platens. The maximum

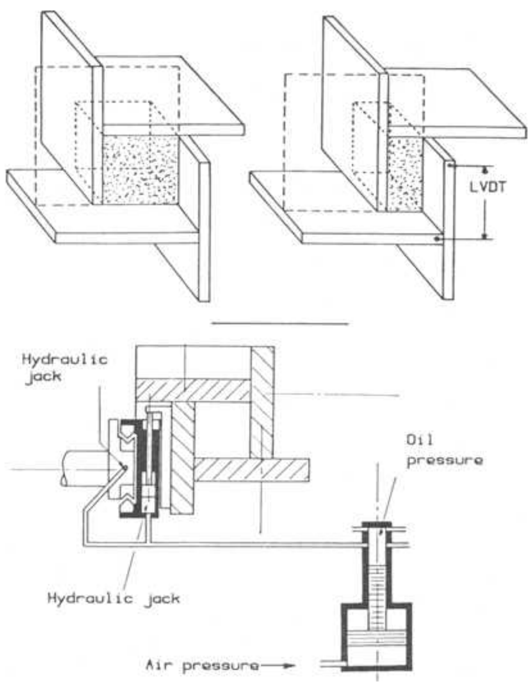

FIG. 1—*Principle of true triaxial apparatus with rigid platens. Detail of closing design.*

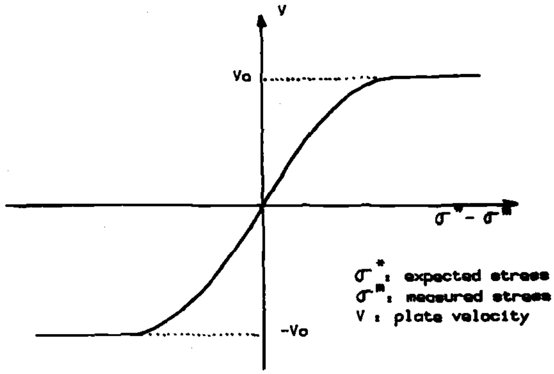

FIG. 2—*Stress-controlled test—principle of the regulation:* $V = F(\sigma^* - \sigma^M)$.

velocity in each direction is 5 mm/min, and the side dimensions can go from 50 mm to 150 mm. Other apparatus of the same type have already been described (see, for example, Refs *5* and *6*). The principle of all these apparatus is the same and their differences lie in the measurements, the control of the test, and the specimen preparation inside or outside the testing box. The author's design is described below.

Measurement

The three normal stresses are measured with three pressure transducers embedded in the platens and in contact with the specimen. Calibration of these three sensors is performed using a special membrane with inside air pressure, instead of the specimen, directly in the testing box. The accuracy can be estimated at 10 kPa in the range 0 to 5 MPa. No control of tangential stress is performed.

The relative displacements of two opposite faces are measured with three linear variable

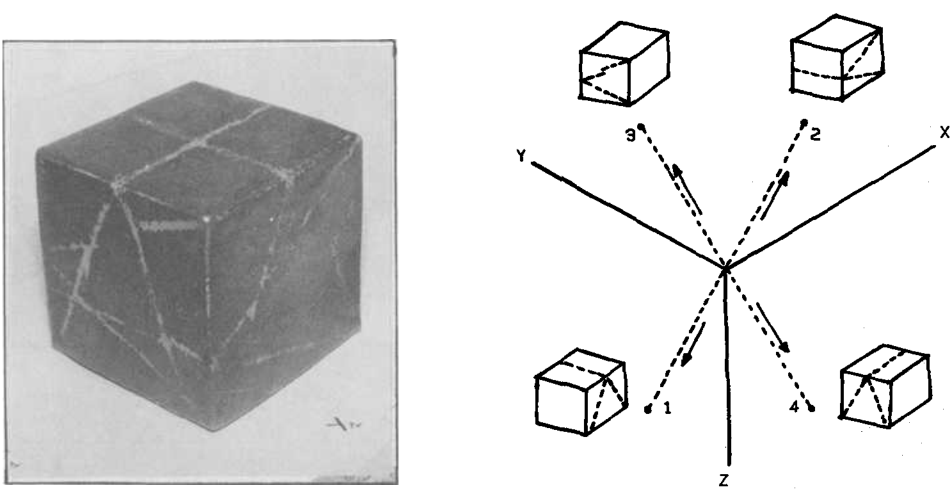

FIG. 3—*Localization of deformation: shear band traces on the painted membrane. Shows photograph of the specimen after testing* (left) *and stress path (1–2–3–4) and successive shear bands.* (right).

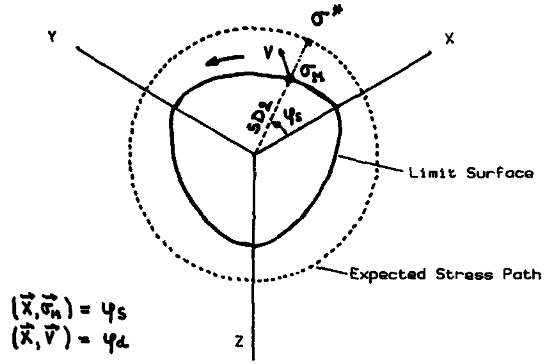

FIG. 4—*Deviatoric stress plane. Notations and principle of the tests.*

differential transformers (LVDT) in the range 0 to 100 mm with an accuracy of 0.05 mm. The strains are evaluated from these displacements without corrections because the sand is fine and the membrane thickness is only 0.3 mm.

Control of the Test

For each of the three directions, strain control or stress control is permitted. However, for a triaxial apparatus with rigid platens, the only basic way of regulation is the displacement of the platens and stress control results necessary by adjustment of strain. If $Vi(t)$ denotes the velocity of the plate i, the stress control is obtained by a relation of the type

$$Vi(t) = F\,(\sigma_i^*(t) - \sigma_i^M(t))$$

where

$\sigma^*(t)$ = expected stress
$\sigma^M(t)$ = measured stress

and F is a function schematically represented on Fig. 2.

For the expected values $Vi(t)$ or $\sigma^*(t)$, three kinds of control are possible:

a. Constant values by use of potentiometers.
b. Linear analogic function of the type

$$S = a \cdot E + b$$

TABLE 1—*Definition and parameters of two circular tests.*

Test	Step in φ_s	Frequency in time, sec	Number of cycles	p, MPa	$SD2/S1$	Friction angle
1	10°	10	5	0.48	0.38	Compression 35°
2	−10°	20	1			Extension 65°

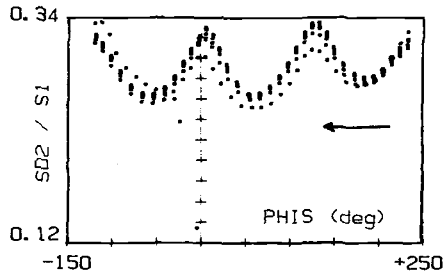

FIG. 5—*Measured values of* SD2/S1 *versus* φ_s *(test 1, five cycles).*

where E is an input value, S is an output value, and a and b are two constants adjustable with potentiometers. Such a function is useful for a linear stress path; then E is a measured stress on a direction and S is the expected stress on another one.

c. More complex paths can be obtained with three digital-to-analog converters. The expected path is defined by points, and the conversion takes place at a chosen frequency in time.

Specimen Preparation

The specimens are prepared in a cubic rubber membrane 0.3 mm thick (100 by 100 by 100 mm^3) inside a mold. The sand is poured and tamped by beds of about 2 cm thickness for dense specimens, or just deposing continuously without falling for loose ones. Then the face used for filling up is closed with a patch. Vacuum, inside the specimen, allows unmolding, greasing, and transporting to the testing box without remolding. When the specimen is maintained laterally by the platens and before closing the box, vacuum is released.

Localization of Deformation

During a test the rupture of the specimen, for large deformation and high stress ratio, cannot be observed directly because the specimen is hidden by platens. So an experimental technique is used, consisting of painting the rubber membrane before greasing it. When shear bands appear, the deformation is very localized, and the paint comes out from the membrane.

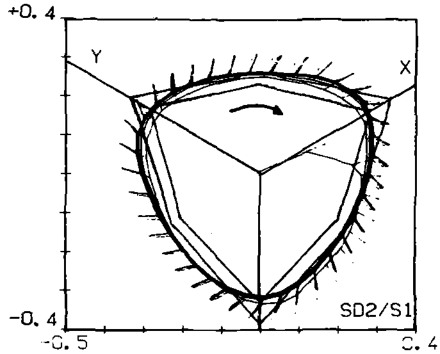

FIG. 6—*Stress path and direction of strain increments (test 1, five cycles). Coulomb criterion 30°, 35°.*

Figure 3*a* shows a sample of fine dense sand after a complex test. The stress path history for this specimen is represented in deviatoric plane (Fig. 3*b*). For each linear path (b = 0.5), the basic mechanism of rupture consists of two narrow shear bands. These two planes intersect along a straight line on the face supporting the major principal stress and give a V-trace on the face supporting the intermediate stress. Although the photograph seems complex at first glance, all the lines can be easily interpreted as a combination of four basic mechanisms, each being activated successively according to the stress path. The angle 2α of the Vs is close to 45°. Referring to the classic slip line theory in plasticity [7], this angle is related to the friction angle by

$$\phi = 90 - 2\alpha \text{ (degrees)}$$

With this formula the estimated friction angle is 45°. The actual value, deduced from the measured stress, is 43°. Such correlation for fine sand was already mentioned by Arthur and Dunstan [8]. Other tests of this kind have been performed, and, whatever the stress paths are, the mechanism of rupture occurs in the same way: the kinematics turn to plane deformation in the direction of the intermediate stress, and the volume change calculated directly from measuring the specimen dimensions seems to flatten, but local measurements with γ-ray absorption technique indicate a very high dilatancy inside the shear bands [9].

Cyclic Circular Stress Path in Deviatoric Plane

Description of Sand

The sand used for the tests described below is a fine quartzic sand (D50 = 0.35 mm; D60/D10 = 2). The maximum and minimum density values are 1.64 and 1.35 measured, respectively, by tamping or air pluviating (height of falling = 1.20 m) and by dry deposit without falling. The initial density for the two tests are 1.55 for test 1 and 1.54 for test 2.

Principle of the Test

If σ_x, σ_y, σ_z are the three principal stresses, they can be expressed by the formulas:

$$\sigma_x = p.(1 + \sqrt{6}.(SD2/S1).\cos(\varphi_s)$$

$$\sigma_y = p.(1 + \sqrt{6}.(SD2/S1).\cos(\varphi_s + 120)$$

$$\sigma_z = p.(1 + \sqrt{6}.(SD2/S1).\cos(\varphi_s - 120)$$

where

$S1$ = trace(σ) = $3p$; p is the mean pressure.
$SD2$ = $(\mathrm{trace}(s^2))^{1/2}$; s is deviatoric stress tensor.
φ_s = the phase angle from the X direction.

The representation of all these parameters is shown in Fig. 4. If $\varphi_s = 2k\pi/3$ the state of stress is a classic state of compression; $\varphi_s = \pi/3 + 2k\pi/3$ corresponds to a classic state of extension.

If φ_s and $S1$ are constant values and $SD2$ is a variable, the stress path is linear from the isotropic state. This is the classic path [10] to obtain point by point a description of the limit surface. It is now well known that the Coulomb criterion is only a rough approximation of

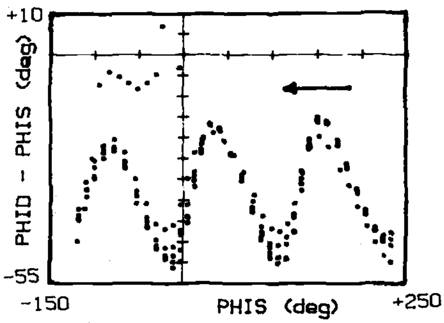

FIG. 7—*Difference angle between stress φs and strain increment φ_D (test 1, five cycles).*

this surface and, in particular, that the measured angle of friction is greater in extension than in compression.

If $S1$ and $SD2$ are constant values and φ_s is a variable, the stress path is circular in the deviatoric plane $S1$ = *Cte* (constant value) with a radius equal to $SD2$. Let us try to impose by the regulation a circle completely at the exterior of the limit surface (see Fig. 4). The material is not strong enough to support the expected state of stress σ^*, and the measured value σ^M will be such that $|\sigma^* - \sigma^M|$ will be different from zero. According to the regulation process described earlier the velocity v will be

$$v = F(\sigma^* - \sigma^M)$$

The material will flow and σ^M will be in the vicinity of the limit surface. The variation of φ_s is imposed step by step at a given frequency in time, and so the actual stress path will give a good description of the whole limit surface.

Experimental Results

Two circular tests are described. The expected values and the parameters for regulation are given in Table 1.

The expected value for the friction angle is close to the actual value in compression, but is very large in extension. Of course, this value will not be reached during the tests.

Test 1—Five clockwise cycles are performed. The results of measurements are plotted in Figs. 5 to 10. At first (Fig. 5), it was observed that the measured values of $SD2/S1$ are not constant but oscillate. The maximum value (0.33) corresponds to an friction angle of 30°

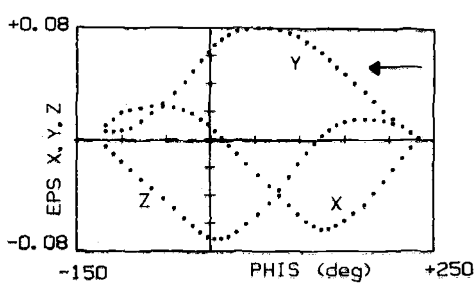

FIG. 8—*Variations of ϵ_x, ϵ_y, ϵ_z during last cycle (test 1).*

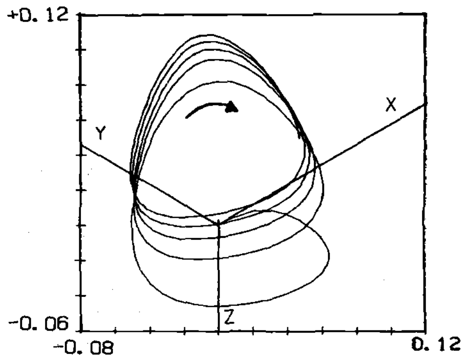

FIG. 9—*Deviatoric strain path (test 1, five cycles).*

and is obtained for the three compression states of stress. The minimum value (0.26—friction angle 35°) is obtained for extension. The periodic oscillations indicate the three symmetries of the limit surface as can be seen in Fig. 6. On the same figure the direction of the total deviatoric strain increment is drawn. This direction coincides neither with that of the stress increment (it would be relevant to linear isotropic elasticity), nor with that of the stress. The difference angle between φ_D and φ_s (φ_D is the phase angle of the strain increment from the X axis) is plotted in Fig. 7. A periodic variation is still found, but the maximum and minimum values are no longer in direct correlation with the stress states of compression or extension. This variation can be approximated by a linear saw-toothed diagram between the two values $-50°$ and $-17°$ with a mean value of $-33.5°$:

$$|\varphi_D - \varphi_s|_{max} = 50° \text{ for } \varphi_s = 230, 110, -10°$$

$$|\varphi_D - \varphi_s|_{min} = 17° \text{ for } \varphi_s = 150, 30, -90°$$

For variation of φ_s from 30° to $-10°$ (the compression state is for $\varphi_s = 0$), $|\varphi_D - \varphi_s|$ decreases, φ_D changes from 13° to $-60°$, and the mean rate is $\Delta\varphi_D/\Delta\varphi_s = 1.82$.

For variation of φ_s from $-10°$ to $-90°$ (the extension state is for $\varphi_s = -60°$), $|\varphi_D - \varphi_s|$ increases, φ_D changes from $-60°$ to $-107°$, and the mean rate is 0.58. So the rate of φ_D versus φ_s is about three times larger in the vicinity of compression than in the vicinity of extension.

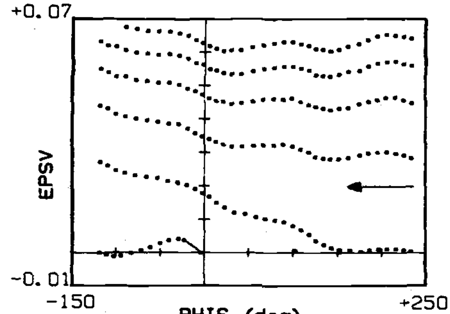

FIG. 10—*Volume change during the five cycles (test 1).*

In analyzing this finding, it is observed that, according to the elastoplasticity theory, the total deviatoric strain increment $d\mathbf{e}$ can be split into two parts:

$$d\mathbf{e} = d\mathbf{e}^e + d\mathbf{e}^p$$

If we suppose linear isotropic elasticity, $d\mathbf{e}^e = d\mathbf{s}/G$ where $d\mathbf{s}$ is the deviatoric stress increment. The plastic part is defined by the flow rule: $d\mathbf{e} = \lambda\mathbf{n}$, where $\mathbf{n}$ is a deviatoric tensor function of stress and hardening parameters. $\mathbf{n}$ defined the direction of plastic strain increment. If we suppose a standard deviatoric flow rule, $\mathbf{n}$ is given by the normal of the limit curve in the deviatoric stress plane, and the $\mathbf{n}$-direction oscillates periodically with φ_s according to the three symmetries of the limit surface. But in this case the mean value of $\varphi_D - \varphi_s$ will be zero. So in the light of this theory a rough interpretation of the results is: the oscillating part of $\varphi_D - \varphi_s$ is mainly due to the plastic deformation and the nonzero mean value is due to the elastic part. A second feature (more physical) is related to a previous observation according to which the main mechanism of large deformation is close to plane deformation. For the stress path under consideration, three mechanisms are activated (plane deformation for x, y, z directions), the three states of compression being the transitions from one to another. This point of view is corroborated in Fig. 8 where the variations of ϵ_x, ϵ_y, ϵ_z are plotted: the small rate of change for φ_D corresponds to maximum (stationary values) of respectively, ϵ_x, ϵ_y, ϵ_z. The deviatoric strain path is plotted in Fig. 9. The tangent to this curve gives the direction of the total deviatoric strain increment (φ_D). We must notice the triangular form: the corners can be associated roughly with state of compression, and the sides can be associated with the three mechanisms of plane deformation.

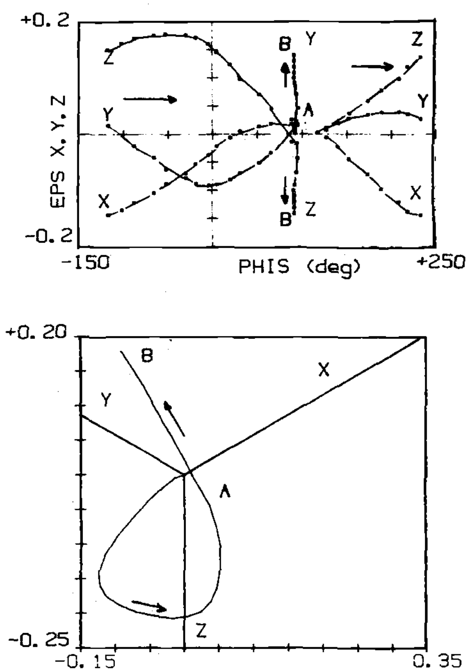

(a)

(b)

FIG. 11—(a) *Variations of* ϵ_x, ϵ_y, ϵ_z. (b) *Deviatoric strain path. The rotation is stopped during path AB (test 2).*

Another important part of the kinematic response of the specimen is the volume change, which is plotted in Fig. 10. The main fact is the very important compaction (7%) for the five cycles with a tendency to stabilization. The density is 1.55 in the initial state and 1.66 at the end of the fifth cycle. For the sand under consideration the initial state is medium and the final state is very dense. This result shows clearly that the volume change cannot be related to the intensity of the stress deviator alone (*SD*2) as it is often admitted for linear stress path. For such linear path, dense sample shows dilatancy when the state of stress reaches a stationary value on the limit surface. In this study, each principal direction *x*, *y*, and *z* is alternatively loaded and unloaded. The observed compaction is due to cyclic loading and unloading even if the state of stress lies on the limit surface. From a practical point of view, in undrained conditions, this tendency to compaction even for dense material, may lead to liquefaction by increasing pore pressure.

Test 2—The second test consists of one circular path with the same value for *S*1 and *SD*2, but the φ_s step is $-10°$ (the rotation is counterclockwise) and the frequency in time is 20 s. This change in frequency produces greater deformation (see Fig. 11) because the material flows for a longer time, but the comments about the stress path, the direction of the strain increment, and the volume change remain unchanged. The new part is that the φ_s evolution has been stopped at the end of this cycle. It corresponds to the AB path on the figures. The expected stress is now constant. In this way it can be verified that the actual state of stress is on the limit surface because the material flows under constant state of stress. The deformation turns in plane deformation on X direction, and the volume increases (Figs. 11–13). The same results are usually obtained for a linear stress path when the state of stress cannot move along the limit surface.

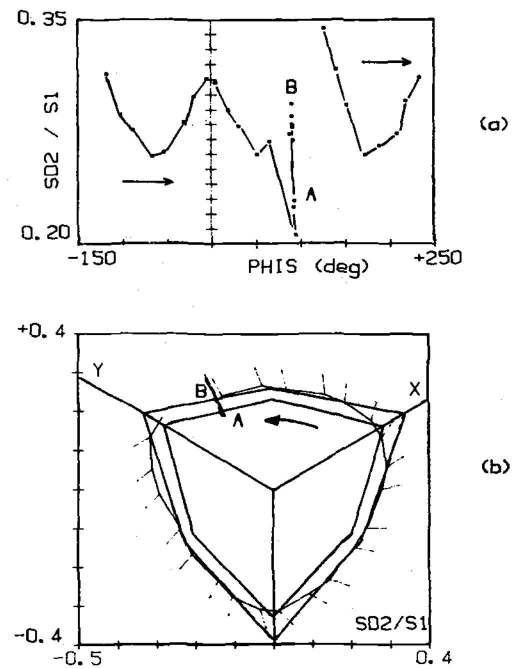

FIG. 12—(a) *Variations of* SD2/S1. (b) *Deviatoric stress path with Coulomb criterion 30°, 35° (test 2).*

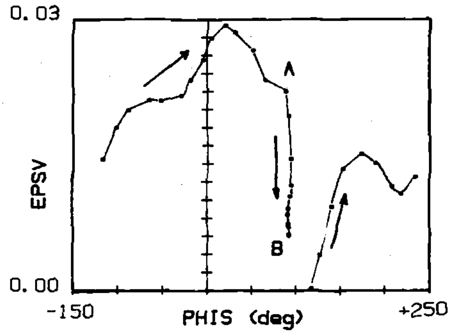

FIG. 13—*Volume change versus* φ_s *(test 2).*

Conclusions

A true triaxial apparatus is a useful tool to study three-dimensional behavior of materials. The conclusions for dry sand are the following:

1. The limit surface exists and is the same whatever the stress paths are.
2. In the vicinity of the limit surface large deformations can occur, but the volume change may be very different if the state of stress is stationary (the material shows dilatancy) or if the state of stress is rotating (the material contracts)
3. The main mechanism of large deviatoric deformation under stationary state of stress is plane deformation with localization in narrow shear bands.

Acknowledgment

This experimental research is partly financially supported by the Centre National de la Recherche Scientifique (CNRS) (Greco 90—Geomateriaux).

References

[*1*] Saada, A. S. and Townsend, F. C. "State of the Art: Laboratory Strength Testing of Soils" in *Laboratory Shear Strength of Soil, ASTM STP 740,* R. N. Yong and F. C. Townsend, Eds., American Society for Testing and Materials, Philadelphia, 1981, pp. 7–77.
[*2*] Lanier, J., *Revue Française de Géotechnique,* No. 20, 1982, pp. 21–29.
[*3*] Lewin, P. I., "Cyclic 3-D Stress Paths and Superposition of Hysteresis Loops" in *Proceedings,* International Symposium on Soils under Cyclic and Transient Loading—SWANSEA, Vol. 1, G. Pande and C. Zienkiewicz, Eds., Balkema, Rotterdam, 1980, pp. 225–229.
[*4*] Matsuoka, H., Koyama, H., and Yamazaki, H., *Soils and Foundations,* Vol. 25, No. 1, 1985, pp. 27–42.
[*5*] Pearce, J. A., "A New Triaxial Apparatus" in *Proceedings,* Stress–Strain Behavior of Soils, Roscoe Memorial Symposium, R. H. G. Parry, Ed., G. T. Foulis and Co., Ltd., England, 1971, pp. 330–339.
[*6*] Goldsheider, M. and Gudehus, G., "Rectilinear Extension of Dry Sand: Testing Apparatus and Experimental Results" in *Proceedings,* Eighth International Conference on Soil Mechanics and Foundation Engineering, Vol. 1–3, Moscow, 1973, pp. 143–149.
[*7*] Hill, R., "*Mathematical Theory of Plasticity,*" Clarendon Press, Oxford, 1950.
[*8*] Arthur, J. R. F. and Dustan, T., "Rupture Layers in Granular Media" in *Proceedings,* International Union of Theoretical and Applied Mechanics. Symposium on Deformation and Failure of Granular Materials, P. A. Vermeer and H. J. Luger, Eds., Balkema, Rotterdam, 1982, pp. 453–459.
[*9*] Desrues, J., Lanier, J., and Stutz, P., *Engineering Fracture Mechanics,* Vol. 21, No. 4, 1985, pp. 909–921.
[*10*] Reades, D. W. and Green, G. E. *Geotechnique,* Vol. 26, No. 4, 1976, pp. 551, 576.

Author Index

S

T

U–Z

Subject Index

A

I

N

O

T

ISBN 0-8031-0983-0